Advances in Experimental Medicine and Biology 1295

Flavia Fontana
Hélder A. Santos *Editors*

Bio-Nanomedicine for Cancer Therapy

Springer

Advances in Experimental Medicine and Biology

Volume 1295

Series Editors

Wim E. Crusio, Institut de Neurosciences Cognitives et Intégratives
d'Aquitaine, CNRS and University of Bordeaux,
Pessac Cedex, France
Haidong Dong, Departments of Urology and Immunology,
Mayo Clinic, Rochester, MN, USA
Heinfried H. Radeke, Institute of Pharmacology & Toxicology, Clinic of the
Goethe University Frankfurt Main, Frankfurt am Main, Hessen, Germany
Nima Rezaei, Research Center for Immunodeficiencies, Children's Medical Center,
Tehran University of Medical Sciences, Tehran, Iran

Advances in Experimental Medicine and Biology provides a platform for scientific contributions in the main disciplines of the biomedicine and the life sciences. This series publishes thematic volumes on contemporary research in the areas of microbiology, immunology, neurosciences, biochemistry, biomedical engineering, genetics, physiology, and cancer research. Covering emerging topics and techniques in basic and clinical science, it brings together clinicians and researchers from various fields.

2019 Impact Factor: 2.450 5 Year Impact Factor: 2.324

More information about this series at http://www.springer.com/series/5584

Flavia Fontana • Hélder A. Santos
Editors

Bio-Nanomedicine for Cancer Therapy

Springer

Editors
Flavia Fontana
Faculty of Pharmacy
University of Helsinki
Helsinki, Finland

Hélder A. Santos
Faculty of Pharmacy
University of Helsinki
Helsinki, Finland

ISSN 0065-2598 ISSN 2214-8019 (electronic)
Advances in Experimental Medicine and Biology
ISBN 978-3-030-58173-2 ISBN 978-3-030-58174-9 (eBook)
https://doi.org/10.1007/978-3-030-58174-9

© Springer Nature Switzerland AG 2021
This work is subject to copyright. All rights are reserved by the Publisher, whether the whole or part of the material is concerned, specifically the rights of translation, reprinting, reuse of illustrations, recitation, broadcasting, reproduction on microfilms or in any other physical way, and transmission or information storage and retrieval, electronic adaptation, computer software, or by similar or dissimilar methodology now known or hereafter developed.
The use of general descriptive names, registered names, trademarks, service marks, etc. in this publication does not imply, even in the absence of a specific statement, that such names are exempt from the relevant protective laws and regulations and therefore free for general use.
The publisher, the authors, and the editors are safe to assume that the advice and information in this book are believed to be true and accurate at the date of publication. Neither the publisher nor the authors or the editors give a warranty, expressed or implied, with respect to the material contained herein or for any errors or omissions that may have been made. The publisher remains neutral with regard to jurisdictional claims in published maps and institutional affiliations.

This Springer imprint is published by the registered company Springer Nature Switzerland AG
The registered company address is: Gewerbestrasse 11, 6330 Cham, Switzerland

Preface

Cancer still represents a heavy societal burden with profound economic implications. Tumors are treated with chemotherapeutic drug molecules with challenging properties for their formulation and unspecific total body toxicity when administered systemically. The application of nanotechnology to medicine, particularly for cancer treatment, has provided physicians with novel weapons in the fight against the diseases. Nanotechnology refers to the development and use of systems characterized by sizes of 1–1000 nm. The use of nanotechnology in cancer treatment has brought along a revolution in the treatment of patients, enabling therapeutic paradigm shifts and ameliorating patients' quality of life. In nanomedicine, the small particles are loaded with anti-cancer drugs, altering their biodistribution compared to the free drug. This research field combines the expertise of engineers and material scientists, pharmacists, physicians, and immunologists to obtain carefully optimized nanoparticles to improve the drug treatment efficacy, while lowering the drug's side effects. The field of nanomedicine draws several parallels from "cooking" where an optimized "recipe" can produce "complex flavored dishes."

Nanotechnology has been, and is currently, playing a major role in cancer treatment, with several formulations for the delivery of chemotherapeutics and multiple others as companion diagnostics. Some of the conventional drug delivery nanosystems have been approved more than 20 years ago, profoundly affecting the treatment options. These nanosystems have also paved the way for research and the application of nanomedicines in other therapeutic indications, such as anesthetics, treatment of iron deficiency, antifungine delivery, and vaccines. The latest approvals have focused on the delivery of nucleic acids for gene therapy, such as in Onpattro®, and the recent developed COVID-19 vaccines. Conventional nanoparticles, however, in most cases only reduce or ameliorate a drug's side effect profile without affecting the efficacy of the drug. Interestingly, the combination of conventional nano-delivery systems with hyperbaric oxygen treatment greatly enhances the therapeutic efficacy.

Conventional nanoparticles are also lacking a complete zip-code, they are immitted in the circulation and the postal system hopes they will find the right target. Peptides can serve as exquisite address labels, facilitating the delivery of drug-loaded nanosystems at the tumor. Alternatively, the combination of cells with nanoparticles in the biohybrid systems modifies the circulation pathway of the nanoparticles by mimicking the natural constituents of the human body. The labelling of these systems with radioactive tags can help in visualizing their biodistribution with potential therapeutic applications in radiotherapy.

Once at the tumor site, particular characteristics of the nanosystems, such as high porosity, and the presence of metals can provide multiple mode of action for the nanocarrier. Together with carrying drugs, they can carry large biomolecules like enzymes or react with lasers to increase the tumor temperature.

Sometimes, however, nanoparticles are not the best choice for all the applications in cancer treatment and can be exchanged for mats of electrospun nanofibers. Nanoneedles represent another alternative particularly for sampling and intracellular drug delivery to specific cell targets.

Research in cancer nanomedicine has resulted into thousands of promising therapies. However, the efficacy has to be evaluated in suitable in vitro models, with the possibility to design automated systems for high-throughput screening. 3D models, and spheroids in particular, are currently considered the state-of-art as in vitro tumor models. Moving further in the development pipeline, solid and translatable in vivo tumor models are highly needed to provide reliable information before starting the clinical trials.

Finally, cancer treatment has been overturned by the discoveries and applications of immunotherapy. In some of the patients, immunotherapy has achieved a complete cure. Nanotechnology plays a role with cancer nanovaccines, providing the immune system with a more powerful response. Moreover, the perfect example of nanosystems is viruses. Viruses have been shaped by millennia of co-evolution with the human body and can be modified to infect and destroy only cancer cells, while establishing a massive immune activation, either alone or combined with other inorganic/organic systems (biohybrid materials).

In this book, we include chapters explaining the basics of nanomedicine, together with the most recent research in cancer immunotherapy. This book is unique in containing both elements to provide the reader with solid basis before moving to the following developments. In this respect, the present book represents a guide on cancer nanotechnology, written by outstanding specialists in the field, for an advanced and specialist readership, while being relevant for the wider readers in academia and in private companies. Moreover, this book is designed with a thought towards the younger generations of under- and post-graduate students, to provide a 101 guide in the world of cancer nanomedicine. Thus, we collected informative and valuable contributions from top-level researchers in material science, pharmacy, biology, radiochemistry, and immunology, working together on the development of advanced nanomedicines/nanoparticles for cancer treatment applications. Overall, this book provides a highly valuable support for the readers in the field of cancer nanomedicine.

We would like to express our gratitude to all the authors and contributors of this book for their cooperation and enthusiasm in writing the book chapters, spacing from classical nanosystems to nanoneedles, to radioactive probes, and in vitro and in vivo models for the screening of nanoparticles, as well as to the latest developments in biohybrid nanoparticles and immunotherapy with cancer vaccines and oncolytic viruses, and the industrial and commercial perspective on nanotechnology in cancer immunotherapy. The concepts presented in each chapter are clarified by selected and explicative examples. We wish the readers will enjoy the contents of the book and hope that this book will promote discussion about the role of nanotechnology in cancer therapy.

Helsinki, Finland

Flavia Fontana
Hélder A. Santos

Contents

Part I 101 Ways on Conventional Nanotherapies and How to Spice It Up

Conventional Nanosized Drug Delivery Systems for Cancer Applications 3
Cristian Vergallo, Muhammad Nadeem Hafeez, Dalila Iannotta, Hélder A. Santos, Nicola D'Avanzo, Luciana Dini, Felisa Cilurzo, Massimo Fresta, Luisa Di Marzio, and Celia Christian

Homing Peptides for Cancer Therapy 29
Prakash Lingasamy and Tambet Teesalu

Radiolabeling of Theranostic Nanosystems 49
Sudeep Das, Surachet Imlimthan, Anu J. Airaksinen, and Mirkka Sarparanta

Boosting Nanomedicine Efficacy with Hyperbaric Oxygen Therapy 77
Xiaoxian Wang, Si Li, Xin Liu, Xian Wu, Ningbing Ye, Xiangliang Yang, and Zifu Li

Part II Shuffle It Up with Innovative Treatment Modalities

Mesoporous Silica Nanoparticles as Carriers for Biomolecules in Cancer Therapy 99
Berrin Küçüktürkmen and Jessica M. Rosenholm

Clearable Nanoparticles for Cancer Photothermal Therapy 121
Jun Zhao, Xin Long, and Min Zhou

Biohybrid Nanosystems for Cancer Treatment: Merging the Best of Two Worlds 135
Flavia Fontana, Raquél Bartolo, and Hélder A. Santos

Electrospun Nanofibers for Cancer Therapy 163
Huanhuan Luo, Tianyang Jie, Li Zheng, Chenglong Huang, Gang Chen, and Wenguo Cui

Nanoneedle-Based Materials for Intracellular Studies 191
Julia E. Sero and Molly M. Stevens

Part III Test, Repeat, and Test Again

In Vitro Assays for Nanoparticle—Cancer Cell Interaction Studies 223
Tomás Bauleth-Ramos and Bruno Sarmento

3D Tumor Spheroid Models for In Vitro Therapeutic Screening of Nanoparticles 243
Simonas Daunys, Agnė Janonienė, Indrė Januškevičienė, Miglė Paškevičiūtė, and Vilma Petrikaitė

In Vitro and In Vivo Tumor Models for the Evaluation of Anticancer Nanoparticles . . . 271
Teresa R. Abreu, Mariana Biscaia, Nélio Gonçalves, Nuno A. Fonseca, and João Nuno Moreira

Part IV It Is All a Matter of Immunity

Nanotechnology for the Development of Nanovaccines in Cancer Immunotherapy . . . 303
Maria Aurora Grimaudo

Viral Nanoparticles: Cancer Vaccines and Immune Modulators . . . 317
Manlio Fusciello, Erkko Ylösmäki, and Vincenzo Cerullo

Industrial Perspective on Immunotherapy . . . 327
Sara Ravasio

Index . . . 349

Part I

101 Ways on Conventional Nanotherapies and How to Spice It Up

Conventional Nanosized Drug Delivery Systems for Cancer Applications

Cristian Vergallo, Muhammad Nadeem Hafeez, Dalila Iannotta, Hélder A. Santos, Nicola D'Avanzo, Luciana Dini, Felisa Cilurzo, Massimo Fresta, Luisa Di Marzio, and Celia Christian

Abstract

Clinical responses and tolerability of conventional nanocarriers (NCs) are sometimes different from those expected in anticancer therapy. Thus, new smart drug delivery systems (DDSs) with stimuli-responsive properties and novel materials have been developed. Several clinical trials demonstrated that these DDSs have better clinical therapeutic efficacy in the treatment of many cancers than free drugs. Composition of DDSs and their surface properties increase the specific targeting of therapeutics versus cancer cells, without affecting healthy tissues, and thus limiting their toxicity versus unspecific tissues. Herein, an extensive revision of literature on NCs used as DDSs for cancer applications has been performed using the available bibliographic databases.

Keywords

Drug delivery systems · Colloidal nanoparticles · Lipid nanoparticles · Liposomes · Polymeric nanoparticles · Metallic nanoparticles · Carbon nanostructure · Nanocrystal · Dendrimers · Hyper-branched polymers · Anticancer therapy · Passive targeting · Active targeting · Aptamers · Therapeutic proteins

1 DDSs Enhancing the Therapeutic Effects of Co-delivered Drugs in Cancer Treatment

Cancer is the most common disease and leading cause of death, and was responsible for an estimated 9.6 million deaths in 2018. Globally, about 1 in 6 deaths is due to cancer [201]. Chemotherapy represents a therapeutic option for cancer treatment that uses drugs, which are administered by different routes, such as intramuscular injection, intravenous push technique, or intravenous infusion, to kill cancer cells [47]. However, several side effects are associated with chemotherapeutics. They include toxic effects and detrimental metabolic activities for healthy cells; in addition, some cancer cells may not be responsive to anticancer drugs, thus developing resistance [75, 184]. Unfavorable toxicity, development of drug resistance, and limited regime in clinical uses are associated with the anticancer treatment by using single chemotherapeutic drugs [159]. To overcome these drawbacks of chemotherapy, in the past decade, the combination of different chemotherapeutic drugs has gained impressive attention. Multiple anticancer drugs are simultaneously used in order to decrease each drug's toxic side effects on normal cells, while, at the same time, enhancing synergistic and additive effects with high therapeutic efficacy on cancer cells. Several NCs, such as lipid-based NCs, metallic/nonmetallic nanoparticles (NPs), nanoshells, nanorattles, quantum dots (QDs), fullerenes, nanotubes

---

Cristian Vergallo and Muhammad Nadeem Hafeez contributed equally with all other contributors.

C. Vergallo · M. N. Hafeez · D. Iannotta · F. Cilurzo · L. Di Marzio
C. Christian (✉)
Department of Pharmacy, University of Chieti-Pescara "G. d'Annunzio", Chieti, Italy
e-mail: c.celia@unich.it

H. A. Santos
Faculty of Pharmacy, University of Helsinki, Helsinki, Finland

N. D'Avanzo · M. Fresta
Department of Health Sciences, University of Catanzaro "Magna Graecia", Catanzaro, Italy

L. Dini
Department of Biology and Biotechnology "Charles Darwin", University of Rome "Sapienza", Rome, Italy

CNR Nanotec, Lecce, Italy

© Springer Nature Switzerland AG 2021
F. Fontana, H. A. Santos (eds.), *Bio-Nanomedicine for Cancer Therapy*, Advances in Experimental Medicine and Biology 1295, https://doi.org/10.1007/978-3-030-58174-9_1

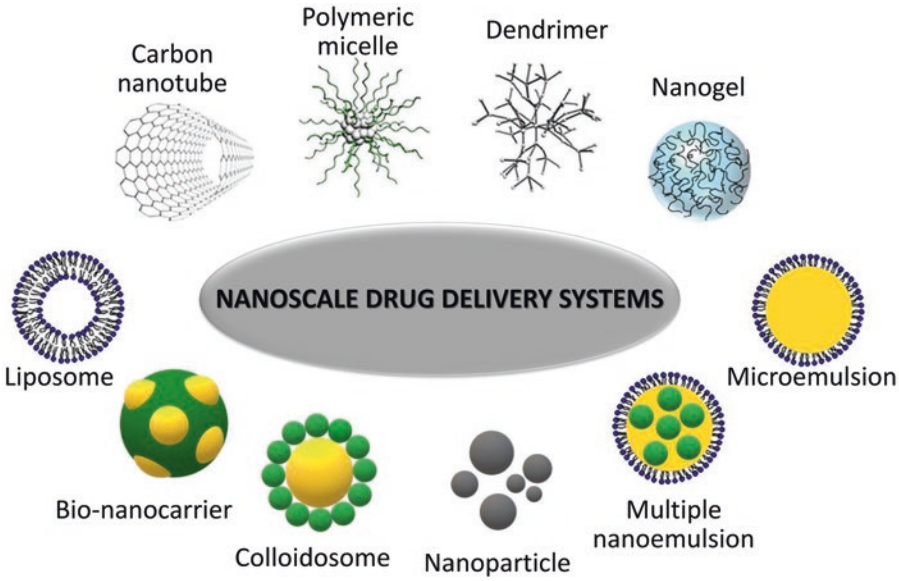

Fig. 1 Nanosized DDSs commonly used to treat different types of cancers

(NTs), carbon nanostructures, monodisperse-nanocrystals, close-packed nanocrystal assemblies, dendrimers, hyperbranched polymers, emulsions, and nanomicelles have been designed and exploited as co-delivery systems to treat different types of cancers. The administration of multiple drugs in drug delivery systems is still prevented by several challenges such as different pharmacokinetic properties and water solubility of the combined drugs, which significantly affect their bio-distribution and blood circulation, the targeting on the tumor site, the bio-accumulation in tissue, and the drug circulation in the blood stream [217, 218].

Examples of nanosized DDSs that have recently been gaining interest from the scientific community and clinicians to enhance the therapeutic effects of co-delivered drugs in combination chemotherapy are shown in Fig. 1. Due to their enhanced bioavailability and blood circulation (e.g., DDSs modified after self-assembling in order to prevent the uptake by the mononuclear phagocyte system), permeability and retention (EPR) effect, nanosized DDSs can target selectively cancer cells [174]. The simultaneous delivery of multiple drugs at targeted tumor tissue is achieved by nanosized DDSs with normalized pharmacokinetics and pharmacodynamics of therapeutic agents. Nanosized DDS-based therapy shows several other advantages over other approaches such as prevention from drug degradation, controlled release of drug, high accumulation rate at the action site, and reduced side effects of drugs on normal body cells [174]. Carrier-free nanodrugs recently emerged as potential generation of nanosized DDSs. Photodynamic therapy (PDT) and photothermal therapy (PTT) have comprehensively been exploited to improve the biosafety and therapeutic efficacy of chemotherapeutic drug treatment of malignant cancers.

The loading of imaging agents into the carrier is another important advantage of nanosized DDSs, resulting in theranostic nanosized DDSs, which allow a rapid biodistribution and an easy pharmacokinetic analysis, as well as a real time tracking of drugs and an enhanced performance of delivery process, thus predicting its/their therapeutic effect(s) [202]. Nanosized DDSs are typically developed by loading multiple anticancer drugs within NCs such as polymer micelles, inorganic NPs, and liposomes. Materials for the synthesis of these NCs should be inert and not exert any dangerous side effects. In fact, they have safety properties and need to prevent such events as inflammation and systemic toxicity. It is also worth mentioning that the average loading capacity of nanosized DDSs is relatively low (<10%). Therefore, it should be highly desirable to develop alternative nanosized DDSs with high drug loading efficiency [218].

2 Lipid-Based NCs

Lipid drug conjugates and lipid based NCs are conventional nanosized DDSs used for cancer treatment. Lipid-drug conjugates are drug molecules that have been covalently modified with lipids, showing several advantages such as improved oral bioavailability, enhanced tumor targeting, reduced toxicity, and increased payloads [94]. Conventional lipid-based NCs increase the water solubility of hydrophobic compounds in the blood stream due to the biopharmaceutical properties of the NCs [126]. Lipids render these nanocarriers suitable for drug delivery and therapeutic applications. A common example of lipid-based NCs is liposomes that mainly consist of phospholipids, which are the main components of the biological cell membranes [61]. Polymer-lipid hybrid NPs have been recently introduced as novel DDSs [203]. They are made up of a polymeric core coated by a phospholipid shell and provide some advantages of both polymeric NPs and liposomes in the form of a unique shell-core structure [208]. The solid core structure of these NPs provides both structural and mechanical stability, which allows a larger surface area, as well as a narrow size distribution [20]. The outer layer of lipid-based NCs is similar to a cell membrane and provides them with high bio-compatible properties [148]. Their improved drug loading and increased encapsulation efficiency [216] allow the delivery of both hydrophobic and hydrophilic drugs, thus promoting the intracellular uptake of payloads [151].

In a recent study, zinc(II)phthalocyanine (photosensitizer) has been combined with thiophenyl and loaded into a lipid NC in order to evaluate its therapeutic efficacy toward cancer treated by PDT. The substitution of thiophenyl in zinc(II) phthalocyanine significantly improves its photodynamic responsiveness, thus representing a useful therapeutic tool to treat hepatocellular carcinoma (HCC) [54]. Albano and coworkers [8], in an effort to minimize the total amount of excipients, formulated solid lipid nanosized DDSs by combining cetyl palmitate with two poloxamers, Pluronic-F68 and F127, as inhibitors of glyco-protein efflux pump. When these polymer-lipid NCs were tested as therapeutics for cancer treatment, both high encapsulation efficiency (more than 90%) and sustained release of docetaxel were obtained. To address the challenges in the therapeutic efficacy of the topotecan and metformin (metabolic modulator) combination, lipid bilayer-camouflaged mesoporous silica NPs were formulated. In addition, a novel ion pairing-assisted loading procedure was developed by using pamoic acid as an in situ trapping agent. It was demonstrated that pamoic acid increased the hydrophobic properties of metformin and topotecan, thus resulting in high significant payload efficiency (>40 and 32 weight (wt)%, respectively) in the mesoporous silica NPs and in a controlled release profile. The synergistic cytotoxicity of both drugs, via cell cycle arrest and depolarization of the mitochondrial membrane, was significantly increased toward MDA-MB-231/4 T1 cells compared to the control. Interestingly, the results of preclinical trials showed pharmacokinetic profiles with 4–7 fold higher circulation and 7.5–10 fold higher concentration at the tumor site for these two drugs, when injected using NPs, than the free drugs [15].

The conjugation of some natural bioactive compounds to lipid based NCs improves their bioavailability and water solubility, and it represents the main challenge of this strategy in drug development. A polymer-lipid hybrid NC was developed by Du et al. [46] to encapsulate the natural compound furanocoumarin. The entrapped compound showed a delayed release compared with the free furanocoumarin. This NC showed similar antitumor efficacy but lower toxicity than the chemotherapeutic anticancer agent doxorubicin (DOX) in a MCF-7 breast tumor model [46].

The combination of diagnostic and therapeutic agents in the same lipid based NCs is an interesting and emerging approach for cancer treatment. Camptothecin (CPT), a liposomal formulation, containing quantum dots, and made up of dimeric CPT glycerophosphorylcholine, significantly inhibits the growth of HepG-2, MCF-7, and HeLa cells, having 62 wt% loading capacity and stability in physiological fluid [58]. Results demonstrated that the resulting NCs can provide a new strategy for synergy therapy of cancer. Similarly, docosahexaenoic acid and DOX have a longer half-life, a higher tumor uptake ratio, lower toxicity and a higher tumor growth inhibition profile when co-loaded into radiolabeled lipid-based NC-Tc-99 m and used to treat a breast cancer murine model [63].

Melphalan and miR-181a were also successfully co-delivered by lipid NCs for the treatment of retinoblastoma [185]. The co-delivery of regulator protein family B-cell lymphoma 2 (BCL-2) siRNA and epirubicin using lipid NCs showed an increased intracellular uptake and drug release in the tumor microenvironment, thus enhancing the anticancer efficacy as measured by the reduction in cell viability and in the expression of P-glycoprotein [212].

Cell penetrating peptides are another promising approaches in targeted cancer treatment, particularly, after their loading in lipid based NCs. Two types of cell penetrating peptides (linear-peptide RGERPPR, RGE, and cyclic-peptide CRGDRGPDC, cRGD) were used to modify gambogic acid-loaded lipid-based NC, and thus obtain gambogic acid-lipid-based NC-RGE, gambogic acid-lipid-based NC-cRGD, and gambogic acid-lipid-based NC-cRGD/RGE. The cellular uptakes of these lipidic formulations were qualitatively and quantitatively evaluated swapping gambogic acid for coumarin-6 as the fluorescent molecule. A high cytotoxicity was obtained for gambogic acid-lipid-based NC-RGE; this result agreed with high intracellular uptake of drug obtained in case of RGE-coumarin 6-lipid-based NC and the higher tumor growth inhibition resulted with RGE-gambogic acid-lipid-based NC [91].

3 Metallic and Nonmetallic NPs, Nanoshells, Nanorattles, and QDs

Metal NPs are submicron scale entities made of pure metals (e.g., gold, platinum, silver, titanium, zinc, cerium, iron, and thallium) or their derivatives (e.g., oxides, hydroxides, sulfides, phosphates, fluorides, and chlorides) [85]. Metallic, nonmetallic NPs, nanoshells, nanorattles, and QDs have several applications in the biomedical area, including cancer therapy. Magneto-plasmonic nanohybrid NCs, having a metallic shell of Au/Ag coated with Fe_3O_4 and poly (co-methacrylic acid-butyl methacrylate-co-acrylamide), co-loading letrozole as the anticancer drug, are used as switchable trimodal temperature/light/pH-triggered and controlled/targeted drug delivery systems for chemo-PTT against MDAMB-231 breast cancer cell. The superparamagnetic internal core provides targeted delivery properties to the plasmonic-magneto-nanohybrid NCs, while phototriggering and photothermal properties depend on the Au/Ag shells [85]. Amoli-Diva and co-workers developed bimetallic plasmonic Ag-Au and Au-Ag (core) NPs. The bimetallic core of NCs is activated by wavelengths to produce heat energy, which not only can increase the surrounding temperature over the upper critical solubility temperature of the polymer to open its valves and promote drug diffusion, but also can kill cancer cells through photo-thermal effects increasing the environment temperature by nearly 18 °C in 5 min. After radiation [10]. Changes of the composition and structure of bimetallic NPs modify the optical resonances that can be tuned over a broad range of wavelengths (e.g., ultra-violet–visible, UV-VIS, and near-infrared, NIR). Optical resonances in the NIR region referred as the "Tissue Transparency Window," which includes wavelengths between 800 and 1200 nm, are the most important because they can penetrate both water and human tissue [200]. Similarly, Au(1,7-phen)Br_3 loaded pH-responsive superparamagnetic NC (nanogels) demonstrated higher cytotoxicity, better pH-triggered-controlled release and significant inhibition of tumor cells against human cervical cancer HeLa cell lines than free drugs and conventional chemotherapeutics [162]. Another study demonstrated that plasmonic hollow Au-Ag nanoshells (tuned to NIR, laser-irradiation), loaded into mesoporous silica, can effectively and efficiently be used to modulate the release of 5-fluorouracil (5-FU) for PTT and prostate cancer therapy [153].

NCs containing metallic and nonmetallic (inorganic-hydroxyapatite, mesoporous silica and Fe_3O_4) nanoshells, and having suitable properties for drug delivery, as therapeutics and targeted agents, represent suitable drug delivery systems for therapeutic use. Inorganic NCs are very promising, because they can be used to study release kinetic and pathway activation by fluorescent probes. The fluorescence signal of tracers could be observed simultaneously with drug release, and thus, this strategy provides several benefits to evaluate the therapeutic effects of the nano-DDSs [55]. Compared with green light (490–570 nm), NIR light (650–900 nm) is more suitable for biological applications due to several advantages, such as minimum photodamage to biological samples, minimal interference from background autofluorescence, and acceptable tissue penetration [196]. Nanocomposites containing graphene QDs (GQDs), concanavalin A, lectin protein, and Fe_3O_4, co-loaded with DOX, were successfully tested for therapeutic/diagnostic applications on HeLa cells lines. The image analysis showed that more than double concentration of DOX was accumulated inside HeLa cells in the presence of an external magnetic field, due to the incorporation of Fe_3O_4 in the NC. The cytotoxicity of DOX was 13% higher than normal cells, thus clearly indicating that these NCs could be used in cancer therapy [50]. DOX targeted delivery is also achieved by using modified GQD-mesoporous silica-NPs with hyaluronic acid for fluorescent imaging [82].

Biosurfactants have been investigated as excipients making NCs by using QDs. They are basically amphipathic molecules having microbial origin that reduce interfacial and surface tension at liquid-solid-gas-interfaces. Bansal and co-workers [16] demonstrated that GQDs NCs conjugated with folic acid (FA) and biosurfactants could be used as therapeutic and diagnostic agents in clinical cancer treatment. In the future, the use of GQD-bioconjugates may allow the detection and treatment of cancer at an early stage. This may increase the life span of cancer patients [16]. Furthermore, black phosphorus QDs are incorporated into liposomes to make DDS with excellent NIR photothermal properties and drug release properties controlled by light. In vitro experiments demonstrate a good biocompatibility and NIR-light-induced chemo-photothermal antitumor efficiency [74]. Finally, ultra-small WS2 QDs co-loaded with DOX and mesoporous organosilicas NPs demonstrated high potentiality as therapeutics for synergistic chemo-PTT [119].

4 Fullerenes, NTs and Carbon Nanostructures

Fullerenes may play an important role in clinical oncology because they form complexes with various anticancer drugs such as cisplatin and DOX. Moreover, fullerenes are versatile delivery platforms because they significantly increase in vitro and in vivo therapeutic/cytotoxic effects of drugs, as shown in vivo in Lewis lung carcinoma [157, 158]. The therapeutic activity of landomycin, an angucycline antibiotic, was also increased using fullerenes as stable and flexible NCs for cancer treatment. Nanocomposites of fullerenes and landomycin show anticancer drug activity in vitro, thus suggesting their potential use in animal models and a future translation in clinics [24]. Water soluble polyhydroxylated fullerenes (PHFs) are functionalized nanomaterials or fullerenols, which can be used as molecular antioxidants and NPs. Compared to fullerenes, PHFs enhanced cellular permeability and solubility and had a lower toxicity [14]. PHF-based NCs conjugated with methotrexate have pH-dependent controlled release of drug, with a significant decrease of IC_{50} value, increased AUC, half-life, and cell cytotoxicity, and lack of toxicity for erythrocytes [14].

Carbon nanotubes (CNTs) are cylindrical fullerenes, the third allotrope of carbon, first discovered by Sumio Iijima in 1991 [93]. CNTs with a minimum diameter of one nanometer, and having length of several micrometers, are graphene sheets rolled in the form of concentric cylinders [51]. According to the number of sheets present in concentric cylinders, CNTs can be divided into two categories: single-walled-CNTs (SWCNTs) and multi-walled-CNTs (MWCNTs). SWCNTs have length of 20–1000 nm and diameter of 0.4–3.0 nm and are made up of a single graphene layer wrapped into a hexagonal cylindrical structure [110]. MWCNTs are composed of several single graphene cylinders, having an inner diameter of 1–3 nm, an outer diameter of 2–100 nm and a length ranging from 1 to several meters [45]. SWCNTs were conjugated with folate and their cell internalization was mediated via folate receptor (FR) pathway thanks to the FA targeting. Results showed that SWCNT-folate NC was not suitable for receptor-mediated cancer cell targeting. However, due to their needle-like structure, which allows easy cellular penetration, SWCNTs can be used as drug delivery systems of nucleic acid into cells [33]. Furthermore, an enhanced intracellular uptake of anticancer drugs, like CPT, was achieved by magnetic halloysite NTs conjugated with chitosan oligosaccharides and FA [44].

Besides CNTs, Khoee and co-workers successfully demonstrated the use of titanium dioxide NTs in cancer therapy. Titanium dioxide NT-loaded liposomes (cholesterol, soy lecithin, and polyethylene glycol or PEG) can be used for the prolonged delivery of 5-FU in the treatment of HeLa cells [106]. The use of longer MWCNTs was limited due to their cytotoxic effects. However, PEGylated MWCNTs of ~300 nm were not toxic and allowed a safe delivery of chemotherapeutic drugs, for example, DOX [219]. Carbon dots can be used as pH-responsive fluorescent therapeutic DDSs for DOX in human gastric cancer cells instead of carbon and titanium dioxide NTs. The fluorescent carbon dots enable the optical labeling and tracking of the drug delivery process for at least 48 h. Carboxyl-rich carbon dots have almost no toxicity to human gastric cancer (MGC-803) and human gastric epithelial (GES-1) cells with a cytocompatibility of over 90% compared to control (untreated) cells [48].

5 Monodisperse Nanocrystals and Close-Packed Nanocrystal Assemblies

Homologous series of monodisperse nanometer size crystals are known as nanocrystals. They are characterized by narrow size distributed systems in terms of the shape, size, surface chemistry, and internal structure. Probes with different properties (electrical, magnetic, and optical) are combined to characterize and develop consistent structural models of nanocrystal samples.

Several anticancer drugs have limitations to intravenous administration because of their poor aqueous solubility. One recent approach to address this issue is to entrap these compounds into colloidal nanocrystals during the nanocrystal assembling. The cores of nanocrystals and the relatively packed nanocrystals are composed of pure drugs, and they are stabilized with various excipients. Nanocrystals improve the treatment efficacy and decrease the side effects of drugs to healthy cells because they target specifically the tumor tissue thus delivering payloads in bulk. Their small size and high energy surfaces cause a rapid dissolution following administration, which limits the nanocrystal capability to accumulate at tumor site [67, 140]. A similar problem was observed with several nanocrystal-based anticancer drugs having pharmacokinetic profiles similar to Abraxane or paclitaxel (PTX) NPs [152, 172]. Among several other benefits, such as reduced hypersensitivity and lower neutropenia, Abraxane dissolves rapidly in biological fluids with an insignificant EPR effect. Several strategies have been investigated till date to interfere with the rapid dissolution of nanocrystal-based anticancer drugs [68, 69]. Among these approaches, the layer-by-layer stabilized coating of polyelectrolytes on nanocrystals is one of the few experimental successes reported, even though polyelectrolyte multilayering of nanocrystals drastically affects the dissolution capability of CPT [178], tamoxifen and PTX [3]. However, several other challenges still need to be addressed, such as opsonization and clearance by the mononuclear phagocyte system, accumulation in spleen and liver, and short half-life [70, 90]. The charged surface of nanocrystals represents one of the causes for the above-mentioned challenges. One possible solution to this challenge comes from masking nanocrystals with PEG, hindering the surface absorption of plasma proteins [150]. PEGylation of polyelectrolyte multilayer nanocrystals has already reported some advantages in vitro, such as slower dissolution than naked NCs, the increased colloidal stability in physiological media, and the lack of toxic effect. Conversely, pharmacokinetic and biodistribution show that these NCs are quickly cleared from the bloodstream and thus accumulated in the mononuclear phagocyte system organs (i.e., liver and spleen). This result may depend on the PEG which modifies the native surface properties of NCs [152].

Closely packed nanocellulose crystals can be successfully linked with chlorotoxin, a polypeptide, using Brønsted acid ionic as a solvent. The resulting close-packed nanocrystals of cellulose and chlorotoxin had significant biocompatibility and enhanced internalization in the U87MG glioblastoma cell line. Thus, this material may be used as DDSs in anticancer therapy [32]. Furthermore, novel PTX nanocrystals were evaluated for their antitumoral efficacy both in vitro and in vivo in comparison with a solution of free drug. Together with a significant lower systemic toxicity, an enhanced accumulation of nanocrystals-PTX was obtained at tumor site in

MCF-7-bearing mice. Moreover, the cytotoxicity was found to be time- and dose-dependent [118].

6 Dendrimers and Hyperbranched Polymers

Highly branched polymers, or dendrimers, were used for the first time in the field of nanotechnology by Vogtle [26]. Dendrimers are well organized 3D nanoscopic macromolecules (5000–500,000 g/mol) characterized by a narrow size distribution. They are distinguished by the number of layers between each cascade (tree like branches), generally known as generations, which possess functional groups at the terminal surface [49]. Their potential interaction with other macromolecules has been widely increased to make them highly functional in terms of host-guest complexes, thus offering wide applications in drug delivery. Herein, we discuss recent updates about dendrimers and hyperbranched polymers in drug delivery, drug conjugation, and their overall toxicity. To avoid any issue like uncontrolled drug release, low efficacy, toxicity, lower half-life, and lower loading capacity associated with NCs, dendrimers represent the solution for the administration of conventional chemotherapeutic drugs. Dendrimers are small in size, and they can penetrate easily in cancer cells. Penetration of dendrimers in deeper layers of 3D spheroid models and tumors depend on their small size (usually below 10 nm) and positive charge [28]. Interestingly, DOX-loaded negatively charged poly(amido amine)-2,3-dimethylmaleic monoamide (PAMAM-DMA) dendrimers had lower toxicity, enhanced cell membrane permeability and cytotoxicity over cancer cells, and are converted into positively charged PAMAM-DMA when exposed to acidic pH at the tumor site [31]. The surface of polyamidoamine G4 (PAMAM G4) dendrimers was modified with PEG to reduce the systemic toxic effect of the dendrimer conjugated with FA while increasing nanocomplex targeting. The FA application to PAMAM G4 improved the cell toxicity of PAMAM G4 and 5-FU-loaded PAMAM G4 in high concentrations due to their increased internalization, while PEGylation increased cell viability in a concentration-dependent manner. This nanocomplex had a good cell growth inhibition of HT-29 human colorectal cancer cells, with low side effects on mice myoblast C2C12 normal ones [142].

Graphene-decorated magnetic dendrimers can be used to co-deliver hydrophobic (curcumin) and hydrophilic (e.g., DOX) drugs to MCF-7 cancer cells. To increase the loading capacity of NCs, edges of graphene oxide sheets were decorated with a magnetic-functionalized polyamidoamine dendrimer with hydrazone groups at the end of the polymer, which not only improved the dispersibility and solubility of sheets but also conferred magnetic property to NCs. These NCs showed a pH-sensitive release for both drugs, and the drug release behavior was also improved by the co-immobilization of payloads [154]. Unimolecular micelles based on PAMAM dendrimers can be used as tumor-selective diagnostic/therapeutic platform owing to their stability, biocompatibility and selectivity. PAMAM dendrimers conjugated with F3, a peptide, and loading DOX exhibit enhanced permeability/internalization into breast cancer cells (e.g., MDA-MB-231) than PAMAM without F3 [207].

7 Emulsions and Micelles

Emulsions are two-phase mixtures of insoluble liquids in which a “continuous phase” surrounds vesicles of the “dispersed phase.” They are stabilized by surfactants to prevent coalescing of the dispersed phase into the macroscopic phase. The continuous phase of an emulsion is generally the aqueous phase, and the drug can be part of this. The stability of emulsions depends upon the diffusion and delivery of drugs from the hydrophobic interior [105]. Microemulsions are transparent oil-in-water systems with a diameter of 100–500 nm [167] which are widely studied as drug carriers, in order to improve the systemic, controlled, and targeted delivery of anticancer drugs [171]. DOX and phthalocyanine co-loaded microemulsions have been incubated with murine breast cancer (4 T1) for 3 h at various concentrations. Less than 10% of 4 T1 viable cells were observed when photodynamic therapy and chemotherapy were combined at a 1.0 J × cm^{-2} laser light dose with 1.0 μM phthalocyanine and 0.5 μM DOX. Additionally, these microemulsions were stable, had a suitable biocompatibility and improved photophysical properties, as well a significant pharmacokinetics profile, and upregulated 15 and 25 genes related to apoptosis and anti-cancer activity, respectively. These interesting features make them promising formulations for clinical trials in anticancer therapy by systemic, topical or transdermal administration [29].

Migotto et al. developed cationic bio-adhesive microemulsions for the intraductal administration of C6 ceramide, a sphingolipid that mediates nonapoptotic as well as apoptotic cell death. C6 ceramide concentration necessary to reduce MCF-7 cells viability to 50% decreased by 4.5-fold after nanoencapsulation compared to free drug; a further decrease of cell viability (2.6-fold) was obtained when tributyrin (a prodrug of butyric acid) was added as component of the oil phase of the nanocarrier. This approach provides a significant synergism between payloads and microemulsions that are per se therapeutic [138]. Gonzales et al. [77] highlighted the pharmacokinetic benefits of microemulsions used as NCs, by developing fluorescent poly(ADP-ribose)polymerase 1 (PARP1) inhibitor (PARPi-FL), as an imaging agent targeting the nuclear enzyme PARP1 in small cell lung cancer, loaded nanoemulsions. Interestingly, this nanoemulsion is accumulated in H-69 and H-82 small cell lung cancer cell lines, where the contrast agent escapes and is then accumulated inside the cell nuclei [77].

Micelles are colloidal suspensions having a small diameter in the range of 5–100 nm. They gained attention from the scientific community thanks to their potential use in cancer therapy and diagnosis [170]. Along with the ability to deliver partially water-soluble anticancer drugs, micelles display also a significant penetration inside the tissue, site specificity (by attaching specific targeting moieties to the outer surface), and drug stability which contribute to their enhanced therapeutic efficacy [87, 127]. Micellar nanosystems are composed of hydrophilic and hydrophobic components self-assembled into nanosized ellipsoid, spherical, or cylindrical structures. Recently, hybrid stimuli-responsive micelles have been developed either by integrating metal NPs (gold, silver, and iron oxide) inside conventional micelles or by combining polymers and lipids into a single composite [87]. Micelles received scientific interest in the field of drug delivery because their diameter facilitates an easy and effective penetration into tumor cells. For example, PTX encapsulated inside polymeric micelles showed good efficacy in patients with advanced metastatic cancer [116, 175]. Similarly, DOX/PTX-loaded micelles [41] and DOX conjugated to pluronic [107] were widely used for cancer treatment. A hydrophobic core of micelles obtained by lipid-conjugated PEG can be used to deliver several poor water drugs, such as PTX, tamoxifen, porphyrin [134], CPT [72], and vitamin K3 [139].

8 Drug Targeting Strategies

One of the main challenges in cancer treatment is drug biodistribution. Drugs reach healthy tissues, damaging them or causing side effects. Because of this redistribution toward other tissues, there is a lower drug concentration in the tumor site. Thus, new targeting strategies have been developed [195]. NCs can achieve targeted delivery, extend half-life, and reduce the systemic toxicity in chemotherapy [36]. Two kinds of drug targeting are being investigated, passive and active [13]. The passive targeting is based on the EPR effect, by exploiting the presence of abnormal fenestrations belonging to the tumor vasculature (Fig. 2a). On the contrary, active targeting depends on NCs conjugating ligands that bind to a specific receptor overexpressed on the surface of the cancer cell (Fig. 2b).

9 Passive Targeting

The EPR effect is caused by the need for tumor cells to access nutrient and oxygen rapidly to fuel their exponential growth. Thus, cancer cells stimulate the growth of new blood vessels by activating vascular endothelial growth factor (VEGF) and other growth factors. These newly formed vessels are structurally and anatomically anomalous. In fact, they have a saccular endothelium with very large fenestra-

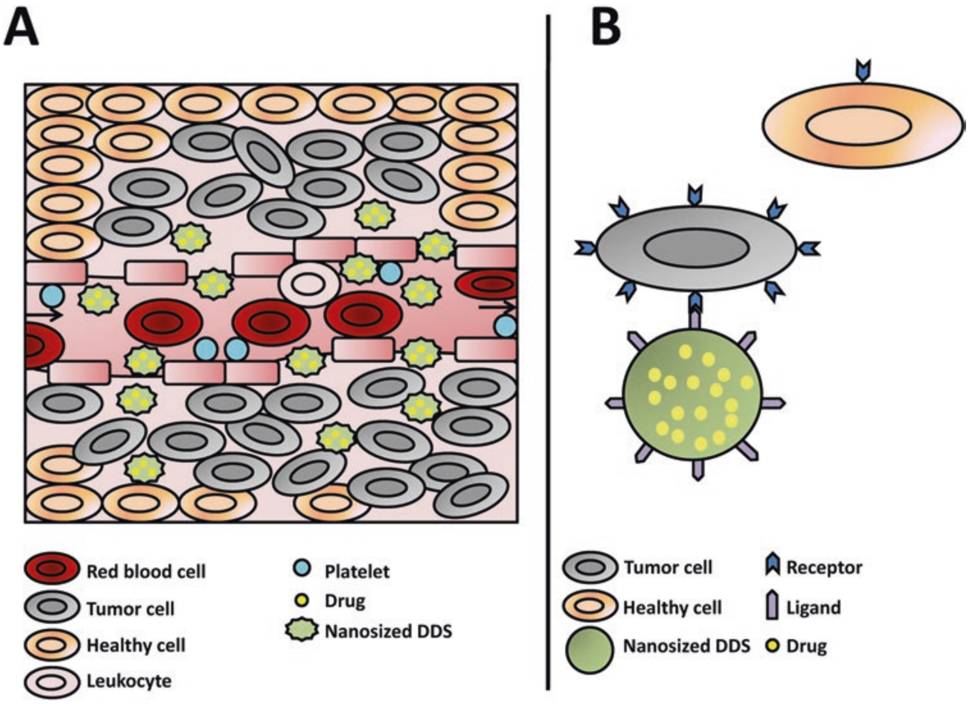

Fig. 2 Passive (**a**) and active (**b**) targeting. Anatomically, tumor microvessels are fenestrated, tortuous, and saccular with irregular and discontinuous patterns of interconnection and branching. Passive targeting takes advantage of these unique pathophysiological properties of tumor vessels, allowing nanosized DDS to accumulate into the tumor tissues. In active targeting, nanosized DDS is recognized and bound to target tumor cells through ligand-receptor interactions by the expression of receptors or epitopes on their cell surface. To achieve high specificity, those receptors/epitopes should be highly expressed on tumor cells, but not on normal ones

tions, without innervations, smooth musculature and lymphatic drainage, exhibiting altered receptors for Angiotensin II [21, 128]. Passive targeting exploits dilated endothelium fenestrations, formed because of the abnormal angiogenesis, to accumulate macromolecules/NPs preferentially in the neoplastic tissues [13, 128, 129]; this phenomenon (EPR effect) occurs by a diffusion-mediated transport, allowing a higher accumulation of macromolecules/NPs into tumor cells rather than in healthy ones [128, 129]. However, there is significant heterogeneity of EPR within and between tumor types. Different tumor types have different pore dimensions in the vasculature and that the maximum pore size changes with the location for a given type of tumor (i.e., primary vs. metastases). In addition, there may be differences in the vessel structure within a single tumor type [155]. Heterogeneous consequences are associated with the EPR effect. For example, the central area of metastatic cancers does not exhibit the EPR effect and shows less accumulation of macromolecules than other parts [141]; it facilitates the transport to tumors of nutrients and oxygen that sustain rapid tumor growth [57].

Erythrocytes normally constitute 40–50% of the total blood volume [190]. Leukocytes and platelets are pushed laterally by the red cells, which tend to accumulate into the vessel core. Thereby, platelets and leukocytes undergo an easy extravasation during inflammation processes [78]. Some NPs have been developed to exploit these underlying phenomena. NPs with the same size of platelets (from ten up to few hundreds of nanometers) flow laterally into the blood vessels and extravasate through the dilated endothelial fenestrations of tumor microvasculature. In addition, the slow blood flow in the tumor microvasculature, due to their anatomical tortuosity, allows NPs to stagnate in the tumor site [13]. The factors exploited in passive targeting, in addition to the anatomical anomalies of the tumor vessels, are the physical characteristics of macromolecules/NPs (e.g., size and shape) as well as the tumor microenvironment, that is, the characteristic of environment around a tumor (e.g., decrease in pH and increase in temperature) [17, 62].

In particular, the tumor microenvironment is characterized by different physicochemical properties in comparison with normal neighboring tissue, such as a lower pH, hyperthermia, and hypoxia [89]. All these differences are useful in the design of stimuli-responsive nanoscale DDSs for cancer therapy.

The responsiveness of DDSs to several stimuli could increase their effectiveness. For this reason, Chitgupi et al. [39] synthesized two liposomal formulations using two different chromophores conjugated to phospholipids, purpurin (690 nm) or pyropheophorbide (665 nm). Basic orange and DOX anthraquinones are loaded as single agents into the two liposomal formulations, and they were then mixed together into a single colloidal suspension. Interestingly, the formulation showed the release of payloads in cancer at a specific wavelength [39]. Fang et al. developed mesoporous carbon NPs modified with hyaluronic acid and GQDs, thus obtaining a dual-responsive targeting drug delivery system capable of providing both in vitro and in vivo synergistic chemo-PTT [56]. Another interesting approach to improve the effectiveness of anticancer DDSs has been proposed recently by Chen et al. and it consists of synthesizing pH/reduction responsive NPs capable of allowing an efficient delivery and a programed release of drugs in vivo. They developed a core of positively charged DOX-loaded lactobionic acid-chitosan-lipoic acid NP which was then coated with a negatively charged dimethylmaleic acid-PEG-chitosan layer to obtain a prolonged circulation time and improve the tumor-targeting effect. NPs targeting the specific tumor tissue were activated by the acidic microenvironment, thus modifying their surface charge from negative to positive with the relative removing of PEG from the surface of NPs. This effect depends on the dimethylmaleic acid-PEG-chitosan layer coating NPs that is pH-responsive to the modification of the microenvironment in tumors. pH-induced responsiveness of NPs caused the rapid release of entrapped DOX and its transfection inside the nuclei where DOX was triggered by the intracellular high concentration of glutathione, and thus activated cellular apoptosis [38].

In order to improve the efficacy of anticancer DDSs, several researches are focusing not only on targeting the general population of cancer cells, but also on others present in the tumor microenvironment [179]. Cancer stem cells (CSCs) are a small subpopulation of cells within tumors with capabilities of self-proliferation, differentiation, and tumorigenicity when transplanted into an animal host [213]. There is a direct correlation between the increase in the number of CSCs and the insurgence of chemoresistance that hinders a successful chemotherapy [122, 213]. Lin et al. recently developed a pH and glutathione sensitive NC co-delivering docetaxel and rubone, a miR-34 activator for targeting cancer stem cells, for a selective targeting of CSCs. Therapeutic NCs are specific for the treatment of taxane-resistant prostate cancer and enter the tumor cells by endocytosis pathway. NCs changed their structure and disassembled in the tumor microenvironment after protonation of the pH-responsive diisopropylaminoethanol, making nanocarriers, with the cleavage of the disulfide bond induced by glutathione under acidic condition. This modification results in a fast release of docetaxel and rubone from NCs, thus providing an upregulation of the intracellular miR-34a (rubone-mediated effect), which modulated the expression of proteins involved in chemoresistance, the increased responsiveness of tumor cells versus docetaxel treatment, and a significant inhibition of taxane-resistant tumor progression [122]. Karandish et al. [99] identified and targeted the neuropilin-1 receptor in both pancreatic and prostate cancer stem cells with stimuli-responsive PEG-PLA-based polymersomes delivering napabucasin, a stemness inhibitor. In particular, napabucasin-loaded polymerosomes decreased significantly the cell viability of prostate and pancreatic stem cells, compared to controls and cancer cells treated with empty formulation, and reduced the expression of stemness proteins like notch-1 and nanog. These DDSs provide some advantages compared to conventional drug delivery systems in prostate and pancreatic cancer therapy because they deeply penetrate into the tumors, thus releasing the entrapped stemness inhibitor, and killing CSCs [99].

Cancer induces an inflammatory response within the organism that leads to a massive accumulation of macrophages on its onset site (tumor associated macrophages, TAMs). TAMs included two entities: M1 and M2. M1 represents macrophages that follow "classical" activation by interferon-γ with either lipopolysaccharide or tumor necrosis factor, whereas M2 represents macrophages that follow "alternative" activation by interleukin 4. M1 macrophages showed a proinflammatory and cytotoxic (antitumoral) function, whereas M2 macrophages are antiinflammatory (protumoral) and promote wound healing [132]. Several studies have shown that the primary tumor growth and the number of metastatic sites can be significantly decreased by decreasing the population of macrophages in tumor tissue, for example, by blocking the recruitment of monocytes or eliminating TAMs already present in the tumor tissue [168]. To this aim, Cao et al. [30]) synthesized PTX-loaded NPs conjugating innovative peptide YI (YINP/PTX) on their surface that can target specifically TAMs and angiogenetic factors. The modified YI peptide increased significantly the specific accumulation of NPs in the tumor tissues [31], thus decreasing the untargeted effect on health tissues and particularly liver [30]. Similarly, Chen et al. [37]) showed that the co-administration of nRGD and lycobetaine-loaded PEGylated liposomes led to an improved tumor penetration and enhanced extravasation [38] which increased the antitumor efficacy against lung carcinoma, likely due to the depletion of TAMs [37].

9.1 Size and Shape

Both size and shape play a crucial role for adhesion of some DDSs, like NPs, to tumor endothelium. Even if several NCs for anticancer drugs have been synthesized in spherical forms, many bacteria and viruses display a nonspherical morphology to evade the immune system [102]. Thus, scientists modified the shape of NCs in order to develop smart and novel DDSs. Recent results showed that discoidal NPs are a good compromise between size (few nanometers) and shape, allowing for a greater adhesion surface [146], a better cellular uptake and antitumor efficacy than classical spherical ones [83]. In fact, they can be margined to the blood vessels thus escaping to macrophage uptake and move through the blood stream. Discoidal shape of nanocarriers also generated a circulating second stage of delivering systems that can transport inside other payloads showing potent anticancer activity versus metastatic tumors and improving the rate and long-term survival in vivo of animal engrafted with metastatic tumor cells [206].

9.2 pH

Several charge-switchable DDSs are developed to improve both the half-life in the bloodstream and their tumor cellular uptake. Due to the accumulation of acid moieties resulting from lower and slower flow of tumor vasculature as well as hypoxic conditions, the tumor microenvironment has a pH value of about 6.5 versus 7.4 of the normal neighboring tissue [81]. These pH differences depend on the ion concentrations that modify the microenvironment and the proton concentration, thus activating some mechanisms that can modulate the internalization and uptake DDSs by different pathways like endocytosis. In particular, protons entry into the endosome, by means of a mechanism called "proton sponge," leads to osmotic swelling and finally to endosome rupture, thus releasing the NCs and its payload into the cytoplasm. Other DDSs have been developed by using organic, inorganic, and hybrid pH-sensitive materials. The easy rupture of some bonds at low pH values allows the drug release at the tumor site [19, 124, 193]. Recently, a novel polymeric micelle-decorated Fe_3O_4/Au core-shell NP has been designed for pH-responsive intracellular co-delivery of 6-mercaptopurine and DOX [75].

The main disadvantage of using pH-sensitive DDSs is that they act in a specific pH range. However, some pH-sensitive DDSs have been translated from bench to clinical application and have been approved by the US Food and Drug Administration (FDA) for treatment of various cancerous diseases [124].

9.3 Temperature

The temperature in different body districts varies according to different factors such as the blood flow and the thermal energy generated by cellular metabolism. Due to their higher metabolic activity and blood flow compared to the surrounding healthy tissue, an increase in the temperature occurs in the tumor tissue [60, 98, 100, 166]. Thus, this increase of temperature at the tumor site could be used by thermo-responsive DDSs. Among the many different stimuli-sensitive delivery systems, temperature-sensitive DDSs offer great potential over their counterparts due to the versatility in their design, the tunability of phase transition temperatures, the passive targeting ability, and in situ phase transitions. In an effort to further control existing temperature-responsive systems, current innovative applications have combined temperature with other stimuli such as pH and light. The result has been the development of highly sophisticated systems, which demonstrate suitable control over drug release and represent huge advances in biomedical research [23]. For example, sulfonamide and hydroethylacrylate monomers have been polymerized with poly(N-isopropylacrylamide) to combine pH and temperature stimuli and thus develop injectable drug delivery systems that do not undergo phase transitions at the lower value of critical solution temperatures in physiological condition [133, 177]. Bikram et al. [22] have developed composite hydrogels of silica-gold nanoshells and poly(N-isopropylacrylamide) co-polymerized with acrylamide to form the photothermal modulated drug delivery system in which NIR light can be used to induce the collapse of the polymeric matrix containing payloads used as drug candidate model [22].

10 Active Targeting

Advances in nanobiotechnology and targeting strategy could improve the delivery of therapeutic molecules into cancer cells, thus improving the treatment effectiveness with minimal side effects on healthy cells [189].

Active targeting uses specific ligands to bind receptors overexpressed in tumor tissues. In literature, many ligands have been used for active targeting. They include peptides (e.g., octreotide, asparagine-glycine-arginine, cyclic peptide iRGD (CCRGDKGPDC) and C-end Rule, or CendR, motif peptide tLyP1), proteins (e.g., transferrin, growth factors, antibodies, and antibody fragments), mono- (e.g., galactose) and polysaccharides, glycosaminoglycans (e.g., hyaluronic acid), aptamers, and other molecules (e.g., FA, bisphosphonates, and biotin) [34, 64, 104, 164, 188]. These ligands are conjugated to NPs loaded with the drugs of interest, in order to release higher amounts of payloads in cancer cells rather than in healthy tissues. The choice of specific ligands to bind the appropriate receptors is very important for the right active targeting [13]. Very useful receptors are epidermal growth factor receptor (EGFR) and folate receptor (FR), which are overexpressed in most cancer cells [120, 147]. Active targeting has several advantages including increasing the drug dosage that is delivered to the tumor tissue with the resulting lower systemic administration, and the higher therapeutic efficacy [113, 194].

Targeting agents are conjugated to the DDS surface, thus increasing their interaction with specific cancer cells and tissues. In particular, many papers demonstrated the targeting cancer cells-overexpressed specific tumor receptors and accumulation of drugs inside cancer cells. However, strategies preserving healthy cells and tissues from the toxicity of drug targeting need to be addressed and are still one of the major challenges in pharmaceutical field [33]. Below, we discuss the main targeting agents that are conjugated to innovative DDSs and provided a smart and specific targeting for anticancer therapy (Fig. 3).

10.1 Peptides and Proteins

Peptides can recognize and bind receptors overexpressed by cancer cells with high affinity. They are poorly immunogenic and quickly excreted via liver and kidneys. Their synthesis is very simple, but it is quite expensive. In addition, peptides are easily exposed to the action of the peptidase enzyme that cleaves and inactivates these macromolecules, thus altering their biological effects.

The blockade of integrin signaling has been demonstrated to be efficient in inhibiting tumor growth, angiogenesis, and metastasis. Among all the integrins, $\alpha v\beta_3$ seems to play a fundamental role during tumor angiogenesis. Integrin $\alpha v\beta_3$ is highly expressed on activated endothelial cells, new-born vessels as well as some tumor cells, but it is not present in the other endothelial cells and most normal tissues and organs [125].

iRGD is a prototypic tumor-specific tissue-penetrating peptide (a 9-amino acid cyclic peptide with sequence CRGDKGPDC), which delivers drugs deeply into the extravascular tumor tissue (Fig. 3b). The pathway triggered by iRGD can be used for the enhanced transport of anticancer drugs administered as combination into the tumors. Indeed, Yang et al. [207]) had higher 4 T1 cells cellular uptake in vitro [209, 210] as well as higher penetration and accumulation of legumain-responsive aggregate gold NPs in breast tumor in vivo when these NPs were co-administered with iRGD [209].

Moreover, the cyclic peptide iRGD has been well established as a tumor-homing and tumor-penetrating peptide. iRGD initially binds the αv integrins expressed on tumor endothelial cells. Subsequently, the cleavage by a protease and the bond with neuropilin-1 allows its internalization [187, 188]. The identity of the iRGD processing protease(s) is unknown [27]. Song et al. [180] reported a DOX loaded liposomes modified with a "tadpole"-like peptide, which was obtained by conjugating covalently the alanine-alanine-asparagine "tail" residual to the cyclic tumor homing peptide iRGD to afford nRGD (multi-target peptide consisting of alanine-alanine-asparagine and cyclic iRGD). This DOX loaded liposomes modified with nRGD showed excellent antitumor efficacy in 4 T1 breast cancer mice than other formulations tested (i.e., free DOX, DOX-loaded PEGylated liposomes, DOX-loaded PEGylated liposomes and modified with iRGD, and DOX-loaded PEGylated liposomes and modified with nRGD), interacting with tumor vascular endothelial cells to achieve efficient tumor penetration, and modulate tumor microenvironment with depletion of tumor associated macrophages [180].

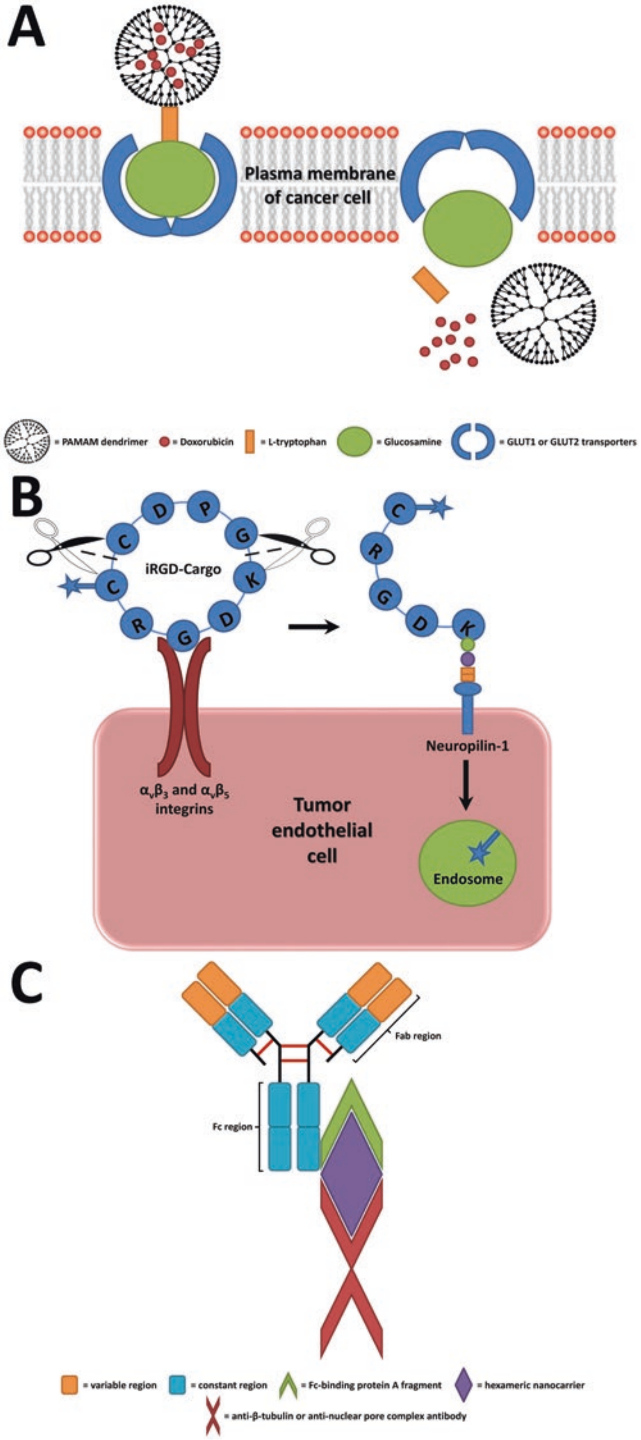
A
Plasma membrane of cancer cell
= PAMAM dendrimer
= Doxorubicin
= L-tryptophan
= Glucosamine
= GLUT1 or GLUT2 transporters
B
iRGD-Cargo
C
D
P
G
K
D
G
R
C
C
R
G
D
K
Neuropilin-1
$\alpha_v\beta_3$ and $\alpha_v\beta_5$ integrins
Tumor endothelial cell
Endosome
C
Fab region
Fc region
= variable region
= constant region
= Fc-binding protein A fragment
= hexameric nanocarrier
= anti-β-tubulin or anti-nuclear pore complex antibody

Fig. 3 New generation of DDSs for the enhanced transport of cancer drugs into tumors. (**a**) GLUTs mediated delivery of anticancer drugs. PAMAM dendrimers modified with L-tryptophan and GlcN permit higher drug loading and the use of GLUT transporters. This DDS allows the DOX release with significant higher cytotoxicity than PAMAM [112]. (**b**) Drug delivery into extravascular tumor tissue by the prototypic tumor-specific tissue-penetrating peptide CRGDKGPDC (iRGD). iRGD peptide homes and penetrates tumors through a three-step process: (1) the RGD sequence motif mediates the binding to $\alpha v\beta_3$ and $\alpha v\beta_5$ integrins expressed on tumor endothelial cells; (2) upon αv binding, a protease cleavage event is activated, revealing the c-terminal CendR motif of the peptide; (3) the peptide, by its CendR motif, binds neuropilin-1, thus activating the endocytotic/exocytotic transport pathway [187, 188] (C) Delivering of functional antibodies to the cytosol as intracellular therapeutics without cytotoxicity by Hex NC. This NC has been generated by combining a α-helical peptide that self-assembles into a hexameric coiled-coil bundle with an Fc-binding protein A fragment. An anti β-tubulin or antinuclear pore complex antibody as cargo allows the intracellular delivery of antibodies. The addition of an endosomolytic motif conjugated to the core improves this delivery [121]

Proteins, such as transferrin and EGF, are also used for active targeting. Transferrin is the major serum glycoprotein which transports iron into cells by receptor-mediated endocytosis, also called clathrin-mediated endocytosis [43]. Since cancer cells have higher transferrin receptor 1 expression than normal cells, this receptor represents a potential targeting to treat cancers by transferrin-conjugated DDSs [173]. However, the administration of elevated doses of transferrin-conjugated DDSs may also cause the death of healthy cells or cells with high proliferative activity [104]. Like transferrin receptor 1, also EGFR is overexpressed in human malignancies (e.g., carcinomas), and its activity enhances tumor growth, invasion, and metastasis [144]. The advantage of using EGF as the targeting moiety is that this can promote the transport of the drug to the nuclear level through an endocytic pathway in highly proliferating cells [34]. In addition, the internalization of DDSs conjugated to EGF is more rapid than those conjugated with other proteins, such as antibodies [164]. However, the use of this ligand may promote cell division because EGF is mitogenic [131, 191]. Antibodies are other ligands used for active targeting. The NC is bound to an antibody in the heavy chains portion, so that the two variable light chain endings can bind a specific receptor expressed on the tumoral cell surface [13]. This allows for a directional targeting effect and a controlled release of the drug simultaneously. V-erb-b2 erythroblastic leukemia viral oncogene homolog 2 (ErbB2) is a growth factor receptor overexpressed in 20–30% of human breast carcinomas as well as other adenocarcinomas. ErbB2 F5-scFv antibody was conjugated to DOX loaded into PEGylated liposomes. These F5-scFv targeted liposomes had antitumor activity and produced significant reduction of the tumor size in xenografted mice compared to nontargeted liposomes loading DOX, Doxil® [143]. Anti VEGF monoclonal antibodies and other VEGF inhibitors block the growth of several tumor cell lines in nude mice as previously reported [64]. Clinical trials with VEGF inhibitors in a variety of malignancies are still ongoing. In particular, a humanized anti VEGF monoclonal antibody (bevacizumab; Avastin®) has been approved by the FDA as a first-line treatment for metastatic colorectal cancer in combination with chemotherapy. VEGF is also implicated in intraocular neovascularization associated with diabetic retinopathy and age-related macular degeneration [64]. Other examples of new targeted DDSs using antibodies are further reported in the Sect. 19. However, targeted DDSs present also some disadvantages. The therapeutic effect could be altered if the bound DDS-antibody is not degraded correctly. Moreover, the antibody binding ability could be decreased if the fractions involved in this bond (antibody and or antigen) are sterically hampered by the presence of the nanocarrier. Finally, the immunoconjugate DDS-antibody could trigger an immune response in vivo by the organism [109, 163].

10.2 Aptamers

Aptamers are short single-stranded DNA or RNA oligonucleotides that can selectively bind to small molecular ligands or protein targets with high affinity and specificity, by acquiring unique three-dimensional structures as previously reported [101]; they have the advantage of being highly specific, relatively small, nonimmunogenic and can be easily stabilized by chemical modifications, thus allowing expansion of their diagnostic and therapeutic potential [101]. They could be conjugated to DDSs by a covalent bond to obtain a high affinity as well as a low immunogenic targeting. In addition, they are stable at different pH and temperature ranges, easily synthesizable, modifiable and excretable by kidneys [114]. However, because aptamers are composed of DNA or RNA oligonucleotides, they are rapidly degraded by exo- and endonucleases [176], thus the half-life of unmodified nucleotide aptamers in blood can be as short as 2 min. [80]. This issue has been solved through PEGylation. Dassie et al. [42] demonstrated that the RNA aptamer A9g functions as a smart drug for metastatic prostate cancer by inhibiting the enzymatic activity of the prostate-specific membrane antigen. A9g was safe in vivo and not immunogenic for human cells. Pharmacokinetic and biodistribution studies in mice have confirmed the targeting specificity and absence of nonspecific on/off-target effects [42]. Since their excellent properties, different aptamers conjugated with DDSs have been developed for cancer therapy. Sgc8c aptamer-DOX conjugates were found cytotoxic for leukemic cells expressing the protein tyrosine kinase 7 [92]. DOX was covalently conjugated with the AS1411 DNA aptamer, which targets plasma membrane nucleolin, a protein that is overexpressed in many cancer cells [115].

10.3 Other Molecules

Several low molecular weight ligand interactions with receptors are used as targeting moieties for DDSs. Among those ligands, folate is often used to target the FR because of its high expression level in most cancer cells compared to healthy cells and tissues. Folate is a very small ligand and has high affinity for its receptor; moreover, it can be easily conjugated with DDSs loading different payloads, and it is cheap, biocompatible, and safe [66].

11 Combined Targeting

The dual targeting of DDSs to tumors by different mechanisms could represent a promising translational approach for anticancer treatment. PEG and its derivatives are used as polymeric materials to synthesize NCs that have both active and passive targeting properties; nowadays, poly(lactic acid) (PLA), PEG, or their combinations are the most used macromolecules to synthesize therapeutic and targeted NPs [95]. PEG is widely used to prevent the opsonization of NPs after their injection in the blood stream. Opsonins are the proteins involved in this process, and interact with the hydrophobic components of NPs, leading to their flagging as "not self" material. NPs flagged by opsonins are then captured by macrophages forming the mononuclear phagocyte system, and, at the end, eliminated from the body. PEGylated NPs are not recognized by opsonins. Thus, their recognition and uptake by the mononuclear phagocyte system is reduced. Consequently, the circulation half-life of various types of NPs, such as polymer-based NPs and hybrid NPs, is widely increased [79, 117, 145]. However, PEG-related immunological issues have received considerable attention. Antibodies against PEG may limit the therapeutic efficacy and/or reduce tolerance of PEG-asparaginase in patients with acute lymphoblastic leukemia and of PEGloticase in patients with chronic gout. In particular, anti PEG immune reaction occurred in 22–25% of healthy volunteers and anti PEG antibodies are present in their blood, compared with a very low 0.2% of anti PEG antibody immune reactions that occurred in the two decades before. This increase may be due to an improvement of the limit of detection of antibodies during the years and to greater exposure to PEG and PEG-containing compounds in cosmetics, pharmaceuticals, and processed food products. Thus, patients should be pre-screened and monitored for anti PEG prior to and throughout the course of treatment with a PEGylated compound [73].

11.1 Anticancer Nanosized DDSs on Market

To overcome chemotherapy-associated drawbacks (see Sect. 1), great progress has been made in the field of anticancer nanomedicine, which led to the development of smart and novel DDSs with characteristics including size not exceeding 200 nm and versatile architecture [2]. The main advantage provided from these nanosized DDSs is the increase of the surface area [53]. To date, several liposomal- and NP-based DDSs for cancer treatment have been approved in different countries. In 1995, Doxil®, lipo-DOX, was the first US-approved (by FDA) nanodrug. Its corresponding equivalent drug approved in the E.U. was Caelyx®, and both are used for the treatment of Kaposi's sarcoma, breast, multiple myeloma, and ovarian neoplasms, and had a better toxicity profile than free DOX hydrochloride. In 1996, FDA approved DaunoXome®, another lipo-DOX formulation, used in cancers and HIV-associated Kaposi's sarcoma. Recently, other liposomal-based drugs have been approved both in the E.U. and USA. In 2009, Mepact®, liposomal mifamurtide, was marketed as a powder which is resuspended into a suspension for infusion to treat osteosarcoma. In 2012, liposomal vincristine sulfate, commercially available as Marqibo®, was marketed to treat Philadelphia chromosome-negative chronic myelogenous leukemia. In 2015, Onivyde®, lipo-irinotecan, was marked as a chemotherapeutic agent to treat metastatic pancreatic cancer [2]. Furthermore, several DDSs are currently under clinical trials, such as AS15 (liposomal adjuvant AS15 containing monophosphoryl lipid-A, Quillaja Saponaria plant extract QS21 and CpG oligodeoxynucleotide, phase II trial), SP1–077 (cisplatin-loaded PEG-liposome treating lung, head, and neck cancers, phase II trial) and ALN-VSP (lipid-based NPs containing VEGF-A and kinesin spindle protein siRNAs, developed for the treatment of advanced cancer and liver metastases, phase I trial) [2]. NP-based DDSs currently in the market include Abraxane®, PTX-loaded albumin NPs, approved in 2005 for non-small cell lung carcinoma and pancreatic neoplasm therapy, and Zevalin®, a monoclonal antibody radio-immunotherapy treatment for relapsed or refractory, low grade or transformed B-cell non-Hodgkin's lymphoma, approved in 2004 [59].

12 Efficacy and Side Effects

DDSs can increase the therapeutic efficacy of several anticancer drugs, by decreasing the drug side effects, and increasing the patient's compliance [123]. Compared to free drugs, DDSs promote drug accumulation preferentially in the disease area. To enhance the DDS effectiveness, many strategies have been developed to increase their targeting toward specific sites. The conjugation of targeting moieties on the surface of NCs is one of the strategies used to increase the accumulation. Recently Ai et al. [4] synthesized integrin targeted iRGD-heparin NPs loading cis-diamminedichloroplatinum(II) to clinically treat gastric cancer. These NPs showed a significant antitumor activity of payload without the weight loss or liver and kidney damage occurring in the nude mice, bearing MKN-45P tumors, that are treated with free diamminedichloroplatinum(II) or untargeted heparin NPs [4].

Interestingly, drugs can become sensible to endogenous and/or exogenous stimuli [161]. Daga et al. [40] developed glutathione-responsive cyclodextrin nanosponge loaded DOX for anticancer therapy. These nanosponges were able to release DOX preferentially in cells having high glutathione content, such as DU145 prostate and HCT116 colon cancer cells, as well as to inhibit the growth of DU145 xenograft tumors more than DOX [40]. Similarly, Argenziano et al. [11] generated strigolactones-loaded glutathione/pH-responsive nanosponges to selectively deliver strigolactones to prostate cancer cells and increase their therapeutic efficacy [11]. Moreover, the therapeutic effectiveness of DDSs can be increased also by co-delivering various anticancer drugs simultaneously (see Sect. 1).

NC protects drugs from degradation after systemic injection, thus increasing their half-time, leading to less frequent administrations, improving patients' compliance and decreasing healthcare costs [75, 130, 205]. Unfortunately, DDSs exhibit some detrimental reactions/side effects strongly correlated with their physicochemical properties and material composition [135]. The side effects include complement activation, which can cause both a rapid drug clearance and a pseudo-allergic reaction in patients [9], and blood adverse reactions such as hemolysis, thrombogenicity, and/or vascular oxidative stress that result in inflammatory responses [135, 137].

13 Physicochemical Properties

Physicochemical properties, such as size, shape, surface chemistry, and polydispersity index (PDI), are fundamental parameters affecting the performance of DDSs (Fig. 4). In particular, they influence primary biopharmaceutical properties such as biodistribution, pharmacokinetic, therapeutic versus side effects of drugs. DDSs can be manipulated and change their physicochemical properties to obtain a personalized medicine for cancer therapy [220]. As a result, DDSs increased the effectiveness of cancer treatments compared to free drugs.

13.1 Size and Shape

Size is directly proportional to the surface area of DDSs interacting with the external environment after administration. Different studies, most of them involving NPs, are currently ongoing to study the mechanisms of DDS cell internalization. The cellular uptake of NPs is a size-dependent process that starts from the interaction between NPs' ligands and the receptors expressed on the cell surface. These interactions provide enough energy to bypass the phospholipid bilayer forming the plasma membrane. Thermodynamically, a NP having a size between 40 and 50 nm can interact and bind receptors to successfully produce membrane wrapping. NPs of ~50 nm bind many receptors and their uptake is limited by the redistribution of receptors on the cell membrane via diffusion to compensate for local depletion. NPs larger than 50 nm bind with high affinity to a great number of receptors and may limit the further binding of additional NPs [7]. Size is also a crucial property that allows NPs to extravasate from the abnormal fenestrations belonging to the tumor vasculature. This extravasation is possible only for DDS with dimensions smaller than 200 nm [108]. Furthermore, the NP size strongly affects the type and the amount of proteins adsorbed on their surface after administration in the blood stream. Plasma proteins, such as serum albumin, complements, immunoglobulins and apolipoproteins, are adsorbed onto the NP surface and form a "protein corona." Basically, there are hard and soft corona proteins that cover the surface of NPs. The protein corona phenomenon can modify the surface properties and targeting on nanoparticles, thus decreasing their specific targeting and modifying their therapeutic response in preclinical and clinical studies [5, 86]. Protein corona also affects the physiological property of DDSs, their circulation lifetime, accumulation, toxicity, cellular uptake, and agglomeration [111, 220].

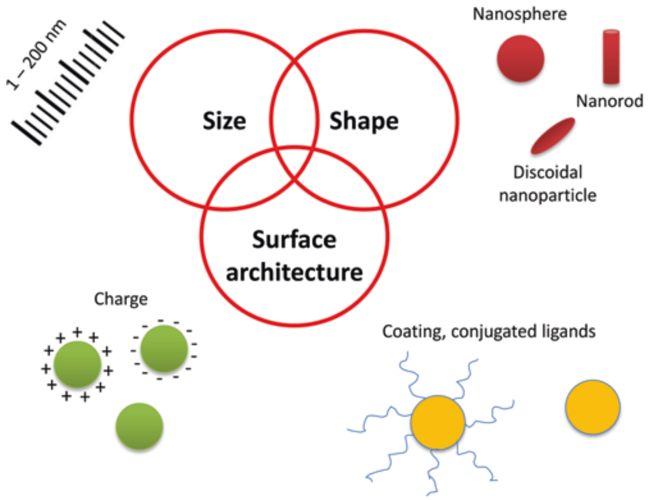

Fig. 4 Main physicochemical properties affecting biopharmaceutics of DDSs

Shape is another crucial characteristic that strongly affects the fate of DDSs because it is involved in several processes occurring after administration, such as biodistribution, macrophage phagocytosis, cell uptake, and targeting [220]. In fact, the shape of NPs can affect their metabolic pathway and the interaction with the cell surface. Spherical shape is better taken up by macrophages and cleared by renal filtration, while discoidal or nonspherical NPs long-circulate inside the blood stream thus avoiding the macrophage uptake and the clearance [103]. This effect depends on the different marginalization of NPs and their distribution in the blood stream. Moreover, opsonins are better adsorbed on the surface of spherical NPs than discoidal or nonspherical one due to their curvature radius that facilitates this interaction and modify the relative surface properties of NPs [86].

13.2 Surface Chemistry

The surface charge plays a crucial role in protein adsorption, which in turn affects the pharmacokinetics and biodistribution of NCs [25]. Circulation time of NCs in blood vessels is highly dependent on charge. For example, highly cationic NPs are rapidly cleared from circulation greater than highly anionic NPs. In contrast, neutral NPs, as well as those with a slight negative charge, show significantly prolonged circulating half-lives [12]. Surface charge affects both internalization and accumulation of NCs in the tumor cells [215]. Conversely to neutral NPs, positively charged NPs show a greater rate of interaction with cancer cells in response to the electrostatic force between the NP surface and the plasma membrane [71, 97]. Xiao et al. [204] showed that the amount of PEG-oligocholic acid NPs accumulated in the tumor was inversely correlated with their surface charge densities (either positive or negative) [204]. Particularly, they demonstrated that the highest tumor accumulation could be achieved by rendering the surface slightly negative. Although it is not good enough for long circulation and tumor accumulation, the positive surface charge improved the tumor extravasation and penetration. For example, He et al. demonstrated that the surface charge density had different impacts on tumor accumulation for negatively and positively charged NPs [88]. Higher surface charge densities caused lower tumor accumulation for negatively charged NPs; however, for positively charged particles, NPs with higher charge densities showed higher accumulation in the tumor [88]. NPs with a higher positive charge density could more efficiently escape from the interstitial space and be internalized by tumor cells and the associated endothelium [220].

14 Health Costs of DDSs in Cancer Therapy

As of 2018, almost 250 therapeutic DDSs were available for clinical use [53], and the perspective assumes the double for 2019 [18]. A small part of these DDSs has been already marketed, whereas all the others are still waiting for approval [1]. On June 2018, US FDA adopted a specific policy for improving their approval [169], whereas European Medicines Agency (EMA) formed a group composed by experts in the field of nanotherapeutics to better outline and review guidelines [65]. Shortening the approval times for new DDSs for cancer therapy could have a net effect on saving public health costs. Targeted drug delivery and conventional medical management have shown to promote a decrease in healthcare use and costs for cancer patients in comparison to conventional medicines. Stearns et al. [182] conducted a retrospective economic evaluation using score-matched analysis by MarketScan commercial claims data on beneficiaries receiving targeted drug delivery and/or conventional medicines for cancer therapy. The survey examined the period from January 1, 2009, to September 30, 2015. In this economic evaluation, involving 536 patients from a large US payer database, the use of targeted drug delivery and conventional medicines versus conventional medicines alone was associated with a significant overall cost savings of $63,498 in the 12 months after the index date and with significantly fewer inpatient visits, shorter hospitalization, and fewer emergency department visits. In the short term and with respect to conventional medical management alone, the use of targeted drug delivery and conventional medicines was associated with significantly higher outpatient and lower inpatient costs [182].

15 Receptors

Receptor-targeted drug delivery has been extensively explored to target/treat cancer cells. Several studies about drug targeting involved the high-affinity receptor for the vitamin FA, also known as FR. The high affinity of the FR toward FA has been also recently confirmed by Kumar et al. [112]. They evaluated the targeted delivery of gum kondagogu-capped gold NPs coupled with FA in both FR positive (MCF-7) and FR negative (A549) cancer cells. A great affinity of these NPs was found toward FR positive cells [112]. In some cases, FA is used to improve the passive targeting of DDS by introducing an active targeting too, thus increasing its effectiveness [189]. Ak et al. [6] synthesized DOX-loaded and glucose/gluconic acid-coated magnetically responsive NPs. Erythrocyte membrane vesicles were used as coating, while folate ligand was anchored to their surface to target the FR. Interestingly, these FR-targeted NCs showed more cytotoxicity against ovarian cancer cells than nontargeted ones [6]. Drug delivery by FR has also proved some effects for other chemotherapeutic agents for the treatment of various cancers, such as PTX and gemcitabine (GEM). In the cytotoxicity study carried out by Erdoğar et al. [52] it was found that the breast cancer cells were more sensitive to cytotoxic effects of PTX delivered by folate-conjugated cyclodextrin NPs than PTX in Cremophor EL® solution [52]. The analysis of parameters that facilitates direct drug delivery into the cancer cells is very important to consequently select a suitable pathway of drug penetration. For example, single-wall carbon nanotubes (SWNTs) below 450 nm could be used as DDSs to transfect nucleic acids into the cells due to direct cell penetration based on their needle-like structure, whereas SWNTs over 450 nm are suitable to target the cells through the FR [33]. The systemic use of free GEM is restricted because of its poor physicochemical properties and nonspecific drug delivery, resulting in dose-dependent adverse effects. With respect to free GEM, fucose-conjugated GO nanosheets provided high loading efficiency of GEM, which was optimized by increasing the drug concentration and maintaining a constant fucose-conjugated GO nanosheets concentration. This strategy provided a sustained pH-dependent drug release, and an affective targeting of GEM toward both human breast cancer MDA-MB-231 cells and human lung cancer A549 cells overexpressing fucose-receptor [84]. The conjugation of several ligands in the same NCs could improve the responsiveness of tumor cells versus these formulations. Wang et al.

[199] synthesized synergetic targeted liposomes which conjugated on their surface both a tumor identification ligand, the antiestrogen receptor (ER) antibody, and an immune targeting ligand, that was the critical segment of Cluster of differentiation 47 (CD47), called self-peptide (SP) [198]. The anti ER antibody recognizes and binds ER-positive breast cancer tissues in a specific way, while SP activates the CD 47-Signal regulatory protein α (CD47-SIRPα) immune response, thus decreasing the phagocytosis of NPs by macrophages. Both the enhanced targeting ability and antiphagocytosis properties improve the tumor uptake of the NCs and prevent their immune clearance [199]. Yang et al. [207, 209, 210] synthesized DOX-loaded micelles made up of hyaluronic acid conjugated with FA via a reduction-sensitive disulfide linkage to form an amphiphilic polymer (HA-ss-FA). Cellular uptake and in vivo biodistribution studies showed that these DOX-loaded micelles targeted specifically tumor tissues and enhanced significantly cellular uptake by CD44 receptor-mediated endocytosis. The cellular uptake of DOX in CD44-positve A549 cells was 1.6-fold more than that in CD44-negative ones. In addition, the biodistribution of HA-ss-FA micelles showed promising results in in vivo tumor targeting in human (HCC-LM3)-bearing nude mice [210].

16 Transporters

Cells have a membrane with different protein transporters that work as channels or pumps driving in and out the molecules according to a specific gradient. The protein transporters protect the internal cell environment and keep its homeostasis for salts, nutrients, and proteins within a physiological range. These protein transporters can allow the specific delivery of anticancer drugs into the cell, thus bypassing the high selectivity of the cell membrane. Glucosamine (2-amino-2-deoxy-D-glucose, GlcN) and N-acetyl glucosamine (GlcNAc) are amino monosaccharides that are components of glycosaminoglycans, which constitute a major part of the matrix of all connective tissues. The entry of GlcN into cells is stimulated by insulin and involves glucose-transporters (GLUTs), GLUT1 and GLUT2. GLUT1 has similar affinity for glucose and GlcN, while GLUT2 has about 20-fold higher affinity for GlcN than glucose [192]. GLUT1 and GLUT2 are expressed in a variety of tumors including breast invasive ductal carcinoma. The same GLUTs are not expressed in normal breast tissue [76]. Thus, the binding of GlcN could be an attractive therapeutic approach for GLUTs mediated delivery of anticancer drugs. Kumar et al. [112] modified poly(amidoamine), or PAMAM dendrimers, obtained by the interactive branching of β-alanine repeat units, with L-tryptophan and GlcN (PTN) for higher drug loading and to use GLUT transporters, respectively. DOX-loaded PTN demonstrated pH-sensitive drug release with significant higher cytotoxicity against breast cancer cells than PAMAM (Fig. 4a) [112]. GLUT1 is overexpressed in breast cancer stem-like cell (CSC) subpopulation [211]. Yi et al. [211] modified glucose-installed poly(ethylene glycol)-block-poly(L-lysine) with lipoic acid at the ω-end (Glu-PEG-PLL-LA). Glu-PEG-PLL-LA was associated with a single siRNA to form an unimer-polyion, which was used to decorate gold NPs through Au-S bonding. With respect to glucose-unconjugated control NPs, conjugated NPs exhibited higher cellular uptake of siRNA payloads in spheroid breast cancer cells (MBA-MB-231), especially in the CSC fraction, probably due to their higher GLUT1 expression level [211]. It was demonstrated that tumor cells compete with host cells for glutamine (Gln), which causes Gln to flux from normal tissues to the tumor [197]. Wang et al. [197] exploited Gln transporter SLC1A5 (solute carrier family 1 member 5) to target the polyglutamine-based NCs delivering therapeutic small interfering RNAs (siRNAs) into orthotopic lung tumor cells. Gamma-ray emitting 111In, which is extensively used for imaging, is also a source of short-range Auger electrons (AE). While exhibiting negligible effect outside cells, these AE become highly toxic near DNA within the cell nucleus. Therefore, these radionuclides can be used as a therapeutic anticancer agent if delivered precisely into the nuclei of tumor target cells [197]. A modular nanotransporter loading AE emitter 111In has also been developed by Rosenkranz et al. [165] to kill human bladder cancer cells overexpressing the EGFR [165].

17 Enzymes

The development of safe and effective stimuli responsive NCs is very important for tumor chemotherapy [214]. In particular, due to their high specificity to bind a certain substrate, molecules responsive to these specific stimuli are enzymes. Prodrug cancer therapy involves the selective activation of prodrug(s) in tumor tissues by exogenous enzyme(s). As a result, the activated prodrug could kill cancer cells. A peptide linker, mimicking the enzyme substrate conjugated between the drug and the polymeric carrier, is responsible for the drug release mechanism [186]. Jiang et al. [96] synthesized hyaluronidase enzyme-responsive targeted NPs for effective delivery of 5-FU in colon cancer. These NPs were threefold more effective than free drug and twofold more effective than 5-FU loaded mesoporous silica NPs [96].

18 Antibodies

Monoclonal antibodies are produced by a single clone of cells. They are engineered to recognize and bind to a single specific antigen as well as highly specific toward a circulating protein or cells that have the corresponding antigenic structure on their surfaces. This high specificity renders antibodies suitable tools for delivering payloads to specific targets, for example, cytotoxic drugs to malignant cells or enzymes to specific cell types [160]. Lim et al. [121] described a self-assembled protein NC capable of delivering functional antibodies to the cytosol and generated intracellular therapeutics without systemic cytotoxicity. This NC has been made by combining a α-helical peptide that is self-assembled into a hexameric coiled-coil bundle with an Fc-binding protein A fragment. Regardless of the pH and the antibody's originating species, the localization of multiple Fc-binding domains on the hexameric core allows to bind the antibody with a subnanomolar affinity. A cytosol-delivering capability of this NC was provided by using anti β-tubulin or antinuclear pore complex antibody as cargo. In addition, an endosomolytic component conjugated to the NC improved the cytosolic delivery effectiveness of the Hex NC. As a result, this modified Hex NC exhibited similar antibody-binding properties but delivered more antibodies to their cytosolic targets at a faster rate than other reported antibody carriers (Fig. 4c) [121].

19 Hybrid DDSs

The current trend of DDSs for cancer targeting and treatment is the synthesis of hybrid DDSs combining the properties of various biomaterials and NCs. Due to their enhanced effect on tumor therapeutics, these multifunctional NCs are widely used in therapy [199]. For example, Prusty et al. [156], synthesized lipid-mediated self-assembly of aptamers, and combined different biomaterials into a single nanoconstruct that targets the hepatocyte growth factor receptor (cMet). This NC consists of lipid derivatives of a cMet-binding aptamer and a separate lipid derivative of GC-rich DNA hairpin loaded with intercalated DOX. Furthermore, multiple 2′,6′-dimethylazobenzene moieties were incorporated into the DOX-binding polymer to trigger the release of the chemotherapeutics by photoisomerization. The resulting NC increased: (i) the serum nuclease resistance, (ii) the relative transfection into the cells mediated by endocytosis, and (iii) the selective photo-release of chemotherapeutics into the targeted cells [156]. Biodegradable core-shell lipid-polymer hybrid NPs can combine the advantages of lipid and polymeric NPs for controlled drug delivery [181]. Song et al. [181] synthetized lipid-polymer hybrid NPs conjugated with EGF co-delivering docetaxel and resveratrol for the treatment of advanced non-small cell lung cancer. In vitro and in vivo studies demonstrated that these NPs have significant synergistic effects, the best tumor inhibition ability, and the lowest systemic toxicity [181]. Zhang et al. [214] used bovine serum albumin and green tea polyphenol to synthesize glutathione and enzyme (trypsin) responsive NCs [215, 216] for DOX delivery [214].

These new-generation DDSs still face multiple challenges. These hurdles include the accessibility/identification of suitable/novel receptors, transporters and enzymes, the lack of knowledge about differential expression between healthy and cancer cells, the selection of ligands (cell surface receptors and transporters), enzymes, immunological kinetics and/or click chemistry (coating molecules and payloads), the improvement of the entrapment efficiency/release of payloads, the drug degradation and the NC stability.

20 Future Perspectives and Conclusions

NC-based DDSs have recently gained attention in nanomedicine for the treatment of various diseases, and particularly cancer. Polymeric, lipid, and hybrid NCs are used to develop safe, biocompatible, and advanced DDSs loading payloads with different physicochemical properties and modulate the cargo release as a specific response to physical and chemical stimuli. Biomaterials used for the synthesis of NCs have different compositions and functional groups that can be simultaneously or not conjugated with peptides, antibodies, and small molecules to provide a selective active targeting. Payloads used for cancer drug delivery are natural and/or synthetic molecules that can affect, as well as NCs per se, the costs of anticancer therapy. Various strategies for targeting have been developed to increase the effectiveness of the therapy and improve patient compliance. Targeting approaches, biomaterials, and payloads as well as biopharmaceutical properties of DDSs affect anticancer therapy and impact the healthcare and patient quality of life. A similar effect was recently obtained for other pathologies, such as metabolic, cardiovascular, and infection diseases. The wide diffusion of selective molecules, providing specific targeting, novel and smart biomaterials as well as natural and synthetic payloads with potent therapeutic efficacy, allowed the synthesis of smart NCs and the development of modern DDSs. This scenario is slowly transforming lethal diseases, such as some cancers, into chronic diseases while developing the medicine for the future, focused on patient's quality of life and overall survival. NCs help nanotechnology and nanomedicines to treat tumor selectively due to the recent development of smart and novel DDSs using physical/chemical stimuli and molecules generated from microenvironment of tumors. These factors are part of the immune systems of patients and are specific targets suitable for personalized medicines. Drug degradation, stability of NCs, and scale-up still remain a major challenge to be address. Although freeze-drying allows stabilizing NCs and preserving NPs as well as payloads from chemical and biological degradation, the lyophilization process can partially inactivate targeting molecules and decrease their selectivity against specific receptors and transporters overexpressed on the surface of cancer cells and tissues. To date, a new frontier for personalized medicines and selective targeting of DDSs is the synthesis of lipid micelles conjugating targeting molecules that are postinserted in preformulated lyophilized NCs that are dissolved in sterile water or saline solution before patient injection. This strategy opens a new scenario in the targeting strategies and allows to preserve both biopharmaceutical properties of NCs either the therapeutic activity of payloads for long storage without affecting targeting properties. Furthermore, targeting molecules that are specific for their tumor markers can be cloned and collected from patients thus improving the efficacy of cancer therapy and decreasing the side effects and related failure. This approach may represent a new frontier for future experimental protocols and clinical studies.

Many studies currently need acute and chronic toxicities of DDSs used in anticancer therapy. The lack of toxicity data depends on missing data (meta-analysis) in this field due to the restricted access of patients to DDSs cure for cancer therapy which remains a second line of treatment for different carcinoma. In addition, several patients with cancer have a limited rate of survival and a low perspective on life for many aggressive carcinomas.

Bibliographic Database Search (Carried Out on March 22, 2019 at 12:30 AM)

The following query string was entered into the search-command-line of the database of the peer-reviewed literature Scopus (Elsevier):

TITLE-ABS-KEY ("nanocarrier" AND "drug delivery" AND "cancer") AND (LIMIT-TO (PUBSTAGE, "final")) AND (LIMIT-TO (PUBYEAR, 2019) OR LIMIT-TO (PUBYEAR, 2018)) AND (LIMIT-TO (DOCTYPE, "ar")) AND (LIMIT-TO (SUBJAREA, "PHAR") OR LIMIT-TO (SUBJAREA, "BIOC") OR LIMIT-TO (SUBJAREA, "CHEM") OR LIMIT-TO (SUBJAREA, "MEDI") OR LIMIT-TO (SUBJAREA, "IMMU")) AND (LIMIT-TO (LANGUAGE, "English")).

The query string was structured to retrieve manuscripts that include in the title/abstract/keywords regarding NCs in the field of the application of DDSs for cancer applications.

Boolean/Proximity Operators and Wildcard Characters

The following Boolean/Proximity operators and Wildcard characters were adopted to define the query strings:

1. "" quotation marks. They allow one to find the terms between the quotation marks in the exact order they are specified (exact sentence), avoiding sentences with reversed terms.
2. () round brackets. They allow to find the composition of complex search expressions by defining the research priorities.
3. AND. It allows to find records in which they are present all the expressions simultaneously.

General Database Settings

The following general settings were adopted:

1. English language.
2. Search by topic (title, abstract, and keywords).
3. Timespan from 2018 to 2019.
4. Document type (articles and reviews).
5. Subject area (pharmacology, (bio)chemistry, medicine, and immunology).

Bibliographic searches by using other bibliographic databases (PubMed, Web Of Science) were also performed.

Manuscript Selection

The selection of manuscripts has been made manually by topic (title, abstract, and keywords), without considering their impact (number of citation or IF/SJR of the Journal). Among the papers (articles and reviews) retrieved in the last 2 years (more than 523 papers, without duplicates), only appropriate findings involving the subject areas of pharmacology, (bio)chemistry, medicine, and immunology were discussed. Older papers were included in the discussion just in case they were essential for the description of various topics. In cases where two or more papers discuss the same topic, the most recent, or the one containing more data, was considered.

Acknowledgments The researches of Nadeem Muhammad Hafeez, and Dalila Iannotta are funded by the Italian Ministry of Instruction, University, and Research under the national project Programma Operativo Nazionale Ricerca e Innovazione (PON) 2014-2020 (CCI 2014IT16M2OP005) Fondo Sociale Europeo, Azione I.1, Dottorati Innovativi con Caratterizzazione Industriale.

References

1. Accomasso, L., Cristallini, C., & Giachino, C. (2018). Risk assessment and risk minimization in nanomedicine: A need for predictive, alternative, and 3Rs strategies. *Frontiers in Pharmacology, 9*, 228.
2. Aftab, S., Shah, A., Nadhman, A., Kurbanoglu, S., Aysıl Ozkan, S., Dionysiou, D. D., Shukla, S. S., & Aminabhavi, T. M. (2018). Nanomedicine: An effective tool in cancer therapy. *International Journal of Pharmaceutics, 540*, 132–149.
3. Agrawal, S., Kelkar, M., De, A., et al. (2018). Newly emerging mesoporous strontium hydroxyapatite nanorods: Microwave synthesis and relevance as doxorubicin nanocarrier. *Journal of Nanoparticle Research, 20*, 230.
4. Ai, S., Zhen, S., Liu, Z., et al. (2018). An iRGD peptide conjugated heparin nanocarrier for gastric cancer therapy. *RSC Advances, 8*, 30012–30020.
5. Al-Ahmady, Z. S., Hadjidemetriou, M., Gubbins, J., et al. (2018). Formation of protein corona in vivo affects drug release from temperature-sensitive liposomes. *Journal of Controlled Release, 276*, 157–167.
6. Ak, G., Yilmaz, H., Güneş, A., et al. (2018). In vitro and in vivo evaluation of folate receptor-targeted a novel magnetic drug delivery system for ovarian cancer therapy. *Artificial Cells, Nanomedicine, and Biotechnology, 46*(Suppl), 926–937.
7. Albanese, A., Tang, P. S., & Chan, W. C. (2012). The effect of nanoparticle size, shape, and surface chemistry on biological systems. *Annual Review of Biomedical Engineering, 14*, 1–16.
8. Albano, J. M., De Morais Ribeiro, L. N., Couto, V. M., et al. (2019). Rational design of polymer-lipid nanoparticles for docetaxel delivery. *Colloids and Surfaces B: Biointerfaces, 175*, 56–64.
9. Alsaleh, N. B., & Brown, J. M. (2018). Immune responses to engineered nanomaterials: Current understanding and challenges. *Current Opinion in Toxicology, 10*, 8–14.
10. Amoli-Diva, M., Sadighi-Bonabi, R., Pourghazi, K., et al. (2018). Tunable surface plasmon resonance-based remote actuation of bimetallic core-shell nanoparticle-coated stimuli responsive polymer for switchable chemo-photothermal synergistic cancer therapy. *Journal of Pharmaceutical Sciences, 107*, 2618–2627.
11. Argenziano, M., Lombardi, C., Ferrara, B., et al. (2018). Glutathione/pH-responsive nanosponges enhance strigolactone delivery to prostate cancer cells. *Oncotarget, 9*, 35813–35829.
12. Arvizo, R. R., Miranda, O. R., Moyano, D. F., et al. (2011). Modulating pharmacokinetics, tumor uptake and biodistribution by engineered nanoparticles. *PLoS One, 6*, e24374.
13. Attia, M. F., Anton, N., Wallyn, J., et al. (2019). An overview of active and passive targeting strategies to improve the nanocarriers efficiency to tumour sites. *The Journal of Pharmacy and Pharmacology, 71*, 1185–1198.
14. Bahuguna, S., Kumar, M., Sharma, G., et al. (2018). Fullerenol-based intracellular delivery of methotrexate: A water-soluble nanoconjugate for enhanced cytotoxicity and improved pharmacokinetics. *AAPS PharmSciTech, 19*, 1084–1092.
15. Banala, V. T., Sharma, S., Barnwal, P., et al. (2018). Synchronized ratiometric codelivery of metformin and topotecan through engineered nanocarrier facilitates in vivo synergistic precision levels at tumor site. *Advanced Healthcare Materials, 7*, 1800300.
16. Bansal, S., Singh, J., Kumari, U., et al. (2019). Development of biosurfactant-based graphene quantum dot conjugate as a novel and fluorescent theranostic tool for cancer. *International Journal of Nanomedicine, 14*, 809.
17. Bazak, R., Houri, M., Achy, S. E., et al. (2014). Passive targeting of nanoparticles to cancer: A comprehensive review of the literature. *Molecular and Clinical Oncology, 2*, 904–908.
18. BBCResearch. (2015). Nanotechnology in medical applications: the global market. http://www.bccresearch.com/market-research/healthcare/nanotechnology-medical-applications-market-hlc069c.html. Accessed 9 Nov 2019.
19. Behr, J. (1997). The proton sponge: A trick to enter cells the viruses did not exploit. *Chimia, 51*, 34–36.
20. Beija, M., Salvayre, R., Lauth-De Viguerie, N., et al. (2012). Colloidal systems for drug delivery: From design to therapy. *Trends in Biotechnology, 30*, 485–496.
21. Bergers, G., & Benjamin, L. E. (2003). Tumorigenesis and the angiogenic switch. *Nature Reviews. Cancer, 3*, 401–410.
22. Bikram, M., Gobin, A. M., Whitmire, R. E., et al. (2007). Temperature-sensitive hydrogels with SiO2-Au nanoshells for controlled drug delivery. *Journal of Controlled Release, 123*, 219–227.
23. Bikram, M., & West, J. L. (2008). Thermo-responsive systems for controlled drug delivery. *Expert Opinion on Drug Delivery, 5*, 1077–1091.
24. Bilobrov, V., Sokolova, V., Prylutska, S., et al. (2019). A novel nanoconjugate of landomycin A with C 60 fullerene for cancer targeted therapy: In vitro studies. *Cellular and Molecular Bioengineering, 12*, 41–51.
25. Blanco, E., Shen, H., Ferrari, M., et al. (2015). Principles of nanoparticle design for overcoming biological barriers to drug delivery. *Nature Biotechnology, 33*, 941–951.
26. Buhleier, E., Wehner, W., & Vögtle, F. (1978). "Cascade"- and "nonskid-chain-like" syntheses of molecular cavity topologies. *Synthesis, 1978*, 155–158.
27. Braun, G. B., Sugahara, K. N., Yu, O. M., et al. (2016). Urokinase-controlled tumor penetrating peptide. *Journal of Controlled Release, 232*, 188–195.
28. Bugno, J., Hsu, H.-J., Pearson, R. M., et al. (2016). Size and surface charge of engineered poly(amidoamine) dendrimers modulate tumor accumulation and penetration: A model study using multicellular tumor spheroids. *Molecular Pharmaceutics, 13*, 2155–2163.
29. Candido, N. M., De Melo, M. T., Franchi, L. P., et al. (2018). Combining photodynamic therapy and chemotherapy: Improving breast cancer treatment with nanotechnology. *Journal of Biomedical Nanotechnology, 14*, 994–1008.
30. Cao, D., Liang, L., Xu, Y., et al. (2018b). Tumor associated macrophages and angiogenesis dual-recognizable nanoparticles for enhanced cancer chemotherapy. *Nanomedicine, 14*, 651–659.
31. Cao, J., Wang, C., Guo, L., et al. (2018a). Co-administration of a charge-conversional dendrimer enhances antitumor efficacy of conventional chemotherapy. *European Journal of Pharmaceutics and Biopharmaceutics, 127*, 371–377.
32. Cellante, L., Costa, R., Monaco, I., et al. (2018). One-step esterification of nanocellulose in a Brønsted acid ionic liquid for delivery to glioblastoma cancer cells. *New Journal of Chemistry, 42*, 5237–5242.
33. Charbgoo, F., Nikkhah, M., & Behmanesh, M. (2018). Size of single-wall carbon nanotube affects the folate receptor-mediated cancer cell targeting. *Biotechnology and Applied Biochemistry, 65*, 328–337.
34. Chaumet, A., Wright, G. D., Seet, S. H., et al. (2015). Nuclear envelope-associated endosomes deliver surface proteins to the nucleus. *Nature Communications, 6*, 8218.
35. Chen, H. H., Lu, I. L., Liu, T. I., et al. (2019). Indocyanine green/doxorubicin-encapsulated functionalized nanoparticles for

effective combination therapy against human MDR breast cancer. *Colloids and Surfaces. B, Biointerfaces, 177*, 294–305.

36. Chen, T., Gong, T., Zhao, T., et al. (2017). A comparison study between lycobetaine-loaded nanoemulsion and liposome using nRGD as therapeutic adjuvant for lung cancer therapy. *European Journal of Pharmaceutical Sciences, 111*, 293–302.
37. Chen, T., Gong, T., Zhao, T., et al. (2018b). A comparison study between lycobetaine-loaded nanoemulsion and liposome using nRGD as therapeutic adjuvant for lung cancer therapy. *European Journal of Pharmaceutical Sciences, 111*, 293–302.
38. Chen, W. L., Yang, S. D., Li, F., et al. (2018a). Programmed pH/reduction-responsive nanoparticles for efficient delivery of antitumor agents in vivo. *Acta Biomaterialia, 81*, 219–230.
39. Chitgupi, U., Shao, S., Carter, K. A., et al. (2018). Multicolor liposome mixtures for selective and selectable cargo release. *Nano Letters, 18*, 1331–1336.
40. Daga, M., Ullio, C., Argenziano, M., et al. (2016). GSH-targeted nanosponges increase doxorubicin-induced toxicity "*in vitro*" and "*in vivo*" in cancer cells with high antioxidant defenses. *Free Radical Biology & Medicine, 97*, 24–37.
41. Danson, S., Ferry, D., Alakhov, V., et al. (2004). Phase I dose escalation and pharmacokinetic study of pluronic polymer-bound doxorubicin (SP1049C) in patients with advanced cancer. *British Journal of Cancer, 90*, 2085–2091.
42. Dassie, J. P., Hernandez, L. I., Thomas, G. S., et al. (2014). Targeted inhibition of prostate cancer metastases with an RNA aptamer to prostate-specific membrane antigen. *Molecular Therapy, 22*, 1910–1922.
43. Dautry-Varsat, A. (1986). Receptor-mediated endocytosis: The intracellular journey of transferrin and its receptor. *Biochimie, 68*, 375–381.
44. Dramou, P., Fizir, M., Taleb, A., et al. (2018). Folic acid-conjugated chitosan oligosaccharide-magnetic halloysite nanotubes as a delivery system for camptothecin. *Carbohydrate Polymers, 197*, 117–127.
45. Dresselhaus, M. S., Dresselhaus, G., & Eklund, P. C. (1996). *Science of fullerenes and carbon nanotubes: Their properties and applications*. Cambridge: Academic Press.
46. Du, M., Ouyang, Y., Meng, F., et al. (2019). Polymer-lipid hybrid nanoparticles: A novel drug delivery system for enhancing the activity of psoralen against breast cancer. *International Journal of Pharmaceutics, 561*, 274–282.
47. Du, X. L., Chan, W., Giordano, S., et al. (2005). Variation in modes of chemotherapy administration for breast carcinoma and association with hospitalization for chemotherapy-related toxicity. *Cancer, 104*, 913–924.
48. Duan, Q., Ma, Y., Che, M., et al. (2019). Fluorescent carbon dots as carriers for intracellular doxorubicin delivery and track. *Journal of Drug Delivery Science and Technology, 49*, 527–533.
49. Dufes, C., Uchegbu, I. F., & Schätzlein, A. G. (2005). Dendrimers in gene delivery. *Advanced Drug Delivery Reviews, 57*, 2177–2202.
50. Dutta Chowdhury, A., Ganganboina, A. B., Tsai, Y. C., et al. (2018). Multifunctional GQDs-Concanavalin A@Fe3O4 nanocomposites for cancer cells detection and targeted drug delivery. *Analytica Chimica Acta, 1027*, 109–120.
51. Elhissi, A., Ahmed, W., Dhanak, V., et al. (2012). Carbon nanotubes in cancer therapy and drug delivery. In K. Subramani & W. Ahmed (Eds.), *Emerging nanotechnologies in dentistry* (1st ed., pp. 347–363). Waltham: William Andrew Publishing (Elsevier).
52. Erdoğar, N., Esendağlı, G., Nielsen, T. T., et al. (2018). Therapeutic efficacy of folate receptor-targeted amphiphilic cyclodextrin nanoparticles as a novel vehicle for paclitaxel delivery in breast cancer. *Journal of Drug Targeting, 26*, 66–74.
53. Etheridge, M. L., Campbell, S. A., Erdman, A. G., et al. (2013). The big picture on nanomedicine: The state of investigational and approved nanomedicine products. *Nanomedicine, 9*, 1–14.
54. Fadeel, D. A., Al-Toukhy, G. M., Elsharif, A. M., et al. (2018). Improved photodynamic efficacy of thiophenyl sulfonated zinc phthalocyanine loaded in lipid nano-carriers for hepatocellular carcinoma cancer cells. *Photodiagnosis and Photodynamic Therapy, 23*, 25–31.
55. Fan, J., Wang, S., Sun, W., et al. (2018). Anticancer drug delivery systems based on inorganic nanocarriers with fluorescent tracers. *AICHE Journal, 64*, 835–859.
56. Fang, J., Liu, Y., Chen, Y., et al. (2018b). Graphene quantum dots-gated hollow mesoporous carbon nanoplatform for targeting drug delivery and synergistic chemo-photothermal therapy. *International Journal of Nanomedicine, 13*, 5991–6007.
57. Fang, J., Nakamura, H., & Maeda, H. (2011). The EPR effect: Unique features of tumor blood vessels for drug delivery, factors involved, and limitations and augmentation of the effect. *Advanced Drug Delivery Reviews, 63*, 136–151.
58. Fang, S., Hou, Y., Ling, L., et al. (2018a). Dimeric camptothecin derived phospholipid assembled liposomes with high drug loading for cancer therapy. *Colloids and Surfaces B: Biointerfaces, 166*, 235–244.
59. Farjadian, F., Ghasemi, A., Gohari, O., Roointan, A., Karimi, M., & Hamblin, M. R. (2019). Nanopharmaceuticals and nanomedicines currently on the market: Challenges and opportunities. *Nanomedicine (London, England), 14*, 93–126.
60. Feng, W., Han, X., Wang, R., et al. (2019). Nanocatalysts-augmented and photo-thermal-enhanced tumor-specific sequential nanocatalytic therapy in both NIR-I and NIR-II biowindows. *Advanced Materials, 31*, e1805919.
61. Fenske, D. B., & Cullis, P. R. (2008). Liposomal nanomedicines. *Expert Opinion on Drug Delivery, 5*, 25–44.
62. Fernandes, C., Suares, D., & Yergeri, M. C. (2018b). Tumor microenvironment targeted nanotherapy. *Frontiers in Pharmacology, 9*, 1230.
63. Fernandes, R. S., Silva, J. O., Mussi, S. V., et al. (2018a). Nanostructured lipid carrier co-loaded with doxorubicin and docosahexaenoic acid as a theranostic agent: Evaluation of biodistribution and antitumor activity in experimental model. *Molecular Imaging and Biology, 20*, 437–447.
64. Ferrara, N., Hillan, K. J., & Novotny, W. (2005). Bevacizumab (Avastin), a humanized anti-VEGF monoclonal antibody for cancer therapy. *Biochemical and Biophysical Research Communications, 333*, 328–335.
65. Flühmann, B., Ntai, I., Borchard, G., et al. (2019). Nanomedicines: The magic bullets reaching their target? *European Journal of Pharmaceutical Sciences, 128*, 73–80.
66. Frigerio, B., Bizzoni, C., Jansen, G., et al. (2019). Folate receptors and transporters: Biological role and diagnostic/therapeutic targets in cancer and other diseases. *Journal of Experimental & Clinical Cancer Research, 38*, 125.
67. Fuhrmann, K., Gauthier, M. A., & Leroux, J.-C. (2014). Targeting of injectable drug nanocrystals. *Molecular Pharmaceutics, 11*, 1762–1771.
68. Fuhrmann, K., Połomska, A., Aeberli, C., et al. (2013). Modular design of redox-responsive stabilizers for nanocrystals. *ACS Nano, 7*, 8243–8250.
69. Fuhrmann, K., Schulz, J. D., Gauthier, M. A., et al. (2012). PEG nanocages as non-sheddable stabilizers for drug nanocrystals. *ACS Nano, 6*, 1667–1676.
70. Ganta, S., Paxton, J. W., Baguley, B. C., et al. (2009). Formulation and pharmacokinetic evaluation of an asulacrine nanocrystalline suspension for intravenous delivery. *International Journal of Pharmaceutics, 367*, 179–186.

71. Gao, J., Yu, B., Li, C., et al. (2019). Ultrasound triggered phase-change nanodroplets for doxorubicin prodrug delivery and ultrasound diagnosis: An in vitro study. *Colloids and Surfaces. B, Biointerfaces, 174*, 416–425.
72. Gao, Z., Lukyanov, A. N., Singhal, A., et al. (2002). Diacyllipid-polymer micelles as nanocarriers for poorly soluble anticancer drugs. *Nano Letters, 2*, 979–982.
73. Garay, R. P., El-Gewely, R., Armstrong, J. K., et al. (2012). Antibodies against polyethylene glycol in healthy subjects and in patients treated with PEG-conjugated agents. *Expert Opinion on Drug Delivery, 9*, 1319–1323.
74. Geng, S., Wu, L., Cui, H., et al. (2018). Synthesis of lipid-black phosphorus quantum dot bilayer vesicles for near-infrared-controlled drug release. *Chemical Communications (Cambridge), 54*, 6060–6063.
75. Ghorbani, M., Mahmoodzadeh, F., Nezhad-Mokhtari, P., et al. (2018). A novel polymeric micelle-decorated Fe3O4/Au core-shell nanoparticle for pH and reduction-responsive intracellular co-delivery of doxorubicin and 6-mercaptopurine. *New Journal of Chemistry, 42*, 18038–18049.
76. Godoy, A., Ulloa, V., Rodríguez, F., et al. (2006). Differential subcellular distribution of glucose transporters GLUT1-6 and GLUT9 in human cancer: Ultrastructural localization of GLUT1 and GLUT5 in breast tumor tissues. *Journal of Cellular Physiology, 207*, 614–662.
77. Gonzales, J., Kossatz, S., Roberts, S., et al. (2018). Nanoemulsion-based delivery of fluorescent PARP inhibitors in mouse models of small cell lung cancer. *Bioconjugate Chemistry, 29*, 3776–3782.
78. Granger, D. N., & Senchenkova, E. (2010). Chapter 7: Leukocyte–endothelial cell adhesion. In D. N. Granger & E. Senchenkova (Eds.), *Inflammation and the microcirculation* (pp. 29–40). San Rafael: Morgan & Claypool Life Sciences.
79. Gref, R., Lück, M., Quellec, P., et al. (2000). 'Stealth' corona-core nanoparticles surface modified by polyethylene glycol (PEG): Influences of the corona (PEG chain length and surface density) and of the core composition on phagocytic uptake and plasma protein adsorption. *Colloids and Surfaces. B, Biointerfaces, 18*, 301–313.
80. Griffin, L. C., Tidmarsh, G. F., Bock, L. C., et al. (1993). In vivo anticoagulant properties of a novel nucleotide-based thrombin inhibitor and demonstration of regional anticoagulation in extracorporeal circuits. *Blood, 81*, 3271–3276.
81. Guaita-Esteruelas, S., Gumà, J., Masana, L., et al. (2018). The peritumoural adipose tissue microenvironment and cancer. The roles of fatty acid binding protein 4 and fatty acid binding protein. *Molecular and Cellular Endocrinology, 462*(Pt B), 107–118.
82. Gui, W., Zhang, J., Chen, X., et al. (2018). N-Doped graphene quantum dot@ mesoporous silica nanoparticles modified with hyaluronic acid for fluorescent imaging of tumor cells and drug delivery. *Microchimica Acta, 185*, 66.
83. Guo, Y., Zhao, S., Qiu, H., et al. (2018). Shape of nanoparticles as a design parameter to improve docetaxel antitumor efficacy. *Bioconjugate Chemistry, 29*, 1302–1311.
84. Gupta, N., Jangid, A. K., Singh, M., et al. (2018). Designing two-dimensional nanosheets for improving drug delivery to Fucose-receptor-overexpressing cancer cells. *ChemMedChem, 13*, 2644–2652.
85. Hadilou, N., Khoshgenab, A. N., Amoli-Diva, M., et al. (2018). Remote trice light, temperature, and pH-actuation of switchable magneto-plasmonic nanocarriers for combinational photothermal and controlled/targeted chemotherapies. *Journal of Pharmaceutical Sciences, 107*, 3123–3133.
86. Hadjidemetriou, M., McAdam, S., Garner, G., et al. (2019). The human in vivo biomolecule Corona onto PEGylated liposomes: A proof-of-concept clinical study. *Advanced Materials, 31*, e1803335.
87. Hanafy, N. A. N., El-Kemary, M., & Leporatti, S. (2018). Micelles structure development as a strategy to improve smart cancer therapy. *Cancers (Basel)*.
88. He, C. B., Hu, Y. P., Yin, L. C., et al. (2010). Effects of particle size and surface charge on cellular uptake and biodistribution of polymeric nanoparticles. *Biomaterials, 31*, 3657–3666.
89. Hao, G., Xu, Z. P., & Li, L. (2018). Manipulating extracellular tumour pH: An effective target for cancer therapy. *RSC Advances, 8*, 22182–22192.
90. Hollis, C. P., Weiss, H. L., Leggas, M., et al. (2013). Biodistribution and bioimaging studies of hybrid paclitaxel nanocrystals: Lessons learned of the EPR effect and image-guided drug delivery. *Journal of Controlled Release, 172*, 12–21.
91. Huang, R., Li, J., Kebebe, D., et al. (2018). Cell penetrating peptides functionalized gambogic acid-nanostructured lipid carrier for cancer treatment. *Drug Delivery, 25*, 757–765.
92. Huang, Y. F., Shangguan, D. H., Liu, H. P., et al. (2009). Molecular assembly of an aptamer-drug conjugate for targeted drug delivery to tumor cells. *Chembiochem, 10*, 862–868.
93. Iijima, S. (1991). Helical microtubules of graphitic carbon. *Nature, 354*, 56–58.
94. Irby, D., Du, C., & Li, F. (2017). Lipid-drug conjugate for enhancing drug delivery. *Molecular Pharmaceutics, 14*, 1325–1338.
95. Jahan, S. T., Sadat, S. M. A., Walliser, M., & Haddadi, A. (2017). Targeted therapeutic nanoparticles: An immense promise to fight against cancer. *Journal of Drug Delivery, 2017*, 9090325.
96. Jiang, H., Shi, X., Yu, X., et al. (2018). Hyaluronidase enzyme-responsive targeted nanoparticles for effective delivery of 5-fluorouracil in colon cancer. *Pharmaceutical Research, 35*, 73.
97. Jin, R., Liu, Z., Bai, Y., et al. (2018). Multiple-responsive mesoporous silica nanoparticles for highly accurate drugs delivery to tumor cells. *ACS Omega, 3*, 4306–4315.
98. Kang, S., Kim, E. H., Hwang, J. E., Shin, J. H., Jeong, Y. S., Yim, S. Y., Joo, E. W., Eun, Y. G., Lee, D. J., Sohn, B. H., Lee, S. H., Lim, B., & Lee, J. S. (2019). Prognostic significance of high metabolic activity in breast cancer: PET signature in breast cancer. *Biochemical and Biophysical Research Communications, 511*, 185–191.
99. Karandish, F., Froberg, J., Borowicz, P., et al. (2018). Peptide-targeted, stimuli-responsive polymersomes for delivering a cancer stemness inhibitor to cancer stem cell microtumors. *Colloids and Surfaces. B, Biointerfaces, 163*, 225–235.
100. Kateb, B., Yamamoto, V., Yu, C., et al. (2009). Infrared thermal imaging: A review of the literature and case report. *NeuroImage, 47*, T154–T162.
101. Kaur, H., Bruno, J. G., Kumar, A., & Sharma, T. K. (2018). Aptamers in the therapeutics and diagnostics pipelines. *Theranostics, 8*, 4016–4032.
102. Kayani, Z., Firuzi, O., & Bordbar, A. K. (2018). Doughnut-shaped bovine serum albumin nanoparticles loaded with doxorubicin for overcoming multidrug-resistant in cancer cells. *International Journal of Biological Macromolecules, 107*, 1835–1843.
103. Key, J., Palange, A. L., Gentile, F., et al. (2015). Soft discoidal polymeric nanoconstructs resist macrophage uptake and enhance vascular targeting in tumors. *ACS Nano, 9*, 11628–11641.
104. Khajavinia, A., Varshosaz, J., & Dehkordi, A. J. (2012). Targeting etoposide to acute myelogenous leukaemia cells using nanostructured lipid carriers coated with transferrin. *Nanotechnology, 23*, 405101.
105. Khatri, S., Lohani, P., & Gandhi, S. (2013). Nanoemulsions in cancer therapy. *Indo Global Journal of Pharmaceutical Sciences, 3*, 124–133.

106. Khoee, M. H., Khoee, S., & Lotfi, M. (2019). Synthesis of titanium dioxide nanotubes with liposomal covers for carrying and extended release of 5-FU as anticancer drug in the treatment of HeLa cells. *Analytical Biochemistry, 572*, 16–24.
107. Kim, S., Shi, Y., Kim, J. Y., et al. (2010). Overcoming the barriers in micellar drug delivery: Loading efficiency, in vivo stability, and micelle-cell interaction. *Expert Opinion on Drug Delivery, 7*, 49–62.
108. Kopeckova, K., Eckschlager, T., Sirc, J., et al. (2019). Nanodrugs used in cancer therapy. *Biomedical Papers of the Medical Faculty of the University Palacky, Olomouc, Czech Republic*.
109. Koshkaryev, A., Sawant, R., Deshpande, M., et al. (2013). Immunoconjugates and long circulating systems: Origins, current state of the art and future directions. *Advanced Drug Delivery Reviews, 65*, 24–35.
110. Kostarelos, K., Lacerda, L., Partidos, C., et al. (2005). Carbon nanotube-mediated delivery of peptides and genes to cells: Translating nanobiotechnology to therapeutics. *Journal of Drug Delivery Science and Technology, 15*, 41–47.
111. Kumar, A., & Dhawan, A. (Eds.). (2019). *Nanoparticle-protein corona: Biophysics to biology*. Cambridge: Royal Society of Chemistry.
112. Kumar, S. S. D., Mahesh, A., Antoniraj, M. G., et al. (2018). Cellular imaging and folate receptor targeting delivery of gum kondagogu capped gold nanoparticles in cancer cells. *International Journal of Biological Macromolecules, 109*, 220–230.
113. Kutova, O. M., Guryev, E. L., Sokolova, E. A., et al. (2019). Targeted delivery to tumors: Multidirectional strategies to improve treatment efficiency. *Cancers (Basel), 11*(1), 68. Pii:E68.
114. Lakhin, A. V., Tarantul, V. Z., Gening, L. V., et al. (2013). Aptamers: Problems, solutions and prospects. *Acta Naturae, 5*, 34–43.
115. Le Trinh, T., Zhu, G. Z., Xiao, X. L., et al. (2015). A synthetic aptamer-drug adduct for targeted liver cancer therapy. *PLoS One, 10*, e0136673.
116. Lee, K. S., Chung, H. C., Im, S. A., et al. (2008). Multicenter phase II trial of Genexol-PM, a Cremophor-free, polymeric micelle formulation of paclitaxel, in patients with metastatic breast cancer. *Breast Cancer Research and Treatment, 108*, 241–250.
117. Li, S. D., & Huang, L. (2006). Surface-modified LPD nanoparticles for tumor targeting. *Annals of the New York Academy of Sciences, 1082*, 1–8.
118. Li, W., Li, Z., Wei, L., et al. (2018). Evaluation of paclitaxel nanocrystals in vitro and in vivo. *Drug Research, 68*, 205–212.
119. Liao, W., Zhang, L., Zhong, Y., et al. (2018). Fabrication of ultrasmall WS2 quantum dots-coated periodic mesoporous organosilica nanoparticles for intracellular drug delivery and synergistic chemo-photothermal therapy. *Oncotargets and Therapy, 11*, 1949.
120. Licciardi, M., Paolino, D., Celia, C., et al. (2010). Folate-targeted supramolecular vesicular aggregates based on polyas-partylhydrazide copolymers for the selective delivery of antitumoral drugs. *Biomaterials, 31*, 7340–7354.
121. Lim, S. I., Lukianov, C. I., & Champion, J. A. (2017). Self-assembled protein nanocarrier for intracellular delivery of antibody. *Journal of Controlled Release, 249*, 1–10.
122. Lin, F., Wen, D., Wang, X., et al. (2019). Dual responsive micelles capable of modulating miRNA-34a to combat taxane resistance in prostate cancer. *Biomaterials, 192*, 95–108.
123. Liu, D., Yang, F., Xiong, F., et al. (2016). The smart drug delivery system and its clinical potential. *Theranostics, 6*, 1306–1323.
124. Liu, J., Huang, Y., Kumar, A., Tan, A., Jin, S., Mozhi, A., & Liang, X. J. (2014). pH-sensitive nano-systems for drug delivery in cancer therapy. *Biotechnology Advances, 32*, 693–710.
125. Liu, Z., Wang, F., & Chen, X. (2008). Integrin alpha(v)beta(3)-targeted cancer therapy. *Drug Development Research, 69*, 329–339.
126. Lopez-Toledano, M. A., Saxena, V., Legassie, J. D., et al. (2019). Advanced lipid technologies® (ALT®): A proven formulation platform to enhance the bioavailability of lipophilic compounds. *Journal of Drug Delivery, 2019*, 1957360.
127. Loppinet, B., & Monteux, C. (2016). Dynamics of surfactants and polymers at liquid interfaces. In P. Lang & Y. Liu (Eds.), *Soft matter at aqueous interfaces* (pp. 137–157). Heidelberg: Springer.
128. Maeda, H., & Khatami, M. (2018). Analyses of repeated failures in cancer therapy for solid tumors: Poor tumor-selective drug delivery, low therapeutic efficacy and unsustainable costs. *Clinical and Translational Medicine, 7*, 11.
129. Maeda, H., Sawa, T., & Konno, T. (2001). Mechanism of tumor-targeted delivery of macromolecular drugs, including the EPR effect in solid tumor and clinical over-view of the prototype polymeric drug SMANCS. *Journal of Controlled Release, 74*, 47–46.
130. Mahmoodzadeh, F., Jannat, B., & Ghorbani, M. (2019). Chitosan-based nanomicelle as a novel platform for targeted delivery of methotrexate. *International Journal of Biological Macromolecules, 126*, 517–524.
131. Mao, J., Ran, D., Xie, C., et al. (2017). EGFR/EGFRvIII dual-targeting peptide-mediated drug delivery for enhanced glioma therapy. *ACS Applied Materials & Interfaces, 9*, 24462–24475.
132. Martinez, F. O., & Gordon, S. (2014). The M1 and M2 paradigm of macrophage activation: Time for reassessment. *F1000Prime Reports, 6*, 13.
133. Mathews, A. S., Ha, C. S., Cho, W. J., et al. (2006). Drug delivery system based on covalently bonded poly[N-isopropylacrylamide-co-2-hydroxyethylacrylate]-based nanoparticle networks. *Drug Delivery, 13*, 245–251.
134. Matsumura, Y., Hamaguchi, T., Ura, T., et al. (2004). Phase I clinical trial and pharmacokinetic evaluation of NK911, a micelle-encapsulated doxorubicin. *British Journal of Cancer, 91*, 1775–1781.
135. Mauricio, M. D., Guerra-Ojeda, S., Marchio, P., et al. (2018). Nanoparticles in medicine: A focus on vascular oxidative stress. *Oxidative Medicine and Cellular Longevity, 2018*, 6231482.
136. McClements, D. J. (2015). Nanoscale nutrient delivery systems for food applications: Improving bioactive dispersibility, stability, and bioavailability. *Journal of Food Science, 80*, N1602–N1611.
137. Michanetzis, G. P., Markoutsa, E., Mourtas, S., et al. (2019). Hemocompatibility of amyloid and/or brain targeted liposomes. *Future Medicinal Chemistry*.
138. Migotto, A., Carvalho, V. F., Salata, G. C., et al. (2018). Multifunctional nanoemulsions for intraductal delivery as a new platform for local treatment of breast cancer. *Drug Delivery, 25*, 654–667.
139. Mu, L., Chrastina, A., Levchenko, T., et al. (2005). Micelles from poly (ethylene glycol)-phosphatidyl ethanolamine conjugates (peg-Pe) as pharmaceutical nanocarriers for poorly soluble drug camptothecin. *Journal of Biomedical Nanotechnology, 1*, 190–195.
140. Müller, R. H., Gohla, S., & Keck, C. M. (2011). State of the art of nanocrystals-special features, production, nanotoxicology aspects and intracellular delivery. *European Journal of Pharmaceutics and Biopharmaceutics, 78*, 1–9.
141. Nagamitsu, A., Greish, K., & Maeda, H. (2009). Elevating blood pressure as a strategy to increase tumor-targeted delivery of macromolecular drug SMANCS: Cases of advanced solid tumors. *Japanese Journal of Clinical Oncology, 39*, 756–766.
142. Narmani, A., Mohammadnejad, J., & Yavari, K. (2019). Synthesis and evaluation of polyethylene glycol-and folic acid-conjugated polyamidoamine G4 dendrimer as nanocarrier. *Journal of Drug Delivery Science and Technology, 50*, 278–286.
143. Nielsen, U. B., Kirpotin, D. B., Pickering, E. M., et al. (2002). Therapeutic efficacy of anti-ErbB2 immunoliposomes targeted by a phage antibody selected for cellular endocytosis.

Biochimica et Biophysica Acta (BBA)-Molecular Cell Research, 1591, 109–118.

144. Normanno, N., De Luca, A., Bianco, C., Strizzi, L., Mancino, M., Maiello, M. R., Carotenuto, A., De Feo, G., Caponigro, F., & Salomon, D. S. (2006). Epidermal growth factor receptor (EGFR) signaling in cancer. *Gene, 366*, 2–16.
145. Owens, D. E., 3rd, & Peppas, N. A. (2006). Opsonization, biodistribution, and pharmacokinetics of polymeric nanoparticles. *International Journal of Pharmaceutics, 307*, 93–102.
146. Palange, A. L., Palomba, R., Rizzuti, I. F., et al. (2017). Deformable discoidal polymeric nanoconstructs for the precise delivery of therapeutic and imaging agents. *Molecular Therapy, 25*, 1514–1521.
147. Paolino, D., Licciardi, M., Celia, C., et al. (2012). Folate-targeted supramolecular vesicular aggregates as a new frontier for effective anticancer treatment in in vivo model. *European Journal of Pharmaceutics and Biopharmaceutics, 82*, 94–102.
148. Peetla, C., Stine, A., & Labhasetwar, V. (2009). Biophysical interactions with model lipid membranes: Applications in drug discovery and drug delivery. *Molecular Pharmaceutics, 6*, 1264–1276.
149. Pelaz, B., Alexiou, C., Alvarez-Puebla, R. A., et al. (2017). Diverse applications of nanomedicine. *ACS Nano, 11*, 2313–2381.
150. Peng, E., Choo, E. S., Tan, C. S., et al. (2013). Multifunctional PEGylated nanoclusters for biomedical applications. *Nanoscale, 5*, 5994–6005.
151. Pokharkar, V. B., Jolly, M. R., & Kumbhar, D. D. (2015). Engineering of a hybrid polymer-lipid nanocarrier for the nasal delivery of tenofovir disoproxil fumarate: Physicochemical, molecular, microstructural, and stability evaluation. *European Journal of Pharmaceutical Sciences, 71*, 99–111.
152. Polomska, A., Gauthier, M. A., & Leroux, J. C. (2017). In vitro and in vivo evaluation of PEGylated layer-by-layer polyelectrolyte-coated paclitaxel nanocrystals. *Small*.
153. Poudel, B. K., Soe, Z. C., Ruttala, H. B., et al. (2018). In situ fabrication of mesoporous silica-coated silver-gold hollow nanoshell for remotely controllable chemo-photothermal therapy via phase-change molecule as gatekeepers. *International Journal of Pharmaceutics, 548*, 92–103.
154. Pourjavadi, A., Asgari, S., Hosseini, S. H., et al. (2018). Codelivery of hydrophobic and hydrophilic drugs by graphene-decorated magnetic dendrimers. *Langmuir, 34*, 15304–15318.
155. Prabhakar, U., Maeda, H., Jain, R. K., et al. (2013). Challenges and key considerations of the enhanced permeability and retention effect for nanomedicine drug delivery in oncology. *Cancer Research, 73*, 2412–2417.
156. Prusty, D. K., Adam, V., Zadegan, R. M., et al. (2018). Supramolecular aptamer nano-constructs for receptor-mediated targeting and light-triggered release of chemotherapeutics into cancer cells. *Nature Communications, 9*, 535.
157. Prylutska, S., Panchuk, R., Gołuński, G., et al. (2017a). C 60 fullerene enhances cisplatin anticancer activity and overcomes tumor cell drug resistance. *Nano Research, 10*, 652–671.
158. Prylutska, S., Politenkova, S., Afanasieva, K., et al. (2017b). A nanocomplex of C60 fullerene with cisplatin: Design, characterization and toxicity. *Beilstein Journal of Nanotechnology, 8*, 1494–1501.
159. Qi, S. S., Sun, J. H., Yu, H. H., et al. (2017). Co-delivery nanoparticles of anti-cancer drugs for improving chemotherapy efficacy. *Drug Delivery, 24*, 1909–1926.
160. Ranade, V. V. (1989). Drug delivery systems-2. Site-specific drug delivery utilizing monoclonal antibodies. *Journal of Clinical Pharmacology, 29*, 873–884.
161. Raza, A., Rasheed, T., Nabeel, F., et al. (2019). Endogenous and exogenous stimuli-responsive drug delivery systems for programmed site-specific release. *Molecules, 24*, 1117.
162. Rezaei, S. J. T., Norouzi, K., Hesami, A., et al. (2018). Au (III) complexes loaded pH-responsive magnetic nanogels for cancer therapy. *Applied Organometallic Chemistry, 32*, e4303.
163. Riley, R. S., June, C. H., Langer, R., et al. (2019). Delivery technologies for cancer immunotherapy. *Nature, 18*, 175–196.
164. Roncato, F., Rruga, F., Porcù, E., et al. (2018). Improvement and extension of anti-EGFR targeting in breast cancer therapy by integration with the Avidin-nucleic-acid-nano-assemblies. *Nature Communications, 9*, 4070.
165. Rosenkranz, A. A., Slastnikova, T. A., Karmakova, T. A., et al. (2018). Antitumor activity of Auger electron emitter 111In delivered by modular nanotransporter for treatment of bladder cancer with EGFR overexpression. *Frontiers in Pharmacology, 9*, 1331.
166. Rossmanna, C., & Haemmerich, D. (2014). Review of temperature dependence of thermal properties, dielectric properties, and perfusion of biological tissues at hyperthermic and ablation temperatures. *Critical Reviews in Biomedical Engineering, 42*, 467–492.
167. Sarker, D. K. (2005). Engineering of nanoemulsions for drug delivery. *Current Drug Delivery, 2*, 297–310.
168. Sawa-Wejksza, K., & Kandefer-Szerszeń, M. (2018). Tumor-associated macrophages as target for antitumor therapy. *Archivum Immunologiae et Therapiae Experimentalis (Warsz), 66*, 97–111.
169. Schatz, A. A., Prejsnar, K. W., McCanney, J., et al. (2019). Policy strategies for the "new normal" in healthcare to ensure access to high-quality cancer care. *Journal of the National Comprehensive Cancer Network, 17*, 105–109.
170. Schramm, L. L., Stasiuk, E. N., & Marangoni, D. G. (2003). 2 surfactants and their applications. *Annual Reports on the Progress of Chemistry, Section C: Physical Chemistry, 99*, 3–48.
171. Shah, P., Bhalodia, D., & Shelat, P. (2010). Nanoemulsion: A pharmaceutical review. *Systematic Reviews in Pharmacy, 1*, 24–32.
172. Sharma, P., Zujovic, Z. D., Bowmaker, G. A., et al. (2011). Evaluation of a crystalline nanosuspension: Polymorphism, process induced transformation and in vivo studies. *International Journal of Pharmaceutics, 408*, 138–151.
173. Shen, Y., Li, X., Dong, D., Zhang, B., Xue, Y., & Shang, P. (2018). Transferrin receptor 1 in cancer: A new sight for cancer therapy. *American Journal of Cancer Research, 8*, 916–931.
174. Shi, J., Kantoff, P. W., Wooster, R., et al. (2017). Cancer nanomedicine: Progress, challenges and opportunities. *Nature Reviews. Cancer, 17*, 20.
175. Shi, Y., Van Der Meel, R., Theek, B., et al. (2015). Complete regression of xenograft tumors upon targeted delivery of paclitaxel via Π-Π stacking stabilized polymeric micelles. *ACS Nano, 9*, 3740–3752.
176. Shigdar, S., Macdonald, J., O'Connor, M., et al. (2013). Aptamers as theranostic agents: Modifications, serum stability and functionalisation. *Sensors (Basel), 13*, 13624–13637.
177. Shim, W. S., Yoo, J. S., Bae, Y. H., et al. (2005). Novel injectable pH and temperature sensitive block copolymer hydrogel. *Biomacromolecules, 6*, 2930–2934.
178. Shutava, T. G., Pattekari, P. P., Arapov, K. A., et al. (2012). Architectural layer-by-layer assembly of drug nanocapsules with PEGylated polyelectrolytes. *Soft Matter, 8*, 9418–9427.
179. Siegler, E. L., Kim, Y. J., & Wang, P. (2016). Nanomedicine targeting the tumor microenvironment: Therapeutic strategies to inhibit angiogenesis, remodel matrix, and modulate immune responses. *Journal of Cellular Immunotherapy, 2*, 69–78.
180. Song, X., Wan, Z., Chen, T., et al. (2016). Development of a multi-target peptide for potentiating chemotherapy by modulating tumor microenvironment. *Biomaterials, 108*, 44–56.
181. Song, Z., Shi, Y., Han, Q., et al. (2018). Endothelial growth factor receptor-targeted and reactive oxygen species-responsive lung cancer therapy by docetaxel and resveratrol encapsulated lipid-polymer hybrid nanoparticles. *Biomedicine & Pharmacotherapy, 105*, 18–26.

182. Stearns, L. J., Narang, S., Albright, R. E., Jr., et al. (2019). Assessment of health care utilization and cost of targeted drug delivery and conventional medical management vs conventional medical management alone for patients with cancer-related pain. *JAMA Network Open, 2*, e191549.
183. Su, Y., Liu, M., Liang, K., et al. (2018). Evaluating the accelerated blood clearance phenomenon of PEGylated nanoemulsions in rats by intraperitoneal administration. *AAPS PharmSciTech, 19*, 3210–3218.
184. Sutradhar, K. B., & Amin, M. D. L. (2014). Nanotechnology in cancer drug delivery and selective targeting. *ISRN Nanotechnology, 2014*, ID939378.
185. Tabatabaei, S. N., Derbali, R. M., Yang, C., et al. (2019). Co-delivery of miR-181a and melphalan by lipid nanoparticles for treatment of seeded retinoblastoma. *Journal of Controlled Release, 298*, 177–185.
186. Taghizadeh, B., Taranejoo, S., Monemian, S. A., et al. (2015). Classification of stimuli-responsive polymers as anticancer drug delivery systems. *Drug Delivery, 22*, 145–155.
187. Teesalu, T., Sugahara, K. N., Kotamraju, V. R., et al. (2009). C-end rule peptides mediate neuropilin-1-dependent cell, vascular, and tissue penetration. *Proceedings of the National Academy of Sciences of the United States of America, 106*, 16157–16162.
188. Teesalu, T., Sugahara, K. N., & Ruoslahti, E. (2013). Tumor-penetrating peptides. *Frontiers in Oncology, 3*, 216.
189. Tesarova, B., Charousova, M., Dostalova, S., et al. (2019). Folic acid-mediated re-shuttling of ferritin receptor specificity towards a selective delivery of highly cytotoxic nickel(II) coordination compounds. *International Journal of Biological Macromolecules, 126*, 1099–1111.
190. Tombak, A. (2019). Introductory chapter: Erythrocytes – Basis of life. In A. Tombak (Ed.), *Erythrocytes* (pp. 1–4). London: IntechOpen.
191. Torrisi, M. R., Lotti, L. V., Belleudi, F., et al. (1999). Eps15 is recruited to the plasma membrane upon epidermal growth factor receptor activation and localizes to components of the endocytic pathway during receptor internalization. *Molecular Biology of the Cell, 10*, 417–434.
192. Uldry, M., Ibberson, M., Hosokawa, M., et al. (2002). GLUT2 is a high affinity glucosamine transporter. *FEBS Letters, 524*, 199–203.
193. Vermeulen, L. M. P., De Smedt, S. C., Remaut, K., et al. (2018). The proton sponge hypothesis: Fable or fact? *European Journal of Pharmaceutics and Biopharmaceutics, 129*, 184–190.
194. Villaverde, G., & Baeza, A. (2019). Targeting strategies for improving the efficacy of nanomedicine in oncology. *Beilstein Journal of Nanotechnology, 10*, 168–181.
195. Wadhawan, A., Chatterjee, M., & Singh, G. (2019). Present scenario of bioconjugates in cancer therapy: A review. *International Journal of Molecular Sciences, 20*, E5243.
196. Wang, B.-H., Fan, J.-L., Wang, X.-W., et al. (2015). A nile blue based infrared fluorescent probe: Imaging tumors that over-express cyclooxygenase-2. *Chemical Communications, 51*, 792–795.
197. Wang, C., Wu, J., Wang, Z., et al. (2018). Glutamine addiction activates polyglutamine-based nanocarriers delivering therapeutic siRNAs to orthotopic lung tumor mediated by glutamine transporter SLC1A5. *Biomaterials, 183*, 77–92.
198. Wang, F., Ye, X., Wu, Y., et al. (2019b). Time interval of two injections and first-dose dependent of accelerated blood clearance phenomenon induced by PEGylated liposomal gambogenic acid: The contribution of PEG-specific IgM. *Journal of Pharmaceutical Sciences-Us, 108*, 641–651.
199. Wang, Y., Wang, Z., Qian, Y., et al. (2019a). Synergetic estrogen receptor-targeting liposome nanocarriers with anti-phagocytic properties for enhanced tumor theranostics. *Journal of Materials Chemistry B, 7*, 1056–1063.
200. Weissleder, R. (2001). A clearer vision for in vivo imaging. *Nature Biotechnology, 19*, 316–317.
201. WHO (2019) Cancer. https://www.who.int/news-room/fact-sheets/detail/cancer. Accessed 8 Nov 2019.
202. Wilhelm, S., Tavares, A. J., Dai, Q., et al. (2016). Analysis of nanoparticle delivery to tumours. *Nature Reviews Materials, 1*, 16014.
203. Wu, X. Y. (2016). Strategies for optimizing polymer-lipid hybrid nanoparticle-mediated drug delivery. *Expert Opinion on Drug Delivery, 13*, 609–612.
204. Xiao, K., Li, Y., Luo, J., et al. (2011). The effect of surface charge on in vivo biodistribution of PEG-oligocholic acid based micellar nanoparticles. *Biomaterials, 32*, 3435–3446.
205. Xuan, M., Shao, J., Zhao, J., et al. (2018). Magnetic mesoporous silica nanoparticles cloaked by red blood cell membranes: Applications in cancer therapy. *Angewandte Chemie (International Ed. in English), 57*, 6049–6053.
206. Xu, R., Zhang, G., Mai, J., et al. (2016). An injectable nanoparticle generator enhances delivery of cancer therapeutics. *Nature Biotechnology, 34*, 414–418.
207. Yang, J., Lu, W., Xiao, J., et al. (2018a). A positron emission tomography image-guidable unimolecular micelle nanoplatform for cancer theranostic applications. *Acta Biomaterialia, 79*, 306–316.
208. Yang, X.-Z., Dou, S., Wang, Y.-C., et al. (2012). Single-step assembly of cationic lipid-polymer hybrid nanoparticles for systemic delivery of siRNA. *ACS Nano, 6*, 4955–4965.
209. Yang, Y., Chen, Q., Li, S., et al. (2018c). iRGD-mediated and enzyme-induced precise targeting and retention of gold nanoparticles for the enhanced imaging and treatment of breast cancer. *Journal of Biomedical Nanotechnology, 14*, 1396–1408.
210. Yang, Y., Zhao, Y., Lan, J., et al. (2018b). Reduction-sensitive CD44 receptor-targeted hyaluronic acid derivative micelles for doxorubicin delivery. *International Journal of Nanomedicine, 13*, 4361–4378.
211. Yi, Y., Kim, H. J., Zheng, M., et al. (2019). Glucose-linked sub-50-nm unimer polyion complex-assembled gold nanoparticles for targeted siRNA delivery to glucose transporter 1-overexpressing breast cancer stem-like cells. *Journal of Controlled Release, 295*, 268–277.
212. Yu, M., Han, S., Kou, Z., et al. (2018). Lipid nanoparticle-based co-delivery of epirubicin and BCL-2 siRNA for enhanced intracellular drug release and reversing multidrug resistance. *Artificial Cells, Nanomedicine, and Biotechnology, 46*, 323–332.
213. Yu, Z., Pestell, T. G., Lisanti, M. P., et al. (2012). Cancer stem cells. *The International Journal of Biochemistry & Cell Biology, 44*, 2144–2151.
214. Zhang, J., Ren, X., Tian, X., et al. (2019c). GSH and enzyme responsive nanospheres based on self-assembly of green tea polyphenols and BSA used for target cancer chemotherapy. *Colloids and Surfaces. B, Biointerfaces, 173*, 654–661.
215. Zhang, L., Hao, P. Y., Yang, D. J., et al. (2019b). Designing nanoparticles with improved tumor penetration: Surface properties from the molecular architecture viewpoint. *Journal of Materials Chemistry B, 7*, 953–964.
216. Zhang, R. X., Cai, P., Zhang, T., et al. (2016). Polymer-lipid hybrid nanoparticles synchronize pharmacokinetics of co-encapsulated doxorubicin-mitomycin C and enable their spatiotemporal co-delivery and local bioavailability in breast tumor. *Nanomedicine, 12*, 1279–1290.
217. Zhang, W., Wen, Y., He, D.-X., et al. (2019a). Near-infrared AIEgens as transformers to enhance tumor treatment efficacy with controllable self-assembled redox-responsive carrier-free nanodrug. *Biomaterials, 193*, 12–21.

218. Zhao, R., Zheng, G., Fan, L., et al. (2018a). Carrier-free nanodrug by co-assembly of chemotherapeutic agent and photosensitizer for cancer imaging and chemo-photo combination therapy. *Acta Biomaterialia, 70*, 197–210.
219. Zhao, X., Tian, K., Zhou, T., et al. (2018b). PEGylated multi-walled carbon nanotubes as versatile vector for tumor-specific intracellular triggered release with enhanced anti-cancer efficiency: Optimization of length and PEGylation degree. *Colloids and Surfaces. B, Biointerfaces, 168*, 43–49.
220. Zhao, Z., Ukidve, A., Krishnan, V., et al. (2019). Effect of physicochemical and surface properties on in vivo fate of drug nanocarriers. *Advanced Drug Delivery Reviews*.

Homing Peptides for Cancer Therapy

Prakash Lingasamy and Tambet Teesalu

Abstract

Tumor-homing peptides are widely used for improving tumor selectivity of anticancer drugs and imaging agents. The goal is to increase tumor uptake and reduce accumulation at nontarget sites. Here, we describe current approaches for tumor-homing peptide identification and validation, and provide comprehensive overview of classes of tumor-homing peptides undergoing preclinical and clinical development. We focus on unique mechanistic features and applications of a recently discovered class of tumor-homing peptides, tumor-penetrating C-end Rule (CendR) peptides, that can be used for tissue penetrative targeting of extravascular tumor tissue. Finally, we discuss unanswered questions and future directions in the field of development of peptide-guided smart drugs and imaging agents.

Keywords

Tumor-homing peptide · Tumor-penetrating peptide · Nanoparticle · Nanomedicine · C-end Rule · Neuropilin-1 · Angiogenic integrins · gC1qR/p32 · Extracellular matrix · Multistep targeting · In vivo peptide phage display · T7 phage · Affinity chromatography

1 Introduction

According to the World Health Organization (WHO), cancer-related deaths are expected to pass the mortality of cardiovascular disease by 2030 [30]. Application of conventional therapies (surgery, radiotherapy, and chemotherapy) for the treatment of solid tumors has resulted in most cases only in incremental increases in the survival of patients with advanced disease [15]. The major chemotherapeutic drugs are low molecular weight chemical agents used to directly or indirectly inhibit the proliferation of rapidly growing cells. In general, the chemotherapy agents kill cancer cells by interacting with the DNA/RNA synthesis function of the cells and the cell cycle function. Chemotherapeutic drugs are categorized into different classes based on their mechanism of action [77]: (1) antimetabolites that mimic the building blocks of RNA and DNA; (2) alkaloids and alkylating agents that directly damage DNA; (3) antitumor antibiotics that interfere with the enzymes involved in DNA replication; (4) topoisomerase inhibitors that inhibit either topoisomerase I or II enzymes involved in unwinding DNA during replication and transcription; (5) mitotic inhibitors that disrupt microtubules causing inhibition of mitosis, or cell division; and (6) steroid hormones involved in estrogen and progesterone and relieve the side effects from other drugs.

Most chemotherapeutic drugs are administered via a systemic route, with the exposure of both healthy and cancerous cells in the body. Unfortunately, a major problem in systemic therapy is that the chemo drugs are nonspecific and attack not only malignant cells but also healthy proliferating cells. Typically only a small fraction of administered drugs reaches its target site(s) and the chemotherapeutics administered over an extended period cause severe toxic side effects, such as damage to the gastrointestinal mucosa and hematopoietic cells, mouth and throat sores, weight loss and cachexia, organ damage, nausea, vomiting, diarrhea, anemia, infections, fatigue, and destruction of the immune system [36].

P. Lingasamy
Laboratory of Cancer Biology, Institute of Biomedicine and Translational Medicine, University of Tartu, Tartu, Estonia

T. Teesalu (✉)
Laboratory of Cancer Biology, Institute of Biomedicine and Translational Medicine, University of Tartu, Tartu, Estonia

Center for Nanomedicine and Department of Cell, Molecular and Developmental Biology, University of California,
Santa Barbara, CA, USA

Cancer Research Center, Sanford Burnham Prebys Medical Discovery Institute, La Jolla, CA, USA
e-mail: Tambet.Teesalu@ut.ee

© Springer Nature Switzerland AG 2021
F. Fontana, H. A. Santos (eds.), *Bio-Nanomedicine for Cancer Therapy*, Advances in Experimental Medicine and Biology 1295, https://doi.org/10.1007/978-3-030-58174-9_2

Administering chemo drugs over extended periods of time leads to the loss of the ability to kill malignant cells and to emergence of resistance. To minimize the side effects, subtherapeutic doses of anticancer drugs are frequently used, the strategy that results in a selection of cancerous cells resistant to the drug, and, ultimately, in more aggressive disease [10]. Monitoring tumor response – clinical symptoms and tumor size – with imaging techniques such as computed tomography (CT), magnetic resonance imaging (MRI), positron emission tomography (PET), and radiography, is critical for effective cancer treatment strategies. Tumor size dynamics (shrinkage vs. progression) is widely used as a criterion for a response; however, some drugs that stabilize disease without an objective response may slow tumor growth sufficiently to improve patient survival [202]. Cancer treatment schemes are based on classification of tumor at diagnosis and clinical symptoms. However, genetic profiles of tumors with the same diagnosis, and hence, sensitivity to therapeutic interventions, can vary, leading to application of nonefficacious treatment strategies and poor prognosis. It has been estimated that the rate of application of inefficient treatment strategies varies from 29.8% to 42.5%, and reaches in some cases even 100% [202].

Cancerous tissue is heterogeneous, with striking regional differences in the tumor structure and physiology that translate into variability in the uptake and distribution of anticancer drugs within tumor tissue. Approved anticancer drugs, even cytotoxic/static compounds with low molecular weight, show inefficient extravasation and penetration of malignant tissue and, therefore, limited therapeutic efficacy [106, 200]. Application of tumor and patient-specific markers for selective delivery of chemotherapeutics to malignant lesions may restrict the damage to healthy tissues and increase therapeutic efficacy [45, 114]. Targeting ligands can also be used for noninvasive patient stratification and better monitoring of treatment response. Therefore, next-generation smart cancer therapeutics should include built-in homing mechanisms that result in their preferential accumulation in malignant tissues [202].

1.1 Next-Generation Cancer Therapies

A recent progress in preclinical and clinical cancer research has led to the development of novel transformative intervention strategies such as immunotherapies, personalized molecular therapies, nanomedicine, and affinity cancer targeting.

1.1.1 Immunotherapy

As part of its normal function, the immune system detects and destroys abnormal cells and most likely prevents or curbs the growth of many cancers. Malignant cells have evolved to avoid destruction by the immune system by a number of mechanisms, including: introducing genetic changes that make them less visible to the immune system, upregulating proteins on their surface that turn off immune cells, and modulating the tumor microenvironment to interfere with how the immune system responds to the cancer cells [32, 69, 75]. The aim of cancer immunotherapies is to restore the ability of the immune system to better recognize and fight against cancer. The first generation of cancer immunotherapies are immune checkpoint inhibitors (anti-CTLA-4 and anti-PD-1/PD-L1) that target natural immune homeostasis pathways to drive antitumor immune responses [32]. In a subset of patients, these checkpoint inhibitors have proven successful in curing metastatic diseases such as nonsmall cell lung cancer and melanoma. Additional immuno-based strategies include T-cell transfer therapy to boost the natural ability of T cells to fight cancer; treatment vaccines, which boost immune system's response to cancer cells, and immune system modulators, which enhance the body's immune response against cancer [35, 92].

The key challenge in cancer immunotherapies is to increase the responder patient population. There is a need for new antitumor immune-activating agents, which are currently in an advanced stages of development in preclinical/clinical studies [22].

1.1.2 Personalized Molecular Therapies

The development of every cancer is driven by a unique set of abnormalities in its genetic makeup that are present only in the tumor and not in normal tissues. While different patients may be diagnosed with what appears to be the same type of cancer, the genetic makeup, underlying mechanisms, and efficient therapeutic disease management strategies vary from patient to patient. Personalized molecular therapies are designed to attack specific mutations and other cancer-related changes in cells to suppress malignant cell proliferation and induce apoptosis by targeting specific molecules that play a critical role in cellular activities. One strategy uses humanized monoclonal antibodies (hMoAb) such as Rituximab (target: CD20), cetuximab (EGFR), and Bevacizumab (VEGF) [11, 23]. The second approach is using tyrosine kinase inhibitors such as cabozantinib (VEGFR2 inhibitor) and vandetanib (a VEGFR and EGFR inhibitor) gefitinib, and imatinib. Personalized molecular therapies require molecular profiling of patients to characterize potential targets for choosing the right drug combinations. However, the off-target toxicities and development of resistance remain significant concerns. The ongoing development of complex genomic and molecular companion diagnostic assays could help to stratify patients and focus on cohorts most likely to respond to drugs.

1.1.3 Nanomedicine

Nanomedicine drugs are seen as the "the magic bullets" that could improve cancer therapy and ameliorate the treatment of malignant disease by being more effective in reaching the target sites, have increased therapeutic efficacy, and cause less adverse side effects. The key revolutionary aspect of nanomedicine lies in the versatility and multifunctionality of the nanocarriers. Multitude of nanoformulations of different compositions, sizes, shapes, and surface properties, have been designed for therapeutic, diagnostic, and theranostic applications. Nanocarriers can accommodate therapeutic and diagnostic payloads of different classes, and can be simultaneously loaded with drugs and imaging agents for theranostic applications – application of a single nanosystems for both detection/diagnosis and therapy of malignant disease [64]. Nanocarrier loading can dramatically extend the drug circulation time and improve the biodistribution for better tolerability and an improved therapeutic outcome. Various classes of NPs are approved for clinical use including liposomes, PEGylated liposomes, albumin NPs, and polymeric micelles. Many more NPs are in clinical and preclinical trials [106]. The first marketed nanodrug Doxil (PEGylated liposomal doxorubicin) was approved by the FDA in 1995 for the treatment of Kaposi's sarcoma [20, 71]. Doxil and other approved nanodrugs are based on existing drugs that have been nanoformulated to improve their biodistribution or pharmacodynamic properties. All clinically approved nanoparticles are nontargeted passive drug delivery vehicles [28, 199]. Accumulation of such nanodrugs in solid tumors is believed to be due to an enhanced permeability and retention (EPR) effect, caused by the abnormal architecture of tumor blood vessels, lack of lymphatic drainage, defective endothelial cells with wide fenestrations, and inadequate pericyte coverage [120, 121, 123, 153]. For nanomedicine to hold its promise of revolutionizing disease prevention, diagnosis, and treatment, the in vivo delivery and biodistribution of nanoparticles must be improved further by strategies such as active targeting.

1.2 Active Cancer Targeting with Affinity Ligands

Malignant cells and cells in tumor stroma express surface molecules that distinguish them from healthy quiescent cells in adult organisms. Targeting of systemically accessible parts of this heterogeneity with affinity ligands (e.g., peptides and antibodies) is also referred to as active (synaphic) targeting [169]. The intended outcome of the synaphic targeting is to achieve what is seen following topical application: high local accumulation with little or no systemic exposure. In contrast to EPR-based passive targeting of tumors that relies on leaky vessels and poor lymphatic drainage that result in the extravasation and accumulation of drugs in the tumor tissue [122], active targeting can be used to improve accumulation of therapeutic payloads in target tissue and their uptake in target cells, leading to increased therapeutic efficacy and reduced off-target side effects [46, 165]. Affinity ligands to tumor vascular signature primarily target specific expression patterns in activated vascular cells (vascular and lymphatic endothelial cells and pericytes), many of which are secondary to the process of angiogenesis – sprouting of new blood vessels from existing vessels. Examples are cell surface angiogenic integrins, growth factor receptors, extracellular proteases, and extracellular matrix proteins. Importantly, by increasing the local drug concentration, active targeting also helps to lower the risk of developing drug resistance [13]. In the last three decades, genomics, proteomics and molecular profiling of cancers, and agnostic techniques such as in vivo peptide phage display, have resulted in the discovery of a number of cancer-specific receptors that can serve as targets for systemic circulating probes. The knowledge facilitated the development of affinity ligands of different classes such as Abs and their fragments, peptides, aptamers, and small molecules [114, 160, 171, 207]. An important challenge related to the ligand-based affinity targeting of vascular heterogeneity in malignant tissues relates to the limitation due to the number of accessible receptors in the tumor tissue [81, 131, 166]. One way to increase the capacity of affinity-based targeting systems is to develop multitargeted vascular targeting ligands and/or ligands that are capable of actively entering tumor parenchyma [48, 115, 159].

A large number of biological ligands, including antibodies, polysaccharides, nucleic acids, peptides, and small molecules, have been studied as agents to facilitate active targeting of malignant disease [210]. Polypeptide-based targeting ligands, including homing peptides, protein domains, and antibodies, have advantages over other classes of targeting ligands in that they can be systematically developed using various biological selection and expression systems. Some major issues of protein ligands include immunogenicity, low stability, and difficulty for site-specific conjugation on nanoparticles [57, 187]. Antibody–drug conjugates (ADCs) are complexes of monoclonal antibodies (mAb) conjugated to drugs or radionuclide therapeutic payloads through chemical linkers. Three FDA-approved ADCs are available for cancer treatment: brentuximab vedotin (target: CD30), trastuzumab emtansine (target: HER2 receptor), and inotuzumab ozogamicin (target: CD22) and many more are in clinical trials [1]. Antibodies are attractive targeting ligands due to high specificity and versatility; however, antibody-based drugs have inherent limitations, such as immunogenicity, and high cost of production on a large scale [23, 111, 171]. Also, antibodies as other proteins of a similar size cannot efficiently extravasate and reach beyond 50 μm in the tumor parenchyma [66, 176].

1.2.1 Tumor-Homing Peptides

Tumor-homing peptides have typically size <20 amino acids and are derived from natural domains of receptor-binding proteins, or have been identified by combinatorial approaches such as ribosomal and phage display. The key advantage of peptides over antibodies as affinity targeting ligands is that due to their small size they possess superior tissue and cell penetration ability [167, 193]. In addition, peptides tend to interact with conserved and functionally important binding pockets on the surface of target molecules, and thus are often biologically active. Importantly and of translational relevance, the small size of peptides renders them relatively nonimmunogenic. The recent advances in peptide synthesis technology allow for fully automated, facile synthesis and manufacturing scale-up of the production in a cost-effective manner – an important aspect considering clinical development and translation, especially considering the cost of large-scale manufacturing of antibodies. Homing peptides can be engineered to involve a range of nonnatural modifications to improve their target binding and/or stability, and to introduce functional groups for site-specific conjugation to proteins, nanocarriers, cytotoxic drugs, radionuclides, and toxins [15, 58, 104, 190].

On downside, peptides generally have lower target binding affinity and stability in biological fluids than antibodies. To compensate for the low affinity and to increase the avidity of target binding, multiple peptides can be used simultaneously. Proteolytic processing may be mechanistically important for triggering interaction of the peptide with its target, for example, activation of the cell and tumor penetration function of neuropilin-1 binding C-end Rule (CendR) peptides requires cleavage of the peptide by a tumor-derived protease to expose the C-terminal arginine residue [9, 167, 192, 193]. In addition, the in vivo half-life of peptides can be modulated by conjugating to albumin-binding elements or polyethylene glycol coupling, substitution of L amino acids with D-amino acids, blocking N- and C-termini, introduction of lactam bridges, and cyclization [113, 146, 203].

In preclinical studies, peptide-based synaphic targeting efforts have led to an impressive improvement in the biodistribution of payloads and their therapeutic efficacy. A big challenge is to translate this success into clinical studies and FDA-approved therapeutic strategies and peptide-targeted anticancer payloads and imaging agents [15, 50, 117, 167, 193, 194].

2 Vascular Heterogeneity and Homing Peptide Discovery

2.1 Vascular Zip Codes

The growth of tumors beyond microscopic lesions depends critically on their ability to ensure the supply of oxygen and nutrients through neovessels generated by angiogenesis and lymphangiogenesis [68, 168]. In the absence of the angiogenic switch to trigger neovascularization, tumor growth is limited to less than 2 mm^3 [133]. The angiogenic tumor blood vessels are morphologically, molecularly, and functionally different from healthy blood vessels. Characteristic microanatomical features of tumor vascular trees include irregular and torturous blood vessels with variable intravascular distances and irregular branching patterns, and the lack of an efficient lymphatic drainage system [44, 130]. Molecularly, the angiogenic signature of tumor neovessels involves upregulation of proangiogenic factors and markers that are not expressed or are expressed at a much lower level in healthy vessels, including angiogenic signaling molecules, adhesion receptors, extracellular matrix components, and enzymes that remodel the extracellular matrix. Examples are members of the angiogenic vascular endothelial growth factor (VEGF) family, basic fibroblast growth factor (bFGF), transforming growth factor (TGF)-α and -β, platelet-derived endothelial growth factor, granulocyte colony-stimulating factor, placental growth factor, epidermal growth factor, interleukin-8, hepatocyte growth factor, αvβ3 and αvβ5 integrins, oncofetal splice variants of fibronectin and Tenascin-C, matrix remodeling proteases – metalloproteinases, and urokinase-type plasminogen activator [158]. As discussed below, in activated cells in tumors some intracellular proteins such as nucleolin and P32/qC1qR are aberrantly expressed at the cell surface of the tumor and are accessible to the circulating affinity probes [41, 76, 137, 173, 182, 216]. The lymphatic endothelial cells are also specialized, as they express markers that are not present in the lymphatics of healthy tissues, or in tumor blood vessels [109]. The term vascular ZIP code refers to this unique vasculo/lymphatic signature that can be applied for systemic synaphic (affinity-based) targeting of diagnostic and therapeutic cargo [164, 194]. Interestingly, the vascular signatures show overlap across a palette of different diseases: cancer, atherosclerosis, inflammation, thrombosis, sepsis, vascular leak syndrome, and tissue regeneration [17, 73, 135, 188]. The likely reason is that all these conditions involve angiogenic/inflammatory components. At the same time, a subset of tumor ZIP codes and the corresponding homing peptides shows exquisite target selectivity and can, for example, differentiate between premalignant lesions and malignant cancer of the same tumor type and location [12, 165]. An important aspect of systemic targeting of the vascular component of tumors is that, unlike mutation-prone tumor cells, nonmalignant cells of the tumor vasculature are genetically stable and less likely to develop drug resistance or mutate the peptide binding sites on receptors [138].

2.2 Peptide Phage Display

Bacteriophages (or phages) are viruses composed of a nucleocapsid that encapsulates the genetic material (DNA or RNA genome) that infects and replicates within the bacteria, but are harmless to humans [2, 21, 83, 112, 195]. The bacteriophage genome can be modified to encode foreign peptide sequences as fusions with the coat protein. George Smith and his Ph.D. student, Stephen F. Parmley were the first to insert foreign DNA fragments into filamentous phage gene encoding p3 protein – one of the minor coat proteins that decorates in five copies the emerging tip of the filamentous phage, to express p3-fusion peptides on the phage surface [183]. Greg Winter subsequently created first phage libraries for humanized antibody discovery, alternative to the hybridoma technology [43]. To contruct peptide display phage libraries, genes encoding phage coat protein are modified to insert a stretch of DNA encoding random peptide sequences at a diversity of about one billion variants per library, close to the total number of theoretical permutations of a random 7-amino acid sequence (1.28E9). Phage display is widely used for peptide and antibody discovery based on different bacteriophage vectors such as T7, T4, M13, and f1. The importance of the phage display technology was acknowledged in 2018 by awarding the Nobel Prize in Chemistry to George P. Smith and Sir Gregory P. Winter "for their contribution in the phage display of peptides and antibodies."

In the context of systemic affinity targeting, in vivo phage display has become an established agnostic tool for the identification of homing peptides and mapping sytemically accessible molecular heterogeneity in normal organs and diseased tissues [143]. This technology has enabled assessment of the extent of the molecular specialization in the vasculature and has contributed to identification of a number of new markers expressed in the tumor neovasculature [143, 165]. For in vivo selection, a peptide phage library is injected into the systemic circulation of animals, typically intravenously, followed by perfusion to remove the background phage, removal of target organs, amplification of the bound phage, and next round of selection (Fig. 1). Unlike in vitro and cell-free selection, in vivo peptide phage selections have an inbuilt mechanism against selecting the promiscuous pan-specific peptides due to their depletion in nontarget vascular beds [194]. For in vivo peptide display, our group prefers to use the lytic T7 bacteriophage system that, compared to lysogenic filamentous phage-based display systems, has a size and aspect ratio more similar to those of clinically developed nanoparticles (in the case of T7 the nucleocapsid diameter is ~55–60 nm, whereas in the case of filamentous phage dimensions are ~6 nm × 900 nm), is less restrictive for the amino acid sequence of displayed peptides, exhibits increased stability, and has a lower mutation rate. In the T7-Select system of Novagen, the peptide-encoding DNA is inserted at the C-terminus of the major coat protein 10A or 10B gene, displaying density of foreign peptides maximum up to 415 identical peptides/phage [50, 167, 194]. High-copy display results in high avidity binding, even in the case of low-affinity peptide ligands, and reduced off-rates. Using phage display, tumor-homing peptides can be discovered using two different strategies: either using cell-free biopanning on purified target receptor (top-down approach), or in vivo selection with no a priori knowledge of the receptors (bottom down, or agnostic screening approach). A representative selection of tumor-targeting peptide identification and application data are stored in TumorHoPe [94] and THPdb [197] databases.

2.2.1 In Vitro Biopanning for Homing Peptide Detection

For top-down selection, the target for affinity delivery is chosen based on its absence in healthy tissues, upregulation in malignancy(ies) of interest, and systemic accessibility in the tumor tissue. The target recombinant protein is expressed, purified, immobilized, and used for peptide phage biopanning. The selection rounds are repeated until enrichment is achieved (usually in 3–6 rounds), followed by sequencing of peptide-encoding genomic DNA using Sanger or next-generation sequencing. The candidate peptide-phages are then back-cloned in the phage genomic DNA (to exclude contribution of mutations elsewhere in the phage capsid to binding) and validated for their target interaction (binding, specificity), and stability. A variation of the theme is to perform different rounds of biopanning on different target proteins to develop multitargeted peptides, as we have recently done for tumor-associated isoforms of extracellular matrix proteins (tenascin C and fibronectin) [115]. In some cases, target receptors fail to maintain the structural integrity during recombinant protein expression and engineered cells overexpressing target molecules can be used for biopanning. In the case of difficult targets, for example, members of highly conserved protein families, the specificity of the peptides can be improved by addition of negative selection steps. A related problem is that cell-free and in vitro selections fail to eliminate promiscuous peptides that nonselectively "stick" to nontarget components and thus lack intended selectivity. One possible way to address this problem is to combine in vitro biopanning with the in vivo selection described in the next section to deplete promiscuous peptides in nontarget organs.

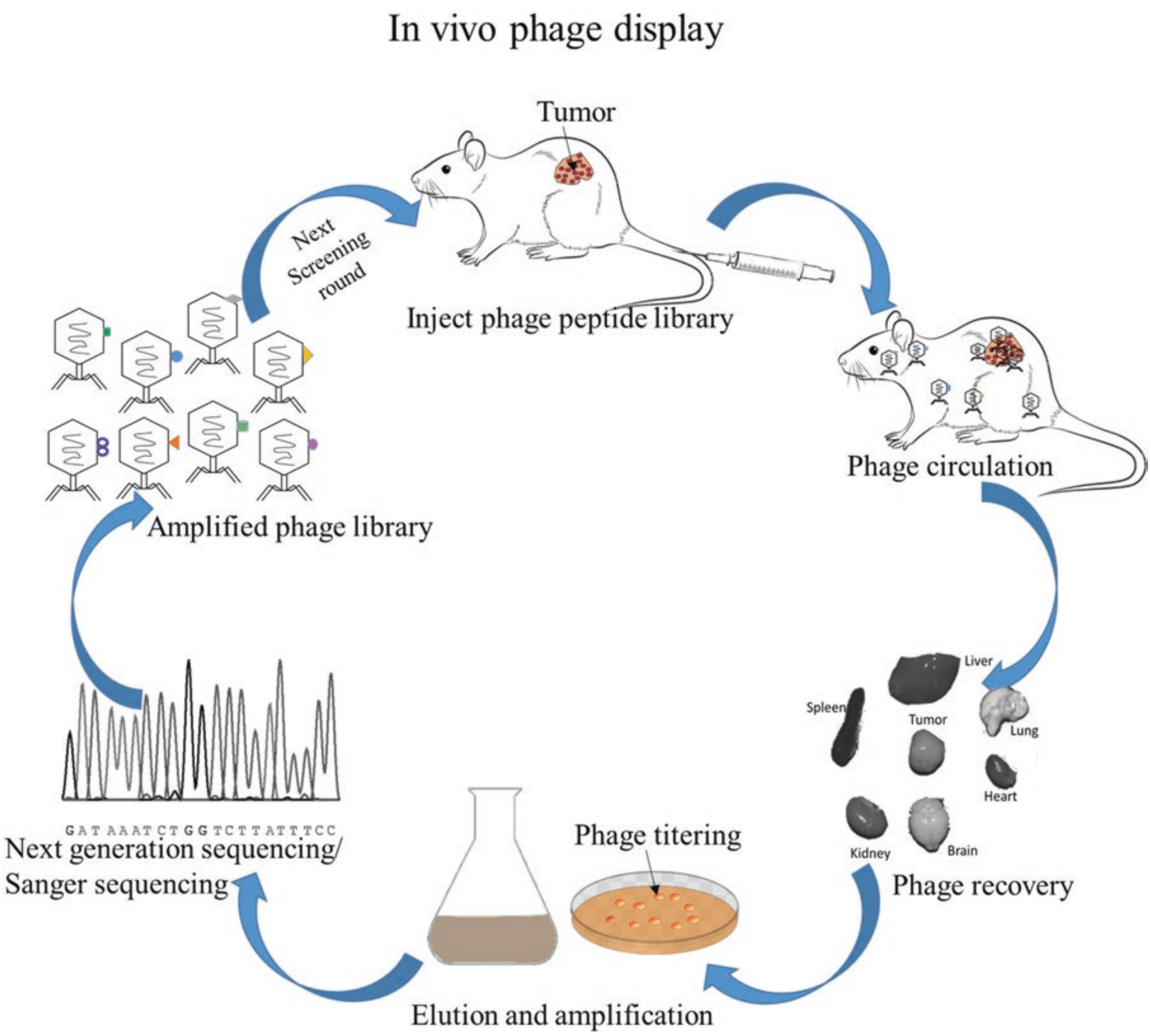
In vivo phage display
Tumor
Next Screening round
Inject phage peptide library
Phage circulation
Amplified phage library
Liver
Spleen
Tumor
Lung
Heart
Kidney
Brain
Phage recovery
Phage titering
GAT AAAT CT GG TCTTATT TCC
Next generation sequencing/
Sanger sequencing
Elution and amplification

Fig. 1 In vivo peptide phage biopanning. The genome of T7 bacteriophage is modified to express foreign peptides on the capsid of bacteriophage particles as C-terminal fusions of coat protein 10A of a bacteriophage. A peptide library is injected through the tail vein of tumor-bearing mice. Ten min to 1 h after injection, the mice are perfused through the heart to remove background unbound phages, and organs are collected for phage amplification in E. coli. The phage recovered from the tumor is amplified and reinjected in mice for additional selection rounds, until enrichment is seen. The phages from each round are subjected to DNA sequencing to identify tumor-targeting candidate peptides

2.2.2 Agnostic In Vivo Peptide Phage Biopanning

In the second approach, phage display is applied to living animals to identify homing peptides that preferentially accumulate in tumors [107, 194]. This approach takes into account the complexity and heterogeneity of the living animals and is closer to clinical applications. In vivo phage screening primarily probes the vascular beds, and peptide phages generally do not penetrate vascular walls into the tumor parenchyma [165]. Variations of in vivo biopanning besides “classic” intravenous route include alternative administration routes: trans- or intradermal, intratumoral, intraperitoneal (IP), subcutaneous (SC), and intranasal – chosen based on the intended target site and screening stringency, and taking into account the desired downstream applications [19, 39, 82, 201]. For detailed protocols on in vivo phage display, the readers are referred to a chapter in the Methods in Enzymology [194]. Briefly, independent of the administration route, the phage particles will be typically allowed to circulate for 10 min to 1 h, followed by perfusion of the circulatory system with a physiological buffer, such as phosphate-buffered saline, to remove the background of the unbound phages (in screens for internalizing peptides, the perfusion is carried out using a low-pH buffer that inactivates target bound noninternalized phages). The target organs and control organs are then collected for assessment of the titer of the recovered phages and amplified for the next round biopanning. These screening rounds are repeated until enrichment is achieved in the tumor tissue. In typical screens under medium-high stringency conditions, during each round of selection the diversity of peptide libraries collapses ~4-fold. Recently, our and other labs have started using next-generation sequencing of the peptide-coding segment of the phage genome and comprehensive assessment of peptide phage biodistribution patterns (custom analysis tool available at http://canbio.ut.ee) [82, 126]. The ability of candidate peptide phages from in vivo biopanning screens to home to intended targets is further validated in individual peptide phage biodistribution studies or in "in vivo play-off assay." In play-off experiments, equimolar mix of candidate and control phages is administered in mice, followed by the assessment of representation of phages in control and target organs to evaluate the robustness and specificity of homing. The distinct advantage of the play-off experiment compared to individual phage homing tests is that they are internally controlled and interanimal variability does not affect the outcome. After validation of peptides in the phage display format, the promising peptides are synthesized and tested for homing as fluorescent monomeric peptides and as targeting ligands of various payloads (drugs, imaging agents, and nanoparticles).

The target receptors of homing peptides need to be established for understanding the mechanistic details of homing and potential bioactivity, for improvement of the efficiency of targeting and delivery, and for development of improved affinity ligands. Affinity chromatography is widely used technique for peptide receptor identification [127]. The peptides immobilized on solid matrices are incubated with tumor tissue and cell lysate for allowing target receptors to bind to the immobilized peptide. The matrix complex is extensively washed and the target receptor is eluted with excess of free peptide. The elutes are analyzed by SDS-PAGE and silver staining, followed by receptor identification by mass spectrometry (MS) [192]. The candidate receptors are then validated using biochemical, immunological, and cell-based assays to confirm the peptide-receptor binding. Besides affinity chromatography, other methods such as chemical cross-linking and enzyme-based proximity labeling (with BioID and hydrogen peroxidase) can be used [24, 37, 79, 97]. However, false-positive receptor identification remains a significant problem in all the receptor hunting technologies.

2.3 Docking-Based Tumor Homing Peptides

2.3.1 Integrin-Targeting Homing Peptides

Already more than 3 decades ago, Ruoslahti and colleagues discovered that RGD tripeptide represents a minimal cell-binding sequence in extracellular matrix protein fibronectin (FN) [148, 149]. The identification of the RGD peptide paved the way for the discovery of many more RGD-containing extracellular matrix proteins such as vitronectin, type I collagen, fibrinogen, von Willebrand factor, osteopontin, and platelet protein gp HIb/IIIa. Ruoslahti and co-workers were also the first to identify transmembrane integrins as receptors for extracellular RGD-containing proteins and synthetic RGD peptides [155, 156, 170]. The integrin family includes 24 structurally related heterodimeric transmembrane proteins consisting of α and β subunits that act as receptors for ECM proteins, including TGF-β, laminin, vitronectin, fibronectin, fibrinogen, and collagens [51]. The RGD-binding site of integrins is formed by sequences from both α and β subunits. Over the years, multiple RGD-derived peptides and RGD-mimetic integrin ligands have been developed for targeted delivery of therapeutics, imaging agents, macromolecules, and nanocarriers. One such example, Cilengitide – c(RGDf-NMeVal) a potent antagonist of αvβ3, has been tested in glioblastoma multiforme phase-III clinical study by Merck [49, 51]. However, the trial failed to produce overall survival endpoints in GBM patients. Other RGD-containing peptides (e.g., cRGDfV, cRGDfK, and RGD4C) have been preclinically tested [102, 125]. The αvβ3 and αvβ5 integrins play important roles in angiogenesis [172]. The variants of RGDs peptide, including CRGDfK, cRGDfC, CRGDyK, have been tested in design of αvβ3 and αvβ5 integrin targeted drug delivery systems in multiple cancers in vivo. The RTDLXXL peptide motif identified by a phage display binds with nanomolar affinity to αvβ6 integrin – another member of the integrin family overexpressed in many solid tumors [99]. These RGD-based integrin targeting probes have been used for noninvasive cancer imaging and for the development of biomarkers. RGD based positron emission tomography (PET) ^{18}F- and ^{68}Ga probes were developed and tested for imaging of solid cancers. Examples are ^{18}F-fluciclatide [177] and ^{68}Ga-linked bombesin-RGD [213] used in probing prostate tumors and metastases, ^{124}I-labelled RGD nanoparticle used in multimodal PET/optical theranostic probes [25], radiolabeled A20FMDV2 peptide explored in targeting αvβ6 in breast cancer [96], and NIR light-guided surgery in preclinical models ovarian carcinoma and gastric cancer [40, 91].

2.3.2 Aminopeptidase N Targeting Homing Peptides

Asn-Gly-Arg (NGR) homing motif first emerged in cell-free peptide phage biopanning against α5β1 integrins that resulted in the selection of different RGD-containing peptides and NGR motif-containing peptides [14, 101]. The relevance of the NGR motif for systemic delivery was confirmed by an in vivo phage display study in mice bearing human breast carcinoma xenografts that led to identification of tumor vasculature-homing peptide CNGRCVSGCAGRC [14, 142]. The minimal cyclic peptide CNGRC inhibited the accumulation of the other NGR motif peptides [14]. NGR does not compete with RGD peptides, suggesting both binds to different receptors. The NGR motif showed specific binding to aminopeptidase N (APN/CD13), a membrane-bound metallopeptidase involved in angiogenesis, cell migration, and proliferation, antigen presentation, and regulation of the activity of hormones and cytokines [119, 142]. The NGR peptide showed a high affinity to CD13 expressed on the surface of the endothelial cells of tumor blood vessels [14]. The CD13 is overexpressed in angiogenic tumor vessels and under other pathologic conditions, such as inflammation and retinal disorders [27, 31, 33, 65, 204].

The NGR peptide is widely used as an affinity ligand to deliver anticancer drugs and imaging agents. Treatment of mice bearing orthotopic neuroblastoma, prostate, lung, and ovarian cancer xenografts with NGR-guided doxorubicin (DOX) liposomes resulted in dramatic destruction of the tumor vasculature and prolonged survival of the mice [60, 144, 145]. CNGRC fusion to proapoptotic $_{D}$(KLAKLAK)$_2$ peptides rendered the peptide selectively toxic for angiogenic endothelial cells [56]. The NGR peptides have been conjugated to different classes of cargoes such as nanoparticles, cytotoxic drugs, therapeutic proteins, proapoptotic peptides, viral particles, DNA/RNA, and imaging agents. The recombinant NGR-hTNFα cytokine, in combination with chemotherapeutics, has been tested in preclinical and clinical trials (phase I, II and III) showing promising efficacy [62, 63, 118]. NGR-hTNFα at low dose in combination with chemotherapeutic drugs (DOX, cisplatin; gemcitabine; pemetrexed, oxaliplatin) exerts synergistic effects and enhanced drug penetration, resulting in increased therapeutic response in various solid tumors in patients [119].

2.3.3 P32/qC1qR Targeting

The p32 is a small acidic mitochondrial chaperone that is expressed intracellularly in resting adult cells and displayed on the surface of tumor endothelial cells (blood and lymphatic), tumor cells, and tumor macrophages. First p32 targeting peptide, Lyp-1 (CGNKRTRGC), was originally identified in an in vivo screen for peptides that home to lymphatic vessels in breast tumors [109]. The Lyp-1 binds p32 in tumor cells, tumor-associated macrophages, and tumor lymphatics. It recognizes lesions from the premalignant lymphatic niche to fully metastatic tumors. Even though many normal cells express intracellular p32, it is a tumor-specific target as only the cell surface p32 present on malignant cells is accessible for cell-impermeable p32 ligands. Extracellular p32 ligands are taken up by the p32-displaying cells and become associated with the mitochondria, suggesting trafficking between the cell surface and the mitochondria. Importantly, p32-binding ligands have an inherent pharmacological activity and display an apoptosis-inducing activity on cultured p32-displaying tumor cells.

Recently we identified a novel ligand of p32, TT1 peptide (active both as a disulfide-bridged cyclic CKRGARSTC and as linearTT1, AKRGARSTA) [137, 178]. Compared to parental LyP-1 peptide, the TT1 peptide showed improved affinity in cell-free binding studies and excellent homing in vivo. In the same study, we reported a high-throughput screening of compound libraries that led to identification of a low molecular weight p32-targeting ligand (Cambridge compound #4014008) that shares the binding site with LyP-1 [137, 178].

Lyp1 and TT1 compete with each other for p32 binding and both contain cryptic tumor-penetrating C-end Rule (CendR) elements (see below). Homing and extravasation of TT1 relies on multistep homing and tumor penetration pathway: first, it binds to P32 protein on cell surface, followed by processing by a tumor-related protease, urokinase-type plasminogen activator (uPA), to expose conditional C-terminal CendR motif (AKRGAR) with newly acquired ability to bind to NRP-1 and to trigger vascular exit and internalization of the peptide [147, 173]. Similarly, Lyp-1 has been shown to be capable of penetrating tumors and to accumulate in the extravascular tumor parenchyma. Both P32 targeting peptides have been evaluated in numerous preclinical studies. The p32 targeting peptides have been evaluated in preclinical efficacy studies as targeting ligands of paclitaxel-albumin nanoparticles, DOX-loaded liposomes and polymersomes. LyP-1 peptide was originally identified as a lymphatic endothelial cell-homing peptide. Besides LyP-1, there are other lymphatic targeting peptides, such as AGR (CAGRRSAYC) and REA (CREAGRKAC) peptides shown to exhibit tumor tissue and stage-specific lymphatic homing patterns [114].

2.3.4 Homing Peptides for Targeting Fibrin–Fibronectin Complexes

Tumors as "wounds that do not heal" are known to contain a meshwork of clotted plasma proteins in the tumor stroma and in the walls of the tumor blood vessels. This tumor ECM complex supports tumor cell migration, survival, and proliferation and could serve as a potential target for affinity probes in the tumor microenvironment. Ruoslahti lab has used in vitro peptide phage library on plasma clots and identified peptides CGLIIQKNEC (CLT1) and CNAGESSKNC (CLT2) that specifically bind to clotted plasma proteins in tumors [150]. In mouse models of orthotopic breast cancer, fluorescein (FAM)-conjugated CLT1 and 2 peptides specifically homed to tumor ECM, whereas nonmalignant tissues remained negative. CLT1 peptide conjugated to PEG-PLA nanoparticles (CNP) loaded with paclitaxel significantly prolonged the survival in glioma-bearing mice [212]. CLT1 peptide conjugated to Gd-DTPA for molecular imaging of fibronectin–fibrin complexes in tumor tissue with magnetic resonance imaging (MRI). CLT1-(Gd-DTPA) demonstrated significant tumor contrast enhancement for at least 60 min in mice bearing HT-29 human colon carcinoma xenografts [208].

CREKA is another clotted plasma protein binding peptide identified by in vivo phage display screen with tumor-bearing MMTV-PyMT transgenic breast cancer mice [181]. CREKA peptide homes to extracellular meshwork in the tumor stroma of MMTV-PyMT tumors and MDA-MB-435 human breast cancer xenografts and also accumulated in malignant but not normal blood vessels [3, 181]. CREKA pentapeptide has a free sulfhydryl group not required for binding activity that is available for conjugation with nanoparticles, drugs, and imaging agents. CREKA-coated iron oxide nanoworms (NWs) act as a self-amplifying nanoparticle-delivery system that causes tumor-specific clotting to trigger binding of additional clot-homing particles. Systemic CREKA-NWs can be used for T2 MRI-based imaging and therapy of orthotopic human prostate cancer modeled in mice [4]. Creka-liposomes loaded with DOX (CREKA-Lipo-Dox), and platelet inhibitor ticagrelor (CREKA-Lipo-T) showed enhanced antitumor and antimetastatic efficacy in metastatic breast cancer model [90, 215]. Systemic treatment of breast tumor mice with CREKA peptide fusion with the truncated extracellular domain of tissue factor (tTF-CREKA) induced tumor-selective intravascular thrombosis, reduced tumor blood perfusion, and resulted in inhibition of tumor growth. tTF-CREKA selectively blocks the tumor blood supply and can be applied to different types of solid tumors [179]. In various other diseases, complexes of CREKA with Fe3O4-PLGA-PFH and SPION nanoparticles have been used for invasive multimodal molecular imaging (ultrasound and photoacoustic imaging) and therapy in thrombosis and myocardial ischemia models in mice and rats [185, 218].

2.3.5 Homing Peptides for Stage-Specific Tumor Targeting

The tumor stage-specific targeting peptides recognize neoplastic vascular signatures during different stages of tumor development [110, 164, 194]. A panel of such peptides and motifs were identified using in vivo phage display in the RIP1-Tag2 transgenic model of islet cell carcinoma, squamous cell carcinomas, pancreatic neuroendocrine tumor, and human MDA-MB-435 breast cancer [73, 93]. The peptides KAA (sequence: CKAAKNK) and KAR (sequence: CKGAKAR) were found to home preferentially to the established tumor over angiogenic islets. The peptides RSR (sequence: CRSRKG) and EYQ (sequence: CEYQLDVE) showed angiogenic islet-specific homing, with little or no binding to tumor vessels and to normal islets of control organs. Finally, VGVA (sequence: FRVGVADV) and RGR (sequence: CRGRRST) were found to home to vasculature of both established tumors and angiogenic islets [93].

Stage-specific tumor-homing peptides have been used successfully for preclinical imaging and efficacy studies. For example, tumor-targeting peptide KAA-guided nanoparticles loaded with anticancer drug gemcitabine showed robust homing to neovessels of pancreatic cancer in mice and therapeutic efficacy [198].

2.3.6 Malignant Extracellular Matrix Targeting Peptides

The extracellular matrix (ECM) is an important element of tissue architecture that provides structural and functional support for its cellular constituents. ECM is dynamic and adapts to changes in the microenvironment by remodeling its composition and topology, resulting in tissue and disease-specific ECM signatures [59, 86]. Compared to cell surface-homing peptide receptors, tumor ECM components are more abundant, thus providing a higher binding capacity [87, 115]. Notably, the oncofetal fibronectin Extra Domain-B (FN-EDB) and Tenascin-C (TNC) are overexpressed in many solid tumors and nearly absent in nonmalignant tissues [34, 140, 180]. There are various monospecific affinity ligands identified over the years to target FN-EDB or TNC, including for FN-EDB (ScFV L19 [132], ZD2 [67]) and TNC (ScFV G11 [180], TNC aptamer [47], and TNC-binding FHK peptide [98]). The FN-EDB and TNC antibodies (FN-EDB ScFV L19, TNC-C ScFV G11, F16, and 81C6) are used for precision delivery of cytokines (e.g., IL2 and TNF) and radionuclides [105, 186]. These ECM protein targeting ligands demonstrated their potential advantage in tumor targeting and delivery in various solid tumors.

Recently, we used cell-free screening to identify a 12 amino acid peptide, PL1 (sequence: PPRRGLIKLKTS), that recognizes two tumor associated ECM molecules: FN-EDB and tenascin-C C domain (TNC-C) [115]. The simultaneous affinity targeting of the two targets with the same affinity ligand allows for more uniform tumor targeting by overcoming the spatiotemporal heterogeneity in expression of target molecules and alleviating issues related to the limited number of available receptors for targeting ligands [81]. Another advantage of a bispecific peptide is that it helps to achieve synergistic targeting and delivery compared to monospecific targeting. The intravenously injected PL1 nanoworms (NWs) and silver nanoparticles (AgNPs) showed robust accumulation in a panel of glioblastoma and prostate carcinoma xenografts modeled in mice [115]. The PL1 nanoparticle accumulation was at least partially angiogenesis-dependent, as nonmalignant angiogenic neovessels induced by VEGF-overexpression we also found to take up PL1-NWs. The homing of nanoworms was dependent on both TNC-C and FN-EDB targeting, as function-blocking antibodies to either target alone decreased the homing, and a cocktail of both antibodies blocked the homing. Further, the experimental therapy of glioblastoma mice with proapoptotic nanoworms resulted in extended survival without apparent toxicity and PL1-NWs bound to the cryosections of clinical glioblastoma, suggesting translational relevance [115].

2.3.7 Hyaluronan Targeting Peptides

Hyaluronic acid (HA) is a nonsulfated glycosaminoglycan (GAG) that is negatively charged and contributes to the mechanical integrity of the ECM network with complex biological functions ranging from matrix organization, cell adhesion, migration, angiogenesis, morphogenesis, wound healing, and inflammatory responses to cancer metastasis [182, 214]. Recently, we reported intraperitoneal in vivo phage display screens using the T7 CX7C library in mice with peritoneal carcinomatosis (xenografts of gastric and colon carcinoma) [82]. This screen led to identification of IP3 (sequence: CKRDLSRRC) 9-residue cyclic peptide that contains a HA-binding motif. Fluorescein-labeled monomeric IP3 peptide bound to immobilized HA in vitro and the intraperitoneal IP3-coated silver nanoparticles and free fluorescent IP3 peptide showed preferential accumulation in peritoneal nodules of carcinomas of colon, gastric, and ovarian origin [82].

Moreover, a synthetic 42-amino acid peptide, BH-P (sequence: CNGRCGGRRAVLGSPRVKWTFLSRGRGGRGVRVKVNEAYRFR), derived from human brain HA binding protein, was reported to bind to HA and possess antitumor activity both in vitro and in vivo [116].

2.3.8 Tumor-Associated Macrophage Targeting Peptides

Tumor-associated macrophages (TAMs) are part of the innate immune system and have been associated with poor prognosis in many types of solid tumors. TAMs promote angiogenesis and tumor cell growth, metastasis, and contribute to the immunosuppressive environment. TAMs are categorized into M1 (M1 TAMs) and M2 macrophages (M2 TAMs). After chemotherapy, M2 TAMs accumulate around blood vessels in tumors, where they promote tumor revascularization and relapse [78, 151]. Pro-tumoral M2-like TAMs in progressing neoplasms typically express characteristic surface molecules, such as various scavenger receptors, for example, the hemoglobin scavenger receptor CD163, scavenger receptor A (SR-A), and mannose receptor-1 (also known as CD206) [18, 174]. These cells secrete growth factors, such as epidermal growth factor (EGF), which stimulates proliferation of carcinoma cells and cytokines, and IL-1, that promote the accumulation of tumor cells at distant sites [38, 136, 205]. Due to the central role that TAMs play in tumor progression and therapeutic resistance, they are recognized as a translationally relevant target for cancer immunotherapy and triggered efforts aimed at their elimination or reprogramming. Protumoral TAMs are not a single uniform population; instead, they are composed of multiple distinct subpopulations with overlapping features depending on a variety of external factors. Defining, differentiating, and targeting these subsets remains a challenging work-in-progress. Over the years a number of affinity ligands to target TAMs have been identified and several compounds are being evaluated in clinical trials. However, these targeting ligands are promiscuous and target other cells besides TAMs. For example, the peptide IDR RP-182 triggers a conformational change in CD206 on M2-like macrophages that shifts M2-like macrophages toward an M1 phenotype [88]. Another group identified by biopanning on isolated M2 macrophages the M2pep peptide (sequence: YEQDPWGVKWWY) that binds CD11b + Ly6G-F4/80high subpopulation of M2 macrophages. M2pep fusion to $_D$(KLAKLAK)$_2$ was able to selectively reduce the M2-like TAM population, but not the M1 macrophages, in tumor-bearing animals [42].

Recently we reported the identification of a peptide (mUNO, sequence: CSPGAK) that binds to mouse CD206 and homes to M2 TAMs in multiple solid tumor models, suggesting that peptide homing is dependent on the presence of M2 TAMs and not on the tumor type [16, 175]. Systemically administered fluorescein-labeled mUNO homes exclusively to CD206^{high} M2 TAMs in metastatic breast cancer, with no accumulation in tumor-free liver [16, 175]. Importantly, M2 TAMs internalize FAM-mUNO complexes, suggesting that the peptide can be used for intracellular payload delivery. Molecular dynamics simulations, docking predictions and fluorescence anisotropy studies suggested that on CD206 mUNO binds to a binding pocket between C-Type Lectin Domains-1 and -2 that is not involved in mannose binding. This observation provides an explanation for the improved selectivity of mUNO towards CD206 compared to mannose-based ligands such as Manocept™.

2.3.9 Nucleolin Targeting Peptides

Nucleolin is a multifunctional phosphoprotein found localized ubiquitously in the nucleolus and cytoplasm in healthy cells and is overexpressed in the cell surface of activated cells in many types of solid tumors [26, 191]. Nucleolin-targeting F3 peptide (sequence: KDEPQRRSARLSAKPAPPKPEPKPKKAPAKK), identified by biopanning with the cDNA phage library, corresponds to 31-aminoacid fragment of the high mobility group protein 2 (HMGN2). The F3 peptide interacts with cell surface-expressed nucleolin on endothelial cells [152] and is able to translocate into the nucleus of tumors cells of different origin [15, 154]. Fluorophore-labeled F3 peptide was found to internalize and translocate in the nuclei in human myeloid leukemia cells and in human breast cancer cells. The cellular uptake of F3 is specific as blocking F3-nucleolin interaction with antibodies abolished binding and internalization. The F3 peptide has been used as a tumor-targeting ligand for nanoparticles, chemotherapeutics, and radiotherapeutic agents [53, 95, 154, 157, 216].

Another nucleolin binding peptide, HB-19 pseudopeptide (5[Kpsi(CH_2N)PR]-TASP), originally identified as a potent inhibitor of HIV-1 infection, inhibits angiogenesis and growth of human breast tumor xenografts orthotopically modeled in mice, and reduces metastasis while causing no toxicities in normal tissues [52, 55, 134].

2.3.10 Epidermal Growth Factor Receptor Targeting Peptide

Members of the EGFR family of receptor tyrosine kinases, including HER1 (EGFR, ErbB1), HER2 (Neu, ErbB2), HER3 (ErbB3), and HER4 (ErbB4), are involved in a wide range of processes, including cell growth, proliferation, survival, migration, and tissue invasion and are overexpressed in many types of solid tumors including breast, colon and nonsmall cell lung cancer (NSCLC) [129, 217]. FDA-approved modulators of the EGFR pathway include monoclonal antibodies (cetuximab and panitumumab) and small molecular inhibitors (gefitinib, erlotinib, and afatinib).

EBP peptide (sequence: CMYIEALDKYAC) was developed by structural modeling of the natural EGFR ligand, EGF [103]. EBP conjugate with DOX showed enhanced anticancer efficacy and reduced systemic toxicity in orthotopic breast cancer xenograft mice [7, 8]. Liposomes functionalized with another EGFR-targeting peptide, D4 (sequence: LARLLT), were found to accumulate in EGFR expressing xenograft tumor tissues [184]. Recently, another EGFR-targeting peptide, GE11 (sequence: YHWYGYTPQNVI), identified by peptide phage display, was found to bind cultured MDA-MB-231 breast cancer cells and was able to systemically deliver gene/drugs to EGFR overexpressing cancer in vivo [74]. Two additional peptidic affinity ligands to EGFR, KCCYSL, and LTVSPWY, were also discovered by phage display and have proven useful for imaging and targeted drug delivery to EGFR-positive tumors [217]. Finally, two EGFR targeting peptides, EDA (sequence: PgYNPTTYQAha) and disruptin (sequence: SVDNPH), were biologically active and inhibit dimerization of EGFR and downstream signaling [5, 6, 70].

2.4 Tumor-Penetrating Peptides

Poor tissue penetration is a serious limitation of drug delivery to tumors, and owing to their size, nanoparticles and antibody drugs, in particular, suffer from this limitation [196]. The barriers are exit from the vasculature and penetration through tumor tissue. The frequently cited “leakiness” of tumor vessels permits passive extravasation, but it is not clear to what extent clinical tumors share this characteristic with the commonly used subcutaneous experimental tumors. Moreover, antiangiogenic treatments cause “normalization” of tumor vasculature [84], making it likely that nanodevices will be deployed with tumors whose vasculature is not leaky. High interstitial pressure in tumors constitutes a major barrier to penetration of extravasated compounds within extravascular tumor tissue, as does abundant fibrotic tissue, which is common in tumors such as pancreatic cancer [72, 85, 167].

About 15 years ago, the tumor homing LyP-1 peptide with the ability to target the lymphatic vessels and hypoxic areas in tumors was identified [108]. Systemically administered LyP-1 phage was found to accumulate in macrophages and lymphatic vessels away from blood vessels. In 2009, we identified a family of internalizing and tumor-penetrating C-end Rule or CendR peptides that contain a R/KXXR/K recognition motif that needs to be carboxyterminally exposed for activity [188, 192]. The CendR receptor NRP-1 is a co-receptor of semaphorins, VEGF family members, and multiple other growth factors that play essential roles in vascular biology and progression of solid tumors [61, 128]. CendR tumor-penetrating peptides (TPP) activate an endocytic transport pathway related to but distinct from macropinocytosis by engaging a complex process that involves binding to a primary, tumor-specific receptor, a proteolytic cleavage, and binding to a second receptor (Fig. 2). The binding to the second receptor NRP-1 activates the transport pathway [139, 192]. The pathway is distinct from known endocytosis pathways and is partially characterized [139].

The first TPP to be discovered was iRGD peptide (sequence: CRGD*K*GPDC or CRGD*R*GPDC) [188] that is clinically developed by San Diego-based DrugCendR Inc. as CEND-1. The iRGD peptide combines the tumor homing ability of the RGD motif with conditional proteolytically activatable CendR tissue penetration switch, rendering it highly potent and tumor-specific. First, the RGD sequence motif drives the recruitment of the peptide to αvβ3 and αvβ5 integrins on the surface of tumor angiogenic vascular endothelial cells and tumor cells. Second, a tumor-derived protease cleaves iRGD to generate fragment with C-terminally exposed CendR motif (CRGDK/R). The truncated peptide loses integrin-binding activity but acquires ability to interact with b1 domain of tissue penetration receptor NRP-1. Interaction with NRP-1 then activates a CendR pathway (endocytotic/exocytotic transport pathway) for enhanced transport of drugs into tumors [188]. The αvβ3 and αvβ5 requirement and involvement of a tumor-derived proteolytic convertase render iRGD activation tumor-specific. The iRGD peptide can carry a payload as large as a nanoparticle deep into tumor tissue. Surprisingly, the cargo does not have to be attached to iRGD; compounds co-administered with iRGD are also transported from the vasculature into the tumor parenchyma [189]. Co-injection of iRGD has resulted in enhanced tumor penetration and accumulation of each of the several compounds tested, and the phenomenon has been observed in a large number preclinical tumor models (transgenic models, xenograft and syngeneic implants of breast, pancreatic, prostate, and ovarian tumors), including metastases [189]. iRGD combination treatment does not affect the extent of the side effects, such as cardiomyopathy caused by

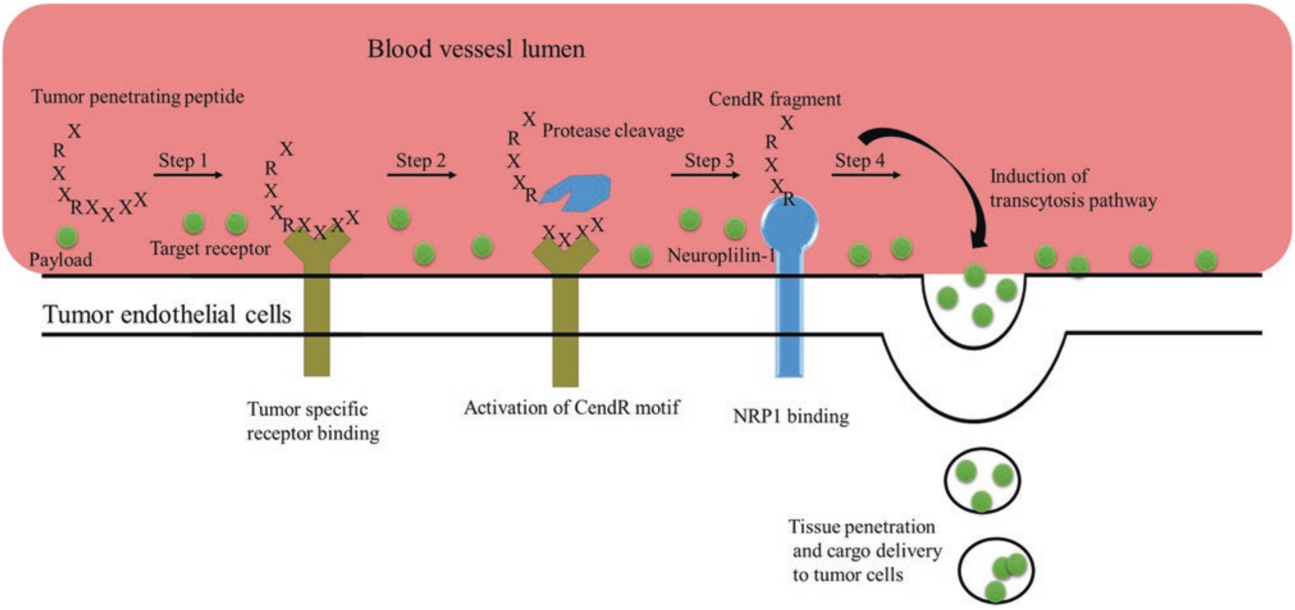
Blood vessesl lumen
Tumor penetrating peptide
Payload
Step 1
Target receptor
Step 2
Protease cleavage
CendR fragment
Step 3
Step 4
Neuroplilin-1
Induction of transcytosis pathway
Tumor endothelial cells
Tumor specific receptor binding
Activation of CendR motif
NRP1 binding
Tissue penetration and cargo delivery to tumor cells

Fig. 2 CendR trans-tissue transport pathway. The TPP cell and tissue penetration pathway is based on a three-step process. First, the peptide is recruited to primary tumor-specific target receptors (e.g., αvβ3/αvβ5 integrin in the case of iRGD; p32/ gC1qR in the case of LyP-1 and TT1). In the second step, the peptide is cleaved by proteases to unmask the cryptic CendR element (R/KXXR/K) at the C-terminus. Finally, the CendR motif interacts with neuropilin-1 (NRP-1) to trigger vascular and tumor tissue penetration

doxorubicin. Thus, iRGD broadens the therapeutic index of cancer drugs.

2.4.1 Novel Tumor-Penetrating Peptides

A defining feature of the CendR system is that the activity of the cell and tissue-penetrating CendR motif is strictly position-dependent and requires carboxy-terminal exposure of consensus element R/KXXR/K. Proteolytic enzymes mediate diverse processes such as extracellular matrix remodeling, immunity, development, protein processing, cell signaling, and apoptosis [54]. Of approximately 700 peptidases of the human degradome, nearly ¼ have cleavage specificities compatible with CendR exposure. Many of the proteases are expressed and secreted in a tissue or disease specific pattern. Incorporation of the CendR element in the context of a protease recognition and cleavage site can be applied for the activation of tissue-penetrating activity at a target site. CendR peptides of novel specificities can be constructed by combining CendR elements with protease cleavage sites and vascular homing modules – either by rational design or screening-based approaches. We have validated the concept by designing cryptic CendR peptides that are activated by urokinase-type plasminogen activator (uPA) [29]. The association of the uPA activity with tumorigenesis and its strong substrate selectivity make it an attractive candidate for protease-activated cancer targeting [29, 124, 182]. Our designer uPA-dependent tumor-penetrating peptide, uCendR, contains the following modules (starting from the N-terminus): a tandem RXXRXXR CendR element in the context of uPA cleavage site, and a vascular homing motif CRGDC. The uCendR peptide is recruited to tumor endothelial cells and tumor cells, followed by cleavage by uPA and NRP-1 dependent penetration into tumor tissue.

Besides angiogenic integrins, other primary receptors have been used for TPP design. For example, the NGR tripeptide tumor homing motif that targets aminopeptidase N (CD13) was embedded in iRGD-derived cyclic peptide scaffold, resulting in internalizing iNGR peptide (sequence: CRNGRGPDC) [9]. The iNGR peptide was found to home to CD13 in tumor vessels and, unlike parental NGR peptide, extravasate, and penetrate deep into the tumor parenchyma. For iNGR peptide-coupled paclitaxel nanoparticles and co-administered DOX, improved biodistribution and antitumor efficacy were observed [211, 219]. In recent studies, the iNGR peptide has been used to potentiate the tumor homing of lanthanide nanoclusters [206], and for targeted co-delivery of chemotherapeutic drugs and photosensitizer to treat treatment-resistant cancer [89].

The p32-targeting LyP-1peptide (sequence: CGNKRTRGC), discussed above, contains a cryptic CendR element, shows robust extravasation and parenchymal penetration in tumor tissue, and is likely to use the CendR pathway for tumor homing and penetration. The truncated version of LyP-1 with exposed CendR motif, tLyP-1 (sequence: CGNKRTR), binds to p32 and internalizes in cells through the CendR pathway [163]. Compared to parental peptide, tLyP-1 improves extravasation of a co-injected nanoparticle into the tumor tissue. As it uses a different primary receptor that iRGD, it may act as complementary peptide for iRGD [163]. Recently, we have identified another P32-targeting cyclic peptide TT1 (sequence: CKRGARSTC) [137]. Similar to Lyp-1 peptide, TT1 (and its linear variant, linTT1, AKRGARSTA) showed homing and internalization in different tumor models in vivo [80, 173, 178]. TT1 and LinTT1 peptides can be activated by cleavage by tumor-derived uPA to carboxyterminally expose the AKRGAR active CendR fragment [178]. Both tLyP-1 and TT1 peptides have applications for targeted drug delivery of anticancer drugs or imaging agents to p32 overexpressing cancers.

2.4.2 Translational Development and Perspectives of TPP Technology

TPP enables specific tumor targeting, increasing the drug accumulation in the tumor, and promoting even drug distribution throughout the tumor. A unique property of TPPs is that the peptides can be used without the need to couple the drug to the targeting agent [189]. The TPP acts through a three-step process involving binding to a receptor present only in tumors, at the surface of tumor vessels, in particular, a subsequent proteolytic cleavage, and transfer to another receptor. The binding of processed TPP to NRP-1 activates a vesicular transport pathway (CendR pathway) that is meant to carry nutrients into tissues [139]. The current hypothesis is that a drug co-administered with TPPs will be transported into tissue as if it were a nutrient. Because TPPs activate the transport pathway only in cancerous tissue, the drug will only accumulate and spread within tumors, not in normal tissues, and the result is enhanced anticancer activity without an increase in side effects. There are currently nearly 200 publications in the scientific literature on applications of prototypic TPP iRGD and the CendR technology for improving the biodistribution and potentiation of a variety of compounds ranging from low molecular weight compounds to macromolecules and nanoparticles, that come from a large number of laboratories located all over the world. In animal studies, iRGD has been shown to enhance the efficacy of kinase inhibitors, cytokines, antibodies, nucleic acid-based therapeutics siRNA, and even anticancer immune cells [209, 220]. The increase in the activity of anti-cancer agents provided by iRGD has been shown for a variety of tumor types. Thus, iRGD/TPP can potentially become a platform technology able of enhancing the activity of a variety of treatment (and imaging) modalities aimed at solid tumors. Alternatively, as the boost in anticancer activity is tumor specific, iRGD has the potential to reduce systemic toxicity of treatments.

The lead indication, currently under Phase I clinical development, is iRGD-enhanced gemcitabine/abraxane therapy for treatment of pancreatic ductal adenocarcinoma (https://clinicaltrials.gov/ct2/show/NCT03517176). Clinical validation of iRGD as a method to enhance antitumor activity of co-administered gemcitabine and abraxane is expected to lead to broader efforts to combine iRGD and other TPPs that are currently in the preclinical development phase with anticancer agents. The use of iRGD will be a therapeutic booster that will not require patients to be removed from standard of care therapy. iRGD-based imaging approaches are also being developed that will serve as functional biomarkers of iRGD-enhanced tumor uptake in the clinic. Preclinical studies with iRGD and contrast agents show robust signals for iRGD-mediated tumor uptake and penetration of the contrast agent in mouse models [193, 220], indicating that iRGD-based imaging approaches could be used for patient stratification. The iRGD peptide is straightforward to manufacture and should provide a cost-effective therapeutic approach to improve the tumor localization, distribution, and efficacy of co-administered therapeutics.

3 Conclusions and Perspectives

Affinity targeting with tumor-homing peptides is an established technology that can be used to achieve improved selectivity and efficacy of anticancer drugs to widen their therapeutic index. The current arsenal of tumor-homing peptides allows targeted drug delivery with great precision to various components in malignant tissues: blood and lymphatic vascular trees, extracellular matrix, immune cells, and fibroblasts (Fig. 3). Translational potential of homing peptides is further strengthened by their small size, low immunogenicity, and biocompatibility. Peptides are usually not species-specific as they target functionally important binding pockets on target molecules, and these sites are highly conserved among species. This circumstance increases the translational potential of peptides. Finally, vascular-homing peptides can be readily identified in an unbiased manner by in vivo phage display.

Among tumor-homing peptides, tumor-penetrating CendR peptides hold a great promise. Activating the CendR pathway in a tumor-specific manner provides a specific way of increasing the activity of conjugated and co-administered anticancer drugs and of enhancing tumor imaging. iRGD and other TPP (tLyP-1, iNGR)-based approaches are the only technologies that enable specific tumor targeting, promote even drug distribution throughout the tumor, and can be used without the need to couple the drug to the targeting agent. Thus, the tumor-penetrating CendR peptides represent a potentially transformative advance in cancer treatment. iRGD is currently undergoing clinical testing, and the next few years are expected to show to what degree the promising preclinical data on TPP are validated in clinical settings.

Refinement of intratumoral precision delivery strategies using the homing peptides is expected to be an important frontier in progress towards more efficacious and more tolerable anticancer strategies. Intratumoral precision delivery

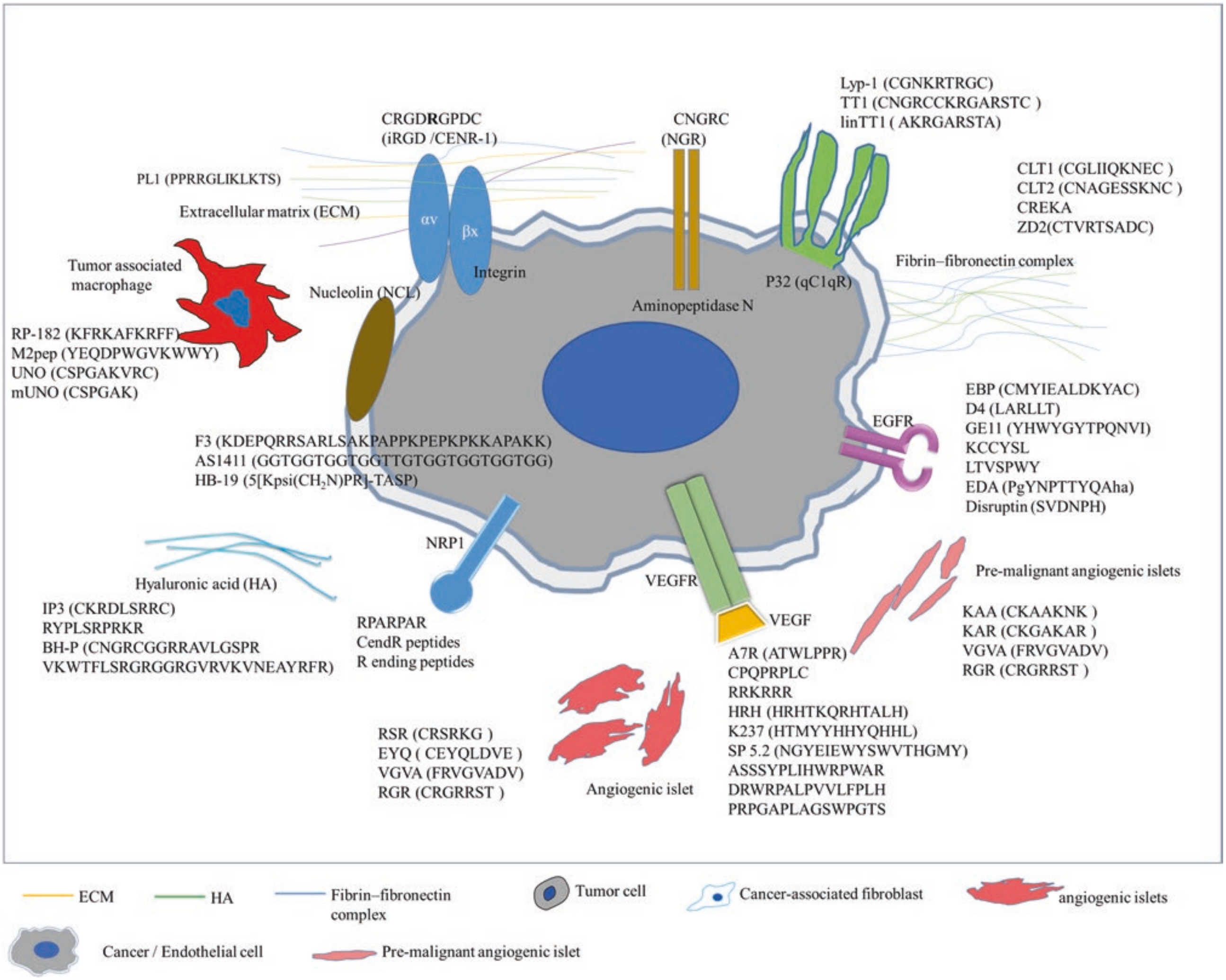
CRGDRGPDC
(iRGD /CENR-1)
PL1 (PPRRGLIKLKTS)
Extracellular matrix (ECM)
αv
βx
Integrin
Tumor associated macrophage
Nucleolin (NCL)
RP-182 (KFRKAFKRFF)
M2pep (YEQDPWGVKWWY)
UNO (CSPGAKVRC)
mUNO (CSPGAK)
F3 (KDEPQRRSARLSAKPAPPKPEPKPKKAPAKK)
AS1411 (GGTGGTGGTGGTTGTGGTGGTGGTGG)
HB-19 (5[Kpsi(CH$_2$N)PR]-TASP)
NRP1
Hyaluronic acid (HA)
IP3 (CKRDLSRRC)
RYPLSRPRKR
BH-P (CNGRCGGRRAVLGSPR
VKWTFLSRGRGGRGVRVKVNEAYRFR)
RPARPAR
CendR peptides
R ending peptides
CNGRC
(NGR)
Aminopeptidase N
Lyp-1 (CGNKRTRGC)
TT1 (CNGRCCKRGARSTC)
linTT1 (AKRGARSTA)
P32 (qC1qR)
CLT1 (CGLIIQKNEC)
CLT2 (CNAGESSKNC)
CREKA
ZD2(CTVRTSADC)
Fibrin–fibronectin complex
EGFR
EBP (CMYIEALDKYAC)
D4 (LARLLT)
GE11 (YHWYGYTPQNVI)
KCCYSL
LTVSPWY
EDA (PgYNPTTYQAha)
Disruptin (SVDNPH)
Pre-malignant angiogenic islets
KAA (CKAAKNK)
KAR (CKGAKAR)
VGVA (FRVGVADV)
RGR (CRGRRST)
VEGFR
VEGF
A7R (ATWLPPR)
CPQPRPLC
RRKRRR
HRH (HRHTKQRHTALH)
K237 (HTMYYHHYQHHL)
SP 5.2 (NGYEIEWYSWVTHGMY)
ASSSYPLIHWRPWAR
DRWRPALPVVLFPLH
PRPGAPLAGSWPGTS
RSR (CRSRKG)
EYQ (CEYQLDVE)
VGVA (FRVGVADV)
RGR (CRGRRST)
Angiogenic islet
ECM
HA
Fibrin–fibronectin complex
Tumor cell
Cancer-associated fibroblast
angiogenic islets
Cancer / Endothelial cell
Pre-malignant angiogenic islet

Fig. 3 Tumor-homing peptides. Overview of tumor-homing peptides and their receptors

may be particularly relevant in the context of immunotherapies, where modulation of precisely defined cell populations (e.g., M2 TAMs, Tregs) may result in profound modulation of therapeutic response. For example, iRGD homes to Treg cells, the main immunosuppressive cells in tumors, and iRGD anticancer drug combination may be able to selectively destroy these cells, while leaving the antitumor immune cells intact.

Homing peptides can have a transformative impact on the clinical development of precision-guided nanodrugs and imaging agents. Where 15 passively targeted nanocarriers are FDA-approved for clinical use, none of the actively targeted nanodrugs have advanced past clinical testing and obtained approval [161]. Most of the nanodrugs approved to date have, compared to conventional drugs, demonstrated reduced toxicity and better tolerability rather than improved efficacy. Currently, there are more anticancer nanodrugs in clinical trials than any other drug classes [162]. In numerous preclinical studies, the application of the affinity targeted nanomedicine results in a high tumor concentration of drugs due to a combination of tumor receptor-dependent uptake and EPR-based accumulation. For example, DOX-loaded anti HER2-guided immunoliposomes showed significantly superior therapeutic results compared to control nontargeted liposomal DOX and free DOX [100, 141].

The final issue that needs to be addressed in the coming years is the limiting number of receptors for targeting ligands – a serious limitation of affinity targeting strategies that limits the capacity of the targeting systems [81]. This issue can be alleviated by using the peptide receptors that are highly abundant and accessible (such as ECM components) or combining targeting peptides of different binding specificities (multitargeting). Additional advantage of multitargeted tumor-homing peptides is that they can be used to overcome uneven tissue distribution of individual targets for more uniform payload delivery. In conclusion, peptide targeted drug therapies will continue to contribute a significant innovation in targeted nanomedicine development for maximal treatment safety and efficacy for cancer therapy and diagnosis in the near future.

Acknowledgment T. Teesalu was supported by the European Regional Development Fund (Project No. 2014-2020.4.01.15-0012) and Estonian Research Council (grants PRG230 and EAG79).

References

1. Abdollahpour-Alitappeh, M., Lotfinia, M., Gharibi, T., et al. (2019). Antibody–drug conjugates (ADCs) for cancer therapy: Strategies, challenges, and successes. *Journal of Cellular Physiology, 234*, 5628–5642.
2. Abedon, S. T., Kuhl, S. J., Blasdel, B. G., & Kutter, E. M. (2011). Phage treatment of human infections. *Bacteriophage, 1*, 66–85.
3. Agemy, L., Kotamraju, V. R., Friedmann-Morvinski, D., et al. (2013). Proapoptotic peptide-mediated cancer therapy targeted to cell surface p32. *Molecular Therapy, 21*, 2195–2204.
4. Agemy, L., Sugahara, K. N., Kotamraju, V. R., et al. (2010). Nanoparticle-induced vascular blockade in human prostate cancer. *Blood, 116*, 2847–2856.
5. Ahsa, A., Ramanand, S. G., Bergin, I. L., et al. (2014). Efficacy of an EGFR-specific peptide against EGFR-dependent cancer cell lines and tumor xenografts. *Neoplasia (United States), 16*, 105–114.
6. Ahsan, A., Ray, D., Ramanand, S. G., et al. (2013). Destabilization of the epidermal growth factor receptor (EGFR) by a peptide that inhibits egfr binding to heat shock protein 90 and receptor dimerization. *The Journal of Biological Chemistry, 288*, 26879–26886.
7. Ai, S., Duan, J., Liu, X., et al. (2011). Biological evaluation of a novel doxorubicin-peptide conjugate for targeted delivery to EGF receptor-overexpressing tumor cells. *Molecular Pharmaceutics, 8*, 375–386.
8. Ai, S., Jia, T., Ai, W., et al. (2013). Targeted delivery of doxorubicin through conjugation with EGF receptor-binding peptide overcomes drug resistance in human colon cancer cells. *British Journal of Pharmacology, 168*, 1719–1735.
9. Alberici, L., Roth, L., Sugahara, K. N., et al. (2013). De Novo design of a tumor-penetrating peptide. *Cancer Research, 73*, 804–812.
10. Alfarouk, K. O., Stock, C.-M., Taylor, S., et al. (2015). Resistance to cancer chemotherapy: Failure in drug response from ADME to P-gp. *Cancer Cell International, 15*, 71.
11. Alibakhshi, A., Abarghooi Kahaki, F., Ahangarzadeh, S., et al. (2017). Targeted cancer therapy through antibody fragments-decorated nanomedicines. *Journal of Controlled Release, 268*, 323–334.
12. Alitalo, K., & Carmeliet, P. (2002). Molecular mechanisms of lymphangiogenesis in health and disease. *Cancer Cell, 1*, 219–227.
13. Andrieu, J., Re, F., Russo, L., & Nicotra, F. (2019). Phage-displayed peptides targeting specific tissues and organs. *Journal of Drug Targeting, 27*, 555–565.
14. Arap, W., Pasqualini, R., & Ruoslahti, E. (1998). Cancer treatment by targeted drug delivery to tumor vasculature in a mouse model. *Science, 279*, 377–380.
15. Araste, F., Abnous, K., Hashemi, M., et al. (2018). Peptide-based targeted therapeutics: Focus on cancer treatment. *Journal of Controlled Release, 292*, 141–162.
16. Asciutto, E. K., Kopanchuk, S., Lepland, A., et al. (2019). Phage-display-derived peptide binds to human CD206 and modeling reveals a new binding site on the receptor. *The Journal of Physical Chemistry. B, 123*, 1973–1982.
17. Augustin, H. G., & Koh, G. Y. (2017). Organotypic vasculature: From descriptive heterogeneity to functional pathophysiology. *Science, 357*, 6353.
18. Azad, A. K., Rajaram, M. V. S., Metz, W. L., et al. (2015). γ-Tilmanocept, a new radiopharmaceutical tracer for cancer sentinel lymph nodes, binds to the mannose receptor (CD206). *Journal of Immunology, 195*, 2019–2029.
19. Bábíčková, J., Tóthová, Ľ., Boor, P., & Celec, P. (2013). In vivo phage display – a discovery tool in molecular biomedicine. *Biotechnology Advances, 31*, 1247–1259.
20. Barenholz, Y. (2012). Doxil® – The first FDA-approved nanodrug: Lessons learned. *Journal of Controlled Release, 160*, 117–134.
21. Barrow, P. A., & Soothill, J. S. (1997). Bacteriophage therapy and prophylaxis: Rediscovery and renewed assessment of potential. *Trends in Microbiology, 5*, 268–271.
22. Baudino, T. A. (2015). Targeted cancer therapy: The next generation of cancer treatment. *Current Drug Discovery Technologies, 12*, 3–20.
23. Beck, A., Goetsch, L., Dumontet, C., & Corvaïa, N. (2017). Strategies and challenges for the next generation of antibody–drug conjugates. *Nature Reviews. Drug Discovery, 16*(5), 315–337.
24. Becker, J. M., & Naider, F. (2015). Cross-linking strategies to study peptide ligand-receptor interactions. In *Methods in enzymology* (pp. 527–547). New York: Academic Press.
25. Benezra, M., Penate-Medina, O., Zanzonico, P. B., et al. (2011). Multimodal silica nanoparticles are effective cancer-targeted probes in a model of human melanoma. *The Journal of Clinical Investigation, 121*, 2768–2780.
26. Berger, C. M., Gaume, X., & Bouvet, P. (2015). The roles of nucleolin subcellular localization in cancer. *Biochimie, 113*, 78–85.
27. Bhagwat, S. V., Lahdenranta, J., Giordano, R., et al. (2001). CD13/APN is activated by angiogenic signals and is essential for capillary tube formation. *Blood, 97*, 652–659.
28. Bobo, D., Robinson, K. J., Islam, J., et al. (2016). Nanoparticle-based medicines: A review of FDA-approved materials and clinical trials to date. *Pharmaceutical Research, 33*, 2373–2387.
29. Braun, G. B., Sugahara, K. N., Yu, O. M., et al. (2016). Urokinase-controlled tumor penetrating peptide. *Journal of Controlled Release, 232*, 188–195.
30. Bray, F., Ferlay, J., Soerjomataram, I., et al. (2018). Global cancer statistics 2018: GLOBOCAN estimates of incidence and mortality worldwide for 36 cancers in 185 countries. *CA: a Cancer Journal for Clinicians, 68*, 394–424.
31. Burg, M. A., Pasqualini, R., Arap, W., et al. (1999). NG2 proteoglycan-binding peptides target tumor neovasculature. *Cancer Research, 59*, 2869–2874.
32. Burugu, S., Dancsok, A. R., & Nielsen TO. (2018). Emerging targets in cancer immunotherapy. *Seminars in Cancer Biology, 52*, 39–52.
33. Cai, J., Kehoe, O., Smith, G. M., et al. (2008). The angiopoietin/Tie-2 system regulates pericyte survival and recruitment in diabetic retinopathy. *Investigative Ophthalmology and Visual Science, 49*, 2163–2171.
34. Carnemolla, B., Castellani, P., Ponassi, M., et al. (1999). Identification of a glioblastoma-associated tenascin-C isoform by a high affinity recombinant antibody. *The American Journal of Pathology, 154*, 1345–1352.
35. Carter, P. J., & Lazar, G. A. (2018). Next generation antibody drugs: Pursuit of the "high-hanging fruit". *Nature Reviews. Drug Discovery, 17*, 197–223.
36. Chabner, B. A., & Roberts, T. G. (2005). Chemotherapy and the war on cancer. *Nature Reviews. Cancer, 5*, 65–72.
37. Chang, L., Chen, Y. J., Fan, C. Y., et al. (2017). Identification of siglec ligands using a proximity labeling method. *Journal of Proteome Research, 16*, 3929–3941.

38. Chanmee, T., Ontong, P., Konno, K., & Itano, N. (2014). Tumor-associated macrophages as major players in the tumor microenvironment. *Cancers (Basel), 6*, 1670–1690.
39. Chen, Y., Shen, Y., Guo, X., et al. (2006). Transdermal protein delivery by a coadministered peptide identified via phage display. *Nature Biotechnology, 24*, 455–460.
40. Cheng, H., Chi, C., Shang, W., et al. (2017). Precise integrin-targeting near-infrared imaging-guided surgical method increases surgical qualification of peritoneal carcinomatosis from gastric cancer in mice. *Oncotarget, 8*(4), 6258.
41. Christian, S., Pilch, J., Akerman, M. E., et al. (2003). Nucleolin expressed at the cell surface is a marker of endothelial cells in angiogenic blood vessels. *The Journal of Cell Biology, 163*, 871–878.
42. Cieslewicz, M., Tang, J., Yu, J. L., et al. (2013). Targeted delivery of proapoptotic peptides to tumor-associated macrophages improves survival. *Proceedings of the National Academy of Sciences, 110*, 15919–15924.
43. Clackson, T., Hoogenboom, H. R., Griffiths, A. D., & Winter, G. (1991). Making antibody fragments using phage display libraries. *Nature, 352*, 624–628.
44. Curnis, F., Arrigoni, G., Sacchi, A., et al. (2002). Differential binding of drugs containing the NGR motif to CD13 isoforms in tumor vessels, epithelia, and myeloid cells. *Cancer Research, 62*, 867–874.
45. Gerber, D. E. (2008). Targeted therapies: A new generation of cancer treatments. *American Family Physician, 77*, 311–319.
46. Danhier, F. (2016). To exploit the tumor microenvironment: Since the EPR effect fails in the clinic, what is the future of nanomedicine? *Journal of Controlled Release, 244*, 108–121.
47. Daniels, D. A., Chen, H., Hicke, B. J., et al. (2003). A tenascin-C aptamer identified by tumor cell SELEX: Systematic evolution of ligands by exponential enrichment. *Proceedings of the National Academy of Sciences of the United States of America, 100*, 15416–15421.
48. Dawar, S., Singh, N., Kanwar, R. K., et al. (2013). Multifunctional and multitargeted nanoparticles for drug delivery to overcome barriers of drug resistance in human cancers. *Drug Discovery Today, 18*, 1292–1300.
49. Dechantsreiter, M. A., Planker, E., Mathä, B., et al. (1999). N-methylated cyclic RGD peptides as highly active and selective α(v)β3 integrin antagonists. *Journal of Medicinal Chemistry, 42*, 3033–3040.
50. Deng, X., Wang, L., You, X., et al. (2017). Advances in the T7 phage display system (Review). *Molecular Medicine Reports, 17*, 714–720.
51. Desgrosellier, J. S., & Cheresh, D. A. (2010). Integrins in cancer: Biological implications and therapeutic opportunities. *Nature Reviews. Cancer, 10*, 9–22.
52. Destouches, D., El Khoury, D., Hamma-Kourbali, Y., et al. (2008). Suppression of tumor growth and angiogenesis by a specific antagonist of the cell-surface expressed nucleolin. *PLoS One, 3*, e2518.
53. Drecoll, E., Gaertner, F. C., Miederer, M., et al. (2009). Treatment of peritoneal carcinomatosis by targeted delivery of the radio-labeled tumor homing peptide 213Bi-DTPA-[F3]2 into the nucleus of tumor cells. *PLoS One, 4*, e5715.
54. Edwards, D. R., Handsley, M. M., & Pennington, C. J. (2009). The ADAM metalloproteinases. *Molecular Aspects of Medicine, 29*, 258–289.
55. El Khoury, D., Destouches, D., Lengagne, R., et al. (2010). Targeting surface nucleolin with a multivalent pseudopeptide delays development of spontaneous melanoma in RET transgenic mice. *BMC Cancer, 10*, 325.
56. Ellerby, H. M., Arap, W., Ellerby, L. M., et al. (1999). Anti-cancer activity of targeted pro-apoptotic peptides. *Nature Medicine, 5*, 1032–1038.
57. Field, L. D., Delehanty, J. B., Chen, Y., & Medintz, I. L. (2015). Peptides for specifically targeting nanoparticles to cellular organelles: Quo vadis ? *Accounts of Chemical Research, 48*, 1380–1390.
58. Fosgerau, K., & Hoffmann, T. (2015). Peptide therapeutics: Current status and future directions. *Drug Discovery Today, 20*, 122–128.
59. Frantz, C., Stewart, K. M., & Weaver, V. M. (2010a). The extracellular matrix at a glance. *Journal of Cell Science, 123*, 4195–4200.
60. Garde, S. V., Forté, A. J., Ge, M., et al. (2007). Binding and internalization of NGR-peptide-targeted liposomal doxorubicin (TVT-DOX) in CD13-expressing cells and its antitumor effects. *Anti-Cancer Drugs, 18*, 1189–1200.
61. Geretti, E., & Klagsbrun, M. (2007). Neuropilins: Novel targets for anti-angiogenesis therapies. *Cell Adhesion & Migration, 1*, 56–61.
62. Gregorc, V., Gaafar, R. M., Favaretto, A., et al. (2018). NGR-hTNF in combination with best investigator choice in previously treated malignant pleural mesothelioma (NGR015): A randomised, double-blind, placebo-controlled phase 3 trial. *The Lancet Oncology, 19*, 799–811.
63. Gregorc, V., Santoro, A., Bennicelli, E., et al. (2009). Phase Ib study of NGR-hTNF, a selective vascular targeting agent, administered at low doses in combination with doxorubicin to patients with advanced solid tumours. *British Journal of Cancer, 101*, 219–224.
64. Gurunathan, S., Kang, M. H., Qasim, M., & Kim, J. H. (2018). Nanoparticle-mediated combination therapy: Two-in-one approach for cancer. *International Journal of Molecular Sciences, 19*(10), 3264.
65. Guzman-Rojas, L., Rangel, R., Salameh, A., et al. (2012). Cooperative effects of aminopeptidase N (CD13) expressed by nonmalignant and cancer cells within the tumor microenvironment. *Proceedings of the National Academy of Sciences of the United States of America, 109*, 1637–1642.
66. Hambley, T. W. (2009). Is anticancer drug development heading in the right direction? *Cancer Research, 69*, 1259–1261.
67. Han, Z., Zhou, Z., Shi, X., et al. (2015). EDB fibronectin specific peptide for prostate cancer targeting. *Bioconjugate Chemistry, 26*(5), 830–836.
68. Hanahan, D., & Folkman, J. (1996). Patterns and emerging mechanisms of the angiogenic switch during tumorigenesis. *Cell, 86*, 353–364.
69. Hanahan, D., & Weinberg, R. A. (2011). Hallmarks of cancer: The next generation. *Cell, 144*, 646–674.
70. Hanold, L. E., Oruganty, K., Ton, N. T., et al. (2015). Inhibiting EGFR dimerization using triazolyl-bridged dimerization arm mimics. *PLoS One, 10*, e0118796.
71. Harris, L., Batist, G., Belt, R., et al. (2002). Liposome-encapsulated doxorubicin compared with conventional doxorubicin in a randomized multicenter trial as first-line therapy of metastatic breast carcinoma. *Cancer, 94*, 25–36.
72. Heldin, C. H., Rubin, K., Pietras, K., & Östman, A. (2004). High interstitial fluid pressure – An obstacle in cancer therapy. *Nature Reviews. Cancer, 4*, 806–813.
73. Hoffman, J. A., Giraudo, E., Singh, M., et al. (2003). Progressive vascular changes in a transgenic mouse model of squamous cell carcinoma. *Cancer Cell, 4*, 383–391.
74. Hossein-Nejad-Ariani, H., Althagafi, E., & Kaur, K. (2019). Small peptide ligands for targeting EGFR in triple negative breast cancer cells. *Scientific Reports, 9*, 2723.

75. Kaufman, H. L., & Scott Wadler, K. A. (2008). *Molecular targeting in oncology*. Totowa, NJ: Humana Press.
76. Hu, Q., Gu, G., Liu, Z., et al. (2013). F3 peptide-functionalized PEG-PLA nanoparticles co-administrated with tLyp-1 peptide for anti-glioma drug delivery. *Biomaterials, 34*, 1135–1145.
77. Huang, C.-Y., Ju, D.-T., Chang, C.-F., et al. (2017). A review on the effects of current chemotherapy drugs and natural agents in treating non–small cell lung cancer. *Biomedicine, 7*, 23.
78. Hughes, R., Qian, B.-Z., Rowan, C., et al. (2015). Perivascular M2 macrophages stimulate tumor relapse after chemotherapy. *Cancer Research, 75*, 3479–3491.
79. Hung, V., Udeshi, N. D., Lam, S. S., et al. (2016). Spatially resolved proteomic mapping in living cells with the engineered peroxidase APEX2. *Nature Protocols, 11*, 456–475.
80. Hunt, H., Simón-Gracia, L., Tobi, A., et al. (2017). Targeting of p32 in peritoneal carcinomatosis with intraperitoneal linTT1 peptide-guided pro-apoptotic nanoparticles. *Journal of Controlled Release, 260*, 142–153.
81. Hussain, S., Rodriguez-Fernandez, M., Braun, G. B., et al. (2014). Quantity and accessibility for specific targeting of receptors in tumours. *Scientific Reports, 4*, 5232.
82. Ikemoto, H., Lingasamy, P., Willmore, A. M. A., et al. (2017). Hyaluronan-binding peptide for targeting peritoneal carcinomatosis. *Tumor Biology, 39*, 1010428317701628.
83. Ivanenkov, V. V., Felici, F., & Menon, A. G. (1999). Targeted delivery of multivalent phage display vectors into mammalian cells. *Biochimica et Biophysica Acta (BBA)-Molecular Cell Research, 1448*, 463–472.
84. Jain, R. K. (2005). Normalization of tumor vasculature: An emerging concept in antiangiogenic therapy. *Science, 307*, 58–62.
85. Jain, R. K., & Baxter, L. T. (1988). Mechanisms of heterogeneous distribution of monoclonal antibodies and other macromolecules in tumors: Significance of elevated interstitial pressure. *Cancer Research, 48*, 7022–7032.
86. Järveläinen, H. (2009). Extracellular matrix molecules: Potential targets in pharmacotherapy. *Pharmacological Reviews, 61*, 198–223.
87. Järveläinen, H., Sainio, A., Koulu, M., et al. (2009). Extracellular matrix molecules: Potential targets in pharmacotherapy. *Pharmacological Reviews, 61*, 198–223.
88. Jaynes, J. M., Sable, R., Ronzetti, M., et al. (2020). Mannose receptor (CD206) activation in tumor-associated macrophages enhances adaptive and innate antitumor immune responses. *Science Translational Medicine, 12*, eaax6337.
89. Jiang, D., Xu, M., Pei, Y., et al. (2019). Core-matched nanoassemblies for targeted co-delivery of chemotherapy and photosensitizer to treat drug-resistant cancer. *Acta Biomaterialia, 88*, 406–421.
90. Jiang, K., Song, X., Yang, L., et al. (2018). Enhanced antitumor and anti-metastasis efficacy against aggressive breast cancer with a fibronectin-targeting liposomal doxorubicin. *Journal of Controlled Release, 271*, 21–30.
91. Jin, Z.-H., Josserand, V., Razkin, J., et al. (2006). Noninvasive optical imaging of ovarian metastases using Cy5-labeled RAFT-c(-RGDfK-)4. *Molecular Imaging, 5*, 188–197.
92. Johansson, A., Hamzah, J., & Ganss, R. (2014). License for destruction: Tumor-specific cytokine targeting. *Trends in Molecular Medicine, 20*, 16–24.
93. Joyce, J. A., Laakkonen, P., Bernasconi, M., et al. (2003). Stage-specific vascular markers revealed by phage display in a mouse model of pancreatic islet tumorigenesis. *Cancer Cell, 4*, 393–403.
94. Kapoor, P., Singh, H., Gautam, A., et al. (2012). Tumorhope: A database of tumor homing peptides. *PLoS One, 7*, e35187.
95. Karamchand, L., Kim, G., Wang, S., et al. (2013). Modulation of hydrogel nanoparticle intracellular trafficking by multivalent surface engineering with tumor targeting peptide. *Nanoscale, 5*, 10327–10344.
96. Keat, N., Kenny, J., Chen, K., et al. (2018). A microdose PET study of the safety, immunogenicity, biodistribution, and radiation dosimetry of 18 F-FB-A20FMDV2 for imaging the integrin α v β 6. *Journal of Nuclear Medicine Technology, 46*, 136–143.
97. Kim, D. I., Jensen, S. C., Noble, K. A., et al. (2016). An improved smaller biotin ligase for BioID proximity labeling. *Molecular Biology of the Cell, 27*, 1188–1196.
98. Kim, M. Y., Kim, O. R., Choi, Y. S., et al. (2012). Selection and characterization of tenascin C targeting peptide. *Molecules and Cells, 33*, 71–77.
99. Kimura, R. H., Teed, R., Hackel, B. J., et al. (2012). Pharmacokinetically stabilized cystine knot peptides that bind Alpha-v-Beta-6 integrin with single-digit nanomolar affinities for detection of pancreatic cancer. *Clinical Cancer Research, 18*, 839–849.
100. Kirpotin, D. B., Drummond, D. C., Shao, Y., et al. (2006). Antibody targeting of long-circulating lipidic nanoparticles does not increase tumor localization but does increase internalization in animal models. *Cancer Research, 66*, 6732–6740.
101. Koivunen, E., Gay, D. A., & Ruoslahti, E. (1993). Selection of peptides binding to the alpha 5 beta 1 integrin from phage display library. *The Journal of Biological Chemistry, 268*, 20205–20210.
102. Kolvunen, E., Wang, B., & Ruoslahti, E. (1995). Phage libraries displaying cyclic peptides with different ring sizes: Ligand specificities of the rgd-directed integrine. *Bio/Technology, 13*, 265–270.
103. Komoriya, A., Hortsch, M., & Meyers, C. (1984). Biologically active synthetic fragments of epidermal growth factor: Localization of a major receptor-binding region. *Isotopenpraxis, 20*, 1351–1355.
104. Kruger, G., Bandyopadhyay, A., & Gao, J. (2017). Cancer-targeting peptides. In *Advances in the discovery and development of peptide therapeutics* (pp. 70–82). Singapore: Springer International Publishing.
105. Kumra, H., & Reinhardt, D. P. (2016). Fibronectin-targeted drug delivery in cancer. *Advanced Drug Delivery Reviews, 97*, 101–110.
106. Kuncic, Z. (2015a). Cancer nanomedicine: Challenges and opportunities. *Medical Journal of Australia, 203*, 204–205.e1.
107. Laakkonen, P., Akerman, M. E., Biliran, H., et al. (2004a). Antitumor activity of a homing peptide that targets tumor lymphatics and tumor cells. *Proceedings of the National Academy of Sciences, 101*, 9381–9386.
108. Laakkonen, P., Akerman, M. E., Biliran, H., et al. (2004b). Antitumor activity of a homing peptide that targets tumor lymphatics and tumor cells. *Proceedings of the National Academy of Sciences of the United States of America, 101*, 9381.
109. Laakkonen, P., Porkka, K., Hoffman, J. A., & Ruoslahti, E. (2002a). A tumor-homing peptide with a targeting specificity related to lymphatic vessels. *Nature Medicine, 8*, 751–755.
110. Laakkonen, P., Zhang, L., & Ruoslahti, E. (2008). Peptide targeting of tumor lymph vessels. In *Annals of the New York academy of sciences* (Vol. 1131, pp. 37–43). John Wiley & Sons, Ltd (10.1111).
111. Lambert, J. M., & Morris, C. Q. (2017). Antibody–drug conjugates (ADCs) for personalized treatment of solid tumors: A review. *Advances in Therapy, 34*(5), 1015–1035.
112. Larocca, D., Kassner, P. D., Witte, A., et al. (1999). Gene transfer to mammalian cells using genetically targeted filamentous bacteriophage. *The FASEB Journal, 13*, 727–734.
113. Lau, J. L., & Dunn, M. K. (2018). Therapeutic peptides: Historical perspectives, current development trends, and future directions. *Bioorganic & Medicinal Chemistry, 26*, 2700–2707.
114. Le Joncour, V., & Laakkonen, P. (2018). Seek & Destroy, use of targeting peptides for cancer detection and drug delivery. *Bioorganic & Medicinal Chemistry, 26*, 2797–2806.

115. Lingasamy, P., Tobi, A., Haugas, M., et al. (2019). Bi-specific tenascin-C and fibronectin targeted peptide for solid tumor delivery. *Biomaterials, 219*, 119373.
116. Liu, N., Lapcevich, R. K., Underhill, C. B., et al. (2001). Metastatin: A hyaluronan-binding complex from cartilage that inhibits tumor growth. *Cancer Research, 61*, 1022–1028.
117. Liu, R., Li, X., Xiao, W., & Lam, K. S. (2017). Tumor-targeting peptides from combinatorial libraries. *Advanced Drug Delivery Reviews, 110–111*, 13–37.
118. Lorusso, D., Scambia, G., Amadio, G., et al. (2012). Phase II study of NGR-hTNF in combination with doxorubicin in relapsed ovarian cancer patients. *British Journal of Cancer, 107*, 37–42.
119. Lu, L., Qi, H., Zhu, J., et al. (2017). Vascular-homing peptides for cancer therapy. *Biomedicine & Pharmacotherapy, 92*, 187–195.
120. Maeda, H. (2010). Tumor-selective delivery of macromolecular drugs via the EPR effect: Background and future prospects. *Bioconjugate Chemistry, 21*(5), 797–802.
121. Maeda, H. (2012). Macromolecular therapeutics in cancer treatment: The EPR effect and beyond. *Journal of Controlled Release, 164*, 138–144.
122. Maeda, H., Nakamura, H., & Fang, J. (2013). The EPR effect for macromolecular drug delivery to solid tumors: Improvement of tumor uptake, lowering of systemic toxicity, and distinct tumor imaging in vivo. *Advanced Drug Delivery Reviews, 65*, 71–79.
123. Maeda, H., Wu, J., Sawa, T., et al. (2000). Tumor vascular permeability and the EPR effect in macromolecular therapeutics: A review. *Journal of Controlled Release, 65*, 271–284.
124. Mahmood, N., Mihalcioiu, C., & Rabbani, S. A. (2018). Multifaceted role of the urokinase-type plasminogen activator (uPA) and its receptor (uPAR): Diagnostic, prognostic, and therapeutic applications. *Frontiers in Oncology, 8*, 24.
125. Marelli, U. K., Rechenmacher, F., Sobahi, T. R. A., et al. (2013). Tumor targeting via integrin ligands. *Frontiers in Oncology, 3*, 222.
126. Matochko, W. L., & Derda, R. (2015). Next-generation sequencing of phage-displayed peptide libraries. *Methods in Molecular Biology, 1248*, 249–266.
127. McFedries, A., Schwaid, A., & Saghatelian, A. (2013). Methods for the elucidation of protein-small molecule interactions. *Chemistry & Biology, 20*, 667–673.
128. Miao, H. Q., & Klagsbrun, M. (2000). Neuropilin is a mediator of angiogenesis. *Cancer Metastasis Reviews, 19*, 29–37.
129. Mitri, Z., Constantine, T., & O'Regan, R. (2012). The HER2 receptor in breast Cancer: Pathophysiology, clinical use, and new advances in therapy. *Chemotherapy Research and Practice, 2012*, 1–7.
130. Nagy, J. A., Chang, S. H., Dvorak, A. M., & Dvorak, H. F. (2009). Why are tumour blood vessels abnormal and why is it important to know? *British Journal of Cancer, 100*, 865–869.
131. Neri, D., & Bicknell, R. (2005). Tumour vascular targeting. *Nature Reviews. Cancer, 5*, 436–446.
132. Nilsson, F., Kosmehl, H., Zardi, L., & Neri, D. (2001). Targeted delivery of tissue factor to the ED-B domain of fibronectin, a marker of angiogenesis, mediates the infarction of solid tumors in mice. *Cancer Research, 61*, 711–716.
133. Nishida, N., Yano, H., Nishida, T., et al. (2006). Angiogenesis in cancer. *Vascular Health and Risk Management, 2*, 213–219.
134. Nisole, S., Krust, B., Callebaut, C., et al. (1999). The anti-HIV pseudopeptide HB-19 forms a complex with the cell-surface-expressed nucleolin independent of heparan sulfate proteoglycans. *The Journal of Biological Chemistry, 274*, 27875–27884.
135. Nolan, D. J., Ginsberg, M., Israely, E., et al. (2013). Molecular signatures of tissue-specific microvascular endothelial cell heterogeneity in organ maintenance and regeneration. *Developmental Cell, 26*, 204–219.
136. Noy, R., & Pollard, J. W. (2014). Tumor-associated macrophages: From mechanisms to therapy. *Immunity, 41*, 49–61.
137. Paasonen, L., Sharma, S., Braun, G. B., et al. (2016). New p32/gC1qR ligands for targeted tumor drug delivery. *Chembiochem, 17*, 570–575.
138. Pagé, M. (2002). *Tumor targeting in cancer therapy*. Totowa: Humana Press.
139. Pang, H.-B., Braun, G. B., Friman, T., et al. (2014). An endocytosis pathway initiated through neuropilin-1 and regulated by nutrient availability. *Nature Communications, 5*, 4904.
140. Park, J., Kim, S., Saw, P. E., et al. (2012). Fibronectin extra domain B-specific aptide conjugated nanoparticles for targeted cancer imaging. *Journal of Controlled Release, 163*, 111–118.
141. Park, J. W., Hong, K., Kirpotin, D. B., et al. (2002). Anti-HER2 immunoliposomes: Enhanced efficacy attributable to targeted delivery. *Clinical Cancer Research, 8*, 1172–1181.
142. Pasqualini, R., Koivunen, E., Kain, R., et al. (2000). Aminopeptidase N is a receptor for tumor-homing peptides and a target for inhibiting angiogenesis. *Cancer Research, 60*, 722–727.
143. Pasqualini, R., & Ruoslahti, E. (1996). Organ targeting in vivo using phage display peptide libraries. *Nature, 380*, 364–366.
144. Pastorino, F., Brignole, C., Di Paolo, D., et al. (2006). Targeting liposomal chemotherapy via both tumor cell-specific and tumor vasculature-specific ligands potentiates therapeutic efficacy. *Cancer Research, 66*, 10073–10082.
145. Pastorino, F., Brignole, C., Marimpietri, D., et al. (2003). Vascular damage and anti-angiogenic effects of tumor vessel-targeted liposomal chemotherapy. *Cancer Research, 63*, 7400–7409.
146. Penchala, S. C., Miller, M. R., Pal, A., et al. (2015). A biomimetic approach for enhancing the in vivo half-life of peptides. *Nature Chemical Biology, 11*, 793–798.
147. Persson, B. E., Kold Olesen, T., & Jensen, J. K. (2009). Degarelix: A new approach for the treatment of prostate cancer. *Neuroendocrinology, 90*, 235–244.
148. Pierschbacher, M. D., & Ruoslahti, E. (1984). Cell attachment activity of fibronectin can be duplicated by small synthetic fragments of the molecule. *Nature, 309*, 30–33.
149. Pierschbacher, M. D., Ruoslahti, E., Sundelin, J., et al. (1982). The cell attachment domain of fibronectin. Determination of the primary structure. *Journal of Biological Chemistry, 257*, 9593–9597.
150. Pilch, J., Brown, D. M., Komatsu, M., et al. (2006). Peptides selected for binding to clotted plasma accumulate in tumor stroma and wounds. *Proceedings of the National Academy of Sciences of the United States of America, 103*, 2800–2804.
151. Pollard, J. W. (2004). Tumour-educated macrophages promote tumour progression and metastasis. *Nature Reviews. Cancer, 4*, 71–78.
152. Porkka, K., Laakkonen, P., Hoffman, J. A., et al. (2002). A fragment of the HMGN2 protein homes to the nuclei of tumor cells and tumor endothelial cells in vivo. *Proceedings of the National Academy of Sciences, 99*, 7444–7449.
153. Prabhakar, U., Maeda, H., Jain, R. K., et al. (2013). Challenges and key considerations of the enhanced permeability and retention effect for nanomedicine drug delivery in oncology. *Cancer Research, 73*, 2412–2417.
154. Prickett, W. M., Van Rite, B. D., Resasco, D. E., & Harrison, R. G. (2011). Vascular targeted single-walled carbon nanotubes for near-infrared light therapy of cancer. *Nanotechnology, 22*, 455101.
155. Pytela, R., Pierschbacher, M. D., Ginsberg, M. H., et al. (1986). Platelet membrane glycoprotein IIb/IIIa: Member of a family of Arg-Gly-Asp-specific adhesion receptors. *Science, 231*, 1559–1562.
156. Pytela, R., Pierschbacher, M. D., & Ruoslahti, E. (1985). Identification and isolation of a 140 kd cell surface glycoprotein with properties expected of a fibronectin receptor. *Cell, 40*, 191–198.
157. Qin, M., Zong, H., & Kopelman, R. (2014). Click conjugation of peptide to hydrogel nanoparticles for tumor-targeted drug delivery. *Biomacromolecules, 15*, 3728–3734.

158. Rajabi, M., & Mousa, S. (2017). The role of angiogenesis in cancer treatment. *Biomedicine, 5*, 34.
159. Ramsay, R. R., Popovic-Nikolic, M. R., Nikolic, K., et al. (2018). A perspective on multi-target drug discovery and design for complex diseases. *Clinical and Translational Medicine, 7*(1), 3.
160. Raucher, D. (2019). Tumor targeting peptides: Novel therapeutic strategies in glioblastoma. *Current Opinion in Pharmacology, 47*, 14–19.
161. Rosenblum, D., Joshi, N., Tao, W., et al. (2018a). Progress and challenges towards targeted delivery of cancer therapeutics. *Nature Communications, 9*, 1–12.
162. Rosenblum, D., Joshi, N., Tao, W., et al. (2018b). Progress and challenges towards targeted delivery of cancer therapeutics. *Nature Communications, 9*, 1410.
163. Roth, L., Agemy, L., Kotamraju, V. R., et al. (2012). Transtumoral targeting enabled by a novel neuropilin-binding peptide. *Oncogene, 31*, 3754–3763.
164. Ruoslahti, E. (2004). Vascular zip codes in angiogenesis and metastasis. *Biochemical Society Transactions, 32*, 397–402.
165. Ruoslahti, E. (2012). Peptides as targeting elements and tissue penetration devices for nanoparticles. *Advanced Materials, 24*, 3747–3756.
166. Ruoslahti, E. (2000). Targeting tumor vasculature with homing peptides from phage display. *Cancer Biology, 10*, 435–442.
167. Ruoslahti, E. (2017). Tumor penetrating peptides for improved drug delivery. *Advanced Drug Delivery Reviews, 110–111*, 3–12.
168. Ruoslahti, E. (2002). Specialization of tumour vasculature. *Nature Reviews. Cancer, 2*, 83–90.
169. Ruoslahti, E., Bhatia, S. N., & Sailor, M. J. (2010). Targeting of drugs and nanoparticles to tumors. *The Journal of Cell Biology, 188*, 759–768.
170. Ruoslahti, E., & Pierschbacher, M. D. (1987). New perspectives in cell adhesion: RGD and integrins. *Science, 238*, 491–497.
171. Ryan, J. M., Wasser, J. S., Adler, A. J., & Vella, A. T. (2016). Enhancing the safety of antibody-based immunomodulatory cancer therapy without compromising therapeutic benefit: Can we have our cake and eat it too? *Expert Opinion on Biological Therapy, 16*, 655–674.
172. Ebbinghaus, S., Hussain, M., Tannir, N., Gordon, M., et al. (2007). Phase 2 study of ABT-510 in patients with previously untreated advanced renal cell carcinoma. In *Clinical cancer research* (pp. 6689–6695). Philadelphia: American Association for Cancer Research.
173. Säälik, P., Lingasamy, P., Toome, K., et al. (2019). Peptide-guided nanoparticles for glioblastoma targeting. *Journal of Controlled Release, 308*, 109–118.
174. Sawa-Wejksza, K., & Kandefer-Szerszeń, M. (2018). Tumor-associated macrophages as target for antitumor therapy. *Archivum Immunologiae et Therapiae Experimentalis (Warsz), 66*, 97–111.
175. Scodeller, P., Simón-Gracia, L., Kopanchuk, S., et al. (2017). Precision targeting of tumor macrophages with a CD206 binding peptide. *Scientific Reports, 7*, 14655.
176. Sharkey, R. M., & Goldenberg, D. M. (2005). Perspectives on cancer therapy with radiolabeled monoclonal antibodies. *Journal of Nuclear Medicine, 46*(Suppl 1), 115S–127S.
177. Sharma, R., Kallur, K. G., Ryu, J. S., et al. (2015). Multicenter reproducibility of 18F-Fluciclatide PET imaging in subjects with solid tumors. *Journal of Nuclear Medicine, 56*, 1855–1861.
178. Sharma, S., Kotamraju, V. R., Mölder, T., et al. (2017). Tumor-penetrating nanosystem strongly suppresses breast tumor growth. *Nano Letters, 17*, 1356–1364.
179. Shi, Q., Zhang, Y., Liu, S., et al. (2018). Specific tissue factor delivery using a tumor-homing peptide for inducing tumor infarction. *Biochemical Pharmacology, 156*, 501–510.
180. Silacci, M., Brack, S. S., Späth, N., et al. (2006). Human monoclonal antibodies to domain C of tenascin-C selectively target solid tumors in vivo. *Protein Engineering, Design & Selection, 19*, 471–478.
181. Simberg, D., Duza, T., Park, J. H., et al. (2007). Biomimetic amplification of nanoparticle homing to tumors. *Proceedings of the National Academy of Sciences of the United States of America, 104*, 932–936.
182. Simón-Gracia, L., Hunt, H., & Teesalu, T. (2018). Peritoneal carcinomatosis targeting with tumor homing peptides. *Molecules, 23*(5), 1190.
183. Smith, G. P. (1985). Filamentous fusion phage: Novel expression vectors that display cloned antigens on the virion surface. *Science, 228*, 1315–1317.
184. Song, S., Liu, D., Peng, J., et al. (2009). Novel peptide ligand directs liposomes toward EGF-R high-expressing cancer cells in vitro and in vivo. *The FASEB Journal, 23*, 1396–1404.
185. Song, Y., Huang, Z., Xu, J., et al. (2014). Multimodal SPION-CREKA peptide based agents for molecular imaging of microthrombus in a rat myocardial ischemia-reperfusion model. *Biomaterials, 35*, 2961–2970.
186. Spenlé, C., Saupe, F., Midwood, K., et al. (2015). Tenascin-C: Exploitation and collateral damage in cancer management. *Cell Adhesion & Migration, 9*, 141–153.
187. Spicer, C. D., Jumeaux, C., Gupta, B., & Stevens, M. M. (2018). Peptide and protein nanoparticle conjugates: Versatile platforms for biomedical applications. *Chemical Society Reviews, 47*, 3574–3620.
188. Sugahara, K. N., Teesalu, T., Karmali, P. P., et al. (2009). Tissue-penetrating delivery of compounds and nanoparticles into tumors. *Cancer Cell, 16*, 510–520.
189. Sugahara, K. N., Teesalu, T., Karmali, P. P., et al. (2010). Coadministration of a tumor-penetrating peptide enhances the efficacy of cancer drugs. *Science, 328*, 1031–1035.
190. Sun, X., Li, Y., Liu, T., et al. (2017). Peptide-based imaging agents for cancer detection. *Advanced Drug Delivery Reviews, 110–111*, 38–51.
191. Tajrishi, M. M., Tuteja, R., & Tuteja, N. (2011). Nucleolin: The most abundant multifunctional phosphoprotein of nucleolus. *Communicative & Integrative Biology, 4*, 267–275.
192. Teesalu, T., Sugahara, K. N., Kotamraju, V. R., & Ruoslahti, E. (2009). C-end rule peptides mediate neuropilin-1-dependent cell, vascular, and tissue penetration. *Proceedings of the National Academy of Sciences of the United States of America, 106*, 16157–16162.
193. Teesalu, T., Sugahara, K. N., & Ruoslahti, E. (2013). Tumor-penetrating peptides. *Frontiers in Oncology, 3*, 216.
194. Teesalu, T., Sugahara, K. N., & Ruoslahti, E. (2012). Mapping of vascular ZIP codes by phage display. *Methods in Enzymology, 503*, 35–56.
195. Tetz, G., & Tetz, V. (2018). Bacteriophages as new human viral pathogens. *Microorganisms, 6*, 54.
196. Tong, R., & Langer, R. (2015). Nanomedicines targeting the tumor microenvironment. *The Cancer Journal, 21*, 314–321.
197. Usmani, S. S., Bedi, G., Samuel, J. S., et al. (2017). THPdb: Database of FDA-approved peptide and protein therapeutics. *PLoS One, 12*, e0181748.
198. Valetti, S., Maione, F., Mura, S., et al. (2014). Peptide-functionalized nanoparticles for selective targeting of pancreatic tumor. *Journal of Controlled Release, 192*, 29–39.
199. Ventola, C. L. (2017). Progress in nanomedicine: Approved and investigational nanodrugs. *Pharmacy and Therapeutics, 42*, 742–755.
200. Vrettos, E. I., Mező, G., & Tzakos, A. G. (2018). On the design principles of peptide–drug conjugates for targeted drug delivery to the malignant tumor site. *Beilstein Journal of Organic Chemistry, 14*, 930–954.
201. Wan, X. M., Chen, Y. P., Xu, W. R., et al. (2009). Identification of nose-to-brain homing peptide through phage display. *Peptides, 30*, 343–350.
202. Weber, W. A. (2009). Assessing tumor response to therapy. *Journal of Nuclear Medicine, 50*, 1S–10S.

203. Werle, M., & Bernkop-Schnürch, A. (2006). Strategies to improve plasma half life time of peptide and protein drugs. *Amino Acids, 30*, 351–367.
204. Wickström, M., Larsson, R., Nygren, P., & Gullbo, J. (2011). Aminopeptidase N (CD13) as a target for cancer chemotherapy. *Cancer Science, 102*, 501–508.
205. Wyckoff, J., Wang, W., Lin, E. Y., et al. (2004). A paracrine loop between tumor cells and macrophages is required for tumor cell migration in mammary tumors. *Cancer Research, 64*, 7022–7029.
206. Yan, J., He, W., Yan, S., et al. (2018). Self-assembled peptide-lanthanide nanoclusters for safe tumor therapy: Overcoming and utilizing biological barriers to peptide drug delivery. *ACS Nano, 12*, 2017–2026.
207. Yan, L., Rosen, N., & Arteaga, C. (2011). Targeted cancer therapies. *Chinese Journal of Cancer, 30*, 1–4.
208. Ye, F., Wu, X., Jeong, E.-K., et al. (2008). A peptide targeted contrast agent specific to fibrin-fibronectin complexes for cancer molecular imaging with MRI. *Bioconjugate Chemistry, 19*, 2300–2303.
209. Yin, H., Zhang, Q., Yang, J., et al. (2017). IRGD as a tumor-penetrating peptide for cancer therapy (Review). *Molecular Medicine Reports, 15*, 2925–2930.
210. Yoo, J., Park, C., Yi, G., et al. (2019). Active targeting strategies using biological ligands for nanoparticle drug delivery systems. *Cancers (Basel), 11*(5), 640.
211. Yu, J., Sun, L., Zhou, J., et al. (2017). Self-assembled tumor-penetrating peptide-modified poly(l-γ-glutamylglutamine)-paclitaxel nanoparticles based on hydrophobic interaction for the treatment of glioblastoma. *Bioconjugate Chemistry, 28*, 2823–2831.
212. Zhang, B., Shen, S., Liao, Z., et al. (2014). Targeting fibronectins of glioma extracellular matrix by CLT1 peptide-conjugated nanoparticles. *Biomaterials, 35*, 4088–4098.
213. Zhang, J., Niu, G., Lang, L., et al. (2017a). Clinical translation of a dual integrin αvβ3- and gastrin-releasing peptide receptor-targeting PET radiotracer, 68Ga-BBN-RGD. *Journal of Nuclear Medicine, 58*, 228–234.
214. Zhang, Y., Sun, T., & Jiang, C. (2018). Biomacromolecules as carriers in drug delivery and tissue engineering. *Acta Pharmaceutica Sinica B, 8*, 34–50.
215. Zhang, Y., Wei, J., Liu, S., et al. (2017b). Inhibition of platelet function using liposomal nanoparticles blocks tumor metastasis. *Theranostics, 7*, 1062–1071.
216. Zhang, Y., Yang, M., Park, J. H., et al. (2009). A surface-charge study on cellular-uptake behavior of F3- peptide-conjugated iron oxide nanoparticles. *Small, 5*, 1990–1996.
217. Zhao, N., Qin, Y., Liu, H., & Cheng, Z. (2018). Tumor-targeting peptides: Ligands for molecular imaging and therapy. *Anti-Cancer Agents in Medicinal Chemistry, 18*, 74–86.
218. Zhong, Y., Zhang, Y., Xu, J., et al. (2019). Low-intensity focused ultrasound-responsive phase-transitional nanoparticles for thrombolysis without vascular damage: A synergistic nonpharmaceutical strategy. *ACS Nano, 13*, 3387–3403.
219. Zhou, J. E., Yu, J., Gao, L., et al. (2017). iNGR-modified liposomes for tumor vascular targeting and tumor tissue penetrating delivery in the treatment of glioblastoma. *Molecular Pharmaceutics, 14*, 1811–1820.
220. Zuo, H. (2019). IRGD: A promising peptide for cancer imaging and a potential therapeutic agent for various cancers. *Journal of Oncology, 2019*, 9367845.

Radiolabeling of Theranostic Nanosystems

Sudeep Das, Surachet Imlimthan, Anu J. Airaksinen, and Mirkka Sarparanta

Abstract

In the recent years, progress in nanotechnology has significantly contributed to the development of novel pharmaceutical formulations to overcome the drawbacks of conventional treatments and improve the therapeutic outcome in many diseases, especially cancer. Nanoparticle vectors have demonstrated the potential to concomitantly deliver diagnostic and therapeutic payloads to diseased tissue. Due to their special physical and chemical properties, the characteristics and function of nanoparticles are tunable based on biological molecular targets and specific desired features (e.g., surface chemistry and diagnostic radioisotope labeling). Within the past decade, several theranostic nanoparticles have been developed as a multifunctional nanosystems which combine the diagnostic and therapeutic functionalities into a single drug delivery platform. Theranostic nanosystems can provide useful information on a real-time systemic distribution of the developed nanosystem and simultaneously transport the therapeutic payload. In general, the diagnostic functionality of theranostic nanoparticles can be achieved through labeling gamma-emitted radioactive isotopes on the surface of nanoparticles which facilitates noninvasive detection using nuclear molecular imaging techniques, such as positron emission tomography (PET) and single-photon emission computed tomography (SPECT), meanwhile, the therapeutic effect arises from the potent drug released from the nanoparticle. Moreover, some radioisotopes can concurrently emit both gamma radiation and high-energy particles (e.g., alpha, beta, and Auger electrons), prompting the use either alone for radiotheranostics or synergistically with chemotherapy. This chapter provides an overview of the fundamentals of radiochemistry and relevant radiolabeling strategies for theranostic nanosystem development as well as the methods for the preclinical evaluation of radiolabeled nanoparticles. Furthermore, preclinical case studies of recently developed theranostic nanosystems will be highlighted.

Keywords

Radiochemistry · Radiolabeling · Nuclear imaging
Molecular imaging · Theranostic nanosystem
Nanotheranostic

1 Introduction

The term *theranostic* coined by the merging of the terms “therapeutic” and “diagnostic,” refers to multifunctional nanosystems that are able to provide both therapeutic (e.g., delivery of a chemotherapeutic payload) and diagnostic (e.g., imaging or therapy monitoring) functions in the same platform. Radioisotopes can be employed in two ways for the development of theranostic nanosystems. First, the nanosystems can be radiolabeled with imaging-compliant isotopes such as those utilized for positron emission tomography (PET) or single-photon emission computed tomography (SPECT), which emit gamma radiation that can be detected and quantified noninvasively outside of the subject using dedicated imaging systems [1]. This will give information on the localization of the nanosystem in the body, including the targeting ability, kinetics of nanomaterial tumor accumulation, the route and rate of nanosystem elimination, and the circulation time. This information provides vital feedback on

S. Das · S. Imlimthan · M. Sarparanta (✉)
Department of Chemistry, University of Helsinki,
Helsinki, Finland
e-mail: mirkka.sarparanta@helsinki.fi

A. J. Airaksinen
Department of Chemistry, University of Helsinki,
Helsinki, Finland

Turku PET Centre, Department of Chemistry, University of Turku,
Turku, Finland

© Springer Nature Switzerland AG 2021

F. Fontana, H. A. Santos (eds.), *Bio-Nanomedicine for Cancer Therapy*, Advances in Experimental Medicine and Biology 1295, https://doi.org/10.1007/978-3-030-58174-9_3

the performance of the nanosystem based on its structure–activity relationship, and guides future structural optimization for improved in vivo behavior. Additionally, when radiolabeled with diagnostic radioisotopes, the nanosystems can be used to screen for patients who will have sufficiently high nanosystem tumor accumulation to permit the attainment of therapeutically relevant payload concentrations in the tumor. In this way, the nanosystem itself can be used for patient stratification instead of a surrogate imaging biomarker. Second, the highly energetic particle radiation (α, β^-, and Auger electrons), arising from radioactive decay of radioisotopes conjugated to the nanosystem, can be employed as a therapeutic strategy either alone or synergistically with chemotherapy [2]. Due to their high molar activity, therapeutic radioisotopes are lucrative payloads for theranostic nanosystem development, as very small amounts of the radioisotope are often enough to impart therapeutically relevant radioactive doses at the tumor. This is in contrast to the feasibility limitations set by a limited drug loading degree in many cancer-targeting nanosystems under development today.

In this chapter, we will give an overview of the current and emerging radiolabeling strategies for the radiolabeling of theranostic nanosystems either for imaging, radiotherapy, or combination of the two, as well as provide a basic outline for the biological evaluation of radiolabeled theranostic nanosystems. Finally, a review of selected contemporary examples of preclinical and clinical studies utilizing radiolabeled theranostic nanosystems is given.

2 Key Concepts in Radiochemistry for Theranostic Nanosystem Development

2.1 Radioactive Decay and Properties of Radiolabeled Tracers

Radioactive decay results when a nucleus has too much mass or an improper proton-to-neutron ratio to remain stable: the nucleus becomes unstable and either emits a bulky particle to reduce its mass (α decay) or transfers one proton to a neutron or neutron to a proton to balance the proton-to-neutron ratio (β^+ or electron capture decay or β^- decay). In α decay, an energetic α particle (a nucleus of a helium atom) is emitted, whereas in a beta decay the outcoming particles are either β^+ (positron) or β^- (electron). In addition to these decays a number of different types of electromagnetic (gamma radiation, X-rays) and electron (conversion and Auger electrons) radiation is emitted while the nuclei formed in excited state in the decay event will de-excite. All these modes of radiation are collectively known as *ionizing radiation.* A stable nucleus can be attained either by a single decay of an unstable nucleus (as for the isotope fluorine-18 (^{18}F in Fig. 1a) or as a result of a decay chain, where the energy is lost in a series of decays through different daughter nuclei like in the case of the alpha emitter actinium-225 (^{225}Ac, Fig. 1b).

The fundamental premise to the use of radiolabeled compounds as *tracers* for the respective nonradiolabeled compounds is that radioactive isotopes behave chemically identically to the nonradioactive isotopes of the same element. The terms tracer, *imaging probe*, and *imaging agent* are used interchangeably in the literature and all refer to radiolabeled compounds used to track a structurally identical nonradiolabeled compound in vivo.

The most important properties of a radioisotope from the theranostic standpoint are the quality and energy of the emitted radiation, the physical half-life ($t_{1/2}$) of the radioisotope, and the chemical characteristics of the element in question. Highly tissue-penetrant gamma radiation is needed for noninvasive nuclear imaging, whereas particle radiation is needed for the deposition of energy into the tumor tissue through the interactions between the tissue and the emitted charged particles. The amount of energy deposited in tissue is determined by the linear energy transfer (LET) value, and it is determined by the path length of the particle in the tissue and the energy of the radiation. Out of the charged particles, helium nuclei (α particles) and Auger electrons have the highest LET values with the path length tens of micrometers (α particles) or mere fractions of a micrometer (Auger electrons), while higher-energy electrons (β particles and conversion electrons) travel millimeters depending on their energy, and consequently have lower LET values as illustrated with an example of radioimmunoconjugates in Fig. 2. The range of the particle radiation in tissue should be matched to the dimensions of the tumor to ensure homogenous deposition of the energy in the tumor tissue as illustrated in Fig. 3.

The radionuclide half-life is determined by Eq. 1,

$$t_{1/2} = \frac{\ln 2}{\lambda} \tag{1}$$

where λ is the decay constant for the radioisotope. The half-life tells us the amount of time required for the radioactivity (A) of the material to decrease to one half of the original value (A_0) and can be used to calculate the amount of radioactivity remaining in a sample at a given time t as shown in Eq. 2.

$$A = A_0 e^{-\lambda t} = A_0 \times 2^{-t/t_{1/2}} \tag{2}$$

The physical half-lives of radioactive isotopes vary from fractions of a second to billions of years. For isotopes relevant for the development and radiolabeling of theranostic nanosystems, the half-lives are most typically in the order of hours to several days. This has a number of practical implications to the nanosystem development and choice of the radio-

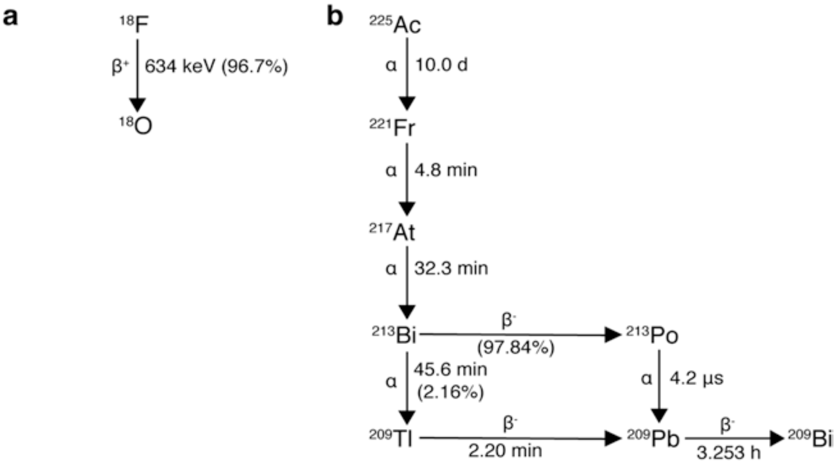
a
^{18}F
β+
634 keV (96.7%)
^{18}O
b
^{225}Ac
α
10.0 d
^{221}Fr
α
4.8 min
^{217}At
α
32.3 min
^{213}Bi
β-
(97.84%)
^{213}Po
α
45.6 min
(2.16%)
α
4.2 μs
^{209}Tl
β-
2.20 min
^{209}Pb
β-
3.253 h
^{209}Bi

Fig. 1 Radioactive decay can occur with a single emission or by multiple decays referred to as a "decay chain". The short-lived positron emitter ^{18}F (**a**) decays predominantly by positron emission (the rest is by electron capture), whereas heavy ^{225}Ac (**b**) decays by a series of alpha and beta decays through a number of daughter nuclei

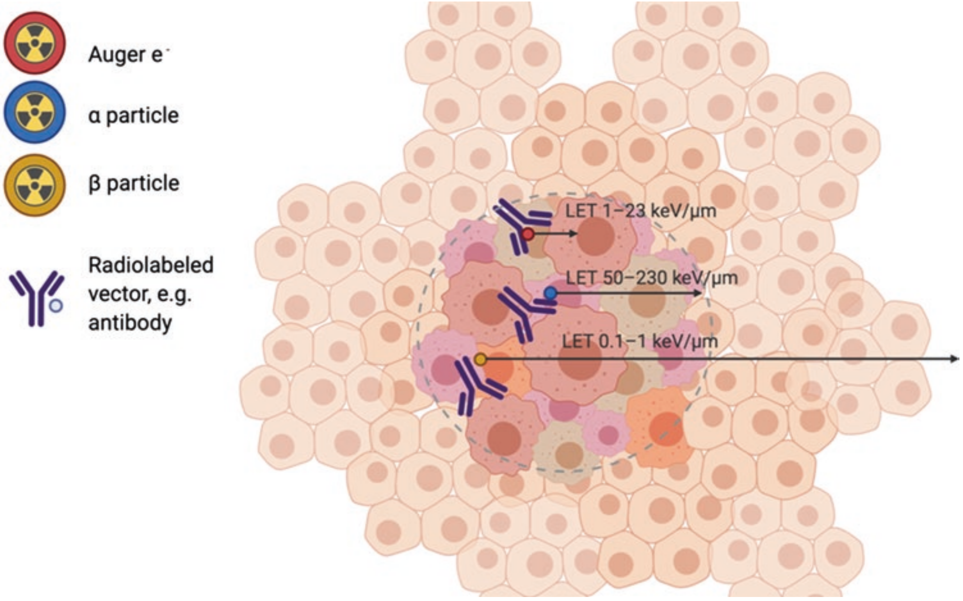
Auger e-
α particle
β particle
Radiolabeled vector, e.g. antibody
LET 1–23 keV/μm
LET 50–230 keV/μm
LET 0.1–1 keV/μm

Fig. 2 Illustration of the track of α-particles, β-particles, and Auger electrons emitted by radiolabeled monoclonal antibodies targeted to cancer cells. The short track length of α-particles (28–100 μm) and Auger electrons (<0.5 μm) results in high linear energy transfer (LET) values of 50–230 keV/μm and 1–23 keV/μm, respectively. β-Particles have a track length of 2–10 mm in tissue resulting in LET of 0.1–1.0 keV/μm. The high LET of α-particles and Auger electrons makes these forms of radiation more powerful for killing cancer cells than β-particles. (Figure adapted from references [3, 4])

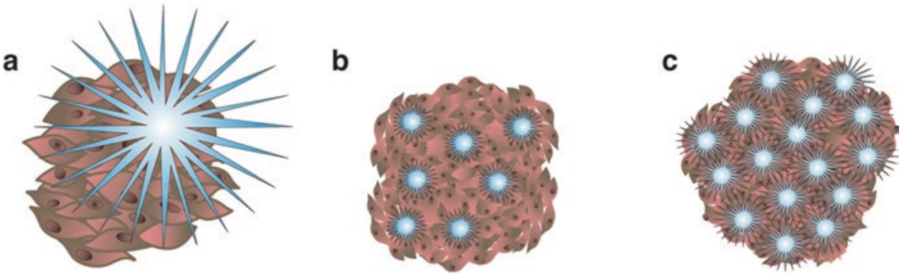

Fig. 3 Matching the range of the radioactive emission to the dimensions of the target is important for the efficacy of the radiotherapy. Subpar effects will be seen in a small tumor treated with long-range (low LET) irradiation (**a**) or in a large mass treated with a short-range (high LET) irradiation with heterogenous distribution (**b**), whereas optimal results are achieved when a relatively homogenous distribution of an intermediate LET radioisotope is attained (**c**). (Figure adapted from reference [5])

labeling strategy. First, the half-life of the isotope sets a practical limit to the maximum theoretical molar activity, the radioactivity per mole (usually expressed in gigabecquerels per micromole, GBq μmol^{-1}), of the isotope that can be produced as shown in Eq. 3, where N is Avogadro's number.

$$\text{molar activity}_{\text{max}} = N \times \frac{\ln 2}{t_{1/2}} \tag{3}$$

Second, as a guideline, the radiosynthetic procedures and purification of the radiolabeled tracer should be completed within ≈ 2 half-lives of the isotope to ensure meaningful molar activity (radioactivity per amount, usually expressed in gigabecquerels per micromole, GBq μmol^{-1}) of the radiolabeled product for in vivo studies. Therefore, in order to obtain maximal molar activity radiolabels are best introduced late in the radiosynthesis, which is often achieved by the use of a *prosthetic group*, a radiolabeled precursor that can be conjugated to the nonradioactive target molecule or material using fast and selective chemistry preferably in a single step [6]. Third, the half-life of the radioisotope constrains the timeframe over which the passage of the radiolabeled compound can be tracked in vivo. For this purpose, the physical half-life of the radioisotope should be matched to the *biological* half-life of the vector, in this case the nanosystem. This is perhaps best illustrated by the case of radiolabeled antibodies, which have biological half-lifes in the order of days, and consequently only longer-lived isotopes such as zirconium-89 (^{89}Zr, $t_{1/2} = 78.41$ h), indium-111 (^{111}In, $t_{1/2} = 2.80$ d), iodine-124 (^{124}I, $t_{1/2} = 4.18$ d), and iodine-131 (^{131}I, $t_{1/2} = 8.03$ d) can be used for the tracking of directly labeled antibodies. Other important concepts in the radiopharmaceutical development are the molar activity mentioned already earlier, specific activity, radiochemical yield, and radiochemical purity, the definitions of which will be reviewed next. The field of radiopharmaceutical chemistry today follows a consensus nomenclature compiled by Coenen *et al.* and set forward in 2017 [7].

The molar activity of a radiolabeled compound is defined as the amount of radioactivity per mole of compound, whereas *specific activity* refers to the amount of radioactivity per mass, most often denoted in GBq mg^{-1} or MBq mg^{-1}. In most cases the exact molecular weight of the nanosystem is not known or reported, thus the specific activity gives a more meaningful denotation on how much radioactivity is incorporated to the nanosystem. Furthermore, if the final radiolabeled product contains a nonradioactive starting material which cannot be removed, as is the case for most nanomaterials, the terms *apparent molar activity* and *apparent specific activity* should be used. The term *radiochemical yield* refers to the quantity (often expressed in percentage of the starting quantity) of the radioisotope incorporated to the radiolabeled product. Although analogous to chemical yield, an important notion of the radiochemical yield is that it needs to be always calculated using starting and final values for the same radioisotope which have been decay-corrected to the same point in time, typically, for example, the end of synthesis (EOS) or the end of bombardment (EOB) for the nuclear reaction producing the radioisotope. The term *radiochemical purity* in turn is analogous to chemical purity and is used to describe the purity of the product with respect to the presence of other radiolabeled compounds in the final product, again decay-corrected to a fixed point in time. Typically, radiochemical purities exceeding 95% are considered adequate in terms of in vivo applications, but this level depends on the identity and pharmacokinetics of the impurity and more stringent criteria to radiochemical purity might need to be applied accordingly.

2.2 Nuclear Reactions for Radionuclide Production

All the radionuclides used in nuclear medicine are artificially manufactured through nuclear reactions of stable isotopes. The production of radionuclides is commonly carried out using either particle accelerators or nuclear reactors. In radionuclide production, a nucleus of a stable element (the "target") is bombarded with nucleons (protons and neutrons) or other nuclei of stable elements, such as helium and deuterium (the "projectile"). The target and the projectile react, forming a product nucleus. In most cases, the primary product nuclei formed in the reaction are in an excited state and further emit out nucleons, small nuclei, or gamma radiation (the "ejectile") to form the final product nucleus. The nuclear reactions are represented by the notation.

$$x + A \to B + y \,\text{or}\, A\left(x,y\right)B \tag{4}$$

where x is the projectile, A is the target, B is the final product after the reaction, and y is the ejectile. Typical reactions used in the radionuclide production are presented in Fig. 4.

The nuclear reactions require energy enough to bring the positively charged projectile and target in contact over the repulsive Coulomb forces ("Coulomb barrier"). On the other hand, the possibly negative reaction Q value, that is, the difference of the masses before and after the nuclear reaction needs to be compensated by a proper projectile energy for enabling the reaction. These two energies define the minimum projectile energy needed for a nuclear reaction.

The probability for certain nuclear reaction to happen is called cross section. A unit of a cross section is called "barn" (b) and 1 b = 10^{-28} m^2. Therefore, the cross section can be thought as an area that the projectile needs to hit – the larger the area, the more probable the reaction is. Cross section is

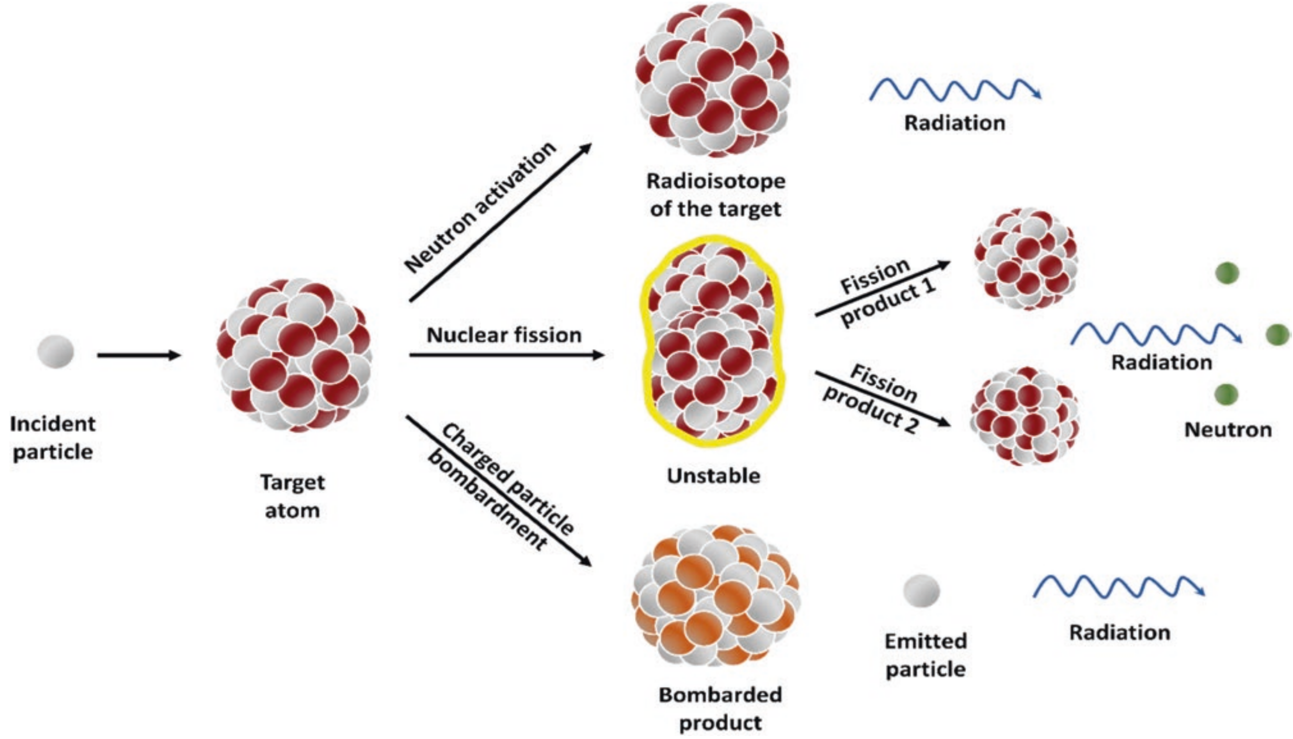

Fig. 4 The most common nuclear reactions in radionuclide production. Neutron activation and nuclear fission are carried out in nuclear reactor while high-energy charged particle bombardment is carried out in accelerators

defined for all the reaction types separately, and it is dependent on the energy of the projectile. Therefore it is important to select an optimal energy for the projectile from the point of view of maximizing the production of the nuclide of interest and minimizing the side reactions leading to impurities. In practice, the target material can be in gaseous, liquid, or solid form. Important things in target design are to ensure a safe manipulation of a highly active target after the irradiation, and to have methods to separate the produced activity from the target material.

Different kinds of charged particles needed for nuclear reactions (e.g., protons, deuterons, and alpha particles) are formed and accelerated in particle accelerators. One most typical of them in radionuclide production is a cyclotron, where the protons are accelerated in the spiraling path. Typical nuclei produced with accelerators are, for example, yttrium-86 (via reaction ^{86}Sr(p,n)^{86}Y), indium-111 (^{112}Cd(p,2n)^{111}In), gallium-67 (^{67}Zn(p,n)^{67}Ga), and fluorine-18 (^{18}O(p,n)^{18}F). For reactions requiring neutrons (e.g., radiative capture (n,γ) and fission), usually pool-type research nuclear reactors are used. In many reactions, especially in radiative capture, thermal neutrons, that is, the neutrons with a speed of about 2000 m/s are utilized. These reactions are used, for example, in production of strontium-89 (^{88}Sr(n,γ)^{89}Sr), technetium-99 (^{98}Mo(n,γ)^{99}Tc), and lutetium-177 (^{176}Lu(n,γ)^{177}Lu). Also (n,p) and (n, α) reactions can be utilised, as well as reactions proceeding through a short-lived intermediate product that decays to the desired radioisotope, such as iodine-131 which is produced via first making tellurium-131 in ^{130}Te(n,γ)^{131}Te reaction, and then letting the ^{131}Te ($t_{1/2}$ = 25 min) to decay by β^- emission to ^{131}I. In nuclear fission reactions (n,fission) neutron splits a heavy nucleus in two pieces with few neutrons emitted in process. Fissions induced by thermal neutrons are resulting in an antisymmetric split with one heavier and one lighter mass nucleus. The commonly used target materials in fission reactions are uranium-235 (^{235}U) and plutonium-239 (^{239}Pu). The most relevant fission products in nuclear medicine are ^{131}I for theranostic applications and ^{99}Mo for the use as radioactive parent in ^{99}Mo/^{99m}Tc generators.

Radioisotope production is globally concentrated on facilities with accelerators and reactors. Smaller medical cyclotrons capable for the production of short-lived positron emitters (^{11}C, ^{13}N, ^{15}O, ^{18}F, ^{89}Zr, ^{124}I) are available at academic institutions and hospitals to account for the use of these isotopes in the clinic and the fact that some of them cannot be transported due to the short half-lives (<2 hours). Additionally, ^{99}Mo/^{99m}Tc and ^{68}Ge/^{68}Ga generators are nowadays nearly ubiquitous in research and hospital laboratories because of their long usable life time which allows the users to dispense the radioisotope on demand. Longer-lived radioisotopes can be purchased through a number of vendors worldwide or acquired through academic collaborations in the case of more rare radioisotopes.

2.3 Principles for the Safe Handling of Radioactive Materials

Working safely with radioactivity requires a number of precautions and specialized working areas which are usually shared between many researchers at a given institute. The type of laboratory and shielding needed and the safe handling practices employed depend on the radioisotope and the amount of radioactivity that needs to be handled at one time. The type of the work also matters as some tasks such as radiotracer administration to animals carry a greater risk of personnel exposure than, for example, the measurement of excised tissue samples in sealed tubes. Safe practices in working with radioactivity need to be followed at every step of the process from the radiolabeling synthesis to biological evaluation to disposal and storage of radioactive waste. The respective national and institutional regulations and guidelines are reviewed during introductory training on radiation safety and the radiation safety officer or department at the institute ensures personnel compliance by offering guidance and continued training. Dose monitoring needs to be offered to personnel working with radioactivity and medical clearance is most often needed prior to starting the work. As a general guideline, the amount of radiation dose accumulated during a procedure can be greatly reduced by using appropriate physical shielding (e.g., a fume hood with a lead-glass window or a remotely controlled synthesis apparatus), by increasing the distance from the radiation source (e.g., by handling radioactive vials with tongs or manipulators), and by minimizing the time spent handling the radioactive source (e.g., by careful planning of the procedure and practicing with mock runs with nonradioactive reagents). Additionally, the benefit gained using radioisotopes should always outweigh the risks associated with their use and the amount of radioactivity used should be kept as low as reasonably possible.

2.4 Radiometric Detection Methods and Nuclear Imaging

The inherent properties of radioactivity contribute to the superior detection sensitivity and ease of quantitation for radiometric methods. First, as most of the radioisotopes employed in radiopharmaceutical development are rare or nonexistent in natural systems as they have been artificially produced in nuclear reactions, there is no “natural” radioactive signal with the same energy spectrum that could hamper the analysis. Naturally abundant radioactive isotopes of elements such as potassium-40 (about 0.012% of natural potassium is ^{40}K) will of course be present in biological samples, but the levels are several orders of magnitude lower to any injected radiotracer and can be excluded from the analysis based on the spectra of the emitted radiation. Second, the aforementioned energy spectra allow for the identification of the desired radionuclide in a mixture of radionuclides and background radiation, enabling the detection of two or more isotopes at the same time if the energies emitted by the isotopes are sufficiently different. Semiconductor gamma spectrometers of superior energy resolution are most often used in these applications. Finally, the number of radioactive disintegrations detected over a given time (*count rate*) is directly proportional to the number of radioactive atoms in the sample which greatly simplifies the quantification.

The quantification of radioactivity is relatively straightforward with radioisotopes emitting highly tissue-penetrant gamma radiation as this can be detected and quantified with minimal sample processing. The radioactivity content in excised tissue samples is, for example, determined simply by measuring the radioactivity in the freshly collected tissue using an automated gamma counter. The commercially available automated counters are the workhorses of both clinical and academic radiochemistry laboratories as they have a large sample handling capacity with automated sample changing, facile operation and robust well-type thallium-doped sodium iodide NaI(Tl) detectors which usually require minimal maintenance over their lifetime. With all radiation detection systems, one needs to take into account the fact that the systems are saturable. This means that the response of the detection system remains linear only over a certain radioactivity range and at activities exceeding this range the response of the detection system deteriorates. The reason for this is the detection system dead time, that is, the time the system remains unresponsive and thus unable to detect the radiation after detection of a radiation event. Care must therefore be taken to maintain the sample activities at the linear range of the detection system. Radioisotopes which do not emit any usable gamma radiation for detection purposes are rare especially in theranostic systems, but if needed, liquid scintillation counting offers a convenient detection method for low-energy β- and α-emitting radioisotopes in biological samples. As the name implies, liquid scintillation counting relies on the detection of the light generated by the absorption of the energy emitted by the radioisotope in the scintillation medium, referred to as a cocktail. The liquid scintillation cocktails are commercially available solutions of solvents capable of absorbing the energy of the emitted radiation and organic scintillator molecules which in turn emit visible light in response to transfer of the energy from the solvent to the scintillator molecule. Unsurprisingly, energy-rich aromatic ring structures and oxazoles compose the backbone for both solvent and scintillator molecules in commercial cocktails. The sample preparation for liquid scintillation counting is slightly more complicated than that for gamma counting, as the homogenized tissue samples need to be solubilized to the solvent and the sample rendered colorless by the addition of, for example, hydrogen peroxide. The sample composition, particularly color and certain compounds, can greatly affect the intensity of the detected light through quenching.

Nuclear imaging refers to the detection of gamma radiation emitted by a radioisotope outside of the living subject and subsequent process of reconstruction of the measured radioactivity distribution to an image. For nuclear imaging in diagnostic purposes, the radioisotope must have gamma emissions, these can either be the two coincident 511-keV annihilation gammas of positron emitters, or single-energy gamma quanta emitted by other isotopes. The former are detected using a technique called positron emission tomography (PET) and the latter by single-photon emission computed tomography (SPECT). The principles of image formation in PET and SPECT imaging are outlined in Fig. 5. Both PET and SPECT are fully translational imaging modalities, meaning that the tracer design, imaging system and setup are the same in small laboratory animals and in the clinic. The instrument design obviously varies as the systems are miniaturized for the imaging of laboratory rodents under inhalation anesthesia, but the detection principle and the study workflow remain the same. Since the molar activity of radiotracers is typically high, they can be administered in doses significantly lower than those used to elicit a pharmacological response. This makes it possible to use expensive and potentially harmful or even toxic substances in vivo without disturbance to the system under study. This *microdosing principle* [8] has made possible the investigational use of radiotracers early on in the drug development pipeline to study the target engagement and elimination of new drugs. For theranostic nanosystems the microdosing principle might not in all cases be directly applicable, as a macrodose of the nanomaterial might be needed for concomitant drug delivery. Nevertheless, the high molar activity of radioisotopes means that they can be used in the radiolabeling reactions in minute amounts and thus with minimal influence on the physicochemical properties of the nanosystem. A caveat in nuclear imaging modalities is the fact that they do not provide any anatomical information on the localization of the tracer except for what can be deduced from the tracer accumulation to nontarget organs and knowledge on their location in the body. Therefore, co-registration of the nuclear image with an image obtained using another imaging modality, for example, X-ray computed tomography (CT) or magnetic resonance imaging (MRI) is often necessary for the precise delineation of the sites of radiotracer accumulation. Conveniently, the large molecular weight of nanomaterials allows for the incorporation of both the radiolabel and a contrast agent for CT or MRI to be incorporated to the same construct, generating a *multimodality* tracer.

3 Radiolabeling Strategies

3.1 Radiometals

Radiometals are radioactive isotopes of metal elements which have become an important tool for radiopharmaceutical drug development in nuclear medicine. Radiometal labels have been employed for a multitude of radiotracers from radiometal-labeled small molecules to peptides, antibodies, and nanoparticles. Radiometal labeling strategies have several advantages over other radiolabeling techniques, for

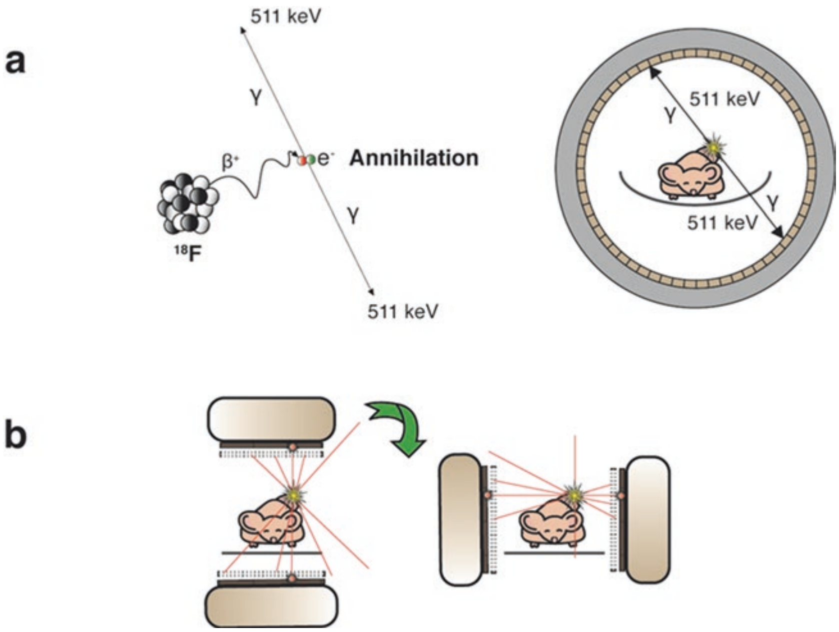

Fig. 5 The principle of detection for positron emission tomography (PET) and single-photon emission computed tomography (SPECT). In PET (**a**), the detectors are arranged on a ring around the subject, and the coincident 511-keV gamma rays from the positron annihilation are detected. In SPECT (**b**), the tomographic image is generated by revolving an array of detectors and a collimator around the subject, and only the gamma quanta which are directly perpendicular to the collimator will pass through to the detectors for registration

example, the easy commercial availability of many radiometals, the pairs of diagnostic and therapeutic radionuclides of the same element, high specific activity, and in often cases favorable radiation dosimetry. The most relevant radiometal isotopes and their properties for SPECT, PET, and theranostics in the clinical and preclinical research have been listed in Table 1.

3.1.1 Chelator-Mediated Radiolabeling with Radiometals

The conjugation of radiometals to radiopharmaceuticals is typically achieved by chelation, the coordination of the radiometal cation by a chelating agent. In order to use the radiometals in biological applications, the radiometal cation must form a stable complex with the chelator to avoid undesirable hydrolysis and transchelation (the displacement of the radiometal by other metal ions in chelator cavity) in vivo. For conjugation to the targeting vector, a number of bifunctional chelating agents (BFCs) have been designed and developed. BFCs generally contain nitrogen (N) and oxygen (O) atoms in their structures that can donate an electron pair to form dative covalent bonds with the metal ions. Moreover, at least one side chain of the BFCs is usually modified with a functional group that can be covalently conjugated to the targeting molecules. The functional groups attached to the carbon backbone of the chelators are preferable due to the availability of all of the N and O atoms for the radiometal coordination, resulting in better stability of metal-chelator complex. A radiometal-labeled radiopharmaceutical consists of three parts: the chelating agent that forms complexes with radiometals, the spacer or linker that is covalently coupled between the chelate and the vector in order to keep the often charged radiometal complex away from the target binding motive, and the biomolecule or targeting vector, such as an antibody, peptide, or nanoparticle (Fig. 6).

Table 1 Overview of radiometals for SPECT, PET, and theranostics

Metal	Radioisotope	Half-life ($t_{1/2}$)	Decay mode	β_{max} MeV (% intensity)	γ keV (% intensity)	Imaging modality	Production method
Scandium (Sc)	^{44}Sc	3.97 h	β^+/EC	1.474 (94.27)	1157 (99.9)	PET	Cyclotron
	^{47}Sc	3.3492 d	β^-	0.600 (31.6)	159.38 (68.3)	SPECT/ theranostic	Cyclotron
Copper (Cu)	^{61}Cu	3.339 h	β^+/EC	1.216 (51)	282.96 (12.2) 656.01 (10.8)	PET	Cyclotron
	^{62}Cu	9.67 m	β^+/EC	2.937 (97.6)	–	PET	Generator
	^{64}Cu	12.701 h	β^+/ β^-/EC	0.653 (17.6)	511 (35.2)	PET/ theranostic	Cyclotron
	^{67}Cu	61.83 h	β^-/γ	0.377 (51)	91.27 (7) 93.31 (16.1) 184.58 (48.7)	SPECT/ theranostic	Cyclotron
Gallium (Ga)	^{66}Ga	9.49 h	β^+/EC	4.153 (51)	833.53 (5.9) 1039.22 (37) 2751.84 (22.7)	PET	Cyclotron
	^{67}Ga	3.262 d	EC/γ	–	93.31 (38.81) 184.58 (21.41) 300.22 (16.64) 393.53 (4.56)	SPECT	Cyclotron
	^{68}Ga	67.71 m	β^+/EC	1.899 (87.72)	–	PET	Generator
Rubidium (Rb)	^{82}Rb	1.258 m	β^+/EC	2.601 (13.13) 3.378 (81.76)	776.52 (15.08)	PET	Generator
Yttrium (Y)	^{86}Y	14.74 h	β^+/EC	1.221 (11.9)	443.13 (16.9)	PET	Cyclotron
	^{90}Y	64 h	β^-	2.280 (99.99)	–	SPECT/ Theranostic	Generator
Zirconium (Zr)	^{89}Zr	78.41 h	β^+/EC	0.902 (22.74)	909.15 (99.04)	PET	Cyclotron
	^{97}Zr	16.749 h	β^-/γ	1.916 (87.8)	743.36 (93.09)	SPECT/ theranostic	Reactor
Technetium (Tc)	^{94m}Tc	52 m	β^+/EC	1.592 (8.9) 1.938 (4.1) 2.438 (67.6) 3.460 (12.8)	871.091 (94)	PET	Cyclotron
	^{99m}Tc	6.01 h	IT	–	140.51 (89)	SPECT	Generator
Indium (In)	^{111}In	2.8047 d	EC/γ	–	171.28 (90.7) 245.35 (94.1)	SPECT	Cyclotron
Lutetium (Lu)	^{177}Lu	6.647 d	β^-/γ	0.177 (11.61) 0.4983 (79.4)	112.95 (6.17) 208.37 (10.36)	SPECT/ theranostic	Reactor

Data retrieved from the NuDat2 database, http://www.nndc.bnl.gov/nudat2

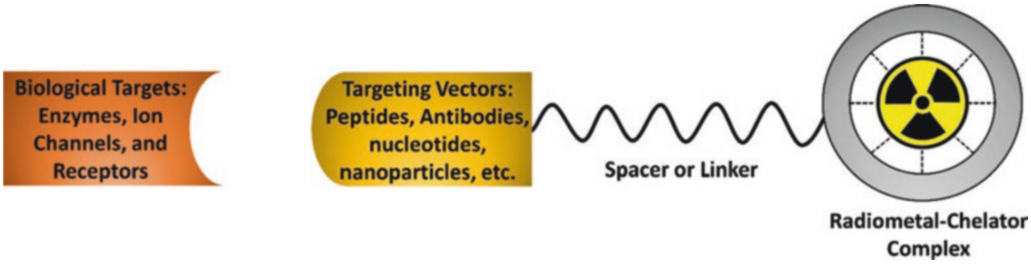
Biological Targets: Enzymes, Ion Channels, and Receptors
Targeting Vectors: Peptides, Antibodies, nucleotides, nanoparticles, etc.
Spacer or Linker
Radiometal-Chelator Complex

Fig. 6 The general design of radiometal-labeled radiopharmaceuticals

The physical and chemical properties of the radiometal-chelator complex affect the overall pharmacokinetic properties of the radiolabeled compounds. Most of the radiometal-chelator complexes are very hydrophilic and have a positive charge leading to rapid clearance from the biological system through renal excretion. Therefore, the chelating agent and the radiometal must be carefully matched to tailor the complex stability and charge. In general, the radiometal-chelator pair is selected based on the chelating agent and radionuclide properties, for example, ionic charge, ionic radius, cavity size in the chelator, the number of donor binding groups, and the rate of metal complex formation and dissociation. Table 2 shows the currently used radiometal chelators and their bifunctional derivatives, and the appropriate radiometal and typical radiolabeling conditions [9]. Since it is preferable to conjugate the chelator to the nanosystem before the radiometal complexation to avoid losses of radioactivity, the radiolabeling condition is as important as other factors mentioned previously as the construct needs to withstand the radiolabeling conditions. Room temperature and neutral pH conditions are superior when the labeled molecules are heat and pH sensitive, such as in the case of nucleotides and antibodies. Moreover, the labeling time is crucial when working with short half-life radiometals, such as scandium-44 (^{44}Sc), copper-62 (^{62}Cu), ^{68}Ga, rubidium-82 (^{82}Rb), and $^{94m/99m}$Tc. Thus, the coordination kinetics must be fast (5–15 min reaction times) and yield high radiolabeling efficiency. Macrocyclic chelators, having inherently constrained geometries where the coordinating groups are close to another creating a “scaffold” metal ion binding sites, undergo only minor conformational and loss in entropy upon radiometal coordination. In contrast, acyclic chelators such as desferrioxamine (DFO) must undergo a more drastic change in their geometry in order to arrange the donor atoms to coordinate with the metal ion [9]. However, despite this thermodynamic favorability of radiometal coordination to macrocycles, they generally require heating (60–90 °C) and longer reaction times (>30 min) to attain radiolabeling at a reasonable yield. In acyclic chelators the coordination often occurs at room temperature within 15 minutes. The radiometal-chelator complex stability should be validated in terms of thermodynamic stability, possibility of transchelation (e.g., Fe^{3+}, EDTA, and DTPA), acid catalyzed dissociation, and stability in physiological conditions relevant to the administration route.

Overall, several factors need to be taken into consideration when designing chelator-mediated radiolabeling of theranostic nanosystems. The choice of the radiometal is the foremost consideration as the physical half-life should be matched to the timeframe of the experiment and the nuclear properties to the theranostic application. From the standpoint of the radiometal-chelator complex, the stability in vitro and in vivo, the radiolabeling conditions (media, pH, time, and temperature), and the conjugation chemistry available for nanosystem labeling all need to be taken into account.

3.1.2 Chelator-Free Radiolabeling

Chelator-based radiometal labeling has been widely employed in nuclear imaging and radiotherapeutic development with radiometals. However, a number of challenges in the chelator-based radiolabeling approach still remain. First, the nanomaterials may not be able to tolerate the severe radiolabeling conditions, such as acidic pH and high temperature, leading to instability and destruction. Second, the incorporation of the hydrophilic chelator onto the surface of nanosystems can change their overall pharmacokinetics, surface charge, and hydrodynamic size, resulting in completely different properties from the native vector. Moreover, the coordination chemistry is vastly different between different chelators and radiometals necessitating a careful evaluation of radiometal and chelator suitability for the application. However, as radiometals can be directly coordinated to certain functional groups that either intrinsically exist in the nanoparticle structure or that are grafted on the surface of nanoparticles, chelate-free strategies have shown potential to maintain the native properties of the nanoparticles in a way that better reflects the behavior of nonradiolabeled nanoparticles in vivo.

Several approaches to chelate-free radiolabeling of nanoparticles have been proposed to match different nanoparticle surface characteristics and modifications. Chelator-free [^{64}Cu]CuS nanoparticles have been developed as a platform for the simultaneous PET/CT imaging and photothermal therapy [10]. The [^{64}Cu]CuS can be formed by direct synthe-

Table 2 Common radiometal chelators, their derivatives, relevant radiometal ions, and radiolabeling conditions

Type	Chelator	Common derivatives	Radiometal ions	Radiolabeling conditions
Acyclic chelators	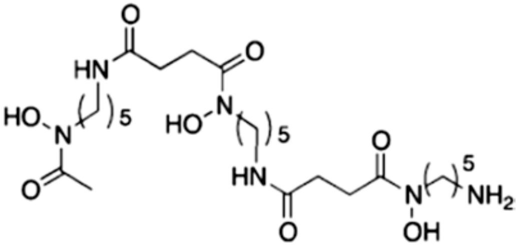 Desferrioxamine (DFO)	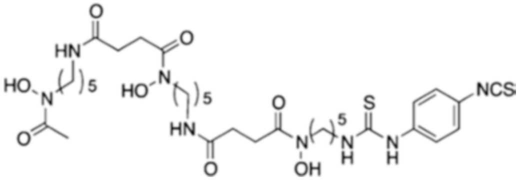 *p*-SCN-Bn-DFO	$^{67/68}Ga^{3+}$ $^{89}Zr^{4+}$	25 °C 30–60 min pH 3.5–7.3
		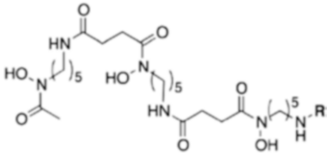 Bifunctional DFO, R = amide, NHS ester, etc.		
	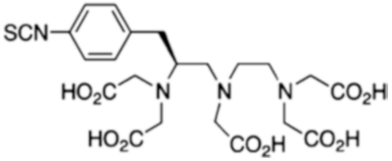 Diethylenetriaminepentaacetic acid (DTPA)	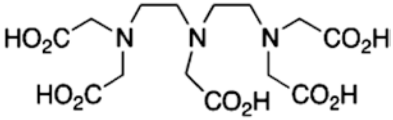 *p*-SCN-Bn-1B-DTPA	$^{44/47}Sc^{3+}$ $^{111}In^{3+}$ $^{177}Lu^{3+}$ $^{86/90}Y^{3+}$	25–75 °C 5–60 min pH 5–5.5
		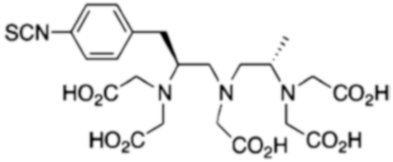 *p*-SCN-Bn-1B4M-DTPA		
		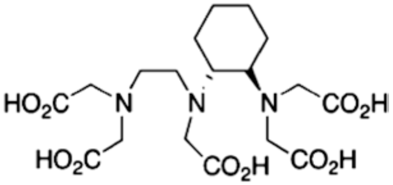 CHX-A”-DTPA		
		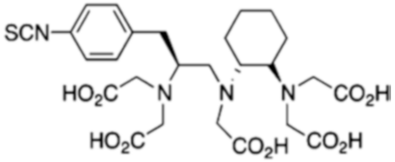 *p*-SCN-Bn-CHX-A”-DTPA		

Macrocyclics	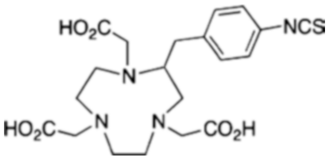 1,4,7-triazacyclononane-1,4,7-triacetic acid (NOTA)	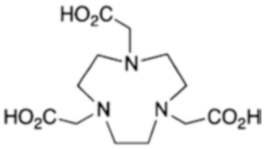 *p*-SCN-Bn-NOTA (C-NOTA)	^{64}Cu^{2+} $^{67/68}$Ga^{3+} $^{44/47}$Sc^{3+} ^{111}In^{3+} ^{177}Lu^{3+} $^{86/90}$Y^{3+}	25–95 °C 5–60 min pH 4–6.5
		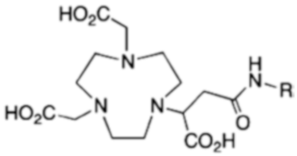 NODASA, R = NHS ester, amine, etc.		
		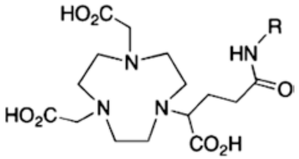 NODAGA, R = NHS ester, amine, etc.		
Macrocyclics (cont.)	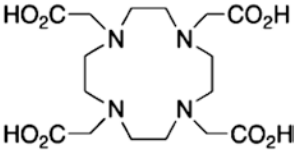 1,4,7,10-tetra-azacyclododecane-1,4,7,10-tetraacetic acid (DOTA)	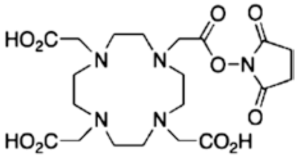 DOTA-NHS-ester	$^{67/68}$Ga^{3+} $^{44/47}$Sc^{3+} ^{111}In^{3+} ^{177}Lu^{3+} $^{86/90}$Y^{3+} ^{212}Pb^{2+} ^{225}Ac^{3+}	25–90 °C 10–120 min pH 4–6
		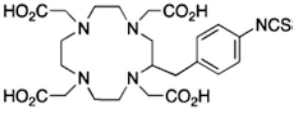 *p*-SCN-Bn-DOTA		
		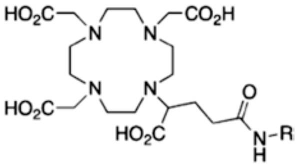 DOTAGA, R = amide, NHS ester, etc.		
		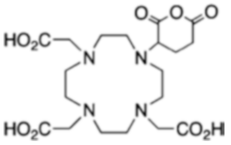 DOTAGA-anhydride		

(continued)

Table 2 (continued)

Type	Chelator	Common derivatives	Radiometal ions	Radiolabeling conditions
	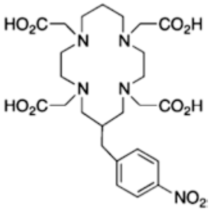 1,4,8,11-tetra-azacyclotetradecane-1,4,8,11-tetraacetic acid (TETA)	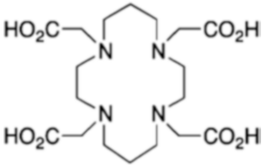 *p*-NO$_2$-Bn-TETA (C-TETA)	$^{64}Cu^{2+}$	25–95 °C 60 min pH 5–7
		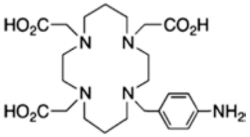 *p*-NH$_2$-Bn-TE3A		
		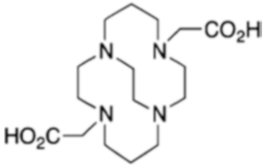 CB-TE2A		

Table adapted from reference [9]

sis from the radioactive precursor in which the ^{64}Cu is incorporated into the building block of CuS and a high radiolabeling yield was achieved. A similar direct radiolabeling approach has been documented in monoclonal antibody radiolabeling with rhenium-188 for radioimmunotherapy [11]. The protein disulfide bridges are firstly reduced with different reducing agents, generating thiol groups (R-SH) that can coordinate with reduced oxidation state of [^{188}Re]ReO_4^- in the presence of stannous chloride ($SnCl_2$) as a reducing agent.

The heat-induced radiolabeling (HIR) of radioactive cations has been employed in the radiolabeling of superparamagnetic iron oxide nanoparticles [12–14]. The thermal stability of iron oxide nanoparticles allows the high heat activation of the iron oxide core to coordinate with radiometals (e.g., ^{64}Cu, ^{89}Zr, ^{111}In, and ^{59}Fe) without changing the structure, magnetic properties, and size of the nanoparticles. In addition, the selective binding of radiometals to the surface of nanoparticles has been reported. The layered double hydroxide (LDH) nanoparticles have demonstrated the potential to be readily radiolabeled with radiometals without the aid of chelators [15]. Bivalent and trivalent cations (e.g., $^{64}Cu^{2+}$ and $^{44}Sc^{3+}$) can form stable coordination with high labeling efficiency into the brucite-like cationic layers of the LDH, while the tetravalent cation such as $^{89}Zr^{4+}$ cannot efficiently label onto the LDH layer due to the lack of compatibility between the ionic radius and the LDH crystal structure. Also, a similar strategy has been applied to investigate the stereotype of chelator-free radiolabeling nanographene with ^{64}Cu [16]. The reduced graphene oxide (RGO) exhibits a superior intrinsically ^{64}Cu radiolabeled to the nanographene due to the transition metal- π-electron interaction where the electron transfer takes place between $^{64}Cu^{2+}$ and π-bond, providing an alternative approach to maintain the properties of nanographene in vivo. The direct implantation method of theranostic radiolanthanoid, dysprosium-159 (^{159}Dy) to thermally hydrocarbonized porous silicon (THCPSi) nanoparticles has been reported [17]. The THCPSi substrates are irradiated with radioactive ion beam (RIB) of ^{159}Dy at the intensity of 10^{10} particles over 39 h, resulting in the implantation of ^{159}Dy ions on the mesoporous layer substrate. The [^{159}Dy]THCPSi nanoparticles demonstrated good stability in vivo after 7 days of intratumoral administration as the ^{159}Dy remained embedded in THCPSi nanoparticles inside the tumor, prompting the use of other RIB-based radiolanthanoids for chelator-free radiolabeling with mesoporous nanoparticles. Overall, the chelator-free radiolabeling strategies reveal the potential of alternative approaches for radiolabeling with radiometals. However, understanding of the coordination mechanism between the radiometal and the nanoparticle itself as well as the stability of the radiometal complex are always warranted before in vivo applications.

3.2 Radiohalogenation

Radiohalogenation can be performed using typical organic chemistry techniques such as nucleophilic and electrophilic substitution. The chemistry is chosen such that the new bond is strong enough to withstand physiological conditions. The carbon-halogen bond energy decreases with increase in size of halogens from $F^- < Cl^- < Br^- < I^-$. The bond strength increases with increasing number of π bonds of the carbon. Aromatic carbon-halogens bonds have higher bond strengths compared to the aliphatic counterparts with hybridization. This makes radioiodination on aromatic substrates less prone to hydrolysis and *β*-elimination. Direct radioiodination technique uses electrophilic and nucleophilic substitutions as well as electrophilic addition to unsaturated compounds in certain cases.

Electron rich aromatic compounds such as those containing the activating hydroxyl, amine and methoxy functionalities can be radioiodinated using electrophilic aromatic substitution. The substitution of the hydrogen at the ortho or para positions relative to the activating groups is called iododeprotonation. The ortho and para positions relative to the electron donating group are substituted due to the higher delocalization of charge in the transition state as shown in Fig. 7 for the dopamine D_2 receptor radioligand, IBZM.

For less activated aromatic rings, the synthesis is carried out in two steps with the formation of an activated derivative followed by the substitution with an electropositive radioiodine. The most commonly used organometallic precursors for iododemetallation are alkylstannyl compounds along with silyl and boronic acid derivatives. Carbon-metal bond is more activated for an electrophilic attack than a carbon-hydrogen bond. The drawback of using tri-alkyltin derivatives is the toxicity of tin compounds. Silyl derivatives are less toxic, a desirable property when the radioiodinated compound is to be used for in vivo studies. The silicon-carbon bond is stronger than tin-carbon bond which results in slower reaction rates for iododesilylation. Boron derivatives also have low toxicity and boron compounds such as boronate

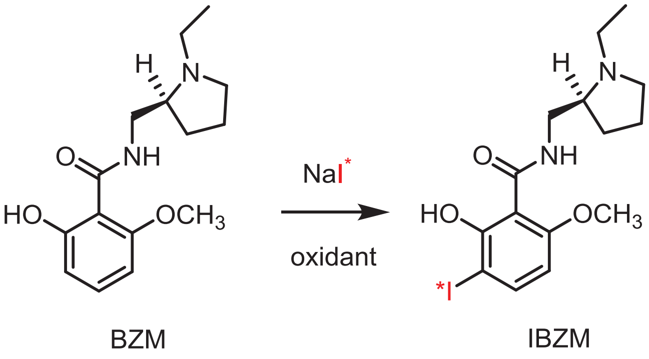

Fig. 7 Iododeprotonation of BZM

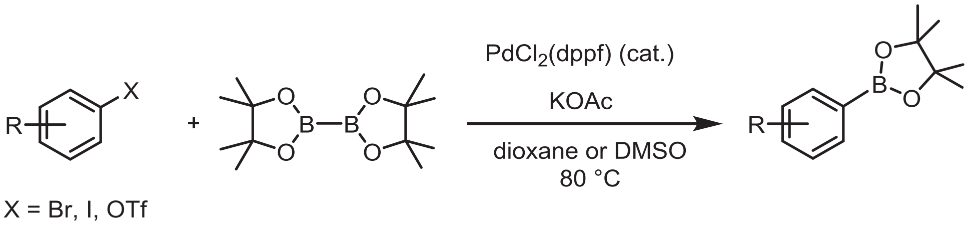

Fig. 8 Miyaura borylation reaction

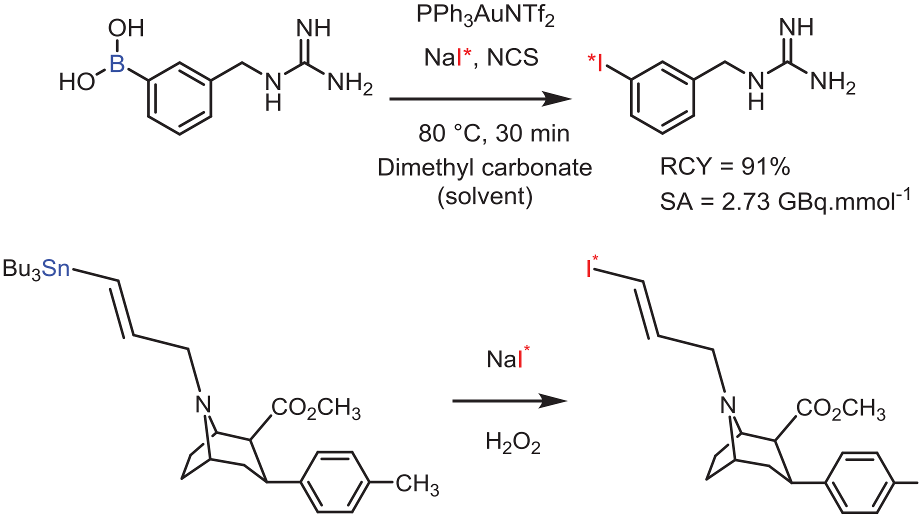

Fig. 9 Synthesis of [^{131}I]MIBG using iododeboronation (top) and PE2I using iododestannylation (bottom)

esters and trifluoroborate salts are air stable crystalline solids making them ideal precursors for halodemetallation reactions [18]. The boronate esters and trifluoroborate salts can be regioselectively prepared using the Miyaura borylation reaction which is the coupling of the bis(pinacolato)diboron with aryl/vinyl halides using palladium catalyst as shown in Fig. 8. Mild basic conditions for the borylation reaction is crucial to prevent activation of the borylated product and undergo Suzuki coupling reaction [19]. The ipso substitution of the metal with the iodine is regioselective under mild oxidative conditions. [^{131}I]MIBG has been prepared using iododeboronation as shown in Fig. 9.

The radioiodine is generally obtained as sodium iodide. It has to be oxidized to its unipositive charged state for electrophilic reactions. It can be oxidized using water soluble oxidants such as chloramine-T, N-chlorosuccimide (NCS), and peracids [20]. Chloramine-T is a strong oxidant but may lead to by-products. Low reaction temperatures and fresh reagents are key to successful oxidation. Polymer bound chloramine called Iodobeads [21] have been developed to reduce the exposure of oxidant sensitive molecules. Iodogen is another chlorine-based oxidant but it is milder and hence can be used with proteins and peptides. Iodogen is water insoluble and it is typically used as a thin film on a glass vial. Iodogen is compatible with common detergents which makes it widely applicable for labeling biologics. Radiolabeled proteins have been shown to have different stabilities depending on the source of the oxidizing agent showing there are fundamental differences among the mechanisms of radioiodination [22]. Structure of some of the oxidants is shown in Fig. 10.

Radioiodination conditions are harsh for sensitive molecules such as peptides and antibodies. To prevent such exposure, indirect radiolabeling methods are used in which prosthetic groups such as Bolton-Hunter reagent are radioiodinated, which can then be conjugated to biomolecules [23]. A typical conjugation of a radioiodinated Bolton-Hunter reagent is shown in Fig. 11. Other spacers which are bifunctional and can be used for radioiodination are shown in Fig. 12. These allow versatile bioconjugation to sulfhydryl and amine containing compounds.

Nucleophilic substitution is carried out in compounds which are functionalized with electron-withdrawing groups where the carbon is functionalized with good leaving groups such as mesylate, triflate, tosylate, or brosylate as shown in Fig. 13.

Aliphatic carbons can use either S_N1 or S_N2 mechanisms and aromatic compounds use S_NAr mechanism. The rate-determining step for a S_NAr reaction is the attack of the nucleophile and formation of the intermediate complex. For increasing the reaction rate, the labeling position needs to be activated by electron withdrawing groups such as -NO_2, aldehyde, ketone, ester, and amide in the ortho- or para-positions or catalyzed by metal salts such as Cu-salts.

For aryl amines the classic Sandmeyer-type reaction can be performed by diazotization of the amine, followed by

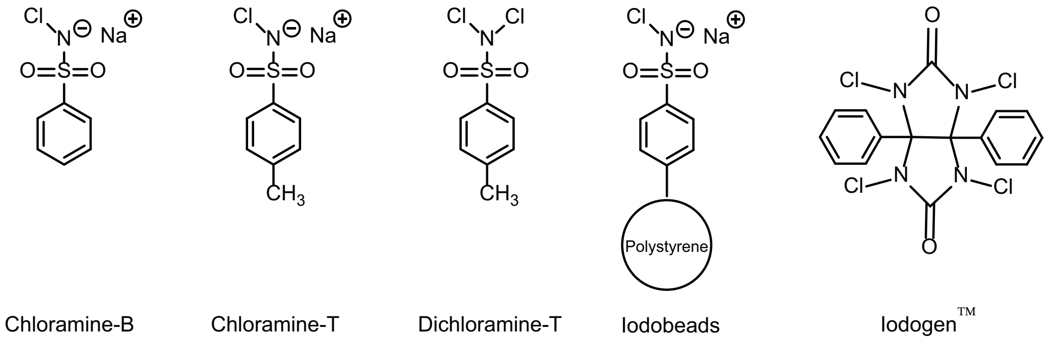
Chloramine-B
Chloramine-T
Dichloramine-T
Iodobeads
Polystyrene
Iodogen™

Fig. 10 Structure of some chlorine-based oxidants

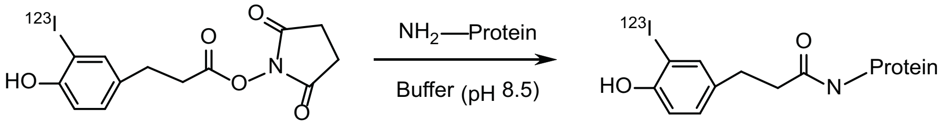
NH2—Protein
Buffer (pH 8.5)

Fig. 11 Conjugation of a protein to a radioiodinated Bolton-Hunter reagent

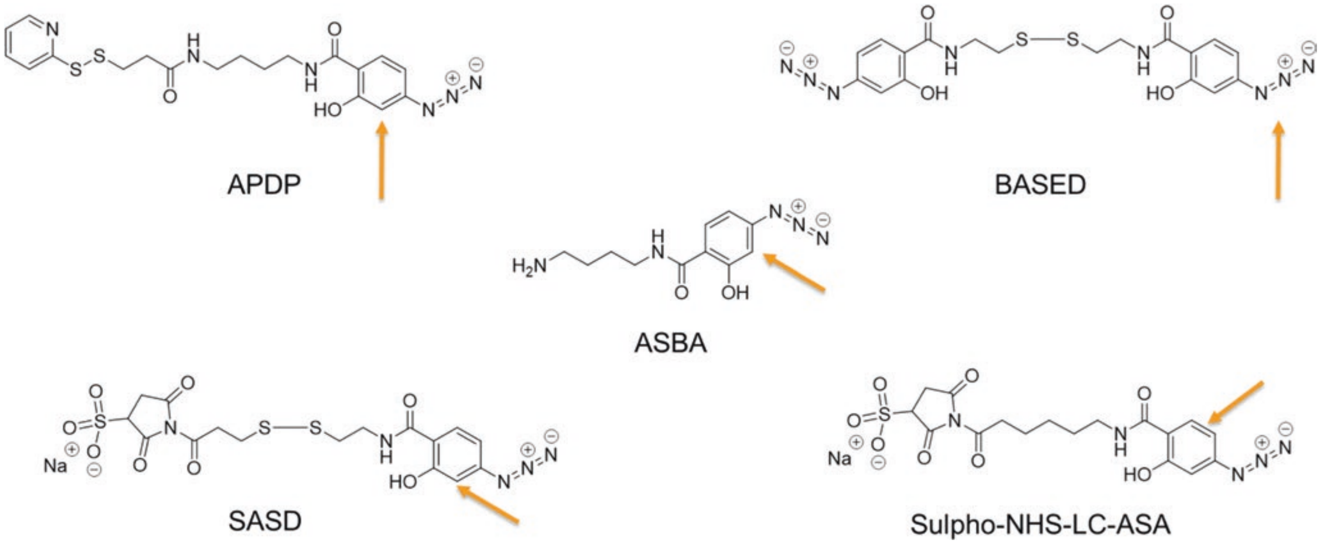
APDP
BASED
ASBA
SASD
Sulpho-NHS-LC-ASA

Fig. 12 Spacers which can be radioiodinated; radioiodination positions have been marked

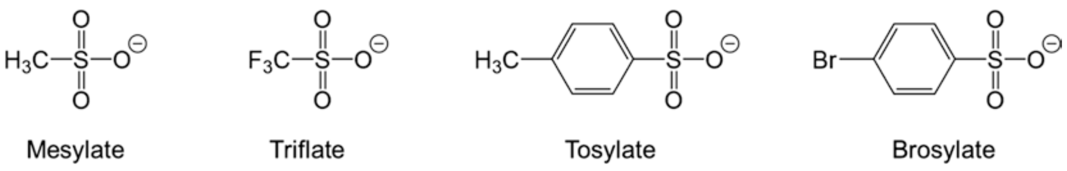
Mesylate
Triflate
Tosylate
Brosylate

Fig. 13 Structure of leaving groups used in nucleophilic substitution reactions

copper(I) catalyzed radioiodination. Limitations of such a reaction are the harsh acidic conditions required for the formation of the diazonium salt and the potentially explosive diazonium salts. A one-pot radioiodination was reported where the diazonium salts were formed under mild reaction conditions. This was achieved using a polymer-supported nitrite reagent and p-toluene-sulphonic acid as a proton source, followed by the direct radioiodination. The solid phase support allows for simple and rapid purification [24].

Substitution of an iodine substituent with radioiodine is called homo/isotopic exchange whereas that of a bromine substituent is called hetero/halogen exchange. These reactions are typically referred to as radioiododehalogenation. Even though commonly used, the isotopic exchange suffers from low molar activity since the parent molecule cannot be separated from the product. When a bromine is being substituted with radioiodine the product can often be separated using chromatographic methods leading to higher specific activity. Ammonium sulphate facilitates solid-phase exchange radioiodination of unactivated aryl iodide. The process involves heating to partial decomposition of the salt to lower pH from 6 to 3 which is essential for the reaction as shown in Fig. 14.

Copper(I) catalyzes nucleophilic reactions by forming a 3-membered intermediate complex. Typically the Cu(I) is produced in situby the reduction of Cu(II) by stannous chloride. The pH is maintained acidic to prevent nucleophilic attack by hydroxyl anions. The nucleophilic reaction can be also performed on boronated compounds as shown in Fig. 15. Higher radiochemical yields were obtained than electrophilic iododeborylation for compounds containing both electron-donating and electron-withdrawing substituents.

3.3 Radiolabeling with Positron-Emitting Radionuclides

The most important positron emitters for radiolabeling of therapeutic nanosystems for diagnostics purposes are ^{18}F, ^{124}I, ^{64}Cu, and ^{89}Zr. All these radionuclides have sufficiently long half-lives for the radiolabeling of theranostic nanosystems, which typically have high molecular mass and slow pharmacokinetics (Table 3). From these nuclides, ^{18}F has the most optimal imaging characteristics, but also the shortest half-life ($t_{1/2}$ = 109.7 min). Therefore, it can be used for tracing nanosystems with faster pharmacokinetics or by adapting a pretargeted radiolabeling strategy. ^{18}F does not have any theranostic nuclide pair, but nevertheless is an excellent choice as a diagnostic radionuclide when tracing therapeutic drug delivery systems, for example, for cancer chemotherapy. ^{124}I, ^{64}Cu, and ^{89}Zr have their theranostic pairs as ^{131}I, ^{67}Cu, and ^{90}Y respectively, which are all β^- emitters and widely used as radiotherapeutic agents in anticancer therapies.

The stability of the radiolabeling position is of utmost importance for both the diagnostic and therapeutic use of the nanosystem. Detached radionuclide may hamper the diagnostic use of a theranostic system, as the nuclear imaging will not be able to make any difference between different radioactive species. Especially if the detached radionuclide is bound to plasma proteins it may be difficult to differentiate whether the signal in circulation or tumor is originating from the protein-bound free radionuclide or from the radiolabeled theranostic nanosystem itself. For the radiotherapeutic use, the radiolabel instability is even more serious because the detached therapeutic radioisotope may cause serious adverse

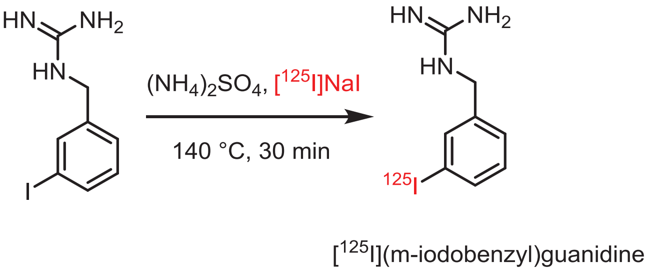

Fig. 14 Nucleophilic exchange reaction for the synthesis of [^{125}I](*m*-iodobenzyl)guanidine

Table 3 Positron emitting diagnostic radionuclides for theranostic systems

Radionuclide	Decay mode	Half-life ($t_{1/2}$)	E_{mean} β^+ in MeV (%)	Theranostic pair
^{18}F	β^+	109.7 m	0.250 (98)	None
^{64}Cu	β^+, β^-	12.7 h	0.278 (9)	^{67}Cu
^{89}Zr	β^+	78.4 h	0.395 (13)	^{90}Y
^{124}I	β^+	4.18 d	0.687 (12)	^{131}I

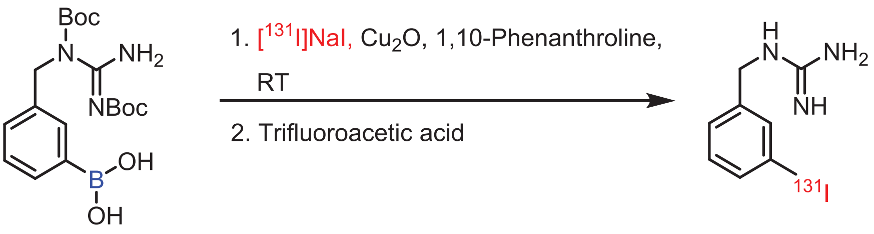

Fig. 15 Copper(I) catalyzed nucleophilic radioiodination of boronated compounds

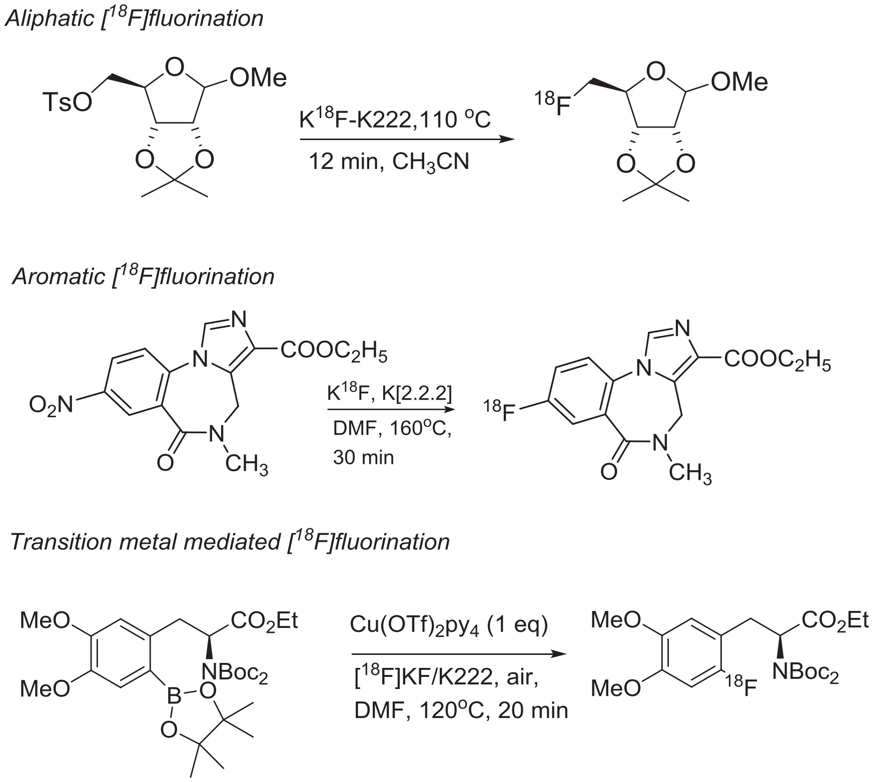

Aliphatic [^{18}F]fluorination

Aromatic [^{18}F]fluorination

Transition metal mediated [^{18}F]fluorination

Fig. 16 Typical reaction conditions for [^{18}F]fluorination

effects in radiation-sensitive healthy tissues such as the bone marrow, kidneys, and the intestinal epithelium. When using a true theranostic nuclide pair with different isotopes of the same element, the diagnostic and therapeutic nuclides exhibit identical chemical and pharmacokinetic properties and therefore the diagnostic system is perfectly suited for reliable evaluation of stability and biodistribution of the therapeutic system. In contrast, when radionuclides with different chemical properties are used, such as in case of ^{89}Zr/^{90}Y, more careful validation of the diagnostic accuracy of the system needs to be carried out before therapeutic use.

In principle, the chemical toolbox available for the radiolabeling of nanosystems is the same as in synthetic chemistry with stable isotopes. The only limitations for the use of short living radionuclides are the time available for the radiosynthesis and characterization, and the limited selection of the radioactive starting materials depending on production method of the selected radioisotope. The radioisotope production determines the chemical species of the produced radioisotope and the solvent or carrier gas in which they are delivered.

Fluorine can form stable covalent bonds with carbon and certain heteroatoms, such as silicon and boron. The formation of the carbon-[^{18}F]fluorine bond is the most difficult to attain and anhydrous reaction conditions and high temperatures are needed in order to achieve high radiochemical yields, even with reactions mediated by transition metals (Fig. 16). In all cases, the stability of the bond is influenced by the groups adjacent to the [^{18}F]fluorine. As fluorine is the most electronegative element in the periodic table, it forms bonds which are strong, but highly polarized and can therefore be hydrolyzed by a nucleophilic attack. This can be overcome if the fluorine is stabilized by functional groups that can inductively compensate the positive partial charge of the fluorine binding atom and/or can sterically hinder it against the attack. The most stable carbon-[^{18}F]fluorine bonds are between fluorine and an aromatic sp^2-carbon, in which the delocalization of the partial positive charge to the aromatic ring can compensate for the bond polarization and decrease vulnerability of the bond against the nucleophilic attack. When fluorine is bound to a sp^3-carbon, there is an additional mechanism which can lead to defluorination of the compound; in favorable conditions [^{18}F]fluorine can be eliminated together with an adjacent proton (Fig. 17). Silicon is one of the least electronegative compounds and predominantly forms bonds as sp^3-hybridized silicon. Polarization of the fluorine bond is most prominent for silicon and careful structure optimization is required in order to achieve stable [^{18}F]fluorination to silicon. In addition to carbon, silicon, and boron, fluorine can form stable coordination complexes together with aluminum by generating an [^{18}F]AlF^{2+} complex, which can be chelated analogously to several radiometals.

The radiolabeling methods for iodine-124 are described in Sect. 3.2. Only the radioiodination to sp^2-carbon is stable in vivo. Radioiodination to a saturated position leads to quick elimination of the radiolabel and accumulation of the free iodine into the thyroid. The detachment of an iodine label can never be completely avoided, but accumulation into thy-

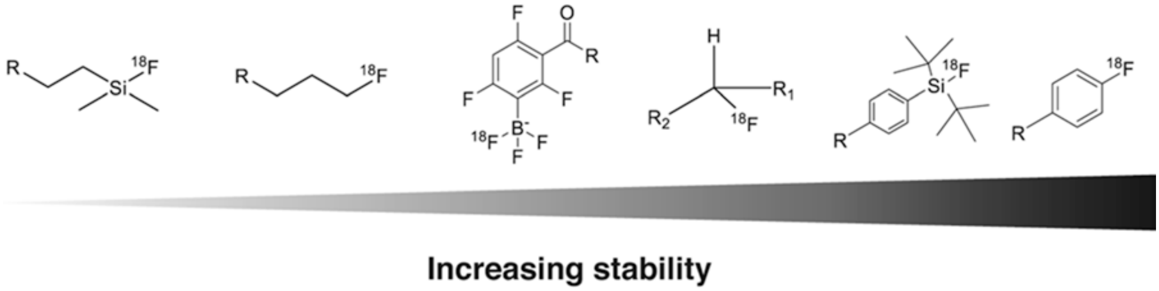

Fig. 17 The bond type and the position influences stability against defluorination

roid can be minimized by pretreating the thyroid with iodine salts. Copper-64 and zirconium-89 are radiometals and can be incorporated to the nanosystems by chelation chemistry. As described already in Sect. 3.1., copper-64 exists predominately in oxidation state II and its coordination number varies between 4 and 6. When using copper-64 for radiolabeling of nanotheranostics systems, it is especially important to notice its susceptibility to bind to endogenous proteins, such as ceruloplasmin and superoxide dismutase. The protein binding competes with binding to a chelator and may cause transchelation of the radiolabel from the nanostructure to the protein. Zirconium-89 is an emerging radionuclide in radiolabeling of nanosystems, due to its long half-life and low positron energy. The main challenge with zirconium-89 is stable chelation – all the existing chelators for $^{89}Zr^{4+}$ have exhibited limited in vivo stability leading to bone accumulation of the detached radiometal over time.

3.4 Pretargeted Radiolabeling Strategies

Instead of using direct labeling of nanosystems prior to their administration it is possible to utilize pretargeted radiolabeling strategies. In a pretargeted strategy, nanosystems are radiolabeled in vivo by using radiotracers which specifically bind to the administered nanosystem either by weak interactions or covalent bonds. One of the most investigated strategies for pretargeted radiolabeling is the biotin-(strept)avidin system, in which the recognition is based on the high-affinity interaction between biotin and avidin [25]. Other investigated pretargeted systems are, for example, systems based on hapten-antibody and DNA-DNA interactions [26, 27]. Recently, pretargeted strategies based on bioorthogonal chemical reactions have been under intensive investigation.

In *bioorthogonal* pretargeted strategies, the recognition between the tracer and a nanosystem is based on a chemical reaction, which leads to the formation of a covalent bond. Notably, the bioorthogonal reactions take place rapidly in physiological media without influencing the biological system. Several reactions have been investigated for the purpose such as Staudinger ligation, strain-promoted cycloadditions and inverse electron-demand Diels-Alder cycloaddition (IEDDA). From these only the IEDDA reaction has been shown to exhibit fast enough kinetics in physiological conditions for use in living animals. In the IEDDA reaction, a cycloaddition product is formed between two functional groups, namely a tetrazine and a strained alkene such as trans-cyclooctene (TCO) (Fig. 18). Typically, a radiolabeled tetrazine is used for radiolabeling of a TCO-conjugated nanosystem due to the improved metabolic stability of functionalized tetrazines. Pretargeted PET imaging based on bioorthogonal chemical reactions has demonstrated great potential in nanotheranostic applications and may allow for the use of short-living radionuclides for tracing long-circulating nanosystems without unnecessary radiation exposure to the patient.

3.5 Radiolabeling with Alpha Emitters

Alpha emitters can be chelated to traditional chelators such as DOTA, but the recoil energy of the ^{225}Ac daughters after an α decay is so energetic that about 30% of the radioactivity is lost from the chelate. Radium-223 (^{223}Ra), lead-211 (^{211}Pb), francium-221 (^{221}Fr), and bismuth-211 (^{211}Bi) are the primary daughter isotopes and cause renal toxicity. ^{225}Ac and its daughter ions are oxophilic making it easy to bind to hydroxyl-rich surfaces such as that of titanium dioxide. To prevent the leaching of ions due to the alpha decay they have to be encapsulated in the nanosystem. TiO_2 nanoparticles were functionalized with peptide fragments targeted to glioma cells with PEG spacer. ^{225}Ac was incorporated by ion exchange on the hydroxyl groups. After 10 days of incubation in physiological buffer, 95% of ^{225}Ac and ^{221}Fr were retained in the nanoparticle core [29]. This type of exchange reactions can also be carried out on nanozeolites. Although produced chemically, nanozeolites have been shown to have low toxicity similar to silicon nanoparticles. ^{223}Ra labeled nanozeolites showed 90% retention after 6 days with up to 5% release of ^{211}Pb and ^{211}Bi [30]. Medically relevant

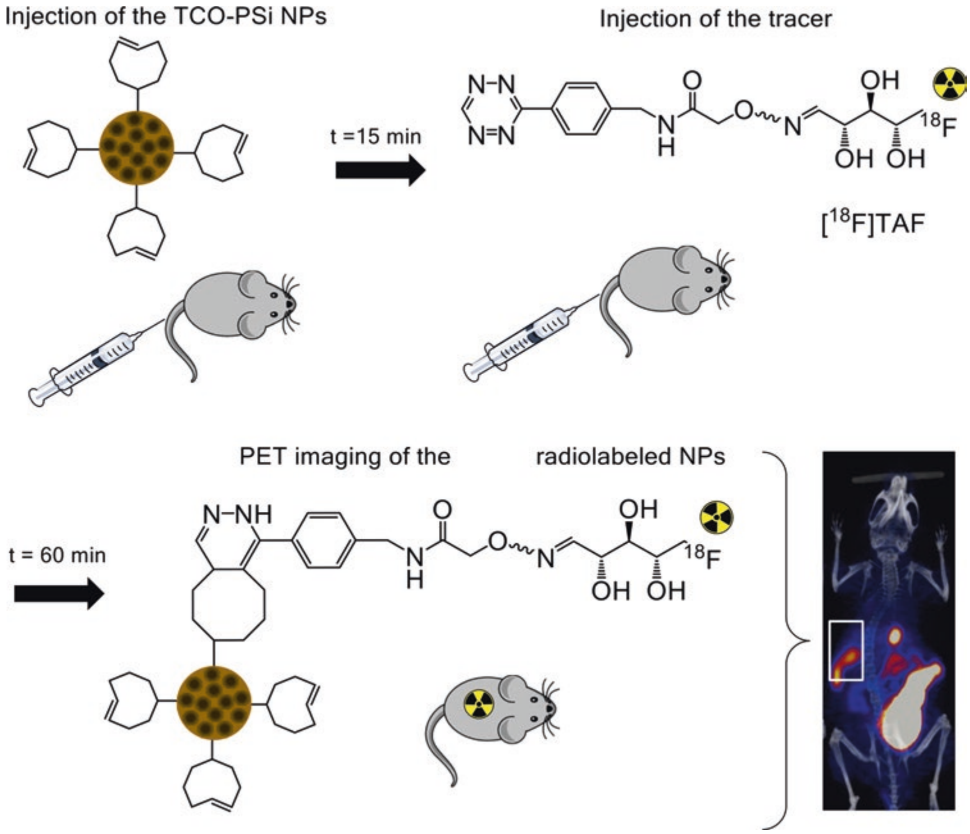
Injection of the TCO-PSi NPs
Injection of the tracer
t =15 min
[18F]TAF
PET imaging of the radiolabeled NPs
t = 60 min

Fig. 18 Pretargeted PET imaging of a TCO-conjugated porous silicon nanosystem (TCO-PSi) in mice. The TCO-PSis were injected 15 minutes before injection of a ^{18}F-labeled tracer, [^{18}F]TAF. PET imaging was performed 60 minutes after injection of the tracer and the TCO-PSis were successfully traced in spleen (delineated by a box). Some accumulation also in liver was observed. The observed high levels of radioactivity in gall bladder, intestines and urinary bladder are caused by elimination of [^{18}F]TAF and its radioactive metabolites. (Figure reprinted with permission from the American Chemical Society from reference [28])

poly(butadiene-b-ethylene oxide) was used to make liposomal vesicles. ^{225}Ac was chelated with ionophores such as calimycin and then incorporated into the liposomes. Recoil-ejected ^{213}Bi and ^{221}Fr could be separated from the unbound liposomes using DOWEX ion exchange resin and were found to be 47% and 31%, respectively [31].

Astatine-211 (^{211}At) is another promising alpha emitter belonging to the halogen series. As for iodine, prosthetic groups such as succinimidyl astatobenzoate (SAB) can be used to functionalize biomolecules. SAB is synthesized from a stannyl precursor using electrophilic halodemetallation reaction with an oxidant as shown in Fig. 19. The limitation of using oxidizing conditions is the multiple oxidation states available for astatine, which leads to low reproducibility and hence limits clinical application. With this respect, At$^-$ is much easier to stabilize and hence nucleophilic reaction conditions are preferable. Nucleophilic substitution of aryliodonium salt containing prosthetic groups using At$^-$ (Fig. 20) was shown to have high radiochemical yields. The aryl group on the aryliodonium salt which should not be radioastatinated was chosen to be electron rich to prevent attack of At$^-$. The p-anisyl group achieved the best radiochemical yields for radioastatination among p- isopropoxyphenyl and 2-thienyl groups [32].

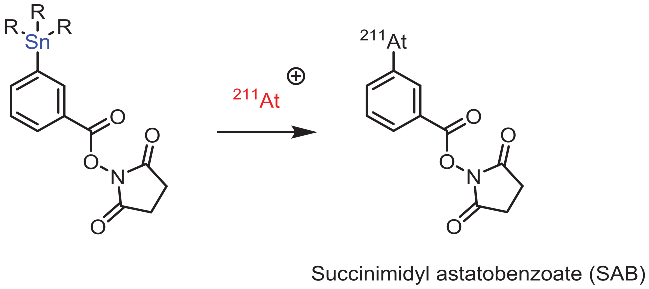

Fig. 19 Synthesis of prosthetic group containing Astatine-211

4 Preclinical Studies with Radiolabeled Tracers

Here, we give an overview of the standard preclinical in vitro, ex vivo, and in vivo methods employed in the biological evaluation of radiolabeled tracers including theranostic nanosystems. The focus is on methods where the output will be a measurement of the amount of radioactivity or visualization of its biodistribution. Conventional therapeutic efficacy and survival studies are to be used alongside to determine the therapeutic efficacy of the nanosystem.

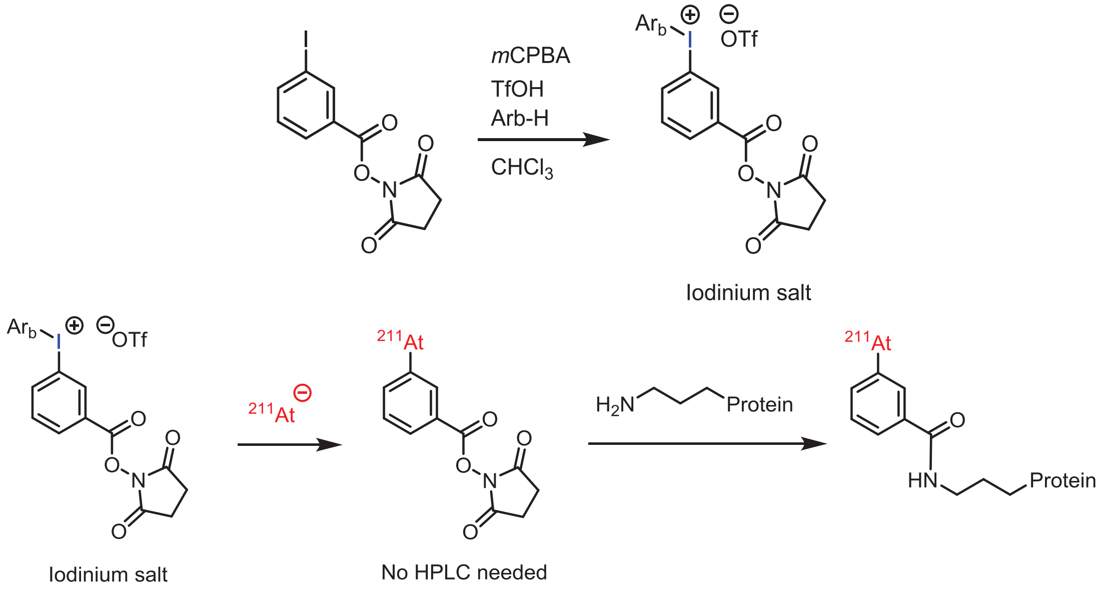

Fig. 20 Using iodinium salts for nucleophilic substitution reactions

4.1 In Vitro Methods

The in vitro methods used in the evaluation of theranostic nanosystems include various radiolabel stability assays in physiologically relevant media and cell uptake studies for the determination of the nanosystem cellular interaction and internalization and to corroborate the specificity of the nanosystem targeting. Additionally, as a proof-of-concept, the therapeutic effects of theranostic nanosystems can be assessed in vitro using various cell viability assays, assays for reactive oxygen species (ROS) and inflammatory markers, as well as by immunofluorescence staining of cells for markers of radiation-induced DNA damage, apoptosis, senescence and by observing the radiation-induced synchronization of the cell cycle with flow cytometry [33].

4.1.1 Radiolabel Stability Assays

Since the chemical identity of a radioactive species cannot be readily identified from nuclear images or radioactivity measurements of excised tissues – in these the radioactive signal is related only to the radioisotope but not its chemical form – radiolabel stability needs to be rigorously evaluated in vitro before proceeding to in vivo studies. Typically, the radiolabeled tracer is incubated in physiological media relevant for the administration route (plasma, serum, simulated gastric or intestinal fluids, simulated lung fluid, or cell culture media) at 37 °C over a period of time and samples are drawn from the incubations at designated time points and analyzed for the fraction of radioactivity remaining in the intact radiotracer. In the case of nanosystems, the nanoparticles are usually removed from the incubation by centrifugation or ultrafiltration and the amount of radioactivity remaining in the collected nanoparticles and in the solution is measured. Alternatively, analytical methods such as size-exclusion chromatography (SEC) thin layer chromatography (TLC) with radioactivity detection can be used to more closely monitor for the presence of the intact radiolabeled nanoparticles and the free radiolabel. In this case, the analytical method needs to be set up so that the retention times for the two are sufficiently different and that a clear separation is obtained. Additionally, the level of radioactivity at the sample needs to be set up to a level that can provide a clear signal even after long incubations. The radiolabel stability should be followed for a duration of time meaningful for the in vivo application and for as long as reasonably permitted by the half-life of the radioisotope. If the theranostic nanosystem is intended for radiotherapy, for example, the stability should be followed for days, for an imaging study with a shorter-lived radioisotope a duration of few hours is often sufficient. The radiolabel stability should be exceeding 95% for the entire duration the stability assay.

4.1.2 Cell Uptake and Internalization Assays

Radioactivity is a convenient tool also for the quantification of the cellular internalization and targeting of theranostic nanosystems. In these assays, the radiolabeled nanoparticles are incubated with the targeted tumor cell line, and at designated time points the amount of radioactivity remaining in the media, on cell surface and in the cell lysate is determined by radioactivity measurement of the fractions. The specificity of the cellular uptake can be studied by preventing the targeting using a large molar excess of a competing ligand or nanosystems modified with, for example, nontargeting control sequences. The time frame for the experiment depends

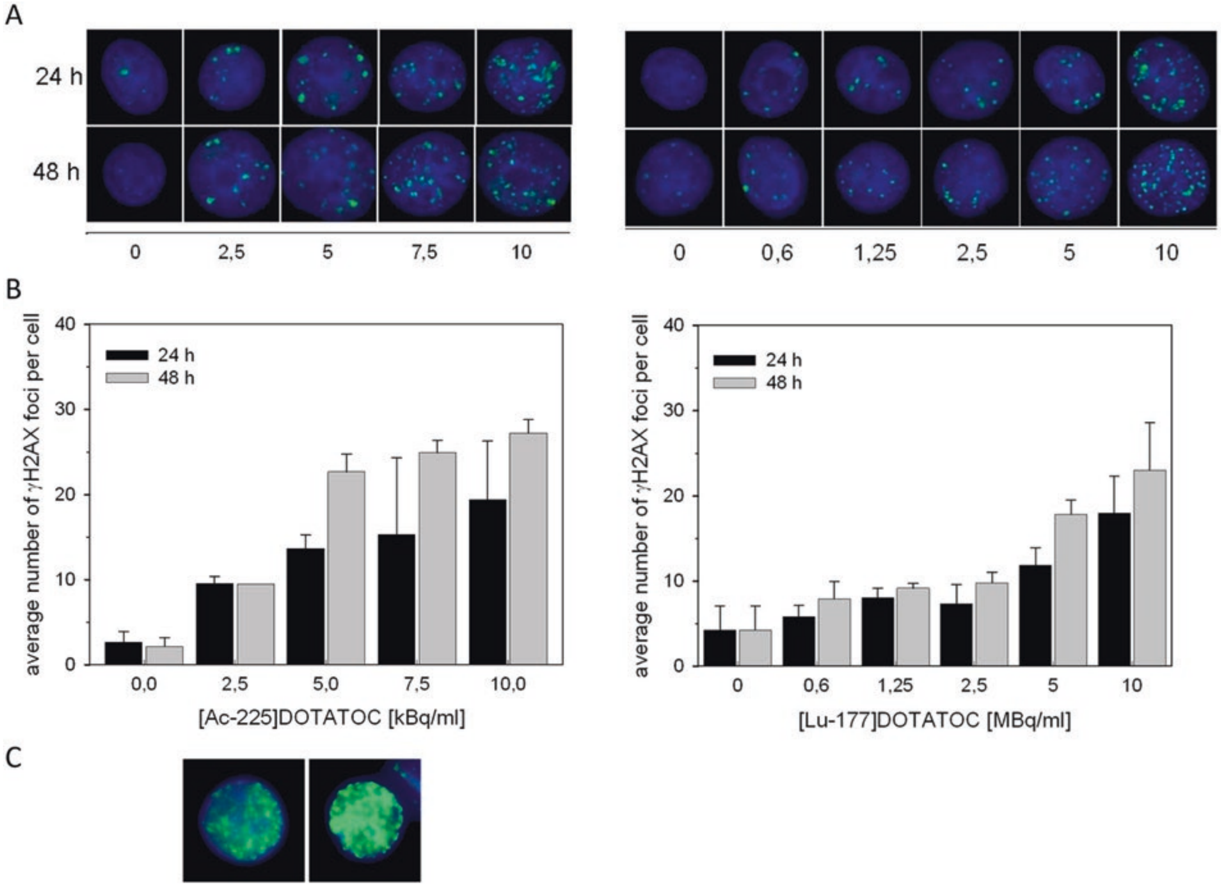

Fig. 21 Histone phosphorylation marker γH2AX can be used to quantify the number of DNA double-strand breaks induced by radiation therapy. Number of γH2AX foci in AR42J cells at 24 and 48 h after incubation with ^{225}Ac-DOTATOC (left) and ^{177}Lu-DOTATOC (right). (**a**) shows representative images from all activity levels, (**b**) shows quantification of cH2AX foci and (**c**) shows two representative examples for pan nuclear staining after high dose ^{225}Ac-DOTATOC treatment. (Figure reprinted with permission from reference [35])

on the system under study, but typically studies over a few hours or even 1–2 doubling times of the cell line can be done depending on the half-life of the radioisotope and its cytotoxicity.

4.1.3 Markers for Radiation-Induced Cellular Damage

Ionizing radiation induces a number of characteristic alterations in mammalian cells, and all of these can be used to determine the radiotherapeutic potential of the theranostic nanosystem. The DNA double-strand breaks induced by high LET α and β^- radiation can be visualized using γH2AX, a marker of histone phosphorylation which occurs in response to the double-strand break [34]. γH2AX has been shown to be a robust marker for radiation damage which is illustrated by the example in Fig. 21. The example from Graf and co-workers nicely illustrates by the number of γH2AX foci in rat pancreatic adenocarcinoma cells the differences between the LET values for theranostic β^- emitter ^{177}Lu and the α emitter ^{225}Ac when delivered by the same vector, the somatostatin receptor targeting peptide DOTATOC [35].

Cells respond to the DNA damage elicited by ionizing radiation by the activation of two main pathways, one leading to apoptosis [36] and the other to premature aging, or senescence [37]. Staining for apoptosis using established markers such as TUNEL (terminal deoxynucleotidyl transferase dUTP nick-end labeling), active caspase-3, or Annexin V is widely used also in the context of radiotherapy to study cellular and tissue-level effects of radiation treatment. Entry into the premature senescence or senescence-associated secretory phenotypes (SASPs) can be studied using a number of hallmark markers for senescence, including senescence-associated β-galactosidase, decreased Ki67, and elevated trimethylated histone H3 lysine 9 (H3K9me3) [38, 39]. The DNA damage resulting from exposure to ionizing radiation activates checkpoint pathways that inhibit the progression of the cells through the G_1 and G_2 phases of the cell cycle and induce a transient delay in the progression through S phase. As a result, an arrest of cells in the G_2/M checkpoint can be seen. This can be studied, for example, by flow cytometry [33, 40].

4.2 Ex Vivo Biodistribution Studies and Autoradiography

The distribution of radiolabeled tracers in the body is in the preclinical setting most commonly determined in an ex vivo biodistribution study, where groups of animals ($n = 3$–5) are sacrificed at predetermined time points after administration and tissue samples are collected to pre-weighed tubes and measured on an automated gamma counter with weighed (approximately 10 μl) standards prepared from the formulated radiotracer solution. The output in biodistibution studies is the percentage of the injected (radioactive) dose per gram of tissue (%ID/g). The injected dose is determined using the standards when the weight of the administered formulation is known (from weighing the syringe before and after administration). Depending on the application, the ex vivo biodistribution studies can be preceded by or conducted alongside small animal PET or SPECT/CT imaging studies discussed next.

Autoradiography is a sensitive imaging technique to study the tissue-level distribution of radiolabeled tracers ex vivo in cryosections prepared from tissue samples. The autoradiographic image can then be overlaid to a histological or immunofluorescence staining image of the same or adjacent section to correlate the radioactivity accumulation, for example, with the presence of the target of the theranostic nanosystem or physiological change elicited by the nanosystem accumulation. Today, most autoradiographic systems employ digital imaging plates instead of conventional X-ray films to record the autoradiographic image. In the digital imaging plate, the energy emitted by the radioisotope is stored by a phosphor layer of europium-doped barium fluoroborate crystals and released through the excitation of the Eu^{2+} to unstable Eu^{3+} when the plate is scanned with a red (633 nm) laser resulting in emission of blue light (390 nm) as the Eu returns to the ground state from the areas of the plate that were exposed to radiation. The emission is called photostimulated luminescence (PSL) and the quantification is often carried out in units of PSL/mm^2. Also real-time autoradiographic systems, where the tissue sample is encased in a parallel ionization multiplier (PIM) chamber are available. In these systems, the signal is accumulated as true counts or count rate per area, and the measurement time can be increased accordingly during the acquisition to improve the signal-to-background ratio in the image. In contrast, in digital autoradiography the autoradiographic trace is lost from the plate during the readout and in the case of short-lived isotopes only a single exposure will be possible.

4.3 Small Animal PET and SPECT/CT Imaging Studies

Small animal PET and SPECT/CT imaging technology allows for the noninvasive imaging of radiotracer biodistribution in laboratory rodents. Imaging studies are typically conducted under inhalation anesthesia, and the commercial imaging systems contain solutions for the administration of anesthesia, warming the animals during the scan and nowadays also platforms for the imaging of multiple animals in a single scan. The power of imaging over the conventional ex vivo biodistribution studies described above is that the entire biodistribution – including organs that are not necessarily sampled for the gamma counting – can be seen in the image and thus possible unexpected accumulation will not go undetected. Furthermore, an individual animal can be followed up longitudinally using imaging, which reduces the number of animals needed for a study as well as allows for the account of inter-individual differences such as tumor heterogeneity or stage and disease progression on the study outcome. The ex vivo biodistribution studies are, however, usually needed at some point of radiotracer development to validate the results of the imaging and to provide quantification for images acquired with SPECT, a semiquantitative method. Imaging can be carried out through a *dynamic* acquisition protocol, where the imaging acquisition is started at the time of the radiotracer injection or immediately after to track the early passage of the radiotracer with sequentially acquired images typically over the first 60 minutes of injection. In *static* acquisition, the signal is collected over a fixed period of time or up to a desired number of counts giving a summed image of the radiotracer distribution. Most small animal imaging systems available today are hybrid systems, where an anatomical imaging modality such as CT or MRI is provided together with the nuclear imaging and workflows can be programed for the sequential acquisition of the two.

4.4 Radiotherapy Studies and Dosimetry

The radiotherapeutic effects of theranostic nanosystems are most commonly determined by following the tumor size and attainment of the experiment humane endpoints after the administration of the radiotherapy. This can be done by conventional caliper measurements for subcutaneous or superficial orthotopic tumors, or, for example, by optical imaging of orthotopic tumors if a luciferase or fluorescent protein-expressing cell line is used, by regular weighing of the animals, and by the use of a technique called body condition scoring [41] to monitor the condition of the animals. In addition, the effects of the radiation exposure on the blood values (such as red blood cell count, hematocrit, white blood cell and platelet counts) of the animals are commonly studied as an indicator for hematological toxicity and when comparing different dosing regimens [42]. Dedicated veterinary systems for blood analysis in the small volumes collected from laboratory rodents are available. Another important factor for the feasibility of the clinical translation of a theranostic nanosystem will be the dosimetry, that is, the radioactive dose imparted by the nanosystem on the tumor and healthy tissues in the body. The dosimetry calculations are determined by measuring the time activity curves (TAC) for the clearance of the radiotracer in selected organs (the %ID/g in each can be determined either by imaging or ex vivo biodistribution) and fitting a typically one or two-phase decay equation in the data. The area under the curve then gives the cumulative uptake which can be converted to the absorbed dose making the necessary assumptions for the absorbed fraction of the radiation and equilibrium absorbed dose constants depending on properties of the radioisotope. Human dosimetry for the same radiotracer can be extrapolated from the mouse data using a number of computational models and reference values such as those set forth by the International Commission for Radiation Protection (ICRP) [42–44].

5 Current Examples of Radiolabeled Theranostic Nanosystems

The nanostructured core of the theranostic nanosystems can be metallic, polymeric, or lipid based such as micelles and liposomes. The surface of the nanosystem is modified to make it biocompatible and functionalized for the conjugation of biological targeting agents, radiolabels, or therapeutic molecules. The surface modifications allow for the extension of the circulation half-life, the tailoring of pharmacokinetics (PK) and biodistribution (BD), the suppression of immunogenicity and antigenicity, the stabilization against enzymatic degradation, reduced efflux of drugs, improved cellular endocytosis, and change in solubility characteristics. Multimodal imaging is often used since the resolution and sensitivity of detection varies across modalities, and different capabilities are needed for addressing phenomena at different levels of organization [45]. The combinations of imaging modalities for multimodal imaging are chosen such that ideally anatomical, physiological and molecular information is acquired with high sensitivity as illustrated by Fig. 22.

While passive targeting is more suited for fast growing tumors and nanoparticles which have a long circulation time, most tumors have unpredictable extravasation of the nanoparticle with varied sizes, shapes, and surface charge. Hence, targeting groups allow specific targeting beyond the effects of enhanced permeating and retention (EPR). This is particularly important in poorly vascularized small metastasis which are below 100 mm^3 [46–48].

Therapeutic agents loaded onto the nanoparticle can be released passively or with the stimuli of light or tumor microenvironment. In certain types of therapy, the external stimuli directly modulate the therapy such as in laser assisted ablation therapy. Well known examples of such therapies are photodynamic therapy (PDT) and photothermal therapy (PTT) where the light stimuli activate the photosensitizer which could be a small molecule or a nanoparticle. The imaging techniques that have been used are PET, SPECT, CT, MRI, optical/photoacoustic imaging, and contrast enhanced ultrasound [49, 50].

Diagnostic and therapeutic radioisotopes such as copper-64 and lutetium-177 can be bound to the same DOTA chelator. They have been loaded onto DOTA containing liposomes and used for PET imaging and therapy. Using PET imaging the optimum PEGylation and its influence on the biodistribution and tumor accumulation can be determined. A high therapeutic dose (114 mGy/MBq) could be delivered to the tumor site for the lutetium-177 loaded liposomes [51]. Liposomal formulations using doxorubicin as a chemotherapeutic agent in combination with rhenium-188 which has therapeutic properties as well SPECT imaging capabilities have been shown to greatly inhibit tumor growth and enhance the median survival time in a murine colon carcinoma model. The therapeutic results were better than singly functional-

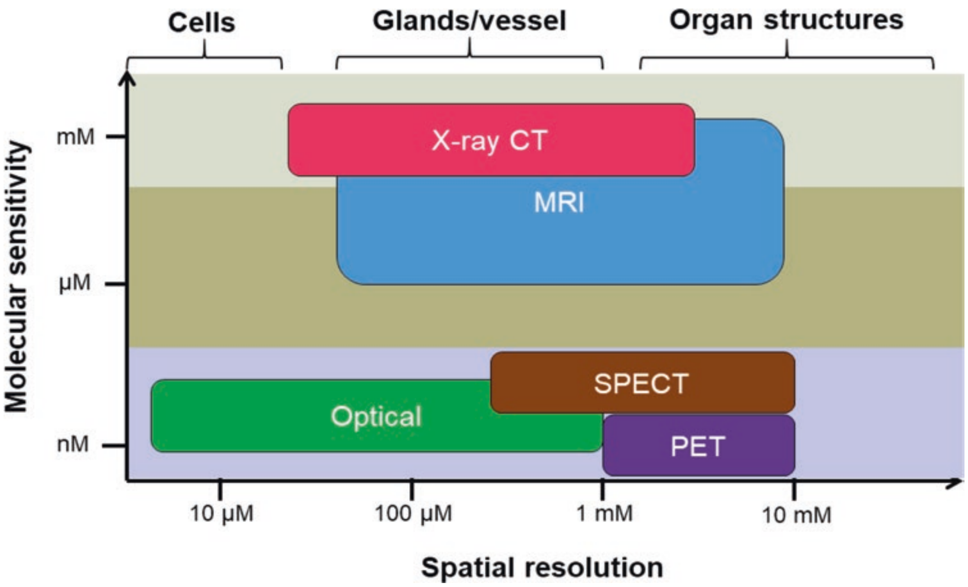

Fig. 22 Precision and sensitivity of detection varies across imaging modalities

ized rhenium-188-liposomes or doxorubicin-liposomes which shows that the synergistic effects of chemotherapy and internal radiation therapy are far more effective in therapy [52]. Multifunctional liposomes have been reported which have been loaded with doxorubicin for therapy, gadolinium ions for MR imaging, IRDye for NIR fluorescence imaging, technetium-99m for SPECT imaging, and copper-64 for PET imaging. In these dipalmitoyl phosphatidylcholine (DSPC)-based liposomes, the drug was encapsulated, technetium-99m was post loaded, while the copper-64 was conjugated to the DOTA chelators available on the liposome surface. The liposomes showed effective and correlated multimodal imaging capabilities in a murine model of head and neck cancer [53]. The drug delivery and therapeutic response was quantified in a clinical study with copper-64 labeled HER2 targeted PEGylated liposomal doxorubicin (Doxil). This study provided evidence that the EPR effect is functional in human tumor and imaging liposomal deposition can identify patients who are ideal for receiving therapeutic liposomes. The concentration, rates of deposition, and washout of the liposomes in human tumor are compable to preclinical models, which is of high significance for future studies [54]. Such image-guided insights are useful to prescreen patients assigned to Doxil in order to identify which patients are likely to respond to therapy and which are not. The release of a doxorubicin from liposomes could be visualized using MRI by using MR contrast agents such as manganese ions which were mixed with doxorubicin and upon simultaneous liberation enhanced contrast due to increase in water exchange rates. Other studies with MRI contrast agents to follow drug release have used ProHance (Gd-HP-DO3A) [55, 56]. Alpha particles have short penetration depth and high linear energy transfer (LET) which gives them an advantage over beta or gamma radiation. Alpha particle emitters such as ^{225}Ac, ^{223}Ra and ^{224}Ra have made it to the clinic. The limitations associated with alpha emitters are that the daughter ions when not retained at the tumor site can cause significant damage to healthy tissue. ^{211}Bi causes renal toxicity which is a limiting factor for performing clinical studies. The ^{225}Ac could be doped into the core of a nanoparticle prepared from lanthanum chloride, gadolinium chloride and cross-linked with sodium tripolyphosphate. The core nanoparticle is then covered with layers of gadolinium phosphate and gold. The magnetic properties of gadolinium phosphate allow easy separation and the gold surface provides biocompatibility and easy attachment of targeting moieties. The multilayered structure allowed 99.9% retention of ^{225}Ac and 98% retention of daughter ions. The gamma rays from the ^{221}Fr allow SPECT/CT imaging. The nanoparticles with antibodies targeted to the thrombomodulin receptors of lung showed predominant lung uptake 1 h post injection [57].

Carbon-based nanomaterials include fullerenes, carbon nanotubes, graphenes, and carbon-based quantum dots. The intrinsic property of one-photon and two-photon fluorescence in the NIR II allows deep tissue optical imaging. Their biocompatibility and ease of functionalization make them interesting candidates for theranostic applications. A ^{64}Cu labeled doxorubicin loaded polydopamine-gadolinium-metallofullerene ($Gd_3N@C_{80}$) core–satellite nanotheranostics was prepared which was capable of MR/photoacoustic/PET imaging and NIR triggered drug delivery in combination with PTT. The gadolinium showed high T1 contrast and was retained well in the particles. The doxorubicin was bound to the polydopamine through π–π stacking and hydrogen-bonding interactions, which were disrupted with NIR, causing the release of doxorubicin. The PTT caused the tumor temperature to reach 46 °C with 808 nm laser in 10 min and the combination therapy slowed the tumor growth and was significantly more effective than the monotherapy [58]. Single wall carbon nanotube (SWCNT) have inherent Raman signature which allows the direct monitoring of the presence of nanotubes in mice tissue. They were covalently attached to DOTA or DFO to chelate to actinium-225 or zirconium-89, respectively. The SWCNT was attached to tumor neovascular-targeting antibody E4G10. The alpha particles from ^{225}Ac have a travelling distance which match the vessel dimensions and delivers high linear energy transfer (LET) to the cells resulting in acute cytotoxicity making it ideal vascular-targeted radioimmunotherapy. The ^{89}Zr labeled constructs allowed PET imaging and determination of pharmacokinetics of the construct [59]. PET imaging and dosimetry of ^{90}Y SIR-Sphere using ^{86}Y and ^{89}Zr radiolabeled surrogates could be performed, and showed in vivo stability for clinical application. Theranostic application could be easily envisioned with the similarity in half lives of ^{89}Zr and ^{90}Y [60].

Gold nanoparticles can be prepared in different geometries, such as nanospheres, nanoshells, nanorods, or nanocages, which along with size affect the photothermal conversion efficiency for photothermal therapy. The absorbed wavelength changes depending on the shape of the particle so it has to be tuned such that it absorbs NIR in the two biologically transparent optical windows available, 650–850 nm and 950–1350 nm. The gold surface is ideal for binding to free thiol which makes it an ideal choice for bioconjugation. Copper sulphide nanoparticles are advantageous to gold nanoparticles as they are considered biodegradable inorganic nanomaterials, the surrounding environment does not affect its absorption wavelength and lastly, the cost of production is much lower. CuS nanoparticles were coupled to ^{64}Cu using chelator-free methods and used for PTT therapy with 800 and 980 nm laser showing better photothermal effects with 980 nm laser. The photothermal conversion efficiencies of the CuS nanoparticles were reported to be much higher than gold nanospheres and SWCNTs with 980 nm laser reaching 99.85 °C at 2 W/cm^2

for 4 min. The biodistribution of the particles was assessed using PET imaging and image guided PTT could be performed with a thermal mapping system equipped with an MRI scanner. In the orthotopic ovarian cancer mice model, this resulted in an effective therapeutic outcome [61]. To improve on the previous results in terms of the tumor availability of the nanoparticle, RGDfK peptides were attached to the CuS nanoparticles to target the αvβ3 integrins and labeled with ^{64}Cu in a chelator-free fashion as before. For the therapy a lower wavelength of 808 nm at 3 W/cm^2 for 2 min was used which increased the tumor temperature to 58.1 °C and resulted in 98% tumor tissue necrosis in U87 tumor-bearing mice [62]. Similar constructs can be used to target other biomarkers such as folate receptors, which are overexpressed in ovarian, breast, lung, and head and neck cancers [63]. CuS nanoparticles were loaded in PLGA microspheres together with the chemotherapeutic paclitaxel and radiolabeled with ^{131}I. These were used for PTT, chemotherapy, radiotherapy, photoacoustic imaging, and SPECT/CT from a single construct. The trimodal combination therapy with NIR irradiation eliminated tumor growth after intratumoral injection at relatively low doses in the orthotopic breast cancer model [64]. Theranostic Gd:CuS@BSA nanoparticles were prepared using copper(II) sulphide and gadolinium(III) ions with bovine serum albumin (BSA) as a scaffold. The 9 nm particles showed high photothermal conversion efficiency and good photostability under near-infrared (NIR) laser irradiation. Mice with ovarian cancer xenograft showed tumor growth inhibition with 5 min irradiation using 980 nm laser irradiation with the tumor temperature going up to 50 °C [65]. Defect-rich multifunctional Cu-doped layered double hydroxide (Cu-LDH) nanoparticles were shown to have pH enhanced NIR PTT as well as pH-sensitive T1 weighted MRI properties. The peculiar microstructures gave these nanoparticles high photothermal conversion at 808 nm and pH sensitivity. Further these particles were loaded with the chemotherapeutic agent 5-FU to combine PTT with chemotherapy and dose-dependent cytotoxicity was observed. Mice with colon cancer xenografts could be MR imaged and showed complete ablation with the combination of PTT and chemotherapy [66].

A melanin-based nanosystem with inherently good biocompatibility, biodegradability, and intrinsic photoacoustic properties was functionalized with tyrosine kinase inhibitor, sorafenib using π–π interaction. In addition, these particles had the natural ability to bind ^{64}Cu or ferric ions for PET or MR imaging studies. PET imaging allowed accurate and sensitive measurement of tissue penetration of the agent whereas the photoacoustic imaging allowed superficial information due to limitations of the penetrability of the NIR laser. Significant tumor shrinkage was observed from a single dose of the agent [67, 68].

Water-soluble superparamagnetic iron oxide (SPIO) nanoparticles such as ferumoxides and ferucarbotrans are clinically approved for MR imaging of the liver diseases. The approval of the SPIO makes them potential candidates for further approval as drug delivery candidates. PEGylated SPIOs were functionalized with cRGD for targeted tumor delivery. They were conjugated with ^{64}Cu using NOTA as chelators for PET imaging. The pH sensitive drug delivery was achieved using hydrazone linked doxorubicin which showed effective release at pH 5.3. Quantifying the PET images showed that targeting the SPIOs with cRGD resulted in doubling of nanoparticle delivery [69].

The drug release from the nanoparticle can be triggered by various external stimuli such as ultrasound, light, thermal, or chemical environment changes. The success of the PDT-based treatment is not without its drawbacks. Since the photosensitizers are always in an “ON” state, patients are typically vulnerable to sunlight even after 4–6 weeks of the PDT therapy. Additionally, the hypoxic conditions of the tumor microenvironment hinder PDT therapy due to its inherent requirement for oxygen to generate reactive oxygen species. A nanoparticle (PcS-MA) formed from the host-guest interactions of water-soluble photosensitizer, zinc(II) phthalocyanine tetrasubstituted with 6,8-disulfonate-2-naphthyloxy groups, and the common anticancer drug, mitoxantrone (MA) were quenched in supramolecular structure and showed no PDT effect or fluorescence signal. Upon interaction with nucleic acids, the construct disassembles resulting in PDT and chemotherapy, and could be imaged using fluorescence. MCF7 tumor-bearing mice which were injected with PcS-MA and irradiated with 1 W/cm^2 for 5 min reached a maximum temperature of 42.7 °C at the tumor site and was able inhibit tumor growth. Thus, such an activatable theranostic strategy could circumvent the drawbacks of traditional PDT in clinical settings [66].

The onset of hypoxia from PDT has been used as a trigger for a hypoxia activated prodrug AQ4N. The liposomal system was prepared by encapsulating AQ4N and hexadecylamine conjugated Ce6 (hCe6) photosensitizer in PEGylated liposomes which had a size of 95 nm. Conjugating the hCe6 with a positron emitter such as ^{64}Cu allowed PET imaging along with the inherently available fluorescence and optoacoustic imaging. All three modalities allowed the visualization of the liposomal delivery in the breast cancer model in mice with PET being the most sensitive. Biodistribution studies with the PET tracer also allowed quantification of the delivered dose. The therapy regiment showed that the synergistic effects of PDT and the hypoxia driven drug activation resulted in stagnation of the tumor growth [70].

Delivery of the drug to the tumor site is a challenge due to the insufficient accumulation of the nanoparticle. The size of the nanoparticle has to be optimized to have the desired blood circulation time. Other constraints which favor small particle size are inefficient tumor vascular extravasation, high interstitial fluid pressure, and dense extracellular matrix. Nanoparticles with smaller size are hence desired because of their high diffusion to the tumor tissue but a size less than 5 nm results in rapid excretion through the kidneys. Another crucial factor is the charge of the nanoparticles which should be preferably positive for improved cellular interaction and internalization. However, immune responses such as opsonization occur more readily on positively charged particles and speeding up the elimination from the bloodstream. Xue et al. developed upPhD theranostic nanovehicles, which had a dual size and charge transformability from the acidic pH of the tumor microenvironment. The monomers (PhD) were synthesized by conjugating cytotoxic doxorubicin and the PDT agent, pheophorbide using pH sensitive hydrazone bonds. The monomers first self-assembled into ultra-small micelles (upPhD) of about 4 nm in size. The upPhDs were then pegylated using pH sensitive imine bonds to form particles (pPhD) with 79 nm in size. When pPhDs were exposed to acidic pH, hydrolysis of the pegylation resulted in reverting to the smaller sized upPhD particles. The strong positive charge of upPhD (43 mV) was reduced to 12 mV upon the formation of the pegylated pPhD particles at neutral pH but reverted back to 35 mV at pH 6.8. The fluorescence of both the monomer components was also quenched in pPhD particles but was regained at a pH of 6.8. In subcutaneous and orthotropic tumor mice models, the pPhD particles showed 100% cure rate and outperformed the upPhD particles showing the importance of charge and size modulation. The large, slightly positive nanovehicles had a long circulation time but could be broken down into ultra-small nanoparticles with high positive charge near the tumor microenvironment, ideal for cell penetration. The particle accumulation at the tumor site could be followed using the fluorescence signal of the monomers as well as by MR imaging of manganese ions bound to the PDT agent [71].

Biomimetic design strategies such as the ones using cell-derived membranes to synthesize natural-mimicking vesicles are particularly interesting due to their excellent biocompatibility, low toxicity, high tumor accumulation, and ability to evade the immune and reticuloendothelial systems. Multicompartment membrane-derived liposomes (MCLs) have been prepared using 4T1 breast cancer cell membranes fused with surfactant, Tween-80, and had a size of 140 nm which was considerably smaller than without Tween-80. The quantitative biodistribution study using DFO conjugated ^{89}Zr showed greater than 9% ID/g in the 4T1 breast cancer tumor model in mice and clearance mostly though the liver. Injection to the lymphatic system allowed imaging of the lymph nodes. PDT agent loaded liposomes showed reduction in the rate of growth of the tumor upon irradiation with 660 nm laser [72].

6 Conclusion

In this chapter, we have outlined the primary ways of introducing therapeutic and diagnostic radioisotopes to theranostic nanosystems of variable compositions and illustrated the vast potential of using radioisotope methods to monitor the behavior of the nanosystems in vivo as well as to deliver efficient therapy. With this knowledge, we are hopeful that the reader is now equipped with an overview on how to go about designing radiolabeled theranostic nanosystems as well as the safe handling of radioisotopes and the principles of the analysis of data based on radioactivity. As we can see, the choice of the available radioisotopes, labeling chemistries, and nanomaterial scaffolds gives rise to an exceptionally wide array of radiolabeled constructs for different purposes. Furthermore, theranostic nanosystems are an ideal platform for the generation of multimodality imaging probes which can provide information on the nanosystem performance across imaging modalities and resolution barriers using the same imaging tracer.

References

1. Kang, H., Hu, S., Cho, M. H., Hong, S. H., Choi, Y., & Choi, H. S. (2018). Theranostic nanosystems for targeted cancer therapy. *Nano Today, 23*, 59–72.
2. Drude, N., Tienken, L., & Mottaghy, F. M. (2017). Theranostic and nanotheranostic probes in nuclear medicine. *Methods, 130*, 14–22.
3. Aghevlian, S., Boyle, A. J., & Reilly, R. M. (2017). Radioimmunotherapy of cancer with high linear energy transfer (LET) radiation delivered by radionuclides emitting α-particles or Auger electrons. *Advanced Drug Delivery Reviews, 109*, 102–118.
4. Ku, A., Facca, V. J., Cai, Z., & Reilly, R. M. (2019). Auger electrons for cancer therapy - a review. *EJNMMI Radiopharmacy and Chemistry, 4*, 27.
5. Eckelman, W. C., Boyd, M., & Mairs, R. J. (2017). Principles of molecular targeting for radionuclide therapy. In H. W. Strauss, G. Mariani, D. Volterrani, & S. M. Larson (Eds.), *Nuclear oncology: From pathophysiology to clinical applications* (pp. 35–65). Cham: Springer International Publishing.
6. Schirrmacher, R., Wängler, B., Bailey, J., Bernard-Gauthier, V., Schirrmacher, E., & Wängler, C. (2017). Small prosthetic groups in 18 F-radiochemistry: Useful auxiliaries for the design of 18 F-PET tracers. *Seminars in Nuclear Medicine, 47*, 474–492.
7. Coenen, H. H., Gee, A. D., Adam, M., Antoni, G., Cutler, C. S., Fujibayashi, Y., et al. (2017). Consensus nomenclature rules for radiopharmaceutical chemistry — Setting the record straight. *Nuclear Medicine and Biology, 55*, v–xi.
8. Bergström, M., Grahnén, A., & Långström, B. (2003). Positron emission tomography microdosing: A new concept with application in tracer and early clinical drug development. *European Journal of Clinical Pharmacology, 59*, 357–366.
9. Price, E. W., & Orvig, C. (2014). Matching chelators to radiometals for radiopharmaceuticals. *Chemical Society Reviews, 43*, 260–290.
10. Zhou, M., Chen, Y., Adachi, M., Wen, X., Erwin, B., Mawlawi, O., et al. (2015). Single agent nanoparticle for radiotherapy and radio-photothermal therapy in anaplastic thyroid cancer. *Biomaterials, 57*, 41–49.

11. Uccelli, L., Martini, P., Pasquali, M., & Boschi, A. (2017). Monoclonal antibodies radiolabeling with Rhenium-188 for Radioimmunotherapy. *BioMed Research International, 2017*, 5923609.
12. Yuan, H., Wilks, M. Q., El Fakhri, G., Normandin, M. D., Kaittanis, C., & Josephson, L. (2017). Heat-induced-radiolabeling and click chemistry: A powerful combination for generating multifunctional nanomaterials. *PLoS One, 12*, e0172722.
13. Boros, E., Bowen, A. M., Josephson, L., Vasdev, N., & Holland, J. P. (2015). Chelate-free metal ion binding and heat-induced radiolabeling of iron oxide nanoparticles. *Chemical Science, 6*, 225–236.
14. Hoffman, D., Sun, M., Yang, L., McDonagh, P. R., Corwin, F., Sundaresan, G., et al. (2014). Intrinsically radiolabelled [(59)Fe]-SPIONs for dual MRI/radionuclide detection. *American Journal of Nuclear Medicine and Molecular Imaging, 4*, 548–560.
15. Shi, S., Fliss, B. C., Gu, Z., Zhu, Y., Hong, H., Valdovinos, H. F., et al. (2015). Chelator-free labeling of layered double hydroxide nanoparticles for in vivo PET imaging. *Scientific Reports, 5*, 16930.
16. Shi, S., Xu, C., Yang, K., Goel, S., Valdovinos, H. F., Luo, H., et al. (2017). Chelator-free radiolabeling of nanographene: Breaking the stereotype of chelation. *Angewandte Chemie (International Ed. in English), 56*, 2889–2892.
17. Jakobsson, U., Mäkilä, E., Airaksinen, A. J., Alanen, O., Etilé, A., Köster, U., et al. (2019). Porous silicon as a platform for radiation theranostics together with a novel RIB-based radiolanthanoid. *Contrast Media & Molecular Imaging, 2019*, 3728563.
18. Kabalka, G. W., & Yao, M.-L. (2009). No-carrier-added radiohalogenations utilizing organoboranes: The synthesis of iodine-123 labeled curcumin. *Journal of Organometallic Chemistry, 694*, 1638–1641.
19. Ishiyama, T., Murata, M., & Miyaura, N. (1995). Palladium(0)-catalyzed cross-coupling reaction of Alkoxydiboron with Haloarenes: A direct procedure for arylboronic esters. *The Journal of Organic Chemistry, 60*, 7508–7510.
20. Hunter, R. (1970). Standardization of the chloramine-T method of protein iodination. *Experimental Biology and Medicine, 133*, 989–992.
21. Conlon, J. M. (1997). The use of IODO-GEN for preparing 125I-labeled peptides and their purification by reversed-phase high performance liquid chromatography. *Methods in Molecular Biology, 73*, 231–237.
22. Krohn, K. A., Knight, L. C., Harwig, J. F., & Welch, M. J. (1977). Differences in the sites of iodination of proteins following four methods of radioiodination. *Biochimica et Biophysica Acta (BBA) - Protein Structure, 490*, 497–505.
23. Bolton, A. E., & Hunter, W. M. (1973). The labelling of proteins to high specific radioactivities by conjugation to a125I-containing acylating agent. Application to the radioimmunoassay. *Biochemical Journal, 133*, 529–538.
24. Sloan, N. L., Luthra, S. K., McRobbie, G., Pimlott, S. L., & Sutherland, A. (2017). A one-pot radioiodination of aryl amines via stable diazonium salts: Preparation of 125I-imaging agents. *Chemical Communications, 53*, 11008–11011.
25. Cauchon, N., Langlois, R., Rousseau, J. A., Tessier, G., Cadorette, J., Lecomte, R., et al. (2007). PET imaging of apoptosis with 64Cu-labeled streptavidin following pretargeting of phosphatidylserine with biotinylated annexin-V. *European Journal of Nuclear Medicine and Molecular Imaging, 34*, 247–258.
26. Honarvar, H., Westerlund, K., Altai, M., Sandström, M., Orlova, A., Tolmachev, V., et al. (2016). Feasibility of Affibody molecule-based PNA-mediated radionuclide pretargeting of malignant tumors. *Theranostics, 6*, 93–103.
27. van Rij, C. M., Frielink, C., Goldenberg, D. M., Sharkey, R. M., Franssen, G. M., Lütje, S., et al. (2014). Pretargeted ImmunoPET of prostate cancer with an anti-TROP-2 x anti-HSG bispecific antibody in Mice with PC3 Xenografts. *Molecular Imaging and Biology, 17*, 94–101.
28. Keinänen, O., Mäkilä, E. M., Lindgren, R., Virtanen, H., Liljenbäck, H., Oikonen, V., et al. (2017). Pretargeted PET imaging of trans-Cyclooctene-modified porous silicon nanoparticles. *ACS Omega, 2*, 62–69.
29. Cędrowska, E., Pruszynski, M., Majkowska-Pilip, A., Męczyńska-Wielgosz, S., Bruchertseifer, F., Morgenstern, A., et al. (2018). Functionalized TiO2 nanoparticles labelled with 225Ac for targeted alpha radionuclide therapy. *Journal of Nanoparticle Research, 20*, 83.
30. Piotrowska, A., Męczyńska-Wielgosz, S., Majkowska-Pilip, A., Koźmiński, P., Wójciuk, G., Cędrowska, E., et al. (2017). Nanozeolite bioconjugates labeled with 223 Ra for targeted alpha therapy. *Nuclear Medicine and Biology, 47*, 10–18.
31. Wang, G., de Kruijff, R. M., Rol, A., Thijssen, L., Mendes, E., Morgenstern, A., et al. (2014). Retention studies of recoiling daughter nuclides of 225Ac in polymer vesicles. *Applied Radiation and Isotopes, 85*, 45–53.
32. Guerard, F., Navarro, L., Lee, Y. S., Roumesy, A., Alliot, C., Cherel, M., et al. (2017). Bifunctional aryliodonium salts for highly efficient radioiodination and astatination of antibodies. *Bioorganic & Medicinal Chemistry, 25*, 5975–5980.
33. Teiluf, K., Seidl, C., Blechert, B., Gaertner, F. C., Gilbertz, K.-P., Fernandez, V., et al. (2014). α-Radioimmunotherapy with 213 Bi-anti-CD38 immunoconjugates is effective in a mouse model of human multiple myeloma. *Oncotarget, 6*, 4692.
34. Kuo, L. J., & Yang, L.-X. (2008). γ-H2AX - A Novel Biomarker for DNA Double-strand Breaks. *In Vivo, 22*, 305–309.
35. Graf, F., Fahrer, J., Maus, S., Morgenstern, A., Bruchertseifer, F., Venkatachalam, S., et al. (2014). DNA double strand breaks as predictor of efficacy of the alpha-particle emitter Ac-225 and the electron emitter Lu-177 for somatostatin receptor targeted radiotherapy. *PLoS One, 9*, e88239.
36. Haimovitz-Friedman, A., Yang, T. J., Thin, T. H., & Verheij, M. (2012). Imaging radiotherapy-induced apoptosis. *Radiation Research, 177*, 467–482.
37. Wang, Y., Boerma, M., & Zhou, D. (2016). Ionizing radiation-induced endothelial cell senescence and cardiovascular diseases. *Radiation Research, 186*, 153–161.
38. Lee, S., & Schmitt, C. A. (2019). The dynamic nature of senescence in cancer. *Nature Cell Biology, 21*, 94–101.
39. Campisi, J., & d'Adda di Fagagna F. (2007). Cellular senescence: When bad things happen to good cells. *Nature Reviews Molecular Cell Biology, 8*, 729.
40. Iliakis, G., Wang, Y., Guan, J., & Wang, H. (2003). DNA damage checkpoint control in cells exposed to ionizing radiation. *Oncogene, 22*, 5834–5847.
41. Ullman-Cullere, M. H., & Foltz, C. J. (1999). Body condition scoring: A rapid and accurate method for assessing health status in mice. *Laboratory Animal Science, 49*, 319–324.
42. Poty, S., Carter, L. M., Mandleywala, K., Membreno, R., Abdel-Atti, D., Ragupathi, A., et al. (2019). Leveraging bioorthogonal click chemistry to improve ^{225}Ac-radioimmunotherapy of pancreatic ductal adenocarcinoma. *Clinical Cancer Research, 25*, 868–880.
43. Keinänen, O., Brennan, J. M., Membreno, R., Fung, K., Gangangari, K., Dayts, E. J., et al. (2019). Dual radionuclide theranostic pretargeting. *Molecular Pharmaceutics, 16*, 4416–4421.
44. Stabin, M. G., & Siegel, J. A. (2003). Physical models and dose factors for use in internal dose assessment. *Health Physics, 85*, 294–310.
45. Gao, X., Guo, L., Li, J., Thu, H. E., & Hussain, Z. (2018). Nanomedicines guided nanoimaging probes and nanotherapeutics for early detection of lung cancer and abolishing pulmonary metas-

tasis: Critical appraisal of newer developments and challenges to clinical transition. *Journal of Controlled Release, 292*, 29–57.

46. Maeda, H., Sawa, T., & Konno, T. (2001). Mechanism of tumor-targeted delivery of macromolecular drugs, including the EPR effect in solid tumor and clinical overview of the prototype polymeric drug SMANCS. *Journal of Controlled Release, 74*, 47–61.
47. Allen, T. M. (2004). Drug delivery systems: Entering the mainstream. *Science, 303*, 1818–1822.
48. Chen, F., Ehlerding, E. B., & Cai, W. (2014). Theranostic nanoparticles. *Journal of Nuclear Medicine, 55*, 1919–1922.
49. Jokerst, J. V., & Gambhir, S. S. (2011). Molecular imaging with theranostic nanoparticles. *Accounts of Chemical Research, 44*, 1050–1060.
50. Zavaleta, C., Ho, D., & Chung, E. J. (2018). Theranostic nanoparticles for tracking and monitoring disease state. *SLAS Technology, 23*, 281–293.
51. Petersen, A. L., Henriksen, J. R., Binderup, T., Elema, D. R., Rasmussen, P. H., Hag, A. M., et al. (2015). In vivo evaluation of PEGylated 64Cu-liposomes with theranostic and radiotherapeutic potential using micro PET/CT. *European Journal of Nuclear Medicine and Molecular Imaging, 43*, 941–952.
52. Chang, Y.-J., Chang, C.-H., Yu, C.-Y., Chang, T.-J., Chen, L.-C., Chen, M.-H., et al. (2010). Therapeutic efficacy and microSPECT/CT imaging of 188Re-DXR-liposome in a C26 murine colon carcinoma solid tumor model. *Nuclear Medicine and Biology, 37*, 95–104.
53. Li, S., Goins, B., Zhang, L., & Bao, A. (2012). Novel multifunctional theranostic liposome drug delivery system: Construction, characterization, and multimodality MR, near-infrared fluorescent, and nuclear imaging. *Bioconjugate Chemistry, 23*, 1322–1332.
54. Lee, H., Shields, A. F., Siegel, B. A., Miller, K. D., Krop, I., Ma, C. X., et al. (2017). (64)Cu-MM-302 positron emission tomography quantifies variability of enhanced permeability and retention of nanoparticles in relation to treatment response in patients with metastatic breast cancer. *Clinical Cancer Research, 23*, 4190–4202.
55. Viglianti, B. L., Abraham, S. A., Michelich, C. R., Yarmolenko, P. S., MacFall, J. R., Bally, M. B., et al. (2004). In vivo monitoring of tissue pharmacokinetics of liposome/drug using MRI: Illustration of targeted delivery. *Magnetic Resonance in Medicine, 51*, 1153–1162.
56. Lammers, T., Aime, S., Hennink, W. E., Storm, G., & Kiessling, F. (2011). Theranostic nanomedicine. *Accounts of Chemical Research, 44*, 1029–1038.
57. Han, Z., McLaughlin, M. F., Woodward, J., Boll, R. A., Wall, J. S., Rondinone, A. J., et al. (2013). Gold coated lanthanide phosphate nanoparticles for targeted alpha generator radiotherapy. *PLoS One, 8*, e54531.
58. Wang, S., Lin, J., Wang, Z., Zhou, Z., Bai, R., Lu, N., et al. (2017). Core-satellite polydopamine-gadolinium-metallofullerene nanotheranostics for multimodal imaging guided combination cancer therapy. *Advanced Materials, 29*.
59. McDevitt, M., McDevitt, M., Alessandro, R., Carlos, H. V., Jason, P. H., Shanna, R. S., et al. (2010). Imaging and treating tumor vasculature with targeted radiolabeled carbon nanotubes. *International Journal of Nanomedicine, 5*, 783.
60. Avila-Rodriguez, M. A., Selwyn, R. G., Hampel, J. A., Thomadsen, B. R., DeJesus, O. T., Converse, A. K., et al. (2007). Positron-emitting resin microspheres as surrogates of 90Y SIR-spheres: A radiolabeling and stability study. *Nuclear Medicine and Biology, 34*, 585–590.
61. Zhou, M., Melancon, M., Stafford, R. J., Li, J., Nick, A. M., Tian, M., et al. (2016). Precision nanomedicine using dual PET and MR temperature imaging-guided photothermal therapy. *Journal of Nuclear Medicine, 57*, 1778–1783.
62. Cui, L., Xiong, C., Zhou, M., Shi, S., Chow, D. S. L., & Li, C. (2018). Integrin αvβ3-targeted [64Cu]CuS nanoparticles for PET/CT imaging and photothermal ablation therapy. *Bioconjugate Chemistry, 29*, 4062–4071.
63. Zhou, M., Song, S., Zhao, J., Tian, M., & Li, C. (2015). Theranostic CuS nanoparticles targeting folate receptors for PET image-guided photothermal therapy. *Journal of Materials Chemistry B, 3*, 8939–8948.
64. Liu, Q., Qian, Y., Li, P., Zhang, S., Wang, Z., Liu, J., et al. (2018). The combined therapeutic effects of 131 iodine-labeled multifunctional copper sulfide-loaded microspheres in treating breast cancer. *Acta Pharmaceutica Sinica B, 8*, 371–380.
65. Yang, W., Guo, W., Le, W., Lv, G., Zhang, F., Shi, L., et al. (2016). Albumin-bioinspired Gd:CuS Nanotheranostic agent for in vivo photoacoustic/magnetic resonance imaging-guided tumor-targeted photothermal therapy. *ACS Nano, 10*, 10245–10257.
66. Li, B., Tang, J., Chen, W., Hao, G., Kurniawan, N., Gu, Z., et al. (2018). Novel theranostic nanoplatform for complete mice tumor elimination via MR imaging-guided acid-enhanced photothermo−/chemo-therapy. *Biomaterials, 177*, 40–51.
67. Fan, Q., Cheng, K., Hu, X., Ma, X., Zhang, R., Yang, M., et al. (2014). Transferring biomarker into molecular probe: Melanin nanoparticle as a naturally active platform for multimodality imaging. *Journal of the American Chemical Society, 136*, 15185–15194.
68. Zhang, R., Fan, Q., Yang, M., Cheng, K., Lu, X., Zhang, L., et al. (2015). Engineering melanin nanoparticles as an efficient drug-delivery system for imaging-guided chemotherapy. *Advanced Materials, 27*, 5063–5069.
69. Yang, X., Hong, H., Grailer, J. J., Rowland, I. J., Javadi, A., Hurley, S. A., et al. (2011). cRGD-functionalized, DOX-conjugated, and 64Cu-labeled superparamagnetic iron oxide nanoparticles for targeted anticancer drug delivery and PET/MR imaging. *Biomaterials, 32*, 4151–4160.
70. Feng, L., Cheng, L., Dong, Z., Tao, D., Barnhart, T. E., Cai, W., et al. (2017). Theranostic liposomes with hypoxia-activated prodrug to effectively destruct hypoxic tumors post-photodynamic therapy. *ACS Nano, 11*, 927–937.
71. Xue, X., Huang, Y., Bo, R., Jia, B., Wu, H., Yuan, Y., et al. (2018). Trojan Horse nanotheranostics with dual transformability and multifunctionality for highly effective cancer treatment. *Nature Communications, 9*, 3653.
72. Yu, B., Goel, S., Ni, D., Ellison, P. A., Siamof, C. M., Jiang, D., et al. (2018). Reassembly of 89Zr-labeled cancer cell membranes into multicompartment membrane-derived liposomes for PET-Trackable tumor-targeted theranostics. *Advanced Materials, 30*, e1704934.

Boosting Nanomedicine Efficacy with Hyperbaric Oxygen Therapy

Xiaoxian Wang, Si Li, Xin Liu, Xian Wu, Ningbing Ye,
Xiangliang Yang, and Zifu Li

Abstract

Nanomedicine has been a hot topic in the field of tumor therapy in the past few decades. Because of the enhanced permeability and retention effect (EPR effect), nanomedicine can passively yet selectively accumulate at tumor tissues. As a result, it can improve drug concentration in tumor tissues and reduce drug distribution in normal tissues, thereby contributing to enhanced antitumor effect and reduced adverse effects. However, the therapeutic efficacy of anticancer nanomedicine is not satisfactory in clinical settings. Therefore, how to improve the clinical therapeutic effect of nanomedicine has become an urgent problem. The grand challenges of nanomedicine lie in how to overcome various pathophysiological barriers and simultaneously kill cancer cells effectively in hypoxic tumor microenvironment (TME). To this end, the development of novel stimuli-responsive nanomedicine has become a new research hotspot. While a great deal of progress has been made in this direction and preclinical results report many different kinds of promising multifunctional smart nanomedicine, the design of these intelligent nanomedicines is often too complicated, the requirements for the preparation processes are strict, the cost is high, and the clinical translation is difficult. Thus, it is more practical to find solutions to promote the therapeutic efficacy of commercialized nanomedicines, for example, Doxil®, Oncaspar®, DaunoXome®, Abraxane®, to name a few. Increasing attention has been paid to the combination of modern advanced medical technology and nanomedicine for the treatment of various malignancies. Recently, we found that hyperbaric oxygen (HBO) therapy could enhance Doxil® antitumor efficacy. Inspired by this study, we further carried out researches on the combination of HBO therapy with other nanomedicines for various cancer therapies, and revealed that HBO therapy could significantly boost antitumor efficacy of nanomedicine-mediated photodynamic therapy and photothermal therapy in different kinds of tumors, including hepatocellular carcinoma, breast cancer, and gliomas. Our results implicate that HBO therapy might be a universal strategy to boost therapeutic efficacy of nanomedicine against hypoxic solid malignancies.

Keywords

Tumor hypoxia · Hyperbaric oxygen therapy · Nanomedicine · Combination therapy

1 Introduction

As a fundamental characteristic of most solid tumors, hypoxia is caused by the imbalance between the supply and the consumption of oxygen due to the aberrant vascular structure and the unrestrained cancer cell proliferation in tumor tissues [1–3]. Hypoxia has been implicated in not only tumor progression and metastasis, but also drug resistance via various means [3, 4]. First, molecular oxygen is indispensable for various cancer treatments, for instance chemotherapy, photodynamic therapy, and radiotherapy. In the hypoxic tumor microenvironment (TME), active oxygen radicals cannot be produced sufficiently to eradicate cancer cells. Second, hypoxia can increase the

---

X. Wang · S. Li · X. Liu · X. Wu · N. Ye
National Engineering Research Center for Nanomedicine, College of Life Science and Technology, Huazhong University of Science and Technology, Wuhan, China

X. Yang · Z. Li (✉)
National Engineering Research Center for Nanomedicine, College of Life Science and Technology, Huazhong University of Science and Technology, Wuhan, China

Key Laboratory of Molecular Biophysics of Ministry of Education, College of Life Science and Technology, Huazhong University of Science and Technology, Wuhan, China

Hubei Key Laboratory of Bioinorganic Chemistry and Materia Medical, Huazhong University of Science and Technology, Wuhan, China
e-mail: zifuli@hust.edu.cn

© Springer Nature Switzerland AG 2021

F. Fontana, H. A. Santos (eds.), *Bio-Nanomedicine for Cancer Therapy*, Advances in Experimental Medicine and Biology 1295, https://doi.org/10.1007/978-3-030-58174-9_4

intracellular expression of hypoxia induced factor (HIF) [5], which is a key transcription factor and regulates crucial pathways including cell cycle arrest, DNA repair, and apoptosis, altogether rendering tumor cells insensitive to cancer treatments [6]. Therefore, alleviating a hypoxic TME can significantly promote the antitumor efficacy of various cancer therapies. To this end, various strategies, including improving intratumor blood flow [7], delivering oxygen to tumor with carriers [8], producing oxygen in situ within tumor [9], and slowing down tumor oxygen consumption [10], have been actively pursued. However, these aforementioned strategies are still under study in the laboratory and have not yet been used in clinical settings.

Boasting the capability of revolutionizing the conventional cancer chemotherapy, nanomedicine has been a research hotspot for the past few decades. With small sizes, typically in the range of 1 to 1000 nm, and large specific surface areas, nanomedicine can prolong the in vivo circulation time of drugs by hydrophilic modification of the surface and accumulate selectively in tumor sites through the passive targeting via the EPR effect. In addition, they can realize active targeting at different levels by surface modifications with targeting ligands, thereby further improving tumor accumulation. As a consequence, nanomedicine can reduce the drug dose under the premise of ensuring the efficacy and mitigating side effects associated with conventional chemotherapeutic agents. For this reason, dozens of nanotherapeutics, for instance Doxil®, Oncaspar®, DaunoXome®, and Abraxane®, have been approved by the Food and Drug Administration (FDA) for the treatment of various malignancies in the past three decades. As expected, these nanoformulations overtly alleviated side effects of the encapsulated chemotherapeutic drugs. Nonetheless, compared with free drugs, nanomedicine provided limited survival benefits to cancer patients. This is because the pathophysiological barriers critically restrict the delivery efficiency of nanomedicine. Due to the pathophysiological barriers, including renal clearance, reticuloendothelial system (RES) clearance, aberrant tumor vasculature, dense extracellular matrix (ECM), interstitial fluid pressure (IFP), and cancer cell fast growing accumulated solid stress, to name a few [11], nanomedicine delivery efficiency has been as low as 0.7% (median) for the past decade [12]. To overcome these physical barriers and obtain a decent delivery efficiency, we proposed that the ideal nanomedicine should possess the following characteristics, including prolonged circulation time in blood, enhanced tumor accumulation, deep penetration, efficient cancer cell cellular internalization, and fast intracellular drug release [13–16], which we collectively termed as "five features" principle for rational design of tumor targeting nanomedicine. Under the guidance of this principle, we have recently achieved drug delivery efficiency of 8% with tumor cell derived microparticles [17]. However, such bio-inspired nanomedicine suffers the issue of potential tumorigenicity. Furthermore, it might take another 10 years and cost additional billion US dollars to translate this bio-inspired nanomedicine to clinical applications. How to promote commercialized nanomedicine delivery efficiency and antitumor efficacy is a pressing unmet need.

Recently, we rationally combined two FDA approved therapies, HBO therapy and Doxil® for enhanced antitumor efficacy. By overcoming tumor hypoxia, HBO therapy not only promotes Doxil® delivery efficiency but also sensitizes cancer cells to Doxil®, altogether contributing to enhanced antitumor efficacy. In this chapter, we will first summarize HBO therapy concisely and the applications of HBO therapy in three different kinds of cancer therapies, including radiotherapy, photodynamic therapy and chemotherapy, from bench and bedside perspectives. The advantages and limitations of HBO therapy as well as other strategies capable of improving tumor hypoxia will be compared. The combination of HBO therapy with nanomedicine will be discussed in detail. Finally, current challenges and future opportunities on boosting nanomedicine efficacy with HBO therapy will be provided.

2 Hyperbaric Oxygen Therapy

According to Underwater & Hyperbaric Medical Society (UHMS), HBO therapy is defined as intermittent respiration of 100% oxygen at more than one atmospheric pressure, typically in the range of 1.4 to 3 atmosphere absolute (ATA, 1 ATA = 101.32 KPa). HBO therapy can increase oxygen in tissue, reduce edema, activate angiogenesis, and increase collagen synthesis [3]. Therefore, HBO is used as the main treatment for decompression disease (DCS), arterial gas embolism, exceptional blood-loss anemia, and severe carbon monoxide poisoning [18]. Table 1 shows the 13 types of HBO indications approved by UHMS [19].

Table 1 Thirteen UHMS approved indications for HBO

Air or gas embolism
Carbon monoxide poisoning; cyanide poisoning
Clostridial myositis and myonecrosis (gas gangrene)
Crush injury, compartment syndrome, and other acute traumatic ischaemia
Decompression sickness
Enhancement of healing in selected problem wounds
Exceptional blood loss (anemia)
Intracranial abscess
Necrotizing soft tissue infections
Osteomeylitis (refractory)
Skin flaps and grafts (compromised)
Delayed radiation injury (soft tissue and bony necrosis)
Thermal burns

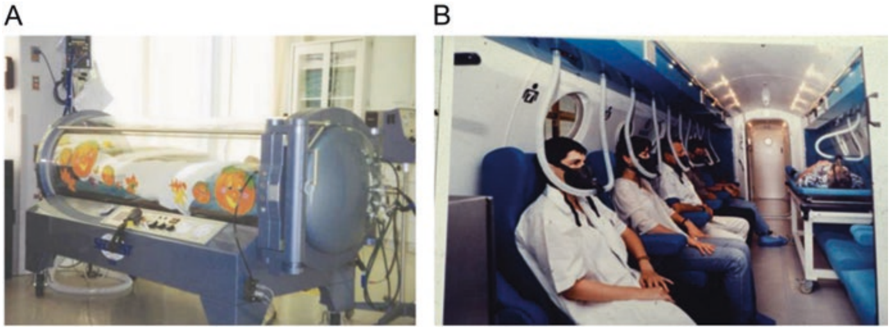

Fig. 1 Hyperbaric chambers. (**a**) Monoplace hyperbaric chamber. (**b**) A multiple walk in hyperbaric chamber. (Reproduced with permission from reference [20, 21], respectively)

Currently, there are numerous ways to perform HBO therapy in clinical settings. Among them, the most commonly used means is hyperbaric chambers, which include monoplace (Fig. 1a) and multiplace chambers (Fig. 1b). Monoplace chambers are normally pressurized with pure (100%) oxygen, while multiplace chambers are usually pressurized with air, with oxygen given via face-mask or endotracheal tube [19]. It is worth noting that fire safety is of utmost importance in these chambers.

2.1 Principle of HBO Therapy

HBO therapy is one of the most effective methods to alleviate tissue hypoxia [2, 3]. The underlying mechanism lies in improving the amount of oxygen dissolved in blood and various tissues by taking pure oxygen at pressures greater than normal atmosphere (1 ATA). Henry's Law states that the number of molecules that will dissolve in a liquid at a given temperature is directly proportional to the partial pressure of that gas. For example, at 37 °C, the amount of oxygen dissolved in the blood is 0.32 vol% when breathing air at normal atmospheric pressure. Administering 100 percent oxygen at sea level (normobaric) pressure increases the amount of oxygen dissolved in the blood 6.53 fold to 2.09 vol%, and at 2 ATA, the dissolved-oxygen content is approximately 4.44 vol%, which is about 14 times the amount of oxygen dissolved in the blood when breathing under normal condition. At this time, the delivery of oxygen in blood is no longer dependent on hemoglobin. HBO therapy not only increases the amount of oxygen dissolved in the blood but also increases the speed and distance of oxygen diffusion from blood vessels to tissues. Fick's first law states that the speed and distance of gas diffusion is directly proportional to the partial pressure of the gas. Under HBO therapy, a large amount of dissolved oxygen in the blood leads to a significant increase in the oxygen partial pressure and the oxygen partial pressure difference between blood vessels and tissues increases, thereby significantly increasing the speed and distance of oxygen diffusion from the blood to tissue. As an example, under the condition of normal atmosphere, the distance of oxygen diffusion in the capillaries of human brain is about 30 μm whereas under the condition of 2 ATA in HBO therapy, the distance of oxygen diffusion can be increased to 100 μm. Therefore, HBO therapy can effectively improve the oxygen partial pressure in tissues, including solid tumors, and alleviate tissue hypoxia.

2.2 Side Effects of HBO Therapy

When used according to standard protocols, with pressures not exceeding 3 ATA and treatment duration limited to a maximum of 120 minutes each time, HBO therapy is safe. However, some adverse effects, such as barotrauma, oxygen poisoning, and decompression [22], may happen during HBO treatment. Barotrauma is caused by pressure imbalance owing to the compression or expansion of closed gas volume, resulting in congestion, edema, and inflammatory response in the compression or decompression process of HBO therapy. Common symptoms in clinic include middle ear barotrauma, inner ear barotrauma, paranasal sinus barotrauma, and pulmonary barotrauma. Such adverse reactions are often caused by the too fast speed of pressure rise and fall or the pathological (such as cold, nasal polyp, etc.) and nonpathological factors (the patient is unable to cooperate with the pressure regulating actions such as swallowing and opening mouth) of patients themselves. These adverse effects can be effectively prevented by consulting and checking the patient's physical conditions in advance and reducing the speed of pressure rise and fall during HBO treatment. Oxygen poisoning refers to the damage of the function and structure of some tissues or organs after the body has inhaled high-concentration oxygen for a certain period of time. Up to now, the mechanism of oxygen poisoning remains elusive, and might be related to oxygen free radicals and enzyme activity in the body. The most sensitive organs to oxygen include brain, lungs, and eyes. Accordingly, oxygen poisoning is usually manifested as convulsion, atelectasis, vision decline, and retinal damage. We can select the patients who are suitable for HBO treatment by oxygen sensitivity test, and strictly control the time of HBO treatment under different pressure conditions or prevent the occurrence of oxygen poisoning by intermittent oxygen inhalation. Decompression sickness is caused by the formation of gas bubbles in the body tissues and blood due to the excessive drop of environmental pressure and the rapid speed of pressure reduction. It is usually nitrogen in the body that forms gas embolism in the process of decompression, resulting in damage to skin, central nervous system, respiratory system, and circulatory system, thus causing adverse reactions. These kinds of situations are often caused by the too fast speed of pressure reduction during HBO treatment and can be solved by slowing down the speed of pressure reduction or carrying out pressure rise treatment again. In other cases, HBO therapy might occasionally cause myopia and cataracts. Overall, HBO treatment is safe when patients are strictly examined and screened and appropriate HBO treatment procedures are established and performed.

2.3 Comparison Between HBO and Other Strategies in Overcoming Tumor Hypoxia

As mentioned above, in addition to HBO therapy, tumor hypoxia can also be alleviated by means of improving intratumor blood flow, delivering oxygen to tumor with carriers, producing oxygen in situ within tumor, and slowing down tumor oxygen consumption. Herein, these five strategies will be compared directly, with the advantages and limitations of each strategy summarized in Table 2.

The most commonly used strategy is to deliver oxygen to tumors via carriers, such as modified hemoglobin (Hb) and perfluorochemicals (PFC). This strategy has been developed by numerous groups and systematically reviewed elsewhere [23]. Nonetheless, this strategy is limited by the available oxygen binding sites within Hb protein or the release of oxygen from PFC to tumor tissue.

Drug molecules, photothermal therapy, or enzymes (such as hyaluronidase, HAase) are used to normalize tumor blood vessels, thereby improving the blood flow in tumor and overcoming tumor hypoxia [23]. For example, Gong et al. demonstrated that HAase could decompose hyaluronic acid, which is the main component of tumor ECM, and increase tumor vascular density and effective vascular area, together resulting in increased tumor perfusion and enhanced therapeutic effect of PDT [7]. This strategy can not only improve the chemotherapy effect by increasing the EPR effect of nanomedicine, but also improve and optimize other types of cancer therapy, such as radiotherapy. However, this strategy is limited by the inherent oxygen binding capacity of Hb in tumor blood vessels. Furthermore, drug molecules, photothermal agents, and enzymes need to accumulate at tumor tissue and reach sufficient concentrations in advance.

In situ production of oxygen within tumor is a strategy to improve tumor hypoxia by catalytic decomposition of endogenous H_2O_2 with MnO_2 or catalase (CAT). As an example, Meng et al. designed a ROS responsive nanoparticle ACF@MnO2, which can react with over-expressed H_2O_2 in tumor tissue, increase oxygen tension, and inhibit HIF-1α, resulting in enhanced therapeutic efficacy in radiotherapy [9]. But this strategy is restrained by the amount of H_2O_2 available in tumor tissue.

Slowing down tumor oxygen consumption is also an effective way to relieve tumor hypoxia. Song et al. developed a Met-HCe6-liposome, in which Met suppressed tumor cell oxygen consumption and therefore improved tumor oxygenation [10]. Nonetheless, this strategy does not increase oxygen content in tumor tissue.

Overall, all these strategies are capable of relieving tumor hypoxia and enhancing various types of cancer therapies, including chemotherapy, PDT, and radiotherapy and have broad applications for the treatment of hypoxic solid tumors. With clear and controllable side effects and contradictions, HBO has more advantages because of its simple operation, low cost and wide clinical applications.

Table 2 Comparison of HBO and other strategies in overcoming hypoxia

Strategy	Principal	Advantages	Limitations	References
HBO therapy	Directly improve oxygen content by physical laws	Easy access Low cost Clinical use	Potential adverse effects	[24, 25]
Delivering oxygen via carriers	Transport oxygen to the tumor site with carriers	Clinical use	Complicated synthesis process	[8, 26]
Improving intratumor blood flow	Normalizing tumor blood vessels with either drug molecules or enzymes	Enhanced EPR effect	Heavily rely on blood vessels	[7, 27]
Producing oxygen in situ	Catalytic decomposition of H_2O_2 to produce O_2 in tumor	Versatile	Limited by H_2O_2	[9, 28]
Decreasing oxygen consumption	Relieve tumor hypoxia by reducing cancer cell oxygen consumption	Simple	Poor efficacy	[10, 29]

2.4 Applications of HBO Therapy in Cancer Therapies

In the early twentieth century, people began to study the relationship between oxygen and cancer radiotherapy. In 1953, Gray et al. confirmed, for the first time, that hypoxia could induce radioresistance and affect the therapeutic effect of radiotherapy [30]. In 1986, HBO was proved to be able to sensitize head and neck tumors to radiotherapy [31]. Since then, increasing attention has been paid to the importance of HBO in cancer therapies, and a large number of studies have utilized HBO as adjuvant therapy for all kinds of malignancies from both bench and bedside applications.

2.4.1 Application of HBO in Radiotherapy

As one of the main treatments, radiotherapy eradicates cancer cells by breaking their DNA double strand with high energy radiation rays. Key to DNA double strand break is the oxidation of DNA radicals induced by radiation while molecular oxygen is indispensable for this oxidation process. Therefore, the sensitivity of cancer cells to radiotherapy is significantly reduced under hypoxic TME.

HBO is the most effective method to solve tissue hypoxia, and it was first used for radiosensitization [32]. HBO has dual functions in cancer radiotherapy. First, it can be used as a radiation sensitizer. Second, it can serve as a therapeutic agent to reduce the damage caused by radiation [33]. As a radiotherapy sensitizer, HBO has improved the therapeutic effect of head and neck tumors, cervical cancer, and glioma to some extent in a series of clinical trials, but the curative effect in the treatment of skin cancer and bladder cancer is unsatisfactory [31, 34]. The results showed that HBO had a better sensitizing effect on radiotherapy when the radiotherapy agent was given with fewer times at a higher dose [34]. As an adjuvant therapy for sensitizing radiotherapy, HBO therapy is usually performed before radiation, and performing radiotherapy 15 minutes after HBO treatment can have a better therapeutic effect and reduce damage to surrounding tissues [35, 36]. In addition to being a radiotherapy sensitizer, HBO can also be used as a therapeutic agent to reduce the damage caused by radiation. Mayer et al. found that HBO treatment can significantly improve urinary and digestive system diseases in patients with prostate cancer after radiotherapy [37]. Feldmeier et al. systematically reviewed 74 studies on the prevention or treatment of radiation-related injuries with HBO. Among them, 67 studies showed that HBO could effectively prevent or cure radiation-induced injuries [38].

2.4.2 Application of HBO in Chemotherapy

Hypoxia was implicated as an important factor in tumor drug resistance and chemotherapy failure [1, 3, 39]. Although the mechanisms of hypoxia-induced drug resistance in tumor cells are related to the types of antitumor agents, in general, hypoxia induces tumor cells to achieve drug resistance through the following mechanisms. First, hypoxia reduces the intracellular concentration of chemotherapy drugs by increasing multidrug resistance protein, or P-Glycoprotein (Pgp), which could pump therapeutic drugs out. Second, hypoxia modulates the metabolic and signaling pathways of tumor cells. Third, hypoxia changes the redox condition of tumor cells. Fourth, hypoxia induces gene instability and mutation in tumor cells.

Using HBO to improve the hypoxic microenvironment of tumor tissues can help chemotherapeutic drugs kill cancer cells more effectively and improve the therapeutic effect of chemotherapy. Ohguri et al. combined HBO with paclitaxel, cisplatin, and hyperthermia for the treatment of non-small cell lung cancers [40]. The results showed that the combined therapy could significantly prolong the survival of patients without severe adverse reactions. Suzuki et al. used cisplatin in combination with HBO for the treatment of gliomas, and found that HBO could significantly increase the average retention time of cisplatin in the brain of cancer patients [41]. In addition to a series of clinical trials, a large number of in vivo and in vitro experiments also confirmed that HBO could indeed increase the therapeutic effect of numerous chemotherapy drugs. Bosco studied the impact of HBO treatment and gemcitabine administration sequence on the killing effect of the PANC-1 cell line in vitro, and demonstrated that simultaneous administration of HBO and chemotherapeutic drugs achieved the highest killing effect than other sequence [42]. Petre et al. studied the killing effect of HBO combined with doxorubicin (DOX) on Mac-2 tumor cell line [43]. The results revealed that the combination killed significantly more tumor cells than that of DOX alone 36 hours post administration. Takiguchi et al. combined HBO with 5-fluorouracil to treat sarcoma [44]. After injection of 5-fluorouracil, HBO treatment was carried out immediately, which together significantly suppressed tumor growth after 17 weeks of successive treatment. Furthermore, it was revealed that the content of 5-fluorouracil in the combination group was significantly higher than that of the control group using 5-fluorouracil alone. In 2009, Moen et al. obtained similar results where the injection of 5-fluorouracil during or immediately after HBO treatment could significantly increase the drug content in tumor tissues [45]. Furthermore, they found that multiple HBO treatments significantly reduced the interstitial fluid pressure and collagen content in tumor tissues of *dimetyl-α-benzantracene* (DMBA) induced breast cancer. Kawasoe et al. utilized HBO as adjuvant therapy in combination with cisplatin for the treatment of osteosarcoma [46]. Their results showed that HBO therapy significantly improved the antitumor effect of low-dose cisplatin, effectively inhibited the growth of tumor and markedly prolonged the survival period of mice. All these results corroborate that HBO has the potential to boost cancer chemotherapy.

2.4.3 Application of HBO in Photodynamic Therapy (PDT)

In cancer PDT, photosensitizers (PS) transfer energy from light to molecular oxygen in TME to form singlet oxygen and other reactive oxygen species (ROS) [47]. Therefore, the antitumor effect of PDT relies on three main parameters: PS, light, and molecular oxygen. As hypoxia is one of the main characteristics of solid tumors [48, 49], and PDT continuously consumes oxygen in tumor tissue, the improvement of the oxygen content in tumor site is a key factor to enhance therapeutic effect of PDT.

HBO therapy, as the most effective way to increase the body's oxygen supply, has therefore been used in combination with PDT to treat tumors for enhanced antitumor efficacy. As early as 1987, Dong et al. utilized HBO to potentiate PDT on transplanted tumor in mice and demonstrated that the combination of HBO and PDT achieved better tumor inhibition than PDT alone [50]. Similar results had been obtained by Robert et al. on fibrosarcoma in mice [51]. In 2001, Tomaselli et al. conducted a clinical trial in 30 lung cancer patients with the combination of HBO and PDT, and their results illustrated that after 1–4 weeks of treatment, the tumor size was significantly reduced and the Karnofsky performance status of patients was significantly improved compared to the group treated with PDT alone [52]. Although the number of patients was small, the combination therapy of HBO and PDT was proved to be safe, efficient and easy to operate. Along the same line, another study in 34 patients with malignant pleura tumor also showed that the combination of HBO and PDT had better antitumor effect than PDT alone [53]. Together, these reports corroborated that the combination therapy of HBO and PDT showed great potential in cancer treatment.

3 Potentiating Nanomedicine Antitumor Efficacy with HBO

Chemotherapy is still one of the three major means of cancer treatments, and nanomedicine plays an increasingly important role in cancer chemotherapy. Doxil® was approved by the FDA in 1995 and became the first chemotherapeutic nanomedicine approved for clinical use. Doxil® is composed of a long circulating liposome and DOX. Because polyethylene glycol (PEG) is coupled on the surface of liposome, the probability of liposome being regulated by protein and engulfed by the reticuloendothelial system (RES) in vivo is reduced and the circulation time of DOX in blood is therefore significantly increased. As the liposome can passively accumulate at tumor tissue through the EPR effect, the content of DOX in the tumor tissue is increased. Correspondingly, the amount of DOX in the normal tissues and organs is decreased, reducing the side effects caused by DOX [54]. Doxil® was approved by the FDA for the treatment of Kaposi's sarcoma, ovarian cancer, and breast cancer in 1995, 1999, and 2003, respectively. In 2007, Europe and Canada granted Doxil® as a combination therapy for multiple myeloma. The approval of Doxil® for cancer treatment aroused great enthusiasm on nanomedicine [55].

However, the clinical efficacy of Doxil® is unsatisfactory. After 10 years since Doxil®'s entry into the market, the US FDA and the European Medicines Evaluation Agency (EMA) investigated the clinical efficacy of Doxil® and found that Doxil® was slightly superior to free DOX in the treatment of Kaposi's sarcoma and ovarian cancer, but exhibited no significant improvement in the treatment of breast cancer and myeloma compared with free DOX. However, all relevant studies corroborated that Doxil® could significantly reduce DOX induced side effects, especially cardiotoxicity. Therefore, Doxil® is only effective in controlling the side effects caused by DOX, but not in improving the antitumor effect. How to improve the clinical antitumor efficacy remains an urgent problem for Doxil®.

Hyperbaric oxygen therapy has already been used in combination with radiotherapy and photodynamic therapy for the clinical combat of hypoxic solid tumors, as it can directly and effectively increase the oxygen content [56, 57]. But HBO therapy is seldom combined with chemotherapeutic agents that kill cancer cells by generating ROS, because HBO may promote the side effects of these chemotherapeutic agents [33]. Accordingly, DOX and HBO are rarely administered at the same time in clinic. Considering Doxil® could significantly reduce DOX induced side effects, we rationally combined two clinical utilized therapies, HBO and Doxil®, hypothesizing enhanced therapeutic efficacy and reduced side effects [58].

Serious side effects prevent the combination of HBO with DOX. Thus, the first in vivo study performed was toxicity test. No obvious damage occurred when HBO therapy was administered alone. For DOX and DOX + HBO, obvious cardiotoxicity was observed. The damage caused by DOX + HBO was more serious than that of DOX to cardiomyocytes. On the contrary, almost no histological damage was detected in the groups of Doxil® and Doxil® + HBO, indicating a decrease in cardiotoxicity. In addition, we also evaluated creatine kinase (CK) activity: the CK value of treatment with DOX alone was significantly higher than that of the control group, confirming its high cardiotoxicity. The CK value of DOX combined with HBO was the highest, which confirmed that HBO exasperated the cardiotoxicity of DOX and supported the absolute contradiction of co-administration of HBO and DOX together. However, no marked difference was observed between the control group

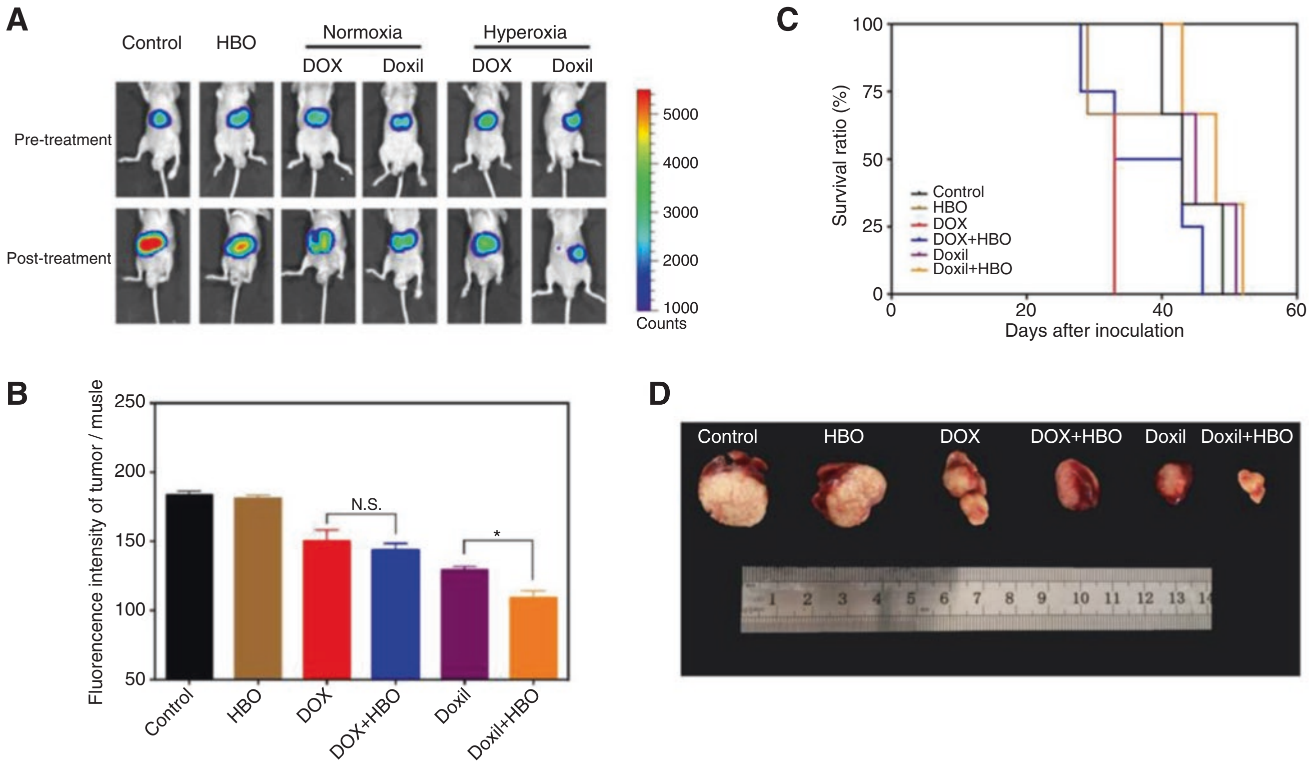

Fig. 2 In vivo antitumor activity of the combination treatment in Luc-Bel7402 orthotopic tumor model. (**a**) Fluorescence imaging of tumor tissue before/after different treatments. (**b**) The ratio of fluorescence intensity of tumor to muscle at the end of the last treatment. (**c**) Survival curve of nude mice in different groups. (**d**) Representative photos of Luc-Bel7402 tumor tissue. Data as mean ± S.E. ($n = 5$). *$P < 0.05$, N.S. represents no significant

and the Doxil® groups (Doxil® and Doxil® + HBO), suggesting that Doxil® could indeed alleviate the side effects of DOX.

After addressing the toxicity issue, we combined HBO with Doxil® and evaluated its antitumor efficacy in orthotopic liver cancer model with the luciferase-transferred cell line Bel7402. The fluorescence in Bel7402 can be easily detected with a live animal imaging system. As shown in Fig. 2a, b, d, the tumors in the combination group (Doxil® + HBO) are the smallest among all the groups. Consequently, Fig. 2c shows that the survival from the combination group is the longest. These results indicate that HBO enhance the antitumor efficacy of Doxil®. Another interesting observation is that HBO selectively benefits the antitumor efficacy of Doxil® but not of free DOX.

It is difficult to monitor the tumor growth in real time in the orthotopic model. Therefore, we performed two in vivo antitumor studies with the combination of HBO and Doxil® on H22 subcutaneous model. The difference in these two models was that tumor volumes in mice were different when the first injection of Doxil® was administrated. One group of mice started with a small initial volume of 80 mm^3 (Fig. 3a, b), whereas the other group began with a relatively bigger initial volume of 150 mm^3 (Fig. 3c, d). Overall, the trends are consistent. HBO boosts the antitumor efficacy of Doxil®. Once again, these two tumor models corroborate that HBO selectively promotes the antitumor efficacy of Doxil® but not of free DOX. It is worth noting that the combination group (HBO + Doxil®) achieves significantly higher tumor inhibition rates for three different models than that of Doxil® alone.

To understand why HBO only benefited the antitumor efficacy of Doxil® but not of free DOX, we performed more studies in terms of pharmacokinetics and pharmacodynamics. We first studied the impact of HBO on tumor hypoxia and Doxil® delivery efficiency. Using a hypoxia-probe, pimonidazole, we evaluated the hypoxic area of tumor tissue after HBO treatment. The hypoxic area stained by pimonidazole significantly decreased by 90% after a single HBO treatment. We further measured the amount of two critical parameters in tissue hypoxia and tumor microenvironment, HIF-1α and vascular endothelial growth factor (VEGF), so as to confirm that alleviation of hypoxic TME could indeed produce an evident effect. The expression of HIF-1 α and VEGF in the HBO group decreased significantly compared with those in the control group. Consistent results were also obtained in western blot assay. Taken together, these aforementioned studies

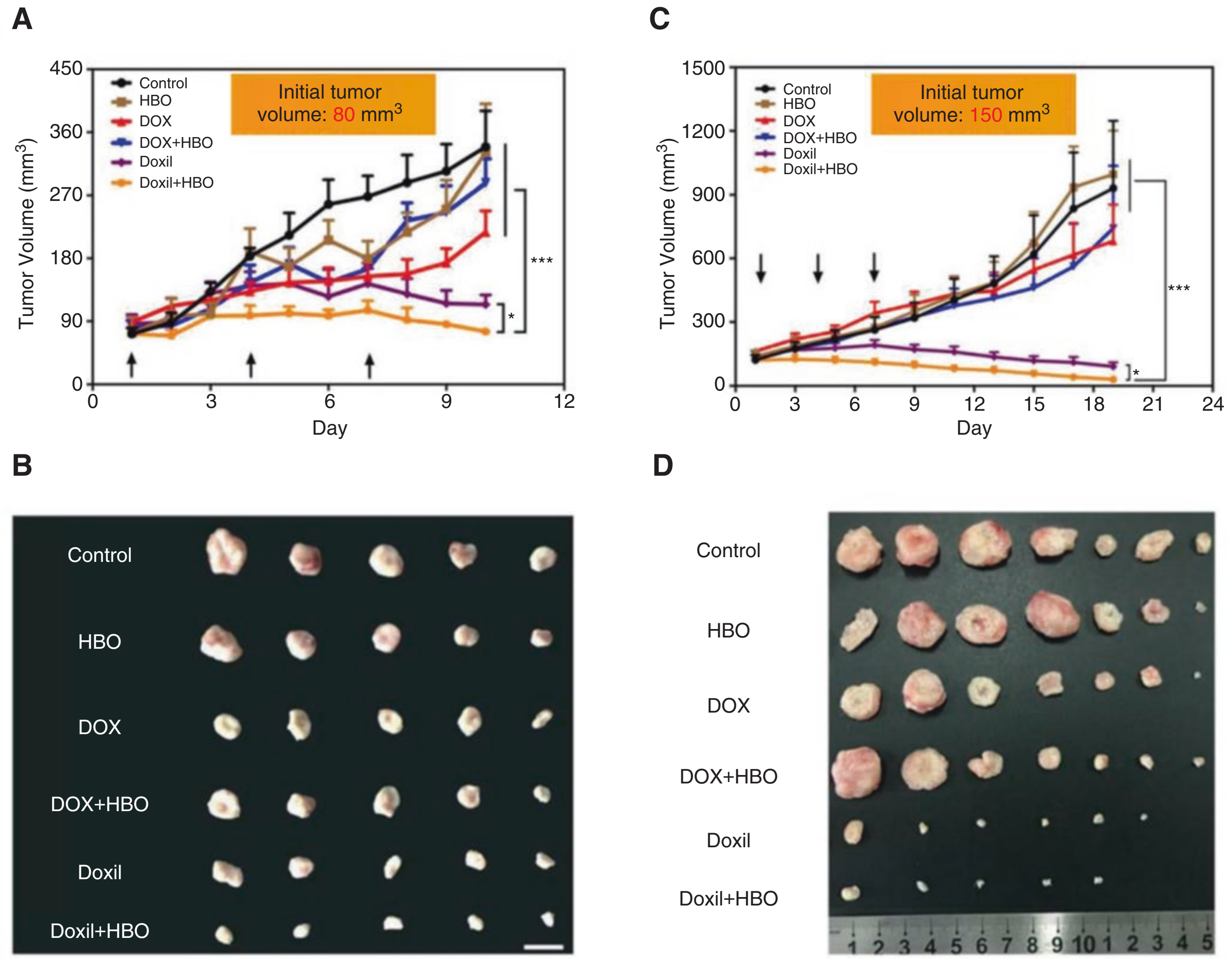

Fig. 3 In vivo antitumor activity of the combination treatment in H22 subcutaneous tumor model. (**a**) Tumor growth curves of H22-bearing mice after different treatments (initial tumor volume of 80 mm^3). (**b**) Representative photos of tumor tissues from different groups at the end of (**a**) ($n = 5$). (**c**) Tumor growth curves of H22-bearing mice after different treatments (initial tumor volume of 150 mm^3). (**d**) Representative photos of tumor tissue from different groups at the end of (**c**) ($n = 7$). Data as mean ± S.E. $*P < 0.05$, $**P < 0.01$, $***P < 0.001$, N.S. represents no significant

support that HBO modulates TME by effectively overcoming tumor hypoxia. Furthermore, HIF-1α mediates the expression of connective tissue growth factor (CTGF), which is the upstream factor mediating the deposition of collagen I. We studied the impact of HBO on CTGF and collagen I. A significant down-regulation of transcription and translation for both CTGF and collagen I after HBO therapy was clearly seen. As collagen I is the main component of fibril in tumor ECM, we further revealed that the deposition of fibers decreased after the HBO treatment (Fig. 4a, b). We hypothesized that decreased deposition of collagen I in ECM would promote the accumulation and deep penetration of Doxil® in tumor tissue. Therefore, we studied the tumor penetration of each group. The fluorescence intensity within the Doxil® + HBO group was significantly higher than that of any other group. It was worth noting that most of the red fluorescence (DOX) in the groups of DOX, DOX + HBO, and Doxil® was co-localized with the green fluorescence of the blood vessel, indicating their poor drug penetration. In stark contrast, the red fluorescence was well dispersed throughout the tumor section in the Doxil® + HBO group. Then, the simulated scatter diagrams were used to calculate the penetration distances based on five confocal images. Doxil® + HBO exhibited the highest penetration distance (Fig. 4c). We also noticed that DOX had a close penetration distance with or without HBO; whereas, Doxil® had a much deeper penetration distance with HBO than that without HBO. Once again, this result indicates that HBO enhances the penetration of Doxil® rather than of free DOX in the tumor site. We further quantified the amount of DOX in tumor tissue (Fig. 4d). Due

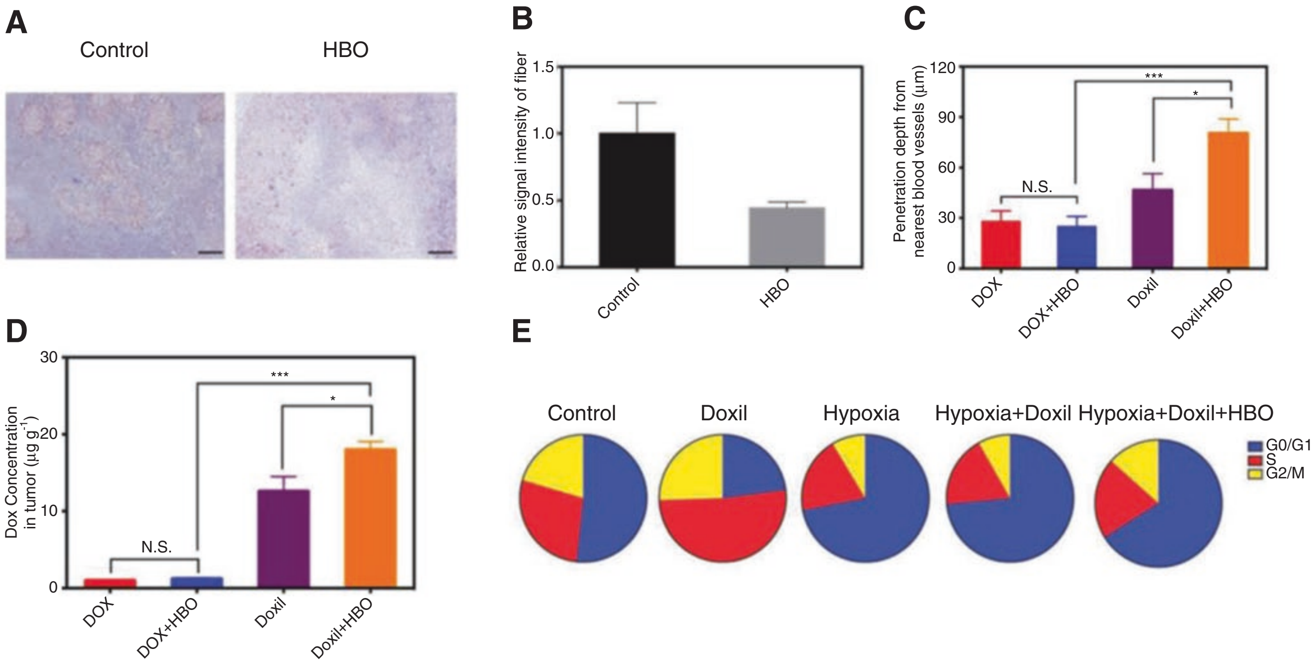

Fig. 4 The combination treatment improved the penetration of the Doxil® by reducing the deposition of collagen and sensitized tumor cells to Doxil® by regulating cell cycle arrest. (**a**) Masson staining of tumor tissue. (**b**) Semi-quantitative analysis of (**a**) (*n* = 5). (**c**) The tumor penetration distance of DOX from the nearest blood vessel was determined with the simulated scatter diagrams method. (**d**) The concentration of DOX in tumor tissue in H22-bearing mice after intravenous injection of free DOX, Doxil® at DOX dosage of 7 mg/kg with and without HBO therapy for 24 h (*n* = 5). (**e**) In vitro cell cycle analysis (*n* = 3). Data as mean ± S.E. $*P < 0.05$, $***P < 0.001$. N.S. as not significant. (Adopted and revised with permission from reference [58])

to its optimum penetration, the Doxil® + HBO group achieves the highest DOX concentration in tumor tissue. Combined with HBO, the concentration of DOX in the HBO + Doxil® group increased by 40% compared with Doxil® whereas HBO had little effect on DOX. Our results reveal that HBO treatment is beneficial for Doxil® in terms of tumor penetration and accumulation but not for free DOX. This could probably be involved in the reason that the circulation time of free DOX is not long enough. DOX has a half-life time $t_{1/2}$ of 8 hours, whereas Doxil® can circulate for 45 hours [59]. Because of its small molecular weight, free DOX is rapidly eliminated after entering blood circulation in vivo. In addition, although HBO treatment decreases tumor fibril deposition, free DOX could not accumulate sufficiently in tumor tissue. Being a small molecular chemotherapeutic drug, DOX is easily drained out from tumor tissue and has a low chance of tumor extravasation, penetration, and accumulation. In contrast, Doxil®, a nanomedicine with a size of around 80 nm, can retain in tumor parenchyma through EPR effect. In this case, the efficacy of HBO-assisted combination therapy with nanomedicine is better than that with small-molecule chemotherapeutic drugs. However, more researches are needed to support this conclusion.

Since most chemotherapeutic agents mainly produce a significant effect on fast growing cells, hypoxia-induced cell cycle arrest makes cancer cells insensitive to these drugs [60, 61]. We revealed the impact of HBO on cell cycle and found that the percentage of cells in the G0/G1 phase decreased from 76% to 73% after HBO treatment. Although it was only 3% decrease, it still constituted a significant difference. Our results implicate that HBO therapy would enhance the sensitivity of cancer cells toward chemotherapeutic drugs by overcoming hypoxia-induced cell cycle arrest in vivo. Cell line was studied under different conditions in vitro to mimic in vivo hypoxic tumor and to better understand the effect of HBO therapy on cell cycle (Fig. 4e). Compared to the control, more cancer cells were arrested in the G0/G1 phase due to hypoxia. Because of this cell cycle arrest, cells were insensitive to Doxil® in hypoxic condition. Compared with 73% of cells arrested in the G0/G1 phase in the hypoxia+Doxil® group, only about 66% cells were trapped after HBO treatment, suggesting that HBO treatment “awakens” some 7% cells. This difference supports that HBO therapy renders tumor cells more sensitive to Doxil® by conquering hypoxia-induced phase arrest. Another important reason for cancer cells insensitivity to chemotherapy is insufficient drug accumulation within cancer cells. The intracellular drug content under different conditions was therefore quantified by flow cytometry. Cells under hypoxia took less but secreted more DOX than the cells under normal condition. As a result, a lower intracellular DOX concentration was detected under hypoxia.

In summary, we rationally combined two FDA approved therapies, HBO and Doxil®, for the first time to treat hypoxic

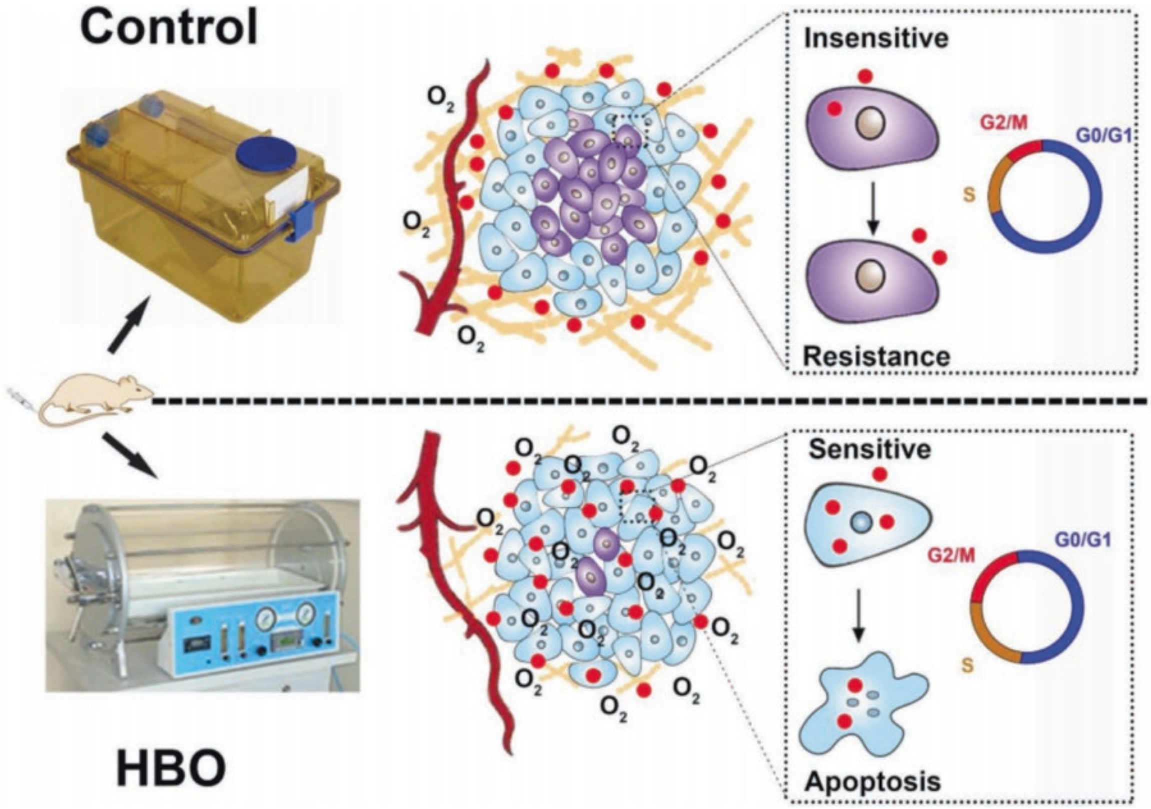

Scheme 1 Schematic illustration of combination therapy based on HBO and Doxil®. By mitigating tumor hypoxia, HBO decreases collagen content, resulting in the enhanced penetration of Doxil® into the tumor. HBO also notably interrupts cancerous cell cycle arrest, rendering cancer cells more sensitive to Doxil®. (Reproduced with permission from reference [58])

hepatocellular carcinoma. By overcoming tumor hypoxia, HBO potentiated Doxil® antitumor efficacy. In detail, HBO overcame hypoxia, resulting in down-regulation of HIF-1α/CTGF/Collagen I and promoted Doxil® delivery efficiency, and in the meantime, escape of cell cycle arrest and enhanced intracellular DOX concentration (Scheme 1). Collectively, these properties contributed to enhanced antitumor efficacy of Doxil®.

As HBO could decrease the collage in tumor ECM, we wondered if HBO would increase tumor metastasis. To address this concern, we first studied tumor metastasis in vitro with transwell assay. Our results indicated that HBO would not increase cancer cell invasion potential, and instead HBO would suppress tumor migration. We further performed the experiment in in vivo settings in mice. After 10 HBO therapies, no significant promotion of metastasis could be observed (Fig. 5). Therefore, HBO would not accelerate tumor metastasis.

Besides, we also investigated the impact of HBO on tumor cell proliferation. Our data showed that HBO did not facilitate tumor cell proliferation. Actually, HBO suppressed the growth of all cells. We further investigated the impact of HBO on tumor stemness by culturing tumor cells in fibrin gels. The results presented in Fig. 6 demonstrated that HBO did not enhance the stemness of tumor cells. Indeed, HBO suppressed the stemness of tumor cells, including HepG-2, MCF-7, and H22 cells.

Collectively, the results from tumor metastasis (Fig. 5), proliferation, and stemness (Fig. 6) corroborated that HBO was safe for cancer treatment. Inspired by these data, we further combined HBO with home-made nanomedicine for enhanced cancer chemotherapy, photodynamic therapy, and photothermal therapy, respectively. All our results confirmed that HBO enhanced the antitumor efficacy of nanomedicine-mediated chemotherapy, photodynamic therapy, and photothermal therapy.

Temozolomide (TMZ) is the first choice for the treatment of gliomas [62]. However, because of the severe toxicity, the dosage in clinic is strictly controlled, leading to insufficient curative effect and poor prognosis [63]. Considering that porous silicon nanoparticles (PSi NPs) have adjustable pore size, large drug loading capacity, autofluorescence property, and favorable biocompatibility [64, 65], we prepared TMZ loaded porous silicon nanoparticles (TMZ/PSi NPs) and combined with HBO for gliomas treatment [66]. We revealed that HBO enhanced C6 cell sensitivity to TMZ and TMZ/PSi NPs by inducing cell cycle arrest in the G2/M phase. Importantly, the combination treatment group (TMZ/

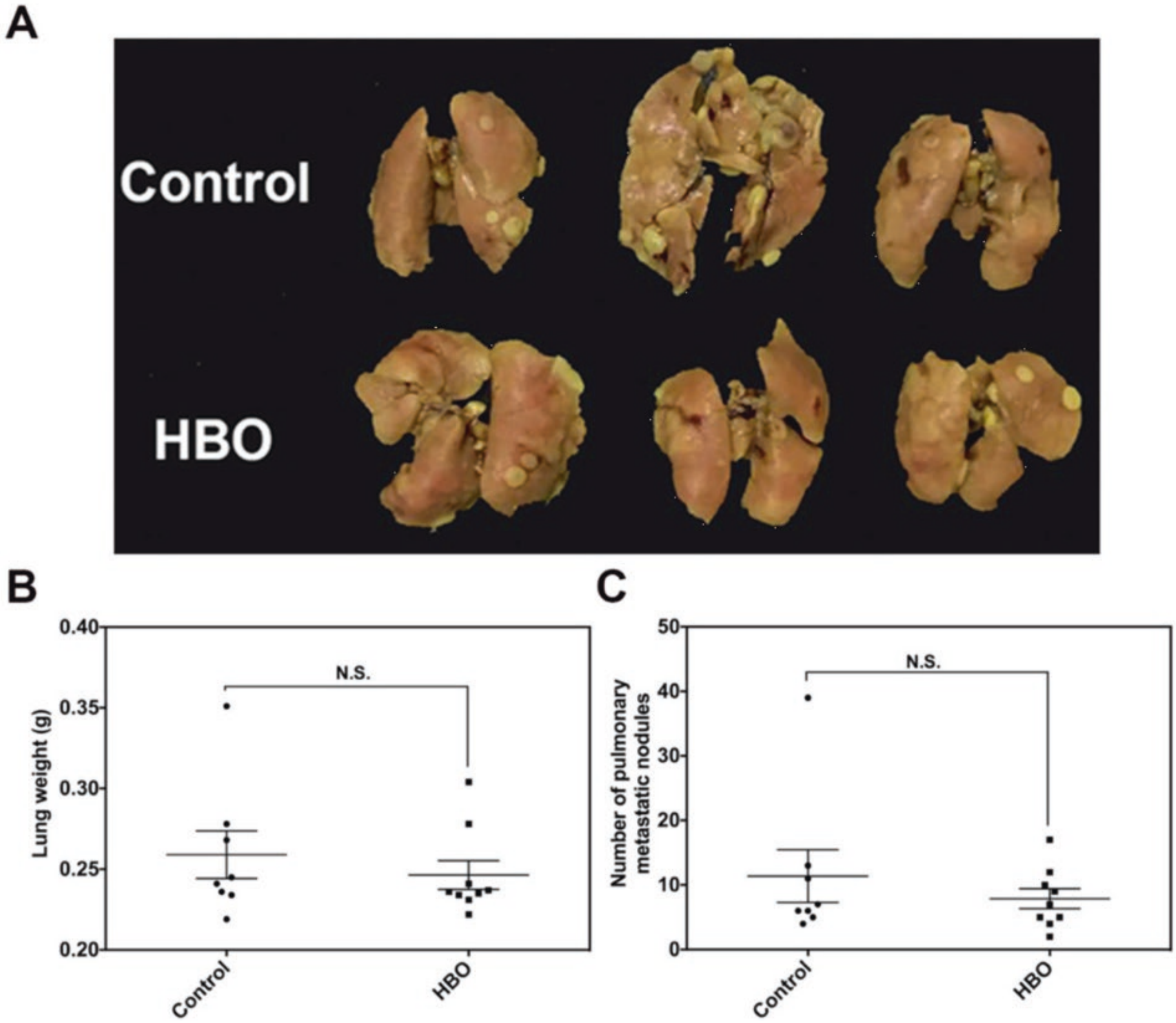

Fig. 5 The impact of HBO on tumor metastasis with a 4 T1 tumor model. (**a**) Representative pictures of lung tissues after treatment, the yellow dots represent metastatic nodules. (**b**) Lung weight after treatment. (**c**) The number of pulmonary metastatic nodules. Data as mean ± S.E. (*n* = 9). N.S. represents not significant

PSi + HBO) achieved the highest tumor inhibition rate (84.2%) among all groups, Fig. 7. Nonetheless, free TMZ group was missing in in vivo antitumor effect evaluation, making it impossible to assess the impact of HBO on free TMZ. It is therefore unclear if HBO selectively boosts antitumor efficacy of TMZ/PSi NPs in gliomas or not.

PDT achieves modest efficacy for the treatment of deep tumors because of hypoxic TME and limited penetration of PS to cancer cells distant from blood vessels. To tackle these issues, we proposed a therapeutic strategy that combined HBO with upconversion nanophotosensitizers (UNPSs) to remodel ECM for enhanced PDT [67] (Scheme 2). The UNPSs were designed to have a Nd3 + −sensitized sandwiched structure, wherein upconversion nanoparticles (UCNPs) served as light transducers to transfer energy from light to the neighboring PS, Rose Bengal (RB), to produce ROS. With HBO, the photodynamic process can generate abundant ROS in hypoxic 4 T1 tumor. We revealed for the first time that HBO-assisted PDT depleted collagen in ECM and thus facilitated the diffusion of oxygen and penetration of UNPSs into the tumor core. Such a synergistic effect ultimately resulted in a significantly enhanced therapeutic efficacy at a low laser power density as compared with that using UNPSs alone, Fig. 8.

Differently from the previous study, in which the deposition of collagen I was inhibited by HBO via the pathway of HIF-1α/CTGF/Collagen I, collagen I was decomposed by PDT generated ROS. Quantitative analysis of the average fluorescence degree of the collagen content in tumor slices revealed that the collagen in UNPSs+NIR + HBO treated group was 14.6, 9.9, and 4.2 times less than PBS, UNPSs+NIR, and HBO groups, respectively. By means of

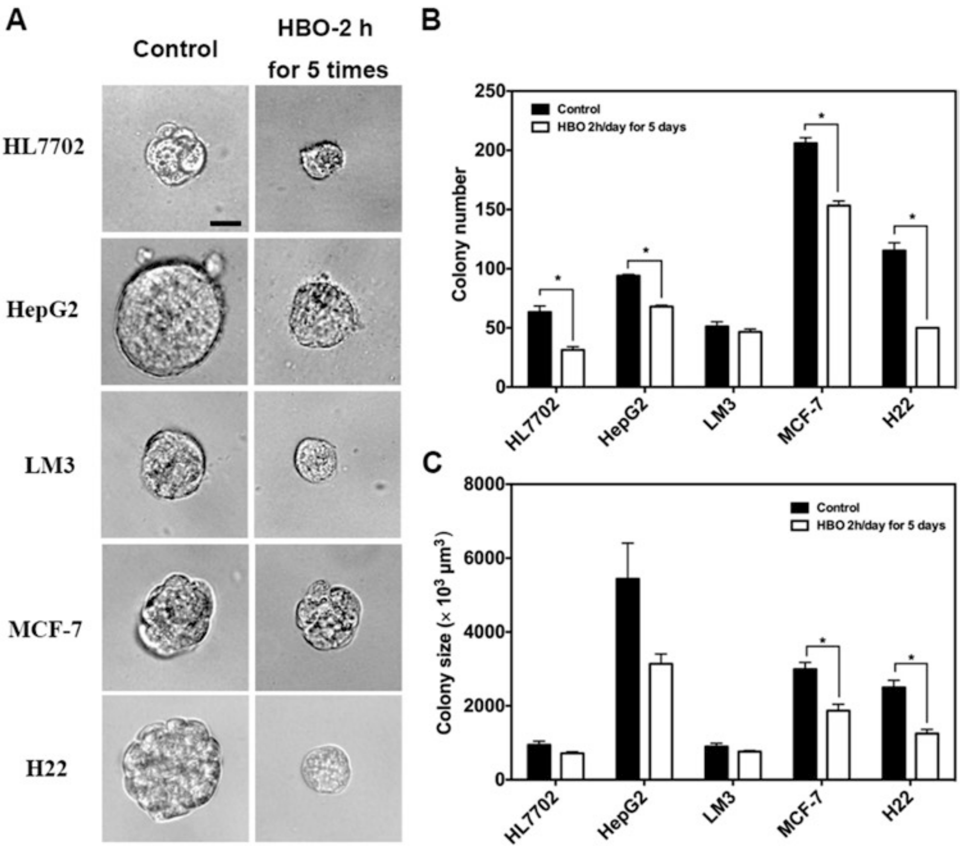

Fig. 6 The effects of HBO treatment on stemness of different tumor cells. (**a**) Pictures of cell colony in Fibrin gels after HBO treatment. The scale bar was 20 μm for all pictures; (**b**) Colony number of different tumor cells in Fibrin gel; (**c**) Colony size of different tumor cells in Fibrin gel. Data as mean ± S.E. (*n* = 5). $*P < 0.05$

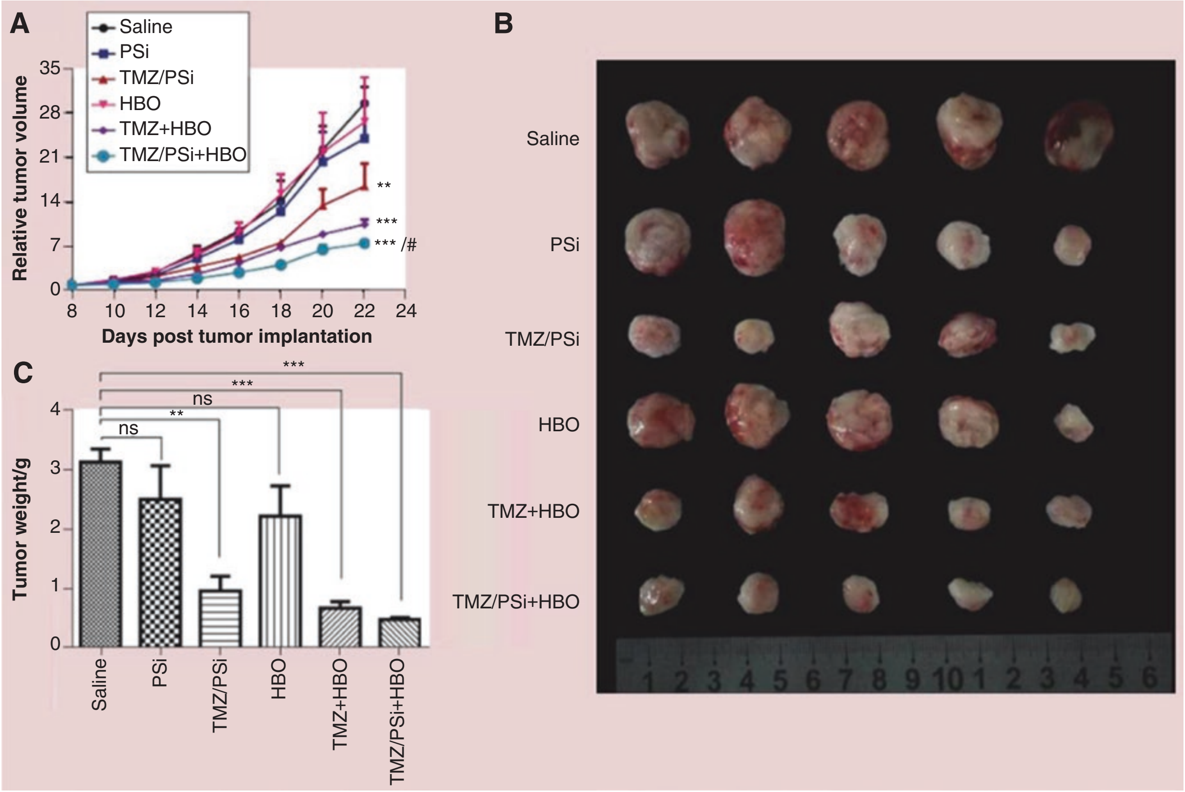

Fig. 7 Antitumor effect of the combination treatment of TMZ/PSi NPs and HBO. (**a**) Changes of tumor volume after treatments. (**b**) Tumors from mice after different treatments. (**c**) Tumor weight. *n* = 5. $**p < 0.01$; $***p < 0.001$; $\#p < 0.05$. N.S. represents no significant. (Reproduced with permission from reference [66])

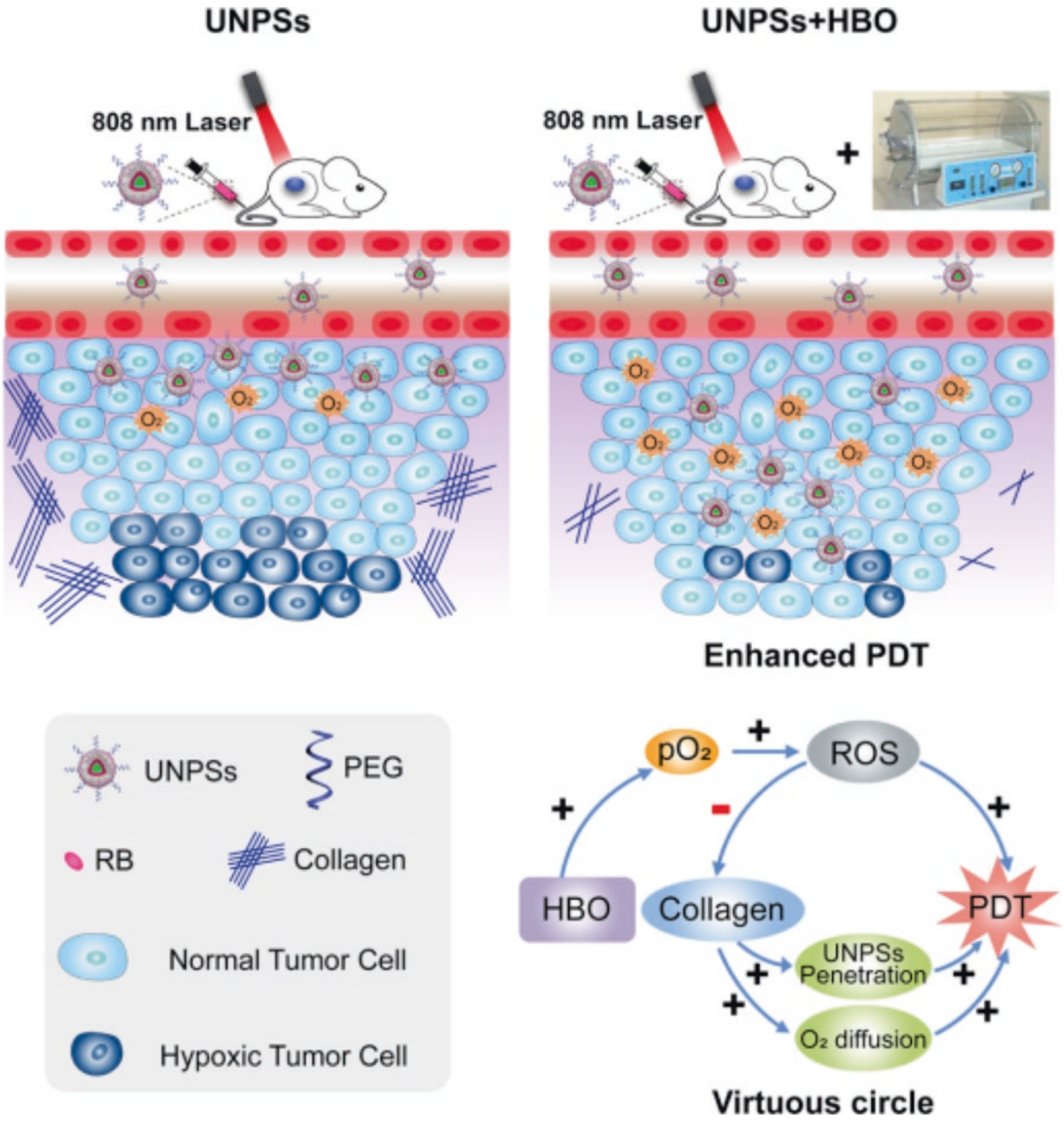

Scheme 2 Schematic illustration of synergizing UNPSs with HBO for depleting collagen in ECM to achieve better oxygenation and deeper penetration of nano-PSs, together contributing to the enhanced PDT antitumor efficacy. (Reproduced with permission from reference [67])

sirius red staining to quantify the [Gly-X-Y] tripeptide helical structure on collagen fibril, we further corroborated that the combination group (UNPSs+NIR + HBO) could reduce the collagen I amount to 35%, whereas the control group (UNPSs+NIR) only decreased it to 83%. The remodeled ECM resulted in deeper penetration of both UNPSs and molecular oxygen, altogether contributing to enhanced PDT.

Our two studies support the hypothesis that HBO decomposed collagen I in cancer treatment. By stark contrast, HBO accelerated collagen synthesis and therefore promoted wound healing [68]. At first sight, these two conclusions seemed to contradict each other. In cancer chemotherapy, HBO overcame tumor hypoxia, interrupted the pathway of HIF-1α/CTGF/Collagen I and ultimately decreased collagen fibril deposition [58]. In PDT, HBO overcame hypoxia and facilitated the formation of ROS, which broke down collagen fibril in the ECM [67]. In ischemic wounds, fibroblast proliferation and collagen synthesis could not proceed effectively without sufficient oxygen [68]. HBO improved hypoxia in wounds and the raised oxygen tension resulted in enhanced fibroblast activity and collagen synthesis [69]. In essence, the fibroblasts in hypoxic TME are markedly different from those in ischemic wounds. For this reason, HBO has played distinctive roles in these different situations, and these results do not conflict each other. Both results are reasonable in different contexts.

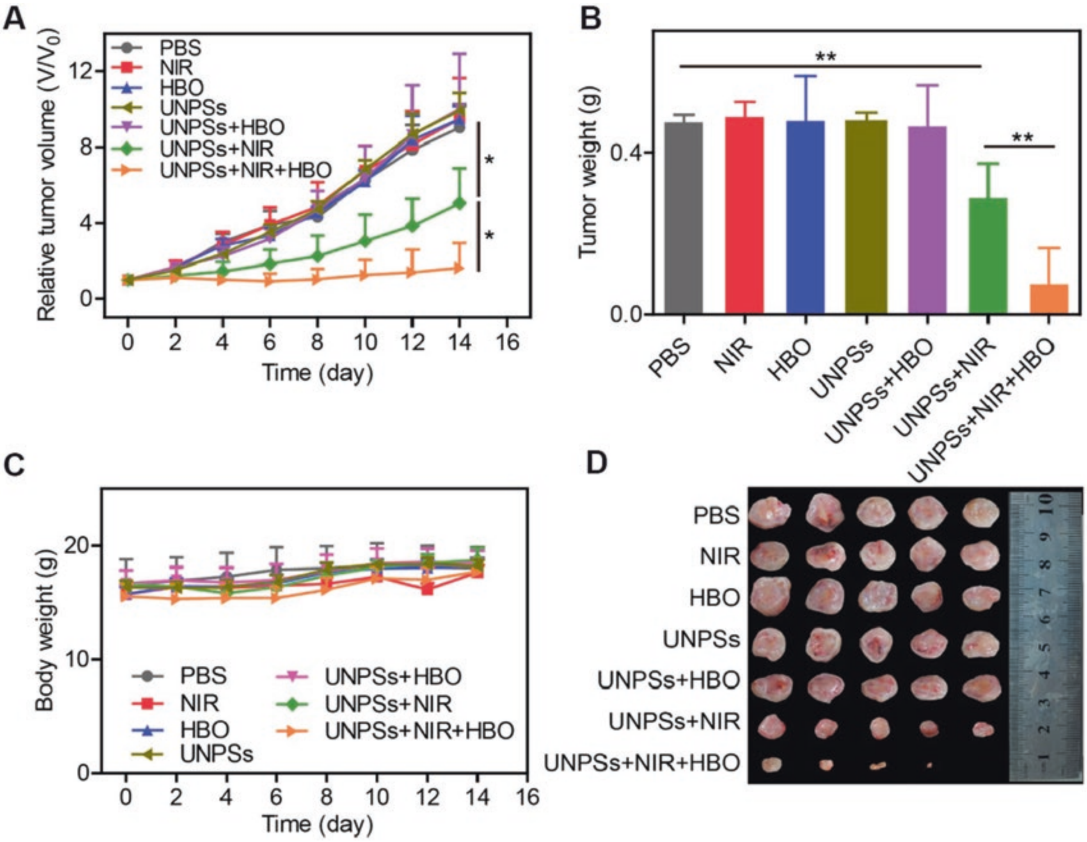

Fig. 8 In vivo PDT evaluation on 4 T1 breast cancer bearing mice. (**a**) Changes of relative tumor growth curves upon different treatments. (**b**) Average weight of excised tumor after different treatments. (**c**) Changing curves of mice body weight upon different treatments. (**d**) Picture of tumors obtained from each group of mice 2 weeks after treatments started. The data were shown as mean ± S.D. ($n = 5$). *$P < 0.05$. **$P < 0.01$. (Reproduced with permission from reference [67])

Extensive evidence suggested that hypoxia played a pivotal role in the formation of cancer stem cells (CSCs), which can lead to drug resistance, tumor recurrence, and poor prognosis [70, 71]. Mild thermal therapy (40–44 °C) could enhance the therapeutic effect of drugs and reduce the killing of normal cells [72]. Hence, we leveraged TMZ/PSi NPs as photothermo−/chemo- therapeutic agent and combined with HBO therapy for elimination of glioma stem cells (GSCs) and inhibition of glioma growth [73] (Scheme 3). By means of spherical colony formation assay, we revealed that combined therapy (TMZ/PSi + PTT + HBO) could effectively inhibit GSCs self-renewal completely compared to TMZ alone (Fig. 9a, b). We further studied specific markers for the self-renewal and stemness maintenance of GSCs (SOX2, Nestin) and hypoxia related molecules HIF-1 and VEGF and revealed that the expression of these four factors decreased in both NCH-421 K and C6 cells after the combined treatment. We also studied the antitumor effect of TMZ/PSi NPs in combination with PTT and HBO in vivo and demonstrated that the combined treatment group (TMZ/PSi + PTT + HBO) achieved the best antitumor effect. Importantly, we studied the expression of tumor stem cell markers in vivo. The expression of SOX2, Nestin, HIF-1α and VEGF decreased consistently after TMZ/PSi NPs combined with PTT and HBO (Fig. 9c). However, several critical control groups are not included in this study, making it impossible to evaluate the contribution from photothermal therapy and HBO therapy on the inhibition of GSCs.

4 Summary and Perspectives

While dozens of nanotherapeutics, such as Doxil®, Oncaspar®, DaunoXome®, and Abraxane®, have been approved by the FDA, their antitumor efficacy in clinical settings is unsatisfactory. Therefore, improving the clinical efficacy of these nanomedicines is of utmost significance. In this chapter, we summarized some of our preliminary results on boosting the nanomedicine efficacy with HBO. In detail, our results demonstrated that HBO promoted tumor inhibition rates of Doxil®, UNPSs, and TMZ/PSi NPs. Despite some progress that has been made on leveraging HBO for enhanced

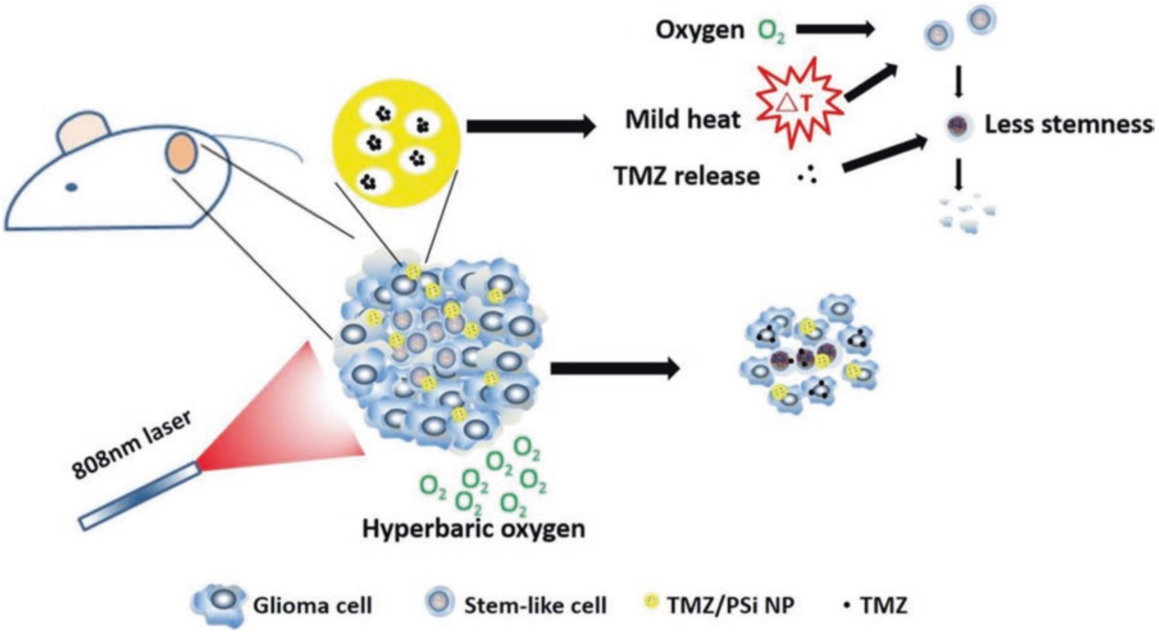

Scheme 3 Scheme of TMZ/PSi nanomedicine combined with mild photothermal therapy and hyperbaric oxygen for treatment of glioma. The mice bearing tumor were intratumor injected with TMZ/PSi NPs followed with PTT and HBO treatments. The combination treatment reduced the stemness and enhanced the sensitivity of glioma tumor cells to TMZ. (Reproduced with permission from reference [73])

therapeutic effect of nanomedicine, there are numerous fundamental challenges and opportunities ahead.

First, the universality of boosting commercialized nanomedicine with HBO needs to be further expanded. The finding that HBO can improve the Doxil® delivery efficiency and antitumor efficacy has significant implications on other commercialized nanomedicine, including Oncaspar®, DaunoXome®, and Abraxane®. However, it is not clear whether other chemotherapeutic nanomedicines also benefit from this combination therapy strategy. Despite HBO promoting the antitumor efficacy of home-made nanotherapeutics, UNPSs, and TMZ/PSi NPs, for photodynamic therapy, chemotherapy, and photothermal therapy, respectively, these nanomedicines are distinctively different from commercialized nanomedicine. Based on the mechanistic studies we performed on the combination of HBO and Doxil®, HBO not only promoted Doxil® tumor penetration and accumulation via decreasing the collagen deposition at the tumor ECM but also sensitized tumor cells to Doxil®, altogether contributing to the enhanced antitumor efficacy. It is worthy to combine HBO with other commercialized nanomedicine, Oncaspar®, DaunoXome®, and Abraxane® and evaluate the antitumor efficacy on versatile hypoxic solid tumors, including breast cancer and pancreatic cancer.

Second, the mechanisms by which HBO sensitizes Doxil® await further investigation. All previous studies involved with HBO for cancer therapy focused solely on oxygen and hypoxic TME. In addition to raised oxygen content, however, HBO exerts another very important impact, which is pressure, typically in the range of 1.4 to 3 ATA. Recently, it was revealed that physical forces exerted a significant influence on tumor immune microenvironment, tumor progression and metastasis, and tumor therapy [74]. Whether elevated pressures exert a beneficial or detrimental effect on Doxil® and other nanomedicine alike is still an open question. To answer this question, more systematic studies, based on the combination of normobaric oxygen or compressed air with Doxil®, are needed.

Third, key to the combination therapy is the clinical efficacy of HBO + Doxil®. While both HBO and Doxil® are approved by the FDA and routinely used in widespread clinics and practices, the clinical translation of their combination is impeded by several concerns. The safety is the most concerning issue. While the combination therapy (HBO + Doxil®) exhibited negligible side effects, the results were obtained in tumor bearing and normal mice. Murine models are incline to underestimate toxicity associated with chemotherapeutic drugs. In particular, HBO increases oxygen tension and generates more ROS nonspecifically through the entire body. HBO might thus exasperate the toxicity in Doxil® in clinics. Another hurdle is the selection of tumor type. In our preliminary study, the combination of HBO and Doxil® achieved enhanced antitumor efficacy on two different hepatocellular carcinoma models, human Bel7402 and murine H22. However, Doxil® has not been approved for liver cancer. Whether the combination therapy could achieve similar

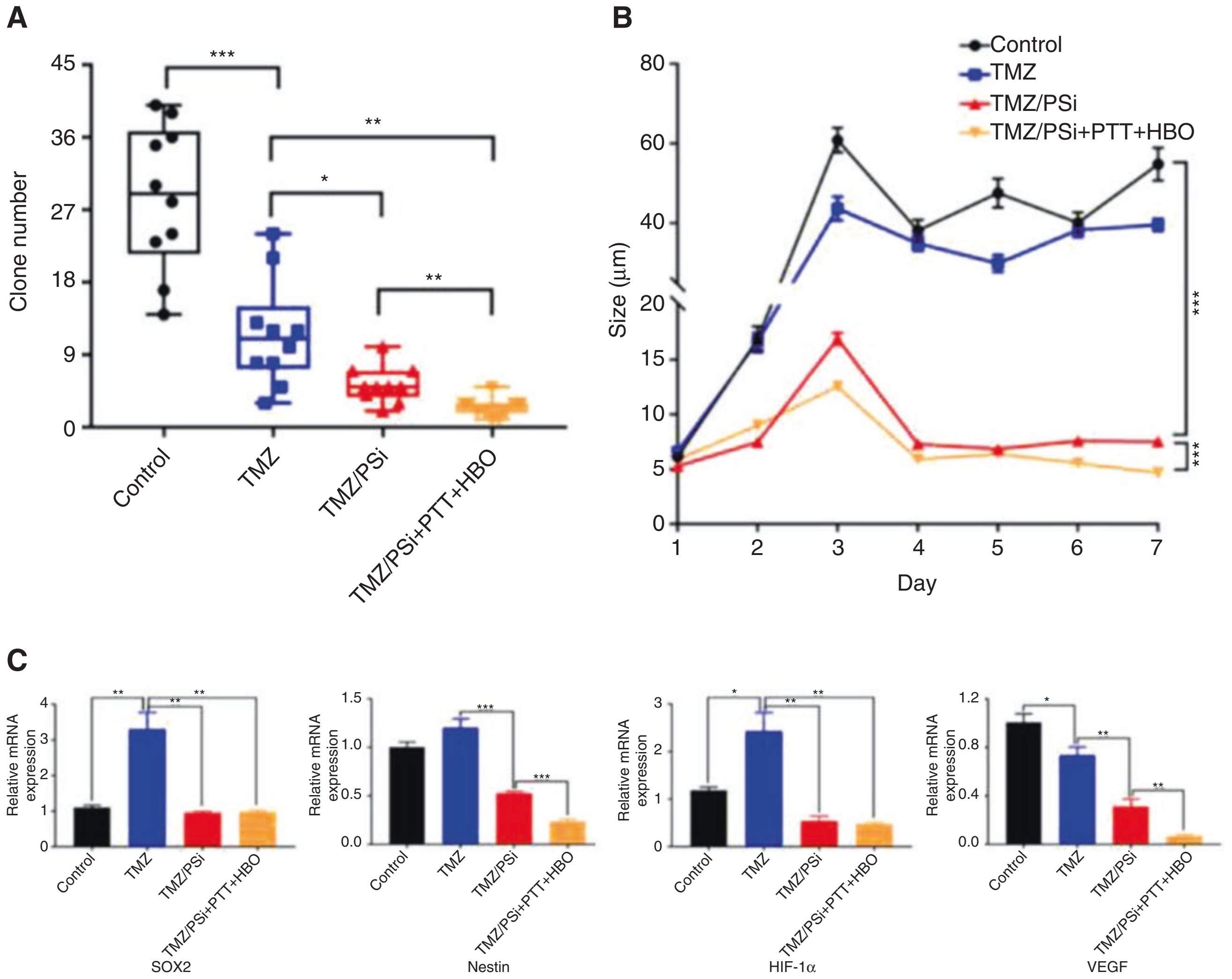

Fig. 9 TMZ/PSi nanomedicine combined with mild photothermal therapy and HBO therapy for treatment of GSCs. (**a**) NCH-421 K cell clone number after different treatments on day 7 ($n = 10$; $^{*}P < 0.05$, $^{**}P < 0.01$, $^{***}P < 0.001$). (**b**) NCH-421 K sphere size in 1 week after different treatments ($n = 4$; $^{***}P < 0.001$). (**c**) mRNA changes of SOX2, Nestin, HIF-1α and VEGF in C6 tumor tissues after combination treatment ($n = 3$; $^{*}P < 0.05$, $^{**}P < 0.01$, $^{***}P < 0.001$). (Reproduced with permission from reference [73])

results in breast cancer is unclear. Different tumors have distinctive pathophysiological features. To initiate a clinical trial on the combination therapy of HBO and Doxil®, the toxicity profile in advanced animal models and the antitumor efficacy on the breast cancer model are essential prerequisites.

Fourth, could HBO boost cancer immune therapies? Hypoxia itself promotes immunosuppressive microenvironment, inhibits immune response, and reduces the activity of effector immune cells, including T cells and NK cells [75]. By overcoming tumor hypoxia, can HBO enhance PD-1 and PD-L1 antibodies-mediated immune therapy? In essence, these antibodies are biomacromolecules with nanometer-scale size. Could HBO promote the delivery of such antibodies? In addition, for chimeric antigen receptor (CAR) T-cell therapy, the difficulty in T-cell infiltration is the key to limit its clinical therapeutic effect on solid tumors [76]. Could HBO promote T cells to enter the tumor core, improve T-cell survival, and boost tumor killing activity? Addressing these questions have significant implications on cancer immune therapies.

Finally, most of the current nanomedicine is developed for the treatment of cancers. Could the combination of HBO and nanomedicine be used for the treatment of other diseases, such as ulcerative colitis? Clinical trials demonstrated that HBO could significantly improve the symptoms of ulcerative colitis [77] while nanomedicine had been used to cure ulcerative colitis with high malignancy [78, 79]. It is tempting to propose that HBO would boost the therapeutic effect of nanomedicine in ulcerative colitis.

Acknowledgments This work was financially supported by grants from the National key research and development program of China (2018YFA0208900), the National Natural Science Foundation of China (31972927, 31700867, and 81627901), the Scientific Research Foundation of Huazhong University of Science and Technology (3004170130), and the Program for HUST Academic Frontier Youth Team (2018QYTD01).

References

1. Al-Waili, N. S., Butler, G. J., Beale, J., Hamilton, R. W., Lee, B. Y., & Lucas, P. (2005). Hyperbaric oxygen and malignancies: A potential role in radiotherapy, chemotherapy, tumor surgery and phototherapy. *Medical Science Monitor, 11*, RA279–RA289.
2. Daruwalla, J., & Christophi, C. (2006). Hyperbaric oxygen therapy for malignancy: A review. *World Journal of Surgery, 30*, 2112–2131.
3. Moen, I., & Stuhr, L. E. B. (2012). Hyperbaric oxygen therapy and cancer – A review. *Targeted Oncology, 7*, 233–242.
4. Shannon, A. M., Bouchier-Hayes, D. J., Condron, C. M., & Toomey, D. (2003). Tumour hypoxia, chemotherapeutic resistance and hypoxia-related therapies. *Cancer Treatment Reviews, 29*, 297–307.
5. Rankin, E. B., & Giaccia, A. J. (2008). The role of hypoxia-inducible factors in tumorigenesis. *Cell Death and Differentiation, 15*, 678–685.
6. Bertout, J. A., Patel, S. A., & Simon, M. C. (2008). The impact of O2 availability on human cancer. *Nature Reviews Cancer, 8*, 967–975.
7. Gong, H., Chao, Y., Xiang, J., Han, X., Song, G., Feng, L., Liu, J., Yang, G., Chen, Q., & Liu, Z. (2016). Hyaluronidase to enhance nanoparticle-based photodynamic tumor therapy. *Nano Letters, 16*, 2512–2521.
8. Song, X., Feng, L., Liang, C., Yang, K., & Liu, Z. (2016). Ultrasound triggered tumor oxygenation with oxygen-shuttle nanoperfluorocarbon to overcome hypoxia-associated resistance in cancer therapies. *Nano Letters, 16*, 6145–6153.
9. Meng, L., Cheng, Y., Tong, X., Gan, S., Ding, Y., Zhang, Y., Wang, C., Xu, L., Zhu, Y., Wu, J., Hu, Y., & Yuan, A. (2018). Tumor oxygenation and hypoxia inducible factor-1 functional inhibition via a reactive oxygen species responsive nanoplatform for enhancing radiation therapy and abscopal effects. *ACS Nano, 12*, 8308–8322.
10. Song, X., Feng, L., Liang, C., Gao, M., Song, G., & Liu, Z. (2016). Liposomes co-loaded with metformin and chlorin e6 modulate tumor hypoxia during enhanced photodynamic therapy. *Nano Research, 10*, 1200–1212.
11. Blanco, E., Shen, H., & Ferrari, M. (2015). Principles of nanoparticle design for overcoming biological barriers to drug delivery. *Nature Biotechnology, 33*, 941–951.
12. Wilhelm, S., Tavares, A. J., Dai, Q., Ohta, S., Audet, J., Dvorak, H. F., & Chan, W. C. W. (2016). Analysis of nanoparticle delivery to tumours. *Nature Reviews Materials, 1*, 16014.
13. Yang, H., Wang, Q., Li, Z., Li, F., Wu, D., Fan, M., Zheng, A., Huang, B., Gan, L., Zhao, Y., & Yang, X. (2018). Hydrophobicity-adaptive nanogels for programmed anticancer drug delivery. *Nano Letters, 18*, 7909–7918.
14. Yong, T., Zhang, X., Bie, N., Zhang, H., Zhang, X., Li, F., Hakeem, A., Hu, J., Gan, L., Santos, H. A., & Yang, X. (2019). Tumor exosome-based nanoparticles are efficient drug carriers for chemotherapy. *Nature Communications, 10*, 3838.
15. Li, Y., Wu, Y., Chen, J., Wan, J., Xiao, C., Guan, J., Song, X., Li, S., Zhang, M., Cui, H., Li, T., Yang, X., Li, Z., & Yang, X. (2019). A simple glutathione-responsive turn-on theranostic nanoparticle for dual-modal imaging and chemo-photothermal combination therapy. *Nano Letters, 19*, 5806–5817.
16. Zhao, H., Xu, J., Huang, W., Zhan, G., Zhao, Y., Chen, H., & Yang, X. (2019). Spatiotemporally light-activatable platinum nanocomplexes for selective and cooperative cancer therapy. *ACS Nano, 13*, 6647–6661.
17. Liang, Q., Bie, N., Yong, T., Tang, K., Shi, X., Wei, Z., Jia, H., Zhang, X., Zhao, H., Huang, W., Gan, L., Huang, B., & Yang, X. (2019). The softness of tumour-cellderived microparticles regulates their drug-delivery efficiency. *Nature Biomedical Engineering, 3*, 729–740.
18. Plafki, C., Peters, P., Almeling, M., Welslau, W., & Busch, R. (2000). Complications and side effects of hyperbaric oxygen therapy. *Aviation, Space, and Environmental Medicine, 71*, 119–124.
19. Gill, A. L., & Bell, C. N. A. (2004). Hyperbaric oxygen: Its uses, mechanisms of action and outcomes. *QJM, 97*, 385–395.
20. Tibbles, P. M., & Edelsberg, J. S. (1996). Hyperbaric-oxygen therapy. *The New England Journal of Medicine, 334*, 1642–1648.
21. Bitterman, H. (2009). Bench-to-bedside review: Oxygen as a drug. *Critical Care, 13*, 205.
22. Heyboer, M., Sharma, D., Santiago, W., & McCulloch, N. (2017). Hyperbaric oxygen therapy: Side effects defined and quantified. *Advances in Wound Care (New Rochelle), 6*, 210–224.
23. Liu, J., Chen, Q., Feng, L., & Liu, Z. (2018). Nanomedicine for tumor microenvironment modulation and cancer treatment enhancement. *Nano Today, 21*, 55–73.
24. Peng, H.-S., Liao, M.-B., Zhang, M.-Y., Xie, Y., Xu, L., Zhang, Y.-J., Zheng, X. F. S., Wang, H.-Y., & Chen, Y.-F. (2014). Synergistic inhibitory effect of hyperbaric oxygen combined with sorafenib on hepatoma cells. *PLoS One, 9*, e100814.
25. Lu, Z., Ma, J., Liu, B., Dai, C., Xie, T., Ma, X., Li, M., Dong, J., Lan, Q., & Huang, Q. (2016). Hyperbaric oxygen therapy sensitizes nimustine treatment for glioma in mice. *Cancer Medicine, 5*, 3147–3155.
26. Song, G., Ji, C., Liang, C., Song, X., Yi, X., Dong, Z., Yang, K., & Liu, Z. (2017). TaOx decorated perfluorocarbon nanodroplets as oxygen reservoirs to overcome tumor hypoxia and enhance cancer radiotherapy. *Biomaterials, 112*, 257–263.
27. Song, G., Liang, C., Gong, H., Li, M., Zheng, X., Cheng, L., Yang, K., Jiang, X., & Liu, Z. (2015). Core-shell MnSe@Bi2Se3 fabricated via a cation exchange method as novel nanotheranostics for multimodal imaging and synergistic thermoradiotherapy. *Advanced Materials, 27*, 6110–6117.
28. Yang, G., Xu, L., Chao, Y., Xu, J., Sun, X., Wu, Y., Peng, R., & Liu, Z. (2017). Hollow MnO2 as a tumor-microenvironment-responsive biodegradable nano-platform for combination therapy favoring antitumor immune responses. *Nature Communications, 8*, 902.
29. Ansiaux, R., Dewever, J., Grégoire, V., Feron, O., Jordan, B. F., & Gallez, B. (2009). Decrease in tumor cell oxygen consumption after treatment with Vandetanib (ZACTIMA™; ZD6474) and its effect on response to radiotherapy. *Radiation Research, 172*, 584–591.
30. Gray, L. H., Conger, A. D., Ebert, M., Hornsey, S., & Scott, O. C. (1953). The concentration of oxygen dissolved in tissues at the time of irradiation as a factor in radiotherapy. *The British Journal of Radiology, 26*, 638–648.
31. Henk, J. M. (1986). Late results of a trial of hyperbaric oxygen and radiotherapy in head and neck cancer: A rationale for hypoxic cell sensitizers? *International Journal of Radiation Oncology, Biology, Physics, 12*, 1339–1341.
32. Brown, J. M., & Wilson, W. R. (2004). Exploiting tumour hypoxia in cancer treatment. *Nature Reviews Cancer, 4*, 437–447.
33. Mayer, R., Hamilton-Farrell, M. R., van der Kleij, A. J., Schmutz, J., Granström, G., Sicko, Z., Melamed, Y., Carl, U. M., Hartmann, K. A., Jansen, E. C., Ditri, L., & Sminia, P. (2005). Hyperbaric oxygen and radiotherapy. *Strahlentherapie und Onkologie, 181*, 113–123.

34. Bennett, M. H., Feldmeier, J., Smee, R., & Milross, C. (2018). Hyperbaric oxygenation for tumour sensitisation to radiotherapy. *Cochrane Database of Systematic Reviews, 4*, CD005007.
35. Dowling, S., Fischer, J. J., & Rockwell, S. (1992). Fluosol and hyperbaric oxygen as an adjunct to radiation therapy in the treatment of malignant gliomas: A pilot study. *Biomaterials, Artificial Cells, and Immobilization Biotechnology, 20*, 903–905.
36. Ogawa, K., Kohshi, K., Ishiuchi, S., Matsushita, M., Yoshimi, N., & Murayama, S. (2013). Old but new methods in radiation oncology: Hyperbaric oxygen therapy. *International Journal of Clinical Oncology, 18*, 364–370.
37. Mayer, R., Klemen, H., Quehenberger, F., Sankin, O., Mayer, E., Hackl, A., & Smolle-Juettner, F. M. (2001). Hyperbaric oxygen – An effective tool to treat radiation morbidity in prostate cancer. *Radiotherapy and Oncology, 61*, 151–156.
38. Feldmeier, J. J., & Hampson, N. B. (2002). A systematic review of the literature reporting the application of hyperbaric oxygen prevention and treatment of delayed radiation injuries: An evidence based approach. *Undersea & Hyperbaric Medicine, 29*, 4–30.
39. Yasuda, H. (2008). Solid tumor physiology and hypoxia-induced chemo/radio-resistance: Novel strategy for cancer therapy: Nitric oxide donor as a therapeutic enhancer. *Nitric Oxide, 19*, 205–216.
40. Ohguri, T., Imada, H., Narisada, H., Yahara, K., Morioka, T., Nakano, K., Miyaguni, Y., & Korogi, Y. (2009). Systemic chemotherapy using paclitaxel and carboplatin plus regional hyperthermia and hyperbaric oxygen treatment for non-small cell lung cancer with multiple pulmonary metastases: Preliminary results. *International Journal of Hyperthermia, 25*, 160–167.
41. Suzuki, Y., Tanaka, K., Negishi, D., Shimizu, M., Yoshida, Y., Hashimoto, T., & Yamazaki, H. (2009). Pharmacokinetic investigation of increased efficacy against malignant gliomas of carboplatin combined with hyperbaric oxygenation. *Neurologia Medico-Chirurgica (Tokyo), 49*, 193–197.
42. Bosco, G., Guizzon, L., Yang, Z., Camporesi, E., Casarotto, A., Bosio, C., Mangar, D., Chen, C., Cannato, M., Toniolo, L., Garetto, G., Nasole, E., & Bassi, C. (2013). Effect of hyperbaric oxygenation and gemcitabine on apoptosis of pancreatic ductal tumor cells in vitro. *Anticancer Research, 33*, 4827–4832.
43. Petre, P. M., Baciewicz, F. A., Tigan, S., & Spears, J. R. (2003). Hyperbaric oxygen as a chemotherapy adjuvant in the treatment of metastatic lung tumors in a rat model. *The Journal of Thoracic and Cardiovascular Surgery, 125*, 85–95.
44. Takiguchi, N., Saito, N., Nunomura, M., Kouda, K., Oda, K., Furuyama, N., & Nakajima, N. (2001). Use of 5-FU plus hyperbaric oxygen for treating malignant tumors: Evaluation of antitumor effect and measurement of 5-FU in individual organs. *Cancer Chemotherapy and Pharmacology, 47*, 11–14.
45. Moen, I., Tronstad, K. J., Kolmannskog, O., Salvesen, G. S., Reed, R. K., & Stuhr, L. E. B. (2009). Hyperoxia increases the uptake of 5-fluorouracil in mammary tumors independently of changes in interstitial fluid pressure and tumor stroma. *BMC Cancer, 9*, 446.
46. Kawasoe, Y., Yokouchi, M., Ueno, Y., Iwaya, H., Yoshida, H., & Komiya, S. (2009). Hyperbaric oxygen as a chemotherapy adjuvant in the treatment of osteosarcoma. *Oncology Reports, 22*, 1045–1050.
47. Dolmans, D. E. J. G. J., Fukumura, D., & Jain, R. K. (2003). Photodynamic therapy for cancer. *Nature Reviews Cancer, 3*, 380–387.
48. Hanahan, D., & Weinberg, R. A. (2000). The hallmarks of Cancer. *Cell, 100*, 57–70.
49. Hanahan, D., & Weinberg, R. A. (2011). Hallmarks of cancer: The next generation. *Cell, 144*, 646–674.
50. Dong, G. C., Hu, S. X., Zhao, G. Y., Gao, S. Z., & Wu, L. R. (1987). Experimental study on cytotoxic effects of hyperbaric oxygen and photodynamic therapy on mouse transplanted tumor. *Chinese Medical Journal, 100*, 697–702.
51. Roberts, D., Cairnduff, F., Dixon, B., & Brown, S. (1995). Modulation of the response of a rodent fibrosarcoma to photodynamic therapy by hyperbaric-oxygen treatment. *Oncology Reports, 2*, 387–390.
52. Tomaselli, F., Maier, A., Sankin, O., Anegg, U., Stranzl, U., Pinter, H., Kapp, K., & Smolle-Jüttner, F. M. (2001). Acute effects of combined photodynamic therapy and hyperbaric oxygenation in lung cancer – A clinical pilot study. *Lasers in Surgery and Medicine, 28*, 399–403.
53. Matzi, V., Maier, A., Sankin, O., Lindenmann, J., Woltsche, M., Smolle, J., & Smolle-Jüttner, F. M. (2004). Photodynamic therapy enhanced by hyperbaric oxygenation in palliation of malignant pleural mesothelioma: Clinical experience. *Photodiagnosis and Photodynamic Therapy, 1*, 57–64.
54. Gabizon, A., Shmeeda, H., & Barenholz, Y. (2003). Pharmacokinetics of Pegylated liposomal doxorubicin: Review of animal and human studies. *Clinical Pharmacokinetics, 42*, 419–436.
55. Shi, J., Kantoff, P. W., Wooster, R., & Farokhzad, O. C. (2017). Cancer nanomedicine: progress, challenges and opportunities. *Nature Reviews Cancer, 17*, 20–37.
56. Bennett, M., Feldmeier, J., Smee, R., & Milross, C. (2008). Hyperbaric oxygenation for tumour sensitization to radiotherapy: A systematic review of randomised controlled trials. *Cancer Treatment Reviews, 34*, 577–591.
57. Maier, A., Anegg, U., Fell, B., Rehak, P., Ratzenhofer, B., Tomaselli, F., Sankin, O., Pinter, H., Smolle-Jüttner, F. M., & Friehs, G. B. (2000). Hyperbaric oxygen and photodynamic therapy in the treatment of advanced carcinoma of the cardia and the esophagus. *Lasers in Surgery and Medicine, 26*, 308–315.
58. Wu, X., Zhu, Y., Huang, W., Li, J., Zhang, B., Li, Z., & Yang, X. (2018). Hyperbaric oxygen potentiates doxil antitumor efficacy by promoting tumor penetration and sensitizing cancer cells. *Advanced Science, 5*, 1700859.
59. Gabizon, A., Catane, R., Uziely, B., Kaufman, B., Safra, T., Cohen, R., Martin, F., Huang, A., & Barenholz, Y. (1994). Prolonged circulation time and enhanced accumulation in malignant exudates of doxorubicin encapsulated in polyethylene-glycol coated liposomes. *Cancer Research, 54*, 987–992.
60. Sanna, K., & Rofstad, E. K. (1994). Hypoxia-induced resistance to doxorubicin and methotrexate in human melanoma cell lines in vitro. *International Journal of Cancer, 58*, 258–262.
61. Raz, S., Sheban, D., Gonen, N., Stark, M., Berman, B., & Assaraf, Y. G. (2014). Severe hypoxia induces complete antifolate resistance in carcinoma cells due to cell cycle arrest. *Cell Death & Disease, 5*, e1067.
62. Tolcher, A. W., Gerson, S. L., Denis, L., Geyer, C., Hammond, L. A., Patnaik, A., Goetz, A. D., Schwartz, G., Edwards, T., Reyderman, L., Statkevich, P., Cutler, D. L., & Rowinsky, E. K. (2003). Marked inactivation of O6-alkylguanine-DNA alkyltransferase activity with protracted temozolomide schedules. *British Journal of Cancer, 88*, 1004–1011.
63. Patil, R., Portilla-Arias, J., Ding, H., Inoue, S., Konda, B., Hu, J., Wawrowsky, K. A., Shin, P. K., Black, K. L., Holler, E., & Ljubimova, J. Y. (2010). Temozolomide delivery to tumor cells by a multifunctional nano vehicle based on poly(β-L-malic acid). *Pharmaceutical Research, 27*, 2317–2329.
64. Guo, S., Wang, Y., Miao, L., Xu, Z., Lin, C. M., Zhang, Y., & Huang, L. (2013). Lipid-coated cisplatin nanoparticles induce neighboring effect and exhibit enhanced anticancer efficacy. *ACS Nano, 7*, 9896–9904.
65. Ju, C., Mo, R., Xue, J., Zhang, L., Zhao, Z., Xue, L., Ping, Q., & Zhang, C. (2014). Sequential intra-intercellular nanoparticle delivery system for deep tumor penetration. *Angewandte Chemie (International Ed. in English), 53*, 6253–6258.

66. Xie, Y., Zeng, X., Wu, X., Hu, J., Zhu, Y., & Yang, X. (2018). Hyperbaric oxygen as an adjuvant to temozolomide nanoparticle inhibits glioma growth by inducing G2/M phase arrest. *Nanomedicine (London, England), 13*, 887–898.
67. Li, J., Huang, J., Ao, Y., Li, S., Miao, Y., Yu, Z., Zhu, L., Lan, X., Zhu, Y., Zhang, Y., & Yang, X. (2018). Synergizing upconversion nanophotosensitizers with hyperbaric oxygen to remodel the extracellular matrix for enhanced photodynamic cancer therapy. *ACS Applied Materials & Interfaces, 10*, 22985–22996.
68. Ishii, Y., Miyanaga, Y., Shimojo, H., Ushida, T., & Tateishi, T. (1999). Effects of hyperbaric oxygen on procollagen messenger RNA levels and collagen synthesis in the healing of rat tendon laceration. *Tissue Engineering, 5*, 279–286.
69. Hunt, T. K., & Pai, M. P. (1972). The effect of varying ambient oxygen tensions on wound metabolism and collagen synthesis. *Surgery, Gynecology & Obstetrics, 135*, 561–567.
70. Talukdar, S., Pradhan, A. K., Bhoopathi, P., Shen, X.-N., August, L. A., Windle, J. J., Sarkar, D., Furnari, F. B., Cavenee, W. K., Das, S. K., Emdad, L., & Fisher, P. B. (2018). MDA-9/Syntenin regulates protective autophagy in anoikis-resistant glioma stem cells. *Proceedings of the National Academy of Sciences of the United States of America, 115*, 5768–5773.
71. Wang, X., Prager, B. C., Wu, Q., Kim, L. J. Y., Gimple, R. C., Shi, Y., Yang, K., Morton, A. R., Zhou, W., Zhu, Z., Obara, E. A. A., Miller, T. E., Song, A., Lai, S., Hubert, C. G., Jin, X., Huang, Z., Fang, X., Dixit, D., Tao, W., Zhai, K., Chen, C., Dong, Z., Zhang, G., Dombrowski, S. M., Hamerlik, P., Mack, S. C., Bao, S., & Rich, J. N. (2018). Reciprocal signaling between glioblastoma stem cells and differentiated tumor cells promotes malignant progression. *Cell Stem Cell, 22*, 514–528.
72. Mallory, M., Gogineni, E., Jones, G. C., Greer, L., & Simone, C. B. (2016). Therapeutic hyperthermia: The old, the new, and the upcoming. *Critical Reviews in Oncology/Hematology, 97*, 56–64.
73. Zeng, X., Wang, Q., Tan, X., Jia, L., Li, Y., Hu, M., Zhang, Z., Bai, X., Zhu, Y., & Yang, X. (2019). Mild thermotherapy and hyperbaric oxygen enhance sensitivity of TMZ/PSi nanoparticles via decreasing the stemness in glioma. *Journal of Nanobiotechnology, 17*, 47.
74. Jain, R. K., Martin, J. D., & Stylianopoulos, T. (2014). The role of mechanical forces in tumor growth and therapy. *Annual Review of Biomedical Engineering, 16*, 321–346.
75. Cubillos-Ruiz, J. R., Bettigole, S. E., & Glimcher, L. H. (2017). Tumorigenic and immunosuppressive effects of endoplasmic reticulum stress in cancer. *Cell, 168*, 692–706.
76. Caruana, I., Savoldo, B., Hoyos, V., Weber, G., Liu, H., Kim, E. S., Ittmann, M. M., Marchetti, D., & Dotti, G. (2015). Heparanase promotes tumor infiltration and antitumor activity of CAR-redirected T lymphocytes. *Nature Medicine, 21*, 524–529.
77. Weisz, G., Lavy, A., Adir, Y., Melamed, Y., Rubin, D., Eidelman, S., & Pollack, S. (1997). Modification of in vivo and in vitro TNF-alpha, IL-1, and IL-6 secretion by circulating monocytes during hyperbaric oxygen treatment in patients with perianal Crohn's disease. *Journal of Clinical Immunology, 17*, 154–159.
78. Lee, Y., Sugihara, K., Gillilland, M. G., Jon, S., Kamada, N., & Moon, J. J. (2020). Hyaluronic acid-bilirubin nanomedicine for targeted modulation of dysregulated intestinal barrier, microbiome and immune responses in colitis. *Nature Materials, 19*, 118–126.
79. Takedatsu, H., Mitsuyama, K., & Torimura, T. (2015). Nanomedicine and drug delivery strategies for treatment of inflammatory bowel disease. *World Journal of Gastroenterology, 21*, 11343–11352.

Part II

Shuffle It Up with Innovative Treatment Modalities

Mesoporous Silica Nanoparticles as Carriers for Biomolecules in Cancer Therapy

Berrin Küçüktürkmen and Jessica M. Rosenholm

Abstract

Mesoporous silica nanoparticles (MSNs) offer many advantageous properties for applications in the field of nanobiotechnology. Loading of small molecules into MSNs is straightforward and widely applied, but with the upswing of both research and commercial interest in biological drugs in recent years, also biomacromolecules have been loaded into MSNs for delivery purposes. MSNs possess many critical properties making them a promising and versatile carrier for biomacromolecular delivery. In this chapter, we review the effects of the various structural parameters of MSNs on the effective loading of biomacromolecular therapeutics, with focus on maintaining stability and drug delivery performance. We also emphasize recent studies involving the use of MSNs in the delivery of biomacromolecular drugs, especially for cancer treatment.

Keywords

Mesoporous silica nanoparticles · Biomolecules · Biological drugs · Biologics · Protein drugs · Stimuli-responsive drug release · Controlled drug release · Photodynamic therapy · Peptide delivery · Protein delivery · Gene delivery · Cancer immunotherapy · Co-delivery · Inorganic drug carriers · Macromolecular drug delivery

B. Küçüktürkmen
Pharmaceutical Sciences Laboratory, Faculty of Science and Engineering, Åbo Akademi University, Turku, Finland

Department of Pharmaceutical Technology, Faculty of Pharmacy, Ankara University, Ankara, Turkey

J. M. Rosenholm (✉)
Pharmaceutical Sciences Laboratory, Faculty of Science and Engineering, Åbo Akademi University, Turku, Finland
e-mail: jerosenh@abo.fi

1 Introduction

Amorphous silica is classified as GRAS (generally recognized as safe) by the FDA and has in nanoparticulate form recently received FDA approval for stage I human clinical trials of fluorescence-based cancer imaging [1–3]. MSNs offer many advantageous properties for applications in the field of nanobiotechnology, e.g., as controllable particle size and pore size, robust morphology, large surface area, ease of inner/outer surface modification, high cargo loading capacity and efficient cargo transfer efficiency, low cytotoxicity, excellent biocompatibility and biodegradability properties, and cost-effective production [4–6]. For all these reasons, MSNs with small particle size but large pore size have great potential to e.g. effectively overcome multiple drug resistance (MDR) by delivering biomacromolecules (peptides, proteins, or nucleic acids) into drug-resistant cancer cells [6]. Numerous MSN nanocarriers smaller than 200 nm in diameter can penetrate tumor tissues due to the enhanced permeability and retention (EPR) effect. However, as for any prospective nanopharmaceuticals, there are some obstacles in the application of MSNs for tumor treatment such as tumor targeting deficiency and strong affinity of MSNs to blood proteins. In order to increase the active targeting ability, zero premature drug release and release at the targeted cancer sites should be considered based on differences between intratumoral and normal cell microenvironments. Therefore, surface functionalization is necessary to equip them with the ability to target tumors and increase the stability of blood circulation in vivo [7, 8]. In addition, the biodegradability of MSNs should be optimized to prevent unwanted accumulation in the body that may cause acute or subacute inflammation or long-term biosecurity risks [9].

Biological medicines (biologicals, biologics) are one of the most promising areas for the implementation of MSNs as drug/gene delivery carriers. It has previously been well documented that proteins maintain increased activity and stability when loaded into the pores of MSNs, since the solid

© Springer Nature Switzerland AG 2021
F. Fontana, H. A. Santos (eds.), *Bio-Nanomedicine for Cancer Therapy*, Advances in Experimental Medicine and Biology 1295, https://doi.org/10.1007/978-3-030-58174-9_5

inorganic framework can efficiently protect proteins from denaturation [10]. To date, MSNs with different morphologies have been synthesized: hollow mesoporous nanocapsules, branched mesoporous nanoparticles, yolk-shell mesoporous structures, and so forth. Particularly in the diagnosis/imaging and treatment of cancer, functional nanoparticles such as magnetite, gold, quantum dots, and anticancer drugs incorporated as core materials in core-shell designs, doped into the mesoporous silica matrix, or loaded into the pore channels have shown great application potential in the field of biological medicines [11].

2 Synthesis of MSNs

MSNs are commonly synthesized using a cetyltrimethylammonium bromide (CTAB) micelle-templated sol-gel technique. The main disadvantage of this method is that the pores of the MSNs produced are small, and the particle size homogeneity is insufficient. In the CTAB micelle-templated sol-gel technique, tetraethyl orthosilicate (TEOS) is first hydrolyzed and produces negatively charged silicate oligomers that approach and interact with positively charged CTAB micelles by electrostatic interaction. The condensation of the silicate oligomers then leads to the collection of silica nanoparticles and micelles (self-assembly). Aggregation ends when the surface net negative charge is high enough to prevent further growth, which results in the formation of MSNs with specific morphologies [4].

Mesoporous silica materials such as MCM-41, SBA-15, MCF, and FMS have been successfully used as supports for the immobilization of biomolecules (see Fig. 1). However, the 2D pore architecture and relatively small pore volume of these materials limit the diffusion and transport of biomolecules. To overcome this problem, researchers have synthesized mesoporous silicas with 3D cubic pore channels such as FDU-12, KIT-5, and KIT-6. These materials have more accessible pores due to the interconnected cage-type pore structures and, thus, can effectively increase the guest species adsorption capacity. The silica framework is negatively charged at neutral pH, making it inherently suitable for loading of biomolecules with an isoelectrical point (IEP/pI) over 7 (i.e., positive charge at neutral pH). However, most therapeutically active proteins and all nucleic acids are negatively charged at neutral pH, creating electrostatic repulsion with the carrier material at suitable loading conditions. Thus, the mesoporous silica surface can be functionalized with different organic groups such as thiol, phenyl, vinyl, amine, and carboxylic acid to increase the application potential in different fields and enhance the affinity to the full range of biomacromolecules [12].

The surfactant-micelle-templating method is a widely used method also in the synthesis of MSNs with large pores, suitable for the encapsulation of macromolecules. In this method, the micelle size is adjusted by adding a swelling agent as well as changing the surfactant. However, the swelling agent tends to induce irregularity or heterogeneity in the resulting structures. It has been reported that when the swelling agents have moderate solubility in the surfactant micelles, well-defined micelle-templated structures with substantially enlarged pores can occur. For example, for Pluronics having a high hydrophobic block fraction, such as Pluronic P123, it is advantageous to use low or moderately soluble swelling agents therein to prevent over-swelling. On the other hand, Pluronics having a low hydrophobic block fraction, such as Pluronic F127, work well with stronger swelling agents and allows the synthesis of silicas and organosilicas with large spherical mesopores. The resulting large-pore silicas and organosilicas with spherical and cylindrical mesopores have thick walls, and thermal treatments can maintain the original pore shape and symmetry to ensure the formation of closed porous silicas. A variety of compounds were shown to act as micelle expanders, including benzene and its alkyl-substituted derivatives (most notably, 1,3,5-trimethylbenzene (TMB), 1,3,5-triethylbenzene (TEB), and 1,3,5-triisopropylbenzene (TIPB)), linear hydrocarbons (hexane), cyclic hydrocarbons (cyclohexane), and long-chain amines [14].

2.1 Large-Pore MSNs for Macromolecular Drugs

Although delivery of small molecules has been shown to be quite successful in numerous examples, even in clinical studies [15], encapsulation of large therapeutic biomolecules such as proteins or DNA is limited due to the small pore size of conventional MSNs ranging from 2 to 5 nm. Compared to traditional MSNs, large-pore MSNs (LPMSNs) with pore sizes reaching the upper limit of mesopores (6–50 nm) have desirable properties for encapsulation of large molecules such as nucleic acids, enzymes, or peptides into their porous structure [16].

Recently, two main approaches have been developed to produce LPMSNs. The first one is a solvent evaporation-induced self-assembly approach using high molecular weight block copolymers as the pore template. In this method, it is essential to use an unusual and costly fluorocarbon surfactant to control particle growth. Although the products obtained in this case have ultra-large pore channels, they have generally had irregular particle morphologies and micrometer particle sizes, which are unsuitable for intracellular delivery applications. The second approach is the use of pore expansion agents such as TMB during the synthesis of MSNs. Unfortunately, the pore expansion agent used causes irregularity and even complete destruction of the resulting mesostructure. Furthermore, the nanoparticles formed generally have a particle size of greater than 250 nm, which is expected to result in rapid removal of the particles from the circulation and a significant reduction in cellular uptake efficiency [11,

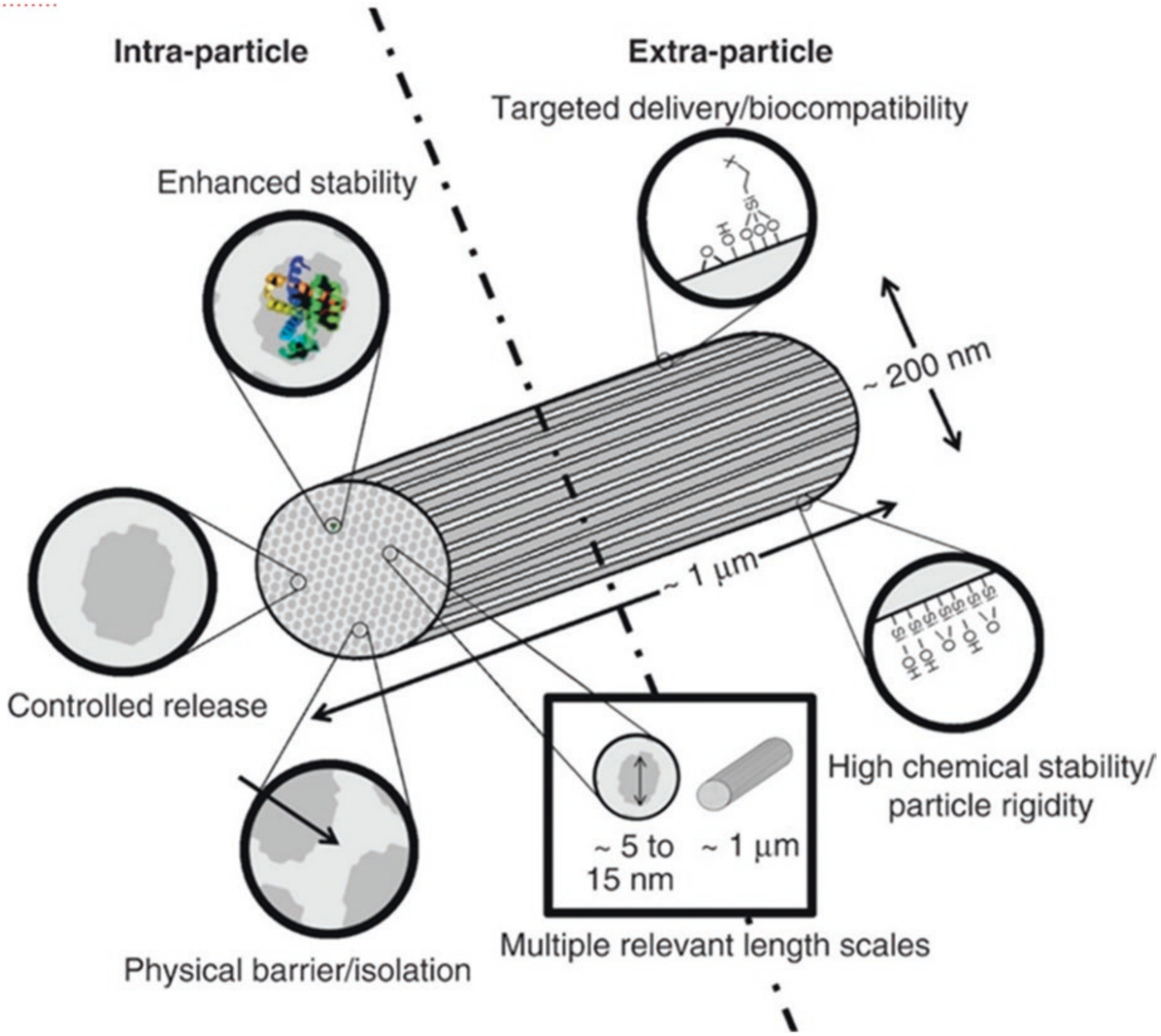

Fig. 1 Design aspects of mesoporous silica SBA-15, highlighting their possible application to address intra- and extra-particle challenges that are especially relevant in biomacromolecular delivery. (Reproduced from J. Siefker et al. [13] under the terms of the Creative Commons Attribution License (http://creativecommons.org/licenses/by/3.0))

16, 17]. Recently, large-pore mesoporous organosilica NPs [18], large-pore hollow dendritic MSNs [19, 20], and extra-large-pore MSNs (XL-MSNs) [21] have been synthesized for the delivery of macromolecules with different structures. Despite extensive efforts to develop large-pore MSNs, there are still some critical limitations to their use in macromolecular drug delivery. Therefore, new approaches and synthetic pathways are already needed for the synthesis of MSNs with accessible large pores (>10 nm), small particle sizes (<200 nm), and well-regulated mesostructures.

Despite recent studies on the preparation of large-pore MSNs using co-solvents, block copolymers, and swelling agents, the preparation of discrete LPMSNs with high colloidal stability remains a challenge for efficient in vivo delivery [21, 22]. Kwon et al. (2017) synthesized uniform XL-MSNs in sizes 100, 150, and 180 nm with large pores over 30 nm for MSN-based in vivo cytokine delivery for immune cell modulation. To prepare large mesopores by providing high colloidal stability, CTAB-stabilized iron oxide nanoparticles were used in the sol-gel reaction as well as a high proportion of ethyl acetate as a pore expansion agent (Fig. 2). To investigate the effect of iron oxide nanoparticles, the MSNs were prepared without CTAB-stabilized iron oxide nanoparticles but with the addition of a high proportion of ethyl acetate. Although the formed MSNs have large pores, the particle morphology was observed to be irregular, and the pore size distribution was not as distinct as XL-MSNs. This suggests that CTAB-stabilized iron oxide nanoparticles serve as the initiator of the silica sol-gel reaction to form uniform XL-MSNs. The prepared XL-MSNs have also been shown to be applicable for loading proteins of different sizes. The loading of ovalbumin (OVA), bovine serum albumin (BSA), and glucose oxidase in 180 nm XL-MSNs was found to be 3.5-, 9.3-, and 6.2-fold higher than that in conventional MSNs, respectively. In this study, bioactive IL-4 was successfully delivered to macrophages by phagocyte targeting

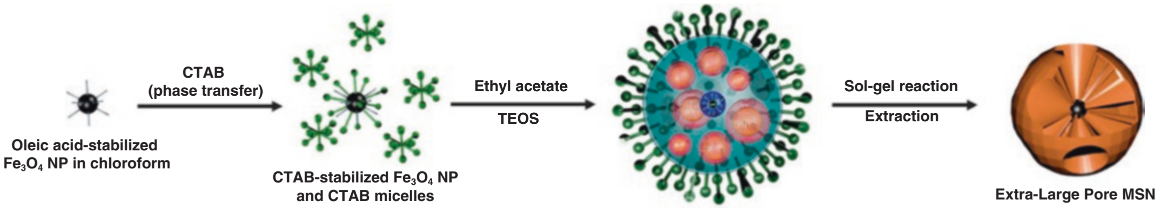

Fig. 2 Synthesis of XL-MSNs. (Reproduced from Kwon et al. [21])

and induced M2 macrophage polarization in vivo [21]. Similar to this study, Cha et al. (2018) synthesized XL-MSNs as a cancer vaccine through the delivery of OVA and CpG oligonucleotide. To prepare large mesopores while maintaining high colloidal stability in MSNs, they employed a large amount of ethyl acetate, an organic additive, as a pore expansion agent in the presence of CTAB-stabilized iron oxide nanoparticles and seed material in a silica sol-gel reaction. Pore size distribution showed that XL-MSNs had bimodal pores that peaked at 3.2 nm and around 25 nm in the range between 10 and 30 nm. Amine-modified XL-MSNs resulted in significantly higher loading of OVA and CpG oligonucleotide compared with conventional small-pore MSNs [22]. In another study, Zhang et al. (2011) synthesized magnetic MSNs using TEOS as the source of silica, cationic surfactant CTAB as template, and TIPB/decane as pore swelling agent. While adding the amount of TIPB in a limited range increased pore size, further use of TIPB resulted in severe particle coalescence and irregular pore structure. On the other hand, effective pore expansion of the magnetic MSNs was achieved by adding a suitable amount of decane together with a limited amount of TIPB. The obtained magnetic MSNs yielded smaller particle sizes (about 40–70 nm in diameter), tunable pore sizes (3.8–6.1 nm), high surface areas, and large pore volumes. In addition, a strong correlation was found between increasing pore size and drug loading, and the maximum loading capacity of the salmon sperm DNA (375 mg/g) was obtained using a magnetic MSN sample with the largest pore size of 6.1 nm [23].

Recently, large-pore dendritic MSNs with hollow cavities have been synthesized and demonstrated superior advantages over dendritic MSNs in protein loading and controlled release. Hollow cavity reduces pore density and increases pore volume and, hence, loading efficiency [19]. Dendritic MSNs with opening pore channels are promising carriers with large pore sizes (34–45 nm). They have a high accessible internal surface area for the delivery of large molecule therapeutic agents such as plasmid DNA (*p*DNA) and proteins into cells. Meka et al. (2016) produced amine-functionalized hollow dendritic MSNs with a core cavity of 170 nm and a mesopore in the shell of 20.7 nm. IgG (658 μg/mg) and β-galactosidase (391 μg/mg) were found to be loaded in high amounts into the MSNs. Cellular uptake of β-galactosidase by hamster ovary cells (CHO-K1) increased, and MSNs maintained its catalytic properties within the cell. In this study, it was stated that using both TEOS and (3-aminopropyl) triethoxysilane (APTES) as the silica source is the most important parameter for the formation of large porous dendritic organic MSNs with hollow cavity. In the absence of APTES, hollow structures were not formed, and in the absence of TEOS, aggregates of amorphous silica molecules were obtained [19]. Hong et al. (2018) synthesized polydopamine and chelated Ti^{4+} modified dendritic MSNs with a central-radial pore structure for phosphopeptide enrichment. The synthesized MSN formulation had a particle size of approximately 150 nm and a wide pore size of 18.8 nm. This formulation was compared with conventional MSN and commercial TiO_2 in terms of phosphopeptide enrichment in various biological samples (including standard phosphoprotein, nonfat milk, human serum, and HeLa cell extracts). Low phosphopeptide detection limit of 0.2 fmol/μL and an extremely high specificity (>95%) of phosphopeptides identified from HeLa cell extracts were obtained [24].

MSNs are also of great importance for enzyme immobilization. Once the enzymes have been loaded into MSNs, their enzymatic activity is maintained over a wide pH range and even after exposure to enzyme degrading agents such as proteases [25]. For use as a support for immobilization of enzymes, it is very important to effectively control both the textural and surface properties of mesoporous silica. If the molecular size of the enzyme is close to the pore size, it is stated that adsorbate molecules have difficulty in reaching the active regions in the mesoporous channels and diffusion limitations occur. It is noted that this diffusion problem can be solved by using large-pore mesoporous silicas with pore diameters greater than twice the largest enzyme size [12]. In the study of Saikia et al. (2019), large-pore cubic mesoporous silica SBA-1 MSNs of 500–700 nm functionalized with COOH were synthesized for papain immobilization. The pore size, specific surface area, and pore volume were increased using the pore-expanding agent TMB in the reaction mixture. The -COOH-functionalized MSNs having a pore size of 5.3 nm exhibited a higher papain adsorption capacity (1138 mg/g) than a pore size of 3.2 nm (995 mg/g). Immobilized papain exhibited higher thermal stability over a wider pH range compared to free papain [12]. Kalantari et al. (2017) synthesized octadecylalkyl-modified mesoporous silica nanoparticles (C18-MSNs) with tunable pore sizes (1.6–13 nm) for lipase immobilization. It has been shown that the pore size slightly larger than the size of the lipase is responsible for the high performance of the immobilized lipase. The optimized C18-MSNs having an average particle size of 60 nm were found to have a high lipase loading capacity of 711 mg/g and a specific activity of 5.23 times higher than that of the free enzyme [26]. Kao et al. (2014) tested the activity and stability of lysozyme immobilized in MSNs of various pore sizes by testing secondary and tertiary structures of proteins by methods such as circular dichroism and activity assay. When the pore size was close to the protein size, the activity of lysozyme in immobilizing in the pores of MSNs was found to be higher than pure lysozyme [10] (Table 1).

3 Gatekeepers for Controlled Drug Release

Recently, the establishment of stimuli-responsive controlled drug release systems for targeted drug delivery has attracted considerable attention. MSNs are ideal nanocarriers for controlled drug or gene delivery sensitive to stimuli because of their superior structural properties. A critical step in developing the stimuli-responsive controlled drug release system is to create "gatekeepers" on the surface of MSNs and to block the drug molecules inside the pores with "zero premature release" and trigger the release of drug molecules upon specific stimulation [34]. These gatekeepers include polymers, cyclodextrin, inorganic nanoparticles, and biomacromolecules developed for efficient capping of the pores [35]. The functional design of the pore surface of MSNs with organic or inorganic moieties defined as gatekeepers may regulate

Table 1 Examples of LPMSNs loaded with macromolecular drugs

Sample	Size (nm)	Pore size (nm)	Pore volume (cm^3/g)	Specific surface area (m^2/g)	Pore expansion agent	Macromolecular drug	Drug loading capacity	Ref.
LPMSN	174–207	8–10	0.6–0.8	220–230	–	Bcl-2 converting peptide	15–43%	[6]
LPMSN	230	10	–	506	–	Cytochrome-c	470 µg/mg	[27]
LPMSN	265, 933	5.4, 14.5	1.82	1061	Mesitylene	Cytochrome-c	415 mg/g	[28]
LPMSN	<150	4.6	1.14	1053	–	Cytochrome-c	230 mg/g	[17]
LPMSN	293	16.7	1.2	315	–	Plasmid-encoding VEGF short hairpin RNA	26.7 µg/mg	[11]
LPMSN	<200	13.4, 27.9	1.09	313	TMB	Twenty-one-nucleotide (oligo) DNA	57 µg/mg	[29]
LPMSN	150	17.2, 20.5	0.46	135	–	pDNA	9.7 µg/g	[30]
XL-MSNs	180	3.6, 30	0.7	450	Ethyl acetate	IL-4	1030 µg/mg	[21]
Amine-modified XL-MSNs	100–200	3.2, 25	1.05	686	Ethyl acetate	OVA CpG oligonucleotide	~1000 mg/g ~80 µg/mg	[22]
Large-pore hollow MSNs	150–200	3.1	1.11	893.8	Decane	TRP2 HGP100	88% 20.6%	[31]
Amine-functionalized hollow dendritic MSNs	242	20.7	2.67	–	–	IgG β-Galactosidase	658 µg/mg 391 µg/mg	[19]
LPMSN Hollow organosilica nanoparticles	100 228–460	3–7 26	–	817 58	TEB	Pepstatin A	32%, 18%	[20]
Mesoporous organosilica nanoparticles	50.75	6.2	2.19	613.9	–	TAT pDNA	66.67 µg/mg	[32]
Carboxylic acid-functionalized LPMSNs	500–700	5.3	0.88	777	TMB	Papain	1138 mg/g	[12]
PEI-functionalized hollow MSNs	270	>5.4	19.36	84.27	–	GFP-DNA	37.98 mg/g	[5]
Large-pore magnetic MSNs	150	12	1.13	411	Hexane	siRNA targeting polo-like-kinase 1	2%	[16]
Large-pore magnetic MSNs	40–70	3.8–6.1	0.44–1.54	700–1100	TIPB/Decane	Salmon sperm DNA	375 mg/g	[23]
PEI-Fe-LPMSN	299	4.6, 9.2	0.3316	217.4	TMB	Twenty-one-nucleotide (oligo) DNA	18 µg/mg	[33]

the release of guest molecules under the control of external stimuli such as certain chemicals, temperature, redox reactions, and photo-irradiation or internal stimuli such as pH, redox, and enzymes [28].

The gatekeepers are opened only in the presence of specific internal or external stimuli, and "zero premature release" is achieved before reaching the targeted cancer cells, so that normal cells are not damaged. Various delivery strategies have been reported targeting cancer-specific stimuli, such as low pH, hypoxia, high H_2O_2, and glutathione (GSH) levels. In recent years, biomolecule-responsive nanosystems have attracted increasing attention as abundant extracellular enzymes (e.g., phospholipase A, hyaluronidase, lipase, and matrix metalloproteinase) which are highly expressed and active within the tumor microenvironment and could be utilized as drug delivery stimuli with enhanced selectivity and sensitivity [36].

3.1 External Stimuli

3.1.1 Magnetic Field

The combination of MSNs with magnetic properties has enabled it to be used in areas such as magnetic targeting and magnetic resonance imaging (MRI). "Magnetofection" studies are carried out to increase the efficiency of DNA transfection by using magnetic MSNs applied under a magnetic field. Although intensive efforts have been made to develop magnetic LPMSNs for macromolecular drug delivery, there are still some critical limitations to their use. The production of magnetic LPMSNs generally consists of complex multistage processes, and particle sizes are often too large (>200 nm) for effective cellular uptake and lead to rapid excretion from the circulation. In addition, low saturation magnetization (<20 emu/g) occurs, often due to the low loading efficiency of the magnetic component. Thus, there is a need for magnetic LPMSNs with small particle size, large open pores, high pore volume, high magnetization density, and controlled release properties for macromolecular drug delivery [16].

There are many studies showing that magnetic-guided conduction can effectively promote the enrichment of nanocarriers in the tumor site. In a study by Li et al. (2018), mesoporous silica-coated iron oxide-based nanoparticles were synthesized, and a peptide sensitive to the MMP-2 enzyme was covalently bound to the surface of nanoparticles to encapsulate doxorubicin (DOX) in the porous cavities (peptide-Fe_3O_4@MSNs/DOX) (Fig. 3). Peptide-Fe_3O_4@MSNs/DOX were cultured with NIH/3T3 and HT1080 cells to test the specificity of normal cells and cancer cells. The cell viability after 24 hours was found still approximately 80% in NIH/3T3 cells, while it was about 50% in HT-1080 cells. In tumor-bearing mice, uptake of peptide-Fe_3O_4@MSNs/DOX into tumor cells by passive targeting was found to be much lower than that treated with magnet. The in vivo peptide-Fe_3O_4@MSNs/DOX- and magnet-treated group was found to have the smallest tumor size, indicating successful suppression of tumor growth. This phenomenon has demonstrated that magnetic-guided conduction can effectively promote the enrichment of nanocarriers in the tumor site [37]. Portilho et al. (2018) developed an intelligent delivery system, based on trastuzumab-loaded radiolabeled magnetic core@shell MSNs for in vivo breast cancer imaging and treatment. The results showed that nanoparticles were 58.9 nm in size with a specific surface area of 872 m^2/g, pore volume of 0.85 cm^3/g, and a pore diameter of 3.15 nm. Entrapment efficiency of trastuzumab into the magnetic core@shell MSNs was found as 97.5%. Biodistribution studies showed systemic uptake of 7.5% and intralesional tumor uptake of 97.37%, whereas less than 3% were absorbed by healthy tissues. During a 6-hour post-injection period, a tumor-limited barrier was not crossed, which supported its use as intralesional nanodrug [38].

Magnetic MSNs have also been used for gene delivery to cancer cells. Xiong et al. (2016) developed a large-pore magnetic core@shell silica nanoparticle for small interfering RNA (siRNA) delivery. These nanoparticles were produced by coating superparamagnetic magnetite nanocrystal clusters with radial large-pore mesoporous silica. To prepare large mesopores, hexane (an organic additive) was used as a pore expander. The amine-functionalized nanoparticles were found to have small particle sizes around 150 nm, large radial mesopores of 12 nm, and magnetization of 25 emu/g. Thus, these nanoparticles were found to have both siRNA loading capacity of 2% and strong magnetic response under an external magnetic field. The tannic acid coating also increased the dispersion stability of the siRNA-loaded carrier and provided a pH-sensitive release. Using tannic acid-coated magnetic silica nanoparticles as the carrier, functional siRNA was successfully delivered to the cytoplasm of human osteosarcoma cancer cells, and the delivery was significantly increased with the help of an external magnetic field [16]. In another study, Hartono et al. (2014) reported the synthesis of LPMSNs loaded with iron oxide and covalently modified by polyethylenimine (PEI) as a carrier for gene delivery. The functionalized LPMSNs were found to have a particle size of 300 nm and a large cavity size of 9.2 nm with an entrance size of 4.6 nm. The amount of oligo-DNA adsorbed by functionalized LPMSNs was 18 µg/mg. Cellular uptake studies showed a 12% intensity increase under magnetic therapy when compared to the group without application of a magnetic field. The functionalized LPMSNs delivered siRNA-PLK1 effectively into osteosarcoma cancer cells resulting in a higher cell viability inhibition of 80%, compared to the 50% reduction when the same siRNA dose was administered by a commercial product, oligofectamine [33].

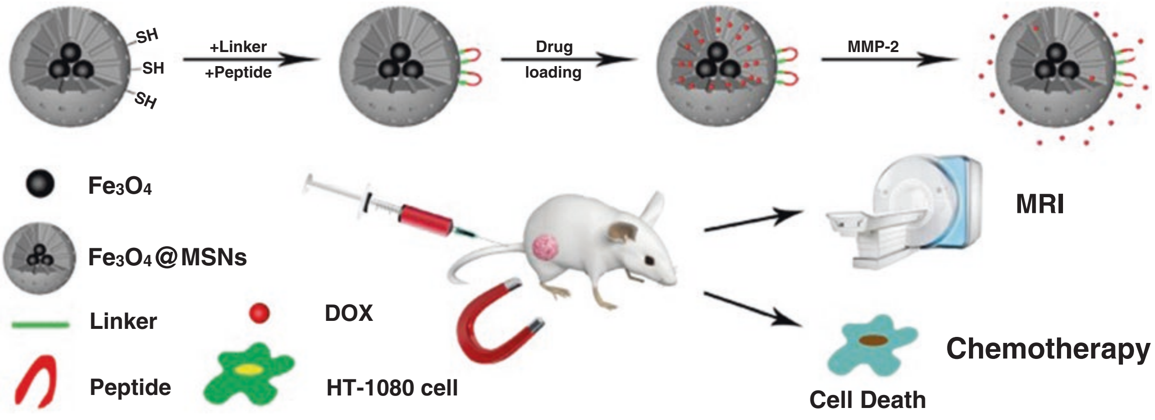

Fig. 3 Schematic illustration of surface-functionalized magnetic MSNs for tumor site-specific delivery. (Reproduced from Li et al. [37])

Albeit not primarily for delivery purposes, the surface of magnetic MSNs can be functionalized with aptamers for targeting to cancer cells. Siminzar et al. (2019) designed mucin-1 (MUC-1)-conjugated mesoporous silica magnetic nanoparticles for the targeted delivery of doxorubicin to breast cancer cells. Superparamagnetic iron oxide nanoparticles (SPIONs) were synthesized using thermal decomposition technique and then coated with mesoporous silica to modify their biocompatibility and reduce undesired cytotoxic effects. Doxorubicin was then loaded into the silica porous structures, which was then grafted with 5′-amine-modified MUC-1 aptamers. Transmission electron microscopy and particle size analysis showed spherical and monodisperse nanoparticles with a size range of 5–27 nm. MUC-1-grafted SPIONs coated with mesoporous silica were applied to MUC-1-positive MCF-7 cells, resulting in higher cytotoxicity and higher uptake [39]. In another study, Sakhtianchi et al. (2019) synthesized an aptamer-functionalized PEG-coated SPION/mesoporous silica core-shell nanoparticle for simultaneous cancer targeted therapy and magnetic resonance imaging. Doxorubicin was loaded into the MSNs, which were then coated with di-carboxylic acid-functionalized polyethylene glycol, and AS1411 aptamers were covalently attached to MSNs. The synthesized nanoparticles were found to be 89 nm in size, and the doxorubicin loading degree was 13.17%. The cytotoxicity assay demonstrated a significantly higher toxicity of decorated MSNs to MCF7 cells. Aptamer-decorated MSNs induced the highest signal intensity reduction in T2-weighted images during in vitro MRI assay [40].

3.1.2 Photodynamic Therapy

Photodynamic therapy (PDT) is a non-invasive and innovative cancer therapy based on the photodynamic effect. In combination with light and molecular oxygen, photosensitizers, which are applied during PDT, produce reactive oxygen species (ROS) to destroy tumor tissues and cells. PDT exhibits its spatiotemporal selectivity because ROS production occurs in the light-exposed region, and the resulting chemical processes take place within about 50 nm of this location. In addition to this inherent selectivity, PDT has demonstrated the advantages of non-invasivity, having a relatively broad-spectrum anticancer effect, allowing repeated treatments without initiating resistance, and providing an immune response. Besides its advantages, the typical PDT approach suffers the drawback that patients must stay in the dark for a long time (usually 4–6 weeks) after treatment, so that the photosensitizers can be removed from the body. Otherwise, photosensitivity of the skin and damage to other tissues may occur [41].

Er et al. (2018) synthesized MSNs targeted with cetuximab, a monoclonal antibody that targets the epidermal growth factor receptor (EGFR), and loaded with zinc(II) 2,3,9,10,16,17,23,24-octa(tert-butylphenoxy)) phthalocyaninato(2-)-N29,N30,N31,N32 (ZnPcOBP) against pancreatic cancer cells to determine the singlet oxygen production, intracellular uptake, and PDT potential in vitro. Upon irradiation, concentration and light fluence-dependent decrease in cell viability was observed in pancreatic cell lines. The results in this study demonstrated that nanoparticles coated with PEG and cetuximab could be an efficient vehicle for delivery of the photosensitizer ZnPcOBP to tumoral pancreatic cells with targeted high EGFR expression [42]. Li et al. (2019) developed a sequential protein-responsive activatable photosensitizer (PcC_4-MSN-O_1) based on zinc(II) phthalocyanine derivative (PcC_4)-entrapped MSNs and a wrapping DNA (O_1) as a biogate. First, MSNs with particle sizes of about 50 nm were synthesized because this size range is claimed to be preferred for tumor passive deposition through the EPR effect. Second, the MSNs were modified with APTES, resulting in positively charged surfaces. Finally, MSN-NH_2 were loaded with PcC_4 and then sealed with the negatively charged O_1 to form a PcC_4-MSN-O_1 nanosystem. In this nanosystem, the loading of

PcC_4 was calculated as 77.6 nmol/mg $MSN\text{-}NH_2$, and the adsorption amount of O_1 was calculated as 0.3 μmol/g PcC_4-MSN. The cytotoxicity of PcC4-MSN-O_1 upon illumination with white light was tested. PcC_4-MSN-O_1 exhibited concentration-dependent phototoxicity against HeLa cells (telomerase overexpressed) but did not show significant phototoxicity against normal cells (HEK-293) under the same conditions, indicating its selective effect on cancer cells. They also investigated the in vivo PDT efficacy of PcC_4-MSN-O_1 on tumor-bearing mice, and compared with the control group (laser irradiation only), the group treated with PcC_4-MSN-O_1 exhibited significant deposition of formulation in HeLa tumors and a significant inhibition in tumor growth in the presence laser irradiation [41].

In another study, Fang et al. (2019) designed a hollow MSN gated with BSA integrated manganese dioxide nanoparticles (BSA-MnO_2) for both chemotherapy and O_2-induced photodynamic therapy. The BSA-MnO_2 nanoparticles were then attached to the surface of hollow mesoporous silica nanospheres (BMHDC) co-loaded with chemotherapeutic drug doxorubicin and photosensitizer chloride e6 (Ce6) by formation of disulfide bonds. BSA-MnO_2 was used not only as a gatekeeper to prevent early release of drugs from hollow MSNs, but also as an oxygen generator to eliminate tumor hypoxia. Furthermore, the BSA component has also been noted to increase the stealthiness of nanoparticles during blood circulation. Under acidic pH and GSH, decomposition of MnO_2 caused the gatekeeper to open and simultaneously release doxorubicin and Ce6 (Fig. 4). In addition, O_2 generation supported the kinetics of O_2 production to improve PDT outcomes. The produced BMHDC nanoplatform was able to effectively limit human cervical carcinoma through synergistic PDT and chemotherapy demonstrated in both in vitro and in vivo experiments [43].

3.1.3 Ultrasound

The surface of the MSNs can be functionalized to control cargo release by ultrasound effect. Paris et al. (2019) demonstrated the possibility of inducing gene transfection using ultrasound-responsive MSNs, without generating significant toxicity to the decidua-derived mesenchymal stem cells (DMSCs), by using a PEI coating. Ultrasound-responsive MSNs were obtained by grafting the polymeric gate poly-(2-(2-methoxyethoxy) ethylmethacrylate-co-2-tetrahydropyranyl methacrylate) to MSNs. When exposed to ultrasound, the monomer tetrahydropyranyl methacrylate in the polymeric coating is converted into a much more hydrophilic monomer (methacrylic acid). This change modifies the overall hydrophilicity of the system and induces a conformational change of the polymeric gate, thus exposing the nanoparticle pores to the environment and enabling cargo release (Fig. 5). This developed nonviral transfection agent was used to transfect DMSCs with an expression plasmid comprising two suicide genes consisting of the sequences for cytosine deaminase and uracil phosphoribosyltransferase, which provided them the capability of converting non-toxic 5-fluorocytosine into toxic 5-fluorouridine monophosphate. It has been found that DMSCs transfected with suicide genes can induce cell death in co-cultured NMU cancer cells when exposed to non-toxic prodrug 5-fluorocytosine [44].

3.2 Internal Stimuli

3.2.1 Release Based on pH

One of the most commonly used stimulants in triggered drug release is pH. In cancer drug delivery, drug carriers coated with gatekeepers can prevent drug release in the bloodstream, but when the nanoparticle reaches the tumor microenvironment by EPR and/or enters the target cell via endocytosis, drug release from the nanocarriers is triggered either around the tumor where pH is lower than in healthy tissue or intracellularly. Because of the abundance of H^+ in the endosomes, the pH in this cellular organ where nanoparticles reside after endocytosis is estimated to be pH 5.0 and is lower than the cytosolic medium of the cell [45].

Many substances and polymers with different chemical structures have been utilized for pH-sensitive functionalization of MSNs. In the study of Shen et al. (2019), benzimidazole-functionalized MSN was prepared to provide pH-triggered release of doxorubicin. β-Cyclodextrin (β-CD) was used as a gatekeeper, and release of doxorubicin sensitive to pH was confirmed by in vitro release experiments [46]. Xiong et al. (2016) developed a large-pore magnetic core@shell silica nanoparticle for siRNA delivery. The acid-liable surface coating of tannic acid was reported to act simultaneously as a pore capping agent for effective protection of siRNA and as a pH-sensitive switch for intracellular release of siRNA [16]. Zahiri et al. (2019) developed a new pH-responsive formulation in which polycarboxylic acid dextran was electrostatically adsorbed to the amine groups on the surface of doxorubicin-loaded dendritic MSNs. They claimed that under physiological condition (pH 7.4), the silica channels were coated and sealed by dextran polysaccharides, but positively charged hydrogen ions in the citrate buffer (pH 5.4) interacted with carboxylate group of dextran and became protonated. Therefore, it has been noted that electrostatic interaction between surface amine groups and dextran carboxylate groups could be compromised by a competitive binding with H^+, resulting in the release of doxorubicin [45]. Liu et al. (2019) introduced a biocompatible, simply structured, and tumor-acidic environmentally sensitive drug delivery system by using $CaCO_3$ as a gatekeeper and cloaking cancer cell membrane on MSNs. It was reported that the synthesized MSNs were monodisperse nanoparticles with a size of about 100 nm, and that the modification of the surface did not affect the morphology of the nanoparticles. Negligible early release at pH 7.4 and rapid release under tumor-acidic

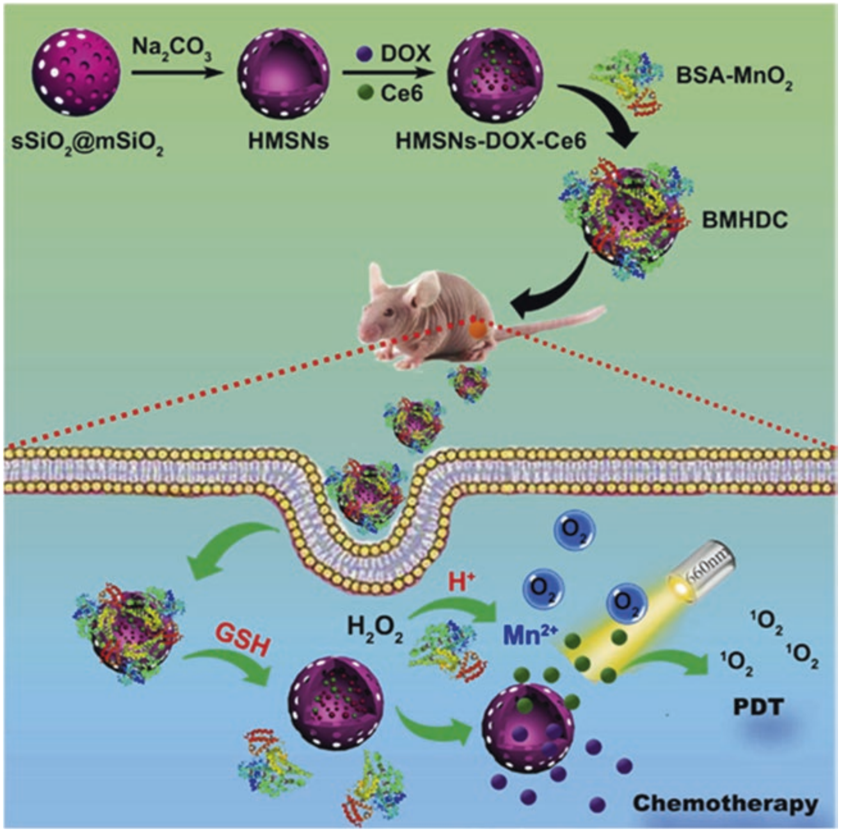

Fig. 4 Schematic representation of drug release from MSNs based on the photodynamic effect. (Reproduced from Fang et al. [43])

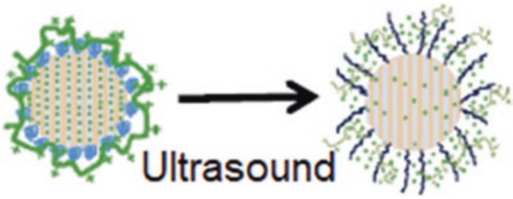

Fig. 5 Schematic representation of MSN before and after ultrasound treatment. (Reproduced from Paris et al. [44])

medium were confirmed. Furthermore, doxorubicin-loaded $CaCO_3$-capped MSNs showed a positive antitumor effect in the LNCaP-AI tumor model, evidenced by significant tumor growth delay, destruction of tumor cells, and reduced tumor cell proliferation [47]. Kuang et al. (2019) prepared doxorubicin-loaded MSNs coated with ZnO, onto which poly-L-lysine (PLL) and 2,3-dimethylmaleic anhydride-functionalized PLL (PLL(DMA)) were subsequently adsorbed on the surface. The outer part of the carriers was negatively charged PLL(DMA), and due to the charge-reversal property, the carriers were found to be difficult to uptake cellularly at pH 7.4, but were able to enter the HeLa cells more easily after accumulation in weakly acidic tumor tissues (pH 6.5), as the hydrolysis of β-carboxylic amide revealed the positive charged PLL. The lower pH in the cancer cell (4.5–6.5) caused the dissolution of the "cap" ZnO to release doxorubicin for cellular apoptosis [48].

3.2.2 Release Based on Glutathione

Recently, glutathione (GSH) has been widely exploited to develop a stimulus-sensitive system by breaking down the disulfide bond in the structures using the large concentration differences between extracellular (2–10 μM) and intracellular (2–10 mM) conditions. Importantly, the GSH concentration in cancer cells was found to be several times higher than normal cells, and this could be utilized by different drug delivery systems for selective cancer treatment [49]. Yang et al. (2016) designed disulfide bond-bridged and large-pore MSNs for intracellular RNase A delivery. These disulfide bond-bridged MSNs exhibited a GSH-sensitive degradation behavior that exhibited a higher rate of degradation in cancer cells but a lower rate in normal cells [49]. Wu et al. (2016) formulated a redox-sensitive gene release by decorating poly(β-amino esters) via a disulfide binder based on the large pore size of HMONs (hollow mesoporous organosilica nanoparticles). These redox-sensitive intelligent nanocarriers were used to co-deliver P-glycoproteins (P-gp) modulator siRNA and anticancer drug doxorubicin to reverse the multidrug resistance of breast cancer cells both in vitro and in vivo [18].

Many studies have shown that GSH-sensitive release is combined with other stimulants to give MSN dual-sensitive properties. Shao et al. (2018) developed oxidative/redox dual-responsive large-pore organosilica nanoparticles to deliver RNase A for cancer treatment. These diselenide-bridged MSNs were able to load cytotoxic RNase A into the internal pores of 8–10 nm by electrostatic interaction. RNase A-loaded MSNs exhibited oxidative/redox dual-responsive protein release behavior and improved in vitro and in vivo anticancer activity with low systemic toxicity [50]. In the study of Zhang et al. (2019), a functionalized dual-sensitive MSN formulation was prepared for both redox-responsive drug release and enzyme-responsive drug release (Fig. 6). Apoptotic peptide (KLAKLAK)$_2$ was attached to the MSN surface by disulfide bonds and was expected to release by responding to GSH in tumor cells. Then they chose reductive agent dithiothreitol (DTT) as an alternative to GSH, to mimic reductive environment inside cells. The release rate of apoptotic peptide from the MSN-SS-KLA with DTT was found to be significantly faster than that without DTT, and the drug release rate increased as DTT concentration increased. This is due to the cleavage of the disulfide bonds between KLA and MSN under reductive conditions. To investigate the effect of enzyme on drug release, BSA was used as the outer layer of the MSN-based drug carrier. Since trypsin is capable of degrading BSA, in vitro release experiments containing trypsin at different concentrations were performed. Drug release rate from the doxorubicin-loaded MSN-SS-KLA/BSA was found to be significantly faster with trypsin than that without trypsin. Therefore, they concluded that a dual-sensitive drug delivery system (doxorubicin@MSN-SS-KLA/BSA) capable of achieving the expected off-on release behavior has great potential for antitumor application as smart carriers [51].

3.2.3 Release Based on Biomolecular Recognition

Recently, biomolecules such as antigen-antibody interaction, hybridization of single-stranded DNA, and enzymes have been used as gatekeepers to control drug release. The development of enzyme-gated MSN makes it possible to prepare specific sequences that can provide fine selectivity in the design of advanced gatekeepers. The enzymes may act as a primary sensor to detect the presence of target compounds to be recognized as the INPUT signal and may further catalyze their conversion into a specific stimulus capable of “opening” the gates. These enzymes can be used as binary systems as control elements and gate molecules or can be immobilized as a control unit [52].

Agostini et al. (2012) prepared an ethylene glycol-capped hybrid material for the controlled release of molecules in the presence of esterase enzyme. The resulting organic-inorganic hybrid solid S1 was synthesized by a two-step procedure. In the first step, the pores of an inorganic MCM-41 support (in the form of nanoparticles) were loaded with the ruthenium complex, and then, in the second step, the pore outlets were functionalized with ester glycol moieties that acted as molecular caps. In the absence of an enzyme, release of the complex from aqueous S1 suspensions at pH 8.0 was inhibited due to the steric barrier imposed by the bulky ester glycol moieties. Upon addition of esterase enzyme, delivery of the ruthenium complex was observed due to enzymatic hydrolysis of the ester bond in the bounded ester glycol derivative which induced the release of oligo(ethylene glycol) frag-

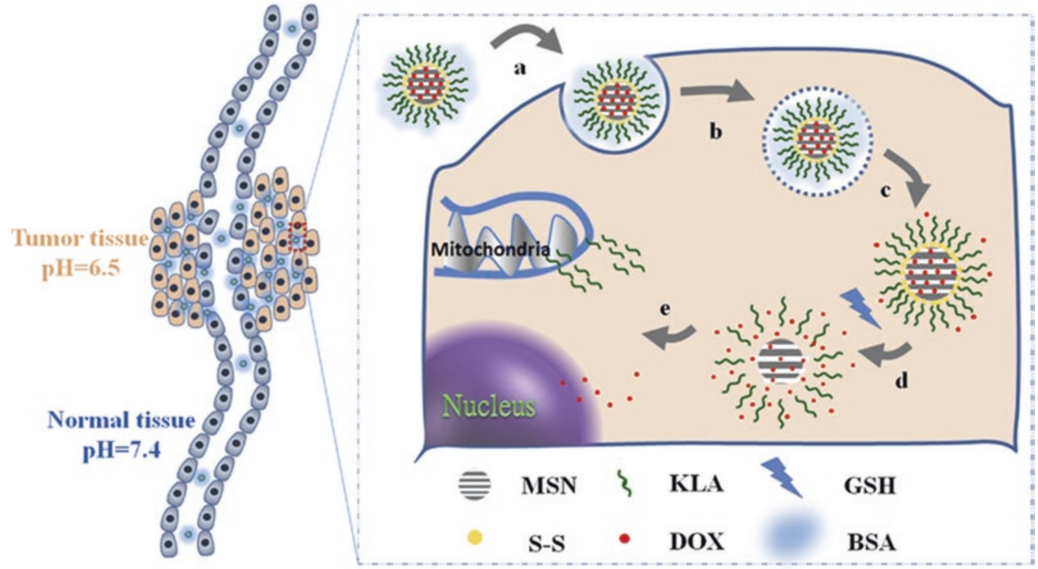

Fig. 6 The cleavage of disulfide bonds by the highly concentrated GSH in the cytoplasm of tumor tissue leading to the release of chemotherapeutics. (Reproduced from Zhang et al. [51])

ments. Hydrolysis of the ester bond allowed the release of the entrapped cargo (Fig. 7). The S1 nanoparticles were not toxic for cells, as demonstrated by cell viability assays with HeLa and MCF-7 cell lines, and were found to be associated with lysosomes as demonstrated by confocal microscopy. However, cells treated with the cytotoxic drug camptothecin-loaded S1 nanoparticles underwent cell death as a result of cellular internalization and subsequent cellular enzyme-mediated hydrolysis followed by opening of the molecular gate that induces the release of camptothecin [53].

Nanosystems responsive to tumor-specific enzymes are considered as a highly attractive approach for intracellular drug release in targeted cancer therapy. The most important point for successful chemo-responsive release is to select the appropriate combination of enzyme media and capping agent to trigger the drug release. In this context, Qiao et al. (2019) developed an enzyme-sensitive drug delivery system that targets the specific intracellular microenvironment in tumor tissues and releases loaded therapeutic agents only in the presence of indoleamine 2,3-dioxygenase 1 (IDO1) enzyme. MSNs were capped with tryptophan-mediated cucurbit[8]uril complex together with Fe_3O_4 to minimize the premature drug leakage to deliver the payload on demand in target tissue. The supramolecular interaction between tryptophan and cucurbit[8]uril is impaired in the presence of IDO1 enzymes which are overexpressed in various cancer cells and intracellular release of therapeutics exclusively in tumor cell. The MTT and FACS results confirmed that drug release is triggered only in the presence of the highly selective IDO1 enzyme and induces significant cytotoxicity against HepG2 cells as well as the superior antitumor effects in vivo [36]. In another study, Yu et al. (2018) constructed a Mg^{2+}-dependent DNAzyme-functionalized hollow MSNs loading with anticancer drug doxorubicin. Mg^{2+}-dependent DNAzyme on the surface of HMSNs nanopores acted as a gatekeeper locking the doxorubicin in the nanostructure of HMSNs and unlocking the nanopores of hollow MSNs to release doxorubicin when triggered by Mg^{2+} ions. These Mg^{2+} ions originated from the biodegradation of hollow MSNs that release Mg^{2+} ions in slightly acidic microenvironment of tumor tissues. In addition, the anticancer activity of chemotherapeutic drugs assisted by these biodegradable smart nanocarriers was increased. Tumor growth of Mg^{2+}-dependent DNAzyme-functionalized hollow MSNs-treated mice compared to control and free doxorubicin groups showed enhanced tumor growth inhibition efficiency, and tumor-suppressing effect of functional hollow MSNs loaded with anticancer drug doxorubicin could reach up to 68.75% [9]. Although different strategies have been developed to achieve chemo-responsive release, particularly in the tumor region, further studies are needed to understand biodistribution and bioaccumulation of these systems and reduce immunogenic responses.

4 Macromolecular Drug Delivery by MSNs for Cancer Diagnosis and Therapy

Cancer has been one of the leading causes of death worldwide for decades. Traditional cancer chemotherapy is still a common treatment, but toxicity problems are inevitable due to the similarity between healthy human and cancerous cells. Cancer is generally believed to be a special site with unique microenvironment with a low pH, high GSH concentration, hypoxia, and tumor-specific enzymes. Therefore, the design of therapeutic nanoplatforms with novel properties that can respond to specific characteristics of the tumor microenvironment has been considered a promising strategy to achieve the desired therapeutic efficacy. In addition, nanoplatforms with flexible properties that can increase blood circulation time and their accumulation in tumors are highly desirable, especially for cancer nanoproducts [43].

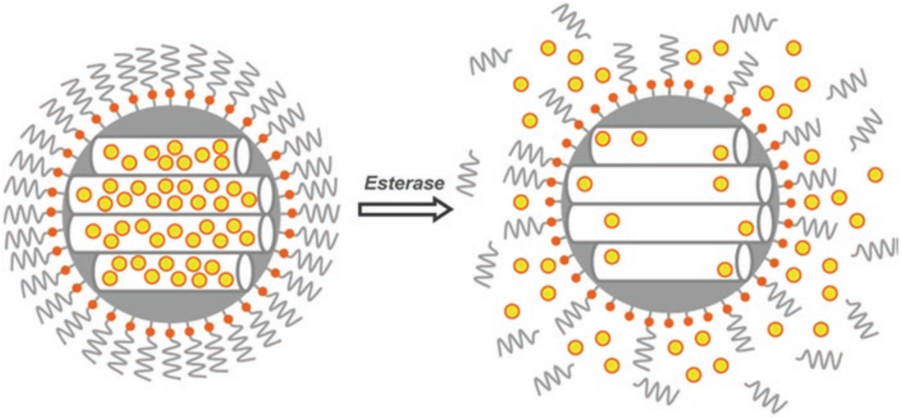

Fig. 7 Hydrolysis of the ester bond in the presence of a specific enzyme (esterase) and the release of the entrapped cargo. (Reproduced from Agostini et al. [53])

4.1 Peptide/Protein Delivery

Intracellular protein delivery allows biomedical applications such as cancer therapy, vaccination, and administration of enzyme-based therapeutics. However, therapeutic proteins are susceptible to high and low pH environments or proteolysis and denaturation, limiting their activity in the body [27, 54]. Therefore, there is a need for novel delivery systems capable of delivering therapeutic proteins to the site of action while maintaining their stability. In this context, the use of MSNs for intracellular protein delivery has many advantages. The large pore volumes of MSNs (>1 cm^3/g) allow for loading a measurable amount of protein into the particles. The chemically and mechanically stable inorganic oxide framework of MSNs protects protein molecules from exposure to proteases and denaturation chemicals. In many applications, such as cancer therapy and immunotherapy, protein therapeutics need to function within cells; however, bare protein cannot automatically cross cell membranes [55]. MSNs have been found to be advantageous not only for the entry of proteins into cells but also for their release into the cytoplasm [28].

There are many studies investigating the use of therapeutic proteins in cancer imaging and therapy through MSNs. Xu et al. (2019) prepared arginine-glycine-aspartic acid-N-εacryllysine (RGD-Acrk)-conjugated MSNs as potential fluorescence imaging nanoprobes of breast cancer tissues in vivo. RGD peptides are known to selectively bind to αVβ3/αVβ5 integrin proteins overexpressed on the surface of breast cancer cells. In vitro confocal and fluorescent imaging showed that these nanoprobes have good binding affinity for the surfaces of breast cancer cells (4T1), resulting in the internalization and accumulation in the cytoplasm of 4T1 cells. RGD-Acrk-conjugated MSN nanoprobe was applied in vivo to detect tumors of breast cancer mice. It has been noted that these nanoprobes are non-toxic, targeted fluorescent probes that selectively accumulate in cancer cells and tissues for early detection and monitoring of tumor growth in vivo [55]. MSNs with large pores and different geometries have been tested for higher loading of peptides/proteins and increased uptake and cytotoxicity of cancer cells. Rahmani et al. (2019) synthesized LPMSNs and hollow MSNs and loaded pepstatin A into both formulations, with a loading efficiency of 32% and 18%, respectively. TEB was used as pore-expanding agent in these formulations. Although LPMSNs have higher loading capacity, pepstatin A-loaded LPMSNs lead to 20% cell death in MCF-7 breast cancer cells, while approximately 60% cell death is observed in hollow MSNs. It has been suggested that this may be due to the release of pepstatin A in cancer cells prior to endocytosis and the binding of pepstatin A to HOSNP with a stronger interaction [20]. In another study, a new type of MSNs featuring a cuboidal-like geometry and large pores (10 ± 1 nm) was synthesized by Yang et al. (2017). The maximum cytochrome-c loading capacity of these cuboidal MSNs was determined to be 470 μg/mg MSNs. To increase the colloidal stability, MSNs/cytC were decorated with a fusogenic lipid bilayer, and the hydrodynamic diameter observed by dynamic light scattering of the nanoparticles was found to be 230 nm. The lipid bilayer acted as a physical barrier and reduced the early release of cytC, thereby retaining the protein better in MSNs. The delivery and bioactivity of cytC using lipid bilayer-coated MSNs resulted in 55% of apoptosis after 48 hours, due to increased uptake and release of cytC into the cytosol of the HeLa cells [27]. Gu et al. (2013) synthesized monodispersed MSNs using cationic surfactants as templating agents, neutral amine of N,N-dimethylhexadecylamine as a pore size mediator, and triblock copolymer of F127 as a particle growth inhibitor/dispersant. The obtained MSNs exhibited a highly ordered mesostructure and tunable pore diameter up to 4.6 nm and monodispersed particle sizes less than 150 nm. A model protein, cytC, was loaded (230 mg/g) in the resultant MSNs. To demonstrate their potential as a protein delivery vehicle, the uptake of the cytC-MSNs by HeLa cancer cells was investigated, and it was determined that MSNs were efficiently internalized into cancer cells and could escape from endosomes [17].

It is important to evaluate the pore width and particle size together for the efficient uptake of macromolecules by the cells. Slowing et al. (2007) synthesized a MCM-41-type MSN with a large pore diameter by adding a pore-expander TMB to a CTAB-templated synthesis. The BJH method yielded two pore size distributions centered on 5.4 nm (major peak) and 14.5 nm (minor). Two different particle size distributions (265 and 933 nm) were measured by dynamic light scattering. The cytochrome-c-encapsulated MSNs were internalized by living human cervical cancer cells (HeLa), and the protein could be released into the cytoplasm. The uptake of MSNs observed in this study was found lower than previously observed for MSNs with the smaller pore size. This difference in uptake efficiency was mainly attributed to the difference in particle size, since the smaller-pore MSNs have an average size around 150 nm, whereas the pore-enlarged MSNs are larger than that [28]. This is the first known example of intracellular protein delivery by MSNs.

A unique advantage of MSNs is the nanoparticle morphology with two independent surfaces (Fig. 1). MSNs have an inner pore surface and an outer surface that can not only serve for different critical functions in the biomacromolecular delivery process (see Fig. 8) but can also be selectively and independently functionalized. Thus, chemical and biological material can be applied together using these surfaces of MSN. For example, Zhang et al. (2019) designed multifunctional MSNs for sub-cellular co-delivery of drug and therapeutic peptide to tumor cells. Firstly, a kind of cell apoptosis peptide $(KLAKLAK)_2$ (KLA) was anchored on the

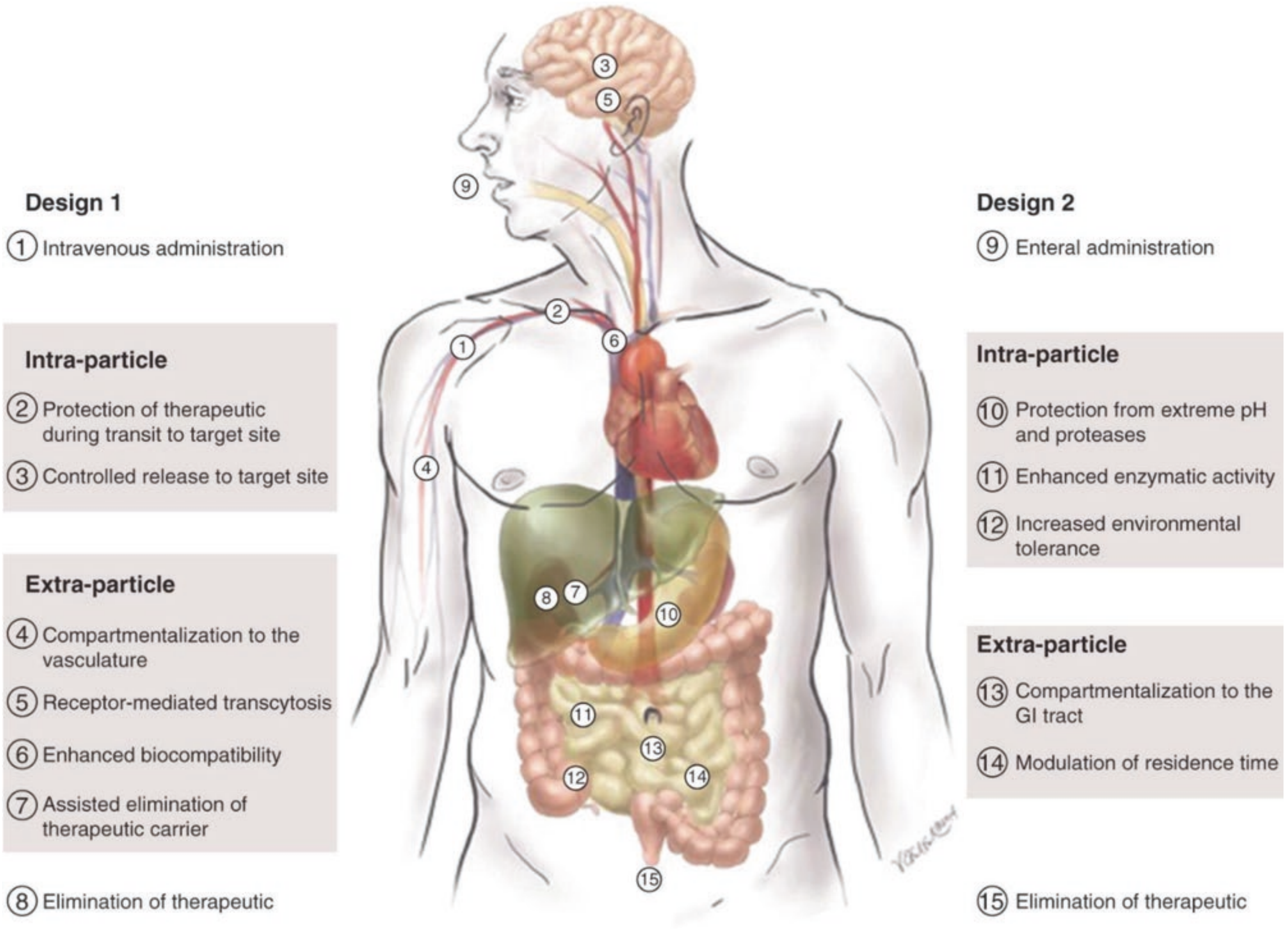
Design 1
① Intravenous administration
Intra-particle
② Protection of therapeutic during transit to target site
③ Controlled release to target site
Extra-particle
④ Compartmentalization to the vasculature
⑤ Receptor-mediated transcytosis
⑥ Enhanced biocompatibility
⑦ Assisted elimination of therapeutic carrier
⑧ Elimination of therapeutic
Design 2
⑨ Enteral administration
Intra-particle
⑩ Protection from extreme pH and proteases
⑪ Enhanced enzymatic activity
⑫ Increased environmental tolerance
Extra-particle
⑬ Compartmentalization to the GI tract
⑭ Modulation of residence time
⑮ Elimination of therapeutic
③
⑤
⑨
②
①
⑥
④
⑧
⑦
⑩
⑪
⑬
⑫
⑭
⑮

Fig. 8 Illustration of how the inner and outer MSN surfaces can be of benefit during the delivery process considering two different routes of administration (IV/parenteral and oral/enteral). (Reproduced with permission © 2019 Virginia E. Fulford)

MSN surface to help the MSN drug carrier escape from endosome after being internalized by tumor cells and release the loaded drug in the cytoplasm. The anticancer drug doxorubicin hydrochloride was then loaded into the pores of MSNs. Then, the drug-loaded MSNs were coated with BSA to achieve a biologically stable MSN-based drug delivery system for cancer synergetic therapy and were able to keep well dispersed in serum for more than 24 hours. After accumulating by EPR effect in the tumor site, the KLA peptide-anchored doxorubicin-loaded BSA-coated MSNs were able to be effectively phagocytosed by HeLa cells and release apoptotic peptide KLA with doxorubicin, which simultaneously respond to reductive stimulus inside the cells. In vitro results showed that the resulting MSN formulation exhibited better inhibition on HeLa cells compared to pure doxorubicin; this demonstrated the success of co-delivery of KLA and doxorubicin to achieve synergetic cancer therapy [51]. In the study of Xu et al. (2018), hydroxyl-, amine-, thiol-, and carboxyl-functionalized MSNs loaded with Bcl-2-converting peptide were synthesized by different surface functionalities to treat multidrug-resistant cancer cells. The resulting large-pore (8–10 nm) MSNs having a small particle size of 174–207 nm exhibited a high Bcl-2-converting peptide loading efficiency of over 40%, especially in those modified with the thiol group. In addition, the amine-modified surface of MSNs has been shown to have a greater effect on the cell apoptosis-inducing effects of peptide compared to others [6]. Tambe et al. (2018) synthesized PEG and triptorelin ligand-conjugated MSNs and characterized them for targeted drug delivery to GnRH-overexpressing cancer cells. Internalization studies showed higher uptake and significant cytotoxicity of doxorubicin-loaded targeted MSNs as compared to doxorubicin-loaded bare MSNs in breast (MCF-7) and prostate (LNCaP) cancer cell lines [56]. Bhattacharyya et al. (2012) synthesized poly(ethylene glycol) (PEG)-coated MSNs with an average particle size of 120 nm containing trypsin inhibitor (TI), a model protein molecule for growth factors. The pore size of the MSNs was expanded by a hydrothermal treatment prior to TI incorporation. 16% loading of TI was achieved for pore-expanded MSNs. In the PEG-coated MSNs, zero-order release was achieved for 4 weeks [57].

As mentioned in the studies above, MSNs allow various modifications to suitably protect the protein structure against physiological conditions. However, although MSN pores are enlarged so that proteins can be loaded, for larger proteins, there is still a size limit. Only small proteins can be loaded successfully because larger ones will not fit in the pores. In this respect, the development of MSN's properties for protein delivery is an area that needs to be improved.

4.2 Gene Delivery

Gene therapy is a promising strategy to treat cancer and other diseases. However, the transfer of a desired gene into host cell nucleus to treat genetic disorders is a complex process with various limitations. Successful gene delivery requires an efficient system to deliver genes to specific cells because naked nucleic acids alone can be rapidly degraded by endogenous nucleases and can be difficult to penetrate through cell membranes. Therefore, an effective gene delivery vector should be able to load a sufficient number of genes, provide a protective environment, and effectively penetrate into cells. In addition, the preparation for an ideal gene carrier should be easy, and the carrier system should not be toxic [5].

4.2.1 pDNA Delivery

MSNs usually have a relatively small 2–3 nm pore size that is not applicable for gene loading and delivery. However, it has been reported that MSNs with pores larger than 5.4 nm are favorable for the absorption of DNA (2000 bp) into the internal pores [58]. The benefit of using LPMSNs as a DNA carrier is to achieve high DNA loading and to provide enhanced protection of DNA against DNase degradation. However, the successful application of LPMSNs for delivery of nucleic acid-based drugs requires surface modification of the silica to produce enough binding affinity for the negatively charged nucleic acids. A variety of techniques have been applied to introduce positively charged functional groups in silica materials, either through noncovalent interactions or by covalent bonding. Amino silanes and polycation polymers have been widely used as chemical agents for modifying silica surfaces [29]. However, there is still a need to develop a simple synthetic methodology for producing MSNs with large pore sizes and ultrasmall particle sizes for intranuclear gene delivery as well as high biocompatibility and transfection efficiency [32].

Numerous studies have been conducted for cancer therapy by introducing genes through MSNs. Niu et al. (2014) developed monodispersed LPMSNs with ordered, accessible, and interconnected pore channels and smaller particle dimensions by employing common polystyrene-b-poly(acrylic acid) as pore template and CTAB as structure-stabilizing agent. By controlling the amount of CTAB added, LPMSNs with different mesostructures (hexagonal, cubic, and lamellar) were synthesized. In addition, the morphology of the MSNs varied from large-pore MSNs to hollow MSNs using block copolymers having shorter or longer PAA lengths as pore templates. The well-defined and monodisperse nanospheres with a hydrodynamic diameter of 293 nm and mesopore diameter of ~16.7 nm were produced. Finally, to assess the loading capacity of amino-functionalized LPMSNs, the plasmid-encoding VEGF short hairpin RNA (pDNA) was selected as model gene. The loading amount of the pDNA was found to be 26.7 μg/mg. The transfection efficiency of pDNA-loaded LPMSNs into human hepatocarcinoma cell line (SMMC-7721 cells) and in vivo tumor gene therapy in SMMC-7721 tumor-bearing mice were also investigated. Compared to the control group, the VEGF mRNA level was downregulated in cells treated with pDNA-loaded amine-modified LPMSNs, which showed remarkable downregulation ability in targeting the VEGF gene. The pDNA-loaded amine-modified LPMSN-treated mice significantly reduced tumor volumes by 47% in 21 days, as compared to the control group. It has been concluded that amine-modified LPMSNs could act as effective plasmid carriers to knockdown VEGF both in vitro and in vivo and demonstrate their potential for application in future cancer treatment [11]. In another study, Chang et al. (2019) developed MSNs that can deliver a Sleeping Beauty system to permanently integrate the asparaginase gene into the genome of human lung adenocarcinoma cells. The Sleeping Beauty (SB) transposon system is a nonviral vector that mediates the stable integration of therapeutic transgenes into the genomes of treated cells and provides sustained expression over a long period of time. Two vectors, the transfer vector pSB-ASNase and the Sleeping Beauty vector SB100, were co-delivered by the PEI-absorbed MSNs into the human lung adenocarcinoma cells. The intracellular asparaginase expression led to the cell cytotoxicity for PC9 and A549 cells. In addition, the combination of the chemotherapy and the asparaginase gene therapy enhanced the cell cytotoxicity of PC9 and A549 cells. The cisplatin treatment alone resulted in 48% cell death of PC9, while co-treatment of the cisplatin and MPT increased the death rate to 69%. Similarly, the doxorubicin treatment alone caused only 22% of A549 cell death, while the doxorubicin and MPT co-treatment increased the cell death to 63% [59].

Gene loading and transfection efficiency were increased by surface modification of LPMSNs with positively charged functional groups, and genes were protected against enzymatic destruction. Zhan et al. (2017) prepared hollow MSNs with large pore size (~10 nm) and functionalized with less toxic 1.8 kD PEI. The maximum loading capacity of green fluorescent protein labeled DNA in the NPs was 37.98 mg/g, an indication that both hollow and large pores contributed to the increase in DNA adsorption. PEI-HMSNs doubled transfection of loaded GFP-DNA plasmid compared to 25 kD PEI confirmed by confocal microscopy [5]. Wu et al. (2015) synthesized mesoporous organosilica nanoparticles (MONs) with micelle/precursor co-templating assembly strategy. Synthesized MONs possessed large nanopores (6.2 nm) and ultrasmall particle sizes (50.75 nm), a large surface area, and a high pore volume. In addition, the unique large mesopores and ultrasmall particle sizes of the MONs have been successfully used for high-throughput intranuclear gene transfer after the stepwise surface conjugations with PEI and TAT pDNA. The loading amount of TAT pDNA was found to be 66.67 μg/mg and two times higher than MSN (33.3 μg/mg). The nuclear targeting gene delivery nanoplatform TAT pDNA-loaded MONs improved protection for loaded genes and enhanced transfection efficiencies of plasmids and was found superior to traditional MSNs of small pore sizes [32]. In another study, Gao et al. (2009) reported LPMSNs with 150 nm in size and uniform pores with the large pore entrance size (17.2 nm) and cavity diameter (20.5 nm) by a low-temperature (10 °C) synthetic method in the presence of a dual surfactant system. Pluronic F127 used as supramolecular template and co-assembled with hydrolyzed silica species to develop a partially ordered mesophase with face-centered cubic symmetry, a fluorocarbon surfactant with high surface activity (FC-4) surrounded the silica particles through interactions and limited their growth. Furthermore, functionalization of these LPMSNs with aminopropyl groups allowed adsorption of *p*DNA and protected it from enzymatic cleavage [30].

4.2.2 Aptamers for Targeted Delivery of MSNs

Aptamers are synthetic single-stranded oligonucleotides and have a three-dimensional structure that specifically recognizes and binds to target molecules with high affinity. They are desirable candidates for systemic administration and treatment because of their excellent molecular recognition capability, high specificity to target molecules, and lower immunogenicity compared to peptides and antibodies [45, 60]. Nejabat et al. (2018) fabricated nucleolin-targeted hybrid nanostructure based on hollow MSNs. The surface of doxorubicin-encapsulated hollow MSNs was coated with acetylated carboxymethyl cellulose and then covalently conjugated to the AS1411 aptamer for targeted delivery to nucleolin overexpressed cancerous cells. The size and shell thickness of surface-modified hollow MSNs were measured as 150 nm and 30 nm, respectively. AS1411 aptamer showed significant enhancement in cellular uptake and cytotoxicity to MCF-7 and C26 cells in vitro compared to non-targeted doxorubicin nanoparticles and free doxorubicin and specifically targeted nucleolin-overexpressing MCF-7 and C26 cells. Furthermore, the in vivo tumor inhibitory effect of AS1411 aptamer-conjugated formulation also confirmed the efficiency in inhibiting tumor growth and improving the survival rate in comparison with non-targeted and free doxorubicin-treated mice [60]. Zahiri et al. (2019) synthesized doxorubicin-loaded dextran-capped MSNs and attached an RNA aptamer against a cancer stem cell marker CD133 covalently to the carboxyl groups of dextran (Fig. 9). The in vitro evaluation of cellular uptake and cytotoxicity demonstrated that the produced nanosystem specifically targets colorectal cancer cells (HT29) [45].

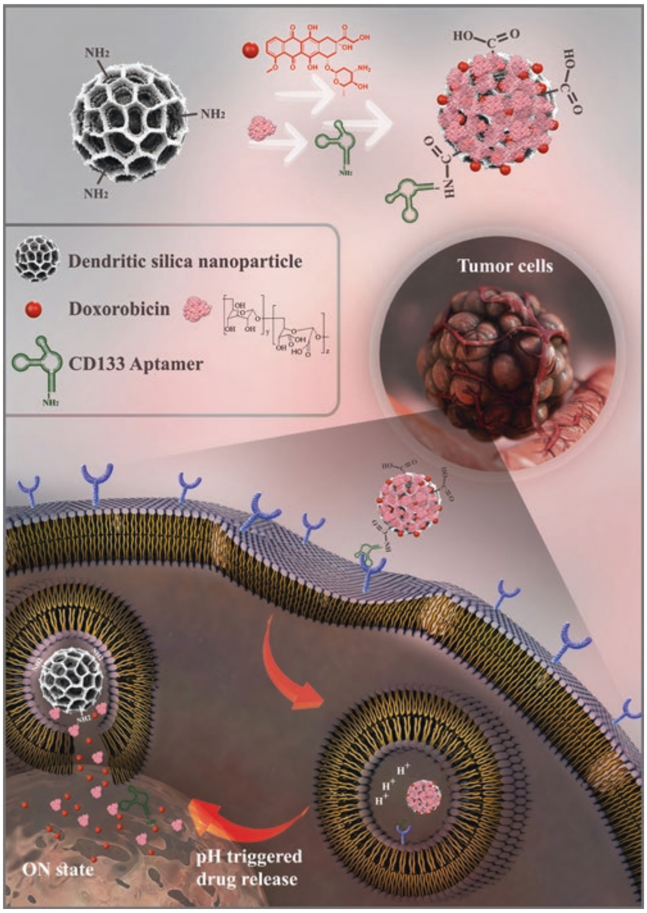

Fig. 9 Conjugation of CD133-RNA aptamer to the surface of MSNs and specific transportation of encapsulated anticancer drug to CD133-overexpressing cancer cells. (Reproduced from Zahiri et al. [45])

Multifunctional MSNs can combine different materials on a functionalized platform. Since the targeting parts can be easily attached to the MSN surface, intelligent designs can be made. Shen et al. (2019) fabricated a HApt aptamer-functionalized pH-sensitive β-CD-capped doxorubicin-loaded MSN (MSN-BM/CD-HApt@DOX) with 218.2 nm in size for targeted delivery and selective targeting of HER2-positive breast cancer. MSN functionalized with 1-methyl-1H-benzimidazole was used to load and obtain pH stimuli-responsive release of the doxorubicin. β-CD exhibited stable hydrophobic interactions with 1-methyl-1H-benzimidazole at physiological pH (7.4), thus introduced as a gatekeeper for encapsulated doxorubicin. HApt was a selective HER2-targeting moiety and biotherapeutic agent, and the β-CD-SH was then functionalized with HApt-SH by disulfide bonding. MSN-BM/CD-HApt@DOX underwent HER2-mediated endocytosis and was found to be more cytotoxic to HER2-positive SKBR3 cells than HER2-negative MCF7 cells. MSN-BM/CD-HApt@DOX also exhibited better uptake and stronger growth inhibition in SKBR3 cells than the control MSN-BM/CDNCApt@DOX functionalized with a scrambled nucleotide sequence on CD. Overall, intracellular delivery of doxorubicin and biotherapeutic agent HApt resulted in synergistic cytotoxic effects in HER2-positive cancer cells compared to doxorubicin or HApt alone [46].

4.2.3 siRNA Delivery

By inhibiting the expression of targeted genes, small interfering RNAs (siRNAs) are considered as promising therapeutics for the treatment of cancer and genetic disorders. However, the use of siRNA as a therapeutic agent is restricted by its poor cellular uptake and short half-life [61]. MSNs have received increasing attention to overcome degradation of siRNA by RNases and to improve intracellular uptake delivery. Hartono et al. (2012) synthesized LPMSNs less than 200 nm in size and functionalized with PLL consisting of cage-like pores organized in a cubic mesostructure. LPMSNs were synthesized by a combination of a dual surfactant system, that is, a combination of triblock copolymer (F127) acting as the cubic pore structure directing agent and a fluorocarbon surfactant (FC-4) to control particle growth. It is noted that the usage of low temperature increases the penetration of the swelling agent TMB into the hydrophobic core of micelles during synthesis, which ultimately results in an extra enlargement of the pore size. The cavity size of LPMSNs was obtained as 27.9 nm, with an entrance size of 13.4 nm. A significant increase of the nanoparticle binding capacity for oligo-DNAs (57 μg/mg) was observed with particle modification by PLL, and functionalized nanoparticles showed a strong ability to deliver oligo-DNA-Cy3 to HeLa cells. Consequently, PLL-functionalized nanoparticles exhibited a strong ability to deliver oligo-DNA-Cy3 (a model for siRNA) to HeLa cells. The system has also been tested to deliver functional siRNAs against minibrain-related kinase (Mirk) and polo-like kinase 1 (PLK1) in osteosarcoma cancer (KHOS) cells, and the cellular viability of osteosarcoma cancer cells was significantly reduced [29].

Recent research has shown that MSN-based gene therapy can be combined with chemotherapy to overcome drug resistance and explore potential therapeutic benefits for the treatment of many complex diseases. Zhang et al. (2019) developed a hybrid MSN using a layer-by-layer assembly method. Hybrid MSNs were coated with hyaluronic acid (HA), and both disulfide bonds and HA coating of hybrid MSNs facilitated controlled drug release in the tumor microenvironment. Hybrid MSN-HA nanoparticles with negative surface charge were grafted with PEI to increase cellular uptake and gene loading efficiency. In vitro release studies indicated that hybrid MSN/HA/PEI can prevent doxorubicin leakage before reaching tumor tissues and is sensitive to intracellular stimuli of hyaluronidase and GSH. Furthermore, the PEI-grafted nanovector showed high siBcl-2 binding efficacy and effectively protected siBcl-2 against enzymatic degradation. Additionally, siBcl-2 and doxorubicin co-loaded hybrid MSNs exhibited the greater growth inhibition against MCF-7 cells compared to single doxorubicin or siBcl-2 showing the synergistic treatment effect of gene and chemical drug on breast cancer [7]. Wang et al. (2018) developed the MSN formulation containing MDR1-siRNA to block MDR1 expression, as well as being able to transport doxorubicin to cancer cells without the effect of multidrug resistance. They modified the surface of MSNs with cationic polymer PEI to obtain positive charge on the surface that would enable them to carry MDR1-siRNA and doxorubicin. Transfection efficacy experiments have shown that modified MSNs are efficiently transfected into doxorubicin-resistant (KBV) cells of human oral squamous carcinoma in vitro. KBV cells transfected with MSNs were able to effectively reduce gene expression of MDR1 (~70% increase after 72 hours of treatment) and induce apoptosis of KBV cells in vitro (24.27% after 48 hours of treatment). MSNs dramatically reduced tumor size (81.64% reduction after 28 days post-treatment) and significantly slowed tumor growth rate compared to the in vivo control group [62]. Wu et al. (2016) used a selective bond breakage strategy based on the difference in stability for the fabrication of large-pore (24 nm) HMONs. The basis of this strategy was found to be the expansion of the pore size in the shell as a result of the selective degradation of the weak Si-C bonds due to the difference in chemical bond stability within the framework where the Si-C bond was significantly weaker than the Si-O bond. Subsequently, these mesopores formed larger pores by continuously fusing or merging with each other with the breakage of more Si-C bonds by increasing the hydrothermal temperature (160 °C). A redox-responsive gene release was provided by functionalization with poly(β-amino esters) via a disulfide linker. These functionalized nanocarriers were further used to co-deliver P-gp modulator siRNA (high RNA loading up to 200 μg/mg) and doxorubicin to reverse the MDR of breast cancer cells. The P-gp expression on MCF-7/ADR membrane was remarkably downregulated by the developed formulation. The introduction of siRNA significantly increased the doxorubicin concentration in MCF-7/ADR cancer cells, further confirmed by cell apoptosis and cell cycle change analyses. Antitumor effect was evaluated in mice bearing MCF-7/ADR tumor xenograft. The tumor volume of the free doxorubicin-treated group was 45.12% of the control group at the end of experiments. Comparatively, the doxorubicin-loaded functionalized HMON group exhibited improved tumor growth inhibitory effect, resulting in a 72.2% reduction in tumor volume. In the functionalized HMON group where siRNA and doxorubicin were loaded together, the highest antitumor activity was obtained, with a tumor volume only 7.61% of the control group [18].

Pan et al. (2018) synthesized an ultra-thin ZIF-8 film for pore blockage on the MSN surface and fabricated a pH-responsive drug delivery system below 100 nm for efficient delivering siRNAs and therapeutic drugs (Fig. 10). The dual delivery of siRNAs and drugs using the ZIF-8-coated MSNs was demonstrated by electrostatic adsorption of Bcl-2 siRNA (98.11%) at the positively charged ZIF-8 film and loading of doxorubicin (59.73%) into the pores. It is noted that the ZIF-8 film can convert the charge of MSN-COOH from negative to positive for efficient loading of siRNA through electrostatic interactions and protect siRNA from nuclease degradation. The pH sensitivity of ZIF-8-coated MSNs was confirmed by release studies and TEM. In addition, the ZIF-8 film was reported to dissociate in the acidic endolysosome and induce the intracellular release of siRNA and doxorubicin, leading to a significantly enhanced chemotherapeutic efficacy for multidrug-resistant cancer cells including MCF-7/ADR and SKOV-3/ADR [63].

4.2.4 MicroRNA Delivery

MicroRNAs (miRNAs) are a class of small endogenous non-coding RNAs of 18–25 nucleotides in length that functions in RNA silencing and gene expression at the post-transcriptional level. Aberrant expressions of miRNAs have been shown to be associated with tumor onset, progression, and metastasis. Unlike siRNAs with one specific target mRNA, miRNAs can achieve gene-silencing effect by regulating multiple mRNAs, making them effective tools for the treatment of complex multigenic diseases such as cancers. Restoring miRNA function by mimicking miRNA and inhibiting the function of a miRNA with antisense miRNA oligonucleotides (anti-miRs) are the two main strategies of modulating miRNA activity [64]. Li et al. (2018) reported MSNs loaded with anti-miR-155 and modified with polydopamine and AS1411 aptamer (modified MSNs) for the targeted treatment of colorectal cancer. Modified MSNs significantly inhibited the expression of miR-155 and NF-κB (P65) in SW480 cells. Due to the high selectivity, modified MSNs effectively inhibited tumor growth in SW480 tumor xenograft nude mice compared to the saline control group. The developed modified MSN formulation was also examined to overcome 5-FU resistance occurring in ~90% of patients with colorectal cancer. Combined treatment of free 5-FU and modified MSNs exhibited higher cytotoxicity on SW480 and SW480/ADR cells, indicating that modified MSNs successfully increased the sensitivity of SW480 cells to 5-FU. The researchers also evaluated combined antitumor therapy in nude mice with SW480 tumor xenograft. Antitumor therapy of free 5-FU and modified MSNs could inhibit tumor growth more effectively than free 5-FU [64].

The surface of MSNs is generally functionalized with positive groups to increase the loading of microRNAs and then coated with polymers to increase miRNA stability. In the study of Hu et al. (2019), anti-miR21 and resveratrol-loaded HA-conjugated MSNs with 155 nm hydrodynamic size were developed to enhance therapeutic efficacy in gastric carcinoma. They modified the MSN surface with PEI to load anti-miR21. Since the presence of a protective coating is believed to increase the stability of charged anti-miR21 and can target cancer tissues, the surface was conjugated

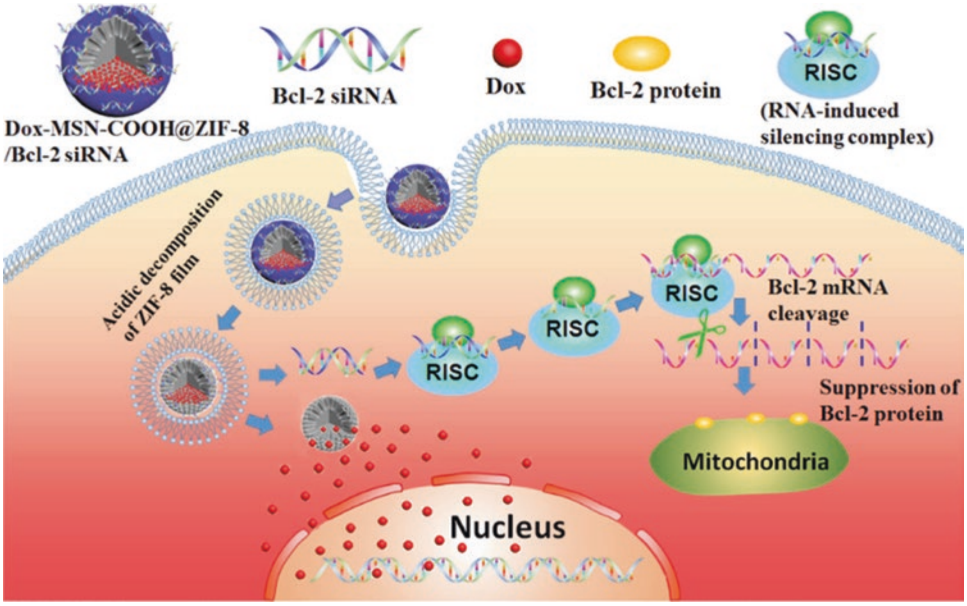

Fig. 10 Schematic view of a pH-sensitive drug delivery system for effective delivery of siRNAs and chemotherapeutics. (Reproduced from Pan et al. [63])

with HA, which specifically targets receptors in the tumor and potentially enhances cellular internalization. Confocal laser scanning microscopy and flow cytometry analysis confirmed higher cellular internalization of HA-conjugated MSNs. In vitro cytotoxicity and apoptosis assays confirmed the superior anticancer effect of the functionalized formulation and synergistic effects of anti-miR21 and resveratrol in gastric cancer cells with apoptosis and cell necrosis mechanisms. A threefold higher tumor regression effect compared to treatment with free resveratrol and a double tumor regression effect compared to MSNs without HA conjugation were achieved with HA-conjugated MSNs [65]. Yang et al. (2019) designed oxaliplatin- and miRNA-204-5p-loaded PEI-based MSNs with surface conjugated with HA. In addition to the tumor-suppressing effect of miR-204-5p, the anticancer effect of oxaliplatin was aimed to increase synergistically. The oxaliplatin loaded in the pores of the MSN and presence of PEI allowed the loading of miRNA. The final particle size was 138.4 nm with a narrow size distribution. Presence of surface-bound HA promoted the selective targeting of its native ligand, CD44 receptors, on the colon cancer cells. The target specificity of functionalized formulation was examined in HT-29 cells, and improved cellular internalization was observed compared to that of untargeted nanoparticles. Oxaliplatin- and miRNA-204-5p-loaded PEI-based MSNs with surface conjugated with HA exhibited a higher cell cytotoxicity than the other formulations, indicating that internalization by CD44 receptor-mediated endocytosis was effective. Furthermore, this formulation caused a marked inhibition of tumor growth [66]. Wang et al. (2018) fabricated doxorubicin-loaded MSNs, conjugated miR-31 onto it, and coated it with PEI/HA. The doxorubicin and miR-31 loading were found to be 6.35 μg/mg and 8.6 nmol/mg, respectively, and drug release was triggered by acidic tumor environment. Co-delivery of miR-31 with doxorubicin within this formulation inhibited the growth of HeLa cells more efficiently than administration of miR-31 or doxorubicin alone [67].

5 MSNs for Cancer Immunotherapy

Cancer immunotherapy is currently one of the most promising strategies for cancer treatment. It stimulates the immune system to increase the effectiveness of cancer therapy. Consequently, both tumor recurrence and metastasis can be prevented. Recent studies have focused on the use of mesoporous silica-based adjuvants due to their excellent properties such as large surface areas, adjustable pore size, various morphologies, easy adjustment of surface properties, and good biocompatibility. However, there are some limitations in the use of MSN-based adjuvants for antitumor immunity. For example, when preparing MSNs with large mesopores to load antigens of larger molecular structure, the particle size also increases and may enter the micron size range. A comparison of antigen-loaded particles of both nanoscaled and micron sizes (17 μm, 7 μm, 1 μm, and 300 nm diameter) has shown that the smaller-sized particles were more readily taken up by bone marrow-derived dendritic cells and consequently also more efficient at stimulating antigen-specific effector immune responses in vivo [68]. Subunit vaccines aiming at induction of cellular (type I) immunity (e.g., cancer vaccines) should thus benefit from encapsulating the antigen in nanoparticles, which consistently outperform microparticles at inducing cytotoxic T cells [69]. In the study of Mathaes et al. (2015), the nanoparticle adjuvant vaccine delivery vehicles displayed a stronger DC activation than the corresponding microparticle counterparts [70]. Furthermore, their therapeutic efficacy as an immunoadjuvant is not satisfactory. Therefore, there is still a need to develop a useful and multifunctional MSN adjuvant to overcome obstacles [71].

Recent studies showed that mesoporous silica materials having different particle sizes, pore structures, and surface functionalities can modulate T cell activation and proinflammatory cytokine production. Xie et al. (2017) developed a monodisperse and stable large-pore hollow MSN formulation for administration of two melanoma-derived antigenic peptides, HGP100 and TRP2, with different hydrophobicities. The loading efficiencies of the peptides were found as 88% and 20.6%, respectively, by adsorption of the hydrophilic HGP100 peptide after the modification of the hollow core of MSNs with NH_2 and hydrophobic TRP2 peptide after COOH modification in porous channels. Hollow MSNs loaded with HGP100 and TRP2 were further encapsulated with liposomes containing the monophosphoryl lipid A (MPLA) adjuvant to improve the stability and biocompatibility of hollow MSNs. This strategy also prevented the leakage of loaded peptides through lipid coating and enhanced antitumor immune responses with the aid of MPLA. The developed hollow MSNs encapsulated HGP100 (in the hollow core) and TRP2 (in the porous channels) together with MPLA-loaded liposomes (on the outer surface of MSNs) stimulated dendritic cells efficiently, resulting in maturation of dendritic cells and secretion of TNF-α, IFN-γ, IL-12, and IL-4. Active CD^{8+} and CD^{4+} T lymphocytes which secreted IFN-γ in local lymph nodes were also significantly increased in vivo. In addition, this formulation led to the inhibition of tumor growth in both B16-F10 prophylactic and lung metastasis models, and the delivery system was thought to have great potential for both preventive and therapeutic cancer vaccination [31]. Lee et al. (2019) reported a click reaction-assisted immune cell targeting (CRAIT) strategy that uses inflammatory $CD11b^+$ cells as active carriers to deliver doxorubicin-loaded MSNs to the less vascularized regions of the tumor. For rapid and catalyst-free reaction in vivo, they

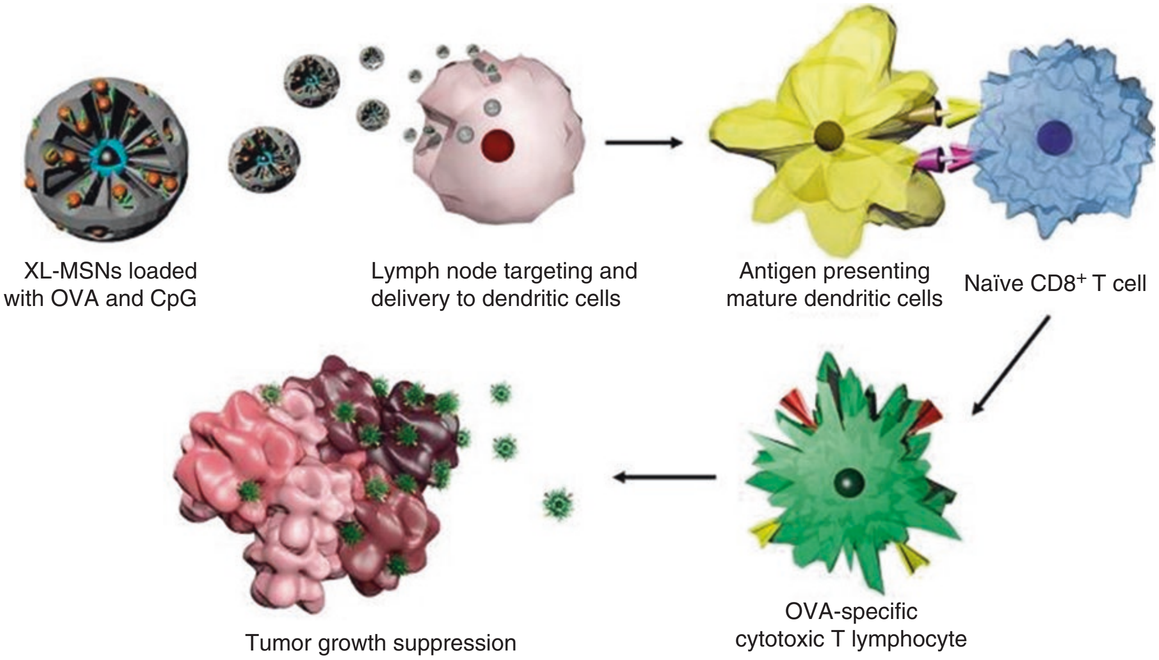
XL-MSNs loaded with OVA and CpG
Lymph node targeting and delivery to dendritic cells
Antigen presenting mature dendritic cells
Naïve CD8⁺ T cell
OVA-specific cytotoxic T lymphocyte
Tumor growth suppression

Fig. 11 Schematic illustration of the overall vaccination process using XL-MSNs loaded with antigen and TLR9 agonist for suppressing tumor growth. (Reproduced from Cha et al. [22])

used tetrazine/trans-cyclooctene (TCO) cycloaddition to selectively target doxorubicin-loaded MSNs to CD11b$^+$ cells in blood circulation and tumor microenvironment. Primary administration of TCO-modified CD11b$^+$ antibodies allowed Tz-functionalized MSNs (MSNs-Tz) to be subsequently conjugated onto CD11b$^+$ cells. Real-time intravital imaging of 4T1 tumor-bearing mice showed that CD11b$^+$ cells tagged with MSNs-Tz are highly mobile, crawling and rolling in tumor vasculatures. CD11b$^+$ cell-mediated delivery showed more uniform distribution and deeper tumor penetration of MSNs-Tz than a conventional passive targeting strategy. In the avascular regions of the tumor, MSNs-Tz delivered by the CRAIT strategy showed two times more accumulation than the nanoparticles transported by the EPR effect. Furthermore, doxorubicin delivery rapidly reduced the tumor burden in an aggressive 4T1 breast cancer model without systemic toxicities [72].

Ding et al. (2018) produced large-pore mesoporous silica-coated upconversion nanoparticles (UCMSs) below 100 nm and evaluated its use as an immunoadjuvant. Merocyanine 540 (MC540) as photosensitizer, chicken OVA as model antigen, and CT26 tumor cell fragment (TF) as tumor antigen were loaded to UCMSs and successfully used in colon cancer tumor-bearing BALB/c mice for in vivo vaccine delivery. The prepared MC540- and OVA-loaded UCMSs showed the best synergistic immunopotentiation effect under near-infrared irradiation at 980 nm. MC540- and TF-loaded UCMS nanovaccine was able to inhibit tumor growth more effectively compared to PDT or immunological therapy alone [73]. In another study, Cha et al. (2018) demonstrated the use of amine-modified XL-MSNs as a cancer vaccine through the delivery of OVA (a model antigenic protein) and CpG oligonucleotide (toll-like receptor 9 (TLR9) agonist). After culture of bone marrow-derived dendritic cells (BMDCs) with antigen and TLR9 agonist-loaded XL-MSNs, the antigen protein and TLR9 agonist were successfully taken up to the cytosol. This led to an increased maturation and antigen presentation of the DCs and increased secretion of proinflammatory cytokines. In the in vivo study, effective targeting to lymph nodes, stimulation of adapted immune responses including antigen-specific cytotoxic T cells, suppression of tumor growth after vaccination, and prevention of tumor growth after substantial vaccination of cancer cells into vaccinated mice due to a significant generation memory T cells were observed (Fig. 11) [22]. These results showed that MSNs for cancer immunotherapy increase the efficacy and clinical potential of immunotherapy as immunoadjuvant.

6 Conclusions and Future Perspectives

The development of various syntheses for LPMSNs has enabled these to be successfully used as delivery vehicles for biomacromolecules. The ceramic silica framework provides efficient protection from the outside environment, providing shelter and stability to the fragile and sensitive biomolecules. The robust inorganic structure further provides ample opportunities for the design of stimuli-responsive drug delivery systems, especially via the gatekeeping approach. Tuning of the surface chemistry of the carrier can ensure maximized affinity between biomolecular cargo and carrier upon loading. Consequently, numerous examples have been showcased for in vitro and in vivo delivery of biomacromolecules with the aid of (LP)MSNs as delivery systems.

Recently, there have been many studies aimed at increasing the pore size in order to load higher amounts of biomacromolecules into MSNs. However, expanding the pore size of MSNs for loading biomacromolecules also causes an increase in the MSN size, which hampers the uptake of the final carrier system by cells. Therefore, it is important to consider the pore size and particle size in parallel. In addition, pore sizes slightly larger than the biomacromolecular size are useful for not limiting the diffusion of the biomolecules to the active sites of mesoporous channels, increasing the amount of loading and enhancing immobilization.

The ability of MSNs to carry multiple bioactive molecules together holds great potential particularly in cancer therapy, to produce a synergistic effect to enhance therapeutic efficacy. Co-delivery of chemotherapeutic agents and biomolecules by MSNs with targeting function can increase the cancer cell accumulation and create synergisms in cancer treatment. Despite the proven efficacy of MSNs in numerous preclinical studies, as with any promising nanopharmaceutical, more efforts are needed for their clinical translation.

References

1. Benezra, M., Penate-Medina, O., Zanzonico, P. B., Schaer, D., Ow, H., Burns, A., et al. (2011). Multimodal silica nanoparticles are effective cancer-targeted probes in a model of human melanoma. *The Journal of Clinical Investigation, 121*(7), 2768–2780.
2. Chen, F., Goel, S., Shi, S., Barnhart, T. E., Lan, X., & Cai, W. (2018). General synthesis of silica-based yolk/shell hybrid nanomaterials and in vivo tumor vasculature targeting. *Nano Research, 11*(9), 4890–4904.
3. Choi, Y. H., & Han, H. K. (2018). Nanomedicines: Current status and future perspectives in aspect of drug delivery and pharmacokinetics. *Journal of Pharmaceutical Investigation, 48*(1), 43–60.
4. Huang, M., Liu, L., Wang, S., Zhu, H., Wu, D., Yu, Z., et al. (2017). Dendritic mesoporous silica nanospheres synthesized by a novel dual-templating micelle system for the preparation of functional nanomaterials. *Langmuir, 33*(2), 519–526.
5. Zhan, Z., Zhang, X., Huang, J., Huang, Y., Huang, Z., Pan, X., et al. (2017). Improved gene transfer with functionalized hollow mesoporous silica nanoparticles of reduced cytotoxicity. *Materials (Basel), 10*(7), 731.
6. Xu, W., Ge, P., Niu, B., Zhang, X., Liu, J., & Xie, J. (2018). Macroporous silica nanoparticles for delivering Bcl2-function converting peptide to treat multidrug resistant-cancer cells. *Journal of Colloid and Interface Science, 527*, 141–150.
7. Zhang, B., Liu, Q., Liu, M., Shi, P., Zhu, L., Zhang, L., et al. (2019). Biodegradable hybrid mesoporous silica nanoparticles for gene/chemo-synergetic therapy of breast cancer. *Journal of Biomaterials Applications, 33*(10), 1382–1393.
8. Chen, C., Tang, W., Jiang, D., Yang, G., Wang, X., Zhou, L., et al. (2019). Hyaluronic acid conjugated polydopamine functionalized mesoporous silica nanoparticles for synergistic targeted chemo-photothermal therapy. *Nanoscale, 11*(22), 11012–11024.
9. Yu, L., Chen, Y., Lin, H., Gao, S., Chen, H., & Shi, J. (2018). Magnesium-engineered silica framework for pH-accelerated biodegradation and DNAzyme-triggered chemotherapy. *Small, 14*(35), e1800708.
10. Kao, K.-C., Lin, T.-S., & Mou, C.-Y. (2014). Enhanced activity and stability of lysozyme by immobilization in the matching nanochannels of mesoporous silica nanoparticles. *The Journal of Physical Chemistry C, 118*(13), 6734–6743.
11. Niu, D., Liu, Z., Li, Y., Luo, X., Zhang, J., Gong, J., et al. (2014). Monodispersed and ordered large-pore mesoporous silica nanospheres with tunable pore structure for magnetic functionalization and gene delivery. *Advanced Materials, 26*(29), 4947–4953.
12. Saikia, D., Deka, J. R., Wu, C. E., Yang, Y. C., & Kao, H. M. (2019). pH responsive selective protein adsorption by carboxylic acid functionalized large pore mesoporous silica nanoparticles SBA-1. *Materials Science & Engineering. C, Materials for Biological Applications, 94*, 344–356.
13. Siefker, J., Karande, P., & Coppens, M.-O. (2014). Packaging biological cargoes in mesoporous materials: Opportunities for drug delivery. *Expert Opinion on Drug Delivery, 11*(11), 1781–1793.
14. Kruk, M. (2012). Access to ultralarge-pore ordered mesoporous materials through selection of surfactant/swelling-agent micellar templates. *Accounts of Chemical Research, 45*(10), 1678–1687.
15. Bukara, K., Schueller, L., Rosier, J., Martens, M. A., Daems, T., Verheyden, L., et al. (2016). Ordered mesoporous silica to enhance the bioavailability of poorly water-soluble drugs: Proof of concept in man. *European Journal of Pharmaceutics and Biopharmaceutics, 108*, 220–225.
16. Xiong, L., Bi, J., Tang, Y., & Qiao, S. Z. (2016). Magnetic core-shell silica nanoparticles with large radial mesopores for siRNA delivery. *Small, 12*(34), 4735–4742.
17. Gu, J., Huang, K., Zhu, X., Li, Y., Wei, J., Zhao, W., et al. (2013). Sub-150 nm mesoporous silica nanoparticles with tunable pore sizes and well-ordered mesostructure for protein encapsulation. *Journal of Colloid and Interface Science, 407*, 236–242.
18. Wu, M., Meng, Q., Chen, Y., Zhang, L., Li, M., Cai, X., et al. (2016). Large pore-sized hollow mesoporous organosilica for redox-responsive gene delivery and synergistic cancer chemotherapy. *Advanced Materials, 28*(10), 1963–1969.
19. Meka, A. K., Abbaraju, P. L., Song, H., Xu, C., Zhang, J., Zhang, H., et al. (2016). A vesicle supra-assembly approach to synthesize amine-functionalized hollow dendritic mesoporous silica nanospheres for protein delivery. *Small, 12*(37), 5169–5177.
20. Rahmani, S., Budimir, J., Sejalon, M., Daurat, M., Aggad, D., Vives, E., et al. (2019). Large pore mesoporous silica and organosilica nanoparticles for pepstatin A delivery in breast cancer cells. *Molecules, 24*(2), 332.
21. Kwon, D., Cha, B. G., Cho, Y., Min, J., Park, E. B., Kang, S. J., et al. (2017). Extra-large pore mesoporous silica nanoparticles for directing in vivo M2 macrophage polarization by delivering IL-4. *Nano Letters, 17*(5), 2747–2756.
22. Cha, B. G., Jeong, J. H., & Kim, J. (2018). Extra-large pore mesoporous silica nanoparticles enabling co-delivery of high amounts of protein antigen and toll-like receptor 9 agonist for enhanced cancer vaccine efficacy. *ACS Central Science, 4*(4), 484–492.
23. Zhang, J., Li, X., Rosenholm, J. M., & Gu, H. C. (2011). Synthesis and characterization of pore size-tunable magnetic mesoporous silica nanoparticles. *Journal of Colloid and Interface Science, 361*(1), 16–24.
24. Hong, Y., Yao, Y., Zhao, H., Sheng, Q., Ye, M., Yu, C., et al. (2018). Dendritic mesoporous silica nanoparticles with abundant Ti(4+) for

phosphopeptide enrichment from cancer cells with 96% specificity. *Analytical Chemistry, 90*(12), 7617–7625.

25. Wang, Y., & Caruso, F. (2005). Mesoporous silica spheres as supports for enzyme immobilization and encapsulation. *Chemistry of Materials, 17*(5), 953–961.
26. Kalantari, M., Yu, M., Yang, Y., Strounina, E., Gu, Z., Huang, X., et al. (2017). Tailoring mesoporous-silica nanoparticles for robust immobilization of lipase and biocatalysis. *Nano Research, 10*(2), 605–617.
27. Yang, J., Tu, J., Lamers, G. E. M., Olsthoorn, R. C. L., & Kros, A. (2017). Membrane fusion mediated intracellular delivery of lipid bilayer coated mesoporous silica nanoparticles. *Advanced Healthcare Materials, 6*(20), 1700759.
28. Slowing, I. I., Trewyn, B. G., & Lin, V. S. (2007). Mesoporous silica nanoparticles for intracellular delivery of membrane-impermeable proteins. *Journal of the American Chemical Society, 129*(28), 8845–8849.
29. Hartono, S. B., Gu, W., Kleitz, F., Liu, J., He, L., Middelberg, A. P., et al. (2012). Poly-L-lysine functionalized large pore cubic mesostructured silica nanoparticles as biocompatible carriers for gene delivery. *ACS Nano, 6*(3), 2104–2117.
30. Gao, F., Botella, P., Corma, A., Blesa, J., & Dong, L. (2009). Monodispersed mesoporous silica nanoparticles with very large pores for enhanced adsorption and release of DNA. *The Journal of Physical Chemistry B, 113*(6), 1796–1804.
31. Xie, J., Yang, C., Liu, Q., Li, J., Liang, R., Shen, C., et al. (2017). Encapsulation of hydrophilic and hydrophobic peptides into hollow mesoporous silica nanoparticles for enhancement of antitumor immune response. *Small, 13*(40), 1701741.
32. Wu, M., Meng, Q., Chen, Y., Du, Y., Zhang, L., Li, Y., et al. (2015). Large-pore ultrasmall mesoporous organosilica nanoparticles: Micelle/precursor co-templating assembly and nuclear-targeted gene delivery. *Advanced Materials, 27*(2), 215–222.
33. Hartono, S. B., Yu, M., Gu, W., Yang, J., Strounina, E., Wang, X., et al. (2014). Synthesis of multi-functional large pore mesoporous silica nanoparticles as gene carriers. *Nanotechnology, 25*(5), 055701.
34. Zheng, Q., Lin, T., Wu, H., Guo, L., Ye, P., Hao, Y., et al. (2014). Mussel-inspired polydopamine coated mesoporous silica nanoparticles as pH-sensitive nanocarriers for controlled release. *International Journal of Pharmaceutics, 463*(1), 22–26.
35. Liu, H. J., & Xu, P. (2019). Smart mesoporous silica nanoparticles for protein delivery. *Nanomaterials (Basel), 9*(4), 511.
36. Qiao, H., Jia, J., Shen, H., Zhao, S., Chen, E., Chen, W., et al. (2019). Capping silica nanoparticles with tryptophan-mediated cucurbit[8]uril complex for targeted intracellular drug delivery triggered by tumor-overexpressed IDO1 enzyme. *Advanced Healthcare Materials, 8*(13), e1900174.
37. Li, E., Yang, Y., Hao, G., Yi, X., Zhang, S., Pan, Y., et al. (2018). Multifunctional magnetic mesoporous silica nanoagents for in vivo enzyme-responsive drug delivery and MR imaging. *Nano, 2*(3), 233–242.
38. Portilho, F. L., Pinto, S. R., de Barros, A., Helal-Neto, E., Dos Santos, S. N., Bernardes, E. S., et al. (2018). In loco retention effect of magnetic core mesoporous silica nanoparticles doped with trastuzumab as intralesional nanodrug for breast cancer. *Artificial Cells, Nanomedicine, and Biotechnology, 46*(sup3), S725–SS33.
39. Siminzar, P., Omidi, Y., Golchin, A., Aghanejad, A., & Barar, J. (2019). Targeted delivery of doxorubicin by magnetic mesoporous silica nanoparticles armed with mucin-1 aptamer. *Journal of Drug Targeting, 28*(1), 92–101..
40. Sakhtianchi, R., Darvishi, B., Mirzaie, Z., Dorkoosh, F., Shanehsazzadeh, S., & Dinarvand, R. (2019). Pegylated magnetic mesoporous silica nanoparticles decorated with AS1411 Aptamer as a targeting delivery system for cytotoxic agents. *Pharmaceutical Development and Technology, 24*(9), 1063–1075.
41. Li, X., Fan, H., Guo, T., Bai, H., Kwon, N., Kim, K. H., et al. (2019). Sequential protein-responsive nanophotosensitizer complex for enhancing tumor-specific therapy. *ACS Nano, 13*(6), 6702–6710.
42. Er, O., Colak, S. G., Ocakoglu, K., Ince, M., Bresoli-Obach, R., Mora, M., et al. (2018). Selective photokilling of human pancreatic cancer cells using cetuximab-targeted mesoporous silica nanoparticles for delivery of zinc phthalocyanine. *Molecules, 23*(11), 2749.
43. Fang, J., Wang, Q., Yang, G., Xiao, X., Li, L., & Yu, T. (2019). Albumin-MnO2 gated hollow mesoporous silica nanosystem for modulating tumor hypoxia and synergetic therapy of cervical carcinoma. *Colloids and surfaces B, Biointerfaces, 179*, 250–259.
44. Paris, J. L., de la Torre, P., Cabanas, M. V., Manzano, M., Flores, A. I., & Vallet-Regi, M. (2019). Suicide-gene transfection of tumor-tropic placental stem cells employing ultrasound-responsive nanoparticles. *Acta Biomaterialia, 83*, 372–378.
45. Zahiri, M., Babaei, M., Abnous, K., Taghdisi, S. M., Ramezani, M., & Alibolandi, M. (2020). Hybrid nanoreservoirs based on dextran-capped dendritic mesoporous silica nanoparticles for CD133-targeted drug delivery. *Journal of Cellular Physiology, 235*(2), 1036–1050.
46. Shen, Y., Li, M., Liu, T., Liu, J., Xie, Y., Zhang, J., et al. (2019). A dual-functional HER2 aptamer-conjugated, pH-activated mesoporous silica nanocarrier-based drug delivery system provides in vitro synergistic cytotoxicity in HER2-positive breast cancer cells. *International Journal of Nanomedicine, 14*, 4029–4044.
47. Liu, C. M., Chen, G. B., Chen, H. H., Zhang, J. B., Li, H. Z., Sheng, M. X., et al. (2019). Cancer cell membrane-cloaked mesoporous silica nanoparticles with a pH-sensitive gatekeeper for cancer treatment. *Colloids and surfaces B, Biointerfaces, 175*, 477–486.
48. Kuang, Y., Chen, H., Chen, Z., Wan, L., Liu, J., Xu, Z., et al. (2019). Poly(amino acid)/ZnO/mesoporous silica nanoparticle based complex drug delivery system with a charge-reversal property for cancer therapy. *Colloids and surfaces B, Biointerfaces, 181*, 461–469.
49. Yang, X., Trinh, H. M., Agrahari, V., Sheng, Y., Pal, D., & Mitra, A. K. (2016). Nanoparticle-based topical ophthalmic gel formulation for sustained release of hydrocortisone butyrate. *AAPS PharmSciTech, 17*(2), 294–306.
50. Shao, D., Li, M., Wang, Z., Zheng, X., Lao, Y. H., Chang, Z., et al. (2018). Bioinspired diselenide-bridged mesoporous silica nanoparticles for dual-responsive protein delivery. *Advanced Materials, 30*, e1801198.
51. Zhang, J., Shen, B., Chen, L., Chen, L., Meng, Y., & Feng, J. (2019). A dual-sensitive mesoporous silica nanoparticle based drug carrier for cancer synergetic therapy. *Colloids and Surfaces B, Biointerfaces, 175*, 65–72.
52. Jimenez-Falcao, S., Joga, N., Garcia-Fernandez, A., Llopis Lorente, A., Torres, D., de Luis, B., et al. (2019). Janus nanocarrier powered by bi-enzymatic cascade system for smart delivery. *Journal of Materials Chemistry B, 7*(30), 4669–4676.
53. Agostini, A., Mondragon, L., Pascual, L., Aznar, E., Coll, C., Martinez-Manez, R., et al. (2012). Design of enzyme-mediated controlled release systems based on silica mesoporous supports capped with ester-glycol groups. *Langmuir, 28*(41), 14766–14776.
54. Deodhar, G. V., Adams, M. L., & Trewyn, B. G. (2017). Controlled release and intracellular protein delivery from mesoporous silica nanoparticles. *Biotechnology Journal, 12*(1), 1600408.
55. Xu, C., Lei, C., & Yu, C. (2019). Mesoporous silica nanoparticles for protein protection and delivery. *Frontiers in Chemistry, 7*, 290.
56. Tambe, P., Kumar, P., Paknikar, K. M., & Gajbhiye, V. (2018). Decapeptide functionalized targeted mesoporous silica nanoparticles with doxorubicin exhibit enhanced apoptotic effect in breast and prostate cancer cells. *International Journal of Nanomedicine, 13*, 7669–7680.

57. Bhattacharyya, S., Wang, H., & Ducheyne, P. (2012). Polymer-coated mesoporous silica nanoparticles for the controlled release of macromolecules. *Acta Biomaterialia, 8*(9), 3429–3435.
58. Solberg, S. M., & Landry, C. C. (2006). Adsorption of DNA into mesoporous silica. *The Journal of Physical Chemistry B, 110*(31), 15261–15268.
59. Chang, J. H., Mou, K. Y., & Mou, C. Y. (2019). Sleeping beauty transposon-mediated asparaginase gene delivery by a nanoparticle platform. *Scientific Reports, 9*(1), 11457.
60. Nejabat, M., Mohammadi, M., Abnous, K., Taghdisi, S. M., Ramezani, M., & Alibolandi, M. (2018). Fabrication of acetylated carboxymethylcellulose coated hollow mesoporous silica hybrid nanoparticles for nucleolin targeted delivery to colon adenocarcinoma. *Carbohydrate Polymers, 197*, 157–166.
61. Pinese, C., Lin, J., Milbreta, U., Li, M., Wang, Y., Leong, K. W., et al. (2018). Sustained delivery of siRNA/mesoporous silica nanoparticle complexes from nanofiber scaffolds for long-term gene silencing. *Acta Biomaterialia, 76*, 164–177.
62. Wang, D., Xu, X., Zhang, K., Sun, B., Wang, L., Meng, L., et al. (2018). Codelivery of doxorubicin and MDR1-siRNA by mesoporous silica nanoparticles-polymerpolyethylenimine to improve oral squamous carcinoma treatment. *International Journal of Nanomedicine, 13*, 187–198.
63. Pan, Q. S., Chen, T. T., Nie, C. P., Yi, J. T., Liu, C., Hu, Y. L., et al. (2018). In situ synthesis of ultrathin ZIF-8 film-coated MSNs for codelivering Bcl 2 siRNA and doxorubicin to enhance chemotherapeutic efficacy in drug-resistant cancer cells. *ACS Applied Materials & Interfaces, 10*(39), 33070–33077.
64. Li, Y., Duo, Y., Bi, J., Zeng, X., Mei, L., Bao, S., et al. (2018). Targeted delivery of anti-miR-155 by functionalized mesoporous silica nanoparticles for colorectal cancer therapy. *International Journal of Nanomedicine, 13*, 1241–1256.
65. Hu, Y., Wang, Z., Qiu, Y., Liu, Y., Ding, M., & Zhang, Y. (2019). Anti-miRNA21 and resveratrol-loaded polysaccharide-based mesoporous silica nanoparticle for synergistic activity in gastric carcinoma. *Journal of Drug Targeting, 27*(10), 1135–1143.
66. Yang, H., Liu, Y., Qiu, Y., Ding, M., & Zhang, Y. (2019). MiRNA-204-5p and oxaliplatin-loaded silica nanoparticles for enhanced tumor suppression effect in CD44-overexpressed colon adenocarcinoma. *International Journal of Pharmaceutics, 566*, 585–593.
67. Wang, F., Zhang, L., Bai, X., Cao, X., Jiao, X., Huang, Y., et al. (2018). Stimuli-responsive nanocarrier for co-delivery of MiR-31 and doxorubicin to suppress high MtEF4 cancer. *ACS Applied Materials & Interfaces, 10*(26), 22767–22775.
68. Joshi, V. B., Geary, S. M., & Salem, A. K. (2013). Biodegradable particles as vaccine delivery systems: Size matters. *The AAPS Journal, 15*(1), 85–94.
69. Slutter, B., & Jiskoot, W. (2016). Sizing the optimal dimensions of a vaccine delivery system: A particulate matter. *Expert Opinion on Drug Delivery, 13*(2), 167–170.
70. Mathaes, R., Winter, G., Siahaan, T. J., Besheer, A., & Engert, J. (2015). Influence of particle size, an elongated particle geometry, and adjuvants on dendritic cell activation. *European Journal of Pharmaceutics and Biopharmaceutics, 94*, 542–549.
71. Ding, D., & Zhu, Q. (2018). Recent advances of PLGA micro/nanoparticles for the delivery of biomacromolecular therapeutics. *Materials Science & Engineering. C, Materials for Biological Applications, 92*, 1041–1060.
72. Lee, S. H., Park, O. K., Kim, J., Shin, K., Pack, C. G., Kim, K., et al. (2019). Deep tumor penetration of drug-loaded nanoparticles by click reaction-assisted immune cell targeting strategy. *Journal of the American Chemical Society, 141*(35), 13829–13840.
73. Ding, B., Shao, S., Yu, C., Teng, B., Wang, M., Cheng, Z., et al. (2018). Large-pore mesoporous-silica-coated upconversion nanoparticles as multifunctional immunoadjuvants with ultrahigh photosensitizer and antigen loading efficiency for improved cancer photodynamic immunotherapy. *Advanced Materials, 30*(52), e1802479.

Clearable Nanoparticles for Cancer Photothermal Therapy

Jun Zhao, Xin Long, and Min Zhou

Abstract

Nanoparticles are important mediators for cancer photothermal therapy (PTT) where they can efficiently convert photon energy into heat and ablate the surrounding cancer cells with superior spatial and temporal precision. Recent decades have witnessed a booming development of numerous formulations of PTT nanoparticles that exhibit outstanding anti-tumor efficacy in preclinical studies. However, their clinical translation has been mined by safety concerns, especially their long-term impact on human body. Biodegradable nanoparticles that can be excreted after PTT, therefore, are gaining popularity due to their biocompatibility and improved safety profiles. This chapter provides an update on the progress in clearable PTT nanoparticles for cancer treatment. We discuss their design, synthesis strategy, and physicochemical properties relevant to photothermal performance. We also review their biodistribution patterns and in vivo anti-tumor efficacy, along with their degradation mechanism and clearance kinetics. Lastly, we present a brief overview of the imaging techniques to noninvasively monitor the degradation of PTT nanoparticles.

Keywords

Clearable nanoparticles · Cancer treatment · Photothermal therapy · Biodegradable · Nanomaterials

1 Introduction

Photothermal therapy (PTT) is an emerging technique with growing popularity in cancer treatment [1]. As a localized therapy, PTT can deliver a specific amount of photon energy to tumor mass with superior temporal and spatial resolution and thereby minimize the toxic side effects that are common for conventional cancer therapies [2]. Recent studies also revealed that localized PTT can elicit an abscopal anti-tumor immune reaction to reject distant tumor metastases and therefore have further expanded the horizon for PTT application [3]. Near-infrared (NIR) laser is the most widely used light source for PTT. However, the lack of tissue absorption to NIR laser greatly limits the efficiency of photo-to-thermal energy conversion. The non-specific laser absorption by tumor and non-tumor tissues may also cause potential thermal damage to the healthy surrounding tissues. To overcome such limitations, NIR-absorbing nanoparticles with tumor-homing capabilities are developed to exert a tumor-specific PTT [4]. A plethora of PTT nanoparticles have been prepared and evaluated in the past decades, including those based on carbon (C) [5], gold (Au) [6], and copper (Cu) [7].

Although PTT nanoparticles have exhibited impressive anti-tumor efficacy in preclinical animal studies and yielded numerous publications including those in highly prestigious journals, none of them has so far received approval for treating cancer patients [8, 9]. Such a dramatic discrepancy has cast a gloomy doubt on the feasibility of clinical translation for not only the PTT nanoparticles but also nanomedicine in general [10]. The foremost concern for the clinical usage of any nanoparticles lies in their safety profile, including acute and long-term toxicities. While extensive studies have shown

---

J. Zhao
School of Basic Medicine, Tongji Medical College, Huazhong University of Science and Technology, Wuhan, Hubei, China

Department of Nuclear Medicine, Tongji Hospital, Tongji Medical College, Huazhong University of Science and Technology, Wuhan, Hubei, China

X. Long
School of Basic Medicine, Tongji Medical College, Huazhong University of Science and Technology, Wuhan, Hubei, China

M. Zhou (✉)
Institution of Translational Medicine, Zhejiang University, Hangzhou, Zhejiang, China

Eye Center, The Second Affiliated Hospital, Zhejiang University School of Medicine, Zhejiang University, Hangzhou, Zhejiang, China
e-mail: zhoum@zju.edu.cn

© Springer Nature Switzerland AG 2021
F. Fontana, H. A. Santos (eds.), *Bio-Nanomedicine for Cancer Therapy*, Advances in Experimental Medicine and Biology 1295, https://doi.org/10.1007/978-3-030-58174-9_6

that the acute toxicities can be mitigated through a careful design of the chemical composition of nanoparticles, the long-term fate of nanoparticles in human body remains poorly understood [11]. Indeed, most PTT nanoparticles are composed of transition metal elements that are not naturally existing in human body, and their continual deposition in normal organs can be hazardous to the already-ailing cancer patients. For example, the deposition of non-degradable nanoparticles in human body is known to cause mesothelioma [12].

Nanoparticles are excreted via two main routes: renal or hepatobiliary route [13]. Nanoparticles with a hydrodynamic diameter below 6 nm are rapidly via kidney into urine, because their size is below the filtration threshold of glomerular membrane [14]. The renal clearance of nanoparticles is desirable due to the rapidity of this process. The hepatobiliary route of non-degradable nanoparticles, on the other hand, is much slower. Gad et al. [15] reported that approximately 85% of injected silica@gold nanoshells was still entrapped in the liver and spleen at 28 days after injection. The nanoshells were not cleared even at 400 days after injection. In this regard, recent research has shifted toward the designing of PTT nanoparticles that can be excreted fairly quickly after PTT. In this chapter, we provide an up-to-date review of this category of nanoparticles, focusing on their synthesis, degradation mechanism, photothermal conversion, biodistribution, and anti-tumor efficacy.

2 Two Important Characteristics of PTT Nanoparticles

The extinction coefficient (α) measures how strongly a laser at a certain wavelength (λ) is absorbed by the dispersion of PTT nanoparticles, usually at the unit mass density. It can be calculated using the Lambert-Beer Law:

$$A(\lambda) = \alpha \times L \times C$$

where $A(\lambda)$ is the absorbance at the wavelength λ, L is the path length (in unit of cm), and C is the concentration of nanoparticles ($g \cdot L^{-1}$). The value of α can then be derived from the slope of the linear fit of $A(\lambda)$ against C.

The photothermal conversion efficiency (η) measures the capability of PTT nanoparticles to convert photon energy into thermal energy [16]. The value of η can be calculated from the time-dependent heating and cooling process of a nanoparticle dispersion. In a typical experiment, the dispersion at a certain particle concentration is first equilibrated at the environmental temperature (T_{en}) and irradiated with the laser until the dispersion reaches its maximum temperature (T_{max}). The laser is then shut off to allow the dispersion to cool down by itself, during which period the dispersion temperature (T_t) and its corresponding time elapsed from the start of cooling (t) are recorded.

A dimensionless driving force temperature (θ) is expressed as:

$$\theta = \frac{T_t - T_{en}}{T_{max} - T_{en}}$$

The time elapsed (t) is then plotted against the negative natural logarithm of θ using the following equation:

$$t = -\tau_s \ln\theta$$

where the time constant (τ_s) can be derived from the slope of linear fit of t against $-\ln(\theta)$.

The value of photothermal conversion efficiency (η) is calculated as:

$$\eta = \frac{hA(T_{max} - T_{en}) - Q_{Dis}}{I(1 - 10^{-A})}$$

where h and A are the coefficient of heat transfer and the surface area of the contained, I is the power density of the laser, A is the absorbance of the nanoparticle dispersion for the laser source, and Q_{Dis} is the heat dissipated due to laser being absorbed by the container. The product of h and A can be calculated using a simplified formula:

$$hA = \frac{m \times C_p}{\tau_s}$$

where m and C_p is the mass and heat capacity of the solvent. The C_p value for water is 4.2 $J \cdot g^{-1}$. Q_{Dis} can be measured independently using a sample container with pure water in a similar laser-heating and cooling experiment as follows:

$$Q_{Dis} = \frac{m \times C_p}{\tau_s} \times (T_{max} - T_{en})$$

3 Enzymatically Degradable Nanoparticles

Carbon-based nanomaterials, including graphene oxide (GO) and reduced graphene oxide (rGO), are useful tools for applications such as biosensors, drug delivery, cellular imaging, and PTT due to their tunable properties. Graphene oxide (GO) sheets consisted of several layers of hexagonal or honeycomb lattice of carbon atoms. While the exact structure of GO sheets is still under debate, one theoretical model proposes that GO consisted of sp^2 basal planes with scattered sp^3 domains, where tertiary alcohols, epoxy functional groups are attached. The edge of GO is decorated with carboxylic acid, keto, and five- or six-membered lactol groups [17]. As a result, GO can absorb NIR light due to the delocalized electron orbitals. The abundant surface functionality groups on GO allow further modification of biocompatible polymers to increase their stability in physiological conditions and alleviate their toxicities. However, the highly oxidized form of GO restricts its efficiency of photothermal conversion; therefore, higher doses of GO as well as higher laser power are required to achieve a satisfactory photothermal therapy [18].

Some recent studies have explored doping GO sheets with other NIR-absorbing nanoparticles, such as copper sulfide (CuS) [19] and iron oxide [20], to improve the photothermal conversion. A more popular method, however, is to restore the network of π electron of GO by synthesizing reduced graphene oxide (RGO). Robinson et al. [21] first broke down micrometric GO sheets by sonicating in the presence of amine-terminated poly(ethylene glycol) (PEG-NH_2) to form 20-nm-sized nano-GO sheets and then reduced them with hydrazine at 80 °C. A dramatic color change from yellow to black indicated the restoration of the π electron network [22], and the reduction was further confirmed by the decrease in oxygen content via Auger spectroscopy. The resultant nano-RGO was further stabilized with amphiphilic C18-poly(maleamide-*alt*-1-octadecene)-*block*-PEG to prevent aggregation. Compared with nano-GO, the nano-RGO exhibited 6.8-fold higher absorbance for 808-nm laser. When both dispersions at 20 mg·L^{-1} was irradiated with the 808-nm laser at 0.6 W·cm^{-2}, 30 °C of temperature elevation was observed for nano-RGO, while that of nano-GO was merely 10 °C. Similar results were also reported by Hashemi et al. [23] to confirm the improvement of RGO in photothermal conversion.

Yan et al. [24] prepared folic acid-functionalized PEG-coated nano-RGO to conduct PTT in combination with immunotherapy via indoleamine-2,3-dioxygenase (IDO) inhibition [25] and programmed cell death ligand 1 (PD-L1) blockade [26]. The formed RGO-PEG-FA nanosheets were about 200 nm in size and 8 nm in thickness. Fluorescence tracking revealed a specific accumulation of RGO-PEG-FA in CT-26 murine colon cancer xenograft as compared to the non-targeting RGO-PEG. At 12 h after intravenous injection of 0.2-mg RGO-PEG-FA per mouse, photothermal therapy with 808-nm laser at 1 W·cm^{-2} for 8 min heated the tumor to over 53 °C, causing an immunogenic cell death that activated dendritic cells and subsequently induced a potent anti-tumor immune response with the help of IDO inhibition and PD-L1 blockade. While the primary tumor was completely suppressed for 16 days after the treatment, an abscopal effect was also observed, where the increased infiltration by T lymphocytes and natural killer (NK) cells significantly suppressed the growth of distant tumor.

Peroxidase-mediated degradation in the presence of hydrogen peroxide is the main route of degradation for carbon-based nanomaterials, including GO and RGO [27]. For example, horseradish peroxidase contains a single protoporphyrin IX heme group at a ferric (Fe^{3+}) oxidation state when inactive. Hydrogen peroxide binds to the ferric center and then is converted to oxywater complex through the His 42 and Arg 38 residues [28] to form Compound I, which is composed of a ferryl oxo iron ($Fe^{4+} = O$) and a porphyrin π cation radical. At a redox potential as high as 950 mV, Compound I can oxidize the epoxy groups of GO into carbonyl groups, subsequently causing the breakage of C-C bonds and disintegration of the GO nanoparticles into even smaller graphene quantum dots [29]. The enzymatic degradation requires a close proximity between the GO surface and the catalytic center of peroxidase. Indeed, minimal degradation was observed when the GO surface was coated with PEG that hinders enzyme docking [30]. The type of peroxidase seems to impact the toxicity of degradation products. While the degradation products by myeloperoxidase are generally nontoxic, those by horseradish peroxidase are able to cause DNA damage [31]. In addition, carbon-based materials can also be degraded by hydrogen peroxide in the presence of ferrous salt via the Fenton reactions [32].

The clearance of GO or RGO nanoparticles is mediated by the phagocytosis via macrophages or giant cells [33]. Yang et al. [18] studied the body clearance of PEGylated GO nanosheets with a size range of 10–50 nm. While GO nanosheets were initially deposited in reticuloendothelial system (RES) organs such as the liver and spleen, a gradual clearance was observed after 3–15 days, and there was no residual GO nanosheets at 3 months after injection [34].

4 Degradation by Oxidation

Chen et al. [35] prepared ultrasmall vanadium disulfide (VS_2) nanodots that can be degraded by oxidation. The nanodots were synthesized by sonicating VS_2 nanosheets in the presence of 1,2-dioleoyl-sn-glycero-3-phosphate (DOPA). As the phosphate group of DOPA formed coordinate bonds with the V^{4+} cations, the interaction between V^{4+} and S^{2-} anions was weakened, causing the dissemination of nanosheets into the ultrasmall nanodots of 2 nm in size. Once formed, the nanodots were encapsulated in situ by the DOPA molecules and self-assembled into liposome-like structures of about 35 nm in size. PEGylation was then performed to further improve their stability under physiological conditions. The semi-conductivity of VS2 nanosheets, with a band gap of 0.77 eV, was preserved in the VS_2@lipid-PEG formulation. As a result, VS_2@lipid-PEG exhibited a strong absorbance to NIR laser with a photothermal conversion efficiency of 31.5%. No deterioration of heating capacity was observed after five laser-on/off cycles, indicating a satisfactory laser stability of VS_2@lipid-PEG. Similar to other transition metal dichalcogenide nanoparticles, VS_2 nanosheets were radiolabeled with $^{99m}Tc^{4+}$ in the absence of chelators with a radiolabeling efficiency of 78.5 ± 2.7%. The ensuing biodistribution study in the 4T1 murine breast cancer xenograft model showed that the tumor uptake of VS_2@lipid-PEG was 5.1 ± 1.2%$ID \cdot g^{-1}$ (percentage of injected dose per gram of tissue) at 24 h after intravenous injection. PTT at 24 h after intravenous injection of VS_2@lipid-PEG at a dose of 20 $mg \cdot kg^{-1}$ using 808-nm laser at 0.6 $W \cdot cm^{-2}$ heated the tumor over 58 °C and completely suppressed tumor growth for up to 14 days. The degradation of VS_2 nanodots was mediated by oxygen dissolved in the medium. Exposure of the nanodots dispersion to open air for 30 days significantly reduced the optical absorbance, while nitrogen protection prevented this reduction. X-ray photoelectron spectroscopy (XPS) confirmed that the V^{3+}/V^{4+} cations in the VS_2 nanodots were oxidized into water-soluble V^{5+} species. Accordingly, VS_2@lipid-PEG was gradually cleared from body after injection. The vanadium concentration in the liver and spleen was only 1.2 ± 0.3%ID/g and 2.9 ± 0.8%ID/g at 30 days post-injection, respectively. In comparison, the liver and spleen uptake of vanadium were as high as 37% ID/g and 20% ID/g, respectively, at 24 h post-injection. In the meanwhile, the level of vanadium in feces gradually increased, suggesting that the excretion was mainly through the hepatobiliary route.

Zhang et al. [36] prepared PEGylated tungsten nitride (WN) nanoparticles that can also be degraded via oxidation. The WN nanoparticles were originally designed as the photocatalyst for water splitting, exhibiting strong absorbance in the NIR region. They were synthesized via a two-step route [37]. First, ammonium tungstate and hydrochloric acid were mixed and dried to form the intermediate H_2WO_4. Then H_2WO_4 was heated at 600 °C in a gaseous ammonia atmosphere to yield the black WN nanoparticles. PEG-thiol (PEG-SH) and 11-mercaptoundecanoic acid-conjugated (2-hydroxypropyl)-β-cyclodextrin (MUA-CD) were added to coat the nanoparticles via W-S bond in a deoxygenated solution. Chemotherapy drug doxorubicin was successfully loaded into the MUA-CD layer at a weight ratio of 9.8%. The resultant nanoparticles were 156 nm in hydrodynamic size with a strong absorbance across the UV to NIR region and a photothermal conversion efficiency of 33%. They remained stable after five cycles of 10-min laser irradiation and 10-min cooling. PTT at 8 h after intravenous injection of PEG-WN-DOX nanoparticles at a dose of 0.6 $mg \cdot kg^{-1}$ using 808-nm laser at 1.5 $W \cdot cm^{-2}$ for 4 min heated the CT-26 tumor to about 52 °C. The combination of doxorubicin chemotherapy and PTT suppressed the tumor growth for 12 days, causing substantial necrosis and apoptosis inside the tumor. After 30 days of exposure to open air, the dispersion of PEG-WN nanoparticles exhibited a steady decrease in NIR absorbance, along with a color shift from black to light blue. Transmission electron microscopy (TEM) also revealed that no particles were present after 30 days. Accordingly, inductively coupled plasma atomic emission spectroscopy (ICP-AES) confirmed that 22% of injected dose (%ID) and 12%ID were excreted via feces and urine, respectively, on the first day of nanoparticle administration. More than 80%ID was already excreted within 1 week.

5 Degradation by H_2O_2

Hydrogen peroxide (H_2O_2), superoxide anion (O_2^-), and hydroxyl radicals (·OH) all belong to the family of reactive oxygen species (ROS) whose levels are elevated in almost all cancer types [38]. While mostly produced by mitochondria, NADPH oxidase (NOX) complexed in cell membrane, peroxisome, and endoplasmic reticulum, the overproduction of ROS is associated with several important oncogenic processes including neoplastic transformation, abnormal growth and proliferation, and resistance to apoptosis [39]. The intratumoral concentration of H_2O_2 can reach as high as 1×10^{-3} M, making it a viable regulator for nanoparticle degradation.

Cupric oxide (Cu_2O) is a p-type semiconductor with strong absorbance for lasers with a wavelength above 600 nm. Coating Cu_2O shell onto noble metal cores is a viable method to prepare novel plasmonic nanoparticles for PTT [40]. Tai et al. [41] prepared Cu@Cu_2O nanoparticles by first reducing $CuCl_2$ with hydrazine in the presence of an amphiphilic polymer poly(styrene-alt-maleic acid) (PSMA). The as-formed Cu-PSMA nanoparticles were then partially oxidized by a brief heating in deionized water with exposure to open air to produce the Cu_2O coating. The resultant Cu@Cu_2O@PSMA nanoparticles were 50 ± 8 nm in hydrodynamic diameter with a spherical Cu/Cu_2O core of 18 ± 6 nm in diameter. The Cu2O coating caused a red shift of the surface plasmon resonance (SPR) peak from a narrow 580 nm of Cu-alone nanoparticles to a broad band spanning from 570 to 800 nm. The PTT efficacy of Cu@Cu_2O@PSMA was examined ex vivo by irradiating a 50-ppm dispersion with 660-nm laser at 0.61 $W \cdot cm^{-2}$. A temperature increase of 28 °C was observed in 10 min. The degradation of Cu@Cu_2O@PSMA was induced by H_2O_2: 30% of the Cu core was degraded in 1 h by 0.3 mM H_2O_2, while 90% of the Cu core was degraded in 1 h once the H_2O_2 concentration increased to 3 mM. X-ray absorption spectroscopy (XAS) revealed that 15 μg of copper was excreted daily via urine after intravenous injection of Cu@Cu_2O@PSMA at a dose of 20 $mg \cdot kg^{-1}$. Interestingly, the Cu_2O protected the copper from a rapid degradation and subsequently mitigated the acute cytotoxicity of Cu^{2+} ions. It is known that the cytotoxicity of Cu-based nanoparticles is caused by the generation of intracellular ROS [42] as well as the release of DNA-damaging Cu^{2+} ions [43]. Such a protection effect was further confirmed in vivo as 75% of the mice injected with 20-mg·kg^{-1} Cu-PSMA died of toxicity, while all the mice injected with 20-mg·kg^{-1} Cu@Cu_2O@PSMA survived.

Miao et al. [44] prepared PEGylated rhenium (Re) nanoclusters for PTT that can degrade into renal clearable ReO_4^- ions. Re is a transition metal with a high atomic number ($Z = 75$). Its radioactive isotope^{188}Re has been evaluated for positron emission tomography (PET) or radiotherapy in clinical trials [45]. Notably, the 50% lethal dose (LD50) of ReO_4^- is 2800 mg/kg, underscoring the biocompatibility of this compound. The Re nanoclusters were synthesized by reducing ammonium perrhenate (NH_4ReO_4) with $NaBH_4$ in the presence of PEG-SH. The resultant nanoclusters were irregular spherical particles of about 1–2 nm in diameter by TEM and about 7.6 nm in hydrodynamic diameter. With a mass extinction coefficient of 2.6 L·g^{-1}·cm^{-1} for 808-nm laser, the nanoclusters exhibited a photothermal conversion coefficient of 33.0% and withstood five laser-on/off cycles without much loss in the heating capacity. Pharmacokinetics study showed a half-life of blood circulation at 2.62 h, indicating a fast blood elimination. Biodistribution study revealed that the liver and spleen are the two major sites for nanocluster deposition. At 6–24 h after intravenously injection, the uptake values were about 25%ID/g for the liver and 15%ID/g for the spleen, respectively. PTT was performed after intratumoral injection of 50-μg Re nanoclusters using 808-nm laser at 1 W·cm^{-2} for 10 min, which completely suppressed the 4T1 tumor xenograft for up to 16 days. The degradation was tested in buffers containing H_2O_2. After incubation with 0.25% to 1% H_2O_2 for 24 h, the nanocluster structures were completely dissolved as indicated by TEM images.

The oxidation process was postulated to be a two-step reaction. First, the Re nanoclusters were partially oxidized into rhenium oxides (ReO_x) by the oxygen dissolved in the dispersion, while the nanocluster structure was maintained. Once H_2O_2 was added to the system, however, ReO_x was further oxidized into water-soluble perrhenate (ReO_4^-) that is nontoxic and renal clearable. The tendency toward oxidation also limited the storage stability of Re nanoclusters. In this regard, vitamin C was added to the dispersion to prevent oxidation by dissolved oxygen. Storage at −20 °C also prevented the premature degradation of the nanoclusters.

Tang et al. [46] prepared hydrangea-structured manganese dioxide (MnO_2) nanoparticles for PTT. The nanoparticles were synthesized by reducing potassium permanganate ($KMnO_4$) with formamide in water. Doxorubicin and aza-BODIPY, a photosensitizer, were then adsorbed to the surface of nanoparticles, which was followed by coating with poly(vinyl pyrrolidinone) (PVP) for surface stabilization. The resultant nanoparticles were about 54 nm in hydrodynamic diameter with a large surface area (117 m^2·g^{-1}) and pores of about 34 nm in diameter. The presence of aza-BODIPY provided the nanoparticles with a strong absorbance at 853 nm. PTT was conducted in an HCT-116 human colon cancer xenograft model at 6 h after intravenous injection of the nanoparticles at a dose of 2 mg·kg^{-1} using a xenon lamp at 20 mW·cm^{-2} for 1 min. There was a moderate elevation of temperature at the tumor site for about 10 °C. Nevertheless, the combination of chemotherapy, PTT, and photodynamic therapy still managed to eradicate the tumor after 4 weeks. The nanoparticles degraded rapidly in the presence of 100 μM H_2O_2: 50% of nanoparticles degraded after 1 h of incubation at pH 7.4, while acidic environment (pH 6.5) further accelerated the degradation. The degradation was accompanied by production of singlet oxygen ($^1O_2$) as well as the release of oxygen, which is favorable for the photodynamic efficacy.

Tian et al. [47] prepared poly(dopamine) melanin nanoparticles as a biodegradable PTT agent. The polymeric nanoparticles were synthesized via self-polymerization of dopamine hydrochloride in a mixture of ethanol, water, and ammonium. A bromodomain and extra-terminal inhibitor, JQ1, was encapsulated in situ to downregulate the expression of programmed cell death ligand 1 (PD-L1). The resultant nanoparticles (PDMN-JQ1) were uniform spheres of 148 ± 3.2 nm in hydrodynamic diameter. The degradation of nanoparticles was evaluated in a buffer with 10 mM H_2O_2, leading to a decrease of UV-Vis absorbance by 80% over 14 days. The dispersion of PDMN-JQ1 at 100 μg/mL in water was irradiated with 808-nm laser at 1 W·cm^{-2} for 300 s, leading to a temperature increase for about 25 °C. Similar photothermal effect was observed after four on-off cycles (300 s on, 400 s off). Notably, intratumoral injection of PDMN-JQ1 followed by photothermal therapy exerted immune-stimulatory effect in the 4T1 model. In both peripheral blood and tumor, the frequency of CD3$^+$, CD4+, and CD8$^+$ T cells increased by more than twofold compared to the PBS control, which was accompanied by the release of TNF-α, IFN-γ, and IL-12 in serum. Memory T cell populations were also higher in the PDMN-JQ1 + laser group. As a result, the photothermal therapy by PDMN-JQ1 successfully suppressed the growth of 4T1 tumor for 30 days after treatment started.

6 Degradation by Reduction

Liu et al. [48] prepared two-dimensional ultrathin manganese dioxide (MnO_2) using a chemical exfoliation method [49] and modified the nanosheet surface with soybean phospholipid to provide dispersion stability under physiological conditions. The resultant nanosheets maintained the crystalline framework of bulk MnO_2 particles, with an average diameter around 295.0 nm and a thickness of 2 nm. The nanosheets absorbed 808-nm laser with an extinction coefficient of 5.0 Lg^{-1} cm^{-1}, with a moderate photothermal conversion efficiency of 21.4%. The photothermal stability was confirmed, and four cycles of laser irradiation (1.5 $W \cdot cm^{-2}$) successfully heated the nanosheet dispersion within 40 min without significant deterioration of heating capacity. PTT was performed in 4T1 tumor model at 4 h after intravenous injection of 60 μg MnO_2 nanosheets using 808-nm laser at 1.5 $W \cdot cm^{-2}$ for 5 min, and the tumor region experienced a temperature elevation from 37 °C to 57 °C. Complete tumor regression was achieved without recurrence up to 18 days after PTT. The degradation of MnO_2 nanosheets was induced in mildly acidic condition (pH 5.0) and reducing environment (GSH 5.0 mM) to mimic the tumor microenvironment, where the nanosheet structure completely disintegrated within 3 min. Notably, degradation also enhanced the nanosheets' contrast for T_1-MR imaging due to the release of paramagnetic Mn^{2+} ions. The r_1 relaxivity was 0.89 $mM^{-1} \cdot s^{-1}$ at neutral condition and then increased to 5.45 $mM^{-1} \cdot s^{-1}$ at pH 5.0 and 4.81 $mM^{-1} \cdot s^{-1}$ in the presence of 5.0 mM GSH. T_1-MRI scan of tumor-bearing mice also showed a rapid increase of T_1 signal at the tumor region within 4 h of nanosheet injection, which then continued to grow until 24 h after injection.

Ascorbic acid is derived from the deficiency of L-gulonolactone oxidase and therefore is not present in living system under normal conditions [50]. Several groups have explored using ascorbic acid to artificially control the degradation of PTT nanoparticles. Liu et al. [51] prepared manganese oxide (Mn_3O_4) capped with bovine serum albumin (BSA) and ethylenediaminetetraacetic acid (EDTA). Hydrophobic oleylamine-coated Mn_3O_4 was first synthesized by hydrothermal treatment of $Mn(NO_3)_2$ and oleylamine at 160 °C for 24 h. The hydrophobic ligand oleylamine was removed by mixing with nitrosyl tetrafluoroborate, after which the ligand-free nanoparticles were resuspended in saturated citric acid solution and coated with polyallylamine and poly(acrylic acid) in a layer-by-layer manner. BSA was finally conjugated using the 1-ethyl-3-(3-dimethylaminopropyl) carbodiimide hydrochloride (EDC) and N-hydroxysuccinimide (NHS) chemistry to improve the nanoparticles' biocompatibility and increase their stability in buffers. EDTA was adsorbed to provide a negative surface charge. The resultant nanoparticles were about 50 nm in hydrodynamic diameter. With a molar extinction coefficient of 6.6×10^8 M^{-1} cm^{-1} at 785 nm, the nanoparticles exhibited a photothermal conversion coefficient of 34.7% and a satisfactory laser stability. MONP-BSA-EDTA also functioned as a dual T_1–T_2 magnetic resonance imaging (MRI) contrast agent ($r_1 = 8.75$ $mM^{-1} \cdot s^{-1}$, $r_2 = 40.09$ $mM^{-1} \cdot s^{-1}$) and successfully delineated the HCT-116 subcutaneous tumor in both T_1 and T_2-MRI scans. After intravenous injection of the nanoparticles at a dose of 10 mg/kg, PTT using 785-nm laser at 0.64 $W \cdot cm^{-2}$ for 3 min heated the tumor to 52 °C and suppressed tumor growth for up to 14 days. The degradation of nanoparticles was initiated by adding ascorbic acid: a complete degradation was confirmed by TEM after 10 min of incubation with 100 ppm ascorbic acid, leaving only sub-10-nm nanoparticles and water-soluble Mn^{2+} cations. While the sub-10-nm nanoparticles can be excreted without causing significant toxicity, the Mn^{2+} cations are known to be toxic. In this regard, the adsorbed EDTA was able to capture Mn^{2+} cations with an efficiency up to 99.74% over a time period of 72 h, therefore substantially mitigating the toxicity. The in vivo degradation was accomplished by intravenous injection of ascorbic acid at a dose of 15 $mg \cdot kg^{-1}$, and more than 50%ID of Mn element was excreted within 3 days of injecting ascorbic acid. Interestingly, ascorbic acid also altered the biodistribution pattern of the Mn_3O_4-BSA-EDTA nanoparticles. Mn uptake was mostly in the kidney (25%$ID \cdot g^{-1}$) and lung (12%$ID \cdot g^{-1}$) at 2 h after ascorbic acid injection, while the Mn uptake was the highest in the liver (20%$ID \cdot g^{-1}$) without ascorbic acid.

Yun et al. [52] prepared BSA-coated cobalt oxide (BSA-Co_3O_4) nanoparticles using a similar chemistry [53]. Doxorubicin was also adsorbed at an encapsulation efficiency of 43.2%. The resultant nanoparticles were about 36 nm in hydrodynamic diameter with strong absorbance in the 600- to 900-nm NIR region. With a molar extinction coefficient of 5.74×10^7 M^{-1} cm^{-1}, BSA-Co_3O_4 exhibited a photothermal conversion efficiency of 46.19% at 808 nm. Inductively coupled plasma mass spectroscopy (ICP-MS) analyses found that the BSA-Co_3O_4 nanoparticles gradually accumulated in the HCT-116 subcutaneous tumor xenograft, with an uptake value of 12%$ID \cdot g^{-1}$ and 15%$ID \cdot g^{-1}$ at 4 h and 24 h after intravenous injection, respectively. PTT was performed at 4–24 h after the intravenous injection of BSA-Co_3O_4-DOX nanoparticles (10 $mg \cdot kg^{-1}$) using 808-nm laser at 1 $W \cdot cm^{-2}$ for 5 min which heated the HCT-116 tumor xenograft to above 45 °C, and the combination of chemo-photothermal therapy eradicated the tumor at 14 days after the treatment started. BSA-Co_3O_4 was stable in the absence of ascorbic acid regardless of pH values. The degradation was initiated by ascorbic acid and further accelerated in mildly acidic condition (pH 5.5), leading to the formation of irregular particles of 3 nm in diameter within 10 min. Interestingly, the degradation process can be monitored noninvasively using MRI. BSA-Co_3O_4 was a typical T_2-MRI contrast agent with a r_2 relaxivity of 5.99 $mM^{-1} \cdot s^{-1}$ and a r_1 relaxivity of 0.17 $mM^{-1} \cdot s^{-1}$ ($r_2/r_1 = 35.24$), while Co^{2+} ions from degraded nanoparticles can be used for T_1-MRI [54]. Within 30 min of ascorbic acid injection, the T_2-MRI intensity at tumor regions decreased by 30%, while the T_1-MRI intensity increased by 60%. Meanwhile, the liver region also brightened on the T_1-MR images.

7 Degradation by pH

Chen et al. [55] prepared pluronic F127-coated molybdenum oxide (MoO_x) nanosheet for encapsulation of doxorubicin and PTT. The MoOx nanosheets were first synthesized by hydrothermal treatment of an emulsion made of $(NH_4)_6Mo_7O_{24}\cdot 4H_2O$ and HCl in water and oleylamine in cyclohexane at 180 °C for 24 h [56]. Pluronic F127 was then coated on the surface of nanosheets to improve their dispersity in water. The resultant nanosheets exhibited a diameter of 80–100 nm with a thickness of about 1.5 nm, and doxorubicin was loaded at a weight ratio of 65%. The nanosheets showed a surface plasmon resonance peak around 800 nm. Consequently, irradiation of the nanosheet dispersion at 10 $\mu g\cdot mL^{-1}$ with an 808-nm laser at 1 $W\cdot cm^{-2}$ for 5 min elevated the temperature to 14.6 °C. The nanosheets also had excellent photothermal stability: showing no change in the ultraviolet-visible (UV-Vis) spectrum after ten cycles of laser irradiation and each cycle yielding similar heating effects. PTT in 4T1 tumor model was conducted at 24 h after intravenous injection of 3-$mg\cdot kg^{-1}$ nanosheets with 808-nm laser at 1 $W\cdot cm^{-2}$. The tumor region reached a peak temperature of 54.9 °C, and the combination of doxorubicin and photothermal therapy eradicated 50% of 4T1 tumor without causing significant toxicities. In contrast to most acid-degradable nanoparticles, the MoO_x nanosheets were stable in acidic buffers with pH lower than 5. Incubation at pH 11.4 for 2 h at 37 °C caused complete disintegration of the nanosheets.

Zhao et al. [57] prepared β-cyclodextrin-capped mesoporous platinum nanoparticle (MPNP) that was degradable at acidic pH values. MPNPs were synthesized by reducing K_2PtCl_4 with ascorbic acid in the presence of poly(ethylene oxide)-block-poly(methyl methacrylate). The nanoparticles were then surface-modified with 1-mercaptoadamantane, loaded with doxorubicin, and then finally capped with β-cyclodextrin. Doxorubicin was loaded at a weight ratio of 7.6%. The resultant nanoparticles were around 58 nm in hydrodynamic diameter with a surface area of 14 $m^2\cdot g^{-1}$ and an average pore size of 2.1 nm. The nanoparticles had strong absorbance in the NIR region. When irradiated with an 808-nm laser at 2 $W\cdot cm^{-2}$, the 200 $\mu g\cdot mL^{-1}$ particle dispersion exhibited a 40 °C temperature increase over 10 min. PTT was evaluated in an MCF-7 human breast cancer model at 24 h after intravenous injection of MPNP-DOX at an equivalent doxorubicin dose of 0.2 $mg\cdot kg^{-1}$ using 808-nm laser at 1 $W\cdot cm^{-2}$ for 5 min. The chemo-photothermal combination therapy suppressed tumor growth for 11 days, causing more tumor necrosis and apoptosis than other treatment groups. Particle degradation was induced by acidic pH values. After 24 h of incubation at pH 5.0 at 37 °C, the particles broke into irregularly shaped debris, while no significant changes were detected after incubation at pH 7.4. ICP-MS also confirmed that the changes of structure were accompanied by a release of Pt ions into the buffer.

8 Laser-Inducible Degradation

Dibaba et al. [58] developed antimony nanoparticles that degraded upon the irradiation with NIR laser. The nanoparticles were synthesized by reducing antimony chloride ($SbCl_3$) with sodium hydroborate ($NABH_4$), which were then loaded with doxorubicin and coated with poly(acrylic acid). The resultant nanoparticles were monodispersed spheres with an average diameter between 34 and 42 nm under TEM and about 112 nm in hydrodynamic diameter. Doxorubicin was absorbed onto the negatively charged surface of antimony nanoparticles with a loading capacity of 26.5 ± 1.1%. X-ray diffraction (XRD) spectrum showed that the nanoparticles consisted of mostly antimony (0) in the trigonal phase with a hexagonal lattice, while a small fraction of antimony oxide (Sb_2O_3) was also present. The photothermal conversion coefficient was 44.6%. While the nanoparticles were stable in both water and phosphate-buffered saline (PBS) for up to 8 days in storage, irradiation with 808-nm laser at 1.5 $W\cdot cm^{-2}$ induced a rapid degradation of the nanoparticles within 10 min, as evidenced by the decrease of absorbance at 808 nm. Theoretical simulation suggested that the degradation was mediated by the splitting of water molecules into H and OH at the antimony surface during laser irradiation, which was followed by the formation of Sb-H and Sb-OH bonds. The release of doxorubicin was accelerated by acidic pH and laser irradiation. Cell culture studies showed that the combination of chemo-photothermal therapy had higher anti-tumor efficacy than the monotherapy groups.

Qiu et al. [59] prepared copper sulfide (CuS)-based surface-enhanced Raman scattering (SERS) probes that degraded upon continuous laser irradiation. Hollow CuS nanoshells were synthesized in a two-step approach. Cu_2O nanoparticles were first formed by adding hydrazine into the alkaline solution of $CuCl_2$ and PVP. Na_2S was then added to convert the Cu_2O nanoparticles into CuS hollow shells by stirring at 60 °C for 2 h [60]. Organic Raman reporter molecules, including 3,3′-diethylthiatricarbocyanine iodide (DTTC), 3,3′-diethylthiacarbocyanine iodide (DTC), and 3,3′-diethylthiadicarbocyanine iodide (DTDC), were then loaded into the cavity of nanoshells to form the SERS probe. The resultant probes were monodispersed spherical shells of about 126 nm in hydrodynamic diameter, with a photothermal conversion efficiency of 52.3%. The probes were intratumorally injected at a dose of 5 $mg\cdot kg^{-1}$ for PTT to prevent tumor regression after the surgical resection of PC-3 M orthotopic human prostate cancer xenograft model. Irradiation with a 980-nm laser at 0.8 W for 5 min heated the residual tumor to over 50 °C and suppressed the tumor relapse for over 45 days. Degradation study was performed using 980-nm laser at a power of 0.8 W. The individual nanoparticles started to agglomerate during the first 3 min of laser irradiation. The dense CuS shell then became loose, and the central cavity was filled with floccule-like clusters in the 4th minute, and a complete disintegration of the nanoshells into sub-20-nm nanoparticles was observed in the 5th minute. The degradation was attributed to the dissemination of the polycrystalline structures of hollow spheres into individual crystals due to laser heating. Interestingly, the photothermal effect was not impaired by the structural change. Similar levels of temperature elevation were produced after five laser-on/off cycles to about 85 °C. A possible explanation was that the photothermal capacity of CuS was due to the d-d energy band transition of Cu^{2+} ions, rather than the structure-dependent surface plasmon resonance [61]. Laser irradiation also accelerated the nanoparticle clearance from the tumor.

At 28 days after nanoparticle injection, only 4.2%ID remained in the laser-treated tumor, while 21.7%ID was present in the control tumor.

We have previously prepared ultrasmall CuS nanodots with a hydrodynamic diameter of only 4.2 nm, by co-precipitation of $CuCl_2$ and Na_2S in the presence of PVP [62]. Pharmacokinetics study showed a rapid distribution phase (half-life = 0.43 ± 0.12 h) and an elimination half-life of 11.69 h. Compared to the 19-nm counterpart, the ultrasmall nanodots had a slower distribution and faster elimination. The nanodots were rapidly cleared via urine: 60%ID was excreted in 4 h, and almost 95%ID was excreted by 24 h. Dynamic light scattering (DLS) and UV-Vis spectrum confirmed that Cu was excreted as intact nanodots. However, the tumor uptake of nanodots, which peaked to 3.62 ± 0.50%ID/g at 2 h after injection and dropped to only 0.22 ± 0.04%ID/g at 24 h after injection, is severely limited by the fast clearance. CuS nanodots exhibited a distinct absorbance peak at 990 nm. PTT was performed at 2 h after intravenous injection of the nanodots at 4 $mg{\cdot}kg^{-1}$ using 808-nm laser at 2.0 $W{\cdot}cm^{-2}$ for 2 min, which heated the 4T1 tumor xenograft to 45.8 °C. Pathological analyses revealed more than 90% of tumor was necrotic, which is consistent with the durable tumor suppression for 17 days (Fig. 1).

In order to improve the tumor uptake of CuS nanoparticles while preserving their renal clearance property, we have recently explored encapsulating the ultrasmall CuS nanodots in laser-degradable matrix. Ji et al. [63] embedded the ultrasmall CuS nanodots into a biodegradable poly(lactic-co-glycolic) acid (PLGA) core and coated it with F-127 micelles. Doxorubicin was co-encapsulated in the PLGA core at the same time. The resultant temperature-sensitive nanoclusters (TSNS) were 40 nm in hydrodynamic diameter, and the CuS nanodots were about 5 nm. Irradiation with 808-nm laser at 2 $W{\cdot}cm^{-2}$ on a 100-μg/mL dispersion elevated the temperature by over 50 °C in 10 min. Pharmacokinetics study found that the blood circulation followed a two-compartment model with a rapid distribution phase (half-life = 0.25 ± 0.12 h) and a slow elimination phase (half-life = 7.20 ± 0.35 h). At 24 h after intravenous injection, the tumor uptake was 8.02%ID/g, more than twofold higher than that of individual 5-nm CuS nanodots (3.27%ID/g). The tumor uptake was corroborated by the photoacoustic imaging, which showed increasing signal intensity at the tumor region within 24 h of particle injection. The combination of chemo-photothermal therapy by TSNS suppressed the tumor growth of 4T1 model for 18 days and significantly suppressed metastases to the liver and lung. In addition, the photothermal therapy also efficiently eliminated cancer stem cells. The degradation of TSNS was induced by laser treatment, which broke down the TSNS into uniform spheres of 6–7 in size (Fig. 2).

Wei et al. [64] prepared doxorubicin-loaded mesoporous silica nanoparticles capped with ultrasmall CuS nanodots. The mesoporous silica nanoparticles were first synthesized via the conventional sol-gel method, followed by loading doxorubicin via physical absorption. The MSN-DOX was then impregnated with $CuCl_2$ solution followed by adding Na2S in the presence of PVP as surfactant stabilizer. CuS ultrasmall nanodots (~5.8 nm) were then formed and sealed the pore opening to prevent the premature release of doxorubicin. The resultant MSN-DOX-CuS nanoparticles were 120 nm in hydrodynamic diameter with a DOX loading ratio of 20.2% by weight. Irradiation of the particle dispersion at 80 μg/mL with 2.0 $W{\cdot}cm^{-2}$ 808-nm laser elevated the temperature for about 50 °C. Pharmacokinetics study showed that MSN-DOX-CuS had a rapid distribution phase (half-life = 0.64 ± 0.17 h) and a prolonged elimination phase (15.87 ± 0.14 h). Biodistribution study found a tumor uptake of 7.14%ID/g at 24 h post-injection, almost two times higher than that of CuS nanodots (3.62%ID/g). The liver uptake was around 22%ID/g, and spleen uptake was around 4%ID/g. Anti-tumor efficacy was examined in MBA-MDA-231 human breast cancer xenograft and HepG2 human live cancer xenograft models. PTT was performed at 24 h after injection using 808-nm laser at 1 $W{\cdot}cm^{-2}$ for 5 min, leading to a temperature increase to 60 °C at the tumor region. The combination of chemo-photothermal therapy induced a complete tumor regression after 21 days from the treatment, which was further confirmed by the ^{18}F-fluorodeoxyglucose (FDG) PET scan and pathology examination. MSN has been established as biocompatible and biodegradable under physiological conditions. The degradation product is soluble silicic acid that can be excreted via urine [65]. The degradation of MSN-DOX-CuS was induced by laser irradiation. There was a significant size reduction and particle agglomeration at 1 h after laser irradiation, while no discrete particular structure was visible at 24 h after. TEM examination of urine samples at 4 h

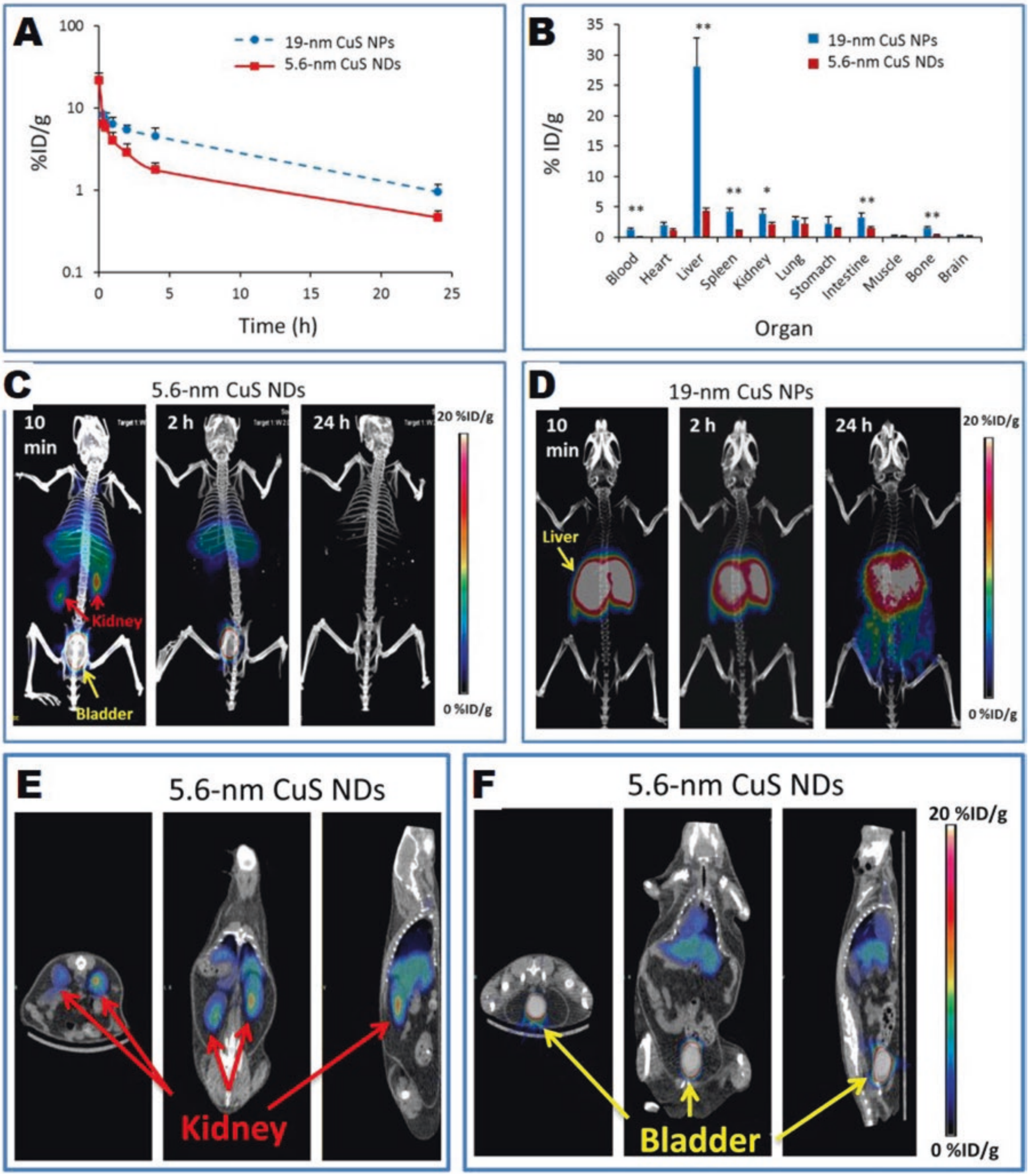

Fig. 1 Pharmacokinetics, biodistribution, and PET/CT images of ^{64}Cu-labeled CuS nanoparticles. (**a**, **b**) Time-activity curves of blood activity (**a**) and biodistribution (**b**) at 24 h after injecting the nanoparticles. (**c**, **d**) Representative co-registered PET/CT maximum intensity projection images. (**e**, **f**) Representative two-dimensional slice of PET/CT images acquired at 10 min after injecting 5.6-nm CuS nanodots. Statistical difference was determined by Student's *t* test ($^{**}p < 0.001$, $^{*}p < 0.01$). (Figure was adapted from Ref. [62] with permission)

after injection found individual CuS nanodots. The UV-Vis spectrum also revealed the characteristic peak of CuS nanodot absorbance at 995 nm, indicating the CuS nanodots detached from the clusters and were excreted separately from the MSN matrix. ICP-MS found that the clearance of silicon element was much slower than that of copper, which is consistent with its hepatobiliary route. Nevertheless, less than 1%ID was present in major organs at 30 days after injection (Fig. 3).

Prasad et al. [66] prepared fluorescent carbon dots of 2–3 nm in diameters by chemical slicing [67] of carbon fibers in concentrated hydrosulfuric acid. The obtained carbon dots were then assembled in liposomes with Janus architecture and an average diameter of about 200 nm. ROS was generated during photothermal therapy. However, photothermal therapy also disrupted the liposomal structure, and the nanoparticles coalesced into smaller particles of

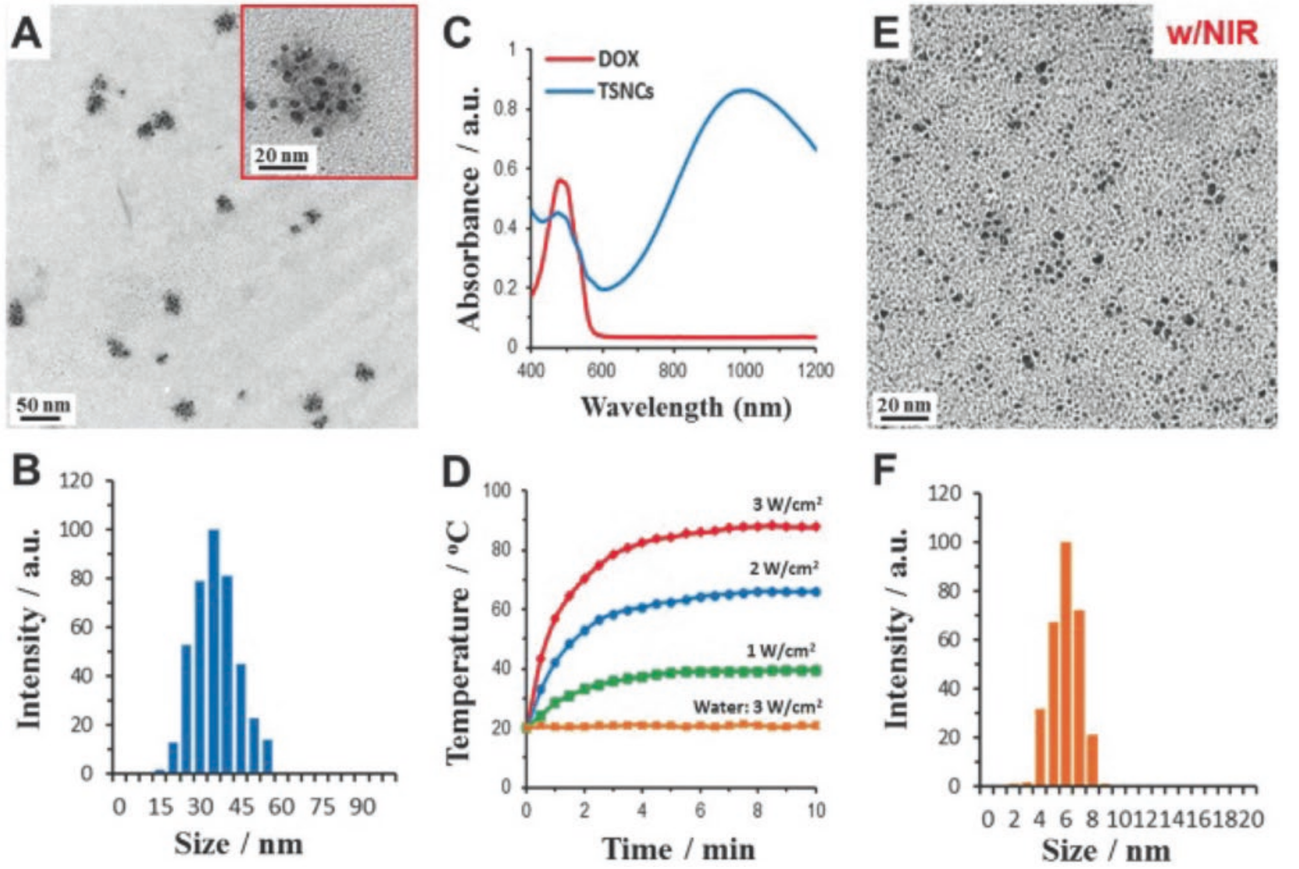

Fig. 2 Characterization of temperature-sensitive nanoclusters (TSNC) based on CuS-embedded PLGA polymeric micelles. (**a**) TEM image of TSNC with high-resolution images in the inset. (**b**) Particle size distribution of TSNC measured with DLS. (**c**) UV-Vis-NIR spectra. (**d**) Temperature elevation curves ex vivo. (**e**) TEM image of laser-degraded TSNC. (**f**) Particle size distribution of laser-degraded TSNC measured with DLS. (Figure was adapted with permission from Ref. [63])

15–40 nm. These particles are expected to be aggregates of even smaller individual carbon dots, therefore enabling their excretion in urine.

9 Degradable Matrix

Hydrogels are used in a wide variety of applications including drug and gene delivery and tissue engineering. Hydrogel-based drug delivery system allows a localized, sustained release of therapeutic cargos to improve drug bioavailability and minimize adverse effects. In addition to the chemotherapy drugs, PTT nanoparticles have also been encapsulated into hydrogels to prevent their premature leakage from the injection site, so that repeated PTT can be applied over an extended time. The use of biodegradable hydrogels, in this regard, allows the gradual clearance of PTT nanoparticles.

Wang et al. [68] embedded poly(amido amine) (PAMAM) dendrimer-encapsulated ultrasmall platinum nanoparticles (2–3 nm in diameter) in an alginate-calcium cross-linked hydrogel. The nanoparticles were synthesized by reducing H_2PtCl_6 with $NaBH_4$ in the presence of PAMAM, followed by acetylation of amine groups with acetic anhydride [69]. The nanoparticles were then mixed with alginate and then cross-linked with $CaCO_3$. Irradiation of the hydrogel with 808-nm laser at 5.8 $W{\cdot}cm^{-2}$ for 10 min resulted in a temperature elevation over 25 °C. Notably, as many as ten PTT treatments were successfully applied over 1 month at the tumor injected with the hydrogel. The degradation of hydrogel was induced by co-injection of small-molecular chelators for the calcium cations, such as EDTA, sodium citrate, and diethylenetriaminepentaacetic acid (DTPA). In situ injection of the chelators initiated the hydrogel degradation within 3 days after injection, which was confirmed by the reduction of photothermal efficiency. Although the study did not elucidate the excretion of individual platinum nanoparticles, they were expected to be cleared with a 2-nm diameter.

Huang et al. [70] embedded gold nanorods into a polypeptide matrix using disulfide bond as the cross-linker and

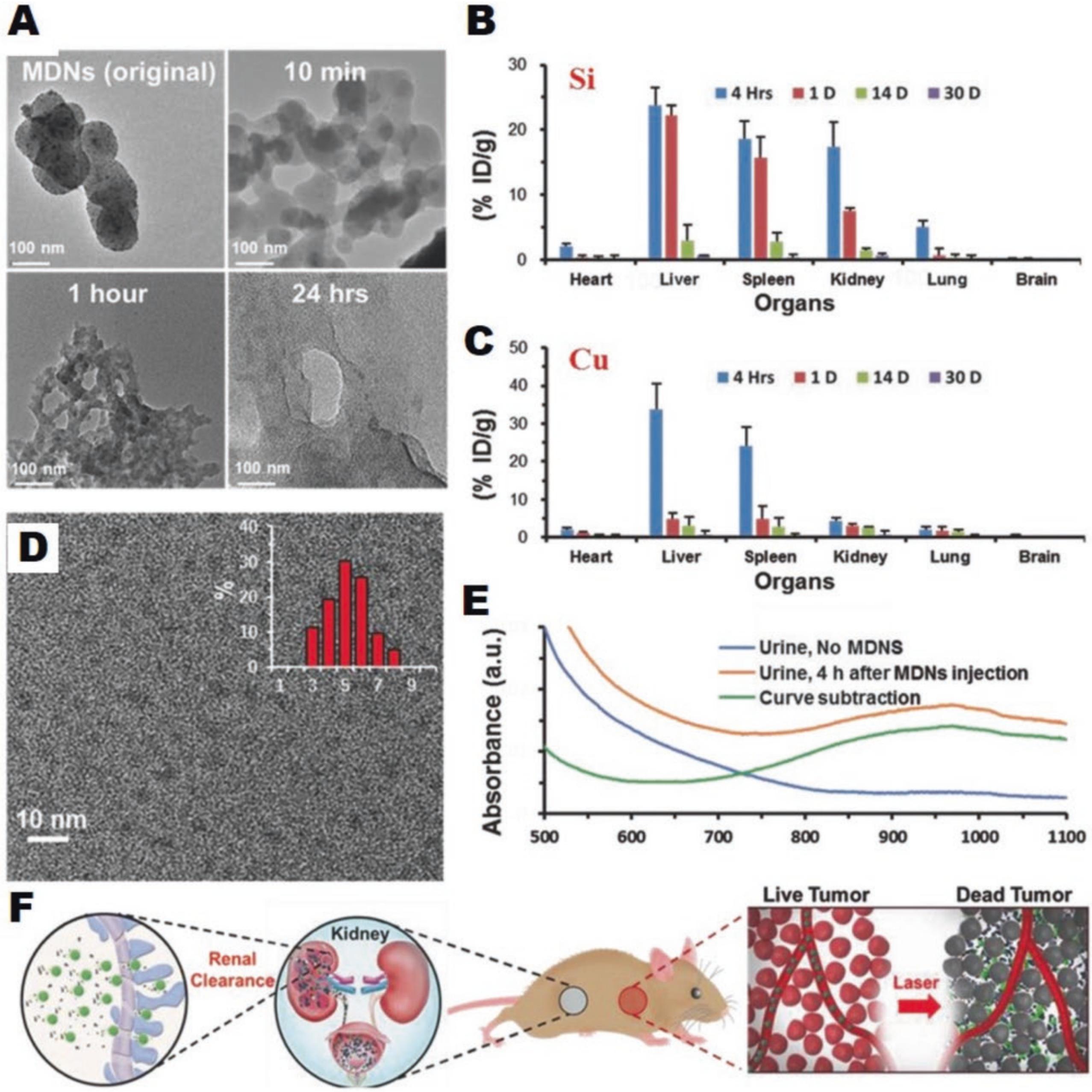

Fig. 3 Degradation and clearance of MSN-DOX-CuS nanoparticles. (**a**) TEM images of nanoparticles after NIR irradiation. (**b**, **c**) Time-dependent element uptake in major organs (*N* = 3). (**d**, **e**) TEM and UV-Vis spectra of urine samples at 4 h after intravenous injection of nanoparticles. (**f**) Schematic illustration of nanoparticle clearance. (Figure was adapted with permission from Ref. [64])

then loaded the matrix with a heat-shock protein (HSP) 90 inhibitor, 17-(allylamino)-17-demethoxygeldanamycin (17-AAG). The resultant matrix was heated to above 45 °C when irradiated with 808-nm laser at 25 W·cm^{-2} for 10 min, which not only killed surrounding cancer cells via thermal effect but also rapidly released 17-AAG to enhance the effects of thermal killing. The hydrogel degraded after adding molecules with thiol groups, such as dithiothreitol (DTT) within 30 min of adding 10 mM dithiothreitol (DTT) at 4 °C.

10 Mesoporous Silicon Nanoparticles

Zhang et al. [71] prepared biodegradable mesoporous silicon/carbon nanoparticles for PTT. The nanoparticles were synthesized in two steps. First, silica nanoparticles (SiO_2) were prepared via sol-gel method, coated with poly(acrylonitrile) that was subsequently oxidized to for the carbon coating. The silica core was then annealed in a hydrogen/argon flow and reduced into silicon. Doxorubicin loading and PEGylation were then performed to give the final multifunctional theranostic nanoparticles (PEG-Si/C-DOX) of hollow architecture with an average diameter around 237 nm. The presence of Si/C provided a strong absorbance for NIR lasers of wavelength between 700 and 1000 nm, with a photothermal conversion efficiency of approximately 40.7%. Biodistribution analyses via the ICP-AES analyses of silicon element found that the tumor uptake was around 19%ID/g at 2 h post intravenous injection and decreased to around 12%ID/g at 12 h post-injection. Photoacoustic imaging (PAI) also corroborated the tumor uptake of nanoparticles, where the PAI signals peaked at 2 h post-injection and then waned off to slightly above baseline at 12 h post-injection. PTT was performed at 24 h after injection of 2 mg·mL^{-1} nanoparticles using 808-nm laser at 1 W·cm^{-2} for 5 min, leading to a temperature increase to 50 °C at the tumor region. The combination of the doxorubicin chemotherapy and photothermal therapy eradicated subcutaneous A549 human lung cancer xenograft, while the photothermal treatment group also suppressed the tumor growth. The degradation study was performed in PBS at 37 °C for over 30 days with continuous shaking: 8.4% of silicon (by weight) was dissolved from the original nanoparticles, which was confirmed by the collapse of the hollow mesoporous structure under TEM examination.

11 Methods to Monitor Degradation

Real-time monitoring of nanoparticle degradation, especially in vivo, provides valuable information about the metabolization and probable fate of nanoparticles after they are administrated. Some indirect methods have been adopted in vitro, including the fluorescence imaging of peroxidase activity for carbon-based material degradation [32] or photoluminescent imaging of degradation products such as the graphene quantum dots degraded from graphene oxide [30]. The changes in r_1 or r_2 relaxivity are also useful for noninvasive detection of Co- and Mn-based nanoparticles through MRI [48, 52].

Photoacoustic imaging is a novel imaging technique via measurement of ultrasonic waves induced by the biological absorption of laser pulses [72]. By switching to tissue-penetrating NIR lasers and NIR-absorbing nanoparticles as contrast agents, photoacoustic imaging was able to detect tumor lesions as deep as 5–7 cm from tissue surface [73]. Shi et al. [74] prepared thermosensitive PEGylated CuS nanoparticles and studied their in vivo degradation with real-time multispectral optoacoustic tomography (MOST). The nanoparticles were prepared via a one-pot reaction by heating $CuCl_2$ and Na_2S in the presence of PEG-SH at 95 °C for 15 min. The resultant nanoparticles were about 11 nm in hydrodynamic diameter. Degradation was induced by the oxygen dissolved in the dispersion, which was further accelerated at 37 °C. As shown by inductively coupled plasma-optical emission spectrometry (ICP-OES), the S^{2-} anions were oxidized to SO_4^{2-}, which forms water-soluble salt with Cu^{2+}. The photoacoustic signals in the liver region were monitored via MOST for up to 7 days after injection. The signal intensity peaked at 3 h and slightly decreased at 24 h after injection. At 7 days after injection, however, the photoacoustic signals returned to baseline, indicating a complete degradation and subsequent clearance of CuS-PEG.

12 Conclusions

Degradable and clearable photothermal nanoparticles are considered as promising agents for targeted cancer therapy. When combined with other therapeutic modalities such as chemotherapy, radiotherapy, and immunotherapy, they are able to generate a significant synergistic response without causing substantial acute or chronic toxicity concerns. However, the superior anti-tumor efficacy of multifunctional PTT nanoparticles has so far been limited to preclinical studies, while the clinical translation has not seen much progress. With the current effort in developing degradable nanoparticles and understanding their fate in vivo, we seem to finally be able to see the light at the end of the tunnel.

References

1. Ryu, J. H., Koo, H., Sun, I. C., Yuk, S. H., Choi, K., Kim, K., & Kwon, I. C. (2012). Tumor-targeting multi-functional nanoparticles for theragnosis: New paradigm for cancer therapy. *Advanced Drug Delivery Reviews, 64*(13), 1447–1458.
2. Fiedler, V. U., Schwarzmaier, H. J., Eickmeyer, F., Muller, F. P., Schoepp, C., & Verreet, P. R. (2001). Laser-induced interstitial thermotherapy of liver metastases in an interventional 0.5 Tesla MRI system: Technique and first clinical experiences. *Journal of Magnetic Resonance Imaging, 13*(5), 729–737.
3. Qi, S., Lu, L., Zhou, F., Chen, Y., Xu, M., Chen, L., Yu, X., Chen, W. R., & Zhang, Z. (2020). Neutrophil infiltration and whole-cell vaccine elicited by N-dihydrogalactochitosan combined with NIR phototherapy to enhance antitumor immune response and T cell immune memory. *Theranostics, 10*(4), 1814–1832.
4. Liu, Y., Bhattarai, P., Dai, Z., & Chen, X. (2019). Photothermal therapy and photoacoustic imaging via nanotheranostics in fighting cancer. *Chemical Society Reviews, 48*(7), 2053–2108.
5. Ashikbayeva, Z., Tosi, D., Balmassov, D., Schena, E., Saccomandi, P., & Inglezakis, V. (2019). Application of nanoparticles and nanomaterials in thermal ablation therapy of cancer. *Nanomaterials (Basel), 9*(9), 1195.
6. Norouzi, M. (2020). Gold nanoparticles in glioma theranostics. *Pharmacological Research, 156*, 104753.
7. Liu, Y., Ji, M., & Wang, P. (2019). Recent advances in small copper sulfide nanoparticles for molecular imaging and tumor therapy. *Molecular Pharmaceutics, 16*(8), 3322–3332.
8. Wilhelm, S., Tavares, A. J., Dai, Q., Ohta, S., Audet, J., Dvorak, H. F., & Chan, W. C. W. (2016). Analysis of nanoparticle delivery to tumours. *Nature Reviews Materials, 1*(5), 16014.
9. Park, K. (2019). Transcending nanomedicine to the next level: Are we there yet? *Journal of Controlled Release, 298*, 213.
10. Park, K. (2019). The beginning of the end of the nanomedicine hype. *Journal of Controlled Release, 305*, 221–222.

11. Halamoda-Kenzaoui, B., Baconnier, S., Bastogne, T., Bazile, D., Boisseau, P., Borchard, G., Borgos, S. E., Calzolai, L., Cederbrant, K., Di Felice, G., Di Francesco, T., Dobrovolskaia, M. A., Gaspar, R., Gracia, B., Hackley, V. A., Leyens, L., Liptrott, N., Park, M., Patri, A., Roebben, G., Roesslein, M., Thurmer, R., Urban, P., Zuang, V., & Bremer-Hoffmann, S. (2019). Bridging communities in the field of nanomedicine. *Regulatory Toxicology and Pharmacology, 106*, 187–196.
12. Poland, C. A., Duffin, R., Kinloch, I., Maynard, A., Wallace, W. A. H., Seaton, A., Stone, V., Brown, S., MacNee, W., & Donaldson, K. (2008). Carbon nanotubes introduced into the abdominal cavity of mice show asbestos-like pathogenicity in a pilot study. *Nature Nanotechnology, 3*(7), 423–428.
13. Longmire, M., Choyke, P. L., & Kobayashi, H. (2008). Clearance properties of nano-sized particles and molecules as imaging agents: Considerations and caveats. *Nanomedicine (London, England), 3*(5), 703–717.
14. Vegt, E., de Jong, M., Wetzels, J. F. M., Masereeuw, R., Melis, M., Oyen, W. J. G., Gotthardt, M., & Boerman, O. C. (2010). Renal toxicity of radiolabeled peptides and antibody fragments: Mechanisms, impact on radionuclide therapy, and strategies for prevention. *Journal of Nuclear Medicine, 51*(7), 1049–1058.
15. Gad, S. C., Sharp, K. L., Montgomery, C., Payne, J. D., & Goodrich, G. P. (2012). Evaluation of the toxicity of intravenous delivery of auroshell particles (gold–silica nanoshells). *International Journal of Toxicology, 31*(6), 584–594.
16. Lin, H., Wang, X., Yu, L., Chen, Y., & Shi, J. (2017). Two-dimensional ultrathin MXene ceramic nanosheets for photothermal conversion. *Nano Letters, 17*(1), 384–391.
17. Bai, H., Jiang, W., Kotchey, G. P., Saidi, W. A., Bythell, B. J., Jarvis, J. M., Marshall, A. G., Robinson, R. A., & Star, A. (2014). Insight into the mechanism of graphene oxide degradation via the photo-Fenton reaction. *The Journal of Physical Chemistry. C, Nanomaterials and Interfaces, 118*(19), 10519–10529.
18. Yang, K., Zhang, S., Zhang, G., Sun, X., Lee, S.-T., & Liu, Z. (2010). Graphene in mice: Ultrahigh in vivo tumor uptake and efficient photothermal therapy. *Nano Letters, 10*(9), 3318–3323.
19. Bai, J., Liu, Y., & Jiang, X. (2014). Multifunctional PEG-GO/CuS nanocomposites for near-infrared chemo-photothermal therapy. *Biomaterials, 35*(22), 5805–5813.
20. Huang, G., Zhu, X., Li, H., Wang, L., Chi, X., Chen, J., Wang, X., Chen, Z., & Gao, J. (2015). Facile integration of multiple magnetite nanoparticles for theranostics combining efficient MRI and thermal therapy. *Nanoscale, 7*(6), 2667–2675.
21. Robinson, J. T., Tabakman, S. M., Liang, Y., Wang, H., Sanchez Casalongue, H., Vinh, D., & Dai, H. (2011). Ultrasmall reduced graphene oxide with high near-infrared absorbance for photothermal therapy. *Journal of the American Chemical Society, 133*(17), 6825–6831.
22. Li, D., Muller, M. B., Gilje, S., Kaner, R. B., & Wallace, G. G. (2008). Processable aqueous dispersions of graphene nanosheets. *Nature Nanotechnology, 3*(2), 101–105.
23. Hashemi, M., Omidi, M., Muralidharan, B., Smyth, H., Mohagheghi, M. A., Mohammadi, J., & Milner, T. E. (2017). Evaluation of the photothermal properties of a reduced graphene oxide/arginine nanostructure for near-infrared absorption. *ACS Applied Materials & Interfaces, 9*(38), 32607–32620.
24. Yan, M., Liu, Y., Zhu, X., Wang, X., Liu, L., Sun, H., Wang, C., Kong, D., & Ma, G. (2019). Nanoscale reduced graphene oxide-mediated photothermal therapy together with IDO inhibition and PD-L1 blockade synergistically promote antitumor immunity. *ACS Applied Materials & Interfaces, 11*(2), 1876–1885.
25. Lu, K., He, C., Guo, N., Chan, C., Ni, K., Weichselbaum, R. R., & Lin, W. (2016). Chlorin-based nanoscale metal-organic framework systemically rejects colorectal cancers via synergistic photodynamic therapy and checkpoint blockade immunotherapy. *Journal of the American Chemical Society, 138*(38), 12502–12510.
26. Ge, R., Liu, C., Zhang, X., Wang, W., Li, B., Liu, J., Liu, Y., Sun, H., Zhang, D., Hou, Y., Zhang, H., & Yang, B. (2018). Photothermal-activatable Fe3O4 superparticle nanodrug carriers with PD-L1 immune checkpoint blockade for anti-metastatic cancer immunotherapy. *ACS Applied Materials & Interfaces, 10*(24), 20342–20355.
27. Lalwani, G., Xing, W., & Sitharaman, B. (2014). Enzymatic degradation of oxidized and reduced graphene nanoribbons by lignin peroxidase. *Journal of Materials Chemistry B, 2*(37), 6354–6362.
28. Filizola, M., & Loew, G. H. (2000). Role of protein environment in horseradish peroxidase compound I formation: Molecular dynamics simulations of horseradish peroxidase−HOOH complex. *Journal of the American Chemical Society, 122*(1), 18–25.
29. Kotchey, G. P., Allen, B. L., Vedala, H., Yanamala, N., Kapralov, A. A., Tyurina, Y. Y., Klein-Seetharaman, J., Kagan, V. E., & Star, A. (2011). The enzymatic oxidation of graphene oxide. *ACS Nano, 5*(3), 2098–2108.
30. Kim, H., Kim, J., Lee, M., Choi, H. C., & Kim, W. J. (2016). Stimuli-regulated enzymatically degradable smart graphene-oxide-polymer Nanocarrier facilitating Photothermal gene delivery. *Advanced Healthcare Materials, 5*(15), 1918–1930.
31. Kagan, V. E., Konduru, N. V., Feng, W., Allen, B. L., Conroy, J., Volkov, Y., Vlasova, I. I., Belikova, N. A., Yanamala, N., Kapralov, A., & Tyurina, Y. Y. (2010). Shvedova, Carbon nanotubes degraded by neutrophil myeloperoxidase induce less pulmonary inflammation. *Nature Nanotechnology, 5*(5), 354–359.
32. Allen, B. L., Kotchey, G. P., Chen, Y., Yanamala, N. V., Klein-Seetharaman, J., Kagan, V. E., & Star, A. (2009). Mechanistic investigations of horseradish peroxidase-catalyzed degradation of single-walled carbon nanotubes. *Journal of the American Chemical Society, 131*(47), 17194–17205.
33. Sydlik, S. A., Jhunjhunwala, S., Webber, M. J., Anderson, D. G., & Langer, R. (2015). In vivo compatibility of graphene oxide with differing oxidation states. *ACS Nano, 9*(4), 3866–3874.
34. Sanchez, V. C., Jachak, A., Hurt, R. H., & Kane, A. B. (2012). Biological interactions of graphene-family nanomaterials: An interdisciplinary review. *Chemical Research in Toxicology, 25*(1), 15–34.
35. Chen, Y., Cheng, L., Dong, Z., Chao, Y., Lei, H., Zhao, H., Wang, J., & Liu, Z. (2017). Degradable vanadium disulfide nanostructures with unique optical and magnetic functions for cancer theranostics. *Angewandte Chemie (International Ed. in English), 56*(42), 12991–12996.
36. Zhang, C., Wang, S. B., Chen, Z. X., Fan, J. X., Zhong, Z. L., & Zhang, X. Z. (2019). A tungsten nitride-based degradable nanoplatform for dual-modal image-guided combinatorial chemo-photothermal therapy of tumors. *Nanoscale, 11*(4), 2027–2036.
37. Wang, Y. L., Nie, T., Li, Y. H., Wang, X. L., Zheng, L. R., Chen, A. P., Gong, X. Q., & Yang, H. G. (2017). Black tungsten nitride as a metallic photocatalyst for overall water splitting operable at up to 765 nm. *Angewandte Chemie International Edition, 56*(26), 7430–7434.
38. Saikolappan, S., Kumar, B., Shishodia, G., Koul, S., & Koul, H. K. (2019). Reactive oxygen species and cancer: A complex interaction. *Cancer Letters, 452*, 132–143.
39. Sabharwal, S. S., & Schumacker, P. T. (2014). Mitochondrial ROS in cancer: Initiators, amplifiers or an Achilles' heel? *Nature Reviews Cancer, 14*(11), 709–721.
40. Zhang, L., Blom, D. A., & Wang, H. (2011). Au–Cu2O Core–Shell nanoparticles: A hybrid metal-semiconductor heteronanostructure with geometrically tunable optical properties. *Chemistry of Materials, 23*(20), 4587–4598.
41. Tai, Y. W., Chiu, Y. C., Wu, P. T., Yu, J., Chin, Y. C., Wu, S. P., Chuang, Y. C., Hsieh, H. C., Lai, P. S., Yu, H. P., & Liao, M. Y. (2018). Degradable NIR-PTT nanoagents with a potential Cu@Cu2O@Polymer structure. *ACS Applied Materials & Interfaces, 10*(6), 5161–5174.

42. Shi, M., Kwon, H. S., Peng, Z., Elder, A., & Yang, H. (2012). Effects of surface chemistry on the generation of reactive oxygen species by copper nanoparticles. *ACS Nano, 6*(3), 2157–2164.
43. Burrows, C. J., & Muller, J. G. (1998). Oxidative nucleobase modifications leading to strand scission. *Chemical Reviews, 98*(3), 1109–1152.
44. Miao, Z., Chen, S., Xu, C. Y., Ma, Y., Qian, H., Xu, Y., Chen, H., Wang, X., He, G., Lu, Y., Zhao, Q., & Zha, Z. (2019). PEGylated rhenium nanoclusters: A degradable metal photothermal nanoagent for cancer therapy. *Chemical Science, 10*(21), 5435–5443.
45. Jeong, J. M., & Chung, J. K. (2003). Therapy with 188Re-labeled radiopharmaceuticals: An overview of promising results from initial clinical trials. *Cancer Biotherapy & Radiopharmaceuticals, 18*(5), 707–717.
46. Tang, Q., Cheng, Z., Yang, N., Li, Q., Wang, P., Chen, D., Wang, W., Song, X., & Dong, X. (2019). Hydrangea-structured tumor microenvironment responsive degradable nanoplatform for hypoxic tumor multimodal imaging and therapy. *Biomaterials, 205*, 1–10.
47. Tian, Y., Wang, X., Zhao, S., Liao, X., Younis, M. R., Wang, S., Zhang, C., & Lu, G. (2019). JQ1-loaded polydopamine nanoplatform inhibits c-MYC/programmed cell death ligand 1 to enhance photothermal therapy for triple-negative breast cancer. *ACS Applied Materials & Interfaces, 11*(50), 46626–46636.
48. Liu, Z., Zhang, S., Lin, H., Zhao, M., Yao, H., Zhang, L., Peng, W., & Chen, Y. (2018). Theranostic 2D ultrathin MnO2 nanosheets with fast responsibility to endogenous tumor microenvironment and exogenous NIR irradiation. *Biomaterials, 155*, 54–63.
49. Chen, Y., Ye, D., Wu, M., Chen, H., Zhang, L., Shi, J., & Wang, L. (2014). Break-up of two-dimensional MnO_2 nanosheets promotes ultrasensitive pH-triggered theranostics of cancer. *Advanced Materials, 26*(41), 7019–7026.
50. Drouin, G., Godin, J. R., & Page, B. (2011). The genetics of vitamin C loss in vertebrates. *Current Genomics, 12*(5), 371–378.
51. Liu, Y., Zhang, G., Guo, Q., Ma, L., Jia, Q., Liu, L., & Zhou, J. (2017). Artificially controlled degradable inorganic nanomaterial for cancer theranostics. *Biomaterials, 112*, 204–217.
52. Yun, T., Liu, Y., Yi, S., Jia, Q., Liu, Y., & Zhou, J. (2018). Artificially controlled degradable nanoparticles for contrast switch MRI and programmed cancer therapy. *International Journal of Nanomedicine, 13*, 6647–6659.
53. Lu, L. T., Dung, N. T., Tung, L. D., Thanh, C. T., Quy, O. K., Chuc, N. V., Maenosono, S., & Thanh, N. T. K. (2015). Synthesis of magnetic cobalt ferrite nanoparticles with controlled morphology, monodispersity and composition: The influence of solvent, surfactant, reductant and synthetic conditions. *Nanoscale, 7*(46), 19596–19610.
54. O'Neill, E. S., Kaur, A., Bishop, D. P., Shishmarev, D., Kuchel, P. W., Grieve, S. M., Figtree, G. A., Renfrew, A. K., Bonnitcha, P. D., & New, E. J. (2017). Hypoxia-responsive cobalt complexes in tumor spheroids: Laser ablation inductively coupled plasma mass spectrometry and magnetic resonance imaging studies. *Inorganic Chemistry, 56*(16), 9860–9868.
55. Chen, Y., Khan, A. R., Yu, D., Zhai, Y., Ji, J., Shi, Y., & Zhai, G. (2019). Pluronic F127-functionalized molybdenum oxide nanosheets with pH-dependent degradability for chemo-photothermal cancer therapy. *Journal of Colloid and Interface Science, 553*, 567–580.
56. Song, G., Hao, J., Liang, C., Liu, T., Gao, M., Cheng, L., Hu, J., & Liu, Z. (2016). Degradable molybdenum oxide nanosheets with rapid clearance and efficient tumor homing capabilities as a therapeutic nanoplatform. *Angewandte Chemie International Edition, 55*(6), 2122–2126.
57. Zhao, W., Li, Z., Yang, H., Ren, C., Lv, F., Gao, S., Ma, H., Jin, Y., Ge, K., Liu, D., Zhang, J., & Liu, H. (2019). Mesoporous platinum nanotherapeutics for combined chemo-photothermal cancer treatment. *ACS Applied Bio Materials, 2*(8), 3269–3278.
58. Dibaba, S. T., Caputo, R., Xi, W., Zhang, J. Z., Wei, R., Zhang, Q., Zhang, J., Ren, W., & Sun, L. (2019). NIR light-degradable antimony nanoparticle-based drug-delivery nanosystem for synergistic chemo-photothermal therapy in vitro. *ACS Applied Materials & Interfaces, 11*(51), 48290–48299.
59. Qiu, Y., Lin, M., Chen, G., Fan, C., Li, M., Gu, X., Cong, S., Zhao, Z., Fu, L., Fang, X., & Xiao, Z. (2019). Photodegradable CuS SERS probes for intraoperative residual tumor detection, ablation, and self-clearance. *ACS Applied Materials & Interfaces, 11*(26), 23436–23444.
60. Ramadan, S., Guo, L., Li, Y., Yan, B., & Lu, W. (2012). Hollow copper sulfide nanoparticle-mediated transdermal drug delivery. *Small, 8*(20), 3143–3150.
61. Wang, Z., Huang, P., Jacobson, O., Wang, Z., Liu, Y., Lin, L., Lin, J., Lu, N., Zhang, H., Tian, R., Niu, G., Liu, G., & Chen, X. (2016). Biomineralization-inspired synthesis of copper sulfide–ferritin nanocages as cancer theranostics. *ACS Nano, 10*(3), 3453–3460.
62. Zhou, M., Li, J., Liang, S., Sood, A. K., Liang, D., & Li, C. (2015). CuS nanodots with ultrahigh efficient renal clearance for positron emission tomography imaging and image-guided photothermal therapy. *ACS Nano, 9*(7), 7085–7096.
63. Ji, J., Ma, F., Zhang, H., Liu, F., He, J., Li, W., Xie, T., Zhong, D., Zhang, T., Tian, M., Zhang, H., Santos, H. A., & Zhou, M. (2018). Light-activatable assembled nanoparticles to improve tumor penetration and eradicate metastasis in triple negative breast cancer. *Advanced Functional Materials, 28*(33), 1801738.
64. Wei, Q., Chen, Y., Ma, X., Ji, J., Qiao, Y., Zhou, B., Ma, F., Ling, D., Zhang, H., Tian, M., Tian, J., & Zhou, M. (2018). High-efficient clearable nanoparticles for multi-modal imaging and image-guided cancer therapy. *Advanced Functional Materials, 28*(2), 1704634.
65. Croissant, J. G., Fatieiev, Y., & Khashab, N. M. (2017). Degradability and clearance of silicon, organosilica, silsesquioxane, silica mixed oxide, and mesoporous silica nanoparticles. *Advanced Materials, 29*(9), 1604634.
66. Prasad, R., Chauhan, D. S., Yadav, A. S., Devrukhkar, J., Singh, B., Gorain, M., Temgire, M., Bellare, J., Kundu, G. C., & Srivastava, R. (2018). A biodegradable fluorescent nanohybrid for photo-driven tumor diagnosis and tumor growth inhibition. *Nanoscale, 10*(40), 19082–19091.
67. Aiyer, S., Prasad, R., Kumar, M., Nirvikar, K., Jain, B., & Kushwaha, O. S. (2016). Fluorescent carbon nanodots for targeted in vitro cancer cell imaging. *Applied Materials Today, 4*, 71–77.
68. Wang, C., Wang, X., Dong, K., Luo, J., Zhang, Q., & Cheng, Y. (2016). Injectable and responsively degradable hydrogel for personalized photothermal therapy. *Biomaterials, 104*, 129–137.
69. Crooks, R. M., Zhao, M., Sun, L., Chechik, V., & Yeung, L. K. (2001). Dendrimer-encapsulated metal nanoparticles: Synthesis, characterization, and applications to catalysis. *Accounts of Chemical Research, 34*(3), 181–190.
70. Huang, H. C., Yang, Y., Nanda, A., Koria, P., & Rege, K. (2011). Synergistic administration of photothermal therapy and chemotherapy to cancer cells using polypeptide-based degradable plasmonic matrices. *Nanomedicine (London, England), 6*(3), 459–473.
71. Zhang, J., Zhang, J., Li, W., Chen, R., Zhang, Z., Zhang, W., Tang, Y., Chen, X., Liu, G., & Lee, C. S. (2017). Degradable hollow mesoporous silicon/carbon nanoparticles for photoacoustic imaging-guided highly effective chemo-thermal tumor therapy in vitro and in vivo. *Theranostics, 7*(12), 3007–3020.
72. Kruger, R. A. (1994). Photoacoustic ultrasound. *Medical Physics, 21*(1), 127–131.
73. Ku, G., Zhou, M., Song, S., Huang, Q., Hazle, J., & Li, C. (2012). Copper sulfide nanoparticles as a New class of photoacoustic contrast agent for deep tissue imaging at 1064 nm. *ACS Nano, 6*(8), 7489–7496.
74. Shi, S., Wen, X., Li, T., Wen, X., Cao, Q., Liu, X., Liu, Y., Pagel, M. D., & Li, C. (2019). Thermosensitive biodegradable copper sulfide nanoparticles for real-time multispectral optoacoustic tomography. *ACS Applied Bio Materials, 2*(8), 3203–3211.

Biohybrid Nanosystems for Cancer Treatment: Merging the Best of Two Worlds

Flavia Fontana, Raquél Bartolo, and Hélder A. Santos

Abstract

During the last 20+ years, research into the biomedical application of nanotechnology has helped in reshaping cancer treatment. The clinical use of several passively targeted nanosystems resulted in improved quality of care for patients. However, the therapeutic efficacy of these systems is not superior to the original drugs. Moreover, despite extensive investigations into actively targeted nanocarriers, numerous barriers still remain before their successful clinical translation, including sufficient bloodstream circulation time and efficient tumor targeting. The combination of synthetic nanomaterials with biological elements (e.g., cells, cell membranes, and macromolecules) is presently the cutting-edge research in cancer nanotechnology. The features provided by the biological moieties render the particles with prolonged bloodstream circulation time and homotopic targeting to the tumor site. Moreover, cancer cell membranes serve as sources of neoantigens, useful in the formulation of nanovaccines. In this chapter, we will discuss the advantages of biohybrid nanosystems in cancer chemotherapy, immunotherapy, and combined therapy, as well as highlight their preparation methods and clinical translatability.

Keywords

Biohybrid · Nanoparticle · Cancer · Immunotherapy · Photothermal therapy

1 Introduction

Biohybrid materials are defined as a combination of biological and non-biological substances [1]. They can range from robots powered by living cells, to bacteria engineered for drug delivery, and to solar cells where the energy conversion is powered by enzymes [2–4]. In the biomedical field, biohybrid materials are researched as drug delivery carriers, vaccine platforms, detoxifying agents, microbots, and scaffolds [5–9]. The broader term of biohybrid materials indicates both biomimetics and biointegrated systems [10]. Biomimetic is the results of a nature-inspired new synthetic material, like the development of specific synthetic hydrogels mimicking specific functions of 3D microenvironment (e.g., presence of growth factors, conductivity, mechanical properties) [11]. Alternatively, biointegration can refer to the addition of organic materials within synthetic scaffolds [10]: examples include the integration of neurons within circuits [12] or cells within hydrogel scaffolds to restore insulin production [13]. All the different types of biohybrid materials have a fundamental role in the development of patient-tailored, personalized medicines [10]. Biohybrid materials can contribute to improved sensing and diagnostic for different biomolecules (e.g., glucose and choline), pathogenic contaminants, and amplification of endogenous signal cascades [14]. Moreover, these materials demonstrated excellent properties for tissue engineering, particularly as artificial extracellular matrices useful for tissue regeneration [14]. Finally, one of the main applications is drug delivery in the form of drug depots or nanocarriers [14]. Enzyme-responsive drug depot can deliver the therapeutics locally with proven efficacy in vivo in neovascularization or wound healing [14, 15]. As for nanocarriers, multiple biohybrid systems (e.g., stimuli-responsive) have been developed for drug delivery in multiple therapeutic applications [16].

F. Fontana · R. Bartolo · H. A. Santos (✉)
Drug Research Program, Division of Pharmaceutical Chemistry and Technology, Faculty of Pharmacy, University of Helsinki, Helsinki, Finland
e-mail: helder.santos@helsinki.fi

© Springer Nature Switzerland AG 2021
F. Fontana, H. A. Santos (eds.), *Bio-Nanomedicine for Cancer Therapy*, Advances in Experimental Medicine and Biology 1295, https://doi.org/10.1007/978-3-030-58174-9_7

In this book chapter, we introduce the last research in terms of nature-derived top-down biohybrids, the use of cells or cell membranes to enhance the properties of nanocarriers, improving their navigation between the different pathophysiological barriers [16]. In the next section, we also introduce the toolboxes and recipes established for the formulation of this type of carriers, followed by the sections illustrating selected applications in cancer chemotherapy, immunotherapy, photothermal therapy, and photodynamic therapy. Finally, we discuss the pros and cons of this approach, together with a clinical outlook.

2 Biohybrids: Toolboxes and Recipes

Biohybrid materials can be classified, according to the structure and/or the preparation method, in top-down and bottom-up approaches. In particular, cell ghosts, cell membrane-wrapped materials, and cellular carriers are top-down techniques starting from whole cells to move to the nanocarriers, while adsorption or direct binding between biological features and the materials are bottom-up, starting from biomolecules to functionalize the nanocarriers. The characteristics and preparation method for each type of material are summarized in Table 1.

In this section, we provide the reader with a toolbox of techniques and protocols widely employed in the preparation of biohybrid nanosystems. Cell ghosts are reformed from the membrane of cells after a process of isolation of the membranes from the cytosolic components, as evaluated by Oieni et al. [20]. The cells are lysed in hypotonic buffer, before undergoing homogenization. The membranes are then purified by cycles of centrifugation and sonication to eliminate all the cytoplasmic contaminants. The nano-ghosts are resuspended in different buffers according to different sources, but Oieni et al. suggested the use of a sucrose buffer to improve the stability of the ghosts. The empty nano-ghosts can be further modified (e.g., PEGylated, labelled with fluorescent probes or radiolabels) and loaded with the payload of interest by electoporation [20]. Different parameters influence the manufacturing of nano-ghosts: duration and speed of the homogenization and centrifugation time and speed influence the purity of the vesicles and the removal of the other contaminants. As for the size uniformity, both extrusion and sonication produce vesicles with an average size distribution of 166 nm. Moreover, nano-ghosts can be stored for short term (up to 1 week) in PBS at −20 °C or −80 °C, without changes in size or zeta (ζ)-potential [20].

The process of enveloping cell membranes around nanocarriers or fibers is somewhat similar with the preparation of cell nano-ghosts. The first steps still rely on the isolation and purification of cell membranes via series of centrifugations [23, 38, 39]. Following the isolation, membrane fragments and vesicles are resuspended in a buffer where the stability of the nanocarrier will be highest: in our own experience, small changes of pH from 7.4 to 7.2 can increase the stability of hydrophobic porous silicon nanoparticles [38], or more elaborate buffer screenings, including the use of glucose or sucrose, are required [40]. Moreover, the physicochemical characteristics of the nanocarrier have an effect on the coating: Luk et al. coated polymeric nanoparticles up to 340 nm with RBC membrane by extrusion, while the coating of positively charged particles still remains an issue (Table 2 and Fig. 1). The negatively stained TEM pictures of positively charged (3-aminopropyl)triethoxysilane thermally carbonized porous silicon (APTS-TCPSi) nanosystems reveal the presence of agglomerates also in the conditions deemed as the best in Table 1 (sucrose 0.3 M, with tip sonication before and after extrusion). The input of energy through tip sonication before the extrusion helps to keep the nanoparticles well suspended in the solution, but it may also introduce new breakage of the particles, exposing different types of surface. As for the sonication following the extrusion, this energy can help in preventing the vesicles from sticking to each other.

Table 1 Properties and preparation methods of the most widely used biohybrid nanosystems[a]

Type	Biological material	Synthetic material	Preparation	References
Cell ghosts	RBC WBC Cancer cells SC	Buffer Drugs pDNA	Homogenization/disruption of original cells Isolation of cell membranes by ultracentrifugation Extrusion/sonication to reform vesicles	[17–22]
Cell membrane-wrapped materials	RBC WBC SC Platelets Cancer cells	Polymeric NPs/nanogels Inorganic NPs Electrospun nanofibers	Homogenization/disruption of original cells Isolation of cell membranes by centrifugation Extrusion/sonication to coat the synthetic material with the membranes	[23–31]
Cellular carriers	RBC SC	Drugs Oncolytic viruses NPs	Direct uptake of NPs within the cells Infection of the cells with oncolytic viruses Conjugation of NPs on the surface of the cells	[32–35]
Adsorption/chemical binding	Biomacromolecules	Polymeric NPs Inorganic NPs	Functionalization of NPs with stealth peptides derived from CD47 Precoating with protein corona of precise composition	[36, 37]

[a] *Abbreviations*: *NPs* nanoparticles, *pDNA* plasmid DNA, *RBC* red blood cells, *SC* stem cell, *WBC* white blood cell

Table 2 Effect of nanocarriers surface charge (positive, APTS-TCPSi, or negative undecylenic acid modified thermally hydrocarbonized porous silicon (UnTHCPSi) and thermally carbonized porous silicon – TCPSi) and hydrophilicity (APTS-TCPSi, TCPSi)/hydrophobicity of the surface (UnTHCPSi)

PSi NPs	Buffers	Tip sonication	Size (nm)	PDI	ζ-potential (mV)	Effect
APTS-TCPSi	Sucrose 0.3 M	Before	Aggregated	n.d.[a]	+ 8.8 ± 1.3	–
		Before and after	304 ± 100	0.30 ± 0.04	−6.3 ± 1.1	++
	Milli-Q water	Before	334 ± 20	0.30 ± 0.049	+31.2 ± 0.5	+
		Before and after	Aggregated	n.d.	−5.7 ± 7.1	–
UnTHCPSi	Sucrose 0.3 M	Before	575 ± 200	0.50 ± 0.07	−21.2 ± 0.3	–
		Before and after	303 ± 200	0.15 ± 0.007	−23.7 ± 0.2	++
	Milli-Q water	Before	649 ± 300	0.24 ± 0.2	−15.1 ± 7.1	+
		Before and after	Aggregated	n.d.	−8.7 ± 0.9	–
TCPSi	Milli-Q water	No sonication	410 ± 180	0.5 ± 0.1	−20.6 ± 6.5	–
		After	Aggregated	n.d.	−19.8 ± 4.9	–
		Before	246 ± 100	0.180 ± 0.03	−22.1 ± 5.2	++
	Sucrose 0.3 M	Before	289 ± 100	0.3 ± 0.07	−23.0 ± 5.9	+

Reproduced with permission from Ref. [40]

[a] *n.d* not disclosed

Another important nanocarrier parameter to evaluate in the formulation of biohybrid cell membrane-coated nanocarriers is the hydrophilicity/hydrophobicity of the system, which will mainly influence the choice of a suitable buffer for the coating [40]. The type of cell membrane, at least considering cell membranes derived from different cancer cell lines, does not seem to influence the coating procedure.

In the case of cellular carriers, nanosystems can be either internalized by the cell or associated/bound with them. As for the internalization, the nanosystems are put into contact with the cells in well plates, left interacting for an appropriate time (different based on the type of particles and on the cells), before rinsing the cells with medium [33, 41]. The retention of the particles within the cells can be quantified in vitro by incubating the cells with fresh medium for different time points, before washing and analysis of the particle content by flow cytometry or more precise quantifications, like inductively coupled plasma-optical emission spectroscopy [33].

In case of association or binding of the nanocarriers on the external membrane, the properties of the particles are fundamental in determining the effectiveness of the attachment and the presence of any modification or toxic effect on the carrier cells [34, 42]. Moreover, the pre-adsorption of proteins (e.g., IgG or albumin) increases the association between commonly used nanocarriers and the RBCs [43]. Alternatively, gentle methods for covalent binding of nanocarriers on the cell membrane employ biotin-avidin reactions, but the authors do not provide any analysis of the toxicity on the carrier cells [44].

Finally, for the modification with biomacromolecules, common chemical reactions like 1-ethyl-3-(3-dimethylaminopropyl)-carbodiimide (EDC)-N-hydroxysuccinimide (NHS) or click chemistry can be useful in the functionalization of the particle surface with the desired molecule [36, 45]. Alternatively, in the case of pre-adsorption of specific protein corona, the particles are pre-incubated in a suitable medium [37].

Notwithstanding the composition and preparation methods of biohybrid materials in biomedical applications, all these systems share few fundamental characteristics that regulate bio-interfacing and its efficacy [46]. First, the presence of cell membranes, cells, or specific biomacromolecules on the surface of the materials provides a stealth coating [16, 47]. The intrinsic stealthiness of the biohybrid component facilitates the prolongation of circulation time in the bloodstream in the case of micro- and nanoparticles and also reduces the inflammatory response and the formation of a fibrotic capsule surrounding bigger implants [48–50]. The mechanisms underlying the prolonged circulation and the stealth effect rely on the presence of specific biomolecules (e.g., CD47) grafted or naturally present on the surface modification of the material, which act as “do-not-eat-me” signal. CD47, naturally found on the surface of cells (e.g., red blood cells, RBCs), interacts with different proteins (e.g., integrins) while having a role in the activation of dendritic cells (DCs) and T cells [51]. Most importantly, CD47 binds with the protein signal-regulatory protein α (SIRPα) expressed on the surface of macrophages, effectively preventing their phenotype shift to M1 proinflammatory and stopping the uptake [36]. CD47 modification has been employed also in combination with major histocompatibility complex (MHC) alloantigen and FS-7-associated surface antigen (FAS) to prevent the rejection in skin grafts [52]. The modification with CD47 preferentially inhibits the uptake by M1 macrophages, while the classical stealth coating of polyethylene glycol (PEG) prevents the uptake in all the populations of macrophages [53].

Secondly, by masking the surface of particles with biological molecules or backpacking them onto cells, the biodistribution of the systems is altered [54, 55]. In particular, the association of particles with macrophages or the coating with leukocyte or neutrophil cell membrane can effectively transport them to the site of inflammation, be it a tumor, an inflamed articulation, or injured blood vessels [29, 56–58].

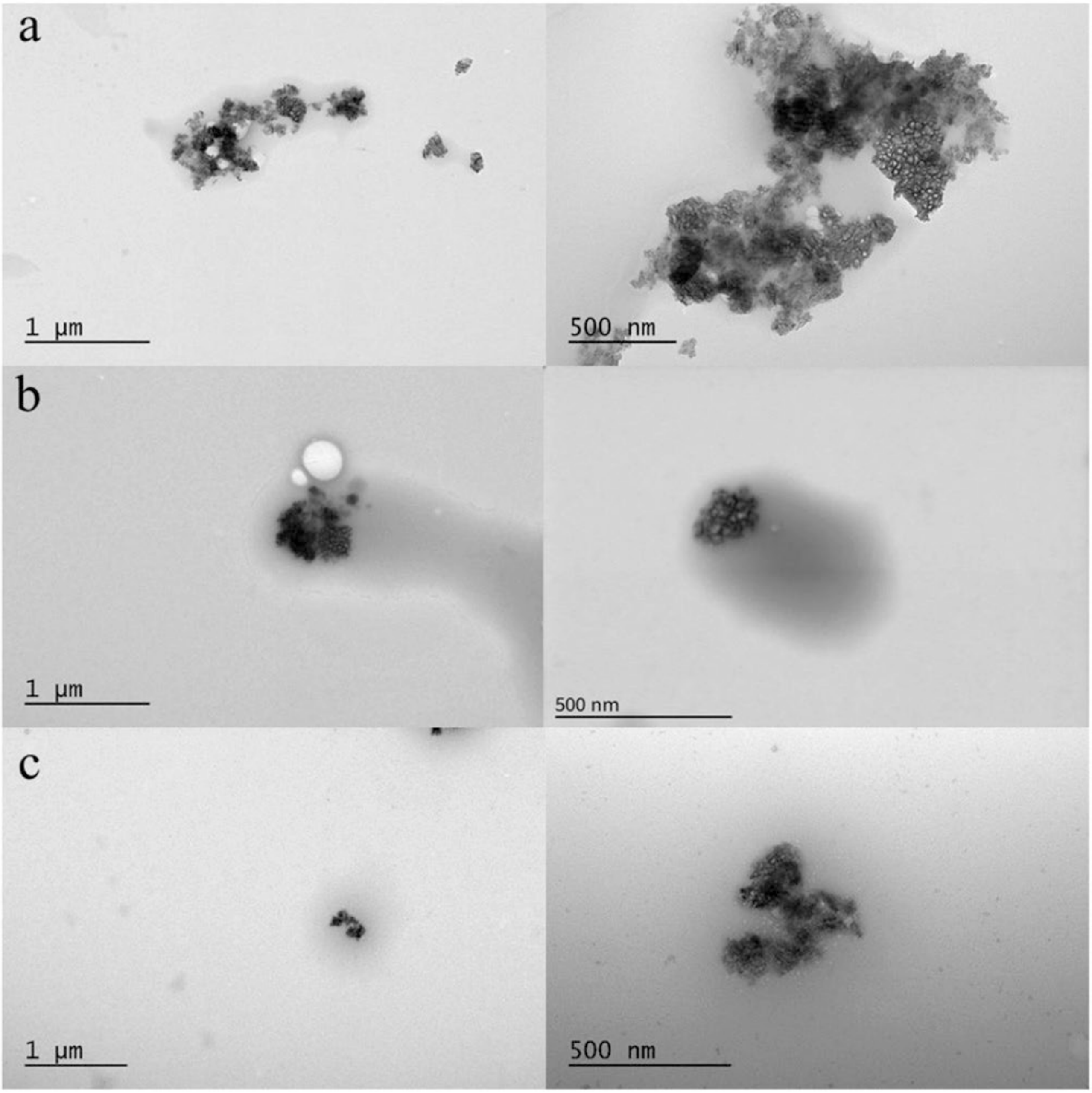

Fig. 1 Negatively stained TEM pictures evaluating the coating with cell membrane in (**a**) positively charged, hydrophilic, APTS-TCPSi; (**b**) negatively charged, hydrophobic, UnTHCPSi; (**c**) negatively charged and hydrophilic TCPSi nanocarriers. (Reproduced with permission from Ref. [40])

Finally, for nano-ghosts and cell membrane coating, the top-down production process allows for the development of reproducible and cost-effective extraction and formulation methods when compared to the always increasing complexity in the bottom-up systems [20, 46].

In this chapter, we will focus on the applications of biohybrid materials in cancer, presenting how this technology has been developed during the last years to achieve homotopic targeting therapies combined with stealthiness to enhance drug delivery, or the role of cancer cell membrane as antigenic source in the development of cancer vaccines.

3 Applications of Biohybrids in Cancer Therapy

3.1 Cancer Therapy

The term “cancer” defines a heterogeneous group of diseases all presenting several hallmarks of uncontrolled proliferation [59–61]. The conventional treatment of cancer is based on surgery, radiotherapy, chemotherapy, hormone therapy, and targeted therapy [62]. However these treatment modalities are plagued by excessive and unspecific toxicity, or by the presence or acceleration of a drug-resistant clonal selection, leading to non-effective treatment [63]. Some of these downsides can be ameliorated by differently formulating the drug molecules to reduce the systemic toxicity and retard the insurgence of drug-resisting clones. The progress in nanotechnology, with the development of micro- and nanosystems, brought along few marketed products whose main feature is the decrease in systemic side effects [64, 65].

Micro- and nanoparticles display a range of advantages over conventional formulations [66]. In particular, loading a compound within a nanosystem results in controlled biodistribution and enhancement in the efficacy or reduction in the toxicity of the compound [67]. These advantageous characteristics are partially provided from the encapsulation of drugs, leading to a control over their release, as well as to increased solubility for poorly water-soluble compounds (e.g., sorafenib represents one of the most famous examples) [68–70]. Moreover, the passive biodistribution of drugs is influenced by the size of NPs and by the systemic conditions of the patient [71]. Indeed, the biodistribution is altered in presence of different diseases (e.g., cardiac ischemia [72], cancer [73], diabetes [74], and obesity [75, 76]) or different patients' ages [77]. Often, disease-specific alteration in the blood circulation (like the enhanced permeation and retention (EPR) effect in cancer and the extravasation through leaky vasculature and subsequent inflammatory cell-mediated sequestration in rheumatology) has been investigated to increase the accumulation of nanotherapeutics in the site of interest [78–80].

Passive targeting of NPs relies on the characteristics of the NPs (size, surface) and the pathophysiological characteristics of the blood vessels to enable the accumulation in the tissue of interest without the presence of any active targeting moiety [81]. One key feature to enable the passive targeting is to provide the nanosystem with the highest level of stealthiness achievable, in order to reduce its interactions with the complement system and with the reticuloendothelial system (RES), increasing its chance to extravasate in the site of interest [81]. The gold standard is represented by the functionalization of the particle surface with hydrophilic polymers, whose function is to create a hydration layer surrounding the NPs, decreasing the interactions with the RES [81]. The most famous example of these polymers is polyethylene glycol (PEG) [82, 83]. Yet, as reported both in clinics and preclinical studies, the recurrent administration of therapeutics decorated with PEG is impaired by the development of anti-PEG antibodies [84]. The widespread use of PEG in different products (e.g., cosmetics) has increased the number of patients presenting a pre-existing immunity to PEG [85]. In practical terms, patients eligible for treatment with PEGylated nanoformulations can have immunoglobulins (Ig) G and M already circulating in the bloodstream. The presence of antibodies against PEG determines a faster clearance of the nanoformulation, causing lower efficacy of the drug [84]. Alternative polymers, like hyaluronic acid or gangliosides, are currently being evaluated as alternative stealth moieties, as well as modifications in the therapeutic schedule [84]. Researchers could take inspiration from the oncolytic virus' field [86, 87], where the problem of neutralizing antibodies has been extensively evaluated in the last years, with possible solutions proposed [88].

Alternatively, the tissue or cell of interest can be actively targeted by functionalizing the surface of the nanosystems with targeting moieties (e.g., peptides, antibodies, aptamers, and sugars) towards receptors expressed in the tissue or cell of interest [89]. The three main functions of active targeting moieties are specific homing, augmenting the retention at the tumor site, and direct involvement in the uptake by target cells [90]. Concerning the homing peptides, these "vascular zip codes" are usually discovered by phage screening and identify peptides suitable for the homing to the vasculature in specific body areas or districts [91]. Such peptides, whose most famous example is RGD, bind to the receptor overexpressed in the tumor vasculature and, if they obey to CendR rule, they mediate the activation of an endocytic/exocytic transport to allow migration from the vessel within the tumor tissue [91]. As for moieties increasing the retention at the tumor site, NPs usually get entrapped within the ECM matrix, close to the extravasation site; instead RGD and similar peptides are useful in increasing the retention in the tumor area [62]. Finally, intracellular delivery of the payload is needed for drugs whose mode of action relies on intracellular delivery (e.g., small interfering RNA, siRNA). To improve the intracellular delivery, active targeting [81] can be employed to provide targeting moieties to a single cancer cell [62]. Targeting moieties frequently described for cancer cell targeting and intracellular delivery include trans-activating transcriptional activator (TAT) peptides, transferrin followed by octaarginine, etc. [92, 93]

However, despite 20+ years of active research in cancer nanomedicine, the proof of concept of a "magic bullet" able to target and kill the cancer cells is still missing. A recent meta-analysis of the preclinical studies and the results of several clinical trials phases II and III have questioned the effectiveness and utility of the currently developed nanomedicines in the treatment of cancer [94, 95], prompting the research for alternative strategies.

Biohybrid systems are currently regarded as a potential solution to improve the clinical efficacy of nanosystems, reducing at the same time the degree of complexity needed for the production of a complex, actively targeted system. In the next section, we will present the applications of biohybrid systems in cancer therapy for the delivery of chemotherapeutics and their combination with other therapies, including photodynamic (PDT) and photothermal therapy (PTT).

3.2 Biohybrid Nanoparticles for Cancer Therapy

The paradigm of a successful cancer therapy requires an effective concentration of drug in the tumor site while lowering as much as possible the systemic side effects. Nanotechnology in general has already contributed to a reduction or change in the side effects while enabling also an increase in the dose administered [62].

The development of biohybrid nanosystems brought along two important contributions towards successful cancer therapy. In particular, particles hitchhiking cells or particles covered with cell membrane show prolonged circulation time when compared with conventional NPs [49, 96]. Moreover, when the particles or viruses are attached or taken up by mesenchymal stem cells, antigen-specific T cells, and macrophages, the fraction delivered to the tumor increased [54, 97]. A similar increase in the NP fraction, and consequently drug, delivered to the tumor was observed for biohybrid NPs coated with membranes derived from homologous tumors or from stem cells, or for nano-ghosts derived from stem cells [30, 98–100]. Therefore, biohybrid nanosystems have been heavily investigated as drug carriers and for combined therapies in cancer treatment.

3.2.1 Biohybrid Systems as Chemotherapeutic Carriers

As a general rule, an optimal nanocarrier for cancer applications has a high drug loading degree, can circulate in the bloodstream for long time, and can specifically target the tumor tissue. Currently, no nanocarrier has all three desirable characteristics. However, biohybrid nanosystems can provide optimal circulation times and homotopic tumor targeting. Next, we will present selected examples of NPs based on the source of the biomaterial and specifically on the cell type. A summary of further examples can be found in Table 3.

Red Blood Cells (RBCs)

When NPs are adsorbed on the membrane or RBCs, they will accumulate in the first organ downstream for the injection point [43]. In practical terms this means that after intravenous administration, the RBCs will go through the lungs, where they will deposit their payload [43]. The enhanced organ targeting to the lungs has been employed for the delivery of doxorubicin (DOX) to established lung metastases (Fig. 2) [96].

The platform developed in the study by Zhao et al. is composed of spherical, positively charged poly(lactic-co-glycolic acid) NPs loaded with DOX, presenting an average size diameter of 136.0 nm [96]. The association with the RBC was carefully optimized in the ratio of NPs/erythrocyte with the ratio 200:1 resulting in 81.6% association, increasable to more than 96% by prolonging the incubation time between the particles and murine RBC. In the case of human RBCs, the association efficiency is lower (between 38.7% and 45.7%). Most importantly, the association of the particles did not induce any morphological change in the RBCs. The proposed mode of action of the system relies on the narrowing of the capillaries in the lungs to increase the shear stress experienced by the particles, which will then detach and deposit in the lungs. This mechanism was proven in vitro, and the administration of the RBC doped with NPs increased the accumulation of the NPs in the lungs, controlling the progression of lung metastasis and prolonging the overall survival of mice in early and late stages of B16F10 Luc model [96]. Finally, the authors evaluated the possibility to extend this system to other chemotherapeutics, demonstrating an efficient binding for NPs loading, among others, camptothecin, paclitaxel, and docetaxel [96].

The use of RBC is quite convenient since the cell source is widely available in the blood banks and will be tailored to the patient based on the blood type. However, the effect of the adsorption of NPs on the RBC has to be carefully evaluated. As reported by Pan et al., by changing the particle type while keeping the concentration constant, polystyrene NPs induced agglutination of the RBC, together with osmotic, mechanical, and oxidative stress. In particular, the adsorption of polystyrene NPs induced changes in the RBC (different stiffness and exposure of phosphatidylserine on the surface) typical of a RBC undergoing apoptosis and thereby rapidly cleared from the circulation. At the same time, lysozyme-dextran nanogel did not show any effect on RBCs [34]. Further studies are needed to optimize the type of particle, type of surface, and size for an optimal adsorption on RBC to prolong the circulation time.

The use of RBC cell membrane to wrap NPs was first proposed in 2013 by Hu et al. as stealth modification preserving the membrane CD47 density as the parent cell [101]. This type of particle coating inhibits the uptake by macrophages and can actively prolong the circulation time of poly(lactic-co-glycolic acid) (PLGA) NPs up to almost 40 h, when a control coated with PEG extends the circulation only up to 16 h [102]. These biohybrid particles can be easily loaded with chemotherapeutics like DOX and paclitaxel (PTX) [103–105]. Moreover, it is possible to modify the membranes with bifunctional linkers, such as succinimidyl-[(N-maleimidopropionamido)-PEG] ester (NHS-PEG-maleimide), to introduce other functions to the RBC, as functional enzymes to disrupt the tumor microenvironment, allowing for a deeper tumor penetration of the nanosystems (Fig. 3) [106]. In this case, human recombinant hyaluronidase was bound to red blood cell membrane via a bi-reactive PEG linker. The linker was attached to the membrane of RBC by EDC/NHS reaction, while the enzyme was success-

Table 3 Examples of biohybrid systems in cancer chemo and combined therapy

Cell type	Material	Type of final formulation	Outcome	Application	Ref
RBC	Screening of 100 nm DOX-loaded particles made of different polymers	RBC as cell carrier of NPs	Increased delivery of NPs to lung metastases after retro-orbital injection in mice	Treatment of melanoma metastasis in the lungs	[134]
	Poly (lactic acid) (PLA) NPs; <100 nm; DOX loaded or chemically conjugated	RBC cell membrane as coating to increase the blood circulation time	Long-term stability of the particles, increased cytotoxicity of DOX in vitro	IV administration of DOX	[103]
	Methoxy poly(ethylene glycol)-*block*-poly (D,L-lactide) NPs loaded with PTX dimer and 5,10,15,20-tetraphenylchlorin for combined photodynamic therapy/ chemotherapy	RBC membranes as outer shell to prolong the blood circulation	Increased therapeutic efficacy in HeLa xenografts	IV administration of PTX chemotherapy combined with photodynamic therapy	[104]
	PTX-loaded polymeric NP, 1,1-dioctadecyl-3,3,3,3-tetramethylindotricarbocyanine iodide inserted into the membrane of the RBC shells for combined photothermal therapy/chemotherapy	RBC membranes as outer shell to prolong the blood circulation	Laser-dependent accumulation at the tumor site. Increased control over tumor growth in 4T1 breast cancer model	IV delivery of a combined photothermal/ chemotherapy	[105]
	Melanin NPs from living cuttlefish; 128 ± 22 nm	RBC membranes as outer shell to prolong the blood circulation	Increased tumor accumulation after 4 h, possibility to image the tumor with ultrasound, control over the tumor growth in A549 lung cancer model	Photoacoustic imaging and PTT of the tumor	[25]
	Iron oxide magnetic nanoclusters; 134 ± 16 nm	RBC membranes as outer shell to prolong the blood circulation	Increased passive tumor accumulation; MRI tumor imaging; control in tumor growth and tumor eradication in MCF breast cancer model by combination of NIR laser and magnetic field	MR imaging of tumor and PTT	[135]
Cancer cells	PLGA NPs; 110 nm	B16.F10 melanoma cancer cell membrane for homotypic targeting and as antigen source MDA-MB-435 cell membrane used for the homotypic targeting assay	First example of biohybrid NPs coated with cancer cell membrane; in vitro proof of concept of homotypic targeting and potential as cancer vaccine	IV homotypic tumor targeting and cancer vaccine	[24]
	PLGA NPs; 79.8 nm	U87 and U87-CXCR4 cancer cells with high and low expression levels of CXCR4	Inhibition of cancer cell migration towards fibroblasts in vitro; reduction in the formation of metastasis in vivo; active vaccination with priming of CD4 and CD8 T cells	Prevention of metastasis formation and cancer vaccine	[136]
	Iron oxide magnetic NPs; DOX loaded; 295 ± 2.8 nm in dextran solution	Human squamous carcinoma cells; HeLa cells; COS-7 cells	Homotypic targeting proven in vitro over three other cell lines and in vivo in two different tumors; control over tumor growth for homotypic tumors with increase in apoptotic cancer cells	Homotypic targeting, MR imaging, chemotherapy	[107]

(continued)

Table 3 (continued)

Cell type	Material	Type of final formulation	Outcome	Application	Ref
	Poly(caprolactone)-pluronic F68 NPs; PTX loaded; ≈ 150 nm	4T1 breast cancer model	Homotypic targeting towards 4T1 demonstrated in vitro and in vivo; high efficacy in controlling tumor growth up to 22 days while avoiding the formation of any metastatic nodule in the lungs	IV injection; homotypic tumor targeting; chemotherapy	[137]
	DOX-loaded gold nanocages	4T1 cells	Almost complete inhibition of tumor growth and metastasis formation	IV injection of combined chemo/photothermal therapy	[98]
	Indocyanine green-loaded PLGA NPs; 197.3 nm	MCF-7 cancer cells; PEGylated	Complete tumor eradication without any relapse in the animals after 18 days	IV administration of PTT active agent with homotypic tumor targeting	[138]
	DOX-indocyanine green NPs; 100 nm	HeLa cells	Control over tumor growth up to 18 days following NIR irradiation and PTT-induced drug release	IV injection of combined chemotherapy/PTT	[139]
	DOX and PD-L1 siRNA-loaded PLGA NPs; 70 nm	HeLa cells	In vitro proof of concept of homotypic targeting	Combined chemo and immunotherapy	[140]
	Mesoporous silica NPs loaded with glucose oxidase	B16.F10 cells	The combination of starvation therapy and checkpoint inhibitors can control tumor growth more efficiently than each of the single treatments	Combined starvation and immunotherapy with immune checkpoint inhibitors	[141]
Stem cell	DOX-loaded PLGA NPs; 150.3 ± 2.7 nm	Mesenchymal stem cells as cell vehicle	Fast uptake in stem cells (1 h); tumor tropism in vitro in different models (including 3D spheroids); tumor tropism to metastasis in 3 h in vivo, determining a decrease in the number of metastatic nodules in the lungs	IV administration of NPs-loaded stem cells for tumor-targeted chemotherapy	[142]
	PTX-loaded PLGA NPs	Mesenchymal stem cells as carrier	Uptake of NPs in stem cells within 4 h; control over the tumor growth of a lung model with approx. 10 times less dose of drug administered	IV administration of NPs-loaded stem cells for chemotherapy	[143]
	PTX-loaded PLGA NPs; 126.3 ± 1.2 nm	Mesenchymal stem cells as carriers	Successful contralateral migration towards the tumor upon injection in the opposite brain hemisphere in vivo, prolonging the mean survival time to 35.5 days	Intracranial administration of stem cells to mediate targeted delivery of chemotherapeutic to gliomas	[144]
	Curcumin-loaded chitosan NPs; 652 ± 10 nm	TRAIL-expressing mesenchymal stem cells	Inhibition of tumor growth in 4T1 breast cancer model; increase in the fraction of apoptotic cells in vitro	Peritumoral injection of stem cells with a combined chemo- and immunotherapy	[145]
	TAT-functionalized, PTX-loaded, PLGA NPs; 225 ± 7 nm	Mesenchymal stem cells as cellular carrier	TAT functionalization increases NPs loading within the cells: Inhibition of tumor growth and prolonged survival in orthotopic model of lung cancer	IV administration of stem cells for targeted tumor chemotherapy	[146]
	Soluble form of TRAIL ligand	Nano-ghosts derived from mesenchymal stem cells; 180 nm	In vitro selective targeting to prostate cancer cells; in vivo safe targeting to the tumor, with improved control over tumor growth	IP injection of tumor-targeting chemotherapeutic	[17]

(continued)

Table 3 (continued)

Cell type	Material	Type of final formulation	Outcome	Application	Ref
	Negatively charged pDNA coding for C-terminal fragment of human matrix metalloprotease-2	Nano-ghosts derived from mesenchymal stem cells; 204 nm	Short-term safe therapy; in vivo efficacy in subcutaneous prostate cancer model and in orthotopic metastatic lung cancer model	IV injection of non-viral vectors for cancer therapy	[19]
	DOX-loaded gelatin nanogels; 140 nm	Mesenchymal stem cell membrane as outer wrapping	In vivo selective tumor targeting and improved efficacy in subcutaneous HeLa tumors	IV administration of tumor-targeting chemotherapeutics	[30]
	Gold NPs, pH-sensitive; 10 nm nanospheres	Mesenchymal stem cells	Accumulation of aggregated gold NPs in stem cells' endosomes; increased tumor targeting resulting in increased PTT effect with increased tumor temperature and antitumor efficacy	Cellular tumor-targeted delivery of gold nanoparticles for PTT	[115]
	Gold NPs coated with alpha-synuclein; 30.2 nm and 19.3 nm; graphene oxide flakes coated with gold NPs	Mesenchymal stem cells	Increased control over tumor growth in HT-1080 human fibrosarcoma subcutaneous model	IV administration of stem cells as carriers for PTT	[116]
	Iron oxide NPs loaded with siRNA against Plk1 gene	Mesenchymal stem cell membrane	Increased tumor accumulation in subcutaneous DU145 xenografts with improved anticancer efficacy	IV injection of a multimodal system for the delivery of siRNA, MR imaging, and PTT	[117]
Immune cells	MFG-LacZ retroviral particles	Antigen-specific T cells	Adsorption of the viral vectors on the T cells; hand-off in the proximity of malignant cells and enhanced by T-cell activation; prolonged overall survival	IV administration of antigen-specific T cells for tumor delivery of viral vectors. Cancer immunotherapy	[147]
	Nanoporous silicon microparticles	Leukocyte cell membranes	In vitro reduced interaction and uptake from cells of the RES; in vivo tumor targeting with lower liver clearance	IV injection of tumor-targeting RES-cloaking microparticles for chemotherapy	[27]
	DOX-loaded mesoporous silica nanocapsules; 47.8 nm	Macrophage cell membrane	Prolonged circulation associated with increased antitumor efficacy in 4T1 breast cancer model	IV injection of tumor-targeting, RES-cloaking NPs for chemotherapy	[148]
	Upconversion NPs; ≈ 80 nm	Macrophage cell membrane	Prolonged stability up to 15 days; increased blood retention time together with tumor accumulation and precise tumor imaging	IV administration of upconversion NPs for imaging purposes	[149]
	Emtansine-loaded liposomes; 64.5 nm	Macrophage cell membrane	Increased targeting to 4T1 metastatic tumor model (lung metastasis); decreased number of metastasis, with a 87.1% inhibition rate	IV administration of tumor-targeting chemotherapy	[122]
	Celasterol-loaded PEG-PLGA NPs; 142.7 ± 2.8 nm	Neutrophil cell membrane	Increased tumor accumulation in GFP-PAnc02 model. Doubled overall survival compared to the free drug	IV injection of pancreas-targeting NPs for chemotherapy	[123]
	Carfilzomib-loaded PLGA NPs; 75.2 ± 5.3 nm	Neutrophil cell membrane	Increased association with cancer cells under shear flow in vitro; depletion of circulating tumor cells and control over the progression of metastasis already formed	IV administration of chemotherapy to prevent and treat lung metastasis in breast cancer models	[124]

(continued)

Table 3 (continued)

Cell type	Material	Type of final formulation	Outcome	Application	Ref
	DOX-loaded liposomes; 121 ± 2 nm hydrated	NK cell membranes	NK receptors-mediated recognition and uptake in cancer cells; increased efficacy against MCF-7 breast cancer xenograft model	IV administration of biomimetic systems for enhanced tumor accumulation and chemotherapy	[125]
	Magnetic iron oxide NPs; ≈ 80 nm	Macrophage cell membrane	Safe nanosystems with cancer-specific targeting and improved anticancer efficacy after PTT treatment	IV administration of stealth nanosystems with enhanced tumor accumulation for PTT	[126]
	Janus polyelectrolyte multilayer microcapsules; silica coated with gold	Leukocyte cell membrane	Mechanism-based study on how the capsules can kill cancer cells also after uptake and the mechanism governing the PTT effect	In vitro proof of concept of PTT mechanism	[127]
	Iron oxide NPs; ≈ 80 nm	Myeloid-derived suppressor cell membranes	Increased tumor targeting compared to RBC-coated NPs; MRI of the tumor and enhanced PTT	IV administration of combined MRI and PTT NPs	[128]
	4,4′,4″,4″′-(porphine-5,10,15,20-tetrayl) tetrakis (benzoic acid)-loaded mPEG-PLGA NPs; 80 ± 1.5 nm	NK cell membrane	Complete eradications of the primary tumors and control over the growth of the distal tumors	PDT with abscopal effect to induce immunogenic cell death, macrophage repolarization, and activation of the immune system	[150]
	NIR dye-loaded and gadolinium-conjugated PLGA NPs; 190 ± 2.8 nm	NK cell membrane	Prolonged circulation time and increased tumor accumulation. Possibility of in vivo NIR fluorescent imaging and ex vivo MRI	IV administration of dual imaging NP probe	[151]
	PTX-loaded PLGA NPs; 165.9 ± 1.0 nm	Cytotoxic T-cell membranes	Enhanced accumulation after low-dose irradiation through chemoattraction; tumor growth inhibition in the 88% of the animals with two complete remissions in gastric cancer model	Combined low-dose irradiation with chemotherapy	[129]
	IR780-loaded mesoporous silica NPs; 105 nm	Chimeric antigen receptor T-cell membrane recognizing GPC3$^+$ cancer cells	Specific tumor targeting both in vitro and in vivo; control over tumor growth and tumor imaging	Multimodal platform for the precise targeting, PTT, and imaging for hepatocellular carcinoma	[152]
Others	Magnetic beads (magnetic NPs); 100 nm	Platelet-leukocyte hybrid cell membrane with a conjugate anti-EpCAM antibody	Increased sensitivity in the isolation in complex samples (full blood) compared to commercial immunomagnetic beads	Immunomagnetic beads for the ex vivo detection and isolation of circulating tumor cells	[130]
	Melanin NPs; 64 nm	RBC-cancer cell (MCF-7) hybrid membrane	Prolonged blood circulation time compared to particles coated only with cancer cell membrane; improved tumor targeting and accumulation compared to RBC membrane-coated particles; possibility of imaging through photoacoustic signal	IV administration of NPs for PTT	[153]

(continued)

Table 3 (continued)

Cell type	Material	Type of final formulation	Outcome	Application	Ref
	DOX-loaded hollow copper sulfide NPs; 190 nm	RBC cancer cell (B16.F10) hybrid membranes	Prolonged circulation together with homotypic targeting. Complete control over melanoma with remissions	IV injection of combined chemo and PTT	[154]
	Iron oxide NPs; 80 nm	Cancer stem cell platelet-hybrid membranes	Prolonged circulation and tumor-targeting ability; enhanced PTT in immunocompetent mice	IV administration of PTT in head and neck squamous cell carcinoma	[155]
	Polypyrrole NPs	RBC-platelet hybrid membranes	Prolonged circulation and targeting provided by platelets upon induction of microthrombosis in the tumor tissue	IV administration of PTT	[132]

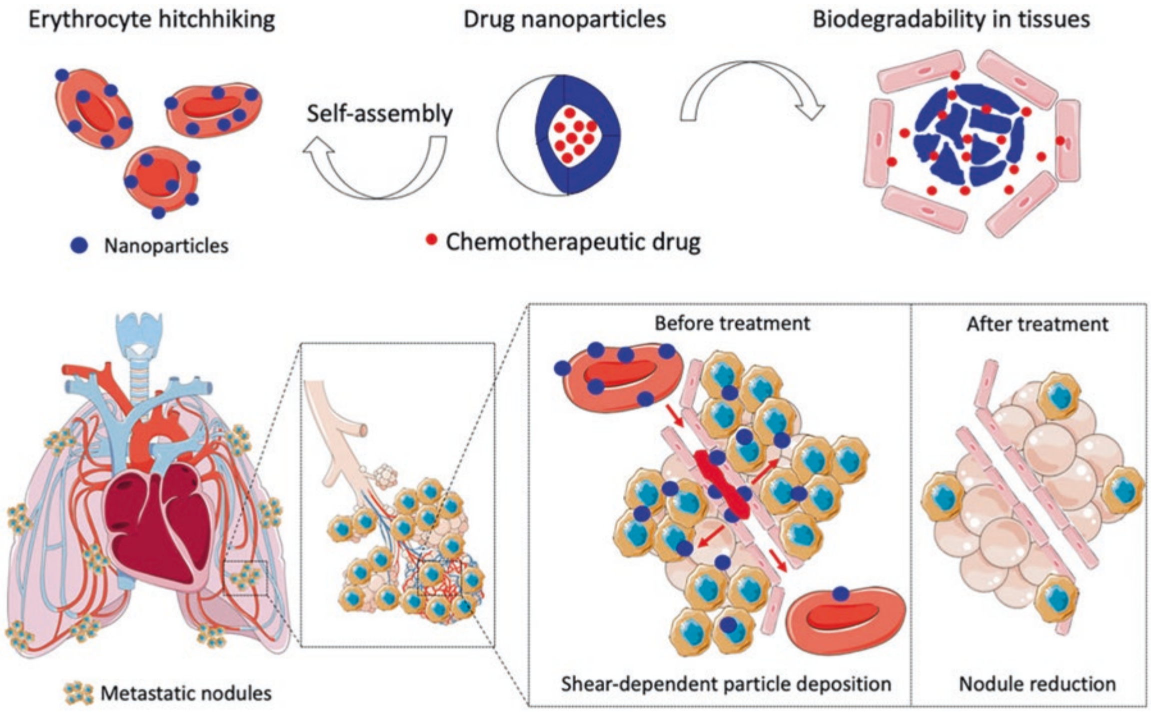

Fig. 2 Schematic illustration of NPs hitchhiking RBC for delivery to lung metastases. Biocompatible and biodegradable drug-loaded NPs are adsorbed on the surface of RBCs. Upon intravenous injection, RBCs pass through the lungs; there they deposit the NPs due to changes in the shear force. The increase in the fraction of NPs available at the tumor site leads to a reduction in the number of metastatic nodules. (Reproduced with permission from Ref. [96] ©2019, The authors)

fully attached to the linker by reaction between thiol groups on the enzyme of interest and maleimide on the linker. Different lengths of the spacer were evaluated, and the longer one (MW: 3400) can retain the enzyme activity better than the shorter ones. The presence of the recombinant extracellular matrix-degrading enzyme can facilitate the diffusion of the particles in in vitro models of matrix-mimicking gels and PC3 prostate cancer extracellular matrix while retaining prolonged circulation time in vivo [106].

Combined Therapy

RBC cell membranes can provide stealth coating to different types of NPs with PTT or PTD properties (melanin NPs, magnetic clusters of iron oxide, near-infrared dyes, photosensitizers like 5,10,15,20-tetraphenylchlorin), altering their biodistribution in favor of a passive tumor accumulation. The enhanced accumulation results in enhanced antitumoral efficacy of the various bare nanosystems.

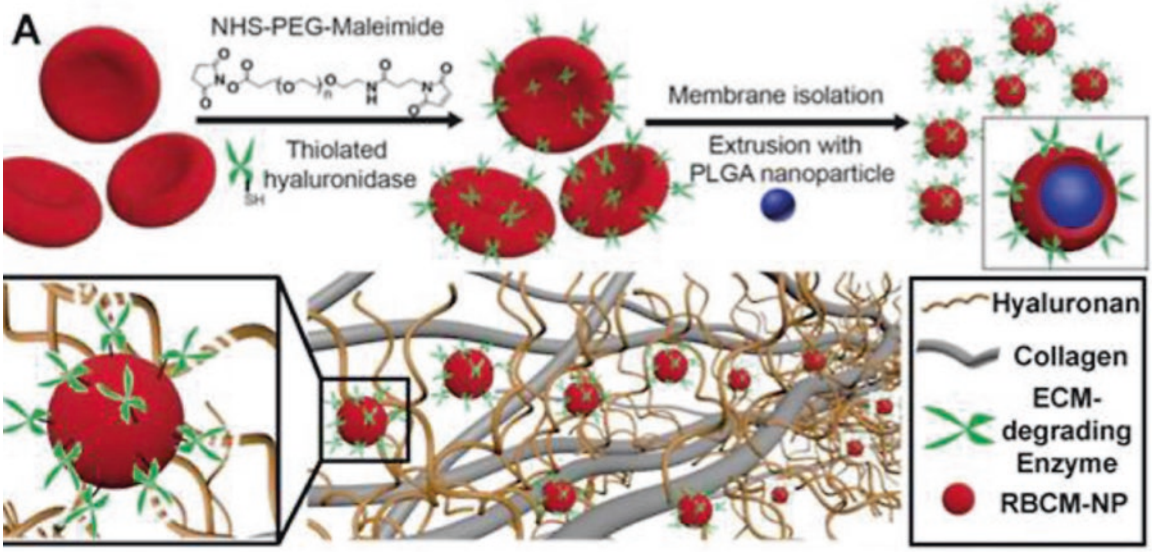

Fig. 3 Schematic illustration of modification of RBC cell membrane with NHS-PEG-maleimide and hyaluronidase. RBCs were modified with a linker, followed by the reaction to attach the hyaluronidase enzyme to the membrane. Biohybrid NPs decorated with hyaluronidase can cut through the hyaluronan in the cell matrix, reaching deeper within the tumor tissue. (Reproduced with permission from Ref. [106], under a Creative Commons License 4.0)

Cancer Cells

The use of cancer cells is limited to the extraction of their membranes or nano-ghosts with the primary aim of achieving tumor-specific targeting. In particular, the use of cell membrane as wrapping moiety was first described by Fang et al. in 2014, highlighting the potential applications as source of antigens for vaccines and for drug delivery [24]. The self-targeting properties of cancer cell membrane-coated particles were proved by Zhu et al., preparing two different sets of DOX-loaded magnetic cell membrane-coated particles, different in the source of the cells used [107]. These particles selectively accumulated in the homologous tumor in vivo. Finally, the tumor self-targeting was demonstrated also in patient-derived xenograft with cisplatinum-loaded NPs [99]. In this study, the authors compared the tumor accumulation of bare gelatin NPs, RBC-coated NPs, or homologous xenograft cells NPs: the normalized accumulation of cancer cell membrane-coated particles was more than double of the RBC-NPs ones. Furthermore, xenografts derived from different patients displayed different membrane signatures, meaning that a selective homotypic tumor accumulation was observed when comparing accumulation in two different patient xenografts [99]. However, some differences in the ability to effectively deliver cisplatin chemotherapy and in its efficacy are present among the different xenografts.

Combination

The exquisite homotypic targeting provided by the presence of cancer cell membrane contributes to an increase in the efficacy of combined therapy with PTT and PDT or the implementation of a theranostic platform for imaging. Furthermore, it is possible to induce starvation in cancer by developing a cascade bioreactor based on glucose oxidase and catalase; the enzymes are loaded within a porphyrin metal-organic framework that is sensitive to NIR irradiation, resulting in PDT (Fig. 4) [108].

The rationale behind the work is to combine the biomimetic properties and homotypic targeting provided by the cancer cell membrane (4T1 cancer cells) with a photodynamic core of metallic organic framework and starvation therapy mediated by the presence of two enzymes, glucose oxidase and catalase. A NIR laser is shone over the tumor, activating the metallic organic frameworks and resulting in the production of ROS, while the two enzymes consume the available glucose, determining the starvation of the cells [108]. This system effectively contributed to a control over the tumor growth.

Stem Cells

Stem cells are highly migratory and are attracted by inflamed areas, like tumors or sites of cardiovascular diseases, migrating selectively towards the tumor site [109, 110]. Owing to tumor-specific targeting properties, stem cells, and in particular mesenchymal stem cells (MSC), have been loaded with NPs, oncolytic viruses, and drugs and modified to add further targeting moieities [111, 112].

However, the use of MSC in the clinics is complicated by their potential to increase the metastatic ability of tumors [113]. This mechanism is primarily due to the secretion of different factors from the MSC; thereby, the development of MSC nano-ghosts, where the cytoplasmic material is

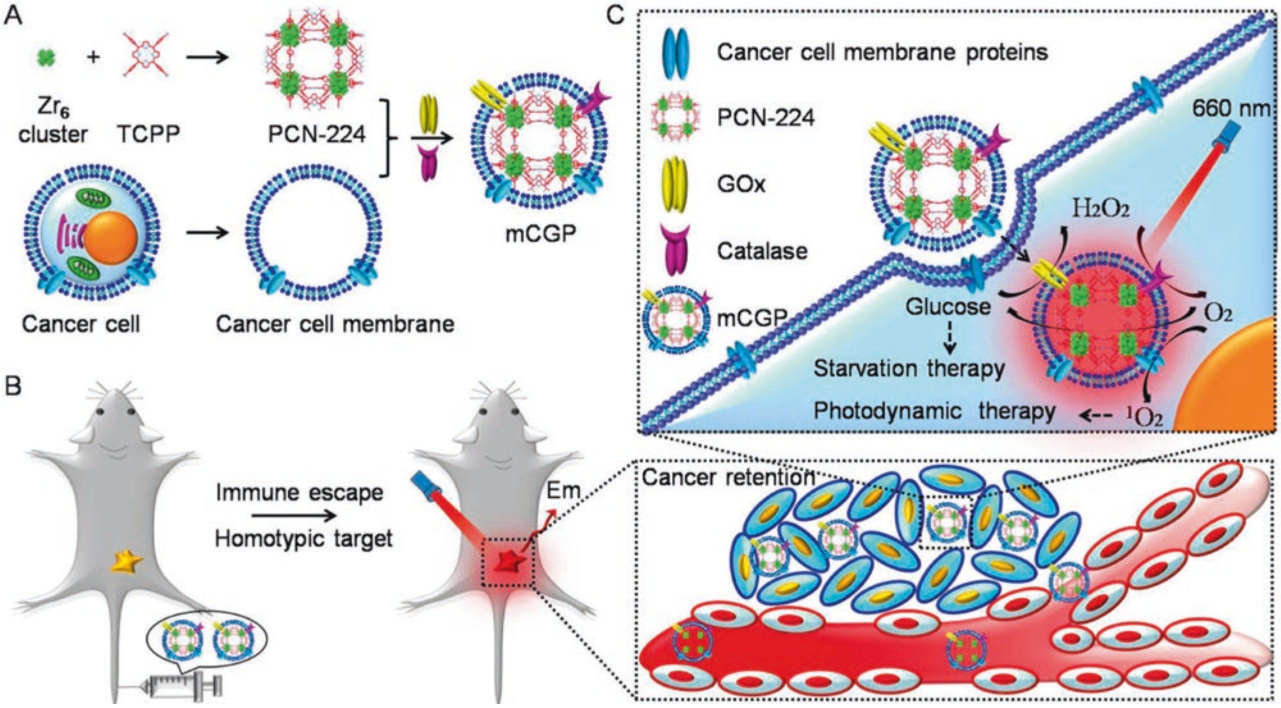

Fig. 4 Schematic illustration of the combined starvation/PDT wrapped with cancer cell membrane. (**a**) Preparation of the nanosystem by combining the photosensitive particles with cancer cell membranes. Glucose oxidase and catalase are then added to the systems. (**b**) Upon intravenous injection, and due to the homotypic targeting provided by the cancer cell membrane, the NPs are accumulating in the tumor site. (**c**) Then, upon uptake of the NPs by the cancer cells, the two enzymes will consume glucose, determining a starvation status in the cancer cells. At the same time, a NIR laser will be shone onto the tumor, interacting with the NP's core and determining the production of reactive oxygen species. (Reproduced with permission from Ref. [108] © 2017, American Chemical Society)

removed from the cells, is currently pursued, as well as the loading of nano-ghosts with antagonists of selected receptors involved in the cross-talk between MSC and cancer cells [114]. The targeting ability of the nano-ghosts can be tailored by changing the culture conditions of the parent MSC. Nano-ghosts derived from MSC cultured in presence of cancer media display higher targeting towards immune cells, while nano-ghosts derived from MSC cultured with proinflammatory cytokines achieve the highest tumor targeting [100].

Combination

The tumor-targeting properties of stem cells and stem cell membranes have been exploited for the loading of different cargos (gold NPs, iron oxide NPs) to enhance their tumor accumulation, improving the PTT efficacy, or providing multimodal systems for delivery of therapeutic cargo, imaging, and PTT [115–117].

Immune Cells

The immune system plays a complex role in its interactions with cancer, as presented in Sect. 3.1. Importantly, immune cells are recruited in the tumor microenvironment [118]. T cells or DCs have been initially proposed as cell therapy, with one treatment successfully in the clinic as cancer vaccine [119]. The costs deriving from the manipulation of cells and the type of facilities needed have sprung the research into alternative biohybrid materials, conserving the features of immune cells. The first examples used membrane derived from leukocytes to create leukolike vectors able to prolong the circulation and extravasate in inflamed areas, accumulating within B16 melanoma tumors [27]. The leukocyte membrane promotes the activation of intercellular adhesion molecule 1 (ICAM) on the endothelial cells, which leads to enhanced vascular permeability, adhesion to the tumor vasculature, and enhanced tumor perfusion (Fig. 5) [120].

Alternatively, membranes derived from macrophages have been investigated for the preferential targeting to inflamed sites, including tumors, for the delivery of chemotherapeutics. The highly effective targeting was combined to a sequentially controlled drug release of PTX from nanogels in the tumor microenvironment and tumor cell responding to the different stimuli in the tumor microenvironment (Fig. 6) [121]. In particular, the macrophage membrane coating allows the NPs to escape the RES while efficiently targeting the tumor site. Upon extravasation, with the lowering of the physiological pH typical of the tumor microenvironment, the poly β-amino esters forming the nanoparticles, modified with 2-aminoethyldiisopropyl groups to tune the pH, expand via proton sponge effect, breaking apart the cell membrane

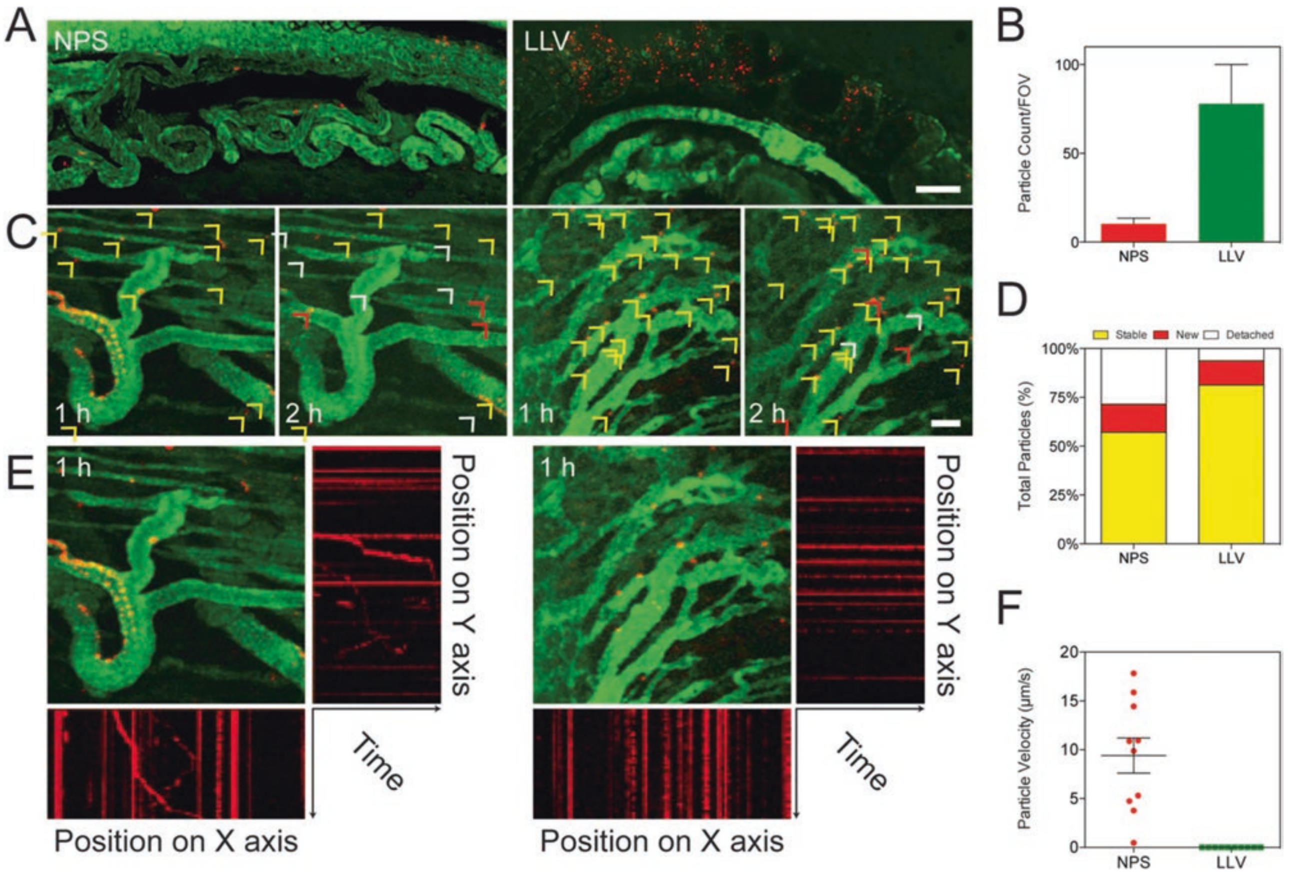

Fig. 5 Comparison between bare NPs and leukolike vectors' interactions with tumor vasculature in a 4T1 tumor model. (**a**) Intravital microscope images showing the presence of the particles in the tumor vasculature (scale bar = 100 μm). (**b**) Number of particles present in the vasculature analyzed from image (**a**). (**c**) Merged images from 20 s movies presenting the stability of the binding between leukolike vectors and the tumor vasculature (scale bar = 50 μm). (**d**) Numerical data quantifying the different fractions of particles (stably bound, newly bound, detached). (**e**) Particle motion analysis to evaluate the movement of single particles on x and y axes. Moving particles present askew lines, while stable particles are identified by straight lines. (**f**) Velocity of the NP movements compared to the bound leukolike vectors. (Reproduced with permission from Ref. [120])

and freeing the cellular peptidic targeting moiety. A D-form oligopeptide of sequence cskc was chosen as the targeting moiety because of its high affinity for the insulin-like growth factor receptor 1, quite commonly expressed by cancer cells. Upon interaction with the receptor and cellular internalization, the further drop in pH recorded into endosomes results in the rupture of the NPs, allowing for an intracellular delivery of PTX. In terms of antitumoral efficacy, the presence of the macrophage cell membrane combined with the targeting peptide can increase the most the number of apoptotic cells intratumorally, prolonging the control over the tumor growth in a 4T1 model.

Moreover, macrophage cell membrane determines an effective targeting of the payload also to metastasis (e.g., the lung metastasis in a breast cancer model) [122]. Interestingly, the cell membrane of neutrophils can help the payload cross the blood-pancreas barrier [123]. Moreover, neutrophils can specifically target the circulating tumor cells responsible for the formation of metastasis [124]. Natural killer (NK) cells routinely patrol the body looking for infected or tumor cells; the combination of DOX-loaded liposomes with cell membrane derived from NK cells increased the circulation time and the tumor targeting, with increased efficacy in a MCF-7 tumor xenograft compared to DOX alone [125].

Combination

The coating with macrophage cell membrane was proposed also to extend the circulation time of iron or gold nanoparticles, as well as Janus microcapsules, increasing their tumor accumulation and their PTT efficacy [48, 126, 127]. Myeloid-derived suppressor cell membranes were wrapped around iron oxide nanoparticles to extend their circulation profile and increase their tumor targeting. These particles were used in PTT, resulting in a decrease in the metabolic activity of the tumor together with reprogramming of tumor-infiltrating macrophages to a proinflammatory phenotype [128]. In an interesting application, low-dose irradiation was needed to increase the delivery of cytotoxic T-cell membrane-coated

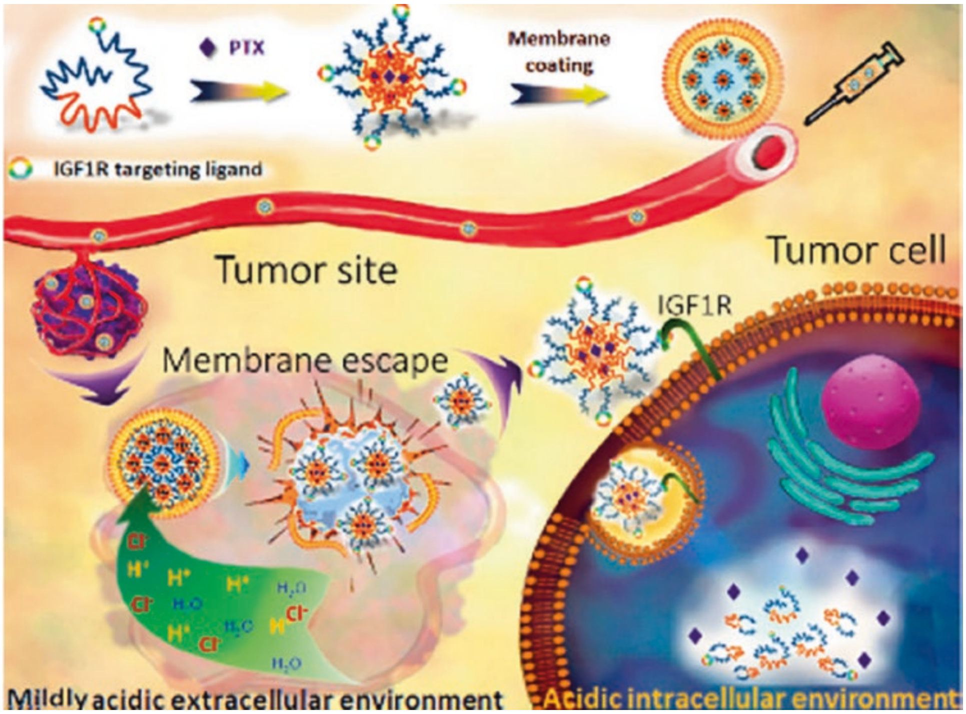

Fig. 6 Schematic illustration of stepwise, stimuli-responsive, biohybrid nanosystem wrapped in macrophage cell membrane. The system is produced by self-assembly of a polymer, can efficiently load PTX, and is then coated with macrophage cell membrane. Upon intravenous administration, the cell membrane ensures a correct targeting to the site of inflammation (the tumor), facilitating the extravasation. Then, in the tumor microenvironment, the system will escape from the cell membrane through a proton sponge effect, releasing the single particles. The targeting moiety present on each particle (insulin-like growth factor 1 receptor, IGF1R) will facilitate the targeting and intracellular uptake of the particles, which will then release the drug at cytoplasmic level, upon a further decrease in the environmental pH. (Reproduced with permission from Ref. [121])

NPs, with almost 90% of growth inhibition in a gastric cancer model in nude mice [129].

Others

In some cases, the optimal properties of a biohybrid nanoparticle derive from the combination of different cells; thereby, hybrid systems have been developed [130]. For example, the membrane of RBCs, which provides extended bloodstream circulation but does not allow the targeting to the site of interest, can be combined with the membrane of platelets, allowing for tumor targeting and retaining the properties of both the original cells [131]. As for the treatment of cancer, the desired properties are prolonged circulation with evasion of the RES and active targeting to the tumor site, to increase the tumor accumulation. Thereby, the stealth effect provided by RBCs can be combined with the homotypic targeting of the cancer cell membranes to prolong circulation time and increase tumor accumulation and efficacy of the cargo. Platelet membrane can represent also a targeting source when the tumor vasculature is injured by radiation and platelets are recruited to the microthrombosis sites created, increasing the distribution of the particles in the tumor tissue and, consequently, the efficacy of PTT [132]. Additionally, cancer cell membranes can be combined with leukocyte membranes in leutusomes, PTX-loaded liposomes formed from the two membranes. Their accumulation at the tumor site was 79% of the injected dose/g of tumor, representing a major increase compared to the tumor accumulation of conventional nanosystems (Fig. 7) [133]. The presence of leukocyte cell membrane features in the coating highly decreased the interactions and the uptake from immune cells. The applications of these particles are not limited only to cancer treatment but can also provide a reliable diagnostic source, as shown by Rao et al., where the combination of platelet membrane and leukocyte membrane allowed for the specific binding to circulating tumor cells provided from platelets while avoiding unspecific interactions with the leukocytes present in the blood sample [130].

4 Applications in Cancer Immunotherapy

4.1 Cancer Immunotherapy

The development of more effective and safer cancer treatments is strongly needed due to the intrinsic limits of conventional cancer therapies (e.g., surgery, radiotherapy,

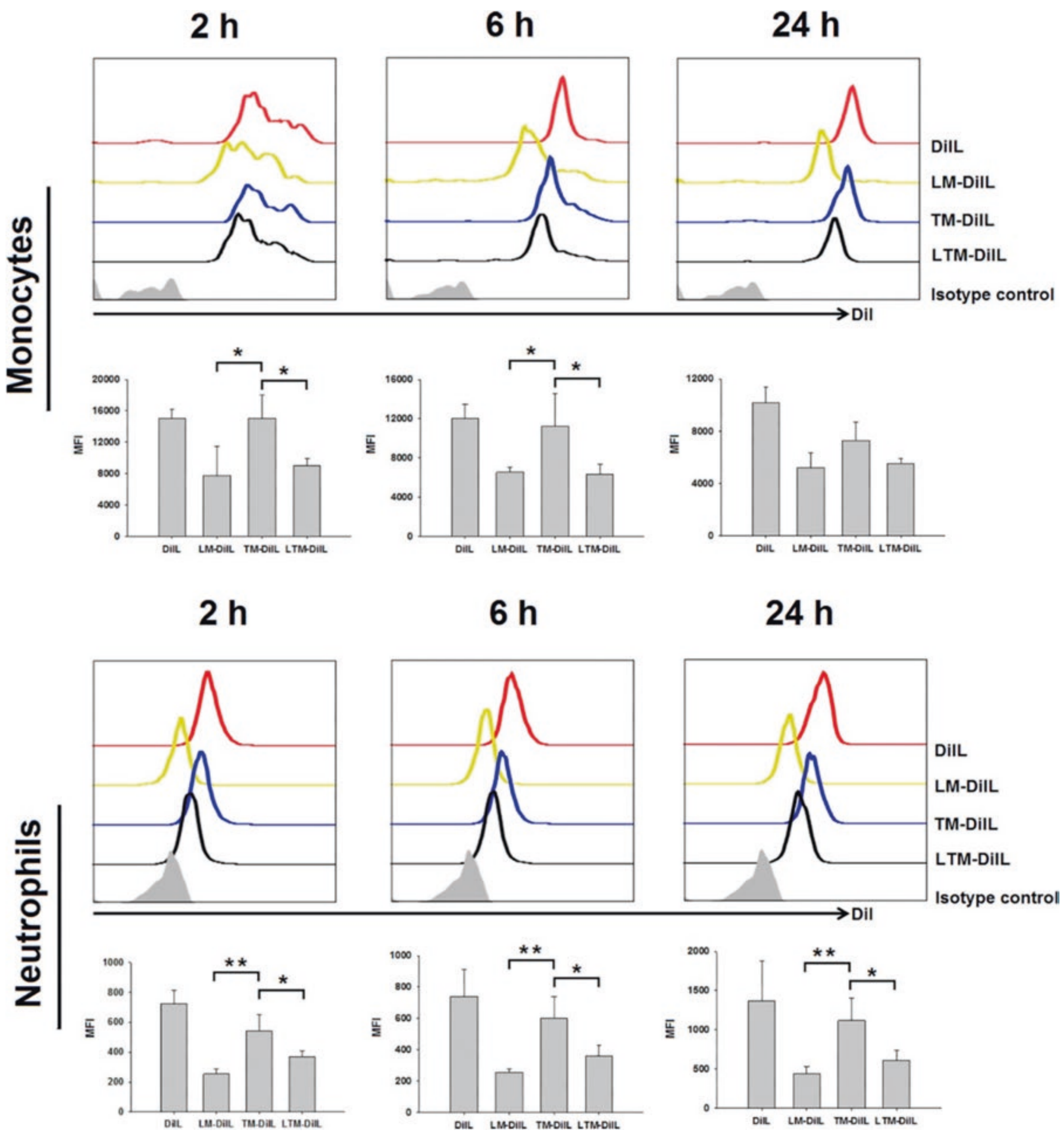

Fig. 7 Stealth effect of leukocyte cell membrane. The addition of leukocyte cell membrane to the cancer cell one reduces the interactions and slows the uptake of the leutusomes by monocytes and neutrophils. For shorter time points (2 h and 6 h), as seen both in the less marked shift of the fluorescence in the cell population and in the quantification of the MFI, the fraction of leutusomes taken up is comparable with systems prepared from the membrane of leukocytes, while the cancer cell membrane-derived systems show a higher uptake. (Reproduced with permission from Ref. [133])

chemotherapy, hormone therapy, and targeted therapy) [62]. The need is especially high against advanced cancer, for which conventional cancer therapies present limited efficacy [156].

Since the introduction of cancer immunotherapy, the paradigm of cancer treatment shifted [157]. Immunotherapy has been regarded as a rising therapeutic approach since the approval of the first marketed immunotherapy for cancer by the US Food and Drug Administration (FDA) in 1986, which consisted in recombinant versions of the cytokine interferon-α (IFNα) for the treatment of hairy cell leukemia [158]. Recently, owing to immune checkpoint inhibitors' (ICIs) clinical success, immunotherapy became a new pillar of cancer treatment [159].

Cancer immunotherapy aims to induce antitumor immune response by stimulating the host immune cells in lymphoid tissues and antitumor immune cells in the tumor microenvironment, such as effector T cells, dendritic cells (DCs), NK cells, and tumor-associated macrophages (M1-like macrophages) to recognize and kill tumor cells [159]. This approach is based on the cancer immunoediting concept,

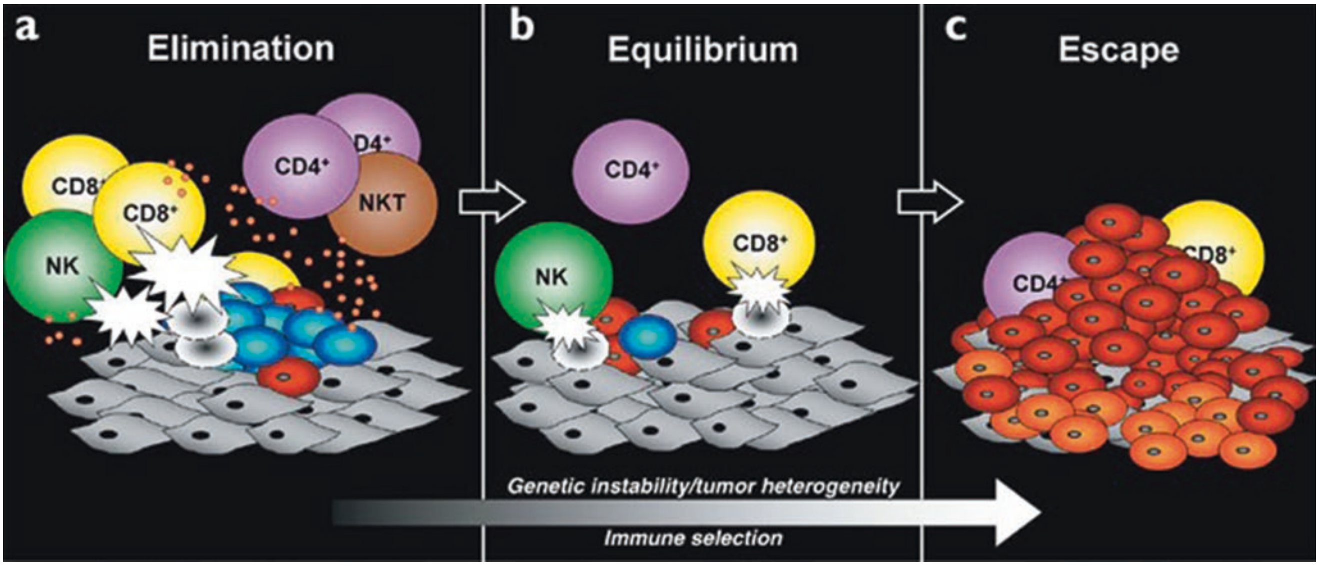

Fig. 8 The process of cancer immunoediting. (**a**) Transformed cells due to danger signals emitted and neoantigens are recognized by a variety of immune cells in the elimination phase. (**b**) This phase can progress to the tumor suppression or evolve to tumor dormancy and editing, the equilibrium phase. (**c**) When the tumor outgrowth is no longer blocked, escape phase starts, and the tumor becomes clinically apparent. The initial tumor cells are depicted in blue, clonal variation of the initial tumor cells are presented in orange, while the stroma and normal cells surrounding the tumor are grey. Leukocytes are directly identified in the figure, while small orange spheres represent cytokines and white flashes the activity of cytotoxic T cells against tumor cells. Reproduced with permission from Ref. [161]

which consists in an extrinsic tumor suppressor mechanism divided into three sequential phases: *elimination*, *equilibrium*, and *escape*. The concept attempts to integrate the diverse effects of the immune system on tumor development and outgrowth [160]. These phases take place only when intrinsic tumor suppressor mechanisms have failed, as shown in Fig. 8.

The first phase, *elimination*, comprises the immune surveillance stage, in which developing tumors are destroyed by a competent immune system long before they become clinically apparent. The second phase may occur when sporadic tumor cells are not destroyed in the elimination phase, entering the *equilibrium* phase. Thus, a state of tumor cells' functional dormancy is maintained by T cells, IL-12, and IFN-γ. In this phase due to the enormous plasticity of the cancer cell genome, edit of tumor immunogenicity occurs, yielding potential resistance to an immune attack. In the third and final phase of the process, the *escape* phase, tumors' outgrowth is no longer blocked by immunity, becoming clinically apparent. It may occur due to (i) lower cellular immunogenicity, adaptive immunity no longer recognizing tumor cells; (ii) increased cell survival, tumor cells becoming insensitive to immune effector mechanisms; or (iii) the formation of a multifaceted immunosuppressive tumor microenvironment (TME) [160, 162].

Therefore, cancer immunotherapy focuses on three main approaches towards an effective antitumor immune response: (1) adoptive T-cell therapy, (2) reversing immunosuppressive TME, and (3) vaccination [162]. By initiating a self-sustaining cycle of cancer immunity, this approach enables a treatment with fewer off-target effects than conventional cancer therapies, which directly kill cancer cells [157, 163].

4.2 Biohybrid NPs for Cancer Immunotherapy

Effective antitumor immunity is related to the presence of T cells directed at cancer neoantigens, which exhibit exquisite tumor specificity [164]. Cancer neoantigens, a class of human leukocyte antigen-bound peptides, derive from tumor-specific mutations [165]. Thus, they allow the immune system to distinguish cancer cells from non-cancer cells [166].

Biohybrid NPs have been gaining increased attention as an attractive candidate for cancer immunotherapy due to their ability to combine the unique functionalities of cellular membranes, which mimic the function of their source cells, and the potentiality of synthetic nanomaterials [136]. By leveraging the complex antigenic profile present on cell membranes, NPs coated with them reveal enhanced immunogenicity. Therefore, cancer vaccines bestowing biohybrid NPs are under hefty investigation to prime tumor-specific immunity [167].

4.2.1 Activation of Antigen-Presenting Cells (APCs)

To generate robust antitumor immune responses in vivo, therapeutic cancer vaccines immunize the patient against neoantigens [168]. Nevertheless, by the time malignant stage is reached, the most immunogenic neoantigens have been potentially eliminated via negative selection [5, 169, 170]. Therefore, to improve vaccine potency, vaccine formulations based on biohybrid nanotechnology typically incorporate cell membrane-coated NPs with immunostimulatory adjuvants to enhance the activation of APCs, boost in situ DCs' maturation, induce T-cell responses, and, lastly, lead to the creation of tumor-specific antitumor immune memory [171, 172].

Cancer Cell Membrane-Coated NPs

In the first proof of concept, Fang et al. developed cancer cell membrane-coated NPs (CCNPs). B16−F10 mouse melanoma cells were coated onto polymeric NP cores made of PLGA polymer with toll-like receptor 4 agonist, monophosphoryl lipid A (MPLA), as an adjuvant attached on the surfaces [24]. The resulting particles facilitated the uptake of membrane-bound neoantigens by APCs for efficient presentation and downstream immune activation. Furthermore, homotypic binding mechanism was observed since the CCNPs and their source cells shared the same cell adhesion molecules, and increased affinity enabled a targeted cancer drug delivery [24]. Therefore, this platform allowed the development of two distinct anticancer modalities, as shown in Fig. 9.

Alternatively, Fontana et al. developed a multistage nanosystem composed of porous silicon (PSi) NPs encapsulated within a polymeric matrix of acetylated dextran as immunostimulant adjuvant core, and they wrapped cell membrane from a human breast cancer cell line (MDA-MB-231) (Fig. 10) [23]. In this proof-of-concept study, the authors demonstrated that the vaccine formulation can efficiently induce the maturation of APC in vitro, together with a selective antitumor ability of PBMC primed against the cell membrane antigens.

Another interesting work swapped inorganic NPs as the vaccine core for oncolytic adenoviruses. Oncolytic adenoviruses can replicate only in cancer cells defective in mechanisms preventing their proliferation. As a result of the viral replication, cancer cells tend to explode, effectively reducing the tumor burden. Furthermore, the immune system has been shaped by millennia of interaction with viruses; thereby, viruses serve as excellent adjuvant platforms. However, the use of oncolytic viruses has also some downsides, including the need for a specific receptor for the cellular internalization whose expression differs among different cancers and the presence or production of neutralizing antibodies in the blood of the patients. Fusciello et al. creatively wrapped oncolytic adenovirus with the cell membrane derived from cancer cell (ExtraCRAd) and evaluated its efficacy as preventive and therapeutic vaccine in different tumor models (Fig. 11) [173]. The vaccination was highly effective in controlling the tumor growth in therapeutic settings, due

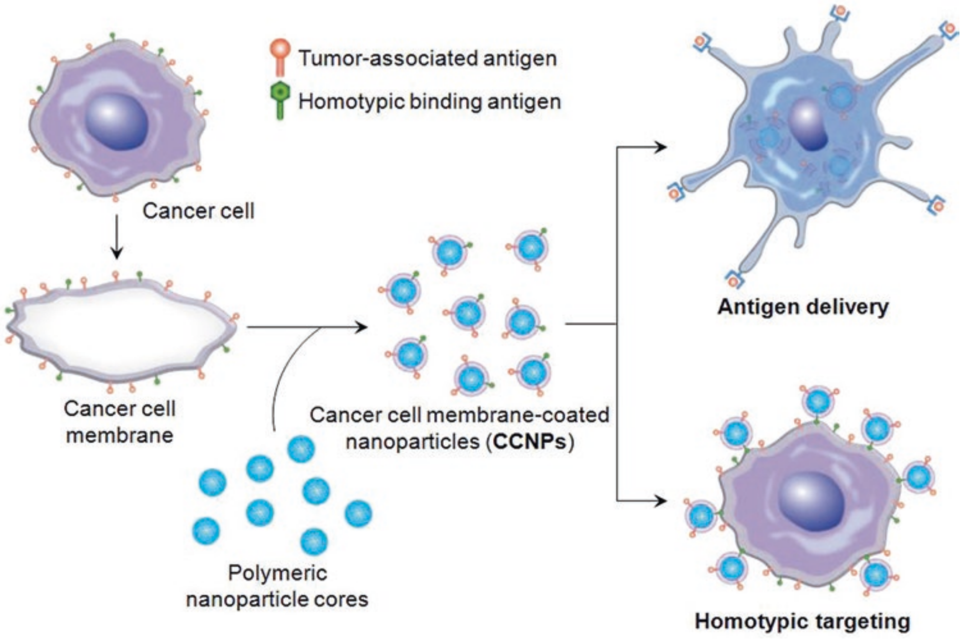
Tumor-associated antigen
Homotypic binding antigen
Cancer cell
Cancer cell membrane
Polymeric nanoparticle cores
Cancer cell membrane-coated nanoparticles (CCNPs)
Antigen delivery
Homotypic targeting

Fig. 9 Cancer cell membrane-coated NPs as cancer vaccines. Schematic presentation of CCNP fabrication. Cancer cell membrane with neoantigens is collected from cancer cells and coated onto polymeric NPs. These biomimetic NPs can be used for antigen delivery and homotypic targeting. (Reproduced with permission from Ref. [24])

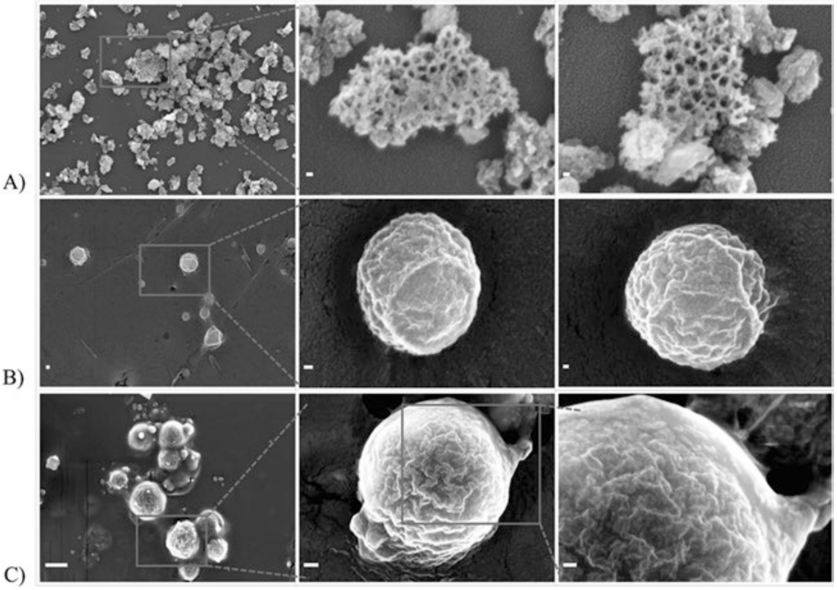

Fig. 10 High-resolution scanning electron microscopy images of the layers in the multistage nanosystem. (**a**) PSi NPs, (**b**) acetalated dextran encapsulating the PSi NP, (**c**) wrapping with cell membrane derived from MDA-MB-231 cells. (Reproduced with permission from Ref. [23])

to the priming of a tumor-specific response. Moreover, the coating of the virus with cell membrane increased the internalization of the virus in a receptor-independent way. The wrapped virus showed also enhanced protection against neutralizing antibodies [173].

RBC Membrane-Coated NPs

Ascribable to their inherent biocompatibility, RBCs, also known as erythrocytes, represent a promising cell-mediated drug delivery system [174]. Within the spleen, damaged or senescent RBCs are eliminated by scavenger cells [175, 176]. There, as cells from the immune system are particularly abundant, damaged RBCs could potentially deliver neoantigens to APCs and induce robust cytotoxic T-cell responses [176].

Guo et al. developed a mannose-RBC membrane-coated PLGA-NP with hpg100(25–33) (a melanoma-associated antigenic peptide) entrapment and MPLA as adjuvant to enhance DCs' targeting and neoantigen presenting efficiency [172]. The entrapment of hpg100(25–33) potentiated vaccine-induced antitumor immune response [177]. Furthermore, mannose-modified NPs delivered the vaccine into draining LNs. Thus, the particles allowed an active targeting of APCs in lymphatic organs, inhibited tumor growth and suppressed tumor metastasis, prolonging the overall survival of the animals in an aggressive melanoma model (Fig. 12) [172].

4.2.2 Combined Therapies with Immunotherapy

As a result of the lack of tumor-infiltrating effector T cells, presentation of neoantigens alone may not be able to overcome the immunosuppressive TME. Therefore, many cancer patients do not respond to single-agent therapy. A combination of multiple cancer therapies may be required to achieve effective tumor elimination and durable tumor inhibition post-treatments [178, 179]. As such, efforts have shifted towards the rational design of combinatorial approaches, as discussed below.

PDT and Immunotherapy

Cytomembrane-Coated NPs

Taking advantage of the features of cancer cells above explained and DCs, Liu et al. created NPs coated with a hybrid cytomembrane [179]. Due to the fusion of cancer cells with DCs and combination with photosensitizers-containing metal-organic frameworks (MOFs), the platform permitted a combination of immunotherapy and PDT (Fig. 13).

The cytomembrane was composed of cancer cells, murine mammary carcinoma tumor (4T1) cells; therefore, it effectively expressed neoantigens. Additionally, DCs are APC, which process and present neoantigens in the form of antigen peptide-MHC (pMHC) molecules on cell surface, regulating in T-cell immunity [180]. Consequently, the fusion of cancer cells and DCs allowed the presentation and processing of neoantigens [179]. Thereby, due to the presence of neoantigens and immunological co-stimulatory molecules derived from the cytomembrane, the platform allowed for targeting of homotypic tumors, had lymph node-homing ability, and increased immune responses [107, 179].

Moreover, the combination of the hybrid cytomembrane and the ultrahigh antitumor effects of MOFs inhibited proliferation of the primary tumors post-PDT treatment by facilitating the diffusion of the produced reactive oxygen species,

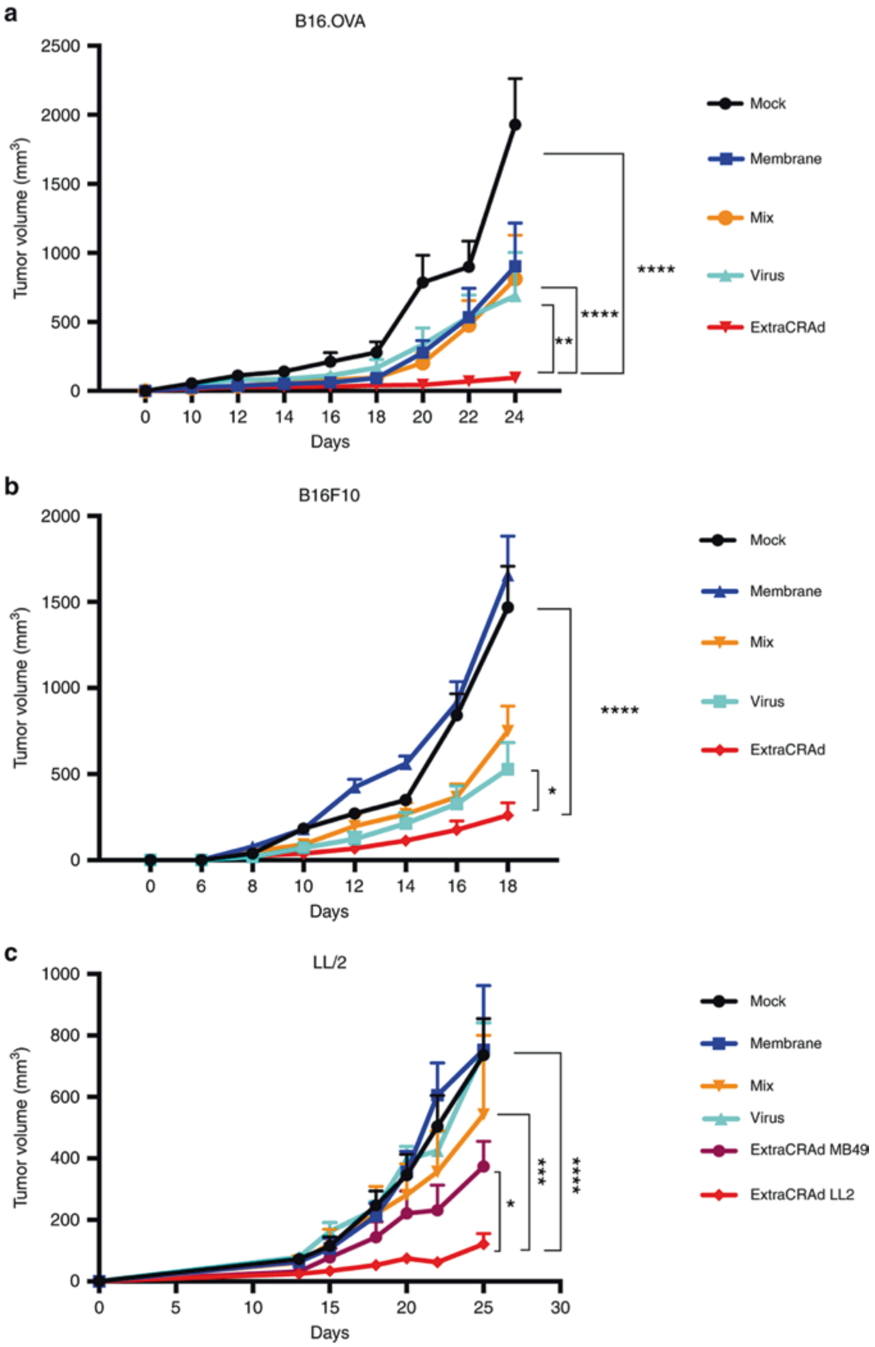

Fig. 11 Therapeutic efficacy of artificially wrapped adenovirus (ExtraCRAd) in melanoma and lung adenocarcinoma models. (**a**) Efficacy in B16.OVA melanoma. (**b**) Efficacy in B16.F10 melanoma. (**c**) Efficacy in LL/2 lung adenocarcinoma model. All the animals were injected four times with the vaccine, every 2 days

while the priming of an immune response suppressed the proliferation of distant tumors [179].

Natural Killer Cell Membrane-Coated NPs

Another strategy was elaborated by Deng et al. by combining immunotherapy based on biohybrid NPs and PDT. The platform was composed of NK cell membranes-cloaked photosensitizer 4,4′,4′′,4′′′-(porphine-5,10,15,20-tetrayl) tetrakis (benzoic acid) (TCPP)-loaded NPs (NK-NPs) with vaccine-like functions in situ [150].

NK cells are innate immune cells with potent cytolytic function, which do not require previous antigen-specific stimulation to eliminate target cells [181]. Moreover, NK cells secrete a variety of cytokines (e.g., tumor necrosis factor-α), promoting the maturation of APCs and, consequently, the production of proinflammatory cytokines and stimulation of T-cell responses [182, 183]. In cancer immunotherapy, NK cell membrane can induce proinflammatory M1 macrophages polarization and stimulate the immune system [150].

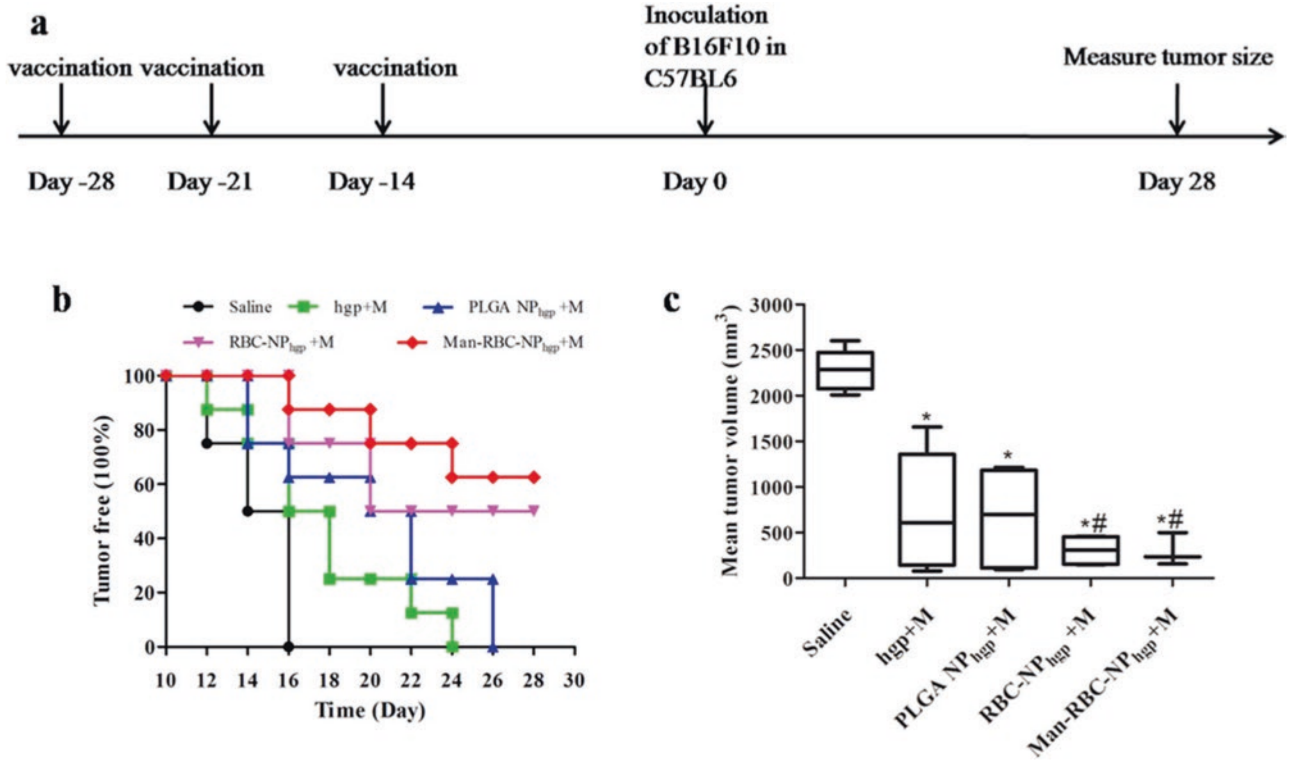

Fig. 12 Efficacy of RBC-coated hybrid NPs as preventive vaccination in B16.F10 melanoma model. (**a**) Schematic of the experiment with three vaccinations, every 7 days; 14 days after the last vaccination, the mice were injected with B16.F10 cells, and the growth of the tumor was then followed. (**b**) Percentage of tumor-free mice over time; (**c**) tumor volume at day 28. (Reproduced with permission from Ref. [172])

Thus, Deng et al. used NK-NPs to induce the polarization of M1 macrophages. Additionally, the loading with TCPP enabled a direct eradication of primary tumor cells through PDT and triggered dying cells to produce damage-associated molecular patterns, leading to the activation of APC. Altogether, this strategy increased the immunogenicity of cancer cells and the immune response. Furthermore, the treatment with the biomimetic nanostructure resulted in an abscopal effect inhibiting distant untreated tumors [150].

PTT and Immunotherapy

Myeloid-Derived Suppressor Cell Membrane-Coated NPs

Myeloid-derived suppressor cells (MDSCs) have emerged as major immune response regulators in cancer due to their immunosuppressive trait [184, 185]. Myeloid cells (e.g., macrophage, DCs, and neutrophils) when terminally differentiated activate in the presence of a pathologic condition towards elimination of potential threats (e.g., abnormal cells, infectious agents, or damaged tissue). When the steady state is not reached, a heterogeneous population of immature myeloid lineage cells, MDSCs, are produced [184]. Therefore, MDSCs are present in low concentration in healthy individuals, but as a result of chronic inflammation mediated by cytokines and chemokines produced by malignant cells, MDSCs are exponentially produced and accumulate in the tumor [185, 186].

By leveraging MDSC intrinsic features, Marvel and Gabrilovich developed a MDSC membrane-coated iron oxide magnetic NP for PTT-induced tumor killing [185]. The MDSC coating allowed an efficient immune escape and tumor targeting. In the tumor, MNP modulated M2 macrophages to M1, which were synergized with PTT-enhanced immunologic cell death [185].

Combined Immunotherapies

The modulation of the suppressive TME is essential for the success of immunotherapy; therefore, the combination of immunotherapies is expected to have a positive impact in increasing efficacy and reducing side effects [167].

Fontana et al. developed thermally oxidized PSi NPs and acetalated dextran formulated into a nanocarrier, which were coated with a layer of cancer cells, B16.F10 and B16.OVA, depending on the disease model to form CCNPs [167]. The biomimicking nanocarrier was administered in synergy with

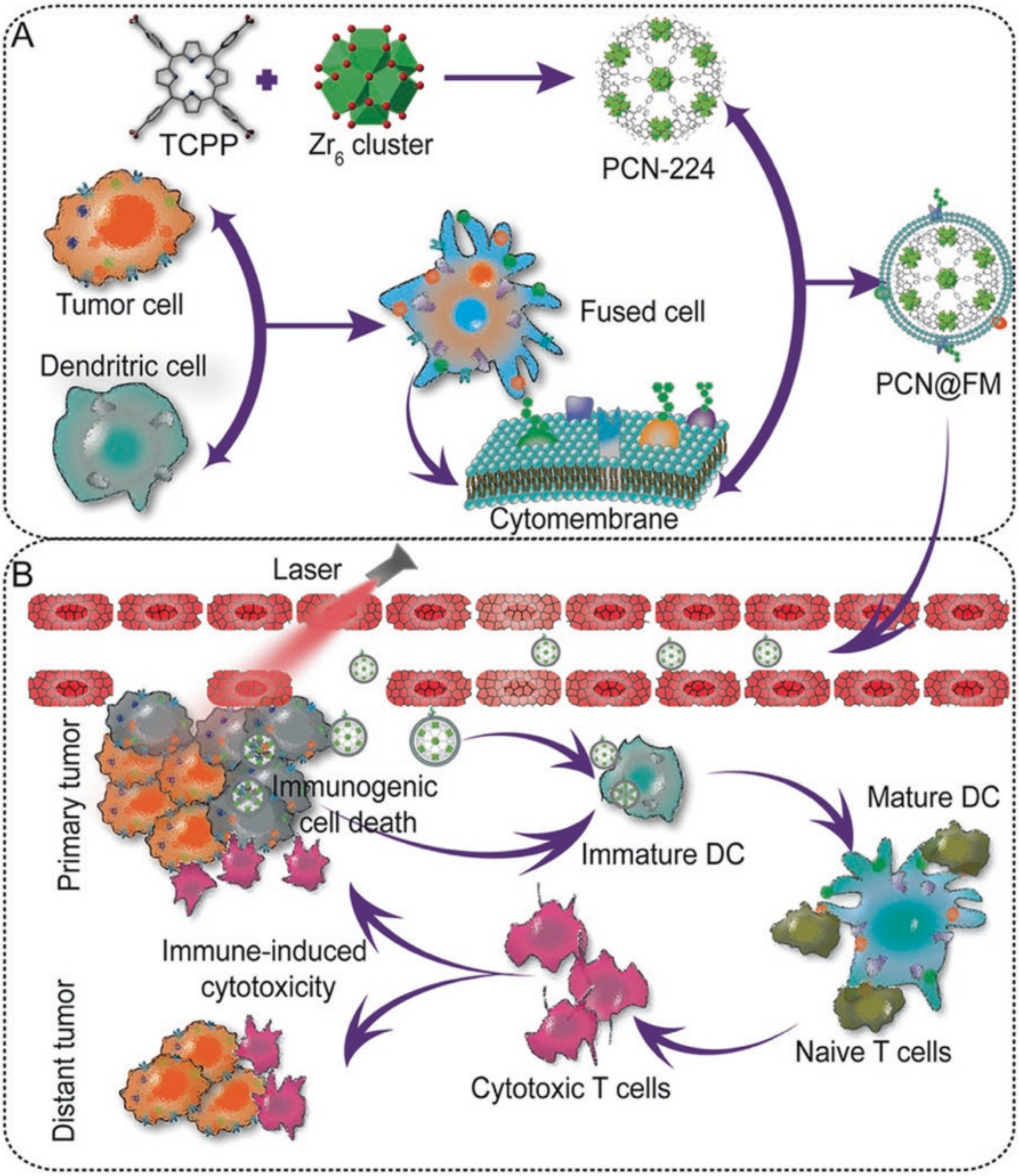
A
TCPP
Zr$_6$ cluster
PCN-224
Tumor cell
Dendritic cell
Fused cell
PCN@FM
Cytomembrane
B
Laser
Primary tumor
Immunogenic cell death
Immature DC
Mature DC
Immune-induced cytotoxicity
Distant tumor
Cytotoxic T cells
Naive T cells

Fig. 13 Schematic of the composition and mechanism of action of cytomembrane-coated MOFs for combined PTT and immunotherapy. (**a**) A NIR-responsive molecule (TCPP) was combined with clusters of zirconium to form MOFs. The cell membranes from 4T1 cells and DCs were then combined in a hybrid cell membrane used to coat the MOF NPs. (**b**) Mode of action of the biohybrid MOFs: after IV injection, the NPs will accumulate in the tumor, where, after NIR irradiation and PTT, cancer cells die, releasing antigens. At the same time, NPs can be uptaken by immature DC, contributing to their maturation and the priming of a tumor-specific immune response able to control the tumor growth also in distal tumors not irradiated with NIR laser. (Reproduced with permission from Ref. [179])

immune checkpoint inhibitors (ICIs), such as CTLA-4 blocking antibodies [187]. As the rate of ICIs-responsive patients remains limited [188], mainly due to the absence of antigen-specific T cells into the TME, this strategy was particularly important to assess the synergistic potential of ICIs and CCNPs [167].

The platform successfully increased the maturation of DCs, the expression of pMHC, and the infiltration rate of DCs and T cells, synergizing with anti-CTLA-4 treatment. Thus, the present strategy elicited an antitumor immune response and improved the antitumor efficacy of ICIs in the treatment of melanoma [167].

5 Advantages, Disadvantages, and Clinical Outlook

The main advantages of biohybrid nanosystems in cancer treatment can be summarized in prolonged circulation (stealthiness), efficient active targeting, and presentation of neoantigens. Each of these characteristics has profoundly innovated the field of nanomedicine.

The surface modification of NPs with PEG has been the gold standard for some decades, with uncountable examples in the clinics or described in the literature. However, the efficiency of this coating is quite limited compared with the normal circulation time of corpuscular elements in the blood. The use of cells or cell membranes has led to a major increase in the blood circulation time, in the order of tens of hours more. Nevertheless, when compared with the actual lifespan of the plain cells (e.g., RBC), this increase is still limited and needs further research and optimization of the physical properties of the system (e.g., shape and elastic modulus), moving away from conventional spherical rigid polymeric particles.

Cells or receptors on their cell membranes provide multiple sources of active targeting to the tissue and cell of interest without the need to introduce foreign targeting agents. The natural affinity and binding of biohybrid systems do not depend on the ratio between targeting agents and PEG or on the formation of the protein corona. However, particularly in the case of cancer cell membrane-coated particles, all the proof-of-concept studies have been in immunodeficient animals, without evaluating the interaction with a complete immune system. In the case of leutusomes, cancer cell membrane was combined with leukocyte cell membrane, minimizing the interactions with RES and increasing the dose delivered to the tumor in a fully immunocompetent model [133]. Thereby, further investigations in immunocompetent animals and in larger animal are needed to effectively demonstrate the homotopic targeting.

The possibility to create a cancer vaccine delivering neoantigens without the need for a costly and time-consuming discovery is providing a powerful alternative. However, the composition of the cell membrane is not homogenous, which means that the membrane composition over the particles is not standardized. Moreover, experiments in larger animals collecting the tumor from biopsy are needed to evaluate whether the amount of material retrieved from a biopsy or a surgery is enough to prepare a nanovaccine.

The main disadvantages are associated with the cost of setting up suitable facilities at hospital or higher level. Some of these particles can be standardized and formulated in advance from a pharmaceutical company (e.g., platelet-based and different formulations of RBC based on the different blood types), while others are intrinsically personalized and require treatment facility at the bedside. Furthermore, the techniques commonly employed for the preparation of these materials are suitable for a small laboratory scale with mg of particles processed, while for the clinics higher amounts are needed. Thereby a suitable scaling-up of the protocols and instrument is fundamental to ensure the clinical success of these innovative systems.

Finally, the regulatory landscape has to convene on an optimal classification for this type of systems to facilitate their development and clinical testing. These systems can be ascribed both to the NPs and the extracellular vesicle categories; thereby, further clarifications from the regulatory bodies may incentivize pharma companies towards biohybrid nanosystems research.

6 Conclusions

Overall, in this book chapter, we presented the recent research on biohybrid materials for cancer treatment, both conventional and immunotherapy-based applications. Biohybrid nanosystems still represent the cutting edge of nanotechnology, providing valid alternatives or solutions to conventional nanoparticles. The use of cell membrane as outer layer of conventional nanoparticles brings along extended circulation, active targeting, and tumor neoantigens enabling more efficient chemo, PTT, PDT, and immunotherapy. In the near future, a careful optimization of the coating, together with an evaluation of the costs for a viable scaling-up and translational applications, will indicate the actual feasibility of the technique into the clinics.

Acknowledgments Prof. H. A. Santos acknowledges financial support from the HiLIFE Research Funds, the Sigrid Jusélius Foundation, and the European Research Council Proof-of-Concept Research Grant (grant no. 825020).

References

1. Gao, J., & Maruyama, A. (2014). Biohybrid materials. In *Encyclopedia of polymeric nanomaterials*. Berlin, Heidelberg: Springer.
2. Ricotti, L., et al. (2017). Biohybrid actuators for robotics: A review of devices actuated by living cells. *Science Robotics, 2*, eaaq0495.
3. Hosseinidoust, Z., et al. (2016). Bioengineered and biohybrid bacteria-based systems for drug delivery. *Advanced Drug Delivery Reviews, 106*, 27–44.
4. Sakimoto, K. K., Kornienko, N., & Yang, P. (2017). Cyborgian material design for solar fuel production: The emerging photosynthetic biohybrid systems. *Accounts of Chemical Research, 50*, 476–481.
5. Kroll, A. V., et al. (2017). Nanoparticulate delivery of cancer cell membrane elicits multiantigenic antitumor immunity. *Advanced Materials, 29*, 1703969.
6. Yan, X., et al. (2017). Multifunctional biohybrid magnetite microrobots for imaging-guided therapy. *Science robotics, 2*, eaaq1155.

7. Pal, A., Tripathi, K., Pathak, C., & Vernon, B. L. (2019). Plasma-based fast-gelling biohybrid gels for biomedical applications. *Scientific Reports, 9*, 1–10.
8. Zhu, Y., et al. (2018). Injectable, porous, biohybrid hydrogels incorporating decellularized tissue components for soft tissue applications. *Acta Biomaterialia, 73*, 112–126.
9. Hu, C. M. J., Fang, R. H., Copp, J., Luk, B. T., & Zhang, L. (2013). A biomimetic nanosponge that absorbs pore-forming toxins. *Nature Nanotechnology, 8*, 336–340.
10. Raman, R., & Langer, R. (2020). Biohybrid design gets personal: New materials for patient-specific therapy. *Advanced Materials, 32*, 1901969.
11. Huang, G., et al. (2017). Functional and biomimetic materials for engineering of the three-dimensional cell microenvironment. *Chemical Reviews, 117*, 12764–12850.
12. Luo, Z., Weiss, D. E., Liu, Q., & Tian, B. (2018). Biomimetic approaches toward smart bio-hybrid systems. *Nano Research, 11*, 3009–3030.
13. Jamal, M., et al. (2013). Bio-origami hydrogel scaffolds composed of photocrosslinked PEG bilayers. *Advanced Healthcare Materials, 2*, 1142–1150.
14. Wagner, H. J., Sprenger, A., Rebmann, B., & Weber, W. (2016). Upgrading biomaterials with synthetic biological modules for advanced medical applications. *Advanced Drug Delivery Reviews, 105*, 77–95.
15. Van Hove, A. H., Burke, K., Antonienko, E., Brown, E., & Benoit, D. S. W. (2015). Enzymatically-responsive pro-angiogenic peptide-releasing poly(ethylene glycol) hydrogels promote vascularization in vivo. *Journal of Controlled Release, 217*, 191–201.
16. Mohammadi, M. R., Corbo, C., Molinaro, R., & Lakey, J. R. T. (2019). Biohybrid nanoparticles to negotiate with biological barriers. *Small, 15*, 1902333.
17. Toledano Furman, N. E., et al. (2013). Reconstructed stem cell nanoghosts: A natural tumor targeting platform. *Nano Letters, 13*, 3248–3255.
18. Krishnamurthy, S., et al. (2016). Monocyte cell membrane-derived nanoghosts for targeted cancer therapy. *Nanoscale, 8*, 6981–6985.
19. Kaneti, L., et al. (2016). Nanoghosts as a novel natural nonviral gene delivery platform safely targeting multiple cancers. *Nano Letters, 16*, 1574–1582.
20. Oieni, J., et al. (2020). Nano-Ghosts: Biomimetic membranal vesicles, technology and characterization. *Methods, 177*, 126–134.
21. Bose, R. J., et al. (2018). Bioengineered stem cell membrane functionalized nanocarriers for therapeutic targeting of severe hindlimb ischemia. *Biomaterials, 185*, 360–370.
22. Dong, X., et al. (2017). Formulation and drug loading features of nano-erythrocytes. *Nanoscale Research Letters, 12*, 1–13.
23. Fontana, F., et al. (2017). Multistaged nanovaccines based on porous silicon@ acetalated dextran@ cancer cell membrane for cancer immunotherapy. *Advanced Materials, 29*, 1603239.
24. Fang, R. H., et al. (2014). Cancer cell membrane-coated nanoparticles for anticancer vaccination and drug delivery. *Nano Letters, 14*, 2181–2188.
25. Jiang, Q., et al. (2017). Red blood cell membrane-camouflaged melanin nanoparticles for enhanced photothermal therapy. *Biomaterials, 143*, 29–45.
26. Xia, Q., Zhang, Y., Li, Z., Hou, X., & Feng, N. (2019). Red blood cell membrane-camouflaged nanoparticles: A novel drug delivery system for antitumor application. *Acta Pharmaceutica Sinica B, 9*, 675–689.
27. Parodi, A., et al. (2013). Synthetic nanoparticles functionalized with biomimetic leukocyte membranes possess cell-like functions. *Nature Nanotechnology, 8*, 61–68.
28. Hu, C. M. J., et al. (2015). Nanoparticle biointerfacing by platelet membrane cloaking. *Nature, 526*, 118–121.
29. Molinaro, R., et al. (2016). Biomimetic proteolipid vesicles for targeting inflamed tissues. *Nature Materials, 15*, 1037–1046.
30. Gao, C., et al. (2016). Stem cell membrane-coated nanogels for highly efficient in vivo tumor targeted drug delivery. *Small, 12*, 4056–4062.
31. Chen, W., et al. (2016). Coating nanofiber scaffolds with beta cell membrane to promote cell proliferation and function. *Nanoscale, 8*, 10364–10370.
32. Hadryś, A., Sochanik, A., McFadden, G., & Jazowiecka-Rakus, J. (2020). Mesenchymal stem cells as carriers for systemic delivery of oncolytic viruses. *European Journal of Pharmacology, 874*, 172991.
33. Paris, J. L., et al. (2016). Decidua-derived mesenchymal stem cells as carriers of mesoporous silica nanoparticles. In vitro and in vivo evaluation on mammary tumors. *Acta Biomateriali, 33*, 275–282.
34. Pan, D. C., et al. (2018). Nanoparticle properties modulate their attachment and effect on carrier red blood cells. *Scientific Reports, 8*, 1–12.
35. Villa, C. H., Anselmo, A. C., Mitragotri, S., & Muzykantov, V. (2016). Red blood cells: Supercarriers for drugs, biologicals, and nanoparticles and inspiration for advanced delivery systems. *Advanced Drug Delivery Reviews, 106*, 88–103.
36. Gheibi Hayat, S. M., Bianconi, V., Pirro, M., & Sahebkar, A. (2019). Stealth functionalization of biomaterials and nanoparticles by CD47 mimicry. *International Journal of Pharmaceutics, 569*, 118628.
37. Simon, J., et al. (2018). Exploiting the biomolecular corona: Precoating of nanoparticles enables controlled cellular interactions. *Nanoscale, 10*, 10731–10739.
38. Balasubramanian, V., et al. (2017). Biomimetic engineering using cancer cell membranes for designing compartmentalized nanoreactors with organelle-like functions. *Advanced Materials, 29*, 1605375.
39. Luk, B. T., et al. (2014). Interfacial interactions between natural RBC membranes and synthetic polymeric nanoparticles. *Nanoscale, 6*, 2730–2737.
40. Fontana, F., et al. (2018). Bioengineered porous silicon nanoparticles@ macrophages cell membrane as composite platforms for rheumatoid arthritis. *Advanced Functional Materials, 28*, 1801355.
41. Yong, T., et al. (2019). Tumor exosome-based nanoparticles are efficient drug carriers for chemotherapy. *Nature Communications, 10*, 1–16.
42. Pan, D., et al. (2016). The effect of polymeric nanoparticles on biocompatibility of carrier red blood cells. *PLoS One, 11*, e0152074.
43. Brenner, J. S., et al. (2018). Red blood cell-hitchhiking boosts delivery of nanocarriers to chosen organs by orders of magnitude. *Nature Communications, 9*, 1–14.
44. Wang, C., et al. (2014). Multifunctional theranostic red blood cells for magnetic-field-enhanced in vivo combination therapy of cancer. *Advanced Materials, 26*, 4794–4802.
45. Song, S., et al. (2019). PEGegylated and CcD47-conjugated nanoellipsoidal artificial antigen-presenting cells minimize phagocytosis and augment anti-tumor T-cell responses. *International Journal of Nanomedicine, 14*, 2465–2483.
46. Fang, R. H., Kroll, A. V., Gao, W., & Zhang, L. (2018). Cell membrane coating nanotechnology. *Advanced Materials, 30*, 1706759.
47. Banskota, S., Yousefpour, P., & Chilkoti, A. (2017). Cell-based biohybrid drug delivery systems: The best of the synthetic and natural worlds. *Macromolecular Bioscience, 17*, 1600361.
48. Xuan, M., Shao, J., Dai, L., Li, J., & He, Q. (2016). Macrophage cell membrane camouflaged Au nanoshells for in vivo prolonged circulation life and enhanced cancer photothermal therapy. *ACS Applied Materials & Interfaces, 8*, 9610–9619.

49. Rao, L., et al. (2015). Red blood cell membrane as a biomimetic nanocoating for prolonged circulation time and reduced accelerated blood clearance. *Small, 11*, 6225–6236.
50. Kim, Y. K., Chen, E. Y., & Liu, W. F. (2016). Biomolecular strategies to modulate the macrophage response to implanted materials. *Journal of Materials Chemistry B, 4*, 1600–1609.
51. Kong, F., et al. (2016). CD47: A potential immunotherapy target for eliminating cancer cells. *Clinical & Translational Oncology, 18*, 1051–1055.
52. Shahzad, K. A., et al. (2018). On-target and direct modulation of alloreactive T cells by a nanoparticle carrying MHC alloantigen, regulatory molecules and CD47 in a murine model of alloskin transplantation. *Drug Delivery, 25*, 703–715.
53. Qie, Y., et al. (2016). Surface modification of nanoparticles enables selective evasion of phagocytic clearance by distinct macrophage phenotypes. *Scientific Reports, 6*, 1–11.
54. Ayer, M., & Klok, H. A. (2017). Cell-mediated delivery of synthetic nano- and microparticles. *Journal of Controlled Release, 259*, 92–104.
55. Letko Khait, N., et al. (2019). Radiolabeling of cell membrane-based nano-vesicles with 14C-linoleic acid for robust and sensitive quantification of their biodistribution. *Journal of Controlled Release, 293*, 215–223.
56. Zhang, W., et al. (2018). Nanoparticle-laden macrophages for tumor-tropic drug delivery. *Advanced Materials, 30*, 1805557.
57. Zhang, Q., et al. (2018). Neutrophil membrane-coated nanoparticles inhibit synovial inflammation and alleviate joint damage in inflammatory arthritis. *Nature Nanotechnology, 13*, 1182–1190.
58. Boada, C., et al. (2020). Rapamycin-loaded biomimetic nanoparticles reverse vascular inflammation. *Circulation Research, 126*, 25–37.
59. Altschuler, S. J., & Wu, L. F. (2010). Cellular heterogeneity: Do differences make a difference? *Cell, 141*, 559–563.
60. Fouad, Y. A., & Aanei, C. (2017). Revisiting the hallmarks of cancer. *American Journal of Cancer Research, 7*, 1016–1036.
61. Hanahan, D., & Weinberg, R. A. (2011). Hallmarks of cancer: The next generation. *Cell, 144*, 646–674.
62. Shi, J., Kantoff, P. W., Wooster, R., & Farokhzad, O. C. (2017). Cancer nanomedicine: Progress, challenges and opportunities. *Nature Reviews. Cancer, 17*, 20–37.
63. Schmitt, M. W., Loeb, L. A., & Salk, J. J. (2016). The influence of subclonal resistance mutations on targeted cancer therapy. *Nature Reviews. Clinical Oncology, 13*, 335–347.
64. Bregoli, L., et al. (2016). Nanomedicine applied to translational oncology: A future perspective on cancer treatment. *Nanomedicine Nanotechnology, Biology and Medicine, 12*, 81–103.
65. Ventola, C. L. (2017). Progress in nanomedicine: Approved and investigational nanodrugs. *Pharmacy and Therapeutics, 42*, 742.
66. Anselmo, A. C., & Mitragotri, S. (2016). Nanoparticles in the clinic. *Bioengineering & Translational Medicine, 1*, 10–29.
67. Bobo, D., Robinson, K. J., Islam, J., Thurecht, K. J., & Corrie, S. R. (2016). Nanoparticle-based medicines: A review of FDA-approved materials and clinical trials to date. *Pharmaceutical Research, 33*, 2373–2387.
68. Wais, U., Jackson, A. W., He, T., & Zhang, H. (2016). Nanoformulation and encapsulation approaches for poorly water-soluble drug nanoparticles. *Nanoscale, 8*, 1746–1769.
69. Liu, D., et al. (2017). A nano-in-nano vector: Merging the best of polymeric nanoparticles and drug nanocrystals. *Advanced Functional Materials, 27*, 1604508.
70. Herranz-Blanco, B., et al. (2015). On-chip self-assembly of a smart hybrid nanocomposite for antitumoral applications. *Advanced Functional Materials, 25*, 1488–1497.
71. Hirn, S., et al. (2011). Particle size-dependent and surface charge-dependent biodistribution of gold nanoparticles after intravenous administration. *European Journal of Pharmaceutics and Biopharmaceutics, 77*, 407–416.
72. Lundy, D. J., Chen, K. H., Toh, E. K. W., & Hsieh, P. C. H. (2016). Distribution of systemically administered nanoparticles reveals a size-dependent effect immediately following cardiac ischaemia-reperfusion injury. *Scientific Reports, 6*, 1–10.
73. Gao, Y., et al. (2017). In vivo biodistribution and passive accumulation of upconversion nanoparticles in colorectal cancer models via intraperitoneal injection. *RSC Advances, 7*, 31588–31596.
74. Lopes, M., et al. (2017). In vivo biodistribution of antihyperglycemic biopolymer-based nanoparticles for the treatment of type 1 and type 2 diabetes. *European Journal of Pharmaceutics and Biopharmaceutics, 113*, 88–96.
75. de Jesus Felismino, C., et al. (2018). Effect of obesity on biodistribution of nanoparticles. *Journal of Controlled Release, 281*, 11–18.
76. Ma, L., et al. (2016). Efficient targeting of adipose tissue macrophages in obesity with polysaccharide nanocarriers. *ACS Nano, 10*, 6952–6962.
77. Pinheiro, W. O., et al. (2019). The influence of female mice age on biodistribution and biocompatibility of citrate-coated magnetic nanoparticles. *International Journal of Nanomedicine, 14*, 3375–3388.
78. Aldayel, A. M., et al. (2018). Lipid nanoparticles with minimum burst release of TNF-α siRNA show strong activity against rheumatoid arthritis unresponsive to methotrexate. *Journal of Controlled Release, 283*, 280–289.
79. Danhier, F. (2016). To exploit the tumor microenvironment: Since the EPR effect fails in the clinic, what is the future of nanomedicine? *Journal of Controlled Release, 244*, 108–121.
80. Park, J., et al. (2019). Alliance with EPR effect: Combined strategies to improve the EPR effect in the tumor microenvironment. *Theranostics, 9*, 8073–8090.
81. Attia, M. F., Anton, N., Wallyn, J., Omran, Z., & Vandamme, T. F. (2019). An overview of active and passive targeting strategies to improve the nanocarriers efficiency to tumour sites. *The Journal of Pharmacy and Pharmacology, 71*, 1185–1198.
82. Khutoryanskiy, V. V. (2018). Beyond PEGylation: Alternative surface-modification of nanoparticles with mucus-inert biomaterials. *Advanced Drug Delivery Reviews, 124*, 140–149.
83. Suk, J. S., Xu, Q., Kim, N., Hanes, J., & Ensign, L. M. (2016). PEGylation as a strategy for improving nanoparticle-based drug and gene delivery. *Advanced Drug Delivery Reviews, 99*, 28–51.
84. d'Avanzo, N., et al. (2020). Immunogenicity of polyethylene glycol based nanomedicines: Mechanisms, clinical implications and systematic approach. *Advances in Therapy, 3*, 1900170.
85. Yang, Q., et al. (2016). Analysis of pre-existing IgG and IgM antibodies against polyethylene glycol (PEG) in the general population. *Analytical Chemistry, 88*, 11804–11812.
86. Lawler, S. E., Speranza, M. C., Cho, C. F., & Chiocca, E. A. (2017). Oncolytic viruses in cancer treatment a review. *JAMA Oncology, 3*, 841–849.
87. Bommareddy, P. K., Shettigar, M., & Kaufman, H. L. (2018). Integrating oncolytic viruses in combination cancer immunotherapy. *Nature Reviews. Immunology, 18*, 498–513.
88. Filley, A. C., & Dey, M. (2017). Immune system, friend or foe of oncolytic virotherapy? *Frontiers in Oncology, 7*, 106.
89. Yoo, J., Park, C., Yi, G., Lee, D., & Koo, H. (2019). Active targeting strategies using biological ligands for nanoparticle drug delivery systems. *Cancers (Basel), 11*, 640.
90. Saha, R. N., Vasanthakumar, S., Bende, G., & Snehalatha, M. (2010). Nanoparticulate drug delivery systems for cancer chemotherapy. *Molecular Membrane Biology, 27*, 215–231.

91. Ruoslahti, E. (2017). Tumor penetrating peptides for improved drug delivery. *Advanced Drug Delivery Reviews, 110–111*, 3–12.
92. Deshpande, P., Jhaveri, A., Pattni, B., Biswas, S., & Torchilin, V. P. (2018). Transferrin and octaarginine modified dual-functional liposomes with improved cancer cell targeting and enhanced intracellular delivery for the treatment of ovarian cancer. *Drug Delivery, 25*, 517–532.
93. Torchilin, V. P. (2008). Tat peptide-mediated intracellular delivery of pharmaceutical nanocarriers. *Advanced Drug Delivery Reviews, 60*, 548–558.
94. Wilhelm, S., et al. (2016). Analysis of nanoparticle delivery to tumours. *Nature Reviews Materials, 1*, 1–12.
95. He, H., Liu, L., Morin, E. E., Liu, M., & Schwendeman, A. (2019). Survey of clinical translation of cancer nanomedicines – lessons learned from successes and failures. *Accounts of Chemical Research, 52*, 2445–2461.
96. Zhao, Z., Ukidve, A., Gao, Y., Kim, J., & Mitragotri, S. (2019). Erythrocyte leveraged chemotherapy (ELeCt): Nanoparticle assembly on erythrocyte surface to combat lung metastasis. *Science Advances, 5*, eaax9250.
97. Willmon, C., et al. (2009). Cell carriers for oncolytic viruses: Fed ex for cancer therapy. *Molecular Therapy, 17*, 1667–1676.
98. Sun, H., et al. (2017). Cancer cell membrane-coated gold nanocages with hyperthermia-triggered drug release and homotypic target inhibit growth and metastasis of breast cancer. *Advanced Functional Materials, 27*, 1604300.
99. Rao, L., et al. (2019). Cancer cell membrane-coated nanoparticles for personalized therapy in patient-derived xenograft models. *Advanced Functional Materials, 29*, 1905671.
100. Lupu-Haber, Y., et al. (2019). Pretreating mesenchymal stem cells with cancer conditioned-media or proinflammatory cytokines changes the tumor and immune targeting by nanoghosts derived from these cells. *Advanced Healthcare Materials, 8*, 1801589.
101. Hu, C. M. J., et al. (2013). 'Marker-of-self' functionalization of nanoscale particles through a top-down cellular membrane coating approach. *Nanoscale, 5*, 2664–2668.
102. Hu, C. M. J., et al. (2011). Erythrocyte membrane-camouflaged polymeric nanoparticles as a biomimetic delivery platform. *Proceedings of the National Academy of Sciences of the United States of America, 108*, 10980–10985.
103. Aryal, S., et al. (2013). Erythrocyte membrane-cloaked polymeric nanoparticles for controlled drug loading and release. *Nanomedicine, 8*, 1271–1280.
104. Pei, Q., et al. (2018). Light-activatable red blood cell membrane-camouflaged dimeric prodrug nanoparticles for synergistic photodynamic/chemotherapy. *ACS Nano, 12*, 1630–1641.
105. Su, J., et al. (2016). Bioinspired nanoparticles with NIR-controlled drug release for synergetic chemophotothermal therapy of metastatic breast cancer. *Advanced Functional Materials, 26*, 7495–7506.
106. Zhou, H., Fan, Z., Lemons, P. K., & Cheng, H. (2016). A facile approach to functionalize cell membrane-coated nanoparticles. *Theranostics, 6*, 1012–1022.
107. Zhu, J. Y., et al. (2016). Preferential cancer cell self-recognition and tumor self-targeting by coating nanoparticles with homotypic cancer cell membranes. *Nano Letters, 16*, 5895–5901.
108. Li, S. Y., et al. (2017). Cancer cell membrane camouflaged cascade bioreactor for cancer targeted starvation and photodynamic therapy. *ACS Nano, 11*, 7006–7018.
109. Müller, F. J., Snyder, E. Y., & Loring, J. F. (2006). Gene therapy: Can neural stem cells deliver? *Nature Reviews Neuroscience, 7*, 75–84.
110. Nakamizo, A., et al. (2005). Human bone marrow-derived mesenchymal stem cells in the treatment of gliomas. *Cancer Research, 65*, 3307–3318.
111. Layek, B., Sadhukha, T., Panyam, J., & Prabha, S. (2018). Nano-engineered mesenchymal stem cells increase therapeutic efficacy of anticancer drug through true active tumor targeting. *Molecular Cancer Therapeutics, 17*, 1196–1206.
112. Duchi, S., et al. (2013). Mesenchymal stem cells as delivery vehicle of porphyrin loaded nanoparticles: Effective photoinduced in vitro killing of osteosarcoma. *Journal of Controlled Release, 168*, 225–237.
113. Mohr, A., & Zwacka, R. (2018). The future of mesenchymal stem cell-based therapeutic approaches for cancer – From cells to ghosts. *Cancer Letters, 414*, 239–249.
114. Timaner, M., et al. (2018). Therapy-educated mesenchymal stem cells enrich for tumor-initiating cells. *Cancer Research, 78*, 1253–1265.
115. Kang, S., et al. (2015). Mesenchymal stem cells aggregate and deliver gold nanoparticles to tumors for photothermal therapy. *ACS Nano, 9*, 9678–9690.
116. Kang, S., et al. (2017). Gold nanoparticle/graphene oxide hybrid sheets attached on mesenchymal stem cells for effective photothermal cancer therapy. *Chemistry of Materials, 29*, 3461–3476.
117. Mu, X., et al. (2018). SiRNA delivery with stem cell membrane-coated magnetic nanoparticles for imaging-guided photothermal therapy and gene therapy. *ACS Biomaterials Science & Engineering, 4*, 3895–3905.
118. Gao, J. Q., Okada, N., Mayumi, T., & Nakagawa, S. (2008). Immune cell recruitment and cell-based system for cancer therapy. *Pharmaceutical Research, 25*, 752–768.
119. Cheever, M. A., & Higano, C. S. (2011). PROVENGE (sipuleucel-T) in prostate cancer: The first FDA-approved therapeutic cancer vaccine. *Clinical Cancer Research, 17*, 3520–3526.
120. Palomba, R., et al. (2016). Biomimetic carriers mimicking leukocyte plasma membrane to increase tumor vasculature permeability. *Scientific Reports, 6*, 34422.
121. Zhang, Y., et al. (2018). Macrophage-membrane-coated nanoparticles for tumor-targeted chemotherapy. *Nano Letters, 18*, 1908–1915.
122. Cao, H., et al. (2016). Liposomes coated with isolated macrophage membrane can target lung metastasis of breast cancer. *ACS Nano, 10*, 7738–7748.
123. Cao, X., et al. (2019). Neutrophil-mimicking therapeutic nanoparticles for targeted chemotherapy of pancreatic carcinoma. *Acta Pharmaceutica Sinica B, 9*, 575–589.
124. Kang, T., et al. (2017). Nanoparticles coated with neutrophil membranes can effectively treat cancer metastasis. *ACS Nano, 11*, 1397–1411.
125. Pitchaimani, A., Nguyen, T. D. T., & Aryal, S. (2018). Natural killer cell membrane infused biomimetic liposomes for targeted tumor therapy. *Biomaterials, 160*, 124–137.
126. Meng, Q. F., et al. (2018). Macrophage membrane-coated iron oxide nanoparticles for enhanced photothermal tumor therapy. *Nanotechnology, 29*, 134004.
127. He, W., Frueh, J., Wu, Z., & He, Q. (2016). Leucocyte membrane-coated janus microcapsules for enhanced photothermal cancer treatment. *Langmuir, 32*, 3637–3644.
128. Yu, G. T., et al. (2018). Myeloid-derived suppressor cell membrane-coated magnetic nanoparticles for cancer theranostics by inducing macrophage polarization and synergizing immunogenic cell death. *Advanced Functional Materials, 28*, 1801389.
129. Zhang, L., et al. (2017). Human cytotoxic T-lymphocyte membrane-camouflaged nanoparticles combined with low-dose irradiation: A new approach to enhance drug targeting in gastric cancer. *International Journal of Nanomedicine, 12*, 2129.
130. Rao, L., et al. (2018). Platelet–leukocyte hybrid membrane-coated immunomagnetic beads for highly efficient and highly specific isolation of circulating tumor cells. *Advanced Functional Materials, 28*, 1803531.

131. Dehaini, D., et al. (2017). Erythrocyte–platelet hybrid membrane coating for enhanced nanoparticle functionalization. *Advanced Materials, 29*, 1606209.
132. Liu, Y., et al. (2018). Erythrocyte-platelet hybrid membranes coating polypyrrol nanoparticles for enhanced delivery and photothermal therapy. *Journal of Materials Chemistry B, 6*, 7033–7041.
133. He, H., et al. (2018). Leutusome: A biomimetic nanoplatform integrating plasma membrane components of leukocytes and tumor cells for remarkably enhanced solid tumor homing. *Nano Letters, 18*, 6164–6174.
134. Zelepukin, I. V., et al. (2019). Nanoparticle-based drug delivery: Via RBC-hitchhiking for the inhibition of lung metastases growth. *Nanoscale, 11*, 1636–1646.
135. Ren, X., et al. (2016). Red blood cell membrane camouflaged magnetic nanoclusters for imaging-guided photothermal therapy. *Biomaterials, 92*, 13–24.
136. Jin, J., et al. (2019). Human cancer cell membrane-coated biomimetic nanoparticles reduce fibroblast-mediated invasion and metastasis and induce T-cells. *ACS Applied Materials & Interfaces, 11*, 7850–7861.
137. Sun, H., et al. (2016). Cancer-cell-biomimetic nanoparticles for targeted therapy of homotypic tumors. *Advanced Materials, 28*, 9581–9588.
138. Chen, Z., et al. (2016). Cancer cell membrane-biomimetic nanoparticles for homologous-targeting dual-modal imaging and photothermal therapy. *ACS Nano, 10*, 10049–10057.
139. Zhang, N., Li, M., Sun, X., Jia, H., & Liu, W. (2018). NIR-responsive cancer cytomembrane-cloaked carrier-free nanosystems for highly efficient and self-targeted tumor drug delivery. *Biomaterials, 159*, 25–36.
140. Chen, M., Chen, M., & He, J. (2019). Cancer cell membrane cloaking nanoparticles for targeted co-delivery of doxorubicin and PD-L1 siRNA. *Artificial Cells, Nanomedicine, and Biotechnology, 47*, 1635–1641.
141. Xie, W., et al. (2019). Cancer cell membrane camouflaged nanoparticles to realize starvation therapy together with checkpoint blockades for enhancing cancer therapy. *ACS Nano, 13*, 2849–2857.
142. Zhao, Y., et al. (2017). Targeted delivery of doxorubicin by nano-loaded mesenchymal stem cells for lung melanoma metastases therapy. *Scientific Reports, 7*, 1–12.
143. Prabha, S., Sadhukha, T. & Layek, B. (2017). Abstract 3103: Nanoengineered mesenchymal stem cells for targeted lung cancer therapy. In 3103.
144. Wang, X., et al. (2018). Mesenchymal stem cells loaded with paclitaxel-poly(lactic-co-glycolic acid) nanoparticles for glioma-targeting therapy. *International Journal of Nanomedicine, 13*, 5231.
145. Kamalabadi-Farahani, M., et al. (2018). Anti-tumour effects of TRAIL-expressing human placental derived mesenchymal stem cells with curcumin-loaded chitosan nanoparticles in a mice model of triple negative breast cancer. *Artificial Cells, Nanomedicine, and Biotechnology, 46*, S1011–S1021.
146. Prabha, S., Moku, G., Layek, B., & Panyam, J. (2019). Abstract 3623: Mesenchymal stem cells engineered with TAT peptide functionalized nanoparticles improve therapeutic efficacy of paclitaxel in an orthotopic lung tumor model. In 3623–3623.
147. Cole, C., et al. (2005). Tumor-targeted, systemic delivery of therapeutic viral vectors using hitchhiking on antigen-specific T cells. *Nature Medicine, 11*, 1073–1081.
148. Xuan, M., Shao, J., Dai, L., He, Q., & Li, J. (2015). Macrophage cell membrane camouflaged mesoporous silica nanocapsules for in vivo cancer therapy. *Advanced Healthcare Materials, 4*, 1645–1652.
149. Rao, L., et al. (2017). Effective cancer targeting and imaging using macrophage membrane-camouflaged upconversion nanoparticles. *Journal of Biomedical Materials Research Part A, 105*, 521–530.
150. Deng, G., et al. (2018). Cell-membrane immunotherapy based on natural killer cell membrane coated nanoparticles for the effective inhibition of primary and abscopal tumor growth. *ACS Nano, 12*, 12096–12108.
151. Pitchaimani, A., et al. (2019). Biomimetic natural killer membrane camouflaged polymeric nanoparticle for targeted bioimaging. *Advanced Functional Materials, 29*, 1806817.
152. Ma, W., et al. (2020). Coating biomimetic nanoparticles with chimeric antigen receptor T cell-membrane provides high specificity for hepatocellular carcinoma photothermal therapy treatment. *Theranostics, 10*, 1281–1295.
153. Jiang, Q., et al. (2019). Erythrocyte-cancer hybrid membrane-camouflaged melanin nanoparticles for enhancing photothermal therapy efficacy in tumors. *Biomaterials, 192*, 292–308.
154. Wang, D., et al. (2018). Erythrocyte-cancer hybrid membrane camouflaged hollow copper sulfide nanoparticles for prolonged circulation life and homotypic-targeting photothermal/chemotherapy of melanoma. *ACS Nano, 12*, 5241–5252.
155. Bu, L. L., et al. (2019). Cancer stem cell-platelet hybrid membrane-coated magnetic nanoparticles for enhanced photothermal therapy of head and neck squamous cell carcinoma. *Advanced Functional Materials, 29*, 1807733.
156. Hu, X., et al. (2019). Tumor lysate-loaded lipid hybrid nanovaccine collaborated with an immune checkpoint antagonist for combination immunotherapy. *Advanced Healthcare Materials, 8*, 1800837.
157. Riley, R. S., June, C. H., Langer, R., & Mitchell, M. J. (2019). Delivery technologies for cancer immunotherapy. *Nature Reviews Drug Discovery, 18*, 175–196.
158. Bezwoda, W. R., Hesdorffer, C. S., Dansey, R. D., & Lewis, D. (1987). Treatment of hairy cell leukaemia with recombinant alpha-interferon. *South African Medical Journal, 72*, 661–662.
159. Nam, J., et al. (2019). Cancer nanomedicine for combination cancer immunotherapy. *Nature Reviews Materials, 4*, 398–414.
160. Schreiber, R. D., Old, L. J., & Smyth, M. J. (2011). Cancer immunoediting: Integrating immunity's roles in cancer suppression and promotion. *Science (80-), 331*, 1565–1570.
161. Dunn, G. P., Bruce, A. T., Ikeda, H., Old, L. J., & Schreiber, R. D. (2002). Cancer immunoediting: From immunosurveillance to tumor escape. *Nature Immunology, 3*(11), 991–998.
162. Lybaert, L., Vermaelen, K., De Geest, B. G., & Nuhn, L. (2018). Immunoengineering through cancer vaccines – A personalized and multi-step vaccine approach towards precise cancer immunity. *Journal of Controlled Release, 289*, 125–145.
163. Rosenberg, S. A. (2014). IL-2: The first effective immunotherapy for human cancer. *Journal of Immunology, 192*, 5451–5458.
164. Leclerc, M., et al. (2019). Recent advances in lung cancer immunotherapy: Input of T-cell epitopes associated with impaired peptide processing. *Frontiers in Immunology, 10*, 1505.
165. Ott, P. A., et al. (2017). An immunogenic personal neoantigen vaccine for patients with melanoma. *Nature, 547*, 217–221.
166. Schumacher, T. N., & Schreiber, R. D. (2015). Neoantigens in cancer immunotherapy. *Science (80-), 348*, 69–74.
167. Fontana, F., et al. (2019). Biohybrid vaccines for improved treatment of aggressive melanoma with checkpoint inhibitor. *ACS Nano, 13*, 6477–6490.
168. Cheung, A. S., Koshy, S. T., Stafford, A. G., Bastings, M. M. C., & Mooney, D. J. (2016). Adjuvant-loaded subcellular vesicles derived from disrupted cancer cells for cancer vaccination. *Small, 12*, 2321–2333.

169. Kim, R., Emi, M., & Tanabe, K. (2007). Cancer immunoediting: from immune surveillance to immune escape. *Immunology, 121*, 1–14.
170. Mittal, D., Gubin, M. M., Schreiber, R. D., & Smyth, M. J. (2014). New insights into cancer immunoediting and its three component phases-elimination, equilibrium and escape. *Current Opinion in Immunology, 27*, 16–25.
171. Li, P. Y., Fan, Z., & Cheng, H. (2018). Cell membrane bioconjugation and membrane-derived nanomaterials for immunotherapy. *Bioconjugate Chemistry, 29*, 624–634.
172. Guo, Y., et al. (2015). Erythrocyte membrane-enveloped polymeric nanoparticles as nanovaccine for induction of antitumor immunity against melanoma. *ACS Nano, 9*, 6918–6933.
173. Fusciello, M., et al. (2019). Artificially cloaked viral nanovaccine for cancer immunotherapy. *Nature Communications, 10*, 1–13.
174. Han, X., Wang, C., & Liu, Z. (2018). Red blood cells as smart delivery systems. *Bioconjugate Chemistry, 29*, 852–860.
175. Banz, A., Cremel, M., Rembert, A., & Godfrin, Y. (2010). In situ targeting of dendritic cells by antigen-loaded red blood cells: A novel approach to cancer immunotherapy. *Vaccine, 28*, 2965–2972.
176. Han, X., et al. (2019). Red blood cell–derived nanoerythrosome for antigen delivery with enhanced cancer immunotherapy. *Science Advances, 5*, eaaw6870.
177. Zhang, Z., et al. (2011). Induction of anti-tumor cytotoxic T cell responses through PLGA-nanoparticle mediated antigen delivery. *Biomaterials, 32*, 3666–3678.
178. Kleponis, J., Skelton, R., & Zheng, L. (2015). Fueling the engine and releasing the break: Combinational therapy of cancer vaccines and immune checkpoint inhibitors. *Cancer Biology & Medicine, 12*, 201–208.
179. Liu, W. L., et al. (2019). Expandable immunotherapeutic nanoplatforms engineered from cytomembranes of hybrid cells derived from cancer and dendritic cells. *Advanced Materials, 31*, 1900499.
180. Yang, P., et al. (2018). Engineering dendritic-cell-based vaccines and PD-1 blockade in self-assembled peptide nanofibrous hydrogel to amplify antitumor T-cell immunity. *Nano Letters, 18*, 4377–4385.
181. Morvan, M. G., & Lanier, L. L. (2016). NK cells and cancer: You can teach innate cells new tricks. *Nature Reviews. Cancer, 16*, 7.
182. Arnon, T. I., Markel, G., & Mandelboim, O. (2006). Tumor and viral recognition by natural killer cells receptors. *Seminars in Cancer Biology, 16*, 348–358.
183. Wehner, R., Dietze, K., Bachmann, M., & Schmitz, M. (2011). The bidirectional crosstalk between human dendritic cells and natural killer cells. *Journal of Innate Immunity, 3*, 258–263.
184. Bronte, V., et al. (2016). Recommendations for myeloid-derived suppressor cell nomenclature and characterization standards. *Nature Communications, 7*, 1–10.
185. Marvel, D., & Gabrilovich, D. I. (2015). Myeloid-derived suppressor cells in the tumor microenvironment: Expect the unexpected. *The Journal of Clinical Investigation, 125*, 3356–3364.
186. Kun, Z., et al. (2019). Tumor derived EDIL3 modulates the expansion and osteoclastogenesis of myeloid derived suppressor cells in murine breast cancer model. *Journal of Bone Oncology, 16*, 100238.
187. Mazzarella, L., et al. (2019). The evolving landscape of 'next-generation' immune checkpoint inhibitors: A review. *European Journal of Cancer, 117*, 14–31.
188. Koyama, S., et al. (2016). Adaptive resistance to therapeutic PD-1 blockade is associated with upregulation of alternative immune checkpoints. *Nature Communications, 7*, 1–9.

Electrospun Nanofibers for Cancer Therapy

Huanhuan Luo, Tianyang Jie, Li Zheng,
Chenglong Huang, Gang Chen, and Wenguo Cui

Abstract

Lately, a remarkable progress has been recorded in the field of electrospinning for the preparation of numerous types of nanofiber scaffolds. These scaffolds present some remarkable features including high loading capacity and encapsulation efficiency, superficial area and porosity, potential for modification, structure for the co-delivery of various therapies, and cost-effectiveness. Their present and future applications for cancer diagnosis and treatment are promising and pioneering. In this chapter we provide a comprehensive overview of electrospun nanofibers (ESNFs) applications in cancer diagnosis and treatment, covering diverse types of drug-loaded electrospun nanofibers.

Keywords

Electrospun fibers · Drug carrier · Cancer diagnosis · Cell capture · Biosensors · Chemosensors · Gas sensors · Immunosensor · Intelligent cancer therapy · Switchable drug release · Immunotherapy · Synergistic therapy

1 Introduction

Cancer is the deadliest disease yet to be cured by humans so far, despite the researches of its treatment technologies being widely supported by funding agencies. Currently, surgery and radiotherapy are still the most commonly used methods for the treatment of non-metastatic and local tumors, while chemotherapy and targeted drugs are the main strategies for the treatment of metastatic and recurrent cancers.

Chemotherapy is the predetermined treatment strategy for most cancer; it is highly toxic to most cancer cells and therefore shows with a relatively high therapeutic efficacy [1]. However, chemotherapeutic drugs have also a series of downsides [2, 3]. In order to overcome these shortcomings, drug delivery systems (DDS) have been widely explored. Typically, DDSs are able to deliver the drugs in a more controlled manner (release time and rate) and allow the drug concentration to be maintained at a level within the effective therapeutic window. Researchers have made a lot of efforts to improve blood circulation and the stability and delivery efficacy of drug delivery systems.

Typically, microparticles [4–6], micelles [7–9], and liposomes [10, 11] have been the most important particle forms of the systemic DDSs (SDDSs). The diameter of the gap between vascular endothelial cells in tumor tissue is larger than in normal tissue, leading to the extravasation of nanoscale particles in the blood circulation, according to the enhanced permeation and retention (EPR) phenomenon [12, 13]. However, the EPR effect has not been proven yet in

---

H. Luo
Shanghai Institute of Traumatology and Orthopaedics, Shanghai Key Laboratory for Prevention and Treatment of Bone and Joint Diseases, Ruijin Hospital, Shanghai Jiao Tong University School of Medicine, Shanghai, China

Jiaxing Key Laboratory of Basic Research and Clinical Translation on Orthopedic Biomaterials, Department of Orthopaedics, The Second Affiliated Hospital of Jiaxing University, Jiaxing, China

T. Jie · W. Cui (✉)
Shanghai Institute of Traumatology and Orthopaedics, Shanghai Key Laboratory for Prevention and Treatment of Bone and Joint Diseases, Ruijin Hospital, Shanghai Jiao Tong University School of Medicine, Shanghai, China

L. Zheng
The central laboratory, The Second Affiliated Hospital of Jiaxing University, Jiaxing, China

C. Huang · G. Chen
Jiaxing Key Laboratory of Basic Research and Clinical Translation on Orthopedic Biomaterials, Department of Orthopaedics, The Second Affiliated Hospital of Jiaxing University, Jiaxing, China

© Springer Nature Switzerland AG 2021
F. Fontana, H. A. Santos (eds.), *Bio-Nanomedicine for Cancer Therapy*, Advances in Experimental Medicine and Biology 1295, https://doi.org/10.1007/978-3-030-58174-9_8

clinical trials of several nanoparticles. The particle size able to exploit EPR to extravasate is in the range between 30 and 200 nm [14].

Nevertheless, anticancer drugs usually circulate around the body in SDDSs [15]. Thereby, a maximum concentration of the drug is reached right after administration and then rapidly cleared by the biological system, which ultimately leads to limitations in the therapeutic effect and significant toxic side effects [16]. Unfortunately, although great efforts have been made by the researchers to avoid excessive distribution in the normal tissues [17], data from the last decade still show that the DDSs' delivery efficiency to tumors was as low as 0.7% (median). Therefore, it is necessary to explore new drug delivery vehicles with different mechanistic principles to improve the delivery efficiency while reducing toxicity and achieving better drug release management.

Local DDSs (LDDSs), whose development began in the 1960s, ensured a certain degree of therapeutic efficiency when a system made of silicone rubber combined with a therapeutic agent was implanted [18]. The drug-loading system implanted into the tumor allowed local drug delivery, avoiding excessive circulation of the drug in the body, thereby limiting its systemic toxic and side effects. The therapeutic dose could be maintained inside the tumor site while ensuring a low concentration of the systemic drugs.

With the advantage of improving the anticancer efficacy while avoiding repeated administrations [19–21], LDDSs have many potential applications in cancer treatment. The first application is in cancer patients whose treatment status is not ideal, such as patients with multiple diseases and elderly patients. In this case, anticancer drug can be loaded within the LDDSs and be implanted into the tumor tissue by a minimally invasive surgery and positioned assisted by the imaging system. The second application is the treatment of malignant tumors such as pancreatic cancer, which is possibly locally infiltrated or systemically disseminated and cannot be readily resected surgically. In this case, therapeutic agents can be delivered from the implanted site to the metastasis tumor through blood and lymphatic circulation and thus efficiently inhibit the cell proliferation and kill tumor cells. The third application is to prevent possible cancer recurrence and eliminate residual cancer cells by implanting the drug-loaded LDDSs into the postoperative cavity site. Therefore, such platforms have gradually been recognized as a promising candidate to address current issues related to DDSs for cancer therapy.

Various forms of LDDSs have been fabricated, such as gels, drug-eluting wafers, films, and rods [21]. In particular, nanofibers synthesized by electrospinning have exhibited unique properties, such as high surface area [22], compatible microstructure [23], various matrix materials [24], and high porosity. These characteristics could promote proliferation, cell adhesion, mass transport properties, and drug delivery [25]. Thereby, these remarkable structure-related characteristics represent an optimal potential for application in cancer therapy. Moreover, the development of advanced electrospinning technology has also provided a new way for the loading and release of insoluble drugs.

Electrospinning is an ideal technology to develop small diameter fibers with a diameter in the range between several nanometers and micrometers. The electrostatic force production of fibers began in the 1930s, after which the electrospinning process has been widely used in many engineering fields, including filtration [26–28], fabrics/masks [29, 30], sensors [31, 32], and energy-related applications [33]. A comprehensive overview of the process of electrospinning and its application in tissue engineering and drug delivery can be found in other works [34–43]. In this chapter, we present a comprehensive overview of electrospun nanofibers for cancer applications, including different types of drug-loaded nanofibers, and their use in the diagnosis and treatment of cancer.

2 Drug-Loaded Electrospun Nanofibers for Cancer Therapy

Electrospun nanofibers for drug delivery were firstly described by Kenawy et al. in 2002 [43]. From then on, electron nanofiber membranes have been regarded as carriers for the delivery of diverse drugs, thanks to their advantageous features including ease of drug incorporation during electrospinning, high superficial area-to-volume ratio, porous and interconnected architecture, and flexibility in material properties which derive from the versatility in polymer composition, allowing for an enhanced control over the drug release profiles [39]. Up to date, the different types of drugs incorporated into the electrospun nanofibers ranged from small molecule drugs to large biomacromolecules such as antibiotics, proteins, DNA, siRNA, and oligo-/polypeptides. Here, we introduce several typical electrospun fibers aimed at cancer therapy.

2.1 Oil-Soluble Drug-Loaded Electrospun Fibers

The majority of small molecule antitumor drugs are hydrophobic, so oil-soluble drug-loaded electrospun fibers are widely reported in cancer therapy [44, 45], due to their remarkable strengths including high operating efficiency, reduced toxicity, and improved therapeutic effect [46].

Zeng et al. [47] studied the influence of surfactants and anticancer drugs on the diameter and uniformity of electron PLLA fibers. Different types of anticancer drugs including doxorubicin hydrochloride (Dox) and paclitaxel (PTX) were also studied. The results indicated that the anticancer drugs were encapsulated inside the nanofibers and their release in the presence of proteinase K followed zero-order kinetics controlled from the degradation of the PLLA nanofibers.

Moreover, Zeng et al. [48] demonstrated the influence of solubility and compatibility of the drugs in the drug-polymer system. The results showed that PLLA has good compatibility with both Dox and PTX.

Electrospun amphiphilic PEG-PLLA diblock copolymer fiber mats containing Dox were successfully prepared using water-in-oil emulsion electrospinning [49]. Compared with the suspension electrospun fiber mats, the emulsion-electrospun fiber mats display better continuous release of Dox.

The long-term delivery of 1,3-bis(2-chloroethyl)-1-nitrosourea (BCNU), one of the most extensively used antineoplastic agents for the treatment of malignant gliomas [50], was assayed by Xu et al. through the fabrication of an electrospun-biodegradable PEG-PLLA diblock copolymer fiber carrier [51]. The results indicated that the BCNU/PEG-PLLA fibers have a significant effect on controlling the release of BCNU and are appropriate for postoperative chemotherapy on cancers. A variety of applications of the oil-soluble nanofibers in cancer drug delivery and therapy are discussed in Table 1.

2.2 Water-Soluble Drug-Loaded Electrospun Fibers

Although a wide variety of agents can be incorporated into electrospun fibers [60], most examples of sustained drug release up to at least 7 days have been primarily limited to small hydrophobic molecule drugs or large biological macromolecules, which are more amenable to sustained release owing to their poor solubility, large size, and preferential partitioning into insoluble polymers. In contrast, small hydrophilic molecule drugs face a major challenge in sustain release because of their high solubility within the release media, poor partitioning, and low solubility in a couple of polymers that are hydrophobic. The drug-polymer compatibility can be correlated with the ability to fully encapsulate drugs and accomplish sustained release. Small hydrophilic molecule drugs, which have low solubility within a nonpolar solvent-polymer system, will more likely partition to the fiber surface and result in uncontrolled release.

The majority of the studies investigating small hydrophilic molecule drug loaded and released from electrospun fibers have focused on antibiotics and some antiviral compounds (Table 2). However, the sustained release of drug molecules from the nanofibers could represent an effective treatment for cancer tharapy [61–64]. The physicochemical diversity of small molecule drugs with respect to parameters such as aqueous solubility, partition coefficient, ionization and pKa, molecular dipole, glass transition, and melt temperature is an important factor that will contribute to its interaction with the solvent and polymer in both solution and the final solid dispersion [65]. Also, the use of model hydrophilic compounds to extrapolate structure-function relationships between the fiber formulation characteristics and the drug release kinetics should be interpreted with caution. For example, a recent study by Carson et al. [66] demonstrated the ability to tune the release of tenofovir, using PCL/PLGA electrospun fibers. The study suggests a relationship between the concentration of PCL/PLGA and the release behavior of tenofovir. The aim is to generalize the PCL/PLGA electrospun fiber platform for other small hydrophilic molecule drugs. However, the release of azidothymidine, maraviroc, raltegravir, and tenofovir disoproxil fumarate was much faster compared to tenofovir when using equivalent PCL/PLGA fiber formulations. These results suggest that even slight differences in the chemical structures of these compounds compared to tenofovir can affect release rates. Therefore, in order to have a deeper understanding of the interaction between the drug, polymer, and solvent in electrospun process, the access to new compounds is essential.

The large drug concentration needed for clinical applications that require high daily dosing (10–100 mg/dose) presents further challenges for a sustained drug release from the

Table 1 Various nanofibers for cancer therapy

Materials	Antitumor drug	Cancer cells	Functions	Ref
PLA	Dichloroacetate	Cervical carcinoma	Reduce tumor volume	[52]
Chitosan nanofibers with hyaluronic acid	PTX	Prostate cancer cells	Inhibit the proliferation of tumors	[53]
PCL/MWCNT	Green tea polyphenol	Hepatocellular carcinoma	High antitumor effect	[54]
PLLA	Titanocene dichloride	Lung tumor cells	Inhibitory activity	[55]
PEG-PLA	Hydroxycamptothecin	MCF-7 cells	High inhibitory activity	[56]
Peptide nanofibers	Self-assembling peptides	Breast cancer cells	Phenotypic reversion	[57]
PLA nanofiber mats	Different	Hepatocellular carcinoma	Local chemotherapy	[58]
PEG-PCL/folate	Hydrophobic doxorubicin	4T1 cells	Efficient and safe	[59]

PLA polylactic acid, *PTX* paclitaxel, *PCL* polycaprolactone, *MWCNT* multi-walled carbon nanotube, *PLLA* poly(L-lactide), *PEG* polyethylene glycol, *MCF-7 cells* human breast cancer cell, *4T1 cells* mouse breast cancer cells

Table 2 Drug release behavior from different electrospun nanofibers

	Drugs			Release (units)			References
Materials	Name	Loading wt.%	1 h	24 h	7d	14d	
Uniaxial fibers							
PLGA	PTX	10	10%	22%	40%	50%	[67]
	Cefoxitin	5	70%	72%	80%	–	[68]
PLA	Tetracycline	5	35%	35%	35%	–	[43]
	Metronidazole	40	5%	25%	45%	–	[69]
	Amoxicillin	7	10%	15%	20%	20%	[70]
PLLA	PTX	15	0–1%	0–1%	–	–	[48]
	DOX hydrochloride	1.6	70%	87%	–	–	[48]
	DOX	1.6	20%	20%	–	–	[48]
Polyurethane	Itraconazole	40	2 μg/cm^2	20 μg/cm^2	–	–	[71]
	Ketanserin	10	2 μg/cm^2	10 μg/cm^2	–	–	[71]
Coaxial fibers							
PEG/PBS	Triclosan	5	75%	–	–	–	[72]
	Curcumin	5	90%	–	–	–	[72]
Different concentrations of zein	Ketoprofen	10	5%	100%	–	–	[73]
PCL/gelatin	Metronidazole	33.4	5%	60%	95%	100%	[74]
PCL/PVA	Metoclopramide hydrochloride	1	5%	55%	65%	68%	[75]
PLLA/PVA	Metoclopramide hydrochloride	1	2%	12%	22%	25%	[75]
PLGA/PVA	Metoclopramide hydrochloride	1	5%	38%	62%	72%	[75]
PCL/PEG	Salicylic acid	10	10%	25%	40%	–	[76]
PEG/PLA	Salicylic acid	15	0.1 mg/ml	0.2 mg/ml	–	–	[76]
PEG/cellulose acetate /gelatin	Amoxicillin	3.7	22%	100%	–	–	[77]
PMMA/nylon 6	Ampicillin	20	100 μg/ml	300 μg/ml	600 μg/ml	800 μg/ml	[78]

PLGA poly(lactic-co-glycolic acid), *PVA* polyvinyl alcohol, *PMMA* poly(methyl methacrylate)

fibers. A higher drug loading often results in increased burst release due to larger amounts of surface-associated drug and the high superficial area of fibers. In fact, the sustained release of small molecule drugs from fibers has been typically performed with low drug loading (below 1 wt.%), which limits the clinical applications for treating and preventing many bacterial and viral infections. For example, Ball et al. [79] fabricated nanofibers evaluating different biodegradable polymers for sustained release. In their studies, several microbicides such as maraviroc, azidothymidine, acyclovir, and glycerol monolaurate were all successfully incorporated into nanofibers without any toxicity to various cells. Although the nanofibers provided sustained release for some of agents abovementioned, they were all loaded at only 1 wt.%, which is not clinically relevant for the proposed applications. In a separate example for the same clinical purpose, Huang et al. [80] loaded tenofovir disoproxil fumarate, a water-soluble antiretroviral prodrug, into fibers electrospun from a polymer which would undergo dissolution in response to the pH change induced by semen. However, none of them demonstrated sustained release of the prodrug or provided any analytical data to describe the solid drug dispersion in the final fibers.

2.3 Protein-Loaded Electrospun Nanofibers

Growth factors (GF) are a group of endogenous proteins having the ability to bind cell surface receptors and promote cellular activities resulting in the regeneration of new tissue [81]. Delivery of exogenous GFs to the tissue of interest is recommended to be an effective therapy for the healing process and tissue production [82].

Chew et al. studied the possibility of encapsulating human b-nerve growth factor (NGF) in a copolymer of ethyl ethylene phosphate and e-caprolactone [83]. Consequently, a continuous release of NGF by diffusion can last for at least 3 months.

Patel et al. studied the effects of immobilizing basic fibroblast growth factor (bFGF) onto nanofibers on neurite extension in vitro in one study [84], while the bFGF was in a soluble manner. In this study, the conjugated nanofibers presented two advantages. One is that the electrospun fibrous scaffolds can function as a delivery vehicle for specific targets without inducing systemic effects. The other is that only a small amount of bFGF is required to achieve its effects, which is similar to those achieved with soluble bFGF in medium.

Sahoo et al. introduced two types of PLGA nanofiber scaffolds integrated with bFGF. Some nanofibers are produced using the easy method of electrospinning and blending (group I) or by the more complex method of coaxial electrospinning (group II) [85]. Although both scaffold groups result in bone marrow stem cell (BMSC) attachment and consequent proliferation, cells cultured on group I revealed amplified collagen construction and upregulated gene expression of specific extracellular matrix (ECM) proteins, representative of fibroblastic differentiation. The results of the study illustrate that the electrospinning method could be used to extend the growth factor release from scaffolds. Important applications of nanofibers in growth factor delivery are listed in Table 3.

2.4 Gene-Loaded Electrospun Fibers

At present, the most popular treatments for cancer therapy are chemotherapy and its combination. However, side effect is one of the major problems in cancer chemotherapy, which would give a fatal damage to other healthy cells [92]. Gene delivery has become a significant technology in biomedical application, including stem cell therapy, cancer therapy, and tissue engineering. Plenty of goals can be achieved by the external stimulus of the targeted cells, such as the differentiation of the targeted cells to the desired cells, such as liver cells or other types of cells [93–95], the activation of apoptosis signal of cancer cells [96, 97], the generation of cellular factors from tissues [98, 99], and the production of cellular therapeutics [100]. Each of the functions of gene delivery is essential and may provide the promising strategies for curing an illness. When a gene malfunction results in a faulty protein, gene therapy can introduce a new specific gene to recuperate the function of that protein by modifying the signal transduction pathway [101]. Researchers are using vectors as their carriers now, due to difficulties correlated with the direct implantation of DNA or RNA into the target cell. And the vectors consist of viral and non-viral vectors. In order to deliver the DNA into the cells, viral vectors are usually modified by nucleic acids. However, different viral vectors are used in different types of gene or tissue. Sometimes, even a very small gene can cause mutation. On the other hand, non-viral vectors are more welcomed because of their big porosity and surface area, controlled toxicity, and the ability to deliver various kinds of genes [102]. Even though some problems associated with electrospun nanofiber scaffolds, such as the inappropriate nucleic acid encapsulation and low transfection efficiency, are still unsolved, nanofiber scaffolds are widely used as non-viral carriers. Several attempts, such as the core/shell, surface modification, coating, encapsulation, incorporation, and interfacing electrostatic interaction, have been investigated to protect the nucleic acid [103–128].

Electrospun nanofibers have been widely used as templates in monitoring the structure and function of extracellular matrices (ECMs), to protect the cellular morphology and deliver molecules to the targeted cells [41, 129]. Therefore, electrospun nanofibers could be widely used in many biomedical applications, including drug or gene delivery and tissue engineering [130]. Highly porous structures of nanofibers have been extensively used as powerful templates in a temporally or spatially regulated way for delivering the intended gene [41, 129, 130] for many purposes, such as tissue engineering, cancer therapy, and stem cell study. Non-viral gene vectors have been mainly introduced into electrospun nanofibers, because they are easier to produce and obtain the ability to maintain integrity [112, 118, 124]. In order to improve the efficiency of gene delivery and prolong the continuous time of gene expression, the viral vectors produced by the combination of the intended gene with viral capsid have been loaded within electrospun nanofibers [88, 111, 131].

Nanofibers represent a potential strategy for cancer therapy to silence the gene expression by delivering small-interfering RNA (siRNA). The delivery of siRNA has been studied in systems such as the encapsulation of microsphere and nanoparticle composition [132, 133]. Although it showed great transfection efficiency and cellular response, it was limited in biomedical application due to its transient effect. Electrospun nanofibers may serve in a potential siRNA delivery, because they can provide a sustained delivery to tumor. It is a report that Rujitanaroj and co-workers identified the feasibility of introducing the siRNA and transfection reagent into nanofibers, which showed a sustained drug release for 28 days and a high efficacy of gene knockout [122]. They introduced plasmid DNA connecting with cell cycle special protein Cdk2 and encoding shRNA into the

Table 3 Different nanofibers used for the delivery of gene

Types of nanofibers	Gene	Cell/tissues	Functions	Ref
CS/PVA nanofibers	Nerve GF	SKNMC cells and U373 cells	Improve the proliferation	[86]
Polyelectrolyte complex	Fibroblast GF	Ovine bone stem cells	Exhibit mitogenic activity	[87]
Polyelectrolyte complex	Angiogenic GF	Skeletal myoblasts isolated	Increase network infiltration	[88]
PLCL nanofibers	VEGF	Pig iliac endothelial cells	Promote proliferation	[89]
PCL nanofiber mesh	Recombinant VEGF	Rat liver	Improve rat liver regeneration	[90]
Biopolymer nanofibers	Fibroblast GF	Rat mesenchymal stem cells	Improve proliferation	[91]

PCL nanofibers [134]. The electrospun nanofibers carrying DNA can deliver the intact and bioactive plasmid DNA for more than 21 days, resulting in 40% decrease proliferation of MCF-7 cells. Stem cells can be used for cancer therapy. Human mesenchymal stem cells can be genetically modified for secreting more effective antitumor agent, such as the apoptosis-inducing ligand related to tumor necrosis factor [135]. Glioblastoma is predicted to be treated by the engineered stem cells. Similar to the traditional stem cell therapy for regenerative medicine, retaining the engineering stem cells in operating cavity is a huge challenge after resecting the glioblastoma. In order to solve this problem, Bago and Pegna et al. [136] designed TRAIL secreting stem cells seeded on the PLA electrospun nanofibers, which could release antitumor protein TRAIL. The results showed that it could control the growth of the glioblastoma left and prolonged the median living time after implanting surgery.

However, the nanofibers could protect the encapsulated DNA from denaturation or degradation and also prolong their release for several months. In a study, the researchers used the copolymer nanofibers consisting of PLGA and PEG-PDLA (poly(ethylene glycol)-poly(D,L-lactide)) as the carriers to deliver plasmid DNA [115]. The release of the plasmid DNA from these promising nanofiber scaffolds can be controlled over 20 h, with a burst release appearing within 2 h. The plasmid DNA released from it showed a higher transfection efficiency and specific protein encoding properties. In another study, various fiber mesh scaffolds were designed and processed by the coaxial electrospinning method. The scaffolds contained the plasmid DNA and a non-viral gene delivery vector inserted both in the core of poly(ethyleneimine)-hyaluronic acid and in the sheath of poly(ethylene) glycol and poly(caprolactone) of the fiber scaffolds. The non-viral vector and plasmid DNA were gradually released from the scaffolds for more than 2 months, increasing the transfection efficiency [124]. Although nanofibers have been modified to protect the encapsulated plasmid, mixing the plasmid and spinning solution alone does not protect it well. As a consequence, the plasmid DNA will be unevenly distributed inside the nanofiber fibers, resulting in slow drug release. Therefore, modifying the surface with cationic polymers may solve these problems. Kim and Yoo et al. prepared DNA-loaded modified nanofibers for the delivery of epidermal gene and controlled release response to matrix metalloproteinases (MMPs). Here, they used MMP-responsive linker connecting the polymer PEG-PCL with linear polyethylenimine (LPEI). When the responsive linker met the MMPs, they will be broken to release the DNA-loaded polymers [109]. And the results showed that over 80% DNA and LPEI could be released from the nanofibers over a period of 72 hours.

Nowadays, the materials for preparing nanofibers are mainly divided into natural polymers and synthetic polymers. In order to successfully deliver genetic material to a target location, researchers also have mixed natural and synthetic polymers to make better fibers. Recently, nanofibers for siRNA delivery have attracted wide attention because of their ability to silence the expression of the specific gene, which is able to develop genetic mutations, resulting in excess cell proliferation that may lead to cancer. To date, siRNA can be delivered into the cell by various electrospun nanofiber scaffolds. As the siRNA delivery scaffolds, PCL nanofibers could help siRNA have a higher loading efficiency and cellular transfection, lower toxicity, and better gene silencing property [103, 105, 114].

Peptide-based nanofiber scaffolds have also been used as a siRNA nanocarrier targeting neurodegenerative disease. The siRNA is able to be released and accumulated in the targeted brain region, which is hopeful for the gene silence and genetic intervention [116]. In addition, scientists first proposed a siRNA delivery system based on zein nanofibers with high loading efficiency and sufficient release of siRNA. Moreover, this zein-based electrospun nanofiber can preserve the efficiency of siRNA successfully [108]. Various nanofibers, other than PCL, such as PEG (polyethylene glycol), PCLEEP (poly(Ɛ-caprolactone-co-ethyl ethylene phosphate)), ZnGa2O4:Cr (chromium-doped zinc gallate), P-G3A3KRK (palmitoyl-GGGAAAKRK peptide), zein, PECL (poly(Ɛ-caprolactone)), PEG-b-P4VP ((poly(ethylene glycol)-b-poly(4-vinylpyridine)), PLGA (poly(lactide-co-glycolide)), LPEI (linear polyethylenimine), ELP (elastin-like polypeptides), PDLLA (poly(D,L-lactide)), and many more are used as a nucleic acid carrier [104, 108, 116, 119–122].

2.5 Other Drug-Loaded Electrospun Nanofibers

Traditional therapeutic practices have been the focus of some practical repurposing in the absence of approved alternative treatment methods. Similar to the novel therapeutic platforms highlighted in the review, the systemic administration of chemotherapeutic drugs has, unsuccessfully, tried to improve delivery efficiencies by incorporating cancer-targeting moiety. A median of only 0.7% of the injected chemotherapeutic agents reach solid tumors upon systemic administration, according to a recent 10-year-long literature survey [128]. Examples of improved systemic treatment using combinatorial chemotherapy and photodynamic therapy nanohybrids [137] or synergistic nanoparticle/chemotherapeutic drug hybrids have been reported [138]; however, interests have changed from the systemic administration to local methods. Electrospun nanofibers may mitigate the current problems with systemic administration; but several obstacles still remain before electrospun nanofiber DDS transition to clinical trials. The essential ones are the potential hazard of residual solvent from the manufacturing process, secondary removal surgery of nonbiodegradable scaffolds, and the biological challenge of foreign-body administration [139]. As the mechanisms involved in hindering systemic drug delivery become better understood, functional ESNF, out-of-the-box DDSs, may be formulated to address these limitations [140]. For instance, active-targeting micelles have been encapsulated in core/shell NFs by coaxially electrospinning micelle-doped poly(vinyl alcohol)/cross-linked gelatin. Compared with the traditional administration of micelles for cancer treatment, the implantable doxorubicin micelle-loaded NF reduced the frequency of administration while retaining high effect against solid tumors [59]. More recently, an implantable hierarchical structured fiber device developed via microfluidic electrospinning could synergistically co-deliver doxorubicin (DOX)-loaded micelles, encapsulated within ESNFs, with the tyrosine kinase inhibitor apatinib (AP), loaded into the ENSF's matrix [141]. This system aims to inhibit P-glycoprotein (P-gp), an ATP-dependent efflux pump, by preventing the overexpression of the protein to overcome multiple drug resistance (MDR). The device was implanted in nude mice bearing multidrug-resistant human mammary adenocarcinoma (MCF-7/Adr) tumors. The sustained release of AP inhibited the P-pg efflux pump continuously, allowing an increased intracellular uptake of DOX. The system presented low systemic toxicity and significantly decreased tumor volumes in comparison to the single drug ESNFs and the intravenously injected mice.

3 Functional Electrospun Nanofibers for Cancer Diagnosis

3.1 Electrospun Nanofibers for Cancer Cell Capture

Electrospun nanofibers present some remarkable features of superficial area and porosity, good biocompatibility, easy preparation and modification, and potential for mimicking natural extracellular matrix. Therefore, they are also widely used in cancer cell capture [142].

3.1.1 Static Cancer Cell Capture

Nanofibers have unique advantages, especially the surface fixation of targeting molecules, enabling the effective and specific capture of cancer cells [142]. Static cancer cell capture refers in particular to the capture of cancer cells using nanofibers under static conditions, including static, mixed, or shaking incubation and blending separation. In general, by incubating nanofibers with blood samples or cell suspensions containing cancer cells for a certain time under static condition, cancer cells attach onto the surface of nanofibers by the interaction with the topographic features of nanofibers and/or the fixed targeting molecules. The nanofibers are then rinsed to remove non-specifically attached blood cells or other cells, leaving the attached cancer cells onto the nanofibers for further analysis.

In a recent study by Zhao et al. [143], HA-modified PVA/PEI nanofibers were prepared (Fig. 1) and applied for cancer cell capture. Suspended HeLa or U87MG cells were incubated with nanofibrous mats in culture medium at 37 °C, 5% CO_2 with a time gradient (10–240 min). By cell counting, scanning electron microscopy (SEM), and qualitative confocal microscopy observation, it was found that the capture efficiency of HA-PVA/PEI-Ac nanofibers to HeLa cells reached 85.0% at 240 min, much higher than PVA/PEI-Ac nanofibers without HA modification. As for U87MG cells (not expressing the CD44 receptor), the capture efficiencies of HA-PVA/PEI-Ac nanofibers and PVA/PEI-Ac nanofibers at the same time points were very close, indicating that HA modification made PVA/PEI nanofibers have specific capture capabilities for cancer cells overexpressing the CD44 receptor. In addition, cellulose acetate (CA) fiber pads modified by folic acid (FA) were cut into 14-mm-diameter circles and placed into a 24-well plate. Subsequently, KB cells overexpressing FA receptor were seeded onto the plate at a density of 5×10^4 cells per well and incubated at 5% CO_2 and 37 °C for a 10–60-minute time gradient. The results showed that KB cells could be captured by FA-modified CA nanofibers with a maximum efficiency of 82.7% at 60 min [143, 144]. In another work by Wang et al. [145], FA-functionalized ɣ-PGA (ɣ-PGA-G2·NH_2-FA NFs) nanofibers were reported to be capable of specifically capturing KB cells through ligand-receptor interactions.

Another work (Fig. 2a) reported that a trap effect of 3D optical fiber network was proposed to capture cancer cells efficiently [142]. Static cell capture experiments were conducted to compare the cancer cell capture function of a smooth PS substrate modified with anti-EpCAM antibody and three other types of 3D fibrous interfaces (nanofibers (NF), microfibers (MF), nanofiber/microbead composites (NFs/MBs)). After incubation for 30 minutes in MCF7 cell suspension, the 3D fibrous interfaces showed a capture efficiency of 67.1–82.2%; however, less than 40.0% of MCF7 cells were captured by the anti-EpCAM-modified smooth PS substrate. The results suggested that 3D fibrous interfaces could significantly improve the capture efficiency of cancer cells, probably due to the efficient capture effect of the 3D fibrous interface (Fig. 2b). For both EpCAM-positive cell lines (MCF7, PC3) and EpCAM-negative cell lines (Daudi, Jurkat, and HeLa), the 3D fibrous network showed high capture efficiency and specificity (shown in Fig. 2b), indicating the great capacity to capture different cell lines. Moreover, in clinical applications, a capture efficiency of 52–63% for

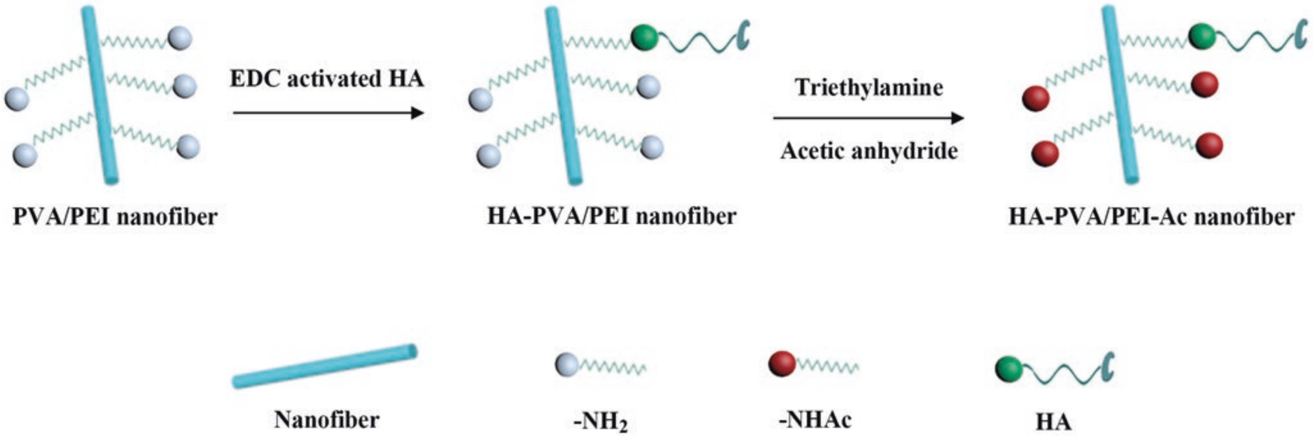

Fig. 1 The preparation of HA-PVA/PEI-Ac nanofibers

spiked MCF7 cells was obtained from whole blood with a 30-minute incubation, indicating the great potential of 3D fibrous interfaces in capturing rare circulating tumor cells (CTCs).

EpCAM-immobilized TiO2 nanofibers (TiNFs) on a silicon substrate were prepared by Zhang et al. with the inorganic nanofibers as the capture substrates [146]. In this work, four cancer cell lines were used, two EpCAM-positive(gastric carcinoma cell line BGC823 and colorectal cancer cell line HCT116) and two EpCAM-negative (chronic myelogenous leukemia cell line K562 and cervical cancer cell line HeLa). The cell lines were used in static cell capture assays to optimize the incubation time and TiNF packing density. Furthermore, to test the clinical applicability of TiNFs, peripheral blood samples from gastric and colorectal cancer patients were used to identify and count CTCs via a generally used tricolor immunocytochemistry method. As for the cell lines, over 45% of spiked HCT116 cells were recovered from the artificial blood samples, while for clinical utility estimation, 0 to 19 CTCs per 0.5 mL blood sample were detected in 7 of 7 gastric cancer patients and 2 of 3 colorectal cancer patients.

Additionally, antibody-immobilized lipid nanofibers were also reported for the capture of lymphoma Granta-22 cells (human mantle cell lymphoma) [147, 148]. Nanofibers modified with anti-CD20 were incubated for 45 min in the suspension of Granta-22 cells, and the captured cells were observed under microscope after being stained with DAPI (40,6-diamidino-2-phenylindole). The results indicated that anti-CD20 immobilization increased the ability of nanofibers to efficiently capture Granta-22 cells. Furthermore, SEM analysis showed that the fibers had the ability to wrap or bury the cancer cells, which might be another important factor in enhancing cell capture in addition to the specific function of antibody.

In a recent study, with the help of poly(carboxybetaine methacrylate) (pCBMA), EpCAM-positive cancer cells were captured using DNA aptamer-modified chitosan nanofibers (CNFs) [149]. After incubation for 50 minutes, the capture efficiency of the human gastric cancer cell line used in this study (Kato III cells) on the aptamer-modified CNFs was as high as 96%, suggesting the great efficiency of the nanostructures of CNFs for cancer cell capture. Additionally, the surface capture effects of naked, pCBMA-coated, and pCBMA-aptamer-coated CNF surfaces were compared, and the results showed that CNFs can effectively inhibit the nonspecific cell adhesion. The clinical application study also revealed that chitosan nanofibers with DNA aptamer had a high capacity of capturing the Kato III cells in whole blood, with more than 1% purity.

Different from the static cells captured by solid fibrous mats described above, ethanol-dispersed nanofibers were also reported to capture EpCAM-positive cancer cells from whole blood or cell culture medium and finally established 3D models [150]. When the cell density is in the range 10–1,000,000 cells/10 m mL, the capture efficiency was 59–67%. In particular, the captured cells could be directly cultured in the ethanol-dispersed nanofibers to form cancer cell clones, indicating the potential use of anti-EpCAM-modified nanofibers in the future.

3.1.2 Dynamic Cancer Cell Capture

For the capture of CTCs, static capture cannot meet the requirements of high-efficiency, high-velocity, and high-sensitivity detection of CTCs because of the specific receptors expressed on the surface of different CTCs and the uneven physical characteristics. The combination of various technologies, especially the application of microfluidic technology for CTC capture and analysis, has attracted wide attention [151]. The geometry size of the microfluidic channel matches the shape and size of the cell quite well. Therefore, by controlling the flow field around cells or by cutting the microstructure of the microfluidic channel, various operations can be performed. In addition, microfluidic

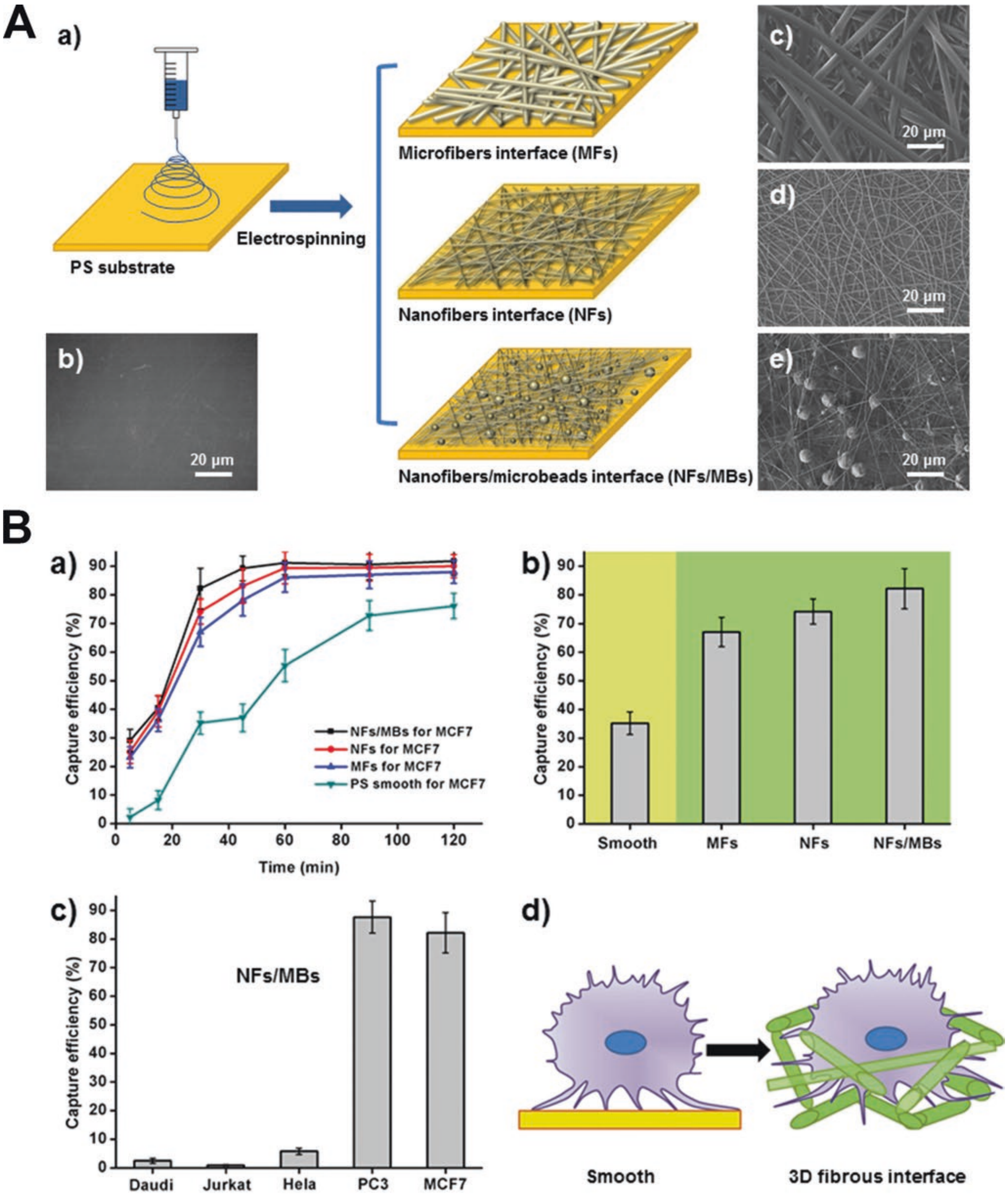

Fig. 2 (**a**) (a) Fabrication of the different types of nanofibers. (b) SEM image of the smooth PS substrate. (c) SEM image of MFs. (d) SEM image of NFs. (e) SEM image of NFs/MBs. (**b**) Capture efficiency of different groups. (a) Different groups of nanofibers at different incubation times. (b) The capture efficiency of MCF7 after incubation for 30 min. (c) Cell capture efficiency of different cells in NFs/MBs. (d) Schematic illustration of the cancer cell capture. (Reprinted with the permission from Ref. [142])

chip has become the most ideal tool for the isolation of CTCs from blood because of its advantages such as small sample demand, small size, and accurate operation [152, 153]. Therefore, the dynamic capture of cancer cells by nanofiber combined with microfluidics chips has been proposed. Cancer cells contained in blood samples or cell suspensions can be captured dynamically by nanofiber-integrated microfluidic chips. Through the interaction with the fiber matrix, cancer cells can be captured on nanofiber mats, while other cells or blood cells that are not captured can flow out from other channels in the chip, determining the separation of cancer cells.

Typically, electrospun nanofibers are used as the substrates, and the microfluidic channels are used as the cover plates for nanofiber-integrated microchips. In order to capture and collect cancer cells, Liu et al. [154] reported the integration of MnO2 nanofibers with a microchannel. MnO2 nanofiber-coated glass substrates and serpentine PDMS microchannels were used to make the nanofiber-integrated microchips. Minimized optimization experiments showed that the capture efficiency was highly dependent on flow rates and decreases dramatically when the flow rates were over 0.2 mLh^{-1}. Nevertheless, the developed microfluidic chip could efficiently and specifically capture EpCAM-positive expression cancer cells such as HCT116.

In another work, a NanoVelcro chip embedded with PLGA nanofiber was reported to isolate CTCs from the blood of prostate cancer patients [142]. The developed NanoVelcro chip is composed of an anti-EpCAM-coated transparent substrate and a PDMS chaotic mixer chip, including three layers. The top layer is a PLGA nanofiber for the immobilization of anti-EpCAM and the capture of CTCs, and the middle layer is a polyphenylene sulfite laser capture microdissection films (PPS LCD) for the separation of the capture cells, while the bottom layer is a glass substrate (Fig. 3). Their results indicated that the NanoVelcro chip embedded with PLGA nanofibers was capable of achieving 82% high capture efficiency at a flow rate of 0.5 mL h^{-1} and was effective in capturing CTCs from blood samples of prostate cancer patients. Moreover, in another study [155], a different PLGA nanofiber-embedded NanoVelcro chip with anti-CD146 was developed for separation and further analysis of single CMCs. Based on these results, it is shown that the NanoVelcro chip integrated with PLGA can capture CMCs efficiently.

Avidin-coated PCL/PEI nanofibers (ABx@NF) were deposited in a microfluidic channel by Son et al. to selectively capture biotinylated cells [156]. Avidin-coated nanofibrous mats were used to selective capture the biotinylated cells through avidin-biotin interaction under continuous flow conditions in the PDMS microchannel. Under an inlet flow rate of 0.5 mL h^{-1}, the capture efficiency of AB100@NF to biotinylated cells reached 98.0%. By controlling the density of biotinylation on the nanofibers, the capture efficiency of biotinylated cells could be precisely regulated.

3.2 Electrospinning Sensors

Although the medical treatment technology is constantly improving, the survival rate of some cancers, such as liver cancer, pancreatic cancer, and other malignant tumors, is still very low, mainly due to a variety of comprehensive factors, such as the relative lag of early diagnosis techniques and the

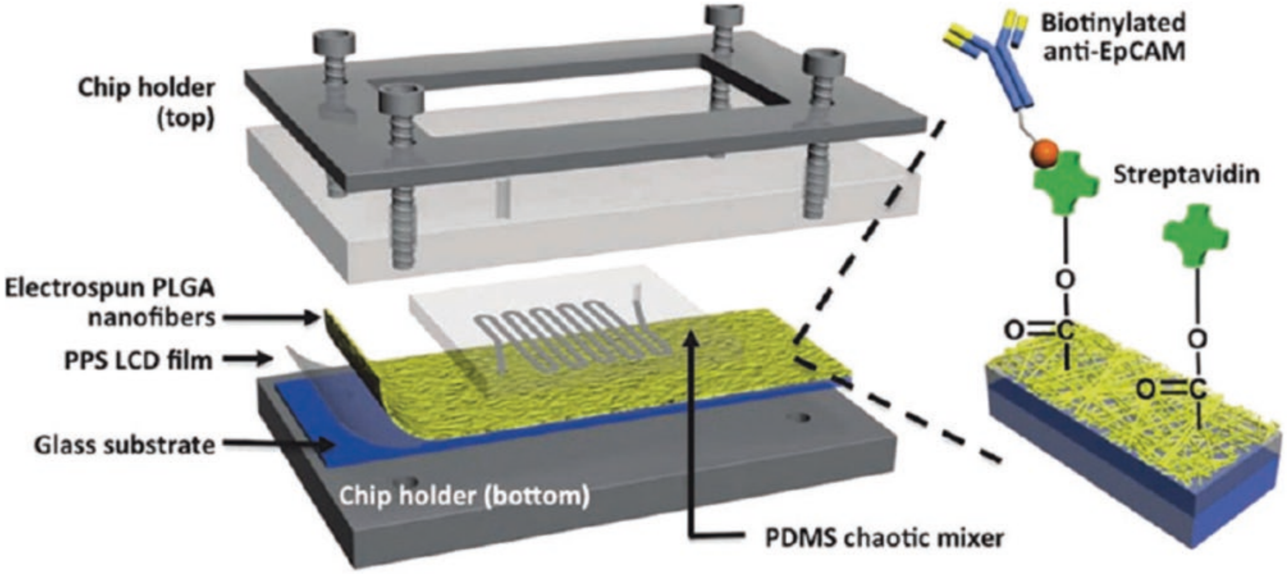

Fig. 3 The design of the NanoVelcro chip embedded with PLGA nanofibers. (Reprinted with the permission from Ref. [142])

lack of standardized treatment [156]. Based on this, biosensors are considered to have an important role in the early diagnosis of cancer because of their rapid detection, low cost, good biocompatibility, and portability. It is worth noting that the development of electrospun nanotechnology can significantly improve the accuracy and sensitivity of biosensors via the amplification of biometric signals. Thus, electrospun nanofibers could be used as an ideal substrate to isolate and detect CTCs [157, 158].

3.2.1 Electrochemical Biosensor

The electrochemical DNA biosensors immobilize a sensor of sequence-specific oligonucleotide probes that can recognize and complement the complementary targeting sequences. Based on this, many researchers have prepared nanofiber-based biosensors. The preparation of the electrochemical biosensor is shown in Fig. 4. This type of sensor can be used to detect macromolecules such as glucose [159–161], genes [162], and proteins [163–165]. A multi-walled carbon nanotube electrochemical biosensor (MWCNT-PA6-PTH) doped with nylon 6/poly(methionine) was prepared, and its detection limit for hybridization detection of mutated K-ras gene was as low as 30 fM [166].

Currently, the most mature biosensing devices are electrochemical biosensors (ECBSs) [167]. This variant of biosensor was derived from microelectronic circuits, which have many advantages such as easy scalability, robustness, portability, and excellent detection limits even though the analyte volume is very small. In principle, the ECBS works by extracting an electrical response signal from a biological analysis which electrochemically reacts with the surface of the working electrode. The response signal can be a measurable potential (potentiometer; significant logarithmic concentration dependence), a dielectric measurable conductivity between two electrodes (conductometric), or a measurable current (current method; significant linear density dependence) [168]. An enzyme is typically used as the recognition element for its selective binding between the bioreceptor and analyte and high catalytic activity [168]. Additionally, immunosensors, in which antibodies can be coupled to electrochemical transducers, have been widely developed to measure cancer markers, particularly in the detection of prostate-specific antigens [169].

As the transducing element of the biosensor, a minimum of three electrodes in the ESNF matrix are needed for electroactive responses. In order to compare the measurement values, the reference electrode, commonly made of silver, is usually separated from the surface reaction and kept at a fixed potential. The working electrode (anode or positive electrode) converts the measured electrochemical response signal; simultaneously the auxiliary electrode connects the electrolyte solution to the working electrode to induce an operating current [170]. The properties of the electrode material can affect the stability, response time, and sensitivity of the biosensor, but the immobilized enzymes often resulted in inadequate electron transfer in signal transduction [171]. This is an adverse effect of the presence of the enzyme on the electrode surface, which inhibits a smooth and rapid exchange of electrons. Therefore, the sensitivities of ECBSs need to be altered before allowing for biomarker detection. In fact, it is possible to improve the signal-to-noise ratio and sensitivity of ECBSs by facilitating the electron transport

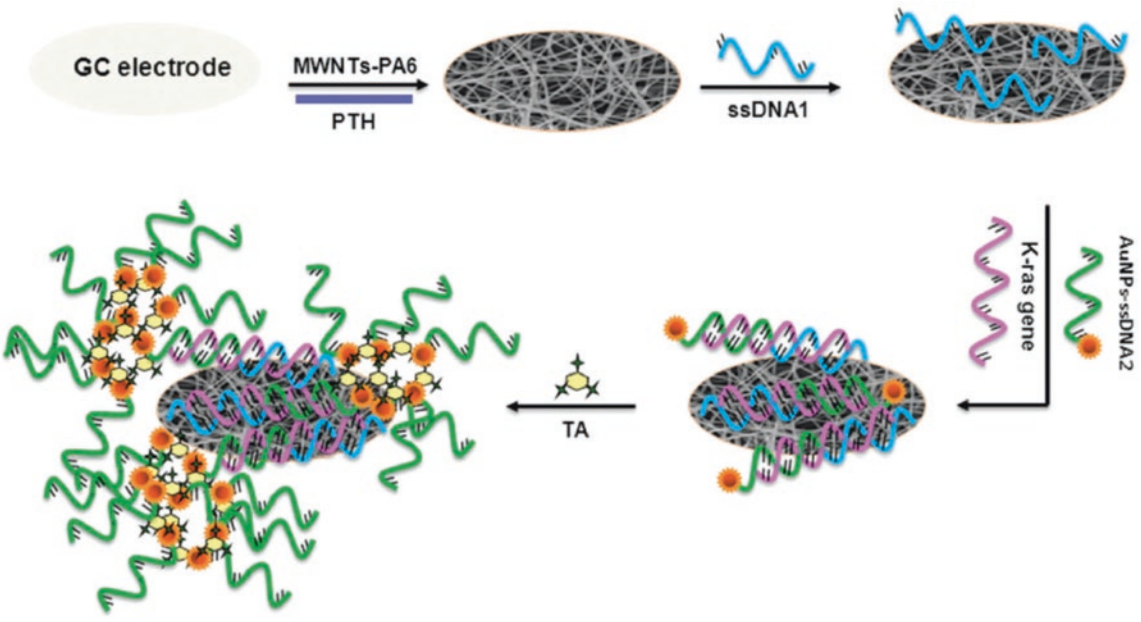

Fig. 4 The scheme of the preparation of the electrochemical biosensor. (Reprinted with permission from Ref. [166])

between the electrode and bioreceptor [172]. Consequently, a transducer with high chemically stable additives and conductive such as metal nanoparticles, quantum dots (QDs), and carbon nanotubes (CNTs) can achieve this requirement [168]. In addition, studies have shown that these nanoscale building blocks have strong adsorption capacity for enzymes, thus improving the sensitivity, response time, and stability of ECBSs by minimizing enzyme expansion [173]. To ensure good absorption performance, these nanoscale building blocks must be evenly and homogeneously distributed, so the dispersion strategies of nanoscale components in ESNFECBS need to be continuously improved.

3.2.2 Fluorescent Chemosensors

Many fluorescent probes consisting of DNA, peptides, and proteins have been developed for molecular biological detection [164, 174]. Fluorescent chemical sensors have evolved into an efficient and simple detection technique and have been widely used in the detection of amines in solution. Recent studies have demonstrated that histamine in the urine is an important marker of cancer, acting as a crucial mediator in the occurrence and development of cancer [175]. Studies on a fluorescent chemosensor based on dendritic zinc porphyrin (Den-Por (Zn)) electrospun nanofibrous membranes showed that the intensity of the fluorescence spectrum is greatly influenced by the concentration of histamine. As described in Fig. 5, for increasing histamine concentrations,

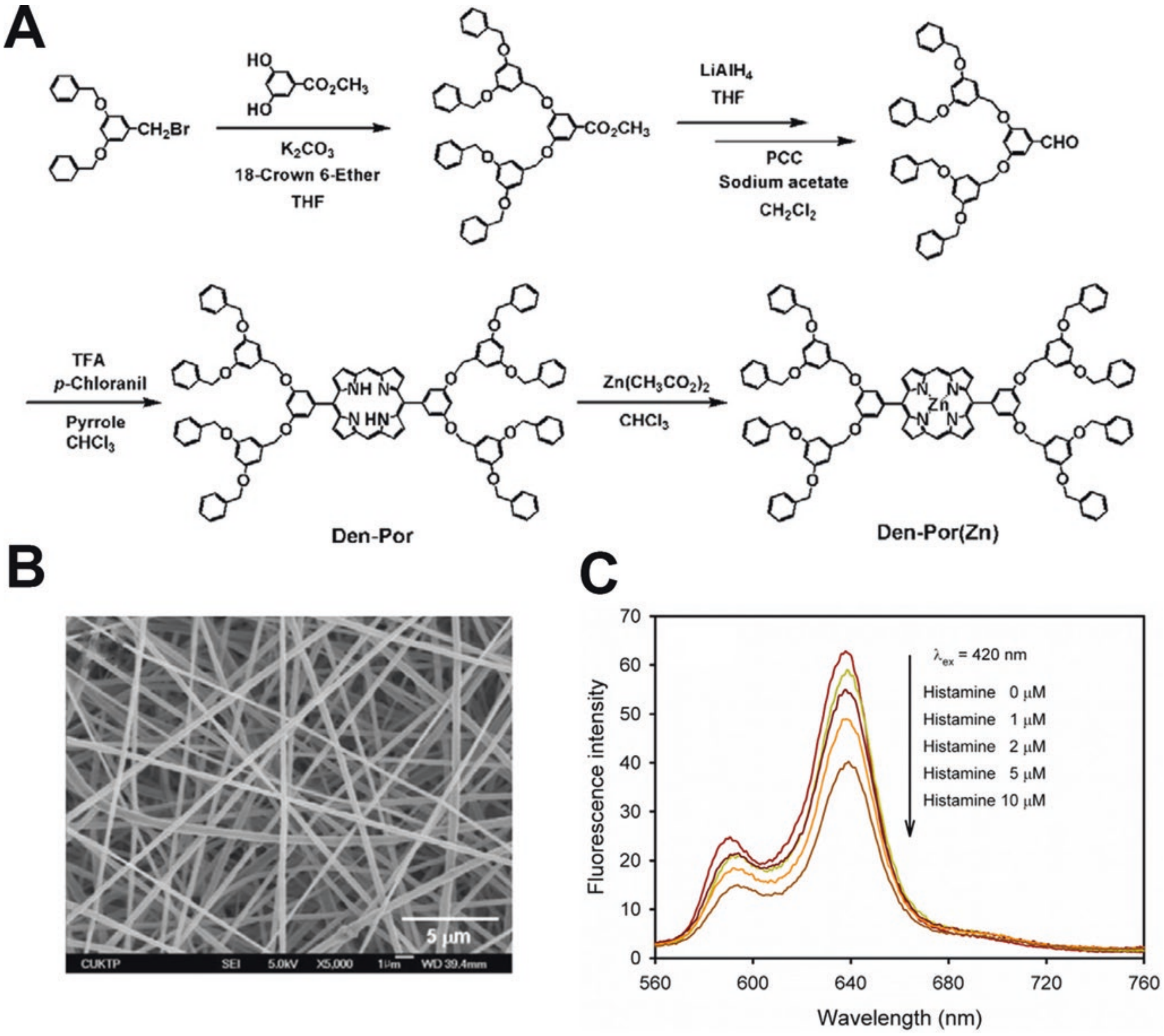

Fig. 5 (**a**) Schematic diagram of the synthetic routes of dendritic porphyrins. (**b**) SEM micrographs of PCL-Por(Zn) nanofibers. (**c**) Fluorescence intensity of the PCL-Por(Zn) exposed to different concentrations of histamine. (Reprinted with permission from Ref. [176])

the fluorescence intensity (λex = 420 nm) was reduced, indicating that the automated system for histamine test at low concentrations is feasible [176].

3.2.3 Gas Sensor for Lung Cancer

At present, hundreds of volatile organic compounds can be detected from the air exhaled by human. Among these molecules, aromatic amines [177] and toluene [178] are well-known biomarkers that can be used to predict lung cancer. Studies based on gas chromatography/mass spectrometry demonstrated that the exhaled toluene level of lung cancer patients (about 80–100 ppb) is two to three times higher than that of healthy people [179]. How to optimize the sensitivity, selectivity, stability, and response speed of the sensor is a great challenge in the future.

Chemically resistive gas sensors based on semiconducting metal oxide nanofibers (such as ZnO [180], SnO_2 [181], In_2O_3 [182], WO_3 [183], ZrO_2, and TiO_2) exhibit good stability, fast response time, excellent gas response, low cost, and high reproducibility. In particular, in order to promote gas sensing reactions, some noble metal nanoparticles such as Au, Pt, and Pd have been used in semiconductor metal oxide nanofibers [184].

By functionalizing the surface of the nanofibers, the gas response can be increased, while the activation energy and the maximum operating temperature of the sensor can be reduced. Kim et al. [185] described an excellent sensor that can be used as a diagnostic biomarker detector (Rair/Rgas = 5.5 at 1 ppm) for lung cancer and was relatively insensitive to H2S through the use of multifunctional semiconductor nanofibers (Rair/Rgas = 1.36 at 1 ppm). These sensors were prepared by the addition of the $PdCl_2$ to the WO_3 nanofibers. As shown in Fig. 6 with the threshold detection level of 20 ppb at 350 °C, the results indicated that the functional nanofibers have an excellent detection performance (Rair/Rgas = 1.32).

3.2.4 Immunosensor

Particularly owning to their accuracy and inherent specificity, immunosensors performing immunoassays based on antigen and antibody interaction have become important in the detection of the biomarkers in body fluids of cancer patients [186]. Nanomaterials are increasingly being used to improve the analytical capabilities of electrodes because of their extremely high diffusion rates and high active catalyst loading [187].

Electrospun nanofibers having epidermal growth factor receptor 2 (EGFR2) and mesoporous zinc oxide (ZnO) conjugated on the surface have been developed for the detection of EGFR2-positive breast cancer. The immunosensor was label-free, highly efficient, highly sensitive, and reproducible [188]. The 3D structure of nanofibers comparatively improved the loading of EGFR2, leading to higher stability, higher reliability, and higher sensitivity of the immunosensor. Therefore, an immunosensor using electrochemical sensor technology possessed high sensitivity (7.76 KΩ μM^{-1}),

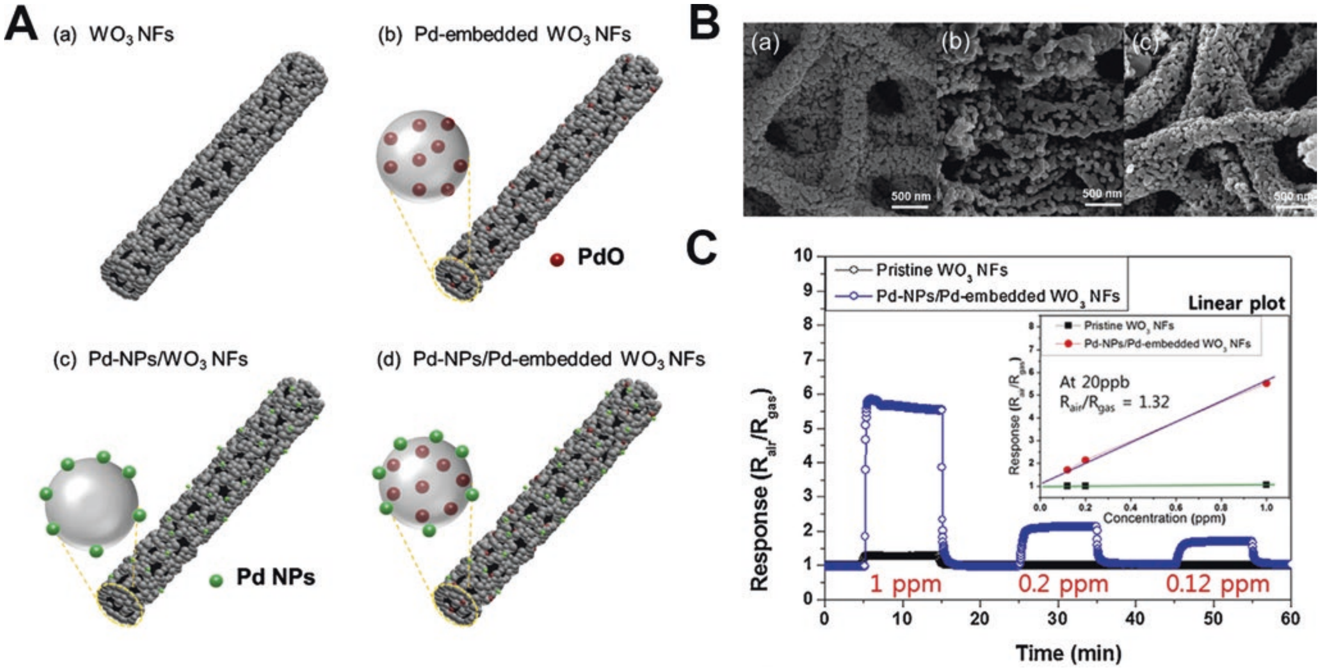

Fig. 6 (**a**) Schematic illustration of different types of (a) WO_3 NFs, (b) Pd-embedded WO_3 NFs, (c) Pd-NPs/WO_3 NFs, and (d) Pd-NPs/Pd-embedded WO_3 NFs. (**b**) SEM images of Pd-embedded WO3 NFs, Pd-NPs/WO3 NFs, and Pd-NPs/Pd-embedded WO3 NFs. (**c**) The cyclic response levels of different types of nanofibers. (Reprinted with permission from Ref. [185])

and thus the detection limit can be as low as 1 fM (4.34×10^{-5} ng mL^{-1}). At the same time, due to the excellent sensitivity of the immunosensor, fast detection (128 s) was possible in a wide detection range of concentrations from 1.0 fM to 0.5 μM.

4 Nanofibers for Intelligent Cancer Therapy

4.1 Nanofibers with Switchable Drug Release for Cancer Therapy

Stimuli-responsive polymers for cancer therapy have attracted extensive attentions around the world in recent years. Stimuli-responsive systems are dependent upon the sensitivity of the responsive materials to the external stimuli. Let's take the nanofiber as an example; compared to other materials, nanofibers stand out among response materials due to their high surface area-to-volume ratio [189, 190]. It is reported that stimuli-responsive electrospun nanofibers can respond to different stimuli, such as magnetic-responsive nanofiber, pH-responsive nanofiber, light-responsive nanofiber, thermal-responsive nanofiber, and so on.

4.1.1 Magnetic-Responsive Nanofiber

As a special type of colloidal solution, magnetic nanoparticles (MNPs) are extensively used in biomedical application. This system is able to give a response to external magnetic environment. When an external magnetic field is applied, the magnetic nanoparticles will be transported to the target area. Therefore, they are widely explored in biomedical application for cancer therapy. Apart from transporting conventional medicine to the tumor, magnetic nanoparticles [191, 192] can also produce magnetic heat to exert tumor treatment effects by the application of alternating magnetic field (AMF) [193–195]. The magnetic thermal agent delivered to the tumor site is able to produce heat (over 42 °C) under external magnetic fields, leading to apoptosis and acute necrosis of tumor cells. However, the application of free magnetic nanoparticles has been greatly limited, because the free magnetic nanoparticles have poor tumor targeting, high variability in the accumulation, and position uncertainty without AMF. In order to solve these problems, magnetic nanoparticles are formulated by electrospinning into electrospun fibers for drug delivery and tumor therapy.

It is significant that magnetic nanoparticles with a reduced cell compatibility in vitro are accepted by the human body. In fact, once they get into cells, they degraded immediately [196]. The magnetic nanoparticles will be degraded into oxygen and iron inside the lysosome of macrophage, and the ratio of degradation will be influenced by several conditions, such as hydrolytic enzymes, related protein, and pH. In particular, the iron oxide nanoparticles degraded in vivo by iron mobilization and other methods [197]. In addition, magnetite is one of the iron oxide derivatives that has been approved by FDA for investigation in vivo [198].

In a study by Feng et al. [199], GO/Fe3O4-IN-PAN nanofibers were prepared by electrospinning to adjust cellular behavior. They cut these nanofibers into pieces and then dissolved them in tert-butanol solvent, which show strong magnetic properties. In order to verify the function of nanofibers to guide cellular behavior, the researches inoculated breast cancer cells on the surface of the magnetic nanofiber membrane. Indeed, the nanofibers show a great biocompatibility with the help of graphene oxide, which is able to promote the adhesion of cell membrane proteins. Finally, it is proved that magnetic fiber membranes can guide part of the behavior of cells. Huang and Soenen et al. [200] prepared polystyrene (PS) nanofibers containing 50 nm iron oxide nanoparticles. To fabricate iron oxide nanoparticles, Fe_3O_4 nanoparticles were dispersed into THF under ultrasonication and then followed by adding PS into mixture for electrospinning. When the fibers were exposed to an AMF, they can produce heat due to their high loading capacity. Relying on their stable structure, the magnetic fibers can be heated to the same temperature several times without releasing Fe3O4 nanoparticles. Actually, researches modified a layer of collagen on the surface of polystyrene fibers to increase the cell adhesion of the fiber membrane. Finally, they incorporated human SKOV-3 tumor cells into the fibers to verify its magnetic thermal capacity. After 10 minutes of the application of AMF, the cells deposited on the fibers died. These systems can be used for in vivo investigation mainly for two reasons: one is that magnetic nanoparticles can be used in a controlled method and the other is that the magnetic nanofibers can be localized in body by magnetic resonance imaging (MRI). Sasikala and Unnithan et al. [201] prepared an implantable composite magnetic nanofiber, which can be applied not only for magnetic thermal therapy but also for responsive drug release to achieve synergistic effect for tumor therapy. This study investigated a protease inhibitor called bortezomib (BTZ), a borate-containing, frequently used in cancer therapy. They first mixed Fe3O4 nanoparticles and PLGA solutions together with ultrasonication and then electrospun them. In addition, a layer of polydopamine was added on the surface of nanofibers by dipping to improve cellular adhesion. These magnetic scaffolds with plenty of catechol moieties had the ability to bind and release bortezomib. They first prepared Fe_3O_4 nanoparticles and PLGA electrospun nanofibers as shown in Fig. 7a, b. Then they mix them together to get the composite magnetic nanofibers, which were observed by both SEM and TEM (Fig. 7c, d), showing an excellent morphology. The TEM image shows the local structure, proving that Fe_3O_4 nanoparticles are successfully encased by the nanofiber. They examined the magnetocaloric

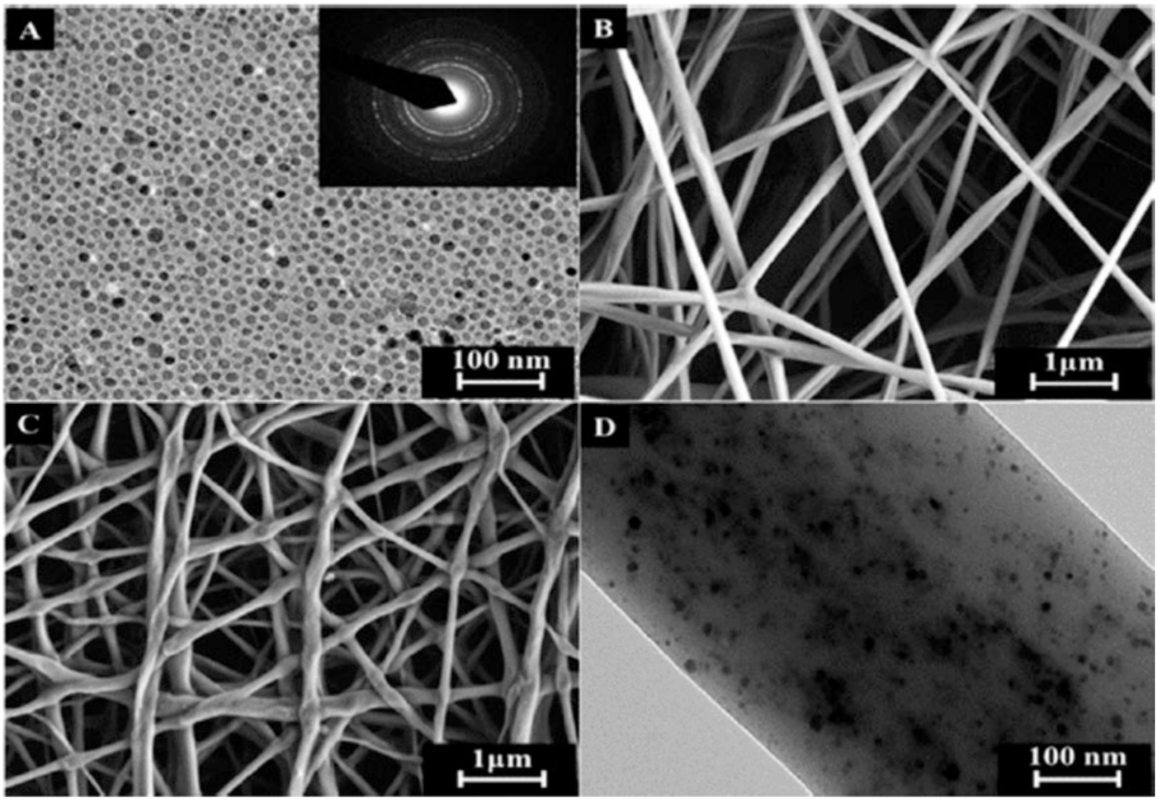

Fig. 7 (**a**) TEM image of Fe3O4 nanoparticles; (**b**) SEM image of PLGA nanofiber; (**c**) SEM image of BTZ-loaded magnetic nanofibers; (**d**) TEM image of BTZ-loaded magnetic nanofibers. (Reprinted with permission from reference [201])

effects of BTZ-loaded magnetic nanofibers on 4T1 tumor cells, demonstrating that 4T1 cancer cells underwent apoptosis and necrosis after three cycles (15 min/24 h) of thermal therapy.

In another study reported by Song and Wang et al. [202], they synthesized polyurethane nanofibers containing superparamagnetic iron nanoparticles for magnetic thermal therapy. This magnetic nanofiber is able to reach the temperature of 43 °C with just the application of an AMF for 70 s. At the same time, Radmansouri and Bahmani et al. [203] prepared TiO_2/cobalt ferrite/chitosan electrospun nanofibers combined with DOX for the synergistic cancer therapy of chemotherapy and magnetic therapy. In order to get higher temperature, they first mixed cobalt ferrite together with TiO2 and then electrospun with chitosan for nanofibers. The fibers achieved a synergistic effect of the components displaying higher cytotoxicity and lower side effect in vivo.

A work [204] (as shown in Fig. 8) reported that they selected the mixture of γ-Fe_2O_3 and Fe_3O_4 as MNPs due to the instability of the single MNPs. DOX and MNPs were mixed and dispersed in the temperature-responsive copolymers of N-hydroxymethylacrylamide and NIPAAM called poly(NIPAAm-coHMAAm). When the magnetic field (AMF) was applied, the MNPs in the nanofibers would produce heat, which can activate the temperature-responsive copolymers to collapse the networks. The swelling ratio of the nanofibers will change by the intervention of AMF. Consequently, the drug release of DOX will also be influenced by the AMF in an "NO-OFF" manner. The majority of cancer cells died when they are incubated with nanofibers under the application of an AMF for 5 minutes. These magnetic-responsive nanofibers can be defined as a switchable drug carrier for smart cancer therapy.

4.1.2 pH-Responsive Nanofibers

The acidic environment of the tumor is being exploited for cancer therapy. At the moment, pH-responsive nanodrugs have been widely used in tumor therapy because they can have a quick release of antitumor drugs in tumor tissues in response to the changeable pH [205]. Demirci and Celebioglu et al. [206] have synthesized a pH-responsive polymer called poly(4-vinylbenzoic acid-co-(ar-vinylbenzyl) trimethylammonium chloride), which was employed as carrier to load ciprofloxacin by electrospinning. The drug release behavior of ciprofloxacin was performed in neutral, acidic, and basic medium to check the pH responsiveness, as shown in Fig. 9. In this study [207], the authors have investigated the drug release nearly for 12 hours. However, the time is not long enough to study the mechanism of drug release. It is known that the solubility of ciprofloxacin is pH dependent. However,

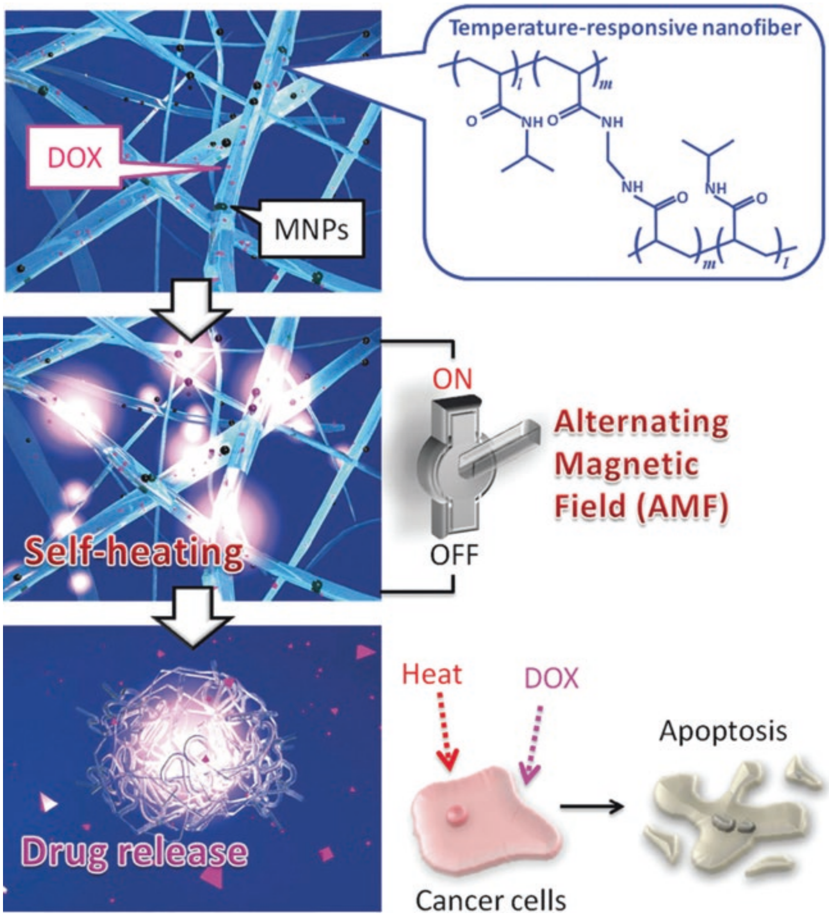
Temperature-responsive nanofiber
DOX
MNPs
ON
Alternating Magnetic Field (AMF)
OFF
Self-heating
Heat
DOX
Apoptosis
Drug release
Cancer cells

Fig. 8 The scheme of magnetic-responsive nanofibers for cancer therapy. (Reprinted with permission from reference [204])

in order to know the release mechanism, it's better to increase the time of drug release, because both ciprofloxacin and polymer are pH-responsive.

In order to study the delivery of 5-fluorouracil (5-Fu), Illangakoon and Yu et al. [208] fabricated pH-responsive nanofibers using the polymer called ES100, an ionic copolymer of methyl methacrylate and methacrylic acid. They first employed a mixture of ethyl cellulose, poly(vinylpyrrolidone), and the drug 5-Fu for electrospinning. Then ES100 was electrospun on the surface of the fibers for pH responsiveness. The results of drug release indicated that the release of drug was controlled due to the pH-responsive ES100. The fibers would break because of the depolymerization of the pH-responsive polymer, which enhanced the release of 5-Fu. Actually, the researchers prepared nanofibers with a core/shell structure. ES100 was for the shell, while Eudragit L100 (EL100) was for the core. This special nanofiber can be used as a carrier for controlled release of drugs at certain pH [209]. Similarly, for the purpose of controlling the drug release, Tran and Hernandez et al. [210] used pH- and temperature-responsive polymers to deliver ibuprofen. A mixture consisting of ibuprofen and PCL represented the control, while the innovative mixture included ibuprofen and the responsive polymer called poly(N-isopropylacrylamide-co-methacrylic acid). As a result, the control nanofibers showed no significant increase in drug release when they were exposed to the temperature at 22–40 °C or at pH 1.7–7.4. But the ibuprofen could be released from the responsive nanofibers in control when the temperature got up to their lower critical solution temperature (LCST) or the pH was below the pKa of acids. However, compared to the environment with temperature higher than 30 °C and pH lower than 2, the ratio of drug release from the nanofibers was ten times higher than at room temperature. Furthermore, other nanofibers were developed from cationic chitosan and PAA and possessed different levels of CS deacetylation. In other words, the property of these nanofibers was determined by the level of CS deacetylation and pH [211]. L-Lactide-co-caprolactone and gelatin were used as a carrier to deliver ciprofloxacin and sodium bicarbonate as nanofibers. The gelatin and sodium bicarbonate are responsive to low pH, while L-Lactide-co-caprolactone had no response to pH [212]. These nanofibers had a good biocompatibility in L929 cell. In addition, they can also promote cell pro-

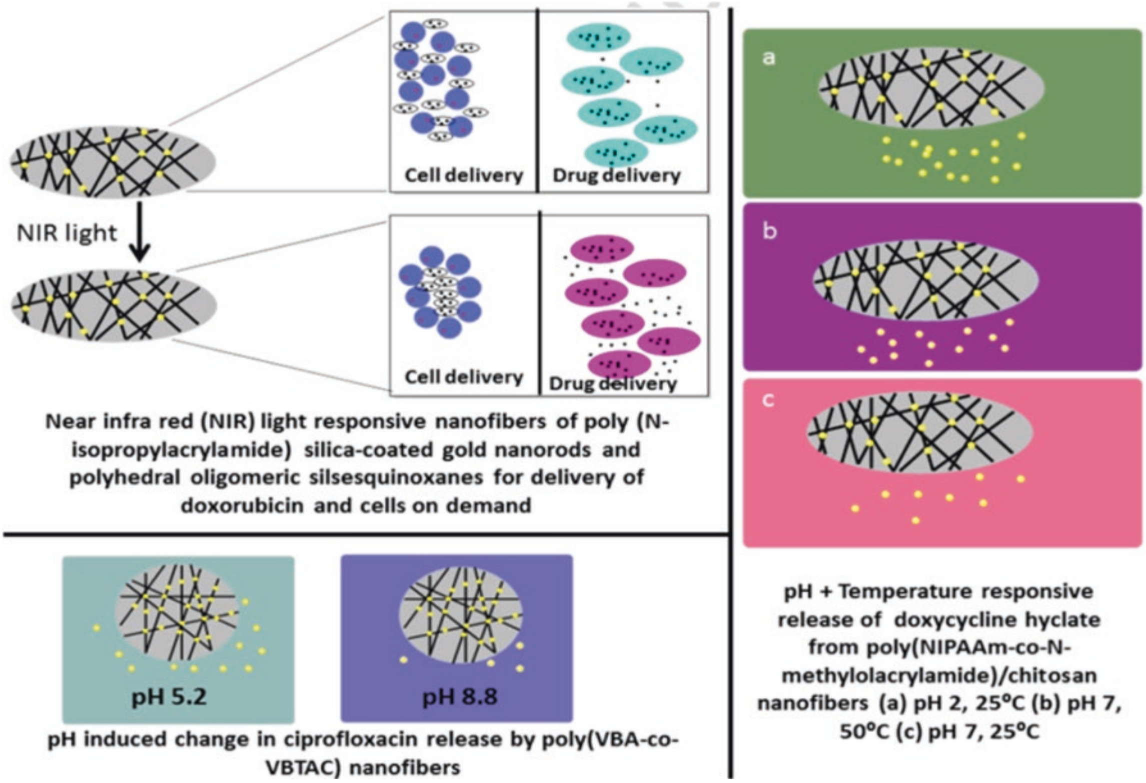
Cell delivery
Drug delivery
NIR light
Cell delivery
Drug delivery
Near infra red (NIR) light responsive nanofibers of poly (N-isopropylacrylamide) silica-coated gold nanorods and polyhedral oligomeric silsesquinoxanes for delivery of doxorubicin and cells on demand
a
b
c
pH + Temperature responsive release of doxycycline hyclate from poly(NIPAAm-co-N-methylolacrylamide)/chitosan nanofibers (a) pH 2, 25°C (b) pH 7, 50°C (c) pH 7, 25°C
pH 5.2
pH 8.8
pH induced change in ciprofloxacin release by poly(VBA-co-VBTAC) nanofibers

Fig. 9 The scheme of drug release from stimuli-responsive nanofibers. (Reprinted with permission from [207])

liferation. DOX was loaded within modified pH-sensitive PCL nanofibers, and drug release experiments were performed at different pH (from 2.5 to 7.4). The results showed that the release of the nanofibers at pH 2.5 was the highest. Furthermore, the cytocompatibility of these nanofibers was also evaluated in HEK cells, and the results indicated that the scaffolds obtained at pH 7.2 had higher cell viability than those at pH 6 because of the difference of release behavior in different pH conditions [213].

In another study reported by Toncheva and Paneva et al. [214], ciprofloxacin was added into poly(L-lactide-co-D,L-lactide) solution in crystalline form for electrospinning. The results of the release study in pH 7.4 showed that there was a burst release of 50% in 400 minutes, and further study of drug release didn't have any significant increase in the amount released, indication of an uncontrolled drug release. Researchers in this study also clarified that the ratio of drug release could be increased by the addition of PEG, because it is easier for release media to permeate by the addition of hydrophilic polymer.

4.1.3 Light-Responsive Nanofiber

Light-responsive materials could be easily focused into the specific area for therapy. This kind of material is often sensitive to the light, and the structure will be changed between the different wavelengths [215].

Ultraviolet Light-Responsive Fibers

Cis-trans isomerization of azobenzene structures usually led to the change of shape, polarity, and dipole moment of the molecule, which have been extensively used in different systems [216–218]. These molecules are able to change from trans structure to cis structure under the irradiation of UV and have a reverse conversion when heated or exposed to the irradiation whose wavelength is over 400 nm.

Cyclodextrins (CDs) thanks to the particular hosting features have been widely studied for more than half a century [219]. CDs are consist of hydrophilic outer surface and hydrophobic inner cavity, which forms a unique combination. It is well known that azobenzene in trans structure is able to bind effectively with CDs, but cannot bind to it in cis structure [220]. Based on the theory of UV-responsive structure, Fu and Xu et al. [221] reported a drug release system of electrospun nanofibers that can be activated by UV light. The block copolymers consisted of glycidyl methacrylate and vinylbenzyl chloride, which were electrospun into nanofibers. Then, they added the azide into the surface of the nanofibers, promoting the reaction with 4-propargyloxyazobenzene. After the reaction was successfully completed, 5-Fu was conjugated with α-CD by the interaction of host to guest. It is reported that electrospun nanofibers showed a great control over the release of 5-Fu under the irradiation of UV light. The drug was released quickly into the solution when the nanofibers were exposed to the UV light and the max release was achieved after irradiating with UV light for 30 minutes. Importantly, this drug release system showed a special response to the UV light. The drug release can happen immediately when exposed to the UV and be quickly interrupted when the UV light disappears.

Near-Infrared Light-Responsive Fibers

A downside of the UV light is its quick attenuation in tissues. Near-infrared (NIR) light could take the place of UV light because of its deep penetration depth in tissues and low risk of damage for healthy organs [222]. The raw materials for synthesizing NIR light-responsive materials are photosensitive structural molecules with strong absorption in the near infrared [223–226]. In particular, gold nanorods (AuNRs) can be used for cell imaging and photothermal therapy because of the adjustable localized surface plasmon resonance [227]. When AuNRs are used as carriers of antitumor drugs, the heat produced by the AuNRs is able to trigger the drug release. Combined with thermal-responsive polymers, AuNRs will produce heat and trigger the depolymerization of the polymers under the irradiation of NIR light, leading to controlled drug release [228–230]. Vyas et al. had reported NIR light-responsive electrospun nanofibers composed of AuNRs and poly(N-isopropylacrylamide-co-polyethylene glycol acrylate) (PNPA), which showed that the drug release of BSA was controlled. By the integration of thermal-responsive pNIPAM with AuNRs, the ratio of drug release would be increased. AuNR was able to increase the temperature of pNIPAM under the irradiation, which decreased the volume of polymer and enhanced the drug release. However, after removing the NIR light, the electrospun nanofibers would suddenly swell and decrease the drug release immediately. This study first demonstrated the ability of electrospun nanofibers to control the drug release under NIR irradiation, with great clinical relevance.

4.1.4 Thermal-Responsive Nanofibers

At present, there are plenty of studies investigating the preparation of thermal-responsive nanodrugs, which are extensively used in biomedical applications because of their degradability and injectability. Their properties could be used for the transport of antitumor drugs to the targeted tumor location and controlled release such as degradable electrospun nanofibers [231]. The study of the synergistic effect of chemotherapy and thermal therapy may have a better therapeutic result as well as decreased dose of the drugs. Liu and Bai et al. [232] have prepared thermal-responsive nanofibers by the copolymers poly(N-vinyl caprolactam-co-methacrylic acid) (PNVCL-co-MAA), loading ketoprofen and captopril inside. The results showed that the nanofibers had a slow release at 40 °C, but burst into release in few seconds at 20 °C, following the mechanism of the Korsmeyer-Peppas model. The authors stated that the polymer was hydrophilic when the temperature was below lower critical solution temperature and the drug release is in diffusion control. In contrast, the polymer was hydrophobic, and the drug release became slower with more dependence of the degradation of polymers for higher temperatures.

Slemming-Adamsen and Song et al. [233] reported an innovative way to add DOX into thermal-responsive pNIPAM-NHS/gelatin nanofibers by the interconnection of N-hydroxysuccinimide (NHS) with N′-(ethylcarbonimidoyl)-N,N-dimethylpropane-1,3-diamine monohydrochloride (EDC). They mixed a solution of pNIPAM-NHS/gelatin with another solution of EDC, NHS, and DOX. In this way, EDC is able to trigger the conjugation by bonding with the carboxyl of the polymers. Then the conjugated EDC polymer will react with NHS by taking the place of EDC with amine ester bond. Finally, the primary amine will replace NHS, acting as a bridge to connect carboxyl polymers with amine polymers. The mixture was then electrospun to get the cross-linked pNIPAM/gelatin nanofibers carrying the antitumor drugs that can be released in response to temperature. In fact, when the temperature was higher than LCST of the polymer, DOX would be released from the cross-linked nanofibers and decreased the cell viability of human cervical cancer cells.

Zhang and Niu et al. [234] prepared thermal-responsive electrospun nanofibers in core/shell structure with a core of PLA and a shell of pNIPAM. First of all, the biodegradable polymers of PLA were used to encapsulate combretastatin A4(CA4)by electrospinning. Then these PLA nanofibers were introduced into the solution of pNIPAM with the aid of cross-linker of N,N-methylenebisacrylamide. The drug-loaded PLA nanofibers were coated and cross-linked with the shell of pNIPAM after exposure to the UV light. They detected the water contact angle at different temperatures around the LCST of the polymers to confirm the wettability of the nanofibers. And they also found the different release behaviors at different temperatures. For instance, the shell of pNIPAM was able to limit the ratio of drug release of CA4 below the LCST. But the release ratio of CA4 would increase significantly above the LCST. Cicotte and Reed et al. [235] used the thermal-responsive pNIPAM electrospun nanofiber films for the attachment and separation of the cells due to their property of fast adhesion to mammal cells. The authors studied the influence of various parameters on the effect of electrospun fibers, such as molecular weight of polymer, collecting time, needle, and so on. Moreover, they investigated the reversible attachment of the pNIPAM nanofibers in MC3T3-E1 cells and EMT6 cells. Once attached, the cells would promote a quick swelling of pNIPAM nanofibers. In recent years, various multi-stimuli-responsive nanoformulations have been designed, such as poly(N-isopropylacrylamide-co-acrylic acid) nanofibers, which are sensitive to pH and temperature. Therefore, we can regulate the release behavior by changing these two parameters [236].

In another study, the authors used pH-responsive polymers Eudragit®L100–55 and thermal-responsive polymers pNIPAM polymers to fabricated multi-stimuli-responsive nanofibers by electrospinning [237]. The nanofibers demonstrated a drug release of ketoprofen sensitive to the pH and temperature and had no cytotoxicity to fibroblast even in a high concentration. Another typical multi-stimuli nanofibers were fabricated by the mixture polymers of poly(N-vinylcaprolactam), ethyl cellulose (EC), and EL100 with twin-jet electrospinning [238]. The ketoprofen loaded in these nanofibers showed a continuous drug release in response to the pH and temperature, and the nanofibers also had a great biocompatibility in fibroblasts. In order to study the cytocompatibility of nanofibers, L929 cells were seeded on the surface of cover slips. After being incubated with the fibers for 1, 3, and 5 days, the cell viability was determined by MTT assay. These nanofibers tend to show a great biocompatibility. However, there are many other kinds of nanofibers displaying better biocompatibility, such as the nanofibers prepared by the mixture of EC and poly(di(ethylene glycol)methyl ether methacrylate) (PDEGMA) [239]. A special stimuli-responsive nanofiber for the delivery of antitumor drugs is constituted of electrospun self-immolative polymer (SIP)/polyacrylonitrile (PAN) fibers [240], which would be depolymerized immediately and released the transported molecules instantly when exposed to external stimulus with the addition of TFA.

4.2 Electrospun Nanofibers for Effective Immunotherapy of Cancer

Self-assembling peptides have been extensively employed in immunotherapy and vaccines due to its outstanding modularity [241]. Rudra and Tian et al. [242] used Q11 (short fibrillizing peptides) as a vaccine adjuvant. When Q11 encapsulated OVA (a 17-amino acid peptide from chicken egg ovalbumin) into the nanofibers, a strong antibody response was observed against OVA, but not observed to Q11. Recently, they have also titrated the concentration of the universal T cell epitope on the nanofibers and discovered that T cell polarization was successfully turned into follicular helper T cell (Tfh) direction [243]. When the protein antigens were fused to a β-tail sequence, they could also be displayed. β-Tail remained soluble during expression and purification, but it could be co-assembled with the help of Q11 [244].

Wen and co-workers [245] introduced the histidine tags (His-tag) into the peptide nanofibers by the co-assembly of EAK16-II (self-assembling peptide) with its histidinylated analogue EAKIIH6. The density of histidine tags can be regulated by the concentration of histidinylated peptide. This design allowed the exhibition of any IgG molecule on the nanofibers by the hexameric adaptor protein A/G [246]. It has been proved that this universal antibody system was capable of self-assembling in the anatomical site when exposed to saline [246–248]. The antibody display systems were beneficial, because it can extremely reduce the body exposure. Wen and Liu et al. [247] prolonged the retention time of antibodies targeting the tumor cytokine and transforming growth factor-β from 24 h to 120 h. This brings along advantages in the immunotherapy for cancer, because the host immunity could be activated by neutralizing the tumor-promoting cytokines, such as TGF-β. More importantly, in order to ease the acute rejection, the antibodies against antigen-presenting cells were displayed at the graft sites in mice skin transplantation model [247]. The results showed that these systems can stay in transplant site for over 7 days and captured donor antigen-presenting cells to attenuate host T cell responses. This antibody display system has been used in the development of functional T cells recently [249]. They introduced the antibody against epithelial cell adhesion molecule into the peptide electrospun nanofibers, which could form 3D clusters with thymic epithelial cells and retained their original morphology. They have detected circulating CD45+CD3+T cells after 5 weeks. The most important is that activated CD4+ T cells and naive CD8+ T cells survived in the secondary lymphoid organs. The research demonstrated that antibody display systems have great potential to recover the immunity of T cells.

4.3 Electrospun Nanofiber Composite for Synergistic Therapy

Synergistic cancer therapy has arisen to great attention in clinical practice to overcome the shortcoming of single cancer treatment and achieved a great success. For example, just making use of localized drug delivery systems (LDDSs) for single chemotherapy may result in a strong drug resistance [250, 251]. In addition, chemotherapy may lead to inevitable side effects. In contrast, the synergistic cancer therapy could achieve a combined efficacy in a low concentration curing multiple drug-resistant cancer cells. Therefore, more and more studies have been carried out in multifunctional nanofibers combining two or more drugs to increase the effect.

Zhang and Wu et al. [252] introduced Pt prodrug micelles and (dichloroacetate) DCA into PVA electrospun nanofibers, forming a new M/DCA nanofiber with dual-drug delivery device as shown in Fig. 10. The different mechanisms of DCA and Pt could have an effective synergistic effect against cancer cells. Compared with systemic therapy, M/DCA micelles showed a prolonged retention time in tumor site, lower toxicity, and greater effect after implantation in vivo.

Effective cancer therapies are able to be achieved by the design of a smart nanofiber systems combining chemotherapy and thermal therapy. Niiyama and co-workers [253] demonstrated the antitumor effects of nanofibers by the

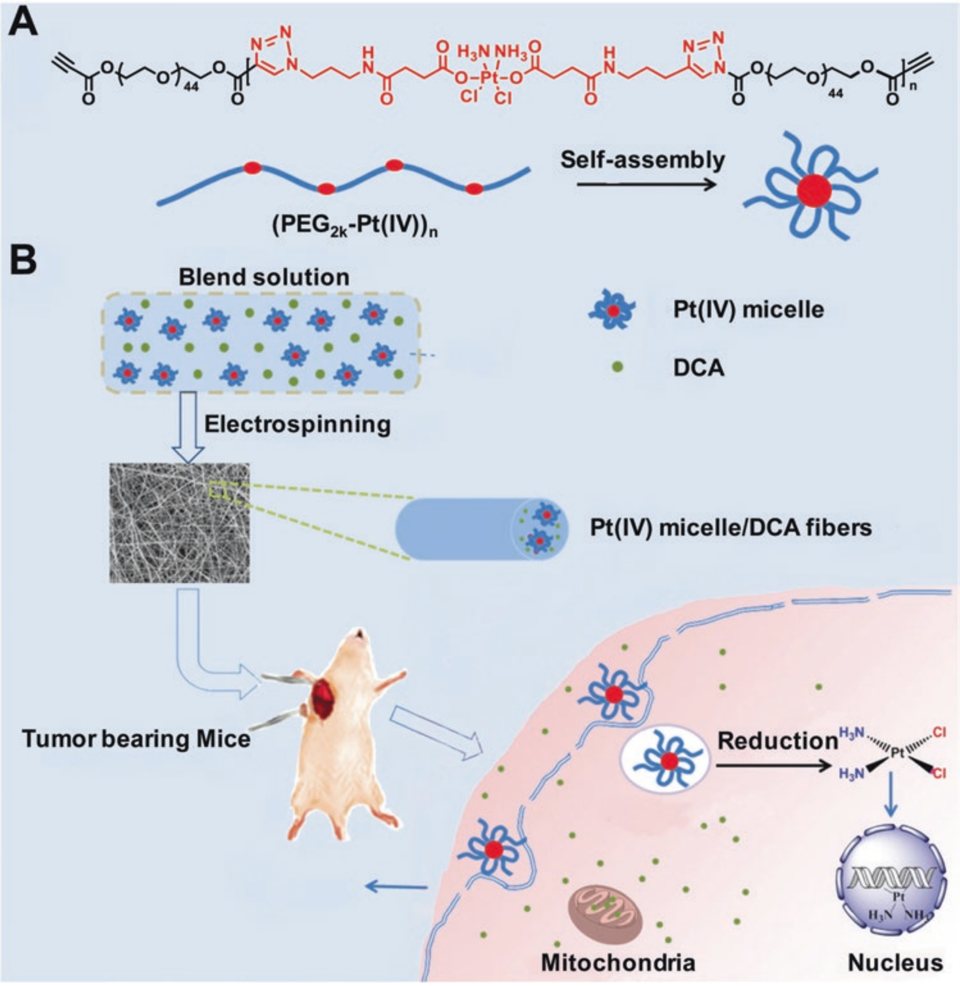

Fig. 10 (**a**) The illustration of the structure of Pt(IV) micelle; (**b**) the fabrication of Pt/DVA nanofibers for synergistic cancer therapy. (Reprinted with permission from [252])

delivery of antitumor drugs. The results of drug release in vitro showed that PTX would be released at least for 6 weeks in a slowly speed. Compared with free PTX, this drug system was able to have a continuous drug release and prolonged therapy. Moreover, the synergistic effect can be achieved by the activation of an alternating magnetic field because the magnetic nanoparticles in nanofibers would produce heat and induce the cancer to apoptosis and enhance the chemotherapy by PTX.

5 Conclusions and Future Perspectives

Electrospun nanofibers have been widely developed as a localized cancer therapy in the past 10 years. This kind of implantable localized drug delivery systems has been recognized as one of most promising approaches for cancer therapy. In this chapter we have summarized different types of drug-loaded nanofibers for cancer therapy, including oil-soluble drug-loaded electrospun fibers, water-soluble drug-loaded electrospun nanofibers, protein-loaded electrospun nanofibers, gene-loaded electrospun nanofibers, and other drug-loaded electrospun nanofibers. These kinds of nanofibers can be widely used in diagnosis and treatment of cancer. Two methods are widely used in the diagnosis: cancer cell capture and electrospinning sensors. Moreover, we have also discussed nanofibers for intelligent cancer therapy. However, there are plenty of challenges before clinical trials.

In order to satisfy the urgent demand in clinical medicine, two scientific researches need to have a breakthrough. One is the degradable nanofibers, which could be degraded gradually in vivo, avoiding a secondary surgery for the removal. The other is the mechanism of the curing molecules released from the electrospun nanofibers to the diseased site. As for the gene therapy, the uptake efficacy of gene is still really low because of the absence of the carriers. Therefore, the combination of nanoparticles and nanofibers has been recognized as a potential approach for cancer gene therapy.

Acknowledgments We thank Zhejiang Provincial Medical and Health Technology Foundation of China (2020RC125).

Notes The authors declare no competing financial interest.

References

1. Qin, S. Y., Zhang, A. Q., Cheng, S. X., Rong, L., & Zhang, X. Z. (2017). Drug self-delivery systems for cancer therapy. *Biomaterials, 112*, 234–247.
2. Singh, M., Kundu, S., Reddy, M. A., Sreekanth, V., Motiani, R. K., Sengupta, S., Srivastava, A., & Bajaj, A. (2014). Injectable small molecule hydrogel as a potential nanocarrier for localized and sustained in vivo delivery of doxorubicin. *Nanoscale, 6*(21), 12849–12855.
3. Cho, K., Wang, X., Nie, S., Chen, Z. G., & Shin, D. M. (2008). Therapeutic nanoparticles for drug delivery in cancer. *Clinical Cancer Research, 14*(5), 1310–1316.
4. Li, Y., Zhou, Y., Gu, T., Wang, G., Ren, Z., Weng, W., Li, X., Han, G., & Mao, C. (2016). A multifunctional Nanocrystalline CaF2:Tm,Yb@mSiO2 system for dual-triggered and optically monitored doxorubicin delivery. *Particle and Particle Systems Characterization, 33*(12), 896–905.
5. Li, Y., Zhou, Y., Li, X., Sun, J., Ren, Z., Wen, W., Yang, X., & Han, G. (2016). A facile approach to Upconversion crystalline CaF2:Yb(3+),Tm(3+)@mSiO2 nanospheres for tumor therapy. *RSC Advances, 6*(44), 38365–38370.
6. Li, Z., Hu, Y., Howard, K. A., Jiang, T., Fan, X., Miao, Z., Sun, Y., Besenbacher, F., & Yu, M. (2016). Multifunctional bismuth selenide nanocomposites for antitumor thermo-chemotherapy and imaging. *ACS Nano, 10*(1), 984–997.
7. Li, W., Peng, J., Tan, L., Wu, J., Shi, K., Qu, Y., Wei, X., & Qian, Z. (2016). Mild photothermal therapy/photodynamic therapy/chemotherapy of breast cancer by Lyp-1 modified Docetaxel/IR820 Co-loaded micelles. *Biomaterials, 106*, 119–133.
8. Zhang, Q., Polyakov, N., Chistyachenko, Y., Khvostov, M., Frolova, T., Tolstikova, T., Alexandr, D., & Su, W. (2018). Preparation of curcumin self-micelle solid dispersion with enhanced bioavailability and cytotoxic activity by mechanochemistry. *Drug Delivery, 25*, 198–209.
9. Xiang, J., Wu, B., Zhou, Z., Hu, S., Piao, Y., Zhou, Q., Wang, G., Tang, J., Liu, X., & Shen, Y. (2018). Synthesis and evaluation of a paclitaxel-binding polymeric micelle for efficient breast cancer therapy. *Science China Life Sciences, 61*, 436.
10. Feng, L., Gao, M., Tao, D., Chen, Q., Wang, H., Dong, Z., Chen, M., & Liu, Z. (2016). Cisplatin-prodrug-constructed liposomes as a versatile theranostic nanoplatform for bimodal imaging guided combination cancer therapy. *Advanced Functional Materials, 26*, 2207–2217.
11. Ngweniform, P., Abbineni, G., Cao, B., & Mao, C. (2009). Self-assembly of drug-loaded liposomes on genetically engineered target-recognizing M13 phage: A novel nanocarrier for targeted drug delivery. *Small, 5*(17), 1963–1969.
12. Fang, J., Nakamura, H., & Maeda, H. (2011). The EPR effect: Unique features of tumor blood vessels for drug delivery, factors involved, and limitations and augmentation of the effect. *Advanced Drug Delivery Reviews, 63*(3), 136–151.
13. Huynh, E., & Zheng, G. (2015). Cancer nanomedicine: Addressing the dark side of the enhanced permeability and retention effect. *Nanomedicine, 10*(13), 1993–1995.
14. Jain, R. K., & Stylianopoulos, T. (2010). Delivering nanomedicine to solid tumors. *Nature Reviews. Clinical Oncology, 7*(11), 653–664.
15. Soussan, E., Cassel, S., Blanzat, M., & Rico-Lattes, I. (2009). Drug delivery by soft matter: Matrix and vesicular carriers. *Angewandte Chemie (International Ed. in English), 48*(2), 274–288.
16. Fu, Y., Chen, X., Mou, X., Ren, Z., Li, X., & Han, G. (2016). A dual-color luminescent localized drug delivery system with ratiometric-monitored doxorubicin release functionalities. *ACS Biomaterials Science & Engineering, 2*(4), 652–661.
17. Huang, S., Duan, S., Wang, J., Bao, S., Qiu, X., Li, C., Liu, Y., Yan, L., Zhang, Z., & Hu, Y. (2016). Folic-acid-mediated functionalized gold nanocages for targeted delivery of anti-miR-181b in combination of gene therapy and photothermal therapy against hepatocellular carcinoma. *Advanced Functional Materials, 26*(15), 2532–2544.
18. Folkman, J., & Long, D. (1964). The use of silicone rubber as a carrier for prolonged drug therapy. *Journal of Surgical Research, 4*(3), 139–142.
19. De Souza, R., Zahedi, P., Allen, C. J., & Piquette-Miller, M. (2010). Polymeric drug delivery systems for localized cancer chemotherapy. *Drug Delivery, 17*(6), 365–375.
20. Ho, E. A., Soo, P. L., Allen, C., & Piquette-Miller, M. (2007). Impact of intraperitoneal, sustained delivery of paclitaxel on the expression of P-glycoprotein in ovarian tumors. *Journal of Controlled Release, 117*(1), 20–27.
21. Wolinsky, J. B., Colson, Y. L., & Grinstaff, M. W. (2012). Local drug delivery strategies for cancer treatment: Gels, nanoparticles, polymeric films, rods, and wafers. *Journal of Controlled Release, 159*(1), 14–26.
22. Xue, J., Xie, J., Liu, W., & Xia, Y. (2017). Electrospun nanofibers: New concepts, materials, and applications. *Accounts of Chemical Research, 50*(8), 1976–1987.
23. Nair, L. S., Bhattacharyya, S., & Laurencin, C. T. (2004). Development of novel tissue engineering scaffolds via electrospinning. *Expert Opinion on Biological Therapy, 4*(5), 659–668.
24. Goyal, R., Macri, L. K., Kaplan, H. M., & Kohn, J. (2016). Nanoparticles and nanofibers for topical drug delivery. *Journal of Controlled Release, 240*, 77–92.
25. Jiang, S., Lv, L. P., Landfester, K., & Crespy, D. (2016). Nanocontainers in and onto nanofibers. *Accounts of Chemical Research, 49*(5), 816–823.
26. Aussawasathien, D., Teerawattananon, C., & Vongachariya, A. (2008). Separation of micron to sub-micron particles from water: Electrospun nylon-6 nanofibrous membranes as pre-filters. *Journal of Membrane Science, 315*(1–2), 11–19.
27. Gopal, R., Kaur, S., Feng, C. Y., Chan, C., Ramakrishna, S., Tabe, S., & Matsuura, T. (2007). Electrospun nanofibrous polysulfone membranes as pre-filters: Particulate removal. *Journal of Membrane Science, 289*(1–2), 210–219.
28. Gopal, R., Kaur, S., Ma, Z., Chan, C., Ramakrishna, S., & Matsuura, T. (2006). Electrospun nanofibrous filtration membrane. *Journal of Membrane Science, 281*(1–2), 581–586.
29. Gorji, M., Jeddi, A. A. A., & Gharehaghaji, A. A. (2012). Fabrication and characterization of polyurethane electrospun nanofiber membranes for protective clothing applications. *Journal of Applied Polymer Science, 125*(5), 4135–4141.
30. Lee, S., & Kay Obendorf, S. (2006). Developing protective textile materials as barriers to liquid penetration using melt-electrospinning. *Journal of Applied Polymer Science, 102*(4), 3430–3437.
31. Kowalczyk, T., Nowicka, A., Elbaum, D., & Kowalewski, T. A. (2008). Electrospinning of bovine serum albumin. Optimization and the use for production of biosensors. *Biomacromolecules, 9*(7), 2087–2090.
32. Rojas, R., & Pinto, N. J. (2008). Using electrospinning for the fabrication of rapid response gas sensors based on conducting polymer nanowires. *IEEE Sensors Journal, 8*(6), 951–953.
33. Dong, Z., Kennedy, S. J., & Wu, Y. (2011). Electrospinning materials for energy-related applications and devices. *Journal of Power Sources, 196*(11), 4886–4904.
34. Khil, M., Chan, D., Kim, H., Kim, I., & Bhattarai, N. (2003). Electrospun nanofibrous polyurethane membrane as wound dressing. *Journal of Biomedical Materials Research, 67B*(2), 675–679.
35. Luo, C. J., Stoyanov, S. D., Stride, E., Pelan, E., & Edirisinghe, M. (2012). Electrospinning versus fibre production methods:

From specifics to technological convergence. *Chemical Society Reviews, 41*(13), 4708–4735.

36. Persano, L., Camposeo, A., Tekmen, C., & Pisignano, D. (2013). Industrial upscaling of electrospinning and applications of polymer nanofibers: A review. *Macromolecular Materials and Engineering, 298*(5), 504–520.
37. Zahedi, P., Rezaeian, I., Ranaei-Siadat, S.-O., Jafari, S.-H., & Supaphol, P. (2009., , n/a–n/a). A review on wound dressings with an emphasis on electrospun nanofibrous polymeric bandages. *Polymers for Advanced Technologies*.
38. Zhou, F.-L., Gong, R.-H., & Porat, I. (2009). Mass production of nanofibre assemblies by electrostatic spinning. *Polymer International, 58*(4), 331–342.
39. Pillay, V., Dott, C., Choonara, Y. E., Tyagi, C., Tomar, L., Kumar, P., du Toit, L. C., & Ndesendo, V. M. K. (2013). A review of the effect of processing variables on the fabrication of electrospun nanofibers for drug delivery applications. *Journal of Nanomaterials, 2013*, 1–22.
40. Rieger, K. A., Birch, N. P., & Schiffman, J. D. (2013). Designing electrospun nanofiber mats to promote wound healing – A review. *Journal of Materials Chemistry B, 1*(36), 4531.
41. Sill, T. J., & von Recum, H. A. (2008). Electrospinning: Applications in drug delivery and tissue engineering. *Biomaterials, 29*(13), 1989–2006.
42. Yoo, H. S., Kim, T. G., & Park, T. G. (2009). Surface-functionalized electrospun nanofibers for tissue engineering and drug delivery. *Advanced Drug Delivery Reviews, 61*(12), 1033–1042.
43. Kenawy, E. R., Bowlin, G. L., Mansfield, K., Layman, J., Simpson, D. G., Sanders, E. H., & Wnek, G. E. (2002). Release of tetracycline hydrochloride from electrospun poly(ethylene-co-vinyl acetate), poly(lactic acid), and a blend. *Journal of Controlled Release, 81*, 57–64.
44. Bala Balakrishnan, P., Gardella, L., Forouharshad, M., Pellegrino, T., & Monticelli, O. (2018). Star poly(ε-caprolactone)-based electrospun fibers as biocompatible scaffold for doxorubicin with prolonged drug release activity. *Colloids and Surfaces B: Biointerfaces, 161*, 488–496.
45. Gabriel, D., Cohen-Karni, T., Huang, D., Chiang, H. H., & Kohane, D. S. (2014). Photoactive electrospun fibers for inducing cell death. *Advanced Healthcare Materials, 3*(4), 494–499.
46. Mohammadian, F., & Eatemadi, A. (2017). Drug loading and delivery using nanofibers scaffolds. *Artificial Cells, Nanomedicine, and Biotechnology, 45*(5), 881–888.
47. Zeng, J., Xu, X., Chen, X., Liang, Q., Bian, X., Yang, L., & Jing, X. (2003). Biodegradable electrospun fibers for drug delivery. *Journal of Controlled Release, 92*(3), 227–231.
48. Zeng, J., Yang, L., Liang, Q., Zhang, X., Guan, H., Xu, X., Chen, X., & Jing, X. (2005). Influence of the drug compatibility with polymer solution on the release kinetics of electrospun fiber formulation. *Journal of Controlled Release, 105*(1–2), 43–51.
49. Xu, X., Yang, L., Xu, X., Wang, X., Chen, X., Liang, Q., Zeng, J., & Jing, X. (2005). Ultrafine medicated fibers electrospun from W/O emulsions. *Journal of Controlled Release, 108*(1), 33–42.
50. Loo, T. L., Dion, R. L., Dixon, R. L., & Rall, D. P. (1966). The antitumor agent, 1,3-bis(2-chloroethyl)-1-nitrosourea. *Journal of Pharmaceutical Sciences, 55*(5), 492–497.
51. Xu, X., Chen, X., Xu, X., Lu, T., Wang, X., Yang, L., & Jing, X. (2006). BCNU-loaded PEG-PLLA ultrafine fibers and their in vitro antitumor activity against Glioma C6 cells. *Journal of Controlled Release, 114*(3), 307–316.
52. Liu, D., Liu, S., Jing, X., Li, X., Li, W., & Huang, Y. (2012). Necrosis of cervical carcinoma by dichloroacetate released from electrospun polylactide mats. *Biomaterials, 33*(17), 4362–4369.
53. Ma, G., Liu, Y., Peng, C., Fang, D., He, B., & Nie, J. (2011). Paclitaxel loaded electrospun porous nanofibers as mat potential application for chemotherapy against prostate cancer. *Carbohydrate Polymers, 86*(2), 505–512.
54. Shao, S., Li, L., Yang, G., Li, J., Luo, C., Gong, T., & Zhou, S. (2011). Controlled green tea polyphenols release from electrospun PCL/MWCNTs composite nanofibers. *International Journal of Pharmaceutics, 421*(2), 310–320.
55. Chen, F. M., Zhang, M., & Wu, Z. F. (2010). Toward delivery of multiple growth factors in tissue engineering. *Biomaterials, 31*(24), 6279–6308.
56. Xie, C., Li, X., Luo, X., Yang, Y., Cui, W., Zou, J., & Zhou, S. (2010). Release modulation and cytotoxicity of hydroxycamptothecin-loaded electrospun fibers with 2-hydroxypropyl-beta-cyclodextrin inoculations. *International Journal of Pharmaceutics, 391*(1–2), 55–64.
57. Mi, K., & Xing, Z. (2015). CD44(+)/CD24(−) breast cancer cells exhibit phenotypic reversion in three-dimensional self-assembling peptide RADA16 nanofiber scaffold. *International Journal of Nanomedicine, 10*, 3043–3053.
58. Liu, S., Wang, X., Zhang, Z., Zhang, Y., Zhou, G., Huang, Y., Xie, Z., & Jing, X. (2015). Use of asymmetric multilayer polylactide nanofiber mats in controlled release of drugs and prevention of liver cancer recurrence after surgery in mice. *Nanomedicine, 11*(5), 1047–1056.
59. Yang, G., Wang, J., Wang, Y., Li, L., Guo, X., & Zhou, S. (2015). An implantable active-targeting micelle-in-nanofiber device for efficient and safe cancer therapy. *ACS Nano, 9*(2), 1161–1174.
60. Zamani, M., Prabhakaran, M. P., & Ramakrishna, S. (2013). Advances in drug delivery via electrospun and electrosprayed nanomaterials. *International Journal of Nanomedicine, 8*, 2997–3017.
61. Kim, Y.-J., ebara, m., & Aoyagi, T. (2013). A smart hyperthermia nanofiber with switchable drug release for inducing cancer apoptosis. *Advanced Functional Materials, 23*, 5753–5761.
62. Liang, P., Zheng, J., Dai, S., Wang, J., Zhang, Z., Kang, T., & Quan, C. (2017). pH triggered re-assembly of nanosphere to nanofiber: The role of peptide conformational change for enhanced cancer therapy. *Journal of Controlled Release, 260*, 22–31.
63. Sadrearhami, Z., Morshed, M., & Varshosaz, J. (2015). Production and evaluation of polyblend of Agar and polyacrylonitrile nanofibers for in vitro release of methotrexate in cancer therapy. *Fibers and Polymers, 16*, 254–262.
64. Kim, Y.-J., Park, M., Kim, M., & Kwon, O. H. (2012). Polyphenol-loaded polycaprolactone nanofibers for effective growth inhibition of human cancer cells. *Materials Chemistry and Physics, 133*, 674–680.
65. Chou, S.-F., Carson, D., & Woodrow, K. A. (2015). Current strategies for sustaining drug release from electrospun nanofibers. *Journal of Controlled Release, 220*, 584–591.
66. Carson, D., Jiang, Y., & Woodrow, K. A. (2016). Tunable release of multiclass anti-HIV drugs that are water-soluble and loaded at high drug content in polyester blended electrospun fibers. *Pharmaceutical Research, 33*(1), 125–136.
67. Xie, J., & Wang, C. H. (2006). Electrospun micro- and nanofibers for sustained delivery of paclitaxel to treat C6 glioma in vitro. *Pharmaceutical Research, 23*(8), 1817–1826.
68. McDonald, P. F., Lyons, J. G., Geever, L. M., & Higginbotham, C. L. (2010). In vitro degradation and drug release from polymer blends based on poly(dl-lactide), poly(l-lactide-glycolide) and poly(ε-caprolactone). *Journal of Materials Science, 45*(5), 1284–1292.
69. He, C. L., Huang, Z. M., Han, X. J., Liu, L., Zhang, H. S., & Chen, L. S. (2006). Coaxial electrospun poly(L-lactic acid) ultrafine fibers for sustained drug delivery. *Journal of Macromolecular Science, Part B, 45*(4), 515–524.
70. Reise, M., Wyrwa, R., Muller, U., Zylinski, M., Volpel, A., Schnabelrauch, M., Berg, A., Jandt, K. D., Watts, D. C., &

Sigusch, B. W. (2012). Release of metronidazole from electrospun poly(L-lactide-co-D/L-lactide) fibers for local periodontitis treatment. *Dental Materials, 28*(2), 179–188.

71. Verreck, G., Chun, I., Rosenblatt, J., Peeters, J., Dijck, A. V., Mensch, J., Noppe, M., & Brewster, M. E. (2003). Incorporation of drugs in an amorphous state into electrospun nanofibers composed of a water-insoluble, nonbiodegradable polymer. *Journal of Controlled Release, 92*(3), 349–360.
72. Llorens, E., Ibanez, H., Del Valle, L. J., & Puiggali, J. (2015). Biocompatibility and drug release behavior of scaffolds prepared by coaxial electrospinning of poly(butylene succinate) and polyethylene glycol. *Materials Science & Engineering. C, Materials for Biological Applications, 49*, 472–484.
73. Yang, J. M., Zha, L. S., Yu, D. G., & Liu, J. (2013). Coaxial electrospinning with acetic acid for preparing ferulic acid/zein composite fibers with improved drug release profiles. *Colloids and Surfaces. B, Biointerfaces, 102*, 737–743.
74. He, M., Xue, J., Geng, H., Gu, H., Chen, D., Shi, R., & Zhang, L. (2015). Fibrous guided tissue regeneration membrane loaded with anti-inflammatory agent prepared by coaxial electrospinning for the purpose of controlled release. *Applied Surface Science, 335*, 121–129.
75. Tiwari, S. K., Tzezana, R., Zussman, E., & Venkatraman, S. S. (2010). Optimizing partition-controlled drug release from electrospun core-shell fibers. *International Journal of Pharmaceutics, 392*(1–2), 209–217.
76. Yu, H., Jia, Y., Yao, C., & Lu, Y. (2014). PCL/PEG core/sheath fibers with controlled drug release rate fabricated on the basis of a novel combined technique. *International Journal of Pharmaceutics, 469*(1), 17–22.
77. Kiatyongchai, T., Wongsasulak, S., & Yoovidhya, T. (2014). Coaxial electrospinning and release characteristics of cellulose acetate-gelatin blend encapsulating a model drug. *Journal of Applied Polymer Science, 131*(8), n/a–n/a.
78. Sohrabi, A., Shaibani, P. M., Etayash, H., Kaur, K., & Thundat, T. (2013). Sustained drug release and antibacterial activity of ampicillin incorporated poly(methyl methacrylate)–nylon6 core/shell nanofibers. *Polymer, 54*(11), 2699–2705.
79. Ball, C., Krogstad, E., Chaowanachan, T., & Woodrow, K. A. (2012). Drug-eluting fibers for HIV-1 inhibition and contraception. *PLoS One, 7*(11), e49792.
80. Huang, C., Soenen, S. J., van Gulck, E., Vanham, G., Rejman, J., Van Calenbergh, S., Vervaet, C., Coenye, T., Verstraelen, H., Temmerman, M., et al. (2012). Electrospun cellulose acetate phthalate fibers for semen induced anti-HIV vaginal drug delivery. *Biomaterials, 33*(3), 962–969.
81. Varkey, M., Gittens, S. A., & Uludag, H. (2004). Growth factor delivery for bone tissue repair: An update. *Expert Opinion Drug Delivery, 1*(1), 19–36.
82. Chen, P., Wu, Q. S., Ding, Y. P., Chu, M., Huang, Z. M., & Hu, W. (2010). A controlled release system of titanocene dichloride by electrospun fiber and its antitumor activity in vitro. *European Journal of Pharmaceutics and Biopharmaceutics, 76*(3), 413–420.
83. Chew, S. Y., Wen, J., Yim, E., & Leong, K. W. (2005). Sustained release of proteins from electrospun biodegradable fibers. *Biomacromolecules, 6*, 2017–2024.
84. Patel, S., Kurpinski, K., Quigley, R., Gao, H., Hsiao, B. S., Poo, M., & Li, S. (2007). Bioactive nanofibers-synergistic effects of nanotopography and chemical signaling on cell guidance. *Nano Letters, 7*(7), 2122–2128.
85. Sahoo, S., Ang, L. T., Goh, J. C., & Toh, S. L. (2010). Growth factor delivery through electrospun nanofibers in scaffolds for tissue engineering applications. *Journal of Biomedical Materials Research. Part A, 93*(4), 1539–1550.
86. Mottaghitalab, F., Farokhi, M., Mottaghitalab, V., Ziabari, M., Divsalar, A., & Shokrgozar, M. A. (2011). Enhancement of neural cell lines proliferation using nano-structured chitosan/poly(vinyl alcohol) scaffolds conjugated with nerve growth factor. *Carbohydrate Polymers, 86*(2), 526–535.
87. Zomer Volpato, F., Almodovar, J., Erickson, K., Popat, K. C., Migliaresi, C., & Kipper, M. J. (2012). Preservation of FGF-2 bioactivity using heparin-based nanoparticles, and their delivery from electrospun chitosan fibers. *Acta Biomaterialia, 8*(4), 1551–1559.
88. Liao, I. C., Chen, S., Liu, J., & Leong, K. (2009). Sustained viral gene delivery through core-shell fibers. *Journal of Controlled Release: Official Journal of the Controlled Release Society, 139*, 48–55.
89. Wang, J., An, Q., Li, D., Wu, T., Chen, W., Sun, B., El-Hamshary, H., Al-Deyab, S. S., Zhu, W., & Mo, X. (2015). Heparin and vascular endothelial growth factor loaded poly(L-lactide-co-caprolactone) nanofiber covered stent-graft for aneurysm treatment. *Journal of Biomedical Nanotechnology, 11*(11), 1947–1960.
90. Yu, Y. Q., Jiang, X. S., Gao, S., Ma, R., Jin, Y., Jin, X., Peng, S. Y., Mao, H. Q., & Li, J. T. (2014). Local delivery of vascular endothelial growth factor via nanofiber matrix improves liver regeneration after extensive hepatectomy in rats. *Journal of Biomedical Nanotechnology, 10*(11), 3407–3415.
91. Kim, T. H., Kim, J. J., & Kim, H. W. (2014). Basic fibroblast growth factor-loaded, mineralized biopolymer-nanofiber scaffold improves adhesion and proliferation of rat mesenchymal stem cells. *Biotechnology Letters, 36*(2), 383–390.
92. Jain, V., Jain, S., & Mahajan, S. (2015). Nanomedicines based drug delivery systems for anti-cancer targeting and treatment. *Current Drug Delivery, 12*(2), 177–191.
93. Maitra, A., Arking, D. E., Shivapurkar, N., Ikeda, M., Stastny, V., Kassauei, K., Sui, G., Cutler, D. J., Liu, Y., Brimble, S. N., et al. (2005). Genomic alterations in cultured human embryonic stem cells. *Nature Genetics, 37*(10), 1099–1103.
94. Lai, K., Kaspar, B., Gage, F., & Schaffer, D. (2003). Sonic hedgehog regulates adult neural progenitor proliferation in vitro and in vivo. *Nature Neuroscience, 6*, 21–27.
95. Gropp, M., Itsykson, P., Singer, O., Ben-Hur, T., Reinhartz, E., Galun, E., & Reubinoff, B. E. (2003). Stable genetic modification of human embryonic stem cells by lentiviral vectors. *Molecular Therapy, 7*(2), 281–287.
96. Walther, W., & Schlag, P. (2013). Current status of gene therapy for cancer. *Current Opinion in Oncology, 25*, 659–664.
97. Réjiba, S., Bigand, C., Parmentier, C., Masmoudi, A., & Hajri, A. (2013). Oncosuppressive suicide gene Virotherapy "PVH1-yCD/5-FC" for pancreatic peritoneal carcinomatosis treatment: NFκB and Akt/PI3K involvement. *PLoS One, 8*, e70594.
98. Jang, J.-H., Houchin, T., Shea, L., Jang, J. H., Houchin, T. L., & Shea, L. D. (2004). Gene delivery from polymer scaffolds for tissue engineering. *Expert Review of Medical Devices, 1*, 127–138.
99. Shea, L., Smiley, E., Bonadio, J., Mooney, D., Shea, L. D., Smiley, E., Bonadio, J., & Mooney, D. J. (1999). DNA delivery from polymer matrices for tissue engineering. *Nature Biotechnology, 17*, 551–554.
100. Yates, F., Daley, G., Yates, F., & Daley, G. Q. (2006). Progress and prospects: Gene transfer into embryonic stem cells. *Gene Therapy, 13*, 1431–1439.
101. Hanna, E., Remuzat, C., Auquier, P., & Toumi, M. (2017). Gene therapies development: Slow progress and promising prospect. *Journal of Market Access Health Policy, 5*(1), 1265293.
102. Nayerossadat, N., Maedeh, T., & Ali, P. A. (2012). Viral and non-viral delivery systems for gene delivery. *Advanced Biomedical Research, 1*, 27.
103. Cao, H., Jiang, X., Chai, C., & Chew, S. Y. (2010). RNA interference by nanofiber-based siRNA delivery system. *Journal of Controlled Release, 144*(2), 203–212.

104. Chen, M., Gao, S., Dong, M., Song, J., Yang, C., Howard, H. A., Kjems, K., & Besenbacher, F. (2012). Chitosan-siRNA nanoparticles encapsulated in PLGA nanofibers for siRNA delivery. *ACS Nano, 6*(6), 4835–4844.
105. Chooi, W. H., Ong, W., Murray, A., Lin, J., Nizetic, D., & Chew, S. Y. (2018). Scaffold mediated gene knockdown for neuronal differentiation of human neural progenitor cells. *Biomaterials Science, 6*(11), 3019–3029.
106. He, S., Xia, T., Wang, H., Wei, L., Luo, X., & Li, X. (2012). Multiple release of polyplexes of plasmids VEGF and bFGF from electrospun fibrous scaffolds towards regeneration of mature blood vessels. *Acta Biomaterialia, 8*(7), 2659–2669.
107. Hu, W. W., & Ting, J. C. (2019). Gene immobilization on alginate/polycaprolactone fibers through electrophoretic deposition to promote in situ transfection efficiency and biocompatibility. *International Journal of Biological Macromolecules, 121*, 1337–1345.
108. Karthikeyan, K., Krishnaswamy, V. R., Lakra, R., Kiran, M. S., & Korrapati, P. S. (2015). Fabrication of electrospun zein nanofibers for the sustained delivery of siRNA. *Journal of Materials Science. Materials in Medicine, 26*(2), 101.
109. Kim, H. S., & Yoo, H. S. (2010). MMPs-responsive release of DNA from electrospun nanofibrous matrix for local gene therapy: In vitro and in vivo evaluation. *Journal of Controlled Release, 145*(3), 264–271.
110. Kim, H. S., & Yoo, H. S. (2013). Matrix metalloproteinase-inspired suicidal treatments of diabetic ulcers with siRNA-decorated nanofibrous meshes. *Gene Therapy, 20*(4), 378–385.
111. Lee, S., Kim, J. S., Chu, H. S., Kim, G. W., Won, J. I., & Jang, J. H. (2011). Electrospun nanofibrous scaffolds for controlled release of adeno-associated viral vectors. *Acta Biomaterialia, 7*(11), 3868–3876.
112. Liang, D., Luu, Y., Kim, K., Hsiao, B., Hadjiargyrou, M., & Chu, B. (2005). In vitro non-viral gene delivery with nanofibrous scaffolds. *Nucleic Acids Research, 33*, e170.
113. Low, W. C., Rujitanaroj, P. O., Lee, D. K., Kuang, J., Messersmith, P. B., Chan, J. K., & Chew, S. Y. (2015). Mussel-inspired modification of nanofibers for REST siRNA delivery: Understanding the effects of gene-silencing and substrate topography on human mesenchymal stem cell neuronal commitment. *Macromolecular Bioscience, 15*(10), 1457–1468.
114. Low, W. C., Rujitanaroj, P. O., Lee, D. K., Messersmith, P. B., Stanton, L. W., Goh, E., & Chew, S. Y. (2013). Nanofibrous scaffold-mediated REST knockdown to enhance neuronal differentiation of stem cells. *Biomaterials, 34*(14), 3581–3590.
115. Luu, Y. K., Kim, K., Hsiao, B. S., Chu, B., & Hadjiargyrou, M. (2003). Development of a nanostructured DNA delivery scaffold via electrospinning of PLGA and PLA–PEG block copolymers. *Journal of Controlled Release, 89*(2), 341–353.
116. Mazza, M., Hadjidemetriou, M., La'zaro, I., Bussy, C., & Kostarelos, K. (2015). Peptide nanofiber complexes with siRNA for deep brain gene silencing by stereotactic neurosurgery. *ACS Nano, 9*(2), 1137–1149.
117. Nie, H., Ho, M. L., Wang, C. K., Wang, C. H., & Fu, Y. C. (2009). BMP-2 plasmid loaded PLGA/HAp composite scaffolds for treatment of bone defects in nude mice. *Biomaterials, 30*(5), 892–901.
118. Nie, H., & Wang, C.-H. (2007). Fabrication and characterization of PLGA/HAp composite scaffolds for delivery of BMP-2 plasmid DNA. *Journal of Controlled Release, 120*(1), 111–121.
119. Pinese, C., Lin, J., Milbreta, U., Li, M., Wang, Y., Leong, K. W., & Chew, S. Y. (2018). Sustained delivery of siRNA/mesoporous silica nanoparticle complexes from nanofiber scaffolds for long-term gene silencing. *Acta Biomaterialia, 76*, 164–177.
120. Qin, L., Yan, P., Xie, C., Huang, J., Ren, Z., Li, X., Best, S., Cai, X., & Han, G. (2018). Gold nanorod-assembled ZnGa2O4:Cr nanofibers for LED-amplified gene silencing in cancer cells. *Nanoscale, 10*(28), 13432–13442.
121. Rujitanaroj, P. O., Jao, B., Yang, J., Wang, F., Anderson, J. M., Wang, J., & Chew, S. Y. (2013). Controlling fibrous capsule formation through long-term down-regulation of collagen type I (COL1A1) expression by nanofiber-mediated siRNA gene silencing. *Acta Biomaterialia, 9*(1), 4513–4524.
122. Rujitanaroj, P. O., Wang, Y. C., Wang, J., & Chew, S. Y. (2011). Nanofiber-mediated controlled release of siRNA complexes for long term gene-silencing applications. *Biomaterials, 32*(25), 5915–5923.
123. Sakai, S., Yamada, Y., Yamaguchi, T., Ciach, T., & Kawakami, K. (2009). Surface immobilization of poly(ethyleneimine) and plasmid DNA on electrospun poly(L-lactic acid) fibrous mats using a layer-by-layer approach for gene delivery. *Journal of Biomedical Materials Research. Part A, 88*(2), 281–287.
124. Saraf, A., Baggett, L., Raphael, R., Kasper, F., & Mikos, A. (2009). Regulated non-viral gene delivery from coaxial electrospun fiber mesh scaffolds. *Journal of Controlled Release: Official Journal of the Controlled Release Society, 143*, 95–103.
125. Wang, W., Zhang, K., & Chen, D. (2018). From tunable DNA/polymer self-assembly to tailorable and morphologically pure core-shell nanofibers. *Langmuir, 34*(50), 15350–15359.
126. Yang, Y., Li, X., Cheng, L., He, S., Zou, J., Chen, F., & Zhang, Z. (2011). Core-sheath structured fibers with pDNA polyplex loadings for the optimal release profile and transfection efficiency as potential tissue engineering scaffolds. *Acta Biomaterialia, 7*(6), 2533–2543.
127. Zou, B., Liu, Y., Luo, X., Chen, F., Guo, X., & Li, X. (2012). Electrospun fibrous scaffolds with continuous gradations in mineral contents and biological cues for manipulating cellular behaviors. *Acta Biomaterialia, 8*(4), 1576–1585.
128. Wilhelm, S., Tavares, A. J., Dai, Q., Ohta, S., Audet, J., Dvorak, H. F., & Chan, C. (2016). Analysis of nanoparticle delivery to tumours. *Nature Reviews Materials, 1*(5), 16014.
129. Agarwal, S., Wendorff, J. H., & Greiner, A. (2009). Progress in the field of electrospinning for tissue engineering applications. *Advanced Materials, 21*(32–33), 3343–3351.
130. Williams, G., Chatterton, N., Nazir, T., Yu, D., Zhu, L.-M., & Branford-White, C. (2012). Electrospun nanofibers in drug delivery: Recent developments and perspectives. *Therapeutic Delivery, 3*, 515–533.
131. Lee, S., Cho, S., Kim, M., Jin, G., Jeong, U., & Jang, J.-H. (2014). Highly moldable electrospun clay-like fluffy nanofibers for three-dimensional scaffolds. *ACS Applied Materials & Interfaces, 6*, 1082–1091.
132. Shimanovich, U., Tkacz, I., Eliaz, D., Cavaco-Paulo, A., Michaeli, S., & Gedanken, A. (2011). Encapsulation of RNA molecules in BSA microspheres and internalization into Trypanosoma Brucei parasites and human U2OS cancer cells. *Advanced Functional Materials, 21*, 3659–3666.
133. Trabulo, S., Resina, S., Lebleu, B., Pedroso de Lima, M., Trabulo, S., Resina, S., Simões, S., Lebleu, B., & Pedroso de Lima, M. C. (2010). A non-covalent strategy combining cationic lipids and CPPs to enhance the delivery of splice correcting oligonucleotides. *Journal of Controlled Release: Official Journal of the Controlled Release Society, 145*, 149–158.
134. Achille, C., Sundaresh, S., Chu, B., & Hadjiargyrou, M. (2012). Cdk2 silencing via a DNA/PCL electrospun scaffold suppresses proliferation and increases death of breast cancer cells. *PLoS One, 7*, e52356.
135. Xie, J. (2015). Expanding two-dimensional electrospun nanofiber membranes in the third dimension by a modified gas-foaming technique. *ACS Bimaterials Science & Engineering, 1*, 991.

136. Bago, R., Pegna, G. J., Okolie, O., Mohiti-Asli, M., Loboa, E., & Hingtgen, S. (2016). Electrospun nanofibrous scaffolds increase the efficacy of stem cell-mediated therapy of surgically resected glioblastoma. *Biomaterials, 90*, 116.
137. Wang, Z., Ma, R., Yan, L., Chen, X., & Zhu, G. (2015). Combined chemotherapy and photodynamic therapy using a nanohybrid based on layered double hydroxides to conquer cisplatin resistance. *Chemical Communications (Camb), 51*(58), 11587–11590.
138. Liu, Y., Zhang, X., Zhou, M., Nan, X., Chen, X., & Zhang, X. (2017). Mitochondrial-targeting Lonidamine-doxorubicin nanoparticles for synergistic chemotherapy to conquer drug resistance. *ACS Applied Materials & Interfaces, 9*(50), 43498–43507.
139. Fu, Y., Li, X., Ren, Z., Mao, C., & Han, G. (2018). Multifunctional electrospun nanofibers for enhancing localized cancer treatment. *Small*, e1801183.
140. Blanco, E., Shen, H., & Ferrari, M. (2015). Principles of nanoparticle design for overcoming biological barriers to drug delivery. *Nature Biotechnology, 33*(9), 941–951.
141. He, Y., Li, X., Ma, J., Ni, G., Yang, G., & Zhou, S. (2019). Programmable codelivery of doxorubicin and Apatinib using an implantable hierarchical-structured Fiber device for overcoming cancer multidrug resistance. *Small, 15*(8), 1804397.
142. Xiao, Y., Shen, M., & Shi, X. (2018). Design of functional electrospun nanofibers for cancer cell capture applications. *Journal of Materials Chemistry B, 6*(10), 1420–1432.
143. Zhao, Y., Fan, Z., Shen, M., & Shi, X. (2015). Hyaluronic acid-functionalized electrospun polyvinyl alcohol/Polyethylenimine nanofibers for Cancer cell capture applications. *Advanced Materials Interfaces, 2*(15), 1500256.
144. Zhao, Y., Zhu, X., Liu, H., Luo, Y., Wang, S., Shen, M., Zhu, M., & Shi, X. (2014). Dendrimer-functionalized electrospun cellulose acetate nanofibers for targeted cancer cell capture applications. *Journal of Materials Chemistry B, 2*(42), 7384–7393.
145. Wang, S., Zhu, J., Shen, M., Zhu, M., & Shi, X. (2014). Poly(amidoamine) Dendrimer-enabled simultaneous stabilization and functionalization of electrospun poly(γ-glutamic acid) nanofibers. *ACS Applied Materials & Interfaces, 6*, 2153.
146. Zhang, N., Deng, Y., Tai, Q., Cheng, B., Zhao, L., Shen, Q., He, R., Hong, L., Liu, W., Guo, S., et al. (2012). Electrospun TiO2 nanofiber-based cell capture assay for detecting circulating tumor cells from colorectal and gastric cancer patients. *Advanced Materials, 24*(20), 2756–2760.
147. Zha, Z., Cohn, C., Dai, Z., Qiu, W., Zhang, J., & Wu, X. (2011). Nanofibrous lipid membranes capable of functionally immobilizing antibodies and capturing specific cells. *Advanced Materials, 23*(30), 3435–3440.
148. Zha, Z., Jiang, L., Dai, Z., & Wu, X. (2012). A biomimetic mechanism for antibody immobilization on lipid nanofibers for cell capture. *Applied Physics Letters, 101*(19), 193701.
149. Sun, N., Liu, M., Jine, W., Zhili, W., Li, X., Jiang, B., & Pei, R. (2016). Chitosan nanofibers for specific capture and nondestructive release of CTCs assisted by pCBMA brushes. *Small, 12*, 5090–5097.
150. Yoon, J., Yoon, H. S., Shin, Y., Kim, S., Ju, Y., Kim, J., & Chung, S. (2017). Ethanol-dispersed and antibody-conjugated polymer nanofibers for the selective capture and 3-dimensional culture of EpCAM-positive cells. *Nanomedicine, 13*(5), 1617–1625.
151. Jackson, J. M., Witek, M. A., Kamande, J. W., & Soper, S. A. (2017). Materials and microfluidics: Enabling the efficient isolation and analysis of circulating tumour cells. *Chemical Society Reviews, 46*(14), 4245–4280.
152. Myung, J. H., & Hong, S. (2015). Microfluidic devices to enrich and isolate circulating tumor cells. *Lab on a Chip, 15*(24), 4500–4511.
153. Liu, Z., Zhang, W., Huang, F., Feng, H., Shu, W., Xu, X., & Chen, Y. (2013). High throughput capture of circulating tumor cells using an integrated microfluidic system. *Biosensors & Bioelectronics, 47*, 113–119.
154. Liu, H.-Q., Yu, X.-L., Cai, B., You, S.-J., He, Z., Huang, Q.-Q., Rao, L., Li, S.-S., Liu, C., Sun, W.-W., et al. (2015). Capture and release of cancer cells using electrospun etchable MnO2 nanofibers integrated in microchannels. *Applied Physics Letters, 106*, 093703.
155. Hou, S., Zhao, L., Shen, Q., Yu, J., Ng, C., Kong, X., Wu, D., Song, M., Shi, X., Xu, X., et al. (2013). Inside back cover: Polymer nanofiber-embedded microchips for detection, isolation, and molecular analysis of single circulating melanoma. *Cells Angewandte Chemie International Edition, 52*(12), 3533–3533.
156. Wu, L., & Qu, X. (2015). Cancer biomarker detection: Recent achievements and challenges. *Chemical Society Reviews, 44*, 2963–2997.
157. Rakovich, T., Mahfoud, O., Mohamed, B., Prina-Mello, A., Crosbie Staunton, K., Van Den Broeck, T., De Kimpe, L., Sukhanova, A., Baty, D., Rakovich, A., et al. (2014). Highly sensitive single domain antibody-quantum dot conjugates for detection of HER2 biomarker in lung and breast cancer cells. *ACS Nano, 8*, 5682.
158. Xu, J.-J., Zhao, W.-W., Song, S., Fan, C., & Chen, H.-Y. (2014). ChemInform abstract: Functional nanoprobes for ultrasensitive detection of biomolecules: An update. *ChemInform, 45*(18), 1601–1611.
159. Yu Ding, Y., Wang, Y., Su, L., Bellagamba, M., Zhang, H., & Lei, Y. (2010). Electrospun Co(3)O(4) nanofibers for sensitive and selective glucose detection. *Biosensors & Bioelectronics, 26*, 542–548.
160. Hu, J., & Easley, C. (2011). A simple and rapid approach for measurement of dissociation constants of DNA aptamers against proteins and small molecules via automated microchip electrophoresis. *The Analyst, 136*, 3461–3468.
161. Hu, J., Sollie, R., & Easley, C. (2010). Improvement of sensitivity and dynamic range in proximity ligation assays by asymmetric connector hybridization. *Analytical Chemistry, 82*, 6976–6982.
162. Wang, X., Wang, X., Wang, X., Chen, F., Zhu, K., & Tang, M. (2013). Novel electrochemical biosensor based on functional composite nanofibers for sensitive detection of p53 tumor suppressor gene. *Analytica Chimica Acta, 765*, 63–69.
163. Davis, B., Niamnont, N., Hare, C., Sukwattanasinitt, M., & Cheng, Q. (2010). Nanofibers doped with dendritic fluorophores for protein detection. *ACS Applied Materials & Interfaces, 2*, 1798–1803.
164. Hu, J., Wang, T., Shannon, C., & Easley, C. (2012). Quantitation of Femtomolar protein levels via direct readout with the electrochemical proximity assay. *Journal of the American Chemical Society, 134*, 7066–7072.
165. Hu, J., Yu, Y., Brooks, J., Godwin, L., Somasundaram, S., Torabinejad, F., Shannon, C., & Easley, C. (2014). A reusable electrochemical proximity assay for highly selective, real-time protein quantitation in biological matrices. *Journal of the American Chemical Society, 136*, 8467–8474.
166. Wang, X., Shu, G., Gao, C., Yang, Y., & Tang, M. (2014). Electrochemical biosensor based on functional composite nanofibers for detection of K-ras gene via multiple signal amplification strategy. *Analytical Biochemistry, 466*, 51–58.
167. Bohunicky, B., & Mousa, S. (2010). Biosensors: The new wave in cancer diagnosis. *Nanotechnology, Science and Applications, 4*, 1–10.
168. Dorothee, G., MacKenzie, R., Janos, V. r. s., & Reimhult, E. (2008). Electrochemical biosensors - sensor principles and architectures. *Sensors, 8*(3), 1400–1458.
169. Wei, Y., Li, X., Sun, X., Ma, H., Zhang, Y., & Wei, Q. (2017). Dual-responsive electrochemical immunosensor for prostate

specific antigen detection based on au-CoS/graphene and CeO 2 /ionic liquids doped with carboxymethyl chitosan complex. *Biosensors and Bioelectronics, 94*, 141–147.

170. Mehrvar, M., & Abdi, M. (2004). Recent developments, characteristics, and potential applications of electrochemical biosensors. *Analytical Sciences: the International Journal of the Japan Society for Analytical Chemistry, 20*, 1113–1126.
171. Marcus, R., & Sutin, N. (1985). Electron transfers in chemistry and biology. *Biochimica Et Biophysica Acta (bba) - Reviews on Bioenergetics, 811*, 265–322.
172. Putzbach, W., & Ronkainen, N. (2013). ChemInform abstract: Immobilization techniques in the fabrication of nanomaterial-based electrochemical biosensors: A review. *Sensors (Basel, Switzerland), 13*, 4811–4840.
173. Tilmaciu, C., & Morris, M. (2015). Carbon nanotube biosensors. *Frontiers in Chemistry, 3*, 1–21.
174. Tyagi, S., & Kramer, F. R. (1996). Molecular beacons: Probes that fluoresce upon hybridization. *Nature Biotechnology, 14*(3), 303–308.
175. Medina, V., & Rivera, E. (2010). Histamine receptors and cancer pharmacology. *British Journal of Pharmacology, 161*, 755–767.
176. Seong, D., Choi, M.-S., & Kim, Y.-J. (2012). Fluorescent chemosensor for the detection of histamine based on dendritic porphyrin-incorporated nanofibers. *European Polymer Journal, 48*, 1988–1996.
177. Kosaki, Y., Izawa, H., Ishihara, S., Kawakami, K., Sumita, M., Tateyama, Y., Ji, Q., Krishnan, V., Hishita, S., Yamauchi, Y., et al. (2013). Nanoporous carbon sensor with cage-in-fiber structure: Highly selective aniline adsorbent toward cancer risk management. *ACS Applied Materials & Interfaces, 5*, 2930–2934.
178. Peng, G., Tisch, U., Adams, O., Hakim, M., Shehada, N., Broza, Y., Billan, S., Abdah-Bortnyak, R., Kuten, A., & Haick, H. (2009). Diagnosing lung cancer in exhaled breath using gold nanoparticles. *Nature Nanotechnology, 4*, 669–673.
179. Yu, H., Xu, L., Cao, M., Chen, X., Wang, P., Jiao, J., & Wang, Y. (2003). Detection volatile organic compounds in breath as markers of lung cancer using a novel electronic nose, 2003.
180. Choi, S.-H., Ankonina, G., Youn, D.-Y., Oh, S.-G., Hong, J.-M., Rothschild, A., & Kim, I.-D. (2009). Hollow ZnO nanofibers fabricated using electrospun polymer templates and their electronic transport properties. *ACS Nano, 3*, 2623–2631.
181. Zhang, Y., He, X., Li, J., Miao, Z., & Huang, F. (2008). Fabrication and ethanol-sensing properties of micro gas sensor based on electrospun SnO2 nanofibers. *Sensors and Actuators B: Chemical, 132*, 67–73.
182. Lee, C., Kim, I.-D., & Lee, J.-H. (2013). Selective and sensitive detection of trimethylamine using ZnO–In2O3 composite nanofibers. *Sensors and Actuators B: Chemical, 181*, 463–470.
183. Choi, S.-J., Kim, S.-J., Koo, W.-T., Cho, H.-J., & Kim, I.-D. (2014). Catalyst-loaded porous WO$_3$ nanofibers using catalyst-decorated polystyrene colloid templates for detection of biomarker molecules. *Chemical Communications, 51*, 2609.
184. Adiguzel, Y., & Kulah, H. (2015). Breath sensors for lung cancer diagnosis. *Biosensors and Bioelectronics, 65*, 121–138.
185. Kim, S.-J., Choi, S.-J., Yang, D.-J., Bae, J., Park, J., & Kim, I.-D. (2014). Highly sensitive and selective hydrogen sulfide and toluene sensors using Pd functionalized WO3 nanofibers for potential diagnosis of halitosis and lung cancer. *Sensors and Actuators B: Chemical, 193*, 574–581.
186. Kimmel, D., Leblanc, G., Meschievitz, M., & Cliffel, D. (2011). Electrochemical sensors and biosensors. *Analytical Chemistry, 84*, 685–707.
187. Scanlon, M., Salaj-Kosla, U., Belochapkine, S., MacAodha, D., Leech, D., Ding, Y., & Magner, E. (2012). Characterization of nanoporous gold electrodes for bioelectrochemical applications. *Langmuir: The ACS Journal of Surfaces and Colloids, 28*, 2251–2261.
188. Ali, M. A., Mondal, K., Singh, C., Malhotra, B., & Sharma Iitk, A. (2015). Anti-epidermal growth factor receptor conjugated mesoporous zinc oxide nanofibers for breast cancer diagnostics. *Nanoscale, 7*, 7234–7245.
189. Frenot, A., & Chronakis, I. (2003). Polymer nanofibers assembled by electrospinning. *Current Opinion in Colloid & Interface Science, 8*, 64–75.
190. Zhang, C.-L., & Yu, S.-H. (2014). Nanoparticles meet electrospinning: Recent advances and future prospects. *Chemical Society Reviews, 43*, 4423–4448.
191. Jordan, A., Scholz, R., Maier-Hauff, K., van Landeghem, F. K., Waldoefner, N., Teichgraeber, U., Pinkernelle, J., Bruhn, H., Neumann, F., Thiesen, B., et al. (2006). The effect of thermotherapy using magnetic nanoparticles on rat malignant glioma. *Journal of Neuro-Oncology, 78*(1), 7–14.
192. Yanase, M., Shinkai, M., Honda, H., Wakabayashi, T., Yoshida, J., & Kobayashi, T. (1998). Intracellular hyperthermia for cancer using magnetite cationic liposomes: An in vivo study. *Japanese Journal of Cancer Research, 89*(4), 463–470.
193. Hervault, A., & Thanh, N. T. (2014). Magnetic nanoparticle-based therapeutic agents for thermo-chemotherapy treatment of cancer. *Nanoscale, 6*(20), 11553–11573.
194. Kobayashi, T. (2011). Cancer hyperthermia using magnetic nanoparticles. *Biotechnology Journal, 6*(11), 1342–1347.
195. Santhosh, P. B., & Ulrih, N. P. (2013). Multifunctional superparamagnetic iron oxide nanoparticles: Promising tools in cancer theranostics. *Cancer Letters, 336*(1), 8–17.
196. Mfiller, R. H., Maaben, S., Weyhers, L. H., Specht, F., & Lucks, J. S. (1996). Cytotoxicity of magnetite-loaded polylactide, polylactide-glycolide particles and solid lipid nanoparticles. *International Journal of Pharmaceutics, 138*, 85–94.
197. Weissleder, R., Bogdanov, A., Neuweltb, E. A., & Papisov, M. (1995). Long-circulating iron oxides for MR imaging. *Advanced Drug Delivery Reviews, 16*, 321–334.
198. Kaminski, M. D., & Rosengart, A. J. (2005). Detoxification of blood using injectable magnetic nanospheres: A conceptual technology description. *Journal of Magnetism and Magnetic Materials, 293*(1), 398–403.
199. Feng, Z.-Q., Shi, C., Zhao, B., & Wang, T. (2017). Magnetic electrospun short nanofibers wrapped graphene oxide as a promising biomaterials for guiding cellular behavior. *Materials Science and Engineering: C, 81*, 314–320.
200. Huang, C., Soenen, S. J., Rejman, J., Trekker, J., Chengxun, L., Lagae, L., Ceelen, W., Wilhelm, C., Demeester, J., & De Smedt, S. C. (2012). Magnetic electrospun fibers for cancer therapy. *Advanced Functional Materials, 22*(12), 2479–2486.
201. Sasikala, A. R. K., Unnithan, A. R., Yun, Y.-H., Park, C. H., & Kim, C. S. (2016). An implantable smart magnetic nanofiber device for endoscopic hyperthermia treatment and tumor-triggered controlled drug release. *Acta Biomaterialia, 31*, 122–133.
202. Song, C., Wang, X. X., Zhang, J., Nie, G. D., Luo, W. L., Fu, J., Ramakrishna, S., & Long, Y. Z. (2018). Electric field-assisted in situ precise deposition of electrospun gamma-Fe2O3/polyurethane nanofibers for magnetic hyperthermia. *Nanoscale Research Letters, 13*(1), 273.
203. Radmansouri, M., Bahmani, E., Sarikhani, E., Rahmani, K., Sharifianjazi, F., & Irani, M. (2018). Doxorubicin hydrochloride - loaded electrospun chitosan/cobalt ferrite/titanium oxide nanofibers for hyperthermic tumor cell treatment and controlled drug release. *International Journal of Biological Macromolecules, 116*, 378–384.
204. Chen, Z., Chen, Z., Zhang, A., Hu, J., Wang, X., & Yang, Z. (2016). Electrospun nanofibers for cancer diagnosis and therapy. *Biomaterials Science, 4*(6), 922–932.

205. Fan, Y., Chen, C., Huang, Y., Zhang, F., & Lin, G. (2017). Study of the pH-sensitive mechanism of tumor-targeting liposomes. *Colloids and Surfaces. B, Biointerfaces, 151*, 19–25.
206. Demirci, S., Celebioglu, A., Aytac, Z., & Uyar, T. (2014). pH-responsive nanofibers with controlled drug release properties. *Polymer Chemistry, 5*(6), 2050–2056.
207. Thakkar, S., & Misra, M. (2017). Electrospun polymeric nanofibers: New horizons in drug delivery. *European Journal of Pharmaceutical Sciences, 107*, 148–167.
208. Illangakoon, U. E., Yu, D. G., Ahmad, B. S., Chatterton, N. P., & Williams, G. R. (2015). 5-fluorouracil loaded Eudragit fibers prepared by electrospinning. *International Journal of Pharmaceutics, 495*(2), 895–902.
209. Han, D., & Steckl, A. J. (2017). Selective pH-responsive core-sheath nanofiber membranes for Chem/bio/med applications: Targeted delivery of functional molecules. *ACS Applied Materials & Interfaces, 9*(49), 42653–42660.
210. Tran, T., Hernandez, M., Patel, D., Burns, E., Peterman, V., & Wu, J. (2015). Controllable and switchable drug delivery of ibuprofen from temperature responsive composite nanofibers. *Nano Convergence, 2*(1), 15.
211. Zhang, R. Y., Zaslavski, E., Vasilyev, G., Boas, M., & Zussman, E. (2018). Tunable pH-responsive chitosan-poly(acrylic acid) electrospun fibers. *Biomacromolecules, 19*(2), 588–595.
212. Sang, Q., Williams, G. R., Wu, H., Liu, K., Li, H., & Zhu, L. M. (2017). Electrospun gelatin/sodium bicarbonate and poly(lactide-co-epsilon-caprolactone)/sodium bicarbonate nanofibers as drug delivery systems. *Materials Science & Engineering. C, Materials for Biological Applications, 81*, 359–365.
213. Jassal, M., Boominathan, V., Ferreira, T., Sengupta, S., & Bhowmick, S. (2016). pH-responsive drug release from functionalized electrospun poly(caprolactone) scaffolds under simulated in-vivo environment. *Journal of Biomaterials Science, Polymer Edition, 27*, 1–34.
214. Toncheva, A., Paneva, D., Maximova, V., Manolova, N., & Rashkov, I. (2012). Antibacterial fluoroquinolone antibiotic-containing fibrous materials from poly(L-lactide-co-D,L-lactide) prepared by electrospinning. *European Journal of Pharmaceutical Sciences: Official Journal of the European Federation for Pharmaceutical Sciences, 47*, 642–651.
215. Ercole, F., Davis, T., & Evans, R. (2010). Photo-responsive systems and biomaterials: Photochromic polymers, light-triggered self-assembly, surface modification, fluorescence modulation and beyond. *Polymer Chemistry, 1*, 37.
216. Gorostiza, P., & Isacoff, E. (2008). Optical switches for remote and noninvasive control of cell signaling. *Science (New York, N.Y.), 322*, 395–399.
217. Yu, Y., Nakano, M., & Ikeda, T. (2003). Directed bending of a polymer film by light. *Nature, 425*(6954), 145–145.
218. Klajn, R., Wesson, P., Bishop, K., & Grzybowski, B. (2009). Writing self-erasing images using metastable nanoparticle "inks". *Angewandte Chemie (International Ed. in English), 48*, 7035–7039.
219. Davis, M., Brewster, M., Davis, M. E., & Brewster, M. E. (2005). Cyclodextrin-based pharmaceutics: Past, present and future. *Nature Reviews. Drug Discovery, 3*, 1023–1035.
220. Wang, Y., Ma, N., Wang, Z., & Zhang, X. (2007). Photocontrolled reversible supramolecular assemblies of an Azobenzene-containing surfactant with α-Cyclodextrin. *Angewandte Chemie (International Ed. in English), 46*, 2823–2826.
221. Fu, G., Xu, L., Yao, F., Li, G., & Kang, E. (2009). Smart nanofibers with a Photoresponsive surface for controlled release. *ACS Applied Materials & Interfaces, 1*, 2424–2427.
222. Weissleder, R. (2001). A clearer vision for in vivo imaging. *Nature Biotechnology, 19*, 316–317.
223. Chen, J., Guo, Z., Wang, H. B., Gong, M., Kong, X. K., Xia, P., & Chen, Q. W. (2013). Multifunctional Fe3O4@C@ag hybrid nanoparticles as dual modal imaging probes and near-infrared light-responsive drug delivery platform. *Biomaterials, 34*(2), 571–581.
224. Kurapati, R., & Raichur, A. (2013). Near-infrared light-responsive graphene oxide composite multilayer capsules: A novel route for remote controlled drug delivery. *Chemical Communications, 49*, 734.
225. Yashchenok, A., Bratashov, D., Gorin, D., Lomova, M., Pavlov, A., Sapelkin, A., Shim, B., Khomutov, G., Kotov, N., Sukhorukov, G., et al. (2010). Carbon nanotubes on polymeric microcapsules: Free-standing structures and point-wise laser openings. *Advanced Functional Materials, 20*, 3136–3142.
226. Zhang, Z., Wang, L., Wang, J., Jiang, X.-M., Li, X., Hu, Z., Yinglu, J., Wu, X., Chen, C., Zhang, Z., Wang, L., Wang, J., Jiang, X., Li, X., Hu, Z., Ji, Y., Wu, X., & Chen, C. (2012). Mesoporous silica-coated gold nanorods as a light-mediated multifunctional theranostic platform for cancer treatment. *Advanced Materials (Deerfield Beach, Fla.), 24*, 1418–1423.
227. Cobley, C., Chen, J., Cho, E., Wang, L., & Xia, Y. (2011). ChemInform abstract: Gold nanostructures: A class of multifunctional materials for biomedical applications. *Chemical Society Reviews, 40*, 44–56.
228. Kang, H., Trondoli, A., Zhu, G., Chen, Y., Chang, Y.-J., Liu, H., Huang, Y.-F., Zhang, X., & Tan, W. (2011). Near-infrared light-responsive Core-Shell Nanogels for targeted drug delivery. *ACS Nano, 5*, 5094–5099.
229. Hribar, K., Lee, M., Lee, D. H., & Burdick, J. (2011). Enhanced release of small molecules from near-infrared light responsive polymer-Nanorod composites. *ACS Nano, 5*, 2948–2956.
230. Wei, Q., Ji, J., & Shen, J. (2008). Synthesis of near-infrared responsive gold Nanorod/PNIPAAm Core/Shell Nanohybrids via surface initiated ATRP for smart drug delivery. *Macromolecular Rapid Communications, 29*, 645–650.
231. Sivakumaran, D., Bakaic, E., Campbell, S., Xu, F., Mueller, E., & Hoare, T. (2018). Fabricating degradable thermoresponsive hydrogels on multiple length scales via reactive extrusion, microfluidics, self-assembly, and electrospinning. *Journal of Visualized Experiments, 2018*, 54502.
232. Liu, L., Bai, S., Yang, H., Li, S., Quan, J., Zhu, L., & Nie, H. (2016). Controlled release from thermo-sensitive PNVCL-co-MAA electrospun nanofibers: The effects of hydrophilicity/hydrophobicity of a drug. *Materials Science and Engineering: C, 67*, 581–589.
233. Slemming-Adamsen, P., Song, J., Dong, M., Besenbacher, F., & Chen, M. (2015). In situ cross-linked pNIPAM/gelatin nanofibers for thermo-responsive drug release. *Macromolecular Materials and Engineering, 300*, 1226–1231.
234. Zhang, H., Niu, Q., Wang, N., Nie, J., & Ma, G. (2015). Thermo-sensitive drug controlled release PLA core/ pNIPAM shell fibers fabricated using a combination of electrospinning and UV photo-polymerization. *European Polymer Journal, 71*, 440–451.
235. Cicotte, K., Reed, J., Nguyen, P., Lora, J., Dirk, E., & Canavan, H. (2017). Optimization of electrospun poly(N- isopropyl acrylamide) mats for the rapid reversible adhesion of mammalian cells. *Biointerphases, 12*, 02C417.
236. Liu, L., Bakhshi, H., Shaohua, J., Schmalz, H., & Agarwal, S. (2018). Composite polymeric membranes with directionally embedded fibers for controlled dual actuation. *Macromolecular Rapid Communications, 39*, 1800082.
237. Li, H., Sang, Q., Wu, J., Williams, G., Wang, H., Niu, S., Wu, J., & Zhu, L.-M. (2018). Dual-responsive drug delivery systems prepared by blend electrospinning. *International Journal of Pharmaceutics, 543*, 1–7.
238. Li, H., Liu, K., Williams, G. R., Wu, J., Wu, J., Wang, H., Niu, S., & Zhu, L.-M. (2018). Dual temperature and pH responsive

nanofiber formulations prepared by electrospinning. *Colloids and Surfaces B: Biointerfaces, 171*, 142–149.

239. Hu, J., Li, H.-Y., Williams, G., Yang, H.-H., Tao, L., & Zhu, L.-M. (2016). Electrospun poly(N-isopropylacrylamide)/ethyl cellulose nanofibers as thermoresponsive drug delivery systems. *Journal of Pharmaceutical Sciences, 105*(3), 1104–1112.
240. Han, D., Yu, X., Chai, Q., Ayres, N., & Steckl, A. (2017). Stimuli-responsive self-Immolative polymer nanofiber membranes formed by coaxial electrospinning. *ACS Applied Materials & Interfaces, 9*, 11858–11865.
241. Wen, Y., & Collier, J. (2015). Supramolecular peptide vaccines: Tuning adaptive immunity. *Current Opinion in Immunology, 35*, 73–79.
242. Rudra, J., Tian, Y., Jung, P., & Collier, J. (2010). A self-assembling peptide acting as an immune adjuvant. *Proceedings of the National Academy of Sciences of the United States of America, 107*, 622–627.
243. Pompano, R., Chen, J., Verbus, E., Han, H., Fridman, A., McNeeley, T., Collier, J., & Chong, A. (2014). Titrating T-cell epitopes within self-assembled vaccines optimizes CD4+ helper T cell and antibody outputs. *Advanced Healthcare Materials, 3*, 1898–1908.
244. Hudalla, G., Sun, T., Gasiorowski, J., Han, H., Tian, Y., Chong, A., & Collier, J. (2014). Gradated assembly of multiple proteins into supramolecular nanomaterials. *Nature Materials, 13*, 829–836.
245. Wen, Y., Roudebush, S. L., Buckholtz, G. A., Goehring, T. R., Giannoukakis, N., Gawalt, E. S., & Meng, W. S. (2014). Coassembly of amphiphilic peptide EAK16-II with histidinylated analogues and implications for functionalization of beta-sheet fibrils in vivo. *Biomaterials, 35*(19), 5196–5205.
246. Zheng, Y., Wen, Y., George, A. M., Steinbach, A. M., Phillips, B. E., Giannoukakis, N., Gawalt, E. S., & Meng, W. S. (2011). A peptide-based material platform for displaying antibodies to engage T cells. *Biomaterials, 32*(1), 249–257.
247. Wen, Y., Liu, W., Bagia, C., Zhang, S., Bai, M., Janjic, J. M., Giannoukakis, N., Gawalt, E. S., & Meng, W. S. (2014). Antibody-functionalized peptidic membranes for neutralization of allogeneic skin antigen-presenting cells. *Acta Biomaterialia, 10*(11), 4759–4767.
248. Wen, Y., Kolonich, H. R., Kruszewski, K. M., Giannoukakis, N., Gawalt, E. S., & Meng, W. S. (2013). Retaining antibodies in tumors with a self-assembling injectable system. *Molecular Pharmaceutics, 10*(3), 1035–1044.
249. Tajima, A., Liu, W., Pradhan, I., Bertera, S., Bagia, C., Trucco, M., Meng, W. S., & Fan, Y. (2015). Bioengineering mini functional thymic units with EAK16-II/EAKIIH6 self-assembling hydrogel. *Clinical Immunology, 160*(1), 82–89.
250. Gottesman, M. M., Fojo, T., & Bates, S. E. (2002). Multidrug resistance in cancer: Role of ATP–dependent transporters. *Nature Reviews Cancer, 2*(1), 48–58.
251. Szakács, G., Paterson, J. K., Ludwig, J. A., Booth-Genthe, C., & Gottesman, M. M. (2006). Targeting multidrug resistance in cancer. *Nature Reviews Drug Discovery, 5*(3), 219–234.
252. Zhang, Z., Wu, Y., Kuang, G., Liu, S., Zhou, D., Chen, X., Jing, X., & Huang, Y. (2017). Pt(iv) prodrug-backboned micelle and DCA loaded nanofibers for enhanced local cancer treatment. *Journal of Materials Chemistry B, 5*(11), 2115–2125.
253. Niiyama, E., Uto, K., Lee, C. M., Sakura, K., & Ebara, M. (2019). Hyperthermia nanofiber platform synergized by sustained release of paclitaxel to improve antitumor efficiency. *Advanced Healthcare Materials, 8*(13), e1900102.

Nanoneedle-Based Materials for Intracellular Studies

Julia E. Sero and Molly M. Stevens

Abstract

Nanoneedles, defined as high aspect ratio structures with tip diameters of 5 to approximately 500 nm, are uniquely able to interface with the interior of living cells. Their nanoscale dimensions mean that they are able to penetrate the plasma membrane with minimal disruption of normal cellular functions, allowing researchers to probe the intracellular space and deliver or extract material from individual cells. In the last decade, a variety of strategies have been developed using nanoneedles, either singly or as arrays, to investigate the biology of cancer cells in vitro and in vivo. These include hollow nanoneedles for soluble probe delivery, nanocapillaries for single-cell biopsy, nano-AFM for direct physical measurements of cytosolic proteins, and a wide range of fluorescent and electrochemical nanosensors for analyte detection. Nanofabrication has improved to the point that nanobiosensors can detect individual vesicles inside the cytoplasm, delineate tumor margins based on intracellular enzyme activity, and measure changes in cell metabolism almost in real time. While most of these applications are currently in the proof-of-concept stage, nanoneedle technology is poised to offer cancer biologists a powerful new set of tools for probing cells with unprecedented spatial and temporal resolution.

Keywords

Nanoneedles · Nanopipettes · Nanocapillaries · Nanoelectrodes · Nanostraws · Nanowires · Nanobiopsy · Nanoparticles · Intracellular sensing · Reactive oxygen species (ROS) · Redox probes · Scanning ion conductance microscopy (SICM) · Fluid force microscopy · Molecular beacons · Surface-enhanced Raman scattering (SERS) · Cancer biomarker · Cell metabolism · Mitochondria · Intracellular pH · Dual carbon electrodes (DCE) · Cytoskeleton

Abbreviations

AFM	Atomic force microscopy
ANE	Asymmetric nanopore electrodes
ATP	Adenosine triphosphate
BNS	Branched nanostraws
CNT	Carbon nanotube
CTC	Circulating tumor cell
CTSB	Cathepsin B
DCE	Dual carbon electrodes
ELISA	Enzyme-linked immunosorbent assay
FET	Field-effect transistor
FIB	Focused ion beam
FRET	Forster resonance energy transfer
GFP	Green fluorescent protein
IP	Immunoprecipitation
iPSC	Induced pluripotent stem cells
LPS	Lysophosphatidic acid
MB	Methylene blue
MEA	Multielectrode array
MFP	Microfluidic probe
MMP	Matrix metalloproteinase
MnSOD	Manganese superoxide dismutase
MS	Mass spectroscopy
NES	Nano-electrospray
NFP	Nanofountain probe
Osbpy	Osmium bipyridine
PEG	Polyethylene glycol
qPCR	Quantitative polymerase chain reaction
RCA	Rolling circle amplification

J. E. Sero
Biology and Biochemistry Department, University of Bath,
Claverton Down, Bath, UK

M. M. Stevens (✉)
Institute for Biomedical Engineering, Imperial College London,
London, UK
e-mail: m.stevens@imperial.ac.uk

© Springer Nature Switzerland AG 2021

F. Fontana, H. A. Santos (eds.), *Bio-Nanomedicine for Cancer Therapy*, Advances in Experimental Medicine and Biology 1295, https://doi.org/10.1007/978-3-030-58174-9_9

RFP	Red fluorescent protein
RNS	Reactive nitrogen species
ROS	Reactive oxygen species
SCIM	Scanning ion conductance microscopy
SECM	Scanning electrochemical microscopy
SEM	Scanning electron microscope
SERS	Surface-enhanced Raman scattering
SOD	Superoxide dismutase
SWCNT	Single-walled carbon nanotube

The 2010s witnessed a "Cambrian explosion" in the fabrication of nanoscale materials. Nanoneedles have emerged as a core technology for probing living cells due to their ability to interface directly with the cytoplasm and cause minimal disruption to normal cellular functions. Here we use the term "nanoneedles" as a catch-all term for high aspect ratio nanostructures, meaning materials with tip diameters of less than ~500 nm and 1–10 microns in length (Fig. 1a). High aspect ratio nanostructures have been fabricated from a variety of materials, from inorganic semiconductors to metals to carbon (Fig. 1b–f). The nanoneedle literature has a varied and often inconsistent nomenclature, including nanowires, nanospears, nanocapillaries, nanostraws, nanopipettes, nanotubes, nanopillars, nanoelectrodes, and more. Nanoneedles can be solid structures, such as porous Si pillars [1] and filled nanoelectrodes [2], or hollow tubes, such as alumina nanostraws [3], quartz nanopipettes [4], and double-barreled nanopipettes. They may be used as single probes for individual cells or as arrays that can interact with cellular populations. Nanoneedles can be used to deliver cargos, remove cellular contents, or measure electrochemical signals – or even all of these at once. Many excellent recent reviews have explored the larger theme of nanoneedles and nanoscale sensors in cell biology [5–9]. In this chapter, we will focus on advances in the use of nanoneedles for intracellular biosensing over the last decade and on how these technologies have been, or could be, applied to cancer research.

1 Types of Nanoneedles Used for Intracellular Sensing

Nanoneedles that directly access the intracellular space can be classified as solid or hollow structures and as single-cell probes or multicell arrays. Solid nanoneedles have been fabricated by a combination of microfabrication techniques, such as wet and dry etching of silicon wafers. These approaches can be tailored to produce nanopillars with well-defined geometries which can be sharpened into conical tips. The processing used to shape nanoneedles can also be used to alter their material properties. For example, wet etching can be used to form solid nanoneedles of mesoporous silicon. Such nanoneedle arrays have been used to deliver cargos, such as nucleic acids, and as carriers of biological probes [10, 11]. Alternatively, nanowires composed of silicon and other inorganic semiconductor materials can be grown on substrates by the vapor-liquid-solid mechanism to produce vertical arrays [12]. Atomic force microscopy (AFM) tips may be sharpened to nanoscale points that can penetrate cell membranes [13]. Hollow nanoneedles include nanostraw arrays, nanopipettes or nanocapillaries, carbon nanotubes, and AFM tips with micro- or nanochannels. Nanostraw arrays are fabricated by coating porous polycarbonate membranes with metals and then etching the support to reveal nanometer-diameter tubes [14]. Fluid force microscopy combines sharpened AFM tips with micro- or even nanofluidic channels [15–17]. Probes such as nanoendoscopes made from carbon nanotubes benefit from being cylindrical, rather than conical or pyramidal, with well-defined radii of 50–200 nm that have less potential to damage cells [18]. Nanoelectrodes can be fabricated in many ways to form either solid or hollow probes. For example, filled nanoelectrodes may be pulled around a conductive material such as Pt wire, filled with Pt black, or flame-etched to expose a nanoscale carbon fiber tip [19, 20]. Hollow nanocapillary electrodes provide multifunctionality, as they can deliver or extract material as well as measure electrochemical signals [21]. Moreover, electrochemical signals can be used to guide probes into position as well as detect analytes [22–24].

Methods for intracellular sensing can be broadly subdivided into direct in situ interfacing with the cytosol, delivery of bioprobes, and extraction of cellular contents. Direct interfacing strategies include insertion of nanoelectrodes, nanoneedle-bound optical or electrochemical sensors, and antibody-functionalized nanoneedles that bind to cytoplasmic proteins. Nanoneedle-mediated delivery can be used to load cells with membrane impermeant chemicals or materials. Cellular contents can be extracted with single nanocapillaries or by using arrays of nanostraws or nanoneedles. Many of these strategies overlap and most can be multiplexed. Readouts for intracellular sensing can be optical (generally fluorescent), mechanical, and/or electrical. Electrical sensors are multifunctional, as they can measure changes in conductance that denote cell penetration, the presence of cell-generated reactive oxygen species (ROS) that are involved in cell metabolism, and the production of ROS such as hydrogen peroxide from enzymatic reactions.

2 The Cell-Nanoneedle Interface

The size of nanoneedles means that they are uniquely able to interact with biological structures on the cellular scale. For example, caveolae are membrane invaginations involved in endocytosis that are similar in size to the smaller end of nanoneedle tips in use today, typically 60–80 nm in diameter

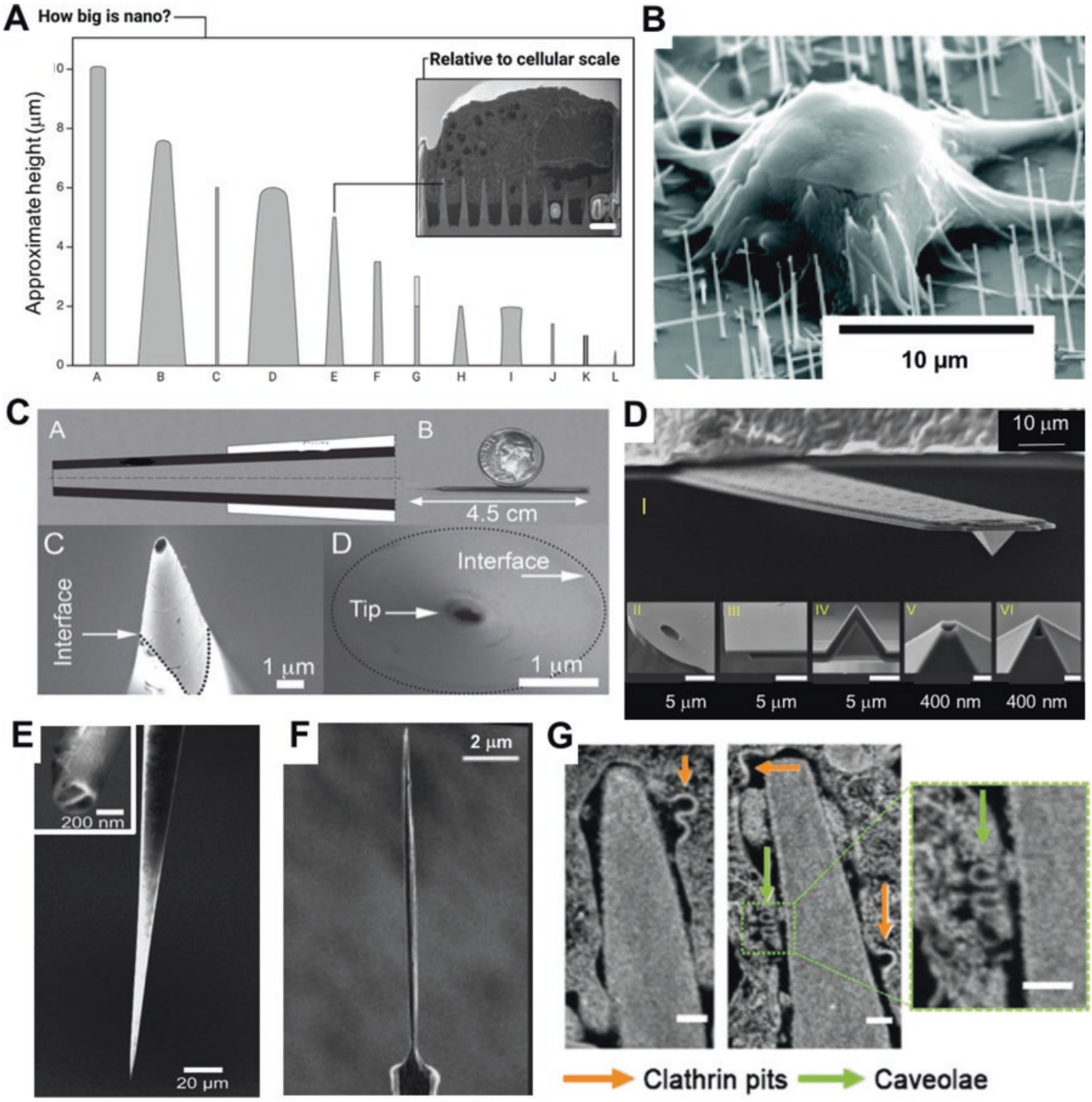

Fig. 1 (**a**) Nanoneedle scales relative to one another and the cellular scale. Scale bar in inset = 2 μm. Nanostructures depicted: (A) Si pillar, (B) diamond nanoneedle, (C) Si nanowire, (D) Plasmonic micropillar, (E) Porous Si nanoneedle, (F) hollow Si nanowire, (G) nanoelectrode, (H) diamond nanoneedle, (I) Si micropillar, (J) quartz nanopillar, (K) hollow nanostraw, (L) carbon fiber nanoelectrode tip. (Reproduced with permission from [9]. Copyright 2020, Wiley). (**b**) SEM of cell adhering to silicon nanowires. (Adapted with permission from [179]. Copyright 2007, American Chemical Society). (**c**) Carbon nanopipettes. (I) Schematic of nanopipette cross section. (II) Photograph of a carbon nanopipette fabricated from a pulled capillary. (III) SEM side view of carbon nanopipette tip. (IV) SEM axial view of a 200 nm carbon nanopipette tip. Dotted lines indicate the quartz-carbon interface. (Reproduced with permission from [2]. Copyright 2014, IOP Publishing). (**d**) SEM images of microchanneled cantilevers for fluidic force microscopy (FluidFM). (I) Perspective view of cantilever with pyramidal tip. (II) Zoomed-in image of the aperture of a tipless probe. (III–IV) Zoomed-in images of the microchannel and hollow pyramid after FIB sectioning. (V) Zoomed-in image of lithographically obtained 300 nm aperture in correspondence with pyramidal apex. (VI) Zoomed-in image of FIB-drilled triangular 300 nm aperture. (Reproduced with permission from [16]. Copyright 2014, Elsevier). (**e**) SEM image of spearhead field-effect transistor dual carbon electrode. Inset: cross section of tip after FIB milling. (Adapted with permission from [109]. Copyright 2016, American Chemical Society). (**f**) SEM of the tip of a conical carbon fiber nanoelectrode used for intracellular vesicle electrochemical cytometry. (Adapted with permission from [125]. Copyright 2015, Wiley). (**g**) FIB-SEM image of engulfed nanoneedle showing two classes of endocytic vesicles, clathrin-coated pits (orange arrows) and caveolae (green arrows). Scale bars = 100 nm. (Adapted with permission from [28]. Copyright 2019, The Authors)

[25, 26]. Caveolae and clathrin pits are clearly visible around mesoporous Si nanoneedles by focused ion beam-scanning electron microscopy (FIB-SEM), in which thin sections of cellular material are milled away and consecutive SEM images are acquired (Fig. 1g) [27, 28]. Furthermore, extracellular matrix components such as collagen fibrils in tissues are on the order of 10–300 nm [29, 30], which is in the mid-range of nanoneedle tips used for intracellular studies. Thus,

distortions of the plasma membrane and underlying cytoskeleton induced by nanoneedles are in the realm of sizes that cells have evolved to experience. However, the extent of cytosolic interaction with different kinds of nanostructures and the circumstances under which membrane penetration occurs are contingent upon a number of factors. The interface between cells and nanoneedles remains an open area of investigation, and many questions remain to be answered about how or when membrane penetration occurs.

In order for nanoneedles to access the cytoplasm, they must breach the plasma membrane and underlying cortical cytoskeleton as well as any extracellular barriers, such as the glycocalyx. When cells settle on nanoneedles by gravity, the plasma membrane has time to adapt to the nanotopography and deform around the nanostructures [31, 32]. Nanoneedles may be thus be engulfed, their cargo may be endocytosed, and/or the cell membrane may be ruptured and resealed around the obstruction (Fig. 2a). Spontaneous penetration is rare in the absence of membrane disruption by applied forces (micromanipulation or hypergravity) or electroporation [33–39]. Chemical modifications such as phospholipids [40] or hydrophobic molecules [41, 42] can also enhance membrane penetration. Current evidence suggests that in addition to the interfacing force between nanoneedle and cell membrane, the key factors for penetration are membrane fluidity, speed of insertion, and tip sharpness [43, 44] (Fig. 2b). The sharpness of the nanoneedle tip is also critical for cell viability, as under some circumstances, tips greater than 400 nm in diameter begin to compromise cellular function [45]. Current in silico models of the cell membrane-nanoneedle interface indicate that these effects are also highly dependent on other geometric parameters, such as the relative spacing between nanoneedles [31, 46]. The architecture of the cortical cytoskeleton and the composition of the plasma membrane play important roles in determining whether nanoneedles can access the cytoplasm [34, 36, 37]. Cancer cells show characteristic changes in stiffness and membrane fluidity [47–49] that may complicate nanoneedle-based experiments but could also be useful as diagnostic metrics [27]. For in-depth discussions of the mechanics of membrane penetration by nanoneedles, see [5, 9].

Electrical conductance is a well-established tool for detecting cellular contact and cell penetration. Changes in ionic current at the probe tip indicate when cell penetration has occurred [2, 50] (Fig. 3a, c, d). Nanoneedle probes are often integrated with scanning ion conductance microscopy (SICM) to precisely control their position and detect cell membrane penetration. SICM works by measuring the increase in resistance in a micro- or nanopipette probe as it approaches a nonconductive or poorly conductive surface.

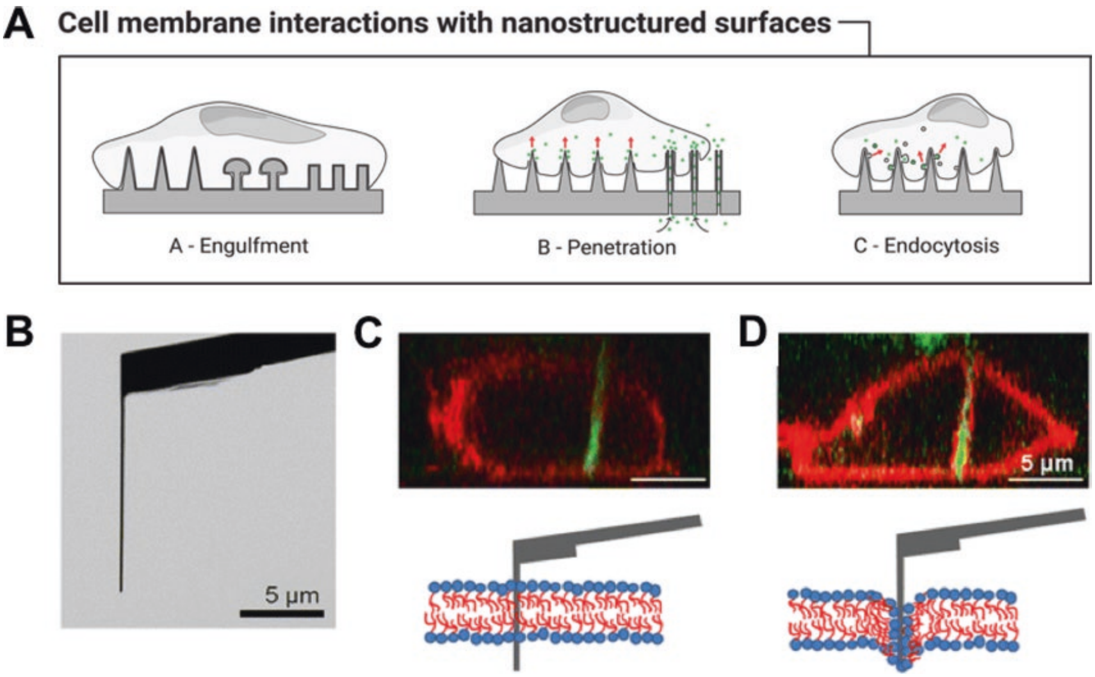

Fig. 2 Nanoneedle-cell interactions. (**a**) Cell membrane interactions on nanoneedle arrays. Cells can engulf nanostructures and spontaneous penetration is rare unless additional membrane rupture is induced, e.g., by electroporation. Endocytosis is enhanced around nanoneedles. (Reproduced with permission from [9]. Copyright 2020, Wiley). (**b**–**d**) Cell penetration by AFM-operated nanoneedles depends on membrane fluidity, insertion speed, temperature, surface chemistry, and cell stiffness. (**b**) Scanning ion microscopy image of AFM cantilever nanoneedle. (**c**) Side view confocal microscopy images and schematics of nanoneedle (green) insertion through the plasma membrane (red). (**d**) Unsuccessful insertion shown by red signal from the membrane surrounding the nanoneedle. (Reproduced under Creative Commons license from [44])

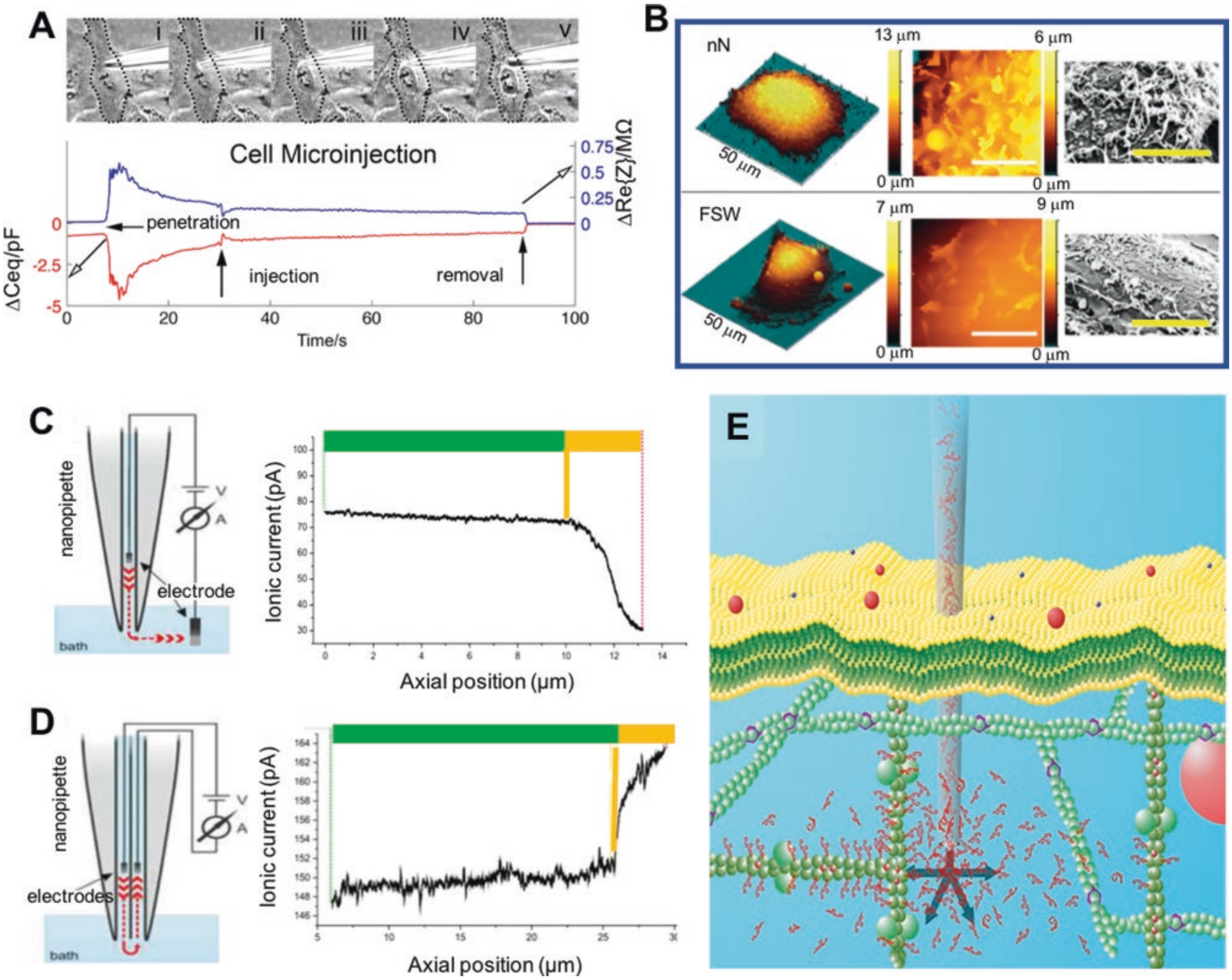

Fig. 3 Hollow nanoelectrodes used for cell surface mapping, detection of membrane penetration, and delivery of biomolecular probes. (**a**) Penetration and microinjection using carbon nanopipettes. Top: micrographs of carbon nanocapillary interfaced with a cell (dotted line) over time. Bottom: changes in capacitance (red) and resistance (blue) over time during cell penetration, injection, and probe removal. (Adapted with permission from [2]. Copyright 2014, IOP Publishing). (**b**) Topographical mapping of the cell surface by scanning ion conductance microscopy (SICM). Increased membrane ruffling was observed on the apical surface of cells seeded on arrays of mesoporous silicon nanoneedles (nN) compared to cells seeded on flat Si wafer (FSW). Left: 3D topographical SICM maps. Middle: 2D SICM scan (10 μm × 10 μm). Right: SEM images of apical membranes. Scale bars = 5 μm. (Adapted with permission from [28]. Copyright 2019, The Authors). (**c**) Single-barreled nanopipette and approach curve. The nanopipette is initially positioned ~20 μm above the cell. The counter electrode is placed in the culture medium and the initial voltage is set to ±60 mV, leading to an ionic current of 70–100 pA. As the tip approaches the cell (green bar) and penetrates the plasma membrane (yellow line), the ionic current decreases sharply (yellow bar). (**d**) Double-barreled nanopipette and approach curve. During the approach, applying positive voltage between electrodes leads to a weak ionic current (green bar). Upon penetrating the cell (yellow line), the ionic current increases (yellow bar). (**e**) Schematic of nanoinjection. Single living cells can be specifically labeled by injecting probes using a nanopipette with tip diameter ~100 nm. Once inside the cell, increasing or reversing the voltage leads to diffusion of the molecules out of the cell by electrophoresis. (Reproduced with permission from [59]. Copyright 2015, American Chemical Society)

This method is commonly used as a noncontact method for mapping cell surface topography [22, 23, 51]. For example, Gopal et al. used SICM to show that seeding human mesenchymal stem cells on nanoneedle arrays led to increased formation of membrane ruffles on the apical surface [28] (Fig. 3b). Electrical conductance measurement can thus be combined with intracellular cargo delivery or sampling using hollow nanocapillaries.

3 Delivery of Molecular Probes to Monitor Cellular Processes

Nanoneedle-based strategies can efficiently introduce a wide range of unbound probes directly into the cytosol, including cell-impermeant molecules, and can even deliver cocktails of cargos for multistep reactions and multiplexed sensing. Intracellular probes label cellular components and are used to monitor biological processes based on electrochemical or fluorescent readouts. Over the last decade, many methods to deliver molecular and nanoparticle probes directly into cells have been developed using nanoneedles [52], nanowires [53], carbon nanotubes [54], nanopipettes [55, 56], nanofluidic devices [15, 57], and nanoelectrodes [58]. Hennig et al. used electrophoretic nanoinjection of fluorescent probes to label DNA, actin, microtubules, and organelles in living cells with signal-to-noise ratios that enabled rapid super-resolution imaging (dSTORM) [59] (Fig. 3e). They showed that nanoneedle tip diameter was an important factor in determining cell viability following electrophoresis, and best results were obtained using nanopipettes with tip diameters of 100 nm or less [45]. Espinosa and colleagues developed "nanofountain probes" (NFP), nanocapillaries fabricated from etched AFM tips with sub-100 nm resolution that act like fountain pens delivering ink through capillary action, to inject cells with fluorescent-labeled nanodiamonds [57] and nucleic acids [60] (Fig. 4a). They found that applying an electrical pulse enhanced NFP cargo delivery without compromising cell viability [61]. They used this localized electroporation system to deliver DNA- and RNA-based molecular beacons that detect specific mRNAs (GAPDH) in live HeLa cells [62]. Molecular beacons are nucleotide hairpins that contain a fluorophore at one end and a quencher at the other; when hybridized to the target, the resulting spatial separation of the 5′ and 3′ ends produces a change in the fluorescent signal [63] (Fig. 4b).

Abnormal protein glycosylation drives cancer cell signaling, adhesion, migration, and stem cell maintenance, and many cell surface tumor markers are glycoproteins [64]. Hollow nanocapillaries called nanostraws are an effective way to deliver cell-impermeable probes [3, 65, 66] (Fig. 5a–d). To fabricate these arrays, nanoporous track-etched polycarbonate membranes are coated with metal (Al, Au, or Pt) by a conformal technique such as atomic-layer deposition, and then the membrane is etched on one side to expose protruding nanostraws. Nanostraws used for cell interfacing experiments are on the order of 100 nm in diameter and 1 μm in height depending on the etch time. The spacing of the nanostraws depends on the

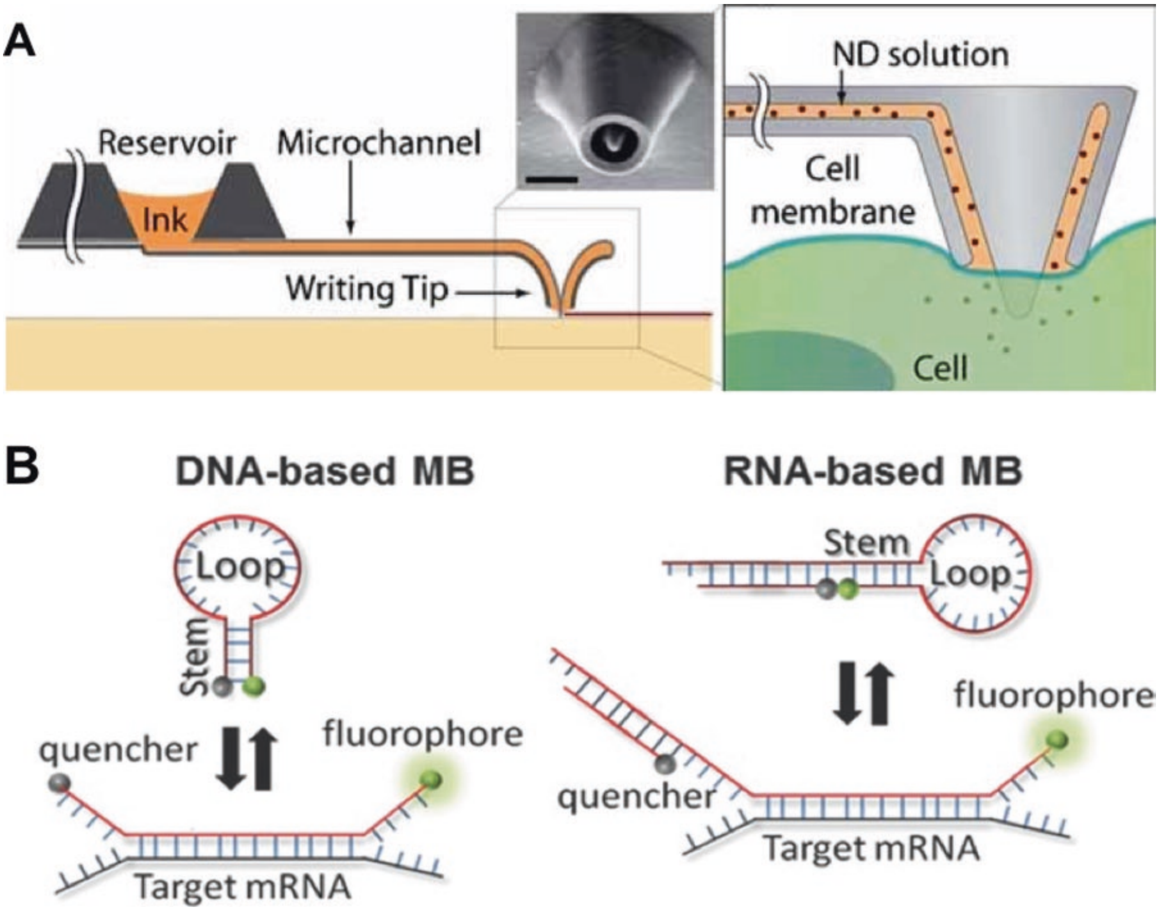

Fig. 4 Nanofountain probe-mediated delivery of fluorescent molecular beacons. (**a**) Schematic of nanofountain probe AFM tip for cell injection. (Copyright (2015) Wiley. Used with permission from [57]). (**b**) Schematic of DNA- and RNA-based molecular beacons (MB) used to detect GAPDH mRNA in live cells. (Copyright (2009) Wiley. Adapted with permission from [62])

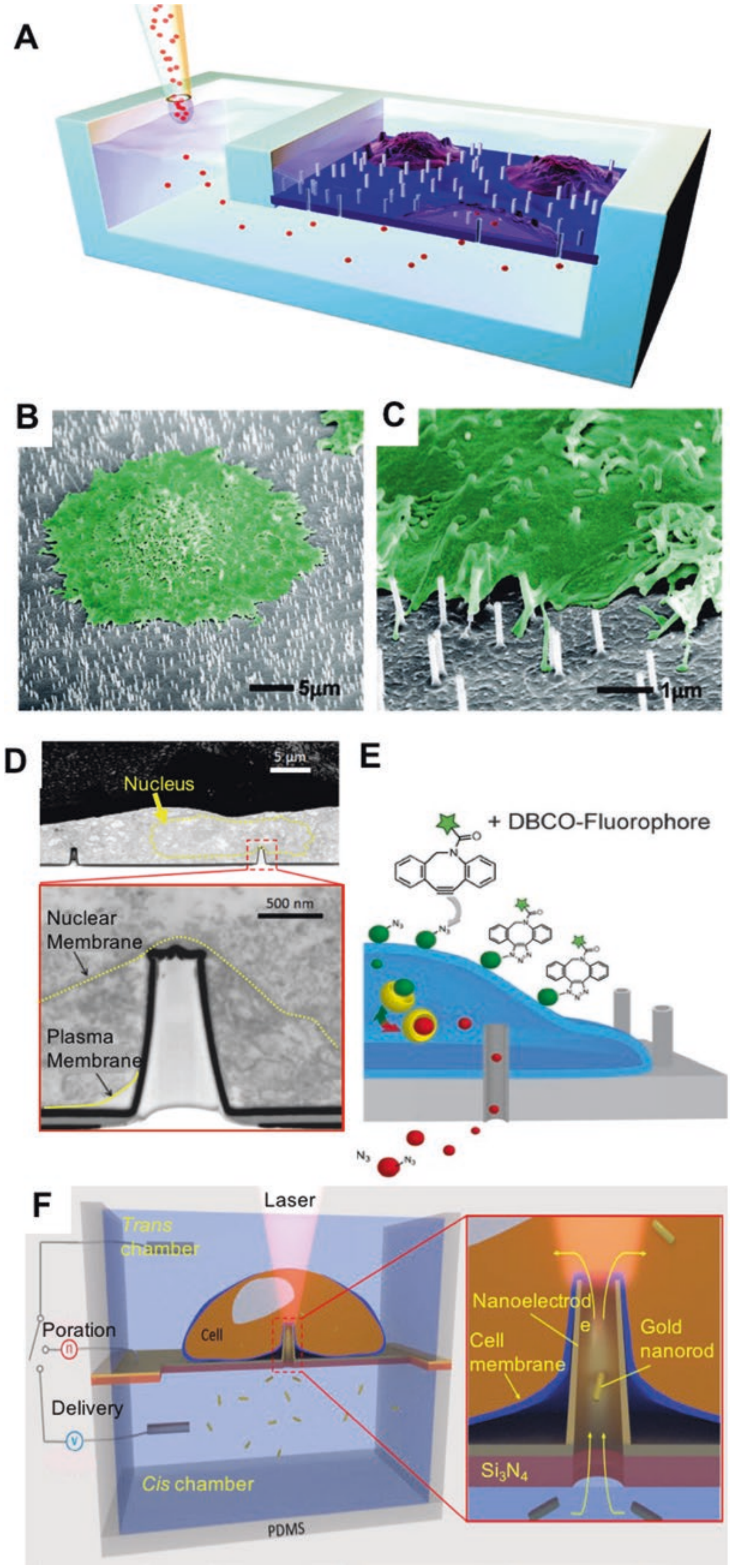
A
B
5μm
C
1μm
D
5 μm
Nucleus
500 nm
Nuclear Membrane
Plasma Membrane
E
+ DBCO-Fluorophore
N₃
F
Laser
Trans chamber
Poration
Cell
Delivery
Cis chamber
PDMS
Nanoelectrode
Cell membrane
Gold nanorod
Si₃N₄

Fig. 5 Nanostraw arrays for cargo delivery and extraction. (**a**) Schematic of nanostraw microfluidic system, cross section (not to scale). (**b**, **c**) SEM images of cells (green) cultured on 100-nm-diameter nanostraws at a density of 10^8 nanostraws/cm^2. (**d**) Top: cross-sectional SEM image of a cell cultured on nanostraw electrodes. Bottom: magnified image of inset showing cell membrane wrapped around the hollow nanostraw and impingement of the nuclear envelope (dashed line). (**e**) Schematic of nanostraw-mediated delivery of azido sugars, which are converted into sialic acid groups and incorporated into cell surface glycoproteins. The azide moiety is then labeled with a fluorophore-conjugated probe (DBCO). (**f**) Schematic of 3D hollow nanoelectrode device for gold nanorod delivery. Electroporation is induced by pulsed voltage. Nanorods are delivered from the lower to the upper chamber through nanostraws due to a direct current potential between two Pt wire electrodes. A laser beam excites the Raman signals of the gold nanorods inside the cell. (**a–c** reproduced with permission from [3]. Copyright 2011, American Chemical Society. **d** and **f** adapted with permission from [83], https://pubs.acs.org/doi/10.1021/acs.nanolett.8b03764. Copyright 2019, American Chemical Society. **e** adapted with permission from [67]. Copyright 2017, Wiley)

porosity of the polycarbonate membrane or ion beam milling parameters. Nanostraw-bearing membranes are overlaid onto microfluidic channels, and cells are seeded in the upper chamber. Agent delivery, or cellular contents extraction, is controlled from the lower channel. Spontaneous contact between the nanostraw interior and cytosol is rare when cells adhere to nanostraw arrays because the plasma membrane has time to engulf the nanostructures while remaining intact [35]. Electroporation of cells on nanostraws increases cargo delivery, for example, improving plasmid transfection efficiency from 5–10% to 60–70% [3, 65]. The electroporation step briefly disrupts the membrane, which can then reseal around nanostraws that have penetrated the cell. Melosh and colleagues used nanostraws to deliver cell-impermeant molecules called azido sugars into cells in order to map protein glycosylation [67]. Loading cells with azido sugars allowed modified glycoproteins to be detected by fluorescent probes conjugated with click chemistry. Other cell-impermeable metabolite or analogue probes, such as modified ATP or synthetic cross-linkers, could be delivered to the cytosol this way [64] (Fig. 5e).

4 Delivery of Probes for Multiplexed Biosensing

In addition to combining cargo delivery and sensing, nanoneedles are now being used for multiplexed cancer marker detection. Biodegradable Si nanoneedles were recently used to deliver multicomponent, enzymatically active probes to detect both miRNA and protein cancer biomarkers using rolling circle amplification and fluorophore-coupled nucleotide probes [68] (Fig. 6). Rolling circle amplification (RCA) is a process in which a short nucleotide primer is amplified to form long single-stranded DNA or RNA molecules through the action of unique polymerases. The whole RCA process can take place at 37°C in a complex biological environment, such as a cell. Mesoporous Si nanoneedles, about 1 μm long and 100 nm in diameter, were fabricated using metal-assisted chemical etching and functionalized with (3-Aminopropyl) triethoxysilane (APTES), a silicon-binding surface chemistry that is frequently used to promote the attachment of probes and biocargos. The nanoneedles were then detached from the substrate and loaded with nucleotide "padlock" probes, FAM- and Cy5-conjugated oligonucleotide probes,

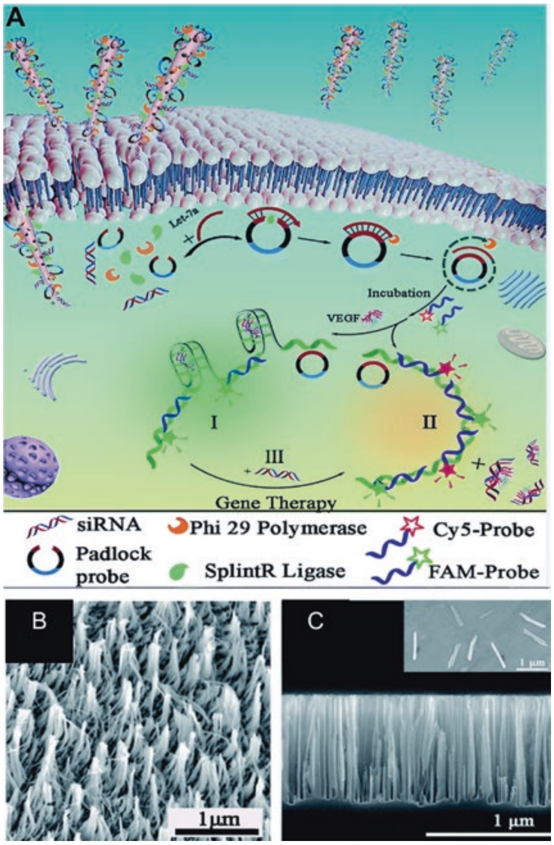

Fig. 6 Porous biodegradable nanosyringes for multiplexed biosensing. (**a**) One-step intracellular rolling circle amplification (RCA). Upon delivery of the "padlock probe," binding of Let-7a miRNA leads to ring formation catalyzed by splintR ligase, followed by amplification catalyzed by phi29 polymerase. An aptamer structure that binds VEGF was designed in the middle of the padlock probe to form a quadruplex in the presence of the protein. In leukemia cells with both Let-7a and VEGF, the RCA products hybridize with the FAM probe, resulting in a green fluorescence (I). In the absence of VEGF, both the Cy5 probe and the FAM probe hybridize to the amplification products, leading to orange fluorescence (II). Cells loaded with siRNA against VEGF therefore showed orange emission due to downregulation of the protein (III). (**b**) SEM top-sectional view of nanoneedles before detachment. (**c**) SEM cross-sectional view of nanoneedles before and after detachment (inset). (Adapted with permission from [68]. Copyright 2019, The Royal Society of Chemistry)

and polymerase and ligase to amplify the padlock probe in the presence of Let-7a miRNA. The padlock probe also contained an VEGF-binding aptamer sequence. The resulting “nanosyringes” were taken up by endocytosis and dissolved within 16 h, similar to porous nanoneedles fabricated by Stevens and colleagues [1, 11, 28, 69]. In the presence of Let-7a transcript and VEGF protein, amplification of the padlock probe and binding to targets produced a green fluorescent signal, whereas in the absence of VEGF, the interaction of FAM and Cy5 produced an orange fluorescent signal. The nanosyringes were also loaded with siRNA targeting VEGF, which resulted in decreased VEGF protein signal due to transcript depletion. Let-7a and VEGF were detected in vitro in cell uptake experiments and in vivo following injection into mouse xenograft tumors. These studies demonstrate the efficacy of using nanoneedles to detect nucleotides and proteins inside cells as part of a multiplexed strategy for tumor detection and gene therapy.

5 Delivery of Nanoparticles as Probes

Nanoneedles have been demonstrated to deliver nanoparticles, such as quantum dots and gold nanoparticles, to the cytosol [1, 70]. Nanoparticles have high surface area-to-volume ratios and the capacity for binding multiple probes. Tang and colleagues showed that Au nanoparticles functionalized with multiple molecular beacons could identify four different intracellular mRNA transcripts [71]. They also developed fluorescent nanoprobes that could distinguish normal and cancer cells based on tumor marker mRNA transcripts (TK1 and GalNAc) and matrix metalloproteinases (MMP-2 and MMP-7) [72]. A number of examples of nanoprobes that target specific MMPs and detect their activity in tumors have been reported [73–75], including one that detects both MMP-2 and urokinase-type plasminogen activator, which is upregulated in many cancers [76]. Gold-coated magnetic nanoparticles modified with redox-labeled DNA probes have also been reported as an ultrasensitive detection method for circulating tumor miRNA in blood [77]. These types of metallic particles could be adapted for intracellular electrochemical sensing by nanoinjection or coupling to nanoneedle probes. Additionally, carbon-based nanomaterials can be utilized to sense a variety of analytes, pH, and even temperature [78].

Biocompatible Au or Au-coated nanoparticles are becoming increasingly popular for label-free sensing using surface-enhanced Raman scattering (SERS). SERS provides highly sensitive and rapid detection of molecules and nanoparticles without the necessity of a fluorescent or reactive probe [79–81]. In 2018, Hanif et al. reported the use of gold-coated nanopipettes (~100 nm tips) functionalized with organic nitrile cyanide to measure Fe^{3+} in live cells [82]. In 2019, De Angelis and colleagues used hollow nanoelectrodes to deliver gold nanorods into cells. Biomolecules colocalized with the gold nanorods could then be detected by the enhanced localized Raman scattering [83] (Fig. 5f). Another novel combination of nanopipettes, nanoparticles, and Raman spectroscopy was reported the same year as a way to measure hypoxia in cells and tumors [84] (Fig. 7). In this study, sharp-edged gold nanostars were coupled to nanopipettes, and SERS was used to measure intracellular redox potential. Clear differences in Raman spectra were observed between triple-negative breast cancer cells and non-tumor MCF10A or nonmetastatic cancer cells in response to hypoxia [84]. The gold nanostar-loaded nanopipettes were then demonstrated to be able to detect hypoxic regions in 3D cell culture and, importantly, in subcutaneous tumors in mice [84]. Nanoneedle-mediated nanoparticle delivery combined with SERS offers a powerful set of tools for cancer research in vitro and tumor detection in vivo.

6 Nanoneedle-Bound Optical Probes

Optical probes can be chemically conjugated to nanoneedles to act as biosensors [85]. An early example of this strategy used a cleavable FRET probe conjugated to an AFM nanoneedle (400 nm tip) to detect caspase-3 activation in live cells [86]. Here, a change in the FRET signal was observed when the Alexa546 fluorophore was cleaved from the GFP portion of the probe by active caspases in apoptotic HeLa cells. Caspase-cleavable fluorescent probes were also used in a nanoneedle “sandwich assay,” in which cells held in place on an adherent nanoneedle array were interfaced with Si nanoneedle arrays decorated with covalently linked TAMRA-labelled peptides [87] (Fig. 8a). In the presence of active caspase in the cytosol, the TAMRA tag was cleaved, resulting in red fluorescence in the cells after removal of the probes (Fig. 8b). In the same study, the sandwich assay was used to monitor protein tyrosine phosphatase (PTP) and protein kinase A (PKA) activity in cells by inserting nanoneedles conjugated with peptide kinase/phosphatase substrates. In the latter cases, however, peptide phosphorylation was determined by MALDI-TOF mass spectroscopy rather than fluorescence [87]. Nakamura and colleagues used fluorescent molecular beacons coupled to arrays of Si nanoneedles by biotinylation to detect GAPDH mRNA [88, 89]. Similar to the sandwich assay [87], nanoneedles were inserted into the apical side of adherent cells. However, in the latter study, penetration was controlled by piezoelectric-driven oscillating mechanism so that force and depth could be precisely controlled, and interfacing times with cells were much shorter (10–30 minutes compared with 24 h) [89].

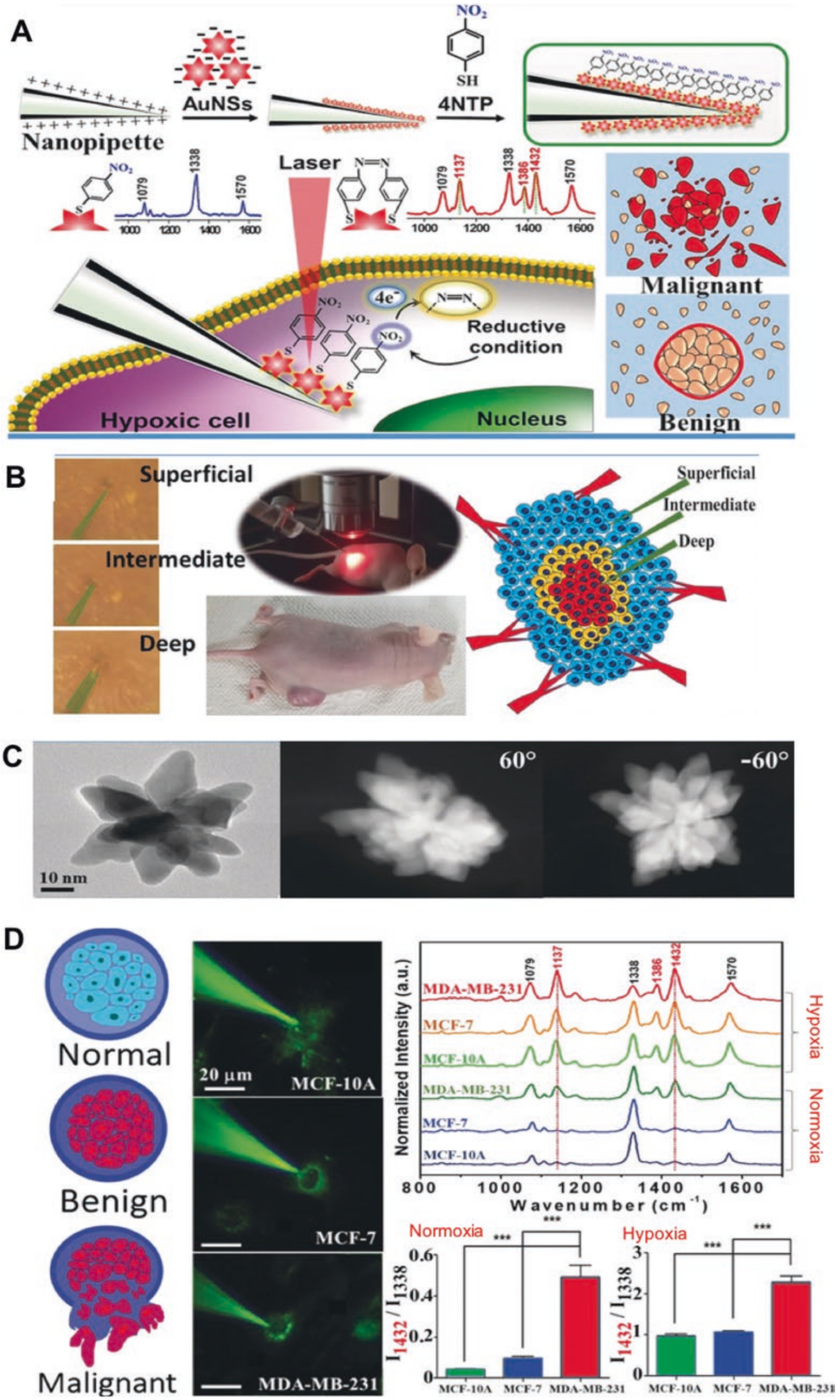
A
Nanopipette
AuNSs
NO2
SH
4NTP
Laser
NO2
1079
1338
1570
1000
1200
1400
1600
N=N
1079
1137
1338
1386
1432
1570
1000
1200
1400
1600
Malignant
Benign
NO2
NO2
NO2
4e-
N=N
Reductive condition
Hypoxic cell
Nucleus
B
Superficial
Intermediate
Deep
Superficial
Intermediate
Deep
C
10 nm
60°
-60°
D
Normal
Benign
Malignant
20 μm
MCF-10A
MCF-7
MDA-MB-231
Normalized Intensity (a.u.)
1079
1137
1338
1386
1432
1570
MDA-MB-231
MCF-7
MCF-10A
MDA-MB-231
MCF-7
MCF-10A
Hypoxia
Normoxia
800
1000
1200
1400
1600
Wavenumber (cm-1)
Normoxia
***
***
0.6
0.4
0.2
0
I1432 / I1338
MCF-10A
MCF-7
MDA-MB-231
Hypoxia
***
***
3
2
1
0
I1432 / I1338
MCF-10A
MCF-7
MDA-MB-231

Fig. 7 Raman-based hypoxia detection using a nanopipette and gold nanostars. (**a**) Schematic of the working principle. Gold nanostars were assembled on nanopipette tips and functionalized with 4-nitrothiophenol (4NTP). Spectral changes for the 4NTP redox group (nitro-NO_2) resulting from intracellular oxygen were quantified. (**b**) In vivo detection of hypoxia in different regions of subcutaneous mouse tumors using the gold nanostar probe. (**c**) 2D TEM and 3D tomography images of Au nanostars showing spikes at tilt angles −60° and 60°. (**d**) Raman probes were used to measure spectra in normal breast myoepithelial cells (MCF10A), nonmetastatic breast cancer cells (MCF7), and metastatic breast cancer cells (MDA-MB-231) under normoxia and hypoxia. (a) Raman probe interacting with cells. (b) Surface-enhanced Raman spectra for cells in each condition. (c) Quantification of peak ratios that are indicative of changes in redox state inside cells (***$p < 0.001$). (Adapted with permission from [84]. Copyright 2019, Wiley)

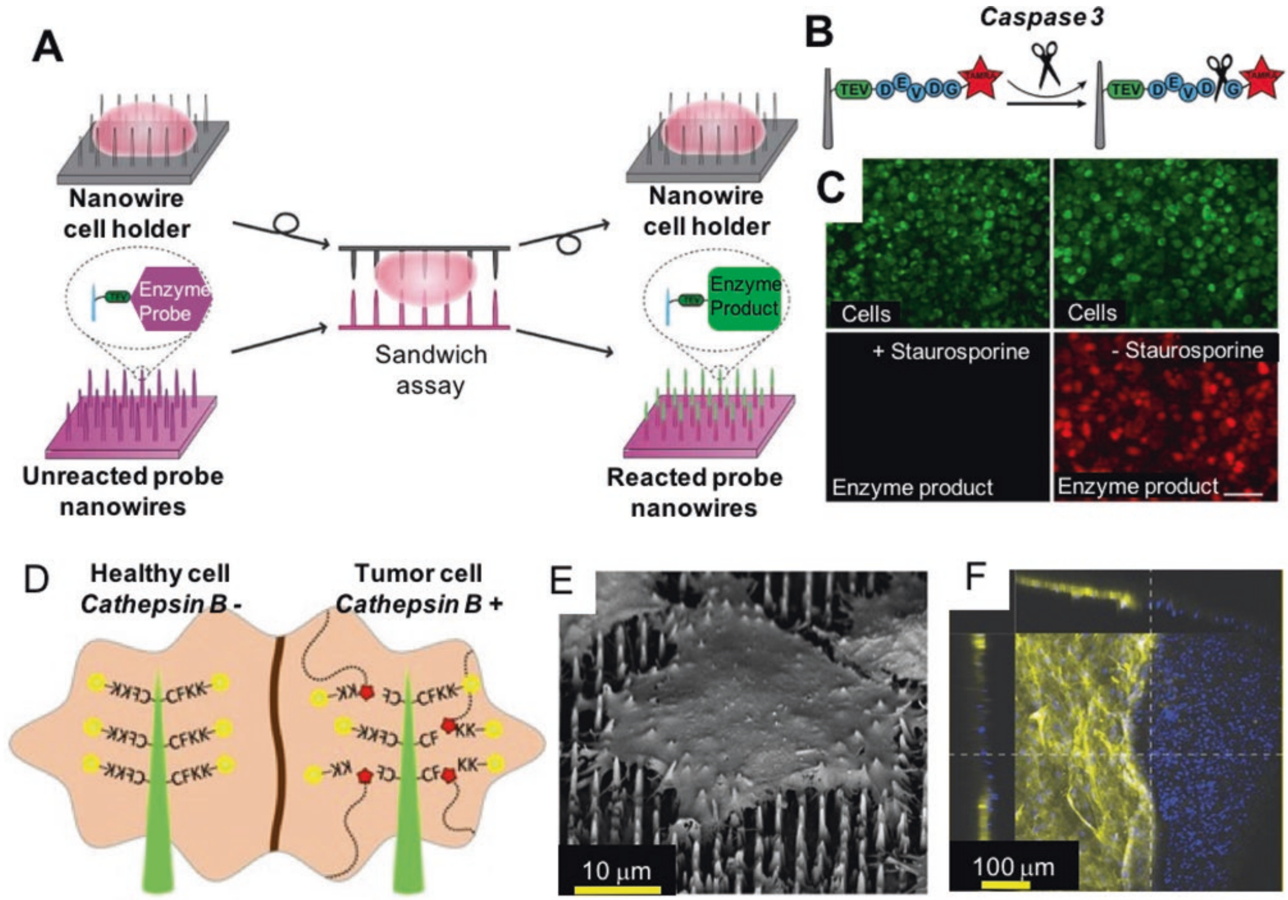
A
Nanowire cell holder
Enzyme Probe
TEV
Unreacted probe nanowires
Sandwich assay
Nanowire cell holder
Enzyme Product
TEV
Reacted probe nanowires
B
Caspase 3
TEV D E V D G
TAMRA
TEV D E V D G
TAMRA
C
Cells
Cells
+ Staurosporine
- Staurosporine
Enzyme product
Enzyme product
D
Healthy cell
Cathepsin B -
Tumor cell
Cathepsin B +
CFKK
CFKK
CFKK
CFKK
CFKK
CF KK
CF KK
E
10 μm
F
100 μm

Fig. 8 Nanoneedle-bound optical probes. (**a**) Nanoneedle "sandwich assay." Cells are immobilized on the one nanoneedle array. Then another array, functionalized with a bound caspase-3 probe (**b**), is interfaced with the cells. When the fluorescent-labeled peptide that immobilizes on the nanoneedles is in contact with active caspase-3 in cells, the red probe is released into the cytoplasm. (**c**) Cells are labeled in green (top). Caspase-3 activity is indicated by red fluorescence in cells treated with staurosporine, which induces apoptosis (bottom). (Adapted with permission from [87]. Copyright 2013, American Chemical Society). (**d**) Porous Si nanoneedle (green) arrays functionalized with the cathepsin B (CTSB) probe (yellow) interface with cells, either by seeding directly on top of the nanoneedle arrays or by pressing against tissue samples. When CTSB (red) is active, the fluorescent probe is cleaved from the peptide substrate. (**e**) A cell growing on a nanoneedle array (SEM). (**f**) Esophageal tissue stamped with nanoneedle biosensor on the tumor margin. Yellow fluorescence indicates CTSB activity in the tumor region. (Adapted under the terms of CC BY license from [10]. Copyright 2015, The Authors)

7 Nanoneedle-Bound Probes for Cancer Biomarkers

Nanoneedles with covalently bound molecular probes have been reported for measuring intracellular pH and enzymatic activities in cancer cells. Dysregulation of pH homeostasis is a common characteristic of tumor cells, which often have higher intracellular pH and lower extracellular pH than healthy cells [90]. Intracellular pH has been measured using nanoneedles with optical and electrochemical functionalization. Chiappini and Stevens used porous Si nanoneedles (tips <100 nm) conjugated with a pH-sensitive fluorophore and a reference fluorophore to measure the pH of interfaced cells by ratiometric imaging. Cells can be injected either from the bottom-up by seeding directly on top of the nanoneedles, or from the top-down by pressing the nanoneedle array against the apical surface [1], which was previously shown not to impair cell viability [11]. Chiappini et al. also used a cleavable TAMRA-peptide probe to sense cytosolic cathepsin B (CTSB) in order to detect cancer cells seeded on Si nanoneedle arrays [10] (Fig. 8d–e). CTSB is a cysteine protease that is a cancer biomarker associated with poor prognosis in many solid tumors [91]. Transformed cells could be distinguished from normal cells in a mixed population based on cleavage of TAMRA by fluorescence microscopy. Furthermore, when nanoneedle sensors were applied to human tissue samples, high CTSB activity was revealed by fluorescence in esophageal tumors and in regions diagnosed by histopathology as having premalignant Barrett's dysplasia (Fig. 8f). Application of the nanosensor array to a tumor margin also showed clear demarcation between diseased and healthy tissue [10]. Proteolytic CTSB activity has

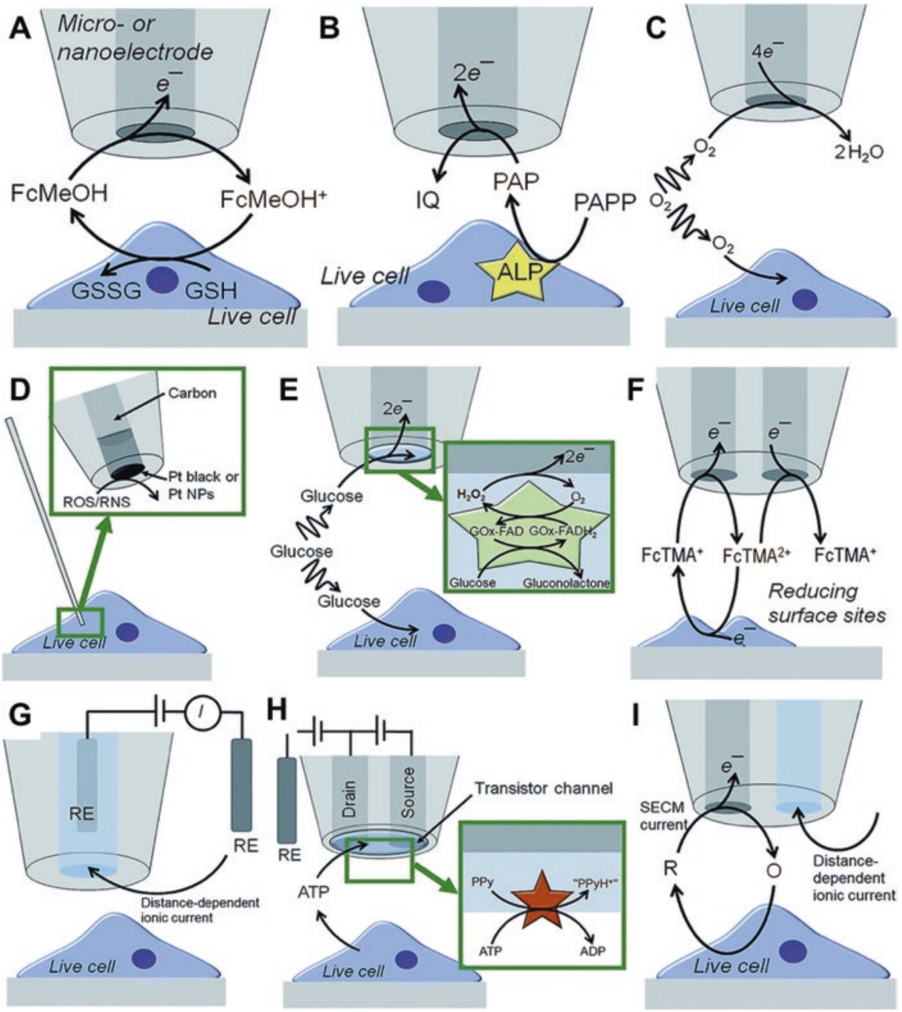
A
Micro- or nanoelectrode
e⁻
FcMeOH
FcMeOH⁺
GSSG
GSH
Live cell
B
2e⁻
IQ
PAP
PAPP
Live cell
ALP
C
4e⁻
O₂
2H₂O
O₂
O₂
Live cell
D
Carbon
Pt black or Pt NPs
ROS/RNS
Live cell
E
2e⁻
Glucose
Glucose
Glucose
Live cell
H₂O₂
2e⁻
O₂
GOx-FAD
GOx-FADH₂
Glucose
Gluconolactone
F
e⁻
e⁻
FcTMA⁺
FcTMA²⁺
FcTMA⁺
Reducing surface sites
e⁻
G
I
RE
RE
Distance-dependent ionic current
Live cell
H
Drain
Source
Transistor channel
RE
ATP
PPy
"PPyH⁺"
ATP
ADP
Live cell
I
e⁻
SECM current
R
O
Distance-dependent ionic current
Live cell

Fig. 9 Schematics of the operating principles of typical electrochemical scanning probe microscopy electrodes. (**a**) SECM feedback (FB) mode. (**b**) SECM substrate generation/tip collection (SG/TC) mode. (**c**) SECM redox (RC) competition mode. (**d**) Pt-based nanoelectrode for noninvasive intracellular recordings. (**e**) Microbiosensor for specific metabolite detection. (**f**) Dual electrode SECM tip. (**g**) SICM for topographic mapping. (**h**) Nano-FET for specific metabolite detection. (**i**) SECM-SICM for constant distance mode electrochemical imaging. (Reproduced under the terms of CC BY license from [94]. Copyright 2018, The Royal Society of Chemistry)

also been measured using peptide-coupled nanoelectrode arrays in breast cancer cell lysates [92].

8 Nanopipette Electrodes to Monitor Cell Metabolism

Nanocapillary electrodes have been used to monitor changes in cell metabolism, which are hallmarks of cancer biology [93]. The range of nanoelectrode varieties used to measure analytes via redox chemistry is summarized in Fig. 9 and reviewed in depth by Lin et al. [94]. For recent reviews of nanoelectrode fabrication, see [58, 95].

Nanocapillaries can be used to deliver unbound probes that produce electrochemically active analytes, such as hydrogen peroxide. Chen and colleagues report delivery of "nanokits" comprised of commercial enzymatic assay components into cells, where metabolites are detected via H_2O_2 generation [96, 97]. They used glass nanocapillaries fabricated with Pt ring electrodes with tips ~200–300 nm in diameter and tip openings of ~130 nm [96]. These nanocapillaries were used to deliver femtoliter quantities of 1) glucose oxidase to detect glucose in HeLa cells and 2) a cocktail of sphingomyelin, alkaline phosphatase, and choline oxidase to measure sphingomyelinase activity in J774 macrophage-like mouse reticulum sarcoma cells [96, 97]. After nanocapillary insertion, voltage was applied to induce electroosmotic flow, resulting in the capillary contents being pumped into the cytosol. Enzymatic reactions that occurred in the vicinity of the electrode were limited by diffusion, so analyte detection was spatially localized [97]. At the same time, intracellular calcium concentrations were measured fluorometrically using Fluo-3. Ca^{2+} did not change significantly during nanocapillary insertion or voltage application, indicating that cells were functioning normally. In another study, Pan et al. used nanocapillary ring electrodes to deliver the contents of an ion assay kit comprised of maltose phosphorylase, maltose, mutarotase, and glucose oxidase into HeLa cells to measure intracellular phosphate ion concentrations [98]. Electroosmotic flow through quartz nanocapillaries with ~100 nm tips has also been employed for ultrafast monitoring of mitochondrial membrane potential in MCF7 breast cancer cells [99]. In this study, Qian and colleagues applied a voltage to inject cells with inactive fluorescent dyes or JC-10, which selectively accumulates in mitochondria and reversibly changes from green to red as membrane potential increases. Red fluorescence, indicating mitochondrial activity, was observed within 20 s after nanoinjection, compared with 20–30 minutes for passive loading by incubation in aqueous JC-10 solution. This method detected rapid changes in mitochondrial metabolism in single cells in response to metformin, a drug used in diabetes and cancer treatment that inhibits mitochondrial electron transport complex I [100].

Over the past 10 years, Pourmand and colleagues have developed a variety of nanopipette electrode probes functionalized with biomolecular sensors to measure a number of metabolic processes implicated in cancer in single cells [6]. In 2015, they reported a method for monitoring intracellular pH using single-cell nanoprobes (tips <100 nm) [101]. These nanoprobes were comprised of quartz nanopipettes coated with chitosan, a polysaccharide biopolymer that undergoes reversible structural changes depending on pH [102], and coupled to a potentiostat with Pt wire. Changes in the ionic current at the nanopipette tip are detected by the electrode as rectification of the output current measured by the system, when stimulated by an oscillating input voltage signal [103, 104]. Nanoprobes were inserted into cells using a custom-built scanning ion conductance microscope. Changes in pH could be monitored in real time as cells were treated with a Cl^- channel blocker, and cytosolic pH measurements were found to be lower in cancer cells than in healthy fibroblasts. The Pourmand group also developed nanopipettes modified with glucose oxidase (GOx) as single-cell, real-time glucose sensors [105] (Fig. 10a–e). In the presence of glucose, GOx activity leads to the production of hydrogen peroxide and current rectification is detected by the nanoelectrode. These studies revealed cell-to-cell variations as well as differences between cell lines, with cancer cells having higher levels of intracellular glucose and increased rates of glucose uptake than normal fibroblasts.

A common feature of cancer cells is switching from oxidative phosphorylation to anaerobic respiration as their main means of ATP generation, which is called the Warburg effect [106]. The final step of glycolysis is the conversion of pyruvate to lactate. A carbon fiber microelectrode coated with lactose oxidase mixed with chitosan, deposited by electrodeposition, was reported to detect lactate fluctuations in brain tissues via H_2O_2 production [107]. This type of probe could also be adapted for intracellular glycolysis measurements. Korchev and colleagues have developed nanometer-scale dual carbon electrodes (DCE) for high-resolution sensing and topological mapping [108]. The addition of polypyrrole (Ppy) to the DCE nanopipette tip enhanced pH sensing and temporal resolution, and the spear shape enhanced spatial resolution. This group also reported a similar spearhead probe consisting of hexokinase immobilized on a pH-sensitive Ppy nano field-effect transistor (FET) as selective ATP biosensor [109] (Fig. 10f). Hexokinase cleavage of ATP leads to a stoichiometric generation of protons, which is detected as a localized change in pH. Thus, carbon nanoelectrodes have many potential applications for investigating oxidative metabolism of living cells.

A new class of nanocapillary probes termed asymmetric nanopore electrodes (ANE) were reported to enable real-time sensing of cellular respiration in breast cancer cells and were used to monitor the effects of anticancer drugs on cell metabolism [110] (Fig. 11). Instead of a wire sealed in the electrode, the ANE's interior is coated with Au and acts as the redox sensing interface which has high temporal and spatial resolution. The tip (~90 nm) of the gold interior of the nanocapillary is polarized as the cathode, and the opposite terminal acts as the anode; an ionic current is generated when the reducing agent NADH diffuses into the tip. Importantly, the ANE was modified with electrochemically reactive 4-thio-catechol (4TC). Reduction of 4TC at the tip led to the generation of H_2 nanobubbles and thus amplified the signal severalfold. Intracellular NADH was measured inside live MCF7 breast cancer cells, and decreases in NADH induced by taxol treatment were reliably detected. This method could be extended to other redox sensors using either reduction-induced H_2 or oxidation-induced O_2 nanobubbles.

9 Multimodal Fluorescent and Electrochemical Detection of mRNA

A multimodal strategy for mRNA detection was reported by Huang et al., who developed "signal-on" or "signal-off" assays based on photocleavable molecular beacons to detect manganese superoxide dismutase (MnSOD) transcripts in MCF7 breast cancer cells in [111] (Fig. 12). MnSOD, or SOD2, is a mitochondrial enzyme that regulates the metabolism of reactive oxygen species (ROS), converting superoxide into hydrogen peroxide. High MnSOD expression is a common feature of tumor cells and is associated with the switch to glycolysis [112]. These experiments used nano fiber-optics to selectively irradiate cells and nanopipettes to record electrochemical signals. In the "signal-on" experiments, single cells were irradiated with UV light, which led to spatially localized activation of DNA probes. The probes consisted of two oligonucleotides, one with a green fluorophore and the other with a red fluorescent quencher. The quencher also contained a photocleavable hairpin. Upon irradiation, the quencher could be displaced from the signal probe, leading to an increase in green fluorescent signal (Fig. 12a, b). In the "signal-off" assays, a nanoelectrode was conjugated to a thiol-modified oligonucleotide and comple-

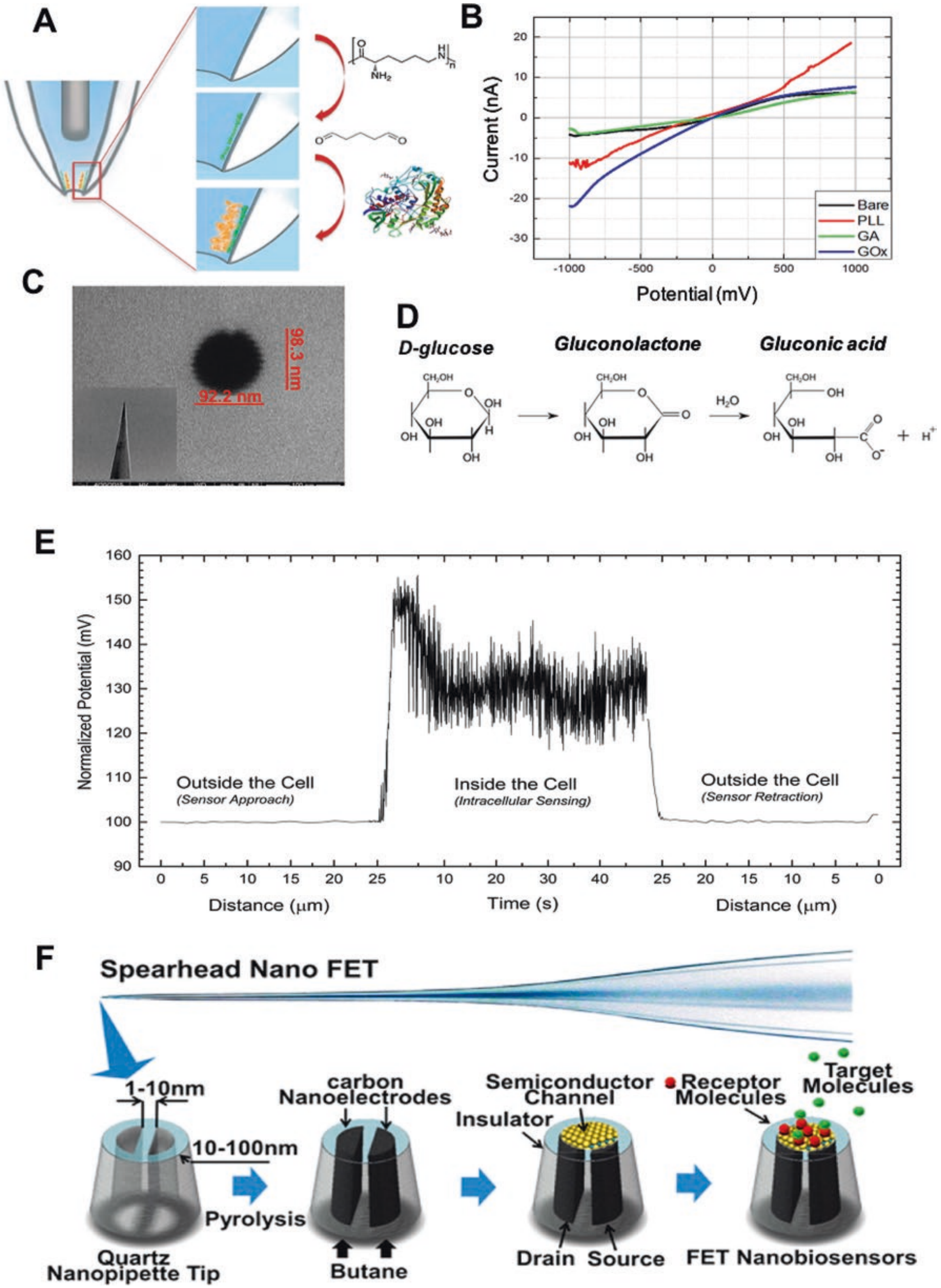
A
NH₂
n
B
Current (nA)
20
10
0
-10
-20
-30
-1000
-500
0
500
1000
Potential (mV)
Bare
PLL
GA
GOx
C
98.3 nm
92.2 nm
D
D-glucose
Gluconolactone
Gluconic acid
CH₂OH
O
OH
H
H₂O
O⁻
+ H⁺
E
Normalized Potential (mV)
160
150
140
130
120
110
100
90
Outside the Cell
(Sensor Approach)
Inside the Cell
(Intracellular Sensing)
Outside the Cell
(Sensor Retraction)
0
5
10
15
20
25
10
20
30
40
25
20
15
10
5
0
Distance (μm)
Time (s)
Distance (μm)
F
Spearhead Nano FET
1-10nm
10-100nm
Quartz
Nanopipette Tip
Pyrolysis
carbon
Nanoelectrodes
Butane
Semiconductor
Channel
Insulator
Drain
Source
Receptor
Molecules
Target
Molecules
FET Nanobiosensors

Fig. 10 Single-cell metabolic nanosensors. (**a**) Schematic of surface modifications for the immobilization of glucose oxidase in the nanopipette tip. The inner surface is coated with poly-L-lysine (PLL) and then treated with glutaraldehyde to cross-link the amino group of PLL to glucose oxidase (GOx). (**b**) Electrochemical characterization of the nanopipette after each step in the fabrication process. (**c**) SEM image of the nanopipette tip. Inset: side view of the nanopipette. (**d**) The chemistry of enzymatic conversion of glucose to gluconic acid. (**e**) Single-cell readings using the glucose nanosensor. As the sensor tip approaches the cell membrane, the potential increases sharply. Once the tip has penetrated the cytoplasm, the potential drops to a steady state of fluctuations caused by localized peroxide generation. After the nanopipette is withdrawn, the potential drops back to baseline. (Adapted with permission from [105]. Copyright 2016, American Chemical Society). (**f**) Spearhead nano-FET. A nanometer-scale field-effect transistor was fabricated by deposition of a thin layer of semiconductor material (polypyrrole) on the tip of dual carbon electrodes, made by pyrolytic decomposition of butane, that serve as drain and source. Redox-generating molecules (e.g., hexokinase) immobilized on the transistor provide selective FET sensing. (Reproduced with permission from [109]. Copyright 2016, American Chemical Society)

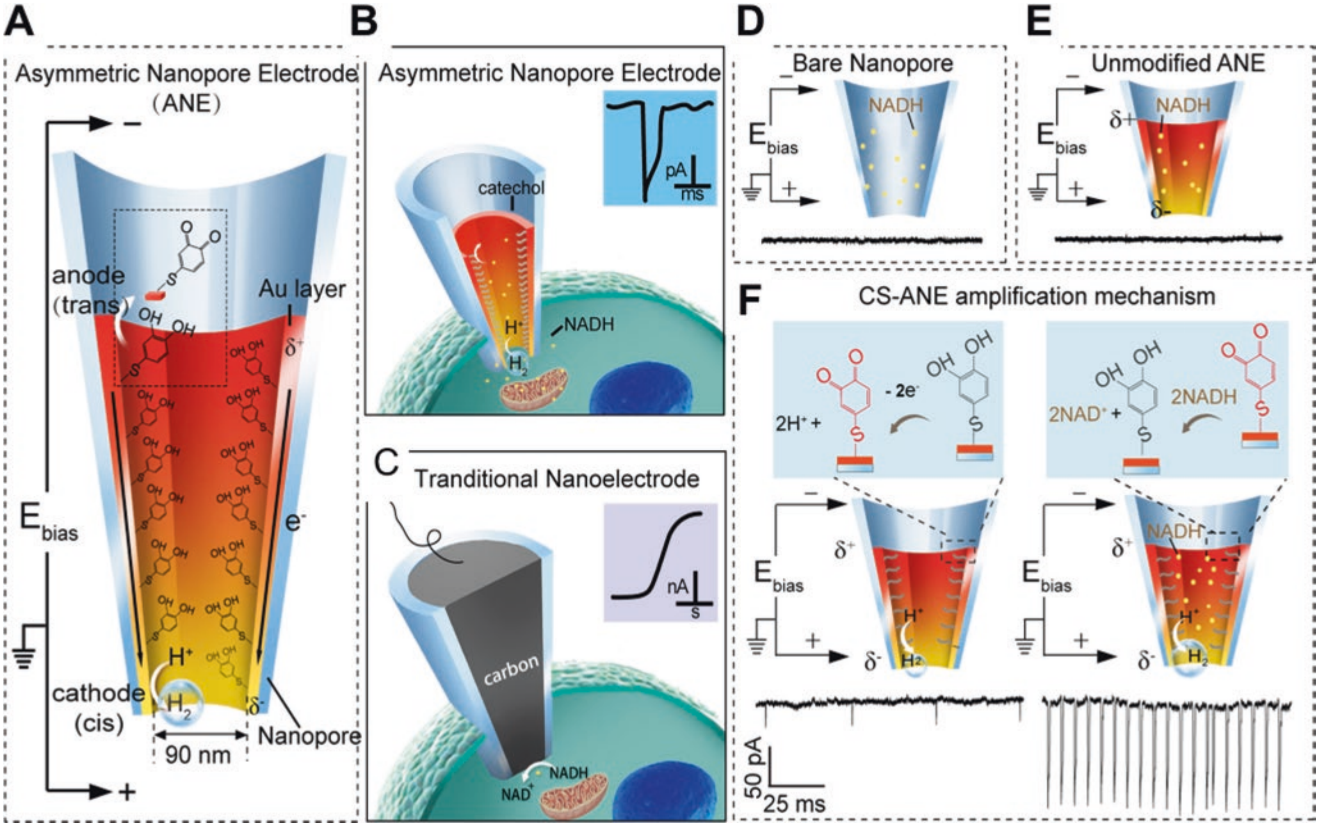

Fig. 11 Wireless asymmetric nanopore electrode (ANE) for real-time sensing of cellular respiration. (**a**) Schematic of the ANE. The applied bias potential drives the potential difference between the two terminals of the Au- and 4-thiol-catechol (4TN)-coated nanopores. The tip opening (*cis*) is polarized as the cathode and the opposite terminal (*trans*) acts as the anode. Reduction occurs at the cathode and oxidation occurs at the anode. (**b**) Intracellular redox species (e.g., NADH) diffuse into the *cis* tip of the ANE, and a pair of redox reactions takes place at the cathode and anode. A transient ionic current response is generated (inset) which allows a high degree of temporal resolution. (**c**) Traditional carbon nanoelectrode schematic with a solid tip that generates a cyclic voltammogram (inset) with poor temporal resolution. (**d**) The bare nanopore does not produce any current in response to NADH. (**e**) The unmodified ANE generates a stable baseline signal. (**f**) The 4TN-coated ANE generates an enhanced current signal due to the generation of H_2 bubbles at the cathode. Left: 4TN is oxidized electrochemically at the anodic pole while a small amount of H_2 is produced at the cathodic pole, generating a weak signal. Right: in the presence of NADH, the catechol conversion is mediated by the redox pair NADH/NAD+, leading to the production of H_2 bubbles and an amplified current response. (Reproduced with permission from [110]. Copyright 2018, American Chemical Society)

mentary methylene blue (MB)-modified hairpin probe. In the absence of irradiation and target mRNA, the nanoelectrode signal was high due to MB redox. When the hairpin was cleaved and MnSOD mRNA was present, displacement of the MB led to depletion of the electrical signal (Fig. 12c, d) [111].

10 Nanopipette Electrodes to Monitor Reactive Oxygen Species Generation

Metabolic reprogramming in cancer leads to changes in the production of ROS and oxidative stress [113, 114]. Platinized carbon nanoelectrodes have long been used to investigate cellular redox chemistry and ROS generation. Pt black is a fine powdered form of Pt that is widely used for improving electrode efficiency by greatly increasing the reactive surface area. Early studies of single-cell ROS detection were performed by Amatore and colleagues in the 1990s using platinized carbon fiber microelectrodes, but cells had to be punctured to release their contents [115]. In 2008, Mirkin and colleagues reported the use of platinized glass nanoelectrodes with ~40 nm tips in diameter to perform intracellular voltammetry in living MCF10A non-tumor breast epithelial cells [116]. Scanning electrochemical microscopy (SECM) [24] was used to position the tip of the electrode, map cell topography, measure membrane potential, and detect redox reactivity inside cells. A current was observed when the probe was in the hydrophilic redox buffer outside the cell and disappeared when the tip penetrated the plasma membrane, indicating that the membrane had resealed around the probe and was not leaky. A redox buffer containing $Ru(NH_3)_6^{3+}$, which cannot cross the plasma membrane, is commonly used to confirm cell penetration and membrane resealing in nanoelectrode studies. SICM-coupled carbon nanoelectrodes functionalized with Pt were reported in 2014 by Korchev and colleagues, who fabricated disk-shaped

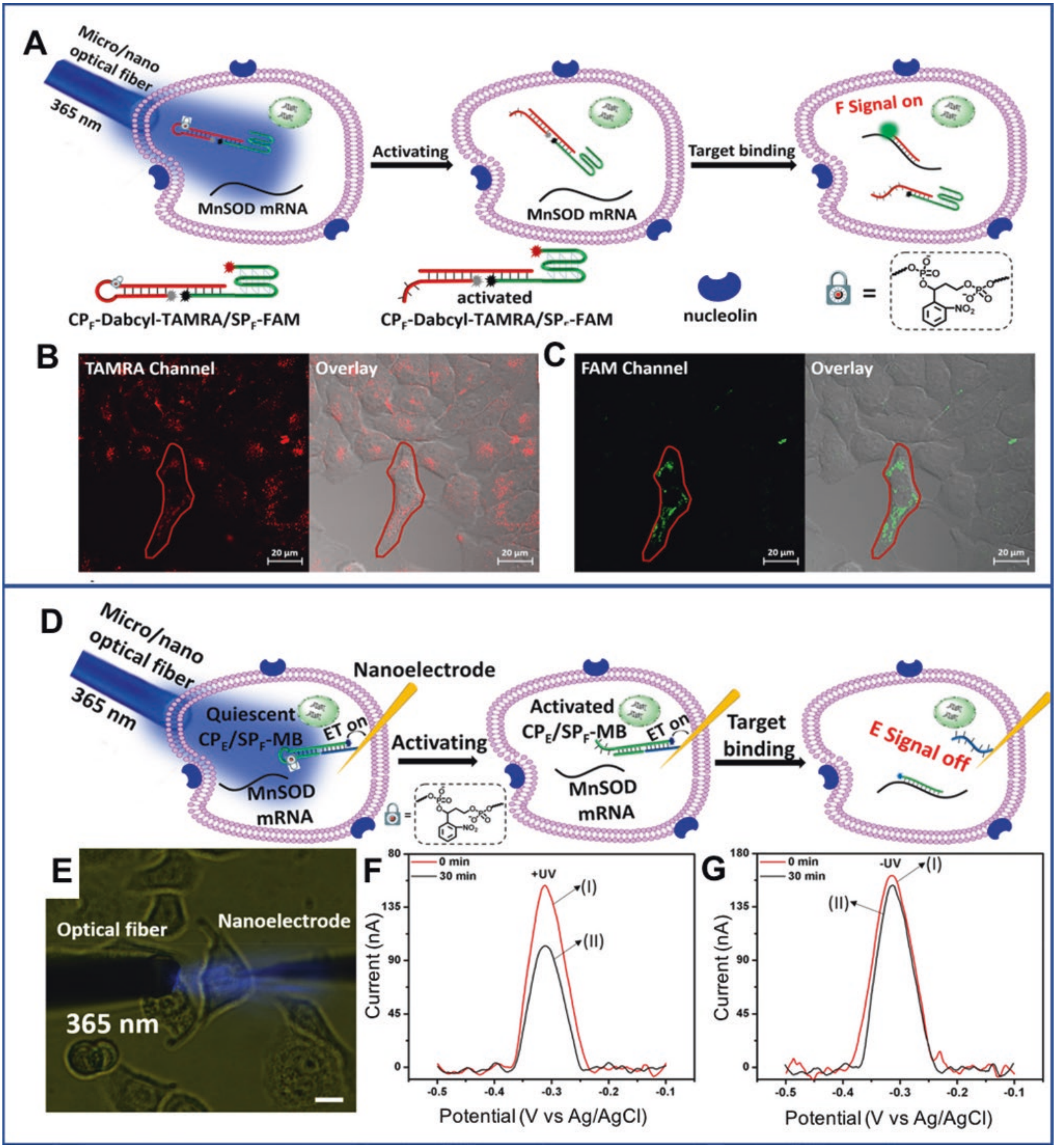
A
Micro/nano optical fiber
365 nm
MnSOD mRNA
Activating
MnSOD mRNA
Target binding
F Signal on
CP_F-Dabcyl-TAMRA/SP_F-FAM
activated CP_F-Dabcyl-TAMRA/SP_F-FAM
nucleolin
=
NO₂
B
TAMRA Channel
Overlay
20 µm
20 µm
C
FAM Channel
Overlay
20 µm
20 µm
D
Micro/nano optical fiber
365 nm
Nanoelectrode
Quiescent CP_E/SP_E-MB
ET on
MnSOD mRNA
Activating
Activated CP_E/SP_E-MB
ET on
MnSOD mRNA
Target binding
E Signal off
=
NO₂
E
Optical fiber
Nanoelectrode
365 nm
F
0 min
30 min
+UV
(I)
(II)
Current (nA)
80
135
90
45
0
-0.5
-0.4
-0.3
-0.2
-0.1
Potential (V vs Ag/AgCl)
G
0 min
30 min
-UV
(I)
(II)
Current (nA)
180
135
90
45
0
-0.5
-0.4
-0.3
-0.2
-0.1
Potential (V vs Ag/AgCl)

Fig. 12 Multimodal mRNA detection of MnSOD mRNA in MCF-7 breast cancer cells. Top box: the "signal-on" strategy. (**a**) Principle of the photoactivated toehold-mediated displacement reaction for the optical mRNA sensing probe. The probe consists of an oligonucleotide with a green fluorophore (FAM), conjugated to a cell surface receptor-binding aptamer, and a hairpin oligonucleotide carrying a quencher red fluorophore (Dabcyl-TAMRA). The hairpin is photocleavable due to the inclusion of an o-nitrobenzylphosphate linker. Binding of the probe aptamer to nucleolin facilitates uptake by cancer cells. A single cell is irradiated with UV light using a micro or nano optical fiber to cleave the probe hairpin, allowing the FAM probe to bind to complementary mRNA. This association displaces the quencher, resulting in green emission from the fluorophore. (**b**) Red TAMRA fluorescence shows uptake of the probe in all cells. (**c**) Green fluorescence is observed only in the photoactivated cell (red line). Bottom box: the "signal-off" strategy. (**d**) Schematic of the electrochemical mRNA sensing probe. The nanoelectrode is functionalized with a thiol-modified capture probe (CP_E) which is bound to a complementary methylene blue (MB)-modified photocleavable hairpin signal probe (SP_E-MB). When the hairpin is cleaved upon UV irradiation in the presence of target mRNA, the electrochemical signal at the nanopipette decreases. (**e**) Micrograph of cells under illumination with intracellular nanoelectrode probe. (**f**) Voltammetric response of a single cell before (I) and after (II) 30 min of UV irradiation. (**g**) Voltammetric recordings of a single cell at 30-min intervals without irradiation. (Adapted with permission from [111]. Copyright 2018, American Chemical Society)

carbon electrodes with radii as small as 5 nm [108]. These nanoelectrodes were used to measure O_2 consumption in brain tissue explants and inside single melanoma cells. In 2018, Pourmand and colleagues used SICM-coupled nanopipettes (~40 nm pore) to specifically detect superoxide (O_2^{*-}) in living cells [117]. These nanoprobes were covalently modified with cytochrome-c, an electron acceptor that converts O_2^{*-} to O_2. Current rectification was sensed by the coupled electrode in the presence of O_2^{*-}. Superoxide levels increased as expected in MCF10A breast myoepithelial cells exposed to carbonyl cyanide 3-chlorophenylhydrazone, a protonophore that induces the generation of ROS in mitochondria, and adding superoxide dismutase (SOD), a ROS scavenging enzyme, had the opposite effect.

Much of the recent work on detecting ROS in live cells has been performed using macrophages, which produce superoxide both to combat pathogens and as part of the monocyte differentiation process [118]. In the former scenario, a macrophage subjects an engulfed pathogen to an intense burst of ROS and reactive nitrogen species (RNS) contained in vacuoles called phagolysosomes, and the debris and leftover ROS/RNS are then ejected from the cell. In the latter, tumor-associated macrophages take on a chronic inflammatory phenotype due in part to the superoxide-mediated signaling. Amatore and colleagues used Pt black-coated nanoelectrodes (>100 nm tips), fabricated using a novel AFM-controlled method, to detect ROS/RNS in live macrophages [119]. However, these probes lacked specificity as the applied potential could oxidize other compounds, such as uric acid. Carbon electrodes coated with the electrocatalyst Prussian Blue were reported to more selectively detect hydrogen peroxide in mouse macrophages [120]. Rawson et al. used single-walled carbon nanotubes (SWCNTs) functionalized with an osmium catalyst, osmium bipyridine (Osbpy), to specifically detect H_2O_2 production in RAW 264.7 cells stimulated with lysophosphatidic acid (LPS) [121] (Fig. 13). Here, the SWCNT electrodes were interfaced with cells by centrifugation. LPS stimulation led to generation of intracellular ROS, and electron transfer from Osbpy to ROS resulted in a drop in current at the nanoelectrode (Fig. 13a). This process could be blocked by the addition of ROS inhibitors (Fig. 13b, c). In 2020, a novel tungsten nanoelectrode was used to selectively measure hydroxyl radicals ($^{*}OH$) in RAW 264.7 macrophages [122]. Tungsten wires were etched to conical nanoneedles and sheathed with Au nanoparticles and then coated with a self-assembled monolayer of 1-hexanethiol, which blocked the electrochemical signal until attacked by $^{*}OH$. Hoechst 33258 and MitoTracker were used to label cellular organelles and establish the subcellular positioning of nanoelectrodes. Hydroxyl bursts were observed following stimulation with LPS. Interestingly, the $^{*}OH$ bursts were many times lower inside cell nuclei than in the cytosol and twofold higher in close proximity to mitochondria, which suggests that these ROS were by-products of mitochondrial respiration.

Two recent studies used nanoelectrodes to measure ROS/RNS specifically inside phagolysosomes of living macrophages [123, 124]. Zhang et al. used cylindrical silicon carbide nanowire electrodes (300–500 nm diameter) inserted into RAW 264.7 macrophages to detect intracellular ROS/RNS. They recorded transient spikes in current, which were determined to be phagolysosomes colliding with the nanowire. A similar study was performed using carbon fiber nanoelectrodes to measure neurotransmitter contents in PC12 cells [125]. Hu et al. also probed RAW 264.7 macrophages but used smaller platinized carbon nanopipettes (tip <100 nm) and distinguished four species of analytes (H_2O_2, $ONOO^-$, NO^*, and NO_2^-). This was accomplished by recording currents over a periodic sequence of potentials, because each ROS/RNS is oxidized at a different potential. Besides investigating macrophages, Mirkin and colleagues previously used similar platinized carbon nanoelectrodes to measure the contributions of four ROS/RNS in non-tumour (MCF10A) and triple-negative breast cancer cell lines (MDA-MB-231 and MDA-MB-468) [126]. They found that ROS/RNS levels were lowest in the non-tumor and highest in the MDA-MB-231 cells. They then measured ROS generation in MCF10A cells treated with diacylglycerol (DAG)-lactone, which induces the activation of protein kinase C (PKC), which is overexpressed in many human breast tumors. A series of oxidative bursts were recorded from about 25 minutes after DAG-lactone addition, suggesting that PKC activity induces oxidative stress which in turn drives cancer malignancy.

11 Nanoelectrodes for Metal Ion Detection

Metal-sensing-functionalized nanoelectrodes show promise as intracellular probes for cancer research. For example, many important signaling pathways that are involved in tumor growth and metastasis rely on calcium ions, such as cell adhesion and actomyosin dynamics [127]. The Pourmand group used nanoprobes conjugated with immobilized calmodulin, a Ca^{2+}-binding protein, to measure extracellular calcium ions [4]. Intracellular calcium ion detection was also achieved by Son et al. using SWCNT FETs in nanocapillaries [128]. The SWCNTs were functionalized with Fluo-4-AM dye, which acted as both an electrochemical sensor for Ca^{2+} binding and as a fluorescent probe.

Although they have not yet been used in living cells, biomolecule-coated quartz nanocapillary electrodes have been developed to measure the levels of various other metal ions in solution. Iron plays a key role in aerobic respiration and ROS generation, and dysfunctional iron metabolism has

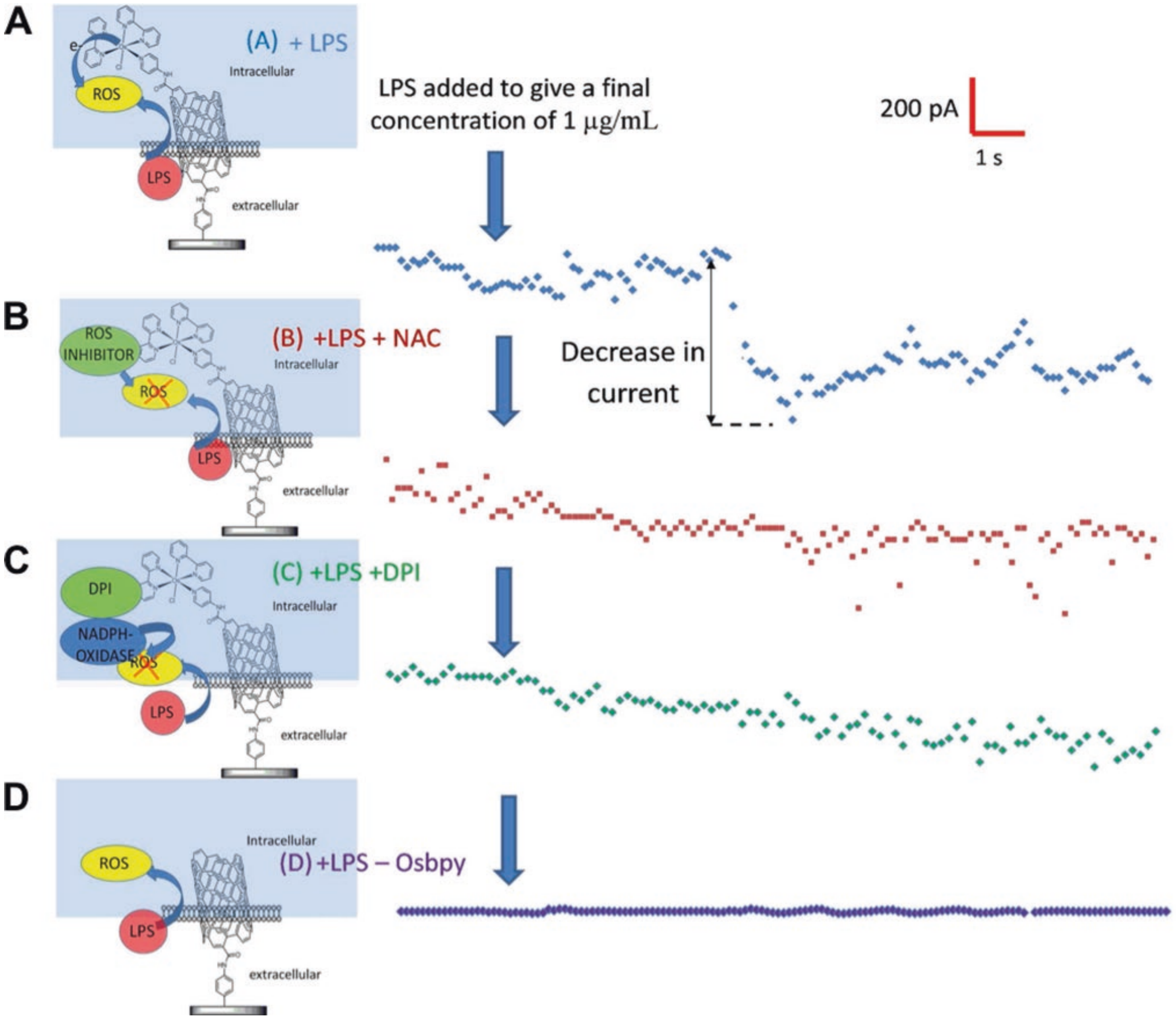

Fig. 13 Reactive oxygen species measurements in live macrophages using single-walled carbon nanotube (SWCNT) probes. Typical current amperograms over time measured in RAW 264.7 macrophages interfaced with SWCNT functionalized with osmium bipyridine (Osbpy) (**a**–**c**) or without functionalization (**d**). (**a**) Addition of LPS induces the generation of ROS. Electron transfer from Osbpy to ROS results in a rapid decrease in current. (**b**, **c**) ROS generation and current decrease is blocked in the presence of ROS inhibitors, N-acetyl cysteine (NAC), and diphenyleneiodonium (DPI). (**d**) No current is observed in the absence of Osbpy. (Reproduced with permission from [121], https://pubs.acs.org/doi/10.1021/acsami.5b06493. Copyright 2015, American Chemical Society. *Further permissions related to the material excerpted should be directed to the ACS*)

been implicated in cancer [129]. An iron-binding protein from *H. influenzae* was used to detect ferrous ions in solution [130]. Other heavy metals also play roles in normal cellular processes and contribute to the production of ROS, DNA damage, inflammation, and tumorigenesis in high concentrations [131, 132]. Divalent copper ion nanopipette sensors have been fabricated from a combination of chitosan and polyacrylic acid [133] and from the copper-binding domain of prion protein [134]. Baker and colleagues used imidazole-modified nanopipettes to measure cobalt ions in solution [135]. An intracellular optical probe could be also adapted from fluorophore-conjugated Si nanowires, which were used to measure free copper ions in liver and HeLa cell lysates by fluorescence quenching [136].

12 Nanoelectrode Arrays for Cell Sensing on the Population Scale

To scale up from the single-cell level, nanoelectrodes can be fabricated as multielectrode arrays (MEA). The majority of these studies have been performed on neuronal cells [137–140] or cardiomyocytes [141], which are the most obvious cell types for electrical assays. It should be noted that the

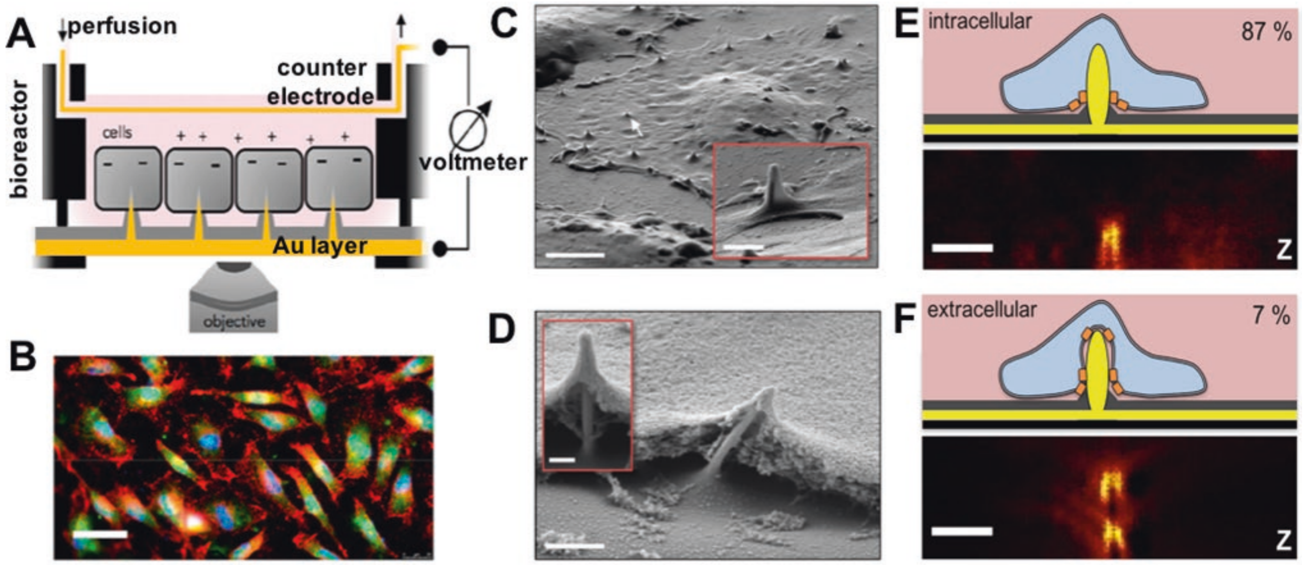

Fig. 14 Gold multielectrode arrays (MEA) used for measuring electrical activity in adherent cells. (**a**) Schematic of the MEA system. (**b**) Fibroblasts seeded on gold nanowire arrays stained to label the plasma membrane (wheat germ agglutinin, red), cytosol (CellTracker, green), and DNA (DAPI, blue). Scale bar = 20 µm. (**c**) SEM images of a fibroblast growing on gold nanowires. White arrow = interfacing electrode. Scale bars = 5 µm and 1 µm (inset). (**d**) SEM images of fracture cross sections of cell-electrode interface. Scale bars = 5 µm and 200 nm (inset). (**e**, **f**) Schematic illustrations (top) and z-projections (bottom) of paxillin staining around nanoelectrodes. In 87% of cases, focal adhesions were only observed around the base of electrodes, and in 7% of cases paxillin was observed along the length of the electrodes. Scale bars = 2 µm. (Adapted with permission from [142], https://pubs.acs.org/doi/10.1021/acs.nanolett.9b00784. Copyright 2019, American Chemical Society. *Further permissions related to the material excerpted should be directed to the ACS*)

majority of systems require cells to be electroporated in situ in order to facilitate intracellular access and sensing of intracellular (rather than extracellular) voltages, which may impart unknown changes on cell electrophysiology. However more recently, en masse electrical activity in electrically coupled cell populations was observed, without the need for electroporation, using Au nanowire arrays in fibroblasts as well as myotubes and neuronal networks [142] (Fig. 14a–d). Cells were found to adhere to the nanowires and remained viable for many days in culture. Paxillin-containing focal adhesions formed around the base or along the side of the nanowires (Fig. 14e, f). The majority of nanowire interfaces had paxillin complexes only at the base, suggesting cytosolic penetration (Fig. 14e). Electrical oscillations recorded by these MEAs were attributed to cellular contractility events involving localized Ca^{2+} waves.

Metal nanoelectrodes can also be combined with SERS to allow both electrical and chemical properties to be sensed from the same cell populations. SERS offers a powerful tool for studying cells interfaced with nanoelectrodes, because Raman spectroscopy provides information about lipids, proteins, and nucleotides. Caprettini et al. plated U2OS osteosarcoma cells on gold MEAs and monitored Raman spectra after electroporation [143]. They detected changes in lipid and amino acid peaks consistent with membrane rupture and resealing and also observed DNA peaks which suggested nuclear penetration or at least nuclear envelope disruption. Mapping physiological and molecular probe-induced electrochemical readouts and Raman spectra from cultured cancer cells or living tissues using MEAs could provide valuable information about cellular activities in wider population contexts.

13 Probing Cytoskeletal Mechanics with Antibody-Conjugated AFM Tips

Cancer cells undergo significant changes in cytoskeletal organization and mechanics. Changes in actomyosin contractility, the formation of actin-based protrusions, and remodeling of cell-cell and cell-matrix adhesions are hallmarks of tumorigenesis and epithelial-to-mesenchymal transition (EMT) [48, 144]. Another cytoskeletal marker of EMT in cancer is the intermediate filament vimentin, which promotes cell stiffening, migration, and loss of E-cadherin at cell-cell junctions [145]. Nakamura and colleagues have used various antibody-conjugated Si nanoneedles operated by AFM to probe the tensile strength of cytoskeletal elements in living cells. High aspect ratio nanoneedles were fabricated by etching AFM tips into 12 µm-long cylinders with diameters of 200 nm and then functionalized with antibodies against the cytoskeletal proteins actin [13] (Fig. 15), tubulin [146], vimentin [44, 147], and nestin [147, 148]. Nanoneedle probes were inserted into cells, allowed to bind targets, and retracted slowly (e.g., 10 µm/s for actin), while the force was measured by AFM cantilever deflection [13]. The pulling forces on the probe

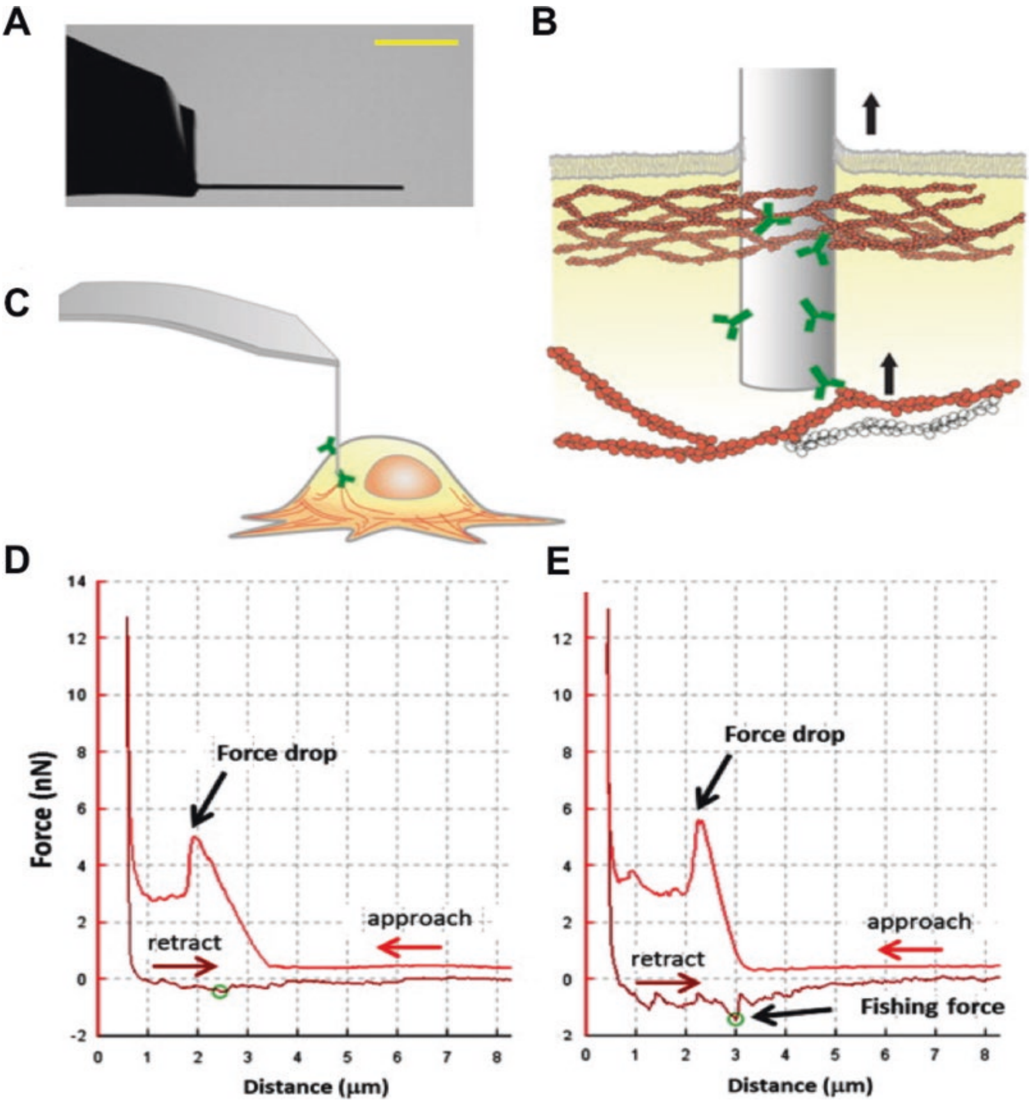

Fig. 15 Antibody-conjugated AFM tips for probing cytoskeletal mechanics. (**a**) Focused ion beam image of nanoneedle etched from an AFM tip. Scale bar = 4 μm. (**b**, **c**) Schematics of antibody-conjugated nanoneedle insertion and binding to actin fibrils. (**d**, **e**) Typical force-distance curves recorded by AFM during approach and retraction of the nanoneedle. The force drop occurs when the nanoneedle initially penetrates the cell membrane. (**d**) Retraction of a nanoneedle with no functionalization results in a smooth force curve. (**e**) Retraction of an anti-actin antibody-conjugated nanoneedle results in a jagged curve and significant "fishing force" peak resulting from antibody-actin unbinding events. (Reproduced with permission from [13]. Copyright 2012, Elsevier)

during the retraction stage, termed "fishing forces," correspond to antibody-target unbinding events (Fig. 15e). Cells could be repeatedly probed (10–20 times) without affecting viability [13, 148]. For anti-actin antibody-conjugated nanoneedles, fishing forces in the 1–2.5 nN range were detected during the retraction stage (twofold higher than observed with nonfunctionalized probes) [13]. Decreased fishing forces, indicative of changes in actin mechanics, induced by treating cells with low doses of cytochalasin D, which depolymerizes F-actin, or Y-27632, which inhibits ROCK-mediated myosin-II activity leading to stress fiber disassembly, were detected by AFM within 5 minutes, before any decrease in actin polymerization could be seen by staining with fluorescent phalloidin. The Nakamura group has also investigated the mechanics of the intermediate filament protein nestin in breast cancer cells. Mouse breast cancer 4T1E cells selected for high metastatic potential had higher fishing forces using anti-nestin conjugated nanoneedles than parental cells, corresponding to higher expression of nestin [148]. Nestin depletion reduced these cells' capacity for directional migration and metastasis [147]. Yamagishi et al. also showed that nestin depletion affected the tensile strength of vimentin, likely via its association with cortical actin, using anti-vimentin functionalized nanoneedles [147].

14 Extraction of Cellular Contents with Nanoneedle Arrays

Antibody-functionalized nanoneedles can also be used to extract proteins from cells. This strategy may be used to perform a spatial biopsy or for immunoprecipitation (IP) or ELISA type assays. Wang et al. used diamond nanoneedle arrays functionalized with protein-binding aptamers to capture and extract cytosolic NF-κB in order to study inflammatory signaling dynamics in cancer cells and neurons [149]. Exposure to double-stranded DNA triggers the degradation of IκB proteins that sequester NF-κB in the cytosol, leading to NF-κB nuclear translocation. The aptamer-conjugated "molecular fishing rods" were interfaced with cells by supergravity, i.e., centrifugation, for 90 seconds and then removed. Temporary disruption of the plasma membrane during this step also allowed for the concurrent delivery of dsDNA into cells. Cells were probed repeatedly following dsDNA exposure for 40 minutes, and captured NF-κB was detected on the nanoneedles by immunofluorescence staining. Fluorescence intensity on the nanoneedles decreased significantly over time in the dsDNA-treated samples but not in controls, indicating (1) that the protein had translocated to the nucleus in response to foreign DNA and (2) that the nanoneedles had penetrated the plasma membrane but not the nucleus.

Antibody-functionalized Si nanowire arrays have also been used to capture proteins from living cells [150] (Fig. 16). A human chronic myelogenous leukemia (CML) cell line that grows in suspension and only weakly interacts with Si nanowires was chosen in order to minimize adhesion to the arrays, which were also blocked with polyethylene glycol (PEG) after functionalization. Nanowires functionalized with anti-RFP antibodies were able to pull out the fluorescent protein from transiently transfected cells. Nanowires bearing anti-c-Abl antibodies pulled out endogenous Bcr-Abl fusion proteins, as shown by immunofluorescence staining. Furthermore, anti-Abl conjugated nanowires were positive for Grb-2, which binds to phosphorylated Brc-Abl, indicating that these arrays could be used to co-IP proteins [150] (Fig. 16d).

15 Extraction of Cellular Contents: Hollow Nanostraw Arrays

Arrays of hollow nanoneedles, or nanostraws, were developed by Melosh and colleagues to allow direct fluid access to cell interiors in order to deliver cargos or sample cellular contents [3] (Fig. 5). The Melosh group has reported using aluminum oxide nanostraws to sample intracellular proteins and mRNA from the same cells repeatedly over many hours and

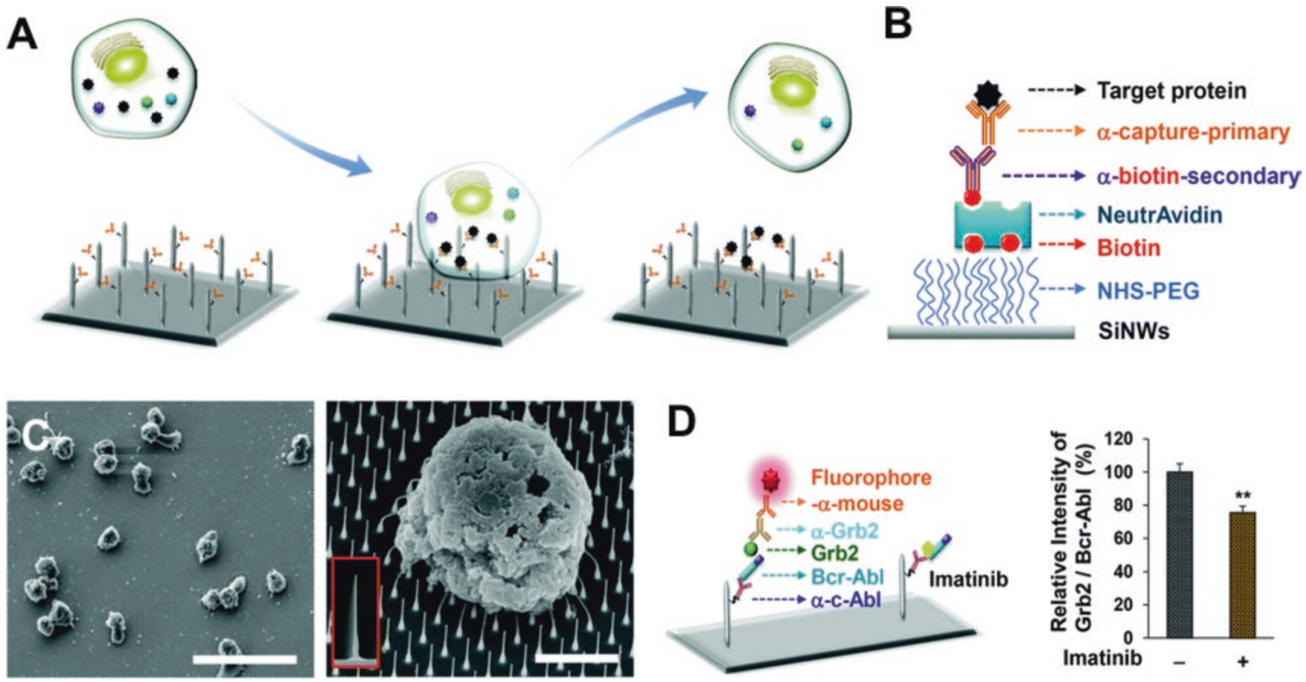

Fig. 16 Silicon nanowire pull-down assay for intracellular sampling. (**a**, **b**) Schematic of the assay. Cells interface transiently with nanowires that are conjugated with biotinylated antibodies for target protein capture. (**c**) SEM images of K562 cells on top of Si nanowires 24 h after plating. Scale bars = 50 μm (left) and 4 μm (right). Inset shows a cross-sectional view of a nanowire at the same scale. (**d**) Co-immunoprecipitation on Si nanowires. Left: schematic of pull-down strategy. Right: intensity of fluorescently labeled secondary antibody relative to negative control (no cell) substrates showing co-IP of Grb2 using anti c-Abl-conjugated nanowires. Data represent mean ± SD ($n = 5$). **$p < 0.01$. (Adapted with permission from [150]. Copyright 2016, Royal Society of Chemistry)

even days in culture with minimal (<5%) cell death [21]. Sampling efficiency was confirmed by measuring fluorescent proteins extracted from GFP-expressing CHO cells. The cells were also transfected with RFP prior to sampling, and extracts showed a gradual increase in red fluorescence over the course of 16 hours. Heat shock protein 27 (HSP27) was also extracted from human iPSC-derived cardiomyocytes over a time course following heat shock. Protein levels were quantified by ELISA and mRNA was measured using qRT-PCR. The levels of protein and mRNA from nanostraw extractions were in good agreement with those from cell lysates and were not present in the absence of electroporation. More recently, Cao et al. reported further optimization of this system for RNA, DNA, and protein delivery [151]. Stamping cells from above with gold nanostraw arrays was also shown to be an efficient means of delivering cargo to adherent cells [152]. This is likely due to the relative speed of insertion compared to cell settling [33, 34, 36]. Magnetic nanoparticles, such as carbon nanotubes, that bind to cytosolic proteins or other molecules can also be loaded into cells and extracted using nanostraws in a magnetic field [153]. Xie and colleagues have also employed hollow nanoneedles with electroporation to repeatedly sample intracellular proteins and deliver cargos [38, 154, 155]. He et al. found that larger alumina nanostraws (450 nm diameter) were able to extract greater quantities of lactate dehydrogenase B (LHDB) from adherent cells, as measured by ELISA [38]. Subsequently, they used a branched nanostraw (BNS) electroporation platform to capture circulating tumor cells (CTC) from a mixed cell suspension, deliver cargos, and extract cytosolic proteins [154] (Fig. 17). MCF7 breast cancer cells were specifically captured by coating nanostraws with antibodies against EpCAM, a CTC marker [156]. The 400-nm-diameter BNS had highly branched surfaces, which facilitated cell capture by greatly increasing surface area (Fig. 17b, c). GFP-encoding plasmid vectors and propidium iodide (which cannot penetrate the intact membrane of living

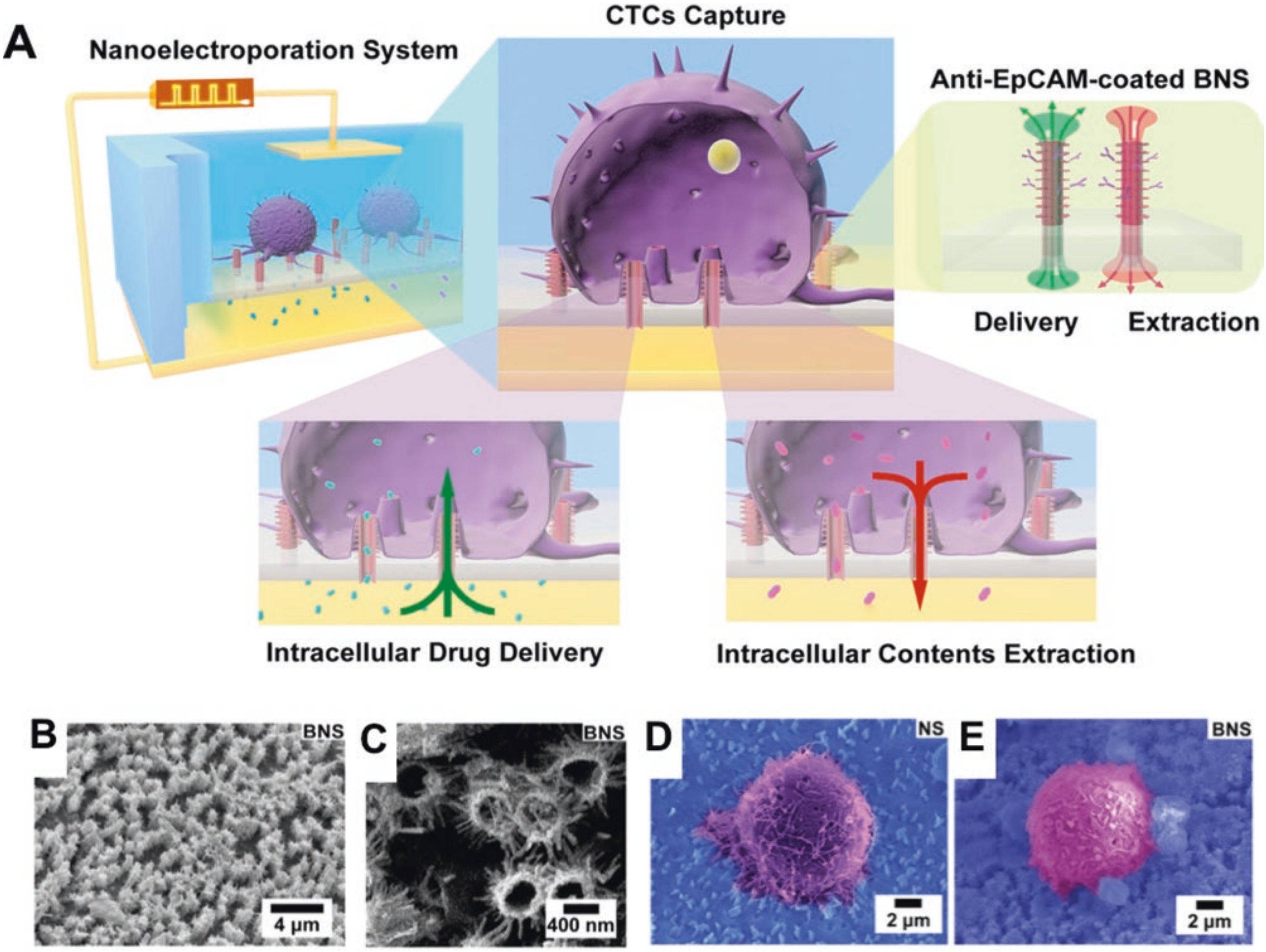
A
Nanoelectroporation System
CTCs Capture
Anti-EpCAM-coated BNS
Delivery
Extraction
Intracellular Drug Delivery
Intracellular Contents Extraction
B
BNS
4 μm
C
BNS
400 nm
D
NS
2 μm
E
BNS
2 μm

Fig. 17 Multifunctional branched nanostraw-electroporation platform for tumor capture and sampling. (**a**) Schematic of the multifunctional branched nanostraw (BNS) platform. Circulating tumor cells (CTCs) are captured on BNS coated with anti-EpCAM antibody. Captured cells are electroporated to introduce cargo and/or sample cellular contents from the underlying microfluidic channel. (**b**, **c**) SEM images of the branched nanostraw array. (**d**, **e**) Captured MCF7 cells on unbranched (**d**) and branched (**e**) nanostraws. (Adapted with Permission from [154]. Copyright 2019, American Chemical Society)

cells) were delivered to cells following electroporation, and cellular proteins were extracted. Intracellular protein sampling was verified by measuring caspase-3 over time after cells were treated with staurosporine to induce apoptosis. Wen et al. also reported fabrication of nanostraw arrays from Au, Pt, and the conductive polymer poly(3,4)ethylenedioxythiophene (PEDOT) and showed that these could be used for both cargo delivery and protein extraction [155].

16 Extraction of Cellular Contents: Single-Cell Nanobiopsy

Measuring proteins, mRNA, and metabolites in single cells is essential for understanding the heterogeneity of cancer cells. Nanoneedles and nanocapillaries have been used to remove genetic material from individual cells with high spatial precision. In 2007, Uehara et al. used a conventional AFM tip to extract mRNA from different points within rat fibroblasts and confirmed the spatial location of *ACTB* mRNA by fluorescence in situ hybridization (FISH) [104]. Nawarathna and Wickramasinghe also used AFM probes coated with Pt to create a dielectrophoretic force that improved nucleotide capture to profile mRNA extracted from living cells, including breast cancer cells [157, 158]. In both cases, the extracted mRNA was analyzed by qPCR. Pourmand and colleagues used SICM to carefully control nanopipette penetration and extracted the contents of single cells using electrowetting [159] (Fig. 18a–d). The nanocapillary was filled with a hydrophobic liquid whose surface tension changes when a voltage is applied. This change causes the aqueous solution to be drawn into the nanopipette under negative voltage and flow out when the bias is reversed. Extracted mRNA transcripts were analyzed by qRT- PCR. In addition, they extracted individual mitochondria labeled with the vital dye MitoTracker and used next-generation sequencing to sequence the mitochondrial DNA. This method was later used to sample mRNA from cell bodies and neurites of individual neurons to measure the spatial localization of transcripts [160]. Nashimoto et al. used double-barreled nanopipettes guided by SICM to sample mRNA from the nucleus or peripheral cytoplasm of MCF7 cells and quantified the abundance of *GAPDH* and *ACTB* transcripts [161]. Another sampling strategy employed a microfluidic probe (MFP) that can simultaneously inject and aspirate liquid using the principle of hydrodynamic flow confinement [162]. Kashyap et al. used vertically oriented MFPs to locally lyse cancer cell cocultured monolayers and collect DNA/RNA from specific subpopulations, though not from individual cells [162].

Fluidic force microscopy (FluidFM) also uses hollow cantilever AFM tips to dispense or collect picoliter or sub-picoliter volumes of liquid [15] (Fig. 1d). FluidFM nanofluidics in the cantilevers act as pressure-controlled nanopipettes. Guillaume-Gentil et al. found that large proportions of the cytoplasm, up to 4 pl, could be extracted from HeLa cells without causing immediate cell death [163]. This method has been employed by sample intracellular protein from cell nuclei and cytoplasm, and extracted contents have been examined by electron microscopy, enzymatic assays, and qPCR [163].

A variety of nanobiopsy methods have been used to perform metabolomic profiling of single cells. (For a review of single-cell metabolomics, see [164].) Much of the work on single-cell sampling for mass spectroscopy (MS) has been done in plants [165–167], but a number have been performed on mammalian cells. For example, Guillaume-Gentil et al. used FluidFM to sample live cells for MALDI mass spectrometry analysis of metabolites in HeLa cells [168]. Previously, Masujima extracted cellular contents for single-cell MALDI-TOF/MS using nano-electrospray (NES) tips [169]. Aerts et al. used patch clamp pipettes to withdraw up to 2 pl of cytoplasm from rat neurons and observed significant cell-to-cell heterogeneity across 60 analyzed metabolites [170] (Fig. 18e, f). Zhang and Vertes sampled human hepatocarcinoma (HepG2) cells and quantified over 60 metabolites [171]. Mitochondria were also captured from live HepG2 cells using a nano-electrospray tip, and MS analysis revealed unique steroids specific to these organelles [172]. Given the extent of metabolic changes that occur in tumors and tumor stroma, analyzing metabolites on the single cell and population scales will provide valuable information for cancer detection and therapeutics.

17 Future Directions

Nanoneedle probes for intracellular sensing have a great potential to provide insight into cancer dynamics and to expand our ability to detect tumor cells in vivo. Single-cell sampling offers an unprecedented level of spatial resolution and characterization of cell-to-cell heterogeneity. Multiplexed fluorescent and electrochemical reporters mean that dynamic processes can be monitored in real time. As probes grow ever smaller, we are more able to interface with living tissues without cellular destruction. Rapid advances are being made in the use of nanowires and nanoelectrode arrays to probe brains and neuronal cells [173, 174], and these technologies may be adapted for tumor diagnostics or super localized therapeutics. Nano fiber-optics are being developed that can illuminate, irradiate, and manipulate cells with ever-finer spatial resolution [175]. Recently, an ultrasensitive nanomechanical AFM detector comprised of a thin tin dioxide wire coated with PEG and studded with gold nanoparticles was shown to be able to sense forces as low as 160 femtonewtons and acoustic signals down to −30 decibels [176]. In 2019, Jayant et al. reported the use of flexible

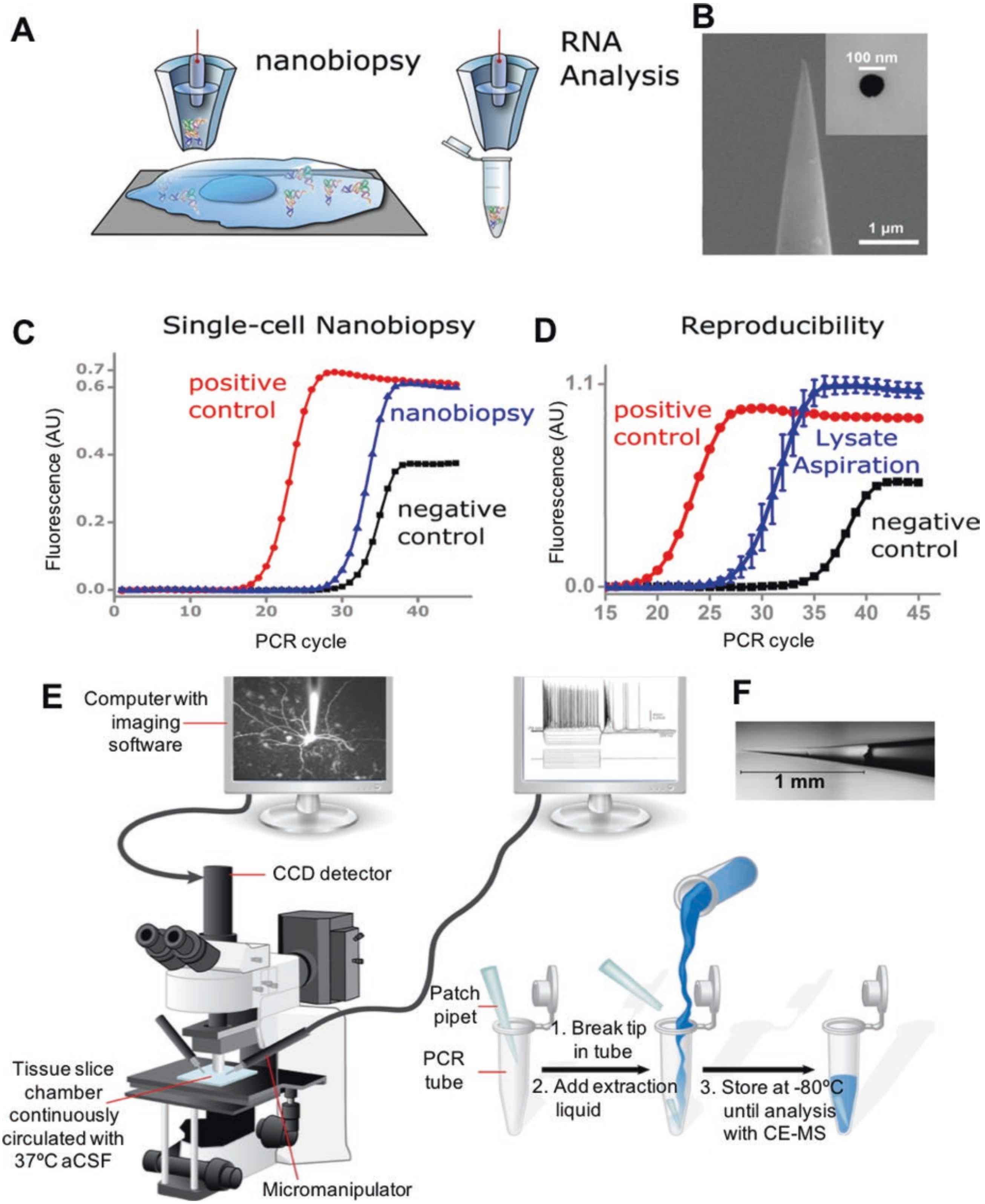
A
nanobiopsy
RNA Analysis
B
100 nm
1 µm
C
Single-cell Nanobiopsy
Fluorescence (AU)
0.7
0.6
0.4
0.2
0.0
0
10
20
30
40
PCR cycle
positive control
nanobiopsy
negative control
D
Reproducibility
Fluorescence (AU)
1.1
0.0
15
20
25
30
35
40
45
PCR cycle
positive control
Lysate Aspiration
negative control
E
Computer with imaging software
CCD detector
Tissue slice chamber continuously circulated with 37°C aCSF
Micromanipulator
Patch pipet
PCR tube
1. Break tip in tube
2. Add extraction liquid
3. Store at -80°C until analysis with CE-MS
F
1 mm

Fig. 18 Extraction of cellular contents for biochemical analysis. (**a**–**d**) Nanobiopsy for mRNA analysis. (**a**) Schematic of nanocapillary needle controlled by SICM to withdraw a small volume of cellular contents. (**b**) SEM of nanocapillary tip (100 nm diameter, inset). (**c**) Post-biopsy qPCR analysis of GFP mRNA from HeLa cells, showing positive control from total cell lysate (~100 cells) in red, negative control (no input) in black, and single-cell nanobiopsy in blue. (**d**) qPCR analysis of four nanobiopsies of the same cell lysate using four different nanoneedles showing good reproducibility. (Adapted with permission from [108]. Copyright 2014, American Chemical Society. **e**–**f**) Patch clamp pipet tip collection of cellular contents for mass spectroscopy. (**e**) Schematic of sample collection. Electrophysiology experiments are conducted on an upright microscope under video observation. Intracellular contents are removed by applying negative pressure. Only cells whose membranes did not rupture during extraction were collected for analysis. Once the patch pipette is removed, the tip is broken off (~1 mm) into a collection tube for MS analysis. (**f**) Photomicrograph of patch tip. (Adapted with permission from [170], https://pubs.acs.org/doi/10.1021/ac500168d. Copyright 2014, American Chemical Society. *Further permissions related to the material excerpted should be directed to the ACS*)

quartz nanopipettes with diameter of 10–25 nm for intracellular electrophysiological recording in the brains of live mice [177]. Another recent innovation was the fabrication of vertical Si nanoneedle arrays on a flexible, transparent elastomer patch which enables direct interfacing with various cell and tissue types as well as real-time imaging [178].

The challenge in the next decade is to bring together this diverse mixture of chemistry, physics, materials science, engineering, and biology to develop platforms that can be readily applied by cancer researchers with clear and targeted readouts. Engineers and cancer researchers will benefit from working together to select from the wide range of nanoneedle innovations those which will provide the most valuable insights into cancer physiology. This can be achieved by clear definitions of biomedical goals (e.g., to build a diagnostic platform that can readily distinguish cancer cells subtypes in vivo or to probe tumor cells to fine-tune personalized medicine) and will be aided by the increasing accessibility of off-the-shelf nanoscale probes for cell biologists and cancer researchers. Most excitingly, there is now substantial evidence that nanoneedle-based approaches can be upscaled using established microfabrication technologies, moving away from the limits of single-cell studies into a regime of network-based analytics and ensemble measurements that can capture the complexity of cancer heterogeneity.

Acknowledgements Thanks to Stuart Higgins (Imperial College, London) for expert advice and invaluable support.

References

1. Chiappini, C., et al. (2015). Biodegradable nanoneedles for localized delivery of nanoparticles in vivo: Exploring the biointerface. *ACS Nano, 9*(5), 5500–5509.
2. Anderson, S. E., & Bau, H. H. (2014). Electrical detection of cellular penetration during microinjection with carbon nanopipettes. *Nanotechnology, 25*(24), 245102.
3. VanDersarl, J. J., Xu, A. M., & Melosh, N. A. (2012). Nanostraws for direct fluidic intracellular access. *Nano Letters, 12*(8), 3881–3886.
4. Vilozny, B., et al. (2011). Reversible cation response with a protein-modified nanopipette. *Analytical Chemistry, 83*(16), 6121–6126.
5. Chiappini, C. (2017). Nanoneedle-based sensing in biological systems. *ACS Sensors, 2*(8), 1086–1102.
6. Bulbul, G., et al. (2018). Nanopipettes as monitoring probes for the single living cell: state of the art and future directions in molecular biology. *Cell, 7*(6), 55.
7. Neves, M., & Martin-Yerga, D. (2018). Advanced nanoscale approaches to single-(bio)entity sensing and imaging. *Biosensors (Basel), 8*(4), 100.
8. McGuire, A. F., Santoro, F., & Cui, B. (2018). Interfacing cells with vertical nanoscale devices: Applications and characterization. *Annual Review of Analytical Chemistry (Palo Alto, California), 11*(1), 101–126.
9. Higgins, S. G., et al. (2020). High-aspect-ratio nanostructured surfaces as biological metamaterials. *Advanced Materials, 32*, e1903862.
10. Chiappini, C., et al. (2015). Mapping local cytosolic enzymatic activity in human esophageal mucosa with porous silicon nanoneedles. *Advanced Materials, 27*(35), 5147–5152.
11. Chiappini, C., et al. (2015). Biodegradable silicon nanoneedles delivering nucleic acids intracellularly induce localized in vivo neovascularization. *Nature Materials, 14*(5), 532–539.
12. Hobbs, R. G., Petkov, N., & Holmes, J. D. (2012). Semiconductor nanowire fabrication by bottom-up and top-down paradigms. *Chemistry of Materials, 24*(11), 1975–1991.
13. Silberberg, Y. R., et al. (2013). Evaluation of the actin cytoskeleton state using an antibody-functionalized nanoneedle and an AFM. *Biosensors & Bioelectronics, 40*(1), 3–9.
14. He, G., et al. (2018). Fabrication of various structures of nanostraw arrays and their applications in gene delivery. *Advanced Materials Interfaces, 5*(10), 1701535.
15. Meister, A., et al. (2009). FluidFM: Combining atomic force microscopy and nanofluidics in a universal liquid delivery system for single cell applications and beyond. *Nano Letters, 9*(6), 2501–2507.
16. Guillaume-Gentil, O., et al. (2014). Force-controlled manipulation of single cells: From AFM to FluidFM. *Trends in Biotechnology, 32*(7), 381–388.
17. van Oorschot, R., et al. (2015). A microfluidic AFM cantilever based dispensing and aspiration platform. *EPJ Techniques and Instrumentation, 2*(1), 4.
18. Singhal, R., et al. (2011). Multifunctional carbon-nanotube cellular endoscopes. *Nature Nanotechnology, 6*(1), 57–64.
19. Shen, M., & Colombo, M. L. (2015). Electrochemical nanoprobes for the chemical detection of neurotransmitters. *Analytical Methods, 7*(17), 7095–7105.
20. Clausmeyer, J., & Schuhmann, W. (2016). Nanoelectrodes: Applications in electrocatalysis, single-cell analysis and high-resolution electrochemical imaging. *Trac-Trends in Analytical Chemistry, 79*, 46–59.
21. Cao, Y., et al. (2017). Nondestructive nanostraw intracellular sampling for longitudinal cell monitoring. *Proceedings of the National Academy of Sciences of the United States of America, 114*(10), E1866–E1874.
22. Hansma, P. K., et al. (1989). The scanning ion-conductance microscope. *Science, 243*(4891), 641–643.
23. Page, A., Perry, D., & Unwin, P. R. (2017). Multifunctional scanning ion conductance microscopy. *Proceedings of the Royal Society A: Mathematical, Physical and Engineering Sciences, 473*(2200), 20160889.
24. Sun, P., Laforge, F. O., & Mirkin, M. V. (2007). Scanning electrochemical microscopy in the 21st century. *Physical Chemistry Chemical Physics, 9*(7), 802–823.
25. Parton, R. G., & Simons, K. (2007). The multiple faces of caveolae. *Nature Reviews. Molecular Cell Biology, 8*(3), 185–194.
26. Wang, Z., et al. (2009). Size and dynamics of caveolae studied using nanoparticles in living endothelial cells. *ACS Nano, 3*(12), 4110–4116.
27. Zhao, W., et al. (2017). Nanoscale manipulation of membrane curvature for probing endocytosis in live cells. *Nature Nanotechnology, 12*(8), 750–756.
28. Gopal, S., et al. (2019). Porous silicon nanoneedles modulate endocytosis to deliver biological payloads. *Advanced Materials, 31*(12), e1806788.
29. Bancelin, S., et al. (2014). Determination of collagen fibril size via absolute measurements of second-harmonic generation signals. *Nature Communications, 5*, 1–8.
30. Maurer, T., et al. (2018). Structural characterization of four different naturally occurring porcine collagen membranes suitable for medical applications. *PLoS One, 13*(10), e0205027.
31. Buch-Manson, N., et al. (2015). Towards a better prediction of cell settling on nanostructure arrays-simple means to complicated ends. *Advanced Functional Materials, 25*(21), 3246–3255.

32. Buch-Manson, N., et al. (2017). Mapping cell behavior across a wide range of vertical silicon nanocolumn densities. *Nanoscale, 9*(17), 5517–5527.
33. Obataya, I., et al. (2005). Mechanical sensing of the penetration of various nanoneedles into a living cell using atomic force microscopy. *Biosensors & Bioelectronics, 20*(8), 1652–1655.
34. Xie, X., et al. (2013). Mechanical model of vertical nanowire cell penetration. *Nano Letters, 13*(12), 6002–6008.
35. Xu, A. M., et al. (2014). Quantification of nanowire penetration into living cells. *Nature Communications, 5*, 3613.
36. Aalipour, A., et al. (2014). Plasma membrane and actin cytoskeleton as synergistic barriers to nanowire cell penetration. *Langmuir, 30*(41), 12362–12367.
37. Xie, X., et al. (2015). Determining the time window for dynamic nanowire cell penetration processes. *ACS Nano, 9*(12), 11667–11677.
38. He, G., et al. (2018). Hollow nanoneedle-electroporation system to extract intracellular protein repetitively and nondestructively. *ACS Sensors, 3*(9), 1675–1682.
39. Dipalo, M., et al. (2018). Cells adhering to 3D vertical nanostructures: Cell membrane reshaping without stable internalization. *Nano Letters, 18*(9), 6100–6105.
40. Duan, X., et al. (2011). Intracellular recordings of action potentials by an extracellular nanoscale field-effect transistor. *Nature Nanotechnology, 7*(3), 174–179.
41. Angle, M. R., et al. (2014). Penetration of cell membranes and synthetic lipid bilayers by nanoprobes. *Biophysical Journal, 107*(9), 2091–2100.
42. Lee, J. H., et al. (2016). Spontaneous internalization of cell penetrating peptide-modified nanowires into primary neurons. *Nano Letters, 16*(2), 1509–1513.
43. Han, S. W., et al. (2005). Gene expression using an ultrathin needle enabling accurate displacement and low invasiveness. *Biochemical and Biophysical Research Communications, 332*(3), 633–639.
44. Kawamura, R., et al. (2016). High efficiency penetration of antibody-immobilized nanoneedle thorough plasma membrane for in situ detection of cytoskeletal proteins in living cells. *Journal of Nanobiotechnology, 14*(1), 74.
45. Simonis, M., et al. (2017). Survival rate of eukaryotic cells following electrophoretic nanoinjection. *Scientific Reports, 7*, 41277.
46. Zhou, J., et al. (2018). The effects of surface topography of nanostructure arrays on cell adhesion. *Physical Chemistry Chemical Physics, 20*(35), 22946–22951.
47. Swaminathan, V., et al. (2011). Mechanical stiffness grades metastatic potential in patient tumor cells and in cancer cell lines. *Cancer Research, 71*(15), 5075–5080.
48. Cross, S. E., et al. (2007). Nanomechanical analysis of cells from cancer patients. *Nature Nanotechnology, 2*(12), 780–783.
49. Handel, C., et al. (2015). Cell membrane softening in human breast and cervical cancer cells. *New Journal of Physics, 17*, 083008.
50. Anderson, S. E., & Bau, H. H. (2015). Carbon nanoelectrodes for single-cell probing. *Nanotechnology, 26*(18), 185101.
51. Novak, P., et al. (2009). Nanoscale live-cell imaging using hopping probe ion conductance microscopy. *Nature Methods, 6*(4), 279–281.
52. Yum, K., et al. (2009). Mechanochemical delivery and dynamic tracking of fluorescent quantum dots in the cytoplasm and nucleus of living cells. *Nano Letters, 9*(5), 2193–2198.
53. Shalek, A. K., et al. (2010). Vertical silicon nanowires as a universal platform for delivering biomolecules into living cells. *Proceedings of the National Academy of Sciences of the United States of America, 107*(5), 1870–1875.
54. Chen, X., et al. (2007). A cell nanoinjector based on carbon nanotubes. *Proceedings of the National Academy of Sciences of the United States of America, 104*(20), 8218–8222.
55. Adam Seger, R., et al. (2012). Voltage controlled nano-injection system for single-cell surgery. *Nanoscale, 4*(19), 5843–5846.
56. Peer, E., et al. (2012). Hollow nanoneedle array and its utilization for repeated administration of biomolecules to the same cells. *ACS Nano, 6*(6), 4940–4946.
57. Loh, O., et al. (2009). Nanofountain-probe-based high-resolution patterning and single-cell injection of functionalized nanodiamonds. *Small, 5*(14), 1667–1674.
58. Ying, Y. L., et al. (2017). Advanced electroanalytical chemistry at nanoelectrodes. *Chemical Science, 8*(5), 3338–3348.
59. Hennig, S., et al. (2015). Instant live-cell super-resolution imaging of cellular structures by nanoinjection of fluorescent probes. *Nano Letters, 15*(2), 1374–1381.
60. Yang, R., et al. (2018). Monoclonal cell line generation and CRISPR/Cas9 manipulation via single-cell electroporation. *Small, 14*(12), e1702495.
61. Kang, W., et al. (2013). Nanofountain probe electroporation (NFP-E) of single cells. *Nano Letters, 13*(6), 2448–2457.
62. Giraldo-Vela, J. P., et al. (2015). Single-cell detection of mRNA expression using nanofountain-probe electroporated molecular beacons. *Small, 11*(20), 2386–2391.
63. Tan, W., Wang, K., & Drake, T. J. (2004). Molecular beacons. *Current Opinion in Chemical Biology, 8*(5), 547–553.
64. Mereiter, S., et al. (2019). Glycosylation in the era of cancer-targeted therapy: Where are we heading? *Cancer Cell, 36*(1), 6–16.
65. Xie, X., et al. (2013). Nanostraw-electroporation system for highly efficient intracellular delivery and transfection. *ACS Nano, 7*(5), 4351–4358.
66. Caprettini, V., et al. (2017). Soft electroporation for delivering molecules into tightly adherent mammalian cells through 3D hollow nanoelectrodes. *Scientific Reports, 7*(1), 8524.
67. Xu, A. M., et al. (2017). Direct intracellular delivery of cell-impermeable probes of protein glycosylation by using nanostraws. *Chembiochem, 18*(7), 623–628.
68. Shen, X., et al. (2019). Biodegradable nanosyringes for intracellular amplification-based dual-diagnosis and gene therapy in single living cells. *Chemical Science, 10*(24), 6113–6119.
69. Hansel, C. S., et al. (2019). Nanoneedle-mediated stimulation of cell mechanotransduction machinery. *ACS Nano, 13*(3), 2913–2926.
70. Pandey, S., et al. (2013). Gold nanorods mediated controlled release of doxorubicin: Nano-needles for efficient drug delivery. *Journal of Materials Science. Materials in Medicine, 24*(7), 1671–1681.
71. Pan, W., et al. (2013). Multiplexed detection and imaging of intracellular mRNAs using a four-color nanoprobe. *Analytical Chemistry, 85*(21), 10581–10588.
72. Pan, W., et al. (2015). Simultaneous visualization of multiple mRNAs and matrix metalloproteinases in living cells using a fluorescence nanoprobe. *Chemistry, 21*(16), 6070–6073.
73. Hong, Y., et al. (2014). Molecular recognition of proteolytic activity in metastatic cancer cells using fluorogenic gold nanoprobes. *Biosensors & Bioelectronics, 57*, 171–178.
74. Lee, H., & Kim, Y. P. (2015). Fluorescent and bioluminescent nanoprobes for in vitro and in vivo detection of matrix metalloproteinase activity. *BMB Reports, 48*(6), 313–318.
75. Sun, L., et al. (2018). MMP-2-responsive fluorescent nanoprobes for enhanced selectivity of tumor cell uptake and imaging. *Biomaterials Science, 6*(10), 2619–2626.
76. Zhan, R., et al. (2020). An Au-Se nanoprobe for the evaluation of the invasive potential of breast cancer cells via imaging the sequential activation of uPA and MMP-2. *Analyst, 145*(3), 1008–1013.
77. Tavallaie, R., et al. (2018). Nucleic acid hybridization on an electrically reconfigurable network of gold-coated magnetic nanoparticles enables microRNA detection in blood. *Nature Nanotechnology, 13*(11), 1066–1071.
78. Li, C., et al. (2020). Intracellular sensors based on carbonaceous nanomaterials: A review. *Journal of the Electrochemical Society, 167*(3), 037540.

79. Navas-Moreno, M., et al. (2017). Nanoparticles for live cell microscopy: A surface-enhanced Raman scattering perspective. *Scientific Reports, 7*(1), 4471.
80. Bruzas, I., et al. (2018). Advances in surface-enhanced Raman spectroscopy (SERS) substrates for lipid and protein characterization: Sensing and beyond. *Analyst, 143*(17), 3990–4008.
81. Szekeres, G. P., & Kneipp, J. (2019). SERS probing of proteins in gold nanoparticle agglomerates. *Frontiers in Chemistry, 7*, 30.
82. Hanif, S., et al. (2017). Organic cyanide decorated SERS active nanopipettes for quantitative detection of hemeproteins and Fe(3+) in single cells. *Analytical Chemistry, 89*(4), 2522–2530.
83. Huang, J. A., et al. (2019). On-demand intracellular delivery of single particles in single cells by 3D hollow nanoelectrodes. *Nano Letters, 19*(2), 722–731.
84. Nguyen, T. D., et al. (2019). Nanostars on nanopipette tips: A Raman probe for quantifying oxygen levels in hypoxic single cells and tumours. *Angewandte Chemie (International Ed. in English), 58*(9), 2710–2714.
85. Yum, K., et al. (2011). Biofunctionalized nanoneedles for the direct and site-selective delivery of probes into living cells. *Biochimica et Biophysica Acta, 1810*(3), 330–338.
86. Kihara, T., et al. (2009). Development of a method to evaluate caspase-3 activity in a single cell using a nanoneedle and a fluorescent probe. *Biosensors & Bioelectronics, 25*(1), 22–27.
87. Na, Y. R., et al. (2013). Probing enzymatic activity inside living cells using a nanowire-cell "sandwich" assay. *Nano Letters, 13*(1), 153–158.
88. Kihara, T., et al. (2010). Development of a novel method to detect intrinsic mRNA in a living cell by using a molecular beacon-immobilized nanoneedle. *Biosensors & Bioelectronics, 26*(4), 1449–1454.
89. Matsumoto, D., et al. (2015). Oscillating high-aspect-ratio monolithic silicon nanoneedle array enables efficient delivery of functional bio-macromolecules into living cells. *Scientific Reports, 5*, 15325.
90. White, K. A., Grillo-Hill, B. K., & Barber, D. L. (2017). Cancer cell behaviors mediated by dysregulated pH dynamics at a glance. *Journal of Cell Science, 130*(4), 663–669.
91. Szpaderska, A. M., & Frankfater, A. (2001). An intracellular form of cathepsin B contributes to invasiveness in cancer. *Cancer Research, 61*(8), 3493–3500.
92. Swisher, L. Z., et al. (2015). Quantitative electrochemical detection of cathepsin B activity in breast cancer cell lysates using carbon nanofiber nanoelectrode arrays toward identification of cancer formation. *Nanomedicine, 11*(7), 1695–1704.
93. DeBerardinis, R. J., & Chandel, N. S. (2016). Fundamentals of cancer metabolism. *Science Advances, 2*(5), e1600200.
94. Lin, T. E., et al. (2018). Electrochemical imaging of cells and tissues. *Chemical Science, 9*(20), 4546–4554.
95. Fan, Y., Han, C., & Zhang, B. (2016). Recent advances in the development and application of nanoelectrodes. *Analyst, 141*(19), 5474–5487.
96. Pan, R., et al. (2016). Nanokit for single-cell electrochemical analyses. *Proceedings of the National Academy of Sciences of the United States of America, 113*(41), 11436–11440.
97. Pan, R., & Jiang, D. (2019). Nanokits for the electrochemical quantification of enzyme activity in single living cells. *Methods in Enzymology, 628*, 173–189.
98. Xu, H., et al. (2019). Phosphate assay kit in one cell for electrochemical detection of intracellular phosphate ions at single cells. *Frontiers in Chemistry, 7*, 360.
99. Qian, R. C., Lv, J., & Long, Y. T. (2018). Ultrafast mapping of subcellular domains via nanopipette-based electroosmotically modulated delivery into a single living cell. *Analytical Chemistry, 90*(22), 13744–13750.
100. Pernicova, I., & Korbonits, M. (2014). Metformin--mode of action and clinical implications for diabetes and cancer. *Nature Reviews. Endocrinology, 10*(3), 143–156.
101. Ozel, R. E., et al. (2015). Single-cell intracellular nano-pH probes. *RSC Advances, 5*(65), 52436–52443.
102. Lee, H. S., et al. (2012). Reversible swelling of chitosan and quaternary ammonium modified chitosan brush layers: Effect of pH and counter anion size and functionality. *Journal of Materials Chemistry, 22*(37), 19605–19616.
103. Cervera, J., et al. (2006). Ionic conduction, rectification, and selectivity in single conical nanopores. *The Journal of Chemical Physics, 124*(10), 104706.
104. Umehara, S., et al. (2009). Label-free biosensing with functionalized nanopipette probes. *Proceedings of the National Academy of Sciences of the United States of America, 106*(12), 4611–4616.
105. Nascimento, R. A., et al. (2016). Single cell "glucose nanosensor" verifies elevated glucose levels in individual cancer cells. *Nano Letters, 16*(2), 1194–1200.
106. Liberti, M. V., & Locasale, J. W. (2016). The Warburg effect: How does it benefit cancer cells? *Trends in Biochemical Sciences, 41*(3), 211–218.
107. Smith, S. K., et al. (2018). Carbon-fiber microbiosensor for monitoring rapid lactate fluctuations in brain tissue using fast-scan cyclic voltammetry. *Analytical Chemistry, 90*(21), 12994–12999.
108. Actis, P., et al. (2014). Electrochemical nanoprobes for single-cell analysis. *ACS Nano, 8*(1), 875–884.
109. Zhang, Y., et al. (2016). Spearhead nanometric field-effect transistor sensors for single-cell analysis. *ACS Nano, 10*(3), 3214–3221.
110. Ying, Y. L., et al. (2018). Asymmetric nanopore electrode-based amplification for electron transfer imaging in live cells. *Journal of the American Chemical Society, 140*(16), 5385–5392.
111. Huang, F., et al. (2018). Photoactivated specific mRNA detection in single living cells by coupling "signal-on" fluorescence and "signal-off" electrochemical signals. *Nano Letters, 18*(8), 5116–5123.
112. Dhar, S. K., et al. (2011). Manganese superoxide dismutase is a p53-regulated gene that switches cancers between early and advanced stages. *Cancer Research, 71*(21), 6684–6695.
113. Moloney, J. N., & Cotter, T. G. (2018). ROS signalling in the biology of cancer. *Seminars in Cell & Developmental Biology, 80*, 50–64.
114. Wang, K., et al. (2019). Targeting metabolic-redox circuits for cancer therapy. *Trends in Biochemical Sciences, 44*(5), 401–414.
115. Arbault, S., et al. (1995). Monitoring an oxidative stress mechanism at a single human fibroblast. *Analytical Chemistry, 67*(19), 3382–3390.
116. Sun, P., et al. (2008). Nanoelectrochemistry of mammalian cells. *Proceedings of the National Academy of Sciences of the United States of America, 105*(2), 443–448.
117. Ozel, R. E., et al. (2018). Functionalized quartz nanopipette for intracellular superoxide sensing: A tool for monitoring reactive oxygen species levels in single living cell. *ACS Sensors, 3*(7), 1316–1321.
118. Zhang, Y., et al. (2013). ROS play a critical role in the differentiation of alternatively activated macrophages and the occurrence of tumor-associated macrophages. *Cell Research, 23*(7), 898–914.
119. Wang, Y., et al. (2012). Nanoelectrodes for determination of reactive oxygen and nitrogen species inside murine macrophages. *Proceedings of the National Academy of Sciences of the United States of America, 109*(29), 11534–11539.
120. Marquitan, M., et al. (2016). Intracellular hydrogen peroxide detection with functionalised nanoelectrodes. *ChemElectroChem, 3*(12), 2125–2129.
121. Rawson, F. J., et al. (2015). Fast, ultrasensitive detection of reactive oxygen species using a carbon nanotube based-electrocatalytic intracellular sensor. *ACS Applied Materials & Interfaces, 7*(42), 23527–23537.
122. Ding, S., et al. (2020). Sensitive and selective measurement of hydroxyl radicals at subcellular level with tungsten nanoelectrodes. *Analytical Chemistry, 92*(3), 2543–2549.

123. Zhang, X. W., et al. (2017). Real-time intracellular measurements of ROS and RNS in living cells with single core-shell nanowire electrodes. *Angewandte Chemie (International Ed. in English), 56*(42), 12997–13000.
124. Hu, K., et al. (2019). Electrochemical measurements of reactive oxygen and nitrogen species inside single phagolysosomes of living macrophages. *Journal of the American Chemical Society, 141*(11), 4564–4568.
125. Li, X., et al. (2015). Quantitative measurement of transmitters in individual vesicles in the cytoplasm of single cells with nanotip electrodes. *Angewandte Chemie (International Ed. in English), 54*(41), 11978–11982.
126. Li, Y., et al. (2017). Direct electrochemical measurements of reactive oxygen and nitrogen species in nontransformed and metastatic human breast cells. *Journal of the American Chemical Society, 139*(37), 13055–13062.
127. Clapham, D. E. (2007). Calcium signaling. *Cell, 131*(6), 1047–1058.
128. Son, D., et al. (2011). Nanoneedle transistor-based sensors for the selective detection of intracellular calcium ions. *ACS Nano, 5*(5), 3888–3895.
129. Petronek, M. S., et al. (2019). Linking cancer metabolic dysfunction and genetic instability through the lens of iron metabolism. *Cancers (Basel), 11*(8), 1077.
130. Bulbul, G., et al. (2019). Employment of iron-binding protein from Haemophilus influenzae in functional nanopipettes for iron monitoring. *ACS Chemical Neuroscience, 10*(4), 1970–1977.
131. Kim, H. S., Kim, Y. J., & Seo, Y. R. (2015). An overview of carcinogenic heavy metal: Molecular toxicity mechanism and prevention. *Journal of Cancer Prevention, 20*(4), 232–240.
132. Leyssens, L., et al. (2017). Cobalt toxicity in humans-A review of the potential sources and systemic health effects. *Toxicology, 387*, 43–56.
133. Actis, P., et al. (2011). Voltage-controlled metal binding on polyelectrolyte-functionalized nanopores. *Langmuir, 27*(10), 6528–6533.
134. Actis, P., et al. (2012). Copper sensing with a prion protein modified nanopipette. *RSC Advances, 2*(31), 11638–11640.
135. Sa, N., Fu, Y., & Baker, L. A. (2010). Reversible cobalt ion binding to imidazole-modified nanopipettes. *Analytical Chemistry, 82*(24), 9963–9966.
136. Miao, R., et al. (2014). Silicon nanowire-based fluorescent nanosensor for complexed Cu2+ and its bioapplications. *Nano Letters, 14*(6), 3124–3129.
137. Abbott, J., et al. (2020). A nanoelectrode array for obtaining intracellular recordings from thousands of connected neurons. *Nature Biomedical Engineering, 4*(2), 232–241.
138. Abbott, J., et al. (2017). CMOS nanoelectrode array for all-electrical intracellular electrophysiological imaging. *Nature Nanotechnology, 12*(5), 460–466.
139. Robinson, J. T., et al. (2012). Vertical nanowire electrode arrays as a scalable platform for intracellular interfacing to neuronal circuits. *Nature Nanotechnology, 7*(3), 180–184.
140. Xie, C., et al. (2012). Intracellular recording of action potentials by nanopillar electroporation. *Nature Nanotechnology, 7*(3), 185–190.
141. Lin, Z. C., et al. (2017). Accurate nanoelectrode recording of human pluripotent stem cell-derived cardiomyocytes for assaying drugs and modeling disease. *Microsystems & Nanoengineering, 3*, 16080.
142. Staufer, O., et al. (2019). Adhesion stabilized en masse intracellular electrical recordings from multicellular assemblies. *Nano Letters, 19*(5), 3244–3255.
143. Caprettini, V., et al. (2018). Enhanced Raman investigation of cell membrane and intracellular compounds by 3D plasmonic nanoelectrode arrays. *Advanced Science (Weinheim), 5*(12), 1800560.
144. Deville, S. S., & Cordes, N. (2019). The extracellular, cellular, and nuclear stiffness, a trinity in the cancer resistome-a review. *Frontiers in Oncology, 9*, 1376.
145. Liu, C. Y., et al. (2015). Vimentin contributes to epithelial-mesenchymal transition cancer cell mechanics by mediating cytoskeletal organization and focal adhesion maturation. *Oncotarget, 6*(18), 15966–15983.
146. Silberberg, Y. R., et al. (2014). Detection of microtubules in vivo using antibody-immobilized nanoneedles. *Journal of Bioscience and Bioengineering, 117*(1), 107–112.
147. Yamagishi, A., et al. (2019). The structural function of nestin in cell body softening is correlated with cancer cell metastasis. *International Journal of Biological Sciences, 15*(7), 1546–1556.
148. Mieda, S., et al. (2012). Mechanical force-based probing of intracellular proteins from living cells using antibody-immobilized nanoneedles. *Biosensors & Bioelectronics, 31*(1), 323–329.
149. Wang, Z. X., et al. (2015). Interrogation of cellular innate immunity by diamond-nanoneedle-assisted intracellular molecular fishing. *Nano Letters, 15*(10), 7058–7063.
150. Choi, S., et al. (2016). Probing protein complexes inside living cells using a silicon nanowire-based pull-down assay. *Nanoscale, 8*(22), 11380–11384.
151. Cao, Y., et al. (2018). Universal intracellular biomolecule delivery with precise dosage control. *Science Advances, 4*(10), eaat8131.
152. Zhang, B., et al. (2019). Nanostraw membrane stamping for direct delivery of molecules into adhesive cells. *Scientific Reports, 9*(1), 6806.
153. Yang, Z., et al. (2014). Molecular extraction in single live cells by sneaking in and out magnetic nanomaterials. *Proceedings of the National Academy of Sciences of the United States of America, 111*(30), 10966–10971.
154. He, G., et al. (2019). Multifunctional branched nanostraw-electroporation platform for intracellular regulation and monitoring of circulating tumor cells. *Nano Letters, 19*(10), 7201–7209.
155. Wen, R., et al. (2019). Intracellular delivery and sensing system based on electroplated conductive nanostraw arrays. *ACS Applied Materials & Interfaces, 11*(47), 43936–43948.
156. Munz, M., Baeuerle, P. A., & Gires, O. (2009). The emerging role of EpCAM in cancer and stem cell signaling. *Cancer Research, 69*(14), 5627–5629.
157. Nawarathna, D., et al. (2011). Targeted messenger RNA profiling of transfected breast cancer gene in a living cell. *Analytical Biochemistry, 408*(2), 342–344.
158. Nawarathna, D., Turan, T., & Wickramasinghe, H. K. (2009). Selective probing of mRNA expression levels within a living cell. *Applied Physics Letters, 95*(8), 83117.
159. Actis, P., et al. (2014). Compartmental genomics in living cells revealed by single-cell nanobiopsy. *ACS Nano, 8*(1), 546–553.
160. Toth, E. N., et al. (2018). Single-cell nanobiopsy reveals compartmentalization of mRNAs within neuronal cells. *The Journal of Biological Chemistry, 293*(13), 4940–4951.
161. Nashimoto, Y., et al. (2016). Evaluation of mRNA localization using double barrel scanning ion conductance microscopy. *ACS Nano, 10*(7), 6915–6922.
162. Kashyap, A., et al. (2016). Selective local lysis and sampling of live cells for nucleic acid analysis using a microfluidic probe. *Scientific Reports, 6*, 29579.
163. Guillaume-Gentil, O., et al. (2016). Tunable single-cell extraction for molecular analyses. *Cell, 166*(2), 506–516.
164. Duncan, K. D., Fyrestam, J., & Lanekoff, I. (2019). Advances in mass spectrometry based single-cell metabolomics. *Analyst, 144*(3), 782–793.
165. Gong, X., et al. (2014). Single cell analysis with probe ESI-mass spectrometry: Detection of metabolites at cellular and subcellular levels. *Analytical Chemistry, 86*(8), 3809–3816.

166. Yin, R., Prabhakaran, V., & Laskin, J. (2018). Quantitative extraction and mass spectrometry analysis at a single-cell level. *Analytical Chemistry, 90*(13), 7937–7945.
167. Yin, R., Prabhakaran, V., & Laskin, J. (2019). Electroosmotic extraction coupled to mass spectrometry analysis of metabolites in live cells. *Methods in Enzymology, 628*, 293–307.
168. Guillaume-Gentil, O., et al. (2017). Single-cell mass spectrometry of metabolites extracted from live cells by fluidic force microscopy. *Analytical Chemistry, 89*(9), 5017–5023.
169. Masujima, T. (2009). Live single-cell mass spectrometry. *Analytical Sciences, 25*(8), 953–960.
170. Aerts, J. T., et al. (2014). Patch clamp electrophysiology and capillary electrophoresis-mass spectrometry metabolomics for single cell characterization. *Analytical Chemistry, 86*(6), 3203–3208.
171. Zhang, L., & Vertes, A. (2015). Energy charge, redox state, and metabolite turnover in single human hepatocytes revealed by capillary microsampling mass spectrometry. *Analytical Chemistry, 87*(20), 10397–10405.
172. Esaki, T., & Masujima, T. (2015). Fluorescence probing live single-cell mass spectrometry for direct analysis of organelle metabolism. *Analytical Sciences, 31*(12), 1211–1213.
173. Zhao, Y. L., et al. (2019). Scalable ultrasmall three-dimensional nanowire transistor probes for intracellular recording. *Nature Nanotechnology, 14*(8), 783–790.
174. Tullii, G., et al. (2019). High-aspect-ratio semiconducting polymer pillars for 3D cell cultures. *ACS Applied Materials & Interfaces, 11*(31), 28125–28137.
175. Li, Y. C., Liu, X. S., & Li, B. J. (2019). Single-cell biomagnifier for optical nanoscopes and nanotweezers. *Light-Science & Applications, 8*, 1–12.
176. Huang, Q., et al. (2017). Nanofibre optic force transducers with sub-piconewton resolution via near-field plasmon-dielectric interactions. *Nature Photonics, 11*(6), 352–355.
177. Jayant, K., et al. (2019). Flexible nanopipettes for minimally invasive intracellular electrophysiology in vivo. *Cell Reports, 26*(1), 266–278 e5.
178. Kim, H., et al. (2018). Flexible elastomer patch with vertical silicon nanoneedles for intracellular and intratissue nanoinjection of biomolecules. *Science Advances, 4*(11), eaau6972.
179. Kim, W., et al. (2007). Interfacing silicon nanowires with mammalian cells. *Journal of the American Chemical Society, 129*(23), 7228–7229.

Part III

Test, Repeat, and Test Again

In Vitro Assays for Nanoparticle—Cancer Cell Interaction Studies

Tomás Bauleth-Ramos and Bruno Sarmento

Abstract

Nanotechnology is a rapid-growing field with an extreme potential to revolutionize cancer treatments. However, despite the rapid advances, the clinical translation is still scarce. One of the main hurdles contributing for this setback is the lack of reliable in vitro models for preclinical testing capable of predicting the outcomes in an in vivo setting. In fact, the use of 2D monolayers, considered the gold-standard in vitro technique, leads to the creation of misleading data that might not be completely observed in in vivo or clinical setting. Thus, there is the need to use more complex models capable of better mimicking the tumor microenvironment. For that purpose, the development and use of multicellular tumor spheroids, three-dimensional (3D) cell cultures which recapitulate numerous aspects of the tumors, represents an advantageous approach to test the developed anticancer therapies. In this chapter, we identify and discuss the advantages of the use of these 3D cellular models compared to the 2D models and how they can be utilized to study nanoparticle-cancer cell interaction in a more reliable way to predict the treatment outcome in vivo.

Keywords

Nanoparticles · Spheroids · Cancer · Tumor microenvironment · 3D · In Vitro · Nanotechnology · Extracellular matrix · Distribution · Efficacy · Toxicity · High throughput screening

1 Introduction

Cancer, a complex and multifactorial disease, is one of the major threats to global health due to its high rates of incidence and mortality. In fact, this disease is one of the leading causes of death worldwide having, according to the report on global burden of cancer worldwide (GLOBOCAN 2018) by the World Health Organization (WHO), been responsible for 9.6 million deaths in 2018. Moreover, it is expected that this value will keep increasing over the years [1].

Commonly, anticancer therapy relies, on the initial stage, on chemotherapy treatment in order to reduce the tumor mass followed, if possible, by surgery to remove the rest of the tumor. Subsequently, chemotherapy and radiotherapy are applied to eliminate the remaining cancer cells [2]. Despite being the main strategy, this method still faces many hurdles as the existence of numerous and severe adverse effects, due to the nonspecificity of these approaches. Furthermore, chemotherapeutics also show lack of efficacy due to their physicochemical characteristics, leading to poor accumulation in the tumor site, short blood circulation, and the existence of tumor resistance mechanisms [3].

Nanoparticles (NPs), owing to their physicochemical properties, have emerged as powerful tools to improve cancer

---

T. Bauleth-Ramos
i3S – Instituto de Investigação e Inovação em Saúde, University of Porto, Porto, Portugal

INEB – Instituto de Engenharia Biomédica, University of Porto, Porto, Portugal

ICBAS, Instituto Ciências Biomédicas Abel Salazar, University of Porto, Porto, Portugal

Drug Research Program, Division of Pharmaceutical Chemistry and Technology, Faculty of Pharmacy, University of Helsinki, Helsinki, Finland

B. Sarmento (✉)
i3S – Instituto de Investigação e Inovação em Saúde, University of Porto, Porto, Portugal

INEB – Instituto de Engenharia Biomédica, University of Porto, Porto, Portugal

CESPU, Instituto de Investigação e Formação Avançada em Ciências e Tecnologias da Saúde & Instituto Universitário de Ciências da Saúde, Gandra, Portugal
e-mail: bruno.sarmento@ineb.up.pt

© Springer Nature Switzerland AG 2021
F. Fontana, H. A. Santos (eds.), *Bio-Nanomedicine for Cancer Therapy*, Advances in Experimental Medicine and Biology 1295, https://doi.org/10.1007/978-3-030-58174-9_10

treatments and counteract the aforementioned hurdles [4–6]. Nowadays, it is possible to produce NPs from a myriad of materials (polymers, lipids, inorganic materials, etc.) and precisely tune their production to achieve specific characteristics [4, 7]. Hence, NPs can be produced to load different types of molecules, control their pharmacokinetic and pharmacodynamic profiles, protect them from degradation, and increase their stability and accumulation in the targeted tissues [8]. Altogether, it permits to boost the therapeutic effect of the treatments while diminishing their off-target side effects.

However, while NPs have been showing promising results in preclinical testing, their clinical translation is still limited [4]. One of the major hurdles for NP clinical translation is the lack of preclinical models that can resemble the heterogeneity of the different tumors and their phenotypes [9–11]. In fact, NP interaction with cancer cells is usually tested in in vitro 2D cellular models which lack the complexity of biological tissues and thereby cannot fully replicate the existence of diverse physiological barriers and the interplay between the different components of the tumors (e.g., cells, extracellular matrix, soluble molecules). Thus, these assays can only provide limited results which ultimately do not correspond to what is observed on an in vivo and clinical setting. It is then imperative to develop new relevant in vitro cancer models capable of better recapitulating the tumor microenvironment (TME) [11].

The development of three-dimensional (3D) cellular models, which mimic several aspects of the TME, can bridge the gap between 2D models and in vivo and ease the development and screening of new nanomedicines for cancer treatment [9, 12]. By using these more accurate models, it is possible to obtain more reliable results and also use them to tune the NP properties based on the biology of the target population, leading to the development of effective therapies [9].

Hence, in this chapter we present an overview on 3D in vitro models to study the interaction between NPs and cancer cells in order to better predict the outcome of the treatments and facilitate the translation of the therapies.

2 2D Versus 3D Models

To date, two-dimensional (2D) cell culture monolayer models have been the gold-standard technique to preclinically develop and study anticancer therapies, due to their easiness, simplicity, reproducibility, quickness, and low cost [13–15]. These models are mostly produced from immortal tumor cell lines, as they are an unlimited self-replicating source capable of growing in large quantities [16]. Additionally, these cell lines are relatively molecular homogeneous, and their genetic profile is known and described [16]. To increase the predictive value of the gathered data, it is possible to use primary cells isolated from living tissue [17, 18]. Although these cells maintain the genomic and phenotypic profiles of the descendant tissue, they are hard to culture and have limited self-replication, which hamper their use [18]. Moreover, 2D models cannot mimic crucial aspects from the tumors, such as the heterogenicity of the TME, composed by various types of cells and noncellular structures as the extracellular matrix (ECM), failing to emulate the in vivo conditions and provide physiological relevance. The existent 3D spatial conformation of tumors results in a heterogeneous and diffusion-limited exposure to various nutrients, signaling molecules, oxygen, and metabolites, among other physical and chemical cues, which cannot be mirrored in 2D cultures [19–22]. Moreover, this 3D spatial organization is also known to influence cell-cell interactions, impacting their morphology, adhesion, viability, proliferation, and biological response to soluble factors and physical stimuli [23–25]. For example, these morphological and biological changes are responsible for a slower proliferation rate of cells in 3D compared to 2D models [26, 27], impacting their response to different compounds, including anticancer molecules [27]. As such, 2D models, by failing to simulate the reciprocal interactions between different cells and the TME, influence the obtained outcomes to the tested therapies, leading in the end to poor prediction of their real in vivo effect.

To avoid the production of misleading preclinical data and improve the translation of new anticancer therapies, there is the need to bridge the gap between 2D models, in vivo whole-animal tumor models, and clinical trials. To that end, 3D cellular models have been extensively studied as they permit the simulation of numerous physiological aspects of the tumors, being more relevant and better predictive models than the 2D ones [12, 20, 28, 29]. In the past decades, various 3D models have been developed, including microfluidic models, scaffold-based models, tumor tissue explant models, and multicellular tumor spheroids (MCTS) [30].

2.1 Multicellular Tumor Spheroid Production Techniques

MCTS are formed without resorting to any exogenous artificial platforms to promote cell growth [31]. To produce MCTS, several techniques can be applied, being the most commonly used agitation-based, hanging drop, and liquid overlay techniques (Fig. 1). All these techniques have as base the use of nonadherent surfaces to promote cell-cell interactions and consequent aggregation [31]. In agitation-based techniques, single-cell suspensions are kept agitating, for example, in spinner flasks, in order to reduce the effect of gravity and promote spontaneous aggregation [32, 33]. While this method is appropriate for long-term culture and

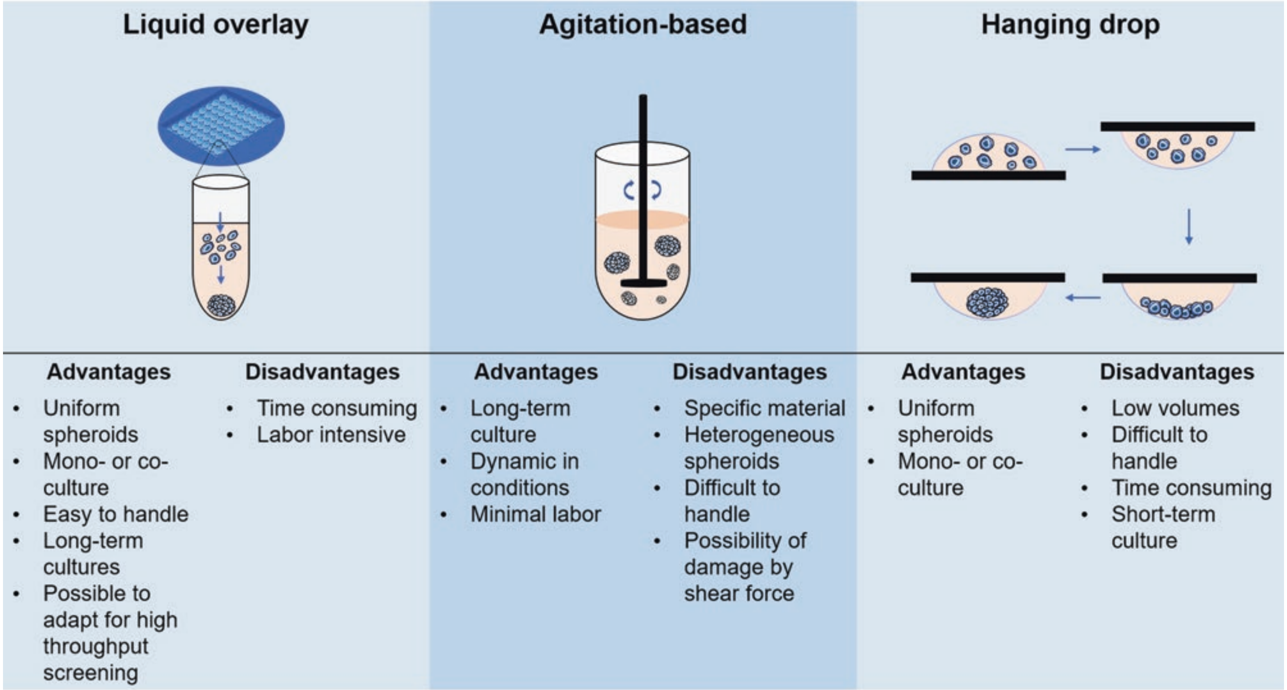

Liquid overlay		Agitation-based		Hanging drop	
Advantages	Disadvantages	Advantages	Disadvantages	Advantages	Disadvantages
• Uniform spheroids • Mono- or co-culture • Easy to handle • Long-term cultures • Possible to adapt for high throughput screening	• Time consuming • Labor intensive	• Long-term culture • Dynamic in conditions • Minimal labor	• Specific material • Heterogeneous spheroids • Difficult to handle • Possibility of damage by shear force	• Uniform spheroids • Mono- or co-culture	• Low volumes • Difficult to handle • Time consuming • Short-term culture

Fig. 1 Multicellular tumor spheroid production techniques, their advantages, and limitations. (Imaged partly generated using Servier Medical Art)

can mimic the dynamic conditions found in the body, it carries several disadvantages as the need of specific material, formation of heterogeneous spheroids, and difficulty to handle [34]. Moreover, the shear fluid force may induce damage and/or changes in the used cells [35]. In the hanging drop method, cell cultures are suspended and due to the gravitational forces cells tend to sediment and spontaneously aggregate in the liquid-air interface [36]. Using this method it is possible to produce uniform spheroids of mono- and co-cultures [37]. However, since spheroids are suspended in a low volume of media, it is time-consuming and difficult to handle and cannot be maintained for long periods [37]. At last, liquid overlay technique represents a more convenient and easier procedure, capable of producing uniform spheroids and which is possible to adapt for high-throughput screening (HTS) [33]. In this technique, cell suspensions are placed in nonadherent surfaces, as agarose or poly(2-hydroxyethyl methacrylate) (poly-HEMA), enhancing cell-cell interactions in spite of the cell-surface interactions [38]. Currently, it is possible to use commercial molds in which these materials (e.g., agarose) are casted, allowing the simultaneous production of numerous spheroids in a homogeneous manner [39, 40].

2.2 MCTS Advantages

MCTS are one of the most commonly used 3D tumor models, consisting of spherical cellular self-aggregates that produce their own ECM, being capable of recapitulating several aspects of the TME, and are recognized as nonvascularized tumor models [41]. This type of model possesses a similar growth kinetics to real tumors, starting with an exponential cell expansion, followed by a delayed growth due to a decrease in proliferative cells, and increase in quiescent and necrotic cells [42]. As the MCTS grow, a gradient of oxygen, nutrients, and metabolic waste is formed, leading to an hypoxic core with necrotic cells and an outer rim formed by proliferative cells in the outer layer and quiescent cells in the inner layer. This hollow structure is estimated to be formed in spheroids with diameter over 400–500 μm, with the outer rim having usually 100–220 μm of thickness [42–45]. Furthermore, combined with the formed 3D spatial organization and its cell-cell and cell-ECM interactions, this leads to cellular heterogeneity, affecting protein expression and leading to different genetic profiles, which were found to resemble the physiological conditions existent in human tumors [46]. These protein expression and genetic changes highly impact the function of different anticancer therapies, inducing several mechanisms of drug resistance [47]. Another aspect of human tumors that is recapitulated in MCTS is the existence of an acidic microenvironment. Due to the generation of a hypoxic core, tumor cells, in response to the lack of oxygen, increase the production of lactate, which promotes an acidification of the microenvironment (pH 6.5–7.2) [28, 48]. This acidic TME directly impacts anticancer molecules protonation, influencing their uptake and efficacy [49].

Additionally, MCTS can be optimized to mimic the cellular heterogeneity of human tumors by co-culturing tumor cells with different stromal cells as fibroblasts, as well as immune and endothelial cells [50, 51]. It is known that the intricate relationship of tumor and stromal cells promotes several pro-tumor events as angiogenesis, invasion, metastasis, and resistance to anticancer drugs [51, 52]. Stromal cells will influence tumor cell activity by secreting soluble factors (e.g., cytokines and growth factors) [53], producing ECM proteins, which interact with different signaling pathways [54] and that create a physical barrier that limits the penetration of different molecules [55, 56]. Altogether, these factors contribute to a higher resistance of the tumor cells to the anticancer treatments when compared with 2D models, resembling in a better fashion what happens in an in vivo situation (Fig. 2).

Also, the ability to produce uniform spheroids with mono- and co-cultures; to tailor their size and controlling their properties, for example, by adjusting the initial cell density and duration of culture; and to use them for HTS purposes makes them valuable tools to study tumor biology and treatment. For instance, spheroids can be used to study the signaling cross talk in the TME, tumor cell growth kinetics, migration and invasion, and the response to several anticancer therapies, including radiotherapy, chemotherapy, immunotherapy, and the use of biomaterials such as nanoparticles [15, 57, 58].

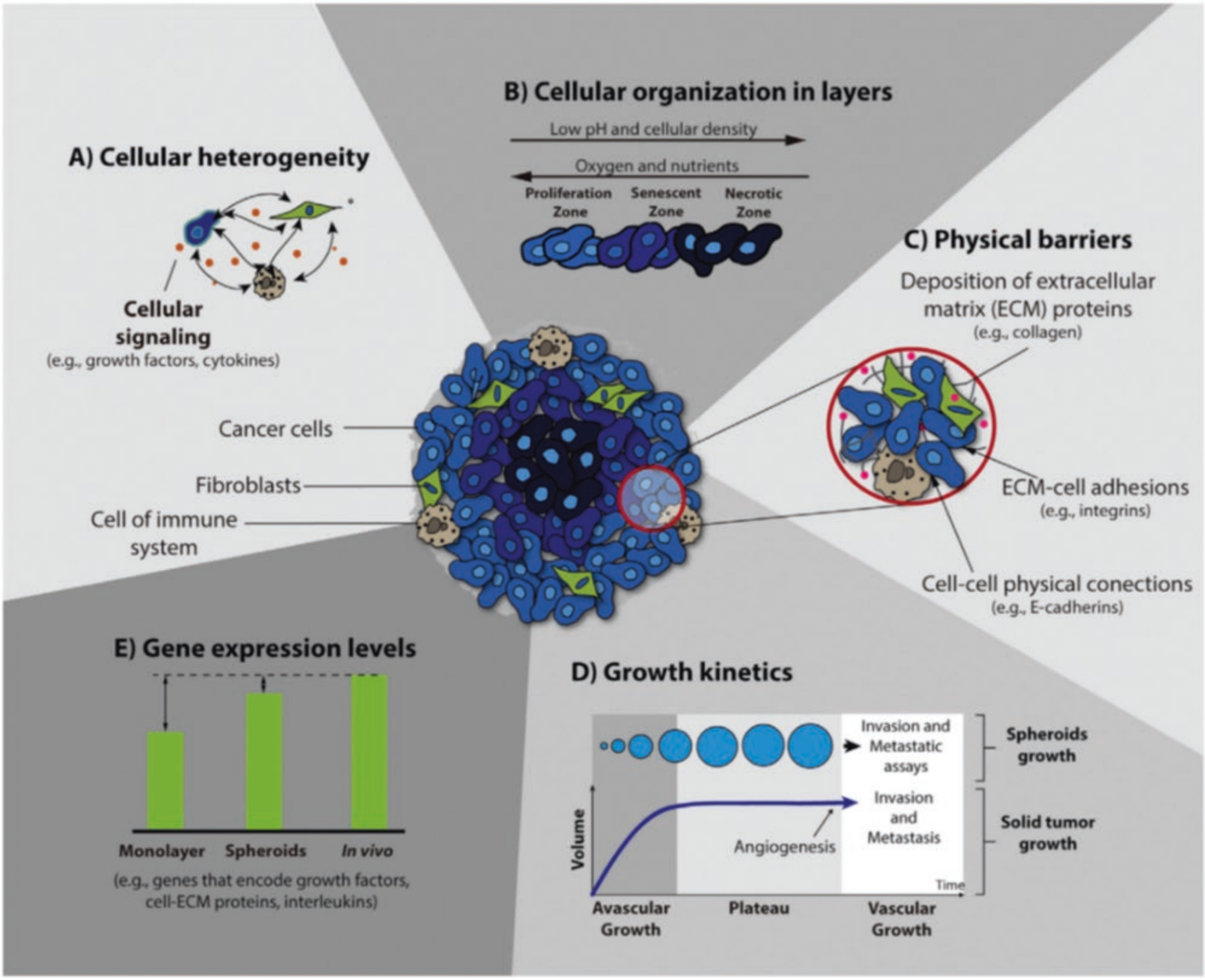
A) Cellular heterogeneity
Cellular signaling
(e.g., growth factors, cytokines)
B) Cellular organization in layers
Low pH and cellular density
Oxygen and nutrients
Proliferation Zone
Senescent Zone
Necrotic Zone
C) Physical barriers
Deposition of extracellular matrix (ECM) proteins
(e.g., collagen)
Cancer cells
Fibroblasts
Cell of immune system
ECM-cell adhesions
(e.g., integrins)
Cell-cell physical conections
(e.g., E-cadherins)
E) Gene expression levels
Monolayer
Spheroids
In vivo
(e.g., genes that encode growth factors, cell-ECM proteins, interleukins)
D) Growth kinetics
Invasion and Metastatic assays
Spheroids growth
Volume
Angiogenesis
Invasion and Metastasis
Solid tumor growth
Time
Avascular Growth
Plateau
Vascular Growth

Fig. 2 Main aspects of 3D spheroids that recapitulate tumor characteristics and are essential for anticancer therapy screening. (**a**) Heterogenicity of tumors (cancer and stromal cells). (**b**) Gradient of nutrients, oxygen, and pH, formation of necrotic core, and senescent and proliferative layers. (**c**) Formation of physical barrier by extracellular matrix deposition and cell-cell interaction. (**d**) Correlation between the growth kinetics of spheroids and solid tumors: initial exponential growth (avascular growth phase) and plateau state. (**e**) Closer gene expression patterns to in vivo solid tumors. (Reprinted with permission from Ref. [55])

2.3 Disadvantages/Limitations

Despite the current advances, the employment of 3D models for preclinical testing still faces several adversities. The major existent shortcomings are the lack of standardization in terms of protocols for spheroid production and evaluation/testing (e.g., characterization, imaging, drug and other therapies screening purposes), high costs, highly laborious, cell-type limitation to form spheroids, and difficulty to produce homogeneous spheroids for HTS purposes [59, 60]. However, the use of 3D models for preclinical testing is growing exponentially [61], and in the next years, with the advances on 3D model formation and standardization of the characterization and testing assays, they will likely substitute 2D cell culture models for in vitro preclinical research [62].

3 Multicellular Tumor Spheroids for Assessing Nanomaterials

One important application of MCTS is to test the cellular association, biocompatibility, and efficacy of nanomaterials, as it can provide valuable data on their interaction and effect in the tumors, as well as in the specifically in the different components of the TME, predicting their impact in vivo. Therefore, it allows to improve the nanoformulations before proceeding to animal studies, reducing the number of used animals and expediting the development of successful therapies. Thus, it is of utmost importance to start testing the developed nanomaterials in more relevant models than the standard 2D cultures, since 2D models can create misleading data.

3.1 Cellular Association/Tumor Penetration

When assessing NP cellular association, the absence of ECM which creates a physical barrier and diffusion gradient through tissue highly impacts the results in 2D when compared to 3D [63, 64]. For instance, even if high cellular uptake is observed both in the 2D and 3D cell models, in the 3D cell model, the NPs might be predominately taken up by cells in the periphery without being able to deeply penetrate in the tumor [42]. This will consequently have an effect on the antiproliferative ability of the developed nanosystems, which might show a higher effect on the 2D cell models (i.e., a lower IC_{50} value) [65, 66]. Furthermore, several studies have shown a correlation between high NPs and drug accumulation and penetration, with an enhanced cytotoxic effect [67, 68]. Thus, the use of MCTS is extremely useful to study the penetration ability of the NPs into the tumors and assess their anticancer efficacy [33].

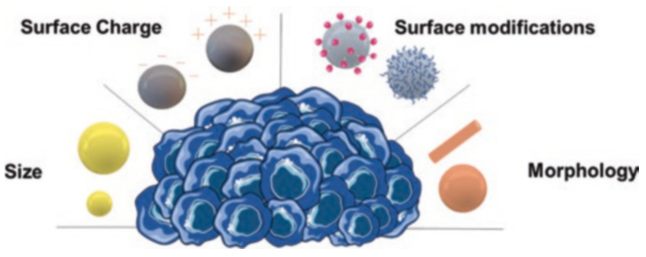

Fig. 3 Illustration of the physicochemical characteristics that affect NP interaction with the tumors. (Imaged partly generated using Servier Medical Art)

It is known that the physicochemical characteristics (e.g., size, charge, morphology, and surface functionalization) of the NPs will highly impact their interaction and penetration into tumors (Fig. 3). Therefore, this subsection will discuss the impact of the NP physicochemical properties on interaction cells in 3D in vitro models and compare to 2D in vitro cellular models and in vivo assays (Table 1).

3.1.1 Size

The size of the NPs is one of the most crucial parameters affecting their interaction with cancer cells. Thus, several studies have been performed to try to analyze its impact in the penetration and uptake of NPs in tumors. For example, in one study, Tchoryk et al. [69] have cultured HCT116 colorectal cancer spheroids and incubated them with polystyrene NPs with different sizes (30, 50, and 100 nm) (Fig. 4). After 24 h incubation, the smaller NPs (30 and 50 nm) were taken up by over 90% of the cells, while the larger particles (100 nm) were only taken up by 22%. Furthermore, while the smaller NPs were able to reach the core of the spheroid, the larger NPs were mainly located in the periphery. This study demonstrated a size-dependent uptake and penetration of NPs into tumors. Another study [70], also using polystyrene NPs but with bigger sizes (20, 100, and 500 nm), has compared in vitro cellular uptake and penetration in 2D monolayers of pancreatic cancer cells (BxPC-3 and PANC-1) and in spheroids prepared with the same cell lines. Interestingly, in this study it was found that there was a size-dependent uptake in BxPC-3 monolayers (20 > 100 > 500 nm), while in PANC-1 monolayers, 100 nm NPs were the ones with higher uptake. This was attributed to the fact that BxPC-3 cells exclusively used clathrin-dependent mechanisms for the uptake of all the NPs and in PANC-1 cells, there were multiple endocytic routes involved in the uptake of 100 nm NPs and only one mechanism for NPs with the other sizes. Further, when incubated with the spheroids, it was observed a size-dependent uptake, showing linear correlation with the BxPC-3 cellular uptake in 2D and no correlation with the data obtained with the PANC-1. This has shown that the mechanisms of uptake, transport, and penetration may vary between the 2D and 3D in vitro models

Table 1 Overview of the main physicochemical characteristics influencing the interaction of NPs with tumor cells. 2D, 3D, and in vivo assays

Size (nm)	Type of NPs	2D model		3D model			In vivo			References
		Cells	Outcome	Cells and cell density at day 0	Technique of production	Outcome	Animal model/cell lines	Route of injection	Outcome	
2 6 15	Gold NPs (spherical, negatively charged)	MCF-7	No observed toxicity Size-dependent uptake: $2 \gg 6 = 15$ NP location: 2 and 6 nm – cytoplasm and nucleus 15 nm – cytoplasm	MCF-7 600 cells/well	Liquid overlay technique	Size-dependent uptake: $2 > 6 > 15$ Time dependency was only observed for NPs with size 2 and 6 nm These NPs were also able to penetrate deeper into the spheroid and localize both in the outer and inner layers 15 nm NPs showed lower penetration and were localized mostly on the outer layers	Balb/c nude mice with MCF-7 cells	IV 5 mg Au/Kg	Rapid elimination from blood in time and size-dependent manner: $15 > 6 > 2$ Size-dependent tumor accumulation: $2 > 6 > 15$	[72]
50 100			No observed toxicity Size-dependent uptake: $50 > 100$ (5-fold higher uptake) Localized on the cytoplasm			Mostly located on the periphery Size-dependent penetration $50 > 100$ (fourfold higher) Time-dependent penetration only for 50 nm NPs			Rapid elimination from blood in time- and size-dependent manner: $100 > 50$ Size-dependent tumor accumulation: $50 > 100$	[71]
30	Polystyrene NPs (negatively charged)	–	–	HCT116 2000 cells/well	Liquid overlay technique	30 nm: 70% uptake after 2 h and >90% after 6 h incubation Have shown the highest penetration ability	–	–	–	[69]
50						50 nm: 80% uptake after 2 h and >90% after 6 h incubation				

100						100 nm: < 10% uptake after 2 h and 22% after 24 h incubation Most of NPs in the periphery, low penetration				
20	Polystyrene NPs (spherical, negatively charged)	BxPC-3 and PANC-1 and NIH3T3	10-fold and 50-fold higher cellular uptake in BxPC-3 than 100 and 500 nm NPs, respectively owest uptake by PANC-1 Only one mechanism of uptake is utilized by PANC-1 cells for internalization	BxPC-3 500 cells/well and PANC-1 120 cells/well and PANC-1/ NIH3T3 (120:12)	Liquid overlay technique	BxPC3 spheroid: 20 nm NPs penetrate more effectively than bigger NPs There was no penetration and almost absent cellular uptake by cells in the periphery of 500 nm NPs Linear correlation with cellular uptake in 2D	–	–	–	[70]
100			Higher cellular uptake in PANC-1 cells than the other NPs Several mechanisms of uptake are utilized by PANC-1 cells for internalization	cells/well		PANC-1 spheroids: 20 nm NPs had higher penetration and reached the core. 100 nm NPs could also penetrate but reached the core in less extent				

(continued)

Table 1 (continued)

Size (nm)	Type of NPs	2D model		3D model			In vivo			References
		Cells	**Outcome**	**Cells and cell density at day 0**	**Technique of production**	**Outcome**	**Animal model/cell lines**	**Route of injection**	**Outcome**	
500			Internalization in BxPC-3 cells was almost absent Only one mechanism of uptake is utilized by PANC-1 cells for internalization			500 nm NPs could only penetrate the surface layers No correlation with 2D data PANC-1/ NIH3T3 spheroids: Less permeable model. NPs could not reach the core. 500 nm NPs only accumulated in the periphery 100 nm NPs accumulated more efficiently than 20 nm NPs due to transcytosis mediated by the fibroblasts				
30	Silica NPs (negatively charged)	–	–	4T1 and 3T3 and 3T3/4T1 (1:1 and 5:1) 18,500 cells/ well	Liquid overlay technique	30 nm NPs had higher penetration in all the spheroids In spheroids without fibroblasts, both NPs were able to penetrate (70–80% positive area) Increased in number of fibroblasts inhibited NP penetration	–	–	–	[106]
100		–	–							
Surface charge (mV)	**Type of NPs**	**2D model**		**3D model**			**In vivo**			**References**
		Cells and cell density at day 0	**Outcome**	**Cells and cell density at day 0**	**Technique of production**	**Outcome**	**Animal model/cell lines**	**Route of injection**	**Outcome**	
53 ± 7	DOTAP liposomes	–	–	Lewis lung carcinoma (LLC) cells. 1000 cells/well	Liquid overlay technique	High-cell bind and higher accumulation in the spheroid. Consequent enhanced cytotoxic effect when loaded with paclitaxel	–	–	–	[67]

−56 ± 3	DOPS liposome			cells/well		Low cell binding but higher penetration into the spheroids than the DOTAP liposomes (cationic NPs)				
24 ± 2	Polystyrene NPs (50 nm)-NH_2	–	–	HCT116 colon cancer cells. 2000 cells/well	Liquid overlay technique	Poor penetration Mostly located in the periphery of the spheroid	–	–	–	[69]
−32 ± 3	Polystyrene NPs (50 nm)-COOH			2000 cells/well		Poor penetration and no accumulation on the periphery				
−32	Plain polystyrene NPs (50 nm)					Fast and high penetration homogeneous distribution within the spheroid				
−20 −40	Silica NPs	–	–	4T1 and 3T3 and 3T3/4T1 (1:1 and 5:1) 18,500 cells/well	Liquid overlay technique	Less negative NPs penetrated less deeply Penetration was inversely correlated to the number of fibroblasts	–	–	–	[106]
21.5–23.5 −22.2 −9 −8	Modified PEG-b-PLA NPs	–	–	MDA-MB-231	Liquid overlay technique	Rapid accumulation of positive NPs in the periphery Negatively charged NPs showed low penetration	Balb/c nude mice with MDA-MB-231 cells	IV	Positive NPs were able to extravasate and accumulate in the tumors, contrary to the other NPs	[107]

Shape	**Type of NPs**	**2D model**		**3D model**			**In vivo**			**References**
		Cells and cell density at day 0	**Outcome**	**Cells and cell density at day 0**	**Technique of production**	**Outcome**	**Animal model/cell lines**	**Route of injection**	**Outcome**	
Spherical Rods	Gold-silica core-shell NPs (negatively charged)	HeLa	Rods were taken up at a higher extension than spheres, leading to higher drug accumulation	HeLa 12,345 cells/well	Liquid overlay technique	Spheres had a more uniform distribution in the spheroids, penetrating deeply into the cell layers (able to penetrate) contrary to the rod NPs	–	–	–	[81]

(continued)

Table 1 (continued)

Size (nm)	Type of NPs	2D model		3D model			In vivo			References
		Cells	Outcome	Cells and cell density at day 0	Technique of production	Outcome	Animal model/cell lines	Route of injection	Outcome	
Spherical (AR = 1) Elongated (AR = 2.8) Elongated (AR = 7.5)	Polystyrene NPs (positively charged)	HeLa	Spherical NPs were taken up at a higher extent Cellular uptake was dependent on the AR. Higher AR, lower uptake	HeLa 800 cells/well	Liquid overlay technique	Elongated NPs with lower AR were able to penetrate and accumulate at a higher extent than the other NPs	–	–	–	[86]
Surface modifications	**Type of NPs**	**2D model**		**3D model**			**In vivo**			**References**
		Cells and cell density at day 0	**Outcome**	**Cells and cell density at day 0**	**Technique of production**	**Outcome**	**Animal model/cell lines**	**Route of injection**	**Outcome**	
iRGD DSS	Lignin NPs	PC3-MM2 MDA-MB-231 A549	Both iRGD and DSS ligands increased uptake PC3-MM2: DSS > iRGD > plain MDA-MB-231: DSS > iRGD = plain A549:	PC3-MM2 5000 cells/well MDA-MB-231 7000 cells/well A549 7000 cells/well	3D bioprinting (magnets)	Both iRGD and DSS ligands increased uptake PC3-MM2: DSS > iRGD > plain MDA-MB-231: DSS = iRGD > plain A549: DSS > iRGD = plain	–	–	–	[88]
			DSS > plain > iRGD			When loaded with a chemotherapeutic, the IC_{50} values were higher than in 2D culture. Moreover, only in the PC3-MM2 cells, the IC_{50} values for modified NPs were lower than for plain NPs				
Anti-FGFR3	Silica NPs			RT4 150,000 cells/well	Liquid overlay technique	Fourfold enhanced internalization of NPs modified with the anti-FGFR3 antibody compared to unmodified NPs NPs modified with antibody partially inhibited cell proliferation and spheroid growth	–	–	–	[90]

tLyP-1	Micelles	4T1	Fourfold enhanced cellular uptake after NP modification	4T1 10,000 cells/ well	Liquid overlay technique	The peptide enhanced the uptake by the spheroids but led to lower penetration than unmodified NPs	4T1	IT IV	IT: NPs modified with the peptide showed stronger penetration ability	[89]
									IV: Peptide-modified NPs had target effect and higher accumulation overtime. Further, these NPs were able to deeply penetrate into the tumors	
Anti-TfR	Lipid magnetic nanovectors	–	–	U-87 MG 25,000 cells/ drop	Hanging drop	NPs modified with antibody had a remarkable enhanced uptake after 48 h compared to unmodified NPs (40% compared to 8%)	–	–	–	[93]
						Enhanced uptake led to enhanced antiproliferative effect after stimulation:				
						Antibody-modified NPs: 49.6% healthy cells, 38.8% necrotic cells, 4.9% apoptotic cells, and 6.7% of late apoptotic cells				
						Unmodified NPs: >96% of healthy cells				

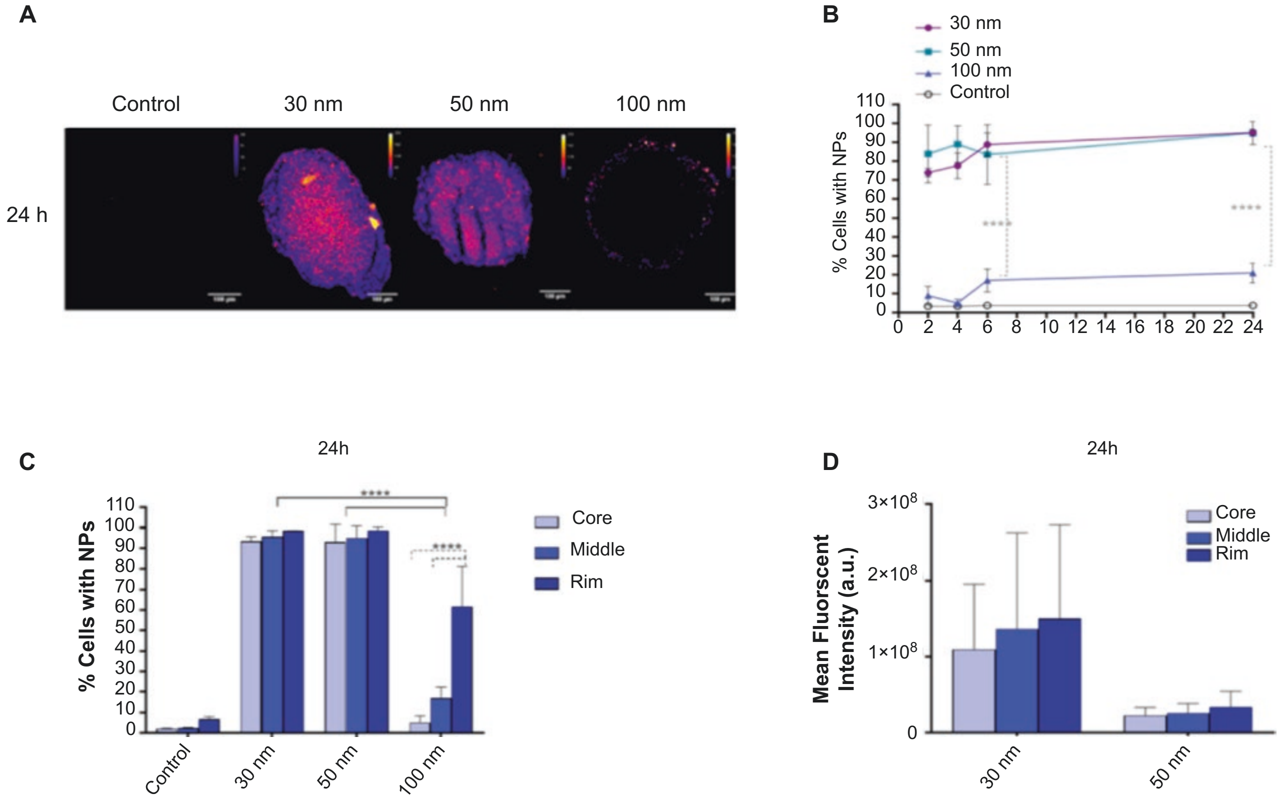

Fig. 4 Size-dependent penetration of polystyrene NPs with sizes of 30, 50, 100 nm after 24 h incubation with HCT116 spheroids. (**a**) Confocal microscopy images of HCT116 spheroid cross-sections after incubation with the NPs. (**b**) Overtime NP penetration into spheroids measured by flow cytometry. (**c**, **d**) Distribution of the NPs in the spheroids. (Adapted with permission from Ref. [69])

and between different 3D models. Like the previously mentioned study, only the smaller NPs could penetrate into the tumors, while the others were mainly retained in the periphery of the spheroid. Moreover, the addition of fibroblasts to the spheroid model significantly enhanced ECM deposition, leading to a poorer penetration of the NPs into the spheroid and blocking their access to the core. However, due to transcytosis mediated by fibroblasts, 100 nm NPs accumulated more efficiently than the other NPs.

Other studies using gold NPs with size ranging from 2 to 100 nm (2, 6, 15, 50, and 100 nm) [71, 72] have also shown a size-dependent uptake and penetration of the NPs in 2D monolayers and spheroids, with the smaller NPs being taken up and penetrating in a higher extent. NPs with size >15 nm were found mainly in the periphery of the spheroids, showing similar pattern to what was observed in the aforementioned studies. Moreover, in these studies, there was correlation between the in vitro results and the in vivo, where it was also observed a size-dependent tumor accumulation after intravenous injection of the NPs.

Taking this into account, it is possible to observe that smaller NPs (<100 nm) have a higher penetration in spheroids [67, 71–73], while larger NPs, despite having limited penetration, may accumulate in spheroids' periphery. Moreover, several studies have found that 50 nm is the optimal size for a better balance between NP penetration and accumulation [71, 74].

3.1.2 Surface Charge

Surface charge is another critical parameter with high influence in NP penetration and accumulation in tumors, and that can be studied using 3D in vitro cellular models [68, 75]. For example, Solomon et al. [67] incubated lung cancer spheroids with positively (53 ± 7 mV) and negatively (−56 ± 3 mV) charged liposomes for 1 h and analyzed their uptake and ability to penetrate in the tumor spheroids. Positively charged NPs were taken up at a higher extent than negatively charged NPs, possibly due to interaction of the NPs with the negatively charged membranes of the cells. Moreover, positively charged NPs accumulated in the periphery of the spheroid, with low capacity of penetration, while the negatively charged NPs were able to penetrate the spheroid. Interestingly, after loading these NPs with a chemotherapeutic drug (paclitaxel), it was observed a higher cytotoxic effect for the positive NPs, attributed to a higher accumulation of the NPs and consequently of the drug, even if in the periphery of the spheroid. Similar findings were obtained in other studies, for example, using positively and negatively charged liposomes in melanoma spheroids [76] and positively and negatively charged gold NPs in breast cancer spheroids [77], with positive NPs accumulating in the periphery and negative NPs being able to penetrate into the core of the spheroids. Moreover, negative gold NPs contrarily to positive NPs were able to induce a higher hyperthermia effect after being radiated by near-infrared laser [77].

The same observations were not totally obtained in a different study performed by Tchoryk et al. [69] In this study, 50 nm polystyrene NPs positively charged (aminated) and negatively charged (carboxylated or plain NPs) were incubated for 24 h with HCT116 colorectal cancer spheroids. As expected, positively charged aminated NPs were highly taken up, and their penetration was limited to the outer cell layers of the spheroids. However, while negatively charged plain NPs were also able to be highly taken up by the cancer cells and penetrate deeply into the spheroid, negatively charged carboxylated NPs were only taken up at a low extent (20% after 24 h) and could barely penetrate the spheroid. The authors justify this due to the different protein content that might be adsorbed to the NPs upon protein corona formation. This highlights that both the surface charge and also the constitution of the NPs have an effect on NP interaction that should be considered. Also, it is hypothesized that the presence of ECM restricts the diffusion of charged NPs due to electrostatic interactions [78].

Altogether, these findings allow to rationally tailor the NPs according to the needs of the treatment, taking into consideration that positively charged NPs are commonly retained in the superficial layers of spheroids, while negatively charged NPs, depending on their surface chemistry, are able to penetrate deeper into the spheroids [67, 79]. Furthermore, while positive charge might impede NP deep penetration into the tumor tissue, it can enhance their retention [79, 80].

3.1.3 Shape

Shape is another factor impacting the NPs' interaction with tumors and whose influence can be studied using MCTS. Some studies in MCTS have shown that rod-shaped NPs have a faster diffusion rate and extended accumulation than spherical NPs [81–83], which is in agreement with in vitro and in vivo observations [84, 85]. For example, Zhang et al. [86] have produced three types of polystyrene NPs with different shapes (spherical and elongated) and aspect ratio (AR) but with fixed volume, identical chemical composition, and similar surface charge (+50 mV) (Fig. 5). The produced NPs were incubated with HeLa cells in 2D monolayer and HeLa spheroids, and their uptake and penetration was evaluated. In the 2D culture, the cellular uptake was directly related to the AR, as a decreased AR lead to higher cellular uptake, with spherical NPs being taken up more extensively than rod-shaped NPs. Contrariwise, short rod-shaped NPs had a higher uptake and penetration in spheroids than spherical NPs and long rod-shaped NPs. However, it is difficult to generate NPs with comparable parameters, for which there is still limited information in the literature and several contradictory reports [42, 83].

3.1.4 Surface Modifications

MCTS are also an important tool to comprehend and evaluate how different surface modifications, for example, to avoid clearance and prolong lifetime of the NPs or to improve treatment by targeting specific cells, etc., affect the penetration in tumors. For example, PEGylation of NPs, commonly used to prolong their blood circulation time, was shown to reduce NP accumulation in spheroids [67, 79, 80] and increase NP penetration [42, 87].

The use of targeting moieties and cell-penetrating peptides can increase the uptake of NPs by the spheroids. In order to assess the efficacy of using targeting moieties on NPs for enhanced tumor uptake and anticancer efficacy, Figueiredo et al. [88] performed an extensive study testing modified lignin NPs in three different cell lines, PC3-MM2 (prostate cancer), MDA-MB-231 (breast cancer), and A549 (lung cancer), both in 2D monolayers and 3D MCTS model (Fig. 6). Here, lignin NPs were modified with either the dentin phosphophoryn-derived (DSS) or with iRGD cell-penetrating peptides, forming spherical NPs with size ca. 300 nm and surface charge of −25 mV. Unmodified and modified NPs were incubated with the cells both in 2D and 3D, and their uptake was analyzed by confocal microscopy and flow cytometry. In both cellular models, NPs modified with DSS had an enhanced internalization in all the cells lines compared to the control, while iRGD-NPs had an enhanced internalization in PC3-MM2 and MDA-MB-231 cells but not on A549. However, in general, the cellular uptake in 2D was superior to the cellular uptake in 3D. The NPs were then loaded with a chemotherapeutic and their anticancer efficacy assessed in the same models. Interestingly, in the 2D models, despite the difference in uptake of modified NPs, there were barely any differences in the IC_{50} of the different treatments. However, in the MCTS models, modified NPs were able to induce an enhanced antiproliferative effect on the PC3-MM2 MCTS model, while no differences were observed on the other models. Nonetheless, the IC_{50} obtained in 2D were lower than the ones obtained in the 3D models, displaying a higher resistance to the treatment that might be encountered in vivo. In another study, Wang et al. [89] have modified NPs with a targeting peptide (tLyP-1), which promotes tumor homing and penetration, and studied its targeting ability in 2D monoculture, in spheroids, and in an in vivo tumor model of 4 T1 breast cancer cells. Modified NPs presented increased uptake in 2D and in the MCTS, being able to penetrate into the spheroid. Furthermore, in vivo, the targeting ligand also enhanced the penetration of NPs after intratumoral injection and enhanced the accumula-

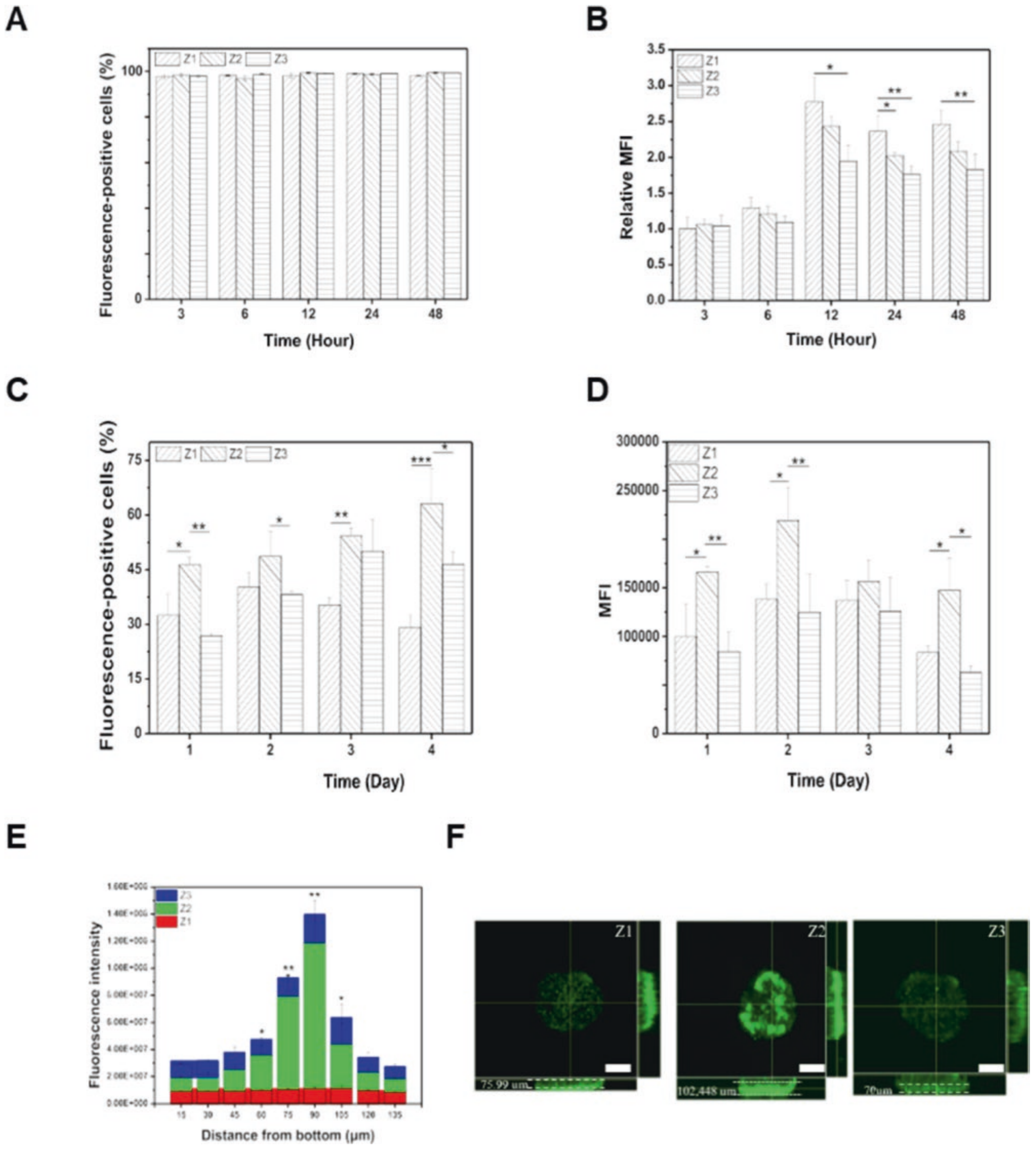

Fig. 5 (**a**) Quantitative cellular uptake of Z1 (spherical, AR = 1), Z2 (elongated, AR = 2.8), and Z3 (elongated, AR = 7.5) polystyrene NPs after incubation with HeLa cell monolayer. (**b**) And respective MFI. (**c**) Quantitative cellular uptake of Z1, Z2, and Z3 polystyrene NPs after incubation with HeLa cell spheroids. (**d**) And respective MFI. (**e**) Analysis of NP penetration in HeLa spheroids. Quantitative fluorescent intensity of different sections. (**f**) Representative fluorescence images of spheroids after 4 days incubation with the different NPs. Scale bars represent 150 μm. (Adapted with permission from Ref. [86])

tion and penetration of NPs in the tumor tissue after intravenous injection, validating the in vitro results. Antibodies can also be used as targeting moieties and tested in 3D cultures. Hortelão et al. [90] have modified mesoporous silica NPs with PEG and antibody anti-fibroblast growth factor receptor 3 (FGFR3), a protein overexpressed in bladder cancer, and

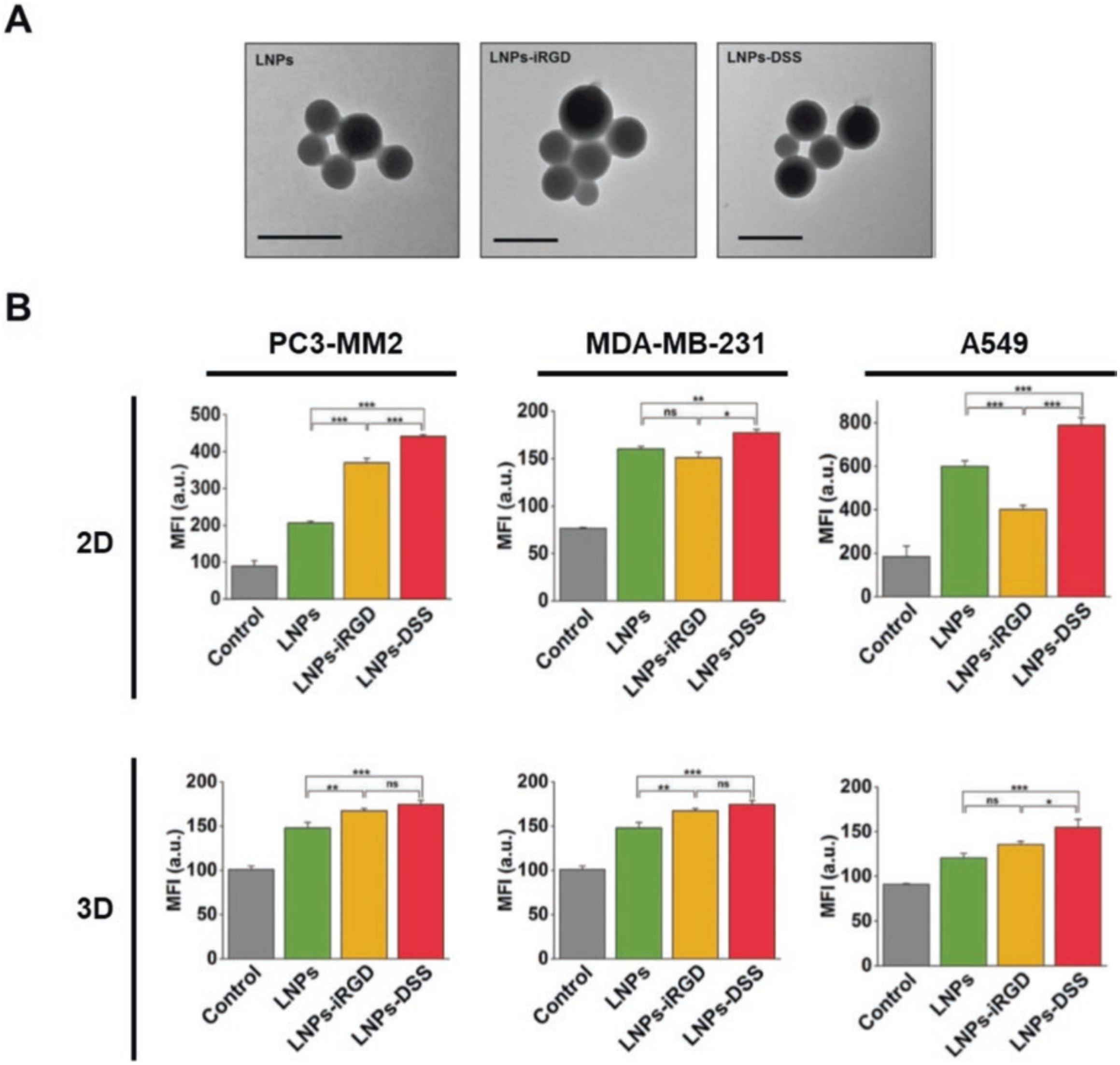

Fig. 6 (**a**) Transmission electron microscopy images of lignin NPs (LNPs) and lignin NPs modified with i-RGD (LNPs-iRGD) and with DSS (LNPs-DSS). Scale bars represent 200 nm. (**b**) Cellular uptake after incubation of unmodified and modified LNPs with either 2D monolayers or spheroids of PC3-MM2, MDA-MB-231, and A549 cells, for 3 h. Results represent mean ± s.d. ($n = 3$). Statistical significance was set at probabilities of $*p < 0.05$, $**p < 0.01$, and $***p < 0.001$, and ns is nonsignificant. (Adapted with permission from Ref. [88])

analyzed their penetration and anticancer efficacy in bladder cancer MCTS. The modification with the antibody enhanced the internalization fourfold compared to the control and induced also antiproliferative effect due to the interaction between the antibody and antigen.

Other studies have also shown the increment of NP uptake by spheroids and deeper penetration when decorated with targeting moieties or coadministered with tumor-homing peptides [91–93]. However, it is necessary to take into consideration that several targeting strategies will only increase the uptake by the superficial layers, and an increment in the penetration will only be achieved if the uptake mechanisms are reversible and the NPs are released again from the cells [42, 94]. Moreover, there is also the possibility of coating the NPs' surface with ECM-degrading enzymes, such as collagenase, or loading the NPs with ECM-degrading drugs to increase their accumulation in the tumor tissue [95–97]. For example, Wang et al. [97] have shown that by functionalizing the surface of nanogels with collagenase, there was an increment on the penetration of the NPs into HepG2 MCTS due to ECM degradation, leading also to higher drug accumulation and enhanced growth inhibition. Furthermore, these results were also confirmed in in vivo assays, where the presence of collagenase leads to an enhanced tumor permeation and antitumor effect.

3.2 Cytocompatibility and Efficacy

MCTS, due to their morphological and biological differences when compared to 2D cultures, are an important tool to assess in vitro the biocompatibility and the anticancer efficacy of the developed NPs, as they might produce different results from 2D cultures [27]. For example, Shi et al. [65] reported much higher IC_{50} values for HCT116 and HCT-8 MCTS (16 and 17 µg/mL, respectively) compared to HCT116 and HCT-8 monolayers (1.4 and 1.1 µg/mL, respectively) after treating the cells with NPs loaded with the chemotherapeutic 5-fluorouracil. The same observation was made in several reports in the literature using various NPs and chemotherapeutics [98–101]. This shows an increased resistance of the cells when cultured in 3D compared to 2D which can be crucial when deciding dosages to test in vivo. Therefore, it must be taken into account when developing NPs for cancer therapy.

Also, since some NPs can promote toxic effect, for example, by promoting inflammation, it is important to develop in vitro models for risk assessment of NPs. In this regard, Leite et al. [102] have evaluated the neurotoxic effect of different types of NPs, gold NPs functionalized with sodium citrate or PEG and polylactic acid NPs, in two 3D neural models, of neurons (LUHMES) and of iPSC-derived brain spheroids. To do so, NPs were incubated with the spheroids, and their viability, morphology, secretion of cytokines, growth factors, and chemokines and gene expression were evaluated. In the monoculture model, NPs have demonstrated some degree of toxicity toward the neurons. However, when incubated with the more complex spheroid model, the NPs did not exert toxic effect probably due to the existent glial cells. Yet, gold NPs promoted some cell physiology alteration that might increase susceptibility to other harmful agents.

Other studies, as, for example, the one performed by Zhou et al. [103], demonstrate the applicability of the MCTS to predict the results in vivo. In this study, the authors developed Ru-Pt bimetallic metallacage encapsulated NPs (5-NPs) as photosensitizers for photodynamic therapy for cancer and tested them in 2D, 3D, and in vivo (Fig. 7). The developed 5-NPs were spherical and had size average of 260 nm. When tested in 2D monolayers of A549 lung cancer cells, these NPs were rapidly taken up, showed high cytocompatibility, and exerted increased toxicity when excited by light. Furthermore, 5-NPs have also shown high cytocompatibility in 3D A549 MCTS model and stimuli-dependent antiproliferative effect. In fact, after light irradiation, spheroids treated with NPs shrank to a volume of 80.4% after 1 day, while the control groups volume growth to ca. 180%. These results were confirmed in vivo, as there was a significant tumor

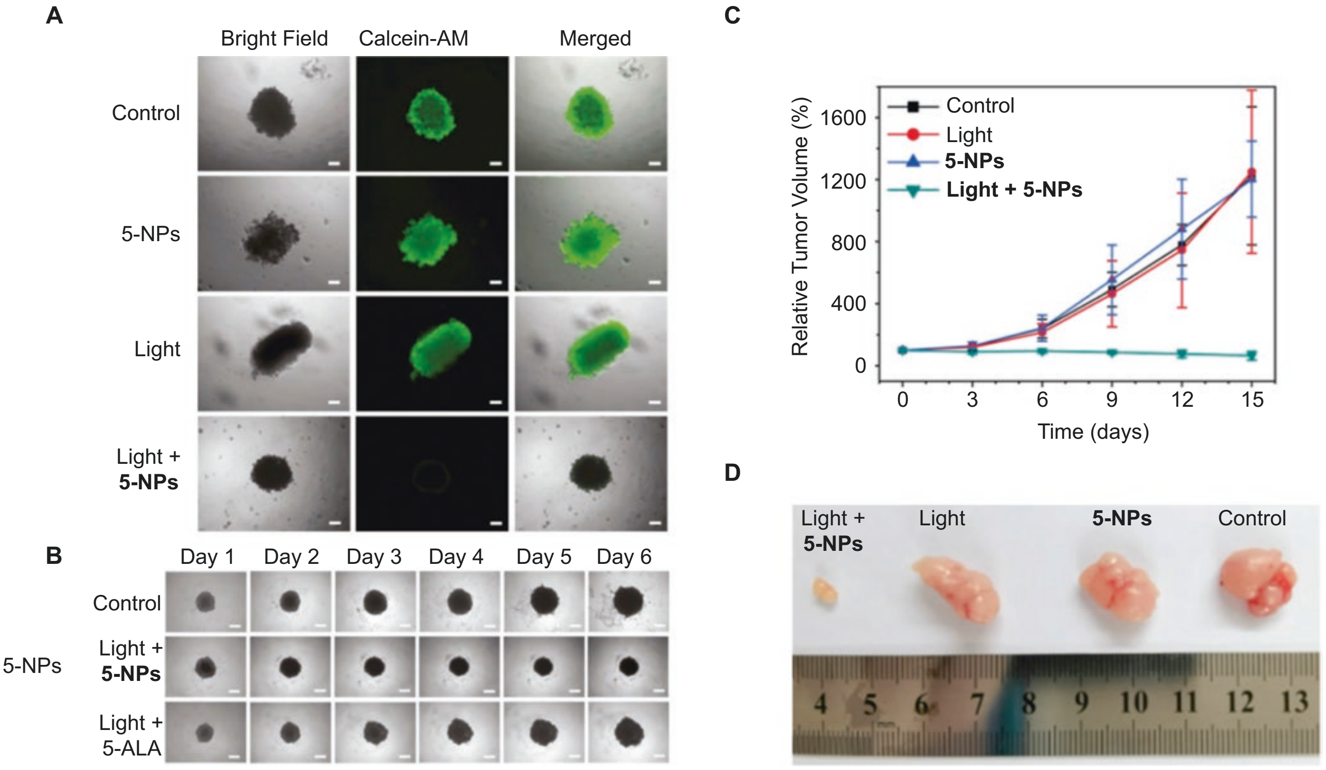

Fig. 7 (**a**) Spheroid viability. Representative confocal microscopy images of spheroids after treatment. (**b**) Representative bright-field images of spheroids after treatments. Scale bars represent 200 µm. (**c**) Mice tumor growth curve after different treatments. (**d**) Representative images of tumors in mice after different treatments. (Adapted with permission from Ref. [103])

reduction (to 65% of original volume) in A549 tumor-bearing animals treated with the 5-NPs intratumorally and irradiated by laser, when compared to the controls which had a 12-fold increase.

4 Conclusions and Future Perspectives

Currently, numerous NPs with different physicochemical characteristics and loaded with different anticancer molecules have been designed and tested for their efficacy in MCTS models and compared to their effect in vivo [42, 68]. Interestingly, the observed results in spheroids regarding NP penetration and accumulation, as well as their effect on tumor growth inhibition, are similar to the ones obtained in vivo [68]. Taking this into account, 3D cellular models, despite not being able to fully recreate every aspect of the tumor milieu, have shown to have a more physiological function than 2D cell cultures, with a consequent superior predictive effect than the 2D monoculture cell models [104, 105].

Despite MCTS being revolutionizing preclinical testing, there are still numerous challenges to be addressed before they can be applied as standard methods for NP testing. Firstly, the focus should be directed to the development of standardized protocols for spheroid formation and evaluation (e.g., metabolic activity, size, development of necrotic core). Next, the protocols for the different assays to assess NP interaction with cancer cells/MCTS should also be standardized (e.g., viability, cellular uptake, penetration, antiproliferative effect) in order to facilitate the comparison of results between different studies. Also, there is the need to perform systematic studies changing only one variable at a time, to allow the proper evaluation of its effect on 2D, 3D, and in vivo models. Finally, fully characterized MCTS models with higher complexity must be developed in order to further mimic the TME and create better predictive tools to ease the translation of NPs to the clinic.

Nevertheless, after surpassing the current challenges, MCTS models have the potential to become the gold-standard in vitro models to assess NPs, highly impacting the design of in vivo studies and accelerating the translation of the developed systems into the clinics.

Acknowledgments T. Bauleth-Ramos acknowledges financial support from Fundação para a Ciência e a Tecnologia (grant no. SFRH/BD/110859/2015). This work was financed by the project NORTE-01-0145-FEDER-000012 by Norte Portugal Regional Operational Programme (NORTE 2020), and COMPETE 2020 – Operacional Programme for Competitiveness and Internationalisation (POCI), under the PORTUGAL 2020 Partnership Agreement, through the (FEDER) Fundo Europeu de Desenvolvimento Regional and by Portuguese funds through (FCT) Fundação para a Ciência e a Tecnologia/Ministério da Ciência, Tecnologia e Ensino Superior in the framework of the project "Institute for Research and Innovation in Health Sciences" UID/BIM/04293/2019.

References

1. Bray, F., Ferlay, J., Soerjomataram, I., Siegel, R. L., Torre, L. A., & Jemal, A. (2018). Global cancer statistics 2018: GLOBOCAN estimates of incidence and mortality worldwide for 36 cancers in 185 countries. *CA: a Cancer Journal for Clinicians, 68*(6), 394–424.
2. Brannon-Peppas, L., & Blanchette, J. O. (2004). Nanoparticle and targeted systems for cancer therapy. *Advanced Drug Delivery Reviews, 56*(11), 1649–1659.
3. Chakraborty, S., & Rahman, T. (2012). The difficulties in cancer treatment. *Ecancermedicalscience, 6*, ed16.
4. Shi, J., Kantoff, P. W., Wooster, R., & Farokhzad, O. C. (2017). Cancer nanomedicine: Progress, challenges and opportunities. *Nature Reviews. Cancer, 17*(1), 20–37.
5. Peer, D., Karp, J. M., Hong, S., Farokhzad, O. C., Margalit, R., & Langer, R. (2007). Nanocarriers as an emerging platform for cancer therapy. *Nature Nanotechnology, 2*(12), 751–760.
6. van der Meel, R., Sulheim, E., Shi, Y., Kiessling, F., Mulder, W. J. M., & Lammers, T. (2019). Smart cancer nanomedicine. *Nature Nanotechnology, 14*(11), 1007–1017.
7. Figueiredo, P., Bauleth-Ramos, T., Hirvonen, J., Sarmento, B., & Santos, H. A. (2018). Chapter 1 – The emerging role of multifunctional theranostic materials in cancer nanomedicine. In J. Conde (Ed.), *Handbook of nanomaterials for cancer theranostics* (pp. 1–31). Elsevier: Amsterdam, The Netherlands.
8. Balasubramanian, V., Liu, Z., Hirvonen, J., & Santos, H. A. (2018). Bridging the knowledge of different worlds to understand the big picture of cancer nanomedicines. *Advanced Healthcare Materials, 7*(1), 1700432.
9. Hare, J. I., Lammers, T., Ashford, M. B., Puri, S., Storm, G., & Barry, S. T. (2017). Challenges and strategies in anti-cancer nanomedicine development: An industry perspective. *Advanced Drug Delivery Reviews, 108*, 25–38.
10. Shreffler, J. W., Pullan, J. E., Dailey, K. M., Mallik, S., & Brooks, A. E. (2019). Overcoming hurdles in nanoparticle clinical translation: The influence of experimental design and surface modification. *International Journal of Molecular Sciences, 20*(23), 6056.
11. Choi, S. Y., Lin, D., Gout, P. W., Collins, C. C., Xu, Y., & Wang, Y. (2014). Lessons from patient-derived xenografts for better in vitro modeling of human cancer. *Advanced Drug Delivery Reviews, 79–80*, 222–237.
12. Thoma, C. R., Zimmermann, M., Agarkova, I., Kelm, J. M., & Krek, W. (2014). 3D cell culture systems modeling tumor growth determinants in cancer target discovery. *Advanced Drug Delivery Reviews, 69–70*, 29–41.
13. Chatzinikolaidou, M. (2016). Cell spheroids: The new frontiers in in vitro models for cancer drug validation. *Drug Discovery Today, 21*(9), 1553–1560.
14. Niu, N., & Wang, L. (2015). In vitro human cell line models to predict clinical response to anticancer drugs. *Pharmacogenomics, 16*(3), 273–285.
15. Nunes, A. S., Barros, A. S., Costa, E. C., Moreira, A. F., & Correia, I. J. (2019). 3D tumor spheroids as in vitro models to mimic in vivo human solid tumors resistance to therapeutic drugs. *Biotechnology and Bioengineering, 116*(1), 206–226.
16. Ibarrola-Villava, M., Cervantes, A., & Bardelli, A. (2018). Preclinical models for precision oncology. *Biochimica Et Biophysica Acta. Reviews on Cancer, 1870*(2), 239–246.
17. Cifola, I., Bianchi, C., Mangano, E., Bombelli, S., Frascati, F., Fasoli, E., Ferrero, S., Di Stefano, V., Zipeto, M. A., Magni, F., Signorini, S., Battaglia, C., & Perego, R. A. (2011). Renal cell carcinoma primary cultures maintain genomic and phenotypic profile of parental tumor tissues. *BMC Cancer, 11*, 244.

18. Fabbrizi Maria, R., Duff, T., Oliver, J., & Wilde, C. (2014). Advanced in vitro systems for efficacy and toxicity testing in nanomedicine. *European Journal of Nanomedicine, 6*, 171.
19. Weiswald, L. B., Bellet, D., & Dangles-Marie, V. (2015). Spherical cancer models in tumor biology. *Neoplasia, 17*(1), 1–15.
20. Pampaloni, F., Reynaud, E. G., & Stelzer, E. H. K. (2007). The third dimension bridges the gap between cell culture and live tissue. *Nature Reviews Molecular Cell Biology, 8*(10), 839–845.
21. Xu, X., Farach-Carson, M. C., & Jia, X. (2014). Three-dimensional in vitro tumor models for cancer research and drug evaluation. *Biotechnology Advances, 32*(7), 1256–1268.
22. Klimkiewicz, K., Weglarczyk, K., Collet, G., Paprocka, M., Guichard, A., Sarna, M., Jozkowicz, A., Dulak, J., Sarna, T., Grillon, C., & Kieda, C. (2017). A 3D model of tumour angiogenic microenvironment to monitor hypoxia effects on cell interactions and cancer stem cell selection. *Cancer Letters, 396*, 10–20.
23. Baker, B. M., & Chen, C. S. (2012). Deconstructing the third dimension – how 3D culture microenvironments alter cellular cues. *Journal of Cell Science, 125*(13), 3015–3024.
24. Lamichhane, S. P., Arya, N., Kohler, E., Xiang, S., Christensen, J., & Shastri, V. P. (2016). Recapitulating epithelial tumor microenvironment in vitro using three dimensional tri-culture of human epithelial, endothelial, and mesenchymal cells. *BMC Cancer, 16*(1), 581.
25. Cavo, M., Fato, M., Peñuela, L., Beltrame, F., Raiteri, R., & Scaglione, S. (2016). Microenvironment complexity and matrix stiffness regulate breast cancer cell activity in a 3D in vitro model. *Scientific Reports, 6*, 35367.
26. Liu, T., Lin, B., & Qin, J. (2010). Carcinoma-associated fibroblasts promoted tumor spheroid invasion on a microfluidic 3D co-culture device. *Lab on a Chip, 10*(13), 1671–1677.
27. Shoval, H., Karsch-Bluman, A., Brill-Karniely, Y., Stern, T., Zamir, G., Hubert, A., & Benny, O. (2017). Tumor cells and their crosstalk with endothelial cells in 3D spheroids. *Scientific Reports, 7*(1), 10428.
28. Hirschhaeuser, F., Menne, H., Dittfeld, C., West, J., Mueller-Klieser, W., & Kunz-Schughart, L. A. (2010). Multicellular tumor spheroids: An underestimated tool is catching up again. *Journal of Biotechnology, 148*(1), 3–15.
29. Haycock, J. W. (2011). 3D Cell culture: A review of current approaches and techniques. In J. W. Haycock (Ed.), *3D cell culture: Methods and protocols* (pp. 1–15). Totowa: Humana Press.
30. Hutmacher, D. W., Horch, R. E., Loessner, D., Rizzi, S., Sieh, S., Reichert, J. C., Clements, J. A., Beier, J. P., Arkudas, A., Bleiziffer, O., & Kneser, U. (2009). Translating tissue engineering technology platforms into cancer research. *Journal of Cellular and Molecular Medicine, 13*(8a), 1417–1427.
31. Knight, E., & Przyborski, S. (2015). Advances in 3D cell culture technologies enabling tissue-like structures to be created in vitro. *Journal of Anatomy, 227*(6), 746–756.
32. Kunz-Schughart, L. A. (1999). Multicellular tumor spheroids: Intermediates between monolayer culture and in vivo tumor. *Cell Biology International, 23*(3), 157–161.
33. Huang, B.-W., & Gao, J.-Q. (2018). Application of 3D cultured multicellular spheroid tumor models in tumor-targeted drug delivery system research. *Journal of Controlled Release, 270*, 246–259.
34. Froehlich, K., Haeger, J.-D., Heger, J., Pastuschek, J., Photini, S. M., Yan, Y., Lupp, A., Pfarrer, C., Mrowka, R., Schleußner, E., Markert, U. R., & Schmidt, A. (2016). Generation of multicellular breast cancer tumor spheroids: Comparison of different protocols. *Journal of Mammary Gland Biology and Neoplasia, 21*(3), 89–98.
35. Achilli, T.-M., Meyer, J., & Morgan, J. R. (2012). Advances in the formation, use and understanding of multi-cellular spheroids. *Expert Opinion on Biological Therapy, 12*(10), 1347–1360.
36. Tung, Y.-C., Hsiao, A. Y., Allen, S. G., Torisawa, Y.-S., Ho, M., & Takayama, S. (2011). High-throughput 3D spheroid culture and drug testing using a 384 hanging drop array. *Analyst, 136*(3), 473–478.
37. Timmins, N. E., & Nielsen, L. K. (2007). Generation of multicellular tumor spheroids by the hanging-drop method. In H. Hauser & M. Fussenegger (Eds.), *Tissue engineering* (pp. 141–151). Totowa: Humana Press.
38. Sutherland, R. M., McCredie, J. A., & Inch, W. R. (1971). Growth of multicell spheroids in tissue culture as a model of nodular carcinomas. *JNCI: Journal of the National Cancer Institute, 46*(1), 113–120.
39. Tang, Y., Liu, J., & Chen, Y. (2016). Agarose multi-wells for tumour spheroid formation and anti-cancer drug test. *Microelectronic Engineering, 158*, 41–45.
40. Costa, E. C., de Melo-Diogo, D., Moreira, A. F., Carvalho, M. P., & Correia, I. J. (2018). Spheroids formation on non-adhesive surfaces by liquid overlay technique: Considerations and practical approaches. *Biotechnology Journal, 13*(1), 1700417.
41. Mehta, G., Hsiao, A. Y., Ingram, M., Luker, G. D., & Takayama, S. (2012). Opportunities and challenges for use of tumor spheroids as models to test drug delivery and efficacy. *Journal of Controlled Release, 164*(2), 192–204.
42. Lu, H., & Stenzel, M. H. (2018). Multicellular tumor spheroids (MCTS) as a 3D in vitro evaluation tool of nanoparticles. *Small, 14*(13), 1702858.
43. Gebhard, C., Gabriel, C., & Walter, I. (2016). Morphological and immunohistochemical characterization of canine osteosarcoma spheroid cell cultures. *Anatomia, Histologia, Embryologia, 45*(3), 219–230.
44. Kunz-Schughart, L. A., Freyer, J. P., Hofstaedter, F., & Ebner, R. (2004). The use of 3-D cultures for high-throughput screening: The multicellular spheroid model. *Journal of Biomolecular Screening, 9*(4), 273–285.
45. Lin, R.-Z., & Chang, H.-Y. (2008). Recent advances in three-dimensional multicellular spheroid culture for biomedical research. *Biotechnology Journal, 3*(9–10), 1172–1184.
46. Katt, M. E., Placone, A. L., Wong, A. D., Xu, Z. S., & Searson, P. C. (2016). In vitro tumor models: Advantages, disadvantages, variables, and selecting the right platform. *Frontiers in Bioengineering and Biotechnology, 4*, 12.
47. Rohwer, N., & Cramer, T. (2011). Hypoxia-mediated drug resistance: Novel insights on the functional interaction of HIFs and cell death pathways. *Drug Resistance Updates, 14*(3), 191–201.
48. Trédan, O., Galmarini, C. M., Patel, K., & Tannock, I. F. (2007). Drug resistance and the solid tumor microenvironment. *JNCI: Journal of the National Cancer Institute, 99*(19), 1441–1454.
49. Swietach, P., Hulikova, A., Patiar, S., Vaughan-Jones, R. D., & Harris, A. L. (2012). Importance of intracellular pH in determining the uptake and efficacy of the weakly basic chemotherapeutic drug, doxorubicin. *PloS One, 7*(4), e35949.
50. Majety, M., Pradel, L. P., Gies, M., & Ries, C. H. (2015). Fibroblasts influence survival and therapeutic response in a 3D co-culture model. *PLoS One, 10*(6), e0127948.
51. Lee, J. W., Shin, D. H., & Roh, J. L. (2018). Development of an in vitro cell-sheet cancer model for chemotherapeutic screening. *Theranostics, 8*(14), 3964–3973.
52. Correia, A. L., & Bissell, M. J. (2012). The tumor microenvironment is a dominant force in multidrug resistance. *Drug Resistance Updates, 15*(1), 39–49.
53. Sun, Y. (2016). Tumor microenvironment and cancer therapy resistance. *Cancer Letters, 380*(1), 205–215.
54. Pickup, M. W., Mouw, J. K., & Weaver, V. M. (2014). The extracellular matrix modulates the hallmarks of cancer. *EMBO Reports, 15*(12), 1243–1253.

55. Costa, E. C., Moreira, A. F., de Melo-Diogo, D., Gaspar, V. M., Carvalho, M. P., & Correia, I. J. (2016). 3D tumor spheroids: An overview on the tools and techniques used for their analysis. *Biotechnology Advances, 34*(8), 1427–1441.
56. Longati, P., Jia, X., Eimer, J., Wagman, A., Witt, M.-R., Rehnmark, S., Verbeke, C., Toftgård, R., Löhr, M., & Heuchel, R. L. (2013). 3D pancreatic carcinoma spheroids induce a matrix-rich, chemoresistant phenotype offering a better model for drug testing. *BMC Cancer, 13*(1), 95.
57. Nath, S., & Devi, G. R. (2016). Three-dimensional culture systems in cancer research: Focus on tumor spheroid model. *Pharmacology and Therapeutics, 163*, 94–108.
58. Ma, H.-L., Jiang, Q., Han, S., Wu, Y., Tomshine, J. C., Wang, D., Gan, Y., Zou, G., & Liang, X.-J. (2012). Multicellular tumor spheroids as an in vivo–like tumor model for three-dimensional imaging of chemotherapeutic and nano material cellular penetration. *Molecular Imaging, 11*(6), 7290.2012.00012.
59. Zanoni, M., Piccinini, F., Arienti, C., Zamagni, A., Santi, S., Polico, R., Bevilacqua, A., & Tesei, A. (2016). 3D tumor spheroid models for in vitro therapeutic screening: A systematic approach to enhance the biological relevance of data obtained. *Scientific Reports, 6*, 19103.
60. Fang, Y., & Eglen, R. M. (2017). Three-dimensional cell cultures in drug discovery and development. *Slas Discovery: Advancing Life Sciences R&D, 22*(5), 456–472.
61. Rodrigues, T., Kundu, B., Silva-Correia, J., Kundu, S. C., Oliveira, J. M., Reis, R. L., & Correlo, V. M. (2018). Emerging tumor spheroids technologies for 3D in vitro cancer modeling. *Pharmacology and Therapeutics, 184*, 201–211.
62. Hoarau-Véchot, J., Rafii, A., Touboul, C., & Pasquier, J. (2018). Halfway between 2D and animal models: Are 3D cultures the ideal tool to study cancer-microenvironment interactions? *International Journal of Molecular Sciences, 19*(1), 181.
63. Li, Y., Wang, J., Wientjes, M. G., & Au, J. L. S. (2012). Delivery of nanomedicines to extracellular and intracellular compartments of a solid tumor. *Advanced Drug Delivery Reviews, 64*(1), 29–39.
64. Ozcelikkale, A., Ghosh, S., & Han, B. (2013). Multifaceted transport characteristics of nanomedicine: Needs for characterization in dynamic environment. *Molecular Pharmaceutics, 10*(6), 2111–2126.
65. Shi, W. B., Le, V. M., Gu, C. H., Zheng, Y. H., Lang, M. D., Lu, Y. H., & Liu, J. W. (2014). Overcoming multidrug resistance in 2D and 3D culture models by controlled drug chitosan-graft poly(caprolactone)-based nanoparticles. *Journal of Pharmaceutical Sciences, 103*(4), 1064–1074.
66. Biondi, M., Guarnieri, D., Yu, H., Belli, V., & Netti, P. A. (2013). Sub-100 nm biodegradable nanoparticles: In vitro release features and toxicity testing in 2D and 3D cell cultures. *Nanotechnology, 24*(4), 045101.
67. Solomon, M. A., Lemera, J., & D'Souza, G. G. M. (2016). Development of an in vitro tumor spheroid culture model amenable to high-throughput testing of potential anticancer nanotherapeutics. *Journal of Liposome Research, 26*(3), 246–260.
68. Millard, M., Yakavets, I., Zorin, V., Kulmukhamedova, A., Marchal, S., & Bezdetnaya, L. (2017). Drug delivery to solid tumors: The predictive value of the multicellular tumor spheroid model for nanomedicine screening. *International Journal of Nanomedicine, 12*, 7993–8007.
69. Tchoryk, A., Taresco, V., Argent, R. H., Ashford, M., Gellert, P. R., Stolnik, S., Grabowska, A., & Garnett, M. C. (2019). Penetration and uptake of nanoparticles in 3D tumor spheroids. *Bioconjugate Chemistry, 30*(5), 1371–1384.
70. Durymanov, M., Kroll, C., Permyakova, A., & Reineke, J. (2019). Role of endocytosis in nanoparticle penetration of 3D pancreatic cancer spheroids. *Molecular Pharmaceutics, 16*(3), 1074–1082.
71. Huo, S., Ma, H., Huang, K., Liu, J., Wei, T., Jin, S., Zhang, J., He, S., & Liang, X. J. (2013). Superior penetration and retention behavior of 50 nm gold nanoparticles in tumors. *Cancer Research, 73*(1), 319–330.
72. Huang, K., Ma, H., Liu, J., Huo, S., Kumar, A., Wei, T., Zhang, X., Jin, S., Gan, Y., Wang, P. C., He, S., Zhang, X., & Liang, X. J. (2012). Size-dependent localization and penetration of ultrasmall gold nanoparticles in cancer cells, multicellular spheroids, and tumors in vivo. *ACS Nano, 6*(5), 4483–4493.
73. Albanese, A., Lam, A. K., Sykes, E. A., Rocheleau, J. V., & Chan, W. C. W. (2013). Tumour-on-a-chip provides an optical window into nanoparticle tissue transport. *Nature Communications, 4*(1), 2718.
74. Tang, L., Yang, X., Yin, Q., Cai, K., Wang, H., Chaudhury, I., Yao, C., Zhou, Q., Kwon, M., Hartman, J. A., Dobrucki, I. T., Dobrucki, L. W., Borst, L. B., Lezmi, S., Helferich, W. G., Ferguson, A. L., Fan, T. M., & Cheng, J. (2014). Investigating the optimal size of anticancer nanomedicine. *Proceedings of the National Academy of Sciences, 111*(43), 15344–15349.
75. Stylianopoulos, T., Poh, M.-Z., Insin, N., Bawendi, M. G., Fukumura, D., Munn, L. L., & Jain, R. K. (2010). Diffusion of particles in the extracellular matrix: The effect of repulsive electrostatic interactions. *Biophysical Journal, 99*(5), 1342–1349.
76. Suzuki, S., Itakura, S., Matsui, R., Nakayama, K., Nishi, T., Nishimoto, A., Hama, S., & Kogure, K. (2017). Tumor microenvironment-sensitive liposomes penetrate tumor tissue via attenuated interaction of the extracellular matrix and tumor cells and accompanying actin depolymerization. *Biomacromolecules, 18*(2), 535–543.
77. Jin, S., Ma, X., Ma, H., Zheng, K., Liu, J., Hou, S., Meng, J., Wang, P. C., Wu, X., & Liang, X. J. (2013). Surface chemistry-mediated penetration and gold nanorod thermotherapy in multicellular tumor spheroids. *Nanoscale, 5*(1), 143–146.
78. Lieleg, O., Baumgartel, R. M., & Bausch, A. R. (2009). Selective filtering of particles by the extracellular matrix: An electrostatic bandpass. *Biophysical Journal, 97*(6), 1569–1577.
79. Kostarelos, K., Emfietzoglou, D., Papakostas, A., Yang, W.-H., Ballangrud, Å., & Sgouros, G. (2004). Binding and interstitial penetration of liposomes within avascular tumor spheroids. *International Journal of Cancer, 112*(4), 713–721.
80. Ernsting, M. J., Murakami, M., Roy, A., & Li, S. D. (2013). Factors controlling the pharmacokinetics, biodistribution and intratumoral penetration of nanoparticles. *Journal of Controlled Release, 172*(3), 782–794.
81. Dias, D. R., Moreira, A. F., & Correia, I. J. (2016). The effect of the shape of gold core–mesoporous silica shell nanoparticles on the cellular behavior and tumor spheroid penetration. *Journal of Materials Chemistry B, 4*(47), 7630–7640.
82. Agarwal, R., Jurney, P., Raythatha, M., Singh, V., Sreenivasan, S. V., Shi, L., & Roy, K. (2015). Effect of shape, size, and aspect ratio on nanoparticle penetration and distribution inside solid tissues using 3D spheroid models. *Advanced Healthcare Materials, 4*(15), 2269–2280.
83. Wang, W., Gaus, K., Tilley, R. D., & Gooding, J. J. (2019). The impact of nanoparticle shape on cellular internalisation and transport: What do the different analysis methods tell us? *Materials Horizons, 6*(8), 1538–1547.
84. Lee, K. L., Hubbard, L. C., Hern, S., Yildiz, I., Gratzl, M., & Steinmetz, N. F. (2013). Shape matters: the diffusion rates of TMV rods and CPMV icosahedrons in a spheroid model of extracellular matrix are distinct. *Biomaterials Science, 1*(6), 581–588.
85. Chauhan, V. P., Popović, Z., Chen, O., Cui, J., Fukumura, D., Bawendi, M. G., & Jain, R. K. (2011). Fluorescent nanorods and nanospheres for real-time in vivo probing of nanoparticle shape-dependent tumor penetration. *Angewandte Chemie International Edition, 50*(48), 11417–11420.
86. Zhang, L., Wang, Y., Yang, D., Huang, W., Hao, P., Feng, S., Appelhans, D., Zhang, T., & Zan, X. (2019). Shape effect of

nanoparticles on tumor penetration in monolayers versus spheroids. *Molecular Pharmaceutics, 16*(7), 2902–2911.

87. You, Y., Hu, H., He, L., & Chen, T. (2015). Differential effects of polymer-surface decoration on drug delivery, cellular retention, and action mechanisms of functionalized mesoporous silica nanoparticles. *Chemistry – An Asian Journal, 10*(12), 2744–2754.
88. Figueiredo, P., Sipponen, M. H., Lintinen, K., Correia, A., Kiriazis, A., Yli-Kauhaluoma, J., Österberg, M., George, A., Hirvonen, J., Kostiainen, M. A., & Santos, H. A. (2019). Preparation and characterization of dentin phosphophoryn-derived peptide-functionalized lignin nanoparticles for enhanced cellular uptake. *Small, 15*(24), 1901427.
89. Wang, Y., Yin, S., Mei, L., Yang, Y., Xu, S., He, X., Wang, M., Li, M., Zhang, Z., & He, Q. (2020). A dual receptors-targeting and size-switchable "cluster bomb" co-loading chemotherapeutic and transient receptor potential ankyrin 1 (TRPA-1) inhibitor for treatment of triple negative breast cancer. *Journal of Controlled Release, 321*, 71–83.
90. Hortelão, A. C., Carrascosa, R., Murillo-Cremaes, N., Patiño, T., & Sánchez, S. (2019). Targeting 3D bladder cancer spheroids with urease-powered nanomotors. *ACS Nano, 13*(1), 429–439.
91. Fan, R., Chuan, D., Hou, H., Chen, H., Han, B., Zhang, X., Zhou, L., Tong, A., Xu, J., & Guo, G. (2019). Development of a hybrid nanocarrier-recognizing tumor vasculature and penetrating the BBB for glioblastoma multi-targeting therapy. *Nanoscale, 11*(23), 11285–11304.
92. Hu, C., Yang, X., Liu, R., Ruan, S., Zhou, Y., Xiao, W., Yu, W., Yang, C., & Gao, H. (2018). Coadministration of iRGD with multistage responsive nanoparticles enhanced tumor targeting and penetration abilities for breast cancer therapy. *ACS Applied Materials & Interfaces, 10*(26), 22571–22579.
93. Marino, A., Camponovo, A., Degl'Innocenti, A., Bartolucci, M., Tapeinos, C., Martinelli, C., De Pasquale, D., Santoro, F., Mollo, V., Arai, S., Suzuki, M., Harada, Y., Petretto, A., & Ciofani, G. (2019). Multifunctional temozolomide-loaded lipid superparamagnetic nanovectors: Dual targeting and disintegration of glioblastoma spheroids by synergic chemotherapy and hyperthermia treatment. *Nanoscale, 11*(44), 21227–21248.
94. Chariou, P. L., Lee, K. L., Pokorski, J. K., Saidel, G. M., & Steinmetz, N. F. (2016). Diffusion and uptake of tobacco mosaic virus as therapeutic carrier in tumor tissue: Effect of nanoparticle aspect ratio. *The Journal of Physical Chemistry B, 120*(26), 6120–6129.
95. Goodman, T. T., Olive, P. L., & Pun, S. H. (2007). Increased nanoparticle penetration in collagenase-treated multicellular spheroids. *International Journal of Nanomedicine, 2*(2), 265–274.
96. Zhang, Y., Liu, Y., Gao, X., Li, X., Niu, X., Yuan, Z., & Wang, W. (2019). Near-infrared-light induced nanoparticles with enhanced tumor tissue penetration and intelligent drug release. *Acta Biomaterialia, 90*, 314–323.
97. Wang, X., Luo, J., He, L., Cheng, X., Yan, G., Wang, J., & Tang, R. (2018). Hybrid pH-sensitive nanogels surface-functionalized with collagenase for enhanced tumor penetration. *Journal of Colloid and Interface Science, 525*, 269–281.
98. Miranda, M. A., Marcato, P. D., Carvalho, I. P. S., Silva, L. B., Ribeiro, D. L., Amaral, R., Swiech, K., Bastos, J. K., Paschoal, J. A. R., dos Reis, R. B., & Bentley, M. V. L. B. (2019). Assessing the cytotoxic potential of glycoalkaloidic extract in nanoparticles against bladder cancer cells. *Journal of Pharmacy and Pharmacology, 71*(10), 1520–1531.
99. Ishiguro, S., Cai, S., Uppalapati, D., Turner, K., Zhang, T., Forrest, W. C., Forrest, M. L., & Tamura, M. (2016). Intratracheal administration of hyaluronan-cisplatin conjugate nanoparticles significantly attenuates lung cancer growth in mice. *Pharmaceutical Research, 33*(10), 2517–2529.
100. Godugu, C., Patel, A. R., Desai, U., Andey, T., Sams, A., & Singh, M. (2013). AlgiMatrix™ based 3D cell culture system as an in-vitro tumor model for anticancer studies. *PLoS One, 8*(1), e53708.
101. Affram, K. O., Smith, T., Ofori, E., Krishnan, S., Underwood, P., Trevino, J. G., & Agyare, E. (2020). Cytotoxic effects of gemcitabine-loaded solid lipid nanoparticles in pancreatic cancer cells. *Journal of Drug Delivery Science and Technology, 55*, 101374.
102. Leite, P. E. C., Pereira, M. R., Harris, G., Pamies, D., dos Santos, L. M. G., Granjeiro, J. M., Hogberg, H. T., Hartung, T., & Smirnova, L. (2019). Suitability of 3D human brain spheroid models to distinguish toxic effects of gold and poly-lactic acid nanoparticles to assess biocompatibility for brain drug delivery. *Particle and Fibre Toxicology, 16*(1), 22.
103. Zhou, Z., Liu, J., Huang, J., Rees, T. W., Wang, Y., Wang, H., Li, X., Chao, H., & Stang, P. J. (2019). A self-assembled Ru–Pt metallacage as a lysosome-targeting photosensitizer for 2-photon photodynamic therapy. *Proceedings of the National Academy of Sciences, 116*(41), 20296–20302.
104. Ramgolam, K., Lauriol, J., Lalou, C., Lauden, L., Michel, L., de la Grange, P., Khatib, A.-M., Aoudjit, F., Charron, D., Alcaide-Loridan, C., & Al-Daccak, R. (2011). Melanoma spheroids grown under neural crest cell conditions are highly plastic migratory/invasive tumor cells endowed with immunomodulator function. *PLoS One, 6*(4), e18784.
105. Horman, S. R., Hogan, C., Reyes, K. D., Lo, F., & Antczak, C. (2015). Challenges and opportunities toward enabling phenotypic screening of complex and 3D cell models. *Future Medicinal Chemistry, 7*(4), 513–525.
106. Priwitaningrum, D. L., Blondé, J.-B. G., Sridhar, A., van Baarlen, J., Hennink, W. E., Storm, G., Le Gac, S., & Prakash, J. (2016). Tumor stroma-containing 3D spheroid arrays: A tool to study nanoparticle penetration. *Journal of Controlled Release, 244*, 257–268.
107. Wang, H.-X., Zuo, Z.-Q., Du, J.-Z., Wang, Y.-C., Sun, R., Cao, Z.-T., Ye, X.-D., Wang, J.-L., Leong, K. W., & Wang, J. (2016). Surface charge critically affects tumor penetration and therapeutic efficacy of cancer nanomedicines. *Nano Today, 11*(2), 133–144.

3D Tumor Spheroid Models for In Vitro Therapeutic Screening of Nanoparticles

Simonas Daunys, Agnė Janonienė, Indrė Januškevičienė, Miglė Paškevičiūtė, and Vilma Petrikaitė

Abstract

The anticancer activity of compounds and nanoparticles is most often determined in the cell monolayer. However, three-dimensional (3D) systems, such as tumor spheroids, are more representing the natural tumor microenvironment. They have been shown to have higher invasiveness and resistance to cytotoxic agents and radiotherapy compared to cells growing in 2D monolayer. Furthermore, to improve the prediction of clinical efficacy of drugs, in the past decades, even more sophisticated systems, such as multicellular 3D cultures, closely representing natural tumor microenvironment have been developed. Those cultures are formed from either cell lines or patient-derived tumor cells. Such models are very attractive and could improve the selection of tested materials for clinical trials avoiding unnecessary expensive tests in vivo. The microenvironment in tumor spheroids is different, and those differences or the interaction between several cell populations may contribute to different tumor response to the treatment. Also, different types of nanoparticles may have different behavior in 3D models, depending on their nature, physicochemical properties, the presence of targeting ligands on the surface, etc. Therefore, it is very important to understand in which cases which type of tumor spheroid is more suitable for testing specific types of nanoparticles, which conditions should be used, and which analytical method should be applied.

Keywords

Tumor spheroid · Multicellular · 3D culture · Nanoparticle · Cellular heterogeneity · Tumorosphere · Screening · Toxicity · Penetration · Bioprinting

1 Introduction

Spheroids are thought to be the most suitable in vitro model for drug testing in oncology due to their ability to reproduce the main features found in solid tumors in vivo, such as cellular heterogeneity, cell-cell signaling, internal structure (composed of different cell layers), extracellular matrix (ECM) deposition, ECM-cell and cell-cell physical interactions, growth kinetics, gene expression, drug resistance, and much more [1]. It is generally recognized that the 3D cell-cell interaction may influence responses such as the cytoskeleton formation while also regulating the signaling related to cell migration and differentiation [2, 3], thereby having an important role in the development of resistance to chemotherapy [4]. Numerous 3D cancer cell models have been specifically developed in cancer research to mimic more closely the natural tumor architecture and display the biological process to as great an extent as possible. These models are constructed in different ways starting from different kinds of cancer cell materials and are divided into multicellular tumor spheroids model (MCTS) [5–7], organotypic slices of cancer tissue [8, 9], multilayered cell cultures [10], and scaffolds [11].

During the last decades, tumor spheroids gained a lot of attention from researchers as they could be used for different applications in nanoparticle development process. It is a convenient model for testing cytotoxicity as 3D cultures much better mimic the real tumor microenvironment compared to

---

S. Daunys · A. Janonienė
Life Sciences Center, Vilnius University, Vilnius, Lithuania

I. Januškevičienė · M. Paškevičiūtė
Laboratory of Drug Targets Histopathology, Institute of Cardiology, Lithuanian University of Health Sciences, Kaunas, Lithuania

V. Petrikaitė (✉)
Life Sciences Center, Vilnius University, Vilnius, Lithuania

Laboratory of Drug Targets Histopathology, Institute of Cardiology, Lithuanian University of Health Sciences, Kaunas, Lithuania

Institute of Physiology and Pharmacology, Academy of Medicine, Lithuanian University of Health Sciences, Kaunas, Lithuania

© Springer Nature Switzerland AG 2021
F. Fontana, H. A. Santos (eds.), *Bio-Nanomedicine for Cancer Therapy*, Advances in Experimental Medicine and Biology 1295, https://doi.org/10.1007/978-3-030-58174-9_11

cells grown in monolayer [12]. It has already proven that data obtained in 3D cultures better represent the results obtained in preclinical or even clinical trials [13, 14]. Also, it is a convenient model to test nanoparticle penetration inside the tumor – this process is critical in vivo and is one of the most important physiological barriers to reach the therapeutic site of action at effective concentrations [15]. Moreover, tumor spheroids could be used for such application when 2D cell models could not be applied at all, e.g., to evaluate nanoparticle effect on cell-cell interaction which represents a critical parameter for spheroid formation [16]. Nowadays more and more attention is paid to high-throughput screening strategies, and there are also many microfluidic devices made both for spheroid formation and their analysis that allow to make the whole process more time- and cost-efficient [17, 18].

However, it is very important to choose the right model for testing different types of nanoparticles or evaluating specific parameters of their penetration, cytotoxicity, or other cancer treatment and development-related processes. There is a huge variety of analytical methods for different application, and all of them have their own strengths and weaknesses; thus, combination of different analytical methods could represent a better choice [16, 19]. Indeed, there is still a lack of standardized protocols that could help to compare the results obtained by different research groups. Thus, it is very important to know the features of the different 3D model systems and specificities of different methods and also to understand how the main critical steps could be related to the possible wrong interpretation of obtained results. This is fundamental particularly when experiments are done with nanoparticles, as many factors related to their nature, size, charge targeting abilities, etc. may influence the results obtained in biological assays [20].

In this chapter, we will discuss the advantages of 3D tumor spheroid models vs. cells grown in monolayer, review methods used for screening nanoparticles in 3D systems, and describe the main challenges of testing nanoparticles in spheroids.

2 3D Tumor Spheroid Model Versus Monolayers of Cancer Cells In Vitro

2.1 Characteristics of 3D Tumor Spheroid

3D spheroids are cellular aggregates, often 100–600 μm of diameter [21, 22], that have been widely used to assemble models of different cancer types in vitro [1]. After formation, these in vitro models are able to mimic various properties and features of real solid tumors. Tumor spheroids can be formed exclusively of cancer cells (homotypic spheroids) or of cancer cells with other cell types (heterotypic spheroids) such as fibroblasts, endothelial cell, or immune cells [1].

Spheroid size and complexity depend on the growth kinetics of individual cell types, cell density during seeding, duration of culture, and spatial limitations, such as the diameter of culture wells [23]. Spheroids can be well-organized, round-shaped, or irregular-shaped aggregates of cells resembling masses or clusters of grapes (Fig. 1) [24].

Similar to solid tumors, the internal structure of spheroids is composed of different cell layers [1, 25]. Normally there are three main layers in spheroids: an outer layer composed of highly proliferating and migratory cells, senescent cells in the middle layer, and necrotic cells in the core layer (Fig. 2) [1, 26]. The peripheral cells closely resemble the in vivo environment of actively proliferating tumor cells next to capillaries, while distant inner cells stay quiescent or die through necrosis and apoptosis [6]. The outer surface of well-formed tumor spheroids is quite smooth, and it is difficult to distinguish individual cells [27]. The high proliferation rate of cells in the spheroid periphery can be explained by their easier access to oxygen and nutrients [28]. The development of a necrotic core and senescent cell layer can be attributed to insufficient oxygen and nutrient supply [28, 29]. However, it is possible to control the formation of the spheroid's necrotic central area, as the necrosis starts only in bigger spheroids (>400 μm in diameter) [27, 30]. This is very important since particular spheroids can be developed to suit specific experiments.

Spheroids can replicate various inside conditions of in vivo tumors. Three-dimensional compact cell architecture, close cell-cell interactions, and junctions in spheroids decrease diffusion of various compounds (nutrients, oxygen, metabolites, etc.) creating various gradients (Fig. 2) [26]. Large tumor spheroids (>500 μm in diameter) display physiochemical gradients similar to micrometastases and small tumors, due to limited diffusion of CO_2, nutrients, metabolic waste, and soluble factors (cytokines, growth factors, and chemokines) [23, 31]. Hypoxia induced by O_2 deficiency triggers changes in gene expression, promoting aerobic glycolysis and lactic acid production to obtain energy [23, 32]. This process is known as the Warburg effect [33]. During this process, lactate accumulates inside of spheroid and acidifies the extracellular space by 0.6 pH units (to 6.5–7.2) [23, 28, 33], which is also common in tumors in vivo. Additionally,

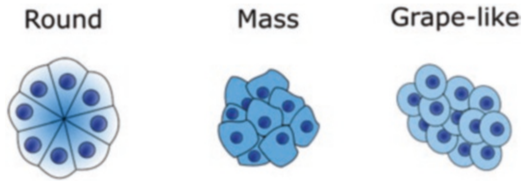

Fig. 1 Different shapes of tumor spheroids

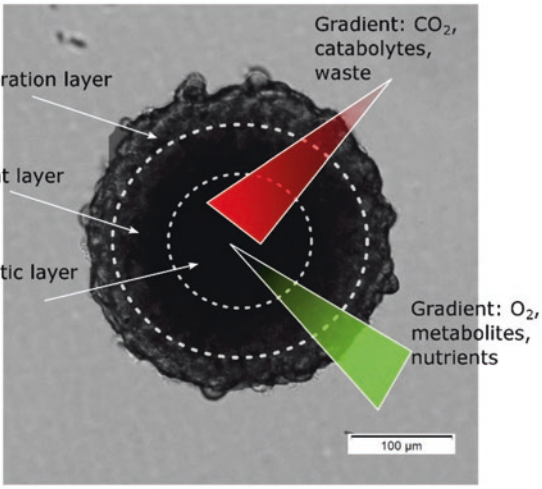
Gradient: CO_2, catabolytes, waste
Proliferation layer
Senescent layer
Necrotic layer
Gradient: O_2, metabolites, nutrients
100 µm

Fig. 2 The structure of pancreatic cancer cell (MIA PACA-2) spheroid. Due to the compact architecture of tumor cells and cell-cell contact, the concentration of oxygen, nutrients, and metabolites decreases toward inner layers of a spheroid. In addition, the concentration of carbon dioxide, catabolites, and waste increases toward inner layers, increasing the rate of cell death and the diameter of the necrotic area

Table 1 Main features of tumor cells in monolayer, spheroids, and in vivo tumors

Features	Cell monolayer	Spheroids	In vivo tumor
Spatial restriction of cells	Yes	No	No
Concentration gradient of O_2, nutrients, and metabolic waste	No	Yes	Yes
Cell heterogeneity	No	Yes	Yes
Hypoxic core	No	Yes	Yes
Biological zones – proliferative, senescent, necrotic	No	Yes	Yes
Glucose flux rate	Low	High	High
Gene expression profile	Different	Similar	Similar
Complex cell architecture	No	Yes	Yes
ECM	No	Yes	Yes

metabolic waste buildup forms in inner layers of spheroid due to the decreased outward diffusion and increases the necrotic death of the cells [23].

Cells within tumor spheroids deposit extracellular matrix (ECM) constituents such as collagen, laminin, fibronectin, tenascin, and other components that are embedded in a gel of glycosaminoglycans and proteoglycans, while monolayer cultures do not produce these elements or produce them in very small quantities [1, 27, 29, 34]. However, the composition of ECM may be different in tumors, spheroids, and monolayer cultures [35]. The polysaccharide gel is involved in cell proliferation, cell differentiation, cell recognition, and tumor cell invasion and metastasis [29]. Some data demonstrate that tumor spheroids produce similar or the same quantities of ECM constituents compared to xenograft tumors from the same cell lines [29]. Different cell types synthesize ECM constituents in xenografts and spheroids. In tumors, fibroblasts produce ECM macromolecules, and the tumor cell might regulate the synthesis to generate a favorable environment for its own growth, whereas in spheroids the tumor cells have to produce the constituents of the ECM by themselves in order to form multicellular arrangements [29]. This microenvironment acts as a regulating factor influencing cell proliferation, differentiation, and tumor growth [36]. In addition, it closely mimics the physical barriers found in real solid tumors, which decrease the free penetration of drugs through the whole mass [1, 36].

Available data show that three-dimensional tumor spheroids resemble the morphology of in vivo tumors much closely rather than monolayer cultures of the same cancer cells.

2.2 3D Culture Comparison to 2D Monolayer Cultures

Available literature shows that most cancer and tumor biological studies are based on two-dimensional (2D) monolayer cell models [37, 38]. Traditional 2D models can be effectively applied for explaining various cancer cell behaviors and interpreting possible mechanisms. However, 2D models cannot effectively mimic the interactions between cells-cells and cells-ECMs of real physiological tissues, due to insufficient structural, mechanical, and biochemical attributions. In most cases, cells in a 3D environment are exposed to other cells or ECMs but in a 2D model are often limited to exposure to fluid, intermediate, and flat culture substrate [37].

Recent studies show that gene expression in 3D spheroids is more similar to real tumors [6]; therefore, a 3D modeling environment can affect or model different cancer cell behavior, such as cell differentiation, drug metabolism, gene expression, and protein synthesis, morphology, proliferation, and viability [39–42]. Cells in a 3D environment behave fundamentally different from cells in a monolayer culture (Table 1). For example, hepatocytes rapidly lose their normal phenotype after they are taken out of the body and put in 2D cell culture, but this loss can be attenuated or even reversed by 3D culturing methodology [43, 44]. Additionally, multipotent mesenchymal stromal cell-derived hepatocytes maintain their key functions, such as albumin and urea synthesis, ammonia, and drug clearance better in a 3D environment compared to 2D monolayer model [45]. Also, oncogenic signals resemble gene expression profiles of orthotopic in vivo models and spontaneous clinical human cancers in 3D model, but not in 2D model [39]. Similar to real human tumors, 3D spheroids are composed of cells with different phenotypes (proliferating, nonproliferating, necrotic). Cellular heterogeneity within these tumor models caused by mass transport limitations resembles multiple phenotypes of cells found in solid epithelial tumors and is more realistic compared to homogeneity found in monolayer culture [46].

Many differences between 2D and spheroid culture are caused by different cell-cell and cell-matrix interactions, which are not represented very well in cell monolayer cultures [43]. A well-defined geometry, stromal elements, and ECM in 3D spheroids make them resemble micrometastases more authentically, compared to 2D cell monolayer. A complex 3D structure and cell-cell and cell-ECM interactions affect cellular RNA and protein expression, the distribution and functions of biomodulators, and also the penetration, binding, and bioactivity of therapeutic drugs and drug candidates [6]. Cells of the spheroid are more resistant to cytotoxic agents and radiotherapy than the same cells grown as monolayers [47, 48]. Increased resistance to cytotoxic agents can be addressed to multiple factors, such as physical penetration barrier, altered signaling pathways of a particular target, modulation of DNA damage and repair mechanisms, and in vivo-like distribution of biological response modifiers and survival signals, which are not so common to 2D monolayer cultures [6]. Due to pathophysiological gradients inside, cell-cell and cell-ECM interactions, spheroids are more versatile drug research model compared to monolayer cultures. For example, spheroids can be used in the study of therapeutic problems related to 3D metabolic and proliferative gradients [26]. Also, the spheroids are more valuable in the studies of tumor cell response to therapeutic agents; therefore, they can serve as excellent models for testing drug delivery systems [26].

In addition to morphology, gene expression, and cell-cell and cell-ECM interactions, 3D spheroids also closely resemble in vivo solid tumors in their growth dynamics [27]. Monolayer cultures grow exponentially, while 3D spheroid's growth, similar to in vivo tumors, can be characterized by an early exponential phase followed by a period of retarded growth (Fig. 3) [49]. The first phase does not depend on external factors, while the second depends on the size of the tumor spheroid and the decreasing diffusion of nutrients and O_2 in the interior of the spheroids. Many mathematical models were applied to demonstrate similarities between solid tumor and tumor spheroid growth. 3D spheroid growth curves, similar to solid tumors, were described with three successive phases – geometric, linear, and plateau (Fig. 3) [27, 49]. The geometric phase relates to early aggregation and proliferation of small spheroids, while the linear and plateau phases represent the development of a nonproliferative inner region and the formation of a necrotic center in the spheroids, respectively [27].

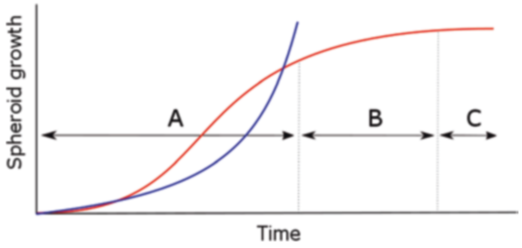

Fig. 3 Schematic comparison between growth of monolayer cell culture and the same cell spheroid. Monolayer cell culture (blue line) grows exponentially over time, while 3D spheroid (red line) growth is characterized by three phases – exponential (A), linear (B), and plateau (C)

Cell monolayer models are easier to manipulate and can be used in high-throughput screening. However, 2D cell models do not reflect the biological features of tumor tissues, therefore limiting its use in research of anticancer agents [50]. Tumor spheroids preserve the characteristics of original tumors (Table 1), making them more convenient in the research of tumor biology/physiology or effects of anticancer agents.

3 Types of Tumor Spheroids

3.1 Tumor Spheroid Cellular Heterogeneity

The concept of 3D spheres is based on the creation of spheroid structures in which cells are located in various layers. This structure mimics the physical and biochemical features of a solid tumor mass in vivo. Morphological analysis of 40 cancer cell lines (originating from glioblastoma, astrocytoma, Wilms' tumor, neuroblastoma, head and neck squamous cell carcinoma, melanoma, and lung, breast, colon, prostate, ovarian, hepatocellular, and pancreatic cancers) cultured as 3D spheroid models has been performed, and three distinct groups were distinguished according to the architecture of spheroid shapes: (1) tight spheroids, (2) compact aggregates, and (3) loose aggregates [51, 52].

On the other hand, tumor spheroids can be formed exclusively of cancer cells (homotypic spheroids) or of cancer cells cultured with other cell types (heterotypic spheroids) such as fibroblasts [1], endothelial cells [53], or immune cells [54]. As an example, homotypic spheroid model could be multicellular tumor spheroids (MCTS) that are microsized cellular aggregates, comprised exclusively of cancer cells grown on synthetic biomaterials that prevent cell adhesion to the substrate while maintaining high cell viability [55]. This type of spheroids can be obtained from single cell lines or even single cells (monocellular or homotypic spheroids) [56, 57]. However, 3D model formed only from cancer cells might be displaying different phenotypes due to homotypic cell-cell interaction, like those of quiescent versus proliferating cells depending upon the cell signaling molecules [58]. Thus, homotypic spheroids do not represent tumor microenvironment in vivo very well and could be useful only when it is enough to include only the interaction of the same types of cancer cells in tumor model.

Heterotypic spheroids are formed from cancer cells and somatic or other types of cells to more closely represent tumor structure and features in vivo. Like in solid tumor tissue, such spheroids consist of a heterogeneous mixture of cells, where cancer cells are surrounded by disorganized blood vessels formed by endothelial cells, lymphatic vessels, infiltrated immune cells (T cells, natural killers (NKs), and macrophages), adipocytes, fibroblasts, and MSCs [59, 60]. Different cell types in the solid tumor have the influence of tumor cell proliferation, invasion, metastasis formation, and drug response [61]. Thus, the best way to more closely mimic the tumor microenvironment heterogeneity and cancer cell-stromal cell (e.g., fibroblast, mesenchymal stromal cells, immune cells, endothelial cells, etc.) interaction in vitro is to create 3D heterotypic spheroids [62].

To improve insight into tumor development and chemotherapeutic approaches, it is most important to understand the interplay between specific tumor microenvironment (TME) components, the associated cellular communication processes, and resultant interactions of this network between cancer cells and the various tumor-associated cell populations. Focusing on heterotypic spheroid models on the molecular communication between stromal cells, mainly MSCs and cancer cells, and the cell-to-cell signaling role and its effect on chemotherapy efficiency could help more understand solid tumor's anticancer drug resistance and tumor's development process [63].

Moreover, heterotypic spheroids can be developed with different ratios of cancer to stromal cells (e.g., fibroblast), since cancer cell behavior and pharmaceutical therapeutic efficacy can be affected by the surrounding stroma [64, 65]. Jaganathan et al. [66] showed that 3D breast tumor models with different ratios of breast cancer cells and fibroblasts (50:50, 70:30, 30:70) determined different drug penetration into tumor spheroids: transport was less efficient into spheroids with more stroma. It has been found that tumor-stroma ratio could be a prognostic factor for cancer with higher stromal components contributing to poor prognosis and increased risk of relapse [67].

Furthermore, cell-cell direct physical contact, which is observed in 3D spheroids, is reported to play an important role in the mechanisms of cancer invasion through actions of adhesion molecules such as N-cadherin and extracellular matrix metalloproteinase inducer [68]. This physical communication and signaling pathways are observed in solid tumors in vivo [69]. For example, the combination of different cell types in spheroid leads to evaluate cell-cell and cell-matrix interaction in a 3D microenvironment where immune cells can infiltrate and migrate toward both tumor cells and fibroblasts, thereby improving the predictability of in vitro testing of immunotherapy agents. This study demonstrated that 3D heterotypic spheroid targeted by immunocytokine (interleukin-2 variant; IgG-IL2v) and tumor- or fibroblast-targeted T-cell bispecific antibody (TCB) are promising candidates for combination treatments in cancer immunotherapy [56]. The 3D heterotypic spheroid model is applied to research of drug targets and immune cell infiltration, activation, and cytotoxicity in response to novel cancer immunotherapy agents.

Three-dimensional cancer cell models represent the different types of cell heterogeneity which is also observed in vivo. Heterogeneous 3D model cultures that combine cancer and stromal cells more precisely represent one of the important features in 3D culture model – heterotypic cell interaction (cross talk) [70]. Among the various types of 3D models, we focus here on spherical cancer models that are classified into four groups: (1) multicellular tumor spheroids (from single-cell suspension), (2) tissue-derived tumorospheres (from cancer cells after partial dissociation of tumor tissues), (3) tumorospheres (from cancer stemlike cells), and (4) organotypic multicellular spheroids (from tumor tissue).

3.2 Multicellular Tumor Spheroids (MCTS)

MCTS (alternative names: spheroids, tumoroids, mixed spheroids, nodules, heterospheroids, organoids [22, 71–75]) is a model generated from single-cell suspension culture and more often is originated from cancer cell lines than tumor cell suspension from tumor tissue (Fig. 4a).

Not all cell lines are able to form compact MCTS [76]. To form MCTS, various methods can be used [76], but the main principle is the same – to provide conditions where adhesive forces between cells are stronger than for the substrate on which cells are plated. In this way, cells due to cell-cell adhesion process form a well-rounded spheroid structure.

The first MCTS was formed from cancer cells in monoculture to represent micrometastasis [77]. Later heterogeneous MCTS became rapidly very popular and led to the study of heterogeneous interaction in MCTS [23]. In addition to cancer cells, the most often used cell types for MCTS formation are immune cells, fibroblasts, and endothelial cells. Stromal cells could be added after MCTS are formed from cancer cells, and thus the stromal cell would be around the MCTS [78, 79], or MCTS could be formed from both cancer and stromal cells mixed in cell suspension at the beginning [70]. These different MCTS formation ways allow to observe MCTS growth, sensitivity to various compounds, and other processes that exist in the tumor.

MCTS can reach a 3-mm-diameter size and differ in compactness depending on the cancer cell line [80]. In larger MCTS, a necrotic core and viable edge are developed due to the growth factor deprivation, nutrients, and oxygen diffusion gradient, as it was described in a previous section. Moreover, the MCTS growth rate resembles a solid tumor

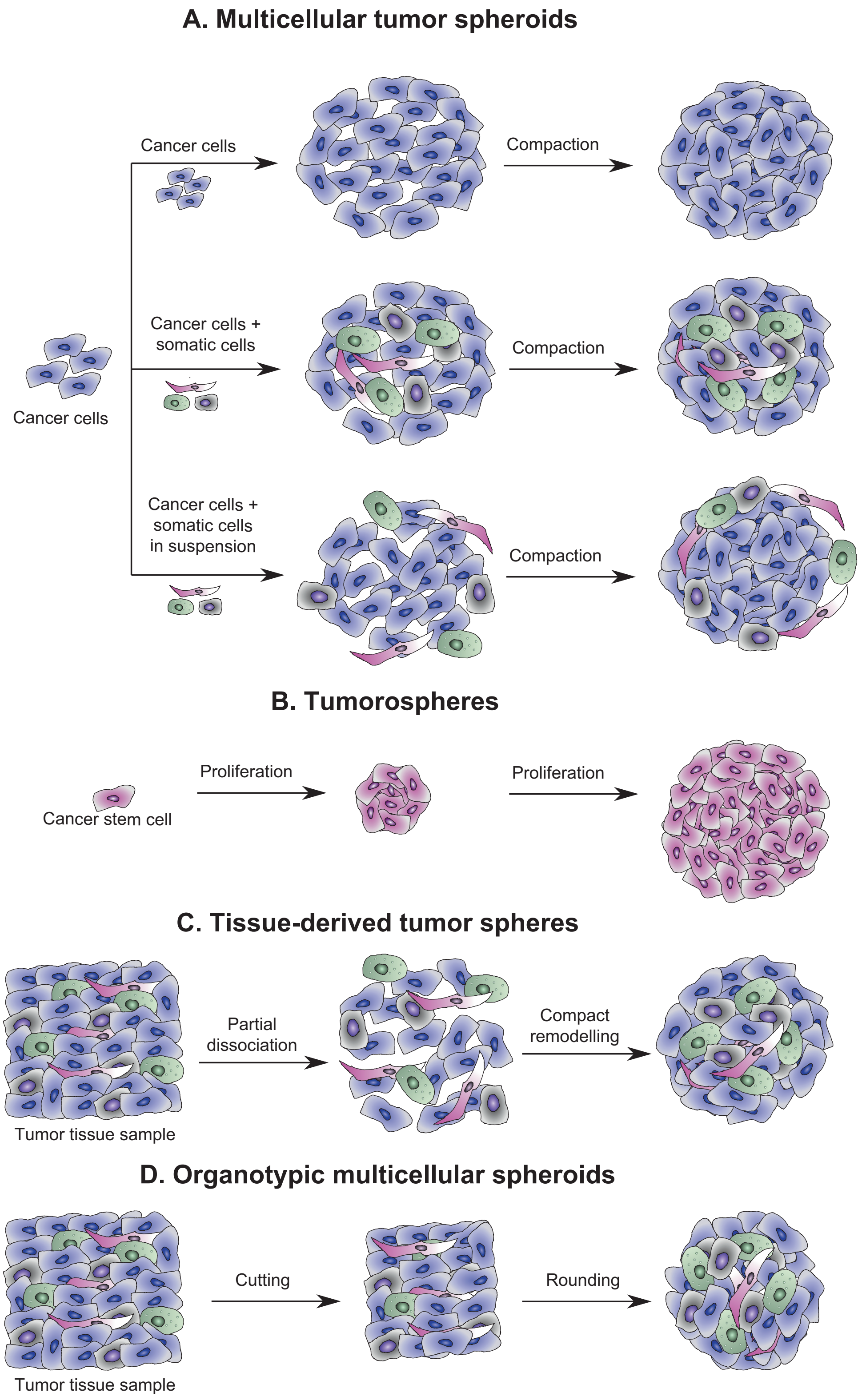
A. Multicellular tumor spheroids
Cancer cells
Cancer cells
Compaction
Cancer cells +
somatic cells
Compaction
Cancer cells +
somatic cells
in suspension
Compaction
B. Tumorospheres
Cancer stem cell
Proliferation
Proliferation
C. Tissue-derived tumor spheres
Tumor tissue sample
Partial
dissociation
Compact
remodelling
D. Organotypic multicellular spheroids
Tumor tissue sample
Cutting
Rounding

Fig. 4 Types of cancer cell spheroids. (**a**) Multicellular tumor spheroids derived from cell suspension from a cell line. (**b**) Tumorospheres are derived from one cancer cell by clonal proliferation. (**c**) Tissue-derived tumor spheres derived from tissue sample after partial tumor tissue dissociation. (**d**) Organotypic multicellular spheroids derived from cut tumor tissue without any sample dissociation

in vivo which is characterized in the early tumor growth stage in patients [81]. In later stages of tumor growth, the rate is slowed down due to the increased amount of necrotic cells [82].

MCTS is a much more accurate model for drug sensitivity or resistance behavior studies than cancer cell monolayer (2D) model. Experts recommend to use the MCTS model in major research for testing or screening anticancer drugs [83]. MCTS models are widely used for modeling and studying multidrug resistance due to different mechanisms: hypoxia, apoptosis inhibition, permeability, and cell cycle changes. Cancer cells are less sensitive to anticancer drugs in MCTS compared to 2D monolayer cell culture models [84, 85]. It indicates that MCTS culture is a convenient model to test various new drugs or treatment strategies and expect the same or very similar effect as in tumors. Cell sensitivity to some compounds or drugs is increased or decreased, but information received from the use of MCTS models can potentially provide more exact results of drug's/compound's activity in vivo.

3.3 Tumorospheres

Tumorospheres is a cancer stemlike cells (CSCs) which are grown in a serum-free medium supplemented with growth factors under nonadherent conditions and are one of the most commonly used cancer spheroid models [86]. In this way, tumorospheres are formed from tumor samples after mechanical and enzymatic dissociation into a single-cell suspension (Fig. 4b). Also, CSC culture could be performed from cell lines, or tumorospheres can be formed with circulating tumor cells (CTCs) from peripheral blood [87].

Knowledge about tumorospheres biology is low, but usually this model aims to study CSC more deeper but not to mimic tumor tissue [88]. It was observed that cells in CSC spheroids are organized hierarchically with self-renewal potential. To evaluate phenotypical changes of CSC is still impossible due to the lack of CSC cell surface markers, but these changes are evaluated by morphological and functional changes [89].

The CSC multi-lineage differentiation ability was observed in several studies by testing their ability to form heterogeneous tumorospheres. In the case of colorectal cancer, three types of CSC tumorospheres were detected [90]: (1) the rare CSCs that maintain growth of tumor/tumorospheres, (2) the tumor (or tumorospheres)-initiating cells (these cells possess limited self-renewal capacity in the later stages of tumorospheres growth), and (3) the latent subgroup of CSCs (these types of CSC were activating tumorospheres growth in the second or later cell passages) [91]. Another evidence of CSC tumorospheres plasticity (ability to change phenotype) was observed in the study which showed that CSC phenotypes are more stable in monolayer-growing cells than in tumorospheres, where phenotypes are changing due to cell interaction and microenvironment influence on cells [92].

Due to heterogeneity and cell plasticity properties, CSC tumorospheres is a useful model to study chemoresistance [93]. After cancer treatment, the remaining CSCs might cause tumor recurrence due to the cell plasticity and increased resistance to drugs. Tumorospheres have a low number of stromal cells, and they lack such microenvironment components as ECM, but it was observed that cancer cells within tumorospheres are able to produce some components of ECM and create a CSC favorable microenvironment [94]. Also, tumorospheres could be cultured with various medium supplements to create different CSC microenvironments (niches). For example, addition of stem cell factor (SCF) and granulocyte colony-stimulating factor (G-CSF) is creating niches like bone marrow where breast cancer metastases are formed [95].

3.4 Tissue-Derived Tumorospheres (TDTS)

TDTS are obtained from partly dissociated tumor tissue, and this model is a contrast to the MCTS model, where spheres are formed from single-cell suspension (Fig. 4c).

TDTS could be categorized into several subcategories: cancer tissue-originated spheroids (CTOs) [96], colospheres [97], and MARY-X spheroids [98]. CTOs are formed from tumor tissue by using mechanical and enzymatic dissociation and can be cultured in suspension without any extracellular matrix [96]. Colospheres is a TDTS model which is formed directly from colorectal cancer tissue by its dissociation [97, 99]. MARY-X is a spontaneously formed spheroid model from inflammatory breast cancer tissue and resembles tight, compact aggregates of cells. Such spheroids could be cultured up to 3 months [98].

TDTS models are obtained by dissociation of various types of tumor tissue including bladder, lung, breast, and prostate cancer [100]. TDTS are formed from tissue after partial dissociation. After all procedures, TDTS are composed only of cancer cells (without nonneoplastic cells) [101]. Thus, in TDTS, strong cell-cell interactions between carcinoma cells are observed, while the interaction between carcinoma and nonneoplastic cells might be lost due to partial tissue dissociation. Moreover, it was observed that especially E-cadherin (residual from tissue sample) has been involved in cell-cell interaction in TDTS models [101].

Due to such cell organization and interaction, and adhesion to each other, cells in TDTS models could avoid anoikis (programmed cell death) and remain viable for several weeks. A major TDTS feature that distinguishes them from other spheroids is their capacity to mimic some tumor microregions by the histological features, gene expression, mutations in various genes, and metastatic properties [101]. For example, MARY-X spheroids display internal lumen-like structures that were observed in in vivo conditions, but this phenomenon wasn't detected in the MCTS model [102]. These cells' properties in TDTS lead them to survive for a longer period and grow larger. TDTS models represent tumors in vivo, but they are not very suitable for transfection or chemosensitivity studies, as it was shown that TDTS were more sensitive to anticancer drugs than in vivo conditions [97].

3.5 Organotypic Multicellular Spheroids (OMS)

The OMS (alternative names: biopsy spheroids, fragment spheroids, organotypic spheroids, organotypic tumor spheroids, primary spheroids, spherules [76, 103–106]) is a 3D model that consists of ex vivo fragments of tumors without any fragment dissociation [107].

To get OMS model, the tumor fragment is cut into small pieces and incubated in a cell culture medium depending on cancer cell types from 2 to 18 days. Then fragments get round shape form and make OMS [106] (Fig. 4d). OMS could be cultured for several weeks. Among various in vitro 3D models, OMS spheres are the closest to in vivo tumor conditions, because all tumor fragment dissociation is used and all cell types and microenvironment components are maintained. Thus OMS biology is similar to the original tumor tissue with macrophages, vessels, fibers of collagen, and fibroblasts [9]. Some studies show that even long-term culturing of OMS did not change the cell properties and maintained cell stability compared to tumors observed in vivo [105].

OMS were used in studies of cancer cell chemosensitivity to anticancer drugs [51, 52, 108]. Cell resistance to anticancer drugs could be explained by cell heterogeneity in tumors and also in OMS. For example, tumor in vivo and OMS in vitro derived from glioblastoma demonstrated resistance to doxorubicin, cisplatin, and etoposide [108], and OMS from human mesothelioma showed resistance to cycloheximide [51]. A few radio-response studies have been also performed on human OMS glioblastoma. Radiation induces a low effect on glioblastoma OMS, which is observed also in in vivo studies, and this resistance may be related to vessel presence in glioblastoma tumor and OMS [109].

Thus, OMS model is useful to explore the new treatment strategies, because it is closest to the real tumors and the response effects in OMS and in patients are similar, and its does not loose tumorigenicity, even after cryopreservation [105].

Table 2 Advantages and disadvantages of commonly used spheroid formation techniques

Method	Advantages	Disadvantages
Magnetic 3D cell culturing	Suitable for forming both mono- and hetero-type spheroids Easy to handle Magnetic tools allow spheroid transferring between containers Spheroids are easily accessible Easy to adjust the spheroid size by seeding different number of cells It is possible to make many spheroids of the same type and size at the same time Spheroids can be made in a few days	Pre-coated low-adhesion plates and special magnetic nanoparticles are expensive Changing medium or spheroid transfer may affect spheroid integrity and is time-consuming
Liquid overlay (forced-floating)	No specialized equipment is needed Suitable for forming both mono- and hetero-type spheroids Spheroid production can be scaled up by using automatic techniques Requires a relatively low volume of medium and testing materials Spheroids are easily accessible Easy to adjust the spheroid size by seeding different number of cells Relatively simple and generally reproducible method	Pre-coated low-adhesion plates are expensive and coating plates is a time-consuming step Short storage time of the coated plates Changing medium or spheroid transfer may affect spheroid integrity and is time-consuming
Hanging drop	Easy to adjust the spheroid size by seeding different number of cells Relatively simple method Suitable for forming both mono- and hetero-type spheroids No need of coating the plates with substrates, as required in liquid overlay culture technique Spheroids show low variability in sizes Spheroids are easily accessible	The volume of the seeding suspension is generally limited and does not provide enough nutrients for a long-term culture Changing medium or spheroid transfer may affect spheroid integrity and is time-consuming Not suitable for high-scale application

(continued)

Table 2 (continued)

Method	Advantages	Disadvantages
Agitation-based methods	Allow long-term culture Suitable for large-scale production Easy to culture cells The motion of culture assists nutrient transport and waste removal mimicking transport in vivo Spheroids are easily accessible	Difficult to control spheroid size Spheroids are nonuniform; thus, manual selection of similarly sized spheroids is mandatory before further assay The collision of the cells with the impeller and a turbulent flow may cause cell damage Specialized equipment and a large amount of culture medium are required
Microfluidics	Suitable for continuous production of highly controlled aggregates Very low reagent consumption Its microscale dimensions are compatible with those of many microstructures and environments native to in vivo systems	Cost of microfluidic devices

4 Tumor Spheroid Formation Techniques

Various techniques have been developed to form 3D cell cultures. They can be classified into two categories: scaffold-free and scaffold-based methods [110]. Scaffold-free methods include magnetic 3D cell culturing (magnetic levitation and magnetic bioprinting), liquid overlay (forced-floating) method, hanging drop, agitation-based methods (spinner flask and rotational culture systems), and microfluidics.

Eligible spheroid formation techniques should be easy to handle, time- and cost-effective, and reproducible. However, there is no perfect method for 3D cell culturing, and all of them have their advantages and disadvantages (Table 2).

4.1 Magnetic 3D Cell Culturing

Using this technique, a cell suspension is incubated with nanoparticles composed of iron, gold, and cell-adhesive peptides (e.g., poly-*L*-lysine) [111]. Nanoparticles electrostatically attach to the cell membranes via cell-adhesive peptides, and the cells obtain magnetic properties [112]. Such magnetized cells are seeded into ultralow attachment multiwell plates and externally affected with a magnetic field to form spheroidal structures [111].

According to the position of the magnets, magnetic 3D cell culture can be classified into two groups: magnetic levitation and magnetic bioprinting (Fig. 5) [113]. Using magnetic levitation method, magnetic drive is placed on the multiwell plate and covered with a lid (the magnets are positioned above the cell suspension). In this way, magnetic forces cause cell levitation and cell-to-cell interaction, which results in spheroid formation [111]. Meanwhile, using bioprinting technique, multiwell plates with seeded cells are placed directly on the top of the magnetic drive (the magnets are positioned under the cell suspension). On the contrary to magnetic levitation, using bioprinting technique, cells start to aggregate at the bottom of the multiwell plate [113].

This is a simple method that does not require a special equipment. Nanoparticles used in these methods must be biocompatible without any effect on cell functions and viability. After magnetization, nanoparticles remain attached to the cells for at most 7–8 days [113]. Using magnetic pens, spheroids can be picked and transferred to other containers [114].

4.2 Liquid Overlay (Forced-Floating) Method

It is a relatively simple and low-cost method based on the cell culturing above nonadhesive surfaces that prevent cells from adhesion to the vessel surface [115]. As a result, forced-floating cells start to attach to each other, thus forming 3D cell aggregates [115]. As nonadhesive surfaces, thin layers of agar/agarose, poly-hydroxyethyl methacrylate (pHEMA), or Matrigel can be used [114].

The most widely used substances are agar and agarose because of their low cost and easy manipulation [116]. In order to prepare the plates, these substances are dissolved in the water or serum-free medium and sterilized. After that, the bottom of the plate is covered with a thin layer of a prepared solution and is kept at room temperature for a few minutes until the solution jellifies. Prepared plates cannot be stored for a long time because water evaporation results in disruption of the coating [116]. It is recommended to use fresh agar or agarose solutions because before usage they must be heated, and heat may reduce the stability of substances or change the concentration of the solution. The formation of spheroids usually takes 1–3 days for most cell lines [116]. It is important to mention that agar influences the growth of fibroblasts because of sulfate groups in its structure [117].

Besides agar or agarose, pHEMA solution in 95% ethanol can be used, as well. Sterilization of pHEMA solution is performed by filtering the solution through 0.22 μm pore mem-

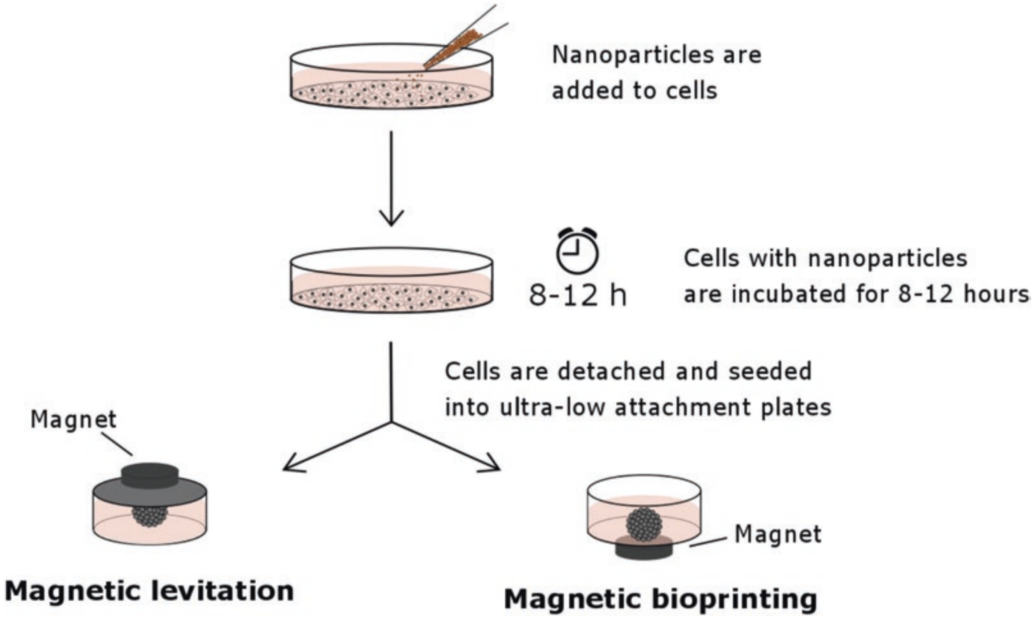
Nanoparticles are added to cells
8-12 h
Cells with nanoparticles are incubated for 8-12 hours
Cells are detached and seeded into ultra-low attachment plates
Magnet
Magnet
Magnetic levitation
Magnetic bioprinting

Fig. 5 Spheroid formation using magnetic 3D cell culturing

brane filters. Such a solution can be stored at 4 °C for 2 months. However, the preparation of this solution is a time-consuming process because it takes a few hours to dissolve pHEMA and the evaporation of ethanol takes around 48 h at 37 °C [116].

Also, commercially available pre-coated plates can be used to reduce the time of preparation, but it significantly increases the expenses.

In order to obtain round-shaped spheroids, it is important to choose plates with U- or V-shaped bottoms. It was observed that spheroids formed in plates with flat surfaces tend to be elongated and disorganized and have an irregular shape [65]. Also, it was observed that horizontal stirring or centrifugation enhances spheroid formation by increasing physical contact among cells [65]. Some cell lines are unable to form dense cellular aggregates; thus, various additives (e.g., methylcellulose) or extracellular matrix components (e.g., fibronectin, laminin, collagen) may be added to the cell suspension. Furthermore, in order to better represent tumor, cancer cells can be mixed with fibroblasts [65]. This also facilitates spheroid formation. It is important to mention that some cell lines do not form compact spheroids. They accumulate next to each other by forming only loose cell aggregates. Spheroid size using this method can be easily adjusted by modifying the number of seeded cells [118].

4.3 Hanging Drop Method

Hanging drop method is a relatively simple technique based on the surface tension to hang small cell suspension droplets on the underside of a tissue culture dish lid [119]. Due to the gravitation force, the cells accumulate at the apex of the droplet (at liquid-air interface) and aggregate into a spheroid [36].

When forming spheroids using this method, a small amount (typically 20–50 μL) of cell suspension is pipetted into the wells of a special tray (Fig. 6a). The cell suspension forms hanging drops that stay in place because of surface tension. At the tip of the drop, accumulated cells form a spheroid (Fig. 6b) [120].

This method does not require any special equipment [121]. Also, in this technique, any matrices or scaffolds, which may affect 3D structures, are not used [120]. Hanging drop method is suitable for cocultivation by mixing cell populations [121]. When the plate is placed directly in an incubator, the medium tends to evaporate fast. Therefore, it is recommended to place the plate in a container with a water reservoir to maintain moisture levels and prevent drying-out [122]. Also, the volume of the test medium is limited to not more than 50 μL since the surface tension cannot keep attached larger volumes [120].

4.4 Agitation-Based Methods

Using the agitation-based methods, cell suspension is kept in motion in special containers by gently stirring in spinner flask bioreactors (spinners) or due to the rotation of the rotational culture systems (rotating wall bioreactors) (Fig. 7). This increases cell-to-cell interactions and prevents cell attachment to the container wall and sedimentation [120, 123].

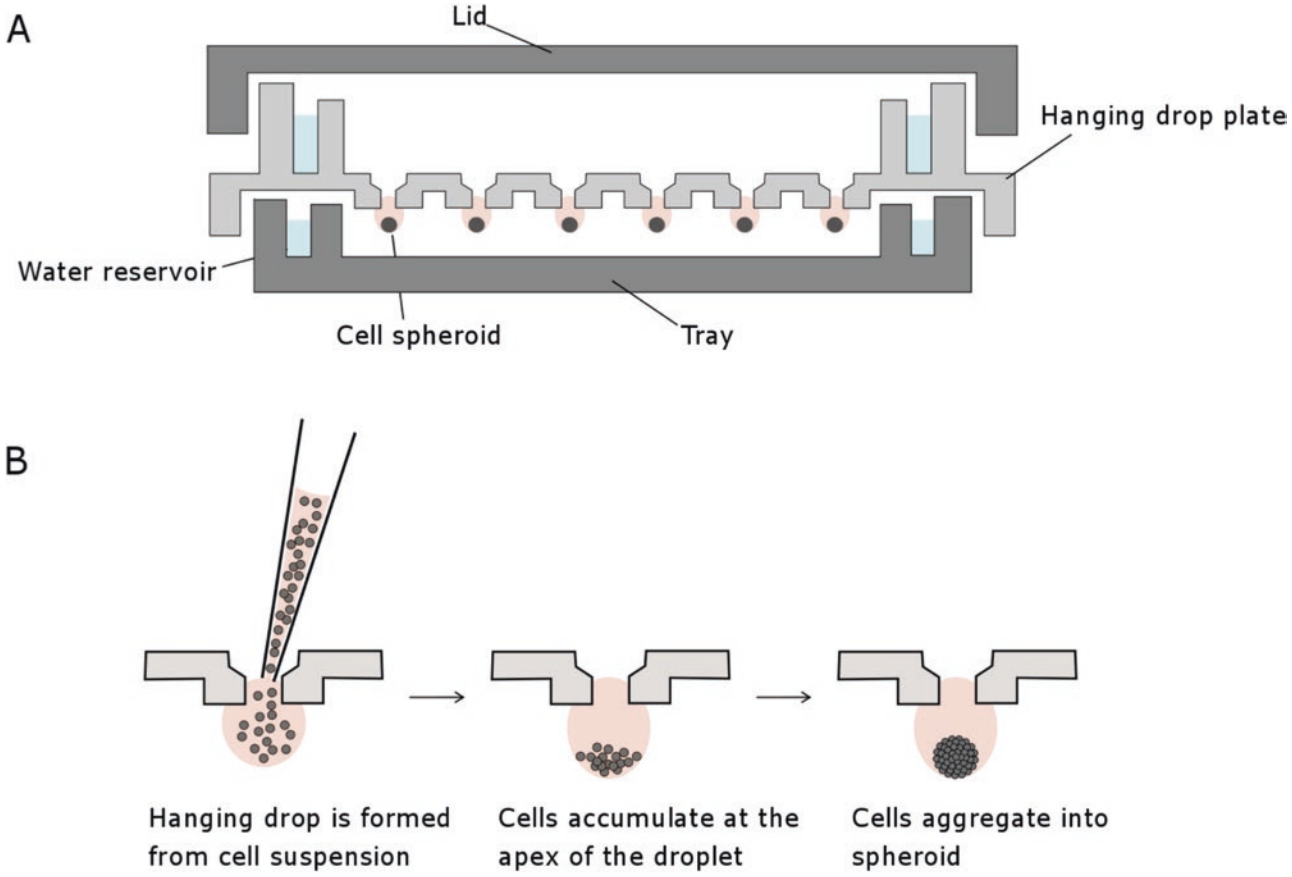
A
Lid
Hanging drop plate
Water reservoir
Cell spheroid
Tray
B
Hanging drop is formed from cell suspension
Cells accumulate at the apex of the droplet
Cells aggregate into spheroid

Fig. 6 Spheroid formation using hanging drop method: (**a**) schematic of hanging drop plate; (**b**) steps of the spheroid formation procedure

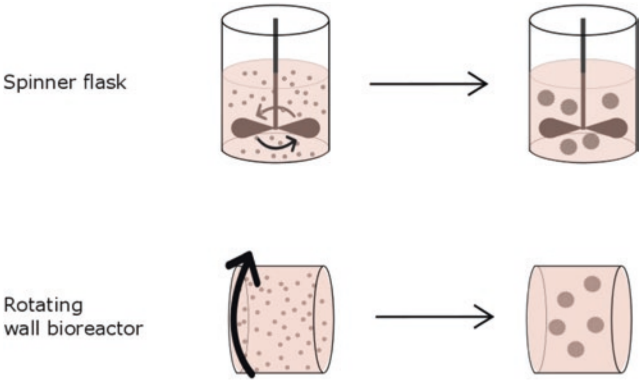
Spinner flask
Rotating wall bioreactor

Fig. 7 Spheroid formation using agitation-based methods: spinner flask bioreactors and rotating wall bioreactors

These methods are not recommended for drug screening because they do not mimic the in vivo microenvironment and require a big volume of cell medium. Depending on the size of bioreactor, approximately 100–300 mL of cell medium may be required [123]. In order to use them for drug screening, spheroids have to be retrieved from the devices and placed into multiwell plates or other cell culture platforms [123]. Also, spheroids formed using these methods are non-uniform; thus, a manual selection of similar-sized spheroids is required for subsequent analysis [123]. To avoid this step, spheroids may be primarily be formed using the liquid overlay method and then transferred to the bioreactor for the culturing [120].

4.4.1 Spinner Flask Bioreactors (Spinners)

Spinner flask bioreactors consist of a container where the cell suspension is placed and a stirring element continuously mixes the cell suspension. Due to the dynamic high-speed stirring, the cells aggregate to each other and form spherical structures [120]. Depending on the size of the bioreactor, spheroid production can be scaled up to produce large yields of spheroids [120].

However, using this method, cells may be damaged due to their collision with the impeller and created turbulent flow. This may affect cell physiology, proliferation, metabolism, and spheroid formation [124]. On the other hand, the flow of fluids improves the transport of nutrients to cells and the removal of waste products [120].

4.4.2 Rotational Culture Systems

The method is very similar to the spinner flask technique. In this approach, instead of using a tank with a rotor, the bioreactor itself rotates about a horizontal axis. This constant rota-

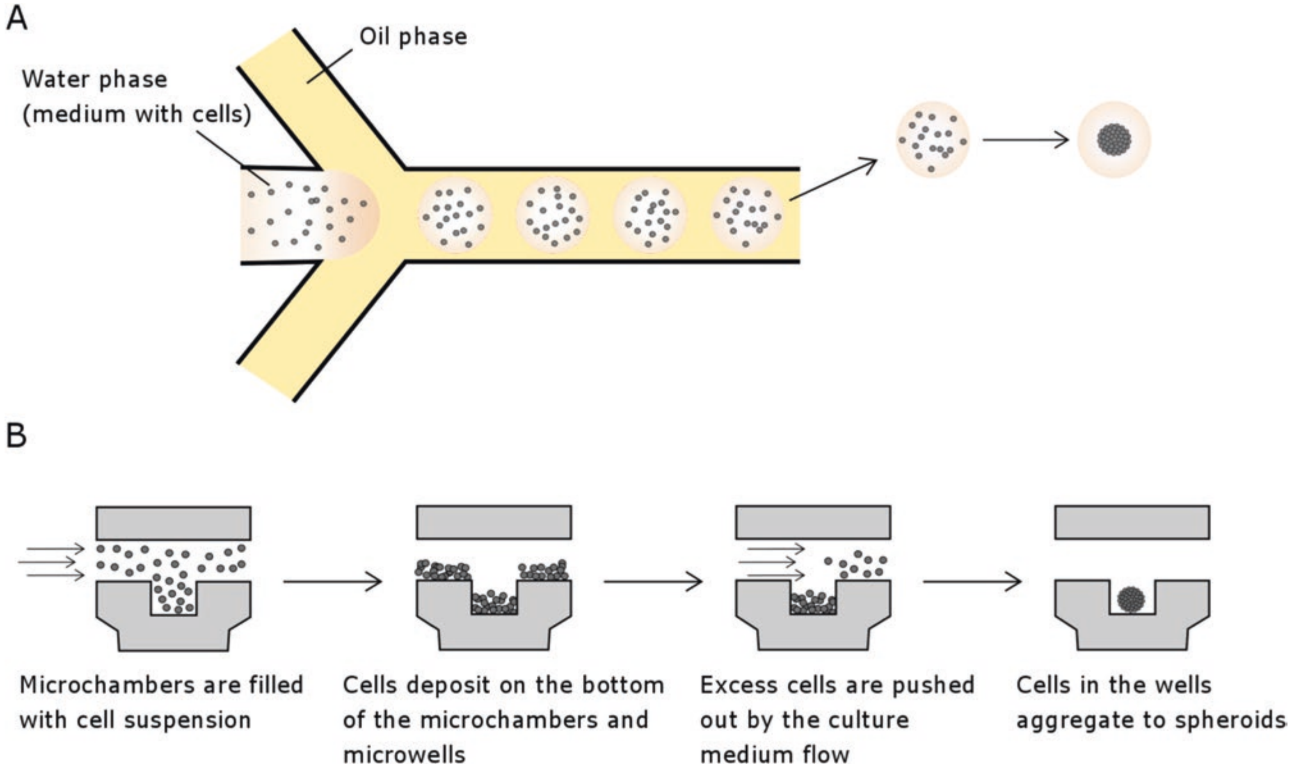
A
Oil phase
Water phase
(medium with cells)
B
Microchambers are filled with cell suspension
Cells deposit on the bottom of the microchambers and microwells
Excess cells are pushed out by the culture medium flow
Cells in the wells aggregate to spheroids

Fig. 8 Application of microfluidics in spheroid generation: (**a**) emulsion-based spheroid formation; (**b**) microwell-based spheroid formation

tion prevents cells from adhesion to the tank walls and creates low sheer force. Rotational culture systems are also suitable for large-scale production of spheroids.

4.5 Microfluidic Cell Culture Platforms

Microfluidics is a technology of using a small volume of fluids in microchannels [123]. The most common microfluidic spheroid formation techniques are emulsion-based spheroid formation and microwell-based spheroid formation [123].

Using emulsion-based spheroid formation method, usually cell suspension in oil is generated (Fig. 8a) [123]. When applying the double-emulsion technique, cell suspension in oil in culture medium or cell suspension in hydrogel in the culture medium is formed [123].

Using microwells, spheroids are formed by filling the microchambers of the device with the cell suspension. The cells enter the microwells and deposit on the bottom, and due to cell-cell interactions, they aggregate to each other by forming spheroid structures. Those cells that did not enter the microwells are pushed out so that they would not clog the microchannels (Fig. 8b) [123].

Microfluidics is suitable for high-throughput drug screening. Also, it requires minimal volumes of reagents. One of the main limitations of this method is difficulty to retrieve formed spheroids.

4.6 Scaffold-Based Culture Systems

In this method, natural or synthetic polymers are used to mimic natural extracellular matrix and serve as physical support matrices on which cells aggregate, differentiate, and proliferate [93, 120, 125]. Cells can migrate in an interstitial space between the fibers of these scaffolds, and by their division and binding to one another, they form 3D cell cultures [110, 120].

The 3D cell culture formation using scaffolds involves either the encapsulation of cells into a base material by mixing cells with scaffold monomers in a liquid state (Fig. 9a) or the preparation of microwells by pouring liquid precursor solutions into micro-molds and, after the formation of hydrogel, seeding them with cells (Fig. 9b) [126].

However, according to studies, scaffold constituents may affect spheroid growth [114]. Natural polymers are based on various extracellular matrix components and include hydrogels, such as collagen, laminin, chitosan, hyaluronic acid, agar, fibrin, or silk fibroin protein [93, 125]. The advantage of natural polymers is high biocompatibility [110, 120]. On the other hand, biodegradation in cell culturing is an unwanted characteristic as it may affect cell growth in unknown ways [110]. Also, scaffolds made from natural materials are highly variable, and their mechanical properties are limited [110]. One of the main commercially available natural polymers used for scaffold preparation is Matrigel. Matrigel consists of collagen IV,

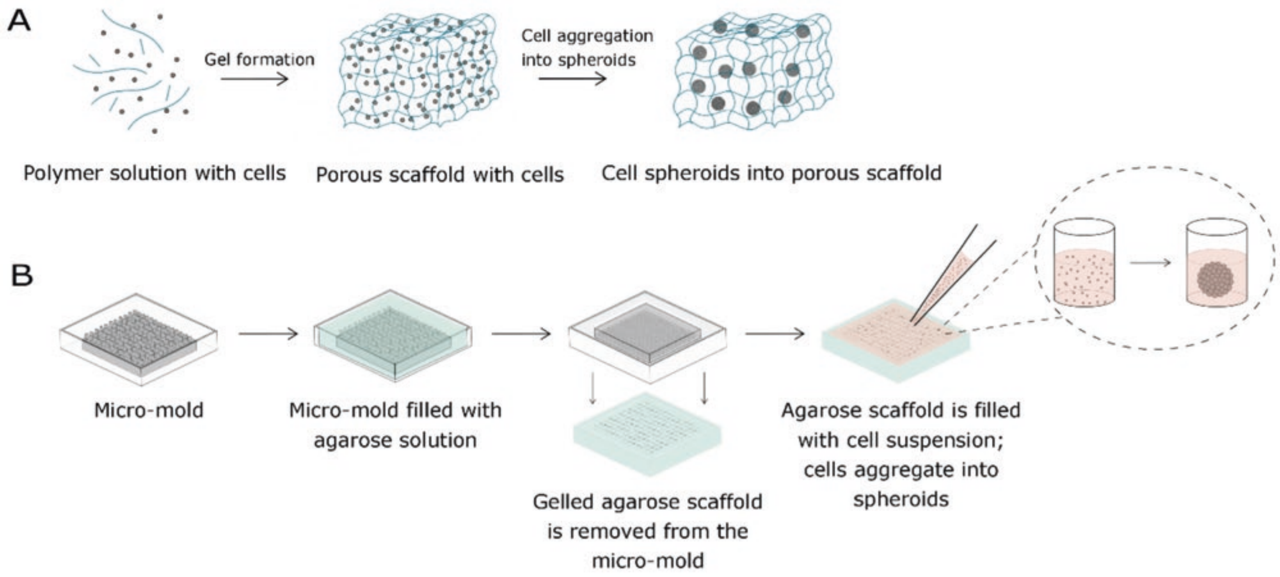
A
Gel formation
Cell aggregation into spheroids
Polymer solution with cells
Porous scaffold with cells
Cell spheroids into porous scaffold
B
Micro-mold
Micro-mold filled with agarose solution
Gelled agarose scaffold is removed from the micro-mold
Agarose scaffold is filled with cell suspension; cells aggregate into spheroids

Fig. 9 Spheroid formation using scaffold-based methods: (**a**) spheroid generation by cell encapsulation into porous matrices; (**b**) spheroid generation using micro-molds

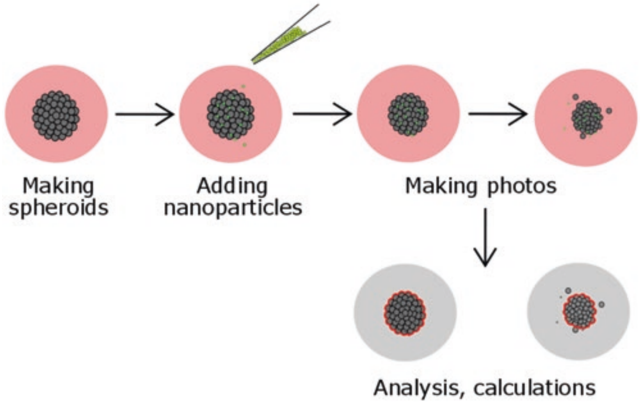
Making spheroids
Adding nanoparticles
Making photos
Analysis, calculations

Fig. 10 Evaluation of nanoparticle toxicity in 3D cultures according to spheroid size change by using microscopy

laminin, perlecan, entactin, matrix metalloproteinase-2, and growth factors that are obtained from Engelbreth-Holm-Swarm mouse tumor basement membranes [127]. This polymer mimics in vivo microenvironment and allows cell-extracellular matrix signaling, natural cell differentiation, and spheroid growth.

Synthetic materials, such as polymers, self-assembled peptides, titanium, and bioactive glasses, are favorable because of their defined chemical composition, adjustable mechanical properties, and reproducibility [110, 125]. On the other hand, synthetic polymers may provide not enough sites for cell adhesion and are less biocompatible [110]. Also, in order to better mimic natural cellular conditions, these polymers may require coating with extracellular matrix proteins [110].

Scaffolds can be distinguished into hydrogels and solid-state scaffolds [125]. Hydrogels are porous polymeric materials with high water content [120, 128]. These microstructures are formed of physically or chemically cross-linked materials, such as hyaluronic acid, collagen, laminin, alginate, agarose, or polyethylene glycol [110, 128]. Their mechanical properties are similar to soft tissues [126]. Hydrogels can be used to produce cell microcarriers that enable the formation of small, up to 500 μM diameter, spheroids using a small volume of medium [120].

Solid-state scaffolds are better reproducible, and their chemical and structural surface features can be easier manipulated [125, 129].

In order to isolate spheroids from scaffolds, they can be enzymatically, mechanically, or chemically disrupted or photodegraded [126, 128]. However, this may affect spheroid integrity [128]. Some hydrogels are temperature-sensitive and may be liquified by changing temperature [128].

5 Methods for Screening Nanoparticles in Spheroids

Nanoparticles are typically tested in cancer cell 2D cultures, as this model is relatively simple and cheap. After in vitro experiments, in most cases, tests are performed in animals. However, in 2010, the European Commission has proposed to replace animals with other models wherever possible, and researchers are widely discussing this request and trying to fulfill it [130]. In order to replace animal models, scientist are developing more sophisticated strategies compared to conventional 2D models that could help to mimic physiological properties of in vivo systems [131, 132]. Despite the advances in 3D systems, they still possess many limitations, especially in assessing the toxicity of nanoparticles [131].

Tumor spheroids are one of the most popular models of 3D cell cultures used as a more advanced system for testing the anticancer effect of nanoparticles in vitro [133].

5.1 Methods for Evaluating Nanoparticle Toxicity in Spheroids

Most often spheroids are used as the model for *nanoparticle cytotoxicity*. One of the most often used methods to estimate the potential effect of tested substances on spheroid growth is to measure the size of spheroids during experiment and compare it with the control (Fig. 10) [134–136]. Spheroid pictures could be taken on any light microscope, and later obtained images might be analyzed by using Image J software (NIH, Bethesda, Maryland, USA) or any other software, also MATLAB program, or different macros [137]. In the case when spheroids are made from fluorescent-labeled cells, their size change could be monitored using a fluorescence microscopy [138].

This is a very simple method that allows noninvasive monitoring of spheroid size and morphology changes over time and to select the endpoint of the experiment at the most convenient time for investigator. In addition, the researcher may employ any other additional method to test the spheroid final status (test the cell viability, analyze histology of spheroid, etc.).

In most cases, spheroids are treated when they reach 300–400 μm [139] or 250–300 μm in diameter [135]. Spheroids could be incubated with nanoparticles for different duration: usually they are treated for 24, 48, or 72 h [136, 139, 140] and sometimes for 4 days [134], 7 days [141, 142], or even 14 days [138] or 30 days [136].

If spheroids are imaged in the same dish where they were produced, some issues could be related to the picture quality. It was observed that images are of better quality when spheroids are imaged in ultralow attachment 96-well plates compared to 96-well hanging drop plates [141]. In some cases, spheroids need to be transferred to different plates for imaging, and there is also a risk of probability to lose them by following this procedure or changing the media. This may affect the results due to the remaining low number of spheroids in some groups [119]. Indeed, as experiments in spheroids are more complicated than in conventional 2D cultures, scientists often use a limited number of spheroids per group. Mostly group consists from 3 to 5 spheroids [139], only sometimes ≥10 spheroids are used [134], and more often the number of spheroids in one group is not mentioned at all.

However, toxicity evaluation in spheroids by microscopy has several disadvantages. Spheroids can become very loose or disintegrate during the experiment, and then analysis becomes quite complicated. Researchers also noticed that the medium change during experiment can also influence the results [134]. Indeed, the evaluation of cytotoxicity by measuring the size of spheroid is questionable since it was found that spheroid size is not necessarily related to DNA content [143].

Also, the effects of nanoparticles on spheroids are quite often evaluated using *cell viability assays*.

For testing nanoparticle toxicity in cells, lactate dehydrogenase release (LDH) [144], 3-(4,5-dimethylthiazol-2-yl)-2,5-diphenyltetrazolium bromide (MTT) [145], and MTS assay [146] are the most widely used methods [147]. Most of them are also applied to test cell viability in spheroids, with only some modifications.

For example, in the case of MTT assay application in spheroids, scientists extend incubation with MTT for up to 1 day (instead of 4 h) [141]. In general, the procedure is the same: 5 mg/mL MTT solution is applied to spheroids at the ratio of 1:100, and after the formazan crystals are formed, they are dissolved in dimethyl sulfoxide. The absorbance is measured at 570 nm and results are calculated using Hill formula (Fig. 11a). This method allows to evaluate cell viability in spheroids only once, usually at the end of the experiment. Thus many different commercial kits were designed (e.g., CellTiter Glo®3D Cell Viability assay, Perfecta3D-Cell viability assay) to perform cell viability studies in spheroids at different time points, up to 72 h or even longer incubation period (Fig. 11b).

Also it is possible to measure cell viability in spheroids by trypan blue assay [148]. In this case, at the end of experiment or separate treatments, spheroids are disrupted and washed, then trypan blue solution is added, and cells are counted by conventional methods in counting chambers or using automated technique [136] (Fig. 11c).

Similarly, LDH release can be determined in spheroids, e.g., using colorimetric assays. The spheroids are treated with a special substrate, and the color that appears after incubation is proportional to the number of cells with disrupted cellular membrane [149]. The mathematical evaluation is done by measuring the absorption [140] (Fig. 11d).

Effects of nanoparticles on mitochondrial membrane potential (MMP) and cell viability could be evaluated by using specific staining with dyes such as MitoTracker® Red CMXRos [140] and analyzing the fluorescence intensity of spheroids. Cell viability in spheroids is also measured by caspase activity assay kits [150]. Specific gene regulatory changes related to potential toxicity of nanoparticles could be analyzed [140]. In some cases, the release of chemokines, cytokines, and growth factors are evaluated, e.g., in 3D cul-

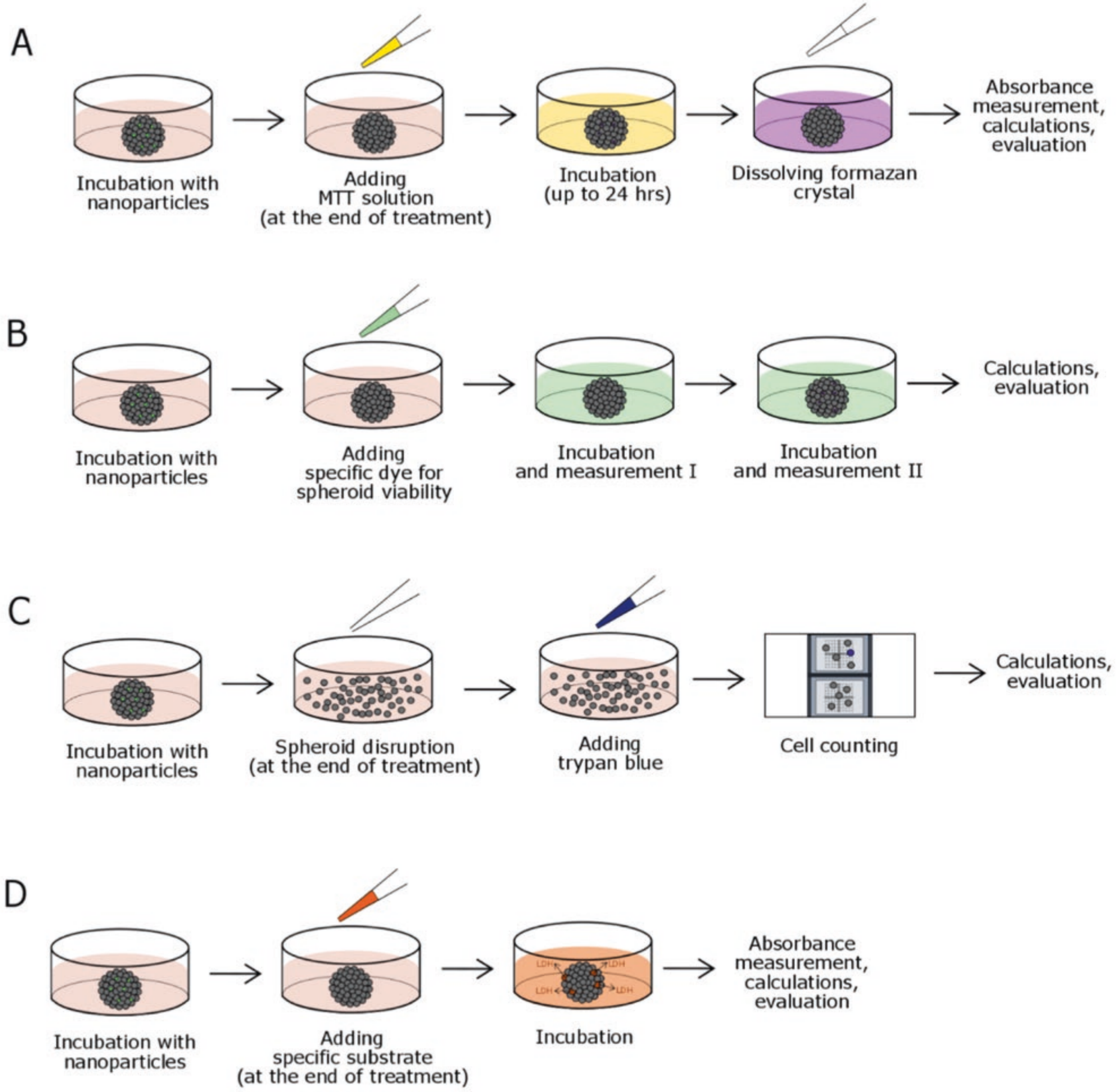
A
Incubation with nanoparticles
Adding MTT solution (at the end of treatment)
Incubation (up to 24 hrs)
Dissolving formazan crystal
Absorbance measurement, calculations, evaluation
B
Incubation with nanoparticles
Adding specific dye for spheroid viability
Incubation and measurement I
Incubation and measurement II
Calculations, evaluation
C
Incubation with nanoparticles
Spheroid disruption (at the end of treatment)
Adding trypan blue
Cell counting
Calculations, evaluation
D
Incubation with nanoparticles
Adding specific substrate (at the end of treatment)
LDH
Incubation
Absorbance measurement, calculations, evaluation

Fig. 11 Main cell viability assays used for testing nanoparticle toxicity in spheroids. (**a**) MTT assay; (**b**) special commercial assay for testing cell viability in spheroids; (**c**) trypan blue assay; (**d**) LDH release assay

tures made from neural cells that produce lower levels of chemokines and cytokines compared to immune cells [140]. However, Leite et al. after analysis of chemokine and cytokine release revealed that nanoparticles tested in neural spheroids do not necessarily induce direct toxicity but are capable to unbalance cell physiology. This means that, in addition to cell viability tests or morphology analysis, additional studies on the secreted factors or gene expression are recommended. It is known that physicochemical reactivity of some nanoparticles, especially metal ones, could lead to the formation of free radicals or reactive oxygen species (ROS) [151]. Thus researchers also test ROS production in spheroids after their treatment.

Immunohistochemistry is an option to analyze *spheroid morphology* [139], especially the bigger ones, and sometimes is also used to test nanoparticle penetration inside them [19, 150]. In most cases after the treatment or at the end of experiment, spheroids are fixed, washed with ethanol, and embedded in agarose gel. Then they are embedded in paraffin, cut into slices (usually 3–4 μm), deparaffinized, dehydrated, and stained with hematoxylin and eosin or specific antibodies for imaging. In some cases, cryosections of spheroids could be made (about 10 μm) [150]. This method enables to analyze the protein expression in the spheroid, thus providing a better understanding of the mechanisms of the tested nanoparticles. Indeed, the process of making spheroid sections requires special skills and is not appropriate in such cases when spheroids are very small or loose.

The morphology changes of spheroids are also analyzed by electron microscopy [118, 140]. This method allows to evaluate the complex structure of 3D cultures, to establish structural features, e.g., the spatial organization of cells. However, both transmission and scanning electron microscopy (TEM and SEM) require even more technical skills than the immunohistochemistry method described above and are therefore used less frequently. Indeed, there are some very detailed protocols specifically designed for spheroid imaging by electron microscopy, with recommendations and tips for researchers [152].

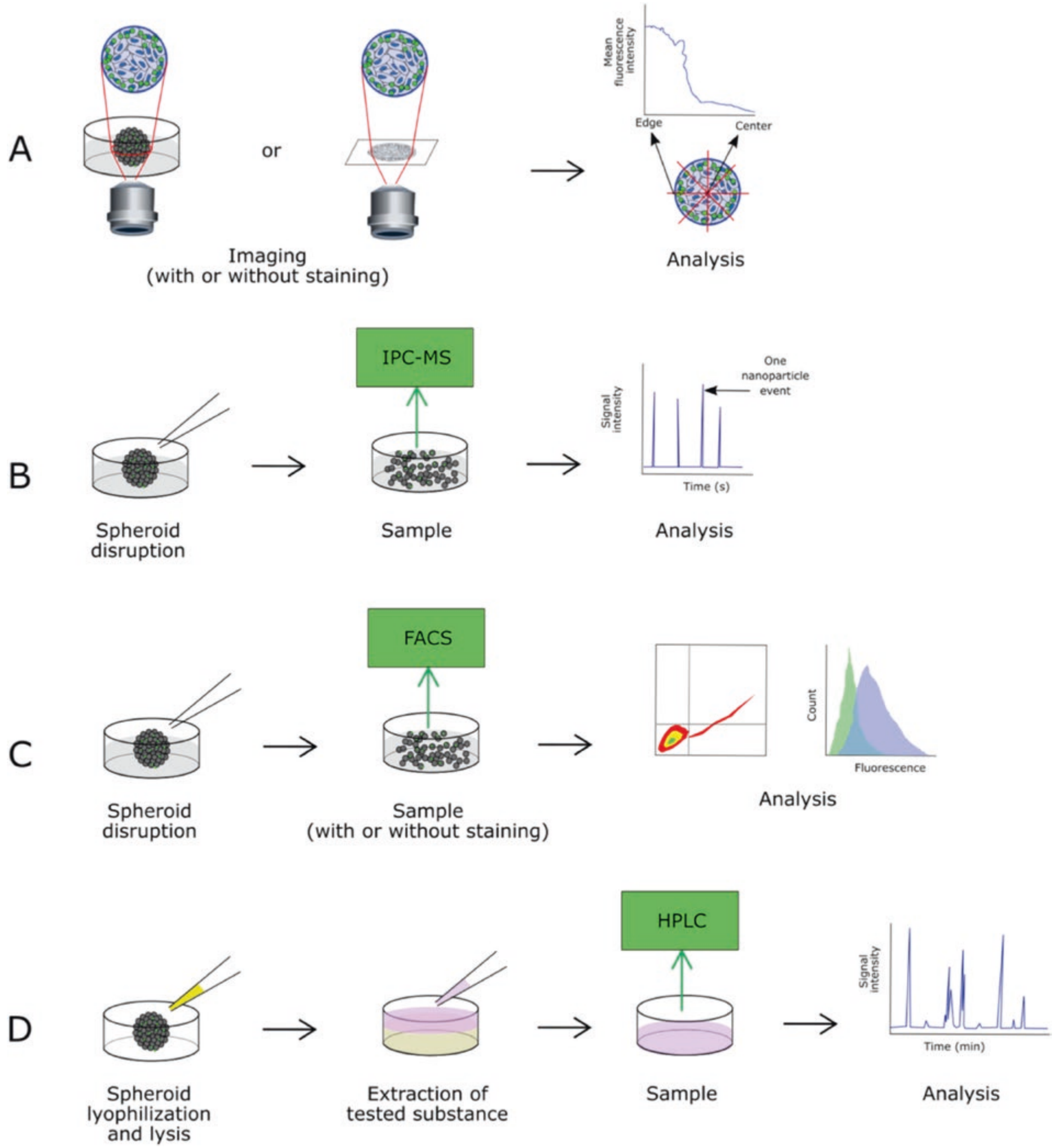
A
or
Imaging
(with or without staining)
Mean fluorescence intensity
Edge
Center
Analysis
B
IPC-MS
Spheroid disruption
Sample
Signal intensity
One nanoparticle event
Time (s)
Analysis
C
FACS
Spheroid disruption
Sample
(with or without staining)
Count
Fluorescence
Analysis
D
HPLC
Spheroid lyophilization and lysis
Extraction of tested substance
Sample
Signal intensity
Time (min)
Analysis

Fig. 12 Methods for evaluating nanoparticle penetration into spheroids. (**a**) Confocal microscopy of the whole spheroid or its section; (**b**) inductively coupled plasma mass spectrometry; (**c**) flow cytometry; (**d**) analytical chromatography

5.2 Methods for Evaluating Nanoparticle Penetration into Spheroids

Tumor spheroids are used quite often to assess nanoparticle penetration inside them, as this process mimics one of the most important barriers to nanoparticle entry into the tumor in vivo. Many factors, such as nanoparticle size, shape, charge, targeting ability, etc., could influence their cell internalization and diffusion into the deeper cellular layers inside spheroid [153]. Accordingly, scientists have developed and adopted many different methods for evaluating the transport of nanoparticles in 3D cultures.

Penetration of fluorescent-labeled nanoparticles or those containing fluorescent materials inside may be easily studied both in live or fixed spheroids by *fluorescent or confocal microscopy* [140, 154, 155] (Fig. 12a). In this case, images are usually analyzed and the depth of nanoparticle penetration and the amount of nanoparticles are estimated. To obtain more accurate results by confocal microscopy, multiple Z-stack images should be captured by scanning spheroids from the bottom up at the same depth interval [156]. However, scientists are discussing the possibility of quenching of fluorescence depending on the depth from the spheroid surface. In order to reduce the quenching effect, cryosections of spheroids could be used. Durymanov et al. tested fluorescent latex beads in pancreatic tumor spheroid 10 μm sections stained with Hoechst 33342 [150].

Several different approaches could be used together to overcome the fluorescence quenching issues. For example, besides confocal microscopy, Leite et al. analyzed penetration of modified gold nanoparticles in spheroids quantitatively by *inductively coupled plasma mass spectrometry* (IPC-MS) method [140] which is considered the gold standard method for metallic detection in cells and organs due to the very high sensitivity of the technique [149, 157] (Fig. 12b). However, this method is not suitable to determine location of nanoparticles within a sample. Thus, ICP-MS is often combined with other techniques, e.g., TEM or other microscopy methods [157]. Multiphoton fluorescent microscopy or two-photon photoluminescence (TPPL) could be used as an alternative imaging strategy to observe internal structure of spheroids and to evaluate fluorescent nanoparticle delivery into live spheroids [118, 158]. Those nondestructive techniques enable to image nanoparticles even in deeper layers of spheroids.

Spheroid incubation with Hoechst 33342 facilitated discrimination between cells in the core and periphery by *flow cytometry* (Fig. 12c). Hoechst 33342 has been recognized about 40 years ago as the dye allowing to distinguish and sort the cells in different layers of 3D cell system [159]. Tchoryk et al. used staining with Hoechst 33342 to evaluate doxorubicin and its liposomal formulation transport into different layers of HCT116 spheroids [19]. Doxorubicin is naturally fluorescent, and it is easy to track it in cells by fluorescent microscopy or fluorescence-activated cell sorter (FACS); thus, it is used quite frequently by many scientists to study nanoparticle transport [155, 160–162]. In the case of doxorubicin or other fluorescent substances or nanoparticles, it is possible to analyze its extent of penetration and also evaluate its accumulation by mean fluorescence intensity in cells [118, 154]. Leite et al. applied double fluorescent signal detection method for evaluation of nanoparticle internalization by flow cytometry: in addition to fluorescence signal from nanoparticles, signal from fluorescent-labeled targeted protein inside spheroid cells was used [140]. However, even more modern techniques are applied, such as imaging flow cytometers, that enable to visualize each single cell separately and to analyze intracellular localization of individual nanoparticles [140].

Instead of the whole nanoparticles, the drug released from them could be tested by *analytical chromatography* (Fig. 12d). Lu et al. [142] evaluated accumulation of albumin-polycaprolactone nanoparticles encapsulating albendazole in pancreatic spheroids. After the treatment, they washed, lyophilized, and lysed the spheroids, then extracted albendazole with acetonitrile, and evaluated its concentration by high-pressure liquid chromatography (HPLC).

In most cases, the spheroids are treated with nanoparticles under static conditions that do not correlate well with the actual situation in vivo. Zhang et al. [156] slightly modified experimental procedure by adding nanoparticles to the HeLa spheroids in 24-well plates and then horizontally rotating them at 50 rpm for different times (1, 2, 3, and 4 days). Fluorescent cells (with nanoparticles) were imaged by confocal microscopy after spheroid disintegration. In order to study the mechanism of penetration, spheroids were pretreated with verapamil for 2 h before adding nanoparticles [156], trypsinized, and then imaged for positively fluorescent cells.

5.3 Evaluation of Other Effects in Spheroids

3D tumor spheroids also allow evaluation of some other effects that could not be tested in monolayer-grown cell cultures. For example, tested nanoparticles can be added to cells prior to spheroid formation to analyze whether they can affect cell-cell interactions [16].

It is also possible to test cell migration from spheroids (antimetastatic effect of nanoparticles). Lu et al. [142], after spheroid treatment with albendazole-loaded nanoparticles, washed them, suspended in collagen, and cultured in collagen-growth medium matrices for 3 days. The cell migration from spheroids was analyzed by contrast phase microscopy.

5.4 High-Throughput Methods Developed for Spheroid Assays

Recently *high-throughput methods* both for spheroid formation and testing are gaining more attention [17, 18, 163]. Scientists acknowledge that current methods (both 2D and 3D) are quite static and do not meet the expectation of closely mimicking physiological conditions in vivo, and this is particularly important for the development of nanoparticles. Microfluidic systems that could simulate body fluid flow, TME, and the gradient of tested materials are becoming more popular [164].

First, they provide an opportunity to perform longer experiments and make them easier, as the device can perfuse spheroids while simulating natural blood flow in vivo [165, 166]. Due to this possibility, some constructed microfluidic systems could serve as models for the study of tumor angiogenesis, as well as tissue ischemia, or even to simulate the transvascular migration of tumor cells [167].

Several systems are used to test nanoparticle uptake, accumulation, and toxicity in 3D cultures. Mitxelena-Iribarren et al. [168] designed a microfluidic platform that could be used for both nanoparticle uptake and toxicity in tumor spheroids. Its advantage is that at the same time it allows different drugs or their nanoformulations to be tested simultaneously. Real-time monitoring device for penetration of nanoparticle into tumor spheroids was designed in order to mimic the dynamic administration of drugs [169]. This system enables to study materials in a mimic-organ level. Polystyrene nanoparticle penetration into spheroids has been tested in a microfluidic device that enables to image quantitatively the depth of penetration by using confocal laser microscopy [170].

Electrical sensing microfluidic device was adopted to test carboplatin nanoparticle efficacy in 3D TME and to evaluate cell susceptibility and resistance [171]. It allows to get the results in less than 12 h, which could save a lot of time for cancer researchers. For drug efficacy evaluation, there are also more elaborated vascularized 3D tumor models, allowing scientists to test TME changes, tumor invasion, and metastasis processes, in the presence or absence of testing compounds or nanoparticles [172].

6 Challenges in Testing of the Nanoparticles in 3D Tumor Spheroids

Despite 3D tumor spheroids mimicking the real tumors closer than 2D models do, some problems may occur during evaluation of nanoparticle effectivity and interpretation of obtained results. Physicochemical properties of nanoparticles, spheroid characteristics, spheroid properties, and the experimental setup might influence the final result (Fig. 13). These determinants should be considered, especially when comparing results obtained by using different nanoparticles.

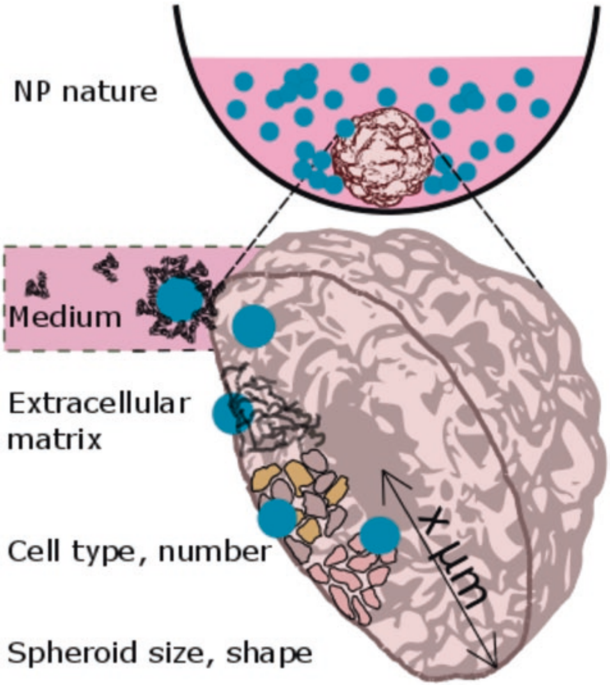

Fig. 13 Some of the factors that influence effectivity testing results of nanoparticles in cancer cell 3D models

6.1 Challenges Arising from Physicochemical Properties of the Nanoparticles

Physicochemical properties of the nanoparticles greatly influence their behavior in vitro and in vivo, including their therapeutic or imaging efficiency, accumulation and penetration in tumor, biodistribution in the organism, and toxicity. Nanoparticles behave and diffuse differently compared to a simple soluble chemical compound [173]. It may agglomerate (reversible process held by weak interactions), aggregate (irreversible process, conditioned by strong physical interaction), and/or sediment, and all these processes affect nanoparticle diffusion and uptake by the spheroid [174]. Medium properties also influence the aforementioned processes.

Agglomeration and aggregation of the nanoparticles is an important issue to consider as it changes the real nanoparticle amount, which could be uptaken by the cells in the spheroid. Nanoparticles that are smaller in size and/or nonspherical are shown to be more easily agglomerated. Moreover, agglomeration of the nanoparticles is also dependent on the parameters of the medium which is used in their dispersion, such as pH, the composition of the salts, ion concentrations, and the presence of serum proteins [173]. As these factors lead to a change in the effective nanoparticle dosages, it should be always considered while comparing the results between different nanoparticles or the same nanoparticle in different media. Agglomeration of the magnetic nanoparticles is found to positively affect the efficiency of the hyperthermia effect to the tissues; however, to this date, this effect has only be studied in 2D tissues [175]. The tendency of the nanoparticles to aggregate, also known as stability, is usually investigated before the in vitro tests; however, the medium used in vitro could contribute to the undetermined aggregation of the nanoparticles [176].

The dose of the nanoparticles reaching the spheroid should be considered in the static conditions as the *sedimentation effect* occurs during the time in some types of the nanoparticles (such as metal, inorganic) [177]. This effect is often related only to 2D experiment failure. After nanoparticles sediment, their concentration on the surface of the seeded cells is increased, and the nanoparticle transportation to the cells could be driven because of diffusion, further showing inadequate response comparing to possible in vivo effect [178]. The uptake of the cells, in this case, is determined to be independent on the physicochemical properties of the nanoparticles (size, shape, surface coating) and even its initial concentration [179]. However, diffusion and sedimentation effects have been deeply investigated on 2D models, and computational analysis methods are developed in order to investigate the particokinetics in a solution [177, 180]. Still, the particle sedimentation and diffusion effects have not been investigated in 3D models yet. In such models, strong particokinetic behavior could lead to the opposite result. Nanoparticle sedimentation and its lowered effective concentration can reduce nanoparticle uptake by spheroids and cells in 3D experiment [136]. Sedimentation in in vivo systems is not considered a problem due to the presence of permanent fluid flow. Inaccuracies arising from sedimentation could be resolved by the use of dynamic flow assays, such as microfluidic devices or other continuous medium mixing devices [181, 182]. Constant flow condition has also been shown to enhance NP penetration into the spheroid [170].

Penetration and accumulation of the nanoparticles inside the spheroid is shown to be dependent on the physicochemical properties of the nanoparticles and might be preliminary predicted by computational analysis [183]. These physicochemical parameters include size, charge, shape, surface properties, ligand attachments, etc. However, computational analysis could not replace experiment, because of a change in medium, or spheroid formation technique could lead to unpredicted penetration, accumulation, and afterward effectivity of nanoparticles.

The size of the nanoparticles plays a huge role in the passage of the nanoparticles into the spheroid. Smaller nanoparticles penetrate deeper in 3D tumor spheroids due to the easier movement through ECM pores [19]. Garcia et al. tested gold nanoparticles of 2, 5, and 14 nm diameter coupled with DNA drug on 3D spheroids and observed that smaller nanoparticles penetrate deeper into the spheroid and can even enter the cell nucleus. Cellular uptake of 14 nm nanoparticles was shown to be higher than those of smaller size, but the payload was less likely to reach the nucleus. Different particle sizes have their advantages as well as disadvantages, and the study again proves that penetration depth does not always correlate with long-term efficiency [184]. Mikhail et al. have compared the size of the block polymer micelles' influence to their penetration into MCTS and tumor xenografts and observed that spheroids properly exhibit size reduction benefits for increased penetration rate into the tumor. However, smaller nanoparticles in vivo are rapidly eliminated from the tumor site and excreted from the organism, while the larger ones achieve prolonged retention [185]. This tendency was also seen with Fe_3O_4 nanoparticles, as smaller ones penetrated better to the spheroid, but larger ones exhibited enhanced accumulation in prolonged experiments, which led to higher multicellular spheroid growth inhibition [186]. This shows that optimal experiment time should be chosen especially when comparing the effect of different size nanoparticles.

It should be noted that NP accumulation could differ because of the cell line used and should be evaluated when comparing the results. For example, it has been shown that pancreatic cancer cells BxPC-3 and PANC-1 uptake polystyrene beads differently, and these results correlate with their accumulation and penetration in 3D models [187]. Furthermore, the spheroids typically exhibit relatively small sizes which only represent small tumors and do not show nanoparticle fate before it reaches the target, in other words, its biodistribution. Small-size nanoparticles, depending on their nature, would probably aggregate, be absorbed by serum proteins, and be excreted by the liver or kidney in the organism. Therefore, this so-called nanoparticles size dilemma is lately been solved by constructing nanoparticles uploaded with smaller ones [188] or by producing shrinking nanoparticles [189].

The charge of nanoparticles also plays a huge role in penetration. Negatively charged nanoparticles diffuse deeper into a spheroid, while positively charged nanoparticles are more easily uptaken by the individual cells, bound by serum proteins and stuck in the periphery of the spheroid [190]. Even so, the accumulation of nanoparticles with positive charge could be greater, due to the nanoparticle-cell interaction as shown with amino group-decorated dendrimers [191]. The penetration depth into the spheroid is often monitored by confocal microscopy, and if the nanoparticles are not fluorescent itself, they are attached with fluorescent molecule markers. These dyes could change the surface characteristics of the nanoparticle and its behavior, and even if the zeta potential remains the same, the behavior could be changed. Tchoryk et al. have compared 50 nm polystyrene nanoparticles and observed that even carboxylated and unmodified nanoparticles had the same zeta potential in HEPES and similar zeta potential in medium; unmodified ones penetrated more deeply into the spheroids than carboxylated ones [19]. Protein corona, which is formed on the surface on the nanoparticles in the presence of proteins, also influences the penetration depth of nanoparticles as it affects the nanoparticle-cell affinity [170]. Protein corona more often forms on the positively charged nanoparticles and further changes its behavior. This should be noted while comparing results obtained from experiments performed in different media. Nanoparticles of different charges behave differently due to ECM used for the spheroid formation, and this is discussed in the bottom section [118].

6.2 Challenges Related to the Spheroid Formation and Growth

A major problem in using 3D spheroids as a system to investigate nanoparticles is that there are *no standardized protocols* for tumor formation and analysis for clinical investigation. The reproducibility of data obtained could be a challenging factor [24]. Nanoparticle's access to its target is dependent on tumor tissue. They could be restored in 3D spheroid models; however, they have to maintain appropriate size, show the binding site barrier, and have the ECM. These are the main challenging factors to maintain them the proper way, and even the absence of only one of the factor could lead to the further failure of the nanoparticle in vivo.

The size of the spheroid is related to nanoparticle activity as they better penetrate into the smaller spheroids than in larger ones [190]. There is a linear dependency of seeded cell number and spheroid size [192]. Hereupon, the challenge arises because different *cell number* for different cell line is needed to form a spheroid; thus, cells have their specific tightness of packing the spheroid [193]. Therefore, the comparison of the results obtained from different cell lines could be misguiding. Bigger spheroids have more cells in it which have to undergo metabolic adaptation due to the lack of the nutrients; in other words, the bigger is the spheroid, the more hypoxic cells are in it [194]. The challenge arises on how to produce spheroids with controllable and reproducible hypoxic regions, as consumption of oxygen is a very important property to the spheroid, but it is not easily assessed [195]. The size of the spheroid should be at least around 300–400 μm to have hypoxia inside of it, as it is known that the diffusion limitation of the oxygen is about 150–200 μm [196]. Yet, not all the spheroids are produced in a perfectly spherical shape, and this is dependent on its *formation technique* [197].

Eccentricity and physical dimensions should be checked to ensure the hypoxic environment presence inside the spheroid [198]. Nanoparticle activity could be reduced due to the presence of hypoxia because hypoxia is often associated with cell resistance to the treatment [199]. Also, the activity of nanoparticles for PDT and ROS producer carriers is dependent on the oxygen amount, and the hypoxic area size influences their activity [200]. The penetration to the deeper regions of the spheroid could be limited for the nanoparticle with negative charge as they would probably be stuck in this acidic hypoxia region [201]. Moreover, the hypoxic region presence monitoring is very important while investigating nanoparticles specifically targeting hypoxic cells.

Cell types used to form spheroid also leads to a diverse nanoparticle activity. Homotypic spheroids could be misguiding due to the lack of stromal cells appearing in the tumor; thus, heterotypic spheroids are also related to therapeutic resistance. Stromal cell existence inside the tumors is also related to nanoparticle failure in vivo, for example, because of the binding site or stromal barrier [202]. To obtain conditions closer mimicking tumors in vivo, heterotypic spheroids are formed often by including fibroblasts inside the spheroid, often by simply mixing them together and then forming a spheroid [14]. However, fibroblast barrier to the effect of nanoparticles could be obscured in such case and give no meaningful results, because fibroblasts, due to their tight adherence, tended to organize in the spheroid core [203]. Therefore, some scientists test how nanoparticles could overcome the barrier by coating spheroids with fibroblasts [204]. Another problem related to heterotypic spheroids is discerning which cells were actually affected by nanoparticles inside of the spheroid [155].

It has been observed that nanoparticles show a reduced diffusion rates in collagen-rich tumors [205]. Therefore, the use of collagen, fibronectin, or other proteins of the so-called *ECM* for spheroid formation is desired for the appropriate experimental model. Nanoparticles diffuse deeper in the spheroid through ECM pores, and their size influences NP movement through the spheroid. Some researchers attach matrix digesting enzymes on the surface of the nanoparticles, which "eat" their way to the spheroid core. ECM together with close cell interaction contributes to an increased interstitial fluid pressure of the spheroid or tumor, which leads to a reduced nanoparticle performance [14]. Moreover, the cell proliferation rate and its behavior could be nonrealistic in the absence of ECM. The presence of negatively charged ECM is a barrier for positively charged nanoparticles [19]. However, some studies reveal that the proteoglycans in the tumor constitute a barrier for negatively charged agents as well [206]. Therefore, the challenge here arises on how to construct a spheroid which mimics tumor ECM as close as possible. Another issue is how to maintain the same ECM amount in spheroids while investigating ECM targeting nanoparticles [207]. Experimental setup where spheroid is surrounded by

ECM, and medium is on the top of it, might also be challenging [192]. To perform longer experiments and maintain spheroids longer, the medium has to be changed. Hereupon, nanoparticle dosage problems could arise not only because of possible nanoparticle sedimentation on collagen layer but also due to their penetration and entanglement within it. Also, it should be noted that spheroid size together with its functionality could vary due to the hydrogel properties when spheroids are cultivated in hydrogels [208].

Medium composition could as well influence spheroid structure, particularly the necrotic core thickness. Baye et al. observed that spheroids grown in the microfluidic device with the constant medium flow with different glucose concentration have the same size, but different necrotic core [209]. When spheroids are grown without constant medium flow, the necrotic core is dependent on medium change periodicity which could also influence nanoparticle penetration inside the spheroid depth.

A lack of *perfusion* is also a dilemma studying nanoparticle effect on cell spheroids. Microfluidic devices have been applied to mimic dynamic organism conditions; however, such systems are not yet applied for massive manufacturing [190].

6.3 Challenges in Observing the Effect

The possibility to observe nanoparticle penetration inside the spheroid is very important. Imaging is complicated in such systems due to the size and spherical shape. The penetration depth of the nanosystems inside the 3D tumor spheroids is sometimes difficult to compare because of completely different systems used. For example, the fluorescence signal of the nanoparticle is measured in one case and by drug or release agent in another. As mentioned before, the fluorescent molecule binding for nanoparticle monitoring could change its behavior in 3D system [118].

It is important to mention that the penetration depth of the nanoparticles inside the spheroid is not a crucial sign of its effectivity. If the tested nanoparticle is a nanocarrier, the release of the payload and its penetration is most important [7]. However, payloads of the nanoparticle track are more complicated, especially for molecules that are not fluorescent [210].

7 Conclusions and Future Perspectives

In the last decades, many types of nanoparticles are increasingly being developed as drug carriers for cancer therapy. Many of them are already applied in clinics for therapeutic and diagnostic purposes. However, the process of nanoparticle introduction into clinical practice remains a great challenge as nanoformulations require more sophisticated models to evaluate and predict their performance in vivo than small-size molecules.

3D tumor spheroids provide a great opportunity to assess nanoparticle suitability for cancer treatment as they mimic the real tumor microenvironment much better than conventional 2D cell cultures do. There is a huge variety of tumor spheroid formation methods with their own advantages and disadvantages. Different types of 3D cultures also possess different properties and are suitable for different purposes. Thus, it is very important to choose the right tumor model for specific nanoparticles and carefully design the whole experiment: to choose the right cell type and spheroid formation technique, to decide when to begin the treatment with nanoparticles and for which duration, to choose the right parameters for the efficacy assessment, and also to choose the right analytical method. Combination of several analytical methods is recommended to evaluate possible effect of nanoparticles as each of them has its own limitations. Experimental results also should be interpreted carefully, especially when comparing them with the data from other research groups or even with the previously obtained results in the same group.

It is important to have in mind that more complex biological system more precisely mimics the real conditions, but at the same time it is more dynamic and it becomes more complicated to control all its variables. Even the cell and nanoparticle are not simple systems; thus, it is of great importance to make the right decision when choosing an optimal model that could be manageable during the whole experiment and provide reproducible and reliable results.

References

1. Costa, E. C., Moreira, A. F., de Melo-Diogo, D., Gaspar, V. M., Carvalho, M. P., & Correia, I. J. (2016). 3D tumor spheroids: An overview on the tools and techniques used for their analysis. *Biotechnology Advances, 34*(8), 1427–1441.
2. Baker, B. M., & Chen, C. S. (2012). Deconstructing the third dimension: How 3D culture microenvironments alter cellular cues. *Journal of Cell Science, 125*(Pt 13), 3015–3024.
3. Huang, S., & Ingber, D. E. (1999). The structural and mechanical complexity of cell-growth control. *Nature Cell Biology, 1*(5), E131–E138.
4. Januškevičienė, I., & Petrikaitė, V. (2019). Heterogeneity of breast cancer: The importance of interaction between different tumor cell populations. *Life Sciences, 239*, 117009.
5. Halfter, K., Hoffmann, O., Ditsch, N., Ahne, M., Arnold, F., Paepke, S., et al. (2016). Testing chemotherapy efficacy in HER2 negative breast cancer using patient-derived spheroids. *Journal of Translational Medicine, 14*, 112. Available from: https://www.ncbi.nlm.nih.gov/pmc/articles/PMC4855689/.
6. Hirschhaeuser, F., Menne, H., Dittfeld, C., West, J., Mueller-Klieser, W., & Kunz-Schughart, L. A. (2010). Multicellular tumor spheroids: An underestimated tool is catching up again. *Journal of Biotechnology, 148*(1), 3–15.
7. Lu, H., & Stenzel, M. H. (2018). Multicellular tumor spheroids (MCTS) as a 3D in vitro evaluation tool of nanoparticles. *Small, 14*(13), e1702858.
8. Vaira, V., Fedele, G., Pyne, S., Fasoli, E., Zadra, G., Bailey, D., et al. (2010). Preclinical model of organotypic culture for phar-

macodynamic profiling of human tumors. *Proceedings of the National Academy of Sciences of the USA, 107*(18), 8352–8356.

9. Lim, C. Y., Chang, J. H., Lee, W. S., Lee, K. M., Yoon, Y. C., Kim, J., et al. (2018). Organotypic slice cultures of pancreatic ductal adenocarcinoma preserve the tumor microenvironment and provide a platform for drug response. *Pancreatology, 18*(8), 913–927.
10. Kyle, A. H., Huxham, L. A., Chiam, A. S. J., Sim, D. H., & Minchinton, A. I. (2004). Direct assessment of drug penetration into tissue using a novel application of three-dimensional cell culture. *Cancer Research, 64*(17), 6304–6309.
11. Fischbach, C., Chen, R., Matsumoto, T., Schmelzle, T., Brugge, J. S., Polverini, P. J., et al. (2007). Engineering tumors with 3D scaffolds. *Nature Methods, 4*(10), 855–860.
12. Lee, J., Lilly, G. D., Doty, R. C., Podsiadlo, P., & Kotov, N. A. (2009). In vitro toxicity testing of nanoparticles in 3D cell culture. *Small, 5*(10), 1213–1221.
13. Shield, K., Ackland, M. L., Ahmed, N., & Rice, G. E. (2009). Multicellular spheroids in ovarian cancer metastases: Biology and pathology. *Gynecologic Oncology, 113*(1), 143–148.
14. Nunes, A. S., Barros, A. S., Costa, E. C., Moreira, A. F., & Correia, I. J. (2019). 3D tumor spheroids as in vitro models to mimic in vivo human solid tumors resistance to therapeutic drugs. *Biotechnology and Bioengineering, 116*(1), 206–226.
15. Barua, S., & Mitragotri, S. (2014). Challenges associated with penetration of nanoparticles across cell and tissue barriers: A review of current status and future prospects. *Nano Today, 9*(2), 223–243.
16. Sambale, F., Lavrentieva, A., Stahl, F., Blume, C., Stiesch, M., Kasper, C., et al. (2015). Three dimensional spheroid cell culture for nanoparticle safety testing. *Journal of Biotechnology, 205*, 120–129.
17. Tsai, H.-F., Trubelja, A., Shen, A. Q., & Bao, G. (2017). Tumour-on-a-chip: Microfluidic models of tumour morphology, growth and microenvironment. *Journal of the Royal Society, Interface, 14*(131), 20170137. Available from: https://www.ncbi.nlm.nih.gov/pmc/articles/PMC5493797/.
18. Trujillo-de Santiago, G., Flores-Garza, B. G., Tavares-Negrete, J. A., Lara-Mayorga, I. M., González-Gamboa, I., Zhang, Y. S., et al. (2019). The tumor-on-chip: Recent advances in the development of microfluidic systems to recapitulate the physiology of solid tumors. *Materials (Basel), 12*(18), 2945. Available from: https://www.ncbi.nlm.nih.gov/pmc/articles/PMC6766252/.
19. Tchoryk, A., Taresco, V., Argent, R. H., Ashford, M., Gellert, P. R., Stolnik, S., et al. (2019). Penetration and uptake of nanoparticles in 3D tumor spheroids. *Bioconjugate Chemistry, 30*(5), 1371–1384.
20. Zhang, J., Tang, H., Liu, Z., & Chen, B. (2017). Effects of major parameters of nanoparticles on their physical and chemical properties and recent application of nanodrug delivery system in targeted chemotherapy. *International Journal of Nanomedicine, 12*, 8483–8493.
21. Groebe, K., & Mueller-Klieser, W. (1996). On the relation between size of necrosis and diameter of tumor spheroids. *International Journal of Radiation Oncology · Biology · Physics, 34*(2), 395–401.
22. Kunz-Schughart, L. A. (1999). Multicellular tumor spheroids: Intermediates between monolayer culture and in vivo tumor. *Cell Biology International, 23*(3), 157–161.
23. Nath, S., & Devi, G. R. (2016). Three-dimensional culture systems in cancer research: Focus on tumor spheroid model. *Pharmacology & Therapeutics, 163*, 94–108.
24. Zanoni, M., Piccinini, F., Arienti, C., Zamagni, A., Santi, S., Polico, R., et al. (2016). 3D tumor spheroid models for in vitro therapeutic screening: A systematic approach to enhance the biological relevance of data obtained. *Scientific Reports, 6*, 19103. Available from: https://www.ncbi.nlm.nih.gov/pmc/articles/PMC4707510/.
25. McIntyre, A., Patiar, S., Wigfield, S., Li, J., Ledaki, I., Turley, H., et al. (2012). Carbonic anhydrase IX promotes tumor growth and necrosis in vivo and inhibition enhances anti-VEGF therapy. *Clinical Cancer Research, 18*(11), 3100–3111.
26. Mehta, G., Hsiao, A. Y., Ingram, M., Luker, G. D., & Takayama, S. (2012). Opportunities and challenges for use of tumor spheroids as models to test drug delivery and efficacy. *Journal of Controlled Release, 164*(2), 192–204.
27. Santini, M. T., & Rainaldi, G. (1999). Three-dimensional spheroid model in tumor biology. *Pathobiology, 67*(3), 148–157.
28. Trédan, O., Galmarini, C. M., Patel, K., & Tannock, I. F. (2007). Drug resistance and the solid tumor microenvironment. *Journal of the National Cancer Institute, 99*(19), 1441–1454.
29. Hamilton, G. (1998). Multicellular spheroids as an in vitro tumor model. *Cancer Letters, 131*(1), 29–34.
30. Lin, R.-Z., Lin, R.-Z., & Chang, H.-Y. (2008). Recent advances in three-dimensional multicellular spheroid culture for biomedical research. *Biotechnology Journal, 3*(9–10), 1172–1184.
31. Groebe, K., & Mueller-Klieser, W. (1991). Distributions of oxygen, nutrient, and metabolic waste concentrations in multicellular spheroids and their dependence on spheroid parameters. *European Biophysics Journal, 19*(4), 169–181.
32. Alvarez-Pérez, J., Ballesteros, P., & Cerdán, S. (2005). Microscopic images of intraspheroidal pH by 1H magnetic resonance chemical shift imaging of pH sensitive indicators. *Magma, 18*(6), 293–301.
33. Koppenol, W. H., Bounds, P. L., & Dang, C. V. (2011). Otto Warburg's contributions to current concepts of cancer metabolism. *Nature Reviews. Cancer, 11*(5), 325–337.
34. Yeon, S.-E., No, D. Y., Lee, S.-H., Nam, S. W., Oh, I.-H., Lee, J., et al. (2013). Application of concave microwells to pancreatic tumor spheroids enabling anticancer drug evaluation in a clinically relevant drug resistance model. *PLoS One, 8*(9), e73345.
35. Mueller-Klieser, W. (1997). Three-dimensional cell cultures: From molecular mechanisms to clinical applications. *The American Journal of Physiology, 273*(4), C1109–C1123.
36. Lazzari, G., Couvreur, P., & Mura, S. (2017). Multicellular tumor spheroids: A relevant 3D model for the in vitro preclinical investigation of polymer nanomedicines. *Polymer Chemistry, 8*(34), 4947–4969.
37. Wang, C., Tang, Z., Zhao, Y., Yao, R., Li, L., & Sun, W. (2014). Three-dimensional in vitro cancer models: A short review. *Biofabrication, 6*(2), 022001.
38. LaBarbera, D. V., Reid, B. G., & Yoo, B. H. (2012). The multicellular tumor spheroid model for high-throughput cancer drug discovery. *Expert Opinion on Drug Discovery, 7*(9), 819–830.
39. Ridky, T. W., Chow, J. M., Wong, D. J., & Khavari, P. A. (2010). Invasive three-dimensional organotypic neoplasia from multiple normal human epithelia. *Nature Medicine, 16*(12), 1450–1455.
40. Loessner, D., Stok, K. S., Lutolf, M. P., Hutmacher, D. W., Clements, J. A., & Rizzi, S. C. (2010). Bioengineered 3D platform to explore cell-ECM interactions and drug resistance of epithelial ovarian cancer cells. *Biomaterials, 31*(32), 8494–8506.
41. Pampaloni, F., Stelzer, E. H. K., Leicht, S., & Marcello, M. (2010). Madin–Darby canine kidney cells are increased in aerobic glycolysis when cultured on flat and stiff collagen-coated surfaces rather than in physiological 3-D cultures. *Proteomics, 10*(19), 3394–3413.
42. Chopra, V., Dinh, T. V., & Hannigan, E. V. (1997). Three-dimensional endothelial-tumor epithelial cell interactions in human cervical cancers. *In Vitro Cellular & Developmental Biology – Animal, 33*(6), 432–442.
43. Fennema, E., Rivron, N., Rouwkema, J., van Blitterswijk, C., & de Boer, J. (2013). Spheroid culture as a tool for creating 3D complex tissues. *Trends in Biotechnology, 31*(2), 108–115.

44. Bierwolf, J., Lutgehetmann, M., Feng, K., Erbes, J., Deichmann, S., Toronyi, E., et al. (2011). Primary rat hepatocyte culture on 3D nanofibrous polymer scaffolds for toxicology and pharmaceutical research. *Biotechnology and Bioengineering, 108*(1), 141–150.
45. Li, J., Tao, R., Wu, W., Cao, H., Xin, J., Li, J., et al. (2010). 3D PLGA scaffolds improve differentiation and function of bone marrow mesenchymal stem cell-derived hepatocytes. *Stem Cells and Development, 19*(9), 1427–1436.
46. Kim, J. B., Stein, R., & O'Hare, M. J. (2004). Three-dimensional in vitro tissue culture models of breast cancer – a review. *Breast Cancer Research and Treatment, 85*(3), 281–291.
47. Zhao, C., Setrerrahmane, S., & Xu, H. (2015). Enrichment and characterization of cancer stem cells from a human non-small cell lung cancer cell line. *Oncology Reports, 34*(4), 2126–2132.
48. Imamura, Y., Mukohara, T., Shimono, Y., Funakoshi, Y., Chayahara, N., Toyoda, M., et al. (2015). Comparison of 2D- and 3D-culture models as drug-testing platforms in breast cancer. *Oncology Reports, 33*(4), 1837–1843.
49. Deisboeck, T. S., Berens, M. E., Kansal, A. R., Torquato, S., Stemmer-Rachamimov, A. O., & Chiocca, E. A. (2001). Pattern of self-organization in tumour systems: Complex growth dynamics in a novel brain tumour spheroid model. *Cell Proliferation, 34*(2), 115–134.
50. Lee, S.-H., Hong, J. H., Park, H. K., Park, J. S., Kim, B.-K., Lee, J.-Y., et al. (2015). Colorectal cancer-derived tumor spheroids retain the characteristics of original tumors. *Cancer Letters, 367*(1), 34–42.
51. Kim, K.-U., Wilson, S. M., Abayasiriwardana, K. S., Collins, R., Fjellbirkeland, L., Xu, Z., et al. (2005). A novel in vitro model of human mesothelioma for studying tumor biology and apoptotic resistance. *American Journal of Respiratory Cell and Molecular Biology, 33*(6), 541–548.
52. Burgués, J. P., Gómez, L., Pontones, J. L., Vera, C. D., Jiménez-Cruz, J. F., & Ozonas, M. (2007). A chemosensitivity test for superficial bladder cancer based on three-dimensional culture of tumour spheroids. *European Urology, 51*(4), 962–969; discussion 969–970.
53. Correa de Sampaio, P., Auslaender, D., Krubasik, D., Failla, A. V., Skepper, J. N., Murphy, G., et al. (2012). A heterogeneous in vitro three dimensional model of tumour-stroma interactions regulating sprouting angiogenesis. *PLoS One, 7*(2), e30753.
54. Courau, T., Bonnereau, J., Chicoteau, J., Bottois, H., Remark, R., Assante Miranda, L., et al. (2019). Cocultures of human colorectal tumor spheroids with immune cells reveal the therapeutic potential of MICA/B and NKG2A targeting for cancer treatment. *Journal for ImmunoTherapy of Cancer, 7*(1), 74.
55. Vinci, M., Gowan, S., Boxall, F., Patterson, L., Zimmermann, M., Court, W., et al. (2012). Advances in establishment and analysis of three-dimensional tumor spheroid-based functional assays for target validation and drug evaluation. *BMC Biology, 10*, 29.
56. Herter, S., Morra, L., Schlenker, R., Sulcova, J., Fahrni, L., Waldhauer, I., et al. (2017). A novel three-dimensional heterotypic spheroid model for the assessment of the activity of cancer immunotherapy agents. *Cancer Immunology, Immunotherapy, 66*(1), 129–140.
57. Lee, J. W., Sung, J. S., Park, Y. S., Chung, S., & Kim, Y. H. (2018). Isolation of spheroid-forming single cells from gastric cancer cell lines: Enrichment of cancer stem-like cells. *BioTechniques, 65*(4), 197–203.
58. Pampaloni, F., Reynaud, E. G., & Stelzer, E. H. K. (2007). The third dimension bridges the gap between cell culture and live tissue. *Nature Reviews. Molecular Cell Biology, 8*(10), 839–845.
59. Bussard, K. M., Mutkus, L., Stumpf, K., Gomez-Manzano, C., & Marini, F. C. (2016). Tumor-associated stromal cells as key contributors to the tumor microenvironment. *Breast Cancer Research, 18*(1), 84.
60. Kucerova, L., & Skolekova, S. (2013). Tumor microenvironment and the role of mesenchymal stromal cells. *Neoplasma, 60*(1), 1–10.
61. Dittmer, J., & Leyh, B. (2015). The impact of tumor stroma on drug response in breast cancer. *Seminars in Cancer Biology, 31*, 3–15.
62. Almendro, V., Marusyk, A., & Polyak, K. (2013). Cellular heterogeneity and molecular evolution in cancer. *Annual Review of Pathology, 8*, 277–302.
63. Plava, J., Cihova, M., Burikova, M., Matuskova, M., Kucerova, L., & Miklikova, S. (2019). Recent advances in understanding tumor stroma-mediated chemoresistance in breast cancer. *Molecular Cancer, 18*, 67. Available from: https://www.ncbi.nlm.nih.gov/pmc/articles/PMC6441200/.
64. Gujam, F. J. A., Edwards, J., Mohammed, Z. M. A., Going, J. J., & McMillan, D. C. (2014). The relationship between the tumour stroma percentage, clinicopathological characteristics and outcome in patients with operable ductal breast cancer. *British Journal of Cancer, 111*(1), 157–165.
65. Costa, E. C., Gaspar, V. M., Coutinho, P., & Correia, I. J. (2014). Optimization of liquid overlay technique to formulate heterogenic 3D co-cultures models. *Biotechnology and Bioengineering, 111*(8), 1672–1685.
66. Jaganathan, H., Gage, J., Leonard, F., Srinivasan, S., Souza, G. R., Dave, B., et al. (2014). Three-dimensional in vitro co-culture model of breast tumor using magnetic levitation. *Scientific Reports, 4*(1), 1–9.
67. Dekker, T. J. A., van de Velde, C. J. H., van Pelt, G. W., Kroep, J. R., Julien, J.-P., Smit, V. T. H. B. M., et al. (2013). Prognostic significance of the tumor-stroma ratio: Validation study in node-negative premenopausal breast cancer patients from the EORTC perioperative chemotherapy (POP) trial (10854). *Breast Cancer Research and Treatment, 139*(2), 371–379.
68. Miki, Y., Ono, K., Hata, S., Suzuki, T., Kumamoto, H., & Sasano, H. (2012). The advantages of co-culture over mono cell culture in simulating in vivo environment. *The Journal of Steroid Biochemistry and Molecular Biology, 131*(3–5), 68–75.
69. Hanahan, D., & Coussens, L. M. (2012). Accessories to the crime: Functions of cells recruited to the tumor microenvironment. *Cancer Cell, 21*(3), 309–322.
70. Thoma, C. R., Zimmermann, M., Agarkova, I., Kelm, J. M., & Krek, W. (2014). 3D cell culture systems modeling tumor growth determinants in cancer target discovery. *Advanced Drug Delivery Reviews, 69–70*, 29–41.
71. Sung, S.-Y., Hsieh, C.-L., Law, A., Zhau, H. E., Pathak, S., Multani, A. S., et al. (2008). Coevolution of prostate cancer and bone stroma in three-dimensional coculture: Implications for cancer growth and metastasis. *Cancer Research, 68*(23), 9996–10003.
72. Kojima, N., Takeuchi, S., & Sakai, Y. (2011). Establishment of self-organization system in rapidly formed multicellular heterospheroids. *Biomaterials, 32*(26), 6059–6067.
73. Weiswald, L.-B., Guinebretière, J.-M., Richon, S., Bellet, D., Saubaméa, B., & Dangles-Marie, V. (2010). In situ protein expression in tumour spheres: Development of an immunostaining protocol for confocal microscopy. *BMC Cancer, 10*, 106.
74. Vamvakidou, A. P., Mondrinos, M. J., Petushi, S. P., Garcia, F. U., Lelkes, P. I., & Tozeren, A. (2007). Heterogeneous breast tumoroids: An in vitro assay for investigating cellular heterogeneity and drug delivery. *Journal of Biomolecular Screening, 12*(1), 13–20.
75. Brouty-Boyé, D., Mainguené, C., Magnien, V., Israel, L., & Beaupain, R. (1994). Fibroblast-mediated differentiation in human breast carcinoma cells (MCF-7) grown as nodules IN VITRO. *International Journal of Cancer, 56*(5), 731–735.

76. Friedrich, J., Ebner, R., & Kunz-Schughart, L. A. (2007). Experimental anti-tumor therapy in 3-D: Spheroids – old hat or new challenge? *International Journal of Radiation Biology, 83*(11–12), 849–871.
77. Sutherland, R. M., Inch, W. R., McCredie, J. A., & Kruuv, J. (1970). A multi-component radiation survival curve using an in vitro tumour model. *International Journal of Radiation Biology and Related Studies in Physics, Chemistry and Medicine, 18*(5), 491–495.
78. Spoettl, T., Hausmann, M., Herlyn, M., Gunckel, M., Dirmeier, A., Falk, W., et al. (2006). Monocyte chemoattractant protein-1 (MCP-1) inhibits the intestinal-like differentiation of monocytes. *Clinical and Experimental Immunology, 145*(1), 190–199.
79. Timmins, N. E., Dietmair, S., & Nielsen, L. K. (2004). Hanging-drop multicellular spheroids as a model of tumour angiogenesis. *Angiogenesis, 7*(2), 97–103.
80. Mayer, B., Klement, G., Kaneko, M., Man, S., Jothy, S., Rak, J., et al. (2001). Multicellular gastric cancer spheroids recapitulate growth pattern and differentiation phenotype of human gastric carcinomas. *Gastroenterology, 121*(4), 839–852.
81. Lin, R.-Z., Chou, L.-F., Chien, C.-C. M., & Chang, H.-Y. (2006). Dynamic analysis of hepatoma spheroid formation: Roles of E-cadherin and beta1-integrin. *Cell and Tissue Research, 324*(3), 411–422.
82. Lawlor, E. R., Scheel, C., Irving, J., & Sorensen, P. H. B. (2002). Anchorage-independent multi-cellular spheroids as an in vitro model of growth signaling in Ewing tumors. *Oncogene, 21*(2), 307–318.
83. Millard, M., Yakavets, I., Zorin, V., Kulmukhamedova, A., Marchal, S., & Bezdetnaya, L. (2017). Drug delivery to solid tumors: The predictive value of the multicellular tumor spheroid model for nanomedicine screening. *International Journal of Nanomedicine, 12*, 7993–8007.
84. Laurent, J., Frongia, C., Cazales, M., Mondesert, O., Ducommun, B., & Lobjois, V. (2013). Multicellular tumor spheroid models to explore cell cycle checkpoints in 3D. *BMC Cancer, 13*(1), 73.
85. Kim, T.-H., Mount, C. W., Gombotz, W. R., & Pun, S. H. (2010). The delivery of doxorubicin to 3-D multicellular spheroids and tumors in a murine xenograft model using tumor-penetrating triblock polymeric micelles. *Biomaterials, 31*(28), 7386–7397.
86. Zhao, W., Luo, Y., Li, B., & Zhang, T. (2016). Tumorigenic lung tumorospheres exhibit stem-like features with significantly increased expression of CD133 and ABCG2. *Molecular Medicine Reports, 14*(3), 2598–2606.
87. Yu, M., Bardia, A., Aceto, N., Bersani, F., Madden, M. W., Donaldson, M. C., et al. (2014). Cancer therapy. Ex vivo culture of circulating breast tumor cells for individualized testing of drug susceptibility. *Science, 345*(6193), 216–220.
88. Valent, P., Bonnet, D., De Maria, R., Lapidot, T., Copland, M., Melo, J. V., et al. (2012). Cancer stem cell definitions and terminology: The devil is in the details. *Nature Reviews. Cancer, 12*(11), 767–775.
89. Dieter, S. M., Ball, C. R., Hoffmann, C. M., Nowrouzi, A., Herbst, F., Zavidij, O., et al. (2011). Distinct types of tumor-initiating cells form human colon cancer tumors and metastases. *Cell Stem Cell, 9*(4), 357–365.
90. Weiswald, L.-B., Bellet, D., & Dangles-Marie, V. (2015). Spherical cancer models in tumor biology. *Neoplasia, 17*(1), 1–15.
91. Chen, R., Nishimura, M. C., Bumbaca, S. M., Kharbanda, S., Forrest, W. F., Kasman, I. M., et al. (2010). A hierarchy of self-renewing tumor-initiating cell types in glioblastoma. *Cancer Cell, 17*(4), 362–375.
92. Calvet, C. Y., André, F. M., & Mir, L. M. (2014). The culture of cancer cell lines as tumorspheres does not systematically result in cancer stem cell enrichment. *PLoS One, 9*(2), e89644.
93. Zhang, S., Balch, C., Chan, M. W., Lai, H.-C., Matei, D., Schilder, J. M., et al. (2008). Identification and characterization of ovarian cancer-initiating cells from primary human tumors. *Cancer Research, 68*(11), 4311–4320.
94. Oskarsson, T., Acharyya, S., Zhang, X. H.-F., Vanharanta, S., Tavazoie, S. F., Morris, P. G., et al. (2011). Breast cancer cells produce tenascin C as a metastatic niche component to colonize the lungs. *Nature Medicine, 17*(7), 867–874.
95. Ma, Y., Liang, D., Liu, J., Axcrona, K., Kvalheim, G., Giercksky, K.-E., et al. (2012). Synergistic effect of SCF and G-CSF on stem-like properties in prostate cancer cell lines. *Tumour Biology, 33*(4), 967–978.
96. Yoshida, T., Okuyama, H., Endo, H., & Inoue, M. (1655). Spheroid cultures of primary urothelial cancer cells: Cancer tissue-originated spheroid (CTOS) method. *Methods in Molecular Biology, 2018*, 145–153.
97. Weiswald, L.-B., Richon, S., Massonnet, G., Guinebretière, J.-M., Vacher, S., Laurendeau, I., et al. (2013). A short-term colorectal cancer sphere culture as a relevant tool for human cancer biology investigation. *British Journal of Cancer, 108*(8), 1720–1731.
98. Theodoraki, M. A., Rezende, C. O., Chantarasriwong, O., Corben, A. D., Theodorakis, E. A., & Alpaugh, M. L. (2015). Spontaneously-forming spheroids as an in vitro cancer cell model for anticancer drug screening. *Oncotarget, 6*(25), 21255–21267.
99. Weiswald, L.-B., Richon, S., Validire, P., Briffod, M., Lai-Kuen, R., Cordelières, F. P., et al. (2009). Newly characterised ex vivo colospheres as a three-dimensional colon cancer cell model of tumour aggressiveness. *British Journal of Cancer, 101*(3), 473–482.
100. Kondo, J., Endo, H., Okuyama, H., Ishikawa, O., Iishi, H., Tsujii, M., et al. (2011). Retaining cell-cell contact enables preparation and culture of spheroids composed of pure primary cancer cells from colorectal cancer. *Proceedings of the National Academy of Sciences of the USA, 108*(15), 6235–6240.
101. Young, S. R., Saar, M., Santos, J., Nguyen, H. M., Vessella, R. L., & Peehl, D. M. (2013). Establishment and serial passage of cell cultures derived from LuCaP xenografts. *The Prostate, 73*(12), 1251–1262.
102. Morales, J., & Alpaugh, M. L. (2009). Gain in cellular organization of inflammatory breast cancer: A 3D in vitro model that mimics the in vivo metastasis. *BMC Cancer, 9*, 462.
103. Ferrante, A., Rainaldi, G., Indovina, P., Indovina, P. L., & Santini, M. T. (2006). Increased cell compaction can augment the resistance of HT-29 human colon adenocarcinoma spheroids to ionizing radiation. *International Journal of Oncology, 28*(1), 111–118.
104. Christensen, K., Aaberg-Jessen, C., Andersen, C., Goplen, D., Bjerkvig, R., & Kristensen, B. W. (2010). Immunohistochemical expression of stem cell, endothelial cell, and chemosensitivity markers in primary glioma spheroids cultured in serum-containing and serum-free medium. *Neurosurgery, 66*(5), 933–947.
105. Sundlisaeter, E., Wang, J., Sakariassen, P. Ø., Marie, M., Mathisen, J. R., Karlsen, B. O., et al. (2006). Primary glioma spheroids maintain tumourogenicity and essential phenotypic traits after cryopreservation. *Neuropathology and Applied Neurobiology, 32*(4), 419–427.
106. Rajcevic, U., Knol, J. C., Piersma, S., Bougnaud, S., Fack, F., Sundlisaeter, E., et al. (2014). Colorectal cancer derived organotypic spheroids maintain essential tissue characteristics but adapt their metabolism in culture. *Proteome Science, 12*, 39.
107. Muthuswamy, R., Berk, E., Junecko, B. F., Zeh, H. J., Zureikat, A. H., Normolle, D., et al. (2012). NF-κB hyperactivation in tumor tissues allows tumor-selective reprogramming of the chemokine microenvironment to enhance the recruitment of cytolytic T effector cells. *Cancer Research, 72*(15), 3735–3743.
108. Chekenya, M., Krakstad, C., Svendsen, A., Netland, I. A., Staalesen, V., Tysnes, B. B., et al. (2008). The progenitor cell

marker NG2/MPG promotes chemoresistance by activation of integrin-dependent PI3K/Akt signaling. *Oncogene, 27*(39), 5182–5194.

109. Musah-Eroje, A., & Watson, S. (2019). A novel 3D in vitro model of glioblastoma reveals resistance to temozolomide which was potentiated by hypoxia. *Journal of Neuro-Oncology, 142*(2), 231–240.
110. Knight, E., & Przyborski, S. (2015). Advances in 3D cell culture technologies enabling tissue-like structures to be created in vitro. *Journal of Anatomy, 227*(6), 746–756.
111. Haisler, W. L., Timm, D. M., Gage, J. A., Tseng, H., Killian, T. C., & Souza, G. R. (2013). Three-dimensional cell culturing by magnetic levitation. *Nature Protocols, 8*(10), 1940–1949.
112. Kuo, C.-T., Wang, J.-Y., Lin, Y.-F., Wo, A. M., Chen, B. P. C., & Lee, H. (2017). Three-dimensional spheroid culture targeting versatile tissue bioassays using a PDMS-based hanging drop array. *Scientific Reports, 7*(1), 4363.
113. Leonard, F., & Godin, B. (2016). 3D in vitro model for breast cancer research using magnetic levitation and bioprinting method. *Methods in Molecular Biology, 1406*, 239–251.
114. Benien, P., & Swami, A. (2014). 3D tumor models: History, advances and future perspectives. *Future Oncology, 10*(7), 1311–1327.
115. Metzger, W., Sossong, D., Bächle, A., Pütz, N., Wennemuth, G., Pohlemann, T., et al. (2011). The liquid overlay technique is the key to formation of co-culture spheroids consisting of primary osteoblasts, fibroblasts and endothelial cells. *Cytotherapy, 13*(8), 1000–1012.
116. Costa, E. C., de Melo-Diogo, D., Moreira, A. F., Carvalho, M. P., & Correia, I. J. (2018). Spheroids formation on non-adhesive surfaces by liquid overlay technique: Considerations and practical approaches. *Biotechnology Journal, 13*(1).
117. Jou, C.-H., Chen, W., Yang, M. J., Hwang, M.-C., Chou, W.-L., Lin, S.-M., et al. (2008). In vitro biocompatibility of three-dimensional chitosan scaffolds immobilized with chondroitin-6-sulfate. *Polymers for Advanced Technologies, 19*(5), 377–384.
118. Ma, H., Jiang, Q., Han, S., Wu, Y., Cui Tomshine, J., Wang, D., et al. (2012). Multicellular tumor spheroids as an in vivo-like tumor model for three-dimensional imaging of chemotherapeutic and nano material cellular penetration. *Molecular Imaging, 11*(6), 487–498.
119. RLF, A., Miranda, M., Marcato, P. D., & Swiech, K. (2017). Comparative analysis of 3D bladder tumor spheroids obtained by forced floating and hanging drop methods for drug screening. *Frontiers in Physiology, 8*, 605. Available from: https://www.frontiersin.org/articles/10.3389/fphys.2017.00605/full.
120. Breslin, S., & O'Driscoll, L. (2013). Three-dimensional cell culture: The missing link in drug discovery. *Drug Discovery Today, 18*(5–6), 240–249.
121. Foty, R. (2011). A simple hanging drop cell culture protocol for generation of 3D spheroids. *Journal of Visualized Experiments*, (51), 2720.
122. Timmins, N. E., & Nielsen, L. K. (2007). Generation of multicellular tumor spheroids by the hanging-drop method. *Methods in Molecular Medicine, 140*, 141–151.
123. Moshksayan, K., Kashaninejad, N., & Saidi, M. S. (2018). Inventions and innovations in preclinical platforms for cancer research. *Inventions, 3*(3), 43.
124. Massai, D., Isu, G., Madeddu, D., Cerino, G., Falco, A., Frati, C., et al. (2016). A versatile bioreactor for dynamic suspension cell culture. Application to the culture of cancer cell spheroids. *PLoS One, 11*(5), e0154610.
125. Joseph, J. S., Malindisa, S. T., & Ntwasa, M. (2018). Two-dimensional (2D) and three-dimensional (3D) cell culturing in drug discovery.
126. Caliari, S. R., & Burdick, J. A. (2016). A practical guide to hydrogels for cell culture. *Nature Methods, 13*(5), 405–414.
127. Hughes, C. S., Postovit, L. M., & Lajoie, G. A. (2010). Matrigel: A complex protein mixture required for optimal growth of cell culture. *Proteomics, 10*(9), 1886–1890.
128. Li, Y., & Kumacheva, E. (2018). Hydrogel microenvironments for cancer spheroid growth and drug screening. *Science Advances, 4*(4), eaas8998.
129. Haycock, J. W. (2011). 3D cell culture: A review of current approaches and techniques. *Methods in Molecular Biology, 695*, 1–15.
130. Animals in scientific research – Environment – European Commission [Internet]. [cited 2019 Dec 27]. Available from: https://ec.europa.eu/environment/chemicals/lab_animals/3r/scientific_conference_non_animal_approaches_en.htm.
131. Fröhlich, E. (2018). Comparison of conventional and advanced in vitro models in the toxicity testing of nanoparticles. *Artificial Cells, Nanomedicine, and Biotechnology, 46*(Suppl 2), 1091–1107.
132. van den Brand, D., Massuger, L. F., Brock, R., & Verdurmen, W. P. R. (2017). Mimicking tumors: Toward more predictive in vitro models for peptide- and protein-conjugated drugs. *Bioconjugate Chemistry, 28*(3), 846–856.
133. Friedrich, J., Seidel, C., Ebner, R., & Kunz-Schughart, L. A. (2009). Spheroid-based drug screen: Considerations and practical approach. *Nature Protocols, 4*(3), 309–324.
134. Hornung, A., Poettler, M., Friedrich, R. P., Weigel, B., Duerr, S., Zaloga, J., et al. (2016). Toxicity of mitoxantrone-loaded superparamagnetic iron oxide nanoparticles in a HT-29 tumour spheroid model. *Anticancer Research, 36*(6), 3093–3101.
135. Bonafè, F., Pazzini, C., Marchionni, S., Guarnieri, C., & Muscari, C. (2019). Complete disaggregation of MCF-7-derived breast tumour spheroids with very low concentrations of α-mangostin loaded in CD44 thioaptamer-tagged nanoparticles. *International Journal of Medical Sciences, 16*(1), 33–42.
136. De Simone, U., Roccio, M., Gribaldo, L., Spinillo, A., Caloni, F., & Coccini, T. (2018). Human 3D cultures as models for evaluating magnetic nanoparticle CNS cytotoxicity after short- and repeated long-term exposure. *International Journal of Molecular Sciences, 19*(7), 1993.
137. Bugno, J., Hsu, H.-J., Pearson, R. M., Noh, H., & Hong, S. (2016). Size and surface charge of engineered poly(amidoamine) dendrimers modulate tumor accumulation and penetration: A model study using multicellular tumor spheroids. *Molecular Pharmaceutics, 13*(7), 2155–2163.
138. Rodallec, A., Sicard, G., Giacometti, S., Carré, M., Pourroy, B., Bouquet, F., et al. (2018). From 3D spheroids to tumor bearing mice: Efficacy and distribution studies of trastuzumab-docetaxel immunoliposome in breast cancer. *International Journal of Nanomedicine, 13*, 6677–6688.
139. Wong, C., Vosburgh, E., Levine, A. J., Cong, L., & Xu, E. Y. (2012). Human neuroendocrine tumor cell lines as a three-dimensional model for the study of human neuroendocrine tumor therapy. *Journal of Visualized Experiments*, (66), e4218.
140. Leite, P. E. C., Pereira, M. R., Harris, G., Pamies, D., dos Santos, L. M. G., Granjeiro, J. M., et al. (2019). Suitability of 3D human brain spheroid models to distinguish toxic effects of gold and poly-lactic acid nanoparticles to assess biocompatibility for brain drug delivery. *Particle and Fibre Toxicology, 16*(1), 22.
141. Bresciani, G., Hofland, L. J., Dogan, F., Giamas, G., Gagliano, T., & Zatelli, M. C. (2019). Evaluation of spheroid 3D culture methods to study a pancreatic neuroendocrine neoplasm cell line. *Frontiers in Endocrinology, 10*, 682. Available from: https://www.frontiersin.org/articles/10.3389/fendo.2019.00682/full.
142. Lu, H., Noorani, L., Jiang, Y., Du, A. W., & Stenzel, M. H. (2017). Penetration and drug delivery of albumin nanoparticles into

pancreatic multicellular tumor spheroids. *Journal of Materials Chemistry B, 5*(48), 9591–9599.

143. Herrera-Martínez, A. D., van den Dungen, R., Dogan-Oruc, F., van Koetsveld, P. M., Culler, M. D., de Herder, W. W., et al. (2019). Effects of novel somatostatin-dopamine chimeric drugs in 2D and 3D cell culture models of neuroendocrine tumors. *Endocrine-Related Cancer, 26*(6), 585–599.
144. Decker, T., & Lohmann-Matthes, M. L. (1988). A quick and simple method for the quantitation of lactate dehydrogenase release in measurements of cellular cytotoxicity and tumor necrosis factor (TNF) activity. *Journal of Immunological Methods, 115*(1), 61–69.
145. Kumar, P., Nagarajan, A., & Uchil, P. D. (2018). Analysis of cell viability by the MTT assay. *Cold Spring Harbor Protocols, 2018*(6).
146. Kabakov, A. E., & Gabai, V. L. (2018). Cell death and survival assays. *Methods in Molecular Biology, 1709*, 107–127.
147. Khalili Fard, J., Jafari, S., & Eghbal, M. A. (2015). A review of molecular mechanisms involved in toxicity of nanoparticles. *Advanced Pharmaceutical Bulletin, 5*(4), 447–454.
148. Strober, W. (2015). Trypan blue exclusion test of cell viability. *Current Protocols in Immunology, 111*, A3.B.1–A3.B.3.
149. Marquis, B. J., Love, S. A., Braun, K. L., & Haynes, C. L. (2009). Analytical methods to assess nanoparticle toxicity. *The Analyst, 134*(3), 425–439.
150. Durymanov, M., Kroll, C., Permyakova, A., O'Neill, E., Sulaiman, R., Person, M., et al. (2019). Subcutaneous inoculation of 3D pancreatic cancer spheroids results in development of reproducible stroma-rich tumors. *Translational Oncology, 12*(1), 180–189.
151. Donaldson, K., Poland, C. A., & Schins, R. P. F. (2010). Possible genotoxic mechanisms of nanoparticles: Criteria for improved test strategies. *Nanotoxicology, 4*, 414–420.
152. Jaros, J., Petrov, M., Tesarova, M., & Hampl, A. (2017). Revealing 3D ultrastructure and morphology of stem cell spheroids by electron microscopy. *Methods in Molecular Biology, 1612*, 417–431.
153. Agarwal, R., Jurney, P., Raythatha, M., Singh, V., Sreenivasan, S. V., Shi, L., et al. (2015). Effect of shape, size, and aspect ratio on nanoparticle penetration and distribution inside solid tissues using 3D spheroid models. *Advanced Healthcare Materials, 4*(15), 2269–2280.
154. Hornung, A., Poettler, M., Friedrich, R. P., Zaloga, J., Unterweger, H., Lyer, S., et al. (2015). Treatment efficiency of free and nanoparticle-loaded mitoxantrone for magnetic drug targeting in multicellular tumor spheroids. *Molecules, 20*(10), 18016–18030.
155. Lee, J. M., Park, D. Y., Yang, L., Kim, E.-J., Ahrberg, C. D., Lee, K.-B., et al. (2018). Generation of uniform-sized multicellular tumor spheroids using hydrogel microwells for advanced drug screening. *Scientific Reports, 8*(1), 17145.
156. Zhang, L., Wang, Y., Yang, D., Huang, W., Hao, P., Feng, S., et al. (2019). Shape effect of nanoparticles on tumor penetration in monolayers versus spheroids. *Molecular Pharmaceutics, 16*(7), 2902–2911.
157. Alkilany, A. M., & Murphy, C. J. (2010). Toxicity and cellular uptake of gold nanoparticles: What we have learned so far? *Journal of Nanoparticle Research, 12*(7), 2313–2333.
158. Rane, T. D., & Armani, A. M. (2016). Two-photon microscopy analysis of gold nanoparticle uptake in 3D cell spheroids. *PLoS One, 11*(12), e0167548.
159. Durand, R. E. (1982). Use of Hoechst 33342 for cell selection from multicell systems. *Journal of Histochemistry & Cytochemistry, 30*(2), 117–122. Available from: https://journals.sagepub.com/doi/10.1177/30.2.6174559.
160. Ozcelikkale, A., Shin, K., Noe-Kim, V., Elzey, B. D., Dong, Z., Zhang, J.-T., et al. (2017). Differential response to doxorubicin in breast cancer subtypes simulated by a microfluidic tumor model. *Journal of Controlled Release, 266*, 129–139.
161. Yang, E., Qian, W., Cao, Z., Wang, L., Bozeman, E. N., Ward, C., et al. (2015). Theranostic nanoparticles carrying doxorubicin attenuate targeting ligand specific antibody responses following systemic delivery. *Theranostics, 5*(1), 43–61.
162. Janoniene, A., Liu, Z., Baranauskiene, L., Mäkilä, E., Ma, M., Salonen, J., et al. (2017). A versatile carbonic anhydrase IX targeting ligand-functionalized porous silicon nanoplatform for dual hypoxia cancer therapy and imaging. *ACS Applied Materials & Interfaces, 9*(16), 13976–13987.
163. Mulholland, T., McAllister, M., Patek, S., Flint, D., Underwood, M., Sim, A., et al. (2018). Drug screening of biopsy-derived spheroids using a self-generated microfluidic concentration gradient. *Scientific Reports, 8*, 14672. Available from: https://www.ncbi.nlm.nih.gov/pmc/articles/PMC6168499/.
164. Mitchell, M. J., Jain, R. K., & Langer, R. (2017). Engineering and physical sciences in oncology: Challenges and opportunities. *Nature Reviews. Cancer, 17*(11), 659–675.
165. Wu, L. Y., Di Carlo, D., & Lee, L. P. (2008). Microfluidic self-assembly of tumor spheroids for anticancer drug discovery. *Biomedical Microdevices, 10*(2), 197–202.
166. Toh, Y.-C., Zhang, C., Zhang, J., Khong, Y. M., Chang, S., Samper, V. D., et al. (2007). A novel 3D mammalian cell perfusion-culture system in microfluidic channels. *Lab on a Chip, 7*(3), 302–309.
167. Wang, X.-Y., Pei, Y., Xie, M., Jin, Z.-H., Xiao, Y.-S., Wang, Y., et al. (2015). An artificial blood vessel implanted three-dimensional microsystem for modeling transvascular migration of tumor cells. *Lab on a Chip, 15*(4), 1178–1187.
168. Mitxelena-Iribarren, O., Zabalo, J., Arana, S., & Mujika, M. (2019). Improved microfluidic platform for simultaneous multiple drug screening towards personalized treatment. *Biosensors & Bioelectronics, 123*, 237–243.
169. Zhuang, J., Zhang, J., Wu, M., & Zhang, Y. (2019). A dynamic 3D tumor spheroid chip enables more accurate nanomedicine uptake evaluation. *Advanced Science (Weinheim), 6*(22), 1901462. Available from: https://www.ncbi.nlm.nih.gov/pmc/articles/PMC6864993/.
170. Huang, K., Boerhan, R., Liu, C., & Jiang, G. (2017). Nanoparticles penetrate into the multicellular spheroid-on-chip: Effect of surface charge, protein corona, and exterior flow. *Molecular Pharmaceutics, 14*(12), 4618–4627.
171. Pandya, H. J., Dhingra, K., Prabhakar, D., Chandrasekar, V., Natarajan, S. K., Vasan, A. S., et al. (2017). A microfluidic platform for drug screening in a 3D cancer microenvironment. *Biosensors & Bioelectronics, 94*, 632–642.
172. Agarwal, P., Wang, H., Sun, M., Xu, J., Zhao, S., Liu, Z., et al. (2017). Microfluidics enabled bottom-up engineering of 3D vascularized tumor for drug discovery. *ACS Nano, 11*(7), 6691–6702.
173. Joris, F., Manshian, B. B., Peynshaert, K., De Smedt, S. C., Braeckmans, K., & Soenen, S. J. (2013). Assessing nanoparticle toxicity in cell-based assays: Influence of cell culture parameters and optimized models for bridging the in vitro-in vivo gap. *Chemical Society Reviews, 42*(21), 8339–8359.
174. Sokolov, S. V., Tschulik, K., Batchelor-McAuley, C., Jurkschat, K., & Compton, R. G. (2015). Reversible or not? Distinguishing agglomeration and aggregation at the nanoscale. *Analytical Chemistry, 87*(19), 10033–10039.
175. Engelmann, U., Buhl, E. M., Baumann, M., Schmitz-Rode, T., & Slabu, I. (2017). Agglomeration of magnetic nanoparticles and its effects on magnetic hyperthermia. *Current Directions in Biomedical Engineering, 3*(2), 457–460. Available from: http://www.degruyter.com/view/j/cdbme.2017.3.issue-2/cdbme-2017-0096/cdbme-2017-0096.xml.
176. Leong, D. T., & Ng, K. W. (2014). Probing the relevance of 3D cancer models in nanomedicine research. *Advanced Drug Delivery Reviews, 79–80*, 95–106.

177. Hinderliter, P. M., Minard, K. R., Orr, G., Chrisler, W. B., Thrall, B. D., Pounds, J. G., et al. (2010). ISDD: A computational model of particle sedimentation, diffusion and target cell dosimetry for in vitro toxicity studies. *Particle and Fibre Toxicology, 7*(1), 36.
178. Frieke Kuper, C., Gröllers-Mulderij, M., Maarschalkerweerd, T., Meulendijks, N. M. M., Reus, A., van Acker, F., et al. (2015). Toxicity assessment of aggregated/agglomerated cerium oxide nanoparticles in an in vitro 3D airway model: The influence of mucociliary clearance. *Toxicology In Vitro, 29*(2), 389–397.
179. Cho, E. C., Zhang, Q., & Xia, Y. (2011). The effect of sedimentation and diffusion on cellular uptake of gold nanoparticles. *Nature Nanotechnology, 6*(6), 385–391.
180. Thomas, D. G., Smith, J. N., Thrall, B. D., Baer, D. R., Jolley, H., Munusamy, P., et al. (2018). ISD3: A particokinetic model for predicting the combined effects of particle sedimentation, diffusion and dissolution on cellular dosimetry for in vitro systems. *Particle and Fibre Toxicology, 15*(1), 6.
181. Grabinski, C., Sharma, M., Maurer, E., Sulentic, C., Mohan Sankaran, R., & Hussain, S. (2016). The effect of shear flow on nanoparticle agglomeration and deposition in in vitro dynamic flow models. *Nanotoxicology, 10*(1), 74–83.
182. Björnmalm, M., Faria, M., Chen, X., Cui, J., & Caruso, F. (2016). Dynamic flow impacts cell–particle interactions: Sedimentation and particle shape effects. *Langmuir, 32*(42), 10995–11001.
183. Gao, Y., Li, M., Chen, B., Shen, Z., Guo, P., Wientjes, M. G., et al. (2013). Predictive models of diffusive nanoparticle transport in 3-dimensional tumor cell spheroids. *The AAPS Journal, 15*(3), 816–831.
184. García, I., Henriksen-Lacey, M., Calvo, J., de Aberasturi, D. J., Paz, M. M., & Liz-Marzán, L. M. (2019). Size-dependent transport and cytotoxicity of mitomycin-gold nanoparticle conjugates in 2D and 3D mammalian cell models. *Bioconjugate Chemistry, 30*(1), 242–252.
185. Mikhail, A. S., Eetezadi, S., Ekdawi, S. N., Stewart, J., & Allen, C. (2014). Image-based analysis of the size- and time-dependent penetration of polymeric micelles in multicellular tumor spheroids and tumor xenografts. *International Journal of Pharmaceutics, 464*(1–2), 168–177.
186. Guo, X., Wu, Z., Li, W., Wang, Z., Li, Q., Kong, F., et al. (2016). Appropriate size of magnetic nanoparticles for various bioapplications in cancer diagnostics and therapy. *ACS Applied Materials & Interfaces, 8*(5), 3092–3106.
187. Durymanov, M., Kroll, C., Permyakova, A., & Reineke, J. (2019). Role of endocytosis in nanoparticle penetration of 3D pancreatic cancer spheroids. *Molecular Pharmaceutics, 16*(3), 1074–1082.
188. Kim, J., Jo, C., Lim, W.-G., Jung, S., Lee, Y. M., Lim, J., et al. (2018). Programmed nanoparticle-loaded nanoparticles for deep-penetrating 3D cancer therapy. *Advanced Materials, 18*, e1707557.
189. Ruan, S., Cao, X., Cun, X., Hu, G., Zhou, Y., Zhang, Y., et al. (2015). Matrix metalloproteinase-sensitive size-shrinkable nanoparticles for deep tumor penetration and pH triggered doxorubicin release. *Biomaterials, 60*, 100–110.
190. Huang, B.-W., & Gao, J.-Q. (2018). Application of 3D cultured multicellular spheroid tumor models in tumor-targeted drug delivery system research. *Journal of Controlled Release, 270*, 246–259.
191. Bugno, J., Poellmann, M. J., Sokolowski, K., Hsu, H., Kim, D.-H., & Hong, S. (2019). Tumor penetration of Sub-10 nm nanoparticles: Effect of dendrimer properties on their penetration in multicellular tumor spheroids. *Nanomedicine: Nanotechnology, Biology and Medicine, 21*, 102059.
192. Charoen, K. M., Fallica, B., Colson, Y. L., Zaman, M. H., & Grinstaff, M. W. (2014). Embedded multicellular spheroids as a biomimetic 3D cancer model for evaluating drug and drug-device combinations. *Biomaterials, 35*(7), 2264–2271.
193. Froehlich, K., Haeger, J.-D., Heger, J., Pastuschek, J., Photini, S. M., Yan, Y., et al. (2016). Generation of multicellular breast cancer tumor spheroids: Comparison of different protocols. *Journal of Mammary Gland Biology and Neoplasia, 21*(3–4), 89–98.
194. Langan, L. M., Dodd, N. J. F., Owen, S. F., Purcell, W. M., Jackson, S. K., & Jha, A. N. (2016). Direct measurements of oxygen gradients in spheroid culture system using electron parametric resonance oximetry. *PLoS One, 11*(2), e0149492.
195. Sheth, D. B., & Gratzl, M. (2019). Electrochemical mapping of oxygenation in the three-dimensional multicellular tumour hemi-spheroid. *Proceedings of the Royal Society A Mathematical Physical and Engineering Sciences, 475*(2225), 20180647.
196. Cui, X., Hartanto, Y., & Zhang, H. (2017). Advances in multicellular spheroids formation. *Journal of the Royal Society Interface, 14*(127).
197. Shi, W., Kwon, J., Huang, Y., Tan, J., Uhl, C. G., He, R., et al. (2018). Facile tumor spheroids formation in large quantity with controllable size and high uniformity. *Scientific Reports, 8*(1), 6837.
198. Grimes, D. R., & Currell, F. J. (2018). Oxygen diffusion in ellipsoidal tumour spheroids. *Journal of the Royal Society Interface, 15*(145), 20180256.
199. Shabana, A. M., Mondal, U. K., Alam, M. R., Spoon, T., Ross, C. A., Madesh, M., et al. (2018). pH-sensitive multiligand gold nanoplatform targeting carbonic anhydrase IX enhances the delivery of doxorubicin to hypoxic tumor spheroids and overcomes the hypoxia-induced chemoresistance. *ACS Applied Materials & Interfaces, 10*(21), 17792–17808.
200. Wang, Z., Zhang, Y., Ju, E., Liu, Z., Cao, F., Chen, Z., et al. (2018). Biomimetic nanoflowers by self-assembly of nanozymes to induce intracellular oxidative damage against hypoxic tumors. *Nature Communications, 9*(1), 3334.
201. Deng, L., Feng, Z., Deng, H., Jiang, Y., Song, K., Shi, Y., et al. (2019). Rational design of nanoparticles to overcome poor tumor penetration and hypoxia-induced chemotherapy resistance: Combination of optimizing size and self-inducing high level of reactive oxygen species. *ACS Applied Materials & Interfaces, 11*(35), 31743–31754.
202. Arakawa, A., Jakubowski, N., Koellensperger, G., Theiner, S., Schweikert, A., Flemig, S., et al. (2019). Quantitative imaging of silver nanoparticles and essential elements in thin sections of fibroblast multicellular spheroids by high resolution laser ablation inductively coupled plasma time-of-flight mass spectrometry. *Analytical Chemistry, 91*(15), 10197–10203.
203. Priwitaningrum, D. L., Blondé, J.-B. G., Sridhar, A., van Baarlen, J., Hennink, W. E., Storm, G., et al. (2016). Tumor stroma-containing 3D spheroid arrays: A tool to study nanoparticle penetration. *Journal of Controlled Release, 244*(Pt B), 257–268.
204. Miao, L., Newby, J. M., Lin, C. M., Zhang, L., Xu, F., Kim, W. Y., et al. (2016). The binding site barrier elicited by tumor-associated fibroblasts interferes disposition of nanoparticles in stroma-vessel type tumors. *ACS Nano, 10*(10), 9243–9258.
205. Jain, R. K., & Stylianopoulos, T. (2010). Delivering nanomedicine to solid tumors. *Nature Reviews. Clinical Oncology, 7*(11), 653–664.
206. Lieleg, O., Baumgärtel, R. M., & Bausch, A. R. (2009). Selective filtering of particles by the extracellular matrix: An electrostatic bandpass. *Biophysical Journal, 97*(6), 1569–1577.
207. Zhang, B., Shen, S., Liao, Z., Shi, W., Wang, Y., Zhao, J., et al. (2014). Targeting fibronectins of glioma extracellular matrix by CLT1 peptide-conjugated nanoparticles. *Biomaterials, 35*(13), 4088–4098.
208. Lee, B. H., Kim, M. H., Lee, J. H., Seliktar, D., Cho, N.-J., & Tan, L. P. (2015). Modulation of Huh7.5 spheroid formation and

functionality using modified PEG-based hydrogels of different stiffness. *PLoS One, 10*(2), e0118123.

209. Baye, J., Galvin, C., & Shen, A. Q. (2017). Microfluidic device flow field characterization around tumor spheroids with tunable necrosis produced in an optimized off-chip process. *Biomedical Microdevices, 19*(3), 59.

210. Lazzari, G., Vinciguerra, D., Balasso, A., Nicolas, V., Goudin, N., Garfa-Traore, M., et al. (2019). Light sheet fluorescence microscopy versus confocal microscopy: In quest of a suitable tool to assess drug and nanomedicine penetration into multicellular tumor spheroids. *European Journal of Pharmaceutics and Biopharmaceutics, 142*, 195–203.

In Vitro and In Vivo Tumor Models for the Evaluation of Anticancer Nanoparticles

Teresa R. Abreu, Mariana Biscaia, Nélio Gonçalves,
Nuno A. Fonseca, and João Nuno Moreira

Abstract

Multiple studies about tumor biology have revealed the determinant role of the tumor microenvironment in cancer progression, resulting from the dynamic interactions between tumor cells and surrounding stromal cells within the extracellular matrix. This malignant microenvironment highly impacts the efficacy of anticancer nanoparticles by displaying drug resistance mechanisms, as well as intrinsic physical and biochemical barriers, which hamper their intratumoral accumulation and biological activity.

Currently, two-dimensional cell cultures are used as the initial screening method in vitro for testing cytotoxic nanocarriers. However, this fails to mimic the tumor heterogeneity, as well as the three-dimensional tumor architecture and pathophysiological barriers, leading to an inaccurate pharmacological evaluation.

Biomimetic 3D in vitro tumor models, on the other hand, are emerging as promising tools for more accurately assessing nanoparticle activity, owing to their ability to recapitulate certain features of the tumor microenvironment and thus provide mechanistic insights into nanocarrier intratumoral penetration and diffusion rates.

Notwithstanding, in vivo validation of nanomedicines remains irreplaceable at the preclinical stage, and a vast variety of more advanced in vivo tumor models is currently available. Such complex animal models (e.g., genetically engineered mice and patient-derived xenografts) are capable of better predicting nanocarrier clinical efficiency, as they closely resemble the heterogeneity of the human tumor microenvironment.

Herein, the development of physiologically more relevant in vitro and in vivo tumor models for the preclinical evaluation of anticancer nanoparticles will be discussed, as well as the current limitations and future challenges in clinical translation.

Keywords

Nanoparticles · Tumor microenvironment · Intratumoral penetration · Preclinical screening · 2D cultures · 3D tumor models · Multicellular tumor spheroids · 3D scaffolds · Microfluidics · Tumor-on-a-chip · Cell line-derived models · Genetically engineered mice · Patient-derived xenografts · Humanized models · Clinical translation

1 Introduction

In the last decades, the active research in the area of cancer cell biology and tumor etiology have unveiled the critical role of the tumor microenvironment (TME) in tumor progression, invasion, and metastasis [1]. It has been recognized that cancer results from a multistep process, supported by the

---

T. R. Abreu · J. N. Moreira (✉)
CNC – Center for Neurosciences and Cell Biology, Center for Innovative Biomedicine and Biotechnology (CIBB), University of Coimbra, Faculty of Medicine (Polo 1), Rua Larga, Coimbra, Portugal

UC – University of Coimbra, CIBB, Faculty of Pharmacy, Pólo das Ciências da Saúde, Azinhaga de Santa Comba, Coimbra, Portugal
e-mail: jmoreira@ff.uc.pt

M. Biscaia · N. Gonçalves
CNC – Center for Neurosciences and Cell Biology, Center for Innovative Biomedicine and Biotechnology (CIBB), University of Coimbra, Faculty of Medicine (Polo 1), Rua Larga, Coimbra, Portugal

N. A. Fonseca
CNC – Center for Neurosciences and Cell Biology, Center for Innovative Biomedicine and Biotechnology (CIBB), University of Coimbra, Faculty of Medicine (Polo 1), Rua Larga, Coimbra, Portugal

TREAT U, SA, Parque Industrial de Taveiro, Lote 44, Coimbra, Portugal

© Springer Nature Switzerland AG 2021
F. Fontana, H. A. Santos (eds.), *Bio-Nanomedicine for Cancer Therapy*, Advances in Experimental Medicine and Biology 1295, https://doi.org/10.1007/978-3-030-58174-9_12

dynamic interactions between malignant and nonmalignant neighboring cells, rather than solely depending on the genetic and epigenetic alterations on both oncogenes and tumor suppressor genes of single cells [2]. The TME is a complex and heterogeneous organ-like structure divided into two main regions: the tumor parenchyma, containing highly proliferative cancer cells, and the stromal compartment, harboring different cell populations, including endothelial cells from the blood and lymphatic vessels, pericytes, cancer-associated fibroblasts (CAFs), and adaptive and innate infiltrating immune cells (Fig. 1). [3]. The stromal cells are settled in an extracellular matrix (ECM) composed of an intricate network of glycoproteins, collagen fibers, hyaluronan, sulfated glycosaminoglycans, and proteoglycans (Fig. 1) [4, 5].

The cross talk between cancer and stromal cells, including cell-matrix dynamic interplay, is driven by both biochemical (i.e., growth and angiogenic factors, cytokines, cell adhesion molecules, etc.) and biophysical (i.e., matrix stiffness, contraction, topography and composition, etc.) cues that provide insights into the tumor three-dimensional architecture and malignant behavior [5, 6]. In fact, tumor stroma-mediated interactions involving CAFs and matrix components have shown to promote malignant phenotypes in benign tissues [7]. Conversely, the addition of nonmalignant components to preestablished epithelial tumors has demonstrated to normalize cell phenotype and regenerate normal tissue organization [8, 9]. These facts further support the critical role of the TME in determining tumor cell fate, by regulating their morphology, signaling pathways, proliferation rates, and metastatic behavior [10].

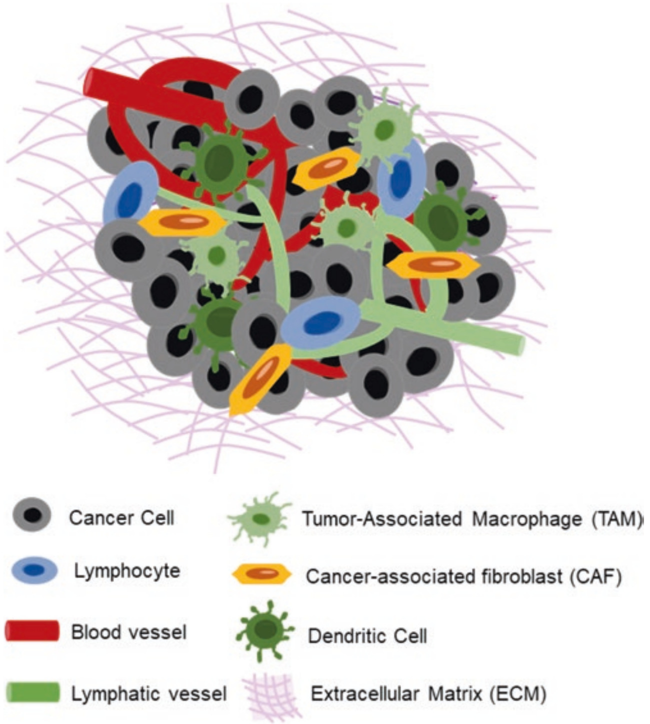
Cancer Cell
Lymphocyte
Blood vessel
Lymphatic vessel
Tumor-Associated Macrophage (TAM)
Cancer-associated fibroblast (CAF)
Dendritic Cell
Extracellular Matrix (ECM)

Fig. 1 Schematic representation of the tumor microenvironment. In the tumor niche, cancer cells are surrounded by other host cellular components including adaptive and innate infiltrating immune cells, endothelial cells from the blood and lymphatic circulation, and cancer-associated fibroblasts. These supporting cells regulate ECM dynamics (i.e., variable composition and three-dimensional arrangement), as well as malignant behavior of cancer cells, upon secreting growth factors, cytokines, and other signaling molecules

To further maintain growth and survival of cancer cells, the tumor exhibits both drug class-specific (e.g., metabolic drug inactivation or lack of drug activation and loss, downregulation or mutation of specific therapeutic tumor targets) and multidrug resistance mechanisms (e.g., overexpression of cell membrane efflux pumps, enhanced antiapoptotic signaling, alterations in cell cycle checkpoints, activation of alternative compensatory signaling pathways, enhanced activation of DNA damage repair mechanisms, etc.) [11, 12]. In addition, the TME's abnormal angiogenic vasculature, with subsequent increase of interstitial pressure in the center of solid tumors, and dense interstitial matrix protect cancer cells from cytotoxic agents by limiting their deeper tumoral penetration [13, 14]. Other intrinsic barriers related to (1) the tumor chemical milieu, which exhibit low partial oxygen pressure, acidic conditions (due to the accumulation of metabolic waste), as well as inhibitory cytokines and growth factors; (2) the inherent tumor cell molecular heterogeneity; and (3) tumor-stroma dynamic interactions further promote microenvironment-mediated drug resistance [15, 16], limiting the pharmacodynamics of both free-drug chemotherapeutics and drug-loaded nanotechnology-based platforms.

Considering the critical role of the TME in the clinical success of anticancer nanotherapies, this chapter will firstly address the specific barriers posed by the TME that affect the pharmacodynamics of nanoparticles at the tumor site. Secondly, the development of physiologically more relevant in vitro and in vivo tumor models, capable of reproducing the TME, will be discussed, further detailing the different types of models available, screening applications, and limitations and challenges to be overcome in clinical translation.

2 The Impact of the Tumor Microenvironment on Cancer Nanomedicine

2.1 Targeting Nanoparticles Toward the Tumor Microenvironment

In the context of cancer treatment, the administration of drug-loaded nanoparticles has shown critical advantages over conventional free-drug chemotherapy, particularly in modulating pharmacokinetics, enabling a significant reduction of treatment-related toxicities [17–20]. The primary rationale for delivering nanoparticles to solid tumors is ascribed to the enhanced permeability and retention (EPR) effect, which predicts that systemically administered nanocarriers tend to accumulate in the tumor site, owing to the tumor's leaky blood vessels and insufficient lymphatic drainage [21, 22]. In fact, most clinically approved nanomedicines for cancer treatment, including liposomes [18, 19, 23–25], albumin-bound nanoparticles [17, 26, 27], and polymeric micelles [28], are exclusively based on EPR-mediated passive targeting. However, from those, few have demonstrated significant clinical benefit, in terms of increased survival and therapeutic efficacy, over free-drug chemotherapy [17, 24]. The cause may be attributed to inefficient tumor drug delivery, owing to the heterogeneity of the EPR effect in patient tumors. Briefly, multiple aspects of nanoparticle's intrinsic properties (e.g., size, shape, charge, surface chemistry, internal composition, etc.) and systemic biodistribution (e.g., circulation halftime, clearance rate by the mononuclear phagocytic system, off-target interactions, tissue penetration, etc.), as well as the tumors' own biological features, can influence the extent of the EPR and subsequent drug distribution throughout the tumor tissue [29]. For example, poorly vascularized tumors show size-dependent restrictions on nanoparticle extravasation and intratumoral penetration, owing to the decreased extent of this effect [30]. Hence, the EPR effect does not enable uniform drug delivery to all regions of the tumor, being highly heterogeneous within and between both tumor types (i.e., intra- and inter-tumor variability) and patients [29, 31].

Although not affecting overall tumor localization, functionalizing nanoparticles' surface with ligands (including antibodies or their fragments) that specifically recognize overexpressed molecules on cancer cells has demonstrated to enhance the mechanism of cellular uptake [32]. Briefly, ligand-mediated targeting enables cell internalization by receptor-mediated endocytosis, leading to increased intracellular drug delivery [33–36]. In this context, long-circulating, ligand-mediated targeted nanocarriers capable of co-delivering synergistic chemotherapeutic combinations specifically at the tumor site are less prone to tumor-mediated resistance mechanisms, in contrast to their nontargeted and free-drug counterparts [37–40].

Given the role of the TME in cancer progression and tumor-mediated drug resistance, as well as its influence on the extent of the EPR effect, several drug-loaded nanoparticles targeting tumor-surrounding cells and other stromal components have been developed [41]. Promising targets include endothelial cells from the tumor vasculature [42, 43], CAFs [44], tumor-infiltrating immune cells such as antigen-presenting cells [45] and tumor-associated macrophages (TAMs) [46, 47], or even matrix components, like the glycoprotein tenascin-C [48, 49] and matrix metalloproteinases [50, 51]. Multi-targeting strategies toward both malignant and nonmalignant cells at the tumor site potentiate nanoparticle-mediated modulation of the tumor pathophysiology, further reducing cancer cell viability [52–55].

A different approach, also exploiting the TME's general features to improve selective drug delivery to the tumor, consists of designing stimuli-responsive nanoparticles. These trigger-dependent nanocarriers only release their payloads when exposed to specific properties of the TME, for instance, its acidic conditions [56–58], abnormal redox environment [59–61], or overexpression of activated matrix metalloproteinases [62, 63], allowing for precise spatiotemporal control of drug release kinetics.

2.2 The Tumors' Intrinsic Barriers to Nanomedicine

It is noteworthy that both ligand-coated and stimuli-responsive nanoparticles also depend on efficient passive targeting to reach their target sites, thus being susceptible to the same limitations of passively targeted nanocarriers [64], except for vascular-targeting nanoplatforms where tumor accumulation does not depend on the EPR effect. Once at the tumor site, both targeted and nontargeted nanoformulations are strongly affected by the intrinsic pathophysiological barriers of the TME [64].

Briefly, systemically administered anticancer nanoparticles, after overriding undesirable clearance by the mononuclear phagocytic and renal systems, flow to different regions of the tumor through blood vessels [65]. The abnormal organization of the angiogenic tumor vasculature, harboring tortuous and hyperpermeable vessels, leads to spatiotemporal heterogeneities in blood perfusion, limiting nanoparticle uniform distribution from the systemic circulation to the tumor [66]. Notwithstanding the potential of the EPR effect in delivering nanomedicines to solid tumors, the combination of leaky tumor vessels with dysfunctional lymphatic drainage results in high interstitial pressure, which has a detrimental effect in nanoparticle extravasation and interstitial transport (Fig. 2) [66]. The composition of the ECM, mainly its content in collagen fibers, also strongly contributes for interstitial hypertension. For example, highly dense, collagen-rich desmoplastic tumors prevent nanoparticle deep intratumoral penetration to a greater extension than low-collagen ones, further promoting their retention in perivascular regions (Fig. 2) [66, 67]. Moreover, the presence of highly proliferative cancer cells within the stroma compartment leads to solid stress, causing vessel compression and collapse, which further hinders nanoparticle interstitial penetration [67].

Apart from the physical barriers, upon reaching the tumor, nanoparticles face a hostile environment featuring hypoxic regions, tight cell-cell and cell-matrix interactions, low pH,

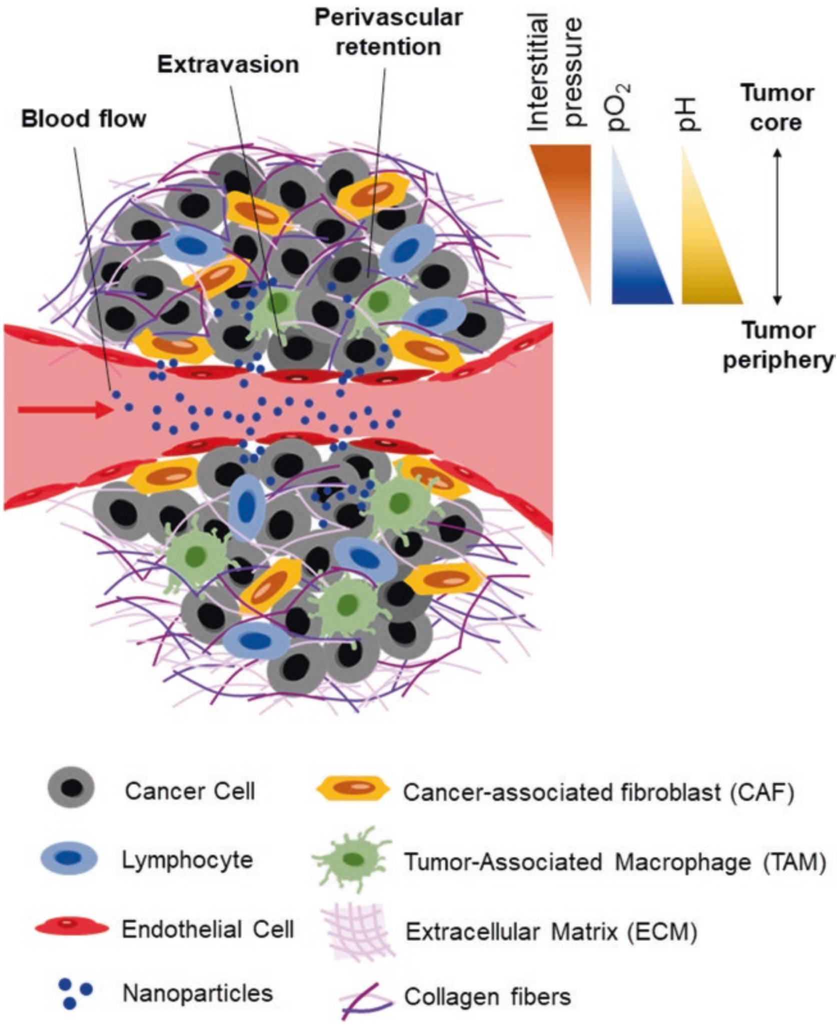

Fig. 2 The barriers of tumor microenvironment to nanomedicine delivery. The tumor vasculature high permeability along with vessel compression (subsequent to the physical forces arising from proliferating cancer and stromal cells) and poor lymphatic drainage lead to spatiotemporal heterogeneities in tumor perfusion, which prevent nanoparticle uniform distribution. Upon extravasation from tumor vessels, nanoparticles face a hostile environment characterized by interstitial hypertension (i.e., high hydrostatic pressure outside the blood vessels further increased by dense ECM rich in collagen fibers), hypoxia, and acidosis. Unwanted interactions with stromal cells, namely, with immune infiltrating cells, may also hinder nanoparticle diffusion. The abnormal tumor vasculature combined with high interstitial pressure and hostile chemical conditions prevents nanoparticle deeper tumoral penetration, promoting their perivascular accumulation. Hence, the TME poses a challenging barrier to the delivery and efficacy of cancer nanomedicine

necrotic core, heterogeneous molecular landscape, etc. that fuel intrinsic drug resistance, as detailed above. Unwanted interactions with stromal cells, such as nonspecific uptake by TAMs, may also hinder nanoparticle diffusion [68]. Surprisingly, Miller and coworkers have shown that TAMs can act as local drug depots, gradually releasing the payload of the internalized therapeutic nanoparticles to the TME [69].

Strategies to overcome these barriers and improve nanoparticle penetration into the tumor interstitium often include complementary preconditioning therapies aiming at normalizing the TME's physiological abnormalities [70]. For example, vascular normalization through inhibition of vascular endothelial growth factor (VEGF)-mediated signaling has demonstrated to enhance the transvascular delivery of intermediate-size nanoparticles (20–40 nm) within the ECM [71]. Another approach consists of ECM normalizing the extracellular matrix upon pretreatment with losartan, an angiotensin II receptor blocker (ARB) responsible for reducing collagen production, leading to a dramatic reduction in stromal collagen. This in turn enabled enhanced tumoral penetration and subsequent therapeutic efficacy of liposomal doxorubicin in desmoplastic tumor models [72].

In summary, the aberrant vasculature, high interstitial pressure, and variable matrix composition of the TME prevent nanoparticle homogeneous intratumoral distribution and subsequent uniform drug delivery throughout the tumor tissue. Moreover, the TME's hostile chemical milieu and heterogeneous molecular landscape limit the biological effects of nanotechnology-based platforms, decreasing their therapeutic benefit. Accordingly, understanding the complex role of the TME on the regulation of nanoparticle antitumor efficacy is of utmost importance upon the rational design of novel nanotechnology-based platforms for cancer treatment, particularly for the ones aiming at targeting and modifying its features. Therefore, given the impact of the TME in anticancer nanomedicines, as well as the potential of nanotechnology to modulate the tumor in its favor, the incorporation of TME's key features on both in vitro and in vivo screening systems emerges as a crucial factor to consider, within the preclinical evaluation of cancer nanomedicine. The generation of tumor models that more closely mimic the pathophysiology of human cancers, in order to provide more predictive therapeutic results, will be discussed below.

3 Preclinical Evaluation of Anticancer Nanoparticles In Vitro

3.1 Conventional Two-Dimensional Systems

3.1.1 General Features and Limitations

The concept of cell culturing was first introduced in 1907 by Harrison, who developed a method for maintaining biologically viable cells (i.e., active proliferation and differentiation) outside their organism of origin [73, 74]. Cell cultures have now been used for over a century as in vitro research models to lighten up the fundamental aspects of cell molecular biology and biochemical pathways, tissue morphogenesis and engineering, regenerative medicine, and mechanisms of disease, as well as to preform pharmaceutical studies [75–77]. In two-dimensional (2D) culture systems, cells previously isolated from living tissues grow homogeneously as monolayers attached to rigid plastic or glass substrates in culture flasks, Petri dishes, multi-well plates, or glass slides, filled with growth medium. These systems present significant advantages being well established models widely available with high robustness, low-cost maintenance, easy handling, and ability to perform high-throughput drug screening tests in a timely manner [78, 79].

Albeit the conventional use of 2D models as reliable tools for biomedical research and drug discovery, they exhibit several limitations, poorly representing the physiological patterns of cell differentiation, morphology, cytoskeletal organization, metabolism, migration, and signal transduction (Fig. 3) [76, 80–82]. Briefly, in a physiological environment, cells grow surrounded by different cell types in a three-dimensional architecture, within a complex matrix containing extracellular ligands responsible for regulating cell adherence and migration pathways [83]. In this network, cell-cell and cell-matrix communications are driven by both biochemical and mechanical cues, which in turn are responsible for maintaining the tissue's specificity and homeostasis [83, 84]. However, on 2D monocultures lacking a supportive matrix, these dynamic interactions and their inherent biological cues and molecular gradients are lost, leading to the dysregulation of innumerous biological processes, including cell migration, functional differentiation, proliferation, signal transduction, and stimuli responsiveness [82, 85]. Without environmental signaling, cultured cells significantly reduce their production of matrix proteins and undergo morphological changes, becoming progressively flatter with increased spreading capacity (i.e., abnormal proliferation leading to unnatural growth kinetics) [81, 86]. Moreover, on 2D conditions, cell surface receptors preferentially cluster on the cell parts directly exposed to the culture media, rich in nutrients, growth factors, and other ligands, rather than on the attached side of the cell. Nonphysiological orientation and clustering of cell receptors are likely to affect not only both intra- and intercellular signaling and subsequent phenotypic differentiation [86, 87] but also the binding efficiency of drugs designed to directly target those receptors [88].

The inherent limitations associated with rigidly adhered monolayer cultures become even more unwieldy in tumor biology studies, where the lack of structural features of the TME, namely, its heterogeneous stromal cell population and complex three-dimensional extracellular matrix, further decreases the physiological relevance of these models [89–91]. The conventional use of immortalized cell lines in cancer research is supported by their well-established genetic and histological classification, for each cancer type [92, 93]. However, it has already been shown that gene expression profiles of cultured tumor cells differ from their corresponding tumor tissues in vivo, which further highlights the impact of the TME three-dimensional architecture and cellular cross talk in determining tumor cell expression patterns, and subsequent biological activity [94–97]. In addition, mRNA splicing patterns have also demonstrated to be altered in tumor cells cultured under 2D conditions [98].

3.1.2 Screening Cancer Nanoparticles in 2D Models

In the field of cancer nanomedicine, established cancer cell lines are routinely used as the main in vitro model, preceding animal studies, for the initial preclinical evaluation of the effectiveness and safety of potentially therapeutic nanoparticles. Consequently, cell-based cytotoxicity assays assume a determinative role on the construction of "stop/go" decisions concerning the initial steps of nanomedicine development [99]. However, testing nanotechnology-based platforms in oversimplified 2D systems lacking general features of the

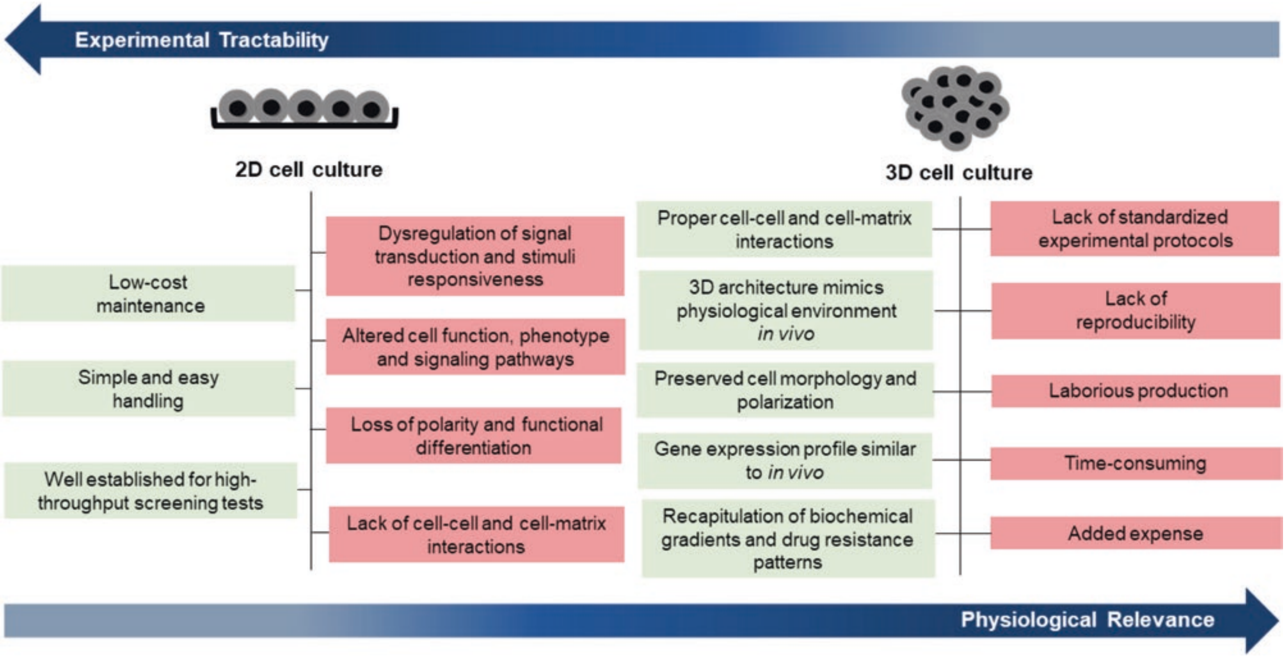
Experimental Tractability
2D cell culture
3D cell culture
Low-cost maintenance
Simple and easy handling
Well established for high-throughput screening tests
Dysregulation of signal transduction and stimuli responsiveness
Altered cell function, phenotype and signaling pathways
Loss of polarity and functional differentiation
Lack of cell-cell and cell-matrix interactions
Proper cell-cell and cell-matrix interactions
3D architecture mimics physiological environment *in vivo*
Preserved cell morphology and polarization
Gene expression profile similar to *in vivo*
Recapitulation of biochemical gradients and drug resistance patterns
Lack of standardized experimental protocols
Lack of reproducibility
Laborious production
Time-consuming
Added expense
Physiological Relevance

Fig. 3 Strengths and limitations of 2D and 3D cell culture systems. Two-dimensional cell culture has been the mainstay of cancer research due to its simplicity, cost-effectiveness, and reproducibility. However, its inherent limitations have prompted the development of 3D cell culture systems. By mimicking normal cell-matrix and cell-cell interactions, complex 3D tumor systems more closely represent the TME. Notwithstanding, the added expense, the laborious production, and the low reproducibility of 3D models decrease their experimental tractability when compared to monoculture systems

TME – herein demonstrated to play a critical role in regulating nanoparticle intratumoral distribution and antitumor efficacy – might lead to misleading results, not reflective of the behavior in vivo [91]. For instance, while tumor cells on static 2D cultures are settled in a uniform environment with unlimited access to nutrients and oxygen, cells on solid tumors are exposed to chemical gradients and heterogeneous fluid supplies that influence their malignant behavior [100]. The lack of physical barriers on 2D models provides nanoparticles straightforward access to tumor cells, enabling uniform drug delivery, which starkly contrasts with their heterogeneous distribution in solid tumors, owing to the intrinsic barriers of the TEM [66]. Moreover, the absence of tumor-stroma interactions precludes the generation and maintenance of microenvironment-mediated drug resistance mechanisms [16, 101], rendering cells on 2D cultures more sensitive to chemotherapeutic nanoparticles [102].

Accordingly, positive results provided by 2D screening platforms, concerning the efficacy of novel nanoformulations, demand critical assessment, avoiding overinterpretation, as nanoparticles are optimized to be highly effective on biased preclinical systems, rather than on real pathophysiological conditions [91].

3.2 Emerging Three-Dimensional Tumor Models

The awareness of the biological limitations and poor predictive power of 2D tumor cell cultures in cancer research and drug discovery has highlighted the critical role of including a third dimension on cell-based assays [103]. This paradigm shift has prompted the development of biomimetic three-dimensional (3D) cell cultures, capable of more closely reflecting the complexity of the human TME in vivo [104]. For example, Mina Bissel's group, one of the pioneers of organotypic tumor models (i.e., coculture of both tumor and stromal cells within a naturally derived ECM in 3D conditions), soon realized the importance of the tumor architecture in vitro [103]. They have shown that breast cancer cells cultured in 3D conditions underwent morphological and polarity changes, generating disorganized proliferative masses that closely resembled the ones observed in vivo during tumor progression [105, 106]. Indeed, it has been demonstrated that gene expression profiles of 2D cultured cells highly differ from those of the same cells cultured in 3D conditions, which in turn are similar to those observed in clinical tumor samples [107–109], such as the upregulation of genes encoding chemokines (e.g., interleukin-8) and angiogenic factors (e.g., angiopoietin and vascular endothelial growth factor) [110].

Nevertheless, despite the large improvement in the pathophysiological relevance, one should be aware of the challenges associated with 3D models, arising from their higher biological complexity [111]. Compared to well-established 2D systems, the generation of 3D models is time-consuming and poorly cost-effective, requires trained handling, and lacks reproducibility between research groups, owing to the inefficient standardization of experimental protocols (Fig. 3) [79]. Moreover, the methods applied to characterize or screen drug-induced modifications in these models must be adjusted to their 3D architecture and physical properties [112] and thus possibly differ from those used to evaluate the same parameters in 2D cultures. This theme will be further assessed on Sect. 3.2.2.

Regarding drug response, in contrast to cells cultured in monolayers, 3D cell systems have revealed significantly reduced sensitivity to chemotherapeutic agents in several studies [113–115], including to anticancer nanoparticles [116]. These outcomes highlight the capacity of 3D systems to reproduce some of the tumor-mediated drug resistance mechanisms, mainly due to their intrinsic tumor tissue-specific properties and cell-cell/cell-matrix dynamic cross talk, which are hardly achieved/maintained in 2D cell cultures [117]. Therefore, the inclusion of a third dimension on the preclinical evaluation of anticancer drugs, mainly anticancer nanoparticles, is of outmost importance to obtain more accurate results, capable of better predicting their antitumor efficacy in vivo. In this respect, the development of 3D in vitro tumor for drug screening has risen dramatically over the past years [102, 118, 119], and currently, a wide range of different 3D models are being applied in the preclinical evaluation of anticancer nanoparticles, as discussed below.

3.2.1 Types of 3D Models and Screening Applications

Multicellular Tumor Spheroids

The concept of multicellular tumor spheroids (MCTS) was first introduced by Costachel and colleagues who demonstrated that cancer cells cultured in a nonadhesive agar substratum were capable of forming proliferative aggregates in suspension (*cell islands*) [120]. MCTS are 3D constructs, with a diameter range from 100 μm to 1000 μm, based on the self-assembly of tumor cells cultured in suspension, deprived from attaching to a growth-promoting substrate [121].

There are several approaches described to generate MCTS, such as the liquid overlay and hanging drop methods, the use of ultralow attachment plates and rotatory bioreactors (e.g., stirred culture vessels/spinner flasks and gyratory rotation systems) for large-scale production, or magnetic levitation/bioprinting techniques [122, 123]. It is noteworthy that the formation of MCTS can be enhanced by the addition, into the culture media, of ECM components, like collagen or fibronectin [124, 125] or materials like methylcellulose [126]. These additional components provide external cell-matrix support amplifying cell-cell and cell-matrix interactions, thus promoting spheroid assembly. Details on these methods can be consulted in Table 1.

These spherical models are one of the most well characterized and versatile methods to culture cancer cells in 3D, allowing for the generation of physiologically relevant in vitro models for the preclinical evaluation of nanoparticles [143, 144]. Briefly, owing to their 3D arrangement and endogenous deposition of extracellular matrix, MCTS present increased cell-cell contacts, including tight junctions, and cell-matrix interactions [121, 145], which are responsible for the discrepancies in gene and protein expression patterns between these cells and their monolayer counterparts [146, 147]. MCTS with ≥200 μm radii (the diffusion limit to oxygen is about 150–200 μm) exhibit differential cell proliferation rates throughout the spheroid, featuring a highly proliferating region on the outer rim and a quiescent region on the inside, owing to the limitations in oxygen and nutrient diffusion [148, 149]. Larger MCTS (≥400–500 μm diameter) present a concentrically layered structure with a necrotic hypoxic core containing apoptotic cells, surrounded by quiescent cells and followed by actively dividing, peripheral tumor cells, closely mimicking the pathophysiological organization of poorly vascularized regions of solid tumors in vivo [145, 148]. Therefore, MCTS are able to emulate both physical and biochemical barriers of the TME, owing to their inherent cell-cell and cell-matrix interactions, as well as gradients in oxygen and glucose distribution, accumulation of metabolic waste leading to acidosis, and different proliferation profiles [117, 149, 150]. Moreover, coculture-derived MCTS, harboring tumor cells and other cell types from the TME, like endothelial cells [151, 152] or stromal fibroblasts [127, 153], constitute more advanced 3D cell cultures capable of better recapitulating in vitro the intercellular signaling pathways and tumor tissue-specific properties observed in vivo. For instance, Priwitaningrum et al. have developed two 3D coculture spheroid models, harboring human breast cancer cells/pancreatic tumor cells and fibroblasts, to evaluate the penetration level of silica and PLGA nanoparticles [154]. In this study, spheroids containing stromal fibroblasts (heterospheroids) presented decreased extent of nanoparticle penetration, relative to tumor cell-derived spheroids (homo-

Table 1 Multicellular tumor spheroid forming methods

Method		Description	Schematic figure	References
Liquid overlay		Culture of suspended cells on a nonadherent surface (e.g., agar, agarose, polyHEMA)	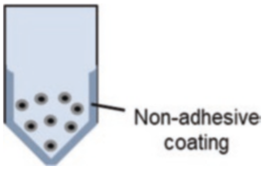	[127, 128]
Matrix-based MCTS	Matrix on top	Cells are seeded on the top of solidified matrix and spontaneously aggregate into spheroids and remain attached to the matrix	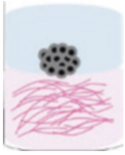	[129–132]
	Matrix embedded	Cells or preformed spheroids are suspended in liquified matrix and dispensed onto pre-coated wells. Cells get embedded within the matrix upon gelation	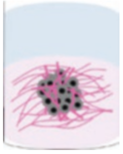	
Ultralow attachment plates (same principle of liquid overlay method)		Cells are seeded in plate wells coated with an inert substrate, which prevents cell attachment. Cells aggregate into visible spheroids	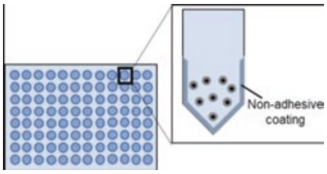	[133, 134]
Bioreactors Computer-controlled culture systems that provide monitoring and automated control of environmental culture variables like temperature, pH, and oxygen.	Spinner Flasks	Cells grow into spherical aggregates in culture flasks with a central magnetic stirrer that ensures continuous distribution of oxygen and nutrients throughout the medium. MCTS are generated under high sheer force owing continuous motion of the stirring bar	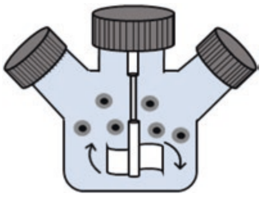	[135–137]
	Rotating culture systems	Cells are cultured in horizontally rotating cylindrical culture vessels with no internal stirring mechanisms. This method allows cells to remain suspended in simulating microgravity conditions with minimal mechanical cell damage	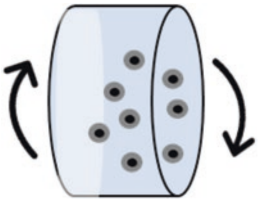	
Hanging drop		Droplets of cell suspension, held by surface tension, are dispensed onto the underside of the lid of culture vessels. Gravity drives cell aggregation at the bottom of the drop, enabling the production of uniform-sized spheroids	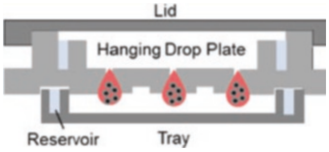	[138, 139]
Magnetic levitation and bioprinting		Cells labeled with magnetic nanoparticles (e.g., SPIONs – Super paramagnetic iron oxide nanoparticles) are pulled up once a magnet is placed on top of the plate (i.e., magnetic levitation) or down, if the magnet is placed beneath the plate (i.e., magnetic bioprinting) and rapidly self-aggregates into spheroids	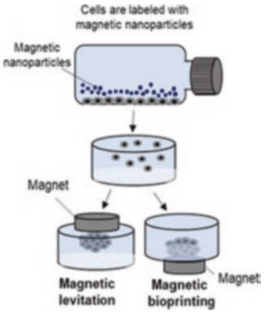 Cells are labeled with magnetic nanoparticles Magnetic nanoparticles Magnet Magnetic levitation Magnetic bioprinting Magnet	[140–142]

spheroids), further highlighting the physical barrier held by the tumor stroma, within the TME [154].

In summary, all these features allow MCTS not only to recapitulate some of the intratumor barriers faced by nanocarriers but also to model tumor-associated drug resistance mechanisms, since cells in these systems are generally more chemoresistant than cells in monolayers [113, 126, 155], and thus provide more accurate results on nanoparticle's antitumor efficacy.

Owing to their tumor biomimetic features, the application of MCTS in the evaluation of novel nanotechnology-based platforms has been emerging since 2004 [156]. Currently, several preclinical studies report the use of 3D MCTS to screen anticancer nanoparticles, namely, their intratumoral distribution and antitumoral effect. For instance, Kim et al. used cervical carcinoma cell-derived 3D MCTS to evaluate the delivery of doxorubicin-loaded triblock polymeric micelles in comparison with free doxorubicin [157]. The penetration of the polymeric micelles was first evaluated by imaging doxorubicin autofluorescence in MCTS sections and further complemented with fluorescein-labeled micelles, both assessed with fluorescence microscopy. While diffusion of doxorubicin alone was limited to the outer layers of the spheroids, drug-loaded micelles were able to penetrate the core and thus improve the efficiency of doxorubicin penetration [157].

MCTS are particularly useful as tumor models in vitro to evaluate both functionalized and stimuli-responsive TME-targeted nanoparticles. In a study performed by Cantisani et al., the delivery efficiency of doxorubicin-loaded biocompatible nanoparticles harboring a MMP2 (matrix metalloproteinase 2)-sensitive cleavable peptide was assessed by confocal microscopy in glioma-derived spheroids, overexpressing MMP2 [158]. Spheroids treated with MMP2-sensitive nanoparticles exhibited higher fluorescence, indicating increased doxorubicin accumulation, and tended to disaggregate after 48 h of incubation, in contrast with nontargeted nanoparticles [158].

Other stimuli-responsive nanoformulations, in which the release of the encapsulated drugs is triggered on the tumor site by an external stimulus, like heat (i.e., thermo-responsive nanoparticles) [159] or light (e.g., nanoparticles loaded with a photosensitizer agent for photodynamic therapy) [160, 161], have also been evaluated on biomimetic MCTS. In these studies, cellular uptake, nanoparticle's intratumoral distribution, and spheroid disassembly (i.e., indicator of tumor cell death) were assessed by optical-based methods, including wide-field optical microscopy and confocal laser scanning (CLS) microscopy [159, 160].

In respect to ligand-mediated targeted nanoparticles, several studies have applied MCTS as models of hypovascularized tumors to evaluate their distribution gradients, intratumoral penetration, and antitumor activity over nontargeted nanoparticles [162, 163]. For instance, MCTS constructed from neuroblastoma cells were used to assess the activity and tumor penetration profile of doxorubicin-encapsulated boronic acid-rich chitosan (CS-PAPBA) nanoparticles, functionalized with the tumor-penetrating peptide iRGD [164]. The intratumoral distribution of both unlabeled and FITC-labeled doxorubicin-loaded CS-PAPBA nanoparticles was analyzed through a CLS microscope, and a growth inhibition assay was performed on the MCTS, to assess CS-PAPBA nanoparticle cytotoxic activity, by measuring the spheroid diameter with an optical microscope. Increased intratumoral penetration of iRGD-conjugated nanoparticles over their free-drug and nontargeted counterparts was observed, but most importantly, the results obtained in 3D conditions were in accordance with the ones of antitumor efficacy in vivo [164].

More recently, Wojnilowicz et al. have used MCTS constructed from prostate cancer cells (PC3 spheroids) to evaluate the gene knockdown efficacy of glycogen-based nanoparticles containing anti-survivin siRNA [165]. These nanoconstructs were able to penetrate the spheroids and mediate survivin downregulation in levels comparable to those observed in 2D cultures [165].

Finally, it is noteworthy that the same nanoparticles can display distinct cellular responses whether they are tested on 2D monolayers or 3D MCTS [166]. For example, in a comparison study, Du et al. demonstrated that paclitaxel-conjugate micelles were significantly more cytotoxic in prostate 3D MCTS in contrast to 2D prostate tumor cell culture, where free paclitaxel exhibited higher antitumor activity instead [134]. In another study, gold nanoparticles exhibited distinct uptake efficiencies and cell growth profiles in colorectal carcinoma cell-derived 2D monolayers and 3D spheroids, further highlighting that the experimental results obtained from 2D cultures do not reflect the 3D cellular behavior [167].

Scaffold- and Matrix-Based 3D Culture Systems

The advances in the field of tissue engineering and biomaterials enabled the design of more advanced matrix- and scaffold-based 3D in vitro tumor models, capable of better reflecting the biochemical and biophysical cues provided by the natural ECM in the TME [168].

The most commonly used biomaterials for constructing these 3D tumor models include naturally derived matrices, hydrogels, and polymeric scaffolds [86]. Among naturally derived matrices, Matrigel™ – a popular laminin-rich extracellular matrix (lrECM), mostly containing type IV collagen and laminin, which is derived from secreted basement membrane extracts of Engelbreth-Holm-Swarm mouse sarcoma cells [169, 170] – is the most prominent one [171, 172], followed by type I collagen gels [173, 174]. It is noteworthy that being composed by natural components, ECM-based matrices often contain residual levels of endogenous chemokines, growth factors, and other undefined constituents that contribute for batch-to-batch variability and subsequent lack of reproducibility [175]. On the other hand, engineered biomimetic hydrogels, either constructed from natural (e.g., self-assembling peptide systems composed of natural amino acids [176]) or synthetic (e.g., PEG, poly(ethylene glycol)-based hydrogel platform [177]) copolymers, present more controllable and reproducible characteristics, offering lot-to-lot uniformity. Polymeric scaffolds are an alternative approach to hydrogels, where the solid and well-defined structure of the former enables tumor cell growth in a specific 3D spatial configuration, closely resembling the organization of the tumor in vivo. Other important features are their high porosity and biodegradable nature, enabling cell attachment and proliferation, as well as scaffold's degradation in accordance with cell growth kinetics [178]. Accordingly, in vitro 3D scaffold-based models have been widely applied in cancer biology studies [179, 180], as well as in the evaluation of efficacy of anticancer drugs [181, 182].

Owing to their recognized physiological relevance, both scaffold- and matrix-based 3D cell culture systems have been applied in the preclinical evaluation of nanoparticles. For example, Xu et al. developed a hyaluronic acid-derived, hydrogel-based 3D prostate cancer model for the in vitro evaluation of doxorubicin-encapsulating nanoparticles [102]. When compared to tumor cells grown in 2D conditions, cells cultured on the crosslinked 3D hydrogel exhibited higher expression of multidrug resistance proteins, closely resembling prostate cancer cells in vivo, and therefore were more resistant to the treatment with both free and encapsulated doxorubicin [102].

In a different context, Belli et al. used a 3D collagen matrix-based culture system, composed of human fibrosarcoma cells, to study the effect of a 3D ECM on the diffusion and uptake kinetics of polystyrene nanoparticles with different sizes (44 and 100 nm) [183]. The intricate network of collagen fibers significantly hampered 100 nm of nanoparticle diffusion, subsequently slowing down cellular uptake, in comparison with their straightforward transport in standard 2D cultures. Moreover, the study points out the influence of the cytoskeleton assembly on nanoparticle internalization. Cells cultured in the 3D collagen model showed a different cytoskeleton arrangement, highlighting the importance of understanding the nano-cellular-matrix dynamic interconnection in biomimetic 3D experimental models [183]. Similarly, Biondi et al. have shown that sub-100 nm doxorubicin-loaded nanoparticles exhibited higher extent of cytotoxic activity than their larger counterparts in a 3D collagen-based model harboring cervix carcinoma cells (HeLa), reinforcing the role of nano-bio interactions on a size-dependent perspective [184].

More recently, an innovative gelatin microscaffold-based 3D coculture system, harboring epithelial breast cancer cells and CAFs, has been developed to evaluate the efficacy of a doxorubicin-loaded MMP2-responsive nanoformulation [158, 185]. In this 3D breast cancer microtissue, both tumor cells and CAFs are embedded in their own ECM, which enables to recapitulate in vitro key features of the TME in vivo, including the overexpression of MMP2. MMP2-dependent drug release was demonstrated, inducing a significant reduction in 3D cell viability, along with the reliability of the 3D microtissue model as a screening platform for drug delivery systems [185].

Tumor Explant Cultures

Unlike the aforementioned 3D models, which are based on the reconstruction of the TME in vitro, tumor explant cultures are alternative 3D systems that maintain the original architecture and composition of the tumor tissue in vivo [186]. In this approach, small samples (1–2 mm) or slices of patient-derived tumor tissues, previously excised during surgery or collected after biopsy, are cultured in ex vivo conditions, on a semiporous membrane, atop a collagen-coated surface or embedded in a 3D gel [187–189]. Of note, since tumor vessels become dysfunctional after excision, tumor slices must be thin enough (200–300 μm thick) to allow sufficient nutrient and oxygen supply through diffusion mechanisms and simultaneously preserve histological features [190, 191].

Regarding their ability to retain tumor's molecular heterogeneity, 3D organization, and microenvironmental barriers, including pathophysiological cell-cell/cell-matrix interactions, ex vivo explants are particularly suitable for drug screening assays, providing the opportunity to evaluate patient-specific biological responses [192–194].

Nevertheless, despite the significant benefits, culturing tumor slices ex vivo harbors critical limitations, such as the dependency on ready access to viable biological material in sufficient quantities, as a consequence of ex vivo short-term cellular viability, and the high intra- and inter-tumor variability of the samples collected. This requires the use of histopathological controls and verification of the tissue content [190, 195].

In respect to cancer nanomedicine, ex vivo cultured tumor slices of 200 μm thick, obtained from non-small cell lung cancer patients, were used to evaluate the delivery and biological activity of chitosan-coated PLGA nanoparticles incorporating anti-telomerase antisense oligonucleotides [196]. The nanoparticles were able to penetrate throughout the tumor slice and inhibit the activity of telomerase in an extent comparable to that observed in 2D primary cultures of non-small cell lung cancer cells (40% and 45% reduction on telomerase activity, respectively) [196].

3D Microfluidic Platforms

Microfluidic technologies offer the opportunity to precisely control, in a spatiotemporal manner, small volumes of fluids within a cell culture device, enabling the generation of 3D gradients of key molecules (e.g., oxygen, nutrients, chemokines, and drugs) in solution [197]. A microfluidic device is a compartmentalized 3D platform harboring microwells interconnected by vasculature mimicking microchannels, etched onto the surface of biocompatible, inert materials, like glass or polydimethylsiloxane (PDMS). These devices enable the simulation in vitro of the physicochemical environment and vascular perfusion in vivo, allowing for an organ-level functionality not achievable with 2D cultures or conventional 3D models [198].

Tumor-on-a-Chip Models

Accordingly, microfluidic-based tumor-on-a-chip models have been developed, in which tumor cells and stromal cells from the TME are cocultured in continuously perfused chambers, within a specific 3D arrangement [199]. The ability to manipulate fluid motion and cell culture substrates allows tumor-on-a-chip models to reproduce the various mechanical cues featuring the TME in vivo, as well as complex cell-cell and cell-matrix interactions mediated by soluble or insoluble biological factors [200].

The development of tumor-on-a-chip models is highly desirable for drug screening assays [201]. Firstly, the ability to reproduce organ/tumor-level pathophysiological functions enables them to closely mimic in vitro the pharmacological responses in vivo. This could provide more accurate results on the antitumor efficacy and safety of potential candidates, early in the process of drug development [200]. Secondly, the optical transparency of these 3D models allows for real-time imaging and quantitative high-resolution analysis of nanoparticle delivery kinetics under flow conditions.

For instance, Albanese et al. have developed a two-layer, PDMS-based tumor-on-a-chip platform harboring multicellular spheroids composed of melanoma cells, embedded in a ECM-mimicking matrix [202]. The spheroids, seeded on the chip's microchannel, were used to test the effect of nanoparticle size, receptor targeting, and flow rate on the tissue accumulation of drug-loaded, fluorescently labeled gold nanoparticles. Association to spheroids was restricted to nanoparticles with mean diameters lower than 110 nm. Forty nanometer transferrin (Tf)-targeted nanoparticles showed significantly increased retention inside the spheroids, in comparison with nontargeted nanoparticles of the same mean size. These in vitro results were confirmed in vivo on a murine xenograft model, in which fluorescently labeled 50 nm Tf-targeted and nontargeted nanoparticles showed higher tumor penetration, over 160 nm nontargeted ones [202].

More advanced tumor-on-a-chip models, designed to specifically mimic certain cancers, such as the breast-cancer-on-chip [203, 204] or colorectal tumor-on-a-chip [205], have been proven highly useful for evaluating the antitumor efficacy of drug-loaded nanoparticles, through live imaging techniques.

Tumor Microenvironment-on-Chip Models

In addition, tumor microenvironment-on-chip platforms with complex 3D architectures have also been developed. For example, Kwak et al. have designed a two-layer tumor microenvironment-on-chip (T-MOC) model with a tumor vessel-mimicking microchannel on the top layer and a central channel, simulating the tumor interstitium, connected with two side channels, simulating the tumor lymphatic vessels, on the bottom layer [206]. Human breast cancer cells embedded in a 3D type I collagen matrix were cultured on the tumor channel, while microvascular endothelial cells were seeded on the porous membrane of the capillary microchannel, mimicking the tumor's endothelium. The T-MOC enabled to study the impact of varying the cutoff pore size of the tumor vasculature, interstitial fluid pressure, ECM's composition, and tumor cell density, in the delivery kinetics of fluorescently labeled nanoparticles. The pores formed by endothelial cells on the capillary channel induced a significant decrease of nanoparticle transmembrane transport. Surprisingly, the high tumor cell density on the tumor channel, rather than the collagen-rich ECM, substantially reduced nanoparticle interstitial transport and extravasation [206].

In a different context, Shin et al. used a single T-MOC 3D platform cultured with spheroids from different human breast cancer cell lines to evaluate the transport behavior and cellular drug response and resistance of doxorubicin-loaded hyaluronic acid nanoparticles, by time-lapse microscopy [116]. Albeit the higher accumulation of nanoparticles over free doxorubicin in the tumor spheroids, namely, on MDA-MB-231-derived ones, cell viability was significantly higher in nanoparticle-treated groups compared to doxorubicin-treated spheroids, suggesting that drug release in the interstitial microchannel was insufficient to promote antitumor activity. The increased cytotoxicity of free doxorubicin over drug-loaded nanoparticles was also observed on 2D models, yet these exhibited higher extent of cell death than the ones in the T-MOC model, likely due to the absence in the former of barriers associated with blood flow, extravasation, interstitial and intracellular transport [116].

More recently, Tang et al. have developed a nonconventional T-MOC, referred to as biomimetic microfluidic tumor microenvironment (bMTM), harboring an in vivo-like microvascular network and a tumor compartment, inhabited by human breast tumor-associated endothelial cells (HBTAEC) and human breast cancer cells, respectively [207]. The bMTM was designed to reproduce in vitro the enhanced permeability and retention (EPR) effect with similar permeability levels to those observed in vivo. Indeed, the results point out the passive accumulation of fluorescently labeled, drug-loaded liposomes in the tumor compartment. Moreover, coculturing highly metastatic MDA-MB-231 cells with HBTAEC promoted enhanced liposome extravasation, owing to their ability to alter endothelial cell morphology and permeability, as demonstrated by immunostaining assays against tight junction proteins, in comparison with nonmetastatic MCF-7 cells [207].

3.2.2 Third Dimension-Associated Challenges

As briefly introduced in Sect. 3.2, owing to their higher biological complexity, 3D models are associated with several challenges mainly regarding system development, screening approaches, and analysis of a vast amount of data [111]. Indeed, monitoring 3D systems mostly requires complex, time-consuming, and cumbersome imaging techniques, which starkly contrasts with the simple and well-established protocols applied to 2D cultures. Notwithstanding most preclinical studies pointing out the pathophysiological relevance of 3D models, it is noteworthy that no study has provided reproducible qualitative and quantitative evidence to validate their use as accurate models of disease, capable of better predicting clinical response over the current animal models [111].

Another relevant point concerns with the applicability of 3D models as platforms to high-throughput (HTS) or high-content screening (HCS) systems. Naturally, the adaptation of 3D approaches, mainly biomimetic MCTS and microfluidic-based models, for high-throughput drug screening assays is highly desirable, over conventional monolayer cultures, owing to their potential higher predictive capacity [208, 209]. Still, one should be aware that to perform both HTS and HCS assays, uniformly miniaturized models designed by simple protocols and further analyzed by cost-effective, automated detection approaches are essential requirements [210]. For instance, some HTS protocols based on uniform-sized 3D tumor spheroids have already been developed, using hanging drop arrays [211], Matrigel™-coated microplates [20], or ultralow attachment/liquid overlay-based multi-well plates [133, 212]. Nevertheless, the lack of standardized methodologies to develop miniaturized systems and automated software tools to perform robust quantitative analysis in all types of 3D models available hinders their further applications in HTS.

Therefore, although the application of robust 3D HTS systems for the preclinical evaluation of new drug candidates is evolving, mainly for anticancer nanoparticles [213], it still has a long road ahead with several challenges to overcome.

4 In Vivo Preclinical Evaluation of Anticancer Nanoparticles

4.1 Animal Models of Cancer

Animal models, mainly rodents, have been extensively used in the evaluation of novel therapeutic anticancer drugs [214, 215], being essential for the identification of new pharmacological targets along with the demonstration of in vivo efficacy [216]. Moreover, they have played a major role in the understanding of human cancer pathophysiology [217, 218], which strongly impacts the performance of nanomedicines.

Although several preclinical studies in vivo have demonstrated consistency in the pharmacokinetics and efficacy of different nanoparticles across several species, including mice, rats, and nonhuman primates [219–221], there is still a great discrepancy between the preclinical performance and the therapeutic efficacy reported on clinical trials [222]**.** One recognized example is Doxil®. Albeit the remarkable therapeutic improvements over free drug revealed in mice [223], its efficacy benefit was not statistically significant in breast cancer patients [19].

To overcome these divergences and improve translation of basic findings into patient benefit, it is of outmost importance to obtain preclinical evidence from several animal models, instead of prioritizing single model experiments [224, 225], among several other issues**.** Accordingly, over the last decade, the variety of preclinical oncological animal models has grown substantially, and a wide range of models are now available for the evaluation of anticancer nanoparticles, each one with its own strengths and limitations (see details on Table 2).

4.1.1 Types of Animal Models and Screening Applications

Cell Line-Derived Syngeneic/Xenograft Models

The simplest animal tumor models are established through the inoculation of cancer cell lines, from either mouse or human origin, into the corresponding immunocompetent mice strain (syngeneic) [230] or immunodeficient mouse strain (xenograft), respectively [240]. In both syngeneic and xenograft models, the inoculation of cancer cell lines may be performed subcutaneously, as in the flank of the mouse (subcutaneous model) [247] or into the matching human tumor organ (orthotopic model) [248, 249]. While subcutaneous models are easier to implement, allowing the fast identification of active compounds, orthotopically implanted tumors could better recapitulate human metastasis and carcinogenesis [250]. However, surgical procedures of an orthotopic tumor implantation are technically challenging, time-consuming, and more expensive than for conventional sub-

Table 2 Characteristics, benefits, and shortcomings of the different animal cancer models

Type of animal model	Description	Advantages	Disadvantages	References
Genetically engineered mouse models (GEMMs)				
	Spontaneous or targeted genetic alterations in oncogenes or tumor suppressor genes of the mouse genome	Autochthonous growth provides native microenvironment. Tumor development driven by relevant genetic alterations.	Costly and time-consuming. Murine host stroma. Variations in tumor growth rates.	[226–229]
Cell line-derived models				
Syngeneic	Inoculation of immortalized murine cancer cell lines into immunocompetent mice	Ease of implementation. Cost-effectiveness. Retention of the host's immunoreactivity. Occurrence of tumor-stroma interactions.	Different features from the original tumor. Little resemblance of tumor complexity and heterogeneity.	[230]
Xenograft	Inoculation of immortalized human cancer cell lines into immunocompromised mice	Ease of implementation. Cost-effectiveness.	Absence of immune cells. Little resemblance of tumor complexity and heterogeneity.	[95, 231]
Patient-derived xenografts (PDX)				
Conventional PDX	Implantation of fragments from freshly resected human tumors into immunocompromised mice	Intact primary tumor tissue that maintains tumor architecture. Reproduces complexity of human disease (genomic heterogeneity and cell diversity). Ability to recapitulate donor patient's response to treatment.	Costly and time-consuming. Absence of immune cells. Low engraftment rate for less aggressive tumors.	[232–234]
Circulating tumor cell-derived xenograft	Implantation of circulating tumor cells from patients into immunocompromised mice	Minimally invasive sampling. Ability to recapitulate donor patient's response to treatment. Enables research of otherwise inaccessible tumor specimens.	Costly and time-consuming. Low levels of CTC in the peripheral blood. Access to technologies to isolate circulating tumor cells. Absence of immune cells. Technically challenging.	[235, 236]
Humanized PDX	Implantation of fragments from freshly resected human tumors into mice with a humanized immune system	Intact primary tumor tissue that maintains tumor architecture. Recapitulates human immune system in mice.	Costly and time-consuming. Technically challenging. Hurdles to achieve complete recapitulation of human immune system.	[237–239]

cutaneous models, therefore limiting the number of available surgically manipulated mice [249]. The establishment of different types of cell line-derived in vivo models is summarized in Fig. 4.

Syngeneic models are easy to implement and retain the host's immunoreactivity, enabling the occurrence of physiological immune interactions between the murine cancer cells and the host stroma elements [230]. Albeit the expression of human targets in xenograft models, the environment surrounding these tumors is derived from the murine host. This leads to differences in the ECM architecture, composition (e.g., percentage in collagen and hyaluronan fibers), and function, consequently affecting the tumor vasculature [241]. Hence, the heterogeneous perfusion and extravasation of nanoparticles into the tumor site, as a result of the physiological barriers presented by the TME [66], may be misrepresented in these models. This could contribute to the differences observed on the kinetics of nanoparticle's tumor accumulation between human tumors and mouse xenograft models [242–244].

For instance, notwithstanding the potent antitumor activity enabled by a micellar formulation of paclitaxel (NK105) in HT-29-derived xenografts implanted into nude mice [245], it did not present superior clinical efficacy over free paclitaxel [246, 247]. The divergence between preclinical and clinical data suggests that these models might be oversimplified (i.e., incapable of replicating human cancer's complexity and heterogeneity) and thus limited in their prediction power of efficacy of nanomedicines [248, 249].

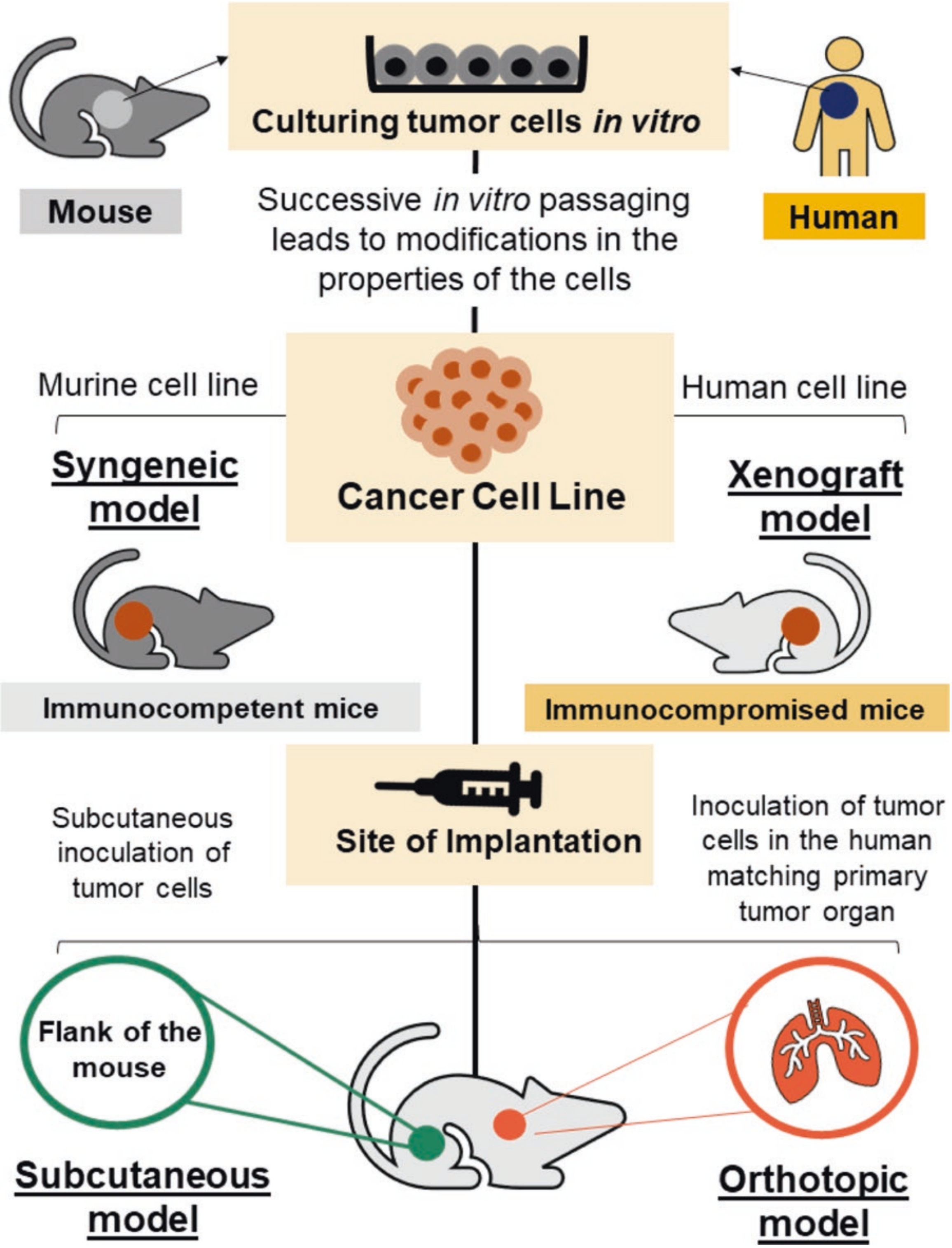
Culturing tumor cells *in vitro*
Mouse
Human
Successive *in vitro* passaging leads to modifications in the properties of the cells
Murine cell line
Human cell line
Cancer Cell Line
Syngeneic model
Xenograft model
Immunocompetent mice
Immunocompromised mice
Site of Implantation
Subcutaneous inoculation of tumor cells
Inoculation of tumor cells in the human matching primary tumor organ
Flank of the mouse
Subcutaneous model
Orthotopic model

Fig. 4 Traditional cell line-derived preclinical mouse cancer models. Preclinical mouse cancer models generated through the inoculation of immortalized cell lines derived from either murine (syngeneic) or human tumors (xenograft), subcutaneously, as in the flank of the mouse (subcutaneous model) or in the human matching primary tumor organ (orthotopic model). Human xenograft tumors are grown in immunocompromised mice, whereas syngeneic tumors are grown in immunocompetent mice. Both murine and human inoculated tumor cells present gene expression profiles that could differ from their original tissues as a result of their in vitro culture. Although the generation of subcutaneous models is technically simple, these models do not reproduce the primary tumor site nor the sites of metastasis. Alternatively, albeit more technically challenging, orthotopically implanted tumors enable, dependent on the tumor, the recapitulation of human metastasis and carcinogenesis

Nevertheless, the most noteworthy limitation associated with cell line-derived syngeneic/xenografts models is the occurrence of phenotypic modifications in cancer cells, as a result of their in vitro passaging [95]. Indeed, emerging evidence have suggested alterations in the genetic content, invasiveness, and capacity to maintain a heterogeneous cell population and in the dependence on specific growth and survival pathways in cell line derived-xenografts, as a consequence of the cell culture process [95, 250, 251].

To circumvent the challenges associated with cell line-derived syngeneic/xenograft models, more advanced preclinical cancer models, capable of better recapitulating human tumor's pathophysiology and heterogeneity and more accurately predicting clinical efficacy, have been developed [252, 253].

Genetically Engineered Mouse Models (GEMM)

Genetically engineered mouse models (GEMMs) are in vivo cancer models where one or several genes from the mouse's genetic profile, expected to be involved in carcinogenesis, have been altered, i.e., mutated, deleted, or overexpressed [233]. Briefly, the genetic alterations may be generated through random integration of exogenous oncogenes into the genome of mouse embryonic stem cells (transgenic GEMM) [254–256] or by homologous recombination in those stem cells, using a targeting vector to introduce several genetic alterations into a specific genomic region (targeted GEMMs) [227–229]. Albeit the long period (2 to 12 months) and the substantial investment required to establish these models, the great progress in CRISPR technologies is fueling rapid and cost-effective generation of new GEMM models [257, 258].

One significant advantage of GEMMs is the spontaneous tumor generation through the action of key human drivers in immunocompetent mice, which enables to better recapitulate the early development of human tumors, in comparison with xenograft models [217]. Therefore, GEMMs display better predictive power relative to cell line-derived xenografts, as demonstrated by several preclinical studies comparing both models [259, 260]. This feature might be attributed to their autochthonous development, which enables to reproduce the critical role of the TME in drug response, unlike xenograft models, in which human tumor cells interact with murine stromal cells in an immunocompromised mouse [226]. This is particularly relevant for the preclinical evaluation of anticancer nanoparticles in highly desmoplastic and hypovascularized tumors, like the pancreatic ductal adenocarcinoma (PDAC), since stromal architecture strongly affects their delivery to tumor cells [66]. In this respect, Frese et al. have studied the antitumor efficacy and pharmacodynamics of paclitaxel-loaded albumin-bound nanoparticles combined with gemcitabine in a previously developed GEMM of PDAC, established through the endogenous expression of mutant *Kras* and *Trp53* alleles in the pancreas [261, 262]. Von Hoff et al. had previously shown that this combination was capable to tackle down the desmoplastic stroma of PDAC xenografts in mice after 28 days of treatment [263]. However, in contrast to Von Hoff et al. observations, Frese and coworkers have demonstrated that the same nanoparticles could not disturb PDAC stromal architecture in GEMMs [261]. These divergent outcomes highlight the role of the abnormal xenograft's TME in enhancing tumor stroma vulnerability to nanomedicines, which might provide misleading results on their therapeutic effect. On the other hand, owing to their ability to preserve tumor cell-stroma cell dynamic interactions [264, 265], GEMMs present higher predictive capacity on nanoparticle's in vivo efficacy [266].

Despite the contribution of GEMMs for our understanding of the molecular pathways underlying tumorigenesis and metastatic behavior of cancer cells [267], as well as for anticancer drug development [226], significant biological discrepancies still exist between murine and human malignancies. For instance, differences in the cytogenetic structure, biology of telomeres, dependence on certain tumor suppressor mechanisms, and target homology might limit drug discovery in these models [268, 269]. To overcome this limitation, preclinical models established from human tumor tissue, featuring the complexity of genetic and epigenetic abnormalities existing in human tumors, are emerging as important platforms to improve the correlation between preclinical and clinical responses.

Patient-Derived Xenograft Models

Patient-derived xenograft (PDX) models are generated through the implantation of fragments from freshly resected human tumors into immunosuppressed mice (e.g., nonobese diabetic (NOD)/severe combined immunodeficiency (SCID)) and, similarly to cell line-derived models, may be implanted subcutaneously or orthotopically [232, 270]. These models have been a valuable preclinical tool for drug development [255, 280] since the early 1980s, when Fiebig and coworkers have observed identical responses to the same cytotoxic agents among lung cancer patients and their corresponding PDXs [271]. In fact, several studies have demonstrated that PDXs, unlike cell line-derived xenografts, maintain patient tumors' histological features, gene expression patterns, and genomic variations even after several passages in immunocompromised mice [233, 234, 272]. Moreover, some reports suggested that PDX models exhibited vascular heterogeneity [273], comprising predominantly human endothelial cells [274, 275]. As a result, nanomedicine behavior is expected to be affected [276].

For example, Delgado and coworkers have shown that in a cohort of 28 PDXs, derived from a single donor tumor, and thus with similar intrinsic sensitivity to liposomal doxorubicin, the stroma morphology and the tumor architecture have significantly affected the nanomedicine's cytotoxicity [277]. Tumors with a highly convoluted tumor-stroma interface (i.e., with most tumor cells in close proximity to blood vessels) were 8.8-fold more responsive to liposomal doxorubicin than tumors with less stroma diffusion, characterized by nests of tumor cells with large necrotic cores (from growth-driven oxygen exhaustion) [277]. Furthermore, Kalra and coworkers have demonstrated that, after the administration of a nanoliposomal formulation of irinotecan, the retention of SN-38 (the active metabolite of irinotecan) was higher in cell line-derived xenografts than in PDXs models and, consequently, the former displayed more robust growth inhibition [278]. Hence, in the context of the preclinical evaluation of anticancer nanoparticles, one major advantage of PDX models is their superior ability to unveil the impact of locoregional features and TME complexity on nanoparticle performance and therapeutic outcome [279, 280].

Notwithstanding the use of PDXs in the preclinical evaluation of novel anticancer nanoparticles holding important advantages, it is noteworthy that these models still have significant limitations that need to be addressed to improve their use in translational cancer research [281]. In this respect, refining PDX models for successful personalized nanomedicine, as well as for preclinical development of immunotherapy-based approaches, has been emerging as an active research area, as further discussed below. The different types of PDX models and their application in preclinical development of anticancer nanoparticles are summarized in Fig. 5.

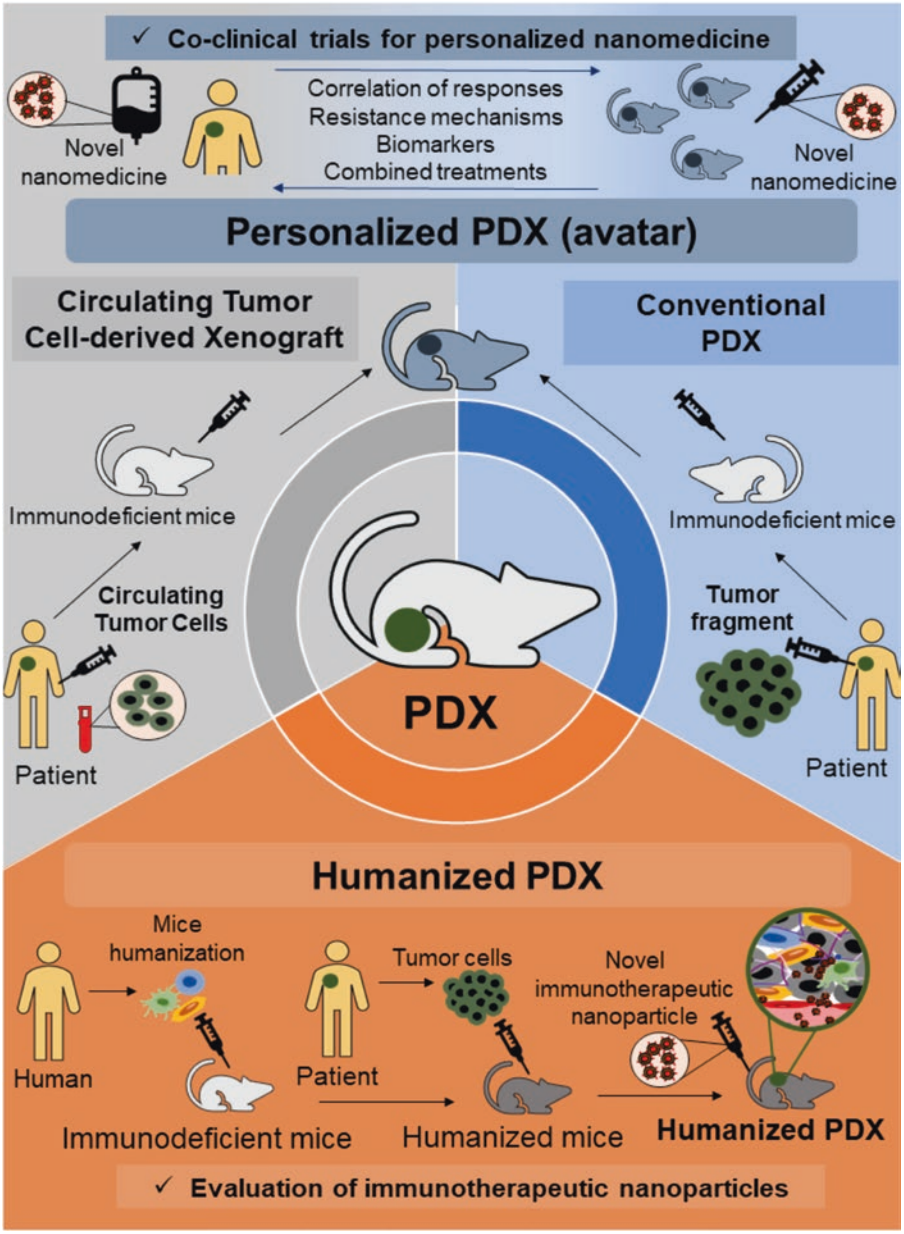
✓ Co-clinical trials for personalized nanomedicine
Novel nanomedicine
Correlation of responses
Resistance mechanisms
Biomarkers
Combined treatments
Novel nanomedicine
Personalized PDX (avatar)
Circulating Tumor Cell-derived Xenograft
Conventional PDX
Immunodeficient mice
Immunodeficient mice
Circulating Tumor Cells
Tumor fragment
PDX
Patient
Patient
Humanized PDX
Mice humanization
Human
Tumor cells
Patient
Novel immunotherapeutic nanoparticle
Immunodeficient mice
Humanized mice
Humanized PDX
✓ Evaluation of immunotherapeutic nanoparticles

Fig. 5 Different types of patient-derived xenograft (PDX) models and their application in preclinical development of anticancer nanoparticles. PDX models are generated through the implantation of human tumor fragments into immunosuppressed mice (conventional PDX) or, alternatively, circulating tumor cells (CTC-derived xenograft). By offering the opportunity to simultaneously evaluate drug response in the patient and in the mouse, as well as to assess key biomarkers of cancer resistance along with the evaluation of novel nanotherapeutic strategies to overcome emergent drug-mediated resistance mechanisms, PDXs are well-suited tools for personalized medicine (personalized PDX/avatar). Moreover, the recent development of humanized models, capable of assembling an anticancer immune response, will provide an opportunity for the preclinical evaluation of cancer immunotherapeutic nanoparticles in a closer setting to human disease

Improving PDX Models with Avatars

Recently, the use of personalized PDXs, also known as *avatars*, as a well-suited tool for personalized medicine has been reported [282, 283]. Herein, the PDX model is developed from a patient enrolled in a clinical trial and treated with the same experimental agents, an approach denominated *co-clinical trial* [253]. This method offers the opportunity to evaluate drug responses simultaneously in the patient and in the mouse model. This subsequently enables the assessment of both key biomarkers on cancer resistance and possible therapeutic alternatives to overcome emergent drug-mediated resistance mechanisms [281, 284, 285]. In fact, personalized PDXs have been recently proposed as appropriate platforms for the co-clinical validation of a cell surface targeted-nanoparticle encapsulating anti-miR 21 oligonucleotides, an oncogenic miRNA involved in PDAC [286–288]. Interestingly, the PDX avatars enabled the identification of miR-21 as a promising noninvasive biomarker aiming at patient stratification for this personalized RNA-based nanotherapy [288].

Notwithstanding the remarkable clinical predictive power of PDXs [289–291], one inherent drawback is the requirement of ready access to fresh and sufficient tumor tissue, which for some tumors is often impracticable or implies invasive biopsies. In this regard, Hodgkinson et al. have developed a different approach to generate PDX models for small cell lung cancer, using circulating tumor cells (CTCs) [292, 293]. It has been demonstrated that the resulting CTC-derived xenografts reflected the donor patient's response to platinum and etoposide chemotherapy [236].

Nonetheless, the process of generating either CTC-derived or conventional PDX models is cumbersome and time-consuming (development can take 4 to 8 months) and presents a low engraftment rate for less aggressive tumors [294, 295]. Thus, albeit the high potential of PDXs as platforms for anticancer drug screening, as well as for personalized medicine, the abovementioned limitations preclude their use in a timely manner [252]. In this context, to improve data reliability and avoid unnecessary efforts, several institutions and pharmaceutical companies have begun to create repositories of PDX models [296, 297]. In fact, Novartis has demonstrated both the reproducibility and the clinical translatability of an approach consisting in a large-scale high-throughput in vivo drug screen, using an extensive, well-characterized PDX collection (1000 PDXs with a diverse set of driver mutations) to model inter-patient response heterogeneity [298]. This strategy established associations between genotype and drug response, besides disclosing mechanisms of resistance, highlighting PDX collections as a well-suited tool for the potential prediction of human clinical trial responses [298].

Humanizing PDX Models

Similarly to cell line-derived xenografts, also PDX models require immunocompromised mice for tumor engraftment and propagation, which renders these models unsuitable for the evaluation of immunotherapeutic approaches, as the ones nanomedicine-based. The absence of an intact immune system is a detrimental factor in the evaluation of nanoparticle's performance, as their potential interaction with immune cells and their distinct accumulation patterns between immunocompromised and immunocompetent mice are neglected [299, 300]. In an effort to tackle these issues, humanized mice have recently started to gather attention as an attractive tool for PDX models (humanized PDX) [238].

Many strategies have been implemented aiming at establishing mice models with a fully competent human immune system, capable of assembling an anticancer immune response and, therefore, better predicting clinical responses [301]. The most commonly used methodology to establish humanized PDXs consists on implanting patient-derived tumor fragments into NOD/SCID/gamma (NSG) mice, upon previous sublethal irradiation and inoculation of human CD34+ hematopoietic stem cells (HSCs) or human peripheral blood mononuclear cells (PBMCs) [237]. An improved humanized non-small cell lung cancer PDX model has recently been developed, in which a strong antitumor response to PD-1 checkpoint inhibitors (pembrolizumab and nivolumab) has been reported, in contrast with the negligible effect in their nonhumanized counterpart [302]. This outcome provided evidence that humanized PDXs recapitulate the human tumor responses to checkpoint blockade, supporting these models as a valuable tool to accurately assess the efficacy of novel immunotherapeutic agents [302].

Besides offering the opportunity to evaluate anticancer immunotherapies, humanized PDX models have already provided many insights into the behaviors of various cancers within their original tumor microenvironments, under the influence of human immune cells [303]. In fact, Morton et al. have demonstrated that the presence of human immune cells in humanized PDXs resulted in altered gene expression within the tumor cells. Moreover, they regulated the expression of genes critical in maintaining the integrity of the native TME, altering cytokine expression, assisting in stromal deposition, and increasing lymphangiogenesis [304].

Although the study of antitumor immune responses and the evaluation of immunotherapeutic nanoparticles have traditionally relied on using cell line-derived syngeneic or GEM models [305], the refinement of humanized PDX models will provide a promising research platform for the preclinical development of novel anticancer immunotherapeutic nanomedicines in a scenery that is closer to human reality, thus contributing to accelerate clinical progress.

4.2 The Challenge of Clinical Translation

Among all the oncological drugs that have been shown to be safe and efficacious in preclinical studies, around 95% fail to demonstrate therapeutic efficacy in clinical trials [249]. Regarding anticancer nanoparticles, albeit their ability to increase intratumoral drug concentration by 100–400% relatively to the conventional free-drug formulations, little attention has been paid to the fact that more than 95% of the administered nanoparticles do not accumulate at the tumor site [306]. Indeed, the high discrepancy between relative size of human tumors and tumors implanted in mice strongly impacts nanoparticle performance [307]. While animal tumors generally grow to more than 10% of the animal's total body weight before treatment, the relative mass of a tumor in a patient is in the range of 0.003–0.01%. As a result, nanoparticles need to circulate through the human vasculature for more than 10 days to have a 50% probability of encountering the tumor, whereas only 6 seconds would be required for the same nanoparticle to reach tumor cells in a mouse model [307]. In addition, variable factors like tumor vasculature, interstitial pressure, and hypoxia may further increase the discrepancies observed between mouse models and patients [308]. Moreover, as a consequence of anatomical, physiological, and biochemical interspecies discrepancies, the specific metabolic rate is increased in mice, often leading to inaccurate estimations of human toxicity and overprediction of drug responses [309, 310]. Therefore, the poor clinical translation of most anticancer nanomedicines may be explained by inadequate preclinical data and overoptimistic efficacy assumptions based on biased animal studies.

In this context, the development of more complex models such as PDXs and GEMMs has emerged as promising alternatives to cell line-derived xenografts, enabling the evaluation of anticancer nanoparticles in a setting that more closely mimics the human TME [282]. Nonetheless, the routinely application of these models is hampered by the significant investment, expertise, and time required to their establishment and maintenance. Also, the lack of human tumor-infiltrating immune cells and the absence of standardized criteria for measuring and interpreting histological, genetic, and stromal drifts of PDX tumors across passages in mice severely hinder the clinical translation of anticancer nanoparticles targeting the TME [215, 311].

Therefore, it is unquestionable that tumor biology should be the major factor driving the design of more rational nanotechnology-based platforms, and this is only achievable with the use of more clinically relevant models [300, 308]. Henceforth, it is expected that the development of animal cancer models that more closely resemble human tumors, together with nanoparticle engineering, will bridge the gap between preclinical studies and clinical trials, improving the clinical translation of nanomedicines.

5 Future Perspectives

The implementation of physiologically more relevant tumor models in the preclinical evaluation of anticancer nanoparticles, both in vitro and in vivo, is of utmost importance to obtain more accurate results and thus bridge the translational gap to the clinic. In this respect, the establishment of early multidisciplinary collaborations, standardized guidelines, and methodologies, as well as the validation of biomimetic 3D in vitro tumor models, will be essential [111, 312]. In 3D tumor models, particularly the ones amenable for HTS, as tumor-on-a-chip models, comparative analysis of cell phenotype, gene expression profile, and metabolic pathways [111] should be performed between the model and living tumor tissues, to ensure their pathophysiological relevance. Concerning complex tumor models in vivo, like PDXs, for example, therapeutic responses should be classified based on quantitative metrics, to enable a more accurate assessment of complete/partial responses and stable/progressive disease in tumor-bearing mice, thereby improving their clinical predictivity [296].

In addition, next-generation models as 3D bioprinting-based tumor models in vitro, enabling the generation of vascular-like networks [313], or humanized mouse models, enabling tumor cell-immune cell interactions essential for evaluating cancer immunotherapeutic nanoparticles [314], are moving the first steps as promising systems for the evaluation of novel nanotechnology-based platforms.

6 Conclusions

The acknowledgment of the TME's critical role in determining nanoparticle's fate in the tumor site, by regulating their intratumoral distribution and therapeutic efficacy, has highlighted the urgent need to generate more physiological in vitro and in vivo preclinical models, capable of better predicting clinical responses.

Despite the routinely use of 2D monocultures in nanoparticle's screening assays, these systems have long been recognized as poor predictors of the activity of nanoformulations. The emergence of 3D models has been a major breakthrough in cancer research and drug discovery, with a vast variety of new biomimetic models arising – tumor spheroids, scaffold-based models, tumor explants, tumor-on-a-chip models, etc. These in vitro tumor models, mainly the ones amenable for HTS analysis, like MCTS and microfluidic-based platforms, offer the opportunity to more accurately evaluate the transport behavior and antitumor efficacy of anticancer nanoparticles, in a TME-mimicking context, starkly contrasting with biased results obtained from 2D conditions. Nonetheless, the incorporation of 3D models in routine high-throughput drug screening systems is challenged by the lack of standardized protocols to develop uniformly miniaturized models and automated detection approaches capable of simultaneously screening thousands of micro-engineered 3D models in a cost-effective manner.

Albeit the promising role of 3D in vitro tumor models in predicting nanoparticle's activity in vivo, validating the efficiency of anticancer nanoparticles in animal cancer models remains irreplaceable at the preclinical stage. In fact, a wide range of in vivo tumor models have been developed, including simple cell line-derived models, either in syngeneic or xenograft mice, and more advanced GEMMs and PDXs, the latter recently evolving to humanized PDXs. Indeed, complex GEMMs and PDX models, capable of more closely resembling the heterogeneity of the human TME, are the most amenable for testing anticancer nanoparticles, owing to their higher predictive capacity.

However, the routinely application of these models in the preclinical evaluation of nanomedicines, over cell-derived xenografts, has been hampered by the significant investment, expertise, and time required to their establishment and maintenance. The absence of pathophysiologically more relevant in vivo tumor models at the preclinical stage is reflected by the discrepancies of nanoparticle's activity between preclinical data and results from clinical trials.

In order to reverse the limited clinical translation of cancer nanomedicine, the alignment of biomimetic 3D tumor models in vitro with more clinically relevant animal cancer models is required.

Acknowledgments This work was supported by the European Regional Development Fund (ERDF), through the COMPETE 2020-Operational Programme for Competitiveness and Internationalisation, and Portuguese national funds via FCT – Fundação para a Ciência e a Tecnologia, I.P. – under projects Cancel Stem (reference POCI-01-0145-FEDER-016390), CENTRO-01-0145-FEDER-000012 (HealthyAging2020), Euronanomed 2 (FCT reference ENMed/0005/2015), and CNC.IBILI (FCT reference UID/NEU/04539/2019).

References

1. Hanahan Douglas, L. M. (2012). Coussens, accessories to the crime: Functions of cells recruited to the tumor microenvironment. *Cancer Cell, 21*, 309–322.
2. Barcellos-Hoff, M. H., Lyden, D., & Wang, T. C. (2013). The evolution of the cancer niche during multistage carcinogenesis. *Nature Reviews. Cancer, 13*, 511–518.
3. Hanahan, D., & Weinberg, R. A. (2011). Hallmarks of cancer: The next generation. *Cell, 144*, 646–674.
4. Dvorak, H. F. (1986). Similarities between tumour stroma generation and wound healing. *The New England Journal of Medicine, 315,* 1650–1659.
5. Lu, P., Weaver, V. M., & Werb, Z. (2012). The extracellular matrix: A dynamic niche in cancer progression. *The Journal of Cell Biology, 196*, 395–406.
6. Pickup, M. W., Mouw, J. K., & Weaver, V. M. (2014). The extracellular matrix modulates the hallmarks of cancer. *EMBO Reports, 15*, 1243–1253.
7. Ao, M., Franco, O. E., Park, D., Raman, D., Williams, K., & Hayward, S. W. (2007). Cross-talk between paracrine-acting cytokine and chemokine pathways promotes malignancy in benign human prostatic epithelium. *Cancer Research, 67*, 4244–4253.
8. Krause, S., Maffini, M. V., Soto, A. M., & Sonnenschein, C. (2010). The microenvironment determines the breast cancer cells' phenotype: Organization of MCF7 cells in 3D cultures. *BMC Cancer, 10*.
9. Ingber, D. E. (2008). Can cancer be reversed by engineering the tumor microenvironment? *Seminars in Cancer Biology, 18*, 356–364.
10. Joyce, J. A., & Pollard, J. W. (2009). Microenvironmental regulation of metastasis. *Nature Reviews. Cancer, 9*, 239–252.
11. Gottesman, M. M. (2002). Mechanisms of cancer resistance. *Annual Review of Medicine, 53*, 615–627.
12. Longley, D., & Johnston, P. (2005). Molecular mechanisms of drug resistance. *The Journal of Pathology, 205*, 275–292.
13. Baxter, L. T., & Jain, R. K. (1990). Transport of fluid and macromolecules in tumors. II. Role of heterogeneous perfusion and lymphatics. *Microvascular Research, 40*, 246–263.
14. Jain, R. K. (1987). Transport of molecules in the tumor Interstitium: A review. *Cancer Research, 47*, 3039–3051.
15. Holohan, C., Van Schaeybroeck, S., Longley, D. B., & Johnston, P. G. (2013). Cancer drug resistance: An evolving paradigm. *Nature Reviews. Cancer, 13*, 714–726.
16. McMillin Douglas, W., Negri, J. M., & Mitsiades, C. S. (2013). The role of tumour-stromal interactions in modifying drug response: Challenges and opportunities. *Nature Reviews Drug Discovery, 12*, 217–228.
17. Gradishar, W. J., Tjulandin, S., Davidson, N., Shaw, H., Desai, N., Bhar, P., Hawkins, M., & O'Shaughnessy, J. (2005). Phase III trial of nanoparticle albumin-bound paclitaxel compared with polyethylated castor oil-based paclitaxel in women with breast cancer. *Journal of Clinical Oncology, 23*, 7794–7803.
18. Guaglianone, P., Chan, K., Delaflor-weiss, E., Hanisch, R., & Jeffers, S. (1994). Phase I and pharmacologic study of liposomal daunorubicin (DaunoXome). *Investigational New Drugs, 12*, 103–104.
19. O'Brien, M. E. R., Wigler, N., Inbar, M., Rosso, R., Grischke, E., Santoro, A., Catane, R., Kieback, D. G., Tomczak, P., Ackland, S. P., Orlandi, F., Mellars, L., Alland, L., & Tendler, C. (2004). Reduced cardiotoxicity and comparable efficacy in a phase III trial of pegylated liposomal doxorubicin HCl (CAELYX™/Doxil®) versus conventional doxorubicin for first-line treatment of metastatic breast cancer. *Annals of Oncology, 15*, 440–449.
20. Hongisto, V., Jernström, S., Fey, V., Mpindi, J. P., Kleivi Sahlberg, K., Kallioniemi, O., & Perälä, M. (2013). High-throughput 3D screening reveals differences in drug sensitivities between culture models of JIMT1 breast cancer cells. *PLoS One, 8*, 2684–2692.
21. Maeda, H., Nakamura, H., & Fang, J. (2013). The EPR effect for macromolecular drug delivery to solid tumors: Improvement of tumor uptake, lowering of systemic toxicity, and distinct tumor imaging in vivo. *Advanced Drug Delivery Reviews, 65*, 71–79.
22. Matsumura, Y., & Maeda, H. (1986). A new concept for macromolecular therapeutics in cancer chemotherapy: Mechanism of tumoritropic accumulation of proteins and the antitumor agent smancs. *Cancer Research, 46*, 6387–6392.
23. Harris, L., Batist, G., Belt, R., Rovira, D., Navari, R., Azarnia, N., Ph, D., Welles, L., & Winer, E. (2000). Liposome-encapsulated

doxorubicin compared with conventional doxorubicin in a randomized multicenter trial as first-line therapy of metastatic breast carcinoma. *American Cancer Society*.

24. Lancet, J. E., Uy, G. L., Cortes, J. E., Newell, L. F., Lin, T. L., Ritchie, E. K., Stuart, R. K., Strickland, S. A., Hogge, D., Solomon, S. R., Stone, R. M., Bixby, D. L., Kolitz, J. E., Schiller, G. J., Wieduwilt, M. J., Ryan, D. H., Hoering, A., Chiarella, M., Louie, A. C., & Medeiros, B. C. (2016). Final results of a phase III randomized trial of CPX-351 versus 7+3 in older patients with newly diagnosed high risk (secondary) AML. *Journal of Clinical Oncology, 34,* 7000–7000.
25. Wang-Gillam, A., Li, C. P., Bodoky, G., Dean, A., Shan, Y. S., Jameson, G., MacArulla, T., Lee, K. H., Cunningham, D., Blanc, J. F., Hubner, R. A., Chiu, C. F., Schwartsmann, G., Siveke, J. T., Braiteh, F., Moyo, V., Belanger, B., Dhindsa, N., Bayever, E., Von Hoff, D. D., & Chen, L. T. (2016). Nanoliposomal irinotecan with fluorouracil and folinic acid in metastatic pancreatic cancer after previous gemcitabine-based therapy (NAPOLI-1): A global, randomised, open-label, phase 3 trial. *Lancet, 387*, 545–557.
26. Sparreboom, A., Scripture, C. D., Trieu, V., Williams, P. J., De, T., Yang, A., Beals, B., Figg, W. D., Hawkins, M., & Desai, N. (2005). Comparative Preclinical and Clinical Pharmacokinetics of a Cremophor-Free, NanoparticleAlbumin-Bound Paclitaxel (ABI-007) and Paclitaxel Formulated in Cremophor (Taxol). *Cancer Therapy Clinical, 11*, 4136–4144.
27. Schmid, P., Adams, S., Rugo, H. S., Schneeweiss, A., Barrios, C. H., Iwata, H., Diéras, V., Hegg, R., Im, S.-A., Wright, G. S., Henschel, V., Molinero, L., Chui, S. Y., Funke, R., Husain, A., Winer, E. P., Loi, S., & Emens, L. A. (2018). Atezolizumab and nab-paclitaxel in advanced triple-negative breast cancer. *The New England Journal of Medicine, 379*, 2108–2121.
28. Lee, K. S., Chung, H. C., Im, S. A., Park, Y. H., Kim, C. S., Kim, S. B., Rha, S. Y., Lee, M. Y., & Ro, J. (2008). Multicenter phase II trial of Genexol-PM, a Cremophor-free, polymeric micelle formulation of paclitaxel, in patients with metastatic breast cancer. *Breast Cancer Research and Treatment, 108*, 241–250.
29. Prabhakar, U., Maeda, H., Jain, R. K., Sevick-Muraca, E. M., Zamboni, W., Farokhzad, O. C., Barry, S. T., Gabizon, A., Grodzinski, P., & Blakey, D. C. (2013). Challenges and key considerations of the enhanced permeability and retention effect for nanomedicine drug delivery in oncology. *Cancer Research, 73*, 2412–2417.
30. Cabral, H., Matsumoto, Y., Mizuno, K., Chen, Q., Murakami, M., Kimura, M., Terada, Y., Kano, M. R., Miyazono, K., Uesaka, M., Nishiyama, N., & Kataoka, K. (2011). Accumulation of sub-100 nm polymeric micelles in poorly permeable tumours depends on size. *Nature Nanotechnology, 6*, 815–823.
31. Yokoia, K., Taneia, T., Godina, B., van de Vena, A. L., Hanibuchib, M., MasakiAika, A., Alexandera, J., & Ferrari, M. (2014). Serum biomarkers for personalization of nanotherapeutics- based therapy in different tumor and organ microenvironments. *Bone, 345*, 48–55.
32. Kirpotin, D. B., Drummond, D. C., Shao, Y., Shalaby, M. R., Hong, K., Nielsen, U. B., Marks, J. D., Benz, C. C., & Park, J. W. (2006). Antibody targeting of long-circulating lipidic nanoparticles does not increase tumor localization but does increase internalization in animal models. *Cancer Research, 66*, 6732–6740.
33. Choi, C. H. J., Alabi, C. A., Webster, P., & Davis, M. E. (2010). Mechanism of active targeting in solid tumors with transferrin-containing gold nanoparticles. *Proceedings of the National Academy of Sciences of the United States of America, 107*, 1235–1240.
34. Cui, Y., Xu, Q., Chow, P. K. H., Wang, D., & Wang, C. H. (2013). Transferrin-conjugated magnetic silica PLGA nanoparticles loaded with doxorubicin and paclitaxel for brain glioma treatment. *Biomaterials, 34*, 8511–8520.
35. Lee, S. M., Park, H., Choi, J. W., Park, Y. N., Yun, C. O., & Yoo, K. H. (2011). Multifunctional nanoparticles for targeted chemophotothermal treatment of cancer cells. *Angewandte Chemie International Edition, 50*, 7581–7586.
36. Gabizon, A., Tzemach, D., Gorin, J., Mak, L., Amitay, Y., Shmeeda, H., & Zalipsky, S. (2010). Improved therapeutic activity of folate-targeted liposomal doxorubicin in folate receptor-expressing tumor models. *Cancer Chemotherapy and Pharmacology, 66*, 43–52.
37. Hu, C. J., & Zhang, L. (2009). Therapeutic nanoparticles to combat cancer drug resistance. *Current Drug Metabolism, 10*, 836–841.
38. Sadava, D., Coleman, A., & Kane, S. E. (2002). Liposomal daunorubicin overcomes drug resistance in human breast, ovarian and lung carcinoma cells. *Journal of Liposome Research, 12*, 301–309.
39. Iinuma, H., Maruyama, K., Okinaga, K., Sasaki, K., Sekine, T., Ishida, O., Ogiwara, N., Johkura, K., & Yonemura, Y. (2002). Intracellular targeting therapy of cisplatin-encapsulated transferrin-polyethylene glycol liposome on peritoneal dissemination of gastric cancer. *International Journal of Cancer, 99*, 130–137.
40. Kobayashi, T., Ishida, T., Okada, Y., Ise, S., Harashima, H., & Kiwada, H. (2007). Effect of transferrin receptor-targeted liposomal doxorubicin in P-glycoprotein-mediated drug resistant tumor cells. *International Journal of Pharmaceutics, 329*, 94–102.
41. Fernandes, C., Suares, D., & Yergeri, M. C. (2018). Tumor microenvironment targeted nanotherapy. *Frontiers in Pharmacology, 9*, 1–25.
42. Murphy, E. A., Majeti, B. K., Barnes, L. A., Makale, M., Weis, S. M., Lutu-Fuga, K., Wrasidlo, W., & Cheresh, D. A. (2008). Nanoparticle-mediated drug delivery to tumor vasculature suppresses metastasis. *Proceedings of the National Academy of Sciences of the United States of America, 105*, 9343–9348.
43. Sugahara, K. N., Teesalu, T., Karmali, P. P., Kotamraju, V. R., Agemy, L., Girard, O. M., Hanahan, D., Mattrey, R. F., & Ruoslahti, E. (2009). Tissue-penetrating delivery of compounds and nanoparticles into tumors. *Cancer Cell, 16*, 510–520.
44. Murakami, M., Ernsting, M. J., Undzys, E., Holwell, N., Foltz, W. D., & Li, S. D. (2013). Docetaxel conjugate nanoparticles that target a-smooth muscle actin-expressing stromal cells suppress breast cancer metastasis. *Cancer Research, 73*, 4862–4871.
45. Saluja, S. S., Hanlon, D. J., Sharp, F. A., Hong, E., Khalil, D., Robinson, E., Tigelaar, R., Fahmy, T. M., & Edelson, R. L. (2014). Targeting human dendritic cells via DEC-205 using PLGA nanoparticles leads to enhanced cross-presentation of a melanoma-associated antigen. *International Journal of Nanomedicine, 9*, 5231–5246.
46. Zhang, X., Tian, W., Cai, X., Wang, X., Dang, W., Tang, H., Cao, H., Wang, L., & Chen, T. (2013). Hydrazinocurcumin Encapsuled nanoparticles "re-educate" tumor-associated macrophages and exhibit anti-tumor effects on breast cancer following STAT3 suppression. *PLoS One, 8*, 1–9.
47. Zhu, S., Niu, M., O'Mary, H., & Cui, Z. (2013). Targeting of tumor-associated macrophages made possible by PEG-sheddable, mannose-modified nanoparticles. *Molecular Pharmaceutics, 10*, 3525–3530.
48. Chen, B., Wang, Z., Sun, J., Song, Q., He, B., Zhang, H., Wang, X., Dai, W., & Zhang, Q. (2016). A tenascin C targeted nanoliposome with navitoclax for specifically eradicating of cancer-associated fibroblasts, nanomedicine nanotechnology. *Biologie et Médecine, 12*, 131–141.
49. Lin, J., Shigdar, S., Fang, D. Z., Xiang, D., Wei, M. Q., Danks, A., Kong, L., Li, L., Qiao, L., & Duan, W. (2014). Improved efficacy and reduced toxicity of doxorubicin encapsulated in sulfatide-containing nanoliposome in a glioma model. *PLoS One, 9*, 1–13.

50. Hatakeyama, H., Akita, H., Ishida, E., Hashimoto, K., Kobayashi, H., Aoki, T., Yasuda, J., Obata, K., Kikuchi, H., Ishida, T., Kiwada, H., & Harashima, H. (2007). Tumor targeting of doxorubicin by anti-MT1-MMP antibody-modified PEG liposomes. *International Journal of Pharmaceutics, 342*, 194–200.
51. Penate Medina, O., Haikola, M., Tahtinen, M., Simpura, I., Kaukinen, S., Valtanen, H., Zhu, Y., Kuosmanen, S., Cao, W., Reunanen, J., Nurminen, T., Saris, P. E. J., Smith-Jones, P., Bradbury, M., Larson, S., & Kairemo, K. (2011). Liposomal tumor targeting in drug delivery utilizing MMP-2- and MMP-9-binding ligands. *Journal of Drug Delivery, 2011*, 1–9.
52. Sengupta, S., Eavarone, D., Capila, I., Zhao, G., Watson, N., Kiziltepe, T., & Sasisekharan, R. (2005). Temporal targeting of tumour cells and neovasculature with a nanoscale delivery system. *Nature, 436*, 568–572.
53. Guo, S., Lin, C. M., Xu, Z., Miao, L., Wang, Y., & Huang, L. (2014). Co-delivery of cisplatin and rapamycin for enhanced anticancer therapy through synergistic effects and microenvironment modulation. *ACS Nano, 8*, 4996–5009.
54. Fonseca, N. A., Gomes-Da-Silva, L. C., Moura, V., Simões, S., & Moreira, J. N. (2014). Simultaneous active intracellular delivery of doxorubicin and C6-ceramide shifts the additive/antagonistic drug interaction of non-encapsulated combination. *Journal of Controlled Release, 196*, 122–131.
55. Gomes-Da-Silva, L. C., Fonseca, N. A., Moura, V., Pedroso De Lima, M. C., Simões, S., & Moreira, J. N. (2012). Lipid-based nanoparticles for siRNA delivery in cancer therapy: Paradigms and challenges. *Accounts of Chemical Research, 45*, 1163–1171.
56. Lv, Y., Hao, L., Hu, W., Ran, Y., Bai, Y., & Zhang, L. (2016). Novel multifunctional pH-sensitive nanoparticles loaded into microbubbles as drug delivery vehicles for enhanced tumor targeting. *Scientific Reports, 6*, 1–9.
57. Gao, N., Xing, C., Wang, H., Feng, L., Zeng, X., Mei, L., & Peng, Z. (2019). PH-responsive dual drug-loaded nanocarriers based on poly (2-Ethyl-2-Oxazoline) modified black phosphorus nanosheets for cancer chemo/photothermal therapy. *Frontiers in Pharmacology, 10*, 1–14.
58. Moura, V., Lacerda, M., Figueiredo, P., Corvo, M. L., Cruz, M. E. M., Soares, R., De Lima, M. C. P., Simões, S., & Moreira, J. N. (2012). Targeted and intracellular triggered delivery of therapeutics to cancer cells and the tumor microenvironment: Impact on the treatment of breast cancer. *Breast Cancer Research and Treatment, 133*, 61–73.
59. Hou, L., Yang, X., Ren, J., Wang, Y., Zhang, H., Feng, Q., Shi, Y., Shan, X., Yuan, Y., & Zhang, Z. (2016). A novel redox-sensitive system based on single-walled carbon nanotubes for chemo-photothermal therapy and magnetic resonance imaging. *International Journal of Nanomedicine, 11*, 607–624.
60. Lin, C. W., Lu, K. Y., Wang, S. Y., Sung, H. W., & Mi, F. L. (2016). CD44-specific nanoparticles for redox-triggered reactive oxygen species production and doxorubicin release. *Acta Biomaterialia, 35*, 280–292.
61. Wu, L., Zhang, L., Shi, G., & Ni, C. (2016). Zwitterionic pH/redox nanoparticles based on dextran as drug carriers for enhancing tumor intercellular uptake of doxorubicin. *Materials Science and Engineering: C, 61*, 278–285.
62. Zhu, L., Kate, P., & Torchilin, V. P. (2012). Matrix metalloprotease 2-responsive multifunctional liposomal nanocarrier for enhanced tumor targeting. *ACS Nano, 6*, 3491–3498.
63. Sun, Z., Li, R., Sun, J., Peng, Y., Xiao, L., Zhang, X., Xu, Y., & Wang, M. (2017). Matrix metalloproteinase cleavable nanoparticles for tumor microenvironment and tumor cell dual-targeting drug delivery. *ACS Applied Materials & Interfaces, 9*, 40614–40627.
64. Rosenblum, D., Joshi, N., Tao, W., Karp, J. M., & Peer, D. (2018). Progress and challenges towards targeted delivery of cancer therapeutics. *Nature Communications, 9*.
65. Wilhelm, S., Tavares, A. J., Dai, Q., Ohta, S., Audet, J., Dvorak, H. F., & Chan, W. C. W. (2016). Analysis of nanoparticle delivery to tumours. *Nature Reviews Materials, 1*, 1–12.
66. Jain, R. K., & Stylianopoulos, T. (2010). Delivering nanomedicine to solid tumors. *Nature Reviews. Clinical Oncology, 7*, 653–664.
67. Chauhan, V. P., & Jain, R. K. (2013). Strategies for advancing cancer nanomedicine. *Nature Materials, 12*, 958–962.
68. Daldrup-Link, H. E., Golovko, D., Ruffell, B., DeNardo, D. G., Castaneda, R., Ansari, C., Rao, J., Tikhomirov, G. A., Wendland, M. F., Corot, C., & Coussens, L. M. (2011). MRI of tumor-associated macrophages with clinically applicable iron oxide nanoparticles. *Clinical Cancer Research, 17*, 5695–5704.
69. Miller, M. A., Zheng, Y. R., Gadde, S., Pfirschke, C., Zope, H., Engblom, C., Kohler, R. H., Iwamoto, Y., Yang, K. S., Askevold, B., Kolishetti, N., Pittet, M., Lippard, S. J., Farokhzad, O. C., & Weissleder, R. (2015). Tumour-associated macrophages act as a slow-release reservoir of nano-therapeutic Pt(IV) pro-drug. *Nature Communications, 6*.
70. Jain, R. K. (2013). Normalizing tumor microenvironment to treat cancer: Bench to bedside to biomarkers. *Journal of Clinical Oncology, 31*, 2205–2218.
71. Jiang, W., Huang, Y., An, Y., & Kim, B. Y. S. (2015). Remodeling tumor vasculature to enhance delivery of intermediate-sized nanoparticles. *ACS Nano*, 8689–8696.
72. Diop-Frimpong, B., Chauhan, V. P., Krane, S., Boucher, Y., & Jain, R. K. (2011). Losartan inhibits collagen I synthesis and improves the distribution and efficacy of nanotherapeutics in tumors. *Proceedings of the National Academy of Sciences of the United States of America, 108*, 2909–2914.
73. Harrison, R. G., Greenman, M. J., Mall, F. P., & Jackson, C. M. (1907). Observations of the living developing nerve fiber. *The Anatomical Record, 1*, 116–128.
74. Harrison, R. G. (1910). The outgrowth of the nerve fiber as a mode of protoplasmic movement. *The Journal of Experimental Zoology, 9*, 787–846.
75. Duval, K., Grover, H., Han, L.-H., Mou, Y., Pegoraro, A. F., Fredberg, J., & Chen, Z. (2017). Modeling physiological events in 2D vs. 3D cell culture. *Physiology, 32*, 266–277.
76. Walpita, D., & Hay, E. (2002). Studying actin-dependent processes in tissue culture. *Nature Reviews. Molecular Cell Biology, 3*, 133–137.
77. Kalashnikova, I., Albekairi, N., Ali, S., Al Enazy, S., & Rytting, E. (2016). Cell culture models for drug transport studies. In *Drug delivery: Principles and applications* (2nd ed., pp. 131–151).
78. Kapałczyńska, M., Kolenda, T., Przybyła, W., Zajączkowska, M., Teresiak, A., Filas, V., Ibbs, M., Bliźniak, R., Łuczewski, Ł., & Lamperska, K. (2018). 2D and 3D cell cultures – A comparison of different types of cancer cell cultures. *Archives of Medical Science, 14*, 910–919.
79. Paridah, M., Moradbak, A., Mohamed, A., Abdulwahab Taiwo Owolabi, F., M. Asniza, & Abdul Khalid, S. H. (2016). 2D and 3D cell culture in drug discovery. *Intech, i*, 13.
80. Bissell, M. J. (1981). The differentiated state of normal and malignant cells or how to define a "normal" cell in culture. *International Review of Cytology, 70*, 27–100.
81. von der Mark, K., Gauss, V., von der Mark, H., & Muller, P. (1977). Relationship between cell shape and type of collagen synthesised as chondrocytes lose their cartilage phenotype in culture. *Nature, 267*, 531–532.
82. Griffith, L. G., & Swartz, M. A. (2006). Capturing complex 3D tissue physiology in vitro. *Nature Reviews. Molecular Cell Biology, 7*, 211–224.

83. Kleinman, H. K., Philp, D., & Hoffman, M. P. (2003). Role of the extracellular matrix in morphogenesis. *Current Opinion in Biotechnology, 14*, 526–532.
84. Bissell, M. J., Rizki, A., & Mian, I. S. (2003). Tissue architecture: The ultimate regulator of breast epithelial function. *Current Opinion in Cell Biology, 15*, 753–762.
85. Cukierman, E., Pankov, R., & Yamada, K. M. (2002). Cell interactions with three-dimensional matrices. *Current Opinion in Cell Biology, 14*, 633–640.
86. Hutmacher Dietmar, W., Loessner, D., Rizzi, S., Kaplan, D. L., Mooney, D. J., & Clements, J. A. (2010). Can tissue engineering concepts advance tumor biology research? *Trends in Biotechnology, 28*, 125–133.
87. Zhang, S. (2004). Beyond the petri dish. *Nature Biotechnology, 22*, 151–152.
88. Luca, A. C., Mersch, S., Deenen, R., Schmidt, S., Messner, I., Schäfer, K. L., Baldus, S. E., Huckenbeck, W., Piekorz, R. P., Knoefel, W. T., Krieg, A., & Stoecklein, N. H. (2013). Impact of the 3D microenvironment on phenotype, gene expression, and EGFR inhibition of colorectal cancer cell lines. *PLoS One, 8*.
89. Tveit, K. M., & Pihl, A. (1981). Do cell lines in vitro reflect the properties of the tumours of origin? A study of lines derived from human melanoma xenografts. *British Journal of Cancer, 44*, 775–786.
90. Bissell, M. J., Radisky, D. C., Rizki, A., Weaver, V. M., & Petersen, O. W. (2002). The organizing principle: Microenvironmental influences in the normal and malignant breast. *Differentiation, 70*, 537–546.
91. Kamb, A. (2005). What's wrong with our cancer models? *Nature Reviews. Drug Discovery, 4*, 161–165.
92. Hahn, W. C., Counter, C. M., Lundberg, A. S., Beijersbergen, R. L., Brooks, M. W., & Weinberg, R. A. (1999). Creation of human tumour cells with defined genetic elements. *Nature, 400*, 464–468.
93. Barretina, J., Caponigro, G., Stransky, N., Venkatesan, K., Margolin, A. A., Kim, S., Wilson, C. J., Lehár, J., Kryukov, G. V., Sonkin, D., Reddy, A., Liu, M., Murray, L., Berger, M. F., Monahan, J. E., Morais, P., Meltzer, J., Korejwa, A., Jané-Valbuena, J., Mapa, F. A., Thibault, J., Bric-Furlong, E., Raman, P., Shipway, A., Engels, I. H., Cheng, J., Yu, G. K., Yu, J., Aspesi, P., De Silva, M., Jagtap, K., Jones, M. D., Wang, L., Hatton, C., Palescandolo, E., Gupta, S., Mahan, S., Sougnez, C., Onofrio, R. C., Liefeld, T., MacConaill, L., Winckler, W., Reich, M., Li, N., Mesirov, J. P., Gabriel, S. B., Getz, G., Ardlie, K., Chan, V., Myer, V. E., Weber, B. L., Porter, J., Warmuth, M., Finan, P., Harris, J. L., Meyerson, M., Golub, T. R., Morrissey, M. P., Sellers, W. R., Schlegel, R., & Garraway, L. A. (2012). The Cancer Cell Line Encyclopedia enables predictive modelling of anticancer drug sensitivity. *Nature, 483*, 603–607.
94. Virtanen, C., Ishikawa, Y., Honjoh, D., Kimura, M., Shimane, M., Miyoshi, T., Nomura, H., & Jones, M. H. (2002). Integrated classification of lung tumors and cell lines by expression profiling. *Proceedings of the National Academy of Sciences of the United States of America, 99*, 12357–12362.
95. Daniel, V. C., Marchionni, L., Hierman, J. S., Rhodes, J. T., Devereux, W. L., Rudin, C. M., Yung, R., Parmigiani, G., Dorsch, M., Peacock, C. D., & Watkins, D. N. (2009). A primary xenograft model of small-cell lung cancer reveals irreversible changes in gene expression imposed by culture in vitro. *Cancer Research, 69*, 3364–3373.
96. Borel, B. (2010). How accurate are cancer cell lines? *Nature, 463*, 858.
97. Gillet, J. P., Calcagno, A. M., Varma, S., Marino, M., Green, L. J., Vora, M. I., Patel, C., Orina, J. N., Eliseeva, T. A., Singal, V., Padmanabhan, R., Davidson, B., Ganapathi, R., Sood, A. K., Rueda, B. R., Ambudkar, S. V., & Gottesman, M. M. (2011). Redefining the relevance of established cancer cell lines to the study of mechanisms of clinical anti-cancer drug resistance. *Proceedings of the National Academy of Sciences of the United States of America, 108*, 18708–18713.
98. Li, C., Kato, M., Shiue, L., Shively, J. E., Ares, M., & Lin, R. J. (2006). Cell type and culture condition-dependent alternative splicing in human breast cancer cells revealed by splicing-sensitive microarrays. *Cancer Research, 66*, 1990–1999.
99. Grainger, D. W. (2014). Cell-based drug testing; This world is not flat. *Advanced Drug Delivery Reviews*, 69–70.
100. Wilding, J. L., & Bodmer, W. F. (2014). Cancer cell lines for drug discovery and development. *Cancer Research, 74*, 2377–2384.
101. Correia, A. L., & Bissell, M. J. (2012). The tumor microenvironment is a dominant force in multidrug resistance. *Drug Resistance Updates, 15*, 39–49.
102. Xu, X., Sabanayagam, C. R., Harrington, D. A., Farach-Carson, M. C., & Jia, X. (2014). A hydrogel-based tumor model for the evaluation of nanoparticle-based cancer therapeutics. *Biomaterials, 35*, 3319–3330.
103. Abbott, A. (2003). Biology's new dimension. *Nature, 424*, 870–872.
104. Pampaloni, F., Reynaud, E. G., & Stelzer, E. H. K. (2007). The third dimension bridges the gap between cell culture and live tissue. *Nature Reviews. Molecular Cell Biology, 8*, 839–845.
105. Bissell, M. J., & Radisky, D. (2001). Putting tumours in context. *Nature Reviews. Cancer, 1*, 46–54.
106. Vidi, P.-A., Bissell, M. J., & Lelièvre, S. A. (2003). Three-dimensional culture of human breast epithelial cells: The how and the why. *Epithelial Cell Culture Protocols, 945*, 193–219.
107. Kenny, P. A., Lee, G. Y., Myers, C. A., Neve, R. M., Semeiks, J. R., Spellman, P. T., Lorenz, K., Lee, E. H., Barcellos-Hoff, M. H., Petersen, O. W., Gray, J. W., & Bissell, M. J. (2007). The morphologies of breast cancer cell lines in three-dimensional assays correlate with their profiles of gene expression. *Molecular Oncology, 1*, 84–96.
108. Ghosh, S., Spagnoli, G. C., Martin, I., Ploegert, S., Demougin, P., Heberer, M., & Reschner, A. (2005). Three-dimensional culture of melanoma cells profoundly affects gene expression profile: A high density oligonucleotide array study. *Journal of Cellular Physiology, 204*, 522–531.
109. Birgersdotter, A., Sandberg, R., & Ernberg, I. (2005). Gene expression perturbation in vitro – A growing case for three-dimensional (3D) culture systems. *Seminars in Cancer Biology, 15*, 405–412.
110. Ghosh, S., Joshi, M. B., Ivanov, D., Feder-mengus, C., Spagnoli, G. C., Martin, I., Erne, P., & Resink, T. J. (2007). Use of multicellular tumor spheroids to dissect endothelial cell – Tumor cell interactions: A role for T-cadherin in tumor angiogenesis. *FEBS Letters, 581*, 4523–4528.
111. Carragher, N., Piccinini, F., Tesei, A., Trask, O. J., Bickle, M., & Horvath, P. (2018). Concerns, challenges and promises of high-content analysis of 3D cellular models. *Nature Reviews Drug Discovery, 17*.
112. Costa, E. C., Moreira, A. F., De Melo-diogo, D., Gaspar, V. M., Carvalho, M. P., & Correia, I. J. (2016). 3D tumor spheroids: An overview on the tools and techniques used for their analysis. *Biotechnology Advances*.
113. Myungjin Lee, J., Mhawech-Fauceglia, P., Lee, N., Cristina Parsanian, L., Gail Lin, Y., Andrew Gayther, S., & Lawrenson, K. (2013). A three-dimensional microenvironment alters protein expression and chemosensitivity of epithelial ovarian cancer cells in vitro. *Laboratory Investigation, 93*, 528–542.
114. Loessner, D., Stok, K. S., Lutolf, M. P., Hutmacher, D. W., Clements, J. A., & Rizzi, S. C. (2010). Bioengineered 3D platform to explore cell-ECM interactions and drug resistance of epithelial ovarian cancer cells. *Biomaterials, 31*, 8494–8506.
115. Barbone, D., Yang, T., Morgan, J. R., Gaudino, G., & Broaddus, V. C. (2008). Mammalian target of rapamycin contributes to the acquired apoptotic resistance of human mesothelioma multi-

cellular spheroids. *The Journal of Biological Chemistry, 283*, 13021–13030.

116. Shin, K., Klosterhoff, B. S., & Han, B. (2016). Characterization of cell-type specific drug transport and resistance of breast cancers using tumor-microenvironment-on- chip. *Molecular Pharmaceutics, 13*, 2214–2223.
117. Geeta, M., Hsiao, A. Y., Ingram, M., Luker, G. D., & Takayama, S. (2012). Opportunities and challenges for use of tumor spheroids as models to test drug delivery and efficacy. *Journal of Controlled Release, 164*, 192–204.
118. Loessner, D., Holzapfel, B. M., & Clements, J. A. (2014). Engineered microenvironments provide new insights into ovarian and prostate cancer progression and drug responses. *Advanced Drug Delivery Reviews, 79*, 193–213.
119. Breslin, S., & O'Driscoll, L. (2013). Three-dimensional cell culture: The missing link in drug discovery. *Drug Discovery Today, 18*, 240–249.
120. Costachel, O., Fadei, L., & Badea, E. (1969). Tumor cell suspension culture on non adhesive substratum. *Zeitschrift für Krebsforschung, 72*, 24–31.
121. Hamilton, G. (1998). Multicellular spheroids as an in vitro tumor model. *Cancer Letters, 131*, 29–34.
122. Santini, M. T., & Rainaldi, G. (1999). Three-dimensional spheroid model in tumor biology. *Pathobiology, 67*, 148–157.
123. Nath, S., & Devi, G. R. (2016). Three-dimensional culture systems in cancer research: Focus on tumor spheroid model. *Pharmacology & Therapeutics, 163*, 94–108.
124. Lin, R.-Z., Chou, L.-F., Chien, C.-C. M., & Chang, H.-Y. (2006). Dynamic analysis of hepatoma spheroid formation: Roles of E-cadherin and β 1-integrin. *Cell and Tissue Research, 324*, 411–422.
125. Meng, Q., Wu, D., Zhang, G., & Qiu, H. (2006). Direct self-assembly of hepatocytes spheroids within hollow fibers in presence of collagen. *Biotechnology Letters, 28*, 279–284.
126. Longati, P., Jia, X., Eimer, J., Wagman, A., Witt, M., Rehnmark, S., Verbeke, C., Toftgård, R., Löhr, M., & Heuchel, R. L. (2013). 3D pancreatic carcinoma spheroids induce a matrix-rich, chemoresistant phenotype offering a better model for drug testing. *BMC Cancer, 2013*(13), 1–13.
127. Costa, E. C., Gaspar, V. M., Coutinho, P., & Correia, I. J. (2014). Optimization of liquid overlay technique to formulate heterogenic 3D co-cultures models. *Biotechnology and Bioengineering, 9999*, 1–14.
128. Carlsson, J., & Yuhas, J. M. (1984). Liquid-overlay culture of cellular spheroids. *Recent Results in Cancer Research, 95*, 1–23.
129. Villaronga, M. Á., Teijeiro, S. Á., Hermida, F., Garzón-Arango, M., Sanz-Moreno, V., & García-Pedrero, J. M. (2018). Analysis of invasive activity of CAF spheroids into Three Dimensional (3D) Collagen Matrices. In *Methods in molecular biology* (pp. 145–154).
130. Vultur, A., Villanueva, J., Krepler, C., Rajan, G., Chen, Q., Xiao, M., Li, L., Gimotty, P. A., Wilson, M., Hayden, J., Keeney, F., & Nathanson, K. L. (2014). MEK inhibition affects STAT3 signaling and invasion in human melanoma cell lines. *Oncogene, 33*, 1850–1861.
131. Ingeson-carlsson, C., Martinez-monleon, A., & Nilsson, M. (2015). Differential effects of MAPK pathway inhibitors on migration and invasiveness of BRAF V600E mutant thyroid cancer cells in 2D and 3D culture. *Experimental Cell Research, 338*, 127–135.
132. Lee, G. Y., Kenny, P. A., Lee, E. H., & Bissell, M. J. (2007). Three-dimensional culture models of normal and malignant breast epithelial cells. *Nature Methods, 4*, 359–365.
133. Vinci, M., Gowan, S., Boxall, F., Patterson, L., Zimmermann, M., Court, W., Lomas, C., Mendiola, M., Hardisson, D., & Eccles, S. A. (2012). Advances in establishment and analysis of three-dimensional tumor spheroid-based functional assays for target validation and drug evaluation. *BMC Biology, 10*, 29.
134. Du, A. W., Lu, H., & Stenzel, M. H. (2015). Core-cross-linking accelerates antitumor activities of paclitaxel-conjugate micelles to prostate multicellular tumor spheroids: A comparison of 2D and 3D models. *Biomacromolecules, 16*, 1470–1479.
135. Rodday, B., Hirschhaeuser, F., Walenta, S., & Mueller-klieser, W. (2011). Semiautomatic growth analysis of multicellular tumor spheroids. *Journal of Biomolecular Screening, 16*, 1119–1124.
136. Jessup, J. M., Coodwin, T. J., & Spaulding, C. (1993). Prospects for use of microgravity-based bioreactors to study three-dimensional host-tumor interactions in. *Journal of Cellular Biochemistry, 51*, 290–300.
137. Ingram, A. M., Techy, G. B., Saroufeem, R., Yazan, O., Narayan, K. S., Goodwin, T. J., Spaulding, G. F., In, S., Cellular, V., Animal, D. B., & Jun, N. (1997). Three-dimensional growth patterns of various human tumor cell lines in simulated microgravity of a Nasa. *In Vitro Cellular & Developmental Biology – Animal, 33,* 459–466.
138. Del Duca, D., Werbowetski, T., & Del Maestro, R. F. (2004). Spheroid preparation from hanging drops: Characterization of a model of brain tumor invasion. *Journal of Neuro-Oncology, 67*, 295–303.
139. Ware, M. J., Colbert, K., Keshishian, V., Ho, J., Corr, S. J., Curley, S. A., & Godin, B. (2016). Generation of homogenous 3D pancreatic cancer cell spheroids using an improved hanging drop technique. *Tissue Engineering Part C, 22*, 1–36.
140. Haisler, W. L., Timm, D. M., Gage, J. A., Tseng, H., Killian, T. C., & Souza, G. R. (2013). Three-dimensional cell culturing by magnetic levitation. *Nature Protocols, 8*.
141. Tseng, H., Gage, J. A., Shen, T., Haisler, W. L., Neeley, S. K., Shiao, S., Chen, J., Desai, P. K., Liao, A., Hebel, C., Raphael, R. M., Becker, J. L., & Souza, G. R. (2015). A spheroid toxicity assay using magnetic 3D bioprinting and real- time mobile device-based imaging. *Scientific Reports, 5*, 1–11.
142. Leonard, F., & Godin, B. (2016). 3D in vitro model for breast cancer research using magnetic levitation and bioprinting method. In *Methods in molecular biology* (pp. 239–251).
143. Ma, H. L., Jiang, Q., Han, S., Wu, Y., Tomshine, J. C., Wang, D., Gan, Y., Zou, G., & Liang, X. J. (2012). Multicellular tumor spheroids as an in vivo-like tumor model for three-dimensional imaging of chemotherapeutic and nano material cellular penetration. *Molecular Imaging, 11*, 487–498.
144. Lu, H., & Stenzel, M. H. (2018). Multicellular tumor spheroids (MCTS) as a 3D in vitro evaluation tool of nanoparticles. *Small, 14*, 1–26.
145. Sutherland, R. M. (1988). Cell and environment interactions in tumor microregions: The spheroid model. *Science (80-.), 240*, 177–184.
146. Oloumi, A., Lam, W., Banath, J. P., & Olive, P. L. (2002). Identication of genes diferentially expressed in V79 cells grown as multicell spheroids. *International Journal of Radiation Biology, 78*, 483–492.
147. Zietarska, M., Maugard, C. M., Filali-mouhim, A., Alam-fahmy, M., Tonin, P. N., & Provencher, D. M. (2007). Molecular description of a 3D in vitro model for the study of epithelial ovarian cancer (EOC). *Molecular Carcinogenesis, 46*, 872–885.
148. Lin, R. Z., & Chang, H. Y. (2008). Recent advances in three-dimensional multicellular spheroid culture for biomedical research. *Biotechnology Journal, 3*, 1172–1184.
149. Curcio, E., Salerno, S., Barbieri, G., De Bartolo, L., Drioli, E., & Bader, A. (2007). Mass transfer and metabolic reactions in hepatocyte spheroids cultured in rotating wall gas-permeable membrane system. *Biomaterials, 28*, 5487–5497.
150. Alvarez-Pérez, J., Ballesteros, P., & Cerdán, S. (2005). Microscopic images of intraspheroidal pH by 1H magnetic resonance chemical shift imaging of pH sensitive indicators. *Magnetic Resonance Materials in Physics, Biology and Medicine, 18*, 293–301.

151. Upreti, M., Jamshidi-Parsian, A., Koonce, N. A., Webber, J. S., Sharma, S. K., Asea, A. A. A., Mader, M. J., & Griffin, R. J. (2011). Tumor-endothelial cell spheroids: New aspects to enhance radiation. *Translational Oncology, 4*, 365–376.
152. Lamichhane, S. P., Arya, N., Kohler, E., Xiang, S., Christensen, J., & Shastri, V. P. (2016). Recapitulating epithelial tumor microenvironment in vitro using three dimensional tri-culture of human epithelial, endothelial, and mesenchymal cells. *BMC Cancer, 16*, 1–12.
153. Holliday, D. L., Brouilette, K. T., Markert, A., Gordon, L. A., & Jones, J. L. (2009). Novel multicellular organotypic models of normal and malignant breast: Tools for dissecting the role of the microenvironment in breast cancer progression. *Breast Cancer Research, 11*, 1–11.
154. Priwitaningrum, D. L., Blonde, J.-B., van Baarlen, J., Hennink, W. E., Storm, G., Le Gac, S., & Prakash, J. (2016). Tumor stroma-containing 3D spheroid arrays: A tool to study nanoparticle penetration. *Journal of Controlled Release*.
155. Karlsson, H., Fryknäs, M., Larsson, R., & Nygren, P. (2012). Loss of cancer drug activity in colon cancer HCT-116 cells during spheroid formation in a new 3-D spheroid cell culture system. *Experimental Cell Research, 318*, 1577–1585.
156. Kostarelos, K., Emfietzoglou, D., Papakostas, A., Yang, W.-H., Ballangrud, Å., & Sgouros, G. (2004). Binding and interestitial penetration of liposomes within asvascular tumor spheroids. *International Journal of Cancer, 112*, 713–721.
157. Kim, T. H., Mount, C. W., Gombotz, W. R., & Pun, S. H. (2010). The delivery of doxorubicin to 3-D multicellular spheroids and tumors in a murine xenograft model using tumor-penetrating triblock polymeric micelles. *Biomaterials, 31*, 7386–7397.
158. Cantisani, M., Guarnieri, D., Biondi, M., Belli, V., Profeta, M., Raiola, L., & Netti, P. A. (2015). Biocompatible nanoparticles sensing the matrix metallo-proteinase 2 for the on-demand release of anticancer drugs in 3D tumor spheroids. *Colloids Surfaces B Biointerfaces, 135*, 707–716.
159. Moreira, A. F., Dias, D. R., Costa, E. C., & Correia, I. J. (2017). Thermo- and pH-responsive nano-in-micro particles for combinatorial drug delivery to cancer cells. *European Journal of Pharmaceutical Sciences, 104*, 42–51.
160. Till, U., Gibot, L., Vicendo, P., Rols, M. P., Gaucher, M., Violleau, F., & Mingotaud, A. F. (2016). Crosslinked polymeric self-assemblies as an efficient strategy for photodynamic therapy on a 3D cell culture. *RSC Advances, 6*, 69984–69998.
161. Gibot, L., Lemelle, A., Till, U., Moukarzel, B., Mingotaud, A. F., Pimienta, V., Saint-Aguet, P., Rols, M. P., Gaucher, M., Violleau, F., Chassenieux, C., & Vicendo, P. (2014). Polymeric micelles encapsulating photosensitizer: Structure/photodynamic therapy efficiency relation. *Biomacromolecules, 15*, 1443–1455.
162. Sims, L. B., Huss, M. K., Frieboes, H. B., & Steinbach-Rankins, J. M. (2017). Distribution of PLGA-modified nanoparticles in 3D cell culture models of hypo-vascularized tumor tissue. *Journal of Nanobiotechnology, 15*, 1–15.
163. Ran, R., Wang, H., Liu, Y., Hui, Y., Sun, Q., Seth, A., Wibowo, D., Chen, D., & Zhao, C. X. (2018). Microfluidic self-assembly of a combinatorial library of single- and dual-ligand liposomes for in vitro and in vivo tumor targeting. *European Journal of Pharmaceutics and Biopharmaceutics, 130*, 1–10.
164. Wang, X., Zhen, X., Wang, J., Zhang, J., Wu, W., & Jiang, X. (2013). Doxorubicin delivery to 3D multicellular spheroids and tumors based on boronic acid-rich chitosan nanoparticles. *Biomaterials, 34*, 4667–4679.
165. Wojnilowicz, M., Besford, Q. A., Wu, Y. L., Loh, X. J., Braunger, J. A., Glab, A., Cortez-Jugo, C., Caruso, F., & Cavalieri, F. (2018). Glycogen-nucleic acid constructs for gene silencing in multicellular tumor spheroids. *Biomaterials, 176*, 34–49.
166. Lugert, S., Unterweger, H., Mühlberger, M., Janko, C., Draack, S., Ludwig, F., Eberbeck, D., Alexiou, C., & Friedrich, R. P. (2019). Cellular effects of paclitaxel-loaded iron oxide nanoparticles on breast cancer using different 2D and 3D cell culture models. *International Journal of Nanomedicine, 14*, 161–180.
167. Rane, T. D., & Armani, A. M. (2016). Two-photon microscopy analysis of gold nanoparticle uptake in 3D cell spheroids. *PLoS One, 11*, 1–13.
168. Hutmacher, D. W. (2010). Biomaterials offer cancer research the third dimension. *Nature Materials, 9*, 90–93.
169. Kleinman, H. K., McGarvey, M. L., Hassell, J. R., Star, V. L., Cannon, F. B., Laurie, G. W., & Martin, G. R. (1986). Basement membrane complexes with biological activity. *Biochemistry, 25*, 312–318.
170. Kleinman, H. K., & Martin, G. R. (2005). Matrigel: Basement membrane matrix with biological activity. *Seminars in Cancer Biology, 15*, 378–386.
171. Poincloux, R., Collin, O., Lizárraga, F., Romao, M., Debray, M., Piel, M., & Chavrier, P. (2011). Contractility of the cell rear drives invasion of breast tumor cells in 3D Matrigel. *Proceedings of the National Academy of Sciences of the United States of America, 108*, 1943–1948.
172. Härmä, V., Virtanen, J., Mäkelä, R., Happonen, A., Mpindi, J. P., Knuuttila, M., Kohonen, P., Lötjönen, J., Kallioniemi, O., & Nees, M. (2010). A comprehensive panel of three-dimensional models for studies of prostate cancer growth, invasion and drug responses. *PLoS One, 5*.
173. Sabeh, F., Shimizu-Hirota, R., & Weiss, S. J. (2009). Protease-dependent versus-independent cancer cell invasion programs: Three-dimensional amoeboid movement revisited. *The Journal of Cell Biology, 185*, 11–19.
174. Chen, L., Xiao, Z., Meng, Y., Zhao, Y., Han, J., Su, G., Chen, B., & Dai, J. (2012). The enhancement of cancer stem cell properties of MCF-7 cells in 3D collagen scaffolds for modeling of cancer and anti-cancer drugs. *Biomaterials, 33*, 1437–1444.
175. Prestwich, G. D. (2008). Evaluating drug efficacy and toxicology in three dimensions: Using synthetic extracellular matrices in drug discovery. *Accounts of Chemical Research, 41*, 139–148.
176. Nagarkar, R. P., & Schneider, J. P. (2008). Synthesis and primary characterization of self-assembled peptide-based hydrogels. In *Methods in molecular biology* (pp. 61–77).
177. Papavasiliou, G., Songprawat, P., Pérez-Luna, V., Hammes, E., Morris, M., Chiu, Y. C., & Brey, E. (2008). Three-dimensional patterning of poly(ethylene glycol) hydrogels through surface-initiated photopolymerization. *Tissue Engineering Part C: Methods, 14*, 129–140.
178. Hutmacher, D. W. (2000). Scaffold design and fabrication technologies for engineering tissues – State of the art and future perspectives. *Journal of Biomaterials Science. Polymer Edition, 12*, 107–124.
179. Kievit, F. M., Florczyk, S. J., Leung, M. C., Veiseh, O., Park, J. O., Disis, M. L., & Zhang, M. (2010). Biomaterials chitosan e alginate 3D scaffolds as a mimic of the glioma tumor microenvironment. *Biomaterials, 31*, 5903–5910.
180. Li, E., Fong, S., Lamhamedi-cherradi, S., Burdett, E., Ramamoorthy, V., Menegaz, B. A., Amin, H. M., Mikos, A. G., & Ludwig, J. A. (2013). Modeling Ewing sarcoma tumors in vitro with 3D scaffolds. *PNAS, 110*.
181. Fischbach, C., Chen, R., Matsumoto, T., Schmelzle, T., Brugge, J. S., Polverini, P. J., & Mooney, D. J. (2007). Engineering tumors with 3D scaffolds. *Nature Methods, 4*, 6–11.
182. Dhiman, H. K., Ray, A. R., & Panda, A. K. (2005). Three-dimensional chitosan scaffold-based MCF-7 cell culture for the determination of the cytotoxicity of tamoxifen. *Biomaterials, 26*, 979–986.

183. Belli, V., Guarnieri, D., Biondi, M., Della Sala, F., & Netti, P. A. (2016). Dynamics of nanoparticle diffusion and uptake in three-dimensional cell cultures. *Colloids Surfaces B Biointerfaces, 149*, 7–15.
184. Biondi, M., Guarnieri, D., Yu, H., Belli, V., & Netti, P. A. (2013). Sub-100 nm biodegradable nanoparticles: In vitro release features and toxicity testing in 2D and 3D cell cultures. *Nanotechnology, 24*.
185. Brancato, V., Gioiella, F., Profeta, M., Imparato, G., Guarnieri, D., Urciuolo, F., Melone, P., & Netti, P. A. (2017). 3D tumor microtissues as an in vitro testing platform for microenvironmentally-triggered drug delivery systems. *Acta Biomaterialia, 57*, 47–58.
186. Vaira, V., Fedele, G., Pyne, S., Fasoli, E., Zadra, G., Bailey, D., Snyder, E., Faversani, A., Coggi, G., Flavin, R., Bosari, S., & Loda, M. (2010). Preclinical model of organotypic culture for pharmacodynamic profiling of human tumors. *Proceedings of the National Academy of Sciences of the United States of America, 107*, 8352–8356.
187. Toda, S., Watanabe, K., Yokoi, F., Matsumura, S., Suzuki, K., Ootani, A., Aoki, S., Koike, N., & Sugihara, H. (2002). A new organotypic culture of thyroid tissue maintains three-dimensional follicles with C cells for a long term. *Biochemical and Biophysical Research Communications, 294*, 906–911.
188. Centenera, M. M., Gillis, J. L., Hanson, A. R., Jindal, S., Taylor, R. A., Risbridger, G. P., Sutherland, P. D., Scher, H. I., Raj, G. V., Knudsen, K. E., Yeadon, T., Tilley, W. D., & Butler, L. M. (2012). Evidence for efficacy of new hsp90 inhibitors revealed by ex vivo culture of human prostate tumors. *Clinical Cancer Research, 18*, 3562–3570.
189. Papini, S., Rosellini, A., De Matteis, A., Campani, D., Selli, C., Caporali, A., Bettuzzi, S., & Revoltella, R. P. (2007). Establishment of an organotypic in vitro culture system and its relevance to the characterization of human prostate epithelial cancer cells and their stromal interactions. *Pathology, Research and Practice, 203*, 209–216.
190. Holliday, D. L., Moss, M. A., Pollock, S., Lane, S., Shaaban, A. M., Millican-Slater, R., Nash, C., Hanby, A. M., & Speirs, V. (2013). The practicalities of using tissue slices as preclinical organotypic breast cancer models. *Journal of Clinical Pathology, 66*, 253–255.
191. Parrish, A. R., Sallam, K., Nyman, D. W., Orozco, J., Cress, A. E., Dalkin, B. L., Nagle, R. B., & Gandolfi, A. J. (2002). Culturing precision-cut human prostate slices as an in vitro model of prostate pathobiology. *Cell Biology and Toxicology, 18*, 205–219.
192. Naipal, K. A. T., Verkaik, N. S., Sánchez, H., van Deurzen, C. H. M., den Bakker, M. A., Hoeijmakers, J. H. J., Kanaar, R., Vreeswijk, M. P. G., Jager, A., & van Gent, D. C. (2016). Tumor slice culture system to assess drug response of primary breast cancer. *BMC Cancer, 16*, 1–13.
193. Gerlach, M. M., Merz, F., Wichmann, G., Kubick, C., Wittekind, C., Lordick, F., Dietz, A., & Bechmann, I. (2014). Slice cultures from head and neck squamous cell carcinoma: A novel test system for drug susceptibility and mechanisms of resistance. *British Journal of Cancer, 110*, 479–488.
194. Grosso, S. H. G., Katayama, M. L. H., Roela, R. A., Nonogaki, S., Soares, F. A., Brentani, H., Lima, L., Folgueira, M. A. A. K., Waitzberg, A. F. L., Pasini, F. S., Góes, J. C. G. S., & Brentani, M. M. (2013). Breast cancer tissue slices as a model for evaluation of response to rapamycin. *Cell and Tissue Research, 352*, 671–684.
195. Centenera, M. M., Raj, G. V., Knudsen, K. E., Tilley, W. D., & Butler, L. M. (2013). Ex vivo culture of human prostate tissue and drug development. *Nature Reviews. Urology, 10*, 483–487.
196. Dong, M., Philippi, C., Loretz, B., Nafee, N., Schaefer, U. F., Friedel, G., Ammon-Treiber, S., Griese, E. U., Lehr, C. M., Klotz, U., & Mürdter, T. E. (2011). Tissue slice model of human lung cancer to investigate telomerase inhibition by nanoparticle delivery of antisense 2′-O-methyl-RNA. *International Journal of Pharmaceutics, 419*, 33–42.
197. Whitesides, G. M. (2006). The origins and the future of microfluidics. *Nature, 442*, 368–373.
198. Bhatia, S. N., & Ingber, D. E. (2014). Microfluidic organs-on-chips. *Nature Biotechnology, 32*, 760–772.
199. Ahn, J., Sei, Y., Jeon, N., & Kim, Y. (2017). Tumor microenvironment on a chip: The progress and future perspective. *Bioengineering, 4*, 64.
200. Esch, E. W., Bahinski, A., & Huh, D. (2015). Organs-on-chips at the frontiers of drug discovery. *Nature Reviews. Drug Discovery, 14*, 248–260.
201. Xu, Z., Gao, Y., Hao, Y., Li, E., Wang, Y., Zhang, J., Wang, W., Gao, Z., & Wang, Q. (2013). Application of a microfluidic chip-based 3D co-culture to test drug sensitivity for individualized treatment of lung cancer. *Biomaterials, 34*, 4109–4117.
202. Albanese, A., Lam, A. K., Sykes, E. A., Rocheleau, J. V., & Chan, W. C. W. (2013). Tumour-on-a-chip provides an optical window into nanoparticle tissue transport. *Nature Communications, 4*, 1–8.
203. Chen, Y., Gao, D., Wang, Y., Lin, S., & Jiang, Y. (2018). A novel 3D breast-cancer-on-chip platform for therapeutic evaluation of drug delivery systems. *Analytica Chimica Acta*.
204. Yang, Y., Yang, X., Zou, J., Jia, C., Hu, Y., Du, H., & Wang, H. (2015). Evaluation of photodynamic therapy efficiency using an in vitro three-dimensional microfluidic breast cancer tissue model. *Lab on a Chip, 15*, 735–744.
205. Carvalho, M. R., Barata, D., Teixeira, L. M., Giselbrecht, S., Reis, R. L., Oliveira, J. M., Truckenmüller, R., & Habibovic, P. (2019). Colorectal tumor-on-a-chip system: A 3D tool for precision onco-nanomedicine. *Science Advances, 5*, eaaw1317.
206. Kwak, B., Ozcelikkale, A., Shin, C. S., Park, K., & Han, B. (2014). Simulation of complex transport of nanoparticles around a tumor using tumor-microenvironment-on-chip. *Journal of Controlled Release, 194*, 157–167.
207. Tang, Y., Soroush, F., Sheffield, J. B., Wang, B., Prabhakarpandian, B., & Kiani, M. F. (2017). A biomimetic microfluidic tumor microenvironment platform mimicking the EPR effect for rapid screening of drug delivery systems. *Scientific Reports, 7*, 1–14.
208. LaBarbera, D. V., Reid, B. G., & Yoo, B. H. (2012). The multicellular tumor spheroid model for high-throughput cancer drug discovery. *Expert Opinion on Drug Discovery, 7*, 819–830.
209. Kunz-Schughart, L. A., Freyer, J. P., Hofstaedter, F., & Ebner, R. (2004). The use of 3-D cultures for high-throughput screening: The multicellular spheroid model. *Journal of Biomolecular Screening, 9*, 273–285.
210. An, W. F., & Tolliday, N. J. (2009). Introduction: Cell-based assays for high-throughput screening. In *Cell-based assays high-throughput screen* (pp. 1–12).
211. Tung, Y. C., Hsiao, A. Y., Allen, S. G., Torisawa, Y. S., Ho, M., & Takayama, S. (2011). High-throughput 3D spheroid culture and drug testing using a 384 hanging drop array. *The Analyst, 136*, 473–478.
212. Friedrich, J., Seidel, C., Ebner, R., & Kunz-Schughart, L. A. (2009). Spheroid-based drug screen: Considerations and practical approach. *Nature Protocols, 4*, 309–324.
213. Cutrona, M. B., & Simpson, J. C. (2019). A high-throughput automated confocal microscopy platform for quantitative phenotyping of nanoparticle uptake and transport in spheroids. *Small, 15*, 1–14.
214. Ruggeri, B. A., Camp, F., & Miknyoczki, S. (2014). Animal models of disease: Pre-clinical animal models of cancer and their applications and utility in drug discovery. *Biochemical Pharmacology, 87*, 150–161.

215. Day, C. P., Merlino, G., & Van Dyke, T. (2015). Preclinical mouse cancer models: A maze of opportunities and challenges. *Cell, 163*, 39–53.
216. Ireson, C. R., Alavijeh, M. S., Palmer, A. M., Fowler, E. R., & Jones, H. J. (2019). The role of mouse tumour models in the discovery and development of anticancer drugs. *British Journal of Cancer*, 1–8.
217. Van Dyke, T., & Jacks, T. (2002). Cancer modeling in the modern era: Progress and challenges. *Cell, 108*, 135–144. https://ac.els-cdn.com/S0092867402006219/1-s2.0-S0092867402006219-main.pdf?_tid=40a45227-b919-44c1-a5fe-cee8af906cae&acdnat=1542170034_6b4705e823f3d5761026210fc414719a.
218. Rosenthal, N., & Brown, S. (2007). The mouse ascending: Perspectives for human-disease models. *Nature Cell Biology, 9*, 993–999.
219. Zuckerman, J. E., Gritli, I., Tolcher, A., Heidel, J. D., Lim, D., Morgan, R., Chmielowski, B., Ribas, A., Davis, M. E., & Yen, Y. (2014). Correlating animal and human phase Ia/Ib clinical data with CALAA-01, a targeted, polymer-based nanoparticle containing siRNA. *PNAS, 111*, 11449–11454.
220. Hrkach, J., Hrkach, J., Von Hoff, D., Ali, M. M., Andrianova, E., Auer, J., Campbell, T., De Witt, D., Figa, M., Figueiredo, M., Horhota, A., Low, S., Mcdonnell, K., Peeke, E., Retnarajan, B., Sabnis, A., Schnipper, E., Song, J. J., Song, Y. H., Summa, J., Tompsett, D., Troiano, G., Hoven, T. V. G., Wright, J., Lorusso, P., Kantoff, P. W., Bander, N. H., Sweeney, C., Farokhzad, O. C., Langer, R., & Zale, S. (2012). Preclinical development and clinical translation of a PSMA-targeted docetaxel nanoparticle with a differentiated pharmacological profile. *Science Translational Medicine, 4*.
221. Schultheis, B., Strumberg, D., Santel, A., Vank, C., Gebhardt, F., Keil, O., Lange, C., Giese, K., Kaufmann, J., Khan, M., & Drevs, J. (2014). First-in-human phase I study of the liposomal RNA interference therapeutic Atu027 in patients with advanced solid tumors. *Journal of Clinical Oncology*.
222. Cook, D., Brown, D., Alexander, R., March, R., & Morgan, P. (2014). Lessons learned from the fate of AstraZeneca's drug pipeline: a five-dimensional framework. *Nature Reviews Drug Discovery, 13*, 419–431.
223. Vail, D. M., Amantea, M. A., Colbern, G. T., Martin, F. J., Hilger, R. A., & Working, P. K. (2004). Pegylated liposomal doxorubicin: Proof of principle using preclinical animal models and pharmacokinetic studies. *Seminars in Oncology, 31*, 16–35.
224. Holen, I., Speirs, V., Morrissey, B., & Blyth, K. (2017). In vivo models in breast cancer research: Progress, challenges and future directions. *Disease Models & Mechanisms, 10*, 359–371.
225. Blyth, K., Carter, P., Morrissey, B., Chelala, C., Jones, L., Holen, I., & Speirs, V. (2016). SEARCHBreast: a new resource to locate and share surplus archival material from breast cancer animal models to help address the 3Rs. *Breast Cancer Research and Treatment, 153*.
226. Sharpless, N. E., & DePinho, R. A. (2006). The mighty mouse: Genetically engineered mouse models in cancer drug development. *Nature Reviews. Drug Discovery, 5*, 741–754.
227. Donehower, L. A., Harvey, M., Slagle, B. L., McArthur, M. J., Montgomery, C. A., Butel, J. S., & Bradley, A. (1992). Mice deficient for p53 are developmentally normal but susceptible to spontaneous tumours. *Nature, 356*, 215–221.
228. Jacks, T., Fazeli, A., Schmitt, E. M., Bronson, R. T., Goodell, M. A., & Weinberg, R. A. (1992). Effects of an Rb mutation in the mouse. *Nature, 359*, 710–713.
229. Groszer, M., Erickson, R., Scripture-Adams, D. D., Lesche, R., Trumpp, A., Zack, J. A., Kornblum, H. I., Liu, X., & Wu, H. (2001). Negative regulation of neural stem/progenitor cell proliferation by the Pten tumor suppressor gene in vivo. *Science (80-.), 294*, 2186–2189.
230. Corbett, T. H., Polin, L., Roberts, B. J., Lawson, A. J., Leopold, W. R., White, K., Kushner, J., Paluch, J., Hazeldine, S., Moore, R., Rake, J., Horwitz, J. P. (2002). Transplantable syngeneic rodent tumors. In B. A. Teicher (Ed.), *Tumor models in cancer research* (pp. 41–71). Humana Press Inc.
231. Rygaard, J., & Povlsen, C. O. (1969). Heterotransplantation of a human malignant tumour to «nude» mice. *Acta Pathologica Microbiologica Scandinavica, 77*, 758–760.
232. Kim, M. P., Evans, D. B., Wang, H., Abbruzzese, J. L., Fleming, J. B., & Gallick, G. E. (2009). Generation of orthotopic and heterotopic human pancreatic cancer xenografts in immunodeficient mice. *Nature Protocols, 4*, 1670–1680.
233. Dangles-Marie, V., Pocard, M., Richon, S., Weiswald, L. B., Assayag, F., Saulnier, P., Judde, J. G., Janneau, J. L., Auger, N., Validire, P., Dutrillaux, B., Praz, F., Bellet, D., & Poupon, M. F. (2007). Establishment of human colon cancer cell lines from fresh tumors versus xenografts: Comparison of success rate and cell line features. *Cancer Research, 67*, 398–407.
234. Derose, Y. S., Wang, G., Lin, Y. C., Bernard, P. S., Buys, S. S., Ebbert, M. T. W., Factor, R., Matsen, C., Milash, B. A., Nelson, E., Neumayer, L., Randall, R. L., Stijleman, I. J., Welm, B. E., & Welm, A. L. (2011). Tumor grafts derived from women with breast cancer authentically reflect tumor pathology, growth, metastasis and disease outcomes. *Nature Medicine, 17*, 1514–1520.
235. Girotti, M. R., Gremel, G., Lee, R., Galvani, E., Rothwell, D., Viros, A., Mandal, A. K., Haw, K., Lim, J., Saturno, G., Simon, J., Baenke, F., Pedersen, M., Rogan, J., Swan, J., & Smith, M. (2015). Application of sequencing, liquid biopsies and patient-derived xenografts for personalized medicine in melanoma. *Cancer Discovery, 44*.
236. Hodgkinson, C. L., Morrow, C. J., Li, Y., Metcalf, R. L., Rothwell, D. G., Trapani, F., Polanski, R., Burt, D. J., Simpson, K. L., Morris, K., Pepper, S. D., Nonaka, D., Greystoke, A., Kelly, P., Bola, B., Krebs, M. G., Antonello, J., Ayub, M., Faulkner, S., Priest, L., Carter, L., Tate, C., Miller, C. J., Blackhall, F., Brady, G., & Dive, C. (2014). Tumorigenicity and genetic profiling of circulating tumor cells in small-cell lung cancer. *Nature Medicine, 20*, 897–903.
237. Pearson, T., Greiner, D. L., & Shultz, L. D. (2008). Creation of "humanized" Mice to study human immunity. In *Current protocols in immunology* (pp. 1–21).
238. Eswaraka, J., & Giddabasappa, A. (2017). Humanized mice and PDX models. In *Patient derived tumor xenograft models: Promise, potential and practice* (pp. 75–89). Elsevier.
239. Rongvaux, A., Willinger, T., Martinek, J., Strowig, T., Gearty, S. V., Teichmann, L. L., Saito, Y., Marches, F., Halene, S., Palucka, A. K., Manz, M. G., & Flavell, R. A. (2014). Development and function of human innate immune cells in a humanized mouse model. *Nature Biotechnology, 32*, 364–372.
240. BOSMA, G. C., CUSTER, R. P., & BOSMA, M. J. (1983). A severe combined immunodeficiency mutation in the mouse. *Nature, 301*, 527–530.
241. Stylianopoulos, T., Martina, J. D., Chauhana, V. P., Jaina, S. R., Diop-Frimponga, B., Bardeesyf, N., Smithg, B. L., Ferroneh, C. R., Horniceki, F. J., Bouchera, Y., Munna, L. L., & Jaina, R. K. (2012). Causes, consequences, and remedies for growth-induced solid stress in murine and human tumors. *PNAS, 109*, 15101–15108. INAUGURAL.
242. Anselmo, A. C., & Mitragotri, S. (2016). Nanoparticles in the clinic. *Bioengineering & Translational Medicine, 1*, 10–29.
243. Park, K. (2013). Facing the truth about nanotechnology in drug delivery. *ACS Nano, 7*, 7442–7447.
244. Gonda, A., Zhao, N., Shah, J. V., Calvelli, H. R., Kantamneni, H., Francis, N. L., & Ganapathy, V. (2017). Engineering tumor-targeting nanoparticles as vehicles for precision nanomedicine. *Physiology & Behavior, 176*, 139–148.

245. Hamaguchi, T., Matsumura, Y., Suzuki, M., Shimizu, K., Goda, R., Nakamura, I., Nakatomi, I., Yokoyama, M., Kataoka, K., & Kakizoe, T. (2005). NK105, a paclitaxel-incorporating micellar nanoparticle formulation, can extend in vivo antitumour activity and reduce the neurotoxicity of paclitaxel. *British Journal of Cancer, 92*, 1240–1246.
246. Kato, K., Chin, K., Yoshikawa, T., Yamaguchi, K., Tsuji, Y., Esaki, T., Sakai, K., Kimura, M., Hamaguchi, T., Shimada, Y., Matsumura, Y., & Ikeda, R. (2012). Phase II study of NK105, a paclitaxel-incorporating micellar nanoparticle, for previously treated advanced or recurrent gastric cancer. *Investigational New Drugs, 30*, 1621–1627.
247. Fujiwara, Y., Mukai, H., Saeki, T., Ro, J., Lin, Y. C., Nagai, S. E., Lee, K. S., Watanabe, J., Ohtani, S., Kim, S. B., Kuroi, K., Tsugawa, K., Tokuda, Y., Iwata, H., Park, Y. H., Yang, Y., & Nambu, Y. (2019). A multi-national, randomised, open-label, parallel, phase III non-inferiority study comparing NK105 and paclitaxel in metastatic or recurrent breast cancer patients. *British Journal of Cancer, 120*, 475–480.
248. Gould, S. E., Junttila, M. R., & De Sauvage, F. J. (2015). Translational value of mouse models in oncology drug development. *Nature Medicine, 21*, 431–439.
249. Stirland, D. L., Nichols, J. W., Miura, S., & Bae, Y. H. (2013). Mind the gap: A survey of how cancer drug carriers are susceptible to the gap between research and practice. *Journal of Controlled Release, 172*, 1045–1064.
250. Pandita, A., Aldape, K. D., Zadeh, G., Guha, A., & James, C. D. (2004). Contrasting in vivo and in vitro fates of glioblastoma cell subpopulations with amplified EGFR. *Genes, Chromosomes and Cancer, 39*, 29–36.
251. De Witt Hamer, P. C., Van Tilborg, A. A. G., Eijk, P. P., Sminia, P., Troost, D., Van Noorden, C. J. F., Ylstra, B., & Leenstra, S. (2008). The genomic profile of human malignant glioma is altered early in primary cell culture and preserved in spheroids. *Oncogene, 27*, 2091–2096.
252. Hidalgo, M., Amant, F., Biankin, A. V., Budinska, E., Byrne, A. T., Caldas, C., Clarke, R. B., de Jong, S., Jonkers, J., Maelandsmo, G. M., Roman-Roman, S., Seoane, J., Trusolino, L., & Villanueva, A. (2014). Patient-derived xenograft models: An emerging platform for translational cancer research. *Cancer Discovery, 4*, 998–1013.
253. Clohessy, J. G., & Pandolfi, P. P. (2018). The mouse hospital and its integration in ultra-precision approaches to cancer care. *Frontiers in Oncology, 8*, 1–6.
254. Brinster, R. L., Chen, H. Y., Messing, A., van Dyke, T., Levine, A. J., & Palmiter, R. D. (1984). Transgenic mice harboring SV40 t-antigen genes develop characteristic brain tumors. *Cell, 37*, 367–379.
255. Stewart, T. A., Pattengale, P. K., & Leder, P. (1984). Spontaneous mammary adenocarcinomas in transgenic mice that carry and express MTV/myc fusion genes. *Cell, 38*, 627–637.
256. Guy, C. T., Cardiff, R. D., & Muller, W. J. (1992). Induction of mammary tumors by expression of polyomavirus middle T oncogene: A transgenic mouse model for metastatic disease. *Molecular and Cellular Biology, 12*, 954–961.
257. Ideno, N., Yamaguchi, H., Okumura, T., Huang, J., Brun, M. J., Ho, M. L., Suh, J., Gupta, S., Maitra, A., & Ghosh, B. (2019). A pipeline for rapidly generating genetically engineered mouse models of pancreatic cancer using in vivo CRISPR-Cas9-mediated somatic recombination. *Laboratory Investigation, 99*, 1233–1244.
258. Oldrini, B., Curiel-García, Á., Marques, C., Matia, V., Uluçkan, Ö., Graña-Castro, O., Torres-Ruiz, R., Rodriguez-Perales, S., Huse, J. T., & Squatrito, M. (2018). Somatic genome editing with the RCAS-TVA-CRISPR-Cas9 system for precision tumor modeling. *Nature Communications, 9*.
259. Singh, M., Lima, A., Molina, R., Hamilton, P., Clermont, A. C., Devasthali, V., Thompson, J. D., Cheng, J. H., Bou Reslan, H., Ho, C. C. K., Cao, T. C., Lee, C. V., Nannini, M. A., Fuh, G., Carano, R. A. D., Koeppen, H., Yu, R. X., Forrest, W. F., Plowman, G. D., & Johnson, L. (2010). Assessing therapeutic responses in Kras mutant cancers using genetically engineered mouse models. *Nature Biotechnology, 28*, 585–593.
260. Omer, C. A., Chen, Z., Diehl, R. E., Conner, M. W., Chen, H. Y., Trumbauer, M. E., Gopal-Truter, S., Seeburger, G., Bhimnathwala, H., Abrams, M. T., Davide, J. P., Ellis, M. S., Gibbs, J. B., Greenberg, I., Hamilton, K., Koblan, K. S., Kral, A. M., Liu, D., Lobell, R. B., Miller, P. J., Mosser, S. D., Neill, T. J. O., Rands, E., Schaber, M. D., Senderak, E. T., Oliff, A., & Kohl, N. E. (2000). Mouse mammary tumor virus-Ki- ras B transgenic mice develop mammary carcinomas that can be growth-inhibited by a farnesyl: Protein transferase inhibitor. *Cancer Research, 60*, 2680–2688.
261. Frese, K. K., Neesse, A., Cook, N., Bapiro, T. E., Lolkema, M. P., Jodrell, D. I., & Tuveson, D. A. (2012). Nab-paclitaxel potentiates gemcitabine activity by reducing cytidine deaminase levels in a mouse model of pancreatic cancer. *Cancer Discovery, 2*, 260–269.
262. Hingorani, S. R., Wang, L., Multani, A. S., Combs, C., Deramaudt, T. B., Hruban, R. H., Rustgi, A. K., Chang, S., & Tuveson, D. A. (2005). Trp53R172H and KrasG12D cooperate to promote chromosomal instability and widely metastatic pancreatic ductal adenocarcinoma in mice. *Cancer Cell, 7*, 469–483.
263. Von Hoff, D. D., Ramanathan, R. K., Borad, M. J., Laheru, D. A., Smith, L. S., Wood, T. E., Korn, R. L., Desai, N., Trieu, V., Iglesias, J. L., Zhang, H., Soon-Shiong, P., Shi, T., Rajeshkumar, N. V., Maitra, A., & Hidalgo, M. (2011). Gemcitabine plus nab-paclitaxel is an active regimen in patients with advanced pancreatic cancer: A phase I/II trial. *Journal of Clinical Oncology, 29*, 4548–4554.
264. Egeblad, M., Nakasone, E. S., & Werb, Z. (2010). Tumors as organs: Complex tissues that interface with the entire organism. *Developmental Cell, 18*, 884–901.
265. Tanaka, H. Y., & Kano, M. R. (2018). Stromal barriers to nanomedicine penetration in the pancreatic tumor microenvironment. *Cancer Science, 109*, 2085–2092.
266. Westphalen, C. B., & Olive, K. P. (2012). Genetically engineered mouse models of pancreatic cancer. *The Cancer Journal, 18*.
267. Walrath, J. C., Hawes, J. J., Van Dyke, T., & Reilly, K. M. (2010). *Genetically engineered mouse models in cancer research* (1st ed.). Elsevier INC.
268. Artandi, S. E., Chang, S., Lee, S.-L., Alson, S., Gottlieb, G. J., Chin, L., & DePinho, R. A. (2000). Telomere dysfunction promotes non-reciprocal translocations. *Nature, 406*, 641–645.
269. Jong, M., & Maina, T. (2010). Of mice and humans: Are they the same? – Implications in cancer translational research. *Journal of Nuclear Medicine, 51*, 501–504.
270. Calles, A., Rubio-Viqueira, B., & Hidalgo, M. (2013). Primary human non-small cell lung unit and pancreatic tumorgraft models-utility and applications in drug discovery and tumor biology. *Current Protocols in Pharmacology*, 1–21.
271. Fiebig, H. H., Neumann, H. A., Hens, H., Koch, H., Kaiser, D., & Arnold, H. (1985). Development of three human small cell lung cancer models in nude mice. *Recent Results in Cancer Research, 97*, 77–86.
272. Uronis, J. M., Osada, T., McCall, S., Yang, X. Y., Mantyh, C., Morse, M. A., Lyerly, H. K., Clary, B. M., & Hsu, D. S. (2012). Histological and molecular evaluation of patient-derived colorectal cancer explants. *PLoS One, 7*.
273. Folaron, M., Merzianu, M., Duvvuri, U., Ferris, R. L., & Seshadri, M. (2019). Profiling the stromal and vascular heterogeneity in patient-derived xenograft models of head and neck cancer: Impact on therapeutic response. *Cancers (Basel), 11*.

274. Gray, D. R., Huss, W. J., Yau, J. M., Durham, L. E., Werdin, E. S., Funkhouser, W. K., & Smith, G. J. (2004). Short-term human prostate primary xenografts: An in vivo model of human prostate cancer vasculature and angiogenesis. *Cancer Research, 64*, 1712–1721.
275. Bieche, I., Vacher, S., Vallerand, D., Richon, S., Hatem, R., De Plater, L., Dahmani, A., Némati, F., Angevin, E., Marangoni, E., Roman-Roman, S., Decaudin, D., & Dangles-Marie, V. (2014). Vasculature analysis of patient derived tumor xenografts using species-specific PCR assays: Evidence of tumor endothelial cells and atypical VEGFA-VEGFR1/2 signalings. *BMC Cancer, 14*, 1–13.
276. Taurin, S., Nehoff, H., & Greish, K. (2012). Anticancer nanomedicine and tumor vascular permeability; where is the missing link? *Journal of Controlled Release, 164*, 265–275.
277. Delgado San Martin, J. A., Hare, J. I., Yates, J. W. T., & Barry, S.T. (2015). Tumour stromal morphology impacts nanomedicine cytotoxicity in patient-derived xenografts. *Nanomedicine Nanotechnology Biology and Medicine*, *11*, 1247–1252.
278. Kalra, A. V., Kim, J., Klinz, S. G., Paz, N., Cain, J., Drummond, D. C., Nielsen, U. B., & Fitzgerald, J. B. (2014). Preclinical activity of nanoliposomal irinotecan is governed by tumor deposition and intratumor prodrug conversion. *Cancer Research, 74*, 7003–7013.
279. Ioannidis, J. P. A., Kim, B. Y. S., & Trounson, A. (2018). How to design preclinical studies in nanomedicine and cell therapy to maximize the prospects of clinical translation. *Nature Biomedical Engineering, 2*, 797–809.
280. Hare, J. I., Lammers, T., Ashford, M. B., Puri, S., Storm, G., & Barry, S. T. (2017). Challenges and strategies in anti-cancer nanomedicine development: An industry perspective. *Advanced Drug Delivery Reviews, 108*, 25–38.
281. Sia, D., Moeini, A., Labgaa, I., & Villanueva, A. (2015). The future of patient-derived tumor xenografts in cancer treatment. *Pharmacogenomics, 16*, 1671–1683.
282. Malaney, P., Nicosia, S. V., & Davé, V. (2014). One mouse, one patient paradigm: New avatars of personalized cancer therapy. *Cancer Letters, 344*, 1–12.
283. Xu, C., Li, X., Liu, P., Li, M., & Luo, F. (2019). Patient-derived xenograft mouse models: A high fidelity tool for individualized medicine (review). *Oncology Letters, 17*, 3–10.
284. Pauli, C., Hopkins, B. D., Prandi, D., Shaw, R., Fedrizzi, T., Sboner, A., Sailer, V., Augello, M., Puca, L., Rosati, R., McNary, T. J., Churakova, Y., Cheung, C., Triscott, J., Pisapia, D., Rao, R., Mosquera, J. M., Robinson, B., Faltas, B. M., Emerling, B. E., Gadi, V. K., Bernard, B., Elemento, O., Beltran, H., Demichelis, F., Kemp, C. J., Grandori, C., Cantley, L. C., & Rubin, M. A. (2017). Personalized in vitro and in vivo cancer models to guide precision medicine. *Cancer Discovery, 7*, 462–477.
285. Chen, Z., Cheng, K., Walton, Z., Wang, Y., Ebi, H., Shimamura, T., Liu, Y., Tupper, T., Ouyang, J., Li, J., Gao, P., Woo, M. S., Xu, C., Yanagita, M., Altabef, A., Wang, S., Lee, C., Nakada, Y., Peña, C. G., Sun, Y., Franchetti, Y., Yao, C., Saur, A., Cameron, M. D., Nishino, M., Hayes, D. N., Wilkerson, M. D., Roberts, P. J., Lee, C. B., Bardeesy, N., Butaney, M., Chirieac, L. R., Costa, D. B., Jackman, D., Sharpless, N. E., Castrillon, D. H., Demetri, G. D., Jänne, P. A., Pandolfi, P. P., Cantley, L. C., Kung, A. L., Engelman, J. A., & Wong, K. K. (2012). A murine lung cancer co-clinical trial identifies genetic modifiers of therapeutic response. *Nature, 483*, 613–617.
286. Duell, E. J., Lujan-Barroso, L., Sala, N., McElyea, S. D., Overvad, K., Tjonneland, A., Olsen, A., Weiderpass, E., Busund, L. T., Moi, L., Muller, D., Vineis, P., Aune, D., Matullo, G., Naccarati, A., Panico, S., Tagliabue, G., Tumino, R., Palli, D., Kaaks, R., Katzke, V. A., Boeing, H., Bueno-de-Mesquita, H. B., Peeters, P. H., Trichopoulou, A., Lagiou, P., Kotanidou, A., Travis, R. C., Wareham, N., Khaw, K. T., Quiros, J. R., Rodríguez-Barranco, M., Dorronsoro, M., Chirlaque, M. D., Ardanaz, E., Severi, G., Boutron-Ruault, M. C., Rebours, V., Brennan, P., Gunter, M., Scelo, G., Cote, G., Sherman, S., & Korc, M. (2017). Plasma microRNAs as biomarkers of pancreatic cancer risk in a prospective cohort study. *International Journal of Cancer, 141*, 905–915.
287. Frampton, A. E., Krell, J., Jamieson, N. B., Gall, T. M. H., Giovannetti, E., Funel, N., Prado, M. M., Krell, D., Habib, N. A., Castellano, L., Jiao, L. R., & Stebbing, J. (2015). MicroRNAs with prognostic significance in pancreatic ductal adenocarcinoma: A meta-analysis. *European Journal of Cancer, 51*, 1389–1404.
288. Gilles, M. E., Hao, L., Huang, L., Rupaimoole, R., Lopez-Casas, P. P., Pulver, E., Jeong, J. C., Muthuswamy, S. K., Hidalgo, M., Bhatia, S. N., & Slack, F. J. (2018). Personalized RNA medicine for pancreatic cancer. *Clinical Cancer Research, 24*, 1734–1747.
289. Bertotti, A., Migliardi, G., Galimi, F., Sassi, F., Torti, D., Isella, C., Corà, D., di Nicolantonio, F., Buscarino, M., Petti, C., Ribero, D., Russolillo, N., Muratore, A., Massucco, P., Pisacane, A., Molinaro, L., Valtorta, E., Sartore-Bianchi, A., Risio, M., Capussotti, L., Gambacorta, M., Siena, S., Medico, E., Sapino, A., Marsoni, S., Comoglio, P. M., Bardelli, A., & Trusolino, L. (2011). A molecularly annotated platform of patient- derived xenografts ("xenopatients") identifies HER2 as an effective therapeutic target in cetuximab-resistant colorectal cancer. *Cancer Discovery, 1*, 508–523.
290. Julien, S., Merino-Trigo, A., Lacroix, L., Pocard, M., Goeŕé, D., Mariani, P., Landron, S., Bigot, L., Nemati, F., Dartigues, P., Weiswald, L. B., Lantuas, D., Morgand, L., Pham, E., Gonin, P., Dangles-Marie, V., Job, B., Dessen, P., Bruno, A., Pierré, A., De Thé, H., Soliman, H., Nunes, M., Lardier, G., Calvet, L., Demers, B., Prévost, G., Vrignaud, P., Roman-Roman, S., Duchamp, O., & Berthet, C. (2012). Characterization of a large panel of patient-derived tumor xenografts representing the clinical heterogeneity of human colorectal cancer. *Clinical Cancer Research, 18*, 5314–5328.
291. Zhang, X., Claerhout, S., Prat, A., Dobrolecki, L. E., Petrovic, I., Lai, Q., Landis, M. D., Wiechmann, L., Schiff, R., Giuliano, M., Wong, H., Fuqua, S. W., Contreras, A., Gutierrez, C., Huang, J., Mao, S., Pavlick, A. C., Froehlich, A. M., Wu, M. F., Tsimelzon, A., Hilsenbeck, S. G., Chen, E. S., Zuloaga, P., Shaw, C. A., Rimawi, M. F., Perou, C. M., Mills, G. B., Chang, J. C., & Lewis, M. T. (2013). A renewable tissue resource of phenotypically stable, biologically and ethnically diverse, patient-derived human breast cancer xenograft models. *Cancer Research, 73*, 4885–4897.
292. Krebs, M. G., Sloane, R., Priest, L., Lancashire, L., Hou, J. M., Greystoke, A., Ward, T. H., Ferraldeschi, R., Hughes, A., Clack, G., Ranson, M., Dive, C., & Blackhall, F. H. (2011). Evaluation and prognostic significance of circulating tumor cells in patients with non-small-cell lung cancer. *Journal of Clinical Oncology, 29*, 1556–1563.
293. Tanaka, F., Yoneda, K., & Hasegawa, S. (2010). Circulating tumor cells (CTCs) in lung cancer: Current status and future perspectives. *Lung Cancer: Targets and Therapy, 1*, 77–84.
294. Lai, Y., Wei, X., Lin, S., Qin, L., Cheng, L., & Li, P. (2017). Current status and perspectives of patient-derived xenograft models in cancer research. *Journal of Hematology & Oncology, 10*, 1–14.
295. Wang, Y., Cui, J., & Wang, L. (2019). Patient-derived xenografts: A valuable platform for clinical and preclinical research in pancreatic cancer. *The Chinese Clinical Oncology, 8*.
296. Byrne, A. T., Alférez, D. G., Amant, F., Annibali, D., Arribas, J., Biankin, A. V., Bruna, A., Budinská, E., Caldas, C., Chang, D. K., Clarke, R. B., Clevers, H., Coukos, G., Dangles-Marie, V., Gail Eckhardt, S., Gonzalez-Suarez, E., Hermans, E., Hidalgo, M., Jarzabek, M. A., De Jong, S., Jonkers, J., Kemper, K., Lanfrancone, L., Mælandsmo, G. M., Marangoni, E., Marine, J. C., Medico, E.,

Norum, J. H., Palmer, H. G., Peeper, D. S., Pelicci, P. G., Piris-Gimenez, A., Roman-Roman, S., Rueda, O. M., Seoane, J., Serra, V., Soucek, L., Vanhecke, D., Villanueva, A., Vinolo, E., Bertotti, A., & Trusolino, L. (2017). Interrogating open issues in cancer precision medicine with patient-derived xenografts. *Nature Reviews Cancer, 17*, 254–268.

297. Evrard, Y. A., Srivastava, A., Randjelovic, J., Arunachalam, S., Bult, C. J., Chen, L., Davies, M., Davies, S., Davis-Dusenbery, B., Digiovanna, J., Doroshow, J. H., Fang, B., Frech, C., Govindan, R., Ha, M. J., Herlyn, M., Jeon, R., Kossenkov, A., Lewis, M. T., Li, S., Meric-Bernstam, F., Miletic, N., Moscow, J. A., Neuhauser, S., Patidar, R., Rebecca, V., Robinson, P. N., Rosains, J., Roth, J., Stankovic, T., Stanojevic, A., Van Tine, B. A., Welm, A. L., Welm, B. E., Wickramasinghe, J., Woo, X., Xiao, M., Zhao, Z., Dean, D. A., Morris, J. S., Chuang, J. H., City, S. L., & Harbor, B. (2019). Investigational Drug Branch, National Cancer Institute, Bethesda, MD. Contact information.
298. Gao, H., Korn, J. M., Ferretti, S., Monahan, J. E., Wang, Y., Singh, M., Zhang, C., Schnell, C., Yang, G., Zhang, Y., Balbin, O. A., Barbe, S., Cai, H., Casey, F., Chatterjee, S., Chiang, D. Y., Chuai, S., Cogan, S. M., Collins, S. D., Dammassa, E., Ebel, N., Embry, M., Green, J., Kauffmann, A., Kowal, C., Leary, R. J., Lehar, J., Liang, Y., Loo, A., Lorenzana, E., Iii, E. R. M., Mclaughlin, M. E., Merkin, J., Meyer, R., Naylor, T. L., Patawaran, M., Reddy, A., Röelli, C., Ruddy, D. A., Salangsang, F., Santacroce, F., Singh, A. P., Tang, Y., Tinetto, W., Tobler, S., Velazquez, R., Venkatesan, K., Von Arx, F., Wang, H. Q., Wang, Z., Wiesmann, M., Wyss, D., Xu, F., Bitter, H., Atadja, P., Lees, E., Hofmann, F., Li, E., Keen, N., Cozens, R., Jensen, M. R., Pryer, N. K., Williams, J. A., & Sellers, W. R. (2015). High-throughput screening using patient-derived tumor xenografts to predict clinical trial drug response. *Nature Medicine, 21*, 1318–1325.
299. Moghimi, S. M., Hunter, A. C., & Andresen, T. L. (2012). Factors controlling nanoparticle pharmacokinetics: An integrated analysis and perspective. *Annual Review of Pharmacology and Toxicology, 52*, 481–503.
300. Moghimi, S. M., & Farhangrazi, Z. S. (2014). Just so stories: The random acts of anti-cancer nanomedicine performance, nanomedicine nanotechnology. *Biologie et Médecine, 10*, 1661–1666.
301. Zitvogel, L., Pitt, J. M., Daillère, R., Smyth, M. J., & Kroemer, G. (2016). Mouse models in oncoimmunology. *Nature Reviews. Cancer, 16*, 759–773.
302. Meraz, I. M., Majidi, M., Meng, F., Shao, R., Ha, M. J., Neri, S., Fang, B., Lin, S. H., Tinkey, P. T., Shpall, E. J., Morris, J., & Roth, J. A. (2019). An improved patient-derived xenograft humanized mouse model for evaluation of lung cancer immune responses.*Cancer Immunology Research, 7,* 1267–1279.
303. Morton, J. J., Bird, G., Refaeli, Y., & Jimeno, A. (2016). Humanized mouse xenograft models: Narrowing the tumor-microenvironment gap. *Cancer Research, 76,* 6153–6158.
304. Morton, J. J., Bird, G., Keysar, S. B., Astling, D. P., Lyons, T. R., Anderson, R. T., Glogowska, M. J., Estes, P., Eagles, J. R., Le, P. N., & Gan, G. (2016). XactMice: humanizing mouse bone marrow enables microenvironment reconstitution in a patient-derived xenograft model of head and neck cancer, *Oncogene, 35,* 290–300.
305. Li, Y., Ayala-Orozco, C., Rauta, P. R., & Krishnan, S. (2019). The application of nanotechnology in enhancing immunotherapy for cancer treatment: Current effects and perspective. *Nanoscale, 11*, 17157–17178.
306. Bae, Y. H., & Park, K. (2011). Targeted drug delivery to tumors: Myths, reality and possibility. *Journal of Controlled Release, 153*, 198–205.
307. Nichols, J. W., & Bae, Y. H. (2012). Odyssey of a cancer nanoparticle: From injection site to site of action. *Nano Today, 7*, 606–618.
308. Björnmalm, M., Thurecht, K. J., Michael, M., Scott, A. M., & Caruso, F. (2017). Bridging bio-nano science and cancer nanomedicine. *ACS Nano, 11*, 9594–9613.
309. Olson, B., Li, Y., Lin, Y., Liu, E. T., & Patnaik, A. (2018). Mouse models for cancer immunotherapy research. *Cancer Discovery, 8*, 1358–1365.
310. Uhl, E. W., & Warner, N. J. (2015). Mouse models as predictors of human responses: Evolutionary medicine. *Current Pathobiology Reports, 3*, 219–223.
311. Tentler, J. J., Tan, A. C., Weekes, C. D., Jimeno, A., Leong, S., Pitts, T. M., Arcaroli, J. J., Messersmith, W. A., & Eckhardt, S. G. (2012). Patient-derived tumour xenografts as models for oncology drug development. *Nature Reviews. Clinical Oncology, 9*, 338–350.
312. Landgraf, M., McGovern, J. A., Friedl, P., & Hutmacher, D. W. (2018). Rational design of mouse models for cancer research. *Trends in Biotechnology, 36*, 242–251.
313. Zahedi-Tabar, Z., Bagheri-Khoulenjani, S., Mirzadeh, H., & Amanpour, S. (2019). 3D in vitro cancerous tumor models: Using 3D printers. *Medical Hypotheses, 124*, 91–94.
314. Choi, Y., Lee, S., Kim, K., Kim, S., Chung, Y., & Lee, C. (2018). Studying cancer immunotherapy using patient-derived xenografts (PDXs) in humanized mice. *Experimental & Molecular Medicine*.

Part IV

It Is All a Matter of Immunity

Nanotechnology for the Development of Nanovaccines in Cancer Immunotherapy

Maria Aurora Grimaudo

Abstract

Up until now, surgery, radiation, and chemotherapy remain the conventional methods used in cancer treatment. However, these treatments are widely associated with severe side effects due to toxicity on normal cells. Consequently, there is an urgent need for novel therapeutic approaches that are able to effectively and selectively target tumor cells without any adverse effects on normal cells. Among the new approaches, cancer immunotherapy seems promising in the fight against tumors thanks to its prolonged efficacy and lower toxicity compared to the traditional treatments.

Research studies suggested that both adjuvants and antigens are essential to induce optimal anti-tumor immunity. Among the different delivery strategies, nanotechnology offers several advantages for the design of cancer vaccines. Indeed, nanocarriers can protect the encapsulated antigens and/or adjuvant from enzymatic degradation, sustain and control the release for the entrapped cargo, and enhance the immune responses.

Several studies reported that different physical characteristics of nanoparticles affect their uptake in cells and the potential to induce cellular responses. Among them, particle size and surface chemistry resulted the most influent.

Clinical trials and recent research papers on the use of nanotechnology in cancer immunotherapy support the idea that this strategy could be successful as weapon against cancer in the near future.

Keywords

Nanovaccines · Cancer immunotherapy · Immune checkpoint inhibitors · Nanotechnology · Liposomes · Polymeric nanoparticles · Micelles · Gold nanoparticles · Inorganic nanoparticles · Hydrogel nanoparticles · Cell membrane coated nanoparticles

1 Cancer Immunotherapy

Despite all the advances in research and in therapy, cancer is still one of the major causes of death worldwide [1], with lung, breast, colorectal, and prostate cancers as globally dominant types (Fig. 1).

Conventional methods for cancer treatment involving surgery, radiation, and chemotherapy are widely associated to severe side effects due to toxicity on normal cells. As a consequence, there is an urgent need for novel therapeutic approaches that are able to effectively and selectively target tumor cells without any adverse effects on other cells [2]. Among them, cancer immunotherapy represents a recent approach in the fight against tumors due to its prolonged efficacy and lower toxicity compared to the traditional antitumor treatments [3, 4].

Despite the existence of natural defense mechanisms against cancer growth (immune-surveillance), the tumor microenvironment often secrets immune suppressive factors such as cytokines, chemokines, and other metabolites for disrupting or escaping from these mechanisms. Additionally, the clonogenic pressure induced from the immune system can alter the antigenic composition of the tumor, promoting the survival of the fittest and least immunogenic tumor cells, a process known as “tumor immunoediting” [5]. In the worst-case scenario, mutations in tumor cells render them insensitive to the immune systems, and the outgrowth of these cells renders the tumors more aggressive and lethal [6, 7].

M. A. Grimaudo (✉)
Nano-Oncology Unit, Translational Medical Oncology Group, Health Research Institute of Santiago de Compostela (IDIS), Santiago de Compostela, Spain
e-mail: Maria.Aurora.Grimaudo@sergas.es

© Springer Nature Switzerland AG 2021

F. Fontana, H. A. Santos (eds.), *Bio-Nanomedicine for Cancer Therapy*, Advances in Experimental Medicine and Biology 1295, https://doi.org/10.1007/978-3-030-58174-9_13

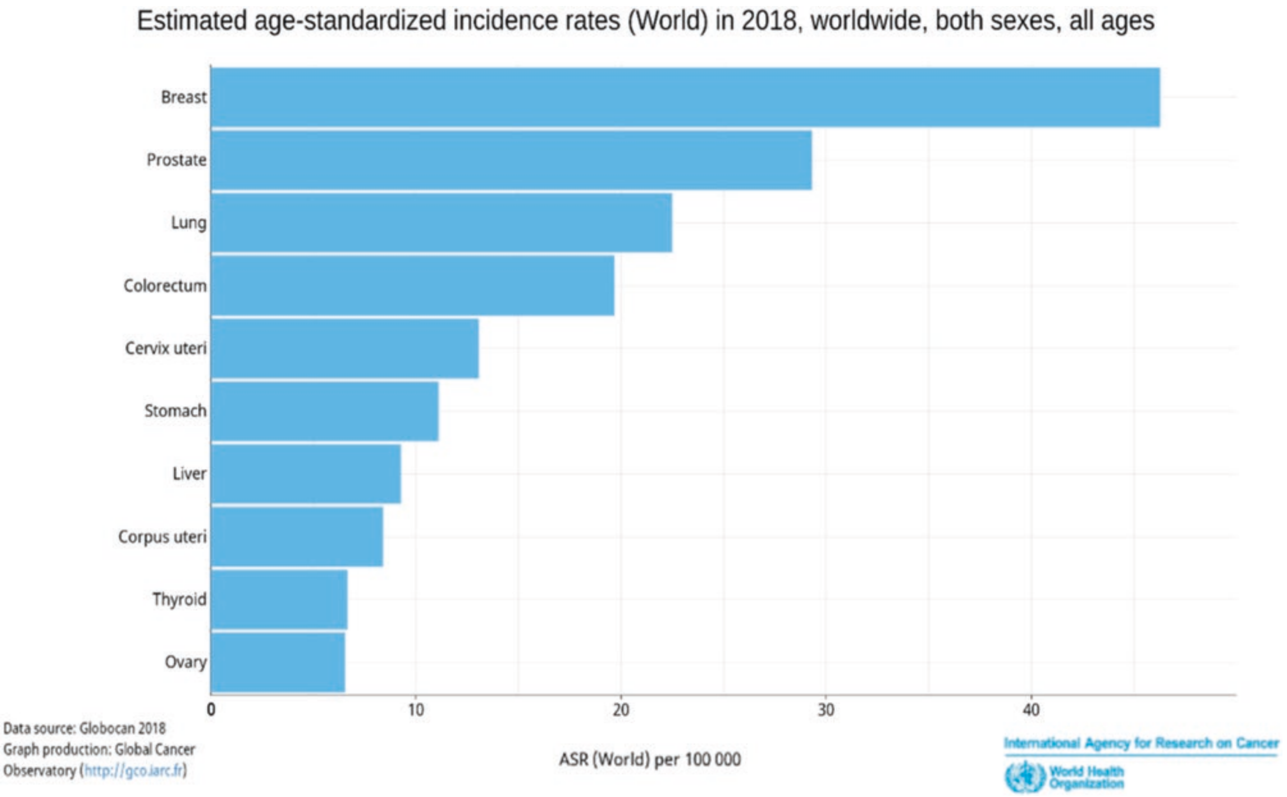

Fig. 1 World incidence rates in 2018 obtained from the International Agency for Research on Cancer–Global Cancer Observatory (https://gco.iarc.fr/)

Generally, immunization is defined as the external stimulation of an immune response against disease causing agents [8]. Particularly, cancer vaccines manipulate the patients' own immune system to recognize and destroy cancer cells. Indeed, the wider goal of immunotherapy is to allow immune system cells to recognize tumor antigens more effectively [9]. Specifically, cancer vaccines elicit potent tumor-specific T lymphocytes (CTLs) capable of decreasing the tumor mass and induce long-term tumor-specific memory response, thus protecting against tumor recurrence [10]. Summarizing, cancer vaccines could potentially stimulate specific antitumor immune responses, induce specific killing of tumor cells with minimal damage to healthy cells, and elicit immune memory for long-term protection against tumors [11].

One of the strategies used in immunotherapy is the delivery of immune adjuvants. Indeed, these molecules can be used for immunostimulatory cancer vaccines as they stimulate the immune system, potentiate the immune responses against antigens, and guide the type of immune response [12]. Conversely to traditional cytotoxic agents, a lower concentration of immunomodulators is required for a robust and durable anticancer immune response, highly decreasing side effects [13]. Based on their principal mechanisms of action, adjuvants can be generally divided into two classes [14, 15]: (a) vaccine delivery systems, such as mineral salts, emulsions, liposomes, and virosomes and (b) immunostimulatory molecular adjuvants, including toll-like receptor (TLR) agonists, STING agonists, costimulatory ligands, and cytokines.

Another attractive strategy for enhancing the anticancer immune response is vaccination with tumor-specific antigens. Indeed, cancer cells express numerous mutations and mutant protein sequences that can be processed into short peptides by antigen presenting cells (APCs). These proteins are then presented on the APC-cell surface by major histocompatibility complex (MHC) molecules and can be recognized by T cells as foreign antigens [16]. However, due to immunosuppression and immune evasion, endogenous cancer antigens, produced by the cancer cells themselves, are unable to elicit significant immune responses. By introducing exogeneous tumor-relevant antigens, cancer vaccines can potentiate antigen-specific anticancer immune response [17].

Summarizing, both adjuvants and antigens are essential to induce optimal anti-tumor immunity. Additionally, the administration of adjuvant together with subunit antigen may dramatically potentiate the immunogenicity [18].

As previously discussed, tumors exhibit several mechanisms for escaping from immune systems surveillance. One of these mechanisms involves the overactivation of immune

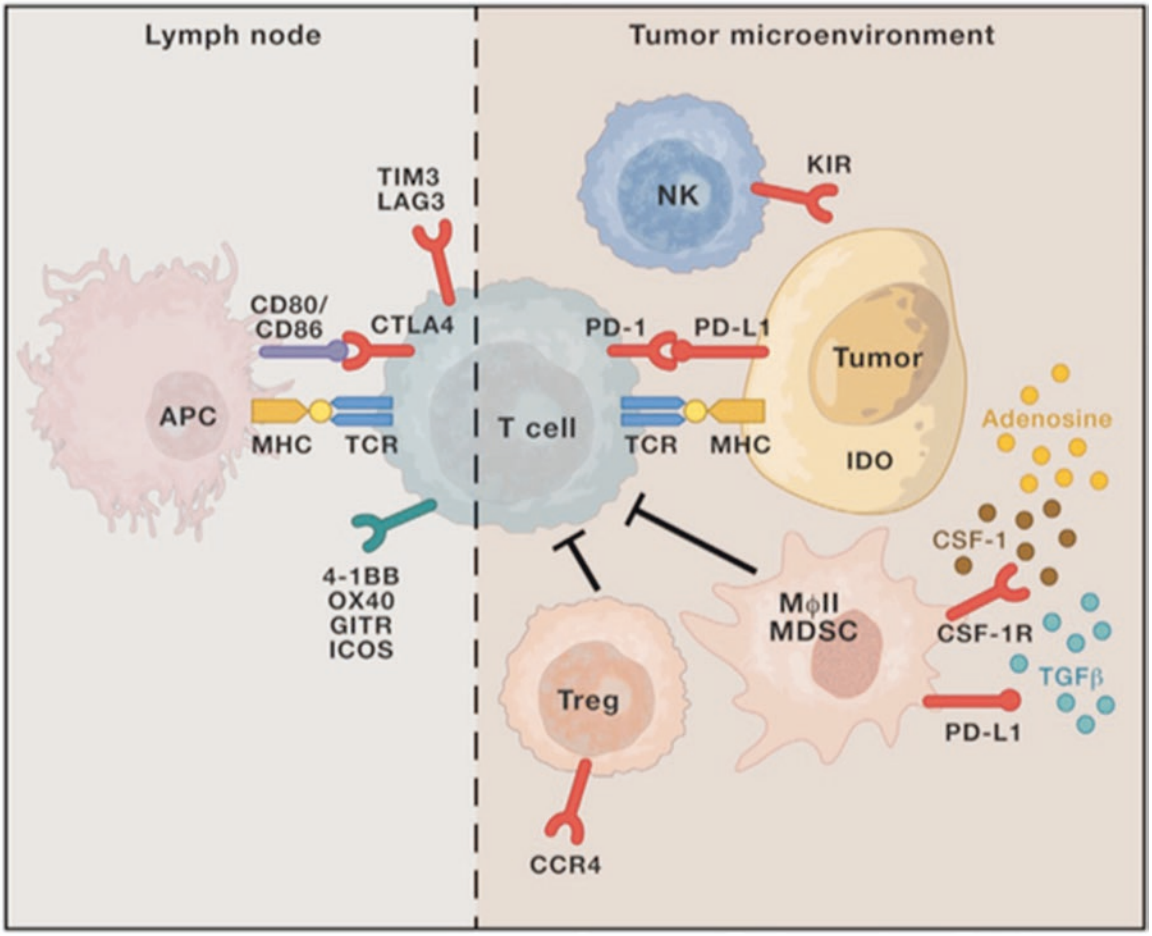

Fig. 2 Mechanisms of immune checkpoint blockade, including CTLA-4, PD-1/PD-L1 axis, IDO, and other immune checkpoints. (Reprinted with permission from [19])

checkpoints pathways. Indeed, these key regulators of the immune system crucial for maintaining immune homeostasis and preventing autoimmunity (Fig. 2) result overactivated in different types of cancer. By this way, effector T cells differentiate into exhausted T cells at late stage of diseases. The inhibitory receptors resulted overexpressed on exhausted T cells and the effector cytokines secretion decreased [3].

For these reasons, different immune checkpoint inhibitors, including cytotoxic T lymphocyte antigen-4 (CTLA-4), programmed cell death protein 1 (PD-L1) axis, indoleamine 2,3-dioxygenase (IDO), cluster of differentiation 47 (CD47), cluster of differentiation 40 (CD40), 4-1BB (CD137), have already received FDA approval or are currently in clinical trials phase (Table 1) [3]. Even though the results of immune checkpoint blockers are promising in cancer immunotherapy, further development is still needed to obtain better therapeutic efficacy and minimize side effects [3].

The tumor microenvironment (TME) also plays an important role in interacting with the host's immune system and modifying the immune response itself. Indeed, the TME is an inflammatory and immunosuppressive environment, where the immune cells recruitment is mediated by secreted chemokines, and their cytotoxic functions are generally suppressed by immunoregulatory cells. As a matter of fact, some immunosuppressive cells, such as tumor-associated macrophages, release immunosuppressive factors which inhibit the

Table 1 FDA-approved immune checkpoint inhibitors

Inhibitor	Target	Clinical trials
Atezolizumab	PD-L1	Colorectal cancer, melanoma, breast cancer, renal cell carcinoma, bladder cancer, non-small cell lung cancer
Avelumab	PD-L1	Bladder cancer, stomach cancer, head and neck cancer, mesothelioma, ovarian cancer, renal cancer, merkel cell carcinoma
Durvalumab	PD-L1	Bladder cancer, head and neck cancer, urothelial carcinoma
Ipilimumab	CTLA-4	Metastatic melanoma, prostate cancer, lung cancer, bladder cancer
Nivolumab	PD-L1	Head and neck cancer, metastatic melanoma, non-small cell lung cancer
Pembrolizumab	PD-L1	Head and neck cancer, metastatic melanoma, non-small cell lung cancer

expression of MHC II, reduce dendritic cells activation, and suppress T-cell differentiation [20].

Recently, nanotechnology has been widely studied for the development of cancer vaccines and the delivery of immunogenic agents. Indeed, in the next section, we will present several advantages of nanotechnology in immunotherapy including their preferential uptake by innate immune cells, such as monocytes, macrophages, and dendritic cells [21].

2 Nanoparticles-Based Approaches for Cancer Immunotherapy

Nanovaccines are typically composed of antigens, adjuvant, and/or nanocarriers [11]. Nanocarriers can protect the encapsulated antigens and/or adjuvant from enzymatic degradation, sustain and control the release for the entrapped cargo, and enhance the immune responses when compared with the antigen and adjuvant in the free form [22].

Nanocarriers are known as particles with a size of 10–100 nm and in some cases up to 1000 nm [23], including liposomes, dendrimers, micelles, and metallic nanoparticles among others (Fig. 3) [24]. Both polymeric and lipid-based nanoparticles can be engineered for efficiently delivering antigens or viral peptides to antigen-presenting cells to stimulate memory T-cell responses against tumors [25].

Overall, NPs could have two roles in the formulation of vaccines. First, they can be a useful tool for passive or active vaccine delivery [26]. Second, due to the inherent antigenicity property, they can stimulate the immune system and create an appropriate immune response [27].

Nanotechnology for tumor drug delivery often leverages on the enhanced permeability and retention effect, meaning that nanocarriers are preferentially accumulated in tumor tissues and drug delivery can be thus efficiently improved [28]. However, in case of nanocarriers application in cancer immunotherapy, nanovaccines should accumulate mostly in lymph nodes, where dendritic cells (DCs) are mostly located and immune system processes can be initiated [29].

Additionally, their physicochemical properties can be tuned for obtaining enhanced immune responses. In particular, particles size, shape, charge, and surface chemistry have been shown to impact innate immune cell interactions, lymphatic drainage, degradation, and biological profile [30].

Lastly, the route of administration of nanovaccines highly impacts distribution and accumulation of nanoparticles into lymph nodes. In case of skin administration, nanoparticles with dimensions minor to 100 nm are rapidly transported into the lymphatic system, where they can interact with immune cells. When larger nanoparticles are administered by the same route, they are accumulated into the skin and are internalized by DCs or monocytes, for migrating subsequently to the lymph nodes. For overcoming the retention in the skin, nanocarriers could be directly administered into the lymph nodes or intravenously. Indeed, intravenous injection could be an easy way to reach both blood and splenic DCs, although some challenges should be overcome, as the formation of the protein corona on the nanoparticles surface in the bloodstream [29].

In summary, the ideal nanocarrier for cancer immunotherapy should be able to: (i) provide colloidal stability against aggregation and undesirable interactions with blood components; (ii) protect their cargo during blood circulation; (iii) specifically target immune cells; and (iv) load a wide range of immunomodulating agents for effectively tuning the tumor microenvironment [22].

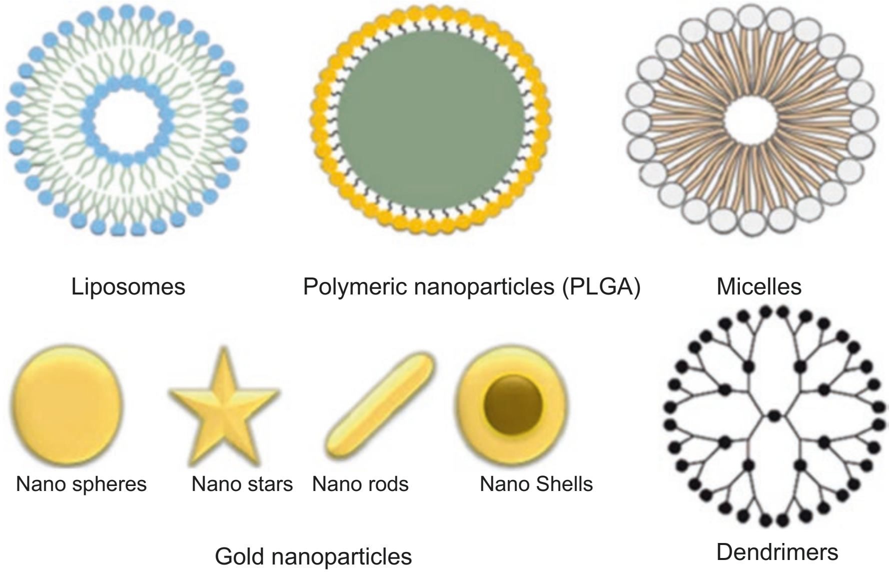

Fig. 3 Different typologies of nanocarriers. (Reproduced from [24], open access article distributed under the terms and conditions of the Creative Commons Attribution (CC BY) license (http://creativecommons.org/licenses/by/4.0/))

Concerning specific immune cells targeting, nanovaccines can be functionally designed to specifically transport antigens to antigen presenting cells (APCs), such as dendritic cells (DCs) and macrophages, ensuring the delivery of both antigen and adjuvant to the same cells population [31]. By this way, systemic distribution and adverse effects are decreased and immune response increased [32].

The simultaneous delivery of an antigen (proteins or small peptides) together with an adjuvant can be regarded as a dual therapeutic delivery [33]. Indeed, by this efficient co-delivery into lymphoid tissues and immune cells, nanovaccines can dramatically potentiate antigen-specific adaptive immune responses for cancer therapy [11].

Summarizing, the potential advantages derived from the administration of nanocarriers are the delivery of therapeutic compounds to a specific target [34]; an improved safety profile of immunostimulatory compounds [35]; finally the nanocarriers themselves may work as adjuvant.

Different nanoformulations delivering antigens, cytokines, chemokines, nucleotides, and toll-like receptor agonists targeting various immune cells have been successfully studied in many preclinical settings, producing promising results [36, 37]. The next sections are going to present the different typologies of nanocarriers and few related examples in cancer immunotherapy.

2.1 Micelles

Polymeric micelles are self-assembled nanoparticles composed of amphiphilic block copolymers widely investigated for cancer therapy [38, 39]. Micelles exhibit a core-shell structure wherein the hydrophobic moieties of the amphiphilic polymer form the inner core, while an outer shell is established by the hydrophilic chains. They are often used to load poorly soluble compound into the core, while the external hydrophilic segment can be functionalized for targeting [40].

Indeed, micelles have been successfully designed for cancer immunotherapy, as presented in comprehensive reviews [4, 6, 11, 18]. For example, Cubillos-Ruiz et al. used linear polyethyleneimine-based (PEI-based) nanomicelles to encapsulate siRNA and found effective uptake by dendritic cells with CD11c and PD-L1 expression in an ovarian cancer mouse model [41]. In another research work, cationic self-assembly micelles of polypeptides were employed for the loading of a model antigen (chicken ovalbumin, OVA), an adjuvant (poly I:C), and a siRNA (STAT3 inhibitor). The systems were targeted to the immunosuppressed dendritic cells in the tumor microenvironment and resulted in the activation of these dendritic cells, priming of cytotoxic T-lymphocytes, and increased survival in a melanoma mouse model (Fig. 4) [42].

2.2 Liposomes

Liposomes are bilayer spherical vesicles constructed from phospholipids and considered as nontoxic agents [43]. Liposomes can increase the retention of the loaded immunostimulants in tumors compared to the free compounds after intratumoral injection, achieving an enhanced immune response. Liposomal encapsulation could also reduce the systemic absorption of the immunostimulant, thereby reducing the toxicity. However, drug release is difficult to control when using liposomes [22]. On the other hand, the liposomal surface is flexible for decoration to enhance the vaccine delivery into immune cells. For example, different polysaccharides or carbohydrates have been used to target lectins overexpressed on dendritic cells, such as curdlan, mannan [44], l-rhamnose [45, 46], and glycan lewis [47]. For all these reasons, liposomes have been widely studied in cancer immunotherapy [48].

Arab et al. [49]. prepared E75 antigen-decorated liposomes consisting of distearoylphosphocholine/distearoylphosphoglycerol/cholesterol (Chol)/DOP to improve immunogenicity of the encapsulated peptide. In vivo results indicated that the formulation dramatically increased the CTL response and significantly prolonged survival time, which was *approx.* 72.4%, expressed as a mean tumor growth delay.

LPD (Liposome-Polycation-Plasmid DNA) nanoliposomes were developed as cationic vehicles containing DOTAP phospholipid. In an in vivo study, the immunostimulatory effect of LPD nanoparticles containing CpG-ODN (CpG oligonucleotides) adjuvant against tumor cells was evaluated in BALB/c mice. LPD-CpG nanoliposomes enhanced IFN-γ production and CTL response induced by the encapsulated multi-epitope peptides derived from the rHER2/neu in TUBO mice model. As a result, mice immunized with encapsulated peptide had significantly lower rates of tumor growth and longer survival time in comparison to mice immunized by free peptide [50].

Faham et al. used a mixture of disteroyl phosphocholine (DSPC) disteroyl phosphoethanolamine (DSPE), cholesterol, and polyethylene glycol (PEG) 750 for preparation of stealth liposomes [51]. The targeting function was obtained by engrafting two peptides derived from high-mobility box (HMGB1) onto the surface of liposomes to induce immune response. Intravenous injection of ovalbumin-loaded liposomes into mice potently induced OVA-specific IFN-γ producing CD8$^+$ T lymphocytes and antibodies. As a result, tumor growth and metastasis were inhibited after vaccination with liposomes in mice challenged with B16-OVA melanoma.

Xu el al [52]. prepared mannose modified lipid-calcium phosphate (LCP) nanoparticles (≈30 nm). Phosphorylated Trp2 peptide (p-Trp2) and CpG ODN were precipitated by

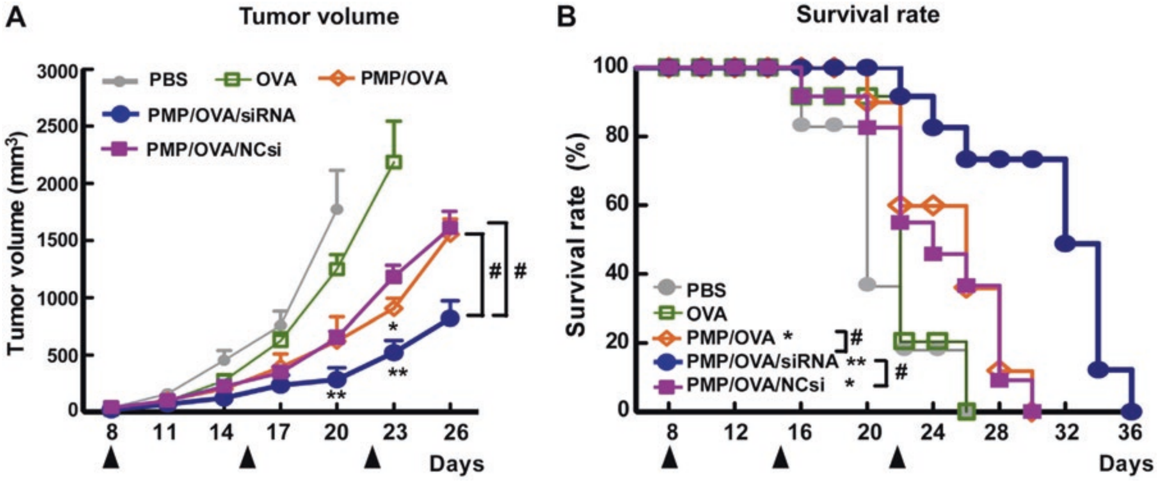

Fig. 4 The anti-tumor effect of polypeptides micelles loading chicken ovalbumin (OVA), an adjuvant (poly I:C) and a siRNA in vivo. B16-OVA tumor-bearing mice were i.p. injected with different vaccines once a week for 3 weeks from day 8 after tumor implantation. The tumor volume (**a**) and survival rate (**b**) were monitored every 2–3 days (black arrows indicate the day of treatment). (Reprinted from [42] with permission)

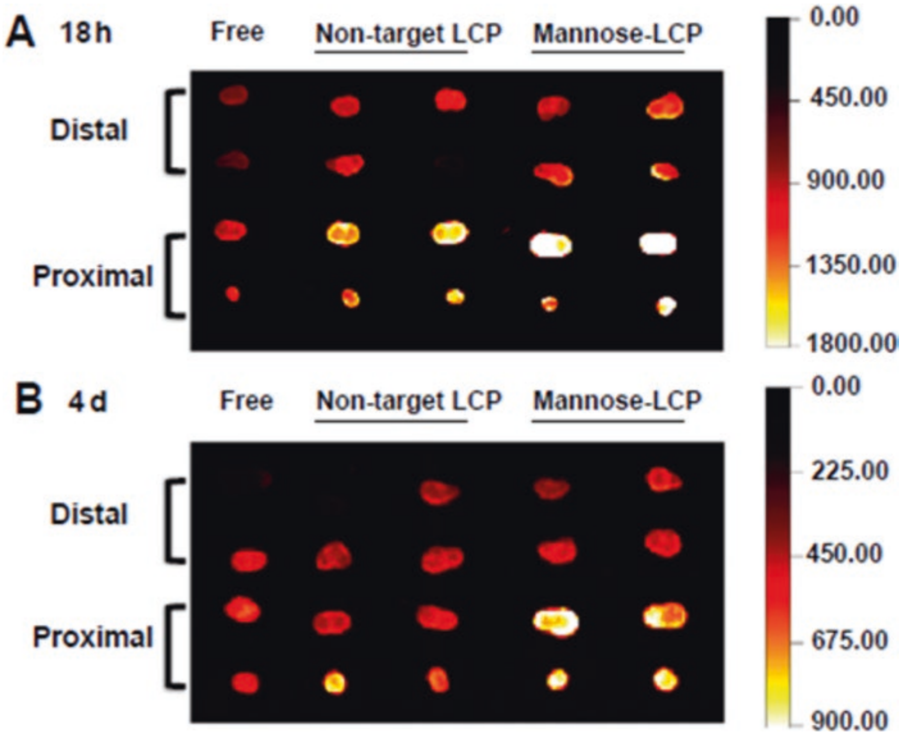

Fig. 5 Distribution of vaccine formulations (mannose targeted nanoparticles loading phosphorylated Trp2 peptide (p-Trp2) and CpG) in lymph nodes. C57BL/6 mice were injected subcutaneously with different formulations and sacrificed after 18 h (**a**) and 4 d (**b**). The lymph nodes along the injection side were then harvested and subjected to fluorescent imaging. (Reprinted from [52] with permission)

calcium ions to form the nanoparticles core, which was then coated with lipids. S.C. injection of the LCP to B16F10 melanoma-bearing mice resulted in high accumulation of the nanoparticles in the lymph nodes (≈35% of the injected dose, Fig. 5), increased DC uptake and enhanced IFN-γ secretion, leading to tumor growth inhibition.

M2-phenotype tumor-associated macrophages (TAMs) have been reported to restrict the functions of DCs and CD8$^+$ T cells. Researchers encapsulated IL-12 into a pH-sensitive poly(β-amino ester) nanoparticle to reverse TAMs from M2 to M1 phenotype. Researchers also developed liposomes dual-targeting scavenger receptors B type 1 (SR-B1) and M2 for delivering cholesterol-modified CSF-1R siRNA to M2 TAMs. By dual-targeting nanoparticles and delivery of CSF-1R siRNA, 52% of M2 TAMs were efficiently targeted and eliminated, obtaining an 87% decrease in tumor size and prolonged survival in B16F10 melanoma mouse model (Fig. 6) [53].

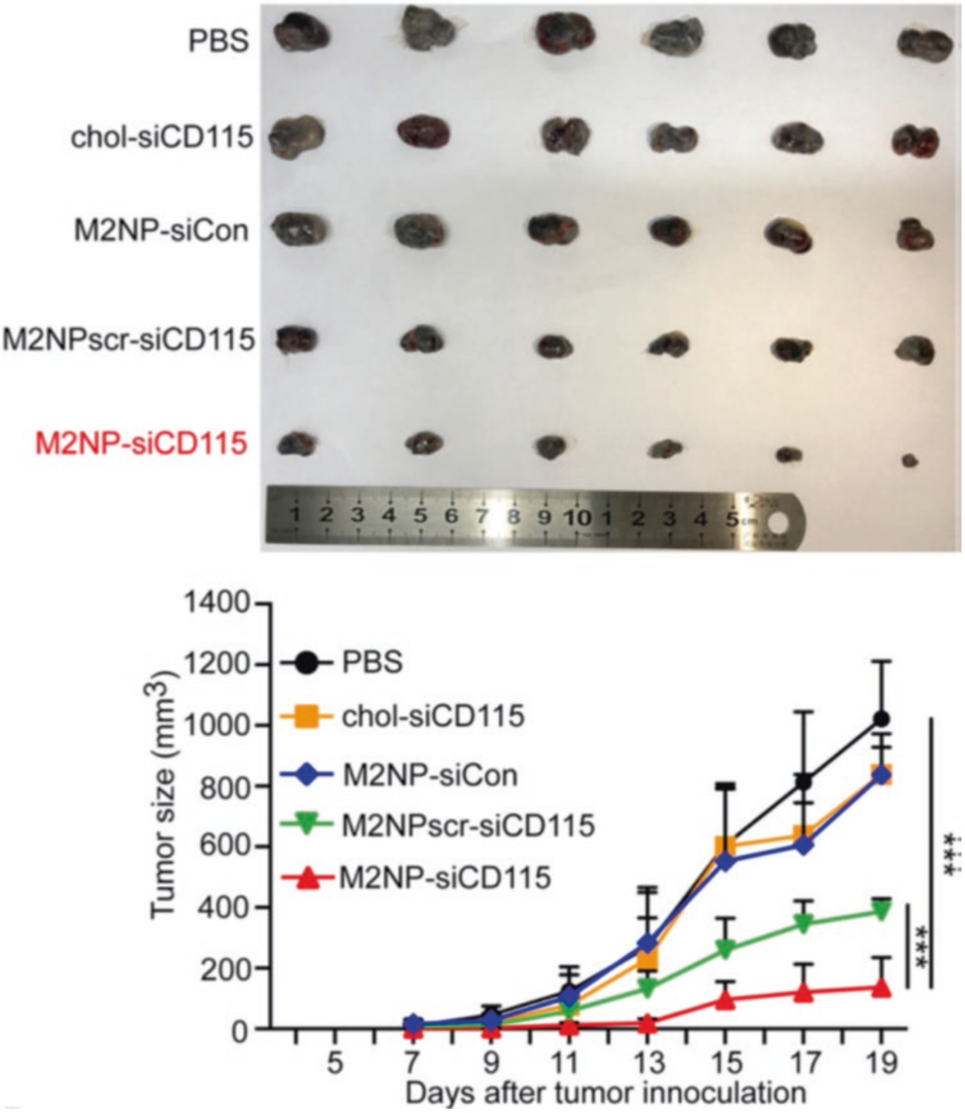

Fig. 6 Tumor growth inhibition effects of siRNA loaded nanoparticles targeting M2 tumor associated macrophages. (Modified from [53] with permission)

2.3 Magnetic and Inorganic Nanoparticles

Gold nanoparticles (AuNPs) have been widely investigated as imaging agents and in combination with phototherapy for cancer treatment thanks to their biocompatibility, tunable surface chemistry, easy control of size and shape, and suitability for computed tomography (CT) imaging [54]. However, the clinical application of AuNPs is hampered by safety issues. Indeed, AuNPs exhibit high affinity for nucleic acids and may affect regular gene expression. Furthermore, the effects of the long-term accumulation of AuNPs in the body have not been completely investigated [22].

Recently, these nanosystems have been also employed for cancer immunotherapy. Activation of DCs by AuNPs can be evidenced by increased phagocytic activity of DCs and subsequent enhanced maturation of T cells and CDC4+ and CD8+ immunoresponses [55]. Lee et al. used CpG and red fluorescent protein (RFP) as a model antigen to track the delivered AuNO-based vaccines to DCs in the target lymph node [56]. Moreover, the researchers injected phosphate buffer saline (PBS), RFP, AuNPs, RFP/AuNPs, or CpG/RFP/AuNPs into the footpads of mice. Compared to other groups, tumor growth was significantly inhibited in groups treated with RFP/AuNPs and CpG/RFP/AuNPs, and the effect of CpG/RFP/AuNPs was significantly higher than that of RFP/AuNPs.

Among inorganic nanoparticles, mesoporous silica nanoparticles (MSNs) exhibit also potent immunostimulating activity by increasing the expression of CD80 and CD86 and induce the secretion of immunostimulating cytokines, which subsequently enhanced CD4+ and CD8+ immune responses. Indeed, these nanocarriers alone (without antigen) were sufficient to inhibit tumor growth and increase survival of tumor-bearing mice [22].

Fontana and coworkers [57] used glass-capillary microfluidics technique to coat thermally oxidized porous silicon nanoparticles with acetalated dextran. Then the obtained nanoparticles were co-extruded with vesicles derived from cancer cell membrane for obtaining core-shell systems. Alternatively, porous silicon nanoparticles were coated with spermidine-modified acetalated dextran and functionalized with a model antigen (Trp2). Authors obtained an increased expression of CD86 and CD80 after peripheral blood monocytes contact with the systems, successfully demonstrating the immunostimulative properties of the designed nanovaccines.

2.4 Hydrogel Nanoparticles

Polysaccharide-based hydrogel nanoparticles are particularly attractive for antigen delivery due to their immunostimulating activities and ability to entrap hydrophilic macromolecules [22].

Park et al. [58] prepared nano-lipogels (nLGs) simultaneously encapsulating a TGF-β receptor I inhibitor (SB505124) and IL-2 for therapy against melanoma. Compounds were encapsulated in nanogels composed of PLA-PEG-PGA coated with different lipids (PC, DSPE-PEG, and cholesterol). nLGs increased the blood circulation half-life of immunoadjuvants by tenfold compared to the free drugs after i.v. injection in animal models. In vivo results showed that nLG enhanced the activation of CD8+ in cells in the tumor by threefold, resulting in improved immune response and anti-tumor efficacy against B16.F10 melanoma. Qiao and coworkers [59] designed pH degradable folated PVA-based nanogels for the dual delivery of docetaxel and IDO1 inhibitor NLG919 to breast cancer cells. Authors successfully promoted immunogenic cell death and infiltration of CD8+ T cells, downregulating at the same time IDO1 mediated immunosuppression in a 4T1-Luc murine breast cancer xenograft mouse model.

2.5 Polymeric Nanoparticles

One of the most used polymers for polymeric nanoparticles preparation is PLGA (poly (lactic-co-glycolic acid)). This copolymer is widely used for preparing particulate drug delivery systems due to its biocompatibility, biodegradability, and FDA-approved status [22]. For example, PLGA microspheres were prepared for the endosomal delivery of CpG-oligonucleotide and OVA to dendritic cells in vitro and for the immunization against melanoma tumor models in vivo, with promising results [60]. PLGA microparticles were also used for in situ immunization against animal models of lymphomas: particulate systems were coloaded with doxorubicin (Dox) and CpG. Authors showed that the intratumoral administration of low-dosage Dox with CpG in combination with the systemic administration of a checkpoint inhibitor resulted in reduced tumor volumes in the tumor models assessed [61].

Rosalia et al. [62] modified a PLGA nanoparticle surface with a monoclonal antibody (mAb) targeting CD40 overexpressed on DCs. The nanoparticles containing ovalbumin (OVA), protein antigen, and TLR 3 agonist displayed sixfold internalization relative to the non-targeted formulation in pre-clinical study in an animal model. In vivo studies demonstrated an increased IFN-γ production, enhanced OVA-specific CD4+ activation, and consequently reduced tumor growth in the B16/OVA tumor model (Fig. 7).

Kwak et al. [63] fabricated polymeric nanoparticles using dermatan sulfate and disulfide-crosslinked polyethyleneimine (CLPEI) for delivering siRNA targeting PD-L1 (siPD-L1). In vivo experiments confirmed enhanced antitumor immunity and upregulation of mature DCs in draining lymph nodes. Indeed, by inducing the immune checkpoint pathway blockade and intrinsic tumorigenesis pathway via mTOR signal, the nanocomplex exhibited tumor suppression on immunocompetent and compromised melanoma-bearing mice.

Huang and coworkers developed a lipid/calcium/phosphate (LCP) nanoparticle for the delivery of MUC1 mRNA, a highly expressed tumor-associated antigen in many cancers. Mannose modified LCP NPs successfully released MUC1 mRNA into the cytosol of DCs and induced an MHC I T-cell response. By combining LCP with anti-CTLA-4, loaded LCP NP successfully induced a strong antigen-specific immune response in mice-bearing triple negative breast cancer [64].

2.6 Cell Membrane-Coated Nanovaccines

Recently, cell membrane camouflage-based nanocarriers have become an interesting biomimetic platform for drug delivery [65]. Cell membranes of interest can be extracted and coated onto the nanoparticle surfaces or formed as building blocks to form nanocarriers. Cancer cell membrane-coated NPs can carry cancer cell membrane antigens, offering a promising a platform as cancer nanovaccines [66]. For example, a B16-F10 melanoma cell membrane was successfully coated on a CgG-loaded PLGA nanoparticle. Cloaked nanocarrier supported maturation of dendritic cells in draining lymph nodes with up-regulation of CD40, CD80, CD86, and MHC-II. Indeed, in vivo 86% of mice vaccinated with cancer membrane-coated nanoparticles remained tumor-free survival for over 4 months, which was more efficient than a mixture of B16-F10 cells and free CpG [67].

Single elements derived from the membrane of cancer cells can be as well employed for the formulation of new cancer nanovaccines [33]. A recent paper proposed the use of

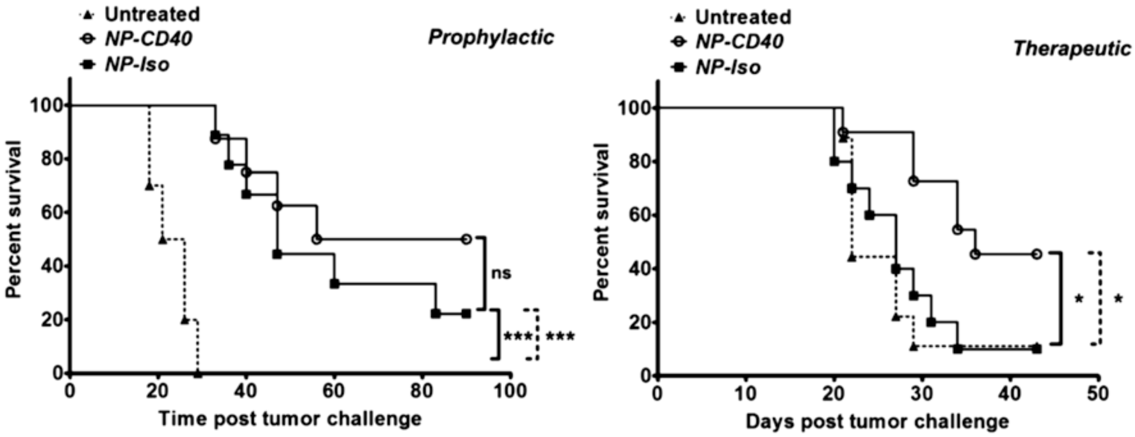

Fig. 7 Animal survival after vaccination (left side) and treatment in B16/OVA tumor model (right side) with nanoparticles containing ovalbumin (OVA), protein antigen, and TLR 3 agonist. (Reprinted from [62] with permission)

plasma membrane-derived vesicle as delivery systems for the co-delivery of adjuvant and antigens; the antigens were conjugated to glycosylphosphatidylinositol (IL-12 and CD80) and incorporated into the vesicle. Successfully, the administration of these systems in animal models led to impressive improvements in the overall survival of the animals compared to the controls [68].

Exosomes have also shown the potential as carriers for vaccine delivery as they are secreted by a variety of cells including T cells, B cells, tumor cells, and APCs [11] and are able to fuse with the membrane of adjacent cells for cell-cell communication [69]. Depending on cell origin, exosomes can be immunostimulatory or immunosuppressive, showing potential applications in immunotherapy of tumor or autoimmune diseases, respectively. Their ability to deliver exogenous vaccines is also valuable for cancer immunotherapy. For example, a therapy with exosomes derived from the ascites of murine T-cell lymphoma has been reported to activate spleenocytes and induced specific CD4+ and CD8+ lymphocytes, leading to increased survival of animals [70]. However, the challenges for exosome-based nanomedicines include the cost and time for preparation at large scales [11, 22].

3 Physicochemical Characteristics Impacting Nanomedicine Application in Immunotherapy

Several studies reported the physical characteristics of NPs affecting their uptake in cells and the potential to induce cellular responses [71]. These characteristics including size, surface coating, etc., influence, as well the processing by immune cells and consequent induction of immune responses [72].

As previously mentioned, different studies demonstrated that nanoparticles can act as vaccine delivery system and are not antigenic themselves. On the other hand, some data suggest that certain NPs could be antigenic because nanoparticle-specific antibodies could be generated after nanoparticle conjugation to serum proteins [35].

The size of NPs plays a decisive role in humoral and/or cellular immune systems response. For example, it has been reported that particles smaller than 500 nm provoke T CD8$^+$ CD4$^+$ Type 1 cells responses, while particles larger than 500 nm stimulate T CD4$^+$ Type 2 cells and produce antibodies [71]. Additionally, nanosized particles in the 10–50 nm easily reach DCs in the lymphatic system, boosting immune system components more effectively [73]. It was also indicated that liposomes with a mean diameter of ≥225 nm induce Th1 responses and strongly promote CTL response, while smaller liposomes could promote humoral immunity through induction of Th2 response and increased IL-5 production [74].

The kinetics of nanoparticle drainage also depends on particle size. Two hundred nm pores in lymphatic vessels walls permits nanoparticles diffusion (with 10–80 nm being the optimal size) while particles exceeding this cut-off require active transport by APCs [30]. Although therapeutic efficacy can be achieved also using large nanoparticles, optimal immune effects are observed with particles showing dimensions of 40–50 nm [75]. Additionally, abnormal vasculature in tumors elicits a greater infiltration of nanoparticles than in normal tissue. As a matter of fact, lymphatic drainage ineffectiveness within tumors increases the accumulation and retention of the nanoparticles inside tumors themselves (enhanced permeability and retention-EPR effect) [13].

A phenomenon well-known for affecting nanoparticles fate is the formation of the protein corona, that is proteins coating on nanoparticle surface. Indeed, nanoparticles are known to modify their native physicochemical properties due to this phenomenon once in contact with biological fluids, such as blood after intravenous injection. These changes in size, surface charge, and aggregation state could potentially affect nanoparticles pharmacokinetics, biodistribution, and finally therapeutic efficacy, as reported by many studies [76].

Nanoparticle uptake by cells involves binding to the cell surface followed by uptake of the nanoparticles by a specific pathway. Among all, nanoparticle uptake can be influenced by particle size, surface charge, surface modification, and hydrophobicity [77]. Indeed, surface charge determines if nanoparticles aggregate adhere to or interact with oppositely charged cells. Surface charge of nanoparticles influences also uptake and interaction with cells [77]. Interestingly, positive charge has an enhancing effect on the uptake rate compared with neutral or negatively charge carriers [78]. For example, positively charged lipids, such as diacyl dimethylammonium-propane (DAP), provide net positive charge to the liposomes enhancing its uptake by APCs to a much higher degree than negatively charged or neutral liposomes [79]. The in vivo scenario is complicated by the presence of negatively charged components in the bio-physiological fluids [80], which possibly immobilize positively charged nanoparticles. Additionally, cationic particles can affect cell membrane integrity or cause hemolysis and platelet aggregation.

Coating nanoparticle surface with hydrophilic molecules such as polyethylene glycol (PEG) permits to effectively balance particle charge [81]. Additionally, PEGylation or nanoparticle coating with other polymers lengthens the circulation time of these systems by inhibiting phagocyte uptake and promoting their accumulation into tumors. Moreover, PEGylation has been reported to optimize lymphatic targeting, potentially increasing nanoparticles interactions with APCs [81]. Unfortunately, these modifications can also inhibit the uptake of these compounds by tumor cells themselves. To overcome this limitation, "active" tumor-targeting approaches involving the conjugation of tumor-specific ligands to the nanoparticles surface have been developed [6].

Lastly, nanoparticles uptake by cells may be influenced by the shape. Uptake studies of protein-coated gold nanoparticles demonstrated that spherical nanoparticles are taken up by cells more effectively than rod-shaped nanoparticles [82, 83]. Elliptical particles were demonstrated to be endocytosed at a slower rate compared to spherical particles [84].

4 Conclusions and Future Perspectives

The potential of novel immunotherapeutics has been demonstrated by a number of recent FDA-approved therapeutic cancer vaccines, including sipuleucel-T (Provenge®, Dendreon, Seattle, WA) against prostate cancer [85] and monoclonal antibodies (mAb) such as ipilumumab (Yervoy®, Bristol-Meyers Squibb, New York, NY), an anti-CTLA-4 mAb used as a first-line therapy for metastatic melanoma [86].

Despite this high enthusiasm for immunotherapy for cancer treatment, the application of nanotechnology in this field presents some challenges. First, the toxicity of nano-based immunotherapy needs to be further characterized. It is unknown if the increased immune activation from nanoparticles will also increase autoimmune side effects. Although immune activation is desired in cancer immunotherapy, an overactivation can be detrimental. Additionally, nanotechnology generally increases the complexity and cost of manufacturing and commercialization of treatments. Strategies aimed at minimizing this economic impact could facilitate clinical translation of nano-based immunotherapy treatments. On the other hand, nanotechnology scalability and reproducibility limit the development and clinical application of nanomedicine. Besides these challenges, preclinical animal models able to mimic human physiology should be improved and standardized.

In conclusion, nanotechnology approach shows tremendous potential for tumor immunotherapy, although some challenges still have to be solved. An example is DepoVax (DPX-0907), a liposome vaccine comprising several TAAs to target to DC, which is under clinical trials for prostate, breast, and ovarian cancers. DepoVax-related clinical data demonstrate that liposomes successfully activate cytotoxic T-cells against tumor at the site of injection [87]. These data and all the research papers in preclinical stage about the use of nanotechnology in cancer immunotherapy support the idea that this strategy could be successful as novel weapons against cancer in future.

References

1. Bray, F., Ferlay, J., Soerjomataram, I., Siegel, R. L., Torre, L. A., & Jemal, A. (2018). Global cancer statistics 2018: GLOBOCAN estimates of incidence and mortality worldwide for 36 cancers in 185 countries. *CA: a Cancer Journal for Clinicians, 68*(6), 394–424.
2. Couzin-Frankel, J. (2013). Breakthrough of the year 2013. Cancer immunotherapy. *Science, 342*(6165), 1432–1433.
3. Deng, H., & Zhang, Z. (2018). The application of nanotechnology in immune checkpoint blockade for cancer treatment. *Journal of Controlled Release, 290*, 28–45.
4. Park, O., Yu, G., Jung, H., & Mok, H. (2016). Recent studies on micro−/nano-sized biomaterials for cancer immunotherapy. *Journal of Pharmaceutical Investigation, 47*, 11.
5. Schreiber, R. D., Old, L. J., & Smyth, M. J. (2011). Cancer immunoediting: Integrating immunity's roles in cancer suppression and promotion. *Science, 331*(6024), 1565–1570.
6. Shao, K., Singha, S., Clemente-Casares, X., Tsai, S., Yang, Y., & Santamaria, P. (2015). Nanoparticle-based immunotherapy for cancer. *ACS Nano, 9*(1), 16–30.
7. Swann, J. B., & Smyth, M. J. (2007). Immune surveillance of tumors. *The Journal of Clinical Investigation, 117*(5), 1137–1146.

8. Zaman, M., Good, M. F., & Toth, I. (2013). Nanovaccines and their mode of action. *Methods, 60*(3), 226–231.
9. Alatrash, G., Jakher, H., Stafford, P. D., & Mittendorf, E. A. (2013). Cancer immunotherapies, their safety and toxicity. *Expert Opinion on Drug Safety, 12*(5), 631–645.
10. Tran, T. H., Tran, T. T. P., Nguyen, H. T., Phung, C. D., Jeong, J.-H., Stenzel, M. H., Jin, S. G., Yong, C. S., Truong, D. H., & Kim, J. O. (2018). Nanoparticles for dendritic cell-based immunotherapy. *International Journal of Pharmaceutics, 542*(1), 253–265.
11. Zhang, Y., Lin, S., Wang, X. Y., & Zhu, G. (2019). Nanovaccines for cancer immunotherapy. *Wiley Interdisciplinary Reviews. Nanomedicine and Nanobiotechnology, 11*(5), e1559.
12. Montomoli, E., Piccirella, S., Khadang, B., Mennitto, E., Camerini, R., & De Rosa, A. (2011). Current adjuvants and new perspectives in vaccine formulation. *Expert Review of Vaccines, 10*(7), 1053–1061.
13. Mi, Y., Hagan, C. T. T., Vincent, B. G., & Wang, A. Z. (2019). Emerging nano−/microapproaches for cancer immunotherapy. *Advanced Science (Weinheim), 6*(6), 1801847.
14. Schijns, V. E. J. C. (2003). Mechanisms of vaccine adjuvant activity: Initiation and regulation of immune responses by vaccine adjuvants. *Vaccine, 21*(9), 829–831.
15. Di Pasquale, A., Preiss, S., Tavares Da Silva, F., & Garcon, N. (2015). Vaccine adjuvants: From 1920 to 2015 and beyond. *Vaccines (Basel), 3*(2), 320–343.
16. Parmiani, G., De Filippo, A., Novellino, L., & Castelli, C. (2007). Unique human tumor antigens: Immunobiology and use in clinical trials. *The Journal of Immunology, 178*(4), 1975–1979.
17. Mellman, I., Coukos, G., & Dranoff, G. (2011). Cancer immunotherapy comes of age. *Nature, 480*, 480.
18. Zhu, G., Zhang, F., Ni, Q., Niu, G., & Chen, X. (2017). Efficient nanovaccine delivery in cancer immunotherapy. *ACS Nano, 11*(3), 2387–2392.
19. Sharma, P., Hu-Lieskovan, S., Wargo, J. A., & Ribas, A. (2017). Primary, adaptive, and acquired resistance to cancer immunotherapy. *Cell, 168*(4), 707–723.
20. Croci, D. O., Zacarias Fluck, M. F., Rico, M. J., Matar, P., Rabinovich, G. A., & Scharovsky, O. G. (2007). Dynamic cross-talk between tumor and immune cells in orchestrating the immunosuppressive network at the tumor microenvironment. *Cancer Immunology, Immunotherapy, 56*(11), 1687–1700.
21. Da Silva, C. G., Rueda, F., Lowik, C. W., Ossendorp, F., & Cruz, L. J. (2016). Combinatorial prospects of nano-targeted chemoimmunotherapy. *Biomaterials, 83*, 308–320.
22. Mahjub, R., Jatana, S., Lee, S. E., Qin, Z., Pauli, G., Soleimani, M., Madadi, S., & Li, S. D. (2018). Recent advances in applying nanotechnologies for cancer immunotherapy. *Journal of Controlled Release, 288*, 239–263.
23. Gheibi Hayat, S. M., & Darroudi, M. (2019). Nanovaccine: A novel approach in immunization. *Journal of Cellular Physiology, 234*(8), 12530–12536.
24. Poilil Surendran, S., Moon, M. J., Park, R., & Jeong, Y. Y. (2018). Bioactive nanoparticles for cancer immunotherapy. *International Journal of Molecular Sciences, 19*(12), 3877.
25. Kuai, R., Ochyl, L. J., Bahjat, K. S., Schwendeman, A., & Moon, J. J. (2017). Designer vaccine nanodiscs for personalized cancer immunotherapy. *Nature Materials, 16*(4), 489–496.
26. Couvreur, P. (2013). Nanoparticles in drug delivery: Past, present and future. *Advanced Drug Delivery Reviews, 65*(1), 21–23.
27. Kreuter, J. (1995). Nanoparticles as adjuvants for vaccines. *Pharmaceutical Biotechnology, 6*, 463–472.
28. Maeda, H., Nakamura, H., & Fang, J. (2013). The EPR effect for macromolecular drug delivery to solid tumors: Improvement of tumor uptake, lowering of systemic toxicity, and distinct tumor imaging in vivo. *Advanced Drug Delivery Reviews, 65*(1), 71–79.
29. Paulis, L. E., Mandal, S., Kreutz, M., & Figdor, C. G. (2013). Dendritic cell-based nanovaccines for cancer immunotherapy. *Current Opinion in Immunology, 25*(3), 389–395.
30. Kelly, H. G., Kent, S. J., & Wheatley, A. K. (2019). Immunological basis for enhanced immunity of nanoparticle vaccines. *Expert Review of Vaccines, 18*(3), 269–280.
31. Reddy, S. T., Swartz, M. A., & Hubbell, J. A. (2006). Targeting dendritic cells with biomaterials: Developing the next generation of vaccines. *Trends in Immunology, 27*(12), 573–579.
32. Lofthouse, S. (2002). Immunological aspects of controlled antigen delivery. *Advanced Drug Delivery Reviews, 54*(6), 863–870.
33. Fontana, F., Liu, D., Hirvonen, J., & Santos, H. A. (2017). Delivery of therapeutics with nanoparticles: what's new in cancer immunotherapy? *Wiley Interdisciplinary Reviews. Nanomedicine and Nanobiotechnology, 9*(1).
34. Peer, D., Karp, J. M., Hong, S., Farokhzad, O. C., Margalit, R., & Langer, R. (2007). Nanocarriers as an emerging platform for cancer therapy. *Nature Nanotechnology, 2*(12), 751–760.
35. Zolnik, B. S., Gonzalez-Fernandez, A., Sadrieh, N., & Dobrovolskaia, M. A. (2010). Nanoparticles and the immune system. *Endocrinology, 151*(2), 458–465.
36. Jiang, W., von Roemeling, C. A., Chen, Y., Qie, Y., Liu, X., Chen, J., & Kim, B. Y. S. (2017). Designing nanomedicine for immuno-oncology. *Nature Biomedical Engineering, 1*, 0029.
37. Liu, Z., Jiang, W., Nam, J., Moon, J. J., & Kim, B. Y. S. (2018). Immunomodulating nanomedicine for cancer therapy. *Nano Letters, 18*(11), 6655–6659.
38. Croy, S. R., & Kwon, G. S. (2006). Polymeric micelles for drug delivery. *Current Pharmaceutical Design, 12*(36), 4669–4684.
39. Letchford, K., & Burt, H. (2007). A review of the formation and classification of amphiphilic block copolymer nanoparticulate structures: Micelles, nanospheres, nanocapsules and polymersomes. *European Journal of Pharmaceutics and Biopharmaceutics, 65*(3), 259–269.
40. Jones, M., & Leroux, J. (1999). Polymeric micelles: A new generation of colloidal drug carriers. *European Journal of Pharmaceutics and Biopharmaceutics, 48*(2), 101–111.
41. Cubillos-Ruiz, J. R., Engle, X., Scarlett, U. K., Martinez, D., Barber, A., Elgueta, R., Wang, L., Nesbeth, Y., Durant, Y., Gewirtz, A. T., Sentman, C. L., Kedl, R., & Conejo-Garcia, J. R. (2009). Polyethylenimine-based siRNA nanocomplexes reprogram tumor-associated dendritic cells via TLR5 to elicit therapeutic antitumor immunity. *The Journal of Clinical Investigation, 119*(8), 2231–2244.
42. Luo, Z., Wang, C., Yi, H., Li, P., Pan, H., Liu, L., Cai, L., & Ma, Y. (2015). Nanovaccine loaded with poly I:C and STAT3 siRNA robustly elicits anti-tumor immune responses through modulating tumor-associated dendritic cells in vivo. *Biomaterials, 38*, 50–60.
43. Parnham, M. J., & Wetzig, H. (1993). Toxicity screening of liposomes. *Chemistry and Physics of Lipids, 64*(1–3), 263–274.
44. Yuba, E., Yamaguchi, A., Yoshizaki, Y., Harada, A., & Kono, K. (2017). Bioactive polysaccharide-based pH-sensitive polymers for cytoplasmic delivery of antigen and activation of antigen-specific immunity. *Biomaterials, 120*, 32–45.
45. Sarkar, S., Salyer, A. C., Wall, K. A., & Sucheck, S. J. (2013). Synthesis and immunological evaluation of a MUC1 glycopeptide incorporated into l-rhamnose displaying liposomes. *Bioconjugate Chemistry, 24*(3), 363–375.
46. Li, X., Rao, X., Cai, L., Liu, X., Wang, H., Wu, W., Zhu, C., Chen, M., Wang, P. G., & Yi, W. (2016). Targeting tumor cells by natural anti-carbohydrate antibodies using Rhamnose-functionalized liposomes. *ACS Chemical Biology, 11*(5), 1205–1209.
47. Boks, M. A., Ambrosini, M., Bruijns, S. C., Kalay, H., van Bloois, L., Storm, G., Garcia-Vallejo, J. J., & van Kooyk, Y. (2015). MPLA incorporation into DC-targeting glycoliposomes favours anti-tumour T cell responses. *Journal of Controlled Release, 216*, 37–46.

48. Sayour, E. J., Mendez-Gomez, H. R., & Mitchell, D. A. (2018). Cancer vaccine immunotherapy with RNA-loaded liposomes. *International Journal of Molecular Sciences, 19*(10), 2890.
49. Arab, A., Behravan, J., Razazan, A., Gholizadeh, Z., Nikpoor, A. R., Barati, N., Mosaffa, F., Badiee, A., & Jaafari, M. R. (2018). A nano-liposome vaccine carrying E75, a HER-2/neu-derived peptide, exhibits significant antitumour activity in mice. *Journal of Drug Targeting, 26*(4), 365–372.
50. Jalali, S. A., Sankian, M., Tavakkol-Afshari, J., & Jaafari, M. R. (2012). Induction of tumor-specific immunity by multi-epitope rat HER2/neu-derived peptides encapsulated in LPD nanoparticles. *Nanomedicine, 8*(5), 692–701.
51. Faham, A., Bennett, D., & Altin, J. G. (2009). Liposomal Ag engrafted with peptides of sequence derived from HMGB1 induce potent Ag-specific and anti-tumour immunity. *Vaccine, 27*(42), 5846–5854.
52. Xu, Z., Ramishetti, S., Tseng, Y. C., Guo, S., Wang, Y., & Huang, L. (2013). Multifunctional nanoparticles co-delivering Trp2 peptide and CpG adjuvant induce potent cytotoxic T-lymphocyte response against melanoma and its lung metastasis. *Journal of Controlled Release, 172*(1), 259–265.
53. Qian, Y., Qiao, S., Dai, Y., Xu, G., Dai, B., Lu, L., Yu, X., Luo, Q., & Zhang, Z. (2017). Molecular-targeted immunotherapeutic strategy for melanoma via dual-targeting nanoparticles delivering small interfering RNA to tumor-associated macrophages. *ACS Nano, 11*(9), 9536–9549.
54. Boisselier, E., & Astruc, D. (2009). Gold nanoparticles in nanomedicine: Preparations, imaging, diagnostics, therapies and toxicity. *Chemical Society Reviews, 38*(6), 1759–1782.
55. Dykman, L. A., & Khlebtsov, N. G. (2011). Gold nanoparticles in biology and medicine: Recent advances and prospects. *Acta Naturae, 3*(2), 34–55.
56. Lee, I. H., Kwon, H. K., An, S., Kim, D., Kim, S., Yu, M. K., Lee, J. H., Lee, T. S., Im, S. H., & Jon, S. (2012). Imageable antigen-presenting gold nanoparticle vaccines for effective cancer immunotherapy in vivo. *Angewandte Chemie (International Ed. in English), 51*(35), 8800–8805.
57. Fontana, F., Shahbazi, M.-A., Liu, D., Zhang, H., Mäkilä, E., Salonen, J., Hirvonen, J. T., & Santos, H. A. (2017). Multistaged nanovaccines based on porous Silicon@Acetalated Dextran@ Cancer cell membrane for cancer immunotherapy. *Advanced Materials (Deerfield Beach, Fla.), 29*(7).
58. Park, J., Wrzesinski, S. H., Stern, E., Look, M., Criscione, J., Ragheb, R., Jay, S. M., Demento, S. L., Agawu, A., Licona Limon, P., Ferrandino, A. F., Gonzalez, D., Habermann, A., Flavell, R. A., & Fahmy, T. M. (2012). Combination delivery of TGF-beta inhibitor and IL-2 by nanoscale liposomal polymeric gels enhances tumour immunotherapy. *Nature Materials, 11*(10), 895–905.
59. Qiao, H., Chen, X., Chen, E., Zhang, J., Huang, D., Yang, D., Ding, Y., Qian, H., Feijen, J., & Chen, W. (2019). Folated pH-degradable nanogels for the simultaneous delivery of docetaxel and an IDO1-inhibitor in enhancing cancer chemo-immunotherapy. *Biomaterials Science, 7*(7), 2749–2758.
60. Heit, A., Schmitz, F., Haas, T., Busch, D. H., & Wagner, H. (2007). Antigen co-encapsulated with adjuvants efficiently drive protective T cell immunity. *European Journal of Immunology, 37*(8), 2063–2074.
61. Makkouk, A., Joshi, V. B., Wongrakpanich, A., Lemke, C. D., Gross, B. P., Salem, A. K., & Weiner, G. J. (2015). Biodegradable microparticles loaded with doxorubicin and CpG ODN for in situ immunization against cancer. *The AAPS Journal, 17*(1), 184–193.
62. Rosalia, R. A., Cruz, L. J., van Duikeren, S., Tromp, A. T., Silva, A. L., Jiskoot, W., de Gruijl, T., Lowik, C., Oostendorp, J., van der Burg, S. H., & Ossendorp, F. (2015). CD40-targeted dendritic cell delivery of PLGA-nanoparticle vaccines induce potent anti-tumor responses. *Biomaterials, 40*, 88–97.
63. Kwak, G., Kim, D., Nam, G. H., Wang, S. Y., Kim, I. S., Kim, S. H., Kwon, I. C., & Yeo, Y. (2017). Programmed cell death protein Ligand-1 silencing with polyethylenimine-dermatan sulfate complex for dual inhibition of melanoma growth. *ACS Nano, 11*(10), 10135–10146.
64. Liu, L., Wang, Y., Miao, L., Liu, Q., Musetti, S., Li, J., & Huang, L. (2018). Combination immunotherapy of MUC1 mRNA Nano-vaccine and CTLA-4 blockade effectively inhibits growth of triple negative breast cancer. *Molecular Therapy, 26*(1), 45–55.
65. Luk, B. T., & Zhang, L. (2015). Cell membrane-camouflaged nanoparticles for drug delivery. *Journal of Controlled Release, 220*, 600–607.
66. Fang, R. H., Hu, C.-M. J., Luk, B. T., Gao, W., Copp, J. A., Tai, Y., O’Connor, D. E., & Zhang, L. (2014). Cancer cell membrane-coated nanoparticles for anticancer vaccination and drug delivery. *Nano Letters, 14*(4), 2181–2188.
67. Kroll, V. A., Fang, R. H., Jiang, Y., Zhou, J., Wei, X., Yu, C. L., Gao, J., Luk, B., Dehaini, D., Gao, W., & Zhang, L. (2017). Nanoparticulate delivery of Cancer cell membrane elicits multiantigenic antitumor immunity. *Advanced Materials, 29*, 1703969.
68. Patel, J. M., Vartabedian, V. F., Bozeman, E. N., Caoyonan, B. E., Srivatsan, S., Pack, C. D., Dey, P., D’Souza, M. J., Yang, L., & Selvaraj, P. (2016). Plasma membrane vesicles decorated with glycolipid-anchored antigens and adjuvants via protein transfer as an antigen delivery platform for inhibition of tumor growth. *Biomaterials, 74*, 231–244.
69. Aryani, A., & Denecke, B. (2016). Exosomes as a Nanodelivery system: A key to the future of Neuromedicine? *Molecular Neurobiology, 53*(2), 818–834.
70. Menay, F., Herschlik, L., De Toro, J., Cocozza, F., Tsacalian, R., Gravisaco, M. J., Di Sciullo, M. P., Vendrell, A., Waldner, C. I., & Mongini, C. (2017). Exosomes isolated from ascites of T-cell lymphoma-bearing mice expressing surface CD24 and HSP-90 induce a tumor-specific immune response. *Frontiers in Immunology, 8*, 286.
71. Jiang, W., Kim, B. Y., Rutka, J. T., & Chan, W. C. (2008). Nanoparticle-mediated cellular response is size-dependent. *Nature Nanotechnology, 3*(3), 145–150.
72. Gregory, A. E., Titball, R., & Williamson, D. (2013). Vaccine delivery using nanoparticles. *Frontiers in Cellular and Infection Microbiology, 3*, 13.
73. Kakwere, H., Ingham, E. S., Allen, R., Mahakian, L. M., Tam, S. M., Zhang, H., Silvestrini, M. T., Lewis, J. S., & Ferrara, K. W. (2017). Toward personalized peptide-based cancer nanovaccines: A facile and versatile synthetic approach. *Bioconjugate Chemistry, 28*(11), 2756–2771.
74. Brewer, J. M., Tetley, L., Richmond, J., Liew, F. Y., & Alexander, J. (1998). Lipid vesicle size determines the Th1 or Th2 response to entrapped antigen. *Journal of Immunology, 161*(8), 4000–4007.
75. Fifis, T., Gamvrellis, A., Crimeen-Irwin, B., Pietersz, G. A., Li, J., Mottram, P. L., McKenzie, I. F., & Plebanski, M. (2004). Size-dependent immunogenicity: Therapeutic and protective properties of nano-vaccines against tumors. *Journal of Immunology, 173*(5), 3148–3154.
76. Barbero, F., Russo, L., Vitali, M., Piella, J., Salvo, I., Borrajo, M. L., Busquets-Fité, M., Grandori, R., Bastús, N. G., Casals, E., & Puntes, V. (2017). Formation of the protein corona: The Interface between nanoparticles and the immune system. *Seminars in Immunology, 34*, 52–60.
77. Kumari, A., & Yadav, S. K. (2011). Cellular interactions of therapeutically delivered nanoparticles. *Expert Opinion on Drug Delivery, 8*(2), 141–151.

78. Munoz Javier, A., Kreft, O., Alberola, A. P., Kirchner, C., Zebli, B., Susha, A. S., Horn, E., Kempter, S., Skirtach, A. G., Rogach, A. L., Radler, J., Sukhorukov, G. B., Benoit, M., & Parak, W. J. (2006). Combined atomic force microscopy and optical microscopy measurements as a method to investigate particle uptake by cells. *Small, 2*(3), 394–400.
79. Nakanishi, T., Kunisawa, J., Hayashi, A., Tsutsumi, Y., Kubo, K., Nakagawa, S., Nakanishi, M., Tanaka, K., & Mayumi, T. (1999). Positively charged liposome functions as an efficient immunoadjuvant in inducing cell-mediated immune response to soluble proteins. *Journal of Controlled Release, 61*(1–2), 233–240.
80. van den Berg, J. H., Oosterhuis, K., Hennink, W. E., Storm, G., van der Aa, L. J., Engbersen, J. F., Haanen, J. B., Beijnen, J. H., Schumacher, T. N., & Nuijen, B. (2010). Shielding the cationic charge of nanoparticle-formulated dermal DNA vaccines is essential for antigen expression and immunogenicity. *Journal of Controlled Release, 141*(2), 234–240.
81. Grimaldi, A. M., Incoronato, M., Salvatore, M., & Soricelli, A. (2017). Nanoparticle-based strategies for cancer immunotherapy and immunodiagnostics. *Nanomedicine (London, England), 12*(19), 2349–2365.
82. Chithrani, B. D., Ghazani, A. A., & Chan, W. C. (2006). Determining the size and shape dependence of gold nanoparticle uptake into mammalian cells. *Nano Letters, 6*(4), 662–668.
83. Huang, X., Teng, X., Chen, D., Tang, F., & He, J. (2010). The effect of the shape of mesoporous silica nanoparticles on cellular uptake and cell function. *Biomaterials, 31*(3), 438–448.
84. Yoo, J. W., Doshi, N., & Mitragotri, S. (2010). Endocytosis and intracellular distribution of PLGA particles in endothelial cells: Effect of particle geometry. *Macromolecular Rapid Communications, 31*(2), 142–148.
85. Sheikh, N. A., Petrylak, D., Kantoff, P. W., Dela Rosa, C., Stewart, F. P., Kuan, L. Y., Whitmore, J. B., Trager, J. B., Poehlein, C. H., Frohlich, M. W., & Urdal, D. L. (2013). Sipuleucel-T immune parameters correlate with survival: An analysis of the randomized phase 3 clinical trials in men with castration-resistant prostate cancer. *Cancer Immunology, Immunotherapy, 62*(1), 137–147.
86. Farkona, S., Diamandis, E. P., & Blasutig, I. M. (2016). Cancer immunotherapy: The beginning of the end of cancer? *BMC Medicine, 14*, 73.
87. Karkada, M., Berinstein, N. L., & Mansour, M. (2014). Therapeutic vaccines and cancer: Focus on DPX-0907. *Biologics, 8*, 27–38.

Viral Nanoparticles: Cancer Vaccines and Immune Modulators

Manlio Fusciello, Erkko Ylösmäki, and Vincenzo Cerullo

Abstract

In the last decades, viruses have gained great interest in the field of immuno-oncology (I-O) for their ability of interacting both with the immune system and the tumour microenvironment. Those pathogens have naturally evolved and been evolutionary to specifically infect hosts, replicate, deliver their genome, and spread. These properties, initially considered a disadvantage, have been investigated and edited to turn viruses into precious allies for molecular biology serving as gene therapy vectors, adjuvants for the immune system, drug cargos, and, lately, anticancer therapeutics. As anticancer drug, one interesting option is viral engineering. Modification of either the viral genome or the outer shell of viruses can change infectivity and tissue targeting and add new functions to the viral particle. Remarkably, in the field of cancer virotherapy, scientists realized that a specific viral genomic depletion would turn the normal tropism of viruses to conditionally replicate in cancer cells only. This category of viruses, named 'Oncolytic viruses', have been investigated and used for cancer treatment in the past decades resulting in the approval of the first oncolytic virus, a herpes simplex virus expressing a stimulating factor, named T-Vec, in 2015. As such, oncolytic viruses achieved positive outcome but still are not able to completely eradicate the disease. This has brought the scientific community to edit those agents, adding to their ability to directly lysate cancer cells, few modifications to mainly boost their interaction with the immune system. Viruses experienced then a renaissance not only as infecting agent but as nanoparticle and cancer vaccines too. These strategies bring new life to the concept of using viruses as viral particles for therapeutic applications.

Keywords

Oncolytic viruses · Gene therapy · Viral vectors · PeptiCrad · PeptiENV · ExtraCRAd · Cancer vaccines · Adenovirus · Capsid surface modification · Peptide-loaded capsid · viRNA · siRNA

1 Introduction

Viral nanoparticles (VNPs) are naturally occurring virus-based bionanomaterial formulations that can be efficiently functionalized with various molecules or genetically engineered to contain a variety of novel properties. VNPs can be bacteriophages, plant or animal viruses, and they can be infectious or non-infectious. VNPs can be tailored for preferred applications by using bioconjugate chemistries that can be applied to link drugs or targeting ligands to the inner or outer capsid shell. Drugs and other molecules can also be encapsulated by VPNs that can be readily disassembled and reassembled. Also, VNPs can be genetically engineered allowing the introduction of precise modifications so that large quantities of identical particles with desired modifications can be manufactured [1–8]. Initially, VNPs have been used as gene delivery vectors because they can deliver foreign genetic material to the infected cell to correct or modify genetic dysfunctions [5, 9]. Some viruses, such as retroviruses, integrate their genetic material into a chromosome of the host cell. Other viruses, such as adenoviruses, introduce

M. Fusciello · E. Ylösmäki
Drug Research Program, Division of Pharmaceutical Biosciences and Digital Precision Cancer Medicine Flagship (iCAN), Faculty of Pharmacy, University of Helsinki, Helsinki, Finland

V. Cerullo (✉)
Drug Research Program, Division of Pharmaceutical Biosciences and Digital Precision Cancer Medicine Flagship (iCAN), Faculty of Pharmacy, University of Helsinki, Helsinki, Finland

Department of Molecular Medicine and Medical Biotechnology and CEINGE, Naples University Federico II, Naples, Italy
e-mail: vincenzo.cerullo@helsinki.fi

© Springer Nature Switzerland AG 2021
F. Fontana, H. A. Santos (eds.), *Bio-Nanomedicine for Cancer Therapy*, Advances in Experimental Medicine and Biology 1295, https://doi.org/10.1007/978-3-030-58174-9_14

their DNA into the nucleus of the infected cell, but the DNA is not integrated into a chromosome. Diverse VNP platforms have been developed exploiting different features of different viruses; from efficient modulation of the tumour microenvironment to vaccination, to various targeted therapies [10–13]. In addition to gene therapy applications, VNPs based on oncolytic viruses (OVs) are promising immunomodulatory agents and can be used in various cancer therapy applications including cancer vaccines. In this chapter, we will discuss oncolytic virus-based VNPs designed to function as cancer vaccines and immunomodulators of the tumour microenvironment (TME).

2 Tumour Microenvironment and Oncolytic Viruses

As normal tissues need to create interconnection with other cells and have a continuous supply of nutrients and resources, cancerous tissue needs to create a highly immunosuppressive environment to be able to survive, grow, and progress. This highly immunosuppressive niche – made of a heterogeneous set of transformed and non-transformed cells including neoplastic cancer cells, mesenchymal cells, hematopoietic cells including innate and adaptive immune cells and myeloid-derived suppressor cells – is identified as the tumour microenvironment (TME) [14]. Within this complex environment, tumours can prosper and release cytokines, chemokines, and other factors affecting the surrounding cells through an interplay between healthy and unhealthy cell subpopulations which supports tumour survival and progression. In optimal conditions, the immune system detects and eliminates malignant cells after their recognition [15]. This so-called immune surveillance is carried out by two main cell subsets responsible for the tumour clearance, that is, cytotoxic CD8$^+$ T cells (CTLs) and Natural Killer cells (NKs) belonging, respectively, to the adaptive and innate immune system [16, 17]. To exert their anti-tumoural activity, CTLs must recognize specific proteins that are produced by cancer cells called tumour-associated antigens (TAAs) or tumour-specific antigens (TSA), presented by major histocompatibility complex class I molecules (MHC-I) on the surface of tumour cells. CTLs tumouricidal activity is carried out both directly through the release of cytotoxic granules containing perforin and granzymes leading to tumour cell lysis, and indirectly through the secretion of cytokines, such as interferon-γ (IFN-γ), tumour necrosis factor-α (TNF-α), and IL-2. These cytokines induce apoptosis of tumour cells and/or further enhance the activation of anticancer immune responses. To evade immune surveillance and suppress the anticancer immune responses mentioned above, tumours are continuously creating a 'cold' immunosuppressive microenvironment with poor inflammation and poor CTL infiltration (Fig. 1). Several mechanisms are activated to foster cancer survival and spreading by unbalancing the immune surveillance: (i) tumour-resident macrophages are polarized towards the immune suppressive M2 phenotype which in turn leads to an increase in the secretion of the pro-angiogenic factor vascular endothelial growth factor (VEGF), responsible for the growth of new blood vessels, leading to more efficient transport of nutrients and oxygen to the TME. (ii) A decrease in the activity of professional APCs priming naïve T cells into specialized tumour-specific T lymphocytes. (iii) The cytokine milieu in the TME induces a decrease in the fraction of T helper type 1 cells, while increasing the number of regulatory T cells (Tregs), responsible for downregulating the immune response. (iv) Finally, the tumour-killing activity of NK cells is strongly inhibited and counterbalanced by the activation of highly immunosuppressive myeloid-derived suppressor cells (MDSCs).

Oncolytic viruses (OVs) have been shown to modulate tumour immunosuppression and revert the 'cold', immune cell deserted TME of low inflammation and poor CTL infiltration, into a 'hot' immune cell-infiltrated and inflamed TME. Cancer cell killing by OVs induce anti-tumour immunity and modulate tumour microenvironment (TME) to less immunosuppressive phenotype. OV-induced inflammation, immune cell, and cytokine infiltration into the TME enhances the immune activation towards cancer cells. OV-mediated lysis of cancer cells release TAAs, TSAs, and neoantigens that can be taken up and processed by antigen presenting cells present in the TME [18]. In addition to the release of antigens, cancer cell lysis by OVs can lead to the release of danger-associated molecular patterns (DAMPs) such as surface-exposed calreticulin (ecto-CRT), secreted adenosine triphosphate (ATP), and released high mobility group box 1 protein (HMGB1), as well as pathogen-associated molecular patterns (DAMPs), including viral components, such as viral nucleic acids, proteins, and capsid components, which in turn are recognized by innate immune cells such as dendritic cells (DCs) that become activated leading to increased recruitment and activation of tumour-specific T cells in the TME [19]. Taken together, tumour cell infection by an OV leads to an inflammatory response and localized cytokine production followed by infiltration of innate and adaptive immune cells that help repolarize the TME towards less immunosuppressive phenotype.

3 Tumour Epitope Peptide-Coated Viral Nanoparticles as Cancer Vaccines

OV-mediated release of tumour-associated antigens and neoantigens by viral oncolysis might not be enough to induce clinically relevant tumour-specific T cell responses or the induced T cell response might be too weak to induce a potent

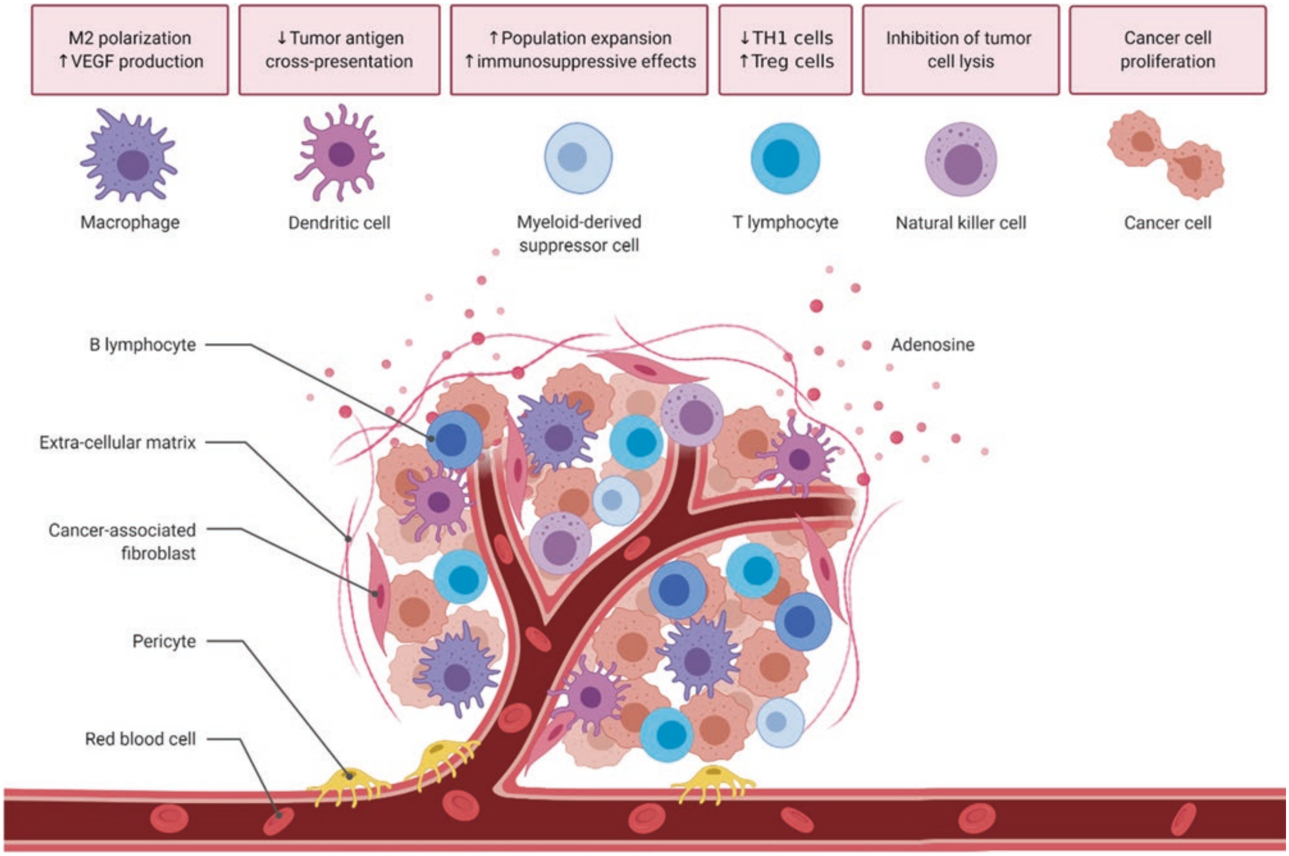
M2 polarization
↑VEGF production
↓Tumor antigen cross-presentation
↑Population expansion
↑immunosuppressive effects
↓TH1 cells
↑Treg cells
Inhibition of tumor cell lysis
Cancer cell proliferation
Macrophage
Dendritic cell
Myeloid-derived suppressor cell
T lymphocyte
Natural killer cell
Cancer cell
B lymphocyte
Extra-cellular matrix
Cancer-associated fibroblast
Pericyte
Red blood cell
Adenosine

Fig. 1 Tumour microenvironment: A schematic representation of the tumour microenvironment with different cell subtypes. Abnormal alterations are represented in the squares on top of the figure for each single cell subpopulation. Those malfunctions allow cancer cells to go undetected, proliferate, and disseminate creating new metastases

clinical response. In an attempt to induce more potent virus-induced T cell response against tumour antigens, various VNPs have been developed by coating modified, tumour antigen epitopes containing peptides onto the outer surface of various viruses [20–23]. Coating of adenovirus capsid with modified tumour epitope peptides (PeptiCRAd, see Fig. 2) has been shown to be an efficient and highly versatile approach to increase the induction of tumour-specific T cell response and enhance the therapeutic efficacy of the peptide-coated VNPs. An oncolytic adenovirus-based VNP coated with major histocompatibility complex I (MHC-I)-restricted tumour epitope derived from human melanoma was shown to induce enhanced T cell responses against this melanoma antigen in a humanized mouse model (an immunocompromised mouse model engrafted with human immune cells) of melanoma leading to a significantly enhanced therapeutic efficacy [20]. Coating of the adenovirus capsid with an MHC-I-restricted tumour epitope together with an MHC-II-restricted Pan HLA-DR reactive epitope increased the efficacy of the adenovirus therapy in weakly immunogenic tumours. This double-coated PeptiCRAd adenovirus was also shown to increase the number of responders to PD-L1 immune checkpoint inhibitor therapy [24]. The PeptiCRAd approach was also successfully used to re-engage pathogen-related CD4$^+$ memory T cell populations to support and enhance tumour-specific T cell responses by coating the adenovirus capsid with pathogen-specific MHC-II-restricted peptides together with tumour-specific MHC-I-restricted peptides [21]. The pathogen-related CD4$^+$ memory T cell populations, initially created by vaccination against tetanus toxoid (tetanus vaccine) or against polio, pertussis, and diphtheria (Polioboostrix vaccine), were readily exploited in order to elicit stronger and more effective melanoma-specific CD8$^+$ effector T cell response by the PeptiCRAd adenoviruses. This approach was also shown to significantly increase the anti-tumour efficacy of anti-PD-1 checkpoint inhibitor therapy [21]. Adenovirus capsid has a negative total charge which makes the capsid surface suitable for electrostatic adhesion of peptides. Peptides, conversely, have different charge varying from positive to negative. Positive peptides can be directly loaded on the adenovirus capsid. Negatively charged peptides will result in repulsion, if loaded as such onto the adenoviral capsid. Therefore, a chemical modification is needed to adapt them for this application. A positive amino acid sequence can be attached to the N-terminus of negatively charged peptides to change the

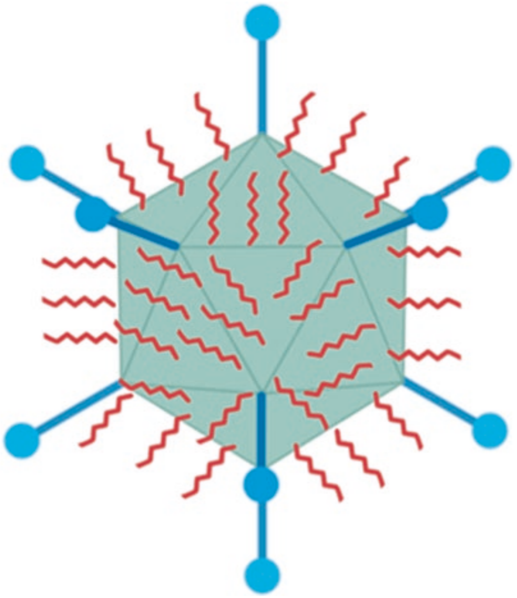

Fig. 2 Schematic representation of a PeptiCRAd Cancer Vaccine VNP Platform. Adenovirus serotype 5 (in light green) was complexed with specific tumour-associated peptides (in red). The assembly was favoured by modifying the net charge of the tumour peptides adding a sequence of six positive lysin amino acids to the sequence of the tumour peptide. The electrostatic interaction resulted in complexing a naked virus with tumour peptides creating a hybrid viral nanoparticle carrying the power of a virus mixed with tumour immunogenicity

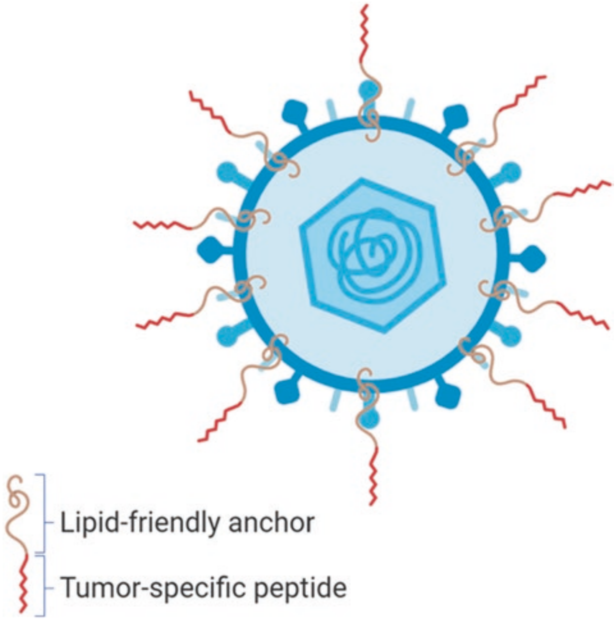

Fig. 3 Schematic representation of a PeptiENV-Cancer Vaccine VNP Platform. Human Herpes virus was loaded with tumour-associated antigens. Antigens were modified with a cell penetrating peptide (lipid friendly anchor) to allow efficient attachment onto the lipid envelop of the virus

net charge from negative to positive for efficient electrostatic interaction. A stretch of lysine residues is usually added to the peptides to create a positive overall charge which will allow the electrostatic assembly.

A very similar peptide coating approach has also been developed for VNPs based on enveloped viruses such as herpes simplex virus 1 (HSV-1) and vaccinia virus (PeptiENV, see Fig. 3) [22]. The coating of enveloped viruses with MHC-I-restricted peptides was shown to induce systemic peptide-specific T cell responses against coated peptides and in therapeutic setting; both peptide-coated HSV-1 and vaccinia virus were shown to improve peptide-specific T cell responses and anti-tumour efficacy [22]. Enveloped viruses contain host cell-derived lipid bilayer as the outer surface. VNPs can be easily engineered to contain tumour epitopes on the surface of the virus particle by adding a cell penetrating, lipid friendly, anchor sequence to the N-terminus of the tumour epitope peptides to allow for efficient coating onto the viral surface.

4 Cancer Membrane-Enveloped Viral Nanoparticles as Cancer Vaccines

The previously described approaches consist of an easy plug-and-play method to combine the power of an oncolytic virus with the reactivity of the immune system towards the tumour antigen epitope present on the viral surface. Unfortunately, the identification of such tumour antigens is very challenging at the moment, making personalized immune virotherapy difficult in absence of specific patient tumour signatures already identified and isolated. Tumour lysate and cancer membrane are a great source of tumour antigens needed by the immune system to mount and orchestrate a targeted anticancer response [25–27]. Such cancer sources alone, when lacking proper activation stimuli, might drive to tolerogenic effect making the immune system unable to spot and process tumour signatures leaving the tumours undetected [28–30]. Viruses, however, serve as great stimuli for the immune system [31]. The fusion of unknown tumour sources and viral adjuvant merged in a viral-like particle made of cancer-derived membrane carrying cancer peptides wrapped around an oncolytic Adenovirus serotype 5 (ExtraCRAd) (Fig. 4). The artificial viral particles were assembled by mechanically constraining the cancer-derived membrane around the virus through extrusion, creating an artificial envelope. In this case, the technology exploits the potent weapon of an oncolytic virus acting as a strong adjuvant supported by the repertoire of cancer antigen present on the membrane used to wrap the virus. When uptaken as such by DCs, different subsets of T cells will be primed against multiple targets allowing the immune system to generate a wider and more differentiated anti-tumoural response against the heterogeneous cancer subclones present in the neoplasia. The wrapping allowed the particle to have an enhanced

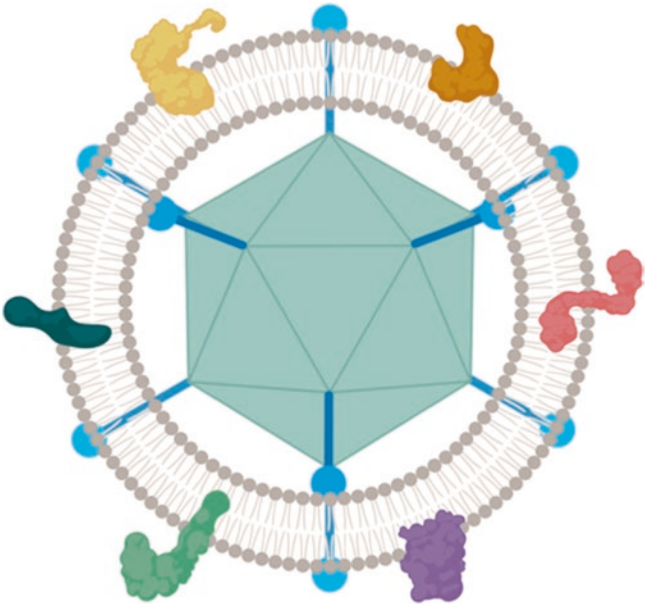

Fig. 4 Schematic representation of the ExtraCRAd Cancer Vaccine VNP Platform. An oncolytic adenovirus serotype 5 (light green) was wrapped into cancer-derived membrane (grey) carrying tumour-specific signature (yellow, green, purple, red). The membrane was mechanically wrapped around the virus with an extrusion process through a porous polycarbonate membrane

infectivity towards cancer cells bypassing the normal interaction between the virus and the host cell receptor. In addition, the artificial shield seemed to protect the virus from anti-viral neutralizing antibodies which lower the efficacy of oncolytic therapy. The platform showed positive outcome in slowing down tumour growth of several murine cancers and eliciting anti-tumoural T lymphocytes presence and activity in the TME. When used in a vaccination set up, the group treated with such platform showed a longer overall survival over the control groups.

A similar approach used on VLPs has been successfully developed with the name of SpyTag/SpyCatcher protein superglue that enables to avoid many of the challenges of binding antigens to virus-like particles [32, 33]. This technology is composed by splitting a protein from the common bacterium, Streptococcus pyogenes, into two parts. One part named SpyTag peptide is bound to antigens, while its partner protein SpyCatcher is bound to the VLP. Spontaneous conjugation will occur with subsequent formation of a strong and unbreakable covalent bond [34]. The process allows for specific assembly of antigens on VLPs to generate an optimal immune response and in addition, carries the benefit of being a plug-and-play method rapid and versatile.

Taken together the above-mentioned strategies represent a valuable and interesting approach to reverse the immune system from fighting a pathogen only, to fighting an external tread and cancer cells at the same time. Those elegant approaches benefit from the use of a pathogen as a stimulator to initiate a complete immune response against a foreign tread. Complexing tumour moieties on the virus allow double activation effect in triggering both antiviral and antitumour CD8. After being engulfed by a dendritic cell, the core virus is disassembled in its simplest structures (peptides) which will then be loaded and presented on MHC II to be recognized by antiviral lymphocytes, start their activation, initiating the hunt of similar peptides throughout the body. At the same time, cancer peptides previously loaded on the pathogen are now loaded and presented on MHC I, where they will serve instead as leading instruction for antitumour cancer cells. The speciality of this method, in addition to the double effect in fighting foreign element (virus) and self-tissue (tumour) at the same time, benefits on the extra help in activation for a more powerful ignition created by the antiviral helper cells attracted by the virus which will then serve as activator for both kind of T cells present in the lymph nodes (Fig. 5).

5 Viral Nanoparticles for Delivery of Nucleic Acids

Enveloped viruses can also act as nanocarriers for RNA-based therapeutics. The challenging in vivo delivery and the lack of adjuvanticity of RNA-based cancer therapeutics have limited the use of therapeutic RNAs. One approach to enhance the delivery of RNA-based therapeutics is to harness enveloped viruses, such as vaccinia virus, as VNP nanocarriers for therapeutic RNA molecules. RNA molecules can be attached onto the viral envelope by the use of cationic liposomes [35]. RNA molecules are first complexed with cationic lipids to obtain RNA-liposome particles. These particles are then attached to VNPs via electrostatic interactions. This approach of engineering VNPs (called viRNA platform, see Fig. 6) can be used to deliver therapeutic RNA molecules of various size and function, such as large self-replicating RNA molecules or small microRNA molecules (miRNAs), inside target cells. In addition to enabling the delivery of RNA molecules, the use of VLPs as nanocarriers can enhance the immunostimulatory properties of the therapeutic RNA.

6 Current Challenges and Future Perspectives

Nanomedicine is a growing field both for diagnosis and for therapy of several diseases. Viruses started to be considered as interesting nanoparticle tools to be used in nanomedicine for cancer immunotherapy due to their interaction with the immune system and the tumour microenvironment. Despite their controversial activity as pathogens, viruses are a great tool to overcome several clinical situations, especially

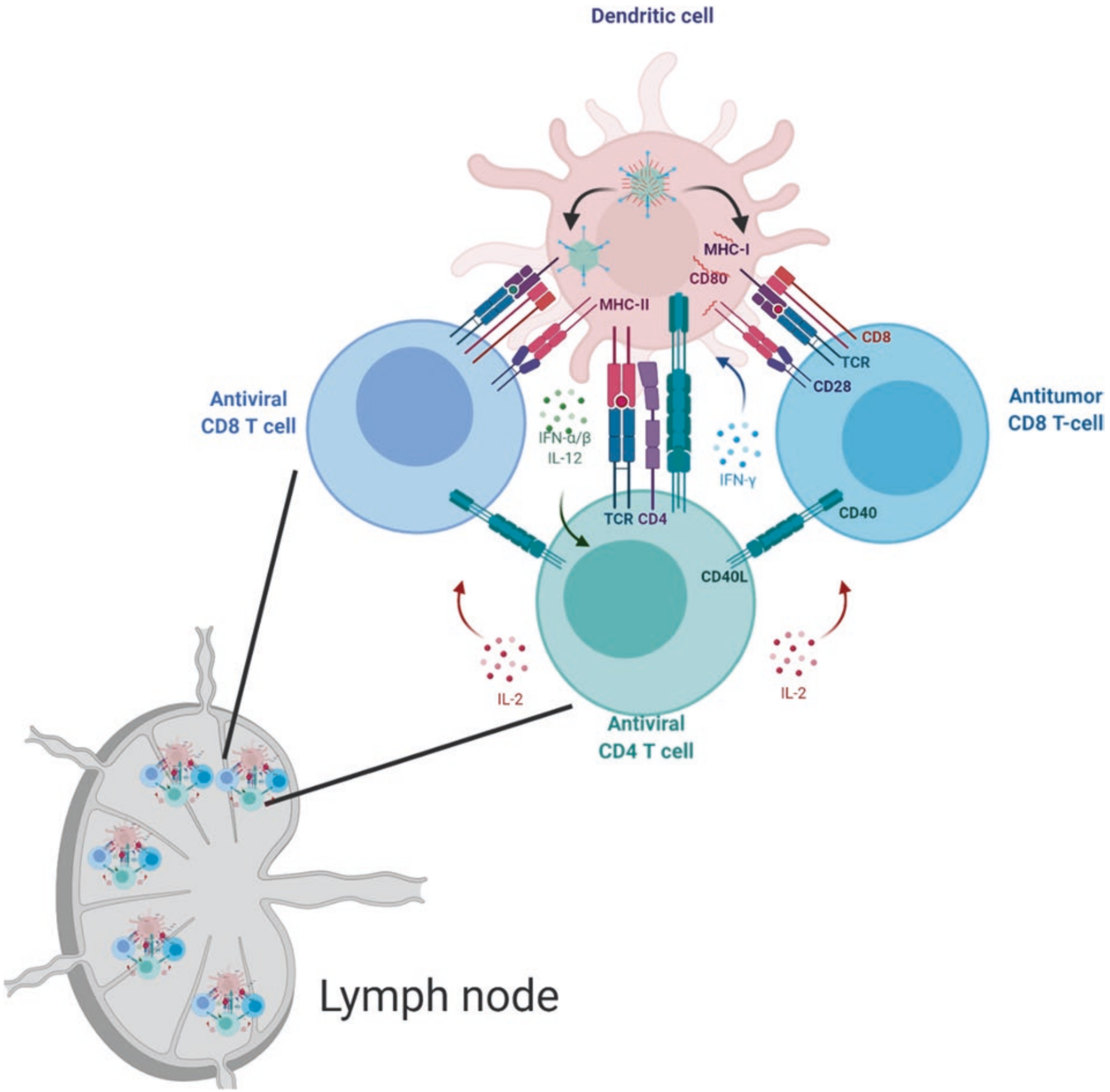

Fig. 5 Schematic representation of tumour peptide-coated viruses in lymph node. After capturing the virus, dendritic cells circulate to the near lymph node. Here they start priming naïve T lymphocytes (antiviral CD8 T-cell) to recognize the viral tread if eventually spotted in the host during patrolling. Tumour antigens instead follow a different priming mechanism and they activate anti-tumour cytotoxic lymphocytes (anti-tumour CD8 T-cell). This method benefits a more powerful activation in the response since antiviral CD4 T-cells kick in attracted by the viral tread but they empower both anti-tumour and antiviral subset as general wide spread effect

related to the immune activity. The strength of their use lays in the tissue-targeting properties, easy production and editing, and stability and storage over time. Despite their great interest, several challenges are still left to be faced. Together with the flexibility and adaptation of viral nanoparticles to several use, viral strategies suffer of major flaws when it comes to their administration and safety. Systemic administration would be the easiest procedure to reach all the organs but represents the main problem since viruses are usually up taken into the liver, displaying a toxic profile, culminating in hepatic failure [36]. In addition, patients undergoing therapies with viruses often have a pre-existing immunity against the viruses [37] or soon develop a strong adaptive one [38]. This means that a host which has encountered a pathogen in his early life has already developed a pathogen- specific response. Typically, immune response against a virus develops soon stable and long-lasting circulating antibodies deputed to neutralize viral spreading, surrounding and blocking the viral particle circulation in the blood. In addition, an early or continuous exposure to a virus results in development of specific anti-viral memory T cells promptly seeking and destroying virus infected

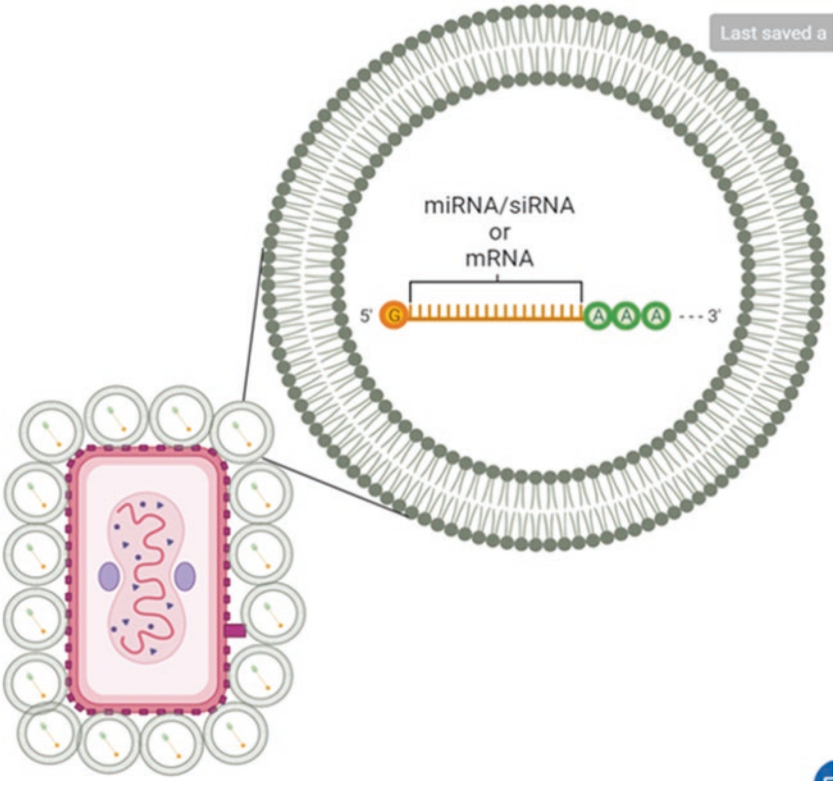

Fig. 6 Schematic representation of viRNA VNP platform. Cationic liposomes (grey) can be complexed with RNA molecules (orange) and then combined with an oncolytic vaccinia virus (light pink). This application exploits the efficient entry of the virus into the host cell simultaneously delivering the RNA molecules for targeted and precise therapeutics

cells. These constitute the challenges for systemic administration of an oncolytic virus, because as non-self agent viruses encounter antiviral neutralizing antibodies that once bond, opsonize the pathogen, lowering its action in reaching distant tissues, resulting in reduction of the therapeutic effect. For that reason, most injections are limited to in situ localized administration which relies on the accessibility of the treatment site and on the operator ability. Few ways to decrease its recognition have been investigated, mostly shielding the virus from neutralizing antibodies with lipid layers, polymers, aptamers, or modifying the capsid structure creating chimeric viruses [35, 39–43].Thus, the route of administration of viral nanoparticles results quite challenging [39, 44, 45]. Despite viral nanoparticles constitute a great opportunity for personalized medicine and customizable strategies acting at different levels, more studies on biodistribution are needed to understand the tropism of viral particles once they undergo specific modifications [46]. Overall, viruses hold a great potential as gene therapy, drug carrier, immune-stimulant, and oncolytic therapeutics. In cancer immunotherapy, the possibility to conjugate cancer-specific signatures assembled on viruses as nanoparticles sounds thrilling. This strategy opens up future application where the anti-viral properties of the immune system are reversed to anti-cancer features. The tumour-associated antigens present on the viral surfaces allow the immune system to orchestrate a specific remarkable anti-cancer response. Those platforms serve as reprogramming tools of the immune system towards cancer tissues. Unfortunately, the limitations encountered by their route of administration and the lack of available cancer peptides to be assembled on viruses make viral nanoparticles use suboptimal. Therefore, new chemical and physical modifications are needed to improve the efficacy of those tools as clinical agents. Viral nanoparticles are under a continuous development and their versatile applicability would able to be implemented in fighting a plethora of different diseases [47–49]. Nanomedicine and viruses used as nanoparticles hold a great potential for present and future disease treatment both as general strategy and as personalized targeted treatment.

References

1. Rajagopal, P., Duraiswamy, S., Sethuraman, S., Giridhara Rao, J., & Krishnan, U. M. (2018). Polymer-coated viral vectors: Hybrid nanosystems for gene therapy. *The Journal of Gene Medicine, 20*(4), e3011.
2. Ramsey, J. D., Vu, H. N., & Pack, D. W. (2010). A top-down approach for construction of hybrid polymer-virus gene delivery vectors. *Journal of Controlled Release, 144*(1), 39–45.
3. Daya, S., & Berns, K. I. (2008). Gene therapy using adeno-associated virus vectors. *Clinical Microbiology Reviews, 21*(4), 583–593.
4. Breuer, C. B., Hanlon, K. S., Natasan, J. S., Volak, A., Meliani, A., Mingozzi, F., et al. (2020). In vivo engineering of lymphocytes after systemic exosome-associated AAV delivery. *Scientific Reports, 10*(1), 4544.

5. Li, C., & Samulski, R. J. (2020). Engineering adeno-associated virus vectors for gene therapy. *Nature Reviews. Genetics, 21*(4), 255–272.
6. Steinmetz, N. F. (2010). Viral nanoparticles as platforms for next-generation therapeutics and imaging devices. *Nanomedicine, 6*(5), 634–641.
7. Grasso, S., & Santi, L. (2010). Viral nanoparticles as macromolecular devices for new therapeutic and pharmaceutical approaches. *International Journal of Physiology, Pathophysiology and Pharmacology, 2*(2), 161–178.
8. Plummer, E. M., & Manchester, M. (2011). Viral nanoparticles and virus-like particles: Platforms for contemporary vaccine design. *Wiley Interdisciplinary Reviews. Nanomedicine and Nanobiotechnology, 3*(2), 174–196.
9. Fischer, A., & Hacein-Bey-Abina, S. (2020). Gene therapy for severe combined immunodeficiencies and beyond. *The Journal of Experimental Medicine, 217*(2), e20190607.
10. Aitken, A. S., Roy, D. G., Martin, N. T., Sad, S., Bell, J. C., & Bourgeois-Daigneault, M. C. (2018). Brief communication; a heterologous oncolytic bacteria-virus prime-boost approach for anticancer vaccination in mice. *Journal of Immunotherapy, 41*(3), 125–129.
11. Lee, K. L., Twyman, R. M., Fiering, S., & Steinmetz, N. F. (2016). Virus-based nanoparticles as platform technologies for modern vaccines. *Wiley Interdisciplinary Reviews. Nanomedicine and Nanobiotechnology, 8*(4), 554–578.
12. Koudelka, K. J., Pitek, A. S., Manchester, M., & Steinmetz, N. F. (2015). Virus-based nanoparticles as versatile nanomachines. *Annual Review of Virology, 2*(1), 379–401.
13. Jeevanandam, J., Pal, K., & Danquah, M. K. (2019). Virus-like nanoparticles as a novel delivery tool in gene therapy. *Biochimie, 157*, 38–47.
14. Najafi, M., Goradel, N. H., Farhood, B., Salehi, E., Solhjoo, S., Toolee, H., et al. (2019). Tumor microenvironment: Interactions and therapy. *Journal of Cellular Physiology, 234*(5), 5700–5721.
15. Durgeau, A., Virk, Y., Corgnac, S., & Mami-Chouaib, F. (2018). Recent advances in targeting CD8 T-cell immunity for more effective cancer immunotherapy. *Frontiers in Immunology, 9*, 14.
16. Molodtsov, A., & Turk, M. J. (2018). Tissue resident CD8 memory T cell responses in cancer and autoimmunity. *Frontiers in Immunology, 9*, 2810.
17. Souza-Fonseca-Guimaraes, F., Cursons, J., & Huntington, N. D. (2019). The emergence of natural killer cells as a major target in cancer immunotherapy. *Trends in Immunology, 40*(2), 142–158.
18. Chen, D. S., & Mellman, I. (2013). Oncology meets immunology: The cancer-immunity cycle. *Immunity, 39*(1), 1–10.
19. Guo, Z. S., Liu, Z., & Bartlett, D. L. (2014). Oncolytic immunotherapy: Dying the right way is a key to eliciting potent antitumor immunity. *Frontiers in Oncology, 4*, 74.
20. Capasso, C., Hirvinen, M., Garofalo, M., Romaniuk, D., Kuryk, L., Sarvela, T., et al. (2016). Oncolytic adenoviruses coated with MHC-I tumor epitopes increase the antitumor immunity and efficacy against melanoma. *Oncoimmunology, 5*(4), e1105429.
21. Tahtinen, S., Feola, S., Capasso, C., Laustio, N., Groeneveldt, C., Ylosmaki, E. O., et al. (2020). Exploiting pre-existing immunity to enhance oncolytic cancer immunotherapy. *Cancer Research, 80*, 2575.
22. Ylosmaki, E., Malorzo, C., Capasso, C., Honkasalo, O., Fusciello, M., Martins, B., et al. (2018). Personalized cancer vaccine platform for clinically relevant oncolytic enveloped viruses. *Molecular Therapy, 26*(9), 2315–2325.
23. Fusciello, M., Fontana, F., Tahtinen, S., Capasso, C., Feola, S., Martins, B., et al. (2019). Artificially cloaked viral nanovaccine for cancer immunotherapy. *Nature Communications, 10*(1), 5747.
24. Feola, S., Capasso, C., Fusciello, M., Martins, B., Tahtinen, S., Medeot, M., et al. (2018). Oncolytic vaccines increase the response to PD-L1 blockade in immunogenic and poorly immunogenic tumors. *Oncoimmunology, 7*(8), e1457596.
25. Harris, J. C., Scully, M. A., & Day, E. S. (2019). Cancer cell membrane-coated nanoparticles for cancer management. *Cancers (Basel), 11*(12), 1836.
26. Liu, W. L., Zou, M. Z., Liu, T., Zeng, J. Y., Li, X., Yu, W. Y., et al. (2019). Cytomembrane nanovaccines show therapeutic effects by mimicking tumor cells and antigen presenting cells. *Nature Communications, 10*(1), 3199.
27. Minciacchi, V. R., You, S., Spinelli, C., Morley, S., Zandian, M., Aspuria, P. J., et al. (2015). Large oncosomes contain distinct protein cargo and represent a separate functional class of tumor-derived extracellular vesicles. *Oncotarget, 6*(13), 11327–11341.
28. Makkouk, A., & Weiner, G. J. (2015). Cancer immunotherapy and breaking immune tolerance: New approaches to an old challenge. *Cancer Research, 75*(1), 5–10.
29. Cheng, F., Gabrilovich, D., & Sotomayor, E. M. (2004). Immune tolerance in breast cancer. *Breast Disease, 20*, 93–103.
30. Barnet, M. B., Blinman, P., Cooper, W., Boyer, M. J., Kao, S., & Goodnow, C. C. (2018). Understanding immune tolerance of cancer: Re-purposing insights from fetal allografts and microbes. *BioEssays, 40*(8), e1800050.
31. Getts, D. R., Chastain, E. M., Terry, R. L., & Miller, S. D. (2013). Virus infection, antiviral immunity, and autoimmunity. *Immunological Reviews, 255*(1), 197–209.
32. Bruun, T. U. J., Andersson, A. C., Draper, S. J., & Howarth, M. (2018). Engineering a rugged Nanoscaffold to enhance plug-and-display vaccination. *ACS Nano, 12*(9), 8855–8866.
33. Zakeri, B., Fierer, J. O., Celik, E., Chittock, E. C., Schwarz-Linek, U., Moy, V. T., et al. (2012). Peptide tag forming a rapid covalent bond to a protein, through engineering a bacterial adhesin. *Proceedings of the National Academy of Sciences of the United States of America, 109*(12), E690–E697.
34. Reddington, S. C., & Howarth, M. (2015). Secrets of a covalent interaction for biomaterials and biotechnology: SpyTag and SpyCatcher. *Current Opinion in Chemical Biology, 29*, 94–99.
35. Ylosmaki, L., Polini, B., Carpi, S., Martins, B., Smertina, E., Feola, S., et al. (2019). Harnessing therapeutic viruses as a delivery vehicle for RNA-based therapy. *PLoS One, 14*(10), e0224072.
36. Adams, D. H., & Hubscher, S. G. (2006). Systemic viral infections and collateral damage in the liver. *The American Journal of Pathology, 168*(4), 1057–1059.
37. Sumida, S. M., Truitt, D. M., Lemckert, A. A., Vogels, R., Custers, J. H., Addo, M. M., et al. (2005). Neutralizing antibodies to adenovirus serotype 5 vaccine vectors are directed primarily against the adenovirus hexon protein. *Journal of Immunology, 174*(11), 7179–7185.
38. Ricca, J. M., Oseledchyk, A., Walther, T., Liu, C., Mangarin, L., Merghoub, T., et al. (2018). Pre-existing immunity to oncolytic virus potentiates its immunotherapeutic efficacy. *Molecular Therapy, 26*(4), 1008–1019.
39. Fisher, K. D., Stallwood, Y., Green, N. K., Ulbrich, K., Mautner, V., & Seymour, L. W. (2001). Polymer-coated adenovirus permits efficient retargeting and evades neutralising antibodies. *Gene Therapy, 8*(5), 341–348.
40. Muharemagic, D., Labib, M., Ghobadloo, S. M., Zamay, A. S., Bell, J. C., & Berezovski, M. V. (2012). Anti-Fab Aptamers for shielding virus from neutralizing antibodies. *Journal of the American Chemical Society, 134*(41), 17168–17177.
41. Wandtke, T., Wozniak, J., & Kopinski, P. (2015). Aptamers in diagnostics and treatment of viral infections. *Viruses-Basel, 7*(2), 751–780.

42. Zhao, N. X., Pei, S. N., Parekh, P., Salazar, E., & Zu, Y. L. (2014). Blocking interaction of viral gp120 and CD4-expressing T cells by single-stranded DNA aptamers. *The International Journal of Biochemistry & Cell Biology, 51*, 10–18.
43. Delgado, C., Francis, G. E., & Fisher, D. (1992). The uses and properties of PEG-linked proteins. *Critical Reviews in Therapeutic Drug Carrier Systems, 9*(3–4), 249–304.
44. Breitbach, C. J., Burke, J., Jonker, D., Stephenson, J., Haas, A. R., Chow, L. Q., et al. (2011). Intravenous delivery of a multi-mechanistic cancer-targeted oncolytic poxvirus in humans. *Nature, 477*(7362), 99–102.
45. Evgin, L., Acuna, S. A., Tanese de Souza, C., Marguerie, M., Lemay, C. G., Ilkow, C. S., et al. (2015). Complement inhibition prevents oncolytic vaccinia virus neutralization in immune humans and cynomolgus macaques. *Molecular Therapy, 23*(6), 1066–1076.
46. Ungerechts, G., Bossow, S., Leuchs, B., Holm, P. S., Rommelaere, J., Coffey, M., et al. (2016). Moving oncolytic viruses into the clinic: Clinical-grade production, purification, and characterization of diverse oncolytic viruses. *Molecular Therapy: Methods & Clinical Development, 3*, 16018.
47. Thomas, C. E., Ehrhardt, A., & Kay, M. A. (2003). Progress and problems with the use of viral vectors for gene therapy. *Nature Reviews. Genetics, 4*(5), 346–358.
48. Guo, Z. S., & Bartlett, D. L. (2017). Editorial of the special issue: Oncolytic viruses as a novel form of immunotherapy for Cancer. *Biomedicine, 5*(3), 52.
49. Prestwich, R. J., Harrington, K. J., Pandha, H. S., Vile, R. G., Melcher, A. A., & Errington, F. (2008). Oncolytic viruses: A novel form of immunotherapy. *Expert Review of Anticancer Therapy, 8*(10), 1581–1588.

Industrial Perspective on Immunotherapy

Sara Ravasio

Abstract

Immunotherapy has revolutionised oncology and represents a fast-growing area of new drug products in anti-cancer therapy. Patients can now benefit from an expanded landscape of treatment options for several tumour types. The value of cancer immunotherapy is well-established thanks to the clinical success following regulatory approval of several immunomodulators and cellular immunotherapies, and both the private and the public sector are investing to provide patients with improved immune-based agents and to extend the indications of already marketed products. Although recent achievements offer the best promise for successful treatment, innovators in the field of cancer immunotherapy still face many challenges toward commercialisation that could be mitigated by a smart drug development strategy.

Keywords

Immunotherapy · Industry · Tumour heterogeneity · Clinical development · Intellectual property · New indications · Resistance to treatment · CAR-T cells · Monoclonal antibody · Biomarker · Patient-centric approach

Abbreviations

Acronym	Definition
ADCC	Antibody-dependent cell-mediated cytotoxicity
AE	Adverse event
AI	Artificial intelligence
AIDS	Acquired immune deficiency syndrome
APC	Antigen-presenting cells
ATMP	Advanced therapy medicinal product
B2M	β2-microglobulin
B-ALL	B-cell precursor acute lymphoblastic leukaemia
BCMA	B-cell maturation antigen
BMS	Bristol–Myers Squibb's
CAR	Chimeric antigen receptor
CAT	Committee for Advanced Therapies
CD	Cluster of differentiation
CDC	Complement-dependent cytotoxicity
CEA	Carcinoembryonic antigen
CRISPR	Clustered Regularly Interspaced Short Palindromic Repeats
CSF1R	Colony-stimulating factor 1 receptor
ctDNA	Circulating tumour DNA
CTLA4	Cytotoxic T-lymphocyte-associated protein
DARPins	Designed ankyrin repeats
DC	Dendritic cells
DLBCL	Diffuse-large B-cell lymphoma
dMMR	Deficient mismatch repair
EBV	Epstein–Barr virus
EGFR	Epidermal growth factor receptor
EMA	European Medicines Agency
Fc	Fragment crystallisable
FDA	Food and Drug Administration
GITR	Glucocorticoid-induced TNFR-related protein
GMP	Good manufacturing practise
GPC3	Glypican-3
HBV	Hepatitis B virus
HER2	Receptor tyrosine-protein kinase erbB-2
HLA	Human leukocyte antigen
HNSCC	Head and neck squamous cell carcinoma
HPV	Human papilloma virus
HSV	Herpes simplex virus
HTA	Health technology assessment
ICI	Immune checkpoint inhibitors
ICOS	Inducible T-cell costimulator
IDO	Idoleamine-2,3 dioxygenase
IgG	Immunoglobulin G

S. Ravasio, PhD (✉)
GSK, Siena, Italy

© Springer Nature Switzerland AG 2021

F. Fontana, H. A. Santos (eds.), *Bio-Nanomedicine for Cancer Therapy*, Advances in Experimental Medicine and Biology 1295, https://doi.org/10.1007/978-3-030-58174-9_15

IL	Interleukin
INFAR	Interferon-alpha receptor
INF-γ	Interferon-γ
IP	Intellectual property
LAG3	Lymphocyte-activation gene 3
MA	Marketing authorisation
mAbs	Monoclonal antibodies
MAGE	Melanoma-associated antigen
MDSC	Myeloid-derived suppressor cells
MHC-I	Major histocompatibility complex I
MRD	Minimal residual disease
MSI	Micro satellite instability
MUC-1	Mucin 1
NGS	Next-generation sequencing
NIH	National Institutes of Health
NK	Natural killer
NSCLC	Non-small cell lung cancer
PASS	Post authorisation safety study
PD1	Programmed cell death protein 1
PDL1	Programmed cell death protein ligand 1
PGE2	Prostaglandin E2
PRO	Patient-reported outcome
PSCA	Prostate stem cell antigen
PSMA	Prostate-specific membrane antigen
PTA	Patent term adjustment
R&D	Research and development
RCC	Renal cell carcinoma
ROS	Reactive oxygen species
RSV	Respiratory syncytial virus
SME	Small- and medium-sized entrepreneurs
SPC	Supplementary protection certificate
STAT3	Signal transducer and activator of transcription 3
STING	Stimulator of interferon genes
TCR	T-cell receptor
TGF-β	Transforming growth factor beta
TIL	Tumour-infiltrating lymphocytes
TLR	Toll-like receptor
TMB	Tumour mutational burden
TME	Tumour microenvironment
TNBC	Triple-negative breast cancer
TNF	Tumour necrosis factor
Treg	T regulatory cells
TRIPS	Trade-Related Aspects of Intellectual Property Rights
USPTO	United States Patent Office
VEGF	Vascular endothelial growth factor
WT1	Wilms tumour protein
WTO	World Trade Organization

1 Introduction

1.1 What Is Cancer Immunotherapy?

Immunotherapy can be defined as a therapeutic procedure aiming to stimulate or suppress the immune system in order to fight a broad range of diseases including infections and cancer.

The idea of exploiting the individual’s immune system to fight disease dates back to the last centuries and it has been widely explored in the field of vaccination. However, before the formal proof of concept that cytotoxic responses could be redirected to destroy malignant tissues, the application of immune-based therapeutic agents to the field of cancer has lagged behind other therapeutic options, such as chemotherapy and radiotherapy.

In this scenario, the description of the durable responses in metastatic melanoma elicited by Ipilimumab (a blocking antibody binding to the checkpoint inhibitor cytotoxic T-lymphocyte-associated protein – CTLA-4) [1] and the efficacy of a monoclonal antibody binding to the checkpoint inhibitor programmed cell death protein 1 (PD-1) [2] represented the dawn of a new era in the treatment of cancer.

The above-mentioned unanticipated clinical observations revealed that, by targeting the so-called checkpoint inhibitors, it was possible to reinvigorate the inherent ability of the host’s immune system to efficiently eradicate cancer. Based on these findings, “Yervoy” (Ipilimumab), developed by Bristol–Myers Squibb, was the first cancer immunotherapeutic agent receiving regulatory approval in the United States. It was soon followed by “Opdivo” (Nivolumab), an anti-PD-1 monoclonal antibody, developed by Ono Pharmaceutical, which received regulatory approval in Japan and later by in the United States.

The discovery of immunostimulatory monoclonal antibodies (mAbs) [3] was more recently followed by the description of adoptive T-cell therapy, which was pioneered by Steven Rosenberg [4], Zelig Eshhar [5], Carl June and Michel Sadelain. Globally, these approaches triggered a revolution of the paradigms of clinical cancer management. Since then, cancer immunotherapy has emerged as a clinically beneficial alternative to conventional treatments for a variety of oncologic malignancies, including melanoma [1, 6, 7], hematologic malignancies – such as refractory Hodgkin lymphoma – [8] non-small cell lung cancer (NSCLC), ovarian cancer [9], prostate cancer, kidney cancer, bladder cancer [10], head and neck squamous cell carcinoma (HNSCC) [11], and renal cell cancer (RCC) [12]. This is acknowledged by the numerous U.S. Food and Drug Administration (FDA) and European Medicines Agency (EMA) approvals of new therapeutic entities and by the rapid expansion for existing agents [13].

Notwithstanding the ground-breaking effect of the emerging field of cancer immunotherapeutic agents on patients care, it should be noted that the seminal discoveries at the basis of cancer immunotherapy date back more than 25 years ago. The route from bench to bedside of the first wave of cancer immune-based agents, such as Ipilimumab, followed drug discovery and development timelines similar to those of canonical drug entites [14].

Indeed, the discovery of the immune checkpoint inhibitor PD-1 dates back to the seminal observations of Dr. Tasuko Honjo at Kyoto University in 1992, whereas the checkpoint inhibitor CTLA-4 was discovered in 1994 by Dr. James P. Allison, through his work at the University of California Berkeley and Memorial Sloan Kettering Cancer Center in New York. The major impact of these discoveries and, in general, of the emerging field of cancer immunotherapy has been acknowledged by the award of the Nobel prize for physiology or medicine in 2018 [15] to Allison for the discovery of CTLA-4 [16] and to Honjo for the discovery of programmed cell death protein 1/programmed cell death protein ligand 1 (PD-1/PD-L1) [17].

The launch of a first generation of cancer immunotherapies based on the pioneering discoveries of Honjo, Allison, and other researchers, including Lieping Chen and Gordon Freeman, is thus a success story of translation of basic science research into clinical treatment. Since then, there has been a tendency toward shortening the clinical development and approval process of cancer immune-based agents [14].

2 How Does Cancer Immunotherapy Work?

The seminal discoveries by Honjo and Allison revealed that interfering with the regulatory mechanisms of the immune system can prove fundamental to treat cancer. In order to fully understand the broad clinical activity, the durable response rates and the distinct characteristics of immune-based agents, it is thus fundamental to provide a detailed explanation of the immunological circuits which they rely on. This analysis is of crucial importance to appreciate the factors that differentiate cancer immunotherapy from traditional cytotoxic or targeted therapies.

Similarly to what is described in the context of immunisation, different immunotherapeutic strategies are available, which comprise passive and active approaches. Passive cancer immunotherapy consists of enhancing existing immune response to tumour cells, while active immunotherapy, by interfering with precise regulatory circuits, directs immune cells to attack tumour cells.

In order to fully comprehend the mechanism of action of immune-based agents, it is crucial to familiarise with a pillar of the adaptive immune response, that is, the concept of self/non-self-discrimination. The discrimination of self/non-self proceeds thanks to the selective recognition of antigenic peptides displayed on the cells' surface bound to major histocompatibility complex I (MHC-I). Antigen recognition occurs via the T-cell receptor (TCR) of Cluster of Differentiation-8+ (CD8)+ T lymphocytes. CD8+T lymphocytes, together with natural killer (NK) cells, are endowed with the ability to kill sister cells as a mechanism of defence for eradicating or controlling intracellular pathogens and tumours.

During their development and maturation, T cells are selected in order to be able to recognise foreign antigens and become able to perform immune-mediated surveillance of the host. Thus, the repertoire of self-reactive TCRs is general very low, although the escape of self-reactive TCRs is associated with autoimmune disorders such as type 1 diabetes and multiple sclerosis.

However, in order to ensure that a targeted immune response is mounted selectively against foreign antigens, the adaptive immune system also developed an additional regulatory circuit, that is representeed by the requirement of a second positive signal in addition to TCR triggering. This concept represents the core of current immunotherapy and is generally referred to as co-stimulation.

T-cell co-stimulation needs to be analysed as a "social" phenomenon that occurs in a complex inter-cellular and receptor-dense environment. Regulatory circuits of the immune system comprise a plethora of molecular and cellular actors [18, 19], including but not limited to T regulatory cells (Treg), checkpoint inhibitors, immunomodulatory cytokines, such as Interleukin-10 (IL-10). These mechanisms have evolved to counterbalance activation stimuli that, if not restrained, could lead to deleterious, mis-targeted immune responses.

It should be noted that lack of proper stimulatory signals may lead to T-cell anergy and T-cell exhaustion. These represent a state of T-cell dysfunction that is typical of many chronic infections and cancer, characterised by poor effector function, sustained expression of inhibitory receptors and a transcriptional state distinct from that of functional effector or memory T cells [20]. The ultimate outcome of this form of T-cell dysfunction is the inability of the adaptive immune system to eradicate an infection or a tumour.

Positive co-stimulation occurs thanks to the fine-tuned action of several receptors expressed on the surface of T cells and antigen-presenting cells (APCs). Binding of CD40 on the surface of APCs to CD40L (CD154) on the T-cell surface stimulates the expression of CD28 and B7 (either B7.1 or

B7.2) by the T cell and APC, respectively. Interaction between CD28 and B7 (mainly CD80 and CD86) is the "second signal" required for efficient T-cell activation and survival.

CD28-B7 binding is also crucial to regulate the intensity of the T-cell response, as it stimulates CTLA-4 (CD152) expression on the T-cell surface. Indeed, CTLA-4 is the competitor of CD28 and its engagement to B7 – which is characterised by a considerably higher affinity compared to CD28–B7 interaction – fully suppresses T-cell response. It is clear that the balance between the contrasting signals triggered by CD28 and CTLA-4 is crucial to fine-tune adaptive immune responses [21].

Accordingly, blocking CTLA-4 with an anti-CTLA-4 antibody such as the above-mentioned Ipilimumab allows efficient interaction between B7 and CD28, thus reinvigorating T-cell responses. It should be noted CTLA-4 is a valuable target also for the treatment of autoimmune disorders, where suppression of CD28-mediated immune responses is pursued; a CTLA-4-immunoglobulin (Ig) fusion protein, named Atabacept, has been successfully employed to interrupt CD28-B7.2 interaction. Actively binding B7-2 with a CTLA-4-Ig fusion protein, like Abatacept, interrupts the interplay between CD28 and B7-2 and thus suppresses CD28-mediated T-cell activation.

Additional regulatory circuits involve T-cell-expressed receptors, such as ICOS (inducible T-cell co-stimulator) and PD-1. PD-1 (PDCD1 or CD279) is expressed on activated T cells, while the expression of its ligand PD-L1 is limited to epithelial and endothelial cells in homeostasis. PD-1/PD-L1 interaction dampens T-cell activation thus protecting PD-L1+ cells. As several cancer cell lineages evolve to escape immune responses by expressing PD-L1, it is straightforward that the use of anti-PD-1 antibodies – such as nivolumab and pembrolizumab – and anti-PD-L1 antibodies – such as atezolizumab, avelumab and durvalumab – can interfere with PD-1/PD-L1 binding and thus sustain T-cell responses.

It is clear that, while cancer cells evolve to take advantage of – and even hijack – the regulatory mechanisms that ensure the safeguard of self tissues, cancer immunotherapy intervenes by releasing inhibitory checkpoints to favour anti-tumour cytotoxic responses [22].

Immune-based agents may be classified as "passive" and "active" based on their ability to engage the host immune system. However, this classification should be applied with a certain degree of plasticity due to the complexity of the drug–host–tumour interaction [23]. In this context, it is widely accepted that the immune checkpoint inhibitors described beforehand represent the archetype of active immunotherapy. Conversely, adoptive T-cell therapies may be classified as passive cancer immunotherapy. It should be noted that passive agents (including tumour-targeting mAbs) often rely on the host immune system in order to achieve their anticancer activity and may de facto constitute active forms of immunotherapy [23].

The development of therapeutic vaccines targeting tumour antigens to arrest cancer progression and preventing recurrence, an example of active immunotherapy, has delivered very little to clinical practise so far [24, 25]. Conversely, adoptive T-cell therapies – exploiting either tumour-infiltrating lymphocytes (TIL) or chimeric antigen receptor (CAR) T cells – have shown remarkable potential.

Isolation and *ex vivo* culture of autologous TILs, followed by perfusion with exogenous IL-2 to patients that are rendered lymphopenic by suitable preconditioning regimens have shown outstanding durable responses [26]. TILs, which are isolated from autologous tumour tissue or from draining lymph nodes, are able to recognise tumour antigens though their native TCR; this allows a broader reactogenicity, which is not restricted to a single human leukocyte antigen (HLA) haplotype and thus prevents unexpected off-target toxicity [27]. Current preclinical and clinical evidences suggest that TILs infiltration could be amenable to broad clinical application.

Alternatively, by genetic manipulation of autologous T cells giving rise to CAR T cells, it is possible to redirect cytotoxic responses to any tumour antigen. Re-infusion of CAR T cells is generally preceded by lympho-depleting chemotherapy to allow *in vivo* expansion of the infused CAR T cells. Engineered CARs encompass a transmembrane receptor, usually consisting of a single-chain antibody domain and intracellular signalling domains. CAR T cells including an anti-CD19 antibody domain and the intracellular signalling domains of CD3ζ, together with additional signalling domains, such as the ones of CD137 or CD28, are able to develop cytotoxic responses toward a target cell population expressing CD19, consisting of B lymphocytes.

Tisagen-lecleucel and axicabtagen-ciloleucel have received FDA approval in 2017 and EMA approval in 2018 for the treatment of relapsed or refractory paediatric B-cell precursor acute lymphoblastic leukaemia (B-ALL) and adult diffuse-large B cell lymphoma (DLBCL) [28, 29]. Importantly, "real-world" CAR T-cell therapy efficacy has been confirmed by independent evaluation by several academic research centres in the United States, supporting remarkable clinical benefit [30].

3 The Value of Cancer Immunotherapy

The cost of cancer care represents one of the fastest growing areas of healthcare-related spending in the United States [31] and globally. It is estimated that due to increased demand for oncology care by an aging population, prolonged survival of cancer patients and changes in oncology practise pattern incorporating newer, more sophisticated treatment options, the total cost of cancer care is going to exceed $175 billion after 2020 [32].

The introduction of cancer immunotherapy to current oncology practise had a profound and multi-level impact on cancer-related expenditure and still represents a revolution for the current value models.

Indeed, the value of a pharmaceutical product needs to be assessed not only from the scientific and clinical standpoint but also from an economic perspective, in a similar way as the health technology assessment (HTA) is evaluated. This means that the social, economic, organisational, and ethical issues of a health intervention or health technology need to be analysed. Specifically, the value of cancer immunotherapy should be evaluated considering its effect on mortality and morbidity, on the patients' quality of life, on the potential reductions in the use of other healthcare interventions and on the cost of the intervention itself [31]. All of these factors present an undeniable economic effect.

As detailed in the previous sections, immune-based agents stimulate cancer eradication through the activation of a pluripotent immune system rather than by inhibiting individual molecular pathways. This, in addition to immunological memory, is associated with long-term benefit in a proportion of patients, some of which can be cured of metastatic disease.

Existing frameworks of value evaluation still fail to capture the positive effects of immunotherapy on a patient's quality of life. Crucial aspects in favour of the value of cancer immunotherapy are the long-term treatment-free survival following treatment with immunotherapy, resulting in dramatic improvements of the patients, as well as that of their family and communities lives, including their returning to productive work. These effects can often be recorded through patient-reported metrics of health. It is also worth noticing that responders to immunotherapy do not need additional subsequent treatment. Additionally, compared to alternative oncologic treatments, the rates and severity of adverse events (AE) are significantly lower [7, 33]. If correctly managed, these AEs can be resolved in few weeks with immunomodulating agents, such as corticosteroid treatment, without interfering either with therapeutic activity or with the patient's wellbeing [31].

Based on these evidences, the value of cancer treatment with immune-based agents should be evaluated in view of anticipated savings in the future accompanied by a dramatic improvement of the quality of life of oncologic patients [31, 34].

Reconciling the reward to innovators who bring new drugs to the market in a field where research and development presents unique challenges needs to be considered side by side to the unique clinical benefits and the "value of hope" offered by cancer immunotherapy. In this context, a patient-centric model is required to negotiate with payers the value of immunotherapy keeping in mind the inherent challenges related to the complexity of the current healthcare fiscal environment and the resulting call for sustainability.

4 The Current Landscape of Cancer Immunotherapy

A landscape analysis of the most recent clinical trials, publications, and patents in the field of cancer immunotherapy reveals an overall growth in this area, which is still characterised by a significant lag time between academic discoveries and industrial applications [35], wherein academic centres lead in target identification, target validation, and early-phase clinical trials, often with sponsorship from the National Institutes of Health (NIH); nonetheless, the last two decades have seen a substantial increase in the involvement of industrial partners, whose expertise can contribute to scale-up for clinical delivery [36, 37].

The same analysis can illustrate a topographical localisation of R&D focusing on immunotherapy, revealing that the field is predominantly US-centric, with more than 70% of the relevant patents of the field granted to US applicants. However, more recently China is also emerging not only as a lead market but also in the clinical landscape, due to the higher number of clinical trials, especially in the CAR T-cell space [30, 36]. The reduced number of CAR T-cells trials in the European Union should be addressed by the scientific community and by local healthcare policy makers [30, 38].

As it was previously described, the term cancer immunotherapy encompasses a wide range of different therapeutic agents. Currently, the most widely exploited agents are immune checkpoint inhibitors (ICI), antibodies or fusion proteins evoking antibody-dependent cell-mediated cytotoxicity (ADCC) or complement-dependent cytotoxicity (CDC), often with modifications within the antibody's Fragment crystallisable (Fc) – the portion of the antibody responsible for effector functions – bispecific antibodies or fusion proteins, cytokines, adjuvants, NK cells, dendritic cells, TILs and CAR-T cells [39].

Checkpoint inhibitor, cytokines and adjuvants can be generally defined as immunomodulators. At least one representative of each of these drug products has received regulatory approval by the FDA (Table 1), mostly for advanced or treatment-resistant cancers, although immunomodulators' approval as first-line options is emerging.

Checkpoint inhibitors are by far the most widely represented class of agents. They are generally conventional antibodies, although antibody-drug conjugates and bi- or tri-specific antibodies are emerging as a second generation of immune checkpoint inhibitors. Of note, based on market records, checkpoint inhibitors mAbs are now competing with the previous generation of mAbs, some of which have dominated the scenes from 2000 onward, such as adalim-

Table 1 FDA-approved immunomodulators. Checkpoint inhibitors, cytokines and adjuvant are listed. Immunoglobulin G (IgG), interferon-alpha receptor (INFAR), Toll-like receptor (TLR)

Checkpoint Inhibitors		
Atezolizumab	"Tecentriq"	Anti-PD-L1, IgG1
Avelumab	"Bavencio"	Anti-PD-L1, IgG1
Cemiplimab	"Libtayo"	Anti-PD-1, IgG4
Durvalumab	"Imfinzi"	Anti-PD-L1, IgG1
Ipilimumab	"Yervoy"	Anti-CTLA-4, IgG1
Nivolumab	"Opdivo"	Anti-PD-1, IgG4
Pembrolizumab	"Keytruda"	Anti-PD-1, IgG4
Cytokines		
Aldesleukin	"Proleukin"	Genetically modified IL-2
Interferon alpha-2a	"Roferon-A"	Agonist of IFNAR1/2 pathway
Interferon alfa-2b	"Intron A"	Agonist of IFNAR1/2 pathway
Peginterferon alfa-2b	"Sylatron", "PEG-Intron"	Agonist of IFNAR1 pathway
Adjuvants		
Poly ICLC	"Hiltonol"	TLR ligand

Table 2 FDA-approved CAR T-cell therapies

CAR-T cells		
Axicabtagene ciloleucel	"Yescarta"	Anti-CD19
Tisagenlecleucel	"Kyrmriah"	Anti-CD19

umab (anti-tumor necrosis factor (TNF)) "Humira" and infliximab (anti-TNF) "Remicade", "Remsima", "Inflectra", rituximab (anti-CD20) "Rituxan", "MabThera", bevacizumab (anti-Vascular endothelial growth factor (VEGF)-A) "Avastin", trastuzumab (anti-HER-2/neu) "Herceptin", or palivizumab (anti-respiratory syncytial virus (RSV)) "Synagis" [40].

The main target that has been explored so far is PD-1, but immunomodulators under evaluation in clinical settings include agents directed to several immunological pathways. Pharmaceuticals targeting chemokine receptors aimed at promoting migration and recruitment of immune cells (e.g. CXCR4) or agents activating co-stimulatory pathways, such as CD40, OX40, ICOS and CD137, hold great promise. In parallel, therapeutic agents blocking immune cells suppression, such as CD73, Lymphocyte-activation gene 3 (LAG3), idoleamine-2,3 dioxygenase (IDO) and glucocorticoid-induced TNFR-related protein (GITR), are currently under clinical evaluation. An alternative approach aims to target CD47, a "don't eat me signal" on tumour cells to promote immune-mediated cancer cells clearance. As a second generation of anti-cancer adjuvants, alternative Toll-like receptors (TLRs) and stimulator of interferon genes (STING) ligands are undergoing clinical evaluation, together with agonist of the signal transducer and activator of transcription 3 (STAT3) pathway.

In parallel to the evaluation of additional targets, a further stream of preclinical and clinical research is focused not only on improving the structural and functional features of already available immune-based agents but also to develop structural alternatives thereof. This is evident from the structural modifications to the Fc portion of checkpoint inhibitor mAbs, such as atezolizumab, durvalumab, wherein the Fc was engineered to avoid ADCC. Moreover, as it is apparent from the list of approved checkpoint inhibitors (Table 1), which are characterised by a different antibody isotype, also the evaluation of the natural functional features of different antibody isotypes may prove valuable to fine-tune the desired therapeutic activity. Furthermore, the design of antibody mimetics, such as designed ankyrin repeats (DARPins) [41], Affibodies, and Anticalins, could provide therapeutic agents with improved characteristics.

Among immunomodulators, Interferon alpha-2b has received FDA approval as adjuvant therapy for patients with high risk of melanoma recurrence, paving the way for additional approvals for cancer immunoprevention [42, 43]. A parallel preventive approach, although effective only in specific cancer types, is represented by preventive vaccines directed to viruses characterised by an oncogenic potential, namely Human Papilloma Virus (HPV), such as "Cervarix" and "Gardasil", and Hepatitis B Virus (HBV) such as "HEPLISAV-B". Therapeutic vaccines are still lagging behind prophylactic vaccines: only Sipuleucel-T ("Provenge"), a vaccine composed of autologous stimulated dendritic cells, has received regulatory approval for prostate cancer.

Following the breakthrough approval of the first two CAR T-cell targeting CD19-expressing B cells (Table 2), the "adoptive therapy" landscape is characterised by substantial clinical research aiming to extend the available targets. Further strategies under investigation to treat B cells malignancies involve targeting of CD22, CD30, CD33, CD123 (also known as IL-3R), B-cell maturation antigen (BCMA), and Epstein–Barr virus (EBV)-related antigens. Alternatively, currently investigated adoptive therapies are directed to different haematological and solid malignancies. In one approach, antigens expressed only in cancer cells are targeted, such as carcinoembryonic antigen (CEA), melanoma-associated antigen (MAGE), cancer/testis antigen 1 also known as LAGE2, LAGE2B or NY-ESO-1, and tyrosine-protein kinase transmembrane receptor ROR1. Alternatively, antigens overexpressed by malignant cells are targeted, such as epidermal growth factor receptor (EGFR), the disialoganglioside GD2, glypican-3 (GPC3), receptor tyrosine-protein kinase erbB-2 (HER2), mesothelin, mucin 1 (MUC-1), prostate stem cell antigen (PSCA), prostate-specific membrane antigen (PSMA) and Wilms tumour protein (WT1).

FDA-approved oncolytic therapy treatment options are so far restricted to T-VEC ("Imlygic"), a modified Herpes simplex virus (HSV) that infects tumour cells and promotes their destruction. Current preclinical and clinical research is focused on evaluating additional virus platform that could be applied to anti-cancer therapies, including Adenovirus, Reovirus and Picornavirus. Remarkably, although the potential of oncolytic virus technology has been explored early in time, the low number of patents in the field suggest that the development of this technology has been slower compared to other subfields of cancer immunotherapy [35]. A similar trend can be observed for cellular vaccines, whose clinical trials had been widely sponsored by industries until 2012. Since 2013, cellular vaccines trials have significantly declined, coinciding with an increased interest to CAR T cells [36].

5 Current Trends

The most promising developments of the fast-evolving field of cancer immunotherapy that will be dealt in detail in the following section are the present focus on combinational therapy aimed at providing synergistic anti-tumour effects, the expansion of current immune-based therapies to new therapeutic indications and the identification of predictive and prognostic biomarkers. A comprehensive overview of additional advances, including the discovery of new checkpoint inhibitors and immunosuppressive mechanisms [44], progresses in the field of T-cell trafficking to tumours [45] and the characterisation of non-synonymous mutations giving rise to neoantigens [46] is provided elsewhere [25].

5.1 Combination Therapy

It is acknowledged that treatments targeting a single molecular cancer pathway have only limited efficacy in most cancers. The results obtained with such a reductionist approach can be significantly improved by administering drug combinations that target multiple mutations and cancer pathways [43, 47].

Combination therapy is thus arising as a new land of opportunities in oncology for multiple reasons. First, the activity of different agents acting on different cellular and molecular targets, potentially with a synergistic effect, is often significantly higher compared to the single agents per se. In parallel, combination therapy can reduce the duration of the treatment, thus limiting the insurgence of treatment-resistant cancer clones and, importantly, reducing the costs and AEs associated with treatment. Additionally, it has been estimated that immunotherapy combinations may actually be less expensive than single agents if they work faster [25].

The idea of combining different immune-based agents arose soon after it was evident that checkpoint inhibitors PD-1 and CTLA-4 use slightly different mechanisms of action; the combination of the first-generation cancer immunotherapies targeting those receptors showed remarkable synergistic anti-tumour effects and has been investigated by more than 250 clinical trials so far [48]. Considering that several immunomodulatory agents have received regulatory approval and the resulting almost infinite number of combinatorial treatment regimens [30], careful preclinical and early-clinical assessment should be performed before clinical testing to avoid the selection of a combination of agents showing antagonistic effect [49] or having positive effects at the expense of safety concerns [7, 50, 51]. Simultaneous targeting of multiple pathways including CTLA-4, PD-1/PD-L1 blockade, transforming growth factor beta (TGF-β), CD40 and ICOS is expected to bring promising clinical results [30] and is generally perceived as the most potent engine for oncology progress [25, 52, 53].

Most frequently, the combined immune-based agent are branded products marketed by different pharmaceutical companies. Agreements aimed at the joint-development of combination therapies may present several advantages. On the one hand, patients can benefit from new therapeutic options undergoing clinical trials and becoming available in due course; on the other hand, the output of R&D pipelines can be maximised.

Not only can immune-based agents be combined between themselves but even combination with standard of care therapies, such as chemotherapy and radiotherapy, have been showing outstanding clinical efficacy. In general, successful combination regimen relies on the use of checkpoint inhibitors and co-stimulatory agents of various nature, provided that a baseline immune response towards tumour neoantigens is present [46]. Several exogenous strategies, such as vaccination and adoptive T-cell transfer, may be employed to create a baseline anti-tumour response [25], which can be supported by several means. Possible combination strategies are focusing on removal of inhibitory signals, by means of acting on checkpoint inhibitors or depleting Tregs, and supply of costimulatory signals, such as by blockade of CD137, CD40 and OX40, together with the manipulation of the tumour microenvironment, for instance, by interfering with TGF-β and by IDO inhibition [25].

In this regard, chemotherapy and radiotherapy were known to exert their antineoplastic effect by triggering TLR4-mediated activation of the innate immune system due to apoptotic cancer cell death [54]. This in turn activates the T-cell compartment of the adaptive immune system, resulting in enhanced anti-tumour responses. To-date immunological effects of chemotherapeutic agents, such as platinum-based drugs, are widely appreciated and the efficacy of therapeutic schemes combining chemotherapy with PD-1/PD-L1 blockade is under evaluation in more than 170 clinical trials in several cancer entities [30, 48].

Radiotherapy has also emerged as a valuable partner for immunotherapy since the description of immune-mediated inhibition of distant lesions following ionising radiation, a phenomenon known as abscopal effect [55]. This phenomenon relies on the amplification of immunostimulatory interferon-γ (INF-γ) -mediated responses that are orchestrated by tumour infiltrating dendritic cells (DC), a professional APC type, upon sensing of tumour DNA [56, 57].

As mentioned previously, responses to immunotherapy are mainly dictated by the pre-existing extent of anti-tumour responses; an additional aspect is the extent of TILs infiltration in the malignant tissue. Technological progress in the precise delivery of radiotherapy is allowing to further appreciate how inflammatory signals associated with various cell death pathways triggered by radiation can possibly convert the tumour into an *in situ* vaccine and promote the regression of metastases outside the field of irradiation, as defined by the abscopal effect [25].

Although the scientific community considers the combination of radiotherapy and PD-1/PD-L1 blockade promising, some negative results have been reported, suggesting that the specific therapeutic interventions, dosage regimens and trials design should be carefully evaluated [30].

5.2 New Indications

Recent studies have suggested that the efficacy of checkpoint inhibitors is not dictated by the specific tumour entity but by the high mutational load due to the presence of mutational defects in the DNA mismatch repair machinery, a condition that is known as micro satellite instability (MSI) [58]. This finding is not surprising considering the mechanism of action of checkpoint inhibitors. Indeed, the higher the mutational load, the higher the presentation of neo-antigens via MHC-I molecules, which would intrinsically result in improved recognition by the CD8+ T cells reinvigorated by checkpoint inhibition. Based on this observation, numerous clinical trials are currently investigating the use of checkpoint inhibitors in different cancer entities.

Conversely, a reduced efficacy is expected against tumour entities which do not express neoantigens or do not express MHC-I molecules – a known mechanism of evasion – as they could not be targeted by T cells despite substantive stimulation [30]. Intriguingly, there is preliminary clinical evidence that also tumour entities characterised by low mutational burden, such as breast cancer, could benefit from treatment with checkpoint inhibitors. As of exemplification, treatment of naïve patients affected by metastatic, triple-negative breast cancer (TNBC) with atezolizumab (anti-PD-L1) in combination with nab-paclitaxel has excitingly shown remarkable efficacy in a phase III trial [59]. Following on this observation, a considerable number of TNBC clinical trials based on targeted immunotherapy have been registered on *clinicaltrials.gov*.

On the other hand, the possibility to expand CAR T-cell therapy horizons to different tumour entities is limited by the ligand that constitutes the extracellular domain allowing targeting of target malignant cells. It is straightforward that targeting novel cancer entities requires significant R&D efforts, whereas the application of fully developed CAR T-cell agents to diverse malignancies of the same cell type could be easier. For example, putatively all B-cell malignancies can be targeted by CAR T employing CD19 as targeting ligand. Indeed, the success of CAR T cells in ALL and DLBCL triggered to the initiation of follow-up trials in these disease entities; clinical trials directed to chronic lymphocytic leukaemia, multiple myeloma and gastrointestinal cancers are also underway. However, as it was detailed in the previous sections, the intrinsic sophisticated complexity of the CAR T-cell technology results into fundamental challenges when aiming to extend its therapeutic indications.

It should be noticed that a new field of therapeutic indication is opening for checkpoint inhibitors, whose application was restricted by standard oncology care to advanced tumour stages, usually consisting of metastatic stage tumours. Remarkably, it is more and more appreciated that improved efficacy is associated with a low tumour burden upon treatment initiation [60]. Thus, treatment with immune-based agent after surgery, a clinical practise known as peri-operative use, is emerging as a promising treatment option.

A similar approach is known as neo-adjuvant therapy and is directed to prime systemic immunity towards tumour antigens (i.e. before primary treatment) aiming to promote long-term tumour surveillance after complete resection of the tumour. This application needs to take into account a correctly orchestrated treatment regimen to allow T cell priming by APCs when neoantigens would still be present [61].

However, it should be reported that several controversial observations were described regarding the application of adjuvant and neo-adjuvant therapy. The FDA approved adjuvant treatment with Ipilimumab for melanoma patients after tumour resection despite the high frequency of reported AEs [62–64]; contrariwise, the EMA approved nivolumab for the same indication, given the lower occurrence of reported AEs [65]. This concept is supported by recent translational findings from an early clinical study in patients with resectable melanoma: in a randomised phase Ib study, neoadjuvant treatment with nivolumab and ipilimumab induced a higher number of tumour-specific T-cell clones than adjuvant treatment [66]. These promising observations, further fuelled by the correlation between improved efficacy of neo-adjuvant therapy and the presence of MSI, are possibly at the basis of the current increase in trials comprising neo-adjuvant treatment with immune-based agents [30]. Despite the current landscape, the previous scepticism towards such treatments should be carefully considered, stimulating investigators to wisely select patients who may benefit from neo-adjuvant treatment based on specific knowledge-based biomarkers, such as minimal residual disease (MRD) by circulating tumour DNA (ctDNA) [30].

5.3 Identification of Predictive and Companion Biomarkers

A major challenge in cancer immunotherapy is the ability to predict efficacy of a given treatment in different patients, given the intrinsic intra- and inter-tumour heterogeneity and variability.

A new frontier of cancer immunotherapy, aiming to maximise the efficacy of the treatment, is the identification of biomarkers. Clinical biomarkers may have diagnostic, predictive, prognostic, or pharmacogenomic value. They could allow a better stratification of patients, classify responders and non-responders, predict outcome and identify patients more likely to develop AEs. Clinically relevant biomarkers support medical decisions and promote a personalised application of immune-based therapeutic schemes, hopefully resulting into increased level of therapeutic successes and reduced side effects.

It should be noted that practical considerations accompany a sound biological rationale for the sake of a broad application of a given clinical biomarker, such as the applicability of the proposed analytical methodologies. This is one of the reasons underlying the fact that to date only few predictive biomarkers for cancer immunotherapy treatments have been robustly validated [47].

For example, the determination of PD-L1 expression by immunohistochemistry on tumour tissue biopsy was approved by the FDA as a diagnostic test to select patients eligible for treatment with therapeutic agents targeting PD-1/PD-L1 axis. However, potential limitations of this biomarker are the variable expression of PD-L1 in a single tumour and by the lack of harmonisation between available assays [31]. Additionally, the observation that PD-L1 expression does not categorise all patients who could potentially benefit from anti-PD-1/PD-L1 therapy calls for the identification of additional and more predictive biomarkers [67].

A parallel approach for predicting responses to checkpoint inhibitors blockade is the determination of MSI, especially by assessing a deficient mismatch repair (dMMR). As detailed in the previous sections, MSI and dMMR determine an increased tumour mutational burden (TMB), which in turn results into an increase in the number of neoantigens. The ultimate biological effect of this phenomenon is a substantive infiltration and activation of pre-existing tumour-specific CD4+ and CD8+ T cells, which render tumours susceptible to checkpoint inhibitors blockade [68]. This approach was approved as a biomarker test for pembrolizumab, in the context of the previously cited target-agnostic indication. However, it was also reported that MSI and dMMR do not always correlate with increased TMB. In contrast, considering that TMB can be observed in the absence of MSI and dMMR, for instance in carcinogen-induced tumours [68, 69], further investigations are needed to assess in which instances MSI and dMMR can be employed as predictive biomarkers.

The identification of reliable, precise companion diagnostic assets is thus an area of current focus both for already marketed and for future immune-based treatments.

A promising approach relies on assessing parameters that could be representative of the tumour's immunogenicity and of the underlying anti-tumour immunity. Accordingly, it was attempted to combine the aforementioned biomarkers to improve their predictivity. However, it was observed that a correlation between TMB and PD-L1 expression is absent [70]. Indeed, a combination of nivolumab and ipilimumab is superior to chemotherapy in patients with high TMB, irrespective of PD-L1 expression [71].

Additionally, correlative data have been generated by measuring changes in target immune cell populations, analysing inflammatory TNB-associated gene expression signatures indicating infiltration by specific immune cell subsets (e.g. myeloid-derived suppressor cells, Treg, effector T cells) and the activation of specific signalling pathways (e.g. INF-γ) [72]. Alternatively, the detection of neoantigens generated by gene fusions has been recently explored to predict responses in patients with low TMB [73]. A significant translational effort is to still to be performed to bring these approaches to the patients' bedside.

An inherent complexity of such approaches resides, in that a tumour biopsy needs to be performed. This implies logistic challenges when repeated biopsies need to be taken and analysed. Additionally, the search for predictive and prognostic biomarkers should not be limited to the tumour itself but should go beyond the malignant lesion. It is thus clear that the identification of soluble biomarkers in peripheral blood would be immensely advantageous and would increase patients' compliance. To this aim, several soluble biomarkers have been identified to predict positive clinical outcome in advanced melanoma patients receiving anti-CTLA-4 Ipilimumab, including C-reactive protein, lactate dehydrogenase, soluble CD25 and vascular endothelial growth factor (VEGF) [74].

PD-1 and PD-L1 are also detectable in peripheral blood in their soluble forms. However, recent studies have questioned the aptitude of soluble PD-1 and soluble PD-L1 as biomarkers for checkpoint blockade [75]. On the contrary, ctDNA is emerging as a suitable biomarker for TMB measurement, early response prediction, pseudo-progression versus disease progression and MRD assessment [30].

However, the identification of genomic mutations poses several technical challenges per se. Indeed, even for routine clinical testing it is necessary to apply sophisticated analytical techniques characterised by high sensitivity and by the possibility to test multiple genomic mutations simultaneously (multiplexing). High-throughput next-generation sequencing (NGS) technologies have thus overcome classic Sanger sequences for biomarker screening, especially considering that NGS technologies can be applied both to customised gene panels and to whole-exome, whole-genome or transcriptome panels [47].

Importantly, genotyping via customised gene panel suits to the challenges inherent to the clinical environment, which include limited availability of biopsy tissue, limitations regarding sample preparation and rapid timeframe required for therapeutic decisions [76]. Only recently, more sophisticated techniques such as whole-exome sequencing are emerging for clinical use. Their application is still limited due to their complexity and to the associated costs, but it is expected that they will become more widely used in the near future. Broad applicability of NGS techniques for biomarker discovery and routine analysis requires the clinical setting to acquire digital capability to handle, analyse and interpret a large quantity of complex genomic data [47].

However, it should be reported that current biomarker-driven trials are designed to allocate to targeted therapies patients whose tumours express the specific driver mutations. Therefore, only the excluded patients will receive immunotherapy. There is thus a need to design future biomarker-driven trials to include immune-based biomarkers [31].

An intriguing scenario suggests that immune-related AEs could also be considered biomarkers for tumour response [77]. Additional studies aimed at evaluating the independency and predictive power of AEs will be carefully monitored by the scientific and industrial community.

The identification of reliable predictive and prognostic biomarkers is expected to play a fundamental role also in guiding the selection of suitable combination approaches. Although predictive and companion biomarkers are considered to be crucial to guide optimisation of the cost and value of cancer immunotherapeutic agents [31], the development of companion diagnostic development lags behind therapeutics, creating scientific and regulatory complexity.

6 Challenges

6.1 Toxicity Management

The use of immune-based therapeutic agents, similarly to any other therapeutic intervention, is associated with AEs. However, a potential barrier to the application of cancer immunotherapy is the concern about its toxicity [25]. Most importantly, unanticipated AEs can dramatically impact not only on a drug product development but also on the valuation of the company itself, as it has occurred to the CAR T-cell-developer Juno Therapeutics [36].

The AEs associated to cancer immunotherapy belong to two main categories: immune-mediated side effects and positive interference with the tumour growth.

In some instances, reactivation of the immune system may sustain the proliferation of tumour cells and cancer stem cells via the production of growth factors. Such deleterious AEs may be prevented by careful *a priori* patient evaluation; importantly, a wise selection of appropriate combination regimens can potentially reduce these AEs in a substantial manner [25]. An additional concern is represented by the integration of the signals triggered by an immunotherapeutic intervention into the complex circuits of the immune system. Indeed, as it was mentioned in the previous sections, several mechanisms maintain a balance between immune activation and immune suppression, thus fine-tuning immune responses. Thus, it is expected that after treatment with ICIs T-cell activation will be gradually dampened by regulatory mechanisms in order to reach homeostasis. However, a sustained action of regulatory mechanisms could result in a temporary or permanent suppression of anti-tumour activity, even resulting in resistance to future activation [25].

Conversely, immune-mediated AEs derive from extensive T-cell activation and present similar characteristics to autoimmune symptoms, including colitis, autoimmune hepatitis, cytokine release, capillary leak syndromes, endocrine or neurological side effects. Immune-mediated AEs require immediate treatment with glucocorticoids to prevent permanent damage [43, 78]. Given that immune-mediated AEs have been considered as predictive biomarkers for response, there is a significant concern regarding the mitigation of immune-mediated effects, as this intervention could result in reduction in therapeutic efficacy. Therefore, there remains a need to investigate the impact of glucocorticoid treatment on the therapeutic efficacy of immune-based agent.

These observations will be fundamental to increase the confidence of patients and physicians dealing with immune-based agents, with a special regard to special patients' populations. Indeed, there is preliminary evidence that cancer immunotherapy could be effective and tolerated also in patients with pre-existing disorders affecting the immune system, such as autoimmune diseases and acquired immune-deficiency syndrome (AIDS) [43]. However, before extending indications to those populations, toxicity management protocols should be robustly validated.

Furthermore, compared to treatment with antibody-based immunotherapy, cellular approaches are still limited to specialised centres, putatively due to the concern that these therapies may present toxicity and may be difficult to manage and costly. It is expected that the remarkable improvements regarding the safety and affordability of CAR T cells and TILs therapies will result in a wider applications [25].

Thus, it is expected that the broader application of cancer immunotherapy in preclinical and clinical settings will allow to decipher its short- and long-term interference with the physiology of the immune system, hopefully leading to improvements not only of the management of AEs but also on the treatment regimens themselves.

6.2 Tumour Heterogeneity and Resistance to Treatment

It is well established that continuous acquisition of aberrant genomic and subgenomic mutation is an hallmark of cancer [79]. Several models have been proposed to decipher how progressive mutations contribute to the development of a heterogeneous population of cells in a malignant lesion.

Considering that several anti-cancer agents are directed to specific targets expressed by malignant cells, tumour heterogeneity is *per se* a cause of therapeutic failures, because cells not expressing the target or expressing a mutated target will be resistant to treatment. The treatment itself, by applying a selective pressure on the tumour, may promote additional heterogeneity due to the exploitation of different cancer signalling networks by different resistant clones.

In general, mechanisms of acquired resistance either reactivate a cancer pathway, or involve secondary genomic mutations in the drug target, or activate alternative signalling pathways; in parallel, epigenetic and transcriptional changes can also play a role [43]. These mechanisms have been widely studied in the context of traditional anti-cancer drugs but a detailed understanding of how tumour heterogeneity and acquired resistance may impact on cancer immunotherapy is still to be achieved.

On the one hand, checkpoint inhibitors, by reactivating pre-existing anti-tumour responses, which are considered to be polyclonal, should be able to target effectively heterogeneous tumour lesions. In a similar manner, infusion of TILs is expected to be able to target heterogeneous cells populations. However, it should be noted that no prediction on efficacy can be made without assessing quantitatively and qualitatively the extent and breath of pre-existing anti-tumour response. Similar evaluations still appear to be inapplicable to clinical settings. Additionally, cancerous lesions may develop resistance to therapies aimed at reinvigorating the immune response by developing strategies to escape immune cell recognition.

On the other hand, approaches like CAR T-cell therapy and anti-cancer vaccines may be significantly affected by tumour heterogeneity and by the development of resistance, because the absence of the target will inevitably result in lack of efficacy.

Recently, the mechanism of resistance were investigated in an exploratory study performed on tissue biopsies from patients with advanced melanoma who became resistance to pembrolizumab treatment [80]. The findings of this study revealed that cancer cells developed resistance mechanisms responsible for evasion and resistance to T-cell-mediated immunity. Among these, mutations of β2-microglobulin (*B2M*), a component of the MHC-I, were able to affect the presentation and the recognition of tumour-antigens by CD8+ T cells, thus impairing cancer cell killing.

This approach clearly shows that the availability of tumour biopsies during the course of treatment could be fundamental to understand resistance mechanisms and apply second-line treatment regimen. However, due the inherent challenges associated with the acquisition of biopsies, the evaluation of less invasive biomarkers is a priority to the field.

6.3 Clinical Development, the Path to Regulatory Approval and Beyond

Cancer immunotherapy is a highly innovative field and comprises some of the so-called advanced therapy medicinal products (ATMPs); the definition of ATMP is particularly suited to adoptive immune cells therapy. Accordingly, cancer immunotherapy requires innovative approaches to trial design, risk-benefit assessments and market access. Hence, many challenges reside in how to balance rapid access to immune-based agents for cancer treatment and establishing new metrics for evaluation in clinical and regulatory settings.

Differently to chemical products or biologicals, ATMPs cannot be standardised and thus require other means of evaluation for product safety, efficacy and potency. Challenges relevant to cancer immunotherapy clinical development include the complexity in designing and interpreting of clinical trials [81, 82] and the selection of appropriate patient populations.

Complex manufacturing processes [81, 83–85] – which is a very common issue in protein production and formulation [86] – and the implementation of Good Manufacturing Practices (GMP) and stringent testing to personalised therapeutic agents, specifically for cell and gene products [87, 88], increase the complexity of the development for immune-based agents. In particular, the logistic complexity of autologous therapies (e.g. TILs and CAR T cells) requires the product to be process in a centralised GMP facility and returned to the treatment centre for infusion into patient; this aspect is expected to increase costs and negatively impact uptake by clinicians [36].

Over and above, heterogeneous regulatory national procedures at member-state level [84] and uncertain reimbursement schemes, which are decisive to determine commercial success [36], are additional prominent challenges that developers of immune-base therapies have to face.

Of note, it has been recently estimated that in Europe 65% of ATMP developers are small- and medium-sized entrepreneurs (SME), while only 35% are large developers. It was also reported that ATMP developers – and especially SMEs – face difficulty with the regulatory requirements as they lack the expertise to address the country-specific requirements deriving, for instance, from different national interpretations of the EU regulation [89].

Since regulatory agencies appreciate the remarkable contribution that cancer immunotherapy is giving to the current therapeutic opportunities of patients affected by cancer, early-stage cooperation between all the parties involved is critical for success in cancer treatment development. Indeed, the regulatory landscape has been acting dynamically so as to promote rationalisation of the path to regulatory approval for immune-based agents. For example, a key initiative facilitating ATMP development was the adoption of European ATMP legislation (Regulation [EC] 1394/2007), which established the Committee for Advanced Therapies (CAT) within the EMA. The CAT is emerging as valuable partner in this field being responsible for assessing quality, safety and efficacy of advanced therapy products. Similarly, the EMA launched a scheme, called PRIME, to enhance support for the development of pharmaceuticals targeting unmet medical need, by promoting early dialogue between the parties and allow an optimised development plan and an acceleration on evaluation.

It is well-established that clinical development represents the most critical phase of a pharmaceutical product's lifecycle for several reasons, which include the challenge residing in the design and interpretation of clinical trials and in the associated costs, which may be considerable. Failure of clinical studies to prove efficacy of a given asset is an enormous risk, which could be mitigated as much as possible by careful preliminary evaluations.

In order to design a successful clinical roadmap, it is advisable to define as early as possible an integrated development roadmap, meaning that the planning of the regulatory process should be started at the earliest convenience and should be integrated with all other aspects of the development process.

The same applies to all other aspects of clinical development; indeed, the strategy for patients' selection should be defined early in development by choosing between an "individualized approach" (e.g. molecular phenotyping) or a subgroup analysis (e.g. expression of a given marker). Given that eligibility criteria based on molecular phenotypic result in an approach analogous to the one personalised medicine, the number of patients who can enrol to the trial and be eligible for treatment will be lower. This may result into poor predictive power of the trial and reduced revenues due to the low number of patients but can be counteracted by high levels of efficacy if the biomarker is highly predictive for efficacy.

This aspect corroborates the current need of predictive, reliable biomarkers to optimise the result of immune-based therapies. On the other hand, despite the trend for a more science-driven individualised approach, the current approach relies on precise patients' stratification, whereas the applicability of purely personalised approaches is still questioned. Additionally, with an increasing number of available biomarkers and assays thereof, independent validation will become a strict regulatory requirement.

It should be noted that in 2017, the FDA approved for the first time a treatment based on a biomarker (genome instability of the tumour) rather than an organ-specific tumour type, paving the way for further similar approvals worldwide.

The unique mechanism of action of immune-based agents creates a challenge for use of traditional efficacy endpoints used to assess clinical benefit of chemotherapy and other cytotoxic agents [90]. The choice of the study objectives and the timing of the assessment are critical, as effective immune response may need more time to develop, and pseudoprogression is often observed [91]. Although clinical benefit is often observed by analysing the tail end of the Kaplan–Meier survival curves, which is characteristic of immunotherapy and can be interpreted as cancer-free survival, it is necessary to avoid prolonged studies to pre-empt the arousal of confounding factors and to reduce costs. Thus, it is also advisable to include among the clinical study endpoints immune-related criteria and the assessment of the immune memory-mediated long-term disease-free survival [43, 92]. Another challenge involves the assessment of efficacy of anti-tumour therapies targeting specific alterations or pathways; due to tumour heterogeneity only a small cohort of patients will be eligible for such treatment, resulting in long-lasting, challenging clinical trials [47]. Therefore, in order to shorten time to market access for patients, it is needed to wisely design clinical trials and to sensibly outline endpoints for rapid assessment of clinical benefit.

An additional layer of complexity derives from the wide application of combinational therapy, where multiple agents are either combined in a sequential manner or co-administered, where even minor differences in the treatment regimen can dictate the trial's success or failure. In this context, assessment of efficacy might become difficult, especially when one agent is significantly more active than the other.

Given that cancer immunotherapy is considered from the regulatory standpoint as any other therapy, regulatory assessment is focused on establishing its risk-benefit profile. It is thus evident that minimisation of the risks associated to access to therapy is required to obtain regulatory approvals;

however, in a fast-evolving field like cancer immunotherapy risk perception and acceptance of uncertainty change as new therapeutic agents get approved. Furthermore, regulators in general require that the risks identified during the evaluation of a marketing authorisation (MA) should be minimised and/or further characterised via a post authorisation safety study (PASS).

In general, it is advisable to design clinical trials to allow collection of samples to perform *post hoc* analysis aimed at identifying biomarkers, comparing assays, and exploring mechanisms of resistance. This approach can drive further innovation which may result into future successful trials. An additional indication is the introduction of patients' questionnaires to evaluate the extent of minor AEs and the effect on the patients' and communities' quality of life; of note, this approach is compliant with the emerging patient-centric vision of cancer immunotherapy.

An additional challenge associated to cancer immunotherapy, which is characterised by a unique risk-benefit profile, is represented by the choice of information to include in product information brochures in order to facilitate both impartial evaluations from clinicians, patients and HTA.

Special considerations apply to cellular therapies, such as CAR T cells. In a scenario where each patient will receive a distinct therapeutic agent, given the autologous nature of the transplanted immune cells, significant challenges arise from the complex logistics for manufacturing and delivery of the product, including transport, import/export, and qualification of process changes where each batch correspond to a different patient. As cellular therapies are considered ATMPs, a risk-based approach is required to enable the control and management of the risks related to the product and manufacturing process, in which a potency assay reflecting the clinical mechanism of action is a crucial parameter. Thus, a strong emphasis on potency and quality is a prerequisite for cellular therapies approval. A comprehensive and detailed primary analysis of challenges encountered by ATMPs developers in Europe is reviewed elsewhere [89].

6.4 Intellectual Property

Immune-based therapeutic agents usually derive from a substantial innovative effort. Rewarding innovators by providing protection to novel inventions against competitors can be achieved by a smart approach to intellectual property (IP) rights.

Indeed, the understanding of the IP landscape in the field of cancer immunotherapy is crucial to define strategies aimed at securing market access and market position, protecting assets from being counterfeited, anticipating possible conflicts to either avoid or exploit them or produce income by royalty payments [39].

Patents and trade secrets appear as the most valuable type of IP rights in the current cancer immunotherapy landscape. Trade secrets are practices or processes by which a party can obtain an economic advantage over competitors, for example the production of an innovative product. Trade secrets, as long as they are not disclosed to the public, grant an unlimited exclusivity to the innovator. However, if the innovative product or process is, even inadvertently, disclosed to the public or if it is easily reverse-engineered, no formal regulation can impair competitors to reproduce the innovative asset. In this regard, it should be noted that it is compulsory to disclose to the public detailed information related to a pharmaceutical product, for example in the regulatory documents and dossier that are submitted in order to obtain a marketing authorisation or in investigator brochures. Hence, a trade secret would be inapplicable to this setting. Additionally, there are also ethical concerns regarding the use of trade secrets in pharmaceutical settings, where the non-disclosure of information could prevent scientific progress and technical development that could be advantageous for patients. Notwithstanding these aspects, trade secrets could be valuable to protect specific technical improvements related to the manufacture of a product, especially when the improvements themselves cannot be protected by a patent.

In contrast to trade secrets, patents grant the right to exclude third parties to make, use, sell, offer to sell, and import an invention for a limited period of time (usually 20 years) and in a limited territory, in exchange for the public disclosure of the invention. Patents can be seen as a mutual contract between an inventor and the public, where the public can benefit from the public disclosure of the invention, which can fuel further innovation, and the inventor can profit from the commercial exploitation of the invention, whose revenues can pay back previous R&D costs and be reinvested in developing additional innovative products.

However, not all inventions are patentable. Inventions need to be new, not obvious and to have an industrial applicability. Additionally, in some jurisdictions, such as in Europe, specific inventions, such as methods of treatments are excluded from patentability, in order to allow medical practitioners to perform such methods of treatments without risking infringement of a patent. Conversely, medical products *per se* are patentable in most jurisdictions.

Given the costs associated with R&D, the private sector will not undertake such investments without the existence of some significant commercial upside to counterbalance the considerable risks of failure. It is thus clear that a solid patent protection is mandatory to ensure exclusive rights on a product, allowing inventors to advance their research objectives and to achieve the commercial availability of a new pharmaceutical product [93].

As it was described in the introduction, the development of most of the current immunotherapeutic agents originates from the discoveries performed by several academic research centres, where inventions often result from collaborations and scientific cross-fertilisation between different researchers. Moreover, the R&D track leading to some of the current ground-braking cancer immunotherapy agents was very circuitous, being characterised by collaboration between multiple companies and research centres. Thus, despite a few players dominating the field, the current landscape still appears dispersed, with multiple acquisitions, transfer of rights, licensing and collaborations agreements having occurred [35]. These factors have contributed to render the current patent landscape of immune-based agents intricate.

In particular, the field of immune checkpoint inhibitors appears to be especially convoluted [39].

For example, the IP rights involved in some of the agreements that were fundamental for the development of the anti-CTLA-4 antibodies ipilimumab from Bristol–Myers Squibb's (BMS) and tremelimumab from Pfizer have shaped their R&D, clinical and commercial route. In detail, the first patent portfolio covering anti-CTLA-4 antibodies originated at the University of California Berkeley from the work of Allison. CTLA-4-related patents were sublicensed to a company called Medarex, which generated the first human anti-CTLA-4 antibody, later called ipilimumab. Medarex also established a collaboration with Pfizer, who had a parallel anti-CTLA-4 program, which included the future tremelimumab; the agreement involved cross-licensing of relevant patents, wherein Medarex was eligible to obtain milestones and royalty payments for sales of any Pfizer anti-CTLA-4 antibodies based on the patents originating from Allison's work. Soon after, while Medarex became a subsidiary of BMS, Pfizer discontinued their program, which was later restarted when tremelimumab was in-licensed by AstraZeneca. It is clear that, if tremelimumab would have been able to reach the market before the patent term expiry of the Allison's portfolio, the sale of tremelimumab would be subject to royalty payment to BMS [39].

The patent landscape related to PD-1 is even more intricate, wherein seminal discoveries resulting in patents directed to PD-1 and PD-L1 were achieved in parallel by several researchers including Tasuku Honjo from Kyoto University, Gordon Freeman from Dana-Farber Cancer Institute, Arlene Sharpe from Harvard Medical School and Lieping Chen from Mayo Clinic. The key players in the field of anti-PD-1 antibodies are BMS and Merck. BMS by acquiring Medarex and collaborating with Ono Pharmaceuticals had access to Honjo's patent estate, which covers broad methods of treatment by administration of anti-PD-1 antibodies. A few months before the approval of ipilimumab, jointly developed by BMS and Ono, pembrolizumab, an anti-PD-1 antibody by Merck was approved by the FDA. This intertwined path resulted in litigation between the parties for patent infringement, as Merck's asset was falling in the broad claims of Honjo's patent estate; the lawsuit came to end in 2017 with Merck agreeing terms to settle the dispute. It should be noted that assuming that Merck's pembrolizumab meets expectations of becoming a "blockbuster" product, the upfront payment and royalties could be considerable [39].

In contrast, the field of anti-PD-L1 antibodies is considerably less conflict-prone. Indeed, despite several players having products in this space, including Genentech, AstraZeneca, MerckSerono and BMS, none of the patents covering those assets comprises broad claims which could interfere with third parties' activities. The reason for this narrow scope resides in the fact that the patents directed to a broad method of treatment by administration of anti-PD-L1 antibodies, which originated from the work of Freeman, were non-exclusively licensed to several parties, all of which thus have freedom to operate in this field [39].

The patent landscape of cellular immunotherapy differs substantially from the checkpoint inhibitor's one. Indeed, given the intrinsic personalised nature of cellular immunotherapy, patent protection is not generally directed to the pharmaceutical product *per se* but usually to constructs, vectors and associated methods that are necessary to obtain a cellular immune-based drug product, such as a CAR T-cell agent. The main IP actors in the CAR T-cell space have been the University of Pennsylvania and St. Jude's Children's Research Hospital, with substantial contributions from their commercial partners Novartis and Juno Therapeutics. These parties have been recently involved in a litigation over the above-described IP [36].

Based on these examples, it is clear how a strategically established patent portfolio is a prerequisite for success in the crowded space of immune-based therapeutic agents. *Ab initio* commitment and diligent planning are required to take advantage of a patent estate. IP can be exploited in a defensive manner, meaning as a tool to aim at market exclusivity by excluding competitors from the market or as an offensive tool, for instance to create revenues by out-licensing or royalties payment. Either ways, expert judgement and advice is needed during the whole life cycle of a product, in order to capture the value of inventions in strong patent claims and in wise negotiation of collaboration and licensing agreements.

Patents are also of primary importance in the protection of the latest innovations of the field. Accordingly, the commercial value of patents covering the use of specific predictive and prognostic biomarkers or kits for detecting the same is significant, given that, in several instances, the testing of a biomarker may be mandatory for the immune-based drug to be granted a MA or to be reimbursed [39]. It could be expected that also combination therapies would be the subject of a separate category patents in the field of cancer immunotherapy. Conversely, considering that patents directed to a new pharmaceutical product usually also encompass claims directed to optional combinations with standard drugs, patents explicitly directed to combinations *per se* may be considered redundant, and are therefore quite rare. An exception to this trend is observed in patents covering assets developed by small biotech companies: in this case, a patent directed to a combination with a well-established drug product from a large pharmaceutical company may be a favourable factor in supporting a potential collaborative research and development agreement between the two companies [39].

A noteworthy challenge to the protection of established IP rights is represented by the fact that the exclusivity granted by a patent estate may be circumvented through special provisions granted by the World Trade Organization (WTO)'s agreement on intellectual property, known as the TRIPS (Trade-Related Aspects of Intellectual Property Rights) Agreement. In exceptional circumstances, a government may allow a third party to produce a patented product without the consent of the patent owner, upon compensation of the patent owner. This provision, known as compulsory licensing, has been introduced to international patent law to ensure access to innovative products in low-income countries, especially in emergency or extreme urgency. However, due to the high costs associated to cancer immunotherapy drug products, there is the possibility that also medium- and high-income countries might advocate compulsory licenses to grant patients access to innovative pharmaceutical products [94].

On the other hand, a crucial aspect that needs to be considered when analysing the impact of IP on cancer immunotherapy is the compensation that specific countries can put into practise to reward innovators for the development of innovative products, especially in the pharmaceutical field.

One example is represented by pilot programs aimed at implementing procedural methods to prioritise examinations of patent applications directed to cancer immunotherapy. It should be noted that the procedure needed to obtain a granted patent is usually long and expensive [93] and may both discourage inventors to file patent applications and delay market access of innovative products. The first and foremost illustration of such initiatives is the "Cancer Immunotherapy Pilot Program" from the United States Patent Office (USPTO). This initiative sets an expedite examination procedure, not requiring any added fees, for patent applications which meet stringent criteria and have at least one claim to a method of treating a cancer using immunotherapy [93]. Since the beginning of the program in 2016, as of January 2019 over 300 petitions requesting participation in the fast-track program have been filed and over 100 patents have been granted. This success has prompted the USPTO to extend the program until June 2020.

Another example is represented by the supplementary protection certificate (SPC) that is available in member-states of the European Union to extend the patent term related to a particular medicinal product. An SPC aims to compensate a patent owner for part of the patent term that was lost due to time needed to obtain a MA. An SPC can extend the term of a patent for up to 5 years, thus granting an additional time frame of exclusivity. Similarly, a request for patent term adjustment (PTA) is available in the United States to compensate for delays caused by the U.S. patent office during the prosecution of a U.S. patent application. Additionally, innovators can qualify for advantageous governmental incentives based on their patent estates. Such measures, usually known as patent box or innovation box, aim to incentivise R&D by applying a lower taxing regimen to patent revenues compared to other commercial revenues.

7 Conclusions

Cancer immunotherapy has progressed from its conceptual design to breakthrough clinical applications [95] and exciting further developments are supported by the pipeline of several pharmaceutical companies, which include new therapeutic paradigms such as personalised medicine [96, 97], combination therapy [98], novel delivery methods [99], biomaterials [98] and new diagnostic procedures [100].

Based on the trajectories of the last decades, wherein clinical translation of immunotherapy was characterised by lengthy translational timelines, false starts and by iterative cycles of scientific research [36], the industrial perspective on cancer immunotherapy is directed to maximise pipeline's value by applying a smart strategy not only to the early phases of drug discovery and preclinical development but also to clinical development and life cycle management.

Similar to the typical drug product development, the current cancer immunotherapy landscape is characterised by industry-driven development of assets directed to targets that have been extensively validated by the academia. It is expected that strategic partnerships and in-licensing of promising assets will become more and more frequent, with academia or smaller biotech companies providing validated assets at the interface between preclinical and phase I clinical trials and the pharmaceutical industries contributing with their expertise to scale up for late-phase development. The application of this scheme may substantially reduce the time to market and the risks associated to R&D, as the pharmaceutical industry will commit to clinical development only of the "best in class" assets, avoiding the risk of long, unsuccessful and expensive early-phase discovery.

Careful planning is required to maximise value and outcome, with the involvement of a multidisciplinary team of experts focussed on integrating all the mandatory stages of drug development into a smart strategy. In line with this approach, there is a tendency to establish collaborations with regulators and players early in clinical development, following the motto "start with the end in mind". Another aspect of this value-oriented strategy is represented by extensive activities involving predictive and prognostic biomarkers. This appears to be a leading tendency in cancer immunotherapy, which may substantially maximise treatment value by reducing – or even abolishing – side effects, and by allowing drug administration to responders only – thus reducing the overall cost of the therapy.

Additionally, the development of cancer immunotherapy represents a milestone in the introduction of personalised medicine, not only to the field of cancer but also to the broader pharmaceutical landscape. Fighting cancer by means of invoking the immune system, whose resources pertain by definition to each individual, implies that allogenic therapies stimulating the immune system (such as immune checkpoint inhibitors and anti-cancer vaccines) may also be considered as a personalised approach. This concept, as it was detailed in the previous sections, presents several challenges and opportunities.

Allogenic therapies are more analogous to standard biopharmaceuticals and, due to significant cost reductions associated with scale in manufacture, quality control and release of a single batch that could be used to treat multiple patients [36], currently they are more appealable to the pharmaceutical industry. This is in contrast to autologous products, such as CAR-T cells and TILs, whose complex value chain still represents a barrier to their extensive application. Despite this additional layer of complexity, the recent approval of CAR T cell therapies is of fundamental importance not only because it paves the way for additional approvals but also because the logistics of the application of such therapies to "real-world" settings will be closely observed by several actors of the pharmaceutical arena, including companies focussed on regenerative medicine. Despite some concerns related to manufacturing, delivery models and cost-effectiveness of autologous therapies, the main focus of the private sector will be the development of more advanced methods for genetic manipulation of immune cells and their bioprocessing [36].

A parallel approach to maximise the value of current cancer immunotherapy is represented by the extensive translational and clinical efforts aimed to broaden the indications of already approved agents. Indeed, by exploiting the physiological polyclonal nature of immune responses, the reactivation of immune system through immunomodulators may result in anti-cancer activity towards a broad spectrum of tumour types. In a similar manner, exploiting the interconnected mechanisms of immune regulation by combining therapeutic agents targeting complementary pathways holds great promise for the treatment of tumours which acquire resistance to therapy. It is expected that this strategy will be fostered by collaboration agreements and joint development between key players that hold exclusive rights in respect to the therapeutic agents amenable for use in combination [35].

The overwhelming curative potential of cancer immunotherapy explains the current enthusiasm and the extensive investments in the field by the public and private sector. During the last decade, the first line of immune-based agents has emerged in clinical trials and in regulatory approvals, with remarkable benefit for patients. Nevertheless, many challenges still need to be overcome to make it universally available. Thus, the clinical community impatiently looks for a second generation of cancer immunotherapy which could be able to address the current challenges facing the field [30].

8 Future Perspectives

The challenges that cancer immunotherapy is facing at present also bring exciting opportunities for further technological innovations.

9 The Tumour Microenvironment

The present generation of immune-based agents acts by targeting immune cells or cancer cells as entities isolated from their context. Despite the remarkable efficacy of current cancer immunotherapy, the understanding of the mechanisms of immune-mediated tumour clearance within the tumour microenvironment (TME) is fundamental to establish a second generation of therapeutic options.

It is acknowledged that the TME, which consists of cancer cells, stroma, vascular elements and infiltrating immune cells, is a complex milieu characterised by an immunosuppressive nature [101]. Cancer cells have been shown to deliver immunosuppressive signals via exosomes and soluble factors, including cytokines, chemokines and inhibitory factors, which are unique to each individual tumour. The resulting level of immunosuppression is generally correlated to T-cell dysfunction and thus to tumour aggressiveness [25].

The success of immune checkpoint inhibitors suggests that interfering with TME-mediated immunosuppressive mechanisms is a valuable therapeutic strategy against cancer. Hence, a second-generation immune-based agents targeting immunosuppressive pathways within the TME is undergoing extensive investigation. In addition, analysis of the immunomodulatory and pro-/anti-inflammatory factors expressed by a tumour may guide the therapeutic intervention targeting the malignant lesion.

Besides CD8+ T cells, the target of current cancer immunotherapy, other immune cells may become primary targets of immune-based therapy, namely Treg and myeloid-derived suppressor cells (MDSC).

Tregs infiltrating the TME are highly immunosuppressive and contribute to impairment of CD8+ T-cells responses. The effect of current checkpoint inhibitors on tumour infiltrating Treg cells is still controversial, and further studies are needed to assess how anti-PD-1 and anti-CTLA-4 therapy impact on this T-cell subpopulation, considering that the maintenance of Treg cells is necessary to safeguard tissue homeostasis. Targeted therapies successful in depleting only tumour infiltrating Tregs may be of great clinical significance.

MDSCs have been shown to promote tumour progression by secretion of inducible nitric oxide synthase, reactive oxygen species (ROS), IL-23, TGF-β, and prostaglandin E2 (PGE2) [25]. Thus, therapies aimed either at depleting MDSC or at blocking their immunosuppressive secretome may represent an important component of novel anti-cancer therapeutic options. The strategies investigated so far include inhibition of IDO, the prevention of MDSC trafficking to the malignant lesion by blocking specific chemokines, targeting colony stimulating factor 1 receptor (CSF1R) on MDSC [102] and blocking IL-23 [103].

These considerations will become crucial also to design therapeutic strategies to enhance efficacy of novel CAR T-cell therapies in the context of solid tumours [30, 104].

10 Technical Developments

Considerable technical developments are expected to improve current therapeutic agents, especially in order to ameliorate their safety profile. Similarly, modifications to mAb scaffolds to fine-tune the drug's pharmacodynamic/pharmacokinetic profile, also CAR T-cells scaffolds are undergoing engineering processes. Improvement of CAR T cells safety profile could be obtained via modification of the CAR itself [105] or by molecular switches inducing programmed cell death [106, 107].

In parallel, the application of new molecular biology technologies, such as CRISPR (Clustered Regularly Interspaced Short Palindromic Repeats), is expected to maximise the throughput and the accessibility of such personalised approaches.

An additional stream of development is represented by research focussing on improving the delivery of immune-based agents to tumours. Such improvements could maximise efficacy and reduce systemic toxicity, resulting in significant benefit for the patients.

11 The Digital Revolution

It was previously described that the identification of novel predictive and prognostic biomarkers is one of the main trends in cancer immunotherapy. It is estimated that non-invasive monitoring and omics-based tests and the broad concept of precision medicine will soon converge within cancer immunotherapy. However, the increasing number of patient-related data does not directly correlate with a more straightforward diagnosis or prognosis. Conversely, a new digital expertise needs to be established in the landscape of cancer immunotherapy to take full advantage of the wealth of data that will become available in the near future thanks to the broad application of NGS technologies for cancer biomarker screening.

In addition to the technical obstacles due to the data-rich technologies *per se*, the challenges related to the management of large datasets need to be carefully considered, starting from the design of appropriate digital architectures ensuring protection of sensitive information and the establishment of the ownership of data [108]. This last aspect is particularly crucial considering that large datasets are currently seen as a valuable basis for drug discovery and development and could represent crucial assets under evaluation in agreements between pharmaceutical companies. Conversely, the scientific community calls for maintaining publicly available databases to sustain research [43]. Preliminary efforts in this direction have been performed by The Cancer Genome Atlas and the International Cancer Genome Consortium [43, 47].

Most of these issues still need to be resolved through close collaboration between the public and the private sectors. In particular, because the legal aspects concerning patients' data storage and analysis, especially by means of machine learning and artificial intelligence (AI), are still unclear, the healthcare system is expected to either downgrade the enthusiasm regarding the application of data science to clinical practise or to proactively invest in the realisation of a legal and technical framework [108].

12 Integration of a Patient-Centric Model

In order to fully define the value of cancer immunotherapy, patient outcome perspective is emerging as a valuable source of data. Indeed, the definition of the value of immune-based therapies would be incomplete if the patients' perspective is not integrated to the evaluations performed by the other counterparts within the healthcare system.

A valuable example of the transition toward a patient-centric model consists of the incorporation of patient-reported outcomes (PROs) in clinical trials. PROs represent the report of the patients' health status performed by the patients themselves and it is widely recognised that PROs are usually accurate in revealing clinical benefit, AEs and changes in disease-related symptoms.

By increasing the engagement of patients in the course of the trial, compliance to the therapeutic scheme can be improved. In this context, it was also estimated that monitoring of clinically relevant symptoms via PROs could improve quality of life and reduced emergency room visits, with an overall increase of the quality-adjusted 1-year survival rates among cancer patients [109]. The same report also suggest that PROs can also address health disparities of patients [31, 109].

An additional strategy to implement a patient-centric model is the engagement of patient advocacy organisations in the discussion regarding patients' and family's needs and regarding disease-specific issues [31].

Trademark Statements

"Avastin" is a trademark of Genentech, Inc.; "Bavencio" is a trademark of MERCK KGaA; "Cervarix" is a trademark of GlaxoSmithKline Biologicals S.A.; "Gardasil" is a trademark of Merck Sharp & Dohme Corp., a New Jersey corporation; "HEPLISAV-B" is a trademark of Dynavax Technologies Corporation; "Herceptin" is a trademark of Genentech, Inc.; "Hiltonol" is a trademark of Oncovir, Inc; "Humira" is a trademark of AbbVie Biotechnology Ltd.; "Imlygic" is a trademark of Amgen Inc.; "Imfinzi" is a trademark of AstraZeneca AB; "Inflectra" is a trademark of Pfizer Limited; "Intron A" is a trademark of MSD International Holdings GmbH; "Keytruda" is a trademark of Merck Sharp & Dohme Corp.; "Kyrmriah" is a trademark of NOVARTIS AG; "Libtayo" is a trademark of Sanofi Biotechnology; "MabThera" is a trademark of F. Hoffmann-La Roche AG; "Opdivo" is a trademark of Bristol-Myers Squibb Company; "PEG-Intron" is a trademark of Schering-Plough Ltd.; "Proleukin" is a trademark of Clinigen Holdings Limited; "Provenge" is a trademark of Dendreon Pharmaceuticals LLC; "Remicade" is a trademark of Janssen Biotech, Inc.; "Remsima" is a trademark of Celltrion, Inc.; "Rituxan" is a trademark of Biogen Inc; "Roferon-A" is a trademark of F. Hoffmann-La Roche AG; "Sylatron" is a trademark of Schering-Plough Ltd.; "Synagis" is a trademark of AbbVie Inc.; "Tecentriq" is a trademark of F. Hoffmann-La Roche AG; "Yervoy" is a trademark of Bristol-Myers Squibb Company; "Yescarta" is a trademark of Kite Pharma, Inc.

Disclaimer

This work was sponsored by GlaxoSmithKline Biologicals SA. S.R. was participating in a post graduate studentship program at Institute for Research in Biomedicine. S.R. is the inventor of a pending patent application entitled "Methods for rapid cDNA production and cloning". S.R. is an employee of GSK Vaccines S.r.l.

References

1. Hodi, F. S., et al. (2010). Improved survival with ipilimumab in patients with metastatic melanoma. *New England Journal of Medicine, 363*(8), 711–723.
2. Robert, C., et al. (2015). Improved overall survival in melanoma with combined dabrafenib and trametinib. *The New England Journal of Medicine, 372*(1), 30–39.
3. Sharma, P., & Allison, J. P. (2015). The future of immune checkpoint therapy. *Science, 348*(6230), 56–61.
4. Rosenberg, S. A., & Restifo, N. P. (2015). Adoptive cell transfer as personalized immunotherapy for human cancer. *Science, 348*(6230), 62–68.
5. Eshhar, Z., Waks, T., Gross, G., & Schindler, D. G. (1993). Specific activation and targeting of cytotoxic lymphocytes through chimeric single chains consisting of antibody-binding domains and the γ or ζ subunits of the immunoglobulin and T-cell receptors. *Proceedings of the National Academy of Sciences of the United States of America, 90*(2), 720–724.
6. Robert, C., et al. (2011). Ipilimumab plus dacarbazine for previously untreated metastatic melanoma. *The New England Journal of Medicine, 364*(26), 2517–2526.
7. Larkin, J., et al. (2015). Combined nivolumab and ipilimumab or monotherapy in untreated Melanoma. *The New England Journal of Medicine, 373*(1), 23–34.
8. Ansell, S. M., et al. (2015). PD-1 blockade with nivolumab in relapsed or refractory Hodgkin's lymphoma. *The New England Journal of Medicine, 372*(4), 311–319.
9. Hamanishi, J., et al. (2015). Safety and antitumor activity of Anti-PD-1 antibody, nivolumab, in patients with platinum-resistant ovarian cancer. *Journal of Clinical Oncology, 33*(34), 4015–4022.
10. Powles, T., et al. (2014). MPDL3280A (anti-PD-L1) treatment leads to clinical activity in metastatic bladder cancer. *Nature, 515*(7528), 558–562.
11. Cohen, E. E. W., et al. (2015). KEYNOTE-040: A phase III randomized trial of pembrolizumab (MK-3475) versus standard treatment in patients with recurrent or metastatic head and neck cancer. *Journal of Clinical Oncology, 33*(15_suppl), TPS6084.
12. Motzer, R. J., et al. (2015). Nivolumab versus everolimus in advanced renal-cell carcinoma. *The New England Journal of Medicine, 373*(19), 1803–1813.
13. Gong, J., Chehrazi-Raffle, A., Reddi, S., & Salgia, R. (2018). Development of PD-1 and PD-L1 inhibitors as a form of cancer immunotherapy: A comprehensive review of registration trials and future considerations. *Journal for Immunotherapy of Cancer, 6*(1), 8.
14. Jardim, D. L., De Melo Gagliato, D., Giles, F. J., & Kurzrock, R. (2018). Analysis of drug development paradigms for immune checkpoint inhibitors. *Clinical Cancer Research, 24*(8), 1785–1794.
15. Altmann, D. M. (2018). A Nobel Prize-worthy pursuit: Cancer immunology and harnessing immunity to tumour neoantigens. *Immunology, 155*(3), 283–284.
16. Leach, D. R., Krummel, M. F., & Allison, J. P. (1996). Enhancement of antitumor immunity by CTLA-4 blockade. *Science, 271*(5256), 1734–1736.
17. Iwai, Y., et al. (2002). Involvement of PD-L1 on tumor cells in the escape from host immune system and tumor immunotherapy by PD-L1 blockade. *Proceedings of the National Academy of Sciences of the United States of America, 99*(19), 12293–12297.
18. Sakaguchi, S., Yamaguchi, T., Nomura, T., & Ono, M. (2008). Regulatory T cells and immune tolerance. *Cell, 133*(5), 775–787.
19. Tanaka, A., & Sakaguchi, S. (2017). Regulatory T cells in cancer immunotherapy. *Cell Research, 27*(1), 109–118.
20. Wherry, E. J., & Kurachi, M. (2015). Molecular and cellular insights into T cell exhaustion. *Nature Reviews Immunology, 15*(8), 486–499.
21. Chen, L., & Flies, D. B. (2013). Molecular mechanisms of T cell co-stimulation and co-inhibition. *Nature Reviews Immunology, 13*(4), 227–242.
22. Gajewski, T. F., Schreiber, H., & Fu, Y. X. (2013). Innate and adaptive immune cells in the tumor microenvironment. *Nature Immunology, 14*(10), 1014–1022.

23. Galluzzi, L., et al. (2014). Classification of current anticancer immunotherapies. *Oncotarget, 5*(24), 12472.
24. Melero, I., et al. (2014). Therapeutic vaccines for cancer: An overview of clinical trials. *Nature Reviews Clinical Oncology, 11*(9), 509.
25. Whiteside, T. L., Demaria, S., Rodriguez-Ruiz, M. E., Zarour, H. M., & Melero, I. (2016). Emerging opportunities and challenges in cancer immunotherapy. *Clinical Cancer Research, 22*(8), 1845–1855.
26. Besser, M. J., et al. (2013). Adoptive transfer of tumor-infiltrating lymphocytes in patients with metastatic melanoma: Intent-to-treat analysis and efficacy after failure to prior immunotherapies. *Clinical Cancer Research, 19*(17), 4792–4800.
27. Raman, M. C. C., et al. (2016). Direct molecular mimicry enables off-target cardiovascular toxicity by an enhanced affinity TCR designed for cancer immunotherapy. *Scientific Reports, 6*, 18851.
28. Neelapu, S. S., et al. (2017). Axicabtagene ciloleucel CAR T-cell therapy in refractory large B-Cell lymphoma. *The New England Journal of Medicine, 377*(26), 2531–2544.
29. Schuster, S. J., et al. (2019). Tisagenlecleucel in adult relapsed or refractory diffuse large B-cell lymphoma. *The New England Journal of Medicine, 380*(1), 45–56.
30. Kruger, S., et al. (2019). Advances in cancer immunotherapy 2019 – Latest trends. *Journal of Experimental and Clinical Cancer Research, 38*(1), 1.
31. Kaufman, H. L., et al. (2017). The value of cancer immunotherapy summit at the 2016 society for immunotherapy of cancer 31st anniversary annual meeting. *Journal for Immunotherapy of Cancer, 5*(1), 1–10.
32. Mariotto, A. B., Robin Yabroff, K., Shao, Y., Feuer, E. J., & Brown, M. L. (2011). Projections of the cost of cancer care in the United States: 2010–2020. *Journal of the National Cancer Institute, 103*(2), 117–128.
33. Hodi, F. S., et al. (2016). Combined nivolumab and ipilimumab versus ipilimumab alone in patients with advanced melanoma: 2-year overall survival outcomes in a multicentre, randomised, controlled, phase 2 trial. *The Lancet Oncology, 17*(11), 1558–1568.
34. Murphy, K. M., Topel, R. H., Murphy, K. M., & Topel, R. H. (2013). The economic value of medical research. *Measuring the Gains from Medical Research, 15*(30), 125–146.
35. Pan, C. L., & Chen, F. C. (2017). Patent trend and competitive analysis of cancer immunotherapy in the United States. *Human Vaccines & Immunotherapeutics, 13*(11), 2583–2593.
36. Bonter, K., Breckenridge, Z., Lachance, S., Delisle, J. S., & Bubela, T. (2017). Opportunities and challenges for the cellular immunotherapy sector: A global landscape of clinical trials. *Regenerative Medicine, 12*(6), 623–636.
37. Barrett, D. M., Grupp, S. A., & June, C. H. (2015). Chimeric antigen receptor– And TCR-modified T cells enter main street and wall street. *Journal of Immunology, 195*(3), 755–761.
38. Hartmann, J., Schüßler-Lenz, M., Bondanza, A., & Buchholz, C. J. (2017). Clinical development of CAR T cells—challenges and opportunities in translating innovative treatment concepts. *EMBO Molecular Medicine, 9*(9), 1183–1197.
39. Storz, U. (2016). Intellectual property issues of immune checkpoint inhibitors. *MAbs, 8*(1), 10–26.
40. Dimitrov, D. S., & Marks, J. D. (2009). Therapeutic antibodies: Current state and future trends–is a paradigm change coming soon? *Methods in Molecular Biology, 525*, 1–27.
41. Stumpp, M. T., Binz, H. K., & Amstutz, P. (2008). DARPins: A new generation of protein therapeutics. *Drug Discovery Today, 13*(15–16), 695–701.
42. Smit, M. A. D., Jaffee, E. M., & Lutz, E. R. (2014). Cancer immunoprevention – The next frontier. *Cancer Prevention Research, 7*(11), 1072–1080.
43. Lee Ventola, C. (2017). Cancer immunotherapy, part 3: Challenges and future trends. *Pharmacy and Therapeutics, 42*(8), 514.
44. Zarour, H. M. (2016). Reversing T-cell dysfunction and exhaustion in cancer. *Clinical Cancer Research, 22*(8), 1856–1864.
45. Melero, I., Rouzaut, A., Motz, G. T., & Coukos, G. (2014). T-cell and NK-cell infiltration into solid tumors: A key limiting factor for efficacious cancer immunotherapy. *Cancer Discovery, 4*(5), 522–526.
46. Türeci, Ö., et al. (2016). Targeting the heterogeneity of cancer with individualized neoepitope vaccines. *Clinical Cancer Research, 22*(8), 1885–1896.
47. Zugazagoitia, J., et al. (2016). Current challenges in cancer treatment. *Clinical Therapeutics, 38*(7), 1551–1566.
48. Tang, J., Shalabi, A., & Hubbard-Lucey, V. M. (2018). Comprehensive analysis of the clinical immuno-oncology landscape. *Annals of Oncology, 29*(1), 84–91.
49. Shrimali, R. K., et al. (2017). Concurrent PD-1 blockade negates the effects of OX40 agonist antibody in combination immunotherapy through inducing T-cell apoptosis. *Cancer Immunology Research, 5*(9), 755–766.
50. Wolchok, J. D., et al. (2013). Nivolumab plus Ipilimumab in advanced melanoma. *The New England Journal of Medicine, 369*, 122–133.
51. Postow, M. A., et al. (2015). Nivolumab and ipilimumab versus ipilimumab in untreated melanoma. *The New England Journal of Medicine, 372*(21), 2006–2017.
52. Smyth, M. J., Ngiow, S. F., Ribas, A., & Teng, M. W. L. (2016). Combination cancer immunotherapies tailored to the tumour microenvironment. *Nature Reviews Clinical Oncology, 13*(3), 143.
53. Melero, I., et al. (2015). Evolving synergistic combinations of targeted immunotherapies to combat cancer. *Nature Reviews Cancer, 15*(8), 457–472.
54. Apetoh, L., et al. (2007). Toll-like receptor 4-dependent contribution of the immune system to anticancer chemotherapy and radiotherapy. *Nature Medicine, 13*(9), 1050–1059.
55. Brix, N., Tiefenthaller, A., Anders, H., Belka, C., & Lauber, K. (2017). Abscopal, immunological effects of radiotherapy: Narrowing the gap between clinical and preclinical experiences. *Immunological Reviews, 280*(1), 249–279.
56. Woo, S. R., et al. (2014). STING-dependent cytosolic DNA sensing mediates innate immune recognition of immunogenic tumors. *Immunity, 41*(5), 830–842.
57. Deng, L., et al. (2014). STING-dependent cytosolic DNA sensing promotes radiation-induced type I interferon-dependent antitumor immunity in immunogenic tumors. *Immunity, 41*(5), 843–852.
58. Alexandrov, L. B., et al. (2013). Signatures of mutational processes in human cancer. *Nature, 500*(7463), 415–421.
59. Schmid, P., et al. (2018). Atezolizumab and nab-paclitaxel in advanced triple-negative breast cancer. *The New England Journal of Medicine, 379*(22), 2108–2121.
60. Joseph, R. W., et al. (2018). Baseline tumor size is an independent prognostic factor for overall survival in patients with melanoma treated with pembrolizumab. *Clinical Cancer Research, 24*(20), 4960–4967.
61. Liu, J., et al. (2016). Improved efficacy of neoadjuvant compared to adjuvant immunotherapy to eradicate metastatic disease. *Cancer Discovery, 6*(12), 1382–1399.
62. Garcia, C. A., et al. (2018). Neurologic immune-related adverse events associated with adjuvant ipilimumab: Report of two cases. *Journal for Immunotherapy of Cancer, 6*(1), 83.
63. Eggermont, A. M. M., et al. (2015). Adjuvant ipilimumab versus placebo after complete resection of high-risk stage III melanoma (EORTC 18071): A randomised, double-blind, phase 3 trial. *The Lancet Oncology, 16*(5), 522–530.

64. Eggermont, A. M. M., et al. (2016). Prolonged survival in stage III melanoma with ipilimumab adjuvant therapy. *The New England Journal of Medicine, 375*(19), 1845–1855.
65. Weber, J., et al. (2017). Adjuvant nivolumab versus ipilimumab in resected stage III or IV melanoma. *The New England Journal of Medicine, 377*(19), 1824–1835.
66. Blank, C. U., et al. (2018). Neoadjuvant versus adjuvant ipilimumab plus nivolumab in macroscopic stage III melanoma. *Nature Medicine, 24*(11), 1655–1661.
67. Colwell, J. (2015). Is PD-L1 expression a biomarker of response? *Cancer Discovery, 5*(12).
68. Fabrizio, D. A., et al. (2018). Beyond microsatellite testing: Assessment of tumor mutational burden identifies subsets of colorectal cancer who may respond to immune checkpoint inhibition. *Journal of Gastrointestinal Oncology, 9*(4), 610.
69. Salem, M. E., et al. (2018). 1835PDComparative molecular analysis between microsatellite instability-high (MSI-H) tumors with high tumor mutational burden (TMB-H) versus MSI-H tumors with TMB-intermediate/low. *Annals of Oncology, 29*(suppl_8), mdy303–mdy005.
70. Carbone, D. P., et al. (2017). First-line nivolumab in stage IV or recurrent non-small-cell lung cancer. *The New England Journal of Medicine, 376*(25), 2415–2426.
71. Hellmann, M. D., et al. (2018). Nivolumab plus ipilimumab in lung cancer with a high tumor mutational burden. *The New England Journal of Medicine, 378*(22), 2093–2104.
72. McDermott, D. F., et al. (2018). Clinical activity and molecular correlates of response to atezolizumab alone or in combination with bevacizumab versus sunitinib in renal cell carcinoma. *Nature Medicine, 24*(6), 749–757.
73. Yang, W., et al. (2019). Immunogenic neoantigens derived from gene fusions stimulate T cell responses. *Nature Medicine, 25*(5), 767–775.
74. Yuan, J., et al. (2016). Novel technologies and emerging biomarkers for personalized cancer immunotherapy. *Journal for Immunotherapy of Cancer, 4*(1), 3.
75. Kruger, S., et al. (2017). Serum levels of soluble programmed death protein 1 (sPD-1) and soluble programmed death ligand 1 (sPD-L1) in advanced pancreatic cancer. *Oncoimmunology, 6*(5), e1310358.
76. Gagan, J., & Van Allen, E. M. (2015). Next-generation sequencing to guide cancer therapy. *Genome Medicine, 7*(1), 1.
77. Haratani, K., et al. (2018). Association of immune-related adverse events with nivolumab efficacy in non-small cell lung cancer. *JAMA Oncology, 4*(3), 374–378.
78. Haanen, J. B., et al. (2017). Management of toxicities from immunotherapy: ESMO Clinical Practice Guidelines for diagnosis, treatment and follow-up. *Annals of Oncology, 28*(suppl_4), iv119–iv142.
79. Hanahan, D., & Weinberg, R. A. (2011). Hallmarks of cancer: The next generation. *Cell, 144*(5), 646–674.
80. Zaretsky, J. M., et al. (2016). Mutations associated with acquired resistance to PD-1 blockade in melanoma. *The New England Journal of Medicine, 375*(9), 819–829.
81. Hanna, E., Rémuzat, C., Auquier, P., & Toumi, M. (2016). Advanced therapy medicinal products: Current and future perspectives. *Journal of Market Access & Health Policy, 4*(1), 31036.
82. Pignatti, F., et al. (2002). The review of drug applications submitted to the European Medicines Evaluation Agency: Frequently raised objections, and outcome. *European Journal of Clinical Pharmacology, 58*(9), 573–580.
83. MacIulaitis, R., D'Apote, L., Buchanan, A., Pioppo, L., & Schneider, C. K. (2012). Clinical development of advanced therapy medicinal products in Europe: Evidence that regulators must be proactive. *Molecular Therapy, 20*(3), 479–482.
84. de Wilde, S., Guchelaar, H. J., Zandvliet, M. L., & Meij, P. (2016). Clinical development of gene- and cell-based therapies: Overview of the European landscape. *Molecular Therapy-Methods & Clinical Development, 3*, 16073.
85. Codinach, M., et al. (2016). Design and validation of a consistent and reproducible manufacture process for the production of clinical-grade bone marrow–derived multipotent mesenchymal stromal cells. *Cytotherapy, 18*(9), 1197–1208.
86. Shire, S. J. (2009). Formulation and manufacturability of biologics. *Current Opinion in Biotechnology, 20*(6), 708–714.
87. Galli, M. C. (2016). ATMPs for cancer immunotherapy: A regulatory overview. *Methods in Molecular Biology, 1393*, 1–10.
88. Viganò, M., Giordano, R., & Lazzari, L. (2017). Challenges of running a GMP facility for regenerative medicine in a public hospital. *Regenerative Medicine, 12*(7), 803–813.
89. ten Ham, R. M. T., et al. (2018). Challenges in advanced therapy medicinal product development: A survey among companies in Europe. *Molecular Therapy-Methods & Clinical Development, 11*, 121–130.
90. Wayteck, L., Breckpot, K., Demeester, J., De Smedt, S. C., & Raemdonck, K. (2014). A personalized view on cancer immunotherapy. *Cancer Letters, 352*(1), 113–125.
91. Hoos, A., et al. (2010). Improved endpoints for cancer immunotherapy trials. *Journal of the National Cancer Institute, 102*(18), 1388–1397.
92. Alatrash, G., Jakher, H., Stafford, P. D., & Mittendorf, E. A. (2013). Cancer immunotherapies, their safety and toxicity. *Expert Opinion on Drug Safety, 12*(5), 631–645.
93. Kovarik, J. E. (2018). Cancer moonshot: Patents for patients. *Trends in Cancer, 4*(8), 515–516.
94. Bognar, C. L. F. B., Bychkovsky, B. L., et al. (2016). Compulsory licenses for cancer drugs: Does circumventing patent rights improve access to oncology medications? *Journal of Global Oncology, 2*(5), 292–301.
95. Couzin-Frankel, J. (2013). Breakthrough of the year 2013. *Cancer Immunotherapy Science, 342*(6165), 1432–1433.
96. Bethune, M. T., & Joglekar, A. V. (2017). Personalized T cell-mediated cancer immunotherapy: Progress and challenges. *Current Opinion in Biotechnology, 48*, 142–152.
97. Capietto, A. H., Jhunjhunwala, S., & Delamarre, L. (2017). Characterizing neoantigens for personalized cancer immunotherapy. *Current Opinion in Immunology, 46*, 58–65.
98. Gotwals, P., et al. (2017). Prospects for combining targeted and conventional cancer therapy with immunotherapy. *Nature Reviews Cancer, 17*(5), 286–301.
99. Francis, D. M., & Thomas, S. N. (2017). Progress and opportunities for enhancing the delivery and efficacy of checkpoint inhibitors for cancer immunotherapy. *Advanced Drug Delivery Reviews, 114*, 33–42.
100. Quandt, D., et al. (2017). Implementing liquid biopsies into clinical decision making for cancer immunotherapy. *Oncotarget, 8*(29), 48507.
101. Munn, D. H., & Bronte, V. (2016). Immune suppressive mechanisms in the tumor microenvironment. *Current Opinion in Immunology, 39*, 1–6.
102. Ries, C. H., et al. (2014). Targeting tumor-associated macrophages with anti-CSF-1R antibody reveals a strategy for cancer therapy. *Cancer Cell, 25*(6), 846–859.
103. Calcinotto, A., et al. (2018). IL-23 secreted by myeloid cells drives castration-resistant prostate cancer. *Nature, 559*(7714), 363–369.

104. Tokarew, N., Ogonek, J., Endres, S., von Bergwelt-Baildon, M., & Kobold, S. (2019). Teaching an old dog new tricks: Next-generation CAR T cells. *British Journal of Cancer, 120*(1), 26–37.
105. Ying, Z., et al. (2019). A safe and potent anti-CD19 CAR T cell therapy. *Nature Medicine, 25*(6), 947–953.
106. Gargett, T., & Brown, M. P. (2014). The inducible caspase-9 suicide gene system as a 'safety switch' to limit on-target, off-tumor toxicities of chimeric antigen receptor T-cells. *Frontiers in Pharmacology, 5*, 235.
107. Di Stasi, A., et al. (2011). Inducible apoptosis as a safety switch for adoptive cell therapy. *The New England Journal of Medicine, 365*, 1673–1683.
108. Panch, T., Mattie, H., & Celi, L. A. (2019). The "inconvenient truth" about AI in healthcare. *Npj Digital Medicine, 2*, 77.
109. Basch, E., et al. (2016). Symptom monitoring with patient-reported outcomes during routine cancer treatment: A randomized controlled trial. *Journal of Clinical Oncology, 34*(6), 557.

Index

A
Abraxane, 7
Active cancer targeting
    ADCs, 31
    expression patterns, 31
    synaphic targeting, 31
    systemic circulating probes, 31
    tumor stroma, 31
Active targeting, 12
Adenovirus, 317, 319–321
Advanced therapy medicinal products (ATMPs), 337
Affinity chromatography, 35
Agarose, 225
Agitation-based methods, 251
    cell suspension, 252
    drug screening, 253
    in vivo microenvironment, 253
    rotational culture systems, 254
    spinner flask bioreactors, 253
    techniques, 224
Aliphatic carbons, 62
Alpha emitters, 66
Alpha particle emitters, 72
(3-Aminopropyl)triethoxysilane (APTES), 198
(3-Aminopropyl)triethoxysilane thermally carbonized porous silicon (APTS-TCPSi) nanosystems, 136
Analytical chromatography, 259
Angiogenic integrins, 40
Angiotensin II receptor blocker (ARB), 274
Animal cancer models, 283
Annexin V, 69
Antiangiogenic treatments, 39
Antibody-dependent cell-mediated cytotoxicity (ADCC), 331
Antibody–drug conjugates (ADCs), 31
Antibody-immobilized lipid nanofibers, 170
Anticancer drugs, 7, 164
Anticancer nanoparticles
    animal models, 282
    cell-cell and cell-matrix communications, 275
    cell culturing, 275
    cultures, 275
    mRNA splicing patterns, 275
    pharmacokinetics, 282
    2D models, 275
Anticancer therapy, 12, 223
Antigen-presenting cells (APCs), 152, 304, 307, 329
    CCNPs, 152, 154
    immunogenic neoantigens, 152
    RBC membrane-coated NPs, 153, 155
    vaccine formulations, 152
Anti-tumor necrosis factor (TNF), 332
Aptamers, 14, 113
Aromatic amines, 175
Aromatic carbon-halogens bonds, 61
Ascorbic acid, 126
Asn-Gly-Arg (NGR) homing motif, 35
Astatine-211 (211At), 67
Asymmetric nanopore electrodes (ANE), 203, 205
Atomic force microscopy (AFM), 192
Auger electrons, 51
Autoradiography, 70
Avatars, 287

B
Basic fibroblast growth factor (bFGF), 166
B-cell maturation antigen (BCMA), 332
Bifunctional chelating agents (BFCs), 56
Biodegradable hydrogels, 130
Biodegradable polymers, 166, 180
Biodistribution analyses, 132, 139
Biohybrid materials
    in biomedical field, 135
    biomimetic, 135
    definition, 135
    personalized, 135
Biohybrid nanosystems
    advantages, 157 (*see also* Biohybrid NPs)
    in cancer chemo and combined therapy, 141–145
    cell ghosts, 136
    cells/receptors, 157
    disadvantages, 157
    natural affinity and binding, 157
Biohybrid NPs
    as chemotherapeutic carriers, 141–145
        cancer cells, 146, 147
        immune cells, 147, 148
        leukocyte membranes, 149, 150
        RBCs, 140, 145, 146
        stem cells, 146, 147
    nano-ghosts, 140
Biohybrid personalized materials, 135
Biohybrids
    characteristics and preparation method, 136
    in cancer therapy
        biodistribution, 139
        drug-resistant clonal selection, 139
        homing peptides, 139
        micro- and NPs, 139
        nanomedicine, 139

© Springer Nature Switzerland AG 2021
F. Fontana, H. A. Santos (eds.), *Bio-Nanomedicine for Cancer Therapy*, Advances in Experimental Medicine and Biology 1295, https://doi.org/10.1007/978-3-030-58174-9

Biohybrids (*cont.*)
      passive targeting, NPs, 139
      PDT and PTT, 139
   nanosystems, 136
   structure/preparation method, 136
Biointegrated systems, 135
Biomacromolecular delivery, 101
Biomacromolecules, 137
Biomarker, 333, 335, 336, 338–340, 343
Biomimetic design strategies, 74
Biomimetic microfluidic tumor microenvironment (bMTM), 281
Biomimetics, 135
Biomolecular recognition
   antigen-antibody interaction, 108
   ester bond, 109
   ethylene glycol-capped hybrid material, 108
   MTT and FACS, 109
Biomolecular sensors, 203
Biomolecules, 100, 108, 117, 199
Bioorthogonal pretargeted strategies, 66
Bioprinting technique, 251
Blood circulation, 163
1,3-Bis(2-chloroethyl)-1-nitrosourea (BCNU), 165
Boolean/Proximity operators, 20
Branched nanostraw (BNS), 212
Breast cancer cells, 110
Bristol–Myers Squibb's (BMS), 340
BSA-coated cobalt oxide (BSA-Co_3O_4), 126

C
Caelyx®, 15
Cancer-associated fibroblasts (CAFs), 272
Carbon-based nanomaterials, 72
Cancer biology, 202
Cancer biomarkers, 198, 201
Cancer cells, 146, 147, 194
Cancer cell spheroids, 248
Cancer diagnosis
   electrospun nanofibers (*see* Electrospun nanofibers)
Cancer immunoediting, 151
Cancer immunotherapy, 116, 303, 305–307, 309, 311, 312, 331, 333
   active, 330 (*see also* Immunotherapy)
   landscape, 331
   mesoporous silica materials, 116
   passive, 329
   vaccination process, 117
   vaccines, 116
   value, 331
Cancer Immunotherapy Pilot Program, 341
Cancer nanomedicine, 274, 275, 280
Cancer neoantigens, 151
Cancer stem cells (CSCs), 10, 90
Cancer therapy
   biohybrids (*see* Biohybrids)
   conventional treatment, 138
   nanotechnology, 139
   synergistic, 176, 177, 180–182
Cancer tissue-originated spheroids (CTOs), 249
Cancer treatment, 30
Cancer vaccines, 318, 320
Cancerous tissue, 30
Capsid surface modification, 317–319
CAR T-cell, 334, 337
Carbon dots, 7
Carbon electrodes, 207
Carbon nanotubes (CNTs), 6, 196
Carboxyl-rich carbon dots, 7
Carcinoembryonic antigen (CEA), 332
Cardiomyocytes, 208
Cardiovascular disease, 29
CAR-T cells, 332, 342
CD 47-Signal regulatory protein α (CD47-SIRPα), 18
CD133-RNA aptamer, 113
CD47 (biomolecules), 137
Cell-based cytotoxicity assays, 275
Cell-cell interactions, 224–226
Cell-ECM interactions, 225
Cell ghosts, 136
Cell line-derived models, 285, 289
Cell line derived-xenografts, 285
Cell-matrix and cell-cell interactions, 276
Cell membrane coated nanoparticles, 310
Cell metabolism, 192, 202, 203
Cell monolayer models, 246
Cell-nanoneedle interface, 192, 194, 195
Cell penetrating peptides, 5
Cell sensing, 208, 209
Cellular heterogeneity, 243, 245–247
Cell viability assays, 256
C-end Rule (CendR), 36
CendR trans-tissue transport pathway, 40
CendR tumor-penetrating peptides (TPP), 39
Cetyltrimethylammonium bromide (CTAB), 100
Chelator-based radiometal labeling, 57, 61
Chelator-mediated radiolabeling, 56–60
Chemically resistive gas sensors, 175
Chemo-photothermal therapy, 127
Chemotherapeutic drugs, 29
Chemotherapy, 3, 81, 82
   drugs, 163, 168
   fluorescent chemosensor, 174
   LDDSs, 181
   nanofibers for cancer therapy, 165
   and photodynamic therapy nanohybrids, 168
   postoperative, 165
   and radiotherapy, 223
   side effect, 167
   synergistic therapy, 177, 180
   and thermal therapy, 181
Chimeric antigen receptor (CAR), 92, 330
Chitosan, 208
Chloramine-T, 62
Chlorine-based oxidants, 63
Chronic myelogenous leukemia (CML), 211
Circulating tumor cells (CTCs), 287
Clinical development, 329, 337, 338, 341, 342
Clinical translation, 288
Cocktail, 54
Co-delivery, 116
Colospheres, 249
Combination therapy, 82, 85, 86, 91, 92, 333
Combretastatin A4(CA4), 180
Committee for Advanced Therapies (CAT), 338
Complement-dependent cytotoxicity (CDC), 331
Complex manufacturing processes, 337
Computed tomography (CT), 309
Connective tissue growth factor (CTGF), 84
Controlled drug release systems, 103
Conventional cancer therapies, 149
Conventional nanosystems, 149
Conventional therapies, 29

Copper sulphide nanoparticles, 72, 73
Copper-64, 66, 72
Coulomb forces, 52
Creative Commons Attribution (CC BY), 306
Cu-doped layered double hydroxide (Cu-LDH) nanoparticles, 73
Cupric oxide (Cu_2O), 124
Cyclic peptide iRGD, 12
Cyclodextrins (CDs), 179
Cytomembrane-coated NPs, 153, 156
Cytoplasm, 194
Cytoskeletal mechanics, 209, 210
Cytoskeleton, 194
Cytosolic cathepsin B (CTSB), 201
Cytotoxic doxorubicin, 74
Cytotoxicity, 244

D
Danger-associated molecular patterns (DAMPs), 318
DaunoXome®, 15
"Decay chain", 51
Dedicated veterinary systems, 70
Deficient mismatch repair (dMMR), 335
Degradable matrix
  hydrogels, 130
Degradation, 132
  acidic pH values, 127
  BSA-Co_3O_4 nanoparticles, 126
  coating Cu_2O, 124
  hydrogen peroxide, 124
  nanodots dispersion, 124
  oxidation, 123
  PEG-WN-DOX nanoparticles, 124
  pH, 127
  photodynamic efficacy, 125
  photothermal effect, 125
  reduction, 125
  VS2 nanosheets, 123
Dendrimers, 8
Dendritic cells (DC), 306, 307, 318, 334
Desferrioxamine (DFO), 57
Diacyl dimethylammonium-propane (DAP), 312
Digital revolution, 343
Dimetyl-α-benzantracene (DMBA), 81
3-(4,5-Dimethylthiazol-2-yl)-2,5-diphenyltetrazolium bromide (MTT), 256, 257
Dipalmitoyl phosphatidylcholine (DSPC)-based liposomes, 72
Distearoylphosphocholine/distearoylphosphoglycerol/cholesterol (Chol)/DOP, 307
Disteroyl phosphocholine (DSPC), 307
Disteroyl phosphoethanolamine (DSPE), 307
Dithiothreitol (DTT), 108
Dosimetry, 56, 70–72
Doxil®, 14, 282
Doxorubicin (DOX), 81, 105, 127, 259, 310
Doxorubicin hydrochloride (Dox), 164, 165
Drug biodistribution, 9
Drug carrier, 177
Drug combinations, 333
Drug degradation, 19
Drug delivery, 135
Drug delivery systems (DDSs)
  advantage, 15
  anticancer, 10
  anticancer nanomedicine, 15
  cancer therapy, 3
    acute and chronic toxicities, 20
    cytotoxic drugs, 19
    FR positive cells, 17
    glycosaminoglycans, 18
    hybrid, 19
    lipid-polymer hybrid, 19
    medical management, 17
    nanosheets, 17
    nanotransporter, 18
    properties, 19
    protein transporters, 18
    receptors, 17
  charge-switchable, 11
  chemotherapeutic drugs, 3, 163
  chemotherapy, 4
  drug circulation, 4
  DU145 prostate and HCT116, 15
  dual targeting, 14
  electrospun nanofibers, 168
  generation, 13
  imaging agents, 4
  LDDSs, 164
  lipid drug, 4
  manuscripts selection, 20
  moieties, 14
  nanocarriers, 11
  nanomicelles, 4
  nanosized, 4
  pH differences, 11
  pharmacokinetic analysis, 4
  physicochemical properties, 16
  SDDSs, 163
  shape, 16
  side effects, 3
  size and shape, 11
  systemic injection, 16
  temperature, 11
  therapeutic efficacy, 15, 17
Drug-loaded electrospun nanofibers
  gene-loaded, 167, 168
  oil-soluble, 164, 165
  protein-loaded, 166–167
  water-soluble, 165, 166
Dual carbon electrodes (DCE), 203

E
E-cadherin, 209
ECM-degrading enzymes, 237
Effective antitumor immunity, 151
Efficacy, anticancer, 235, 237–239
Electrical conductance, 194
Electrical sensing microfluidic device, 260
Electrochemical biosensors (ECBSs), 173, 174
Electrochemical DNA biosensors, 173
Electroporation, 198
Electrospinning sensors
  early diagnosis, 173
  ECBSc, 173
  electrochemical, 173
  fluorescent chemosensors, 174, 175
  gas sensor, 175
  immunosensors, 175
Electrospun nanofibers
  biomacromolecules, 164
  as carriers, 164

Electrospun nanofibers (*cont.*)
  for cell capture
    dynamic cancer cell capture, 170–172
    fabrication, 171
    static cancer cell capture, 169, 170
  drug release behavior, 166
  electrostatic force production, 164
  properties, 164
  thermal-responsive, 180
Emulsion-based spheroid formation method, 254
Emulsions, 8
  microemulsions, 8
  nanoencapsulation, 8
  phase, 8
Endocytic pathway, 14
Endocytosis pathways, 39
Engelbreth-Holm-Swarm mouse sarcoma cells, 279
Enhanced permeability and retention (EPR) effect, 31, 139, 273, 282
  heterogeneity, 273
  nanomedicines, 273
Enzymatic degradation, 123
Enzymatically degradable nanoparticles, 122
  nano-RGO, 123
  RGO-PEG-FA nanosheets, 123
Enzyme-responsive drug, 135
Epidermal growth factor (EGF), 38
Epidermal growth factor receptor (EGFR), 39, 332
Epstein–Barr virus (EBV)-related antigens, 332
Erythrocyte membrane vesicles, 17
Erythrocytes, 10
1-Ethyl-3-(3-dimethylaminopropyl)-carbodiimide (EDC)-N-hydroxysuccinimide (NHS), 137
European Medicines Evaluation Agency (EMA), 17, 82, 329
External stimuli
  cytotoxicity assay, 105
  intelligent delivery system, 104
  magnetic-guided conduction, 104
  magnetic MSNs, 104, 105
  magnetic properties, 104
  PDT, 105, 106
  siRNA, 104
  trastuzumab, 104
  ultrasound, 106
Extracellular matrix (ECM), 37, 167, 224–227, 234, 235, 237, 272
ExtraCRAd, 320, 321
Extra-large-pore MSNs (XL-MSNs), 101
Ex vivo biodistribution study, 72

F
Fibroblast growth factor receptor 3 (FGFR3), 232, 236
Field-effect transistor (FET), 203
Flow cytometry, 259
Fluidic force microscopy (FluidFM), 192, 213
Fluorescence in situ hybridization (FISH), 213
Fluorescence tracking, 123
Fluorescent carbon dots, 129
Fluorescent chemosensors, 174, 175
[18F]fluorination, 65
Focused ion beam-scanning electron microscopy (FIB-SEM), 193
Fragment crystallisable (Fc), 331
FS-7-associated surface antigen (FAS), 137
Fullerenes, 6

G
Gangliosides, 139
Gas sensors, 175
Gene delivery, 112
  aptamers, 113
  PC9 and A549 cells, 112
  siRNA, 114
  therapy, 112
Gene loading and transfection efficiency, 112
Gene-loaded electrospun fibers, 167, 168
Gene therapy, 112, 318, 323
Generations, 8
Genetically engineered mouse models (GEMMs), 285
  advantage, 285
Genomic mutation, 337
Glioma stem cells (GSCs), 90
Glucocorticoid-induced TNFR-related protein (GITR), 332
Glucocorticoid treatment, 336
Glucose oxidase (GOx), 203
Glutathione (GSH), 107
  diselenide-bridged MSNs, 108
  disulfide bonds, 108
  sensitive properties, 108
Glycocalyx, 194
Gold nanoparticles (AuNPs), 72, 309, 312
Good Manufacturing Practices (GMP), 337
GQD-bioconjugates, 6
Graphene-decorated magnetic dendrimers, 8
Growth factors (GF), 166, 167

H
Hanging drop method, 250, 252, 253
γH2AX, histone phosphorylation, 69
Health technology assessment (HTA), 331
Heat-induced radiolabeling (HIR), 61
Heat-shock protein (HSP), 131
Hemoglobin (Hb), 80
Herpes simplex virus (HSV), 332–333
Herpes simplex virus 1 (HSV-1), 320
Heterogeneous 3D model cultures, 247
Heterogenicity, 226
Heterotypic spheroid models, 247
Heterotypic spheroids, 247
High-content screening (HCS) systems, 282
Highly energetic particle radiation, 50
Highly tissue-penetrant gamma radiation, 50
High-mobility box (HMGB1), 307
High-resolution scanning electron microscopy, 153
High-throughput screening (HTS), 226
Homing peptides, 36
  CLT1 and 2 peptides, 36
  CREKA, 37
  ECM, 37
  neoplastic vascular signatures, 37
  tTF-CREKA, 37
Homo/isotopic exchange, 64
Homogeneous distribution, 231
Homotypic spheroids, 246, 262
Human dosimetry, 71
Human fibrosarcoma cells, 280
Human Papilloma Virus (HPV), 332
Human recombinant hyaluronidase, 140
Hyaluronic acid (HA), 38, 139
Hybrid MSN-HA nanoparticles, 114

Hybrid stimuli-responsive micelles, 9
Hydrogel nanoparticles, 310
Hydrogels, 254, 255, 263
Hydrogen peroxide (H_2O_2), 124
Hydroxyl bursts, 207
Hyperbaric oxygen (HBO) therapy
  antitumor efficacy, 78
  applications
    cancer therapies, 81
    chemotherapy, 81
    PDT, 82
    radiotherapy, 81
  biomacromolecules, 92
  cancer therapies, 78
  characteristics, 77
  clinical trials, 92
  Doxil®, 91
  HBO+Doxil®, 91
  HBO therapy, 79
  intratumor blood flow, 78
  molecular oxygen, 77
  monoplace chambers, 79
  nanoformulations, 78
  nanomedicine, 78, 91
  nanotherapeutics, 90
  pathophysiological barriers, 78
  physical barriers, 78
  principles, 79
  side effects, 79, 80
  surface modifications, 78
  tumor hypoxia, 80
  UHMS, 78
Hyperbranched polymers, 8
Hypoxia, 244
Hypoxia induced factor (HIF), 78
Hypoxic tumor microenvironment (TME), 77

I
Idoleamine-2,3 dioxygenase (IDO), 332
Imaging agent, 50
Imaging-compliant isotopes, 49
Imaging probe, 50
Immune-based agents, 333
Immune-based therapeutic agents, 336
Immune cells, 147, 148
Immune checkpoint blockade, 305
Immune checkpoint inhibitors (ICI), 305, 331
Immune system, 147
Immunization, 304
Immunohistochemistry, 257
Immunomodulators, 332
Immunoprecipitation (IP), 211
Immunosensors, 173, 175
Immunostimulatory molecular adjuvants, 304
Immunotherapy, 328, 329, 334
  antitumor immune response, 150
  approaches, 151
  biohybrid NPs
    APCs (*see* Antigen-presenting cells (APCs))
    cancer neoantigens, 151
    CCNPs, 152
    cellular membranes, 151
    immunogenicity, 152
  cancer immunoediting, 151
    elimination phase, 151
    equilibrium phase, 151
    escape phase, 151
  combined therapies, 153, 155, 156
  electrospun nanofibers (*see* Electrospun nanofibers)
  and PDT
    cytomembrane-coated NPs, 153, 156
    NK cell membrane-coated NPs, 154, 155
  and PTT, 155
  as therapeutic approach, 150
  in TME, 150
  TGF-β, 181
  tumor suppressor mechanism, 151
In vivo assays, 227, 234, 237, 238
In vivo peptide phage biopanning, 34
In vivo play-off assay, 35
In vivo whole-animal tumor models, 224
Inductively coupled plasma mass spectrometry (IPC-MS), 259
Industry-driven development, 341
Inorganic nanoparticles, 309
Integrin-targeting homing peptides, 35
Integrins, 137
Intellectual property (IP), 339
Intelligent cancer therapy
  electrospun nanofibers
    for effective immunotherapy, 181
    for synergistic therapy, 181, 182
  nanofibers with switchable drug release (*see* Switchable drug release)
Intercellular adhesion molecule 1 (ICAM), 147
Internal stimuli
  electrostatic interaction, 106
  GSH, 107
  LNCaP-AI tumor model, 107
  pH, 106
  pH-sensitive switch, 106
  substances and polymers, 106
  tumor microenvironment, 106
Inter-tumour heterogeneity, 335
Intracellular pH, 201, 203
Intracellular protein delivery, 110
Intracellular sensing, 192
Intratumoral penetration, 273, 279
Inverse electron-demand Diels-Alder cycloaddition (IEDDA), 66
Iodine-124, 65
Iodinium salts, 68
Iododeprotonation, 61
Iodogen, 62
Ionizing radiation, 50, 69

K
Kaplan–Meier survival curves, 338

L
Lactate dehydrogenase B (LHDB), 212
Lambert-Beer Law, 122
Large-pore MSNs (LPMSNs), 100
  approaches and synthetic pathways, 101
  CTAB-stabilized iron oxide nanoparticles, 101
  discrete, 101
  macromolecular drugs, 103
  OVA and CpG, 102
  XL-MSNs, 101
Laser-inducible degradation, 127
  photothermal effect, 128

Laser irradiation, 128
Leukocyte cell membrane, 143, 144, 147, 149, 150, 157
Linear energy transfer (LET) value, 50
Lipid-based NCs, 4
  bioactive compounds, 5
  gambogic, 5
  melphalan and miR-181, 5
  pamoic acid, 5
  polymer, 5
  RGE-coumarin 6, 5
  synergistic cytotoxicity, 5
  therapeutic efficacy, 5
Lipid/calcium/phosphate (LCP), 307, 310
Liposome-Polycation-Plasmid DNA (LPD), 307
Liposomes, 4, 6, 304, 306, 307, 311, 312
Liquid overlay, 250–252
Liquid scintillation cocktails, 54
Localized drug delivery systems (LDDSs), 164, 181
Lodobeads, 62
Lymphocyte-activation gene 3 (LAG3), 332

M
Macrocyclic chelators, 57
Macromolecular drug delivery, 109
Macrophage cell membrane, 148, 149
Magnetic 3D cell culturing, 250–252
Magnetic bioprinting, 251
Magnetic MSNs, 104
Magnetic nanoparticles (MNPs), 176, 177, 182
Magnetofection, 104
Major histocompatibility complex (MHC), 304
Major histocompatibility complex class I molecules (MHC-I), 318
Malignant cells, 30
Manocept ™, 38
Marketing authorisation (MA), 339
Mass spectrometry (MS), 35, 213
MATLAB program, 256
Matrigel™, 279
Matrix- and scaffold-based 3D
  collagen model, 280
  ECM-based, 279
  MMP2-dependent drug, 280
  spatial configuration, 280
Matrix metalloproteinases (MMPs), 168
Medical treatment technology, 172
Melanoma-associated antigen (MAGE), 332
Mesoporous organosilica nanoparticles (MONs), 113
Mesoporous silica materials, 100
Mesoporous silica nanoparticles (MSNs), 309
  advantage, 110
  biodegradability, 99
  biological medicines, 99, 100
  blood proteins, 99
  CD44 receptors, 116
  conventional, 101, 102
  COOH-functionalized, 102
  CTAB, 100
  dendritic, 102
  enzyme immobilization, 102
  human clinical trials, 99
  LPMSNs, 100
  lysozyme immobilized, 103
  mesoporous silica SBA-15, 101
  miRNAs, 115
  morphologies, 100
  multifunctional, 113
  nanocarriers, 99
  PEG-coated MSNs, 111
  Pluronic F127, 100
  siRNAs, 114, 115
  surface-functionalized magnetic, 105
  synthesis, 100
Metal ion detection, 207, 208
Metal nanoelectrodes, 209
Metal NPs, 5
Metallic nanoparticles, 3
Metastatic colorectal cancer, 14
Micelles, 9, 306–308
Microdosing principle, 55
Microfabrication techniques, 192
Microfluidic-based tumor-on-a-chip models, 281
Microfluidic probe (MFP), 213
Microfluidic technologies, 281
Microfluidics, 251
  description, 254
  electrical sensing device, 260
  emulsion-based spheroid formation method, 254
  high-throughput drug screening, 254
  microwell-based spheroid formation, 254
  polystyrene nanoparticle penetration, 260
  tumor angiogenesis, 260
MicroRNAs (miRNAs), 115
Minimal residual disease (MRD), 335
Mitochondria, 203, 207, 213
Mitochondrial membrane potential (MMP), 256
Miyaura borylation reaction, 62
Molecular beacons, 196, 199, 203
Monoclonal antibodies (mAbs), 18, 328
Mononuclear phagocytic system, 273
Multicellular tumor spheroids (MCTS), 277
  advantages, 225, 226
  application, 279
  biomimetic, 279
  cell-cell adhesion process, 247
  cellular association/tumor penetration, 227
    physicochemical characteristics, 227–233
    shape, 235, 236
    size, NPs, 227, 234
    surface charge, 234, 235
    surface modifications, 235–237
    3D cell model, 227
  cellular heterogeneity, 225
  cytocompatibility and efficacy, 238, 239
  disadvantages/limitations, 227
  drug sensitivity/resistance behavior, 249
  features, 279
  forming methods, 277, 278
  growth rate, 247
  hanging drop method, 225
  heterospheroids, 247
  micrometastasis, 247
  micro-sized cellular aggregates, 246
  mixed spheroids, 247
  multidrug resistance, 249
  nodules, 247
  organoids, 247
  size and cell line, 247
  spheroids, 247
  stimuli-responsive nanoformulations, 279
  stromal cells, 247
  techniques, 224

  3D spheroids, 226
  3D tumor models, 225
  tumoroids, 247
  2D monolayers, 279
Multielectrode arrays (MEA), 208, 209
Multimodal imaging, 71
Multimodality tracer, 55
Multispectral optoacoustic tomography (MOST), 132
Myeloid-derived suppressor cells (MDSCs), 155, 318, 342

N

Nanobiopsy methods, 213, 214
Nanobiotechnology, 12
Nanocapillaries, 192, 196, 202, 207, 213
Nanocapillary electrodes, 192
Nanocarriers, 135
  characterisits, 136
  effect, surface charge, 137
  hydrophilicity/hydrophobicity, 137
  nature-derived top-down biohybrids, 136
  pre-adsorption, proteins, 137
Nanocellulose crystals, 7
Nanocrystals, 7
Nanoelectrode arrays, 208, 209
Nanoelectrodes, 192, 195, 196, 202, 203, 205–208
Nano-electrospray (NES), 213
Nanofibers
  fabrication, 171
Nanofluidic devices, 196
Nanofountain probes (NFP), 196
Nano-ghosts, 136, 138, 146, 147
Nano-lipogels (nLGs), 310
Nanomedicine, 321, 323
  physical characteristics, 311
Nanomedicine antitumor efficacy
  breast cancer, 90
  cancer cells, 85
  chemotherapeutic agents, 85
  chemotherapy, 82
  CTGF, 84
  DOX, 84
  Doxil®, 82, 83, 85, 86
  flow cytometry, 85
  fluorescence, 83
  GSCs, 90
  hypothesis, 89
  in vivo antitumor activity, 83, 84
  mild photothermal therapy, 91, 92
  orthotopic liver cancer model, 83
  orthotopic model, 83
  photodynamic therapy, 82
  pimonidazole, 83
  quantitative analysis, 87
  radiotherapy, 82
  TMZ/PSi, 86–88
  tumor cells, 86, 88
  tumor metastasis, 87
Nanomedicine drugs, 31
Nanoneedles
  biochemical analysis, 214
  cancer biomarkers, 201
  cancer heterogeneity, 215
  cancer physiology, 215
  cell biology, 192
  cell interactions, 194
  cell-nanoneedle interface, 192, 194, 195
  cell sensing, 208, 209
  cellular contents, 211
  cellular scale, 193
  cytoskeletal mechanics, 209, 210
  intracellular sensing, 213
  metal ion detection, 207, 208
  molecular probes, 195, 196, 198
  monitor cell metabolism, 202, 203
  monitor cellular processes, 195, 196, 198
  mRNA, 203, 205
  multimodal mRNA detection, 206
  multiplexed biosensing, 198, 199
  multiplexed fluorescent, 213
  nano fiber-optics, 213
  nanoelectrode arrays, 208, 209
  nanoelectrodes, 207, 208
  nanoparticle probes, 199
  nanopipette electrodes, 202, 203
  nanoprobes, 198, 199
  nanoscale materials, 192
  nanostraws, 211–213
  nanostructures, 192
  nanowires, 213
  optical probes, 199, 201
  Raman-based hypoxia detection, 200
  ROS, 205, 207, 208
  single-cell metabolic nanosensors, 204
  single-cell nanobiopsy, 213
  solid structures, 192
  types, 192
Nanoparticle cytotoxicity, 256
Nanoparticle penetration
  and accumulation, 261
  fluorescent/confocal microscopy, 259
  methods of evaluation, 258
  modified gold, 259
  polystyrene, 260
  tumor spheroids, 259
Nanoparticles (NPs), 199
  biohybrids (*see* Biohybrid NPs)
  with cancer cells, 224
  CCNPs, 152, 154
  cytomembrane-coated, 153, 156
  factors, 260
  5-NPs, 238
  gold, 234
  iron/gold, 148
  lignin (LNPs), 235, 237
  molecules, 224
  monoculture model, 238
  NK cell membrane-coated, 154, 155
  passive targeting, 139
  PEGylation, 235
  physicochemical characteristics, 227
  physicochemical properties, 223, 260
  polystyrene, 227
  in preclinical testing, 224
  RBC membrane-coated NPs, 153, 155
  shape, 235
  size, 227
  3D cell model, 227
  in 3D tumor spheroids
    agglomeration and aggregation, 260
    imaging, 263
    penetration and accumulation, 261, 262

Nanoparticles (NPs) (*cont.*)
        physicochemical properties, 260
        sedimentation effect, 261
        spheroid formation and growth, 262–263
Nanoparticle toxicity
    cell viability assays, 257
    disadvantages, 256
    evaluation in 3D cultures, 255
    microfluidic platform, 260
    testing, in cells, 256
Nanopipettes, 192, 194–196, 199, 204, 207, 213
Nanostraw arrays, 192
Nanostraws, 192, 196, 197, 211–213
Nanosyringes, 199
Nanosystems, 50, 109, 137
Nanotechnology, 140, 306, 312
Nanotheranostics, 66, 72
Nanotopography, 194
Nanovaccines, 306, 307, 310
    formulation of vaccines, 306
Nanowires, 192, 196, 207, 209, 211
National Institutes of Health (NIH), 331
Natural killer (NK) cell membrane-coated NPs, 154, 155
Natural killer (NK) cells, 329
Neo-adjuvant therapy, 334
Neoantigens, 151
Neuronal cells, 208
Neuropilin-1, 32
New indications, 334
Next-generation cancer therapies
    immunotherapy, 30
    nanomedicine, 31
    personalized molecular therapies, 30
    preclinical and clinical, 30
Next-generation sequencing (NGS), 336
NGR peptides, 36
NIR-absorbing nanoparticles, 132
Non-small cell lung cancer (NSCLC), 81, 328
Non-viral carriers, 167
Nuclear imaging, 55, 57, 64, 70
Nuclear medicine, 52, 55
Nucleic acids, 196
Nucleolin, 38
Nucleophilic substitution, 62

O
Oil-soluble drug-loaded electrospun fibers, 164, 165
Oncological drugs, 287
Oncolytic adenoviruses, 152
Oncolytic viruses (OVs), 318
Onivyde®, 15
Opsonins, 15
Optical probes, 199, 201
Organic materials, 135
Organotypic multicellular spheroids (OMS)
    biology, 250
    cancer cell chemosensitivity, 250
    cell culture medium, 250
    cell resistance, 250
    description, 250
    from human mesothelioma, 250
    treatment strategies, 250
Ovalbumin (OVA), 101, 308, 310
Oxidation process, 125
Oxidative stress, 205

P
P32/qC1qR Targeting, 36
Paclitaxel (PTX), 164, 182
Pancreatic cancer therapy, 11
Pancreatic ductal adenocarcinoma (PDAC), 285
Parallel ionization multiplier (PIM) chamber, 70
Passive targeting, 10, 15
Patient-centric model, 331, 339, 343, 344
Patient-derived xenograft (PDX) models, 285, 286
    Avatars, 287
    and GEMMs, 288
    clinical predictive power, 287
    human immune system, 287
    humanized, 287
Patient-reported outcomes (PROs), 343
Patent term adjustment (PTA), 341
PEGylated nanoformulations, 139
PeptiCrad, 319, 320
Peptide-based synaphic targeting, 32
Peptide-coated viral nanoparticle, 318–320, 322
Peptide phage display, 33
    homing peptides, 35
    in vitro biopannin, 33
    in vivo phage screening, 34
    peptide-encoding DNA, 33
    receptor hunting technologies, 35
    systemic affinity targeting, 33
    target recombinant protein, 33
Peptides, 12
Peptidic targeting moiety, 148
PeptiENV, 320
Perfluorochemicals (PFC), 80
Peroxidase-mediated degradation, 123
Personalized molecular therapies, 30
P-glycoprotein (Pgp), 81
Phagolysosomes, 207
Pharmaceutical industry, 342
Pharmacokinetics, 125, 129
Phosphate buffer saline (PBS), 309
Photoacoustic imaging (PAI), 132
Photodynamic therapy (PDT), 4, 82, 105, 139
    BSA-MnO_2 nanoparticles, 106
    and cetuximab, 105
    combined starvation with cancer cell membrane, 147
    cytomembrane-coated NPs, 153, 156
    NK cell membrane-coated NPs, 154–155
    photodynamic effect, 107
    theranostic platform for imaging, 146
Photoluminescent imaging, 132
Photosensitizers (PS), 82
Photostimulated luminescence (PSL), 70
Photothermal conversion efficiency, 122
Photothermal efficiency, 130
Photothermal therapy (PTT), 80, 121, 123, 129, 132, 139
    application, 121
    characteristics, 122
    chemotherapeutics, 139
    cytomembrane-coated MOFs, 156
    designing, 122
    MDSCs, 155
    nanoparticles, 121
    tumor accumulation, 148
Photo-to-thermal energy conversion, 121
Platelet-leukocyte hybrid cell membrane, 144
Poly(carboxybetaine methacrylate) (pCBMA), 170
Poly(2-hydroxyethyl methacrylate) (poly-HEMA), 225

Polyacrylic acid, 208
Polydimethylsiloxane (PDMS), 281
Polyethylene glycol (PEG), 82, 211, 307, 312
Polyethyleneimine-based (PEI-based) nanomicelles, 307
Polyethylenimine (PEI), 104
Polylactic acid (PLA), 165, 166, 168, 180
Polymeric nanoparticles, 310
Polypeptide-based targeting ligands, 31
Porous silicon nanoparticles (PSi NPs), 86
Positron emission tomography (PET)
  imaging-compliant isotopes, 49
  pretargeted imaging, 66, 67
  principle of detection, 55
  radiometals, 56
Positron-emitting radionuclides, 64–66
Post authorisation safety study (PASS), 339
Pretargeted PET imaging, 66, 67
Pretargeted radiolabeling strategies, 66, 67
Prostate-specific membrane antigen (PSMA), 332
Prostate stem cell antigen (PSCA), 332
Protein adsorption, 16
Protein corona, 16, 262
Protein kinase A (PKA) activity, 199
Protein kinase C (PKC), 207
Protein-loaded electrospun nanofibers, 166, 167
Proteins, 14
Protein transporters, 18
Protein tyrosine phosphatase (PTP), 199
Proteolytic processing, 32

R
Radioactivity, 68
Radiochemical purity, 52
Radiochemical yield, 52
Radiochemistry
  automated gamma counter, 54
  theranostic nanosystem (*see* Theranostic nanosystem)
Radiohalogenation, 61–64
Radioiodinated Bolton-Hunter reagent, 63
Radioiododehalogenation, 64
Radioisotope production, 53
Radioisotopes, 49
Radiolabeled nanoparticles, 68
Radiolabeled theranostic nanosystems, 50
  alpha particle emitters, 72
  biomimetic design strategies, 74
  carbon-based nanomaterials, 72
  copper sulphide nanoparticles, 72, 73
  diagnostic and therapeutic radioisotopes, 71
  drug release, 73
  EPR effect, 72
  gold nanoparticles, 72
  liposomal system, 73
  melanin-based nanosystem, 73
  micelles and liposomes, 71
  multifunctional liposomes, 72
  multimodal imaging, 71
  passive targeting, 71
  PDT therapy, 73
  SWCNT, 72
  therapeutic agents, 71
  upPhDs, 74
Radiolabeled tracers
  in vitro methods
    assays for ROS and inflammatory markers, 68
    autoradiography, 70
    cell uptake and internalization assays, 68, 69
    ex vivo biodistribution study, 70
    radiation-Induced cellular damage, 69
    radiolabel stability assay, 68
  small animal PET, 70
  SPECT/CT imaging technology, 70
  theranostic nanosystems, 67
Radiolabeling
  with positron-emitting radionuclides, 64–66
  pretargeted strategies, 66, 67
  radiohalogenation, 61–64
  radiometals (*see* Radiometals)
Radiometal chelators, 58–60
Radiometals
  chelator-based labeling, 57, 61
  chelator-mediated radiolabeling, 56–60
  labeling strategies, 55
  radiopharmaceutical drug development, 55
  SPECT, PET and theranostics, 56
Radionuclide production, 52
Radiosynthesis, 52
Radiotherapy, 70, 81
Radiotracer administration, 54
Raman scattering, 199
Raman signature, 72
Ratiometric imaging, 201
R&D track, 340
Reactive nitrogen species (RNS), 207
Reactive oxygen species (ROS), 68, 82, 192, 203, 205, 207, 208, 343
Real-time autoradiographic systems, 70
Receptor-targeted drug delivery, 17
Red blood cells (RBCs), 140, 145, 146
Red fluorescent protein (RFP), 309
Reduced graphene oxide (RGO), 61
Research on Cancer–Global Cancer Observatory, 304
Resistance to treatment, 337
Reticuloendothelial system (RES), 82, 139
Rolling circle amplification (RCA), 198
Rotational culture systems, 254

S
Sandmeyer-type reaction, 62
Sandwich assay, 199
Scaffold-based culture systems, 254, 255
Scaffold-free methods, 251
Scanning electrochemical microscopy (SECM), 205
Scanning ion conductance microscopy (SICM), 194
Screening cancer nanoparticles, 276
Screening nanoparticles, in spheroids
  albendazole-loaded nanoparticles, 259
  cancer cell 2D cultures, 255
  colorimetric assays, 256
  high-throughput methods, 260
  MMP and cell viability, 256
  monolayer-grown cell cultures, 259
  nanoparticle penetration, evaluation, 258, 259
  nanoparticle toxicity, evaluation, 255–257
  3D cell cultures, 256
  trypan blue assay, 256
Self-assembling peptides, 181
Senescence-associated secretory phenotypes (SASPs), 69
Signal transducer and activator of transcription 3 (STAT3), 332
Silicon, 65
Single wall carbon nanotube (SWCNT), 72, 207

Single-photon emission computed tomography (SPECT)
  principle of detection, 55
  radiometals, 56
Small- and medium-sized entrepreneurs (SME), 338
Small animal PET, 70
Small-interfering RNA (siRNA), 104, 114, 167, 168
SPECT/CT imaging technology, 70
Spherical cancer models, 247
Spheroid formation techniques
  advantages and disadvantages, 250–251
  eligible techniques, 251
  scaffold-free methods, 251
Spheroid morphology, 257
Spheroids
  fibroblasts, 234
  gold NPs, 234
  HeLa cells, 235, 236
  heterogeneous, 225
  in vivo, 235
  MCTS (*see* Multicellular tumor spheroids (MCTS))
  melanoma, 235
  mono- and co-cultures, 226
  pancreatic cancer cell, 245
  poly-HEMA, 225
  screening nanoparticles, methods (*see* Screening nanoparticles, in spheroids)
  sizes, 227
  solid tumors in vivo, 243
  spheroid viability, 238
  targeting moieties and cell-penetrating peptides, 235
  3D spheroids, 226
Spheroids formation techniques
  agitation (*see* Agitation-based methods)
  hanging drop method, 252, 253
  liquid overlay method, 251, 252
  magnetic 3D cell culturing, 251, 252
  microfluidic cell culture platforms (*see* Microfluidics)
  scaffold-based culture systems, 254, 255
Spinner flask bioreactors, 253
SpyTag/SpyCatcher protein, 321
Stem cells, 146, 147
Stimulator of interferon genes (STING), 332
Stimuli-responsive polymers, 176
Stroma cells, 226, 272
Subgenomic mutation, 337
Succinimidyl astatobenzoate (SAB), 67
Superoxide dismutase (SOD), 207
Superparamagnetic iron oxide (SPIO) nanoparticles, 73
Superparamagnetic iron oxide nanoparticles (SPIONs), 105
Supplementary protection certificate (SPC), 341
Surface-enhanced Raman scattering (SERS), 199, 209
Surfactant-micelle-templating method, 100
Suzuki coupling reaction, 62
Switchable drug release
  light-responsive materials, 179
    NIR-responsive fibers, 180
    ultraviolet light-responsive fibers, 179–180
  magnetic-responsive nanofiber, 176–177
  pH-responsive nanofibers, 177–179
  stimuli-responsive electrospun nanofibers, 176
  stimuli-responsive polymers, 176
  thermal-responsive nanofibers, 180–181
Synergistic therapy, 176, 177, 180–182
Syngeneic and xenograft models, 282
  cell line-derived, 285
  physiological immune, 283
  subcutaneous models, 284
Synthetic materials, 255
Systemic DDSs (SDDSs), 163

T
Taxane-resistant tumor progression, 10
T-cell bispecific antibody (TCB), 247
T-cell receptor (TCR), 329
T-cell transfer therapy, 30
Technical developments, 343
Temozolomide (TMZ), 86
Temperature-sensitive nanoclusters (TSNC), 130
Theranostic nanosystem
  detection methods, 54, 55
  nuclear imaging, 55
  radioactive decay, 50
    decay chain, 51
    electromagnetic and electron radiation, 50
    ionizing radiation, 50
    proton-to-neutron ratio, 50
  radiochemical yield, 52
  radiolabeled monoclonal antibodies, 51
  radiolabeled tracers
    development and radiolabeling, 50
    imaging agent, 50
    imaging probe, 50
    LET value, 50
    molar activity, 52
    radiochemical purity, 52
    radiosynthetic procedures and purification, 52
    subpar effects, 51
  radionuclide production, 52, 53
  radiopharmaceutical development, 52
Theranostic nanosystems, 49, 57, 70
Theranostic nanosystemsafe handling, radioactive materials, 54
Theranostic system, 64
Therapeutic, 49
Thermally hydrocarbonized porous silicon (THCPSi) nanoparticles, 61
3D cancer cell models, 243
3D cell-cell interaction, 243
Three-dimensional (3D) cellular models, 224
Three-dimensional cancer cell models, 224, 247
3D cultures, 243, 245, 247, 255–260, 263
3D heterotypic spheroid model, 247
3D in vitro models, 227
3D spatial organization, 224
Three-dimensional tumor models, 279, 288, 289
  architecture and physical properties, 277
  genes encoding chemokines, 277
  TME, 276
3D tumor spheroid
  cells, 244
  cellular aggregates, 244
  cellular heterogeneity, 245
  complex 3D structure, 246
  cytotoxic agents, 246
  ECM constituents, 245
  gene expression, 245
  in monolayer, spheroids and in vivo tumors, 245
  in vivo tumors, 244
  internal structure, 244
  layers, 244
  microenvironment, 245
  peripheral cells, 244
  polysaccharide gel, 245

  shape, 244
  size and complexity, 244
  vs. 2D monolayer cultures, 245–246
Thrombosis and myocardial ischemia models, 37
Tissue-derived tumorospheres (TDTS)
  cell-cell interactions, 249
  colospheres, 249
  CTOs, 249
  histological features, 249
  MARY-X spheroids, 249
  MCTS model, 249
  subcategories, 249
  tumor tissue, 249
T lymphocytes (CTLs), 304
Toll-like receptors (TLRs), 332
Toxicity, 228, 238
Trade-Related Aspects of Intellectual Property Rights (TRIPS), 341
Traditional 2D models, 245
Traditional cancer chemotherapy, 109
Transfection efficacy experiments, 114
Transmission electron microscopy, 105
T regulatory cells (Treg), 329
Triple-negative breast cancer (TNBC), 334
Tumor accumulation, 141, 143, 146–149
Tumor associated macrophages (TAMs), 11, 38, 273, 274, 308
Tumor explant cultures, 280
Tumor-homing peptides, 32
  and receptors, 42
Tumor hypoxia, 78, 80
Tumor immunoediting, 303
Tumor-infiltrating immune cells, 273
4T1 tumor model, 148
Tumor microenvironment (TME), 10, 271, 272, 277, 305
  angiogenic vasculature, 272
  in anticancer nanomedicines, 275
  barriers, 274
  biomimicking nanocarrier, 155
  cancer immunotherapy, 150, 151
  in cancer progression, 273
  cancer treatment, 272
  clinical translation, 272
  features, 273, 275
  functional enzymes, 140
  heterogenicity, 224
  immune cells, 147
  immunosuppressive, 153
  matrix composition, 274
  nanogels, 147
  role, 272
  targeting moiety, 149
  therapeutic nanoparticles, 274
  3D cellular models, 224
  2D models, 224
Tumor microenvironment-on-chip platforms, 281
Tumor pathophysiology, 273
Tumor spheroids, 244
  cellular heterogeneity, 246–247
  formation techniques (*see* Spheroid formation techniques)
  homotypic spheroid model, 246
  MCTS (*see* Multicellular tumor spheroids (MCTS))
  in nanoparticle development process, 243
  nanoparticle effect, on cell-cell interaction, 244
  OMS, 250
  size and complexity, 244
  TDTS (*see* Tissue-derived tumorospheres (TDTS))
  tumorospheres, 249
  types, 248
Tumorospheres
  biology, 249
  cancer stemlike cells, 247
  clonal proliferation, 248
  in colorectal cancer, 249
  CSCs, 249
  heterogeneity and cell plasticity properties, 249
  stromal cells, 249
  TDTS, 249, 250
  tissue-derived, 247
Tumor-penetrating peptides
  CendR peptides, 40
  CendR system, 40
  iRGD, 41
  LyP-1 phage, 39
  LyP-1peptide, 40
  NRP-1 activates, 41
  tissue penetration, 39
  TT1 and LinTT1 peptides, 41
  tumor targeting, 41
  uCendR peptide, 40
Tumors' intrinsic barriers
  anticancer nanoparticles, 273
Tumour-associated antigens (TAAs), 318
Tumour heterogeneity, 337, 338
Tumour-infiltrating lymphocytes (TIL), 330
Tumour microenvironment (TME), 318, 319, 342
Tumour mutational burden (TMB), 335
Tumour neoantigens, 333
Tumour-specific antigens (TSA), 318
T2-weighted images, 105
Two-dimensional (2D) cell culture monolayer models, 224
Two-dimensional (2D) culture systems, 275
2D pore architecture, 100
2D screening platforms, 276

U
Ultra-large pore channels, 100
Ultra-small micelles (upPhD), 74
Ultrasmall nanodots, 128
Ultrasonic waves, 132
Ultrasound
  polymeric coating, 106
Ultrasound-responsive MSNs, 106
Underwater & Hyperbaric Medical Society (UHMS), 78
Uniform drug delivery, 273
United States Patent Office (USPTO), 341
Upconversion nanoparticles (UCMSs), 117
Upconversion nanophotosensitizers (UNPSs), 87

V
Vaccine delivery systems, 304
Vascular endothelial growth factor
    (VEGF), 9, 32, 83, 274, 318
Vascular heterogeneity
  angiogenic tumor blood vessels, 32
  tumor ZIP codes, 32
  vascular trees, 32
  vascular ZIP code, 32
Vascular leak syndrome, 32
Vascular zip codes, 139

Viral nanoparticles (VNPs), 317
  membrane envelop, 320
  RNA molecules, 321
  tumour epitope peptides, 319
viRNA, 321, 323

W
Warburg effect, 244
Water-soluble drug-loaded electrospun fibers, 165, 166
Water-soluble SPIO nanoparticles, 73
Whole-exome sequencing, 336
World Trade Organization (WTO), 341

Z
Zero premature release, 104
Zirconium-89, 66